

# ***RIKEN Accelerator Progress Report***

2018

vol. 52

理化学研究所 仁科加速器科学研究センター  
*RIKEN Nishina Center for Accelerator-Based Science*





*RIKEN Accelerator Progress Report* 2018

vol. **52**

理化学研究所 仁科加速器科学研究センター  
*RIKEN Nishina Center for Accelerator-Based Science*  
Wako, Saitama, 351-0198 JAPAN

## **RIKEN Accelerator Progress Report 2018 vol.52**

This is an unabridged version of the 52nd volume of RIKEN Accelerator Progress Report (hereinafter referred to as APR), the official annual report of the Nishina Center for Accelerator-Based Science.

A PDF version of APR can be downloaded from our website.  
[http://www.nishina.riken.jp/researcher/APR/index\\_e.html](http://www.nishina.riken.jp/researcher/APR/index_e.html)

### **Published by**

RIKEN Nishina Center for Accelerator-Based Science  
2-1 Hirosawa, Wako-shi, Saitama 351-0198 JAPAN

### **Director of RIKEN Nishina Center for Accelerator-Based Science**

Hideto En'yo

### **Editorial Board**

H. Ueno (Editor-in Chief), J. Zenihiro, T. Isobe, Y. Ichikawa, A. Kohama, E. Hiyama, T. Matsuzaki, R. Seidle, T. Doi, T. Tada, T. Tamagawa, K. Takahashi, Y. Higurashi, K. Ozeki, T. Sumikama, K. Morimoto, H. Sato, M. Watanabe, T. Ikeda, I. Watanabe, H. Haba, T. Abe, K. Tanaka, Y. Watanabe, H. Nagahama, M. Wada, Y. Tsuburai, M. Yamamoto, E. Fujino and I. Yoshida

### **Contact**

[Progress@ribf.riken.jp](mailto:Progress@ribf.riken.jp)

All rights reserved. This report or any portion thereof may not be reproduced or used in any form, including photostatic print or microfilm, without written permission from the Publisher.  
Contents of the manuscripts are the authors' responsibility. The Editors are not liable for the content of the report.

RIKEN Nishina Center for Accelerator-Based Science, September 2019

## PREFACE

In fiscal year 2018, RIKEN entered its 4th midterm, which will last for seven years. For this new midterm period, we have modified the Center's organization. The former RIBF Research Division was split into three divisions, the Nuclear Science and Transmutation Research Division, Research Facility Development Division, and Accelerator Application Research Division. The change makes our infrastructure components, application research, and nuclear transmutation research more visible. We merged the Theoretical Research Division into the Subnuclear Research Division, reflecting the recent promotions of the leading theorists in the Nishina Center.

We made this change, in part, because from this midterm, the RIKEN Nishina Center is categorized as a strategic research center, switched from the former infrastructure center. This means that we need to place more emphasis on our research strategy than on our user support as an accelerator facility. With this organizational change, we can pursue the enhancement of both RIKEN's own strategic research and user support for the community.

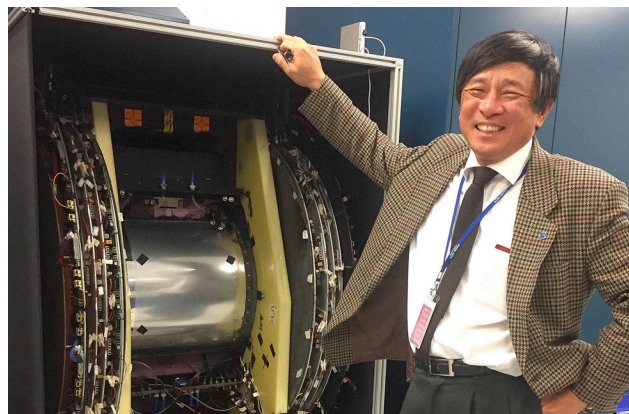
The Heisei era ended in April 2019. Considering the festive mood for the era change, I feel that it was much more natural for the Japanese imperial transition to have taken place through abdication rather than by passing of the Emperor. However, as stated by the Heisei Emperor, we have experienced so many disasters over the 30 Heisei years, and the one of the largest was the accident at the Fukushima Nuclear Power Plant. We still remember that many of us went there to perform radiation measurements of the local people and soil in Fukushima.

Nuclear energy is one of the most important social knowledges born from nuclear science. Unfortunately, with the radioactive waste generated by nuclear reactors becoming a social problem, because of the Fukushima disaster, and the decommissioning of the "Monju" plan, the nuclear energy cycle of our nation has failed. As nuclear physicists, we must now reconsider energy issues and identify the correct path for the use of nuclear energy by scientifically reconstructing its usefulness. Continuing operation of large nuclear power plants is not necessarily the only way to achieve this goal.

The Nishina Center has spearheaded a research effort to transform radioactive waste into short-lived nuclides with the use of the accelerator through the ImpACT Project. The patent "Radioactive Waste Processing Method," which originated from the Project, was awarded the 21st Century Invention Award for FY2018 by the Japan Institute of Invention and Innovation. The award ceremony was attended by Imperial Prince Takamatsunomiya Nobuhito. This is a very small step toward the real goal of the nuclear energy problem, but we have to pursue solutions patiently and continuously.

The year 2019 was proclaimed the International Year of the Periodic Table of Chemical Elements by UNESCO. The opening ceremony was held in Paris in January, and the Year will conclude at the closing ceremony scheduled for Tokyo on December 5. The 150th anniversary of the creation of the periodic table by Mendeleev as well as the recent completion of the 7th row of the table will be celebrated. Tokyo was chosen as the venue of the closing ceremony because of the discovery of nihonium.

The scientific goal of the Nishina Center is to obtain more research results from experiments conducted at the RIBF, promote facility expansion and reinforcement of the RIBF, and discover elements 119 and 120. We have already begun experiments to search for element 119. Trial operation of the superconducting RILAC will begin soon, providing a substantial boost to the search experiment. Only God knows whether the elements will be discovered in the near future or in 10 years.



A handwritten signature in black ink, appearing to read "H. En'yo".

*Hideto En'yo*  
*Director*

*RIKEN Nishina Center for Accelerator-Based Science*



## C O N T E N T S

Page

## PREFACE

## I . HIGHLIGHTS OF THE YEAR

First observation of $^{20}\text{B}$ and $^{21}\text{B}$ ..... S. Leblond <i>et al.</i>	1
Gamow–Teller giant resonance in $^{132}\text{Sn}$ ..... M. Sasano, J. Yasuda <i>et al.</i>	2
First spectroscopy of the near drip-line nucleus $^{40}\text{Mg}$ ..... H. L. Crawford, P. Fallon <i>et al.</i>	3
Interplay between nuclear shell evolution and shape deformation revealed by magnetic moment of $^{75}\text{Cu}$ ..... Y. Ichikawa <i>et al.</i>	4
Mass measurements of neutron-rich Ni isotopes in Rare RI Ring ..... A. Ozawa <i>et al.</i>	5
Discovery of $^{60}\text{Ca}$ and Implications For the Stability of $^{70}\text{Ca}$ ..... O. B. Tarasov	6
Nuclear surface diffuseness revealed in nucleon-nucleus diffraction ..... W. Horiuchi and A. Kohama	7
Proton- and deuteron-induced reactions on $^{107}\text{Pd}$ and $^{93}\text{Zr}$ at 20–30 MeV/nucleon ..... M. Dozono <i>et al.</i>	8
Transverse momentum dependent fragmentation measurements in Belle ..... R. Seidl	9
Measurement of elliptic flow of single electrons from semi-leptonic decay of charm and bottom hadrons in Au+Au collisions at $\sqrt{s_{NN}} = 200$ GeV ..... Y. Ueda <i>et al.</i>	10
The chiral propulsion effect ..... Y. Hirono <i>et al.</i>	11
Superconducting RILAC booster ..... N. Sakamoto <i>et al.</i>	12
Remodeling of acceleration cavity resonators for RIKEN Ring Cyclotron ..... K. Yamada <i>et al.</i>	13
He gas stripper with $\text{N}_2$ gas-jet curtain ..... H. Imao <i>et al.</i>	14
Upgrade of particle selection system for Rare RI Ring experiments ..... Y. Abe <i>et al.</i>	15
Aberration correction study for high-resolution optics of BigRIPS using sextupole magnets ..... T. Nishi <i>et al.</i>	16
In-gas-jet laser ionization spectroscopy at KISS ..... Y. Hirayama <i>et al.</i>	17
Microgram-order palladium isotope separation by odd-mass-selective photoionization ..... T. Sonoda and T. Kobayashi	18
Introducing silver atoms into superfluid helium for precision laser spectroscopy ..... W. Kobayashi <i>et al.</i>	19
Magnetic properties of Alkali-metal Superoxide, $\text{NaO}_2$ ..... F. Astuti <i>et al.</i>	20
Mass spectrometric speciation of mononuclear Re carbonyls in the gas phase ..... Y. Wang <i>et al.</i>	21
Practical synthesis of $^{211}\text{At}$ -labeled immunoconjugate by double click method for $\alpha$ -emission cancer radiotherapeutics ..... K. Fujiki and K. Tanaka <i>et al.</i>	22
Activation cross sections of $\alpha$ -induced reactions on $^{\text{nat}}\text{Zn}$ for Ge and Ga production ..... M. Aikawa <i>et al.</i>	23

A novel mutation induced by Ar-ion-irradiation affect grain length and improve yield in rice .....	24
R. Morita <i>et al.</i>	
Recent progress in overcoming interspecific hybrid sterility in rice .....	25
Y. Koide <i>et al.</i>	
Improved and robust method to efficiently deplete repetitive elements from complex plant genomes .....	26
H. Ichida and T. Abe	

## II. RESEARCH ACTIVITIES I (Nuclear, Particle and Astro-Physics)

### 1. Nuclear Physics

Breakup of $^9\text{C}$ studied at SAMURAI .....	27
A. I. Chilug, V. Panin <i>et al.</i>	
Cluster structure of neutron-rich beryllium isotopes investigated by cluster quasi-free scattering reaction .....	28
P. Li, D. Beaumel	
Particle identification in $^{11}\text{Li}(p, n)$ experiment at SAMURAI .....	29
Y. Hirai <i>et al.</i>	
Neutron-gamma separation performance of PANDORA in SAMURAI30 experiment .....	30
Y. Hirai <i>et al.</i>	
Gamow-Teller resonance in $^{14}\text{Be}(p, n)$ reaction .....	31
J. Gao and L. Stuhl	
Systematic study of one-proton and two-proton knockout reactions by deuterium target .....	32
M. Miwa <i>et al.</i>	
Study of spin-isospin response of $^{11}\text{Li}$ (SAMURAI30 experiment) .....	33
L. Stuhl <i>et al.</i>	
Overview of the experimental setup of SAMURAI30 to measure the $^{11}\text{Li}(p, n)$ reaction in inverse kinematics .....	34
M. Sasano, L. Stuhl <i>et al.</i>	
Neutron-neutron correlation in Borromean nucleus $^{11}\text{Li}$ via the $(p, pn)$ reaction .....	35
Y. Kubota <i>et al.</i>	
Particle identification of light charged particle by $S\pi\text{RIT-TPC}$ in Sn-Sn isotopic reactions .....	36
M. Kaneko <i>et al.</i>	
Recent results of collective flow for $S\pi\text{RIT-TPC}$ experiment .....	37
M. Kurata-Nishimura <i>et al.</i>	
New implant-decay correlation method for $\beta$ -delayed neutron emission measurements with the BRIKEN setup .....	38
O. Hall <i>et al.</i>	
Progress on the measurements of $P_n$ -values and half-lives for understanding the formation of the r-process rare-earth peak .....	39
A. Tarifeño-Saldivia	
$\beta$ decays of the heaviest $N = Z - 1$ nuclei and proton instability of $^{97}\text{In}$ .....	40
J. Park <i>et al.</i>	
Beta-gamma spectroscopy of neutron-rich $^{150}\text{Ba}$ .....	41
R. Yokoyama <i>et al.</i>	
Preliminary results on $\beta$ -decay of the $T_z = -1$ nucleus $^{66}\text{Se}$ at RIBF .....	42
P. Aguilera <i>et al.</i>	
Study of $\beta$ -decay of $^{71}\text{Kr}$ .....	43
A. Sveczer <i>et al.</i>	
Coexisting single-particle and octupole states in $^{133}\text{Sn}$ .....	44
G. Simpson <i>et al.</i>	
Inelastic scattering of neutron-rich Ni and Zn isotopes off a proton target .....	45
M. L. Cortés <i>et al.</i>	
Magnetic-moment measurement of the isomeric state of $^{130}\text{Sn}$ in the vicinity of doubly-magic nucleus $^{132}\text{Sn}$ .....	46
G. Georgiev <i>et al.</i>	
Track distortion due to ion back flow in CAT-S at RIBF113: $^{132}\text{Sn}(d, d')$ measurement .....	47
S. Ota <i>et al.</i>	
First mass measurements of neutron-rich calcium isotopes, $^{55-57}\text{Ca}$ .....	48
S. Michimasa <i>et al.</i>	

Re-measurement of the ${}^4\text{He}({}^8\text{He}, {}^8\text{Be})$ reaction S. Masuoka, S. Shimoura <i>et al.</i>	49
Evaluation of ${}^{79}\text{Se}(n, \gamma){}^{80}\text{Se}$ reaction by measuring ${}^{77,79}\text{Se}(d, p){}^{78,80}\text{Se}$ reactions N. Imai, M. Dozono <i>et al.</i>	50
Fine tuning of isochronism in Rare RI Ring using resonant Schottky monitor F. Suzaki <i>et al.</i>	51
Preliminary analysis of the mass measurement experiment in the south-western region of ${}^{132}\text{Sn}$ with Rare RI Ring H. F. Li <i>et al.</i>	52
First online experiment of $\alpha$ -ToF detector with MRTOF-MS T. Niwase <i>et al.</i>	53
$\beta$ - $\gamma$ spectroscopy of ${}^{195}\text{Os}$ at KISS M. Ahmed <i>et al.</i>	54
Feasibility study of ${}^{199}\text{Pt}$ $Q$ -moment measurement using in-gas-jet laser ionization spectroscopy at KISS H. Choi <i>et al.</i>	55
Electric field gradient of ZnO crystal measured by $\beta$ -NQR of ${}^{23}\text{Ne}$ H. Nishibata <i>et al.</i>	56
${}^7\text{Be}$ target production to measure ${}^7\text{Be}(d, p)$ reaction for the primordial ${}^7\text{Li}$ problem in Big-Bang Nucleosynthesis A. Inoue <i>et al.</i>	57
New measurement of ${}^8\text{Li}(\alpha, n){}^{11}\text{B}$ reactions Y. Mizoi <i>et al.</i>	58
Trojan Horse Method-based study of the ${}^{18}\text{F}(p, \alpha){}^{15}\text{O}$ reaction at astrophysical energies: update on the 2015 run S. Cherubini <i>et al.</i>	59
Gamow-Teller transitions in ${}^6\text{He}$ with PANDORA L. Stuhl <i>et al.</i>	60
$\beta$ -NMR measurements for ${}^{21}\text{O}$ at HIMAC A. Gladkov <i>et al.</i>	61
RI beam production at BigRIPS in 2018 Y. Shimizu <i>et al.</i>	62
Measurement of production cross-section and momentum distribution of isotopes produced from ${}^{18}\text{O}$ beam H. Takeda <i>et al.</i>	64
Cross-section measurement of neutron-rich isotopes produced from an RI beam of ${}^{132}\text{Sn}$ using a two-step scheme H. Suzuki <i>et al.</i>	65
<b>2. Nuclear Physics (Theory)</b>	
Improvement of functionals in density functional theory using inverse Kohn-Sham method and density functional perturbation theory D. Ohashi, T. Naito <i>et al.</i>	67
Coulomb exchange functional with generalized gradient approximation for self-consistent Skyrme Hartree-Fock calculations T. Naito, X. Roca-Maza <i>et al.</i>	68
Joint project for large-scale nuclear structure calculations in 2018 N. Shimizu <i>et al.</i>	69
Bubble nuclei within the self-consistent Hartree-Fock mean field plus pairing approach L. Tan Phuc <i>et al.</i>	70
Dineutron correlation and large quadrupole collectivity in deformed Mg isotopes near neutron drip line M. Yamagami	71
Isoscalar and isovector spin responses in $sd$ -shell nuclei H. Sagawa and T. Suzuki	72
Self-consistent constrained HFB in odd-A nuclei K. Sugawara-Tanabe and K. Tanabe	73
Nuclear symmetry energy and the breaking of the isospin symmetry: how do they reconcile with each other? X. Roca-Maza <i>et al.</i>	74
Neutron-proton pairing correlations and deformation for $N = Z$ nuclei in $pf$ -shell using deformed BCS and HFB approach E. Ha <i>et al.</i>	75

Spin-singlet and spin-triplet pairing correlations on shape evolution in $sd$ -shell $N = Z$ Nuclei .....	76
E. Ha <i>et al.</i>	
Low-lying collective excited states in non-integrable pairing models based on stationary phase approximation to the path integral .....	77
F. Ni <i>et al.</i>	
Study of giant dipole resonance in hot rotating light mass nucleus $^{31}\text{P}$ .....	78
D. Mondal <i>et al.</i>	
<b>3. Nuclear Data</b>	
Verification test of $^{107}\text{Pd}$ transmutation .....	79
Y. Miyake <i>et al.</i>	
Measurement of neutron production from 7 MeV/nucleon $\alpha$ incidence on a Bi target .....	80
K. Sugihara <i>et al.</i>	
EXFOR compilation of RIBF data in 2018 .....	81
S. Jagjit <i>et al.</i>	
<b>4. Hadron Physics</b>	
Preliminary result of the transverse single spin asymmetry in very forward $\pi^0$ production in 510 GeV $p^\dagger + p$ collisions .....	83
M. H. Kim	
The stability of energy scale for RHICf photon measurement during the 2017 operation .....	84
K. Sato <i>et al.</i>	
Cross section and longitudinal single-spin asymmetry $A_L$ for forward $W^\pm \rightarrow \mu^\pm \nu$ production in polarized $p + p$ collisions at $\sqrt{s} = 510$ GeV .....	85
R. Seidl	
Progress in analysis technique for extracting light-antiquark flavor asymmetry by SeaQuest at Fermilab .....	86
K. Nagai <i>et al.</i>	
Forward hadron calorimeter R&D .....	87
Y. Goto <i>et al.</i>	
Development of the intermediate silicon tracker for sPHENIX experiment at RHIC .....	88
I. Nakagawa	
Tracking performance simulation for INTT at sPHENIX .....	89
T. Todoroki <i>et al.</i>	
Preparation status of the J-PARC E16 experiment in 2018 .....	90
S. Yokkaichi	
Spectroscopy of pionic atoms in $^{122}\text{Sn}(d, ^3\text{He})$ reaction and angular dependence of the formation cross sections .....	91
T. Nishi <i>et al.</i>	
Isotope identification in nuclear emulsion plate for double-hypernuclear study .....	92
S. Kinbara <i>et al.</i>	
<b>5. Hadron Physics (Theory)</b>	
Short range $\pi J/\psi - D\bar{D}^*$ interaction .....	93
Y. Yamaguchi <i>et al.</i>	
Proton decay matrix elements at physical quark mass .....	94
Y. Aoki <i>et al.</i>	
The $\pi\gamma \rightarrow \pi\pi$ transition and the $\rho$ radiative decay width from lattice QCD .....	95
S. Meinel <i>et al.</i>	
Neutron stars from an effective quark theory of QCD .....	96
T. Tanimoto	
<b>6. Particle Physics</b>	
Baryon spectrum of an SU(4) composite Higgs theory .....	97
E. T. Neil <i>et al.</i>	
Updated empirical formulae of the masses of elementary particles .....	98
Y. Akiba	
A model of the empirical mass formulae of elementary particles .....	99
Y. Akiba	

**7. Astrophysics and Astro-Glaciology**

High-sensitivity sulfur isotopic measurements for Antarctic ice core analyses .....	101
K. Takahashi <i>et al.</i>	
Mass Measurements with the Rare-RI Ring for the $A = 130$ r-process Abundance Peak .....	102
S. Naimi	

**8. Accelerator**

Construction of New 28-GHz ECR ion source for RILAC .....	103
T. Nagatomo <i>et al.</i>	
Development of prototype superconducting linac for low-beta ions .....	104
N. Sakamoto <i>et al.</i>	
Performance test of bulk-niobium cavities for new superconducting linear accelerators .....	105
K. Yamada <i>et al.</i>	
Input power coupler for SRILAC .....	106
K. Ozeki <i>et al.</i>	
Development of RIKEN 28 GHz SC-ECRIS for the production of intense metal ion beam .....	107
Y. Higurashi <i>et al.</i>	
Beam energy adjuster for super-heavy element synthesis at RIKEN Ring Cyclotron .....	108
K. Yamada <i>et al.</i>	
Operation of high-temperature oven for 28-GHz superconducting ECR ion source .....	109
J. Ohnishi <i>et al.</i>	
Laser Energy Dependence of Plasma Instability by Solenoid Magnetic Field .....	110
T. Karino <i>et al.</i>	
Evaluation of beam orbit calculation method for the injection line of AVF cyclotron and performance evaluation of pepper-pot emittance monitor .....	111
Y. Kotaka <i>et al.</i>	
Updating control units around the AVF cyclotron .....	112
M. Komiyama <i>et al.</i>	
Reconstruction of RF system controller for RIKEN Ring Cyclotron .....	113
K. Yamada <i>et al.</i>	
Radiation monitoring for cycrotrons in RIBF .....	114
M. Nakamura <i>et al.</i>	
Development of beam interlock system driven by change in current of the magnet .....	115
K. Kumagai and A. Uchiyama	
Design of reliable control with star-topology fieldbus communication for an electron cyclotron resonance ion source at RIBF .....	116
A. Uchiyama	
Operation report for Nishina and RIBF water-cooling systems .....	117
T. Maie <i>et al.</i>	
Pressure measurement of plasma window with large diameter .....	118
N. Ikoma <i>et al.</i>	
Maintenance of vacuum conditions of RILAC .....	119
S. Watanabe <i>et al.</i>	

**9. Instrumentation**

Application of the Generic Electronics for Time Projection Chamber (GET) readout system for heavy radioactive isotope collision experiments .....	121
T. Isobe <i>et al.</i>	
PANDORA, a large volume low-energy neutron detector with real-time neutron-gamma discrimination .....	122
L. Stuhl <i>et al.</i>	
Measurement of total kinetic energy using LaBr <sub>3</sub> (Ce) crystal in ZeroDegree spectrometer for two-step experiment .....	123
H. Suzuki <i>et al.</i>	
Prototype of new delay line with chip inductors for the PPAC .....	124
H. Sato <i>et al.</i>	
Development of electronics to allow vertex determination in the KISS MSPGC .....	125
P. Schury <i>et al.</i>	

Development of Plastic Scintillator Barrel for WASA at GSI .....	126
R. Sekiya <i>et al.</i>	
Energy dependence study of cylindrical drift chamber used for the MTV experiment .....	127
F. Goto <i>et al.</i>	
Development of long and high-density data bus for sPHENIX INTT detector .....	128
T. Hachiya <i>et al.</i>	
Performance evaluation of sensor module for INTT at sPHENIX .....	129
A. Suzuki <i>et al.</i>	
Slit system between the foci F2 and F3 of the BigRIPS separator .....	130
K. Yoshida <i>et al.</i>	
Fast beam interlock system for BigRIPS separator .....	131
K. Yoshida	
Thermal model simulation of high-power rotating target for BigRIPS separator .....	132
Z. Korkulu <i>et al.</i>	
Primary beam intensity calibration method using charge-states distribution .....	133
D. S. Ahn <i>et al.</i>	
Angle-tunable degrader system for OEDO .....	134
J. W. Hwang <i>et al.</i>	
Development of dispersion-matching optics of primary beam for SRC-BigRIPS system .....	135
S. Y. Matsumoto <i>et al.</i>	
SHE-Mass-II: an MRTOF-MS for Super Heavy Nuclei .....	136
M. Wada <i>et al.</i>	
Status and future plans of the MRTOF MS constructed at the SLOWRI facility .....	137
M. Rosenbusch <i>et al.</i>	
Development of multiple reflection time of flight mass spectrograph at KISS .....	138
J. Y. Moon <i>et al.</i>	
Offline test for RF carpet transportation in RF ion guide gas cell at the SLOWRI facility .....	139
A. Takamine <i>et al.</i>	
Study of extraction yield of multi-nucleon transfer reaction products by using cooled argon gas cell .....	140
Y. Hirayama <i>et al.</i>	
Yield analysis using target sliding system at KISS .....	141
Y. X. Watanabe <i>et al.</i>	
Present status of ERIS at the SCRIT electron scattering facility .....	142
T. Ohnishi <i>et al.</i>	
Electron-beam-current control at RTM injector .....	143
M. Watanabe <i>et al.</i>	
Modification of dc-to-pulse converter FRAC .....	144
S. Sato <i>et al.</i>	
Precise magnetic field measurement of WiSES .....	145
H. Wauke <i>et al.</i>	
MPV – Parallel Readout Extension of VME .....	146
H. Baba <i>et al.</i>	
Validation method to merge digital data acquisition with analog data-acquisition system in SAMURAI30 experiment .....	147
J. Gao, L. Stuhl	
Development of 1.5-mm thick liquid hydrogen target .....	148
S. Koyama and D. Suzuki	
Profile measurement of a large target cell of liquid hydrogen .....	149
M. Miwa <i>et al.</i>	
The stability of the liquid hydrogen target system during the SAMURAI 30 experiment .....	150
X. Sun <i>et al.</i>	
Design of an Ion Source for the eSHE project Toward Pioneering Electron Scattering on Superheavy Elements .....	151
S. Naimi	
Absolute optical absorption cross-section of Rb atoms injected into superfluid helium using energetic ion beams .....	152
K. Imamura <i>et al.</i>	

Baseline correction system of laser-microwave double resonance spectrum for atoms injected into superfluid helium by laser sputtering .....	153
M. Sanjo <i>et al.</i>	
Attempt to measure relaxation time of atomic bubble surrounding alkaline atoms in superfluid helium .....	154
Y. Takeuchi <i>et al.</i>	
Development of offline ion source for collinear laser spectroscopy of RI beams .....	155
M. Tajima <i>et al.</i>	
Development of active nuclear spin maser with time-separated feedback scheme for Xe-EDM search .....	156
T. Sato <i>et al.</i>	
Epithermal neutron spin filter with dynamic nuclear polarization using photo-excited triplet electron .....	157
S. Takada <i>et al.</i>	
Measurement of impurity nuclides in 10.75 MeV/nucleon $^{136}\text{Xe}$ beam in the atmosphere .....	158
T. Kambara and A. Yoshida	
Computing and network environment at the RIKEN Nishina Center .....	159
T. Ichihara <i>et al.</i>	
CCJ operations in 2018 .....	160
S. Yokkaichi <i>et al.</i>	

### III. RESEARCH ACTIVITIES II (Material Science and Biology)

#### 1. Atomic and Solid State Physics (Ion)

Effects of asymmetrically-introduced splayed columnar defects on the peak effect in $(\text{Ba}, \text{K})\text{Fe}_2\text{As}_2$ .....	161
T. Tamegai <i>et al.</i>	
Control of the electrical conductivity in diamond by ion implantation .....	162
H. Yamazaki <i>et al.</i>	
Investigation of single event effects observed in SiC-SBDs .....	163
Y. Nakada <i>et al.</i>	
Energy dependence of MeV-ion microbeam size extracted from tapered glass capillary optics .....	164
M. Ikekame <i>et al.</i>	
Development of UV microbeam irradiation system by glass capillary optics .....	165
S. Kawamura <i>et al.</i>	

#### 2. Atomic and Solid State Physics (Muon)

Magnetic ordered states of hole-doped pyrochlore iridates $(\text{Y}_{1-x-y}\text{Cu}_x\text{Ca}_y)_2\text{Ir}_2\text{O}_7$ investigated by $\mu\text{SR}$ .....	167
J. Angel <i>et al.</i>	
Generalization of muon spin relaxation function to study the pseudogap state of the underdoped $\text{La}_{2-x}\text{Sr}_x\text{CuO}_4$ .....	168
M. D. Umar and I. Watanabe	
Magnetic order in defective reduced graphene oxides (rGO) investigated using $\mu\text{SR}$ .....	169
R. Asih <i>et al.</i>	
Ground state of quasi-one dimensional competing spin chain $\text{Cs}_2\text{Cu}_2\text{Mo}_3\text{O}_{12}$ .....	170
T. Goto and K. Matsui	
Superconductivity in single crystals of $\lambda$ -(BETS) $_2\text{GaCl}_4$ studied by transverse-field $\mu\text{SR}$ .....	171
D. P. Sari <i>et al.</i>	
$\mu\text{SR}$ study on ferrimagnetism of Na-K alloy clusters incorporated into zeolite LSX under high-pressure helium gas .....	172
T. Nakano <i>et al.</i>	
Quantum effects of muon on the electronic state of $\text{La}_2\text{CuO}_4$ .....	173
M. R. Ramadhan <i>et al.</i>	
<i>Ab-initio</i> calculation and $\mu\text{SR}$ study of the covalency effect in $\text{YBa}_2\text{Cu}_3\text{O}_6$ .....	174
I. Ramli <i>et al.</i>	
Studies of electrical conductivity in 12-mer single-stranded DNA by using scanning tunneling microscope .....	175
H. Rozak <i>et al.</i>	
Magnetic ordering of $(\text{Eu}_{1-x}\text{Ca}_x)_2\text{Ir}_2\text{O}_7$ studied using muon spin relaxation ( $\mu\text{SR}$ ) .....	176
U. Widyaiswari <i>et al.</i>	
$\mu\text{SR}$ study of the Cu-spin correlation in the electron-underdoped $\text{Pr}_{1.3-x}\text{La}_{0.7}\text{Ce}_x\text{CuO}_{4+\delta}$ ( $x = 0.05$ ) single crystals .....	177
T. Adachi <i>et al.</i>	

Reduction in Néel Temperature of La <sub>2</sub> CuO <sub>4</sub> Nanoparticles ..... S. Winarsih <i>et al.</i>	178
Muon spin relaxation after hydrogen absorption-desorption process in Pd ..... M. Mihara <i>et al.</i>	179
Negative muon spin rotation with low-density gas target under transverse magnetic field to solve the proton radius puzzle ..... S. Kanda <i>et al.</i>	180
Measurement of total muonium emission yield from silica aerogel using $\mu$ SR method ..... K. Ishida <i>et al.</i>	181
<b>3. Radiochemistry and Nuclear Chemistry</b>	
Extraction behavior of rutherfordium as a cationic fluoride complex with a TTA chelate extractant from HF/HNO <sub>3</sub> acidic solutions ..... A. Yokoyama <i>et al.</i>	183
Coprecipitation experiment of element 102, No, with Sm(OH) <sub>3</sub> using NH <sub>3</sub> and NaOH solution ..... H. Ninomiya <i>et al.</i>	184
Complex formation of Fr with crown ethers ..... Y. Komori <i>et al.</i>	185
Anion and cation exchange of Pa in HF/HCl mixture solution for Db chemistry ..... T. Yokokita and H. Haba	186
Study of anion exchange equilibrium of Zr and Hf in H <sub>2</sub> SO <sub>4</sub> for Rf experiment ..... T. Yokokita <i>et al.</i>	187
Development of <sup>211</sup> At-labeled antibody for targeted alpha therapy ..... Y. Kanayama <i>et al.</i>	188
RI imaging tracers for Na <sup>+</sup> /K <sup>+</sup> dynamics in a living body ..... S. Motomura <i>et al.</i>	189
Measurement of activation cross sections of alpha particle induced reactions on iridium up to an energy of 50 MeV ..... S. Takács <i>et al.</i>	190
Cross-section measurement of $\alpha$ -induced reactions on <sup>nat</sup> Er for <sup>169</sup> Yb production ..... M. Saito <i>et al.</i>	191
Activation cross sections of alpha-induced reactions on <sup>nat</sup> In for <sup>117m</sup> Sn production ..... M. Aikawa <i>et al.</i>	192
Investigation of alpha particle induced reactions on natural silver in the 40–50 MeV energy range ..... F. Ditrói <i>et al.</i>	193
Production cross sections of deuteron-induced reactions on natural palladium for Ag isotopes ..... N. Ukon <i>et al.</i>	194
Production cross sections of <sup>111</sup> Ag in deuteron-induced nuclear reactions on natural palladium ..... K. Ooe <i>et al.</i>	195
Production cross sections of Mo, Nb and Zr radioisotopes from $\alpha$ -induced reaction on <sup>nat</sup> Zr ..... T. Murata <i>et al.</i>	196
Activation cross sections of deuteron-induced reactions on niobium up to 24 MeV ..... M. Aikawa <i>et al.</i>	197
New cross section data for production of zirconium-89 by alpha-induced reaction on yttrium target ..... T. Murata <i>et al.</i>	198
Cross section measurement of the deuteron-induced reaction on <sup>89</sup> Y to produce <sup>89</sup> Zr ..... M. Sakaguchi <i>et al.</i>	199
Activation cross sections of alpha particle induced reactions on natural nickel up to 50 MeV ..... S. Takács <i>et al.</i>	200
Measurement of half-lives of <sup>181</sup> , <sup>182a</sup> , <sup>182b</sup> , <sup>183</sup> , <sup>184m</sup> Re and <sup>187</sup> W ..... Y. Komori and H. Haba	201
Production of Np isotopes in nuclear reactions for standard material in accelerator mass spectrometry ..... Y. Hayakawa <i>et al.</i>	202
Column chromatography of astatine using weak base anion exchange resin ..... H. Ikeda <i>et al.</i>	203

Speciation analysis of oxidation states of astatine extracted into ethanol-water solutions Y. Shin <i>et al.</i>	204
Purification of $^{121m}\text{Te}$ by anion exchange chromatography T. Kubota <i>et al.</i>	205
Production of arsenic RI tracer from gallium oxide target by alpha beam irradiation H. Ikeda <i>et al.</i>	206
Production of $^{44m}\text{Sc}$ for multiple-isotope PET T. Fukuchi <i>et al.</i>	207
Adsorption experiments of $^{88}\text{Y}$ and $^{143}\text{Pm}$ on in $\text{HNO}_3$ T. Yokokita <i>et al.</i>	208
<b>4. Radiation Chemistry and Biology</b>	
Development of new cultivar of Hibiscus by C-ion beam irradiation S. Ochiai <i>et al.</i>	209
Effect of heavy ion beam irradiation on germination and mutation rate in local Toraja rice R. Sjahril <i>et al.</i>	210
Isolation of the chalky grain mutant 13–45 in rice ( <i>Oryza sativa L.</i> ) T. Katsube-Tanaka <i>et al.</i>	211
Molecular analysis of the stay-green mutant <i>dye1</i> induced by carbon ion beams in rice H. Yamatani <i>et al.</i>	212
An early-flowering einkorn wheat mutant with deletions of <i>PHYTOCLOCK 1/LUX ARRHYTHMO</i> and <i>VERNALIZATION 2</i> exhibits a high level of <i>VERNALIZATION 1</i> expression induced by vernalization K. Murai <i>et al.</i>	213
Effects of carbon-ion irradiation to male gametes on double fertilization in <i>Cyrtanthus mackenii</i> T. Hirano <i>et al.</i>	214
Death of pollen tetrads caused by chromosomal rearrangement Y. Kazama <i>et al.</i>	215
Estimation of efficient dose for heavy-ion beam mutagenesis by whole-genome mutational analysis in <i>Arabidopsis thaliana</i> K. Ishii <i>et al.</i>	216
Characterization of L-cysteine requiring mutants derived from heavy-ion-beam irradiated cells in the unicellular green alga <i>Parachlorella kessleri</i> T. Yamazaki <i>et al.</i>	217
Increase of lipid production upon outdoor cultivation of heavy-ion beam irradiation mutant <i>Parachlorella kessleri</i> PK4 and identification of its genetic variations T. Takeshita <i>et al.</i>	218
Pleiotropic mutant of plant-symbiotic edible mushroom <i>Tricholoma matsutake</i> induced by argon-ion beam H. Murata <i>et al.</i>	219
Comparison of biological effect between low- and high-LET irradiation on DSB repair in the filamentous fungus <i>Neurospora crassa</i> L. Ma <i>et al.</i>	220
Effect of different conditions of the mutant isolation system on rotifers by using heavy-ion beam irradiation K. Tsuneizumi <i>et al.</i>	221
The inhibitor of DNA-PK suppressed DNA repair after heavy-ion irradiation in quiescent mammalian cells M. Izumi and T. Abe	222
Phosphorylation and accumulation of low-dose high-LET heavy ion-induced bystander signaling molecules M. Tomita <i>et al.</i>	223
CR-39 imaging method to estimate microbeam profiles produced by tapered glass capillary optics Y. Hikima <i>et al.</i>	224
Stability test of ion microbeams produced by tapered glass capillary optics for biological use T. Ikeda <i>et al.</i>	225
<b>IV. OPERATION RECORDS</b>	
Program Advisory Committee meetings for nuclear physics and for materials and life experiments K. Yoneda <i>et al.</i>	227

Beam-time statistics of RIBF experiments .....	228
K. Yoneda and H. Ueno	
Electric power consumption of RIKEN Nishina Center in 2018 .....	229
E. Ikezawa <i>et al.</i>	
Operation report of the ring cyclotrons in the RIBF accelerator complex .....	230
J. Shibata <i>et al.</i>	
RILAC operation .....	231
E. Ikezawa <i>et al.</i>	
Operation report on the RIKEN AVF cyclotron for 2018 .....	232
K. Kobayashi <i>et al.</i>	
Present status of the liquid-helium supply and recovery system .....	233
T. Dantsuka <i>et al.</i>	
Present status of the BigRIPS cryogenic plant .....	234
K. Kusaka <i>et al.</i>	
Radiation safety management at RIBF .....	235
K. Tanaka <i>et al.</i>	
Operation of the Pelletron tandem accelerator .....	237
T. Ikeda <i>et al.</i>	
Fee-based activities by the industrial application research team .....	238
A. Yoshida <i>et al.</i>	

## V. EVENTS

DIS2018 International Workshop .....	239
Y. Goto, for the QNP2018 LOC	
RIKEN Open Day 2018 .....	240
K. Yoshida and T. Uesaka	
Workshop on “The r-process and unstable nuclei in multi-messenger astronomy” .....	241
N. Nishimura <i>et al.</i>	
TESLA Technology Collaboration Meeting 2019 at RIKEN Nishina Center .....	242
N. Sakamoto	
Participation in Hokkaido Science Festival .....	243
N. Miyauchi	
QNP2018 International Conference .....	244
Y. Goto, for the QNP2018 LOC	
RIBF “Hodan-kai” meeting on the future of exotic nuclear physics .....	245
T. Matsumoto	
Symposium on “Science and Technology Explored with Periodic Table” celebrating the “IYPT2019 in Japan” .....	246
H. Sakurai	

## VI. ORGANIZATION AND ACTIVITIES OF RIKEN NISHINA CENTER

### (Activities, Members, Publications & Presentations)

1. Organization .....	247
2. Finances .....	248
3. Staffing .....	248
4. Research publication .....	249
5. Management .....	250
6. International Collaboration .....	253
7. Awards .....	255
8. Brief overview of the RI Beam Factory .....	256
Nuclear Science and Transmutation Research Division	
Radioactive Isotope Physics Laboratory .....	258

Spin isospin Laboratory .....	267
Nuclear Spectroscopy Laboratory .....	273
High Energy Astrophysics Laboratory .....	278
Superheavy Element Research Group .....	283
Superheavy Element Production Team .....	285
Superheavy Element Device Development Team .....	289
Astro-Glaciology Research Group .....	291
Nuclear Transmutation Data Research Group .....	294
Fast RI Data Team .....	296
Slow RI Data Team .....	298
Muon Data Team .....	299
High-Intensity Accelerator R&D Group .....	302
High-Gradient Cavity R&D Team .....	303
High-Power Target R&D Team .....	304
Research Facility Development Division	
Accelerator Group .....	305
Accelerator R&D Team .....	307
Ion Source Team .....	309
RILAC Team .....	310
Cyclotron Team .....	311
Beam Dynamics & Diagnostics Team .....	313
Cryogenic Technology Team .....	315
Infrastructure Management Team .....	316
Instrumentation Development Group .....	317
SLOWRI Team .....	319
Rare RI-ring Team .....	323
SCRIT Team .....	325
Research Instruments Group .....	328
BigRIPS Team .....	329
SAMURAI Team .....	332
Computing and Network Team .....	335
Detector Team .....	337
Accelerator Applications Research Division	
Beam Mutagenesis Group .....	340
Ion Beam Breeding Team .....	341
Plant Genome Evolution Research Team .....	345
RI Application Research Group .....	347
Nuclear Chemistry Research Team .....	348
Industrial Application Research Team .....	355
Subnuclear System Research Division	
Quantum Hadron Physics Laboratory .....	357
Strangeness Nuclear Physics Laboratory .....	362
Radiation Laboratory .....	365
Meson Science Laboratory .....	369

RIKEN BNL Research Center .....	375
Theory Group .....	376
Experimental Group .....	378
Computing Group .....	382
RIKEN Facility Office at RAL .....	389
Safety Management Group .....	394
User Liaison Group .....	396
RIBF User Liaison Team .....	397
Outreach Team .....	398
Partner Institutions .....	399
Center for Nuclear Study, Graduate School of Science, The University of Tokyo .....	400
Wako Nuclear Science Center, IPNS (Institute of Particle and Nuclear Studies), KEK (High Energy Accelerator Research Organization) .....	411
Events (April 2018 – March 2019) .....	414
Press Releases (April 2018 – March 2019) .....	415

## **VII. LIST OF PREPRINTS**

List of Preprints (April 2018 – March 2019) .....	417
---	-----

## **VIII. LIST OF SYMPOSIA, WORKSHOPS & SEMINARS**

List of Symposia & Workshops (April 2018 – March 2019) .....	419
List of Seminars (April 2018 – March 2019) .....	419

# I. HIGHLIGHTS OF THE YEAR

<< Selection process of highlights >>

Highlights are selected by a two-step process. In the first step, a referee who reviews a manuscript decides whether she/he would recommend it as one of the highlights.

Members of the editorial board then make additional recommendations if they think an important contribution has not been recommended by the referee.

The second step involves the editor-in-chief proposing a list of highlights based on the recommendation given above to the editorial board. After discussing the scientific merits and uniqueness of the manuscripts from viewpoints of experts/non-experts, the editorial board makes the final decision.



## First observation of $^{20}\text{B}$ and $^{21}\text{B}^\dagger$

S. Leblond,<sup>\*1</sup> F. M. Marqués,<sup>\*1</sup> J. Gibelin,<sup>\*1</sup> N. A. Orr,<sup>\*1</sup> Y. Kondo,<sup>\*2</sup> T. Nakamura,<sup>\*2</sup> J. Bonnard,<sup>\*3</sup> N. Michel,<sup>\*4,\*5</sup> N. L. Achouri,<sup>\*1</sup> T. Aumann,<sup>\*6,\*7</sup> H. Baba,<sup>\*8</sup> F. Delaunay,<sup>\*1</sup> Q. Deshayes,<sup>\*1</sup> P. Doornenbal,<sup>\*8</sup> N. Fukuda,<sup>\*8</sup> J. W. Hwang,<sup>\*9</sup> N. Inabe,<sup>\*8</sup> T. Isobe,<sup>\*8</sup> D. Kameda,<sup>\*8</sup> D. Kanno,<sup>\*2</sup> S. Kim,<sup>\*9</sup> N. Kobayashi,<sup>\*2</sup> T. Kobayashi,<sup>\*10</sup> T. Kubo,<sup>\*8</sup> J. Lee,<sup>\*8</sup> R. Minakata,<sup>\*2</sup> T. Motobayashi,<sup>\*8</sup> D. Murai,<sup>\*11</sup> T. Murakami,<sup>\*12</sup> K. Muto,<sup>\*10</sup> T. Nakashima,<sup>\*2</sup> N. Nakatsuka,<sup>\*12</sup> A. Navin,<sup>\*13</sup> S. Nishi,<sup>\*2</sup> S. Ogoshi,<sup>\*2</sup> H. Otsu,<sup>\*8</sup> H. Sato,<sup>\*8</sup> Y. Satou,<sup>\*9</sup> Y. Shimizu,<sup>\*8</sup> H. Suzuki,<sup>\*8</sup> K. Takahashi,<sup>\*10</sup> H. Takeda,<sup>\*8</sup> S. Takeuchi,<sup>\*8</sup> R. Tanaka,<sup>\*2</sup> Y. Togano,<sup>\*2,\*7</sup> A. G. Tuff,<sup>\*14</sup> M. Vandebrouck,<sup>\*3</sup> and K. Yoneda<sup>\*8</sup>

It is well established that the shell structure of the nucleus, that leads to an enhanced stability for systems with “magic” numbers of protons ( $Z$ ) and/or neutrons ( $N$ ) of 2, 8, 20... is modified as the limits of particle stability, or driplines, are approached. Neutron numbers between 8 and 20 correspond to the filling of the  $sd$ -shell neutron single-particle orbitals. Approaching the driplines, the energies of these orbitals evolve, leading for example to the disappearance of the  $N = 20$  magic number for  $Z = 10$ –12 and to the appearance of new shell closures at  $N = 14, 16$  in the oxygen isotopes. In this respect, the most neutron-rich boron isotopes, which lie below doubly-magic  $^{22}, ^{24}\text{O}$  and straddle the neutron dripline, are of considerable interest.

After removing one or two nucleons from secondary beams of  $^{22}\text{N}$  and  $^{22}\text{C}$ , produced at the RIBF of the RIKEN Nishina Center, with a carbon reaction target, beam-velocity  $^{19}\text{B}$  fragments and neutrons were detected in the forward direction using the SAMURAI setup including the NEBULA neutron array. The relative energy between the  $^{19}\text{B}$  fragment and the first detected neutron is shown in Fig. 1. A prominent resonance-like structure was observed at about 2.5 MeV above the one-neutron decay threshold (Fig. 1) that, guided by theoretical considerations, has been identified as the  $1^-, 2^-$  ground-state doublet of  $^{20}\text{B}$ , with energies  $E_r = 1.56 \pm 0.15$  and  $2.50 \pm 0.09$  MeV. A weaker higher-lying peak was also observed at  $4.86 \pm 0.25$  MeV.

The data acquired for  $^{21}\text{B}$  in the  $^{19}\text{B}$  plus one- (Fig. 1) and two-neutron channels were consistent with the population of a resonance  $2.47 \pm 0.19$  MeV above

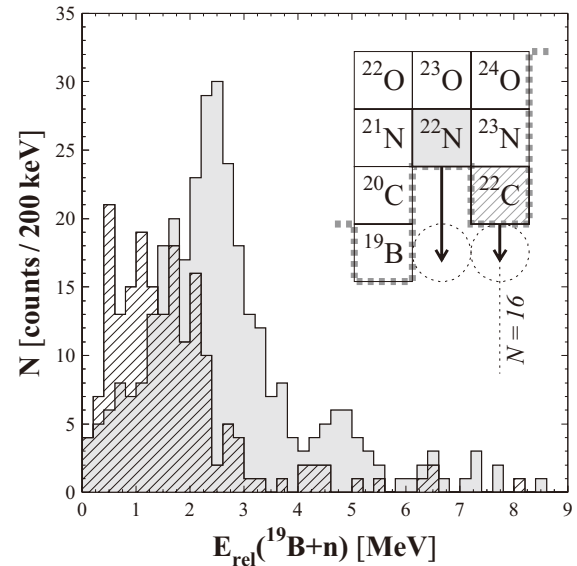


Fig. 1. Relative energy spectrum of  $^{19}\text{B}+n$  events following proton-removal from  $^{22}\text{N}$  (gray) and  $^{22}\text{C}$  (hatched histogram). The gray dotted line in the inset delineates the neutron dripline.

the two-neutron emission threshold, and thus tentatively assigned to be the expected  $3/2^-$  ground state. These results allowed the first determinations to be made of the ground-state masses of  $^{20}, ^{21}\text{B}$ , which are in agreement with the extrapolations of the most recent atomic-mass evaluations taking into account the  $^{19}\text{B}$ ,  $^{22}\text{C}$  and  $^{23}\text{N}$  mass measurements. In this spirit, the present  $^{20}, ^{21}\text{B}$  masses will permit mass-surface extrapolations in this region to be made with improved precision and further from stability. In addition,  $^{21}\text{B}$  was found to exhibit direct two-neutron decay.

The identification and first spectroscopy of  $^{20}, ^{21}\text{B}$  opens the way to the exploration of structure and correlations beyond the dripline below  $^{24}\text{O}$ . In particular, improvements in secondary-beam intensities and neutron detection should permit  $n$ - $n$  correlations in the decay of  $^{21}\text{B}$  to be investigated and its first excited state to be located. This, coupled with work underway to investigate the excited states of  $^{22}\text{C}$ , will provide direct insights into the  $N = 16$  shell closure beyond the neutron dripline as well as stringent tests of a new generation of *ab initio* and related theoretical models.

<sup>†</sup> Condensed from the article in Phys. Rev. Lett. **121**, 262502 (2018), see also references therein.

<sup>\*1</sup> LPC-Caen

<sup>\*2</sup> Department of Physics, Tokyo Institute of Technology

<sup>\*3</sup> Institut de Physique Nucléaire, Orsay

<sup>\*4</sup> NSCL/FRIB Laboratory, Michigan State University

<sup>\*5</sup> School of Physics, Peking University

<sup>\*6</sup> Institut für Kernphysik, Technische Universität Darmstadt

<sup>\*7</sup> ExtreMe Matter Institute EMMI, GSI

<sup>\*8</sup> RIKEN Nishina Center

<sup>\*9</sup> Department of Physics and Astronomy, Seoul National University

<sup>\*10</sup> Department of Physics, Tohoku University

<sup>\*11</sup> Department of Physics, Rikkyo University

<sup>\*12</sup> Department of Physics, Kyoto University

<sup>\*13</sup> GANIL, CEA/DRF-CNRS/IN2P3

<sup>\*14</sup> Department of Physics, University of York

## Gamow–Teller giant resonance in $^{132}\text{Sn}$

M. Sasano,<sup>\*1</sup> J. Yasuda,<sup>\*2</sup> L. Stuhl,<sup>\*1,\*6</sup> R. G. T. Zegers,<sup>\*3</sup> H. Baba,<sup>\*1</sup> W. Chao,<sup>\*1</sup> M. Dozono,<sup>\*1</sup> N. Fukuda,<sup>\*1</sup> N. Inabe,<sup>\*1</sup> T. Isobe,<sup>\*1</sup> G. Jhang,<sup>\*1,\*13</sup> D. Kamaeda,<sup>\*1</sup> T. Kubo,<sup>\*1</sup> M. Kurata-Nishimura,<sup>\*1</sup> E. Milman,<sup>\*1</sup> T. Motobayashi,<sup>\*1</sup> H. Otsu,<sup>\*1</sup> V. Panin,<sup>\*1</sup> W. Powell,<sup>\*1</sup> M. Sako,<sup>\*1</sup> H. Sato,<sup>\*1</sup> Y. Shimizu,<sup>\*1</sup> H. Suzuki,<sup>\*1</sup> T. Suwat,<sup>\*1</sup> H. Takeda,<sup>\*1</sup> T. Uesaka,<sup>\*1</sup> K. Yoneda,<sup>\*1</sup> J. Zenihiro,<sup>\*1</sup> T. Kobayashi,<sup>\*1,\*4</sup> T. Sumikama,<sup>\*1,\*4</sup> T. Tako,<sup>\*4</sup> T. Nakamura,<sup>\*5</sup> Y. Kondo,<sup>\*5</sup> Y. Togano,<sup>\*5</sup> M. Shikata,<sup>\*5</sup> J. Tsubota,<sup>\*5</sup> K. Yako,<sup>\*6</sup> S. Shimoura,<sup>\*6</sup> S. Ota,<sup>\*6</sup> S. Kawase,<sup>\*6</sup> Y. Kubota,<sup>\*6</sup> M. Takaki,<sup>\*6</sup> S. Michimasa,<sup>\*6</sup> K. Kisamori,<sup>\*6</sup> C. S. Lee,<sup>\*6</sup> H. Tokieda,<sup>\*6</sup> M. Kobayashi,<sup>\*6</sup> S. Koyama,<sup>\*7</sup> N. Kobayashi,<sup>\*7</sup> H. Sakai,<sup>\*1</sup> T. Wakasa,<sup>\*2</sup> S. Sakaguchi,<sup>\*2</sup> A. Krasznahorkay,<sup>\*8</sup> T. Murakami,<sup>\*9</sup> N. Nakatsuka,<sup>\*9</sup> M. Kaneko,<sup>\*9</sup> Y. Matsuda,<sup>\*10</sup> D. Mucher,<sup>\*11</sup> S. Reichert,<sup>\*11</sup> D. Bazin,<sup>\*3</sup> and J. W. Lee<sup>\*12</sup>

Among collective modes,<sup>1)</sup> the Gamow-Teller (GT) giant resonance is an interesting excitation mode. It is a  $0\hbar\omega$  excitation characterized by the quantum-number changes in orbital angular momentum ( $\Delta L = 0$ ), spin ( $\Delta S = 1$ ), and isospin ( $\Delta T = 1$ ), and it is induced by the transition operator  $\sigma\tau$ . In stable nuclei in medium or heavier mass regions ( $A > 50$ ), the collectivity in this mode exhibits the GT giant resonance (GTGR), which provides information that is critically important for understanding the isovector part of the effective nucleon-nucleon interaction<sup>2)</sup> and the symmetry potential of the equation of state.<sup>3)</sup> In particular, the understanding of the short-range repulsive part of the effective interaction, *i.e.*, so-called Landau-Migdal (LM) force in the spin-isospin channel, is crucial in the prediction of the onset of the pion condensation in nuclear matters such as a neutron star.<sup>4)</sup> Recently, we have been rapidly expanding the domain of GTGR studies at RIBF in the nuclear chart.<sup>5,6)</sup> This provides a new opportunity to evaluate the strength of the LM force and the so-called LM parameter  $g'$  for an unstable nucleus.

In this study, an experiment at RIBF was performed in March 2014 to extract the GT transition strengths over a wide excitation energy range covering their giant resonances on the key doubly magic nucleus  $^{132}\text{Sn}$ . The purpose of the experiment was to calibrate the  $g'$  parameter through observing the GTGR in  $^{132}\text{Sn}$ . This is also an essential step toward establishing the comprehensive theoretical models for the nuclei located between  $^{78}\text{Ni}$  and  $^{208}\text{Pb}$ . Details of the experimental setups and analysis are already given in previous progress reports and the results have been recently published in Ref. 7). Data for the GTGR were ob-

tained almost in the same quality as the stable-beam experiments, which opens up a new age of GR studies with RI beams in the field of experimental nuclear physics. The obtained  $g'$  parameter was  $0.68 \pm 0.07$ . In comparison to the values obtained for the stable nuclei  $^{90}\text{Zr}$  and  $^{208}\text{Pb}$ , it indicates that  $g'$  is kept almost constant over a region of isospin asymmetry from  $(N - Z)/A = 0.11$  to 0.24 and from mass number  $A = 90$  to 208. It also indicates that pion condensation occurs in the inner part of a neutron star whose mass is 1.4 times heavier than the solar mass.

We are grateful to the RIKEN RIBF accelerator crew and CNS, University of Tokyo, for their efforts and support to operate the RI beam factory. We thank M. Ichimura, E. Litvinova, C. Robin, Y. F. Niu, G. Colo, H. Z. Liang, and Z. M. Niu for our valuable discussions. This work was supported in part by a Grant-in-Aid for Scientific Research (No. 274740187), Grant-in-Aid for the Japan Society for the Promotion of Science (JSPS) Research Fellow (No. 265720), JSPS KAKENHI Grant No. 16H02179 from the Japan Society for the Promotion of Science, MEXT KAKENHI Grant No. 24105005, US NSF PHY-1430152 (JINA Center for 606 the Evolution of the Elements), US NSF PHY-1565546, and the Hungarian NKFI Foundation [K124810].

### References

- 1) M. N. Harakeh, A. M. van der Woude, *Giant Resonances* (Oxford University Press, Oxford, 2001).
- 2) S. Fracasso, G. Colo, *Phys. Rev. C* **72**, 064310 (2005).
- 3) P. Danielewicz, *Nucl. Phys. A* **727**, 233 (2003).
- 4) A. B. Migdal, *Rev. Mod. Phys.* **50**, 107 (1978).
- 5) M. Sasano *et al.*, *Phys. Rev. Lett.* **107**, 202501 (2011).
- 6) M. Sasano *et al.*, *Phys. Rev. C* **86**, 034324 (2012).
- 7) M. Sasano *et al.*, *Phys. Rev. Lett.* **121**, 132501 (2018).

\*1 RIKEN Nishina Center

\*2 Department of Physics, Kyushu University

\*3 NSCL, Michigan State University

\*4 Department of Physics, Tohoku University

\*5 Department of Physics, Tokyo Institute of Technology

\*6 CNS, University of Tokyo

\*7 Department of Physics, University of Tokyo

\*8 MTA, Atomki

\*9 Department of Physics, Kyoto University

\*10 Department of Physics, Konan University

\*11 Department of Physics, Technical University Munich

\*12 Department of Physics, Korea University

## First spectroscopy of the near drip-line nucleus $^{40}\text{Mg}^\dagger$

H. L. Crawford,<sup>\*1</sup> P. Fallon,<sup>\*1</sup> A. O. Macchiavelli,<sup>\*1</sup> P. Doornenbal,<sup>\*2</sup> N. Aoi,<sup>\*3</sup> F. Browne,<sup>\*2</sup> C. M. Campbell,<sup>\*1</sup> S. Chen,<sup>\*2</sup> R. M. Clark,<sup>\*1</sup> M. L. Cortés,<sup>\*2</sup> M. Cromaz,<sup>\*1</sup> E. Ideguchi,<sup>\*3</sup> M. D. Jones,<sup>\*1</sup> R. Kanungo,<sup>\*4,\*5</sup> M. MacCormick,<sup>\*6</sup> S. Momiyama,<sup>\*7</sup> I. Murray,<sup>\*6</sup> M. Niikura,<sup>\*7</sup> S. Paschalis,<sup>\*8</sup> M. Petri,<sup>\*8</sup> H. Sakurai,<sup>\*2,\*7</sup> M. Salathe,<sup>\*1</sup> P. Schrock,<sup>\*9</sup> D. Steppenbeck,<sup>\*9</sup> S. Takeuchi,<sup>\*2,\*10</sup> Y. K. Tanaka,<sup>\*11</sup> R. Taniuchi,<sup>\*7</sup> H. Wang,<sup>\*2</sup> and K. Wimmer<sup>\*7</sup>

Magnesium isotopes offer an opportunity to experimentally study the transition from well-bound to weakly-bound nuclei and its influence on the excited states, which may reflect the correlations at the limits of stability. While knowledge on the heaviest Mg isotopes is limited, an overall consistent picture of the structure along  $Z = 12$  has emerged between  $N = 20$  and  $N = 28$ , of persistent prolate deformation from  $^{32}\text{Mg}$  to  $^{38}\text{Mg}$ ,<sup>1)</sup> which likely extends to  $^{40}\text{Mg}$ .<sup>2)</sup>

$^{40}\text{Mg}$  represents a particularly intriguing case for study. Theoretical expectations and experimental systematics suggest  $^{40}\text{Mg}$  to be a well-deformed prolate rotor as well, structurally very similar to  $^{36,38}\text{Mg}$ . However, the occupation of the relatively weakly-bound  $2p_{3/2}$  neutron orbital near the Fermi surface may add a new degree of freedom. In this report, the first  $\gamma$ -ray spectroscopic information of  $^{40}\text{Mg}$  is presented and discussed in the context of the systematics along the magnesium isotopes.

Experimentally, a drastically different prompt  $\gamma$ -ray spectrum is observed for  $^{40}\text{Mg}$  (see Fig. 1 (c)) as compared to  $^{36,38}\text{Mg}$  (see Fig. 1 (a), (b)), contrary to expectations. The tentatively assigned  $2_1^+ \rightarrow 0_1^+$  transition at 500(14) keV is 20% below that in  $^{38}\text{Mg}$ , a trend that is outside the shell-model and other state-of-the-art theoretical predictions. The second  $\gamma$ -ray transition is even more puzzling. Given that  $^{40}\text{Mg}$  is very near the neutron dripline, and the low- $\ell$   $\nu 2p_{3/2}$  orbital sits at the Fermi surface, the observed spectrum may be an indication of the manifestation of weak-binding effects, as discussed fully in the published Letter.

The experiment was carried out at the Radioactive Isotope Beam Factory (RIBF) at RIKEN Nishina Center. An intense (450 pA) primary beam of  $^{48}\text{Ca}$  was fragmented on a rotating production target, producing a secondary cocktail beam centered on  $^{41}\text{Al}$ . This beam was transported through BigRIPS<sup>3)</sup> and was incident upon a thick polyethylene secondary target at the focal

plane in front of ZeroDegree, which was tuned to center  $^{40}\text{Mg}$  reaction residues. Prompt  $\gamma$  rays depopulating the excited states in  $^{40}\text{Mg}$  and other reaction residues were detected in the DALI2 spectrometer,<sup>5)</sup> which consists of 186 large-volume NaI(Tl) detectors surrounding the secondary target.

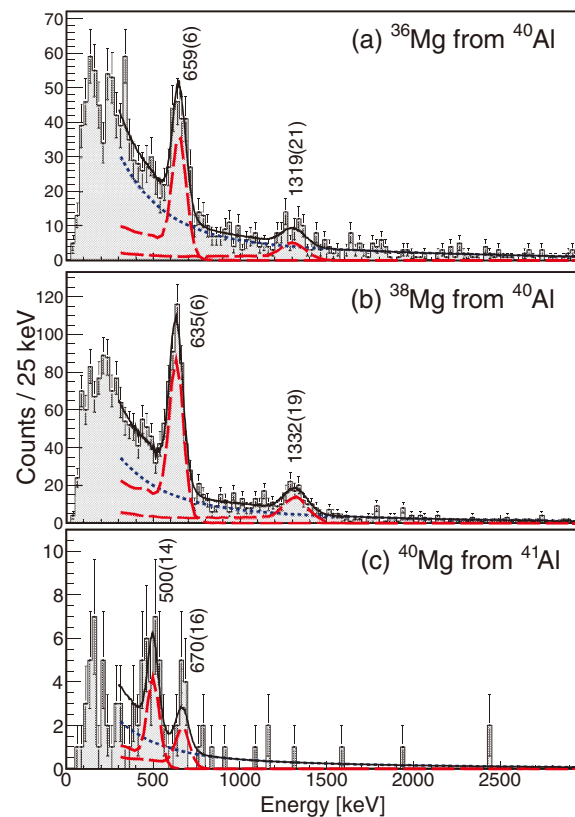


Fig. 1. (color online) Prompt  $\gamma$ -ray spectrum associated with (a)  $^{36}\text{Mg}$ , (b)  $^{38}\text{Mg}$  and (c)  $^{40}\text{Mg}$  (populated in  $-1p$  removal from  $^{41}\text{Al}$ ). Spectra were fit using the simulated DALI2 response (red dashed curves) and a smooth background (dotted blue line); the solid black line represents the total fit.

<sup>†</sup> Condensed from the article in press in Phys. Rev. Lett. (2019)

<sup>\*1</sup> NSD, Lawrence Berkeley National Laboratory

<sup>\*2</sup> RIKEN Nishina Center

<sup>\*3</sup> RCNP, Osaka University

<sup>\*4</sup> Astronomy & Physics Department, Saint Mary's University

<sup>\*5</sup> TRIUMF

<sup>\*6</sup> Institut de Physique Nucléaire, IN2P3-CNRS, Université Paris-Sud, Université Paris-Saclay

<sup>\*7</sup> Department of Physics, University of Tokyo

<sup>\*8</sup> Department of Physics, University of York

<sup>\*9</sup> CNS, University of Tokyo, RIKEN Campus

<sup>\*10</sup> Department of Physics, Tokyo Institute of Technology

<sup>\*11</sup> GSI Helmholtzzentrum für Schwerionenforschung GmbH

### References

- 1) P. Doornenbal *et al.*, Phys. Rev. Lett. **111**, 212502 (2013).
- 2) H. L. Crawford *et al.*, Phys. Rev. C **89**, 041303 (2014).
- 3) T. Kubo *et al.*, Prog. Theor. Exp. Phys. **2012**, 03C003 (2012).
- 4) Y. Mizoi *et al.*, RIKEN Accel. Prog. Rep. **38**, 297 (2005).
- 5) S. Takeuchi *et al.*, Nucl. Instrum. Methods Phys. Res. A **763**, 596 (2014).

## Interplay between nuclear shell evolution and shape deformation revealed by magnetic moment of $^{75}\text{Cu}^\dagger$

Y. Ichikawa,<sup>\*1</sup> H. Nishibata,<sup>\*1,\*2</sup> Y. Tsunoda,<sup>\*3</sup> A. Takamine,<sup>\*1</sup> K. Imamura,<sup>\*1,\*4</sup> T. Fujita,<sup>\*1,\*2</sup> T. Sato,<sup>\*1,\*5</sup> S. Momiyama,<sup>\*6</sup> Y. Shimizu,<sup>\*1</sup> D. S. Ahn,<sup>\*1</sup> K. Asahi,<sup>\*1,\*5</sup> H. Baba,<sup>\*1</sup> D. L. Balabanski,<sup>\*1,\*7</sup> F. Boulay,<sup>\*1,\*8,\*9</sup> J. M. Daugas,<sup>\*1,\*9</sup> T. Egami,<sup>\*10</sup> N. Fukuda,<sup>\*1</sup> C. Funayama,<sup>\*5</sup> T. Furukawa,<sup>\*11</sup> G. Georgiev,<sup>\*12</sup> A. Gladkov,<sup>\*1,\*13</sup> N. Inabe,<sup>\*1</sup> Y. Ishibashi,<sup>\*1,\*14</sup> T. Kawaguchi,<sup>\*10</sup> T. Kawamura,<sup>\*2</sup> Y. Kobayashi,<sup>\*1,\*15</sup> S. Kojima,<sup>\*5</sup> A. Kusoglu,<sup>\*7,\*12,\*16</sup> I. Mukul,<sup>\*17</sup> M. Niikura,<sup>\*6</sup> T. Nishizaka,<sup>\*10</sup> A. Odahara,<sup>\*2</sup> Y. Ohtomo,<sup>\*1,\*5</sup> T. Otsuka,<sup>\*1,\*3,\*6,\*18</sup> D. Ralet,<sup>\*12</sup> G. S. Simpson,<sup>\*19</sup> T. Sumikama,<sup>\*1</sup> H. Suzuki,<sup>\*1</sup> H. Takeda,<sup>\*1</sup> L. C. Tao,<sup>\*1,\*20</sup> Y. Togano,<sup>\*1,\*5</sup> D. Tominaga,<sup>\*10</sup> H. Ueno,<sup>\*1</sup> H. Yamazaki,<sup>\*1</sup> and X. F. Yang<sup>\*18</sup>

Exotic nuclei are characterized by a number of excess neutrons (or protons) relative to stable nuclei. Their shell structure, which represents single-particle motion in a nucleus, may vary owing to nuclear force and excess neutrons, in a phenomenon called shell evolution. This effect could be counterbalanced by collective modes causing deformations of the nuclear surface. We studied the interplay between shell evolution and shape deformation by focusing on the magnetic moment of an isomeric state of the neutron-rich nucleus  $^{75}\text{Cu}$ ,<sup>1)</sup> where low-lying states of the Cu isotopes exhibit an intriguing behavior involving the shell evolution.<sup>2-4)</sup>

The magnetic moment measurement was carried out at the BigRIPS at RIBF. Spin alignment as large as 30% was achieved in the isomeric state of  $^{75}\text{Cu}$  by a scheme of two-step projectile fragmentation with a technique of momentum-dispersion matching,<sup>5)</sup> incorporating an angular-momentum selecting proton removal from  $^{76}\text{Zn}$ . The magnetic moment was determined using the time-differential perturbed angular distribution (TDPAD) method. Owing to the high spin alignment realized by the refined two-step scheme, the observed oscillation for the 66.2-keV  $\gamma$  rays in the TDPAD spectrum had a significance greater than  $5\sigma$ . The magnetic moment of the 66.2-keV isomer with spin parity  $3/2^-$  was determined to be  $\mu = 1.40(6) \mu_N$  for the first time.

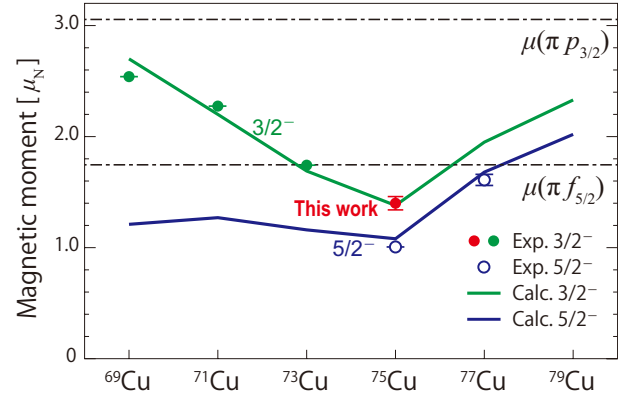


Fig. 1. Systematics of magnetic moments for odd- $A$  Cu isotopes. Filled and open circles represent experimental data for  $3/2^-$  and  $5/2^-$  states, respectively. Filled red circle represents the result obtained in this work. Solid green and blue lines represent MCSM calculations for  $3/2^-$  and  $5/2^-$  states, respectively, with  $20 \leq (N, Z) \leq 56$  model space.<sup>6)</sup>  $\mu(\pi p_{3/2})$  and  $\mu(\pi f_{5/2})$  denote the proton Schmidt values for  $p_{3/2}$  and  $f_{5/2}$ , respectively.

The magnetic moment, thus obtained, demonstrated a considerable deviation from the Schmidt value,  $\mu = 3.05 \mu_N$ , for the  $p_{3/2}$  orbital. Figure 1 shows the systematics of magnetic moments of the  $3/2^-$  and  $5/2^-$  states, where deviation from the Schmidt values appears to be maximal at  $^{75}\text{Cu}$ . The analysis of the magnetic moment with the help of Monte Carlo shell model (MCSM) calculations<sup>6)</sup> reveals that the trend of the deviation corresponds to the effect of core excitation and the low-lying states in  $^{75}\text{Cu}$  are, to a large extent, of a single-particle nature on top of a correlated  $^{74}\text{Ni}$  core, elucidating the crucial role of the shell evolution even in the presence of collective mode.

### References

- 1) C. Petrone *et al.*, Phys. Rev. C **94**, 024319 (2016).
- 2) T. Otsuka *et al.*, Phys. Rev. Lett. **95**, 232502 (2005).
- 3) S. Franchoo *et al.*, Phys. Rev. Lett. **81**, 3100 (1998).
- 4) K. T. Flanagan *et al.*, Phys. Rev. Lett. **103**, 142501 (2009).
- 5) Y. Ichikawa *et al.*, Nat. Phys. **8**, 918 (2012).
- 6) Y. Tsunoda *et al.*, Phys. Rev. C **89**, 031301(R) (2014).

<sup>†</sup> Condensed from the letter in Nat. Phys. **15**, 321 (2019)

<sup>\*1</sup> RIKEN Nishina Center

<sup>\*2</sup> Department of Physics, Osaka University

<sup>\*3</sup> Center for Nuclear Study, University of Tokyo

<sup>\*4</sup> Department of Physics, Meiji University

<sup>\*5</sup> Department of Physics, Tokyo Institute of Technology

<sup>\*6</sup> Department of Physics, University of Tokyo

<sup>\*7</sup> ELI-NP, IFIN-HH

<sup>\*8</sup> GANIL, CEA/DSM-CNRS/IN2P3

<sup>\*9</sup> CEA, DAM, DIF

<sup>\*10</sup> Department of Advanced Sciences, Hosei University

<sup>\*11</sup> Department of Physics, Tokyo Metropolitan University

<sup>\*12</sup> CSNSM, CNRS/IN2P3, Université Pris-Sud

<sup>\*13</sup> Department of Physics, Kyungpook National University

<sup>\*14</sup> Department of Physics, University of Tsukuba

<sup>\*15</sup> Department of Informatics and Engineering, University of Electro-Communications

<sup>\*16</sup> Department of Physics, Istanbul University

<sup>\*17</sup> Department of Particle Physics, Weizmann Institute

<sup>\*18</sup> Intsituuat voor Kern-en Srralingsfysica, K. U. Leuven

<sup>\*19</sup> LPSC, Université Grenoble Alpes, CNRS/IN2P3

<sup>\*20</sup> School of Physics, Peking University

## Mass measurements of neutron-rich Ni isotopes in Rare RI Ring

A. Ozawa,<sup>\*1</sup> Y. Abe,<sup>\*2</sup> D. Nagae,<sup>\*2</sup> S. Naimi,<sup>\*2</sup> F. Suzaki,<sup>\*2</sup> Y. Yamaguchi,<sup>\*2</sup> M. Wakasugi,<sup>\*2</sup> H. Arakawa,<sup>\*3</sup> S. Hosoi,<sup>\*3</sup> Y. Inada,<sup>\*3</sup> K. Inomata,<sup>\*3</sup> T. Kobayayashi,<sup>\*3</sup> K. Nishimuro,<sup>\*3</sup> S. Omika,<sup>\*3</sup> M. Sakaue,<sup>\*3</sup> K. Yokota,<sup>\*3</sup> T. Yamaguchi,<sup>\*3</sup> R. Kagesawa,<sup>\*1</sup> D. Kamioka,<sup>\*1</sup> T. Moriguchi,<sup>\*1</sup> M. Mukai,<sup>\*1</sup> S. Ota,<sup>\*4</sup> N. Kitamura,<sup>\*4</sup> S. Masuoka,<sup>\*4</sup> S. Michimasa,<sup>\*4</sup> D. S. Ahn,<sup>\*1</sup> H. Baba,<sup>\*1</sup> N. Fukuda,<sup>\*1</sup> Y. Shimizu,<sup>\*1</sup> H. Suzuki,<sup>\*1</sup> H. Takeda,<sup>\*1</sup> Z. Ge,<sup>\*5</sup> H. Li,<sup>\*5</sup> S. Suzuki,<sup>\*5</sup> K. Wang,<sup>\*5</sup> Q. Wang,<sup>\*5</sup> M. Wang,<sup>\*5</sup> Y. Litvinov,<sup>\*6</sup> Z. Podolyak,<sup>\*7</sup> and T. Uesaka<sup>\*2</sup>

Nuclear mass measurements are important to investigate nuclear structure and pathway of nucleosynthesis. Neutron separation energies ( $S_n$  and  $S_{2n}$ ), which can be deduced from the nuclear masses, are very sensitive to the nuclear shell structure. In nucleosynthesis,  $S_n$  is a key parameter to determine the pathway of the r-process. Ni isotopes have a magic number for the protons ( $Z = 28$ ) and three doubly magic isotopes ( $N = 20, 28, 50$ ). Ni isotopes close to  $^{78}\text{Ni}$  are assumed to lie on the r-process path. Thus, the mass measurements for neutron-rich Ni isotopes are anticipated. Until now, in neutron-rich Ni isotopes, masses up to  $^{73}\text{Ni}$  have been evaluated in Atomic Mass Evaluation.<sup>1)</sup> The mass of  $^{74}\text{Ni}$  has been reported in Ref. 2). However, the error bar is quite large (approximately 1 MeV). Thus, in this experiment, we performed the mass measurements for neutron-rich Ni isotopes ( $^{74,76}\text{Ni}$ ) in Rare RI Ring (R3).

The experimental setup in this measurement is essentially the same as that in the previous experiment at R3.<sup>3)</sup> We improved beam optics after installing the OEDO system.<sup>4)</sup> The primary beam of  $^{238}\text{U}$  accelerated in SRC up to 345 MeV/nucleon was impinged on a Be target. Secondary beams including  $^{74,76}\text{Ni}$  isotopes were produced through in-flight reaction. We adjusted the thickness of the degraders located at F1 and F2 in BigRIPS such that the beam energies of  $^{74,76}\text{Ni}$  became approximately 160 MeV/nucleon, which is the suitable energy for individual ion injection.<sup>5)</sup>

Particle identification in BigRIPS was done by TOF between F2 and F3, which were measured by two plastic scintillators, and  $\Delta E$  at F3, that was measured by an ionization chamber (IC). In this experimental setting, a typical count rate for  $^{76}\text{Ni}$  in F3 was approximately 0.16 cps for the full primary beam intensity (approximately 60 particles nA). The plastic scintillator at F3 also provided trigger signals for the kicker magnets in R3. To maintain the trigger rate of the kicker magnets within 100 Hz, we applied TOF- $\Delta E$  gates to the trigger signals, as described in Ref. 6). A typical particle identification spectrum at F3 (for the case of  $^{74}\text{Ni}$ ) is shown in Fig. 1. In this experiment, momentum dispersive focus was applied at F5 in BigRIPS. We placed two PPACs there to measure the momentum of the beams ( $B\rho$ ). At S0, *i.e.*, at the entrance of SHARAQ, we located a TOF counter,

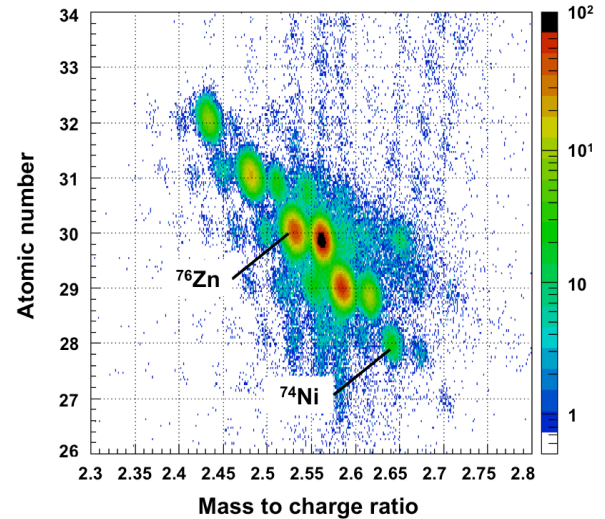


Fig. 1. A typical particle identification spectrum as measured at F3 for  $^{74}\text{Ni}$  mass measurement.

which is a similar to the one used inside R3.<sup>7)</sup> This TOF counter provided a start signal to the TOF in R3.

We also measured the TOFs of each particle between F3 and S0, which were converted to the  $\beta$  of their beams. The particle injected into R3 was extracted after approximately 700  $\mu\text{s}$  using the same kicker magnets. After the extraction, the particle was collided with a plastic scintillator, which provided a stop signal for the TOF in R3 and IC. Finally, it was stopped in an NaI scintillator. In the measurement of  $^{74}\text{Ni}$  ( $^{76}\text{Ni}$ ), the isochronous optics of R3 were tuned using  $^{76}\text{Zn}$  ( $^{78}\text{Zn}$ ) such that the width of TOF in R3 was the narrowest for this nucleus, thereby resulting in a width of approximately 3 ps. Furthermore, we carefully tuned the septum magnets and magnets at the injection line of R3 to increase the transmission efficiencies of  $^{74,76}\text{Ni}$  from F3 to R3. The achieved values for  $^{74}\text{Ni}$  and  $^{76}\text{Ni}$  were approximately 0.5% and 2.8%, respectively. In this experiment, we accumulated the events for  $^{74}\text{Ni}$  ( $^{76}\text{Ni}$ ) for approximately 5 h (10 h). To deduce the masses, the TOF in R3 should be corrected by the corresponding  $\beta$  or  $B\rho$ . The analysis of data is still ongoing.

### References

- 1) M. Wang *et al.*, *Chin. Phys.* **41**, 030003 (2017).
- 2) A. Estrade *et al.*, *Phys. Rev. Lett.* **107**, 172503 (2011).
- 3) D. Nagae *et al.*, *RIKEN Accel. Prog. Rep.* **50**, 18 (2017).
- 4) Y. Yamaguchi *et al.*, *RIKEN Accel. Prog. Rep.* **51**, 165 (2018).
- 5) Y. Yamaguchi *et al.*, *RIKEN Accel. Prog. Rep.* **49**, 18 (2016).
- 6) Y. Abe *et al.*, in this report.
- 7) D. Nagae *et al.*, *RIKEN Accel. Prog. Rep.* **49**, 181 (2016).

<sup>\*1</sup> Institute of Physics, University of Tsukuba  
<sup>\*2</sup> RIKEN Nishina Center  
<sup>\*3</sup> Department of Physics, Saitama University  
<sup>\*4</sup> CNS, University of Tokyo  
<sup>\*5</sup> IMP, CAS, Lanzhou, China  
<sup>\*6</sup> GSI Helmholtz Center, Darmstadt, Germany  
<sup>\*7</sup> NPI, University of Surrey

# Discovery of $^{60}\text{Ca}$ and Implications For the Stability of $^{70}\text{Ca}^\dagger$

O. B. Tarasov,<sup>\*1,\*2</sup> D. S. Ahn,<sup>\*2</sup> D. Bazin,<sup>\*1,\*2</sup> N. Fukuda,<sup>\*2</sup> A. Gade,<sup>\*1</sup> M. Hausmann,<sup>\*1</sup> N. Inabe,<sup>\*2</sup> S. Ishikawa,<sup>\*3</sup> N. Iwasa,<sup>\*3</sup> K. Kawata,<sup>\*4</sup> T. Komatsubara,<sup>\*2</sup> T. Kubo,<sup>\*1,\*2</sup> K. Kusaka,<sup>\*2</sup> D. J. Morrissey,<sup>\*1,\*2</sup> M. Ohtake,<sup>\*2</sup> H. Otsu,<sup>\*2</sup> M. Portillo,<sup>\*1,2</sup> T. Sakakibara,<sup>\*3</sup> H. Sakurai,<sup>\*2</sup> H. Sato,<sup>\*2</sup> B. M. Sherrill,<sup>\*1,\*2</sup> Y. Shimizu,<sup>\*2</sup> A. Stolz,<sup>\*1</sup> T. Sumikama,<sup>\*2</sup> H. Suzuki,<sup>\*2</sup> H. Takeda,<sup>\*2</sup> M. Thoennessen,<sup>\*1</sup> H. Ueno,<sup>\*2</sup> Y. Yanagisawa,<sup>\*2</sup> and K. Yoshida<sup>\*2</sup>

The landscape of atomic nuclei is delineated by the nucleon drip lines beyond which no bound states of lighter or heavier isotopes exist. The location of the neutron drip line provides a key benchmark for nuclear models and the quest to understand the nuclear force. The proton-magic calcium isotopes span the magic neutron numbers 20, 28, 32, 34, and possibly 40 and 50. The calcium chain is just within reach of ab-initio models<sup>1)</sup> as well as the broadly applicable mean-field and configuration-interaction models. Observation of  $^{59}\text{Ca}$  and  $^{60}\text{Ca}$  would test the predictive power of ab-initio models as compared to the energy density functionals (EDFs), and indicate if the success of the ab-initio approaches in describing the masses of the calcium isotopes. Measurements at NSCL<sup>2,3)</sup> have demonstrated that the fragmentation of  $^{76}\text{Ge}$  and  $^{82}\text{Se}$  beams using a two-stage separator can be used to produce new neutron-rich isotopes in the calcium region. We report here the continuation of this work at the RIKEN RIBF facility, using a higher beam energy and intensity, and so accessing the one-order-of-magnitude lower production cross sections needed to explore the stability of  $^{59,60}\text{Ca}$ .

The discovery of  $^{60}\text{Ca}_{40}$  and seven other neutron-rich nuclei near the limits of stability is reported from the projectile fragmentation of 345 MeV/nucleon  $^{70}\text{Zn}$  beam with an intensity of 225 particle nA on Be targets at the RI Beam Factory operated by RIKEN Nishina Center and CNS, University of Tokyo. During a 99.5 hour measurement,  $^{47}\text{P}$ ,  $^{49}\text{S}$ ,  $^{52}\text{Cl}$ ,  $^{54}\text{Ar}$ ,  $^{57}\text{K}$ ,  $^{59,60}\text{Ca}$ , and  $^{62}\text{Sc}$ , the most neutron-rich isotopes of the respective elements, were observed for the first time. In addition, one event consistent with  $^{59}\text{K}$  was observed. The produced fragments were analyzed and unambiguously identified using the BigRIPS two-stage in-flight separator tuned according to LISE<sup>++</sup> calculations.<sup>4)</sup> Two aluminum wedge-shaped degraders at the F1 and F5 dispersive planes were used at full BigRIPS momentum acceptance to separate and purify the RI beams. The particle identification (PID) was conducted using the ToF- $B\rho$ - $\Delta E$ -TKE method described in the appendix to the previous work.<sup>5)</sup>

The results are compared with the drip-line predic-

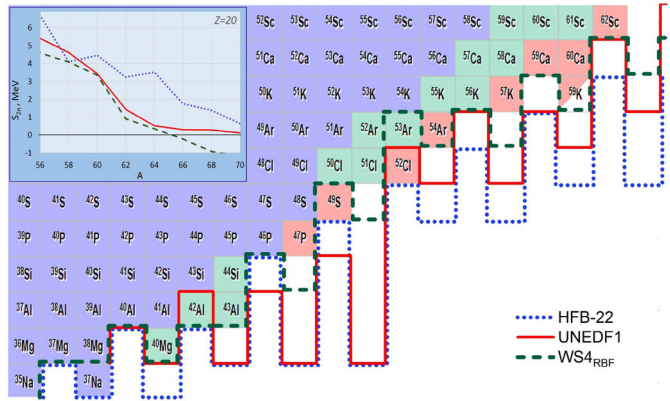


Fig. 1. The region of the chart of nuclides studied in this work. Nuclei highlighted by red background were discovered in this work, green squares denote nuclei discovered at the NSCL since 2007.<sup>2,3,8,9)</sup> The neutron drip lines predicted by the HFB-22,<sup>6)</sup> UNEDF1,<sup>10)</sup> and WS4<sub>RBF</sub><sup>11)</sup> mass models are indicated by the blue dotted, red solid, and green dashed lines, respectively. The model WS4<sub>RBF</sub> appears to underestimate the bindings of isotopes in this region. HFB-22 and UNEDF1 seem to better predict the drip line. The inset shows the predicted  $S_{2n}$  values for even neutron-rich calcium isotopes.

tions of a wide variety of mass models. The two isotopes  $^{49}\text{S}$  and  $^{52}\text{Cl}$ , discovered in this work, emerge as key discriminators between different models. EDFs in best agreement with the limits of existence in the explored region, HFB-22<sup>6)</sup> and UNEDF0,<sup>7)</sup> predict the even-mass Ca isotopes to be bound out to at least  $^{70}\text{Ca}$  (see Fig. 1), at odds with ab-initio models that predict the neutron drip line in Ca to be closer to  $^{60}\text{Ca}$  with  $^{59}\text{Ca}$  unbound.

## References

- 1) G. Hagen *et al.*, Phys. Rev. Lett. **108**, 242501 (2012).
- 2) O. B. Tarasov *et al.*, Phys. Rev. Lett. **102**, 142501 (2009).
- 3) O. B. Tarasov *et al.*, Phys. Rev. C **87**, 054612 (2013).
- 4) O. B. Tarasov, D. Bazin, Nucl. Instrum. Methods Phys. Res. B **266**, 4657 (2008), <http://lise.nslc.msu.edu>.
- 5) O. B. Tarasov *et al.*, Phys. Rev. C **80**, 034609 (2009).
- 6) S. Gorieli *et al.*, Phys. Rev. C **88**, 024308 (2013).
- 7) M. Kortelainen *et al.*, Phys. Rev. C **82**, 024313 (2010).
- 8) O. B. Tarasov *et al.*, Phys. Rev. C **75**, 064613 (2007).
- 9) T. Baumann *et al.*, Nature **449**, 1022 (2007).
- 10) M. Kortelainen *et al.*, Phys. Rev. C **85**, 024304 (2012).
- 11) N. Wang *et al.*, Phys. Lett. B **734**, 215 (2014).

<sup>†</sup> Condensed from the article in Phys. Rev. Lett. **121**, 022501 (2018)

<sup>\*1</sup> NSCL/FRIB, Michigan State University

<sup>\*2</sup> RIKEN Nishina Center

<sup>\*3</sup> Department of Physics, Tohoku University

<sup>\*4</sup> Center for Nuclear Study, University of Tokyo

# Nuclear surface diffuseness revealed in nucleon-nucleus diffraction<sup>†</sup>

S. Hatakeyama,<sup>\*1</sup> W. Horiuchi,<sup>\*1</sup> and A. Kohama<sup>\*2</sup>

A systematic study of the nuclear surface density of neutron-rich nuclei is interesting, as it reveals the neutron number dependence of the nuclear structure dominated by nuclear dynamics at around the nuclear surface. The study can also be extended to understand the properties of the equation of state of asymmetric nuclear matter. However, it is difficult to probe the neutron density by using traditional electron scattering. In this paper, we use a proton target as a probe of the surface density. Extended systematic studies have shown that it is advantageous to use proton to study the neutron and proton radii because it has more sensitivity to the neutrons at low-incident energy.<sup>1,2)</sup> To know more than the nuclear radii, we study the proton-nucleus elastic scattering, focusing on the reactions of small scattering angles up to a few diffraction peaks.

Here, we employ the optical-limit approximation of the Glauber model. As the input to the theory, a two-parameter Fermi (2 pF) density,  $\rho(r) = \frac{\rho_0}{1 + \exp(\frac{r-R}{a})}$ , is assumed. The parameter  $R$  is chosen to give the same root-mean-square (rms) radius with several choices of  $a$ . By calculating differential elastic scattering cross sections (DECS), it is found that the first peak position does not change and that its magnitude increases with smaller diffuseness (sharper surface). The magnitude of the DECS at the first peak position must have information on the nuclear surface.

We perform a “numerical experiment” to deduce the nuclear “diffuseness” from the reaction data. We have the DECS obtained from the realistic densities, the Skyrme-Hartree-Fock (HF) + BCS method used in Refs. 2) and 3). Regarding the DECS used as experimental data, we determine  $R$  and  $a$  in such a way that the DECS with the 2 pF density matches the first peak position and its magnitude of the DECS obtained by the HF+BCS density. The extracted  $a$  values are displayed in Fig. 1. We can clearly see the isotope dependence of the nuclear surface, indicating shell evolution, weak binding, and nuclear deformation, which crucially change the density profile at around the nuclear surface.<sup>3)</sup> We find that the extracted  $a$  values have a robust structure information that is independent of the choice of the incident energy.

To extract detailed structure information of unstable nuclei, separation of proton and neutron diffuseness is important because neutron diffuseness is expected to be more sensitive to the ground-state structure of neutron-rich isotopes as it is dominated by the neutron motion at the nuclear surface. We investigate the possibility of utilizing the incident energy dependence of the nucleon-nucleon total cross sections.<sup>1,2)</sup> Again, we perform a nu-

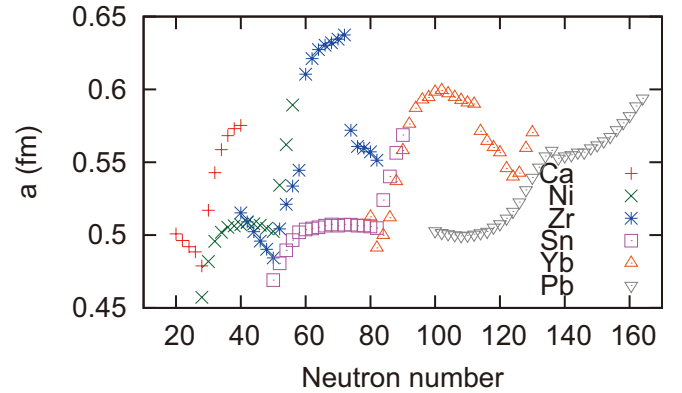


Fig. 1. Nuclear “diffuseness” extracted from the “numerical experiment” at an incident energy of 550 MeV.

merical experiment. We respectively assume 2 pF densities for protons and neutrons and determine these four parameters to reproduce the first peak positions and their DECS at low and high incident energies. We calculate the diffuseness parameters and rms radii of the protons and neutrons for  $^{120}\text{Sn}$ ,  $^{208}\text{Pb}$ , and neutron-rich  $^{132}\text{Sn}$  with several sets of two incident energies among 200, 300, 550, and 800 MeV. For  $^{120}\text{Sn}$  and  $^{208}\text{Pb}$ , the extracted diffuseness parameters are scattered around 0.4–0.6 fm depending on the incident energies chosen, though the rms radii are converged within  $\sim 0.5\%$ . In such cases where the proton and neutron surfaces are located at almost the same position, the separation of the proton and neutron surface profiles might be difficult, whereas in the case of  $^{132}\text{Sn}$ , all the extracted values are consistent with each other within 0.003 fm for protons and neutrons.

In summary, we have performed a numerical experiment using the theoretically obtained DECS of high-energy nucleon-nucleus scattering based on the Glauber model starting from the nucleon-nucleon total cross sections. We have shown that first diffraction peak reflects the nuclear density profile at around the nuclear surface, and have proposed a way to quantify it with the diffuseness parameter of the 2 pF function, which can be determined uniquely. This method is advantageous for application to studies of unstable nuclei since the experimental data is limited to forward angles in the inverse kinematics. This can also be useful for extracting the information of the proton and neutron surfaces, although the separation of the proton and neutron surfaces may be possible only for such neutron (proton)-rich systems in which the surfaces of the proton and neutron surfaces are well separated.

## References

- 1) W. Horiuchi *et al.*, Phys. Rev. C **89**, 011601(R) (2014).
- 2) W. Horiuchi *et al.*, Phys. Rev. C **93**, 044611 (2016).
- 3) W. Horiuchi *et al.*, Phys. Rev. C **96**, 035804 (2017).

<sup>†</sup> Condensed from the article in Phys. Rev. C **97**, 054607 (2018)

<sup>\*1</sup> Department of Physics, Hokkaido University

<sup>\*2</sup> RIKEN Nishina Center

# Proton- and deuteron-induced reactions on $^{107}\text{Pd}$ and $^{93}\text{Zr}$ at 20–30 MeV/nucleon

M. Dozono,<sup>\*1</sup> N. Imai,<sup>\*1</sup> S. Michimasa,<sup>\*1</sup> T. Sumikama,<sup>\*2</sup> N. Chiga,<sup>\*2</sup> S. Ota,<sup>\*1</sup> O. Beliuskina,<sup>\*1</sup> S. Hayakawa,<sup>\*1</sup> K. Iribe,<sup>\*3</sup> C. Iwamoto,<sup>\*1</sup> S. Kawase,<sup>\*4</sup> K. Kawata,<sup>\*1</sup> N. Kitamura,<sup>\*1</sup> S. Masuoka,<sup>\*1</sup> K. Nakano,<sup>\*4</sup> P. Schrock,<sup>\*1</sup> D. Suzuki,<sup>\*2</sup> R. Tsunoda,<sup>\*1</sup> K. Wimmer,<sup>\*5</sup> D. S. Ahn,<sup>\*2</sup> N. Fukuda,<sup>\*2</sup> E. Ideguchi,<sup>\*6</sup> K. Kusaka,<sup>\*2</sup> H. Miki,<sup>\*7</sup> H. Miyatake,<sup>\*8</sup> D. Nagae,<sup>\*2</sup> M. Nakano,<sup>\*9</sup> S. Ohmika,<sup>\*2</sup> M. Ohtake,<sup>\*2</sup> H. Otsu,<sup>\*2</sup> H. J. Ong,<sup>\*6</sup> S. Sato,<sup>\*9</sup> H. Shimizu,<sup>\*1</sup> Y. Shimizu,<sup>\*2</sup> H. Sakurai,<sup>\*2</sup> X. Sun,<sup>\*2</sup> H. Suzuki,<sup>\*2</sup> M. Takaki,<sup>\*1</sup> H. Takeda,<sup>\*2</sup> S. Takeuchi,<sup>\*7</sup> T. Teranishi,<sup>\*3</sup> H. Wang,<sup>\*2</sup> Y. Watanabe,<sup>\*4</sup> Y. X. Watanabe,<sup>\*8</sup> H. Yamada,<sup>\*7</sup> H. Yamaguchi,<sup>\*1</sup> R. Yanagihara,<sup>\*6</sup> L. Yang,<sup>\*1</sup> Y. Yanagisawa,<sup>\*2</sup> K. Yoshida,<sup>\*2</sup> and S. Shimoura<sup>\*1</sup>

The nuclear transmutation of long-lived fission products (LLFPs), which are produced in nuclear reactors, is one of the candidate techniques for the reduction and/or reuse of LLFPs. To design optimum pathways for the transmutation process, several nuclear reactions have been studied by using LLFPs as secondary beams. The studies indicate that proton- and/or deuteron-induced spallation reactions at intermediate energies (100–200 MeV/nucleon) are sufficiently effective for the LLFP transmutation.<sup>1–3</sup> We note that protons/deuterons lose their energies in materials; therefore, measurements at lower reaction energies are definitely desired for the application of transmutation. In this study, the isotopic production cross sections of proton- and deuteron-induced reactions on  $^{107}\text{Pd}$  and  $^{93}\text{Zr}$  at 20–30 MeV/nucleon were measured under an inverse kinematics condition. The experiment was conducted at the OEDO<sup>4</sup>) beamline at RIBF. This was the first physics experiment using OEDO. Detailed descriptions of the setup and procedure can be found in Ref. 5).

Figure 1 shows the preliminary results for the isotopic production cross sections of the proton-induced reactions on  $^{107}\text{Pd}$ . Considering the energy loss of the beam in the target, the measured cross sections are the ones averaged over 25–30 MeV/nucleon. The sensitivity threshold of the measurement was 5 mb because of statistics. We determined the cross sections for five isotopes ( $^{107–105}\text{Ag}$  and  $^{106,105}\text{Pd}$ ).

The results show significant production of Ag isotopes; about 70% of the total cross section is exhausted by Ag isotopes. This can be understood by the compound-nuclear process:  $^{107}\text{Pd} + p \rightarrow ^{108}\text{Ag}^*$ . The Ag isotopes are probably produced by the evaporation of neutrons from the highly excited compound nucleus  $^{108}\text{Ag}^*$ . Actually, the trend is completely different from the high-energy spallation reaction case,<sup>2</sup>) in which the contribution of Ag isotopes is less than 10%.

The curves in Fig. 1 show the excitation functions

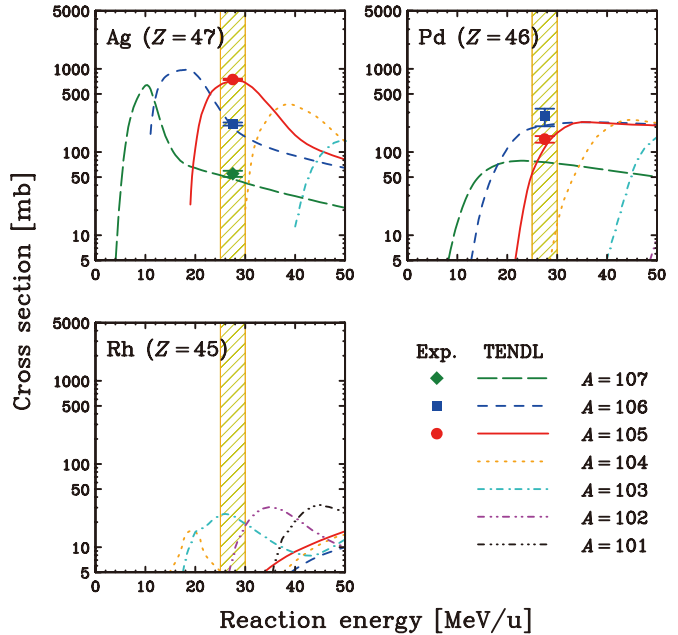


Fig. 1. Isotopic production cross sections of the proton-induced reactions on  $^{107}\text{Pd}$ .

evaluated by TENDL-2017.<sup>6</sup>) The cross sections of Ag and Pd isotopes were reasonably reproduced by the evaluation. On the other hand, the cross sections of  $^{103,102}\text{Rh}$  were considerably overestimated; TENDL predicted significant values for  $^{103,102}\text{Rh}$ , but they were not detected in the experiment.

The present data, as well as higher-energy data, would provide an effective guideline for a possible solution of LLFP transmutation. The results will be finalized soon, and the preparation for publication is in progress. Regarding the  $^{93}\text{Zr}$  data, the analysis for particle identification is ongoing.

This work was funded by the ImPACT Program of the Council for Science, Technology and Innovation (Cabinet Office, Government of Japan).

## References

- 1) H. Wang *et al.*, Phys. Lett. B **754**, 104 (2016).
- 2) H. Wang *et al.*, Prog. Theor. Exp. Phys. **2017**, 021D01 (2017).
- 3) S. Kawase *et al.*, Prog. Theor. Exp. Phys. **2017**, 093D03 (2017).
- 4) S. Michimasa *et al.*, Prog. Theor. Exp. Phys., accepted.
- 5) M. Dozono *et al.*, RIKEN Accel. Prog. Rep. **51**, 99 (2018).
- 6) A. J. Koning *et al.*, Nucl. Data Sheets **113**, 2841 (2012).

<sup>\*1</sup> Center for Nuclear Study, the University of Tokyo

<sup>\*2</sup> RIKEN Nishina Center

<sup>\*3</sup> Department of Physics, Kyushu University

<sup>\*4</sup> Department of Advanced Energy Engineering Science, Kyushu University

<sup>\*5</sup> Department of Physics, the University of Tokyo

<sup>\*6</sup> Research Center for Nuclear Physics, Osaka University

<sup>\*7</sup> Department of Physics, Tokyo Institute of Technology

<sup>\*8</sup> WNSC, IPNS, KEK

<sup>\*9</sup> Department of Physics, Rikkyo University

# Transverse momentum dependent fragmentation measurements in Belle<sup>†</sup>

R. Seidl<sup>\*1</sup>

The Belle experiment at the asymmetric  $e^+e^-$  collider KEKB provides a very large data set for not only the study of flavor physics but also the study of the strong interaction, QCD. The clean initial state allows very effective measurements of fragmentation functions. Fragmentation functions describe the formation of confined, final state hadrons out of asymptotically-free high-energetic partons. These fragmentation functions (FF) therefore tell us about the confinement process in itself. They also can be seen as tools used in order to extract flavor and/or spin information in parton distribution functions via their different sensitivities. The transverse momentum dependence of distribution and fragmentation functions is of particular importance as it is closely related to the three-dimensional structure of the nucleon planned to be measured in great detail at the Electron-Ion-Collider, EIC, and the Collins and Sivers effects. In Belle, one has the unique chance to study the transverse momentum dependence in single hadron fragmentation using the event-shape variable thrust as the reference axis and as proxy for the initial quark-anti-quark axis. For this analysis, data sample of  $655 \text{ fb}^{-1}$  collected at the center-of-mass energy of  $\sqrt{s} = 10.58 \text{ GeV}$  was used. Single charged pions, kaons and protons were selected as a function of fractional energy  $z = 2E_h/\sqrt{s}$ , the thrust value  $T$  and the transverse momentum. The raw distributions were corrected for particle mis-identification, momentum smearing, backgrounds from other processes, reconstruction and acceptance as well as initial-state radiation, similar to the description of previous results.<sup>1,2)</sup> The resulting transverse momentum dependent cross sections are shown in Fig. 1 for  $0.85 < T < 0.9$ . The behavior is overall very similar between particle species with protons having generally narrower distributions. As expected by theory, the low transverse momentum region  $P_{hT} < 1 \text{ GeV}$  can be successfully described by Gaussians. However, unlike theory predictions of a rather simple fractional energy dependence, the widths of these Gaussian fits are increasing at small fractional energies while they decrease again at higher fractional energies. In these fits, pions and kaons show similar widths while those of proton are significantly smaller, as can be seen in Fig. 2. When compared for different thrust values, the widths are largest at low thrust, where the events are more spherical while they become smaller as the events become more collimated.

These results will be used in global fragmentation analyses in order to increase the precision of the al-

ready existing transverse spin data from RHIC and semi-inclusive scattering and inform on the data to be taken at the EIC.

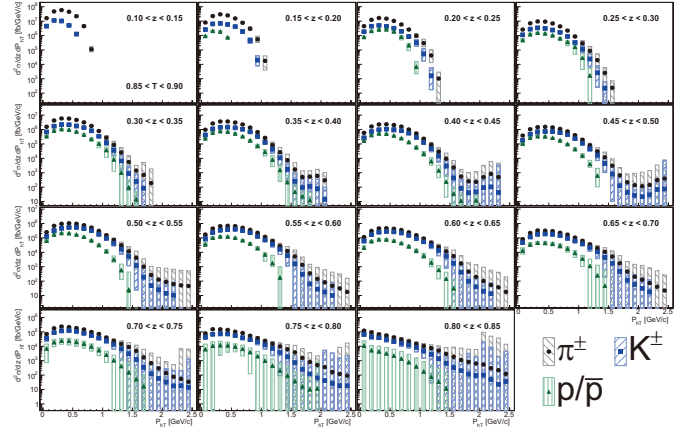


Fig. 1. Differential cross sections for pions (black circles), kaons (blue squares) and protons (green triangles) as a function of  $P_{hT}$  for the indicated  $z$  bins and thrust  $0.85 < T < 0.9$ . The error boxes represent the systematic uncertainties. Due to the large uncertainties in them,  $z$  bins above 0.85 are not displayed.

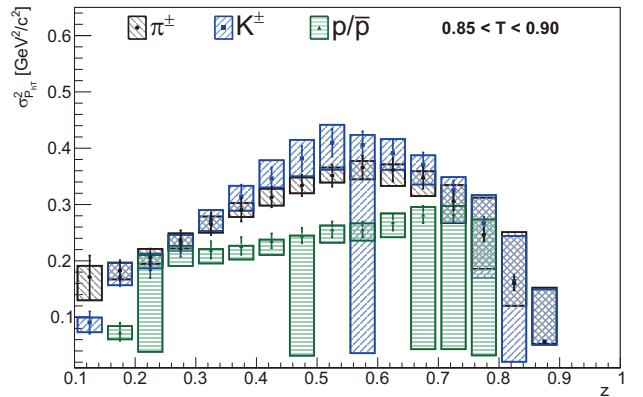


Fig. 2. Gaussian widths as a function of  $z$  for pions (black circles and boxes), kaons (blue squares and boxes) and protons (green triangles and boxes) and thrust  $0.85 < T < 0.9$ . The error boxes represent the corresponding systematic uncertainties as described in the text.

## References

- 1) R. Seidl *et al.* [Belle Collaboration], Phys. Rev. D **96**, 032005 (2017).
- 2) R. Seidl *et al.* [Belle Collaboration], Phys. Rev. D **92**, 092007 (2015).

<sup>†</sup> Condensed from the article accepted in Phy. Rev. D  
<sup>\*1</sup> RIKEN Nishina Center

# Measurement of elliptic flow of single electrons from semi-leptonic decay of charm and bottom hadrons in Au + Au collisions at $\sqrt{s_{NN}} = 200$ GeV

Y. Ueda<sup>\*1,\*2</sup> for the PHENIX Collaboration

Heavy flavors (HFs), charm ( $c$ ) and bottom ( $b$ ) quarks, are suitable probes for the study of quark gluon plasma (QGP). HFs are mainly produced from the hard scattering at the early stage of collisions because they have large masses ( $M_c \approx 1.3$  GeV/ $c^2$ ,  $M_b \approx 4.2$  GeV/ $c^2$ ). HFs reflect the space-time evolution of the QGP well. The perturbative QCD calculations can be applied to the  $c$  and  $b$  quarks at the initial hard scattering in the collisions. It means that the yield of the  $c$  and  $b$  quarks is calculated precisely. Also, the  $b$  quark mass is about three times as heavy as the  $c$  quark mass. The measurement with  $c$  and  $b$  quark separation shows the quark mass dependence of their quantities and behaviors in the QGP. Therefore, the  $c$  and  $b$  quark measurement is essential for QGP research. The modification of  $c$  and  $b$  quarks provides information about QGP.

A Silicon Vertex Tracker (VTX) consisting of 4 layers of silicon detectors was installed at the RHIC-PHENIX experiment in 2011 to reconstruct charged particle trajectories and their Distances of Closest Approach (DCA) to the primary collision vertex. The DCA is related to the decay length of the particles. As the decay lengths of  $c$  and  $b$  hadrons are different enough ( $D^0 \sim 123$   $\mu\text{m}$ ,  $B^0 \sim 455$   $\mu\text{m}$ ), we can statistically separate electrons from the semileptonic decays of  $c$  and  $b$  hadrons using the DCA, even with a lower integrated luminosity. In 2014, the PHENIX collected about 15 billion minimum bias events from Au + Au collisions at  $\sqrt{s_{NN}} = 200$  GeV, which is 10 times larger than the previous dataset obtained in 2011. Additionally, the systematic uncertainties are reduced because the photonic background estimation and the VTX are improved.

For the HF study, we measure the centrality dependence of the nuclear modification factors<sup>1)</sup> and the azimuthal anisotropy ( $v_2$ ) of the  $c$  and  $b$  electrons.  $v_2$  is originated from the initial geometry of the QGP. It then

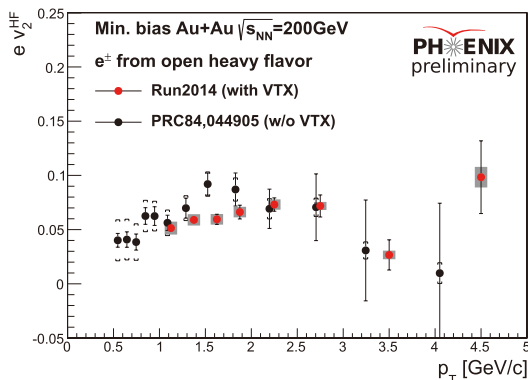


Fig. 1. Comparison of HF  $v_2$  using 2007 dataset and 2014 dataset.

\*1 RIKEN Nishina Center

\*2 Department of Physics, Hiroshima University

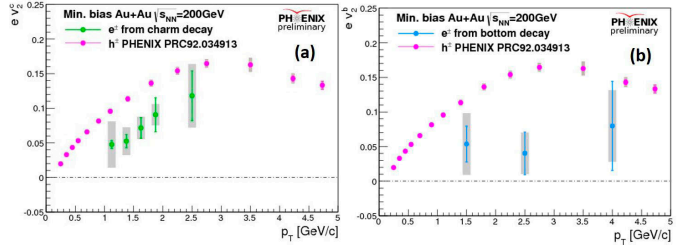


Fig. 2. Compared of charged hadron  $v_2$  with (a) charm and (b) bottom electron  $v_2$ .

expands the pressure gradient with the QGP evolution.  $v_2$  reflects the hydrodynamic property of the QGP, *e.g.*,  $\eta/s$ , well. Therefore, the  $c$  and  $b$  electron separation measurement of  $v_2$  is essential for the study of the flow effect. We installed the high-resolution detector FVTX at the RHIC-PHENIX experiment in 2012 for the  $c$  and  $b$  electron  $v_2$  separation measurement. The FVTX detector precisely measures the reaction plane, which is the reference of the  $v_2$  measurement. We measure the  $c$  and  $b$  electron  $v_2$  with smaller uncertainties using this detector.

A comparison of HF electron  $v_2$  using the 2014 dataset (black point) and the 2004 dataset (red point) is shown in Fig. 1. The new result is consistent with the previous result. On the other hand, the uncertainties became smaller because of the higher statistics in the 2014 dataset and the higher resolution provided by the FVTX detector.

The HF  $v_2$  is statistically separated into  $c \rightarrow e$   $v_2$  and  $b \rightarrow e$   $v_2$  using the DCA information. The DCA region is separated into 2 DCA regions:  $c$  and  $b$  rich regions. The  $c/b$  electron  $v_2$  ( $v_2^{c/b}$ ) is described with the calculated  $b$  fraction  $f_b(c/b)$  and background (BG) fraction  $f_{BG}(c/b)$  for the  $c/b$  rich region using the following formulas.

$$v_2^{\text{meas}}(c) = f_b(c) \cdot v_2^b + (1 - f_b(c)) \cdot v_2^c + f_{BG}(c) \cdot v_2^{\text{BG}}(c)$$

$$v_2^{\text{meas}}(b) = f_b(b) \cdot v_2^b + (1 - f_b(b)) \cdot v_2^c + f_{BG}(b) \cdot v_2^{\text{BG}}(b)$$

Here,  $v_2^{\text{meas}}(c/b)$  and  $v_2^{\text{BG}}(c/b)$  are the measured inclusive electron  $v_2$  and BG  $v_2$  for the  $c/b$  rich region, respectively. The  $c$  and  $b$  electron  $v_2$  are separately calculated by solving these equations.

A comparison of (a)  $c$  electron  $v_2$  (red point) and (b)  $b$  electron  $v_2$  (blue point) with the charged hadron  $v_2$  (pink point) is shown in Fig. 2. It is the first measurement of  $b$  electron  $v_2$  at RHIC. The  $c$  and  $b$  electron  $v_2$  are smaller than the charged hadron  $v_2$ . Also, the  $c$  electron  $v_2$  seems to be larger than the  $b$  electron  $v_2$ . Unfortunately, the large uncertainty makes  $b$  electron  $v_2$  consistent with zero. We will improve the method for the  $c$  and  $b$  electron  $v_2$  separation measurement.

## Reference

- 1) K. Nagashima for the PHENIX Collaboration., Nucl. Phys. A **967**, pp. 644–647 (2017).

# The chiral propulsion effect<sup>†</sup>

Y. Hirono,<sup>\*3</sup> D. E. Kharzeev,<sup>\*1,\*2,\*3</sup> and A. V. Sadofyev<sup>\*4</sup>

The physics of chiral media has attracted a significant attention recently. Remarkably, it appears that the quantum chiral anomaly significantly affects the macroscopic behavior of chiral media and induces new transport phenomena,<sup>1,2)</sup> such as the Chiral Magnetic and Chiral Vortical Effects (CME and CVE, respectively). CME and CVE refer to the generation of electric currents along an external magnetic field or vorticity in the presence of a chirality imbalance. The resulting currents are non-dissipative due to the protection by the global topology of the gauge field. These chiral effects are expected to occur in a variety of systems: the quark-gluon plasma, Dirac and Weyl semimetals, primordial electroweak plasma, and cold atoms. In quark-gluon plasma, the chirality imbalance can be produced by topological fluctuations of QCD, or by the combination of electric and magnetic fields that accompany heavy-ion collisions.

Consider the motion of a vortex filament in a fluid. It can be described by the localized induction equation (LIE),

$$\dot{\mathbf{X}} = C\mathbf{X}' \times \mathbf{X}'', \quad (1)$$

where  $\mathbf{X} = \mathbf{X}(t, s)$  denotes the position of a vortex,  $t$  is the time,  $s$  is the arc-length parameter, the dot and the prime indicate the derivatives with respect to  $t$  and  $s$  respectively, and  $C$  is a parameter dependent on the properties of the fluid. Interestingly, the LIE (1) can be mapped to the non-linear Schrödinger equation (NLSE) by the so-called Hasimoto transformation,

$$\psi(t, s) = \kappa(t, s) \exp \left[ i \int^s \tau(t, s') ds' \right], \quad (2)$$

where  $\kappa(t, s)$  is the curvature and  $\tau(t, s)$  is the torsion of a vortex. NLSE is known to be a completely integrable system which has solitonic solutions and an infinite sequence of commuting conserved charges. The LIE possesses solutions that represent helical excitations propagating along the vortex; they are known as Hasimoto solitons.

Let us now consider a system in which parity is broken by the presence of magnetic helicity; the corresponding term in the action is

$$S_\chi = \int dt \mu \mathcal{H}, \quad (3)$$

where  $\mu$  is the ‘‘chiral’’ chemical potential,  $\mathcal{H}$  is the

magnetic helicity given by  $\mathcal{H} = \frac{e^2}{4\pi^2} \int d^3x \mathbf{A} \cdot \mathbf{B}$ , where  $\mathbf{A}$  is the vector potential and  $\mathbf{B}$  is the magnetic field. It is worth mentioning that taking the derivative of this action with respect to the vector potential, one readily finds the CME current:  $\mathbf{J}_{\text{CME}} = \delta S_\chi / \delta \mathbf{A} \propto \mathbf{B}$ . Supplementing the non-relativistic Abelian Higgs model with the term given by Eq. (3), one can find the equation of motion for a quantized magnetic vortex at finite  $\mu$ , as derived by Kozhevnikov:

$$\dot{\mathbf{X}} = C\mathbf{X}' \times \mathbf{X}'' + \mu \left[ \mathbf{X}''' + \frac{3}{2}(\mathbf{X}'')^2 \mathbf{X}' \right], \quad (4)$$

where a tangential term  $\frac{3}{2}\mu(\mathbf{X}'')^2 \mathbf{X}'$  is added to keep the arc-length-preserving property.

In this paper we are interested in the behavior of chiral solutions. We can find a simple explicit solution of the FME (4) having the form of a helix,

$$\mathbf{X}_{\text{helix}}(t, s) = \frac{1}{A^2} \begin{pmatrix} \kappa_0 \cos[A(s - v_p t)] \\ \kappa_0 \sin[A(s - v_p t)] \\ \tau_0 A(s - v_g t) \end{pmatrix}, \quad (5)$$

where the constants  $\kappa_0$  and  $\tau_0$  give the curvature and the torsion of the helix,  $A = \sqrt{\kappa_0^2 + \tau_0^2}$ , and the phase and group velocities are given by  $v_p = \tau_0 + \mu(\tau_0^2 - \frac{\kappa_0^2}{2})$ ,  $v_g = -\frac{\kappa_0^2}{\tau_0} - \frac{3\kappa_0^2}{2}\mu$ . Note that the sign of  $\tau_0$  determines the handedness of the helix. The radius  $R$  and the pitch  $\ell$  of the helix are given by  $R = \kappa_0 / (\kappa_0^2 + \tau_0^2)$ ,  $\ell = 2\pi\tau_0 / (\kappa_0^2 + \tau_0^2)$ .

Using the map between the FME and the Hirota equation, we find a propagating solitonic solution of the FME,

$$\mathbf{X}_{\text{sol}}(t, s) = \begin{pmatrix} -\frac{2\epsilon}{\epsilon^2 + \tau_0^2} \operatorname{sech}[\epsilon\xi] \cos[\eta] \\ -\frac{2\epsilon}{\epsilon^2 + \tau_0^2} \operatorname{sech}[\epsilon\xi] \sin[\eta] \\ s - \frac{2\epsilon}{\epsilon^2 + \tau_0^2} \tanh[\epsilon\xi] \end{pmatrix}. \quad (6)$$

where  $\eta \equiv \tau_0 s + (\epsilon^2 - \tau_0^2)t + \mu\tau_0(3\epsilon^2 - \tau_0^2)$ ,  $\xi \equiv s - (2\tau_0 + \mu(3\tau_0^2 - \epsilon^2))t$ , and  $\epsilon$  and  $\tau_0$  are constants. This soliton has a constant torsion given by  $\tau_0$  and propagates in the  $z$  direction. Its speed is modified by  $\mu$  and reduces to the original Hasimoto soliton at  $\mu = 0$ .

To summarize, we have found that in chirally imbalanced media there exist helical excitations that carry energy along the vortex (the Chiral Propulsion Effect).

## References

- 1) K. Fukushima, D. E. Kharzeev, H. J. Warringa, Phys. Rev. D **78**, 074033 (2008) [arXiv:0808.3382 [hep-ph]].
- 2) D. E. Kharzeev, Prog. Part. Nucl. Phys. **75**, 133 (2014) [arXiv:1312.3348 [hep-ph]].

<sup>†</sup> Condensed from the article in Phys. Rev. Lett. **121**, 142301 (2018)

<sup>\*1</sup> RIKEN Nishina Center

<sup>\*2</sup> Department of Physics and Astronomy, Stony Brook University

<sup>\*3</sup> Department of Physics, Brookhaven National Laboratory

<sup>\*4</sup> Los Alamos National Laboratory

## Superconducting RILAC booster<sup>†</sup>

N. Sakamoto,<sup>\*1</sup> M. Dantsuka,<sup>\*1</sup> H. Hara,<sup>\*3</sup> H. Imao,<sup>\*1</sup> E. Kako,<sup>\*2</sup> O. Kamigaito,<sup>\*1</sup> K. Kusaka,<sup>\*1</sup> K. Miyamoto,<sup>\*3</sup> H. Nakai,<sup>\*2</sup> H. Okuno,<sup>\*1</sup> K. Ozeki,<sup>\*1</sup> H. Sakai,<sup>\*2</sup> K. Sennyu,<sup>\*3</sup> K. Suda,<sup>\*1</sup> K. Umemori,<sup>\*2</sup> T. Watanabe,<sup>\*1</sup> Y. Watanabe,<sup>\*1</sup> K. Yamada,<sup>\*1</sup> and T. Yanagisawa<sup>\*3</sup>

The RIKEN Heavy-Ion Linac (RILAC) is undergoing an upgrade to enable it to further investigate super-heavy elements and produce of radioactive isotopes for medical applications. In this project, a new superconducting (SC) electron cyclotron resonance ion source and SC booster linac (SRILAC) are being developed and constructed. The SRILAC consists of 10 TEM quarter-wavelength resonators that are operated at 73 MHz and contained in three cryomodules (CMs). The goals of the upgrade are listed in Table 1. It should be noted that the fundamental frequency of the reference radio frequency (RF) signal has been chosen as 36.5 MHz because it is the frequency for the RF system of the RIBF accelerators.

As shown in Fig. 1, the SRILAC consists of three CMs—CM1, CM2, and CM3—with a room-temperature medium-energy beam transport (MEBT) between them. The CMs do not contain superconducting magnets. The design of the CMs is a modification of a prototype CM developed at RIKEN.<sup>1–3)</sup>

The operational parameters of the CMs are listed in Table 2. The gap length of the cavity is optimized for  $\beta = 0.08$  particles with a transit time factor (TTF) of 0.9. The gap voltage is 1.2 MV, which corresponds to an acceleration gradient  $E_{acc}$  of 6.8 MV/m with a synchronous phase of  $-25^\circ$ . After the fabrication of the ten SC-cavities, all cavities were tested and passed the acceptance test.<sup>5)</sup>

The SC-cavities are cooled by 4-K liquid helium provided by a liquid helium cryogenic system using a HELIAL MF refrigerator (Air Liquide).

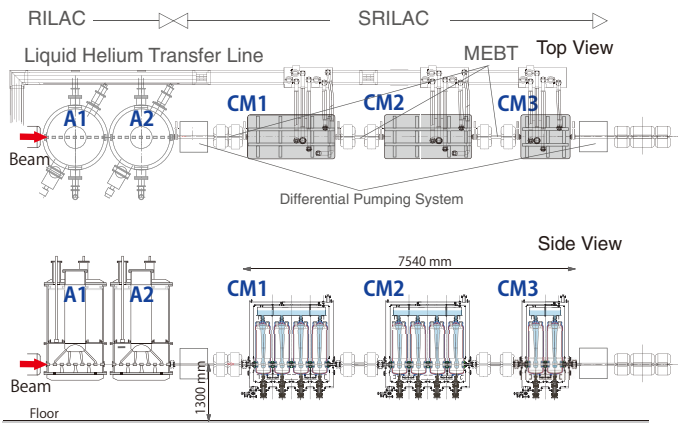


Fig. 1. Layout of the Superconducting RILAC (SRILAC).

Table 1. Specifications of RILAC before and after upgrade.

Upgrade	Before	After
Number of tanks	12 DTLs	8 DTLs, 3 CMs
Frequency (MHz)	37.75/75.5	36.5/73.0
Total $V_{acc}$ (MV)	25 ( $A/q = 5$ )	39 ( $A/q = 6$ )

Table 2. Operational parameters of the SRILAC.

Frequency (MHz)	73.0 (c. w.)
$E_{inj}$ (MeV/nucleon)	3.6
$E_{ext}$ (MeV/nucleon)	6.5 for $A/q = 6$
Number of cavities	10
Cavity type	TEM, $\lambda/4$
Max. gap voltage (MV)	1.2
Synchronous phase ( $^\circ$ )	$-25$
Max. acc. gradient (MV/m)	6.8
Target $Q_0$ (at $E_{acc} = 6.8$ MV/m)	$1 \times 10^9$
Beam current ( $\mu A$ )	$\leq 100$
$Q_{ext}$	$1-4.5 \times 10^6$
Amplifier output (kW)	7.5

For the MEBT, a newly designed beam energy position monitor will be employed instead of the traditional wire scanners. Because beam measurement is non-destructive, ideally there is neither outgassing nor spattering to produce particulates in the high-vacuum sections.

Because the SRILAC will be installed in the existing facility, it is important to have an isolation system indicated as a differential pumping system in Fig. 1 to prevent contamination of the SC-cavities, which deteriorates the performance of the SC-cavities.

Full assembly of the CM will be finished in the first quarter of 2019 and its installation in the accelerator building is scheduled for March 2019. After installing the MEBT, including the differential pumping systems, cooling and RF testing will be performed during the second quarter of 2019 with the aim of full beam commissioning in the third quarter of 2019.

### References

- 1) K. Ozeki *et al.*, *Cryomodule and power coupler for RIKEN Superconducting QWR*, LINAC2016, East Lansing, September 2016, TUPLR061, p. 598.
- 2) K. Yamada *et al.*, *First Vertical Test of Superconducting QWR Prototype at RIKEN*, LINAC2016, East Lansing, September 2016, THPLR040, p. 939.
- 3) N. Sakamoto *et al.*, SRF2017, WEYA01; K. Yamada *et al.*, PASJ 14th Annual Meeting, TUOL02.
- 4) <http://www.jst.go.jp/impact/en/program/08.html>
- 5) K. Yamada *et al.*, *Performance test of bulk-niobium cavities for new superconducting linear accelerator*, in these reports.

<sup>†</sup> Condensed from the proceedings of LINAC2018, Beijing, September 2018, WE2A03, p. 620.

<sup>\*1</sup> RIKEN Nishina Center

<sup>\*2</sup> KEK, Tsukuba

<sup>\*3</sup> MHI-MS, Kobe

# Remodeling of acceleration cavity resonators for RIKEN Ring Cyclotron

K. Yamada,<sup>\*1</sup> K. Suda,<sup>\*1</sup> N. Sakamoto,<sup>\*1</sup> and O. Kamigaito<sup>\*1</sup>

The RIKEN Ring Cyclotron (RRC)<sup>1)</sup> has two acceleration cavities that consist of variable-frequency half-wavelength resonators constructed over 30 years ago. The design range of resonant frequency is between 20 and 45 MHz. Additionally, the resonant frequency can be varied by moving two movable boxes,<sup>2)</sup> as shown in Fig. 1. During the acceleration of  $^{238}\text{U}$ , which is one of the most important beams in the operation of RIBF, the maximum beam current in the RRC was limited by large beam losses in the electrostatic deflection channel (EDC) that were caused by small turn separations and a space-charge effect owing to the insufficient acceleration voltage of the cavity resonators. The  $^{238}\text{U}$  beam was accelerated in a fixed-frequency mode using RILAC<sup>2,3,4)</sup> as an injector. Consequently, the RRC resonators have to be operated at a low frequency of 18.25 MHz, which is less than the designed lower limit. To resonate at this low frequency, the capacitance was increased by bringing the movable box close to the location of 20 mm from the dee electrode, which caused the extremely low shunt-impedance and frequent discharge. Moreover, the acceleration voltage could not be raised above 80 kV/gap. Therefore, we decided to increase the acceleration voltage at 18.25 MHz operation by remodeling the inner component of the stems and dee electrode, excluding the outer box of the resonator and the movable boxes, respectively.

The frequency range of the RRC resonator was shifted to the lower side by inserting notches in the stem that was originally straight. Because the RRC resonator had not operate at a frequency higher than 39 MHz in recent years, the frequency range after remodeling was set to be 16–38 MHz. Although this slant type stem is similar to the early design<sup>5)</sup> of the RRC resonator, the shunt-impedance, voltage distribution, and frequency range were optimized by changing the notch sizes based on 3D electromagnetic calculation using Microwave Studio (MWS).<sup>6)</sup> Figure 1 shows a calculation model of MWS for the original resonator and the modified resonator. It was expected that the shunt-impedance could be doubled at 18.25 MHz by this remodeling.

The remodeling work on site was carried out from February to March 2018. We performed a low power RF test with a network analyzer in April. According to the test results, it was found that the frequency range and quality factor  $Q_0$  were almost consistent with the expected values for each resonator. Figure 2 shows an image of the inside of the resonator after modification. Simultaneously, the old-degraded power supplies for the grid of tetrodes in RF power amplifiers were updated for stable operation.

The new resonators were used for the machine time

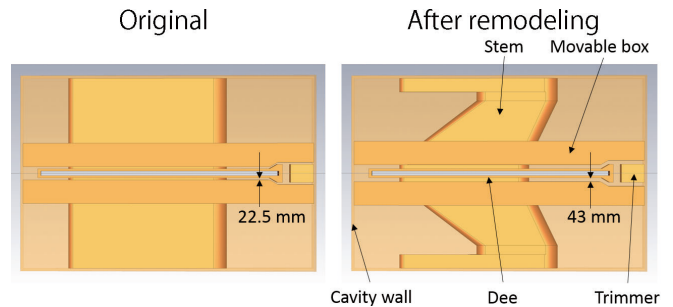


Fig. 1. Calculation models of the original cavity (left panel) and remodeling cavity (right side) used in the MWS.

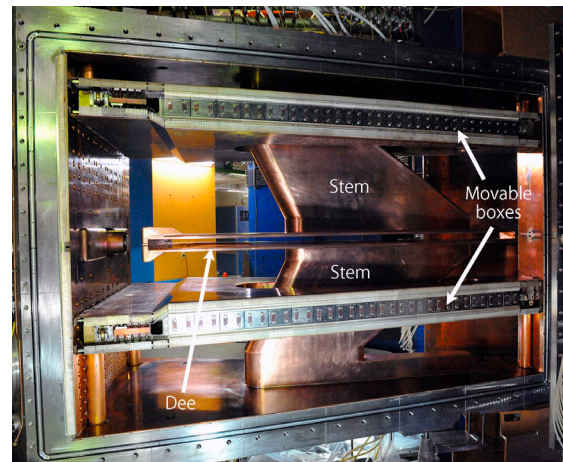


Fig. 2. Inside view of the remodeled RRC cavity.

from May and showed good performance in the operation from 18.25 MHz to 32.6 MHz. Especially, a stable operation with the voltage of 120 kV/gap was realized for 18.25 MHz owing to the shunt-impedance improvement and discharge decrement. However, owing to the water leakage from the cooling channel in the vacuum due to the production problem, we are currently considering countermeasures.

## References

- 1) Y. Yano, Proc. 13th Int. Cyclo. Conf., 102 (1992).
- 2) T. Fujisawa *et al.*, Nucl. Instrum. Methods Phys. Res. A **292**, 1 (1990).
- 3) K. Yamada *et al.*, Proc. of IPAC12, TUOBA02, 1071 (2012).
- 4) K. Suda *et al.*, Nucl. Instrum. Methods Phys. Res. A **722**, 55 (2013).
- 5) K. Ogiwara *et al.*, RIKEN Accel. Prog. Rep. **18**, 172 (1984).
- 6) <https://www.cst.com/products/cstmws>.

<sup>\*1</sup> RIKEN Nishina Center

## He gas stripper with N<sub>2</sub> gas-jet curtain

H. Imao,<sup>\*1</sup> H. Okuno,<sup>\*1</sup> H. Hasebe,<sup>\*1</sup> N. Ikoma,<sup>\*1,\*2</sup> and O. Kamigaito<sup>\*1</sup>

The present intensity of uranium beams injected into the first stripper is reaching  $\sim 10^{13}/s$  at the RIBF. This has given rise to various types of difficulties in the operation of He gas stripper. A small fraction of beam loss in the He gas stripper<sup>1,2)</sup> causes serious hardware troubles or radioactivities. The qualities of beams injected to the He stripper become worse at high-intensity operations owing to the space charge effect in the RIKEN ring cyclotron (RRC) placed 7 m upstream of the He stripper. The diameter of the orifices in the He stripper must be enlarged for the efficient transmission of high-intensity beams. In contrast, a small leak of He gas to the RRC becomes a serious problem at high-intensity operations. The RRC has only 14 cryopumps with total pumping speed of 120 m<sup>3</sup>/s for N<sub>2</sub>. Owing to the small pumping capacity of He gas, the leaked He gas is accumulated in the RRC gradually. Collisions between U ions and He atoms in the RRC can easily change their charges and cause beam loss. For the acceleration of high-intensity uranium beams, such beam loss induces further losses by the local pressure rise due to the gas desorption (dynamic vacuum).

To solve these inevitable problems, we invented the N<sub>2</sub> gas-jet curtain method. By using curtain-like nitrogen gas-jet that separates two rooms (Fig. 1), we can block the helium flow to the low-pressure side and the leaked gas is exchanged to N<sub>2</sub> from He.

Based on the concept, we designed and developed the

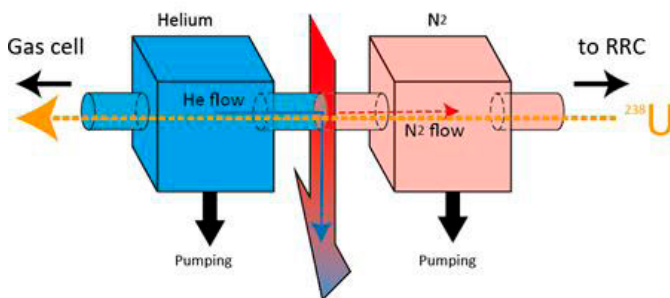


Fig. 1. Concept of N<sub>2</sub>-jet curtain. The jet separates two rooms.

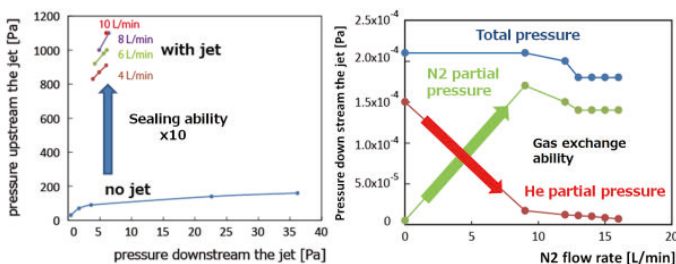


Fig. 2. Performance of N<sub>2</sub>-jet curtain.

<sup>\*1</sup> RIKEN Nishina Center

<sup>\*2</sup> Department of Energy and Environment Science, Nagaoka University of Technology

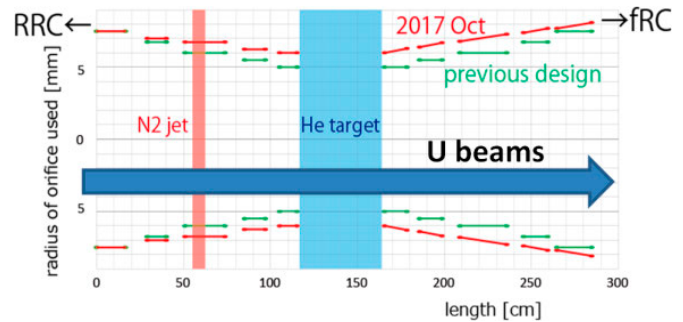


Fig. 3. Enlargement of diameters of tapered tube orifices.

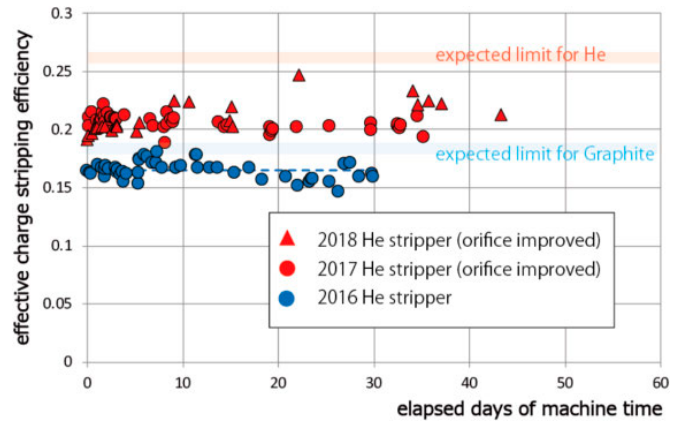


Fig. 4. Comparison of effective charge stripping efficiencies.

actual device to make the N<sub>2</sub> gas-jet curtain optimized with CFD calculations. The device was installed in the He stripper and tested. Figure 2 shows the demonstrated performance of the N<sub>2</sub> gas-jet curtain method. It is evident that the sealing abilities significantly increased. The gas that leaked downstream was successfully exchanged to nitrogen, as we desired. In addition, the N<sub>2</sub> gas-jet curtain worked as a pre-stripper. Initial stripping in N<sub>2</sub>-jet curtain ( $\sim 30 \mu\text{g}/\text{cm}^2$ ) reduced the required pressure of He gas up to  $\sim 15\%$ .

By utilizing the gas-jet curtain, we enhanced the orifice diameters as shown in Fig. 3. The 4D acceptance of the system is 1.5 times higher than that of previous systems.

The improved system was applied in the user runs in 2017 and 2018. The output intensities were increased with more than 25% owing to the increasing transmission efficiencies (Fig. 4). No serious pressure rise in the RRC was observed. The N<sub>2</sub> gas-jet curtain method was greatly contributed to the enhanced output intensity (71 pA at 345 MeV/nucleon) achieved in 2017.

### References

- 1) H. Imao *et al.*, Phys. Rev. ST Accel. Beams **15**, 123501 (2012).
- 2) H. Imao *et al.*, in Proc. IPAC'13, Shanghai, paper **THPPA01 & THPWO038** (2013).

## Upgrade of particle selection system for Rare RI Ring experiments

Y. Abe,<sup>\*1</sup> Y. Yamaguchi,<sup>\*1</sup> M. Wakasugi,<sup>\*1</sup> D. Nagae,<sup>\*1</sup> F. Suzaki,<sup>\*1</sup> and for the Rare RI Ring collaboration

We developed a particle selection system for Rare RI Ring experiments. This system selects particles to be injected into R3 using the flight time and energy loss ( $\Delta E$ ) information obtained at F3 in the BigRIPS focal plane. In the early stage of development,<sup>1)</sup> the signals from detectors were processed using the standard NIM modules with a processing time of at least 60 ns. Because it is necessary to transmit the trigger signal to the kicker magnets as soon as possible, we developed dedicated modules with the particle-selection function. A conceptual circuit diagram is shown in Fig. 1. Because these modules are placed at F3, they are remote-controlled through the ethernet communication. The signal processor consists of two types of modules. One is for particle selection (module A). This processes the raw signals related to the flight time and energy loss information.

Each particle arrives at a certain time relative to the RF Phase. The module A applies coincidence or veto logic with time window created by the RF signal and controls the output signal rate by adjusting the dead time of the module. Therefore, the particle is temporally separated and the output rate is appropriately adjusted. The module A has a window-type discrimination function and can select a certain pulse height signal depending on the energy loss. In combination with both functions, in principle, it is possible to select a single isotope. The required processing time is approximately 15 ns. The other module (module B) combines OR-logic with the signals from two or more types of module A. Because module A can control the rate of output signal in the given time window, it is possible to control the abundance of isotopes to be injected into R3. The processing time required in module B is also approximately 15 ns. Furthermore, module B can limit the total rate of the output signal and adjust the delay of the signal used as the excitation trigger for the kicker magnets.

We practically used the modules in the R3 experiments in fall 2018.<sup>2,3)</sup> The target nuclei chosen in the experiments were the neutron-rich Ni and Pd isotopes. In these experiments, a 2 mm-thick plastic scintillation detector was installed additionally at F3 to get  $\Delta E$  information for particle selection. Figure 2 (a) shows a typical particle-identification (PID) plot and  $^{77}\text{Ga}$  has the high-

est abundance. The abundance of other isotopes could be increased by selectively getting rid of the Ga events, as shown in Fig. 2 (b), where  $^{76}\text{Zn}$  is the measure component. We increased the purity of nuclei in the more neutron-rich side by shifting the time window and adjusting the output rate. Their purities can be higher than that of  $^{77}\text{Ga}$ , as shown in Fig. 2 (c). Owing to this system, we succeeded in the mass measurement of neutron-rich nuclei. This system is useful not only for R3 experiments but also other experiments on exotic nuclei.

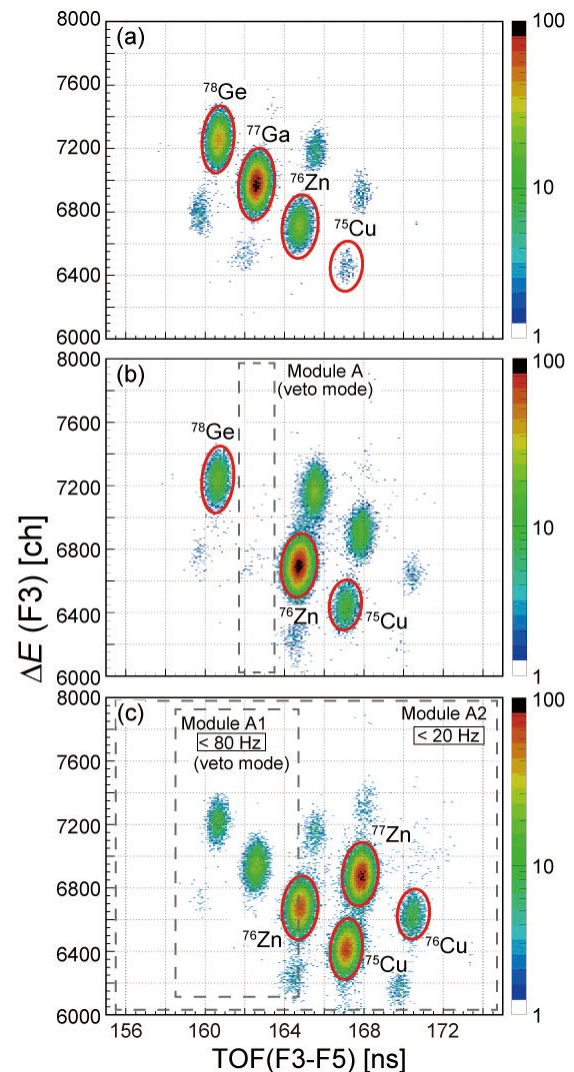


Fig. 2. (a) Typical PID plot of the secondary particles with TOF and  $\Delta E$ . (b) Ga isotope was ridded by the selection system. (c) Typical example of abundance control. Broken-lines show the time window and frequency of the output rate set by each module A.

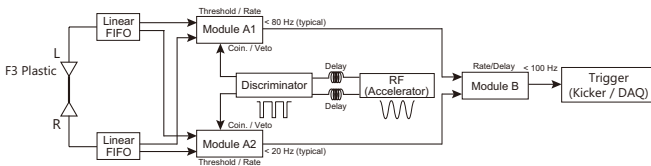


Fig. 1. Conceptual circuit diagram for particle selection and abundance tuning. Frequency of the output signal is adjustable.

<sup>\*1</sup> RIKEN Nishina Center

### References

- 1) Y. Abe *et al.*, RIKEN Accel. Prog. Rep. **50**, 186 (2017).
- 2) A. Ozawa *et al.*, in this report.
- 3) S. Naimi *et al.*, in this report.

# Aberration correction study for high-resolution optics of BigRIPS using sextupole magnets

T. Nishi,<sup>\*1</sup> D. S. Ahn,<sup>\*1</sup> N. Fukuda,<sup>\*1</sup> N. Fukunishi,<sup>\*1</sup> H. Geissel,<sup>\*1,\*2</sup> N. Inabe,<sup>\*1</sup> K. Itahashi,<sup>\*1</sup> K. Kusaka,<sup>\*1</sup> S. Y. Matsumoto,<sup>\*1,\*3</sup> Y. Shimizu,<sup>\*1</sup> T. Sumikama,<sup>\*1</sup> H. Suzuki,<sup>\*1</sup> M. Takaki,<sup>\*4</sup> H. Takeda,<sup>\*1</sup> Y. K. Tanaka,<sup>\*1,\*2</sup> T. Uesaka,<sup>\*1</sup> Y. Yanagisawa,<sup>\*1</sup> and K. Yoshida<sup>\*1</sup>

We performed a test experiment in May 2018 to develop new optics of BigRIPS with higher order aberrations diminished by sextupole magnets. The optics is designed for spectroscopy of deeply bound pionic atoms<sup>1)</sup> and search for double Gamow-Teller giant resonance.<sup>2)</sup> Until now, we have achieved double the resolving power with the new optics compared to a standard design; however higher order aberrations remain. For example, the correlation between the horizontal position and the angle at F5 strongly depends on momentum, which is referred to as  $(x|a\delta)$ . In other words, the focal plane at F5 is inclined at  $87^\circ$  (almost parallel to the beam axis). This causes position-dependent deterioration of the resolution coupled with multiple scattering. To improve this condition, we developed a new optics using sextupoles.

Taking advantage of the mirror-symmetrical configuration of the magnets in BigRIPS, we designed a new optical setting as shown in Fig. 1. Trajectories in several corresponding sections, namely between F0-F1 and F1-F2, and between F3-F5 and F5-F7, are designed to be symmetric at the first order. The field strengths of the sextupoles are also constrained to have (anti) symmetry in the same sections based on the sextupole coupling coefficients.<sup>3)</sup> Through these constraints, many aberrations will be canceled out, and others are expected to have simple responses to the field strengths of the sextupoles.

In the test experiment, we systematically varied the field strengths of the sextupoles and measured the aberrations. We utilized fragments of  $^{12}\text{C}$  produced by a primary  $^{18}\text{O}$  beam of 230 MeV/nucleon and a 30 mm thick Be target. The  $^{12}\text{C}$  distributions in terms of angle and momentum are large enough to have a nearly flat distribution in the acceptance of BigRIPS. We detected  $^{12}\text{C}$  by PPACs at F3, F5, and F7 and a plastic scintillator at F7. Aberration coefficients such as  $(x|a^2)$  or  $(x|a\delta)$  were evaluated at F3 and F5. During the measurement, we applied very narrow momentum gates of 0.1%, which were set by time of flights between F0 and F7 using the RF and F7 scintillator signals.

As a result, we found clear dependence of aberration coefficients on the sextupole settings as expected; further, we optimized the settings to suppress the aberrations. Figure 2 shows correlation between position and angle in the horizontal direction at F5, where our main detectors will be installed, with the sextupoles all off

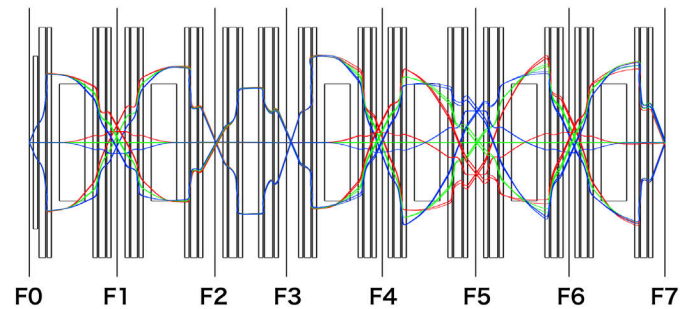


Fig. 1. Calculated horizontal trajectories based on third-order matrix elements by simulation code. Blue, green, and yellow correspond to +1.0%, 0.0% and -1.0% of deviations, respectively. The sextupole magnets are also taken into account in the calculation.

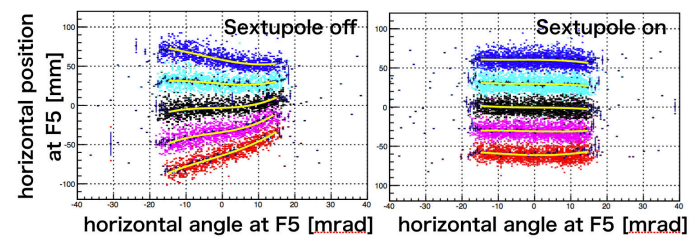


Fig. 2. Position and angle correlation at F5 focal plane. Blue, sky blue, black, pink, and red correspond to the deviations of +1.0%, +0.5%, 0.0%, -0.5%, and -1.0%, respectively. (Left) All of the sextupole magnets are off. (Right) All of the sextupole magnets are optimized.

(left) and all on after optimization (right). The different colors represent different momenta. The left panel indicates a clear third order angular dependence, which also depends on the momentum. In the right panel, all angular dependencies almost disappear.

In conclusion, we successfully controlled the aberrations using the sextupoles by maintaining strict conditions of symmetry. After optimization, dominant aberrations were clearly corrected. This study is a part of our work to develop a dispersion-matched optical system of SRC - BigRIPS. We performed another test experiment to study the optical properties between SRC and F0 in June 2018 as found in Ref. 4).

## References

- 1) K. Itahashi *et al.*, RIBF Proposal **135**, (2015).
- 2) T. Uesaka *et al.*, RIBF Proposal **141**, (2015).
- 3) K. L. Brown, SLAC Report No. **91**, (1970).
- 4) S. Y. Matsumoto *et al.*, in this report.

\*1 RIKEN Nishina Center

\*2 GSI Helmholtzzentrum für Schwerionenforschung GmbH

\*3 Department of physics, Kyoto University

\*4 CNS, University of Tokyo

## In-gas-jet laser ionization spectroscopy at KISS

Y. Hirayama,<sup>\*1</sup> Y. X. Watanabe,<sup>\*1</sup> P. Schury,<sup>\*1</sup> M. Mukai,<sup>\*2</sup> H. Choi,<sup>\*3</sup> M. Ahmed,<sup>\*1,\*2</sup> Y. Kakiguchi,<sup>\*1</sup>  
M. Oyaizu,<sup>\*1</sup> M. Wada,<sup>\*1</sup> and H. Miyatake<sup>\*1</sup>

We developed the KEK Isotope Separation System (KISS)<sup>1</sup> to study the nuclear properties of neutron-rich isotopes with neutron numbers around  $N = 126$ . To study the nuclear structures at KISS, we measured the hyperfine structure (HFS) of  $^{199}\text{Pt}$  and  $^{196, 197, 198}\text{Ir}$  to determine the magnetic dipole moment and the change in charge radius using the in-gas-cell laser ionization spectroscopy technique.<sup>2)</sup>

The present resolution of  $\Gamma = 12$  GHz (FWHM) in the HFS spectra measured by the in-gas-cell laser ionization technique was governed by pressure broadening (typically  $\Gamma_p = 10$  GHz in FWHM), Doppler broadening ( $\Gamma_D = 1.1$  GHz), and laser bandwidth ( $\Gamma_L = 3.4$  GHz). To improve the resolution, the in-gas-jet (collinear) laser ionization technique was successfully established by the KU Leuven group<sup>3)</sup> to obtain precise laser spectroscopy. In the case of in-gas-jet laser ionization technique,  $\Gamma_p$  and  $\Gamma_D$  were drastically reduced to 0.05 and 0.3 GHz owing to the spectroscopy in low-pressure and low-temperature gas jet, respectively.  $\Gamma_L$  can be improved to be 0.1 GHz by applying a narrow-band laser system. Finally, the evaluated resolution will be  $\Gamma = 0.35$  GHz in FWHM.

To determine the electromagnetic moments and isotope shifts with higher precision, we have been developing an in-gas-jet laser ionization spectroscopy technique at KISS. We developed and installed a Laval nozzle to obtain a gas jet with uniform velocity distribution,<sup>3)</sup> S-shaped pseudo-radio frequency quadrupole (S-RFQ) for the production and transportation of laser-induced singly charged ions by collinear laser spectroscopy, and a new narrow-band laser system. The designed Mach number of the Laval nozzle is 6.3, and the expected diameter and velocity of the gas jet are approximately 4 mm and 538 m/s, respectively. The laser system consists of a pumping laser of Nd:YAG (EdgeWave, 355 nm, 60 W), narrow-band seed laser (TOPTICA, DLC DL Pro HP), and dye-amplifier (Sirah).

Figure 1 shows the HFS spectra of  $^{198}\text{Pt}$  ( $I^\pi = 0^+$ ) and  $^{194}\text{Pt}$  ( $I^\pi = 0^+$ ) measured using the in-gas-cell and in-gas-jet laser ionization techniques, respectively. No HFS was observed due to  $I^\pi = 0^+$  of both isotopes. Therefore, the widths measured by both techniques are the intrinsic resolutions of the techniques. The widths obtained using the in-gas-cell and in-gas-jet laser ionization techniques were 12.5(5) and 0.6(1) GHz in

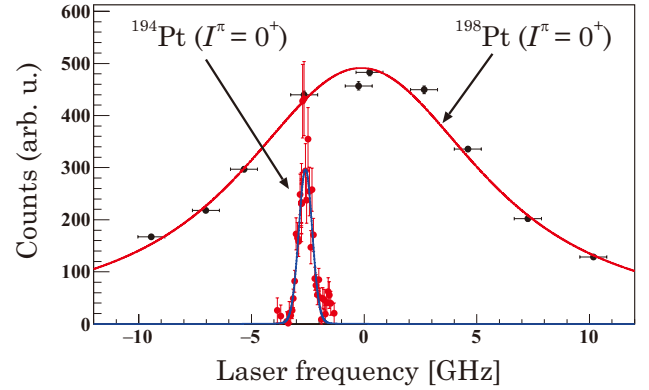


Fig. 1. HFS spectra of  $^{198}\text{Pt}$  ( $I^\pi = 0^+$ ) and  $^{194}\text{Pt}$  ( $I^\pi = 0^+$ ) measured using the in-gas-cell and in-gas-jet laser ionization techniques, respectively, under the gas cell pressure of 80 kPa (background gas-pressure 50 Pa). For the in-gas-cell laser ionization spectroscopy, the ionization scheme in Ref. 2) was used. We used the combination of  $\lambda_1 = 225.000$  nm and  $\lambda_2 = 355$  nm for the in-gas-jet laser ionization spectroscopy. Horizontal axis shows the deviation from each  $\lambda_1$  of the applied ionization schemes. Horizontal uncertainties stemmed from wavemeters were 0.6 and 0.06 GHz for the in-gas-cell and jet spectroscopy, respectively.

FWHM, respectively. Thus, we significantly improved the resonance width by applying the in-gas-jet laser ionization technique. The gas-jet velocity was deduced to be 537(5) m/s from the Doppler shift of the HFS spectra of  $^{194}\text{Pt}$  measured by the in-gas-jet collinear. The gas-jet velocity was significantly consistent with the designed value of 538 m/s. From the measurements, we confirmed that the experimental equipment used in this study was successful.

However present width of 0.6 GHz is broader than our expected width of 0.35 GHz owing to the Doppler broadening effect. To achieve the expected width, we will optimize the background gas-pressure to create a gas jet with uniform velocity distribution.<sup>3)</sup> Despite the present width of 0.6 GHz, we could measure the electromagnetic moments and isotope shift more precisely. The feasibility study by simulating the  $^{199}\text{Pt}$  HFS spectra was performed and reported in this progress report by H. Choi.<sup>4)</sup>

### References

- 1) Y. Hirayama *et al.*, Nucl. Instrum. Methods Phys. Res. B **412**, 11 (2017).
- 2) Y. Hirayama *et al.*, Phys. Rev. C **96**, 014307 (2017).
- 3) Y. Kudryavtsev *et al.*, Nucl. Instrum. Methods Phys. Res. B **297**, 7 (2013).
- 4) H. Choi *et al.*, in this progress report.

<sup>\*1</sup> Wako Nuclear Science Center (WNSC), Institute of Particle and Nuclear Studies (IPNS), High Energy Accelerator Research Organization (KEK)

<sup>\*2</sup> Department of Physics, University of Tsukuba

<sup>\*3</sup> Seoul National University

## Microgram-order palladium isotope separation by odd-mass-selective photoionization

T. Sonoda,<sup>\*1</sup> T. Kobayashi,<sup>\*2</sup> T. Fujiwara,<sup>\*2</sup> Y. Nagata,<sup>\*2</sup> H. Ishiyama,<sup>\*1</sup> V. Sonnenschein,<sup>\*3</sup> M. Oohashi,<sup>\*3</sup> A. Takamine,<sup>\*1</sup> M. Rosenbusch,<sup>\*1</sup> I. Katayama,<sup>\*1</sup> H. Tomita,<sup>\*3</sup> T. M. Kojima,<sup>\*1</sup> P. Schury,<sup>\*4</sup> and K. Midorikawa<sup>\*2</sup>

High-level radioactive wastes generated from nuclear power plants contain small percentages of platinum group metals such as palladium, rhodium, zirconium, and plutonium, which are valuable resources for industrial applications. A novel research project has been started by the Impulsing Paradigm Change through Disruptive Technologies Program (ImPACT, Project manager: R. Fujita), which includes (1) the separation of those valuable metals from fission waste, (2) the separation of long-lived and short-lived nuclei, and (3) the nuclear mutation from long-lived to short-lived nuclei. One of the key techniques in (2) was successfully advanced in the method using odd-mass-selective laser excitation.<sup>1)</sup> The separation of even- and odd-mass-number isotopes of Pd using orthogonally polarized lasers was demonstrated with ionization that was 10,000 times more efficient<sup>1)</sup> than the scheme used so far. From a practical perspective, the yields on the separation of even- and odd-mass-number isotopes must be comparable to Avogadro's number of atoms for a large amount of nuclear waste.

We demonstrated stable Pd isotope separation on a microgram order by photoionization using a high-power, high repetition rate pulsed laser system.<sup>2)</sup> The experimental apparatus is shown in Fig. 1. The Pd vapor was produced by an electron beam that irradiated Pd samples in a crucible. Two linearly polarized beams with parallel polarization were applied for the selectively resonant ionization of odd-mass Pd isotopes among stable six isotopes ( $^{102}, ^{104}, ^{105}, ^{106}, ^{108}, ^{110}\text{Pd}$ ). We succeeded in the dominant photoionization of the  $^{105}\text{Pd}$ .

Two Frequency doubled Nd:YAG InnOSlab lasers (EdgeWave) individually pumped two dye lasers having a pulse width of 10 ns and repetition rate of 10 kHz.

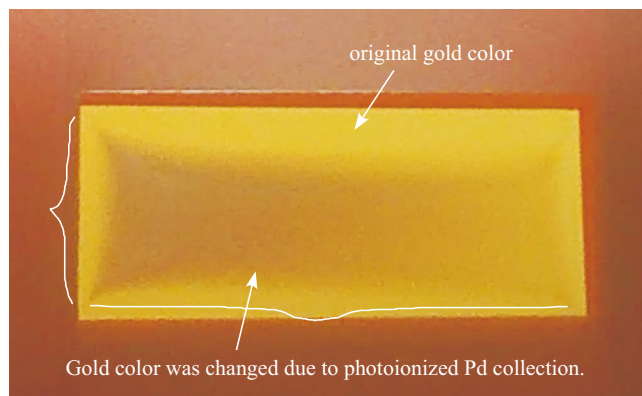
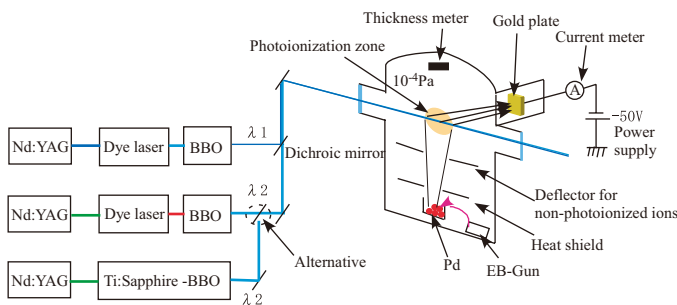


Fig. 2. The gold plate implanted by selectively ionized  $^{105}\text{Pd}$  (total deposition time is 3 h 23 min).

Also, there is an intra-cavity SHG in a Ti:Sapphire laser system pumped by Nd:YAG, whose repetition rate and pulse width are 10 kHz and 35 ns, respectively. The first excitation wavelength ( $\lambda_1$ ) of 244.9 nm was produced by the first dye laser after frequency doubling in a BBO crystal, which excites Pd atoms into the  $4d^9(^2D_{3/2})5p[1/2]$  state. The typical power of  $\lambda_1$  was 100 mW. The second dye laser or Ti:Sa laser produces the second excitation wavelength ( $\lambda_2$ ) of 361.023 nm via frequency doubling in a BBO crystal placed at the external (dye) and internal (Ti:Sa) cavity configuration. The  $\lambda_2$  excites Pd atoms to the Rydberg autoionizing state  $4d^9(^2D_{3/2})9d[3/2]$ . We used dye or Ti:Sa, depending on the situation. The typical power of  $\lambda_2$  in the case of Ti:Sa was 2 W, while that in the case of dye was 1.5 W. Photoionized  $^{105}\text{Pd}$  ions were collected on the gold plate on which a collection voltage of  $-50$  V was applied. The distance between the gold plate and the ionization area was about 5 cm. We confirmed the yields of Pd ions and identified the Pd element from the off/on resonant frequency by monitoring with a current meter. The typical current level attributed to the photoionized Pd was  $10 \mu\text{A}$ .

Figure 2 shows the gold plate after collecting photoionized  $^{105}\text{Pd}$  ions for 3 h and 23 min. From the value of the total deposition current, we deduce the total number of  $^{105}\text{Pd}$  to be  $3.0 \times 10^{17}$ , which corresponds to a weight of  $50 \mu\text{g}$ . For the first time, we confirmed Pd isotope separation in microgram orders by using odd-mass-selective laser excitation.

### References

- 1) C. Locke *et al.*, Appl. Phys. B **123**, 240 (2017).
- 2) T. Sonoda *et al.*, Nucl. Instrum. Methods Phys. Res. A **877**, 118 (2018).

\*1 RIKEN Nishina Center

\*2 RIKEN Center for Advanced Photonics

\*3 Faculty of Engineering, Nagoya University

\*4 High Energy Accelerator Research Organization (KEK)

## Introducing silver atoms into superfluid helium for precision laser spectroscopy

W. Kobayashi,<sup>\*1,\*2</sup> K. Imamura,<sup>\*1,\*3</sup> M. Sanjo,<sup>\*1,\*2</sup> T. Fujita,<sup>\*1,\*4</sup> A. Takamine,<sup>\*1</sup> T. Furukawa,<sup>\*5</sup> H. Ueno,<sup>\*1</sup> and Y. Matsuo<sup>\*1,\*2</sup>

In the Optical Radioisotope atom Observation in Condensed Helium as Ion-catcher (OROCHI), the short-lived and low-yield radioisotope (RI) atoms generated as high-energetic ion beams at accelerator facilities are stopped in a very narrow region in superfluid helium (He II) owing to the high density of He II. Laser-RF and laser-microwave (MW) double resonance spectroscopy for the atoms enable the determination of the nuclear spin and electromagnetic moment, respectively, through the measurements of Zeeman splitting and hyperfine splitting (HFS). Even without the high energy ion beams, by using the laser ablation technique, we can supply stable isotope atoms into He II. We have successfully measured HFSs of alkali atoms, <sup>85, 87</sup>Rb and <sup>133</sup>Cs in He II.<sup>1,2)</sup> Consequently, we found that the HFSs differ from the ones in vacuum by a little less than 1% and the achieved precision was sufficient even for the study of hyperfine anomalies. Currently, we are attempting to apply this method to group 11 atoms to verify whether a similar difference appears in atoms other than alkali metal elements. The HFS of the stable isotope <sup>197</sup>Au atom in He II was measured using this technique.<sup>3)</sup> To discuss the differential hyperfine anomalies between isotopes, it is necessary to measure the HFSs of at least two isotopes. Silver is a good candidate with two stable isotopes, <sup>107</sup>Ag and <sup>109</sup>Ag, whose natural abundance ratio is almost 1:1. Previously, however, we faced difficulties in the preparation of Ag atoms in He II.<sup>4)</sup> In this report, we describe how we solved this problem.

In offline experiments, atoms are introduced into He II by laser ablation and laser dissociation. As the first step, a metal sample placed above He II surface is ablated by a second-harmonic pulse of a Nd:YAG laser in the same manner as Ref. 4). Only Ag clusters, among the particles generated by the ablation, can be immersed into He II because the energy barrier for a thermalized atom is too high to penetrate the surface of liquid helium. Next, the clusters are required to be dissociated by a dissociation laser to produce atoms for the application of our spectroscopic technique. If dissociation occurs, highly excited atoms are generated and the plasma emission from those atoms should be observed. When we used a femtosecond Ti:Sa laser for Ag atoms, however, even plasma emission was not observed, as reported in Ref. 4).

It has been reported that Ag clusters in superfluid

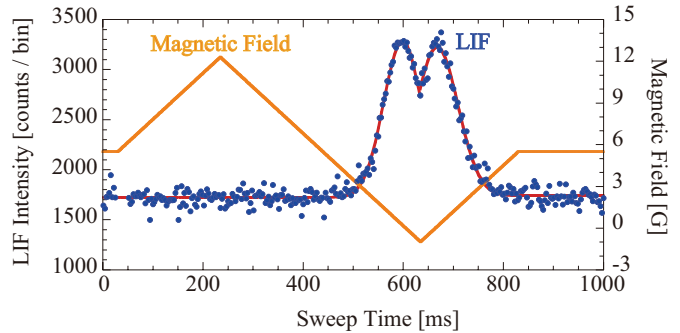


Fig. 1. Variation of LIF intensity with sweeping a magnetic field.

helium droplets have an absorption at the around 330–360 nm instead of 800 nm.<sup>5)</sup> Considering this characteristic of Ag clusters, we used the third-harmonic pulse of Nd:YAG laser (wavelength: 355 nm, repetition rate: 20 Hz, pulse width: 5 ns, pulse energy: 8 mJ) for the dissociation. Consequently, plasma emission was observed. From this result, it was revealed that laser wavelength selection is crucial for the dissociation of Ag clusters, which was not the case for Rb, Cs, and Au clusters.

Next, we generated spin polarization by an optical pumping method. The Ag atoms in He II were optically pumped and polarized by irradiation with a circularly polarized pumping laser, which was the fourth-harmonic pulse of a neodymium-doped yttrium vanadium oxide (Nd:YVO<sub>4</sub>) laser (wavelength: 335.5 nm, repetition rate: 20 kHz, pulse width: ~25 ns, pulse energy ~1.5 μJ). When optical pumping is achieved, the intensity of laser-induced fluorescence (LIF) due to the pumping laser is decreased because we optically pumped the atoms into a dark state. Spin polarization was confirmed by the observation of the variation in LIF intensity while sweeping a magnetic field (0–12 G). Figure 1 shows the decrease in LIF intensity when a sufficient magnetic field was applied. We preliminarily confirmed from this spectrum that we achieved a spin polarization of 50%. This result also leads to the conclusion that we successfully introduced Ag atoms into He II and observed LIF. The HFS measurement for Ag atoms in He II is in progress.

### References

- 1) T. Furukawa, Doctoral thesis, Osaka University (2007).
- 2) K. Imamura *et al.*, *Hyperfine Interact.* **230**, 73 (2014).
- 3) T. Fujita *et al.*, *RIKEN Accel. Prog. Rep.* **47**, 212 (2014).
- 4) T. Fujita *et al.*, *RIKEN Accel. Prog. Rep.* **50**, 196 (2017).
- 5) E. Loginov *et al.*, *Phys. Rev. Lett.* **106**, 233401 (2011).

\*1 RIKEN Nishina Center

\*2 Department of Advanced Sciences, Hosei University

\*3 Department of Physics, Okayama University RIIS

\*4 Department of Physics, Osaka University

\*5 Department of Physics, Toho University

## Magnetic properties of Alkali-metal Superoxide, NaO<sub>2</sub>

F. Astuti,<sup>\*1,\*2</sup> M. Miyajima,<sup>\*3</sup> T. Kambe,<sup>\*3</sup> T. Nakano,<sup>\*4</sup> and I. Watanabe<sup>\*1,\*2</sup>

Magnetism in the p-electron system has attracted attention for the possibility of new types of magnetic informative materials. Alkali-metal superoxides, AO<sub>2</sub> (A = Na, K, Rb, Cs), present an interesting example of magnetic materials on the basis of unpaired p-electrons. The magnetic ordering of KO<sub>2</sub>, RbO<sub>2</sub>, and CsO<sub>2</sub> have been observed at temperatures 7 K, 15 K, and 9.6 K, respectively using specific heat.<sup>1)</sup> However, the magnetic ground state in NaO<sub>2</sub> is not yet clarified.

Clear anomalies from the measurement of magnetic susceptibility were observed at a temperature between 230 and 200 K in NaO<sub>2</sub>. These anomalies were consistent with the expected structural phase transition, as discussed in the previous study.<sup>1)</sup> The magnetic susceptibility,  $\chi$ , drops sharply below 40 K, as shown in Fig. 2 (a). We checked that the sample quality was good and the anomalies in magnetic susceptibility could be reproduced in all NaO<sub>2</sub> sample batches (see sample condition in Fig. 1). The sudden change of susceptibility value toward zero is an indication of spin gap state as observed in other spin gap systems, NaTiSi<sub>2</sub>O<sub>6</sub> and TiOCl.<sup>2,3)</sup> Mahanti *et al.* reported that NaO<sub>2</sub> has some similarities with one-dimensional spin system.<sup>4)</sup>

There was no emergence of muon-spin precession from the previous zero-field (ZF)  $\mu$ SR experiment in NaO<sub>2</sub> down to 0.3 K measured at the RIKEN-RAL Muon Facility and DOLLY PSI, which indicated the absence of magnetic ordering. To further study the magnetic properties in NaO<sub>2</sub>, we measured the depolarization rate in ZF close to anomaly  $\sim$  40 K (observed by magnetic susceptibility) using CHRONUS spectrometer at the RIKEN-RAL Muon Facility.

The temperature dependence of exponential relaxation rate,  $\lambda$ , measured using ZF- $\mu$ SR showed an anomaly at a temperature below 40 K that was significantly consistent with the anomaly observed by magnetic susceptibility measurement, as shown in Fig. 2 (a). This indicated the possibility of magnetic transition around this temperature.<sup>5)</sup> The red line in Fig. 2 (b) is the fitting line that utilizes the following function:  $\lambda(T) = \lambda_0/[1 + A \exp(-\frac{2\Delta}{T})]$ , in which A is the constant and  $\Delta$  is the spin-gap value.<sup>6)</sup> The obtained result of  $\Delta$  is estimated to be  $\sim$  35 K. The possibility of the formation of spin gap in NaO<sub>2</sub> must be further explored using other experimental techniques.



Fig. 1. Some sample batches of NaO<sub>2</sub> used for  $\mu$ SR experiment. Labels indicate the number of sample batches. Bright and dense yellow color imply that sample quality is good.

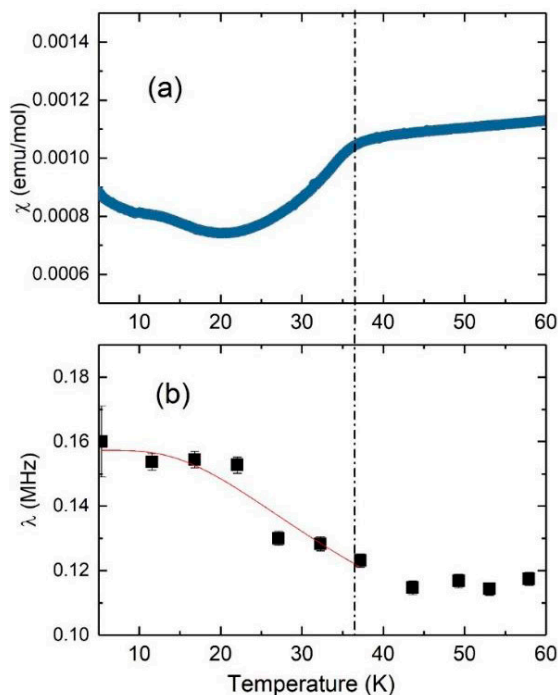


Fig. 2. (a) Magnetic susceptibility of NaO<sub>2</sub> and (b) Temperature dependence of exponential relaxation rate,  $\lambda$ , measured using ZF- $\mu$ SR at various temperature above and below 40 K.

### References

- 1) A. Zumsteg *et al.*, Phys. Cond. Matter **17**, 267–291 (1974).
- 2) M. Isobe *et al.*, J. Phys. Soc. Jpn, **71**, 1423 (2002).
- 3) A. Seidel *et al.*, Phys. Rev. B **67**, 020405(R) (2002).
- 4) S. D. Mahanti *et al.*, Solid State Commun. **18**, 159–162 (1976).
- 5) S. J. Blundell *et al.*, J. Phys. Condens. Matt. **9**, 119 (1997).
- 6) P. J. Baker *et al.*, Phys. Rev. B **75**, 094404 (2007).

<sup>\*1</sup> Department of Condensed Matter Physics, Hokkaido University

<sup>\*2</sup> RIKEN Nishina Center

<sup>\*3</sup> Department of Physics, Okayama University

<sup>\*4</sup> Graduate School of Science and Engineering, Ibaraki University

# Mass spectrometric speciation of mononuclear Re carbonyls in the gas phase

Y. Wang,<sup>\*1,\*2</sup> Y. Wittwer,<sup>\*3,\*4</sup> J. Zhang,<sup>\*2</sup> J. Yang,<sup>\*2</sup> H. Haba,<sup>\*1</sup> Y. Komori,<sup>\*1</sup> T. Yokokita,<sup>\*1</sup> S. Cao,<sup>\*2</sup> F. Fan,<sup>\*2</sup> R. Eichler,<sup>\*3,\*4</sup> A. Türler,<sup>\*4</sup> and Z. Qin<sup>\*2</sup>

For the chemical characterization of bohrium carbonyls,  $\text{Bh}(\text{CO})_n$ , a gas-phase chemical study of rhenium (Re) carbonyls was conducted at RIBF, RIKEN.<sup>1)</sup> However, the experiments provided low chemical yields, making it necessary to further study the formation of mononuclear Re carbonyls. In this study, a laser-ablation time-of-flight mass-spectrometer (LA-TOF-MS) was modified to obtain the mass spectra of mononuclear Re carbonyl ions. High-purity CO and He gas mixtures were used to deduce the most stable species. Moreover, the influence of impurities on the formation of the carbonyls was also investigated by adding  $\text{O}_2$  and  $\text{H}_2$  to the gas mixture, because both were expected to have a significant influence on Re.<sup>2)</sup>

Figure 1 shows the schematic of our LA-TOF-MS setup. Each measurement starts with the pulse valve opening (120  $\mu\text{s}$ ), thereby releasing a supersonic gas jet. The gas is directed over the target surface, where an ablation laser (Nd: YAG laser, 532 nm, 10 Hz, 15 mJ/pulse) induces a plasma to generate free metal atoms and ions. Some of the plasma is rapidly cooled by the gas. Then it is transported through a skimmer to a positive electric field, where a short pulsed high voltage is applied (20  $\mu\text{s}$ , 10 Hz, +1400 V). After free drifting, the cations reach a micro-channel plate (MCP) detector and the flight time is measured. An extension pipe (*i.d.* = 4 mm; length = 60 mm) is added downstream of the metal target in to increase the reaction time and strengthen the interaction between Re ions and CO gas. This was done to identify the most stable products formed in the gas phases, which are similar to those of our gas chromatography experiment.<sup>1,3)</sup>

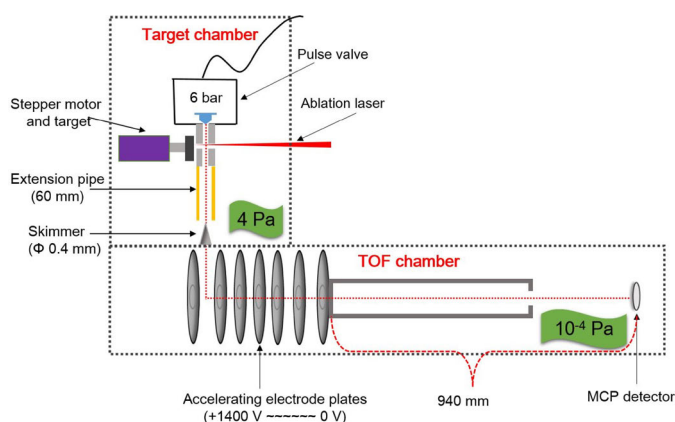


Fig. 1. Schematic of the LA-TOF-MS technique.

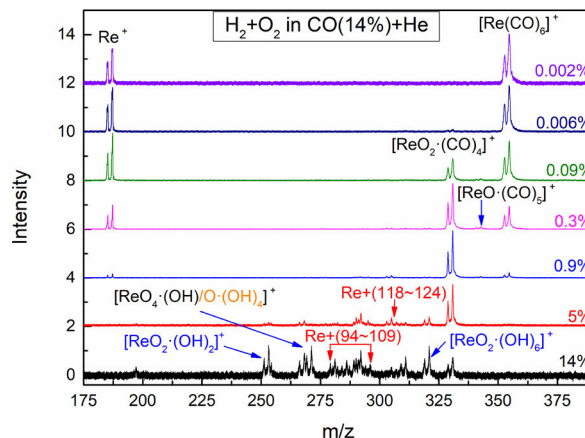


Fig. 2. Mass spectra with a Re target using  $\text{H}_2$  and  $\text{O}_2$  in CO and He gas mixture ( $C_{\text{CO}}$  is 14%, while both  $C_{\text{H}_2}$  and  $C_{\text{O}_2}$  vary from 14% to 0.002% in the same steps).

Because the ion mass is proportional to the square-root of its flight time, the mass number of each cation can be determined, and then the chemical formula can be deduced. Using He seeded by CO ( $C_{\text{CO}} = 14\%$ ) as the carrier gas,  $\text{Re}^+$  and  $[\text{Re}(\text{CO})_6]^+$  ions can be clearly identified in the mass spectrum. No intermediates or other products can be observed owing to the added extension pipe. Then,  $\text{H}_2$ ,  $\text{O}_2$ , and  $\text{H}_2/\text{O}_2$  gas mixtures are added to the carrier gas as impurities. Only few  $[\text{Re}(\text{CO})_5 \cdot (\text{H}_2)]^+$  can be observed when 14% of  $\text{H}_2$  is added to the carrier gas. No other Re carbonyl hydrides appear when  $C_{\text{H}_2}$  is lower than 5%, while large amount of  $[\text{ReO}_2 \cdot (\text{CO})_4]^+$  can be observed when  $\text{O}_2$  is added to the carrier gas. Therefore,  $\text{H}_2$  does not have a significant influence on the formation of  $[\text{Re}(\text{CO})_n]^+$ . The mass spectra of  $\text{O}_2$  gas mixtures are very similar to Fig. 2. Figure 2 shows the mass spectra of adding  $\text{H}_2$  and  $\text{O}_2$  to the CO and He carrier gas ( $C_{\text{CO}}$  was fixed at 14%;  $C_{\text{H}_2}$  and  $C_{\text{O}_2}$  varied from 14% to 0.002% in the same steps). Despite the small quantities of hydroxides visible in both figures, the only significant reaction products are  $[\text{ReO}_2 \cdot (\text{CO})_4]^+$  and  $[\text{Re}(\text{CO})_6]^+$ .  $[\text{ReO}_2 \cdot (\text{CO})_4]^+$  disappears completely when  $C_{\text{O}_2}$  is 0.002%. Therefore, we conclude that the formation of Re carbonyl ions is not sensitive to trace amounts of  $\text{H}_2$ , while even 0.09% of  $\text{O}_2$  will significantly increase the product yield of Re carbonyl oxide ions and decrease the product yield of Re carbonyl ions.

## References

- 1) Y. Wang *et al.*, RIKEN Accel. Prog. Rep. **50**, 25 (2017).
- 2) Y. Wang *et al.*, Phys. Chem. Chem. Phys. **17**, 13228 (2015).
- 3) Y. Wang *et al.*, Phys. Chem. Chem. Phys. **21**, 7147 (2019).

\*1 RIKEN Nishina Center

\*2 Institute of Modern Physics, Chinese Academy of Sciences

\*3 Laboratory of Radiochemistry, Paul Scherrer Institute

\*4 Department of Chemistry and Biochemistry, University of Bern

# Practical synthesis of $^{211}\text{At}$ -labeled immunoconjugate by double click method for $\alpha$ -emission cancer radiotherapeutics<sup>†</sup>

K. Fujiki,<sup>\*1,\*2</sup> Y. Kanayama,<sup>\*3</sup> S. Yano,<sup>\*4</sup> N. Sato,<sup>\*4</sup> T. Yokokita,<sup>\*4</sup> P. Ahmadi,<sup>\*1,\*2</sup> Y. Watanabe,<sup>\*3</sup> H. Haba,<sup>\*4</sup> and K. Tanaka<sup>\*1,\*2,\*5</sup>

In this paper, a facile synthesis of an  $^{211}\text{At}$ -labeled immunoconjugate that is used as an  $\alpha$ -emission molecular targeting therapy is described. We synthesized a tetrazine probe modified with closo-decaborate(2-), which is a prosthetic group that forms a bioavailable stable complex with  $^{211}\text{At}$ . Our one-pot three-component double-click labeling method,<sup>1)</sup> which consists of RIKEN click<sup>2-4)</sup> and tetrazine ligation,<sup>5)</sup> was utilized to introduce the decaborate to HSA (human serum albumin) or trastuzumab (anti-HER2 antibody) using decaborate-tetrazine **1** and TCO (*trans*-cyclooctene)-aldehyde **2** without reducing the antibody binding affinity, as shown in Fig. 1. The average number of molecules attached to HSA was determined as 2 decaborate moieties (a **1** + **2** molecule underwent a 1,065 MW increase) by the MALDI-TOF mass spectroscopic analysis in comparison to the intact HSA molecular weight.

Next, the astatination of decaborate-trastuzumab was conducted by treating solutions of decaborate-trastuzumab with  $\text{Na}[^{211}\text{At}]$  in the presence of chloramine T as an oxidant over 5 min at room temperature. As shown in Fig. 2, the labeling was performed using 1  $\mu\text{M}$  decaborate-trastuzumab in 0.05% PBS-T and  $\text{Na}[^{211}\text{At}]$ , 75 MBq, in PBS to furnish  $^{211}\text{At}$ -labeled trastuzumab with a specific activity of 1.7 MBq/ $\mu\text{g}$  in 49% RCY. The potential loss of antigen recognition activity in the  $^{211}\text{At}$ -labeled trastuzumab with a high specific activity was assessed by measuring the dissociation

constant  $K_d$  of the obtained  $^{211}\text{At}$ -labeled trastuzumab. This value was found to be 1.0 nM, indicating no impairment to the affinity. Reacting 0.1  $\mu\text{M}$  decaborate-trastuzumab with  $\text{Na}[^{211}\text{At}]$ , 104 MBq, in PBS provided  $^{211}\text{At}$ -labeled trastuzumab in 30% RCY with a very high specific activity of 15 MBq/ $\mu\text{g}$ .

An intratumor injection of 6.3  $\mu\text{g}$  of the  $^{211}\text{At}$ -labeled trastuzumab with 1.4 MBq in BALB/c nude mice implanted with HER2-expressing epidermoid cancer cells yielded effective suppression of tumor growth, as shown in Fig. 3. Our work provides one of the most practical  $^{211}\text{At}$ -labeling methods to develop molecular cancer radiotherapeutics.

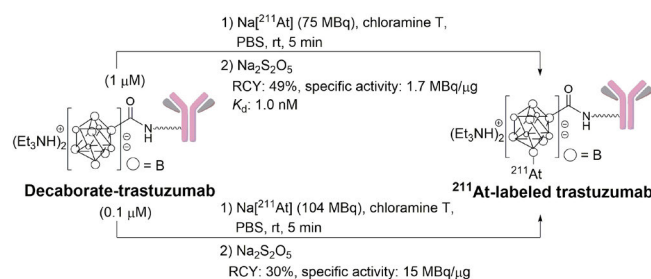


Fig. 2. Radiolabeling of decaborate-trastuzumab. RCY (Radiochemical yield) was obtained from the radioactivity of the purified radiolabeled product against the added  $\text{Na}[^{211}\text{At}]$ .

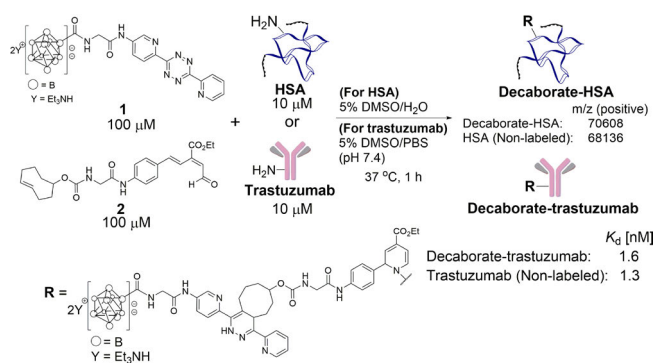


Fig. 1. Preparation of decaborate-HSA/trastuzumab via the one-pot three-component double-click labeling method. Dissociation constants ( $K_d$ ) of the decaborate-trastuzumab measured by the QCM method.

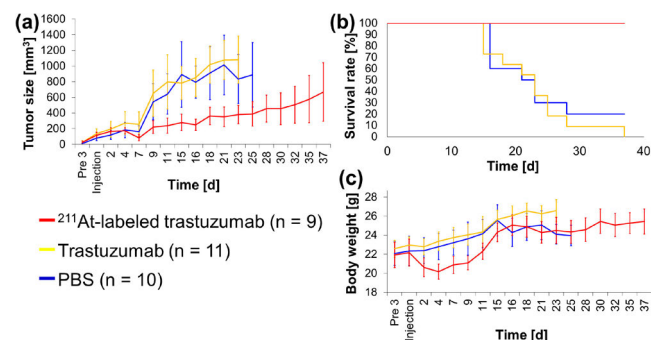


Fig. 3. Therapeutic efficacies of  $\alpha$ -emitting  $^{211}\text{At}$ -labeled trastuzumab, trastuzumab, or PBS after intratumor injection.

## References

- 1) K. Fujiki *et al.*, *Sci. Rep.* **7**, 1912 (2017).
- 2) K. Tanaka *et al.*, *Angew. Chem. Int. Ed.* **47**, 102 (2008).
- 3) K. Tanaka *et al.*, *Angew. Chem. Int. Ed.* **49**, 8195 (2010).
- 4) K. Fujiki, K. Tanaka, *e-EROS Encyclopedia of Reagents for Organic Synthesis* (Wiley, Germany, 2018), published online. DOI: 10.1002/047084289X.rm02050
- 5) M. L. Blackman, M. Royzen, J. M. Fox, *J. Am. Chem. Soc.* **130**, 13518 (2008).

<sup>†</sup> Condensed from the article in *Chem. Sci.* **10**, 1936 (2019)

<sup>\*1</sup> Biofunctional Synthetic Chemistry Laboratory, RIKEN

<sup>\*2</sup> GlycoTargeting Research Laboratory, RIKEN

<sup>\*3</sup> Laboratory for Pathophysiological and Health Science, RIKEN

<sup>\*4</sup> RIKEN Nishina Center

<sup>\*5</sup> Biofunctional Chemistry Laboratory, Kazan Federal University

# Activation cross sections of $\alpha$ -induced reactions on $^{nat}\text{Zn}$ for Ge and Ga production<sup>†</sup>

M. Aikawa,<sup>\*1,\*2</sup> M. Saito,<sup>\*3,\*2,\*4</sup> S. Ebata,<sup>\*1,\*5</sup> Y. Komori,<sup>\*2</sup> and H. Haba<sup>\*2</sup>

Gallium-68 ( $T_{1/2} = 67.71$  min) is used in positron emission tomography (PET). The production of  $^{68}\text{Ga}$  is important for its application in PET. In addition to  $^{68}\text{Ga}$ , the production of its long-lived parent,  $^{68}\text{Ge}$  ( $T_{1/2} = 270.95$  d), is worthy of investigation for a  $^{68}\text{Ga}$  generator. One of the reactions to produce  $^{68}\text{Ge}$  is the  $\alpha$ -induced reaction on  $^{nat}\text{Zn}$ . Two sets of experimental data<sup>1,2)</sup> could be found in the EXchange FORmat (EXFOR) library. The two datasets deviate from each other. Therefore, we measured the cross sections of  $\alpha$ -induced reactions on  $^{nat}\text{Zn}$  for  $^{68}\text{Ge}$  production.

The experiment was performed at the AVF cyclotron of the RIKEN RI Beam Factory using standard methods, stacked foil activation method, and off-line  $\gamma$ -ray spectrometry. Thin metallic foils of  $^{nat}\text{Zn}$  (99.9% purity, Nilaco Corp., Japan) and  $^{nat}\text{Ti}$  (99.6% purity, Nilaco Corp., Japan) were stacked as the target. The stacked target was irradiated by a 51.5 MeV  $\alpha$  beam. The incident beam energy was measured by the time-of-flight method using a plastic scintillator monitor.<sup>3)</sup> The irradiation of the  $\alpha$  beam lasted for 2 hours. The average intensity was 82.0 nA, which was measured by a Faraday cup. The decrease in the energy of projectiles in the target was estimated using the SRIM code.<sup>4)</sup>  $\gamma$  spectra from the irradiated foils were measured with a high-resolution HPGe detector.

To assess the beam parameters and target thicknesses, the cross sections of the  $^{nat}\text{Ti}(\alpha, x)^{51}\text{Cr}$  monitor reaction were derived. Consequently, we could confirm that our results were significantly consistent with the recommended values.<sup>5)</sup>

The 1077.34-keV  $\gamma$ -line ( $I_\gamma = 3.22\%$ ) from the  $^{68}\text{Ga}$  decay was measured after a long cooling time of approximately 80 days. Directly produced  $^{68}\text{Ga}$  could completely get decayed in this period and the decay of  $^{68}\text{Ga}$  was in equilibrium with that of its parent  $^{68}\text{Ge}$ . The cross sections of  $^{68}\text{Ge}$  are shown in Fig. 1 with previous experimental data<sup>1,2)</sup> and TENDL-2017 data.<sup>6)</sup> The peak position of our result is consistent with the experimental data, although the amplitude is slightly larger. The tendency of TENDL-2017 data is different from the experimental data.

The integral yield of  $^{68}\text{Ge}$  was estimated from the

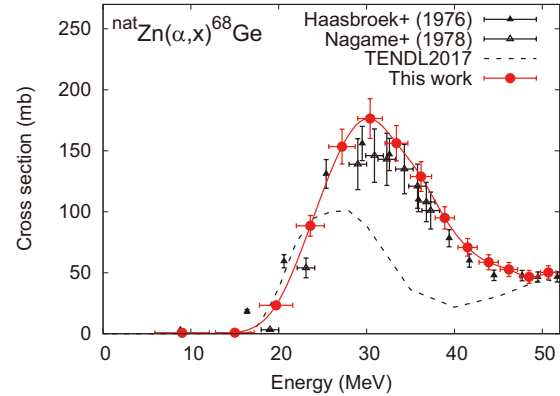


Fig. 1. Excitation function of  $^{nat}\text{Zn}(\alpha, x)^{68}\text{Ge}$  reaction.

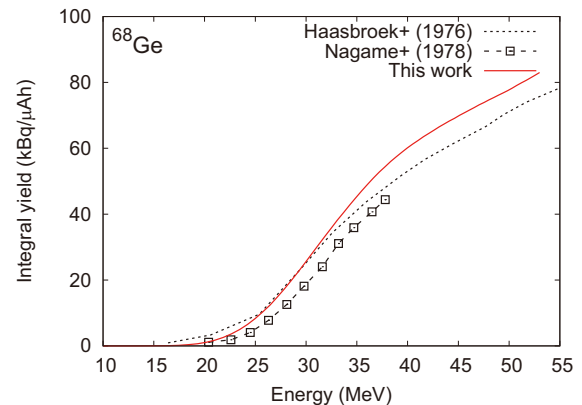


Fig. 2. Integral yield of  $^{68}\text{Ge}$ .

cross sections measured in this work and stopping powers calculated by the SRIM code.<sup>4)</sup> The derived integral yield is shown in Fig. 2 with the previously obtained experimental data.<sup>1,2)</sup> The values obtained in our result are greater than other data above 30 MeV as expected from the cross sections measured in this work.

## References

- 1) F. J. Haasbroek *et al.*, CSIR Res. Rep. FIS **91**, 1 (1976).
- 2) Y. Nagame *et al.*, Int. J. Appl. Radiat. Isot. **29**, 615 (1978).
- 3) T. Watanabe *et al.*, Proc. 5th Int. Part. Accel. Conf. (IPAC2014), 3566 (2014).
- 4) SRIM: the Stopping and Range of Ions in Matter, <http://www.srim.org/>.
- 5) A. Hermanne *et al.*, Nucl. Data Sheets **148**, 338 (2017).
- 6) A. J. Koning *et al.*, Nucl. Data Sheets **113**, 2841 (2012).

<sup>†</sup> Condensed from the article in Nucl. Instrum. Methods Phys. Res. B **427**, 91 (2018)

<sup>\*1</sup> Faculty of Science, Hokkaido University

<sup>\*2</sup> RIKEN Nishina Center

<sup>\*3</sup> Graduate School of Science, Hokkaido University

<sup>\*4</sup> Present address: Graduate School of Biomedical Science, Hokkaido University

<sup>\*5</sup> Present address: School of Environment and Society, Tokyo Institute of Technology

## A novel mutation induced by Ar-ion-irradiation affect grain length and improve yield in rice

R. Morita,<sup>\*1</sup> H. Ichida,<sup>\*1</sup> Y. Hayashi,<sup>\*1</sup> H. Abe,<sup>\*1</sup> Y. Shirakawa,<sup>\*1</sup> K. Ichinose,<sup>\*1</sup> T. Kazama,<sup>\*2</sup> K. Toriyama,<sup>\*2</sup> T. Sato,<sup>\*1,\*2</sup> and T. Abe<sup>\*1</sup>

Rice serves as an important staple food for more than half of the world's population. The size of a rice grain, which is one of the most important agronomic traits, is correlated with its yield. The grain size is a polygene-controlled quantitative trait, resulting in substantial variations in the size and shape of grains. Although several genes influencing the grain size have been cloned from rice cultivars, it is necessary to identify novel genes that determine the grain size to meet the increasing food demands of the growing world population.

To identify a novel gene that can determine the grain size, we isolated a rice mutant that exhibited a significant increase in grain weight from 159 independent M2 lines raised from Ar-ion-irradiated (5 Gy, 290 keV $\mu\text{m}^{-1}$ ) rice seeds. In the mutant, the grain length increased ( $5.46 \pm 0.01$  mm, Avr.  $\pm$  SE) in comparison with that of the wild-type (WT) Nipponbare ( $5.26 \pm 0.02$  mm, Fig. 1). Given that the grain width and thickness were not altered in the mutant, the increased grain weight was considered to be the result of the increase in grain length. We designated this mutant as *long grain1* (*lin1*).

We tested whether the yield increased in the *lin1* mutant under field conditions in 2014 and 2016 in a paddy field. Three plots of the *lin1* mutant and wild-type Nipponbare plants were formed in a paddy field. In each plot, 49 plants (7  $\times$  7 plants, 30 cm inter-plant spacing) were planted. The outermost plants were excluded from sampling to avoid the border effect. Therefore, 25 plants (5  $\times$  5 plants grown in the 1.44 m<sup>2</sup>) in the center of each plot were used to calculate the yield. The 1000-grain weight was 27.6 g and 25.9 g in 2014, and 27.1 g and 26.3 g in 2016 in the *lin1* mutant and Nipponbare, respectively (Table 1). The number of panicles, spikelets, and percentage fertility were not significantly different between the *lin1* mutant and WT in both years, suggesting that there was no tradeoff between grain length

Table 1. Agronomic traits and grain yield of WT and *lin1*.

Year	Line name	Panicle number	Spikelet number	Fertility (%)	1000-grain weight (g)	Yield (g/m <sup>2</sup> )
2014	WT	23.8	124.9	93.7	25.9	803.5
	<i>lin1</i>	24.8	120.6	94.3	27.6	869.3
2016	WT	20.8	121.0	87.0	26.3	642.3
	<i>lin1</i>	21.3	126.5	92.0	27.1	747.8

and number of panicles, number of spikelets, and percentage fertility in this mutant. Consequently, the grain yield (g/m<sup>2</sup>) was 8.2% and 16.4% higher in the *lin1* mutant compared with that of the WT in 2014 and 2016, respectively. These results demonstrated that the mutated *lin1* allele could improve the rice grain yield.

We performed the whole-genome sequencing and genetic linkage analyses to identify the yield-related gene, *LIN1*. Thus, a 1 bp deletion in the coding sequence of *Os06g0675200* gene on chromosome 6 was ascertained to be linked with the grain length. To confirm that *Os06g0675200* corresponded with the *LIN1* gene, we introduced a 1 bp insertion in the gene of Nipponbare using the CRISPR/Cas9-mediated genome editing system. As with the *lin1* mutant, the transgenic plants displayed enhanced grain length compared with that of WT, thereby indicating that the inactivation of the gene by the 1 bp insertion and subsequent frameshift reproduced the observed phenotype of the *lin1* mutant and supported the conclusion that *Os06g0675200* is the *LIN1* gene.

To investigate whether the mutant allele of *LIN1* has already been utilized in rice breeding, we conducted the sequence polymorphism analysis using the TASUKE genome browser,<sup>1)</sup> which collectively provides polymorphisms among rice cultivars. We used information from 25 varieties (15 temperate *japonica* and ten *indica*), for which the sequencing coverage of the entire coding sequence of *LIN1* was available. All temperate *japonica*- and six *indica*-varieties harbored the wild-type *LIN1* allele. In contrast, four *indica* varieties shared an identical T to C substitution, which caused a non-synonymous substitution in the amino acid sequence of *LIN1*. These results revealed that the increase in grain yield achievable by the inactivation of *LIN1* might be limited in such variants that already harbor mutant *LIN1* alleles. Thus, the *lin1* mutation reported in this study may be useful to further increase the grain yield in both temperate *japonica* and *indica* rice varieties.



Fig. 1. Seeds and brown grains of Nipponbare (a and c) and *lin1* mutant (b and d). Bar = 5 mm.

<sup>\*1</sup> RIKEN Nishina Center

<sup>\*2</sup> Graduate School of Agricultural Science, Tohoku University

### Reference

- 1) M. Kumagai *et al.*, *Bioinformatics* **29**, 1806 (2013).

## Recent progress in overcoming interspecific hybrid sterility in rice

Y. Koide,<sup>\*1</sup> K. Onishi,<sup>\*2</sup> Y. Hayashi,<sup>\*3</sup> T. Abe,<sup>\*3</sup> Y. Fukuta,<sup>\*4</sup> Y. Okumoto,<sup>\*5</sup> and A. Kanazawa<sup>\*1</sup>

Inter-specific hybridization enables breeders to transfer valuable genes from one species to another for improving crops. However, reproductive barriers, which are also known as “species barriers,” often prevent gene flow between two species. In two cultivated rice species (*Oryza sativa* and *O. glaberrima*), hybrid sterility is considered as the main reproductive barrier. To date, more than 10 loci for hybrid sterility between these species have been found.<sup>1)</sup> Among these loci, the *HYBRID STERILITY 1* ( $S_1$ ) locus on the short arm of chromosome 6 has been frequently detected,<sup>2)</sup> suggesting that the  $S_1$  locus is the major cause of the sterility barrier. Here, we review the recent progress in overcoming the hybrid sterility caused by the  $S_1$  locus and highlight the usefulness of a forward genetic screening for a mutant with a “neutral” allele of hybrid sterility loci.

In 1990, Sano<sup>3)</sup> showed that the hybrid between a strain of *O. sativa* and near-isogenic lines (NILs) containing a segment of chromosome 6 from *O. glaberrima* in the genetic background of *O. sativa* exhibited partial sterility in pollen and seeds. This phenomenon was explained by the genetic interaction between the  $S_1^g$  allele (formerly the  $S_1$  allele of Sano<sup>3)</sup>) and  $S_1^s$  allele (formerly the  $S_1^s$  allele of Sano<sup>3)</sup>), which were derived from *O. glaberrima* and *O. sativa*, respectively. The  $S_1^g$  allele acts as a “gamete eliminator,” and both male and female gametes possessing the  $S_1^s$  allele are aborted only in the heterozygote ( $S_1^g/S_1^s$ ).<sup>4)</sup> Although these studies revealed the genetic nature of the  $S_1$  locus, it was still unclear how we can overcome the sterility barrier.

Recently, significant progress has been made by artificial mutagenesis using genome editing<sup>5)</sup> or heavy-ion beam irradiation.<sup>6)</sup> Koide *et al.*<sup>6)</sup> used Acc108 (a variety of *O. sativa*) and NIL, which contain the  $S_1^g$  allele and the  $S_1^s$  allele at the  $S_1$  locus, respectively. They obtained a total of 2,478  $F_1$  seeds for heavy-ion beam irradiation via artificial pollination. From 1,817  $F_1$  hybrids ( $M_1$  generation) irradiated with carbon-ion beam (LET 30 keV/nucleonm, 150 Gy) at the RIKEN RI-beam factory, Wako, Japan, they obtained one plant that had a panicle with >50% seed fertility from the  $M_1$  population (Fig. 1). Then, they developed the  $M_2$  family through self-pollination of the  $M_1$  plant and obtained the mutant Acc108 $S_1M$ , which does not induce

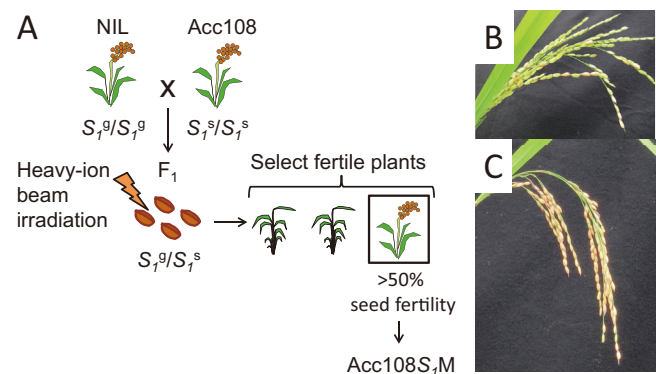


Fig. 1. Forward genetic screening for a mutant with a “neutral” allele of the hybrid sterility locus,  $S_1$ . (B) A sterile rice panicle observed in the  $M_1$  plant. The seed sterility was due to the hybrid sterility locus,  $S_1$ . (C) A fertile panicle observed in the  $M_1$  plant. Seed sterility did not occur because of a mutation induced at the  $S_1$  locus.

sterility in either the hybrid with the  $S_1^g$  carrier or that with the  $S_1^s$  carrier.

The results of the crossing experiments, genetic mapping, and nucleotide sequencing suggested that the causative mutation of Acc108 $S_1M$  was a 5-bp deletion in the peptidase-coding gene (denoted by *SSP*) in the  $S_1$  locus. These results indicated that the *SSP* was one of the essential genes for inducing hybrid sterility in heterozygotes ( $S_1^g/S_1^s$ ) and Acc108 $S_1M$  has a neutral allele “ $S_1^{mut}$ ” at the  $S_1$  locus.<sup>6)</sup>

In summary, recent studies<sup>5,6)</sup> have focused on the  $S_1$  locus and have shown how to obtain a neutral allele through reverse or forward genetic approaches. In general, the number of hybrid sterility loci that have been annotated and characterized in crop gene pools is still limited. In such a case, a forward genetic screening is more practical than approaches in which gene identification is a prerequisite, *e.g.*, genome editing, for creating neutral alleles. Although these two approaches have their own specific advantages, recent studies have demonstrated a technique that allows broader access to desirable traits in distantly related species during crop breeding.

### References

- 1) K. Doi *et al.*, *Curr. Opin. Plant Biol.* **11**, 144–148 (2008).
- 2) A. Garavito *et al.*, *Genetics* **185**, 1425–1440 (2010).
- 3) Y. Sano, *Genetics* **125**, 183–191 (1990).
- 4) Y. Koide *et al.*, *New Phytol.* **179**, 888–900 (2008).
- 5) Y. Xie *et al.*, *Mol. Plant* **10**, 1137–1140 (2017).
- 6) Y. Koide *et al.*, *Proc. Natl. Acad. Sci. USA*, **115**, E1955–E1962 (2018).

<sup>\*1</sup> Research Faculty of Agriculture, Hokkaido University

<sup>\*2</sup> Department of Agro-Environmental Science, Obihiro University of Agriculture and Veterinary Medicine

<sup>\*3</sup> RIKEN Nishina Center

<sup>\*4</sup> Japan International Research Center for Agricultural Sciences

<sup>\*5</sup> Faculty of Agriculture, Kyoto University

## Improved and robust method to efficiently deplete repetitive elements from complex plant genomes<sup>†</sup>

H. Ichida\*<sup>1</sup> and T. Abe\*<sup>1</sup>

Wheat is one of the most important staple food crops around the world, occupying 17% (one-sixth) of the global crop acreage and serving as a food source for approximately 40% of the world's population. Despite the availability of a high-quality reference genome sequence, whole genome re-sequencing of wheat is still a major challenge owing to its large and complex genome. Wheat has an estimated haploid genome size of 15.4–15.8 Gb, of which 84.7% is made up of repetitive sequences. To successfully apply genome sequencing to practical agricultural breeding situations, the establishment of an effective strategy to eliminate highly abundant repetitive elements within the genome is required.

Duplex-specific nuclease (DSN) provides an enzymatic method to reduce the whole-genome redundancy and normalization. However, this method has not been widely used in the genome analysis of agricultural crops owing to its sensitivity to reaction conditions and difficulty in DNA recovery after the treatment. We developed an improved design for Illumina-compatible sequencing adapters that avoids duplex formation within a typical annealing temperature range ( $\sim 68^{\circ}\text{C}$ ) and accidental degradation by the DSN enzyme. The newly designed adapter includes the 21 bp sequences immediately adjacent to the original TruSeq adapter and forms a hairpin-like structure by placing the necessary adapter sequences in a complementary orientation at the 5' and 3' ends of a single oligonucleotide at room temperature during library preparation. Using this design, all necessary sequence elements for Illumina sequencing could then be added using full-length adapter primers during the recovery PCR, which generates a library with exactly the same structure as the original TruSeq libraries.

We compared the relative abundance of 18S and 25S rDNA elements in genomic DNA and the DNA libraries before and after DSN treatment (DSN<sup>-</sup> and DSN<sup>+</sup>, respectively) in rice and diploid, tetraploid, and hexaploid wheat cultivars by quantitative PCR. In summary, the relative abundances of 18S and 25S rDNA were reduced to 1.15% and 3.54% of the DSN<sup>-</sup> samples in rice. The effectiveness of the DSN treatment was essentially the same among the three wheat genomes. In particular, the relative abundance of 18S rDNA was decreased to 7.13%, 4.95%, and 4.33% considering the DSN<sup>-</sup> in diploid, tetraploid, and hexaploid cultivars, respectively. The relative abun-

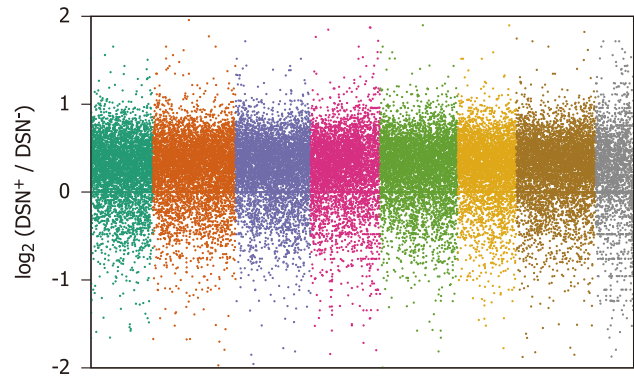


Fig. 1. Comparison of read counts before and after duplex-specific nuclease-based repeat depletion in gene regions. Reprinted from *Plant Science*, <https://doi.org/10.1016/j.plantsci.2018.10.021>, with permission from Elsevier.

dance of 25S rDNA was also decreased to 21.73%, 8.96%, and 7.54% considering DSN<sup>-</sup>. These results indicate that the DSN treatment effectively depleted repetitive sequences in different wheat cultivars, which have much larger and more complex genomes compared with rice.

We evaluated the enzymatic depletion of highly repetitive elements by DSN treatment in an actual Illumina sequencing run using the diploid wheat cultivar KU104-1, which has an estimated genome size of 6.1 Gb, as a model. The sequencing reads mapped on the regions encoding Ty1-Copia and Ty3-Gypsy were decreased by 61.6% and 33.4%, respectively, compared with the DSN<sup>-</sup> samples. DNA-type repetitive elements were also successfully depleted by the DSN treatment. In particular, reads mapped to DNA-type transposons and simple sequence repeats (SSRs) were respectively reduced by 17.1% and 9.0% compared with the untreated control. Therefore, we conclude that this method should be useful in a broad range of species in which genomic approaches are not currently applicable owing to their large and complex genome structures and the consequent high expenses of sequencing and analysis.

<sup>†</sup> Condensed from the article in *Plant Science*, 280, 455-460 (2019)

\*<sup>1</sup> RIKEN Nishina Center

## **II. RESEARCH ACTIVITIES I**

### **(Nuclear, Particle and Astro-Physics)**



# 1. Nuclear Physics



# Breakup of ${}^9\text{C}$ studied at SAMURAI

A. I. Chilug,<sup>\*1,\*2,\*3</sup> V. Panin,<sup>\*3,\*4</sup> L. Trache,<sup>\*1</sup> T. Motobayashi,<sup>\*3</sup> Z. Halasz,<sup>\*5</sup> for HI-p collaboration

During the NP1412-SAMURAI29R1 experiment, the  ${}^9\text{C}$  breakup reaction into  ${}^8\text{B}+p$  was studied by Coulomb dissociation and nuclear breakup. By using the invariant mass technique and the detailed balance theorem,<sup>1)</sup> it is possible to determine the reaction cross section for the astrophysical process  ${}^8\text{B}(p,\gamma){}^9\text{C}$  using two alternative indirect methods: Coulomb dissociation<sup>1)</sup> and by applying the ANC technique for nuclear breakup (NB).<sup>2)</sup>

The radiative proton capture  ${}^8\text{B}(p,\gamma){}^9\text{C}$  is being investigated due to its astrophysical importance as a possible bypass of the  $3\alpha$ -process leading to the CNO cycle in low metallicity massive stars, by a sequence of protons and alpha capture reactions on nuclei close to the proton drip line.<sup>3)</sup> From the previous experiments, a large spread of results was obtained for the determined astrophysical  $S_{18}$  factor (see Ref. 4)), and hence a new set of accurate measurements is necessary.

The experiment was performed in RIKEN at the RIBF facility during the SAMURAI Oxygen18 campaign in the spring of 2018, as part of the HI-p program. The primary beam  ${}^{18}\text{O}$  at 230 AMeV hit a Be production target. The  ${}^9\text{C}$  secondary beam, having intensities up to  $4.7 \cdot 10^4$  pps, was separated by using the two-stage separator BigRIPS and delivered to the SAMURAI area. Fig. 1 shows the PID of the beam at the entrance of the SAMURAI area. The aim of the experiment is to perform inclusive and exclusive measurements of the  ${}^9\text{C}$  breakup reaction products using a dedicated detection system set at the superconducting magnetic spectrometer SAMURAI. For the study of  ${}^9\text{C}$  breakup in a nuclear field, a natural carbon target ( $425 \mu\text{m}$  thick) was used, and for the Coulomb dissociation measurement, we set a Pb target ( $150 \mu\text{m}$  thick). The detection system used during the experiment comprised two scintillator detectors (SBT1&2) for beam PID (in combination with the BigRIPS scintillators) and for triggering the data acquisition system. Two drift chambers (BDC1&2) were used to measure the position and angle of the beam. The target was followed by 4 Si detectors to track the reaction products along with another drift chamber (FDC0). Two plastic scintillators (HODF&HODP) were placed behind the SAMURAI exit window to measure the energy loss and the time of flight for particle identification. Finally, two proton drift chambers (PDC1&2) were used for magnetic rigidity analysis of the emitted protons.

The tracking system mentioned above is made of 4 position sensitive Si detectors (GLAST) with a large active area ( $87.5 \times 87.5 \text{ mm}^2$ ) and high granularity (each silicon detector has 128 strips), which were arranged in two pairs, an placed downstream of the reaction target.

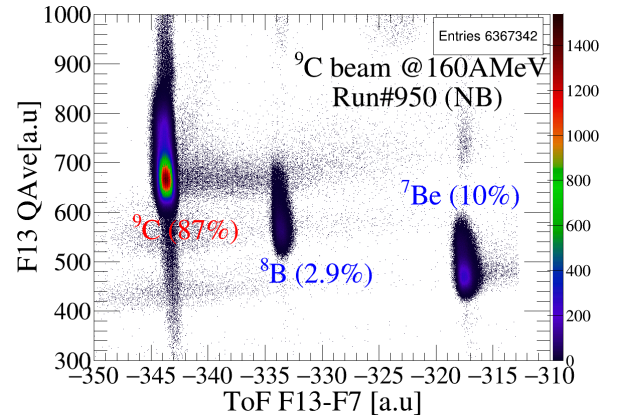


Fig. 1. The purity and PID of the secondary beam.

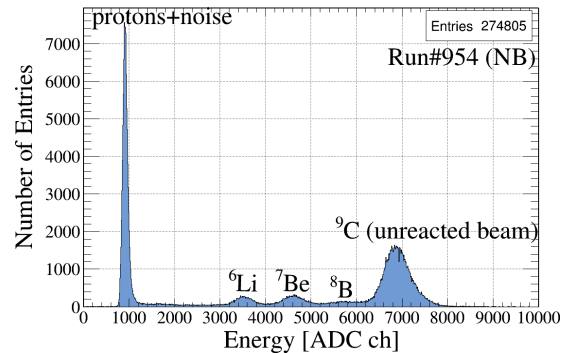


Fig. 2. Signals of the reaction products in the Si system.

This system was newly introduced for all 4 HI-p experiments. In order to simultaneously track the protons and heavy fragments, the signals from the Si detectors were processed with new Dual Gain Preamplifiers (DGP) designed at RIKEN and packed at ATOMKI. A high dynamic range was assured for the entire system. Thus, the system could measure the energy loss of the protons (around 200 keV) in coincidence with the heavy fragments (up to 600 MeV). The signals from the DGP were fed into the ASIC system based on HINP16 chips.<sup>5)</sup> Two Motherboards (MB) with 16 slots each for connecting 16 HINP boards, each of them having 2 ASIC chips, processed a total of 1024 output signals from the silicon detectors. The PID of the reaction products in the Si detectors can be seen in Fig. 2.

The Si system was used in the beam for the first time. It worked well, and in combination with the existing detection systems, assured the experimental goals presented in the submitted proposal. The data analysis is in progress.

## References

- 1) G. Baur *et al.*, Nucl. Phys. A **458**, 188–204 (1986).
- 2) L. Trache *et al.*, Phys. Rev. Lett. **87**, 271102 (2001).
- 3) M. Wiescher *et al.*, Astrophys. J. **343**, 352–364 (1989).
- 4) T. Fukui *et al.*, Few-body Syst. **54** 1583–1586 (2013).
- 5) G. L. Engel *et al.*, Nucl. Instrum. Methods Phys. Res. A **573**, 418–426 (2007).

<sup>\*1</sup> Horia Hulubei National Institute for R&D in Physics and Nuclear Engineering (IFIN-HH)

<sup>\*2</sup> Faculty of Physics, University of Bucharest

<sup>\*3</sup> RIKEN Nishina Center

<sup>\*4</sup> Département de Physique Nucléaire, IRFU, CEA, Université Paris-Saclay

<sup>\*5</sup> Institute of Nuclear Research (ATOMKI), Debrecen

# Cluster structure of neutron-rich beryllium isotopes investigated by cluster quasi-free scattering reaction

P. Li<sup>\*1</sup> and D. Beaumel<sup>\*2,\*3</sup> for the SAMURAI12 collaboration

Clustering is known for long as an important and general feature of atomic nuclei. So far alpha-particle clustering has dominated cluster states studies among all other possible partitioning. Thus, nuclei with even and equal numbers of protons and neutrons (the so-called alpha-conjugate nuclei) have been extensively studied. A few decades ago, some general properties of clustering in nuclei have been stressed, *e.g.* its preferential occurrence close to cluster decay thresholds rather than in ground-states.<sup>1)</sup> The situation might be somewhat different in exotic nuclei for which well developed cluster configurations may occur in ground-states, even though located well below the corresponding cluster threshold. The SAMURAI12 experiment aims to investigate the cluster structure of neutron-rich beryllium isotopes using the cluster quasifree scattering reaction ( $p, p\alpha$ ) in inverse kinematics. Such an approach has been recently emphasized as a suitable method to investigate how  $\alpha$  cluster states are spatially developed.<sup>2)</sup> Beryllium isotopes are of special interest in relation with clustering. The  $^8\text{Be}$  nucleus is famous for its developed  $\alpha$ - $\alpha$  structure, well reproduced by *ab initio* calculations. Antisymmetrized Molecular dynamics calculations predict the occurrence of  $\alpha$ - $\alpha$  core up to the dripline, neutrons occupying molecular orbits around this core. The purpose of the SAMURAI12 experiment is to study the ( $p, p\alpha$ ) reaction on neutron-rich Beryllium isotopes up to the dripline.

The experiment was performed using the SAMURAI large-acceptance spectrometer during the spring campaign of 2018. Secondary  $^{10,12,14}\text{Be}$  beams at nearly 150A MeV were produced by fragmentation of a 230A-MeV  $^{18}\text{O}$  primary beam, using the BigRIPS separator. To study the ( $p, p\alpha$ ) reaction in inverse kinematics, a new setup combining several elements was developed. The first component was the solid hydrogen target (SHT) system associated with the ESPRI setup.<sup>4)</sup> This system allows to prepare a target foil of typically 1–3 mm thickness with a diameter of 3 cm, well adapted for our study. A new target chamber dedicated to the SAMURAI12 experiment has been built with new apertures allowing detection of protons at the relevant angles. A new target frame was also built for the production of a 2 mm thick foil which was used in the experiment. For recoil proton detection, the ESPRI Recoil Proton Spectrometer (RPS) system was implemented. It is composed of 3 stages: 1. Multiwire drift chamber (MWDC) for scattering angle determi-

nation, 2. plastic detector of 4 mm thickness and 3. NaI rods. The system was installed in a two-arm configuration identical to the one used during the SAMURAI13 experiment.<sup>4)</sup> The two arms were placed at 95 cm from target, covering an angular range of  $50^\circ$ – $70^\circ$ , corresponding to about  $40^\circ$ – $70^\circ$  in center of mass (CM) for the free  $p + \alpha$  elastic scattering. Detection of alpha clusters was insured by two telescopes composed of Silicon and CsI(Tl) detectors placed at forward angles to cover the angular range  $4^\circ$ – $12^\circ$ . The first layer was a double-sided Silicon detector (DSSD),  $62 \times 62$  mm active area with 32 strips on each side. The second stage was composed of CsI(Tl) crystals  $2.5 \times 2.5$  cm<sup>2</sup>, 6 cm long, from the FARCOS array. Energy range of the clusters was 100 ~ 150 MeV/nucleon. A dedicated energy calibration run with a (secondary) alpha beam was used in order to achieve precise energy calibration needed to deduce the missing mass. The detection of the  $^4,6,8\text{He}$  beam-like velocity residues near zero degrees produced in the  $^{10,12,14}\text{Be}(p, p\alpha)$  reactions was performed using the SAMURAI spectrometer and its standard detectors.<sup>5)</sup> The residue scattering angle was measured using the Forward Drift Chamber 0 (FDC0) placed upstream of the SAMURAI entrance. After the exit window of SAMURAI, rigidity measurement and particle identification of the residues were insured by the Forward Drift Chamber 2 (FDC2), and the HODP and HODF walls of plastic hodoscopes composed of 16 and 24 slats of BC408 scintillators, (of dimensions  $120 \times 10 \times 1$  cm<sup>3</sup>), respectively. For complementary invariant mass studies, the neutron multi-detector NEBULA was also included in the setup. The data analysis is undergoing, presently focusing on the calibrations runs of forward telescopes with alpha secondary beams. A detailed uniformity response study of CsI(Tl) modules is being performed owing to the position information provided by the DSSD.

## References

- 1) K. Ikeda, N. Tagikawa, H. Horiuchi, Prog. Theor. Phys. **464**, (1968).
- 2) M. Lyu *et al.*, Phys. Rev. C **97**, 044612 (2018).
- 3) Y. Matsuda *et al.*, Nucl. Instrum. Methods Phys. Res. A **643**, 6 (2011).
- 4) S. Chebotaryov *et al.*, Prog. Theor. Exp. Phys. **2018**, 053D01 (2018).
- 5) T. Kobayashi *et al.*, Nucl. Instrum. Methods Phys. Res. B **317**, 294 (2013).

\*1 Hong Kong University

\*2 Institut de Physique Nucléaire, Orsay

\*3 RIKEN Nishina Center

## Particle identification in $^{11}\text{Li}(p, n)$ experiment at SAMURAI

Y. Hirai,<sup>\*1</sup> L. Stuhl,<sup>\*2</sup> M. Sasano,<sup>\*3</sup> J. Gao,<sup>\*3,\*4</sup> K. Yako,<sup>\*2</sup> T. Wakasa,<sup>\*1</sup> D. S. Ahn,<sup>\*3</sup> H. Baba,<sup>\*3</sup> A. Chilug,<sup>\*5,\*3</sup> S. Franchoo,<sup>\*6</sup> Y. Fujino,<sup>\*7</sup> J. Gibelin,<sup>\*6</sup> I. S. Hahn,<sup>\*8</sup> Z. Halász,<sup>\*9</sup> T. Harada,<sup>\*10</sup> M. N. Harakeh,<sup>\*11,\*12</sup> D. Inomoto,<sup>\*1</sup> T. Isobe,<sup>\*3</sup> H. Kasahara,<sup>\*1</sup> D. Kim,<sup>\*13</sup> G. G. Kiss,<sup>\*9</sup> T. Kobayashi,<sup>\*14</sup> Y. Kondo,<sup>\*15</sup> Z. Korkulu,<sup>\*3</sup> S. Koyama,<sup>\*16</sup> Y. Kubota,<sup>\*3</sup> A. Kurihara,<sup>\*15</sup> H. N. Liu,<sup>\*17</sup> M. Matsumoto,<sup>\*15</sup> S. Michimasa,<sup>\*2</sup> H. Miki,<sup>\*15</sup> M. Miwa,<sup>\*18</sup> T. Motobayashi,<sup>\*3</sup> T. Nakamura,<sup>\*15</sup> M. Nishimura,<sup>\*3</sup> H. Otsu,<sup>\*3</sup> V. Panin,<sup>\*3</sup> S. Park,<sup>\*8</sup> A. T. Saito,<sup>\*15</sup> H. Sakai,<sup>\*3</sup> H. Sato,<sup>\*3</sup> T. Shimada,<sup>\*15</sup> Y. Shimizu,<sup>\*3</sup> S. Shimoura,<sup>\*2</sup> A. Spiridon,<sup>\*5</sup> I. Stefanescu,<sup>\*5</sup> X. Sun,<sup>\*3,\*4</sup> Y. L. Sun,<sup>\*17</sup> H. Suzuki,<sup>\*3</sup> Y. Togano,<sup>\*7</sup> T. Tomai,<sup>\*15,\*3</sup> L. Trache,<sup>\*5</sup> D. Tudor,<sup>\*5,\*3</sup> T. Uesaka,<sup>\*3</sup> H. Yamada,<sup>\*15</sup> M. Yasuda,<sup>\*15</sup> K. Yoneda,<sup>\*3</sup> K. Yoshida,<sup>\*3</sup> J. Zenihiro,<sup>\*3</sup> and N. Zhang<sup>\*19,\*2</sup>

The details of the particle identification (PID) of the incoming secondary cocktail beam and the reaction residues in the SAMURAI30 experiment are reported.

A secondary cocktail beam of unstable  $^{11}\text{Li}$  and  $^{14}\text{Be}$  was produced via the fragmentation reaction of a 230 MeV/nucleon  $^{18}\text{O}$  primary beam on a 14-mm-thick  $^9\text{Be}$  target. In the experimental setup<sup>1)</sup> around the SAMURAI spectrometer,<sup>2)</sup> two 1-mm-thick plastic scintillators (SBT1,2) were installed for the detection of beam particles. The SBTs were used to produce the beam trigger (threshold was set to  $Z > 2$ ). The beam PID was performed on an event-by-event basis by measuring the energy loss in the SBTs and the ToF of the beam particles in BigRIPS between F7 and F13. The secondary cocktail beam consisted of  $^{11}\text{Li}$  at 182 MeV/nucleon with an intensity of  $2.5 \times 10^5$  particle/s and  $^{14}\text{Be}$  at 198 MeV/nucleon with an intensity of  $1 \times 10^5$  particle/s with purities of 48% and 19%, respectively. The triton contamination was below 30%. Figure 1 shows the incoming beam PID spectrum.

The secondary beam was transported onto a 10-mm-thick liquid hydrogen target.<sup>3,4)</sup> The reaction residues entered SAMURAI after passing through the forward drift chamber, FDC0. The magnetic field of the spectrometer was set to 2.75 T. At the focal plane of SAMURAI, a wall (HODF24 detector) of 24 plastic scintillator bars with dimensions of  $1200^W \times 100^H \times 10^D$  mm<sup>3</sup> was installed, to measure the trajectories, energy loss, and ToF (from SBTs) of the reaction residues. Further downstream, an additional wall, HODP, with 16 plastic bars (same as HODF24 bars) was installed. The 2 bars of

HODF24 that were hit by the unreacted beam were excluded from the trigger. Figure 2 shows a typical PID spectrum in HODF24 for events generated by the  $^{11}\text{Li}$  or  $^{14}\text{Be}$  beams. Using the PID information, the reaction channels for  $^{11}\text{Li}(p, n)^{11}\text{Be}^{5)}$  and  $^{14}\text{Be}(p, n)^{14}\text{B}^{6)}$  can be identified.

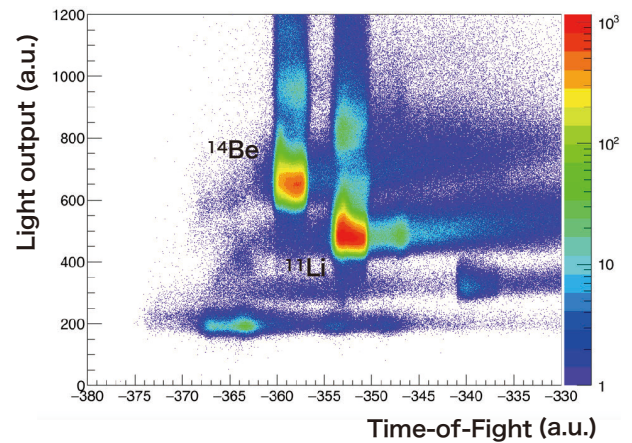


Fig. 1. An incoming PID spectrum of the SBT detector. The separation of  $^{11}\text{Li}$  and  $^{14}\text{Be}$  is clear.

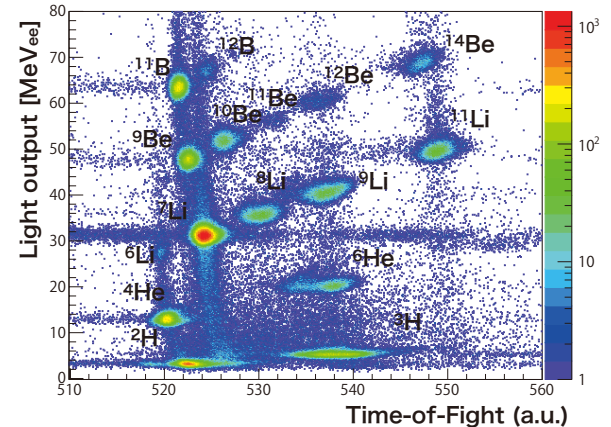


Fig. 2. A PID spectrum in the focal plane of SAMURAI, measured by one bar (bar ID = 7) of HODF24.

<sup>\*1</sup> Department of Physics, Kyushu University  
<sup>\*2</sup> Center for Nuclear Study, University of Tokyo  
<sup>\*3</sup> RIKEN Nishina Center  
<sup>\*4</sup> School of Physics, Peking University  
<sup>\*5</sup> Horia Hulubei Nat. Inst. of Phys. and Nucl. Eng.  
<sup>\*6</sup> LPC CAEN  
<sup>\*7</sup> Department of Physics, Rikkyo University  
<sup>\*8</sup> Department of Physics, Ewha Womans University  
<sup>\*9</sup> ATOMKI, Institute for Nuclear Research, HAS  
<sup>\*10</sup> Department of Physics, Toho University  
<sup>\*11</sup> KVI - CART, University of Groningen  
<sup>\*12</sup> GSI Helmholtzzentrum für Schwerionenforschung  
<sup>\*13</sup> Department of Physics, Korea University  
<sup>\*14</sup> Department of Physics, Tohoku University  
<sup>\*15</sup> Dept. of Physics, Tokyo Institute of Technology  
<sup>\*16</sup> Department of Physics, University of Tokyo  
<sup>\*17</sup> Dépt. Physique Nucl., CEA, Univ. Paris-Saclay  
<sup>\*18</sup> Dept. of Physics, Saitama University  
<sup>\*19</sup> Institute of Modern Physics, Chinese Acad. of Sci.

### References

- 1) M. Sasano *et al.*, in this report.
- 2) T. Kobayashi *et al.*, Nucl. Instrum. Methods Phys. Res. B **317**, 294 (2013).
- 3) X. Sun *et al.*, in this report.
- 4) M. Miwa *et al.*, in this report.
- 5) L. Stuhl *et al.*, in this report.
- 6) J. Gao *et al.*, in this report.

# Neutron-gamma separation performance of PANDORA in SAMURAI30 experiment

Y. Hirai,<sup>\*1</sup> L. Stuhl,<sup>\*2</sup> M. Sasano,<sup>\*3</sup> J. Gao,<sup>\*3,\*4</sup> K. Yako,<sup>\*2</sup> T. Wakasa,<sup>\*1</sup> D. S. Ahn,<sup>\*3</sup> H. Baba,<sup>\*3</sup> A. Chilug,<sup>\*5,\*3</sup> S. Franchoo,<sup>\*6</sup> Y. Fujino,<sup>\*7</sup> J. Gibelin,<sup>\*6</sup> I. S. Hahn,<sup>\*8</sup> Z. Halász,<sup>\*9</sup> T. Harada,<sup>\*10</sup> M. N. Harakeh,<sup>\*11,\*12</sup> D. Inomoto,<sup>\*1</sup> T. Isobe,<sup>\*3</sup> H. Kasahara,<sup>\*1</sup> D. Kim,<sup>\*13</sup> G. G. Kiss,<sup>\*9</sup> T. Kobayashi,<sup>\*14</sup> Y. Kondo,<sup>\*15</sup> Z. Korkulu,<sup>\*3</sup> S. Koyama,<sup>\*16</sup> Y. Kubota,<sup>\*3</sup> A. Kurihara,<sup>\*15</sup> H. N. Liu,<sup>\*17</sup> M. Matsumoto,<sup>\*15</sup> S. Michimasa,<sup>\*2</sup> H. Miki,<sup>\*15</sup> M. Miwa,<sup>\*18</sup> T. Motobayashi,<sup>\*3</sup> T. Nakamura,<sup>\*15</sup> M. Nishimura,<sup>\*3</sup> H. Otsu,<sup>\*3</sup> V. Panin,<sup>\*3</sup> S. Park,<sup>\*8</sup> A. T. Saito,<sup>\*15</sup> H. Sakai,<sup>\*3</sup> H. Sato,<sup>\*3</sup> T. Shimada,<sup>\*15</sup> Y. Shimizu,<sup>\*3</sup> S. Shimoura,<sup>\*2</sup> A. Spiridon,<sup>\*5</sup> I. Stefanescu,<sup>\*5</sup> X. Sun,<sup>\*3,\*4</sup> Y. L. Sun,<sup>\*17</sup> H. Suzuki,<sup>\*3</sup> Y. Togano,<sup>\*7</sup> T. Tomai,<sup>\*15,\*3</sup> L. Trache,<sup>\*5</sup> D. Tudor,<sup>\*5,\*3</sup> T. Uesaka,<sup>\*3</sup> H. Yamada,<sup>\*15</sup> M. Yasuda,<sup>\*15</sup> K. Yoneda,<sup>\*3</sup> K. Yoshida,<sup>\*3</sup> J. Zenihiro,<sup>\*3</sup> and N. Zhang<sup>\*19,\*2</sup>

The neutron-gamma discrimination ability of PANDORA (Particle Analyzer Neutron Detector Of Real-time Acquisition)<sup>1)</sup> was studied for SAMURAI 30<sup>2,3)</sup> experiment using <sup>11</sup>Li(*p*, *n*) reactions.<sup>4)</sup> The method of separating neutron and gamma events is based on charge integration, where the PSD (Pulse-Shape Discrimination) parameter is  $(Q_{\text{Long}} - Q_{\text{Short}})/Q_{\text{Long}}$ , where  $Q_{\text{Long}}$  and  $Q_{\text{Short}}$  are derived from the charge integrated in the long gate and short gate of each end of a PANDORA bar, respectively.  $\text{PSD}_{\text{mean}}$  can be defined as the arithmetic average of PSD because PANDORA is a double-ended read-out. Figure 1 presents a two-dimensional plot of  $\text{PSD}_{\text{mean}}$  vs.  $Q_{\text{Long}}$  (light output) of a PANDORA bar. The locus in the higher PSD region corresponds to

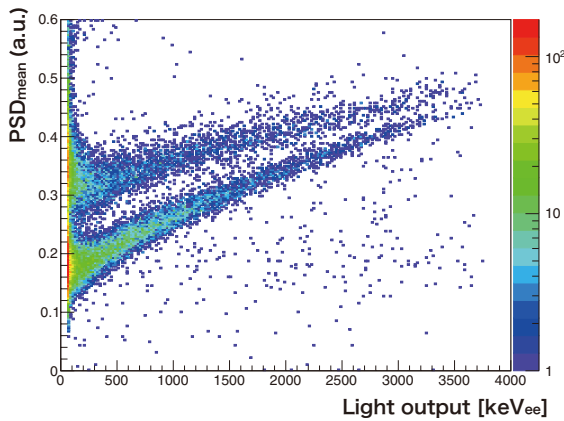


Fig. 1.  $\text{PSD}_{\text{mean}}$  as a function of light output (bar ID = 7).

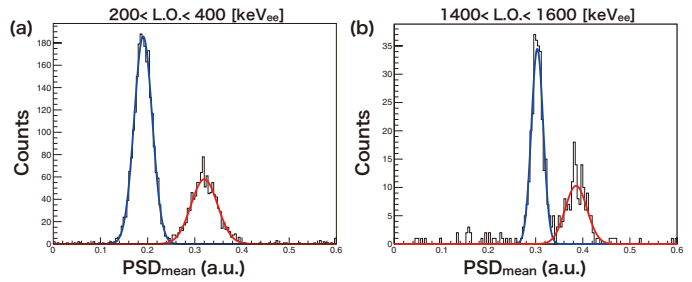


Fig. 2.  $\text{PSD}_{\text{mean}}$  distributions for the light output (a) from 200 to 400 and (b) from 1400 to 1600 [keV<sub>ee</sub>]. The blue and red lines shows gamma and neutron events, respectively.

the neutron-like events, while the distribution in the low PSD range represents the gamma-like events.

To evaluate the discrimination performance of PANDORA, Figure-of-Merit (FoM) is used. FoM is defined as:

$$\text{FoM} = \frac{\Delta_{\gamma-n}}{L_{\gamma-\text{FWHM}} + L_{n-\text{FWHM}}}, \quad (1)$$

where  $\Delta_{\gamma-n}$  is the PSD difference between the neutron and gamma component peaks.  $L_{\gamma-\text{FWHM}}$  and  $L_{n-\text{FWHM}}$  are the full widths at half maxima of the gamma and neutron distributions, respectively. In this work, we used the window method, detailed in Ref. 1). Figure 2 shows the one-dimensional  $\text{PSD}_{\text{mean}}$  projections in 200 keV<sub>ee</sub> wide window centered at light outputs of 300 keV<sub>ee</sub> (a) and 1500 keV<sub>ee</sub> (b), respectively. The calculated FoM values are  $1.17 \pm 0.01$  (a) and  $0.98 \pm 0.03$  (b). We achieved better FoM value than previous studies.<sup>5-7)</sup> Owing to the optimized digital read-out, large gain setting, and improved scintillation material, we achieved better FoM value than previous studies.

References

- 1) L. Stuhl, *et al.*, Nucl. Instrum. Methods Phys. Res. A **866**, 164 (2017).
- 2) M. Sasano *et al.*, in this report.
- 3) L. Stuhl *et al.*, in this report.
- 4) Y. Hirai *et al.*, in this report.
- 5) S. A. Pozzi, *et al.*, Nucl. Instrum. Methods Phys. Res. A **723**, 19 (2013).
- 6) D. Cester, *et al.*, Nucl. Instrum. Methods Phys. Res. A **735**, 202 (2014).
- 7) P. Blanc, *et al.*, Nucl. Instrum. Methods Phys. Res. A **750**, 1 (2014).

\*1 Department of Physics, Kyushu University  
 \*2 Center for Nuclear Study, University of Tokyo  
 \*3 RIKEN Nishina Center  
 \*4 School of Physics, Peking University  
 \*5 Horia Hulubei Nat. Inst. of Phys. and Nucl. Eng.  
 \*6 LPC CAEN  
 \*7 Department of Physics, Rikkyo University  
 \*8 Department of Physics, Ewha Womans University  
 \*9 ATOMKI, Institute for Nuclear Research, HAS  
 \*10 Department of Physics, Toho University  
 \*11 KVI - CART, University of Groningen  
 \*12 GSI Helmholtzzentrum für Schwerionenforschung  
 \*13 Department of Physics, Korea University  
 \*14 Department of Physics, Tohoku University  
 \*15 Dept. of Physics, Tokyo Institute of Technology  
 \*16 Department of Physics, University of Tokyo  
 \*17 Dépt. Physique Nucl., CEA, Univ. Paris-Saclay  
 \*18 Dept. of Physics, Saitama University  
 \*19 Institute of Modern Physics, Chinese Acad. of Sci.

## Gamow-Teller resonance in $^{14}\text{Be}(p, n)$ reaction

J. Gao,<sup>\*1,\*3</sup> L. Stuhl,<sup>\*2</sup> M. Sasano,<sup>\*1</sup> Y. Hirai,<sup>\*4</sup> K. Yako,<sup>\*2</sup> T. Wakasa,<sup>\*4</sup> for SAMURAI30 Collaboration

A charge-change ( $p, n$ ) experiment, SAMURAI30, on  $^{14}\text{Be}$  and  $^{11}\text{Li}$  nuclei was performed on the SAMURAI spectrometer.<sup>1,2)</sup> In this report, we present the status of the analysis of  $^{14}\text{Be}(p, n)^{14}\text{B}^*$  channel.

We used inverse kinematics with a secondary beam of  $^{14}\text{Be}$  at 198.4 MeV/nucleon and a 10 mm thick liquid hydrogen target, rotated by  $45^\circ$ .<sup>3,4)</sup> The low-energy neutron detector setup, consisted of PANDORA<sup>5)</sup> and WINDS scintillator arrays, covered the laboratory angular range of  $47.8^\circ$  to  $133.9^\circ$  and were employed to detect the recoil neutrons. Signals from those detectors were recorded by a digital data acquisition system, which was operated in parallel with the standard SAMURAI DAQ system by sharing the same trigger signal.<sup>6)</sup> The neutron time-of-flight was measured to reconstruct the missing mass spectra.

Figure 1 shows the laboratory angle vs. laboratory energy spectrum of the detected neutrons when  $^{13}\text{B}$  is selected in the HODF24 hodoscope, three curves (in 0–5 MeV, 5–10 MeV, and 15–20 MeV of excitation energies) evidently appeared. The left and right wings of the scintillator array are drawn separately. The colored solid lines indicate the excitation energy of  $^{14}\text{B}$ . The dotted lines indicate the corresponding center-of-mass angles. The signal-to-noise ratio is expected to be improved by the neutron-gamma discrimination analysis.<sup>7)</sup>

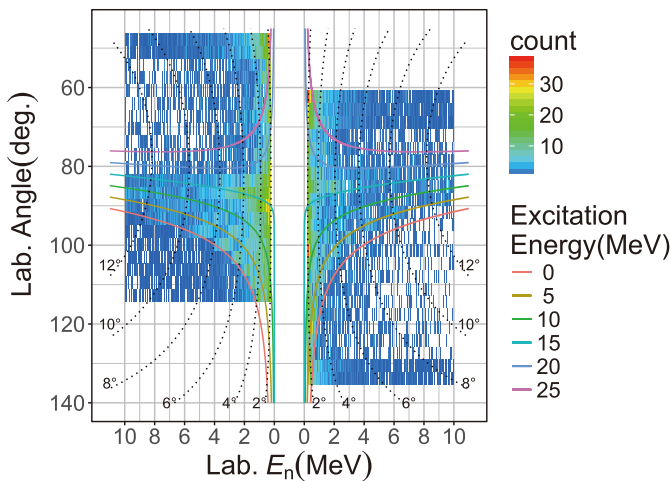


Fig. 1. Kinematic correlation of neutron angle and energy when  $^{13}\text{B}$  is detected downstream of SAMURAI.

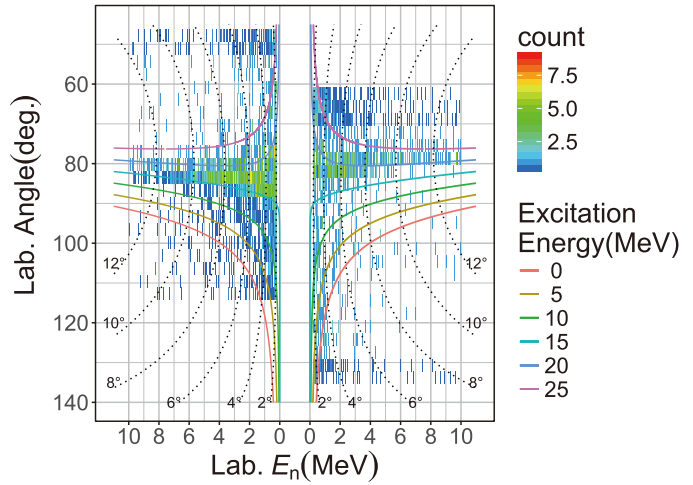


Fig. 2. Kinematic correlation of neutron angle and energy when  $^{12}\text{Be}$  and deuteron are detected downstream of SAMURAI.

Figure 2 shows the laboratory angle vs. laboratory energy spectrum of neutrons when both  $^{12}\text{Be}$  and deuteron are selected in the HODF24 hodoscope.

These curves show that the  $^{14}\text{B}$  excitation energy can be derived from the missing mass spectrum of neutrons, thereby implying that our experiment was successfully performed. In the future, we will tag the other decay channels of excited  $^{14}\text{B}$  and finally derive the Gamow-Teller strength.

We express our gratitude to the RIKEN and CNS staff for the stable operation of the accelerators during the measurement. This work is funded by the China Scholarship Council, KAKENHI project 16H06716, the Japan Society for the Promotion of Science, and Kurata Grant from the Kurata Memorial Hitachi Science and Technology Foundation.

### References

- 1) M. Sasano *et al.*, in this report.
- 2) T. Kobayashi *et al.*, Nucl. Instrum. Methods Phys. Res. B **317**, 294(2013).
- 3) M. Miwa *et al.*, in this report.
- 4) X. Sun *et al.*, in this report.
- 5) L. Stuhl *et al.*, Nucl. Instrum. Methods Phys. Res. A **866**, 164 (2017).
- 6) J. Gao *et al.*, in this report.
- 7) Y. Hirai *et al.*, in this report.

\*1 RIKEN Nishina Center

\*2 Center for Nuclear Study, University of Tokyo

\*3 School of Physics, Peking University

\*4 Department of Physics, Kyushu University

# Systematic study of one-proton and two-proton knockout reactions by deuterium target

M. Miwa,<sup>\*1,\*2</sup> T. Uesaka,<sup>\*2</sup> Y. Kubota,<sup>\*3</sup> H. Wang,<sup>\*2</sup> P. Doornenbal,<sup>\*2</sup> A. Obertelli,<sup>\*3</sup> H. Otsu,<sup>\*2</sup>  
and for the SEASTAR Collaboration

Roy J. Glauber<sup>1)</sup> first stated that an additive law does not always hold true in nuclear reactions. He showed that the interaction cross-sections in deuteron induced reactions are smaller than the sum of those in proton- and neutron-induced reactions under the same conditions. The reduction in cross-section is due to hiding one nucleon from the other in the target nucleus. This is called an “eclipse” effect.

This effect is thoroughly investigated for the interaction cross-section but not for individual reaction channels. In this work, we investigate the deuteron and proton induced one-proton and two-proton knockout reactions for neutron-rich beams and discuss their systematic behavior.

The experiment was performed after the third SEASTAR campaign<sup>4)</sup> in May 2017, using the SAMURAI spectrometer and MINOS target. A cocktail beam including neutron-rich K, Ca, Sc, Ti, and V was produced through projectile fragmentation reactions of a primary <sup>70</sup>Zn beam at 345 MeV/nucleon impinging on a beryllium target. The experimental setup was the same as that in the SEASTAR experiment, except that liquid hydrogen in the target container was replaced by liquid deuterium. In the following analysis, we used the data for liquid hydrogen as well. The liquid hydrogen and deuterium targets with thicknesses of 1.1 and 2.6 g/cm<sup>2</sup>, respectively, were used as secondary targets. Beams of <sup>51</sup>K, <sup>52–54</sup>Ca, <sup>56–57</sup>Sc, <sup>58–60</sup>Ti, and <sup>61–62</sup>V with an initial energy of  $\sim 240$  MeV/nucleon lost their energies by  $\sim 90$  MeV/nucleon in the target. Therefore, the cross-sections evaluated in this work are averaged over the energy range. The secondary beam and fragments were identified event by event using the  $\Delta E$ -TOF- $B\rho$  method.

The systematic of interaction and one- and two-proton knockout reactions for the neutron-rich beams were obtained. In the data analysis, the MINOS-TPC tracking was not required and the cross-section was obtained by counting the number of relevant isotopes in the focal plane detectors of the SAMURAI spectrometer. Owing to large acceptance of the SAMURAI spectrometer, all beam particles and the products of one- and two-proton knockout reactions were collected. Figure 1 summarizes the data for the cross-section ratio of a deuteron target to a proton target plotted for nuclides in the cocktail beam. The green, blue, and red plots represent interaction, one-, and two-proton knockout reaction cross-sections respectively. The ratios of interaction cross-sections had an almost constant value  $\sim 1.2$

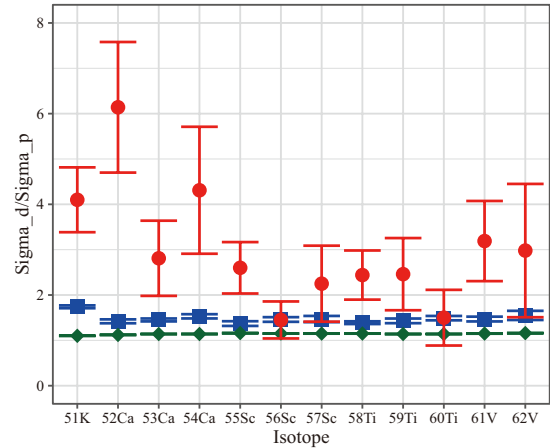


Fig. 1. Ratio ( $\sigma_d/\sigma_p$ ) of cross-sections of a deuteron target to a proton target. The horizontal axis is the beam isotope. The green, blue, and red plots represent the interaction, one-proton, and two-proton knockout the reaction cross-sections respectively.

for all isotopes. This is qualitatively attributed to the eclipse effect as mentioned above. The ratios of one-proton knockout cross-sections had slightly larger values  $\sim 1.5$ . This is due to the difference in elementary processes. The cross-sections for p-n scattering were 60% larger than those for p-p scattering. Thus, the cross-section comprising deuterium and a neutron is larger than that of hydrogen. It should be noted that the ratios of interaction and one-proton knockout reaction cross-section exhibited very small isotope dependences.

In contrast, the result of two-proton knockout cross-sections shows a significantly large deuteron/proton ratio. This value cannot be understood by the eclipse effect and/or the difference in elementary processes. We presume it originates from unknown mechanisms, which might enhance the cross-section of two-proton knockout with a deuterium target. Practically, the large values indicate the usefulness of a deuterium target in the production of neutron-rich nuclei via two-proton knockout reactions.

the data for neutron knockout reactions and channels with one and more neutron evaporation were also recorded. The systematic data can provide a comprehensive understanding of deuteron induced reactions.

## References

- 1) R. J. Glauber, Phys. Rev. **100**, 242 (1955).
- 2) A. Obertelli *et al.*, Eur. Phys. J. A **50**, 8 (2014).
- 3) H. Wang *et al.*, Phys. Lett. B **754**, 104 (2016).
- 4) P. Doornenbal, A. Obertelli, RIKEN Proposal for Scientific Program, (2013).

\*1 Department of Physics, Saitama University

\*2 RIKEN Nishina Center

\*3 Institut für Kernphysik, Technische Universität Darmstadt

## Study of spin-isospin response of $^{11}\text{Li}$ (SAMURAI30 experiment)

L. Stuhl,<sup>\*1</sup> M. Sasano,<sup>\*2</sup> J. Gao,<sup>\*2,\*3</sup> Y. Hirai,<sup>\*4</sup> K. Yako,<sup>\*1</sup> T. Wakasa,<sup>\*4</sup> D. S. Ahn,<sup>\*2</sup> H. Baba,<sup>\*2</sup> A. Chilug,<sup>\*5,\*2</sup> S. Franchoo,<sup>\*6</sup> Y. Fujino,<sup>\*7</sup> J. Gibelin,<sup>\*8</sup> I. S. Hahn,<sup>\*9</sup> Z. Halász,<sup>\*10</sup> T. Harada,<sup>\*11</sup> M. N. Harakeh,<sup>\*12,\*13</sup> D. Inomoto,<sup>\*4</sup> T. Isobe,<sup>\*2</sup> H. Kasahara,<sup>\*4</sup> D. Kim,<sup>\*14</sup> G. G. Kiss,<sup>\*10</sup> T. Kobayashi,<sup>\*15</sup> Y. Kondo,<sup>\*16</sup> Z. Korkulu,<sup>\*2</sup> S. Koyama,<sup>\*17</sup> Y. Kubota,<sup>\*2</sup> A. Kurihara,<sup>\*16</sup> H. N. Liu,<sup>\*18</sup> M. Matsumoto,<sup>\*16</sup> S. Michimasa,<sup>\*1</sup> H. Miki,<sup>\*16</sup> M. Miwa,<sup>\*19</sup> T. Motobayashi,<sup>\*2</sup> T. Nakamura,<sup>\*16</sup> M. Nishimura,<sup>\*2</sup> H. Otsu,<sup>\*2</sup> V. Panin,<sup>\*2</sup> S. Park,<sup>\*9</sup> A. T. Saito,<sup>\*16</sup> H. Sakai,<sup>\*2</sup> H. Sato,<sup>\*2</sup> T. Shimada,<sup>\*16</sup> Y. Shimizu,<sup>\*2</sup> S. Shimoura,<sup>\*1</sup> A. Spiridon,<sup>\*5</sup> I. Stefanescu,<sup>\*5</sup> X. Sun,<sup>\*2,\*3</sup> Y. L. Sun,<sup>\*18</sup> H. Suzuki,<sup>\*2</sup> Y. Togano,<sup>\*7</sup> T. Tomai,<sup>\*16,\*2</sup> L. Trache,<sup>\*5</sup> D. Tudor,<sup>\*5,\*2</sup> T. Uesaka,<sup>\*2</sup> H. Yamada,<sup>\*16</sup> M. Yasuda,<sup>\*16</sup> K. Yoneda,<sup>\*2</sup> K. Yoshida,<sup>\*2</sup> J. Zenihiro,<sup>\*2</sup> and N. Zhang<sup>\*20,\*1</sup>

The spin-isospin responses of  $^{11}\text{Li}$  and  $^{14}\text{Be}$  neutron drip line nuclei were measured in charge-exchange ( $p, n$ ) reactions. Until recently, only the spin-isospin collectivity in stable isotopes was investigated.<sup>1)</sup> There is no available data for nuclei with large isospin asymmetry factors, where  $(N - Z)/A > 0.25$ . The ( $p, n$ ) reactions at intermediate beam energies ( $E/A > 100$  MeV) and small scattering angles can excite Gamow-Teller (GT) states up to high excitation energies in the final nucleus, without  $Q$ -value limitation. The combined setup of PANDORA<sup>2)</sup> and SAMURAI spectrometer<sup>3)</sup> with a thick liquid hydrogen target (LHT)<sup>4)</sup> allowed us to perform the experiment with high luminosity. In this setup,<sup>5)</sup> PANDORA was used for the detection of the recoil neutrons while SAMURAI was used to tag the decay channel of the reaction residues.

The secondary cocktail beam of  $^{11}\text{Li}$  and  $^{14}\text{Be}$  was transported onto the 10 mm-thick LHT.<sup>6)</sup> The neutron detector setup on the left and right sides of LHT consisted of 27 PANDORA and 13 WINDS<sup>7)</sup> plastic scintillator bars. The neutron kinetic energies were deduced by the time-of-flight (ToF) technique (1.25 m flight path). The ToF time reference was taken from SBT1,2 plastic scintillators. The left and right wings with respect to the beam line covered the laboratory recoil angular region of  $47^\circ$ – $113^\circ$  and  $62^\circ$ – $134^\circ$ , respectively, with  $3.25^\circ$  steps. PANDORA was optimized to detect neutrons with a kinetic energy of 0.1–5 MeV. The light output threshold was set to be 60 keV<sub>ee</sub>. The digital data-acquisition (DAQ) of PANDORA was combined<sup>8)</sup> with standard

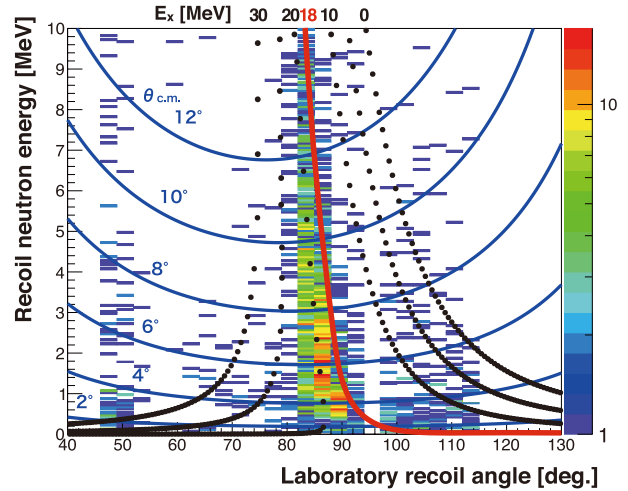


Fig. 1. Recoil neutron energy spectrum as a function of scattering angle in the laboratory frame.

DAQ of SAMURAI.

The reaction residues were momentum analyzed by the SAMURAI spectrometer, using HODF24 and HODP detectors.<sup>9)</sup> Figure 1 shows a preliminary plot of kinetic energy as a function of laboratory scattering angle for recoil neutrons associated with  $^{11}\text{Li}$  beam. We required the simultaneous detection of  $^9\text{Li}$  and  $d$  in HODF24 and neutron detection<sup>10)</sup> in PANDORA.

A clear kinematical correlation between the measured kinetic energy and the laboratory scattering angle, above 18 MeV excitation energy ( $E_x$ ), was obtained. This forward scattering peak ( $2^\circ$ – $7^\circ$  in the center-of-mass system) suggests a GT transition. The  $^{11}\text{Li} + d$  decay channel of  $^{11}\text{Be}$  is observed for the first time. Reconstruction of the excitation-energy spectrum up to about 30 MeV, including the GT giant resonance region, is ongoing.

### References

- 1) K. Nakayama *et al.*, Phys. Lett. B **114**, 217(1982).
- 2) L. Stuhl *et al.*, Nucl. Instrum. Methods Phys. Res. A **866**, 164 (2017).
- 3) T. Kobayashi *et al.*, Nucl. Instrum. Methods Phys. Res. B **317**, 294 (2013).
- 4) X. Sun *et al.*, in this report.
- 5) M. Sasano *et al.*, in this report.
- 6) M. Miwa *et al.*, in this report.
- 7) K. Yako *et al.*, RIKEN Accel. Prog. Rep. **45**, 137 (2012).
- 8) J. Gao *et al.*, in this report.
- 9) Y. Hirai *et al.*, in this report.
- 10) Y. Hirai *et al.*, in this report.

<sup>\*1</sup> Center for Nuclear Study, University of Tokyo  
<sup>\*2</sup> RIKEN Nishina Center  
<sup>\*3</sup> School of Physics, Peking University  
<sup>\*4</sup> Department of Physics, Kyushu University  
<sup>\*5</sup> Horia Hulubei Nat. Inst. of Phys. and Nucl. Eng.  
<sup>\*6</sup> Inst. de Physique Nuclaire, Univ. Paris-Saclay  
<sup>\*7</sup> Department of Physics, Rikkyo University  
<sup>\*8</sup> LPC CAEN  
<sup>\*9</sup> Department of Physics, Ewha Womans University  
<sup>\*10</sup> ATOMKI, Institute for Nuclear Research, HAS  
<sup>\*11</sup> Department of Physics, Toho University  
<sup>\*12</sup> KVI - CART, University of Groningen  
<sup>\*13</sup> GSI Helmholtzzentrum für Schwerionenforschung  
<sup>\*14</sup> Department of Physics, Korea University  
<sup>\*15</sup> Department of Physics, Tohoku University  
<sup>\*16</sup> Dept. of Physics, Tokyo Institute of Technology  
<sup>\*17</sup> Department of Physics, University of Tokyo  
<sup>\*18</sup> Dépt. Physique Nucl., CEA, Univ. Paris-Saclay  
<sup>\*19</sup> Dept. of Physics, Saitama University  
<sup>\*20</sup> Institute of Modern Physics, Chinese Acad. of Sci.

# Overview of the experimental setup of SAMURAI30 to measure the $^{11}\text{Li}(p, n)$ reaction in inverse kinematics

M. Sasano,<sup>\*1</sup> L. Stuhl,<sup>\*2</sup> J. Gao,<sup>\*1,\*3</sup> Y. Hirai,<sup>\*4</sup> K. Yako,<sup>\*2</sup> T. Wakasa,<sup>\*4</sup> D. S. Ahn,<sup>\*1</sup> H. Baba,<sup>\*1</sup> A. Chilug,<sup>\*5,\*1</sup> S. Franchoo,<sup>\*6</sup> Y. Fujino,<sup>\*7</sup> J. Gibelin,<sup>\*6</sup> I. S. Hahn,<sup>\*8</sup> Z. Halász,<sup>\*9</sup> T. Harada,<sup>\*10</sup> M. N. Harakeh,<sup>\*11,\*12</sup> D. Inomoto,<sup>\*4</sup> T. Isobe,<sup>\*1</sup> H. Kasahara,<sup>\*4</sup> D. Kim,<sup>\*13</sup> G. G. Kiss,<sup>\*9</sup> T. Kobayashi,<sup>\*14</sup> Y. Kondo,<sup>\*15</sup> Z. Korkulu,<sup>\*1</sup> S. Koyama,<sup>\*16</sup> Y. Kubota,<sup>\*1</sup> A. Kurihara,<sup>\*15</sup> H. N. Liu,<sup>\*17</sup> M. Matsumoto,<sup>\*15</sup> S. Michimasa,<sup>\*2</sup> H. Miki,<sup>\*15</sup> M. Miwa,<sup>\*18</sup> T. Motobayashi,<sup>\*1</sup> T. Nakamura,<sup>\*15</sup> M. Nishimura,<sup>\*1</sup> H. Otsu,<sup>\*1</sup> V. Panin,<sup>\*1</sup> S. Park,<sup>\*8</sup> A. T. Saito,<sup>\*15</sup> H. Sakai,<sup>\*1</sup> H. Sato,<sup>\*1</sup> T. Shimada,<sup>\*15</sup> Y. Shimizu,<sup>\*1</sup> S. Shimoura,<sup>\*2</sup> A. Spiridon,<sup>\*5</sup> I. Stefanescu,<sup>\*5</sup> X. Sun,<sup>\*1,\*3</sup> Y. L. Sun,<sup>\*17</sup> H. Suzuki,<sup>\*1</sup> Y. Togano,<sup>\*7</sup> T. Tomai,<sup>\*15,\*1</sup> L. Trache,<sup>\*5</sup> D. Tudor,<sup>\*5,\*1</sup> T. Uesaka,<sup>\*1</sup> H. Yamada,<sup>\*15</sup> M. Yasuda,<sup>\*15</sup> K. Yoneda,<sup>\*1</sup> K. Yoshida,<sup>\*1</sup> J. Zenihiro,<sup>\*1</sup> and N. Zhang<sup>\*19,\*2</sup>

In this report, we provide an overview of the setup used in the SAMURAI30 experiment performed at the RI Beam Factory (RIBF) of RIKEN Nishina Center in the spring of 2018.

The experiment was performed to measure the  $(p, n)$  reaction on  $^{11}\text{Li}$ <sup>1)</sup> and  $^{14}\text{Be}$ .<sup>2)</sup> A secondary cocktail beam was produced via the fragmentation reaction of a 230 MeV/nucleon  $^{18}\text{O}$  primary beam on a 14 mm-thick  $^9\text{Be}$  target installed at the F0 focal plane of the BigRIPS separator. The secondary cocktail beam consisted of  $^{11}\text{Li}$  at 182 MeV/nucleon and  $^{14}\text{Be}$  at 198 MeV/nucleon with purities of 48% and 19%, respectively. The total beam intensity was  $5 \times 10^5$  particle/s.

The SAMURAI spectrometer<sup>3)</sup> was used as the key device to tag the  $(p, n)$  reaction channel through particle identification of beam residual nuclei.<sup>4)</sup> The large acceptance by the SAMURAI spectrometer was crucial to detect a wide range of residual nuclei with different mass and proton numbers in the same setup.

Figure 1 shows a schematic view of the experimental setup around the SAMURAI spectrometer. Two 1-mm-thick plastic scintillators (SBT1, 2) were installed downstream of STQ25 for the detection of beam particles. Two multi-wire drift chambers were installed (BDC1, 2) to tune the beam focus. The secondary beam was transported onto a liquid hydrogen (LH) target with a thickness and diameter of 10 and 60 mm, respectively<sup>5,6)</sup> (rotated by  $45^\circ$ ) at the secondary target position of SAMURAI (F13).

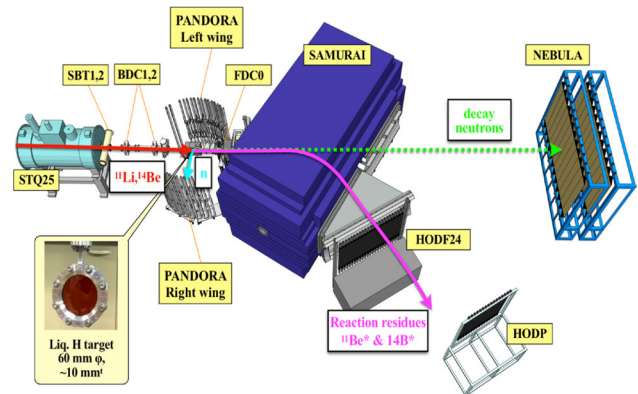


Fig. 1. The schematic view of the experimental setup around the SAMURAI spectrometer.

The PANDORA neutron detector setup consisted of 40 plastic scintillators and was placed on the left and right sides of the LH target. The neutron-gamma pulse-shape discrimination (PSD) capability of PANDORA in combination with a new DAQ system based on digitizers<sup>7)</sup> enables the reduction of the gamma-ray background originating from the environment as well as from the beam.<sup>8)</sup> PANDORA was optimized to detect neutrons with a kinetic energy of 0.1–5 MeV. The reaction residues entered SAMURAI after passing through the forward drift chamber, FDC0. The magnetic field of the spectrometer was set to 2.75 T. At the focal plane of SAMURAI, walls consisting of 24 and 16 plastic scintillator bars, HODF24 and HODP, were installed to momentum analyze the reaction residues. NEBULA was used to detect the fast decay neutrons of the reaction products (decays by  $1n$  and  $2n$  emissions).

We are grateful to the RIKEN accelerator staff and CNS, University of Tokyo, for their continuous efforts to accomplish this stable beam acceleration.

## References

- 1) L. Stuhl *et al.*, in this report.
- 2) J. Gao *et al.*, in this report.
- 3) T. Kobayashi, *et al.*, Nucl. Instrum. Methods Phys. Res. B **317** 294 (2013).
- 4) Y. Hirai *et al.*, in this report.
- 5) X. Sun *et al.*, in this report.
- 6) M. Miwa *et al.*, in this report.
- 7) J. Gao *et al.*, in this report.
- 8) Y. Hirai *et al.*, in this report.

\*1 RIKEN Nishina Center

\*2 Center for Nuclear Study, University of Tokyo

\*3 School of Physics, Peking University

\*4 Department of Physics, Kyushu University

\*5 Horia Hulubei Nat. Inst. of Phys. and Nucl. Eng.

\*6 LPC CAEN

\*7 Department of Physics, Rikkyo University

\*8 Department of Physics, Ewha Womans University

\*9 ATOMKI, Institute for Nuclear Research, HAS

\*10 Department of Physics, Toho University

\*11 KVI - CART, University of Groningen

\*12 GSI Helmholtzzentrum für Schwerionenforschung

\*13 Department of Physics, Korea University

\*14 Department of Physics, Tohoku University

\*15 Dept. of Physics, Tokyo Institute of Technology

\*16 Department of Physics, University of Tokyo

\*17 Dépt. Physique Nucl., CEA, Univ. Paris-Saclay

\*18 Dept. of Physics, Saitama University, Saitama

\*19 Institute of Modern Physics, Chinese Acad. of Sci.

# Neutron-neutron correlation in Borromean nucleus $^{11}\text{Li}$ via the $(p, pn)$ reaction

Y. Kubota,<sup>\*1,\*2</sup> A. Corsi,<sup>\*3</sup> G. Authelet,<sup>\*3</sup> H. Baba,<sup>\*2</sup> C. Caesar,<sup>\*4</sup> D. Calvet,<sup>\*3</sup> A. Delbart,<sup>\*3</sup> M. Dozono,<sup>\*1</sup> J. Feng,<sup>\*5</sup> F. Flavigny,<sup>\*6</sup> J. -M. Gheller,<sup>\*3</sup> J. Gibelin,<sup>\*7</sup> A. Giganon,<sup>\*3</sup> A. Gillibert,<sup>\*3</sup> K. Hasegawa,<sup>\*8,\*2</sup> T. Isebe,<sup>\*2</sup> Y. Kanaya,<sup>\*9,\*2</sup> S. Kawakami,<sup>\*9,\*2</sup> D. Kim,<sup>\*10,\*2</sup> Y. Kiyokawa,<sup>\*1</sup> M. Kobayashi,<sup>\*1</sup> N. Kobayashi,<sup>\*11</sup> T. Kobayashi,<sup>\*8,\*2</sup> Y. Kondo,<sup>\*12,\*2</sup> Z. Korkulu,<sup>\*13,\*2</sup> S. Koyama,<sup>\*11,\*2</sup> V. Lapoux,<sup>\*3,\*2</sup> Y. Maeda,<sup>\*9</sup> F. M. Marqués,<sup>\*7</sup> T. Motobayashi,<sup>\*2</sup> T. Miyazaki,<sup>\*11</sup> T. Nakamura,<sup>\*12,\*2</sup> N. Nakatsuka,<sup>\*14,\*2</sup> Y. Nishio,<sup>\*15,\*2</sup> A. Obertelli,<sup>\*3,\*2</sup> A. Ohkura,<sup>\*15,\*2</sup> N. A. Orr,<sup>\*7</sup> S. Ota,<sup>\*1</sup> H. Otsu,<sup>\*2</sup> T. Ozaki,<sup>\*12,\*2</sup> V. Panin,<sup>\*2</sup> S. Paschalis,<sup>\*4</sup> E. C. Pollacco,<sup>\*3</sup> S. Reichert,<sup>\*16</sup> J. -Y. Roussé,<sup>\*3</sup> A. T. Saito,<sup>\*12,\*2</sup> S. Sakaguchi,<sup>\*15,\*2</sup> M. Sako,<sup>\*2</sup> C. Santamaria,<sup>\*3,\*2</sup> M. Sasano,<sup>\*2</sup> H. Sato,<sup>\*2</sup> M. Shikata,<sup>\*12,\*2</sup> Y. Shimizu,<sup>\*2</sup> Y. Shindo,<sup>\*15,\*2</sup> L. Stuhl,<sup>\*2</sup> T. Sumikama,<sup>\*8,\*2</sup> M. Tabata,<sup>\*15,\*2</sup> Y. Togano,<sup>\*12,\*2</sup> J. Tsubota,<sup>\*12,\*2</sup> T. Uesaka,<sup>\*2</sup> Z. H. Yang,<sup>\*2</sup> J. Yasuda,<sup>\*15,\*2</sup> K. Yoneda,<sup>\*2</sup> and J. Zenihiro<sup>\*2</sup>

Dineutron is a hypothetical bound state of two neutrons in a nuclear medium and spatially localized pair, which is different from the one obtained via the BCS mechanism.<sup>1)</sup> The neutron-neutron correlation from the dineutron is expected to appear in various circumstances such as the surface of weakly bound neutron-rich systems and inner crust of the neutron stars. With the advent of RI beam facilities, extended experimental studies on the dineutron correlation on  $^{11}\text{Li}$  have been conducted such as  $E1$  strength measurement using the Coulomb breakup reaction<sup>2)</sup> and neutron momentum measurement using the carbon-induced knockout reaction.<sup>3)</sup> Dineutron correlation has been experimentally indicated through the smaller opening angle of two neutrons with respect to the core but its signature was integrated over the whole volume or limited region of the system owing to the methodology.<sup>4)</sup> The kinematically complete measurement of the quasi-free  $(p, pn)$  reaction was thus performed with  $^{11}\text{Li}$ ,  $^{14}\text{Be}$ , and  $^{17,19}\text{B}$  to obtain the correlation angle  $\theta_{nf}$  as well as the missing momentum  $k$ , which provides radial information about the neutron in its initial state.

The measurement was performed at RIBF using the SAMURAI spectrometer.<sup>5)</sup> For higher statistics, the 15-cm-thick liquid hydrogen target MINOS<sup>6)</sup> was used with a 200 kpps  $^{11}\text{Li}$  beam. The  $(p, pn)$  setup composed of the neutron detector WINDS,<sup>7)</sup> recoil proton detector, and gamma-ray detector array DALI2<sup>8)</sup> was newly configured to realize the kinematically complete

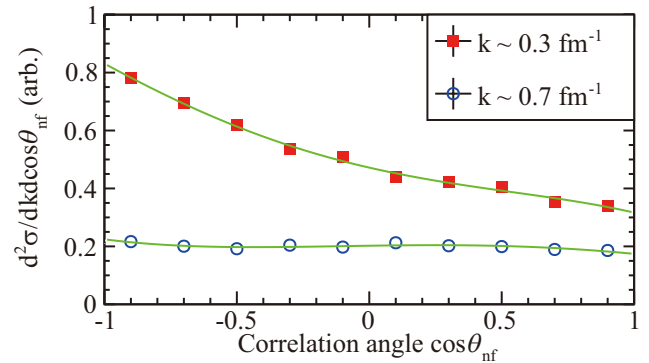


Fig. 1.  $\cos \theta_{nf}$  dependence of the double differential cross-section for each missing momentum  $k$ . The horizontal and vertical axes show the correlation angle and double differential cross-section, respectively. Each spectrum is scaled for the comparison. Errors are smaller than the symbols.

measurement.

Figure 1 shows the  $\cos \theta_{nf}$  dependence of the double differential cross-section at  $k \sim 0.3$  and  $0.7 \text{ fm}^{-1}$ , corresponding to the outer and inner part of  $^{11}\text{Li}$ , respectively. The figure exhibits apparent  $k$ -dependence of the correlation angle. The large negative slope at  $k \sim 0.3 \text{ fm}^{-1}$  is the signature of the dineutron correlation in this region. The slope is almost flat at  $k \sim 0.7 \text{ fm}^{-1}$ , indicating a weak correlation. This result reveals that the dineutron correlation is favored in the outer region of  $^{11}\text{Li}$ , which is qualitatively consistent with the theoretical predictions.<sup>1)</sup>

<sup>\*1</sup> Center for Nuclear Study, University of Tokyo

<sup>\*2</sup> RIKEN Nishina Center

<sup>\*3</sup> CEA, Saclay

<sup>\*4</sup> Department of Physics, Technische Universität Darmstadt

<sup>\*5</sup> Department of Physics, Peking University

<sup>\*6</sup> IPN Orsay

<sup>\*7</sup> LPC Caen

<sup>\*8</sup> Department of Physics, Tohoku University

<sup>\*9</sup> Department of Applied Physics, University of Miyazaki

<sup>\*10</sup> Department of Physics, Ehwa Womans University

<sup>\*11</sup> Department of Physics, University of Tokyo

<sup>\*12</sup> Department of Physics, Tokyo Institute of Technology

<sup>\*13</sup> MTA Atomki

<sup>\*14</sup> Department of Physics, Kyoto University

<sup>\*15</sup> Department of Physics, Kyushu University

<sup>\*16</sup> Department of Physics, Technische Universität München

## References

- 1) A. B. Migdal, Soviet J. Nucl. Phys. **16**, 238 (1973).
- 2) T. Nakamura *et al.*, Phys. Rev. Lett. **96**, 252502 (2006).
- 3) H. Simon *et al.*, Phys. Rev. Lett. **83**, 496 (1999).
- 4) Y. Kikuchi *et al.*, Prog. Theor. Exp. Phys. **2016** 103D03 (2016).
- 5) T. Kobayashi *et al.*, Nucl. Instrum. Methods Phys. Res. B **317**, 294 (2013).
- 6) A. Obertelli *et al.*, Eur. Phys. J. A **50**, 8 (2014).
- 7) J. Yasuda *et al.*, Nucl. Instrum. Methods Phys. Res. B **376**, 393 (2016).
- 8) S. Takeuchi *et al.*, Nucl. Instrum. Methods Phys. Res. A **763**, 596 (2014).

# Particle identification of light charged particle by S $\pi$ RIT-TPC in Sn-Sn isotopic reactions

M. Kaneko,<sup>\*1,\*2</sup> J. Barney,<sup>\*2,\*3</sup> G. Cerizza,<sup>\*2,\*3</sup> J. Estee,<sup>\*2,\*3</sup> W. G. Lynch,<sup>\*3</sup> T. Isobe,<sup>\*2</sup> G. Jhang,<sup>\*2,\*3</sup>  
 M. Kurata-Nishimura,<sup>\*2</sup> P. Lasko,<sup>\*5,\*2</sup> J. Łukasik,<sup>\*5</sup> T. Murakami,<sup>\*1,\*2</sup> P. Pawłowski,<sup>\*5,\*2</sup> C. Santamaria,<sup>\*2,\*7</sup>  
 M. B. Tsang,<sup>\*3</sup> J. W. Lee,<sup>\*4,\*2</sup> and Y. Zhang<sup>\*6,\*2</sup> for the S $\pi$ RIT collaboration

The nuclear equation of state (EOS) is one of the most attractive subjects in nuclear physics and astrophysics. Intermediate energetic heavy ion collisions (HIC) with high isospin asymmetry provide us critical knowledge to constrain the density dependence of the symmetry energy, which contributes to the asymmetric nuclear EOS. Various types of models have predicted that the spectrum of  $\pi^-/\pi^+$  from HIC has a high sensitivity to the symmetry energy;<sup>1,2)</sup> however, the lack of experimental data and the model dependence are still a problem. At intermediate energies, since the  $\pi$  meson production is dominated by the decay of the  $\Delta$  resonance state, which is excited from the inelastic nucleon-nucleon scattering, nucleon dynamics in the participant region indirectly influences the final yield of  $\pi$  mesons. Recent progress in calculations based on AMD shows that the cluster correlation alters the nucleon dynamics and has a considerable influence on the final yield of  $\pi^-/\pi^+$  as well as the sensitivity of the symmetry energy.<sup>3)</sup> Therefore, precise information on the cluster production in HIC is desired. In order to estimate the relative production rate of light clusters emitted from Sn-Sn reactions at 270 MeV per nucleon,<sup>4)</sup> mass evaluation for the light charged particles is ongoing, which will be described in this report.

The SAMURAI Pion Reconstruction and Ion Tracker Time Projection Chamber<sup>5)</sup> was placed into the gap of the SAMURAI dipole magnet at 0.5 T, which allows us to measure the energy deposit per unit length ( $dE/dx$ ) and the magnetic rigidity of the charged particles individually. In order to calibrate  $dE/dx$  and to estimate the resolution of particle identification, the numerical mass is calculated as follows. The mean  $dE/dx$  for relativistic charged particles in a material is described well by the Bethe equation,<sup>6)</sup>  $-\langle dE/dx \rangle = f_{\text{Bethe}}(\beta)$ , where  $\beta$  is the velocity of the incident particle. Furthermore,  $\beta^2 = (zR)^2/(m^2 + (zR)^2)$ , where  $z$  is the charge, and  $R$  and  $m$  are the rigidity and mass, respectively. If the experimental locus of  $dE/dx$  and the rigidity for a certain particle species can be fit by  $g(\beta) = a \times f_{\text{Bethe}}(\beta) + b$  with fixed  $z$  and  $m$  (for an example of proton,  $z = 1$  and  $m = 938.272 \dots \text{ MeV}/c^2$ ), the empirical  $dE/dx$  calculator is obtained. Finally, by solving the equation

$$(dE/dx)_{\text{measured}} - (a \times f_{\text{Bethe}}(\beta) + b) = 0 \quad (1)$$

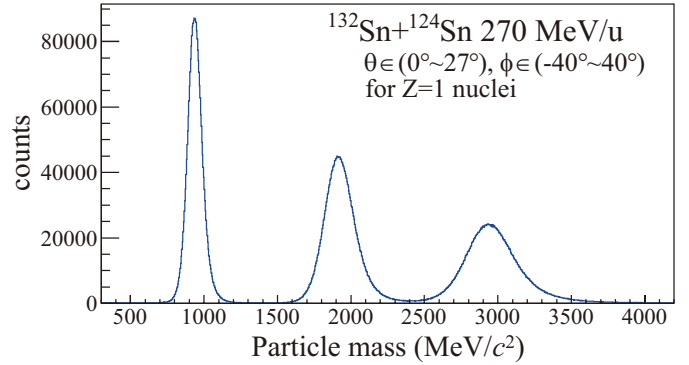


Fig. 1. Mass spectrum calculated from  $dE/dx$  and rigidity by using Eq. (1).  $\theta$  and  $\phi$  are polar and azimuthal angles in the laboratory frame, respectively.

in terms of mass with  $z$  for a certain particle and the obtained coefficients  $a$  and  $b$ , we can calculate the mass from the measured  $dE/dx$  and rigidity. Figure 1 shows the mass spectrum calculated by Eq. (1) for a restricted angle, where the coefficients  $a$  and  $b$  are obtained by fitting the proton locus of  $dE/dx$  and rigidity. The protons, deuterons, and tritons are well resolved, but the peak positions are slightly shifted for deuterons and tritons since only the proton locus is considered for the fitting.

In Ref. 6), a highly-skewed Landau distribution is introduced to calculate the energy loss, which considers the fluctuations of the energy loss during interactions with a thin absorber material. Investigation on the resolution using Landau formula is also ongoing.

This work is supported by the Japanese MEXT KAKENHI Grant No. 24105004, the U.S. DOE under Grant Nos. DE-SC0004835, DE-SC0014530, DE-NA0002923, the U.S. NSF Grant No. PHY-1565546, and the Polish NSC Grant Nos. UMO-2013/09/B/ST2/04064 and UMO-2013/10/M/ST2/00624. The computing resources for analyzing the data were provided by the HOKUSAI system at RIKEN.

## References

- 1) B. A. Li *et al.*, Phys. Rev. C **71**, 014608 (2005).
- 2) M. B. Tsang *et al.*, Phys. Rev. C **95**, 044614 (2017).
- 3) N. Ikeno *et al.*, Phys. Rev. C **97**, 069902 (2018).
- 4) J. Barney *et al.*, RIKEN Accel. Prog. Rep. **50**, 49 (2017).
- 5) R. Shane *et al.*, Nucl. Instrum. Methods Phys. Res. A **784**, 513 (2015).
- 6) <http://pdg.lbl.gov/2018/reviews/rpp2018-rev-passage-particles-matter.pdf>.

<sup>\*1</sup> Department of Physics, Kyoto University  
<sup>\*2</sup> RIKEN Nishina Center  
<sup>\*3</sup> NSCL and Dept. of Phys. & Ast., Michigan State University  
<sup>\*4</sup> Department of Physics, Korea University  
<sup>\*5</sup> Institute of Nuclear Physics, PAN  
<sup>\*6</sup> Department of Physics, Tsinghua University  
<sup>\*7</sup> Lawrence Verkeley National Laboratory, UC Verkeley

## Recent results of collective flow for S $\pi$ RIT-TPC experiment

M. Kurata-Nishimura,<sup>\*1</sup> J. Barney,<sup>\*2,\*1</sup> G. Cerizza,<sup>\*2,\*1</sup> J. Estee,<sup>\*2,\*1</sup> B. Hong,<sup>\*3</sup> T. Isobe,<sup>\*1</sup> G. Jhang,<sup>\*2,\*1</sup> M. Kaneko,<sup>\*4,\*1</sup> H. S. Lee,<sup>\*7</sup> J. W. Lee,<sup>\*3,\*1</sup> J. Łukasik,<sup>\*5</sup> W. G. Lynch,<sup>\*2</sup> A. B. McIntosh,<sup>\*8</sup> T. Murakami,<sup>\*4,\*1</sup> P. Pawłowski,<sup>\*5,\*1</sup> H. Sakurai,<sup>\*1</sup> C. Santamaria,<sup>\*2,\*1</sup> R. Shane,<sup>\*2</sup> D. Suzuki,<sup>\*1</sup> M. B. Tsang,<sup>\*2</sup> and S. J. Yennello<sup>\*8</sup> for S $\pi$ RIT Collaboration

The SAMURAI Pion-Reconstruction and Ion-Tracker-Time-Projection Chamber (S $\pi$ RIT-TPC)<sup>1)</sup> project aims to constrain a nuclear equation of state (EoS) at supra-saturation density using heavy ion collisions. The S $\pi$ RIT-TPC was designed to measure  $\pi^-/\pi^+$  production ratio depending on isospin asymmetry. Since the pions are expected to be produced through the  $\Delta$  resonance formation,  $\pi^-/\pi^+$  ratio is related to some kind of neutron-to-proton squared ratio which is then supposed to be sensitive to the symmetry energy at high densities.<sup>3)</sup>

Additionally, measurements of collective flow with proton and neutron are proposed as a useful probe<sup>2)</sup> to nuclear EOS, because neutrons are repelled from dense region as a result of the repulsive isospin symmetry potential with increase of density, while protons are opposite.

The first experiment had been performed in April 2016 with <sup>132</sup>Sn and <sup>108</sup>Sn beams at 270 MeV/nucleon on <sup>112</sup>Sn and <sup>124</sup>Sn targets at SAMURAI in RIBF. Neutrons were detected by NeuLAND<sup>4)</sup> covering the mid-rapidity region. In this paper, recent results of the collective flow for proton and neutron will be discussed.

A track reconstruction was done using S $\pi$ RITROOT software and particle identification ability is discussed in Ref. 5).

An orientation angle of reaction plane,  $\Psi$  was determined with summing up a transverse momentum of light charged fragments, p, d, t, <sup>3</sup>He, and <sup>4</sup>He event by event, as following.

$$\vec{Q} = \begin{pmatrix} Q \cos \Psi \\ Q \sin \Psi \end{pmatrix} = \sum_{k=1}^N \omega_k \begin{pmatrix} \cos \phi_k \\ \sin \phi_k \end{pmatrix} \quad (1)$$

$$\omega_k = \begin{cases} 1 & \text{if rapidity in the center of mass} > 0 \\ -1 & \text{otherwise} \end{cases}$$

Since the distribution of  $\Psi$  was distorted due to a rectangular shape of S $\pi$ RIT-TPC, it was corrected applying a re-centering and a shifting method.<sup>6)</sup> The azimuthal angle distributions with respect to  $\Psi$  were plotted for protons measured with <sup>132</sup>Sn + <sup>124</sup>Sn in Fig. 1. In these plots,  $\Psi$  was determined with all light fragments excluding itself to avoid auto correlation. Red lines shows fitting results with a formula

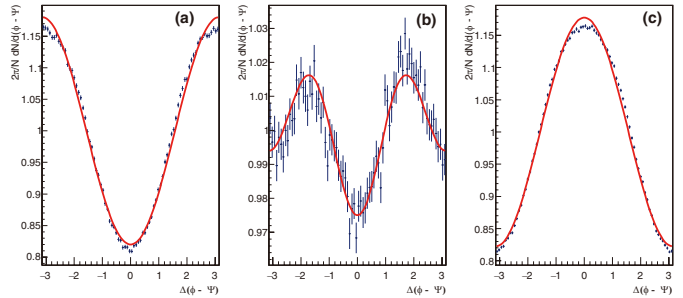


Fig. 1. Azimuthal angle distributions of proton with respect to  $\Psi$ . The rapidity coverages in the center of mass are (a) target-rapidity:  $-4.0 \sim -0.06$ , (b) mid-rapidity:  $-0.06 \sim 0.06$ , and (c) Beam-rapidity:  $0.06 \sim 4.0$ . Red lines indicate fitting with Eq. (2).

$$\frac{2\pi}{N} \frac{dN}{d\phi} = 1 + 2v_1 \cos(\phi) + 2v_2 \cos(2\phi) + \dots \quad (2)$$

The negative and positive  $v_1$  were observed in the target (a) and beam rapidity region (c), which is the evidence of directed flow. The negative  $v_2$  was observed in the mid rapidity region (b), which indicates out-of-plane elliptic flow of protons. The strength of  $v_1$  and  $v_2$  are needed to be corrected with a reaction plane resolution to compare between <sup>132</sup>Sn + <sup>124</sup>Sn and <sup>108</sup>Sn + <sup>112</sup>Sn collisions. Neutron's collective flow was also observed within a limited acceptance. Simulation and further analysis are necessary to extract EoS information. Addition to neutron to proton ratio, <sup>3</sup>H to <sup>3</sup>He analysis is ongoing, which is expected to serve in resolving ambiguities caused by the effective-mass splitting between neutrons and proton.

This work is supported by the U.S. Department of Energy under Grant Nos. DE-SC0004835, DE-SC0014530, DE-NA0002923, US National Science Foundation Grant No. PHY-1565546, the Japanese MEXT KAKENHI (Grant-in-Aid for Scientific Research on Innovative Areas) grant No. 24105004, and the Polish National Science Center (NCN), under contract Nos. UMO-2013/09/B/ST2/04064 and UMO-2013/10/M/ST2/00624.

### References

- 1) R. Shane *et al.*, Nucl. Instrum. Methods Phys. Res. A **784**, 513 (2015).
- 2) B. -A. Li *et al.*, Phys. Rev. Lett. **85**, 4221 (2000).
- 3) N. Ikeno *et al.*, Phys. Rev. C **97**, 069902 (2018).
- 4) NeuLAND Technical Design Report, <http://www.fair-center.eu/fileadmin/fair/experiments/NUSTAR/Pdf/TDRs/NeuLAND-TDR-Web.pdf>, accessed: 2016/01/21.
- 5) M. Kaneko *et al.*, in this report.
- 6) J. -Y. Ollitrault *et al.*, Nucl. Phys. A **638**, 195c (1998).

<sup>\*1</sup> RIKEN Nishina Center

<sup>\*2</sup> NSCL and Dept. of Phys. & Ast., Michigan State University

<sup>\*3</sup> Department of Physics, Korea University

<sup>\*4</sup> Department of Physics, Kyoto University

<sup>\*5</sup> IFJ PAN

<sup>\*6</sup> Faculty of Physics, Astronomy and Applied Computer Science, Jagiellonian University

<sup>\*7</sup> Rare Isotope Science Project, Institute for Basic Science

<sup>\*8</sup> Cyclotron Institute, Texas A&M University

## New implant-decay correlation method for $\beta$ -delayed neutron emission measurements with the BRIKEN setup

O. Hall,<sup>\*1</sup> A. Estrade,<sup>\*2,\*3</sup> J. Liu,<sup>\*4</sup> G. Lorusso,<sup>\*3,\*5</sup> K. Matsui,<sup>\*3</sup> F. Montes,<sup>\*6</sup> N. Nepal,<sup>\*2</sup> S. Nishimura,<sup>\*3</sup> V. H. Phong,<sup>\*3,\*7</sup> J. Agramunt,<sup>\*8</sup> D. S. Ahn,<sup>\*3</sup> A. Algora,<sup>\*8</sup> H. Baba,<sup>\*3</sup> S. Bae,<sup>\*9</sup> N. T. Brewer,<sup>\*10</sup> C. G. Bruno,<sup>\*1</sup> R. Cabellero-Folch,<sup>\*11</sup> F. Calvino,<sup>\*12</sup> T. Davinson,<sup>\*1</sup> I. Dillmann,<sup>\*11</sup> C. Domingo-Pardo,<sup>\*8</sup> S. Go,<sup>\*13</sup> C. J. Griffin,<sup>\*1</sup> R. Grzywacz,<sup>\*10,\*13</sup> T. Isobe,<sup>\*3</sup> D. Kahl,<sup>\*1</sup> G. Kiss,<sup>\*3</sup> S. Kubono,<sup>\*3</sup> M. Labiche,<sup>\*14</sup> A. I. Morales,<sup>\*8</sup> B. C. Rasco,<sup>\*10</sup> K. P. Rykaczewski,<sup>\*10</sup> H. Sakurai,<sup>\*3</sup> Y. Shimizu,<sup>\*3</sup> T. Sumikama,<sup>\*3</sup> H. Suzuki,<sup>\*3</sup> H. Takeda,<sup>\*3</sup> J. L. Tain,<sup>\*8</sup> A. Tarifeño-Saldivia,<sup>\*12</sup> A. Tolosa-Delgado,<sup>\*8</sup> P. J. Woods,<sup>\*1</sup> R. Yokoyama,<sup>\*11</sup> for the BRIKEN collaboration

With the observation of a binary neutron-star merger accompanied by the spectroscopic identification of  $r$ -process nucleosynthesis<sup>1)</sup> taking place in 2017, there have been major developments in identifying a site of the  $r$ -process. These new observations will increase the demand for precise nuclear data that is necessary to reach a clearer understanding of the  $r$ -process mechanisms thought to be occurring in these environments.

In June 2017, an experiment was performed to study the decay properties of the  $\beta$ -delayed neutron emitters in the mass region  $A = 130$  near the doubly magic nucleus  $^{132}\text{Sn}$ . The active-stopper array AIDA<sup>2)</sup> was placed at F11 with the nuclei of interest being implanted and detected alongside their subsequent decays in the silicon detector stack. Neutrons emitted from the  $\beta$ -decay of the implanted ions were detected by the BRIKEN neutron counter array<sup>3,4)</sup> surrounding AIDA. The neutron counter array consisted of 140 gas-filled  $^3\text{He}$  counters, which were held inside a large moderation block made of high-density polyethylene.

In carrying out analysis on the data, a new method of correlating beta events with implanted ions was developed. As the detectors that comprise the AIDA detector stack are double-sided silicon strip detectors (DSSDs), positional information of both high energy implant and low energy decay events is obtained. With  $\beta$ -decay energies of 100 s of keV and a narrow strip pitch of  $560\ \mu\text{m}$ , decay events will be spread across multiple strips. This results in a trade-off between detection efficiency and a background from electronic

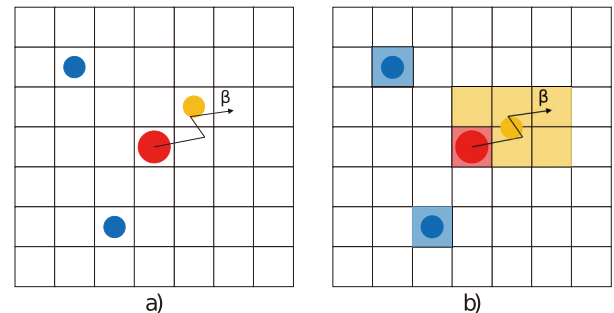


Fig. 1. Comparison between the old correlation method (a) and the new method (b). In both images the red circle indicates an implant particle, the orange circle a beta particle and the blue circles as noise events.

noise for low energy signals, which is sensitive to the detection threshold and the correlation method.

In previous experiments single points have been assigned to the location of the implants and betas with correlation performed based upon the beta points that fall within an area around the implant signal, typically a  $7 \times 7$  pixel square shown in Fig. 1 a). The new method instead takes into account all of the strips that fire during an event and assigns an area for both implant and decay signals. Correlations can then be performed by searching for an overlap between the areas of the beta and implant events as shown in Fig. 1 b). This new method has been shown to reduce the amount of noise correlated with implants whilst maintaining the beta-detection efficiency of the previous method, as noise events that would otherwise fall within the  $7 \times 7$  area will now be rejected.

The data analysis for the experiment is ongoing. The data shows the potential of the BRIKEN setup to extend the systematics of  $\beta$ -delayed neutron emission probabilities along the  $N = 82$  and  $Z = 50$  shell closures south and east of  $^{132}\text{Sn}$ . The results will improve the reliability of nuclear data for  $r$ -process models.

### References

- 1) E. Pian *et al.*, *Nature* **551**, 67–70 (2017).
- 2) C. J. Griffin *et al.*, *Proc. XIII Nuclei in the Cosmos* **1**, 97 (2014).
- 3) A. Tarifeño-Saldivia *et al.*, *J. Instrum.* **12**, 04006 (2017).
- 4) B. C. Rasco *et al.*, *Nucl. Instrum. Methods Phys. Res.* **911**, 78–86 (2018).

\*1 School of Physics and Astronomy, University of Edinburgh  
 \*2 College of Science and Engineering, Central Michigan University  
 \*3 RIKEN Nishina Center  
 \*4 Department of Physics, The University of Hong Kong  
 \*5 National Physics Laboratory  
 \*6 NSCL and Department of Physics and Astronomy, Michigan State University  
 \*7 Faculty of Physics, VNU Hanoi University of Science  
 \*8 Instituto de Física Corpuscular  
 \*9 Department of Physics, Seoul National University  
 \*10 Oak Ridge National Laboratory  
 \*11 TRIUMF  
 \*12 Universitat Politècnica de Catalunya  
 \*13 Department of Physics and Astronomy, University of Tennessee  
 \*14 STFC Daresbury Laboratory

## Progress on the measurements of $P_n$ -values and half-lives for understanding the formation of the r-process rare-earth peak

A. Tarifeño-Saldivia,<sup>\*1</sup> G. G. Kiss,<sup>\*2</sup> J. L. Tain,<sup>\*3</sup> A. Estrade,<sup>\*4</sup> J. Agramunt,<sup>\*3</sup> T. Davinson,<sup>\*5</sup> I. Dillmann,<sup>\*10</sup> N. Fukuda,<sup>\*6</sup> R. Grzywacz,<sup>\*9</sup> O. Hall,<sup>\*5</sup> A. I. Morales,<sup>\*3</sup> A. Navarro,<sup>\*1</sup> N. Nepal,<sup>\*4</sup> S. Nishimura,<sup>\*6</sup> K. P. Rykaczewski,<sup>\*7</sup> N. T. Szegedi,<sup>\*2</sup> A. Sveiczer,<sup>\*2</sup> A. Tolosa-Delgado,<sup>\*3</sup> P. Vi,<sup>\*8</sup> R. Yokoyama<sup>\*9</sup> for the BRIKEN collaboration<sup>\*11</sup>

The Rare Earth Peak (REP) is a small, but clearly distinctive, peak around mass  $A \sim 160$  in the elemental solar system abundances created by the rapid neutron-capture process (r-process). In contrast to the r-process abundance peaks associated with neutron shell closures (*e.g.*  $A \sim 130, 195$ ), which are formed during the  $(n, \gamma) \leftrightarrow (\gamma, n)$  equilibrium, the REP is formed later after the neutron exhaustion. Thus, the understanding of the REP formation offers a unique probe for the study of the late times environmental conditions in the r-process site. According to theoretical models,<sup>1)</sup> masses,  $\beta$ -decay rates,  $\beta$ -delayed neutron emission probabilities ( $P_n$ ) and the capture rates play a key role in the formation of the REP. The most influential nuclei to the REP formation have been determined by sensitivity studies to be the neutron-rich region with mass  $A \sim 160$  from Cs to Gd.<sup>2)</sup> The physical input for these sensitivity studies is based on current nuclear model calculations. Recently, several of the half-lives in the REP region have been measured by the EURICA collaboration at RIBF in the RIKEN Nishina Center.<sup>3)</sup> More recently, the largest and most efficient  $\beta$ -delayed neutron detector of its kind has been built by the BRIKEN collaboration,<sup>4)</sup> at the RIKEN Nishina Center, for a systematic study of the decay properties of the most exotic neutron-rich nuclei, including the REP nuclei, accessible currently by experimental means. A detailed description of the BRIKEN detector and the scientific program of the BRIKEN project is provided by Tain *et al.*<sup>5)</sup>

The NP1612-RIBF148 experiment make use of BRIKEN for the measurement of  $\beta$ -delayed neutron emission probabilities and half-lives in the REP nuclei region. The experiment has been allocated with 10 days of total beamtime. An exploratory experimental run (2.5 days in total) was carried out in 2017 with a setting centered on  $^{167}\text{Sm}$ , the heaviest most exotic accessible REP nuclei. This run has provided data for

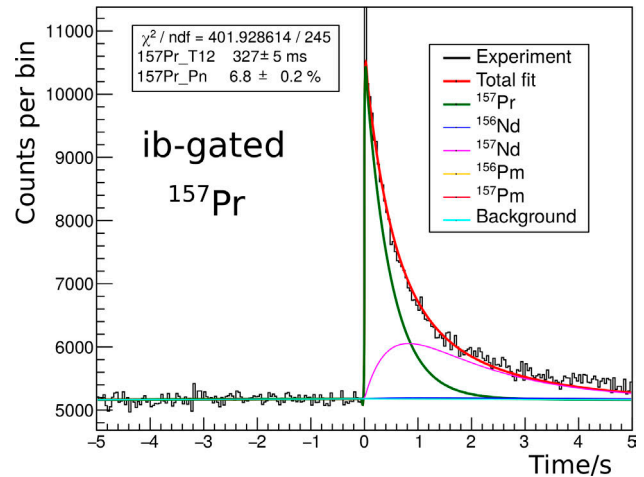


Fig. 1. Preliminary analysis from partial data for the  $\beta$ -decay for  $^{157}\text{Pr}$ .

measurement of some new half-lives in the region from Gd to Pm.<sup>6)</sup> However the statistics for precise measurement of  $P_n$ -values was rather poor. In 2018 a new experimental run has been carried using a total of 5.0 days of beamtime. The 2018 run has used a setting centered on  $^{165}\text{Pm}$ , providing data for measurement of  $P_n$ -values in the region from Ce to Eu. In Fig. 1 is presented the preliminary analysis of partial data for the case of  $^{157}\text{Pr}$ . The analysis make use of the approach developed by Tolosa-Delgado *et al.*<sup>7)</sup> for a consistent fit of parameters of the decay chain in implant- $\beta$ -gated and implant- $\beta$ -neutron-gated time correlation histograms. The preliminary analysis yielded a half-live of 327 ms, in agreement with the previous EURICA measurement (295 ms +10% -4%), and a new  $P_n$ -value of 6.8%.

In summary, three quarters of the allocated beamtime for the experiment have been completed. The coverage region of the experimental data from 2017 and 2018 runs, for measurement of the REP  $P_n$ -values and half-lives, extends from Ce to Gd nuclei. The detailed data analysis of this region is ongoing.

### References

- 1) A. Arcones *et al.*, Phys. Rev. C **83**, 045809 (2011).
- 2) M. R. Mumpower *et al.*, Phys. Rev. C **85**, 045801 (2012).
- 3) J. Wu *et al.*, Phys. Rev. Lett. **118**, 072701 (2017).
- 4) A. Tarifeño-Saldivia *et al.*, J. Instrum. **12**, P04006 (2017).
- 5) J. L. Tain *et al.*, Acta Phys. Pol. B **49**, 417–428 (2018).
- 6) A. Tarifeño-Saldivia *et al.*, RIKEN Accel. Prog. Rep. **51**, 55 (2018).
- 7) A. Tolosa-Delgado *et al.*, Nucl. Instrum. Methods Phys. Res. A **925**, 133–147 (2019).

<sup>\*1</sup> Universitat Politècnica de Catalunya (UPC)

<sup>\*2</sup> Institute for Nuclear Research (Atomki)

<sup>\*3</sup> Instituto de Física Corpuscular (IFIC)

<sup>\*4</sup> University College of Science and Engineering, Central Michigan University (CMU)

<sup>\*5</sup> School of Physics and Astronomy, University of Edinburgh

<sup>\*6</sup> RIKEN Nishina Center

<sup>\*7</sup> Oak Ridge National Laboratory

<sup>\*8</sup> Faculty of Physics, VNU University of Science

<sup>\*9</sup> Department of Physics and Astronomy, University of Tennessee

<sup>\*10</sup> TRIUMF

<sup>\*11</sup> [www.wiki.ed.ac.uk/display/BRIKEN/Home](http://www.wiki.ed.ac.uk/display/BRIKEN/Home)

# $\beta$ decays of the heaviest $N = Z - 1$ nuclei and proton instability of $^{97}\text{In}^\dagger$

J. Park,<sup>\*1,\*2</sup> R. Krücken,<sup>\*1,\*2</sup> D. Lubos,<sup>\*3,\*4,\*5</sup> R. Gernhäuser,<sup>\*3</sup> M. Lewitowicz,<sup>\*6</sup> S. Nishimura,<sup>\*4</sup> and H. Sakurai<sup>\*4,\*7</sup> for the EURICA Collaboration

Interesting nuclear structure phenomena can be observed at the limits of neutron or proton binding, providing sensitive probes of shell evolution and/or collective behaviors. Studies have found the doubly magic  $^{100}\text{Sn}$  to be stable against proton emission, confirming the robustness of the  $N, Z = 50$  shells. Searches for even more neutron-deficient nuclei below  $^{100}\text{Sn}$  resulted in a discovery of new isotopes, while also reaching the proton dripline for Rh and Ag isotopes.<sup>1)</sup>

From a decay spectroscopy experiment at the RIBF, half-lives,  $\beta$ -decay endpoint energies, and  $\beta$ -delayed proton emission branching ratios of  $N = Z - 1$  nuclei  $^{91}\text{Pd}$ ,  $^{95}\text{Cd}$ ,  $^{97}\text{In}$  and  $^{99}\text{Sn}$  were measured with the wide-range active silicon strip stopper array for  $\beta$  and ion detection<sup>2)</sup> (WAS3ABi). The results, summarized in Table 1, are consistent with  $\beta$  decays of mirror nuclei containing a mixture of Gamow-Teller and Fermi decay components.

The apparent stability of  $^{97}\text{In}$  against proton emission was investigated. Based on the deficit in the  $\beta$ -decay amplitude of the parent nucleus, an isomeric state in  $^{97}\text{In}$  decaying to  $^{96}\text{Cd}$  via one-proton emission was proposed. Although this decay branch has not been detected directly, the observation of a  $\gamma$ -ray transition belonging to the  $\beta$  decay of  $^{96}\text{Cd}$  was a supporting evidence for the proton-emitting isomer. The missing proton events were hypothesized to have occurred in a time range between the ions' flight through the BigRIPS and ZeroDegree separators ( $\sim 600$  ns) and the 600- $\mu\text{s}$  deadtime of WAS3ABi.

From the shell model perspective,  $^{97m}\text{In}$  is formed by promoting a  $\pi 1p_{1/2}$  proton into the  $\pi 0g_{9/2}$  orbital, leaving an unpaired proton in the  $\pi 1p_{1/2}$  orbital and resulting in a spin-parity of  $(1/2^-)$ . The large spin difference and parity change suppress a  $\gamma$ -ray decay branch to the  $(9/2^+)$  ground state. Experimental half-life limits on the isomer were converted into a hypothetical proton energy range through a theory on proton emission.<sup>3)</sup> As shown in Fig. 1, the lower angular momentum barrier for proton emission from the  $\pi 1p_{1/2}$  orbital compared to the  $\pi 0g_{9/2}$  orbital would facilitate proton emission from the isomer. This result is con-

Table 1. Half-lives,  $\beta$ -decay endpoint energies,  $\log ft$  values and  $\beta$ -delayed proton emission branching ratios of  $^{91}\text{Pd}$ ,  $^{95}\text{Cd}$ ,  $^{97}\text{In}$  and  $^{99}\text{Sn}$ .

Nucleus	$T_{1/2}$ (ms)	$Q_{EC}$ (MeV)	$\log ft$	$b_{\beta p}$ (%)
$^{91}\text{Pd}$	32(3)	11.8(22)	3.4(5)	$3.0^{+1.1}_{-0.9}$
$^{95}\text{Cd}$	32(3)	10.2(17)	3.1(5)	$4.5^{+1.2}_{-1.0}$
$^{97}\text{In}$	28(5)	10.0(30)	3.0(9)	$1.7^{+1.7}_{-0.8}$
$^{97m}\text{In}$	1.3–230 $\mu\text{s}$			
$^{99}\text{Sn}$	24(4)	14.7(36)	3.8(7)	$3.9^{+3.4}_{-1.7}$

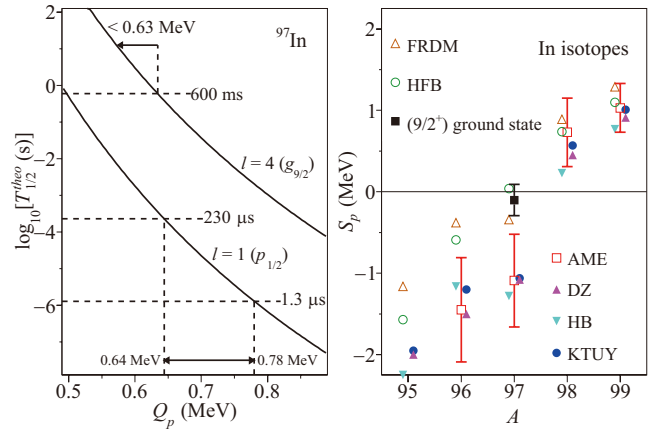


Fig. 1. Left: theoretical  $T_{1/2}$  as a function of emitted proton energy  $Q_p$  and orbital angular momentum  $l$ . Right: experimental proton separation energy  $S_p$  of the ground state of  $^{97}\text{In}$  compared with different mass predictions.<sup>4–9)</sup>

sistent with a few mass models which predict  $^{97}\text{In}$  to undergo  $\beta$  decay as opposed to proton emission.

## References

- 1) I. Čeliković *et al.*, Phys. Rev. Lett. **116**, 162501 (2016).
- 2) S. Nishimura, Prog. Theor. Exp. Phys. **2012**, 03C006 (2012).
- 3) D. S. Delion, R. J. Liotta, R. Wyss, Phys. Rep. **424**, 113 (2006).
- 4) J. Duflo, A. P. Zuker, Phys. Rev. C **52**, R23 (1995).
- 5) P. Möller, J. R. Nix, W. D. Myers, W. J. Swiatecki, At. Data Nucl. Data Tables **59**, 185 (1995).
- 6) S. Goriely, N. Chamel, J. M. Pearson, Phys. Rev. C **88**, 061302(R) (2013).
- 7) H. Koura, T. Tachibana, M. Uno, M. Yamada, Prog. Theor. Phys. **113**, 305 (2005).
- 8) M. Wang *et al.*, Chin. Phys. C **41**, 030003 (2017).
- 9) H. Herndl, B. A. Brown, Nucl. Phys. A **627**, 35 (1997).

<sup>†</sup> Condensed from the article in Phys. Rev. C **97**, 051301(R) (2018)

<sup>\*1</sup> Department of Physics and Astronomy, University of British Columbia

<sup>\*2</sup> TRIUMF

<sup>\*3</sup> Physik Department, Technische Universität München

<sup>\*4</sup> RIKEN Nishina Center

<sup>\*5</sup> Excellence Cluster Universe, Technische Universität München

<sup>\*6</sup> Grand Accélérateur National d'Ions Lourds (GANIL)

<sup>\*7</sup> Department of Physics, University of Tokyo

## Beta-gamma spectroscopy of neutron-rich $^{150}\text{Ba}^\dagger$

R. Yokoyama,<sup>\*1</sup> E. Ideguchi,<sup>\*2</sup> G. Simpson,<sup>\*3</sup> Mn. Tanaka,<sup>\*2</sup> S. Nishimura,<sup>\*4</sup> P. Doornenbal,<sup>\*4</sup>  
 P. -A. Söderström,<sup>\*4</sup> G. Lorusso,<sup>\*4</sup> Z. Y. Xu,<sup>\*5</sup> J. Wu,<sup>\*4,\*6</sup> T. Sumikama,<sup>\*7</sup> N. Aoi,<sup>\*2</sup> H. Baba,<sup>\*4</sup> F. Bello,<sup>\*8</sup>  
 F. Browne,<sup>\*9,\*4</sup> R. Daido,<sup>\*10</sup> Y. Fang,<sup>\*10</sup> N. Fukuda,<sup>\*4</sup> G. Gey,<sup>\*3,\*4,\*11</sup> S. Go,<sup>\*1,\*4</sup> N. Inabe,<sup>\*4</sup> T. Isobe,<sup>\*4</sup>  
 D. Kameda,<sup>\*4</sup> K. Kobayashi,<sup>\*12</sup> M. Kobayashi,<sup>\*1</sup> T. Komatsubara,<sup>\*13</sup> T. Kubo,<sup>\*4</sup> I. Kuti,<sup>\*14</sup> Z. Li,<sup>\*6</sup>  
 M. Matsushita,<sup>\*1</sup> S. Michimasa,<sup>\*1</sup> C. -B. Moon,<sup>\*15</sup> H. Nishibata,<sup>\*10</sup> I. Nishizuka,<sup>\*7</sup> A. Odahara,<sup>\*10</sup> Z. Patel,<sup>\*16,\*4</sup>  
 S. Rice,<sup>\*16,\*4</sup> E. Sahin,<sup>\*8</sup> L. Sinclair,<sup>\*17,\*4</sup> H. Suzuki,<sup>\*4</sup> H. Takeda,<sup>\*4</sup> J. Taprogge,<sup>\*18,\*19</sup> Zs. Vajta,<sup>\*14</sup>  
 H. Watanabe,<sup>\*20</sup> A. Yagi,<sup>\*10</sup> and T. Inakura<sup>\*21</sup>

Intruder orbitals due to the strong  $l \cdot s$  coupling in atomic nuclei can cause higher-order interactions, for example, octupole-deformed shapes energetically favored in certain nuclei. Octupole correlations ( $\lambda = 3$ ) are caused by the interactions between orbits with  $\Delta j = \Delta l = 3$ . Nuclei with  $Z$  or  $N = 34, 56, 88,$  and  $134$  possess such orbits at or close to the Fermi surface and are expected to have strong octupole correlations. Recently, static octupole deformation was reported in the  $Z \sim 88, N \sim 134$  (Ra) region by Gaffney *et al.*<sup>(2)</sup> and at  $Z \sim 56, N \sim 88$  (Ba) by Bucher *et al.*<sup>(3)</sup> However, the result that  $^{148}\text{Ba}$  may have strong octupole correlation as  $^{144}\text{Ba}$  does<sup>(4)</sup> raised a question whether  $^{150}\text{Ba}$  also possess strong octupole correlation.

Neutron-rich Ba ( $Z = 56$ ) isotopes were produced at RIBF and measured by means of  $\beta$ - $\gamma$  spectroscopy at the F11 focal plane of the ZeroDegree spectrometer. An active stopper, WAS3ABi,<sup>(5)</sup> and HPGe array, EURICA,<sup>(6)</sup> were used for  $\beta$ -ion correlation and  $\gamma$ -ray detection, respectively. The  $\gamma$ -ray spectrum of the  $^{150}\text{Cs}$  decay within 0.2 s after implantation is shown in Fig. 1. The estimated continuum background is overlaid. Two peaks at 100 and 597 keV were assigned as transitions in  $^{150}\text{Ba}$  after a log-likelihood ratio test requiring  $4\sigma$  significance. From the systematics of  $^{144}\text{--}^{148}\text{Ba}$ , the 100-keV and 597-keV  $\gamma$  rays were assigned as  $2_1^+ \rightarrow 0^+$  and  $3^- \rightarrow 2_1^+$  decay, which are also consistent with their intensities.

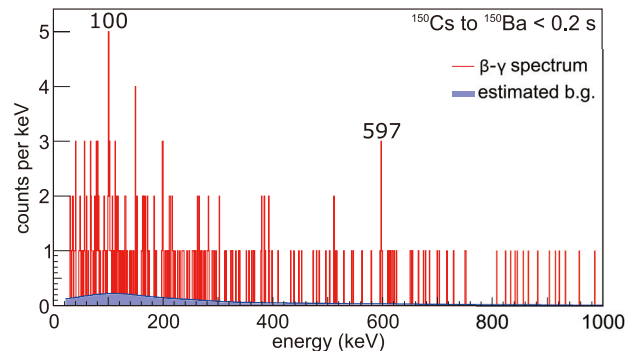


Fig. 1. A  $\gamma$ -ray spectrum from the  $\beta$  decay of  $^{150}\text{Cs}$ .

A calculation with the Hartree-Fock method and the random-phase approximation (RPA) was newly performed.<sup>(7,8)</sup> The calculation predicted that  $^{150}\text{Ba}$  has a large ground-state octupole deformation,  $\beta_{30} = 0.15$ , as those of the even-even  $A = 144$  to  $148$  isotopes. The RPA calculation predicted a  $J = 3$  excitation of  $^{150}\text{Ba}$  at 0.76 MeV, which may be the observed 697 keV state. The calculated state has  $B(E3) = 35$  W.u., indicating that the state is an octupole collective state rather than a single particle one.

In summary, the newly measured  $E(2_1^+)$  and possibly  $E(3^-)$  of  $^{150}\text{Ba}$  indicate that the quadrupole deformation of  $^{150}\text{Ba}$  is larger than that of  $^{148}\text{Ba}$ , and there may exist a negative-parity  $J = 3$  band with a large octupole collectivity. A newly performed HF-plus-RPA calculation predicted a static octupole deformation in the  $A = 140$  to  $150$  Ba isotopes and excited states with octupole collectivity at around 1 MeV. The results show that  $^{150}\text{Ba}$  has a large octupole collectivity and that the region of octupole correlations around  $Z = 56, N = 88$  may be wider than expected.<sup>(9,10)</sup>

### References

- 1) I. Ahmad *et al.*, Ann. Rev. Nucl. Pt. Sci. **43** 71 (1993).
- 2) L. P. Gaffney *et al.*, Nature **497**, 199 (2013).
- 3) B. Bucher *et al.*, Phys. Rev. Lett. **116**, 112503 (2016).
- 4) W. Urban *et al.*, Nucl. Phys. A **613**, 107 (1997).
- 5) S. Nishimura *et al.*, Prog. Theor. Exp. Phys. **2012**, 03C006 (2012).
- 6) P.-A. Söderström *et al.*, Nucl. Instrum. Methods Phys. Res. B **317**, 649 (2013).
- 7) T. Nakatsukasa *et al.*, Phys. Rev. C **76**, 024318 (2007).
- 8) T. Inakura *et al.*, Phys. Rev. C **80** 044301 (2009).
- 9) P. Möller *et al.*, At. Data Nucl. Data Tables **109**, 1 (2016).
- 10) S. E. Agbemava *et al.*, Phys. Rev. C **93**, 044304 (2016).

<sup>†</sup> Condensed from the article in Prog. Theor. Exp. Phys. **2018**, 041D02

<sup>\*1</sup> Center for Nuclear Study, The University of Tokyo

<sup>\*2</sup> Research Center for Nuclear Physics, Osaka University

<sup>\*3</sup> LPSC, Université Grenoble-Alpes, CNRS/IN2P3

<sup>\*4</sup> RIKEN Nishina Center

<sup>\*5</sup> Department of Physics, The University of Tokyo

<sup>\*6</sup> Department of Physics, Peking University

<sup>\*7</sup> Department of Physics, Tohoku University

<sup>\*8</sup> Department of Physics, University of Oslo

<sup>\*9</sup> School of Computing Engineering and Mathematics, University of Brighton

<sup>\*10</sup> Department of Physics, Osaka University

<sup>\*11</sup> ILL, Grenoble

<sup>\*12</sup> Department of Physics, Rikkyo University

<sup>\*13</sup> Department of Physics, University of Tsukuba

<sup>\*14</sup> MTA Atomki, Hungarian Academy of Science, Hungary

<sup>\*15</sup> Department of Display Engineering, Hoseo University

<sup>\*16</sup> Department of Physics, University of Surrey

<sup>\*17</sup> Department of Physics, University of York

<sup>\*18</sup> Instituto de Estructura de la Materia, CSIC

<sup>\*19</sup> Departamento de Física Teórica, Universidad Autónoma de Madrid

<sup>\*20</sup> Department of Physics, Beihang University

<sup>\*21</sup> Department of Physics, Niigata University

# Preliminary results on $\beta$ -decay of the $T_z = -1$ nucleus $^{66}\text{Se}$ at RIBF

P. Aguilera,<sup>\*1,\*2</sup> B. Rubio,<sup>\*2</sup> F. Molina,<sup>\*1</sup> J. Agramunt,<sup>\*2</sup> A. Algora,<sup>\*2</sup> V. Guadilla,<sup>\*2</sup> A. Montaner-Piza,<sup>\*2</sup> A. I. Morales,<sup>\*2</sup> S. E. A. Orrigo,<sup>\*2</sup> B. Blank,<sup>\*3</sup> P. Ascher,<sup>\*3</sup> M. Gerbaux,<sup>\*3</sup> T. Goigoux,<sup>\*3</sup> J. Giovinozzo,<sup>\*3</sup> S. Grévy,<sup>\*3</sup> T. Kurtukian Nieto,<sup>\*3</sup> C. Magron,<sup>\*3</sup> D. Nishimura,<sup>\*4</sup> J. Chiba,<sup>\*4</sup> H. Oikawa,<sup>\*4</sup> Y. Takei,<sup>\*4</sup> S. Yagi,<sup>\*4</sup> D. S. Ahn,<sup>\*5</sup> P. Doornenbal,<sup>\*5</sup> N. Fukuda,<sup>\*5</sup> N. Inabe,<sup>\*5</sup> G. Kiss,<sup>\*5</sup> T. Kubo,<sup>\*5</sup> S. Kubono,<sup>\*5</sup> S. Nishimura,<sup>\*5</sup> Y. Shimizu,<sup>\*5</sup> C. Sidong,<sup>\*5</sup> P. A. Söderström,<sup>\*5</sup> T. Sumikama,<sup>\*5</sup> H. Suzuki,<sup>\*5</sup> H. Takeda,<sup>\*5</sup> V. H. Phong,<sup>\*5</sup> J. Wu,<sup>\*5</sup> H. Sakurai,<sup>\*4,\*5</sup> Y. Fujita,<sup>\*6</sup> M. Tanaka,<sup>\*6</sup> W. Gelletly,<sup>\*2,\*7</sup> F. Diel,<sup>\*8</sup> D. Lubos,<sup>\*9</sup> G. de Angelis,<sup>\*10</sup> D. Napoli,<sup>\*10</sup> C. Borcea,<sup>\*11</sup> A. Boso,<sup>\*12</sup> R. B. Cakirli,<sup>\*13</sup> E. Ganioglu,<sup>\*13</sup> G. de France,<sup>\*14</sup> S. Go,<sup>\*15</sup> and K. Wimmer<sup>\*16</sup>

In this paper, the preliminary results of the analysis of the NP1112-RIBF82 experimental campaign are presented. The main goal of this study is the  $T_z = -1$   $^{66}\text{Se}$   $\beta$ -decay.

$^{66}\text{Se}$  was produced using a primary beam of  $^{78}\text{Kr}$  with 345 MeV/nucleon and a target of Be. The nuclei of interest were separated and identified at the BigRIPs mass separator by the  $\Delta E$ -ToF- $B\rho$  method (see Fig. 1 inset). The nuclei of interest were implanted in three Double-Sided Silicon Strip Detectors (DSSSDs) named WAS3ABi, surrounded by the EUROBALL-RIKEN Cluster Array<sup>1)</sup> (EURICA).

The  $\beta$  and  $\gamma$  spectra were obtained by the correlations between implants and decays within a  $\pm 400$  ms time

window. Backward correlation times were used to subtract random correlations. In Fig. 1, the  $\beta$  spectrum with background subtraction is shown. A similar procedure was applied to obtain the  $\gamma$ -spectrum, considering that EURICA was triggered by WAS3ABi. In Fig. 2 the  $\gamma$ -spectrum is shown.

We present here the first experimental results on the  $\beta$ -delayed gamma decay of  $^{66}\text{Se}$ . Two gamma lines were previously observed in the isomeric decay<sup>2)</sup> and in-beam study<sup>3)</sup> of  $^{66}\text{As}$ . They correspond to the gamma-deexcitation of two levels with  $J^\pi = 1^+$  and  $2^+$  at 836 keV and 964 keV energy respectively. Through our analysis, we could identify three additional levels by implant- $\gamma$  and implant- $\gamma$ - $\gamma$  correlation analysis (see Fig. 3).

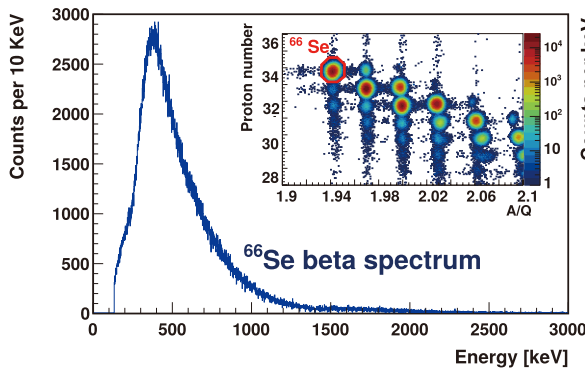


Fig. 1. Beta spectrum from  $^{66}\text{Se}$  decay with background subtracted and PID selection of  $^{66}\text{Se}$  implants identified by the BigRIPs mass separator.

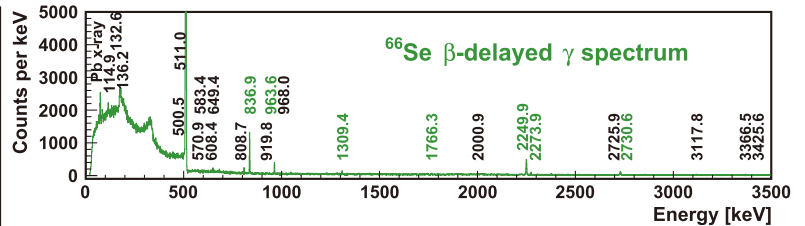


Fig. 2. Gamma spectrum following  $^{66}\text{Se}$  decay, background subtracted. In green,  $\gamma$  lines identified in  $^{66}\text{Se}$   $\beta$ -decay.

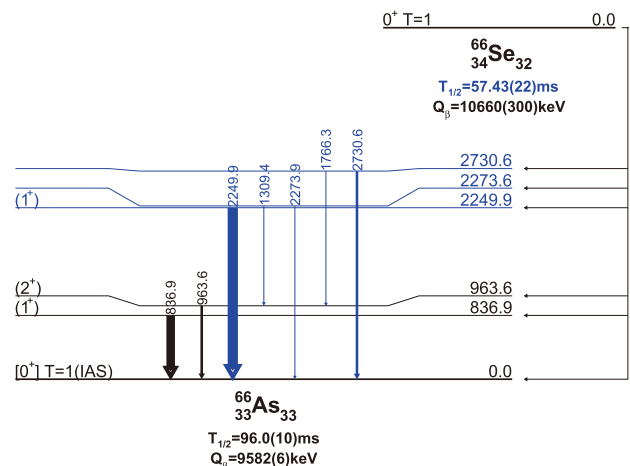


Fig. 3. (Color online) Preliminary level scheme for  $^{66}\text{Se}$  decay. Levels previously known in the literature are shown in black, blue lines correspond to this work.

\*1 Chilean Nuclear Energy Commission  
 \*2 IFIC, CSIC-Universidad de Valencia  
 \*3 Centre d'Etudes Nucléaires de Bordeaux-Gradignan  
 \*4 Department of Physics, Tokyo City University  
 \*5 RIKEN Nishina Center  
 \*6 Department of Physics, Osaka University  
 \*7 Department of Physics, Surrey University  
 \*8 Institute of Nuclear Physics, Universität zu Köln  
 \*9 Physics Department E-12, Technische Universität München  
 \*10 Istituto Nazionale di Fisica Nucleare, Laboratorio Nazionale di Legnaro  
 \*11 National Institute for Physics and Nuclear Engineering, IFIN-HH  
 \*12 Istituto Nazionale di Fisica Nucleare, Sezione di Padova  
 \*13 Department of Physics, Istanbul University  
 \*14 Grand Accélérateur National d'Ions Lourds  
 \*15 Department of Physics, Tennessee University  
 \*16 Atomki, Debrecen

## References

- 1) B. Rubio *et al.*, RIKEN Accel. Prog. Rep. **49**, 27 (2015).
- 2) R. Grzywacz *et al.*, Phys. Lett. B **429**, 247 (1998).
- 3) R. Grzywacz *et al.*, Nucl. Phys. A **682**, 41c (2001).

## Study of $\beta$ -decay of $^{71}\text{Kr}$

A. Sveiczler,<sup>\*1,\*2,\*3</sup> A. Algora,<sup>\*1,\*2</sup> A. I. Morales,<sup>\*1</sup> B. Rubio,<sup>\*1</sup> G. Kiss,<sup>\*2</sup> J. Agramunt,<sup>\*1</sup>  
 V. Guadilla,<sup>\*1</sup> A. Montaner-Pizá,<sup>\*1</sup> S. E. A. Orrigo,<sup>\*1</sup> A. Horváth,<sup>\*3</sup> G. de Angelis,<sup>\*4</sup> D. Napoli,<sup>\*4</sup> F. Recchia,<sup>\*5</sup>  
 S. Lenzi,<sup>\*5</sup> A. Boso,<sup>\*5</sup> S. Nishimura,<sup>\*6</sup> V. H. Phong,<sup>\*6</sup> J. Wu,<sup>\*6</sup> P. -A. Söderström,<sup>\*6</sup> T. Sumikama,<sup>\*6</sup> H. Suzuki,<sup>\*6</sup>  
 H. Takeda,<sup>\*6</sup> D. S. Ahn,<sup>\*6</sup> H. Baba,<sup>\*6</sup> P. Doornebal,<sup>\*6</sup> N. Fukuda,<sup>\*6</sup> N. Inabe,<sup>\*6</sup> T. Isobe,<sup>\*6</sup> T. Kubo,<sup>\*6</sup>  
 S. Kubono,<sup>\*6</sup> H. Sakurai,<sup>\*6</sup> Y. Shimizu,<sup>\*6</sup> C. Sidong,<sup>\*6</sup> B. Blank,<sup>\*7</sup> P. Ascher,<sup>\*7</sup> M. Gerbaux,<sup>\*7</sup>  
 T. Goigoux,<sup>\*7</sup> J. Giovinozzo,<sup>\*7</sup> S. Grévy,<sup>\*7</sup> T. Kurtukián Nieto,<sup>\*7</sup> C. Magron,<sup>\*7</sup> W. Gelletly,<sup>\*1,\*8</sup> Zs. Dombrádi,<sup>\*7</sup>  
 Y. Fujita,<sup>\*9</sup> M. Tanaka,<sup>\*9</sup> P. Aguilera,<sup>\*10</sup> F. Molina,<sup>\*10</sup> J. Eberth,<sup>\*11</sup> F. Diel,<sup>\*11</sup> D. Lubos,<sup>\*12</sup> C. Borcea,<sup>\*13</sup>  
 E. Ganioglu,<sup>\*14</sup> D. Nishimura,<sup>\*15</sup> H. Oikawa,<sup>\*15</sup> Y. Takei,<sup>\*15</sup> S. Yagi,<sup>\*15</sup> W. Korten,<sup>\*16</sup> G. de France,<sup>\*17</sup>  
 P. Davies,<sup>\*18</sup> J. Liu,<sup>\*19</sup> J. Lee,<sup>\*19</sup> T. Lokotko,<sup>\*19</sup> I. Kojouharov,<sup>\*20</sup> N. Kurz,<sup>\*20</sup> and H. Shaffner<sup>\*20</sup>

In this paper, we present the preliminary results of the analysis of the experiment NP1112-RIBF93, in particular, the ones related to our study of the  $\beta$ -decay of  $^{71}\text{Kr}$ . The main objective of the NP1112-RIBF93 experiment is to study p-n pairing and isospin-related features in the structure of  $^{70,71}\text{Kr}$  through their  $\beta$ -decays.

$^{71}\text{Kr}$  nuclei were produced in the fragmentation of a  $^{78}\text{Kr}$  primary beam with an energy of 345 MeV/nucleon. The high intensity beam provided by the accelerator complex of the RI Beam Factory (RIBF) enabled us to achieve primary beam currents around 40 pA. The primary beam impinged on a 5 mm thick Be target to produce a cocktail beam. After the separation and selection in the BigRIPS separator (see Fig. 1), the nuclei were implanted in the WAS3ABi active stopper, surrounded by the EURICA  $\gamma$ -ray spectrometer.<sup>1)</sup>

Standard  $\beta$ - $\gamma$  and  $\beta$ - $\gamma$ - $\gamma$  coincidence techniques were applied to study the  $\beta$ -decay of  $^{71}\text{Kr}$ . New  $\gamma$  transitions have been identified based on the comparisons between the half-lives obtained from implant- $\beta$ - $\gamma$  correlations and the half-life values determined from the corresponding correlations of previously identified  $\gamma$ -rays that belong to the  $^{71}\text{Kr}$  decay (198, 207 and 397-keV transitions). In total, 4 new  $\gamma$  transitions have been identified. After the identification of all  $\gamma$ -rays that belong to this decay,  $\gamma$ - $\gamma$  coincidences were also studied. A new half-life value was determined using the implant- $\beta$ - $\gamma$  time correlations with coincidence conditions on the strongest identified  $\gamma$ -rays of the decay. Several factors

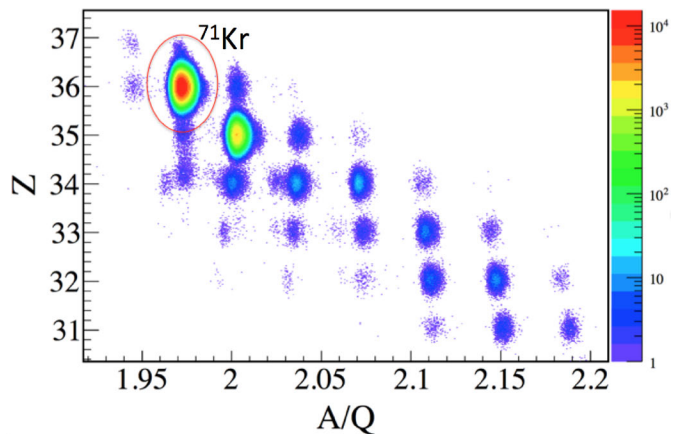


Fig. 1. Identification plot for the isotopes produced in  $^{78}\text{Kr}$  fragmentation for the  $^{71}\text{Kr}$  setting.

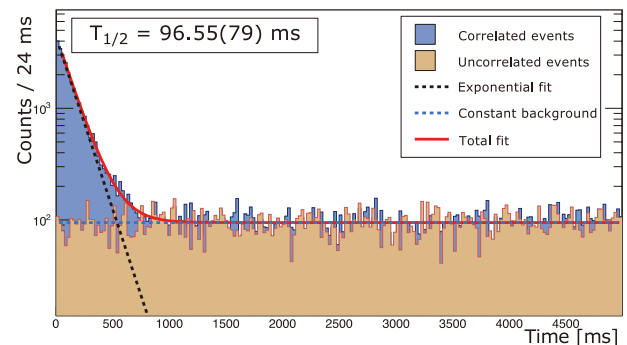


Fig. 2. Half-life of  $^{71}\text{Kr}$  determined in this work.

\*1 IFIC, CSIC-Univ. Valencia  
 \*2 MTA ATOMKI  
 \*3 ELTE-Budapest  
 \*4 INFN-Legnaro  
 \*5 INFN-Padova  
 \*6 RIKEN Nishina Center  
 \*7 CEN Bordeaux-Gradignan  
 \*8 Department of Physics, Surrey University  
 \*9 Osaka University  
 \*10 CCHEN  
 \*11 Institute of Nucl. Physics, Universität zu Köln  
 \*12 Physik Department, Technische Universität München  
 \*13 IFIN-HH, Bucarest  
 \*14 Department of Physics, University of Istanbul  
 \*15 Tokyo Univ. Sci.  
 \*16 IRFU, CEA, Université Paris-Saclay  
 \*17 GANIL-Caen  
 \*18 Department of Physics, York University  
 \*19 Department of Physics, University of Hong Kong  
 \*20 GSI

that can influence the quality of the fit and the final value were taken into account as in our previous  $^{70}\text{Br}$  study.<sup>2)</sup> Figure 2 shows the half-life of the  $^{71}\text{Kr}$  decay obtained with this method. The half-life obtained of  $T_{1/2} = 96.55(79)$  ms for this decay was significantly consistent with the previous measurements and it is the most precise value reported until now in the literature. Presently, a new decay scheme is being constructed. The analyses of the  $^{70,71}\text{Kr}$   $\beta$  and the possible  $^{71}\text{Kr}$  isomer decays are still in progress.

### References

- 1) S. Nishimura, Prog. Theor. Exp. Phys. 03C006 (2012).
- 2) A. I. Morales *et al.*, Phys. Rev. C **95**, 064327 (2017).

# Coexisting single-particle and octupole states in $^{133}\text{Sn}$

G. Simpson,<sup>\*1</sup> J. Keatings,<sup>\*2</sup> A. Jungclaus,<sup>\*3</sup> J. Taprogge,<sup>\*4</sup> S. Nishimura,<sup>\*5</sup> P. Doornenbal,<sup>\*5</sup> G. Lorusso,<sup>\*5</sup> P. -A. Söderström,<sup>\*5</sup> T. Sumikama,<sup>\*5</sup> J. Wu,<sup>\*5</sup> Z. Y. Xu,<sup>\*5</sup> T. Isobe,<sup>\*5</sup> H. Sakurai,<sup>\*5</sup> and the EURICA RIBF-85 collaboration<sup>\*5</sup>

The experimental study of single valence particle (hole) nuclei provides crucial experimental data for nuclear structure studies. In particular the energies of low-lying levels in these nuclei can provide the effective single-particle (hole) energies used in shell-model calculations.<sup>1)</sup> In experiment RIBF-85,<sup>1,2)</sup> which was part of the EURICA campaign, the single valence neutron nucleus  $^{133}\text{Sn}$  was studied following the  $\beta$ - and  $\beta$ -n decay of  $^{133,134}\text{In}$  parent nuclei. This has allowed the energies of several single-particle states to be verified and the  $\gamma$  decays of new levels observed. To date all single-particle states in the  $N = 82$ –126 valence shell have been directly experimentally identified in  $^{133}\text{Sn}$ , except the  $\nu i_{13/2}$  one.<sup>3–5)</sup> Furthermore the recent report of enhanced quadrupole and octupole strength in  $^{132}\text{Sn}$ <sup>6)</sup> allows searches for more complex states to be performed. The co-existence of spherical single-particle and collective states appears to be a ubiquitous feature of the nuclear landscape.

The high  $Q_\beta$  and  $Q_{\beta-n}$  values of 14135(60) keV and 11110(270) keV for the  $\beta$  and  $\beta$ -n decays of  $^{133,134}\text{In}$ , respectively, make them ideal for studying a wide range of states in  $^{133}\text{Sn}$ . The differing spins of the ground states of these nuclei [(9/2<sup>+</sup>) and (4<sup>-</sup> – 7<sup>-</sup>)] mean that levels with different spin ranges should be populated.

The experimental  $\gamma$ -ray spectrum obtained following the decay of selected and implanted  $^{133}\text{In}$  ions is presented in Fig. 1. Many transitions previously assigned to  $^{132}\text{Sn}$  are observed.<sup>7)</sup> A new  $\gamma$  decay of energy 1779 keV is assigned to  $^{133}\text{Sn}$  as this transition was observed following both the  $\beta$  decay of  $^{133}\text{In}$  and the  $\beta$ -n decay of  $^{134}\text{In}$ . The 1561-keV transition, previously reported in several experiments is confirmed.<sup>3–5)</sup> However, no evidence was found for the 513- and 854-keV  $\gamma$  decays of the  $\nu p_{3/2}$  and  $\nu p_{1/2}$  states from parent  $^{133}\text{In}$  nuclei.<sup>4)</sup> This shows that  $^{133}\text{In}$  was much more strongly populated in its  $\pi g_{9/2}^{-1}$  ground state, than the  $\pi p_{1/2}^{-1}$  long-lived isomer. The  $\gamma$  decay of the 854-keV  $\nu p_{3/2}$  state was however observed following the  $\beta$ -n decay of  $^{134}\text{In}$ .

The 1561-keV transition receives more than one third of the total feeding intensity following the  $\beta$ -n decay of  $^{134}\text{In}$ . The weak population of the 1779-keV state in  $^{133}\text{Sn}$  following  $\beta$ -n decay means that it may have a positive parity.

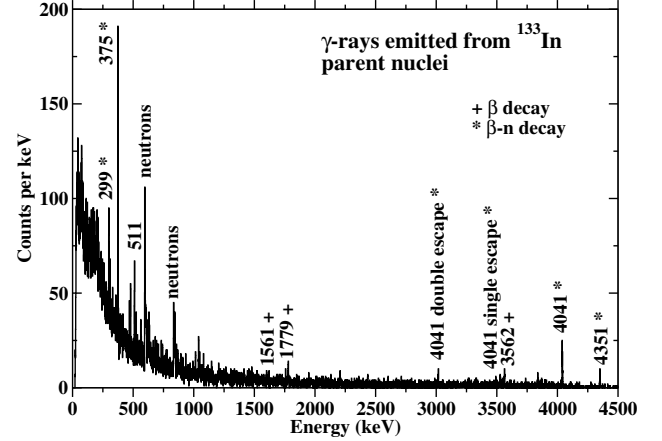


Fig. 1.  $\gamma$ -ray spectrum obtained from the  $\beta$ -decay of  $^{133}\text{In}$  in the current work.

Octupole excitations are amongst the first few excited states in  $^{132}\text{Sn}$ <sup>7)</sup> and have recently been shown to possess enhanced collectivity.<sup>6)</sup> As the 1779-keV state has not been populated in transfer reaction experiments then its isospin quantum number is probably different to that of the neighboring states<sup>4,5,8)</sup> The 1779-keV state probably has a  $\nu f_{7/2}^1 \otimes 3^-$  configuration and is lowered in energy due to an attractive proton-neutron interaction.

Following the  $\beta$  decay of  $^{133}\text{In}$  the  $\log ft$  value for the 1779-keV state was measured to be 6.9(1). This is compatible with either a first-forbidden transition or a hindered allowed Fermi one. Here the hindrance occurs due to  $\Delta T \neq 0$  between the initial and final states, which impedes Fermi transitions. This underlines the complex nature of the octupole state, which contains multiple particle-hole excitations.

Evidence of coexisting single-particle and octupole states at an energy of  $\sim 1.6$  MeV in  $^{133}\text{Sn}$  is presented. It is a theoretical challenge to reproduce these states.

## References

- 1) J. Taprogge *et al.*, Phys. Rev. Lett. **112**, 132501 (2014).
- 2) G. Simpson *et al.*, Phys. Rev. Lett. **113**, 132502 (2014).
- 3) P. Hoff *et al.*, Phys. Rev. Lett. **77**, 1020 (1996).
- 4) J. M. Allmond *et al.*, Phys. Rev. Lett. **112**, 172701 (2014).
- 5) V. Vaquero *et al.*, Phys. Rev. Lett. **118**, 202505 (2017).
- 6) D. Rosiak *et al.*, Phys. Rev. Lett. **121**, 252501 (2018).
- 7) B. Fogelberg *et al.*, Phys. Rev. Lett. **73**, 2413 (1994).
- 8) K. Jones *et al.*, Phys. Rev. C **84**, 034601 (2011).

<sup>\*1</sup> LPSC, Grenoble

<sup>\*2</sup> School of Engineering, University of the West of Scotland

<sup>\*3</sup> IEM, CSIC Madrid

<sup>\*4</sup> Departamento de Física Teórica, Universidad Autónoma de Madrid

<sup>\*5</sup> RIKEN Nishina Center

## Inelastic scattering of neutron-rich Ni and Zn isotopes off a proton target<sup>†</sup>

M. L. Cortés,<sup>\*1,\*2</sup> P. Doornenbal,<sup>\*3</sup> M. Dupuis,<sup>\*4</sup> S. M. Lenzi,<sup>\*5</sup> F. Nowacki,<sup>\*6</sup> A. Obertelli,<sup>\*7,\*3</sup> S. Péru,<sup>\*4</sup> N. Pietralla,<sup>\*1</sup> V. Werner,<sup>\*1</sup> K. Wimmer,<sup>\*8</sup> and the NP1312-RIBF118 collaboration.

One of the most important insight on nuclear structure obtained from studies performed at radioactive ion beam facilities is the modification of the shell closures with varying number of protons and neutrons.<sup>1)</sup> This shell-evolution has been widely studied, in particular on the neutron-rich side of the nuclear chart. Experimental evidence suggests, for example, the appearance of new magic numbers at  $N = 32, 34$  in Ca isotopes,<sup>2,3)</sup> as well as the disappearance of the shell closures at  $N = 8, 20$  and  $28^1$ ) in various neutron-rich isotopes. For the Ni isotopic chain, the reduced transition probability,  $B(E2)\uparrow$ , measured between  $N = 28$  and  $N = 40$ , shows a parabolic trend which indicates a subshell closure at  $N = 40$ . A measurement of the  $B(E2)\uparrow$  value of  $^{70}\text{Ni}$  indicated an enhanced collectivity for  $N = 42$ ,<sup>4)</sup> thus a possible weakening of the  $Z = 28$  gap towards  $^{78}\text{Ni}$ . In contrast, measurements of  $^{72,74}\text{Ni}$ <sup>5,6)</sup> show a reduced  $B(E2)\uparrow$  value for these isotopes, corroborating the magic character of the  $N = 50$  and  $Z = 28$  shell gaps.

In the experiment, performed at the RIBF as part of the first SEASTAR campaign, a  $^{238}\text{U}$  primary beam with an energy of 345 MeV/nucleon and an average intensity of 12 pnA impinged on a 3 mm thick  $^9\text{Be}$  target at the entrance of BigRIPS.<sup>7)</sup> After selection and identification,  $^{72,74}\text{Ni}$  and  $^{76,80}\text{Zn}$  ions were focused on the MINOS device,<sup>8)</sup> composed of a 102(1) mm long liquid hydrogen target surrounded by a Time Projection Chamber (TPC). Due to the low efficiency of MINOS for the  $(p, p')$  reaction, the information of the TPC was not used, leading to a decrease of the resolution of 1 MeV  $\gamma$ -rays from a typical 9% using MINOS, to 14%. Reaction products were identified using the ZeroDegree spectrometer,<sup>7)</sup> and  $\gamma$  rays were detected with the DALI2 array,<sup>9)</sup> composed of 186 NaI(Tl) detectors. The full-energy-peak efficiency of the array was determined using a detailed Geant4 simulation and was found to be 14% at 1.33 MeV with an energy resolution of 6.2% (FWHM) for a stationary source.

Direct proton inelastic scattering cross sections to the  $2_1^+$  and  $4_1^+$  states were inferred from the  $\gamma$ -ray spectrum of each isotope. Such cross sections were analyzed considering two reaction models. First, a microscopic

approach, based on transition densities obtained from Quasiparticle Random Phase Approximation (QRPA) and the Jeukenne-Lejeune-Mahaux (JLM) potential,<sup>10)</sup> was used to calculate theoretical inelastic scattering cross sections. To deal with the high energies of the beam in front of the target ( $\approx 270$  MeV), an extension of the JLM folding model above 200 MeV/nucleon was developed. This approach provided the theoretical cross sections for inelastic scattering to the  $2_1^+$  state of  $^{72,74}\text{Ni}$  and  $^{80}\text{Zn}$ . By comparing the theoretical and experimental cross sections, neutron-to-proton matrix element ratios,  $M_n/M_p$ , were obtained. The results suggest that for the Ni isotopes ( $M_n/M_p > (N/Z)$ ), which implies that the contribution of the neutrons to the collectivity is enhanced. For  $^{80}\text{Zn}$ , the calculation yields ( $M_n/M_p < (N/Z)$ ), which is in agreement with an increased role of the protons to the collectivity. Second, deformation lengths for the first quadrupole excitation of each isotope were obtained using the ECIS-97<sup>11)</sup> code. The calculations included a collective vibrational model and used the KD02 global optical potential.<sup>12)</sup> From the deformation lengths a matter deformation parameter  $\beta_2(p, p')$  was obtained and compared with previously measured charge deformations,  $\beta_2(\text{EM})$ . For the Ni isotopes  $\beta_2(p, p')$  is slightly higher than  $\beta_2(\text{EM})$ , consistent with a previous measurement on  $^{74}\text{Ni}$ <sup>13)</sup> and with the conservation of the  $Z = 28$  gap for neutron-rich Ni isotopes. The opposite effect is observed for  $^{80}\text{Zn}$ , thus suggesting that the shell closure for  $N = 50$  is conserved when approaching  $Z = 28$ . This work represents a step towards a consistent interpretation of the  $(p, p')$  data and will be beneficial for the extraction of useful physics parameters linked to nuclear structure calculations.

### References

- 1) O. Sorlin *et al.*, Prog. Part. Nucl. Phys. **61**, 602 (2008).
- 2) F. Wienholtz *et al.*, Nature **498**, 346 (2013).
- 3) D. Steppenbeck *et al.*, Nature **502**, 207 (2013).
- 4) O. Perru *et al.*, Phys. Rev. Lett. **96**, 232501 (2006).
- 5) K. Kolos *et al.*, Phys. Rev. Lett. **116**, 122502 (2016).
- 6) T. Marchi *et al.*, Phys. Rev. Lett. **113**, 182501 (2014).
- 7) T. Kubo *et al.*, Prog. Theor. Exp. Phys. **2012** (2012).
- 8) A. Obertelli *et al.*, Eur. Phys. J. A **50**, 8 (2014).
- 9) S. Takeuchi *et al.*, Nucl. Instrum. Methods Phys. Res. A **763**, 596 (2014).
- 10) J.-P. Jeukenne *et al.*, Phys. Rev. C **16**, 80 (1977).
- 11) J. Raynal, Phys. Rev. C **23**, 2571 (1981).
- 12) A. Koning *et al.*, Nucl. Phys. A **713**, 231 (2003).
- 13) N. Aoi *et al.*, Phys. Lett. B **692**, 302 (2010).

<sup>†</sup> Condensed from the article in Phys. Rev. C **97**, 044315 (2018)

<sup>\*1</sup> Institut für Kernphysik, Technische Universität Darmstadt

<sup>\*2</sup> GSI Helmholtzzentrum für Schwerionenforschung GmbH

<sup>\*3</sup> RIKEN Nishina Center

<sup>\*4</sup> CEA, DAM, DIF

<sup>\*5</sup> Dipartimento di Fisica e Astronomia, Università di Padova

<sup>\*6</sup> IPHC, CNRS/IN2P3, Université de Strasbourg

<sup>\*7</sup> IRFU, CEA, Université Paris-Saclay

<sup>\*8</sup> Department of Physics, University of Tokyo

# Magnetic-moment measurement of the isomeric state of $^{130}\text{Sn}$ in the vicinity of doubly-magic nucleus $^{132}\text{Sn}$

G. Georgiev,<sup>\*1,\*2,\*3</sup> Y. Ichikawa,<sup>\*1</sup> D. S. Ahn,<sup>\*1</sup> T. Asakawa,<sup>\*4</sup> K. Asahi,<sup>\*1</sup> H. Baba,<sup>\*1</sup> K. Doi,<sup>\*4</sup> N. Fukuda,<sup>\*1</sup> A. Gladkov,<sup>\*1,\*5</sup> T. Gray,<sup>\*3</sup> G. Häfner,<sup>\*2,\*6</sup> K. Kawata,<sup>\*1,\*7</sup> A. Kusoglu,<sup>\*8</sup> W. Kobayashi,<sup>\*4</sup> G. J. Lane,<sup>\*1,\*3</sup> R. L. Lozeva,<sup>\*2</sup> C. Mihai,<sup>\*9</sup> R. Mihai,<sup>\*9</sup> Y. Nakamura,<sup>\*10</sup> M. Niikura,<sup>\*11</sup> H. Nishibata,<sup>\*1</sup> A. Odahara,<sup>\*12</sup> S. Pascu,<sup>\*9</sup> M. Sanjo,<sup>\*4</sup> Y. Sasaki,<sup>\*4</sup> T. Sato,<sup>\*1</sup> Y. Shimizu,<sup>\*1</sup> C. Sotty,<sup>\*9</sup> A. Stuchbery,<sup>\*3</sup> T. Sumikama,<sup>\*1</sup> H. Suzuki,<sup>\*1</sup> M. Tajima,<sup>\*1</sup> A. Takamine,<sup>\*1</sup> Y. Takeuchi,<sup>\*4</sup> H. Takeda,<sup>\*1</sup> A. Toda,<sup>\*5</sup> A. Turturica,<sup>\*9</sup> H. Ueno,<sup>\*1</sup> and H. Yamazaki<sup>\*1</sup>

The  $^{130}\text{Sn}$  nucleus is located in the vicinity of the doubly-magic nucleus  $^{132}\text{Sn}$  and known to have an isomeric state at an energy level of 2435 keV with a half-life of 1.61  $\mu\text{s}$ .<sup>1-3</sup> Its spin parity has been tentatively assigned to be  $10^+$  where a configuration of two neutron holes coupled in parallel in the  $h_{11/2}$  orbital is expected to be predominated. The purity of the configuration can be a good indicator of the magicity near  $^{132}\text{Sn}$ . Therefore, we measured the magnetic moment of the isomeric state of  $^{130}\text{Sn}$ .

The experiment was conducted at the BigRIPS at the RIBF. The two-step fragmentation scheme<sup>4</sup> was employed to produce spin-aligned  $^{130}\text{Sn}$  beam. In the reaction at F0,  $^{132}\text{Sn}$  was produced by a fission reaction of a 345-MeV/nucleon  $^{238}\text{U}$  beam on a  $^9\text{Be}$  target with a thickness of 6 mm. A wedge-shaped aluminium degrader with a mean thickness of 6 mm was placed at the first momentum-dispersive focal plane F1, where the momentum acceptance at F1 was  $\pm 1.4\%$ . The secondary  $^{132}\text{Sn}$  beam was introduced to a second target of wedge-shaped aluminum with a mean thickness of 2 mm, placed at the momentum-dispersive focal plane F5. The  $^{130}\text{Sn}$  nuclei including those in the isomeric state  $^{130\text{m}}\text{Sn}$ , were produced by removing two neutrons from  $^{132}\text{Sn}$ . The  $^{130}\text{Sn}$  beam was subsequently transported to F7 under the condition that the momentum dispersion between F5 and F7 was matched to that between F3 and F5. The slit width at F7 was set to  $\pm 9$  mm. The intensity and purity of  $^{130}\text{Sn}$  in the tertiary beam were 30 cps and 30%, respectively.

The  $^{130}\text{Sn}$  beam was introduced to the experimental apparatus for time-differential perturbed angular distribution (TDPAD) measurement, which was placed at the focal plane F12. The TDPAD apparatus consisted of a dipole magnet, a Cu crystal stopper, Ge detectors, and a plastic scintillator. The Cu stopper was 3.0 mm

in thickness and  $30 \times 30$  mm<sup>2</sup> in area. The dipole magnet provided a static magnetic field of  $B_0 = 0.150$  T.  $^{130\text{m}}\text{Sn}$  was implanted into the Cu stopper and  $\gamma$  rays were detected with four Ge detectors located in a plane perpendicular to  $B_0$  at a distance of 7.0 cm from the stopper and at every 90 degrees. Two LaBr<sub>3</sub> detectors were also placed at 90 degrees with respect to each other so as not to interfere with the Ge detectors. The plastic scintillator with a thickness of 0.1 mm was placed upstream of the stopper. Its signal provided the time-zero trigger. The TDPAD apparatus enabled us to determine the  $g$ -factor of  $^{130\text{m}}\text{Sn}$  by observing the changes in anisotropy of the de-excitation  $\gamma$  rays emitted from spin-aligned  $^{130\text{m}}\text{Sn}$  in synchronization with the spin precession in the presence of an external field.

In this experiment, we observed two cascade  $\gamma$  rays from  $^{130}\text{Sn}$  with energies of 97 keV and 391 keV. The  $R(t)$  ratio representing the change in the anisotropy of  $\gamma$  rays was obtained according to

$$R(t) = \frac{N_{13}(t) - \epsilon N_{24}(t)}{N_{13}(t) + \epsilon N_{24}(t)}, \quad (1)$$

where  $N_{13}(t)$  and  $N_{24}(t)$  are the aggregates of the photo-peak count rates in the two pairs of Ge detectors placed diagonally to each other, and  $\epsilon$  denotes a correction factor for the difference in detection efficiency. The same applies to the LaBr<sub>3</sub> detectors. Theoretically,  $R(t)$  is expressed as a function of  $t$  as,

$$R(t) = \frac{3A_{22}}{4 + A_{22}} \cos 2(\omega_L t + \alpha), \quad (2)$$

in terms of the rank-two anisotropy parameter  $A_{22} = AB_2F_2$ , where  $A$  denotes the degree of spin alignment,  $B_2$  is the statistical tensor for complete alignment, and  $F_2$  is the radiation parameter. The Larmor frequency  $\omega_L$  is given by  $\omega_L = g\mu_N B_0/\hbar$ , where  $g$  is the  $g$ -factor of  $^{130\text{m}}\text{Sn}$  in the unit of nuclear magneton  $\mu_N$ .  $\alpha$  is the initial phase of the precession depending on the detector arrangement. The detailed analysis and deduction of the  $g$ -factor are in progress.

## References

- 1) R. L. Lozeva *et al.*, Phys. Rev. C **77**, 064313 (2008).
- 2) D. Kameda *et al.*, Phys. Rev. C **86**, 054319 (2012).
- 3) S. Pietri *et al.*, Phys. Rev. C **83**, 044328 (2011).
- 4) Y. Ichikawa *et al.*, Nat. Phys. **8**, 918 (2012).

\*1 RIKEN Nishina Center

\*2 CSNSM, CNRS/IN2P3, Université Paris-Saclay

\*3 Department of Physics, Australian National University

\*4 Department of Advanced Sciences, Hosei University

\*5 Department of Physics, Kyungpook National University

\*6 Department of Physics, University of Cologne

\*7 Center for Nuclear Study, University of Tokyo

\*8 Department of Physics, Istanbul University

\*9 NIPNE, IFIN-HH

\*10 Department of Physics, Meiji University

\*11 Department of Physics, University of Tokyo

\*12 Department of Physics, Osaka University

## Track distortion due to ion back flow in CAT-S at RIBF113: $^{132}\text{Sn}(d, d')$ measurement

S. Ota,<sup>\*1</sup> H. Tokieda,<sup>\*1</sup> C. Iwamoto,<sup>\*1</sup> M. Dozono,<sup>\*1</sup> U. Garg,<sup>\*2</sup> S. Hayakawa,<sup>\*1</sup> K. Kawata,<sup>\*1</sup> N. Kitamura,<sup>\*1</sup> M. Kobayashi,<sup>\*1</sup> S. Masuoka,<sup>\*1</sup> S. Michimasa,<sup>\*1</sup> A. Obertelli,<sup>\*3,\*4</sup> D. Suzuki,<sup>\*4</sup> R. Yokoyama,<sup>\*1</sup> J. Zenihiro,<sup>\*4</sup> R. Kojima,<sup>\*1</sup> H. Baba,<sup>\*4</sup> O. Beliuskina,<sup>\*1</sup> S. Chebotaryov,<sup>\*4</sup> P. Egelhof,<sup>\*5</sup> T. Harada,<sup>\*6</sup> M. N. Harakeh,<sup>\*7</sup> K. Howard,<sup>\*2</sup> N. Imai,<sup>\*1</sup> M. Itoh,<sup>\*8</sup> Y. Kiyokawa,<sup>\*1</sup> C. S. Lee,<sup>\*1</sup> Y. Maeda,<sup>\*9</sup> Y. Matsuda,<sup>\*8</sup> E. Milman,<sup>\*4</sup> V. Panin,<sup>\*4</sup> H. Sakaguchi,<sup>\*10</sup> P. Schrock,<sup>\*1</sup> S. Shimoura,<sup>\*1</sup> L. Stuhl,<sup>\*4</sup> M. Takaki,<sup>\*1</sup> K. Taniue,<sup>\*9</sup> S. Terashima,<sup>\*11</sup> T. Uesaka,<sup>\*4</sup> Y. N. Watanabe,<sup>\*12</sup> K. Wimmer,<sup>\*1,\*4,\*12</sup> K. Yako,<sup>\*1</sup> Y. Yamaguchi,<sup>\*1</sup> Z. Yang,<sup>\*4</sup> and K. Yoneda<sup>\*4</sup>

The equation of state (EoS) of nuclear matter not only governs the femto-scale quantum many-body system, namely nuclei, but also plays an important role in the structure of neutron stars and in supernova phenomena. In particular, the EoS of isospin asymmetric nuclear matter has attracted much interest from the viewpoint of the existence of heavy neutron stars. Although the asymmetric term of incompressibility,  $K_\tau$ , can be a benchmark for various EoSs thanks to the direct accessibility via the measurements of isoscalar giant monopole resonances,<sup>1)</sup> the ambiguity of the  $K_\tau$  is still larger than those of other EoS parameters. The measurement of deuterium inelastic scattering off  $^{132}\text{Sn}$  was performed at RIBF in RIKEN, aiming at a more precise determination of the  $K_\tau$  value.

An active target CAT-S has been employed for the measurement<sup>2)</sup> to measure the forward angle scattering, which is sensitive to the monopole transition, together with the backward angle scattering. A cocktail beam of  $^{132}\text{Sn}$ ,  $^{133}\text{Sb}$ , and  $^{134}\text{Te}$  having the total intensity of  $3.2 \times 10^5$  particles per second bombarded the CAT-S filled with 0.4-atm pure deuterium gas. A set of three 400- $\mu\text{m}$  thick THGEMs is used for the electron multiplication device in TPC of CAT-S. In this paper, we report the observed field distortion due to the injection of the high-intensity heavy-ion beam and its treatment in the tracking procedure.

There is a phenomena called ion back flow (IBF) where the ions produced in the THGEMs go back to the drift region through the hole of the THGEMs. The drift velocity of the ion is as slow as 0.01 cm/ $\mu\text{s}$  and a significant number of ions exists along the beam axis like a wall if the IBF rate is large. Since the geometrical configuration and voltage settings of THGEMs in RIBF113 were not optimized for the reduction of the IBF rate, the effect of space charge due to the ions is

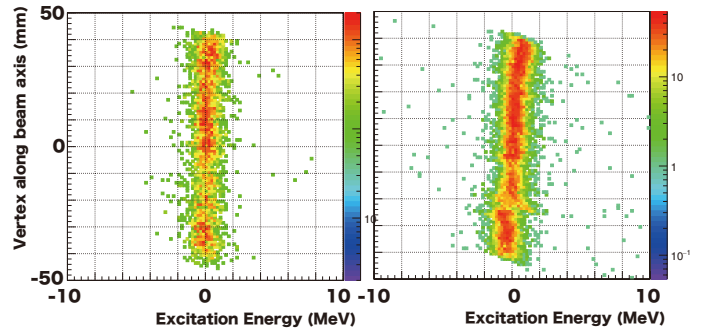


Fig. 1. Corrected (left) and uncorrected (right) correlation.

observed. This effect on the trajectory of recoil particle is observed in the vertex position dependence of the excitation energy (shown in the right panel of Fig. 1), because the position displacement along the beam axis changes the angle of trajectory. A locus around the excitation energy of zero corresponds to elastic scattering. Large deviations at the entrance ( $Z = -50$ ) and exit ( $Z = 50$ ) are clearly seen. The field distortion is estimated by using the finite element solver (FENICS project) assuming a certain ion density along the beam axis in the active volume. The resultant position displacement between the electron generated point and the observed point are estimated by the simulation of electron transportation taking the estimated field distortion into account. Left panel of Fig. 1 shows the result with taking the position displacement into account in tracking procedure. In this procedure, the IBF rate of 32% is assumed. Now the locus of elastic scattering becomes straight and the effect of the IBF is compensated. The best estimator of the IBF rate can be obtained by comparing the widths of elastic peaks assuming various IBF rates.

The excitation energy with beam particle identification is obtained and significant statistics is observed in the GMR energy region in excitation energy spectrum of each isotope. The analysis to finalize the excitation energy spectra at forward angle is ongoing and the further analysis for backward angle will be performed.

### References

- 1) T. Li *et al.*, Phys. Rev. Lett. **99**, 162503 (2007).
- 2) S. Ota *et al.*, J. Radioanal. Nucl. Chem. **305**, 907–911 (2015).

<sup>\*1</sup> Center for Nuclear Study, the University of Tokyo

<sup>\*2</sup> Department of Physics, University of Notre Dame

<sup>\*3</sup> Le Centre CEA de Saclay

<sup>\*4</sup> RIKEN Nishina Center

<sup>\*5</sup> GSI Helmholtzzentrum für Schwerionenforschung GmbH

<sup>\*6</sup> Department of Physics, Toho University

<sup>\*7</sup> KVI, Center for Advanced Radiation Technology

<sup>\*8</sup> Cyclotron and Radio Isotope Center, Tohoku University

<sup>\*9</sup> Department of Applied Physics, University of Miyazaki

<sup>\*10</sup> Research Center for Nuclear Physics, Osaka University

<sup>\*11</sup> Dept. of Nucl. Sci. and Tech., Beihang University

<sup>\*12</sup> Department of Physics, the University of Tokyo

# First mass measurements of neutron-rich calcium isotopes, $^{55-57}\text{Ca}^\dagger$

S. Michimasa,<sup>\*1</sup> M. Kobayashi,<sup>\*1</sup> Y. Kiyokawa,<sup>\*1</sup> S. Ota,<sup>\*1</sup> D. S. Ahn,<sup>\*2</sup> H. Baba,<sup>\*2</sup> G. P. A. Berg,<sup>\*3</sup> M. Dozono,<sup>\*1</sup> N. Fukuda,<sup>\*2</sup> T. Furuno,<sup>\*4</sup> E. Ideguchi,<sup>\*5</sup> N. Inabe,<sup>\*2</sup> T. Kawabata,<sup>\*4</sup> S. Kawase,<sup>\*6</sup> K. Kisamori,<sup>\*1</sup> K. Kobayashi,<sup>\*7</sup> T. Kubo,<sup>\*8,9</sup> Y. Kubota,<sup>\*2</sup> C. S. Lee,<sup>\*1</sup> M. Matsushita,<sup>\*1</sup> H. Miya,<sup>\*1</sup> A. Mizukami,<sup>\*10</sup> H. Nagakura,<sup>\*7</sup> D. Nishimura,<sup>\*11</sup> H. Oikawa,<sup>\*10</sup> H. Sakai,<sup>\*2</sup> Y. Shimizu,<sup>\*2</sup> A. Stolz,<sup>\*9</sup> H. Suzuki,<sup>\*2</sup> M. Takaki,<sup>\*1</sup> H. Takeda,<sup>\*2</sup> S. Takeuchi,<sup>\*12</sup> H. Tokieda,<sup>\*1</sup> T. Uesaka,<sup>\*2</sup> K. Yako,<sup>\*1</sup> Y. Yamaguchi,<sup>\*1</sup> Y. Yanagisawa,<sup>\*2</sup> R. Yokoyama,<sup>\*13</sup> K. Yoshida,<sup>\*2</sup> and S. Shimoura<sup>\*1</sup>

The mass of atomic nuclei is a fundamental quantity as it reflects the sum of all interactions within the nucleus, which is a quantum many-body system comprised of two kinds of fermions, protons and neutrons. Changes in the shell structures in nuclei far from stability can be directly probed by mass measurements.

The shell evolution of the neutron  $2p_{1/2}$  and  $1f_{5/2}$  orbitals in neutron-rich calcium region has attracted considerable attention in recent years. The presence of a large subshell gap at  $N = 34$  between the orbitals in the Ca isotopes was theoretically predicted,<sup>1)</sup> and the measurement of  $E(2_1^+)$  in  $^{54}\text{Ca}$  suggested the possible emergence of a sizable subshell closure at  $N = 34$ .<sup>2)</sup> One of the most critical information on the existence of the subshell gap at  $N = 34$  is the atomic masses of the calcium isotopes beyond  $N = 34$ . We performed the first mass measurements of neutron-rich Ca isotopes beyond  $N = 34$  to probe the shell evolution of the neutron  $2p_{1/2}$  and  $1f_{5/2}$  orbitals.

The experiment was performed at the Radioactive Isotope Beam Factory (RIBF) at RIKEN, which is operated by RIKEN Nishina Center and Center for Nuclear Study, University of Tokyo. The masses were measured directly by using the TOF- $B\rho$  technique. Neutron-rich isotopes were produced by fragmentation of a  $^{70}\text{Zn}$  primary beam at 345 MeV/nucleon in a  $^9\text{Be}$  target. The fragments were separated by the BigRIPS separator,<sup>3)</sup> and transported in the High-Resolution Beam Line to the SHARAQ spectrometer.<sup>4)</sup> Details on the experimental setup and analysis procedure can be found in the previous report.<sup>5)</sup>

We discussed the evolution of the empirical  $\delta e$  shell gaps<sup>6)</sup> of neutron-rich Ca isotopes from the atomic masses of  $^{55-57}\text{Ca}$ , as shown in Fig. 1. The  $\delta e$  value is identical with  $S_{2n}(N) - S_{2n}(N + 1)$ , where  $S_{2n}(N)$  is the two-neutron separation energy of a nucleus with

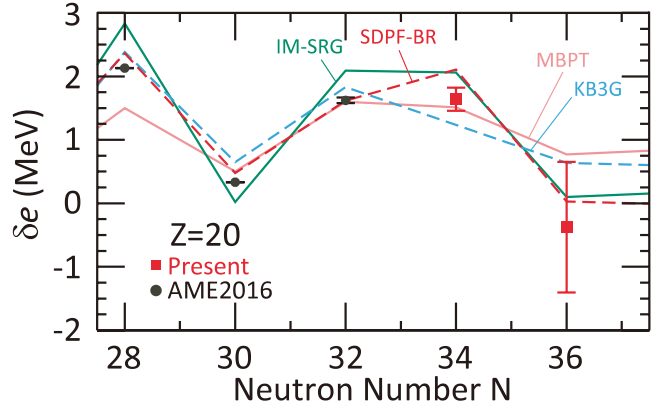


Fig. 1. The empirical  $\delta e$  shell gaps in neutron-rich Ca isotopes. Squares indicate values determined for the first time, and circles are literature values from AME2016.<sup>7)</sup> The solid lines show theoretical predictions.<sup>8-11)</sup>

neutron number  $N$ , and the empirical energy gaps across the Fermi surface in the nuclei is evaluated. In the figure, the squares represent the experimental  $\delta e$  values determined for the first time, while the circles represent the literature values obtained from AME2016.<sup>7)</sup> The solid lines indicate the theoretical predictions by using KB3G,<sup>8)</sup> MBPT,<sup>9)</sup> IM-SRG,<sup>10)</sup> and modified SDFP-MU (SDPF-BR)<sup>11)</sup> interactions. The empirical energy gap at  $N = 34$  is close to that at  $N = 32$ , and slightly smaller than that at  $N = 28$ . Thus, the experimental result indicates a sizable energy gap of subshells in  $^{54}\text{Ca}$ , which is comparable to that in  $^{52}\text{Ca}$ . However the gap is not as large as recent predictions by SDFP-BR and IM-SRG interactions. We are preparing a physics article to report the shell evolution in neutron-rich Ca isotopes beyond  $N = 34$ .

## References

- 1) T. Otsuka *et al.*, Phys. Rev. Lett. **87**, 082502 (2001).
- 2) D. Steppenbeck *et al.*, Nature **502**, 207 (2013).
- 3) T. Kubo, Nucl. Instrum. Methods Phys. Res. B **204**, 97 (2003).
- 4) T. Uesaka *et al.*, Prog. Theor. Exp. Phys. **2012**, 03C007 (2012).
- 5) M. Kobayashi *et al.*, RIKEN Accel. Prog. Rep. **50**, 59 (2017).
- 6) W. Satuła, *et al.*, Phys. Rev. Lett. **81**, 3599 (1998).
- 7) M. Wang *et al.*, Chin. Phys. C **41**, 030003 (2017).
- 8) A. Poves *et al.*, Nucl. Phys. A **694**, 157 (2001).
- 9) J. D. Holt *et al.*, Phys. Rev. C **90**, 024312 (2014).
- 10) J. Simonis *et al.*, Phys. Rev. C **96**, 014303 (2017).
- 11) Y. Utsuno *et al.*, Phys. Rev. C **86**, 051301 (2012).

<sup>†</sup> Condensed from the article in Phys. Rev. Lett. **121**, 022506 (2018)

<sup>\*1</sup> Center for Nuclear Study, The University of Tokyo

<sup>\*2</sup> RIKEN Nishina Center

<sup>\*3</sup> Dept. of Physics, University of Notre Dame, USA

<sup>\*4</sup> Dept. of Physics, Kyoto University

<sup>\*5</sup> RCNP, Osaka University

<sup>\*6</sup> Dept. of Advanced Energy Engineering Sciences, Kyushu University

<sup>\*7</sup> Dept. of Physics, Rikkyo University

<sup>\*8</sup> FRIB, MSU, USA

<sup>\*9</sup> NSCL, MSU, USA

<sup>\*10</sup> Dept. of Physics, Tokyo University of Science

<sup>\*11</sup> Dept. of Physics, Tokyo City University

<sup>\*12</sup> Dept. of Physics, Tokyo Institute of Technology

<sup>\*13</sup> Dept. of Physics & Astronomy, University of Tennessee

## Re-measurement of the ${}^4\text{He}({}^8\text{He}, {}^8\text{Be})$ reaction

S. Masuoka,<sup>\*1</sup> S. Shimoura,<sup>\*1</sup> M. Takaki,<sup>\*1</sup> S. Ota,<sup>\*1</sup> S. Michimasa,<sup>\*1</sup> M. Dozono,<sup>\*1</sup> C. Iwamoto,<sup>\*1</sup>  
 K. Kawata,<sup>\*1</sup> N. Kitamura,<sup>\*1</sup> M. Kobayashi,<sup>\*1</sup> R. Nakajima,<sup>\*1</sup> H. Tokieda,<sup>\*1</sup> R. Yokoyama,<sup>\*1</sup> D. S. Ahn,<sup>\*2</sup>  
 H. Baba,<sup>\*2</sup> N. Fukuda,<sup>\*2</sup> T. Harada,<sup>\*3</sup> E. Ideguchi,<sup>\*4</sup> N. Imai,<sup>\*1</sup> N. Inabe,<sup>\*2</sup> Y. Kondo,<sup>\*5</sup> T. Kubo,<sup>\*2</sup>  
 Y. Maeda,<sup>\*6</sup> F. M. Marqués,<sup>\*7</sup> M. Matsushita,<sup>\*1</sup> T. Nakamura,<sup>\*5</sup> N. Orr,<sup>\*7</sup> H. Sakai,<sup>\*2</sup> H. Sato,<sup>\*2</sup> P. Schrock,<sup>\*1</sup>  
 L. Stuhl,<sup>\*1,\*2</sup> T. Sumikama,<sup>\*2</sup> H. Suzuki,<sup>\*2</sup> H. Takeda,<sup>\*2</sup> K. Taniue,<sup>\*6</sup> T. Uesaka,<sup>\*2</sup> K. Wimmer,<sup>\*8</sup> K. Yako,<sup>\*1</sup>  
 Y. Yamaguchi,<sup>\*1</sup> Y. Yanagisawa,<sup>\*2</sup> K. Yoshida,<sup>\*2</sup> and J. Zenihiro<sup>\*2</sup>

In our previous study, the candidate resonance of  $4n$  system (tetra-neutron) was found using the  ${}^4\text{He}({}^8\text{He}, {}^8\text{Be})4n$  reaction with a 186 MeV/nucleon  ${}^8\text{He}$  beam.<sup>1)</sup> A new measurement with better statistics and better accuracy was performed to evidence the existence of the tetra-neutron system.<sup>2)</sup>

The intensity of the  ${}^8\text{He}$  beam ( $3.5 \times 10^6$  particles per second at the liquid helium target) was approximately twice compared to that of the previous experiment. A pair of cathode readout drift chambers (CRDCs) was used at the final focal plane of the SHARAQ spectrometer. To improve the resolution, the positions and angles of the CRDCs were precisely calibrated in the software analysis by using the reference data of a  ${}^4\text{He}$  beam. We achieved position resolutions of 0.40 and 0.62 mm FWHM and angular resolutions of 1.12 and 1.87 mrad FWHM in the horizontal and vertical directions, respectively. Ion optical analysis was then performed to evaluate the ion transport matrix elements of both the beam line and the SHARAQ spectrometer. The scattering angle of the reaction was deduced from the angle measured by the CRDCs after taking the ion transport matrix into account. Higher order aberrations were thus corrected for. We obtained a resolution of 4.7 and 2.8 mrad FWHM in the horizontal and vertical directions, respectively.

In the previous experiment, the systematic uncertainty was 1.25 MeV mostly due to the fact that no reference data were measured in the momentum region of the tetra-neutron resonance. In this experiment, we measured the  ${}^1\text{H}({}^3\text{H}, {}^3\text{He})n$  reaction by using a  ${}^3\text{H}$  beam at 310 MeV/nucleon (8.3 Tm) and a  $\text{CH}_2$  target. The advantage of this reaction is that the rigidity of both the beam and the ejectile are the same as that of the  ${}^4\text{He}({}^8\text{He}, {}^8\text{Be})4n$  reaction at 186 MeV/nucleon. Therefore, the reaction of reference and the reaction of physics can be measured in the same momentum window without changing the magnet settings.

Figure 1 (a) shows the kinematical curve of the  ${}^1\text{H}({}^3\text{H}, {}^3\text{He})n$  reaction. The scattering angle is plotted

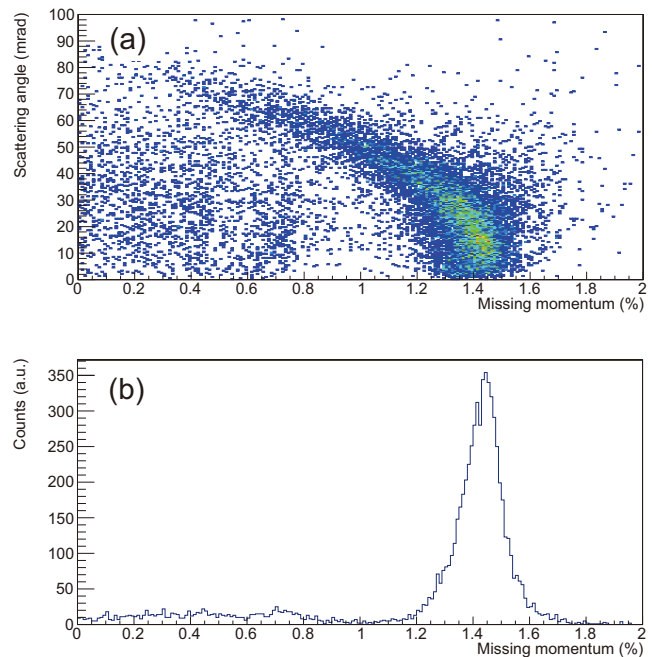


Fig. 1. (a) Plot of the scattering angle against the missing momentum. The kinematical curve of  ${}^1\text{H}({}^3\text{H}, {}^3\text{He})n$  reaction is visible. (b) Missing momentum spectrum after correcting for the scattering angle in (a).

against the missing momentum, which is given by the momentum difference between the  ${}^3\text{H}$  beam and the  ${}^3\text{He}$  ejectile. Figure 1 (b) shows the spectrum of the missing mass momenta after correcting for the scattering angle dependence. Given the known  $Q$ -value of the  ${}^1\text{H}({}^3\text{H}, {}^3\text{He})n$  reaction, the missing mass momentum of the peak seen in the figure was taken as a reference. The uncertainty of the excitation energy of  $4n$  is evaluated to be 26 keV RMS due to the uncertainty of the peak position in Fig. 1 (b).

Further analysis is ongoing.

### References

- 1) K. Kisamori *et al.*, Phys. Rev. Lett. **116**, 052501 (2016).
- 2) S. Masuoka *et al.*, RIKEN Accel. Prog. Rep. **50**, 198 (2017).

<sup>\*1</sup> Center for Nuclear Study, the University of Tokyo  
<sup>\*2</sup> RIKEN Nishina Center  
<sup>\*3</sup> Department of Physics, Toho University  
<sup>\*4</sup> Research Center for Nuclear Physics, Osaka University  
<sup>\*5</sup> Department of Physics, Tokyo Institute of Technology  
<sup>\*6</sup> Faculty of Engineering, University of Miyazaki  
<sup>\*7</sup> Laboratoire de Physique Corpusculaire, IN2P3-CNRS, ENSICAEN et Université de Caen  
<sup>\*8</sup> Department of Physics, the University of Tokyo

## Evaluation of $^{79}\text{Se}(n, \gamma)^{80}\text{Se}$ reaction by measuring $^{77, 79}\text{Se}(d, p)^{78, 80}\text{Se}$ reactions

N. Imai,<sup>\*1</sup> M. Dozono,<sup>\*1</sup> S. Michimasa,<sup>\*1</sup> T. Sumikama,<sup>\*2</sup> S. Ota,<sup>\*1</sup> S. Hayakawa,<sup>\*1</sup> K. Iribe,<sup>\*2,\*3</sup> C. Iwamoto,<sup>\*1</sup> S. Kawase,<sup>\*4</sup> K. Kawata,<sup>\*1,\*2</sup> N. Kitamura,<sup>\*1</sup> S. Masuoka,<sup>\*1</sup> K. Nakano,<sup>\*4</sup> P. Schrock,<sup>\*1</sup> D. Suzuki,<sup>\*2</sup> R. Tsunoda,<sup>\*1</sup> K. Wimmer,<sup>\*2,\*5</sup> D. S. Ahn,<sup>\*2</sup> O. Beliuskina,<sup>\*1</sup> N. Chiga,<sup>\*2</sup> N. Fukuda,<sup>\*2</sup> E. Ideguchi,<sup>\*2,\*6</sup> K. Kusaka,<sup>\*2</sup> H. Miki,<sup>\*2,\*7</sup> H. Miyatake,<sup>\*8</sup> D. Nagae,<sup>\*2</sup> M. Nakano,<sup>\*2,\*9</sup> S. Ohmika,<sup>\*2</sup> M. Ohtake,<sup>\*2</sup> H. Otsu,<sup>\*2</sup> H. J. Ong,<sup>\*2,\*6</sup> S. Sato,<sup>\*2,\*9</sup> H. Shimizu,<sup>\*1</sup> Y. Shimizu,<sup>\*2</sup> H. Sakurai,<sup>\*2,\*5</sup> X. Sun,<sup>\*2</sup> H. Suzuki,<sup>\*2</sup> M. Takaki,<sup>\*1</sup> H. Takeda,<sup>\*2</sup> S. Takeuchi,<sup>\*2,\*7</sup> T. Teranishi,<sup>\*2,\*3</sup> Y. Watanabe,<sup>\*4</sup> Y. X. Watanabe,<sup>\*8</sup> H. Yamada,<sup>\*2,\*7</sup> H. Yamaguchi,<sup>\*1</sup> L. Yang,<sup>\*1</sup> R. Yanagihara,<sup>\*6</sup> K. Yoshida,<sup>\*2</sup> Y. Yanagisawa,<sup>\*2</sup> and S. Shimoura<sup>\*1</sup>

The first excited state at 95.7 keV in  $^{79}\text{Se}$ , which is located on the path of the  $s$ -process nucleosynthesis, has a tiny branch of  $\beta$  decay to  $^{79}\text{Br}$ . Depending on the temperature of the astrophysical site, some ground states of  $^{79}\text{Se}$  can be excited to produce  $^{79}\text{Br}$ . The ratio of  $^{80}\text{Se}$  to  $^{79}\text{Se}$  in a meteorite indicates the temperature of the site.<sup>1)</sup> However, the neutron capture reaction on  $^{79}\text{Se}$  which is the main reaction flow in the  $s$ -process has not been measured.

The nucleus is known as one of the long-lived fission products (LLFP) of nuclear waste. To design the facility to transmute the nucleus, a neutron capture cross-section on the nucleus was conceptualized. However, because both the neutron and LLFPs are unstable, the measurement of neutron-induced cross-section is quite challenging. Alternatively, the reaction cross-section can be indirectly determined through a surrogate reaction.

It is generally assumed that the  $(n, \gamma)$  cross-section is composed of two parts; the formation of compound state and the subsequent decay. The first term can be calculated using the optical model potentials with global parametercharres. In contrast, the theoretical estimates of the second process is quite challenging owing to high level density and complicated decay scheme, and need to be evaluated by the experiment.<sup>2)</sup> This work aims to determine the  $\gamma$  emission probability,  $P_\gamma$ , from the unbound states of  $^{80}\text{Se}$  populated by the  $(d, p)$  reaction as a surrogate for the  $^{79}\text{Se}(n, \gamma)^{80}\text{Se}$  reaction. The method can be verified by comparing the cross-sections of  $^{77}\text{Se}(n, \gamma)^{78}\text{Se}$  determined by directly measuring the  $^{77}\text{Se}(d, p)^{78}\text{Se}$  reaction with the direct measurement at  $E_n = 550$  keV.<sup>3)</sup>

The experiment was performed by using the OEDO beam line<sup>4)</sup> as one of the first physics experiments. The  $^{77, 79}\text{Se}$  beams produced by BigRIPS were energy-degraded at F5 and the beam was spatially focused on a 4-mg/cm<sup>2</sup> thick polyethylene deuteride target by OEDO. The beam energy was adjusted to be

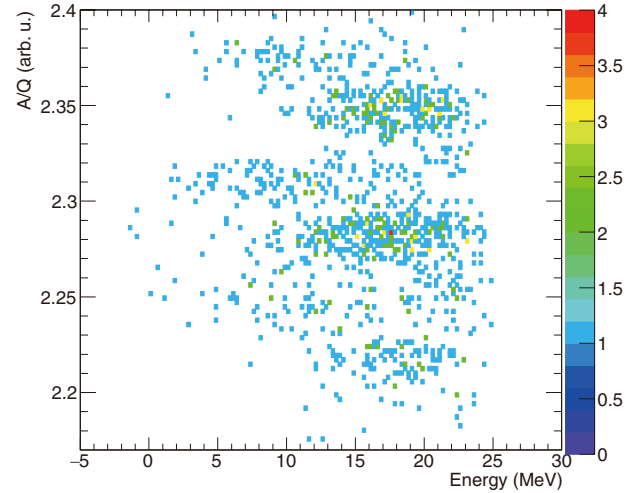


Fig. 1.  $A/Q$  measured at S1 focal plane as a function of the excitation energy in  $^{80}\text{Se}$ . See the text for details.

20 MeV/nucleon at the target. The recoiled particles were identified by employing the six SSD-CsI(Tl) array called TiNA, which covered  $100^\circ$  to  $150^\circ$  in the laboratory frame. The excitation energies of the state populated in  $^{78}\text{Se}$  ( $^{80}\text{Se}$ ) were determined using TiNA and incident beam momentum. The momenta of the outgoing nuclei were analyzed by the first half of the SHARAQ spectrometer.

Figure 1 presents the mass-to-charge ( $A/Q$ ) ratio determined by the spectrometer as a function of the excitation energy of  $^{80}\text{Se}$ . The locus at  $A/Q = 2.3$  is the  $^{80}\text{Se}^{33+}$  while  $A/Q = 2.27$  is  $^{79}\text{Se}^{33+}$ . The locus of  $^{80}\text{Se}$  clearly indicates that  $^{80}\text{Se}$  survived at an energy higher than 10 MeV of the one neutron separation energy of  $^{80}\text{Se}$ . The fraction of  $(N+1, Z)$  nuclei to  $(N, Z)$  residues allows us to determine  $P_\gamma$  as a function of excitation energy. Further analysis is ongoing.

This work was funded by the ImPACT Program of Council for Science, Technology and Innovation (Cabinet Office, Government of Japan).

### References

- 1) F. Kappler *et al.*, Rep. Prog. Phys. **52**, 945 (1989).
- 2) J. E. Escher *et al.*, Rev. Mod. Phys. **84**, 353 (2012).
- 3) S. Kawada, M. Igashira, T. Katabuchi, M. Mizumoto, J. Nucl. Sci. Tech. **47**, 643 (2010).
- 4) S. Michimasa *et al.*, Prog. Theo. Exp. Phys., accepted (2019).

<sup>\*1</sup> Center for Nuclear Study, University of Tokyo

<sup>\*2</sup> RIKEN Nishina Center

<sup>\*3</sup> Department of Physics, Kyushu Univ.

<sup>\*4</sup> Department of Advanced Energy Engineering Science, Kyushu Univ.

<sup>\*5</sup> Department of Physics, Univ. of Tokyo

<sup>\*6</sup> RCNP, Osaka University

<sup>\*7</sup> Department of Physics, Tokyo Institute of Technology

<sup>\*8</sup> WNSC, IPNS, KEK

<sup>\*9</sup> Department of Physics, Rikkyo University

# Fine tuning of isochronism in Rare RI Ring using resonant Schottky monitor

F. Suzaki,<sup>\*1</sup> Y. Abe,<sup>\*1</sup> M. Wakasugi,<sup>\*1</sup> Y. Yamaguchi,<sup>\*1</sup> and the Rare RI Ring collaboration

Rare RI Ring (R3)<sup>1)</sup> is a storage ring that measure the masses of highly unstable exotic nuclei. According to the r-process, the masses of neutron-rich nuclei are crucial to understand nucleosynthesis. We employed a time-of-flight mass spectrometry method in an isochronous storage ring (R3). Because the target precision in mass determination was  $10^{-6}$ , isochronism with a precision of  $10^{-6}$  was required. R3 has a hexagonal symmetric structure that alternates between the sector section and straight section. The sector section consists of four bending magnets. The two magnets on both ends are equipped with ten trim coils to tune the isochronous condition. A monitor that measures the isochronous condition with  $10^{-6}$  precision is required for precise isochronism tuning. This can be achieved through revolution time measurement for several sample particles with evenly distributed momentum over acceptance. However, it is not practical because it takes a long time. In this paper, we report another way using a resonant Schottky pick-up,<sup>2)</sup> which measures the revolution frequency with a precision of  $10^{-6}$ , to evaluate the isochronism. The revolution frequency of an accumulated single-ion is temporally varied, as already shown in Ref. 3), because the momentum is smoothly decreased with time owing to the collision with the residual gas under the vacuum level of  $10^{-5}$  Pa. The advantage of the new method is that the isochronism over the full range of momentum acceptance is precisely monitored with a single event, and the measurement is completed within a few seconds.

We practically applied this method to measure the isochronism of R3 using  $^{78}\text{Ge}^{32+}$  beam with an energy of 166 MeV/nucleon, and attempted to fine tune the isochronism. Figure 1 shows the momentum dependence of the revolution frequency. The momentum acceptance of R3 and the beam transport line up to R3 is limited to  $\pm 0.3\%$  and the good field region in R3 is provided within  $\pm 0.3\%$ . Although a particle with momentum less than  $-0.3\%$  can be accumulated, its isochronism is unestablished. Therefore, we discuss here the isochronism within the momentum region of  $\pm 0.3\%$ . The black line indicates the momentum-dependent revolution frequency under the expected setting of the trim-coil current. The initial momentum, which is indicated at the right edge of the plot, was obtained from the horizontal position measured at the dispersive focal point F5 in BigRIPS. The third-order correlation between the revolution frequency and momentum remains. It is suppressed by fine tuning the trim-coil

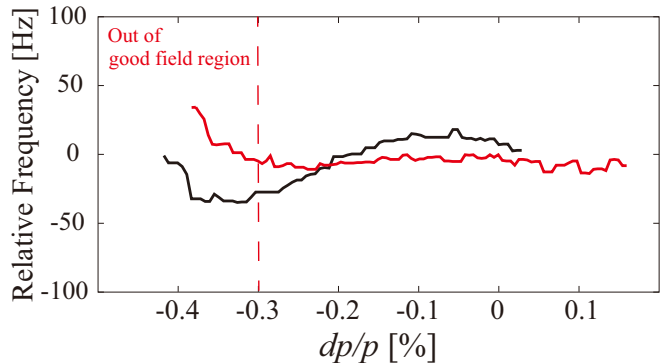


Fig. 1. Revolution frequency as a function of momentum converted from the accumulation time. The black and red solid lines indicate the revolution frequency before and after the fine tuning procedure, respectively. Two lines correspond to one event each. We subtracted the center frequency of the observational range from each revolution frequency. The momentum region less than  $-0.3\%$  is out of the acceptance. Third-order correlation between the revolution frequency and momentum disappeared owing to fine tuning. The isochronism was obtained to be  $5.4 \times 10^{-6}$ .

current using the known response functions of each trim-coil current to the isochronism. Among the ten horizontally arranged trim coils, the currents for the inner trim coils were slightly decreased by a few percent and those for the outer trim coils were oppositely increased in this case. This tuning procedure was repeated for some time. The red line shows the revolution frequency after the tuning procedure and it is nearly constant within the momentum acceptance. We can reduce the variation in frequency within the momentum acceptance from 46 Hz before tuning to 15 Hz after tuning. This corresponds to the isochronism of  $5.4 \times 10^{-6}$ . The data outside the acceptance are ignored because they are out of the good field region. We succeeded in the quick tuning of isochronism with a resonant Schottky pick-up and frequency variation within the momentum acceptance was easily achieved in the order of  $10^{-6}$ .

## References

- 1) Y. Yamaguchi *et al.*, Nucl. Instrum. Methods Phys. Res. B **317**, 629 (2013).
- 2) F. Nolden *et al.*, Nucl. Instrum. Methods Phys. Res. A **659**, 69 (2011).
- 3) F. Suzaki *et al.*, Proc. of 13th Int. Conf. on Heavy Ion Acc. Tech., 98 (2015).

<sup>\*1</sup> RIKEN Nishina Center

# Preliminary analysis of the mass measurement experiment in the south-western region of $^{132}\text{Sn}$ with Rare RI Ring

H. F. Li,<sup>\*1,\*2,\*3</sup> S. Naimi,<sup>\*1</sup> D. Nagae,<sup>\*1</sup> Y. Abe,<sup>\*1</sup> F. Suzaki,<sup>\*1</sup> Y. Yamaguchi,<sup>\*1</sup> M. Wakasugi,<sup>\*1</sup> S. Omika,<sup>\*4</sup> K. Inomata,<sup>\*4</sup> H. Arakawa,<sup>\*4</sup> S. Hosoi,<sup>\*4</sup> K. Nishimuro,<sup>\*4</sup> Y. Inada,<sup>\*4</sup> T. Kobayashi,<sup>\*4</sup> D. Kajiki,<sup>\*4</sup> D. Hamakawa,<sup>\*4</sup> W. B. Dou,<sup>\*4</sup> T. Yamaguchi,<sup>\*4</sup> M. Mukai,<sup>\*5</sup> T. Moriguchi,<sup>\*5</sup> R. Kagesawa,<sup>\*5</sup> D. Kamioka,<sup>\*5</sup> A. Ozawa,<sup>\*5</sup> S. Suzuki,<sup>\*2</sup> Z. Ge,<sup>\*2</sup> C. Y. Fu,<sup>\*2</sup> Q. Wang,<sup>\*2</sup> M. Wang,<sup>\*2</sup> S. Ota,<sup>\*6</sup> S. Michimasa,<sup>\*6</sup> N. Kitamura,<sup>\*6</sup> S. Masuoka,<sup>\*6</sup> D. S. Ahn,<sup>\*1</sup> H. Suzuki,<sup>\*1</sup> N. Fukuda,<sup>\*1</sup> H. Takeda,<sup>\*1</sup> Y. Shimizu,<sup>\*1</sup> Y. A. Litvinov,<sup>\*7</sup> G. Lorusso,<sup>\*8</sup> and T. Uesaka<sup>\*1</sup>

Mass measurement experiments were conducted at Rare RI Ring (R3)<sup>1)</sup> in 2018. Neutron-rich  $^{122}\text{Rh}$ ,  $^{123,124}\text{Pd}$ , and  $^{125}\text{Ag}$  nuclides were measured in two settings.<sup>2)</sup> The principle of the mass measurement in the R3 can be described by the following equation:

$$\frac{m_1}{q_1} = \frac{m_0}{q_0} \frac{T_1}{T_0} \sqrt{\frac{1 - \beta_1^2}{1 - \left(\frac{T_1}{T_0} \beta_1\right)^2}} \quad (1)$$

where  $T_1$  and  $T_0$  are the revolution times of nucleus of interest and reference nucleus, respectively, and  $\beta_1$  is the velocity of the nucleus of interest.<sup>3)</sup> The unknown mass  $m_1$  is determined relative to the mass of reference nucleus  $m_0$ . When a particle is injected into R3 using the kicker magnet,<sup>1)</sup> it circulates for approximately 0.7 ms. The particle is then extracted to ELC using the same kicker magnet. The detector setup in R3 is shown in Fig. 1 We measured the time-of-flight (TOF) from F3 to S0 to determine the velocities of each particle and from S0 to ELC to determine  $T_1$  and  $T_0$ .

To obtain the revolution time of the particle in R3, we need to know the turn number of each particle before the extraction. For this purpose, we used detectors at R-MD4 of R3, which were composed of the E-MCP detector,<sup>4)</sup> a plastic scintillator, and a CsI(Tl) telescope.

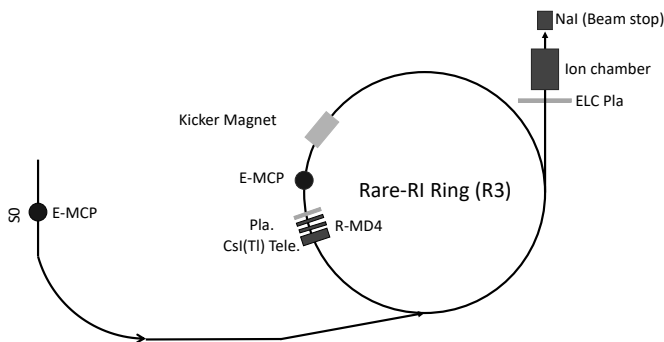


Fig. 1. Schematic view of the detector setup at R3.

Table 1. TOF, revolution times, and deduced turn numbers of nuclide in the two settings.

Nuclei	$^{128}\text{Sn}$	$^{127}\text{In}$	$^{126}\text{Cd}$	$^{125}\text{Ag}$
Rev. time [ns]	394.00	397.642	405.44	405.44
R3 TOF [ns]	724922.66	724897.19	724904.61	724904.61
Turns	1840	1823	1806	1788

$^{127}\text{Sn}$	$^{126}\text{In}$	$^{125}\text{Cd}$	$^{124}\text{Ag}$	$^{123}\text{Pd}$
391.69	395.28	399.04	402.99	407.09
724293.23	724204.20	724284.13	724561.00	724621.44
1849	1832	1815	1798	1780

First, the telescope detectors and plastic scintillator at R-MD4 were placed on the central orbit and the injection time spectrum was recorded. Second, the detectors were moved to the inner side of the ring, 85 mm away from the central orbit, which corresponds to the extraction orbit. The TOF of the nuclei, circulating in R3, can be determined from these two measurements. Third, we inserted the E-MCP detector with a thin foil into the central orbit of the ring to measure the revolution time of the nuclei. The turn number of each nucleus was determined based on the TOF obtained by the first two steps and the revolution time obtained by the third step. The TOF in the R3, revolution time measured by the E-MCP detector, and the deduced turn number are listed in Table 1. For  $^{122}\text{Rh}$  and  $^{124}\text{Pd}$ , the turn numbers could not be clearly determined owing to the low statistics of the revolution times. However, the revolution times of  $^{122}\text{Rh}$  and  $^{124}\text{Pd}$  could be precisely estimated based on the mean  $B\rho$  value and central orbit length, which were calibrated by the data of other nuclei.

To determine the mass, besides  $T_{0,1}$ , we also need to calculate  $\beta_1$  for each event.  $\beta_1$  will be determined by the TOF between the F3 achromatic focus of BigRIPS and S0 and the corresponding path length that will be calibrated by the reference nuclei in the future.

## References

- 1) Y. Yamaguchi *et al.*, Nucl. Instrum. Methods Phys. Res. B **317**, 629(2013).
- 2) S. Naimi *et al.*, in this report.
- 3) A. Ozawa *et al.*, Prog. Theor. Exp. Phys. **2012**, 03C009 (2012).
- 4) Y. Abe *et al.*, JPS Conf. Proc. **1**, 013059 (2014).
- 5) D. Nagae *et al.*, RIKEN Accel. Prog. Rep. **51**, 168 (2018).

\*1 RIKEN Nishina Center  
 \*2 Institute of Modern Physics, Chinese Academy of Sciences  
 \*3 University of Chinese Academy of Sciences  
 \*4 Department of Physics, Saitama University  
 \*5 Institute of Physics, University of Tsukuba  
 \*6 Center for Nuclear Study, University of Tokyo  
 \*7 GSI Helmholtzzentrum für Schwerionenforschung  
 \*8 NPL, University of Surrey

## First online experiment of $\alpha$ -ToF detector with MRTOF-MS

T. Niwase,<sup>\*1,\*2</sup> M. Wada,<sup>\*3</sup> P. Schury,<sup>\*3</sup> Y. Ito,<sup>\*4</sup> S. Kimura,<sup>\*1</sup> D. Kaji,<sup>\*1</sup> M. Rosenbusch,<sup>\*1</sup> Y. X. Watanabe,<sup>\*3</sup> Y. Hirayama,<sup>\*3</sup> H. Miyatake,<sup>\*3</sup> J. Y. Moon,<sup>\*3,\*7</sup> H. Ishiyama,<sup>\*1</sup> K. Morimoto,<sup>\*1</sup> H. Haba,<sup>\*1</sup> T. Tanaka,<sup>\*1,\*2</sup> S. Ishizawa,<sup>\*1,\*4</sup> A. Takamine,<sup>\*1</sup> K. Morita,<sup>\*1,\*2</sup> and H. Wollnik<sup>\*5</sup>

We have the measured masses of more than 80 short-lived nuclei using a multi reflection time-of-flight mass spectrograph (MRTOF-MS)<sup>1)</sup> and plan to measure super heavy nuclei. For this purpose, we developed a new innovative detector, named  $\alpha$ -ToF,<sup>2)</sup> which is capable of performing correlation measurement of the time-of-flight signal and successive  $\alpha$  decay signals. It can reliably discriminate true events from background events.

The first online experiment of the  $\alpha$ -ToF detector was performed at SHE-Mass-II<sup>3)</sup> coupled with the gas-filled recoil Ion Separator GARIS-II.<sup>4)</sup> A short-lived radium isotope was produced in the  $^{159}\text{Tb}(^{51}\text{V}, 5n)^{207}\text{Ra}$  reaction by a 219.1 MeV primary beam with an intensity of 1.0 pμA. The 460 μg/cm<sup>2</sup> thick Tb target was produced by sputtering of the target material on a 3.0 μm thick Ti backing foil. The reaction products (fusion-evaporation residues: ERs) were separated in-flight from the projectiles and other background products. The ERs were captured in a cryogenic He gas catcher through Mylar foil windows, and the thermalized ions were extracted from the gas catcher by an rf-carpet and further transported to the MRTOF-MS via multiple ion traps.

The SHE-Mass-II facility has a single triplet ion trap, which directly connects the gas catcher to the MRTOF to achieve high efficiency. However, such configuration might suffer from contaminant ions from the gas catcher, therefore, we placed a Bradbury-Nielsen ion gate between the trap and the MRTOF to reduce the contamination. Unfortunately, the gate was broken just before the measurement due to a discharge accident. A preliminary time-of-flight spectrum for  $^{207}\text{Ra}^{2+}$  is shown in Fig. 1. Many background counts are seen in the raw spectrum (Fig. 1 (a)). On gating the spectrum by the  $\alpha$ -ray energy of  $^{207}\text{Ra}$  with a coincident time of two half-life periods, such backgrounds were reduced by a factor of 40 (Fig. 1 (b)), while the true event number was preserved with 36% efficiency, which agrees with the solid angle of the Si detector and the limited coincidence time.

Figure 2 (a) shows a part of the two-dimensional spectrum for the time-of-flight and the  $\alpha$ -energy while Fig. 2 (b) shows a decay time spectrum of  $^{207}\text{Ra}$ . The decay time is the interval between the time-of-flight

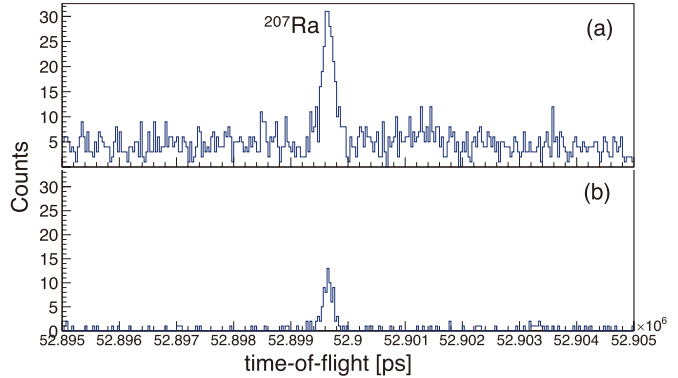


Fig. 1. A part of the time-of-flight spectrum of  $^{207}\text{Ra}$ . (a) is a raw spectrum while (b) shows coincident events with  $\alpha$ -rays from  $^{207}\text{Ra}$  for a coincident time of two half-lives of  $^{207}\text{Ra}$ .

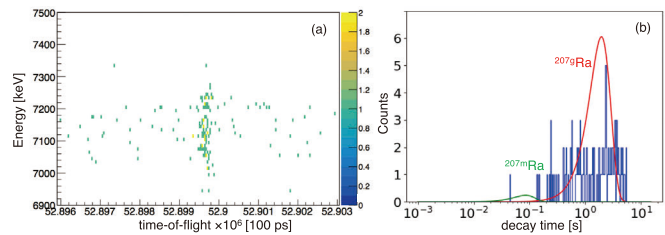


Fig. 2. (a) Two-dimensional spectrum of the time-of-flight and  $\alpha$ -decay energy. (b) decay spectrum of  $^{207}\text{Ra}$ . The solid lines indicate the literature values of the decay profiles, namely  $T_{1/2} = 1.3$  s and 59 ms with an intensity ratio of 1:20.

signal and the  $\alpha$ -ray signal. From this spectrum, the half-life of  $^{207}\text{Ra}$  is found to be 1.33(50) s, which agrees with the literature value.<sup>5)</sup> We also observed a few early events, which are consistent with the decay from the isomeric state of  $^{207m}\text{Ra}$  having a half-life of 59 ms.

In this first online experiment, we confirmed that the  $\alpha$ -ToF detector can reduce the background in a time-of-flight spectrum and obtain decay properties of short-lived nuclei.

### References

- 1) P. Schury *et al.*, Nucl. Instrum. Methods Phys. Res. B **335**, 39 (2014).
- 2) T. Niwase *et al.*, RIKEN Accel. Prog. Rep. **51**, 157 (2018).
- 3) M. Wada *et al.*, RIKEN Accel. Prog. Rep. **52**, (2019).
- 4) D. Kaji *et al.*, Nucl. Instrum. Methods Phys. Res. B **317**, 311 (2013).
- 5) F. G. Kondev, S. Lalkovski *et al.*, Nucl. Data Sheets **112**, 707 (2011).

\*1 RIKEN Nishina Center

\*2 Department of Physics, Kyushu University

\*3 KEK, Wako Nuclear Science Center

\*4 Japan Atomic Energy Agency

\*5 Department of Physics, Yamagata University

\*6 Department of Chemistry and Biochemistry, New Mexico State University

\*7 Institute for Basic Science, Rare Isotope Science Project

## $\beta$ - $\gamma$ spectroscopy of $^{195}\text{Os}$ at KISS

M. Ahmed,<sup>\*1</sup> Y. X. Watanabe,<sup>\*2</sup> Y. Hirayama,<sup>\*2</sup> M. Mukai,<sup>\*1</sup> J. H. Park,<sup>\*3</sup> P. Schury,<sup>\*2</sup> Y. Kakiguchi,<sup>\*2</sup> S. Kimura,<sup>\*4</sup> A. Ozawa,<sup>\*1</sup> M. Oyaizu,<sup>\*2</sup> M. Wada,<sup>\*2</sup> and H. Miyatake<sup>\*2</sup>

Almost a half of nuclei in nature heavier than iron are considered to have been synthesized in the rapid neutron capture process (r-process) under an explosive stellar environment with a temperature higher than  $10^9$  K and a neutron density higher than  $10^{20}$  cm<sup>-3</sup>. The r-process goes through the region of extremely neutron-rich nuclei under such an explosive condition. The peak at the mass number of 195, called as the 3rd peak, on the observed solar r-abundance distribution is considered to be originated from the waiting point nuclei with the neutron number ( $N$ ) of 126 on the r-process path. The astrophysical environment such as the temperature and the neutron density is not known for the formation of the 3rd peak. To investigate those conditions, the properties such as lifetimes and masses of the waiting point nuclei are important. However, they are too far from the  $\beta$ -stability line to experimentally access. Therefore, some theoretical prediction is employed for the physical values of the nuclear properties concerning the r-process in order to perform the nucleosynthesis simulation to survey the explosive stellar conditions. Thus a reliable theoretical nuclear model is required to precisely predict those nuclear properties to elucidate the astrophysical environments of the r-process. The region of the neutron-rich nuclei around  $N = 126$  is predicted as a competitive region of the first-forbidden (FF) and the allowed Gamow-Teller (GT)  $\beta$ -decays.<sup>1)</sup> Such competition makes it difficult to theoretically predict their half-lives, and those predicted values in various theoretical models are deviated from each other. The systematic experimental investigation of nuclear properties of the neutron-rich nuclei around  $N = 126$  is important for the selection of reliable theoretical model and improvement of their predictions.

Neutron-rich osmium isotopes are candidates to study their nuclear structures because they have the filled single particle orbits  $h_{11/2}$  for protons, which contribute to the GT  $\beta$ -transitions for the nuclei around  $N = 126$ . We have performed  $\beta$ - $\gamma$  spectroscopy of  $^{195}\text{Os}$  at KEK Isotope Separation System (KISS)<sup>2)</sup> to study its  $\beta$ -decay scheme, which is unknown so far. The  $^{195}\text{Os}$  isotopes were produced by multi-nucleon transfer reactions between the  $^{136}\text{Xe}$  beam (50 pA on target) with energy of around 10 MeV/nucleon and a  $^{198}\text{Pt}$  target. They were collected, separated and extracted by the KISS, and finally the  $^{195}\text{Os}$  ions of its ground state and isomeric state were transported with the rate of 14(2) cps to the measurement area. They were implanted into an alu-

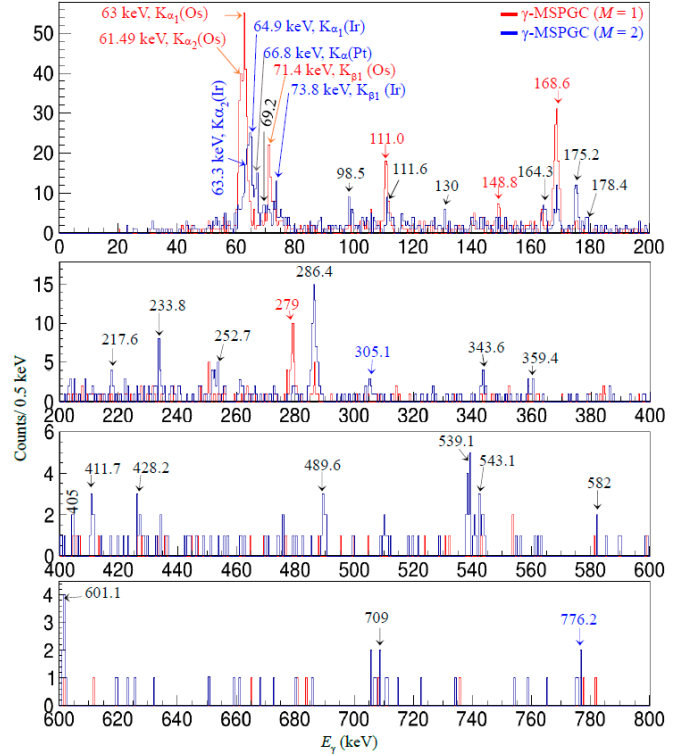


Fig. 1. Measured  $\gamma$ -ray energy spectra in coincidence with the MSPGC detector hit patterns  $M = 1$  (red line) and  $M = 2$  (blue line).

minized Mylar tape, which was surrounded by the Multi-Segmented Proportional Gas Counter (MSPGC)<sup>3)</sup> and four High-Purity Germanium (HPGe) clover detectors. The MSPGC was used to detect  $\beta$ -rays, X-rays and conversion electrons, and the HPGe clover detectors were used to detect  $\gamma$ -rays. Figure 1 shows measured  $\gamma$ -ray energy spectra in coincidence with the MSPGC detector hit patterns  $M = 1$  (red line) and  $M = 2$  (blue line). The hit patterns  $M = 1$  and  $M = 2$  are sensitive to X-rays and  $\beta$ -rays, respectively. We have found 28  $\gamma$ -ray peaks in total with some characteristic X-rays. 22  $\gamma$ -ray peaks denoted by black labels agree with energies in the literature for  $\gamma$ -rays from  $^{194}\text{Ir}(n, \gamma)^{195}\text{Ir}$  reactions and  $\beta$ -delayed  $\gamma$ -rays of  $^{195}\text{Ir}$ . We found 6  $\gamma$ -ray peaks for the first time. The lifetime measurements and  $\gamma$ - $\gamma$  coincidence analyses reveal that two of them with blue labels are  $\beta$ -delayed  $\gamma$ -rays of  $^{195}\text{Os}$ , and four of them with red labels are  $\gamma$ -rays associated with a newly found isomeric decay of  $^{195}\text{Os}$ . Further analysis for the  $\beta$ -decay scheme and the isomeric decay of  $^{195}\text{Os}$  is in progress.

### References

- 1) I. N. Borzov, Phys. Rev. C **67**, 025802 (2003).
- 2) Y. Hirayama *et al.*, Nucl. Instrum. Methods Phys. Res. B **353**, 4 (2015).
- 3) M. Mukai *et al.*, Nucl. Instrum. Methods Phys. Res. A **884**, 1 (2018).

<sup>\*1</sup> Department of Physics, University of Tsukuba

<sup>\*2</sup> Wako Nuclear Science Center (WNSC), Institute of Particle and Nuclear Studies (IPNS), High Energy Accelerator Research Organization (KEK)

<sup>\*3</sup> Institute for Basic Science (IBS)

<sup>\*4</sup> RIKEN Nishina Center

# Feasibility study of $^{199}\text{Pt}$ $Q$ -moment measurement using in-gas-jet laser ionization spectroscopy at KISS

H. Choi,<sup>\*1</sup> Y. Hirayama,<sup>\*2</sup> Y. X. Watanabe,<sup>\*2</sup> P. Schury,<sup>\*2</sup> M. Mukai,<sup>\*2</sup> M. Ahmed,<sup>\*2,\*3</sup> M. Oyaizu,<sup>\*2</sup> M. Wada,<sup>\*2</sup> and H. Miyatake<sup>\*2</sup>

KEK Isotope Separation System (KISS)<sup>1)</sup> has been developed to study nuclei in the region of neutron magic number  $N = 126$ . We investigated the nuclear structure of  $^{199}\text{Pt}$  and Ir isotopes by measuring their hyperfine structures (HFSs) through the in-gas-cell laser ionization technique.<sup>2)</sup> In the measurement, we obtained precise values of magnetic dipole moments  $\mu = +0.75(8) \mu_N$  and  $\mu = -0.57(5) \mu_N$  for  $^{199g}\text{Pt}$  and  $^{199m}\text{Pt}$ , respectively. However the errors of electric quadrupole moments were quite large,  $Q_g = +1.7(17) \text{ b}$  and  $Q_m = +3.5(21) \text{ b}$ . To improve the spectral resolution, we developed an in-gas-jet laser ionization spectroscopy technique at KISS. In the laser system, a diode laser (TOPTICA, DLC DL Pro HP, 450 nm) is used for the seed laser of a pulsed dye-amplifier (Sirah), which creates UV light ( $\lambda_1 = 225 \text{ nm}$ ) for the excitation to the state  $5d^8 6s 6p^5 F_2$ . A Nd:YAG laser (EdgeWave) is used to pump the dye amplifier and for ionization as the second step ( $\lambda_2 = 355 \text{ nm}$ ). Compared to in-gas-cell ionization, we improved the resolution from 12.5(5) GHz to 0.6(1) GHz in the full width of the half maximum owing to the low density and temperature conditions of the gas jet.<sup>3)</sup> From this result, we are expecting to obtain a much more precise value of electromagnetic moments and isotope shift for  $^{199}\text{Pt}$  through the in-gas-jet laser ionization spectroscopy technique.

The feasibility of  $^{199}\text{Pt}$  HFS measurement through the in-gas-jet laser ionization spectroscopy was investigated by the Monte Carlo simulation. Based on the HFS spread and present resolution of 0.6 GHz by the in-gas-jet method, we determined the measurement step  $\Delta\nu_1 = 0.27 \text{ GHz}$ . From the yield of  $^{199g+m}\text{Pt}$ , we determined the measurement time of 10 min for each data point, which corresponds to a measurement of 20 h. A Voigt function with Gaussian width  $\Gamma_G = 316(27) \text{ MHz}$  and Lorentzian width  $\Gamma_L = 110(76) \text{ MHz}$ , which were determined from the off-line measurement of  $^{196}\text{Pt}$  ( $I^\pi = 0^+$ ), was used in a response function of the resonance peak. Relative intensities between each resonance peak were computed via the Racah coefficient. We assumed the unknown electric quadrupole hyperfine coupling constant of the atomic excited state of  $^{199g}\text{Pt}$  to be 1 GHz.

Figure 1 shows the simulated hyperfine splitting spectrum of  $^{199g+m}\text{Pt}$ . The vertical axis indicates the expected  $\beta$ -ray events detected by MSPGC<sup>4)</sup> during the 10 min beam accumulation. The total  $\beta$ -ray events were evaluated to be 4915 counts. Figure 2 shows the simulated HFS spectrum of  $^{199m}\text{Pt}$  nuclei obtained by gat-

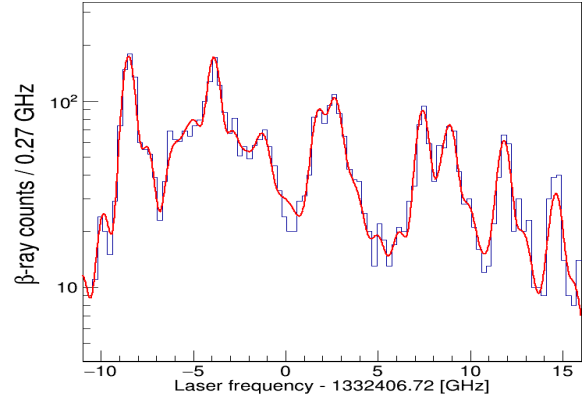


Fig. 1. Simulated HFS spectrum of  $^{199g+m}\text{Pt}$ . Red line indicates the simultaneous fitting function.

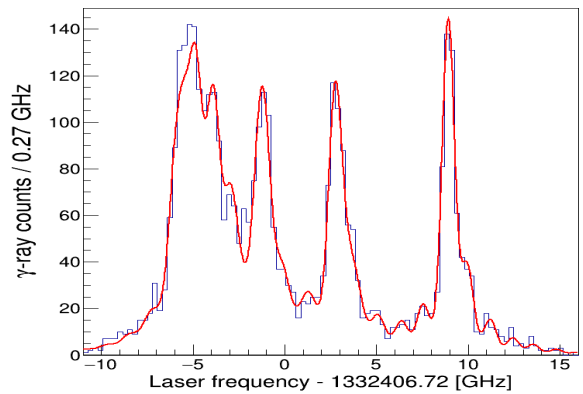


Fig. 2. Simulated HFS spectrum of  $^{199m}\text{Pt}$  obtained by gating on 392-keV  $\gamma$ -ray.

ing on a 392 keV  $\gamma$ -ray. Total  $\gamma$ -ray events detected by the four super clover Ge detectors were evaluated to be 3941 counts. In the analysis, the spectra in Figs. 1 and 2 were simultaneously fitted using the common parameters (electromagnetic hyperfine coupling constants) for  $^{199i}\text{Pt}$  ( $i = g, m$ ). The reduced chi-square of fitting was 1.13. In the simulation, we assumed  $\mu_g = +0.75 \mu_N$  and  $Q_g = +1.7 \text{ b}$ , and  $\mu_m = -0.57 \mu_N$  and  $Q_m = +3.5 \text{ b}$  for  $^{199g}\text{Pt}$  and  $^{199m}\text{Pt}$  respectively. The evaluated electromagnetic moments from the fitting were  $\mu_g = +0.7434(58) \mu_N$ ,  $Q_g = +1.75(10) \text{ b}$ ,  $\mu_m = -0.5740(49) \mu_N$ , and  $Q_m = +3.42(10) \text{ b}$ . From the simulation, we confirmed that the 20 h measurement is enough to achieve precise values of electromagnetic moments for  $^{199}\text{Pt}$ .

## References

- 1) Y. Hirayama *et al.*, Nucl. Instrum. Methods Phys. Res. B **353**, 4 (2015).
- 2) Y. Hirayama *et al.*, Phys. Rev. C **96**, 014307 (2017).
- 3) Y. Hirayama *et al.*, in this progress report.
- 4) M. Mukai *et al.*, Nucl. Instrum. Methods Phys. Res. A **884**, 1 (2018).

<sup>\*1</sup> Seoul National University

<sup>\*2</sup> Wako Nuclear Science Center (WNSC), Institute of Particle and Nuclear Studies (IPNS), High Energy Accelerator Research Organization (KEK)

<sup>\*3</sup> Department of Physics, University of Tsukuba

# Electric field gradient of ZnO crystal measured by $\beta$ -NQR of $^{23}\text{Ne}$

H. Nishibata,<sup>\*1</sup> A. Gladkov,<sup>\*1,\*2</sup> T. Kawaguchi,<sup>\*3</sup> H. Ueno,<sup>\*1</sup> Y. Ichikawa,<sup>\*1</sup> A. Takamine,<sup>\*1</sup> T. Sato,<sup>\*1</sup> K. Kawata,<sup>\*1,\*4</sup> H. Yamazaki,<sup>\*1</sup> W. Kobayashi,<sup>\*3</sup> M. Sanjo,<sup>\*3</sup> L. C. Tao,<sup>\*5</sup> Y. Namamura,<sup>\*6</sup> T. Asakawa,<sup>\*3</sup> Y. Sasaki,<sup>\*3</sup> K. Totsuka,<sup>\*3</sup> K. Doi,<sup>\*3</sup> T. Yada,<sup>\*3</sup> K. Asahi,<sup>\*1</sup> Y. Ishibashi,<sup>\*7</sup> K. Imamura,<sup>\*8</sup> T. Fujita,<sup>\*9</sup> G. Georgiev,<sup>\*10</sup> J. M. Daugas,<sup>\*11</sup> and S. Fujiyama<sup>\*12</sup>

This report presents the results of the experimental program NP1612-RRC47, which is a part of a project to measure the ground-state magnetic dipole ( $\mu$ ) and electric quadrupole ( $Q$ ) moments of neutron-rich Ne isotopes.

The structures of neutron-rich Ne have attracted much attention because of their exotic structures in the ground states, such as large deformation and p-wave halo, as suggested by some of the experiments.<sup>1)</sup> In order to investigate such structures, measurements of  $\mu$  and  $Q$  moments are one of the most effective ways; however, up to now, there exist no moment data for neutron-rich Ne isotopes. In our project, we approach the ground-state moments of neutron-rich Ne isotopes by means of  $\beta$ -detected nuclear magnetic resonance ( $\beta$ -NMR). As the first step of this project, we performed an experiment to determine an appropriate single crystal with an electric field gradient at the Ne stopping site for  $\beta$ -NMR measurement of the Ne isotopes. In the present experiment, we applied a  $\beta$ -NQR method<sup>2)</sup> to the spin-polarized  $^{23}\text{Ne}$ , whose ground-state moments and spin were well known.<sup>3)</sup>

The experiment was performed by using RIKEN projectile fragment separator (RIPS). A radioactive  $^{23}\text{Ne}$  was produced by the one-neutron pickup reaction of  $^{22}\text{Ne}$  (70 MeV/nucleon) with a 0.25-mm-thick Be target. The  $^{23}\text{Ne}$  spin polarization was obtained by injecting the primary beam with a tilt angle of  $2^\circ$  with respect to the Be target at the focal plane F0 and selecting the mo-

Table 1. Comparison between the experimental  $|q|$  and the calculated ones.

Exp.	Calc.	
	Zn site	O site
31(3)	30	45
$\times 10^{19} [\text{V}/\text{m}^2]$	$\times 10^{19} [\text{V}/\text{m}^2]$	$\times 10^{19} [\text{V}/\text{m}^2]$

mentum of  $^{23}\text{Ne}$  at the dispersive focal plane F1. The obtained spin polarization of  $^{23}\text{Ne}$  was approximately 8%.

Figure 1 shows a layout of the experimental setup. In the figure, the spin-polarized  $^{23}\text{Ne}$  beam comes from left to right side and stops in a ZnO single crystal in vacuum. The crystal was cooled down to  $\sim 47$  K to achieve a long spin-lattice relaxation time. A static magnetic field of 0.5 T was applied to the crystal. An oscillating magnetic field was applied by a pair of coils perpendicular to the static magnetic field through a vacuum chamber wall, made of fiber-reinforced plastics. The  $\beta$  rays from the  $\beta$  decay of  $^{23}\text{Ne}$  were detected by two telescopes, which consist of three 1.0-mm-thick plastic scintillators, placed at  $0^\circ$  and  $180^\circ$  along the polarization direction.

The obtained NQR spectrum for the ZnO crystal has been already shown in the previous report.<sup>4)</sup> The observation of the resonance indicated that the ZnO single crystal is available for the Ne NMR measurement and ensures sufficient spin-lattice relaxation time. From the obtained  $\nu_Q (= eQq/h) = 1.08(5) \times 10^3$  kHz and the literature  $Q$  moment value of  $^{23}\text{Ne}$ ,  $Q = 145(13)$  emb,<sup>3)</sup> the electric field gradient  $q$  was obtained as  $|q| = 31(3) \times 10^{19} \text{ V}/\text{m}^2$ .

For a deeper insight, the obtained electric field gradient was compared with those calculated by using the gauge including projector augmented waves (GIPAW) approach.<sup>5)</sup> Table 1 compares the experimental electric field gradient with those calculated for substitutional sites of Zn and O. As seen in the table, the experimental value is very close to that for the O site. It may suggest that the implanted  $^{23}\text{Ne}$  tends to stop at the substitutional Zn site.

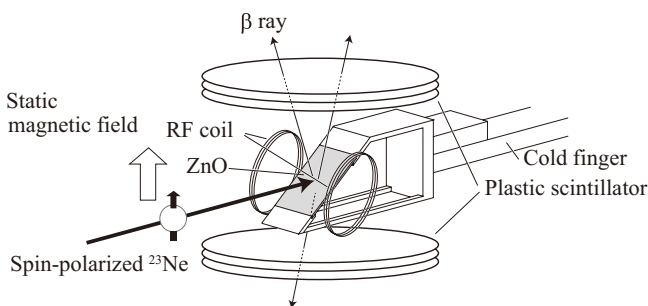


Fig. 1. Experimental setup.

\*1 RIKEN Nishina Center  
 \*2 Department of Physics, Kyungpook National University  
 \*3 Department of Physics, Hosei University  
 \*4 Center for Nuclear Study, University of Tokyo  
 \*5 School of Physics, Peking University  
 \*6 Department of Physics, Meiji University  
 \*7 Cyclotron and Radioisotope Center, Tohoku University  
 \*8 Department of Physics, Okayama University  
 \*9 Department of Physics, Osaka University  
 \*10 CSNSM, CNRS/IN2P3, Université Paris-Sud  
 \*11 CEA, DAM, DIF  
 \*12 RIKEN, Condensed Molecular Materials Laboratory

## References

- 1) T. Nakamura *et al.*, Phys. Rev. Lett. **112**, 142501 (2014) and references therein.
- 2) D. Nagae *et al.*, Nucl. Instrum. Methods Phys. Res. B **266**, 4612 (2008).
- 3) W. Geithner *et al.*, Phys. Rev. C **71**, 064319 (2005).
- 4) H. Nishibata *et al.*, RIKEN Accel. Prog. Rep. **2017**, 75 (2018).
- 5) C. J. Pickard, F. Mauri, Phys. Rev. B **63**, 245101 (2001).

# ${}^7\text{Be}$ target production to measure ${}^7\text{Be}(d, p)$ reaction for the primordial ${}^7\text{Li}$ problem in Big-Bang Nucleosynthesis

A. Inoue,<sup>\*1</sup> A. Tamii,<sup>\*1</sup> S. Cha,<sup>\*2</sup> K. Y. Chae,<sup>\*2</sup> S. Hayakawa,<sup>\*3</sup> N. Kobayashi,<sup>\*1</sup> S. Nakamura,<sup>\*1</sup> T. Shima,<sup>\*1</sup> H. Shimizu,<sup>\*3</sup> H. Yamaguchi,<sup>\*3</sup> L. Yang,<sup>\*3</sup> and Z. Yang<sup>\*1</sup>

The overestimation of primordial  ${}^7\text{Li}$  abundance in the standard Big-Bang nucleosynthesis (BBN) model is one of the known and unresolved problems. A recent theoretical BBN model predicted a primordial  ${}^7\text{Li}$  abundance that was approximately three times larger than the recent precise observation.<sup>1)</sup> Light nuclei were produced up to  ${}^7\text{Be}$  by nuclear reactions in several hundred seconds following the Big Bang.

${}^7\text{Li}$  nuclei were predominantly produced by the electron capture decay of  ${}^7\text{Be}$  in the standard BBN model. The decay half life of  ${}^7\text{Be}$ , 53.22 days, is much longer than the timescale of the production of light nuclei after the Big Bang. Thus, one possible scenario to solve the  ${}^7\text{Li}$  problem is that  ${}^7\text{Be}$  was destroyed in the timescale of the nuclear reactions. There are several possibilities to destroy  ${}^7\text{Be}$ , for example, the  ${}^7\text{Be}(d, p){}^8\text{Be}$ ,  ${}^7\text{Be}(n, \alpha)$ , or  ${}^7\text{Be}(n, p)$  reactions.<sup>2)</sup> We focus on the  ${}^7\text{Be}(d, p){}^8\text{Be}$  reaction because its contribution is suggested to be larger than that of  ${}^7\text{Be}(n, \alpha){}^4\text{He}$ .<sup>3,4)</sup> The goal of the experiment is to measure the cross-section of the  ${}^7\text{Be}(d, p){}^8\text{Be}$  reaction in the BBN energy region of 100–400 keV. We plan to measure the  ${}^7\text{Be}(d, p){}^8\text{Be}$  reaction with a  ${}^7\text{Be}$  target because the available data are insufficient for the accuracy or energy range.<sup>5,6)</sup> We are also motivated to measure the reaction in direct kinematics because it implements a good energy resolution. The method allows us to reconstruct the kinematics of the reaction by measuring the outgoing proton without measuring the two alpha particles. We apply the *implantation target method* to produce the  ${}^7\text{Be}$  target.  ${}^7\text{Be}$  particles were implanted by irradiating a gold target with a  ${}^7\text{Be}$  beam.

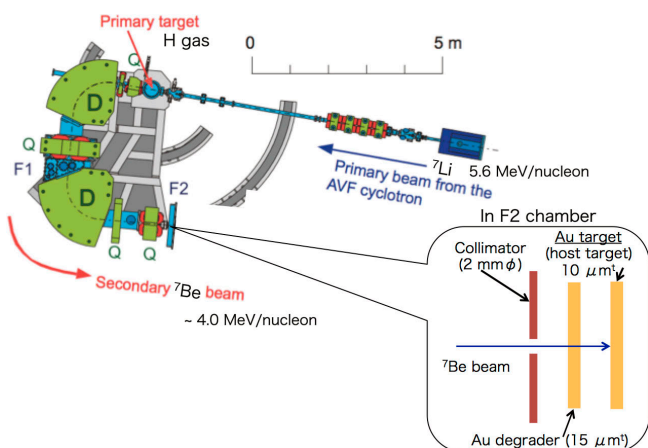


Fig. 1. Experimental setup at CRIB. The enlarged schematic picture shows the inside of the F2 chamber.

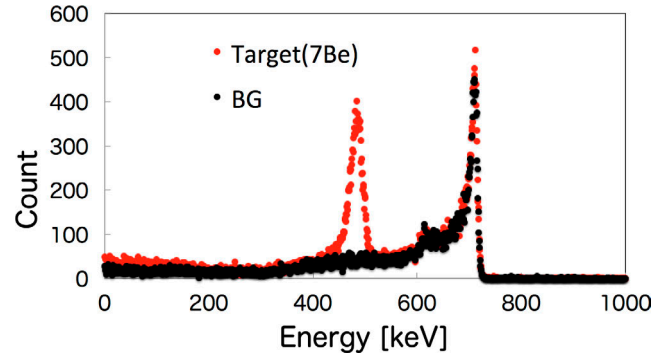


Fig. 2.  $\gamma$ -ray energy spectrum of the implanted  ${}^7\text{Be}$  (red dotted plot) and background spectrum (black dotted plot).

We performed an experiment to produce a  ${}^7\text{Be}$  implanted target at CRIB, Center for Nuclear Study (CNS) in April, 2018. The experimental setup is shown in Fig. 1.<sup>7)</sup> The primary beam was  ${}^7\text{Li}^{2+}$  at 5.6 MeV/nucleon. The secondary beam was produced by the  ${}^1\text{H}({}^7\text{Li}, {}^7\text{Be})$  reaction. The secondary beam energy was 4.0 MeV/nucleon. The  ${}^7\text{Be}$  beam was directed on to a 10  $\mu\text{m}$  thick gold target as the host material after an energy degrader made of gold with a thickness of 15  $\mu\text{m}$  and 2 mm $\phi$  collimator determined the implanted beam position.

We evaluated the amount of implanted  ${}^7\text{Be}$  by detecting 477 keV  $\gamma$ -rays with a LaBr<sub>3</sub> detector after the implantation. The  $\gamma$ -ray is emitted in the electron capture process of  ${}^7\text{Be}$  with a branching ratio of 10.5%. We achieved an implantation of  $1.9 \times 10^{12}$   ${}^7\text{Be}$  particles as expected after one day of irradiation. Figure 2 shows the measured  $\gamma$ -ray spectrum. We improved the beam optics for the the high intensity  ${}^7\text{Be}$  beam since 2017, which enabled the production of the  ${}^7\text{Be}$  target with a high intensity beam.

The  ${}^7\text{Be}$  target was carried to the Japan Atomic Energy Agency (JAEA) to measure the  $(d, p)$  reaction in June, 2018. The outgoing protons were successfully measured by three layered silicon detectors with the thickness of 500  $\mu\text{m}$  each at 2 different angles, 30° and 45°. Currently, analyses are being conducted to obtain the cross-section of the  ${}^7\text{Be}(d, p)$  reaction.

## References

- 1) R. H. Cyburt *et al.*, J. Cosmol. Astropart. Phys. **11**, 012 (2008).
- 2) M. Barbagallo *et al.*, Phys. Rev. Lett. **117**, 152701 (2016).
- 3) S. Q. Hou *et al.*, Phys. Rev. C **91**, 055802 (2015).
- 4) T. Kawabata *et al.*, Phys. Rev. Lett. **118**, 052701 (2017).
- 5) R. W. Kavanagh *et al.*, Nucl. Phys. **18**, 493 (1960).
- 6) C. Angulo *et al.*, Astrophys. J. **630**, L105 (2005).
- 7) H. Yamaguchi *et al.*, Nucl. Instrum. Methods Phys. Res. A **589**, 150 (2008).

<sup>\*1</sup> Research Center for Nuclear Physics, Osaka University

<sup>\*2</sup> Department of Physics, Sungkyunkwan University

<sup>\*3</sup> Center for Nuclear Study, Graduate School of Science, University of Tokyo

## New measurement of ${}^8\text{Li}(\alpha, n){}^{11}\text{B}$ reactions

Y. Mizoi,<sup>\*1,\*2,\*3</sup> H. Baba,<sup>\*3</sup> A. Bracco,<sup>\*4,\*5</sup> F. Camera,<sup>\*4,\*5</sup> S. M. Cha,<sup>\*6</sup> K. Y. Chae,<sup>\*6</sup> S. Cherubini,<sup>\*3,\*7,\*8</sup> H. S. Choi,<sup>\*9</sup> N. N. Duy,<sup>\*6</sup> T. Fukuda,<sup>\*3,\*10</sup> S. Hayakawa,<sup>\*2</sup> Y. Hirayama,<sup>\*11</sup> N. Imai,<sup>\*2</sup> H. Ishiyama,<sup>\*3</sup> A. Kim,<sup>\*12</sup> D. H. Kim,<sup>\*6</sup> N. Kitamura,<sup>\*2</sup> S. Kubono,<sup>\*2,\*3</sup> M. S. Kwag,<sup>\*6</sup> S. Michimasa,<sup>\*2</sup> M. Mihara,<sup>\*3,\*13</sup> H. Miyatake,<sup>\*11</sup> S. Ota,<sup>\*2</sup> R. G. Pizzone,<sup>\*7</sup> H. Shimizu,<sup>\*2,\*3</sup> N. K. Uyen,<sup>\*6</sup> R. Wakabayashi,<sup>\*3,\*13</sup> Y. X. Watanabe,<sup>\*11</sup> O. Wieland,<sup>\*4</sup> H. Yamaguchi,<sup>\*2</sup> L. Yang,<sup>\*2</sup> N. Zhang,<sup>\*2,\*14</sup> and Z. C. Zhang<sup>\*14</sup>

The  ${}^8\text{Li}(\alpha, n){}^{11}\text{B}$  reaction is considered to be the key reaction in the inhomogeneous Big Bang and type-II supernova nucleosyntheses, and we have been providing cross-section data<sup>1-7)</sup> on this reaction for more than two decades. The previous results<sup>1-7)</sup> are summarized in Fig. 1, in which the Gamow-peak widths are also drawn. The energy regions of  $T_9 = 1$  and 2 are important for the Big Bang and supernova nucleosyntheses, respectively.

As shown in Fig. 1, the cross-sections obtained by the previous experiments have large differences around  $E_{\text{cm}} = 1.0$  MeV. The previous experiments were performed by two different methods: inclusive and exclusive. The former detected either  ${}^{11}\text{B}^{1,2)}$  or neutron<sup>4,6)</sup> and the latter<sup>3,5,7)</sup> detected both  ${}^{11}\text{B}$  and neutron by measuring their kinetic energies and angles. The cross-sections of the former results are five times larger than the latter ones systematically. We could estimate that the sources of the discrepancies might originate from the experimental methods, but we have no experimental fact to determine them. To solve this problem, we designed a new *inclusive* measurement, in which we measured the  $\gamma$ -rays emitted from  ${}^{11}\text{B}^*$ s. The previous experiment did not measure the  $\gamma$ -rays. Therefore this experiment will provide new data to understand the  ${}^8\text{Li}(\alpha, n){}^{11}\text{B}$  reaction. Considering that the expected  $\gamma$ -ray energies are between 2 and 8 MeV, we selected a large volume  $3.5' \times 8''$  LaBr<sub>3</sub>:Ce detector<sup>8)</sup> provided by INFN Milano. We also installed plastic and  ${}^6\text{Li}$ -

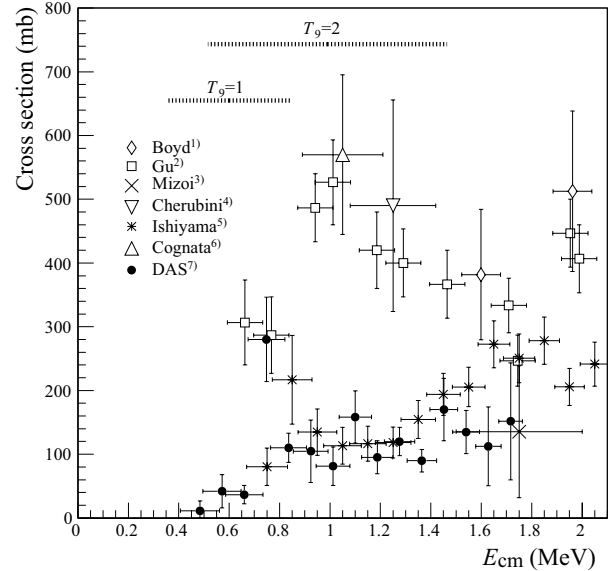


Fig. 1. Excitation functions of  ${}^8\text{Li}(\alpha, n){}^{11}\text{B}$  reaction.

glass scintillators to detect neutrons by covering wide energy ranges between a few ten keV to 10 MeV.

This experiment was performed at CRIB in September 2018. We placed a gas-target cell at F3, in which  ${}^4\text{He}$  gas was filled at a pressure of 1.0 atm. The  ${}^8\text{Li}$  beam, whose intensity was typically 300 kHz, was produced by the  ${}^7\text{Li}(d, p){}^8\text{Li}$  reaction. The primary  ${}^7\text{Li}$  beam had an energy of 6.0 MeV/nucleon and an intensity of 250 particle nA. The  $\text{D}_2$ -gas production target had a thickness of 1.9 mg/cm<sup>2</sup>. The energies of  ${}^8\text{Li}$  particles measured inside the  ${}^4\text{He}$ -gas target were between  $E_{\text{cm}} = 0.9$  and 1.9 MeV.

We successfully obtained data with sufficient statistics. Although we faced difficulties in data analysis owing to the large background originating from thermal neutrons, we could identify the  $\gamma$ -rays emitted from  ${}^{11}\text{B}^*$ s. We will further present the results to solve the controversial discrepancies.

### References

- 1) R. N. Boyd *et al.*, Phys. Rev. Lett. **68**, 1283 (1992).
- 2) X. Gu *et al.*, Phys. Lett. B **343**, 31 (1995).
- 3) Y. Mizoi *et al.*, Phys. Rev. C **62**, 065801 (2000).
- 4) S. Cherubini *et al.*, Eur. Phys. J. **20**, 355 (2004).
- 5) H. Ishiyama *et al.*, Phys. Lett. B **640**, 82 (2006).
- 6) M. La Cognata *et al.*, Phys. Lett. B **664**, 157 (2008).
- 7) S. K. Das *et al.*, Phys. Rev. C **95**, 055805 (2017).
- 8) A. Gaiz *et al.*, Nucl. Instrum. Methods Phys. Res. A **729**, 910 (2013).

<sup>\*1</sup> Center for Physics and Mathematics, Institute for Liberal Arts and Sciences, Osaka Electro-Communication University

<sup>\*2</sup> Center for Nuclear Study, the University of Tokyo

<sup>\*3</sup> RIKEN Nishina Center

<sup>\*4</sup> Istituto Nazionale di Fisica Nucleare (INFN) - Sezione di Milano

<sup>\*5</sup> Dipartimento di Fisica dell'Università degli Studi di Milano

<sup>\*6</sup> Department of Physics, Sungkyunkwan University

<sup>\*7</sup> Istituto Nazionale di Fisica Nucleare (INFN) - Laboratori Nazionali del Sud (LNS)

<sup>\*8</sup> Dipartimento di Fisica ed Astronomia, Università di Catania

<sup>\*9</sup> Department of Physics and Astronomy, Seoul National University

<sup>\*10</sup> Research Center for Nuclear Physics (RCNP), Osaka University

<sup>\*11</sup> Wako Nuclear Science Center (WNSC), Institute of Particle and Nuclear Studies (IPNS), High Energy Accelerator Research Organization (KEK)

<sup>\*12</sup> Department of Physics, Ewha Womans University

<sup>\*13</sup> Department of Physics, Osaka University

<sup>\*14</sup> Institute of Modern Physics (IMP), Chinese Academy of Science (CAS)

## Trojan Horse Method-based study of the $^{18}\text{F}(p, \alpha)^{15}\text{O}$ reaction at astrophysical energies: update on the 2015 run

S. Cherubini,<sup>\*1,\*2,\*3</sup> G. D'Agata,<sup>\*1,\*2</sup> M. Gulino,<sup>\*1,\*3,\*4</sup> M. La Cognata,<sup>\*1</sup> S. Palmerini,<sup>\*1</sup> R. G. Pizzone,<sup>\*1</sup> S. Romano,<sup>\*1,\*2</sup> R. Sparta,<sup>\*1</sup> C. Spitaleri,<sup>\*1,\*2</sup> H. Yamaguchi,<sup>\*5</sup> K. Abe,<sup>\*5</sup> O. Beliuskina,<sup>\*5</sup> S. Hayakawa,<sup>\*5</sup> D. M. Kahl,<sup>\*5</sup> Y. Sakaguchi,<sup>\*5</sup> S. Kubono,<sup>\*3</sup> D. Suzuki,<sup>\*3</sup> N. Iwasa,<sup>\*6</sup> K. Y. Chae,<sup>\*7</sup> M. Kwag,<sup>\*7</sup> H. S. Jung,<sup>\*8</sup> D. N. Binh,<sup>\*9</sup> V. Guimarães,<sup>\*10</sup> and S. Bishop<sup>\*11</sup>

The first experiment where the Trojan Horse Method (THM)<sup>1,2)</sup> was applied to measure the cross-section of an astrophysically important reaction, namely  $^{18}\text{F}(p, \alpha)^{15}\text{O}$  at nova energies,<sup>3,4)</sup> using a radioactive beam was published in Phys. Rev. C **92**, 015805 (2015).

To improve the results of that study, a new experiment was performed at the RIKEN Nishina Center using the CRIB apparatus from the University of Tokyo during the fall of 2015. Similar to the previous work, the primary beam of  $^{18}\text{O}$  delivered by the AVF cyclotron was used to produce a  $^{18}\text{F}$  radioactive beam with intensity in the range of  $10^5$ – $10^6$  pps.

After the standard CRIB apparatus, the radioactive beam of  $^{18}\text{F}$  was tracked by two PPACs and finally used to bombard thin (100–200  $\mu\text{g}/\text{cm}^2$ )  $\text{CD}_2$  targets. The THM aimed to study a suitably chosen reaction proceeding via a quasi-free mechanism with three bodies in the final state<sup>1)</sup> ( $^{18}\text{F}(d, \alpha)^{15}\text{O}n$  in this case) to infer pieces of information for the purpose of astrophysics,  $^{18}\text{F}(p, \alpha)^{15}\text{O}$  in this case.

The distance between the PPACs was substantially optimized on the basis of the experience acquired in the previous experiment. Additionally, detection system based on the ASTRHO (Array of Silicons for Trojan HORse) setup was upgraded. In particular, 8 bidimensional position sensitive silicon detectors (45  $\times$  45  $\text{mm}^2$  active area, 500  $\mu\text{m}$  thick, made by Hamamatsu Photonics K. K., Solid State Division) mounted in a square geometry were used to detect the outgoing particle with an exit angle of approximately  $10^\circ$  to  $40^\circ$ . A set of two double-sided multi-strip silicon detectors (50  $\times$  50  $\text{mm}^2$ , 500  $\mu\text{m}$  thick, produced by Micron Semiconductor Ltd) was used to detect the particles with exit angle ranging from approximately  $4^\circ$  to  $10^\circ$ .

One of the main problems encountered in the analysis of data in the previous work came from the existence of various reaction channels with three parti-

cles in the final state. Although it was shown that the events originating from the reaction channels of interest could be disentangled from those from other channels by applying various types of cuts in the phase space, the possibility of having a direct identification in the  $Z$  of the outgoing particles, at least for the heavier ones, was a major goal in this experiment. To this end, a  $\Delta E$  stage was added in front of the double-sided multi strip detectors mentioned above to ensure that a  $\Delta E$ - $E$  telescope covered the angles ranging between approximately  $4^\circ$  to  $10^\circ$ . This resulted in a higher detection efficiency because we could accept regions of the phase space that had to be discarded in the previous data analysis.

The 2015 experimental run was also optimized to cover the phase of space region relevant to the neutron induced  $^{18}\text{F}(n, \alpha)^{15}\text{N}$  reaction. The importance of having a method to measure the cross-sections of the reaction induced by neutrons on radioactive species is clear, specially if the half-life of the radioactive isotopes involved in the entrance channel of the reaction are of the order of 1 h or less.

The experiment was successfully performed in the fall of 2015 over a period of 18 days divided into two runs. Unfortunately, while we expected to obtain highly enhanced accumulated statistics with respect to the previous experiment, the number of relevant THM events only increased by a factor of approximately 2. In contrast, the events that can be associated with the  $^{18}\text{F}(n, \alpha)^{15}\text{N}$  reaction in the THM framework, were abundant and well discriminated.

The analysis of both channels is being finalized. Some preliminary results have been presented at various meetings and conferences, and we plan to publish the final results of these studies within this year.

### References

- 1) R. E. Tribble *et al.*, Rep. Prog. Phys. **77**, 106901 (2014).
- 2) S. Cherubini *et al.*, Astrophys. J. **457**, 855, (1996).
- 3) A. S. Adekola *et al.*, Phys. Rev. C **83**, 052801(R) (2011).
- 4) A. M. Laird *et al.*, Phys. Rev. Lett. **110**, 032502 (2013).

\*1 INFN-LNS

\*2 Dipartimento di Fisica e Astronomia, Università di Catania

\*3 RIKEN Nishina Center

\*4 Università di Enna KORE

\*5 Center for Nuclear Study, The University of Tokyo

\*6 Department of Physics, Tohoku University

\*7 Department of Physics, Sungkyunkwan University

\*8 Department of Physics, Chung-Ang University

\*9 30 MeV Cyclotron Center, Tran Hung Dao Hospital

\*10 Universidade de São Paulo, Instituto de Física, Departamento de Física Nuclear

\*11 Technische Universität München

# Gamow-Teller transitions in ${}^6\text{He}$ with PANDORA

L. Stuhl,<sup>\*1,\*2</sup> J. Gao,<sup>\*2,\*3</sup> M. Sasano,<sup>\*2</sup> K. Yako,<sup>\*1</sup> Y. Kubota,<sup>\*2</sup> Z. Yang,<sup>\*2</sup> J. Zenihiro,<sup>\*2</sup> V. Panin,<sup>\*2</sup>  
Z. Korkulu,<sup>\*2</sup> E. Takada,<sup>\*4</sup> H. Baba,<sup>\*2</sup> and T. Uesaka<sup>\*2</sup>

We started a program at RIBF aiming to study the spin-isospin responses of light drip line nuclei. An experiment<sup>1)</sup> with 5 days of beam time was approved to investigate  ${}^{11}\text{Li}$  and  ${}^{14}\text{Be}$  nuclei. The charge-exchange ( $p, n$ ) reactions at intermediate beam energies ( $E/A > 100$  MeV) and small angles can selectively excite the Gamow-Teller (GT) states up to high excitation energies in the final nucleus. Therefore, ( $p, n$ ) reactions in inverse kinematics applying the missing mass reconstruction<sup>2,3)</sup> provide the best and efficient tool to study the  $B(\text{GT})$  strength values of unstable isotopes in a wide excitation energy region, without  $Q$ -value limitation. In a pilot measurement of the mentioned experiment, we studied the case of  ${}^6\text{He}$  at HIMAC facility in Chiba to investigate the Gamow-Teller transitions in  ${}^6\text{He}$  and commission our new plastic scintillator-based neutron detector PANDORA (Particle Analyzer Neutron Detector Of Real-time Acquisition)<sup>4)</sup> and its pulse shape discrimination (PSD) capability.

The secondary beam properties and details of the experimental setup are described in another contribution in this volume.<sup>5)</sup> By using PANDORA with our digital data acquisition system,<sup>6)</sup> we could detect the neutrons having kinetic energies of a few tens of keV. Neutron and gamma-like events could be separated by defining  $\text{PSD}_{\text{mean}}$  value as the arithmetic mean of PSD values<sup>1)</sup> of two single-end read-outs of each bar. From the measured neutron time-of-flight and recoil angle (in the laboratory angle range of  $75^\circ$ – $99^\circ$ ), the excitation energy of the residual nucleus can be reconstructed. Figure 1 shows the calculated kinematical correlations for the  ${}^6\text{He}(p, n)$  charge-exchange reaction at 123 MeV/nucleon

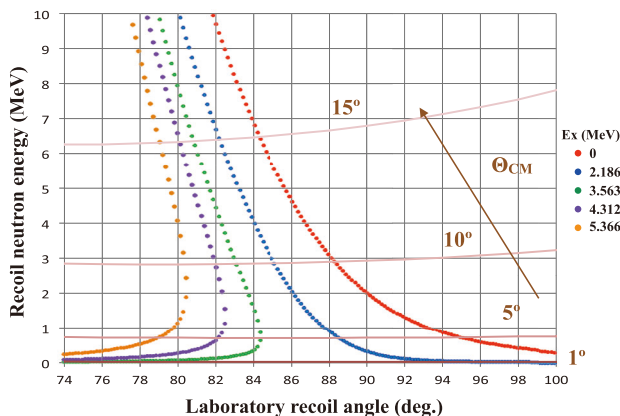


Fig. 1. Correlations between recoil neutron energy and laboratory kinematics for fixed excitation energies.

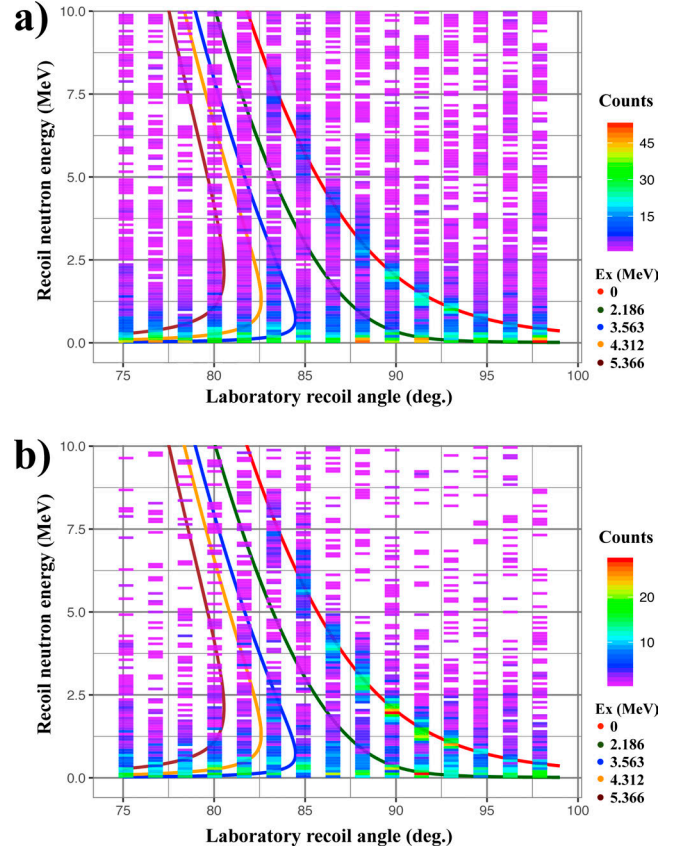


Fig. 2. Neutron spectra as functions of both recoil neutron energy and recoil angle in the  ${}^6\text{He}(p, n)$  reaction without gating on neutron-like events (a) and with gate on neutron-like events (b).

energy.

Selecting the incident  ${}^6\text{He}$  particles and the identification of  ${}^6\text{Li}$  reaction residue produced from the ( $p, n$ ) reaction, a clear kinematical correlation can be seen on the Fig. 2 (a) scatter plot. This matches with the calculated curve and corresponds to transitions to the ground state in  ${}^6\text{Li}$ . After gating on neutron-like events by  $\text{PSD}_{\text{mean}}$ , the improvement of the kinematic locus in Fig. 2 (b) presents the effectiveness of PANDORA and its PSD capability. The data shown here were accumulated within 9 h. Further analysis with larger statistics is in progress.

This work was supported by KAKENHI 16H06716 and the Japan Society for the Promotion of Science.

## References

- 1) L. Stuhl *et al.*, RIKEN Accel. Prog. Rep. **48**, 54 (2015).
- 2) M. Sasano *et al.*, Phys. Rev. Lett. **107**, 202501 (2011).
- 3) M. Sasano *et al.*, Phys. Rev. C **86**, 034324 (2012).
- 4) L. Stuhl *et al.*, Nucl. Instrum. Methods Phys. Res. A **866**, 164 (2017).
- 5) M. Sasano *et al.*, RIKEN Accel. Prog. Rep. **51**, 78 (2018).
- 6) J. Gao *et al.*, RIKEN Accel. Prog. Rep. **51**, 146 (2018).

\*1 Center for Nuclear Study, University of Tokyo

\*2 RIKEN Nishina Center

\*3 School of Physics, Peking University

\*4 National Institute of Radiological Sciences (NIRS)

## $\beta$ -NMR measurements for $^{21}\text{O}$ at HIMAC

A. Gladkov,<sup>\*1,\*2</sup> H. Nishibata,<sup>\*1</sup> K. Kawata,<sup>\*1,\*3</sup> H. Yamazaki,<sup>\*1</sup> T. Sato,<sup>\*1</sup> Y. Ichikawa,<sup>\*1</sup> A. Takamine,<sup>\*1</sup> M. Sanjo,<sup>\*1,\*4</sup> W. Kobayashi,<sup>\*1,\*4</sup> T. Asakawa,<sup>\*1,\*4</sup> Y. Sasaki,<sup>\*1,\*4</sup> M. Tajima,<sup>\*1</sup> K. Asahi,<sup>\*1</sup> and H. Ueno<sup>\*1</sup>

The interest in the shell evolution in the region of neutron-rich oxygen isotopes has its origin in the multiple studies on  $^{23}\text{O}$ , which have revealed the anomalous nuclear properties of this isotope. The appearance of the new neutron magic number at  $N = 16$  as well as the formation of the halo structure in  $^{23}\text{O}$  have been experimentally indicated.<sup>1,2)</sup> Thus, the information on the nuclear structure of the neighboring isotopes, such as  $^{19,21}\text{O}$ , can provide the systematic picture of the change in the nuclear properties in this region.

In parallel with the interest in the nuclear structure, the  $^{21}\text{O}$  isotope has a large potential in materials science studies. Owing to its advantages in the beta-ray-detected NMR measurements, as compared to other oxygen isotopes with known electromagnetic moments,<sup>3)</sup>  $^{21}\text{O}$  appeared to be a good candidate to serve as the electromagnetic probe to investigate the atomic-scale properties of the oxygen-containing systems.

Previously, we have reported on the measurement of nuclear moments of  $^{21}\text{O}$  at RIKEN RIBF.<sup>3)</sup> However, even though the obtained values provide certain information on the nuclear structure, the improvements in the precision of  $Q$ -moment measurement are desirable to successfully implement  $^{21}\text{O}$  in the studies described above.

Thus, we prepared and performed precision measurements on the nuclear magnetic dipole and electric quadrupole moments for the ground-state of  $^{21}\text{O}$  using the  $\beta$ -NMR method at HIMAC, Chiba. The secondary beam of  $^{21}\text{O}$  was produced at the SB2<sup>4)</sup> separation line of the facility by using the  $^{22}\text{Ne}$  primary beam on the 1-mm-thick Be target at an energy of 70 MeV/nucleon and beam intensity of  $7.8 \cdot 10^8$  particles per spill. The isotope separation was done in two stages through the momentum and momentum-loss analyses. The latter was realized using a 3.5-mm-thick Al wedge-shaped energy degrader installed at the F1 focal plane. Beam purity of nearly 100% was achieved for the secondary beam after the separation. To ensure the polarization of  $^{21}\text{O}$ , an emission angle of  $\theta = 2.6^\circ \pm 1^\circ$  was applied using the beam swinger located upstream of the SB2 beam line and the outgoing momentum window was selected to be  $p_f = p_0 \times (0.984 \pm 0.020)$  considering the one neutron pick-up mechanism involved in the reaction. The particle identification was done using  $\Delta E$ -ToF. The time of flight (ToF) was measured between the F1 and F3 focal planes of the beam line.

After the isotope separation, the secondary beam of  $^{21}\text{O}$  was delivered to the  $\beta$ -NMR apparatus installed downstream the beam line. The well-established method of  $\beta$ -NMR in combination with AFP technique<sup>5)</sup> was applied to measure the electromagnetic moments. The following sequence was implemented in the measurements. The stopper crystal placed in a 5000 G static magnetic field  $B_0$  was irradiated by the secondary beam during the first two spills from synchrotron. After the beam implantation, the oscillating magnetic field was applied to the stopper perpendicular to  $B_0$  by using the tank circuit containing five variable remotely controlled vacuum capacitors of 50–2000 pF. The following six spills (9.9 s) were artificially skipped and the  $\beta$ -rays from  $^{21}\text{O}$   $\beta$ -decay were counted by the plastic scintillator telescopes located above and below the stopper. In the next cycle, the beta-rays were counted without the application of the RF field and the ratio between the two measurements was taken to extract the AP value and therefore, the resonant frequency. The 0.5-mm-thick CaO crystal and 0.5 mm-thick  $\text{TiO}_2$  single crystal were used in the  $g$ -factor and  $Q$ -moment measurements, respectively.

The analysis of the data acquired during the experiment is in progress and the results will be reported later.

### References

- 1) C. Nociforo *et al.*, Phys. Lett. B **605**, 79 (2005).
- 2) D. Cortina-Gil *et al.*, Phys. Rev. Lett. **93**, 062501 (2004).
- 3) A. Gladkov *et al.*, RIKEN Accel. Prog. Rep. **50**, 74 (2017).
- 4) M. Kanazawa *et al.*, Nucl. Phys. A **746**, 393 (2004).
- 5) D. Nagae *et al.*, Nucl. Instrum. Methods Phys. Res. B **266**, 4612 (2008).

\*1 RIKEN Nishina Center

\*2 Department of Physics, Kyungpook National University

\*3 Center for Nuclear Study, The University of Tokyo

\*4 Department of Advanced Sciences, Hosei University

## RI beam production at BigRIPS in 2018

Y. Shimizu,<sup>\*1</sup> N. Fukuda,<sup>\*1</sup> H. Takeda,<sup>\*1</sup> H. Suzuki,<sup>\*1</sup> D. S. Ahn,<sup>\*1</sup> N. Inabe,<sup>\*1</sup> K. Kusaka,<sup>\*1</sup> M. Ohtake,<sup>\*1</sup>  
Y. Yanagisawa,<sup>\*1</sup> T. Komatsubara,<sup>\*1</sup> H. Sato,<sup>\*1</sup> K. Yoshida,<sup>\*1</sup> and T. Uesaka<sup>\*1</sup>

The radioactive isotope (RI) beam production at the BigRIPS fragment separator<sup>1)</sup> in 2018 is presented here. Table 1 summarizes the experimental programs that involved the use of the BigRIPS separator during this period and the RI beams produced for each experiment.

In the spring beam time, the  $^{18}\text{O}$  beam campaign was performed with seven experiments. The  $^{10,12,14}\text{Be}$  beams were delivered to the SAMURAI spectrometer to study the cluster structure of neutron-rich Beryllium isotopes. The  $^{14}\text{O}$  beam was produced to investigate the single-particle structure and nucleon correlation in exotic nuclei using knockout reactions. Cocktail beams of  $^{14}\text{Be}$ ,  $^{11}\text{Li}$ , and  $^8\text{He}$  were produced to measure the spin-isospin responses of the neutron drip-line nuclei.  $^9\text{C}$  beam was produced to study the single-particle structure of  $^8\text{B}$  relevant to nuclear astrophysics. Two machine studies were performed to develop the dispersion-matched ion-optical system of the SRC and BigRIPS.<sup>2,3)</sup> The BigRIPS group has measured the production cross-sections of the proton-rich nuclei for the Li-F region and the momentum distribution of  $^{10}\text{C}$  beam in the machine study.<sup>4)</sup>

In the autumn beam time, the  $^{238}\text{U}$  beam campaign was conducted with seven experiments.  $^{134,136}\text{Sn}$  beams were produced to study the unbound  $\gamma$ -decaying states in  $^{133,135}\text{Sn}$ . The first physics experiments using the Rare-RI Ring were performed to measure the precise masses of  $^{74,76}\text{Ni}$ ,  $^{122}\text{Rh}$ , and  $^{124}\text{Pd}$  isotopes. The BRIKEN experiment was performed to measure the beta-delayed multi-neutron emission probabilities in the rare-earth region using the cocktail beam around  $^{165}\text{Pm}$ . The first experiment with the VANDLE array setup was performed to study the beta-delayed neutron emission in the vicinity of  $^{78}\text{Ni}$  using the cocktail beam around  $^{82}\text{Cu}$ . The  $^{132}\text{Sn}$  beam was used to produce the tertiary  $^{130}\text{Sn}$  beam using a two-step scheme with a momentum-dispersion matching technique<sup>5)</sup> at F5. The tertiary  $^{130}\text{Sn}$  beam was delivered to F12 for the magnetic moment measurement using the time-differential perturbed angular distribution method.

The number of experiments using RI beams at the BigRIPS separator is tallied in Table 2 for various primary beams in each year. A total of 174 experiments have been performed so far. Figure 1 shows the RI beams produced in 2018 at the BigRIPS separator on

Table 1. List of experimental programs and RI beams produced at the BigRIPS separator in 2018.

Primary beam (Period)	Proposal No.	Course	RI beams
$^{18}\text{O}$ 230 MeV/nucleon (May 15 – Jun. 8)	NP1612-SAMURAI12R1	SAMURAI	$^{10,12,14}\text{Be}$ , $^4\text{He}$
	NP1512-SAMURAI31	SAMURAI	$^{14}\text{O}$
	MS-EXP18-03	BigRIPS	$^9\text{C}$
	NP1412-SAMURAI30	SAMURAI	$^{14}\text{Be}/^{11}\text{Li}/^8\text{He}$
	MS-EXP18-04	BigRIPS	$^{17,18}\text{F}$ , $^{13,14,15}\text{O}$ , $^{12,13,17,18}\text{N}$ , $^{9,10,11,14}\text{C}$ , $^{8,13,14}\text{B}$ , $^{7,10,11}\text{Be}$ , $^6\text{Li}$
	NP1412-SAMURAI29R1	SAMURAI	$^9\text{C}$
	MS-EXP18-02	BigRIPS	$^9\text{C}$
$^{238}\text{U}$ 345 MeV/nucleon (Oct. 16 – Dec. 10)	NP1712-RIBF162		$^{134,136}\text{Sn}$
	NP1612-RIBF149	ZeroDegree	
	NP1612-RIRING2	Rare-RI Ring	$^{74,76}\text{Ni}$
	NP1612-RIBF148-03	ZeroDegree	$^{165}\text{Pm}$
	NP1712-RIRING1R1	Rare-RI Ring	$^{124}\text{Pd}$ , $^{122}\text{Rh}$
	NP1512-RIBF136	ZeroDegree	$^{82}\text{Cu}$
	INSPECTION18	BigRIPS	
NP1712-RIBF143R1	F12	$^{132}\text{Sn}$	

<sup>\*1</sup> RIKEN Nishina Center

Table 2. Number of experiments performed using RI beams in each year.

Year	$^{238}\text{U}$	$^{124}\text{Xe}$	$^{86}\text{Kr}$	$^{78}\text{Kr}$	$^{70}\text{Zn}$	$^{48}\text{Ca}$	$^{18}\text{O}$	$^{16}\text{O}$	$^{14}\text{N}$	$^4\text{He}$	$^2\text{H}$	Yearly total
2007	4		1									5
2008	2					4						6
2009	3					3			3	1		10
2010						10	1		2		1	14
2011	4	2					2					8
2012	6	3			1	4	6					20
2013	4	2					3					9
2014	11				1	3		1			1	17
2015	15			6		4					1	26
2016	13	1				6	2					22
2017	13				4	2	3					22
2018	7						7					14
Total	82	8	1	6	6	36	24	1	5	1	3	173

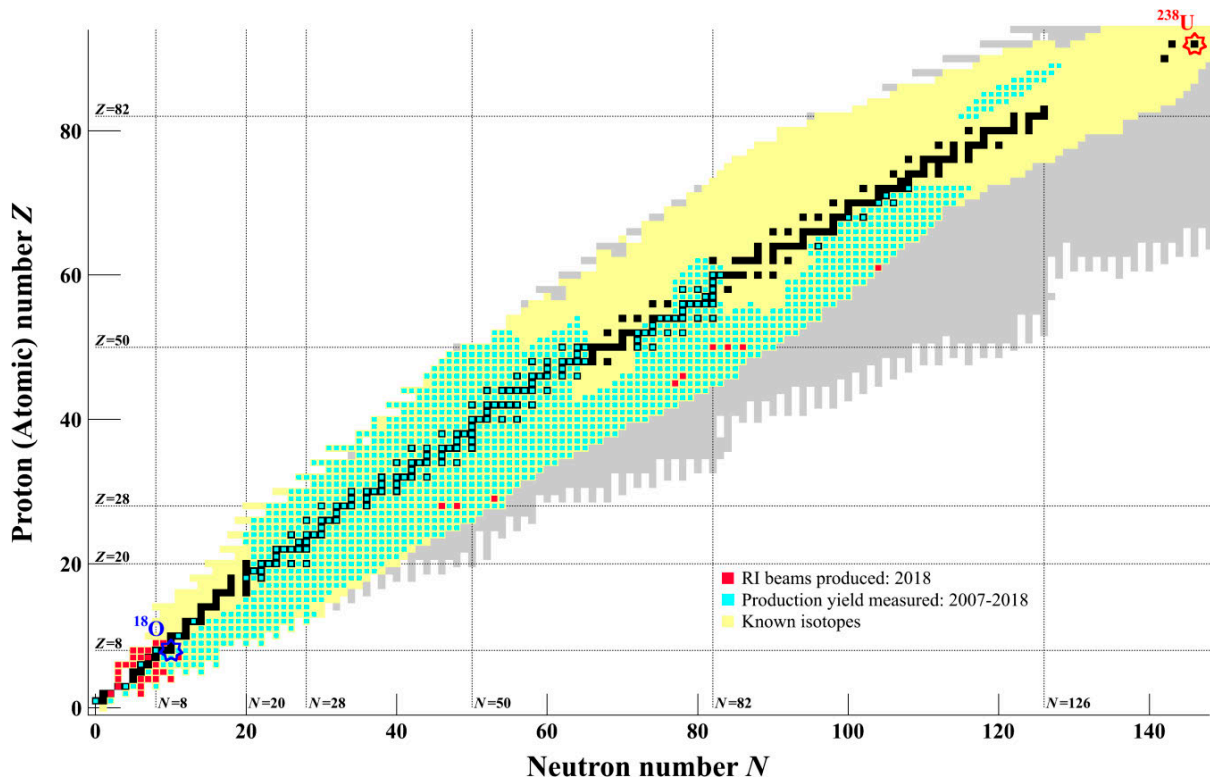


Fig. 1. RI beams produced in 2018 and the production yield measured from March 2007 to December 2018 at the BigRIPS separator.

the table of nuclides with red squares. The number of RI beams produced in 2018 is 40. The production yields for 1608 RI beams have been measured from March 2007 to December 2018 and they are indicated using cyan. The yellow color indicates the known isotopes. The number of new isotopes is approximately 140.

References

- 1) T. Kubo, Nucl. Instrum. Methods Phys. Res. B **204**, 97 (2003).
- 2) S. Y. Matsumoto *et al.*, in this report.

- 3) T. Nishi *et al.*, in this report.
- 4) H. Takeda *et al.*, in this report.
- 5) Y. Ichikawa *et al.*, Nature Phys. **8**, 918 (2012).

# Measurement of production cross-section and momentum distribution of isotopes produced from $^{18}\text{O}$ beam

H. Takeda,<sup>\*1</sup> N. Fukuda,<sup>\*1</sup> H. Suzuki,<sup>\*1</sup> Y. Shimizu,<sup>\*1</sup> D. S. Ahn,<sup>\*1</sup> N. Inabe,<sup>\*1</sup> K. Yoshida,<sup>\*1</sup> and T. Uesaka<sup>\*1</sup>

The production yields and production cross-sections of  $^6\text{Li}$ ,  $^7,^{10},^{11}\text{Be}$ ,  $^8,^{13},^{14}\text{B}$ ,  $^9,^{10},^{11},^{14}\text{C}$ ,  $^{12},^{13},^{17},^{18}\text{N}$ ,  $^{13},^{14},^{15}\text{O}$ , and  $^{17},^{18}\text{F}$  produced from an  $^{18}\text{O}$  beam at 230 MeV/nucleon were systematically measured with the BigRIPS separator.<sup>1)</sup> By combining with previously measured cross-sections of other isotopes, the cross-section data of almost all nuclei that can be produced from  $^{18}\text{O}$  has been completed, except for some stable nuclei and  $^3\text{H}$ . In addition, the momentum distribution was measured for a wide range for  $^{10}\text{C}$ .

The secondary beam was produced from the  $^{18}\text{O}$  beam on a 2 mm-thick Be target at F0. The momentum slit at F1 was set at  $\pm 3\%$ . An 8 mm-thick Al achromatic degrader was used at F1 to purify the secondary beam. The particle identification was performed by using the  $\Delta E$  vs. TOF information in the second stage of BigRIPS. For each cross-section measurement, the  $B\rho$  setting was tuned for the peak of the momentum distribution of the target isotope. The production cross-sections were deduced from the measured production rates and the transmission efficiency of the BigRIPS separator estimated with the simulation code LISE<sup>++</sup>.<sup>2)</sup>

The measured production cross-sections are shown in Fig. 1. The upper and lower panels show the results for proton-rich ( $A/Z \leq 2$ ) and neutron-rich ( $A/Z > 2$ ) isotopes, respectively. The filled circles are the measured data at this time, while open circles are previously measured ones. The magenta, blue, and green lines are predictions of EPAX 3.1a,<sup>3)</sup> EPAX 2.15,<sup>4)</sup> and FRACS 1.1,<sup>5)</sup> respectively.

The measured cross-sections of the proton-rich B–O isotopes are 1/2–1/10 of the EPAX 3.1a predictions. The closer to the proton dripline, the larger the deviation becomes. The results of FRACS 1.1 are almost the same as those of EPAX 3.1a, while EPAX 2.15 underestimates the cross-sections of isotopes near the stability line. For the neutron-rich isotopes, all the models reproduced the measured cross-sections relatively well compared to the proton-rich side.

The momentum distribution of  $^{10}\text{C}$  was measured by changing the first  $B\rho_{01}$  from  $-12\%$  to  $+12\%$  for the peak momentum value in 3% steps. The yield ratio to the peak value is plotted as a function of the momentum deviation in Fig. 2. The red circles show the measured values. The distribution was not well reproduced by the LISE<sup>++</sup> calculation with the “Universal parametrization” model<sup>6)</sup> (green line). We need to modify the  $\sigma_{\text{conv}}$  and  $\text{coef}$  parameters, which correspond to the width and low-momentum tail of the distribution, to reproduce the measured distribution (blue line). Detailed analysis is in progress.

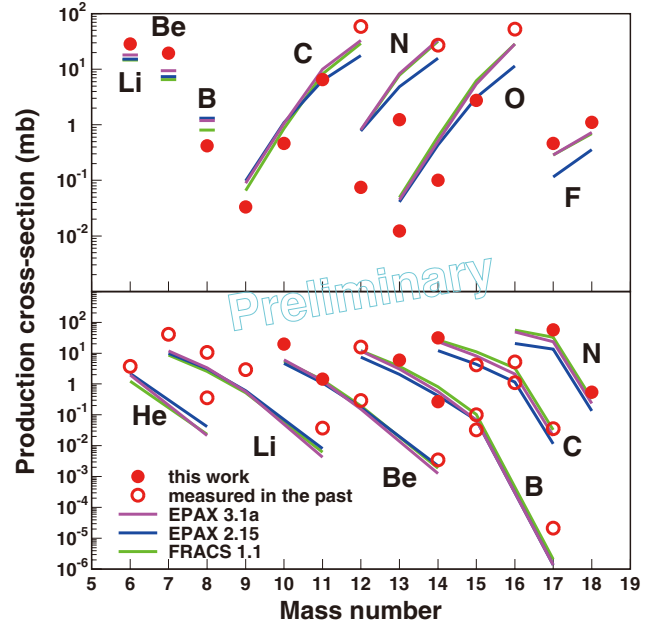


Fig. 1. Production cross-sections of isotopes produced in the  $^{18}\text{O} + \text{Be}$  reaction. The upper and lower panels show the results for proton-rich ( $A/Z \leq 2$ ) and neutron-rich ( $A/Z > 2$ ) isotopes, respectively.

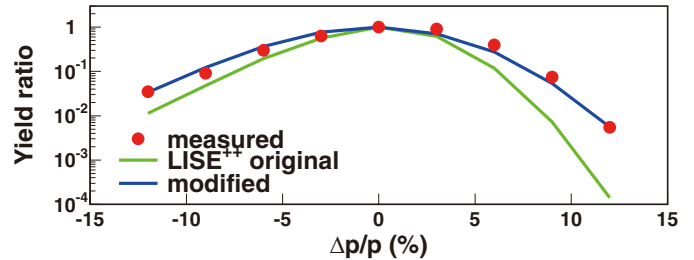


Fig. 2. Momentum distribution of  $^{10}\text{C}$  produced in the  $^{18}\text{O} + \text{Be}$  2 mm reaction at 230 MeV/nucleon. The original model (green line) used in the LISE<sup>++</sup> did not reproduce the measured distribution (red circles) well. Modification of the parameters were needed (blue line).

## References

- 1) T. Kubo, Nucl. Instrum. Methods Phys. Res. B **204**, 97 (2003).
- 2) O. B. Tarasov, D. Bazin, Nucl. Instrum. Methods Phys. Res. B **266**, 4657 (2008).
- 3) K. Sümmerer, Phys. Rev. C **86**, 014601 (2012).
- 4) K. Sümmerer, B. Blank, Phys. Rev. C **61**, 034607 (2000).
- 5) B. Mei, Phys. Rev. C **95**, 034608 (2017).
- 6) O. Tarasov, Nucl. Phys. A **734**, 536 (2004).

<sup>\*1</sup> RIKEN Nishina Center

# Cross-section measurement of neutron-rich isotopes produced from an RI beam of $^{132}\text{Sn}$ using a two-step scheme

H. Suzuki,<sup>\*1</sup> K. Yoshida,<sup>\*1</sup> N. Fukuda,<sup>\*1</sup> H. Takeda,<sup>\*1</sup> Y. Shimizu,<sup>\*1</sup> D. S. Ahn,<sup>\*1</sup> T. Sumikama,<sup>\*1</sup> N. Inabe,<sup>\*1</sup> T. Komatsubara,<sup>\*1</sup> H. Sato,<sup>\*1</sup> Z. Korkulu,<sup>\*1</sup> K. Kusaka,<sup>\*1</sup> Y. Yanagisawa,<sup>\*1</sup> M. Ohtake,<sup>\*1</sup> H. Ueno,<sup>\*1</sup> S. Michimasa,<sup>\*2</sup> N. Kitamura,<sup>\*2</sup> K. Kawata,<sup>\*2</sup> N. Imai,<sup>\*2</sup> O. B. Tarasov,<sup>\*3,\*1</sup> D. P. Bazin,<sup>\*3,\*1</sup> T. Kubo,<sup>\*4,\*1</sup> J. Nolen,<sup>\*5,\*1</sup> and W. F. Henning<sup>\*5,\*6,\*1</sup>

The production cross sections of neutron-rich radioactive isotopes (RI), including  $^{125-128}\text{Pd}$  produced from a less-exotic RI beam of  $^{132}\text{Sn}$ , were measured using BigRIPS and ZeroDegree at the RIKEN RI Beam Factory (RIBF) in November 2017.

A two-step reaction scheme was proposed<sup>1)</sup> for the efficient production of mid-heavy very-neutron-rich RIs. In this scheme, a long-lived neutron-rich RI such as  $^{132}\text{Sn}$ , whose half-life is 40 s, is produced by an ISOL in the first step, and accelerated by post-accelerators. In the second step, more exotic nuclei, such as  $^{125-128}\text{Pd}$ , are produced by a fragmentation reaction. With this scheme, one may obtain greater yields of very neutron-rich RIs than those obtained by direct production through the in-flight fission of a  $^{238}\text{U}$  beam, which is currently a very popular method to produce them. To evaluate the yields of RIs by the two-step scheme with a  $^{132}\text{Sn}$  beam, we measured the production cross sections of neutron-rich Pd isotopes beyond  $^{125}\text{Pd}$ , up to which the cross sections had already been measured at GSI together with the neighboring RIs.<sup>2)</sup>

In the experiment, the  $^{132}\text{Sn}$  beam was produced at BigRIPS by the in-flight fission of a 40-pnA 345-MeV/nucleon  $^{238}\text{U}^{86+}$  beam impinging on a 4-mm-thick Be target. The  $^{132}\text{Sn}$ -beam energy was 278 MeV/nucleon, the intensity was 35 kHz, and the purity was 50%. The neutron-rich Pd isotopes were produced by the fragmentation with a 6-mm-thick Be target at the entrance of ZeroDegree. The particle identification (PID) was performed by deducing the atomic number  $Z$ , the mass-to-charge ratio  $A/Q$ , and the mass number  $A$  of the RIs based on the TOF- $B\rho$ - $\Delta E$ -TKE method in ZeroDegree. Two settings—the  $^{126}\text{Pd}$  setting and the  $^{128}\text{Pd}$  setting—were applied for measuring the cross sections of  $^{125,126}\text{Pd}$  and  $^{127,128}\text{Pd}$ , respectively.

The  $Z$  vs  $A/Q$  PID plot of the  $^{128}\text{Pd}$  setting is shown in Fig. 1. Many fully-stripped isotopes are observed with the partially-stripped ones.  $^{127,128}\text{Pd}^{46+}$  are well identified in the plot. The events in the two blobs on the right side of  $^{128}\text{Pd}^{46+}$  are the H-like ions of  $^{126,127}\text{Pd}^{45+}$ . From the yields of RIs, their transmission in ZeroDegree, and the beam dose of  $^{132}\text{Sn}$ , the production cross sections were deduced. In Fig. 2, the cross sections obtained

in this experiment at RIBF and the ones at GSI<sup>2)</sup> are shown with the cross-section formulae COFRA1.0<sup>3)</sup> and EPAX3.1a.<sup>4)</sup> Both formulae reproduce the experimental cross sections fairly well. Further detailed analyses are in progress.

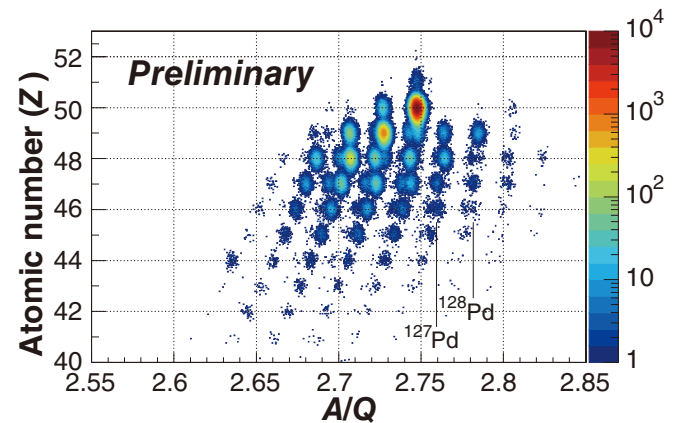


Fig. 1. The  $Z$  versus  $A/Q$  PID plot of  $^{128}\text{Pd}$  setting in ZeroDegree. Partially-stripped contaminants are included in the plot with the fully-stripped  $^{127,128}\text{Pd}$ .

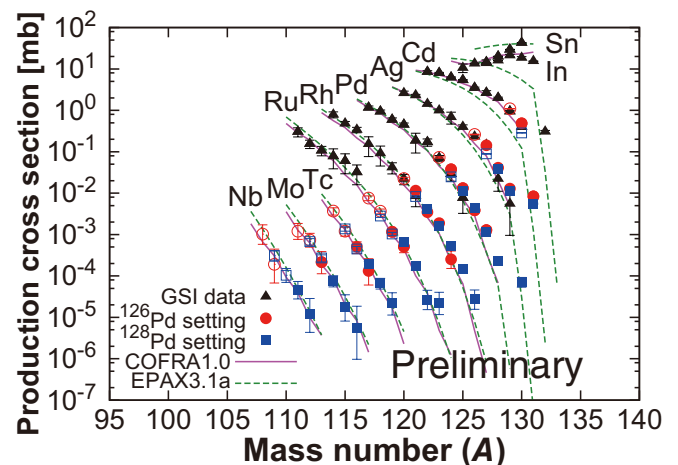


Fig. 2. The experimental cross sections of neutron-rich RIs produced from  $^{132}\text{Sn}$  beams at RIBF and GSI<sup>2)</sup> with cross-section formulae COFRA1.0<sup>3)</sup> and EPAX3.1a.<sup>4)</sup>

<sup>\*1</sup> RIKEN Nishina Center

<sup>\*2</sup> Center for Nuclear Study, University of Tokyo

<sup>\*3</sup> National Superconducting Cyclotron Laboratory, Michigan State University

<sup>\*4</sup> Facility for Rare Isotope Beams, Michigan State University

<sup>\*5</sup> Division of Physics, Argonne National Laboratory

<sup>\*6</sup> Physik Department, Technische Universität München

## References

- 1) K. Helariutta *et al.*, *Eur. Phys. J. A* **17**, 181 (2003).
- 2) D. Pérez-Loureiro *et al.*, *Phys. Lett. B* **703**, 552 (2011).
- 3) COFRA web page, <http://www.usc.es/genp/cofra>.
- 4) K. Sümmerer, *Phys. Rev. C*, **86**, 014601 (2012).



## **2. Nuclear Physics (Theory)**



# Improvement of functionals in density functional theory using inverse Kohn-Sham method and density functional perturbation theory<sup>†</sup>

D. Ohashi,<sup>\*1,\*2</sup> T. Naito,<sup>\*1,\*2</sup> and H. Z. Liang<sup>\*2,\*1</sup>

The density functional theory (DFT) is one of the most successful approaches to calculate the ground-state properties. The ground-state density  $\rho_{\text{gs}}$  and energy  $E_{\text{gs}}$  are obtained by solving the Kohn-Sham (KS) equation.<sup>1,2)</sup> The ground-state energy is given by  $E_{\text{gs}} = T_0[\rho_{\text{gs}}] + \int v_{\text{ext}}(\mathbf{r}) \rho_{\text{gs}}(\mathbf{r}) d\mathbf{r} + E_{\text{Hxc}}[\rho_{\text{gs}}]$ , where  $T_0$  is the KS kinetic energy,  $v_{\text{ext}}$  is the external field, and  $E_{\text{Hxc}}[\rho]$  is the Hartree-exchange-correlation energy density functional (EDF). However, the accuracy of DFT calculations depends on the determination of  $E_{\text{Hxc}}[\rho]$  as it is unknown. The inverse Kohn-Sham (IKS) method was proposed toward the improvement of EDFs. Nevertheless, the actual method to improve EDFs has not been explicitly determined.

In this work, for the first time, a new way to improve EDFs by the combination of the IKS method and density functional perturbation theory (DFPT) is proposed. In this method, a conventional  $\tilde{E}_{\text{Hxc}}[\rho]$  is assumed to be close enough to  $E_{\text{Hxc}}[\rho]$  and the difference is considered in the first-order DFPT with small  $\lambda$  as  $E_{\text{Hxc}}[\rho] = \tilde{E}_{\text{Hxc}}[\rho] + \lambda E_{\text{Hxc}}^{(1)}[\rho] + O(\lambda^2)$ . In addition,  $\rho_{\text{gs}}(\mathbf{r})$  and  $E_{\text{gs}}$  are expanded perturbatively. The perturbation is assumed to not affect the external field, and  $\rho_{\text{gs}}(\mathbf{r})$  is assumed to be given.

Under the assumptions, we calculate  $E_{\text{gs}}$  based on the first-order DFPT and on the IKS method. By comparing them, the following equation for  $E_{\text{Hxc}}^{(1)}[\rho]$  is obtained:

$$\begin{aligned} & \lambda E_{\text{Hxc}}^{(1)}[\tilde{\rho}_{\text{gs}}] - \lambda E_{\text{Hxc}}^{(1)}[\rho_{\text{gs}}] + \lambda \int \frac{\delta E_{\text{Hxc}}^{(1)}[\rho_{\text{gs}}]}{\delta \rho(\mathbf{r})} \rho_{\text{gs}}(\mathbf{r}) d\mathbf{r} \\ &= \sum_{i=1}^N \varepsilon_i + \tilde{E}_{\text{Hxc}}[\rho_{\text{gs}}] - \int \frac{\delta \tilde{E}_{\text{Hxc}}[\rho_{\text{gs}}]}{\delta \rho(\mathbf{r})} \rho_{\text{gs}}(\mathbf{r}) d\mathbf{r} - \tilde{E}_{\text{gs}}, \end{aligned}$$

where  $\varepsilon_i$  is the single-particle energy obtained from  $\rho_{\text{gs}}$  using the IKS method. Because it is difficult to solve this equation, we assume  $E_{\text{Hxc}}^{(1)}[\rho] = \sum_k A_k \int [\rho(\mathbf{r})]^{\alpha_k} d\mathbf{r}$  and iteratively determine its value. Finally,  $\tilde{E}_{\text{Hxc}}[\rho]$  is improved to be  $\tilde{E}_{\text{Hxc}}[\rho] + \lambda E_{\text{Hxc}}^{(1)}[\rho]$ .

As benchmark calculations,  $\rho_{\text{gs}}(\mathbf{r})$  is calculated from the known  $E_{\text{Hxc}}^{\text{target}}[\rho]$  and we attempt to reproduce it from a less accurate  $\tilde{E}_{\text{Hxc}}$ . Here, we use the Hartree and LDA exchange functional as  $E_{\text{Hxc}}^{\text{target}}$  and the Hartree one as  $\tilde{E}_{\text{Hxc}}$ . The pairs of noble-gas atoms He-Ne and Xe-Rn are used because two unknowns  $A_i$  and  $\alpha_i$  should be determined at each iteration. Addi-

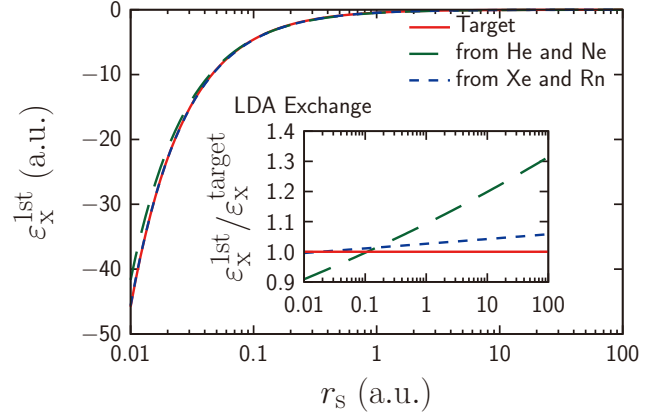


Fig. 1. Exchange energy density  $\varepsilon_x^{\text{1st}}(r_s)$  calculated in the first iteration and ratios  $\varepsilon_x^{\text{1st}}(r_s)/\varepsilon_x^{\text{target}}(r_s)$ . The Hartree atomic unit is used here.

tionally, they are easy to handle owing to their spherical symmetry.

It is found that  $A_1$  and  $\alpha_1$  are obtained within 7.2% and 1.0% errors in He-Ne, and within 2.3% and 0.2% errors in Xe-Rn, respectively, from the LDA results.

The calculated exchange energy density at the first iteration,  $\varepsilon_x^{\text{1st}}(r_s)$ , and its ratio to the LDA are shown in Fig. 1 for the pairs of He-Ne and Xe-Rn with dashed and dot lines, respectively, while the LDA exchange functional is represented with a solid line. The energy density  $\varepsilon_x(\rho)$  and the Wigner-Seitz radius  $r_s$  are defined as  $E_x[\rho] = \int \varepsilon_x(\rho) \rho(\mathbf{r}) d\mathbf{r}$  and  $r_s = [3/(4\pi\rho)]^{1/3}$ , respectively. The Xe-Rn pair reproduces the LDA functional within a few percents.

Moreover, it is found that the ground-state energy becomes closer to the LDA as the iteration proceeds. The ground-state energies of He, Ne, Xe, and Rn are finally reproduced within 0.4%, 0.003%, 0.002%, and 0.0003% errors, respectively, comparing with 28%, 8%, 2%, and 2% errors at the zeroth step. It is also found that the ground-state density is improved by the iterations.

To summarize, our method accurately reproduces the LDA functionals. The accuracy of ground-state energies and densities are improved by two to three orders and one to two orders of magnitude, respectively. This method can be effective for nuclear DFT as well.

## References

- 1) P. Hohenberg, W. Kohn, Phys. Rev. **136**, B864 (1964).
- 2) W. Kohn, L. J. Sham, Phys. Rev. **140**, A1133 (1965).
- 3) Y. Wang, R. G. Parr, Phys. Rev. A **47**, R1591 (1993).
- 4) Q. Zhao, R. G. Parr, J. Chem. Phys. **98**, 543 (1993).

<sup>†</sup> Condensed from arXiv:1812.09285 [physics.chem-ph]

<sup>\*1</sup> Department of Physics, The University of Tokyo

<sup>\*2</sup> RIKEN Nishina Center

# Coulomb exchange functional with generalized gradient approximation for self-consistent Skyrme Hartree-Fock calculations<sup>†</sup>

T. Naito,<sup>\*1,\*2</sup> X. Roca-Maza,<sup>\*3,\*4</sup> G. Colò,<sup>\*3,\*4</sup> and H. Z. Liang<sup>\*2,\*1</sup>

Recently, it was shown that the Coulomb energy density functionals of the generalized gradient approximation (GGA) give almost the same accuracy as that of the exact-Fock energy<sup>1)</sup> by using the experimental charge density distribution as inputs of the functional. As a step further, we carry out the corresponding self-consistent Skyrme Hartree-Fock calculation by using the Perdew-Burke-Ernzerhof GGA (PBE-GGA) Coulomb exchange functional<sup>2)</sup> instead of the exact-Fock. The GGA Coulomb exchange functionals have been proposed as

$$E_{C_x}[\rho_{ch}] = -\frac{3e^2}{16\pi\epsilon_0} \left(\frac{3}{\pi}\right)^{1/3} \int [\rho_{ch}(\mathbf{r})]^{4/3} F(s(\mathbf{r})) d\mathbf{r}, \quad (1)$$

where  $F$  is the enhancement factor due to the density gradient,  $F \equiv 1$  is the hold for the local density approximation (LDA), and  $\rho_{ch}$  is the charge distribution. Here,  $s$  denotes the dimensionless density gradient

$$s = \frac{|\nabla\rho_{ch}|}{2k_F\rho_{ch}}, \quad k_F = (3\pi^2\rho_{ch})^{1/3}. \quad (2)$$

In particular, the enhancement factor  $F$  in the PBE-GGA Coulomb exchange functional is assumed to be<sup>2)</sup>

$$F(s) = 1 + \kappa - \frac{\kappa}{1 + \mu s^2/\kappa}, \quad (3)$$

in order to satisfy some physical conditions.<sup>3)</sup> Accordingly, the parameter  $\kappa = 0.804$  is determined for any value of  $\mu$  by the Hölder inequality. In contrast, two different values of  $\mu$  have been widely used in the studies of atoms<sup>2)</sup> and solids.<sup>4)</sup> For the PBE-GGA functional,  $\mu = 0.21951$  is determined by the random phase approximation of the homogeneous electron gas. Since this  $\mu$  can be a different value for nuclear systems, the free parameter of the PBE-GGA Coulomb exchange functional,  $\mu$ , is multiplied by a factor  $\lambda$ . For the nuclear part, the SAMi functional<sup>5)</sup> is used in the self-consistent calculation. For comparison, the exact-Fock energies are also calculated, where the exact-Fock calculation is carried out using the first-order perturbation theory.<sup>6)</sup>

The deviation of the Coulomb exchange energy  $E_{C_x}$  in the PBE-GGA from that in the LDA,  $\Delta E_{C_x}^{LDA}$ , and the deviation from that in the exact-Fock  $\Delta E_{C_x}^{exact}$ ,

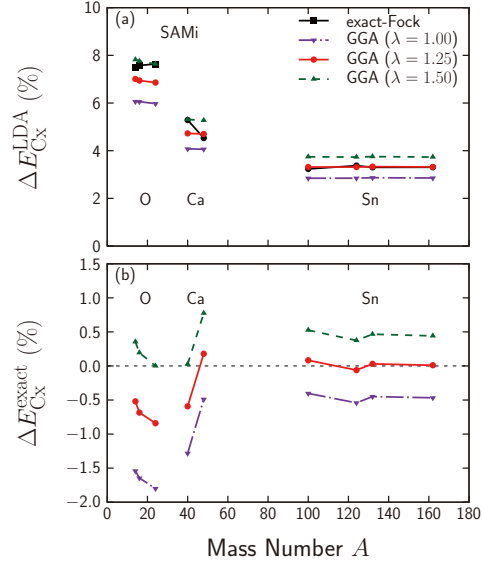


Fig. 1. Deviation between the PBE-GGA and the LDA,  $\Delta E_{C_x}^{LDA}$ , and the deviation between the PBE-GGA and the exact-Fock  $\Delta E_{C_x}^{exact}$ , defined as Eq. (4).

$$\Delta E_{C_x}^{LDA} = \frac{E_{C_x} - E_{C_x}^{LDA}}{E_{C_x}}, \quad \Delta E_{C_x}^{exact} = \frac{E_{C_x} - E_{C_x}^{exact}}{E_{C_x}}, \quad (4)$$

are shown as functions of mass number  $A$  in Figs. 1(a) and (b), respectively.

In conclusion,  $\lambda$  does not have an obvious isospin dependence, and  $\lambda = 1.25$  reproduces the exact-Fock calculation well in general. Here, note that the PBE-GGA Coulomb potential is the local potential and hence the numerical cost of the self-consistent calculation is  $O(N^3)$ , while the exact-Fock Coulomb potential is the non-local potential and hence the numerical cost is  $O(N^4)$ . This scheme helps to achieve a better description and understanding of the observables in which the Coulomb interaction plays important roles, such as the mass difference of the mirror nuclei and the energy of the isobaric analog state.

## References

- 1) T. Naito, R. Akashi, H. Liang, Phys. Rev. C **97**, 044319 (2018).
- 2) J. P. Perdew, K. Burke, M. Ernzerhof, Phys. Rev. Lett. **77**, 3865 (1996).
- 3) J. P. Perdew, K. Burke, Y. Wang, Phys. Rev. B **54**, 16533 (1996).
- 4) J. P. Perdew, *et al.*, Phys. Rev. Lett. **100**, 136406 (2008).
- 5) X. Roca-Maza, G. Colò, H. Sagawa, Phys. Rev. C **86**, 031306 (2012).
- 6) X. Roca-Maza, L.-G. Cao, G. Colò, H. Sagawa, Phys. Rev. C **94**, 044313 (2016).

<sup>†</sup> Condensed from the article in Phys. Rev. C **99**, 024309 (2019)

<sup>\*1</sup> Department of Physics, The University of Tokyo

<sup>\*2</sup> RIKEN Nishina Center

<sup>\*3</sup> Dipartimento di Fisica, Università degli Studi di Milano

<sup>\*4</sup> INFN, Sezione di Milano

## Joint project for large-scale nuclear structure calculations in 2018

N. Shimizu,<sup>\*1</sup> J. Menéndez,<sup>\*1</sup> T. Miyagi,<sup>\*1</sup> S. Yoshida,<sup>\*2</sup> T. Otsuka,<sup>\*3,\*1,\*2</sup> and Y. Utsuno<sup>\*4,\*1</sup>

We have been promoting a joint project for large-scale nuclear structure calculations since the year 2002, based on a collaboration agreement between the RIKEN Accelerator Research Facility (currently RIKEN Nishina Center) and the Center for Nuclear Study, the University of Tokyo. This agreement was completed successfully in March 2018 successfully. Based on this project, 62 original papers and 56 proceedings have been published and some are being prepared under various collaborations with many experimentalists (*e.g.* Refs. 1–3)). In 2018, we performed several theoretical studies for understanding the nuclear structure. Among these studies, we briefly show three theoretical achievements: a statistical method for the uncertainty quantification of shell-model studies,<sup>4)</sup> the development of an *ab initio* nuclear structure calculation,<sup>5)</sup> and the theoretical estimation of nuclear matrix elements that are required for surveying physics beyond the standard model.<sup>3,6–9)</sup>

We proposed a novel method to quantify the theoretical uncertainty stemming from the effective interactions of the nuclear shell model.<sup>4)</sup> In this method, the uncertainty is discussed by estimating the probability distribution of the parameter set of the effective interaction in the multidimensional parameter space. This enables us to quantify an extent of the agreement between the theoretical results and experimental data in a statistical manner, and the resulting confidence intervals show unexpectedly large variations. In addition, we pointed out that a large deviation of the confidence interval of the energy in the shell-model calculations from the corresponding experimental data can be used as an indicator of some exotic property, *e.g.*,  $\alpha$  clustering.

In order to investigate the medium-mass nuclei based on the underlying nuclear interactions in an *ab initio* way, the unitary-model-operator approach (UMOA)<sup>5)</sup> was developed. In the UMOA, the many-body Hamiltonian is transformed by a unitary transformation such that one-particle-one-hole and two-particle-two-hole excitations do not occur. We calculated the binding energies and radii of  $^4\text{He}$ ,  $^{16}\text{O}$ , and  $^{40}\text{Ca}$  using the similarity-renormalization-group (SRG) evolved chiral effective-field-theory interaction consisting of two-nucleon and three-nucleon forces. The resulting binding energies and radii were consistent with the recent *ab initio* results obtained using the same Hamiltonian, and we significantly underestimated the radii compared to the experimental

data. To clarify the origin of this underestimation, we also calculated the radii using the effective operators obtained from consistent SRG evolution in two- and three-body spaces. It turned out that the SRG evolution of the radius operator gives a minor modification and the underestimation still remains. For a unified description of the binding energies and radii, a further understanding of the nuclear force itself is essential.

We also studied two-neutrino double-beta decays and double-electron capture. We developed an effective theory that, based on data on beta decays and electron capture, describes well measured double-beta transitions, making predictions for several unknown decays.<sup>6)</sup> Subsequently, we calculated the double electron-capture half-life of  $^{124}\text{Xe}$  into the final nucleus  $^{124}\text{Te}$ .<sup>7)</sup> Our large-scale shell model results predicted a half-life of about  $10^{22}$  y, which is shorter than that predicted by other theoretical approaches, suggesting that an observation of the double-electron capture of  $^{124}\text{Xe}$  is within the reach of current experimental searches.

In addition, we performed shell-model calculations to study the possible scattering of dark matter off atomic nuclei. These interactions could reveal the nature of dark matter, and we investigated how to discriminate experimentally the signal from different dark matter–nucleus couplings.<sup>8)</sup> In addition, together with the XENON collaboration, we analyzed for the first time, the coupling of dark matter particles to the pions exchanged between two nucleons,<sup>3)</sup> a contribution that has so far not been constrained experimentally. Finally, we calculated the more general dark matter–nucleus interactions that can receive coherent contributions from several nucleons in fluorine, silicon, argon, germanium, and xenon targets.<sup>9)</sup>

### References

- 1) Md. S. R. Laskar *et al.*, Phys. Rev. C **99**, 014308 (2019).
- 2) C. Loelius *et al.*, Phys. Rev. Lett. **121**, 262501 (2018).
- 3) XENON collaboration, M. Hoferichter, P. Klos, J. Menéndez, A. Schwenk, Phys. Rev. Lett. **122** 071301 (2019).
- 4) S. Yoshida, N. Shimizu, T. Togashi, T. Otsuka, Phys. Rev. C **98**, 061301(R) (2018).
- 5) T. Miyagi, T. Abe, R. Okamoto, T. Otsuka, Phys. Rev. C **96**, 054312 (2017).
- 6) E. A. Coello Pérez, J. Menéndez, A. Schwenk, Phys. Rev. C **98**, 044501 (2018).
- 7) E. A. Coello Pérez, J. Menéndez, A. Schwenk, arXiv:1809.04443.
- 8) A. Fieguth, M. Hoferichter, P. Klos, J. Menéndez, *et al.*, Phys. Rev. D **97**, 103532 (2018).
- 9) M. Hoferichter, P. Klos, J. Menéndez, A. Schwenk, Phys. Rev. D **99**, 055031 (2019).

<sup>\*1</sup> Center for Nuclear Study, The University of Tokyo

<sup>\*2</sup> Department of Physics, The University of Tokyo

<sup>\*3</sup> RIKEN Nishina Center

<sup>\*4</sup> Japan Atomic Energy Agency

# Bubble nuclei within the self-consistent Hartree-Fock mean field plus pairing approach<sup>†</sup>

L. Tan Phuc,<sup>\*1,\*2</sup> N. Quang Hung,<sup>\*1</sup> and N. Dinh Dang<sup>\*3</sup>

A bubble structure is the depletion of nucleon density at its center, which is caused by the absence of the nucleon on the  $s$ -orbitals. The peak of the  $s$ -wave function at  $r = 0$  significantly contributes to the nucleon density. Therefore, the absence of the  $s$ -wave creates the bubble structure. The pairing correlation and the low-lying excitations affect this bubble structure. In this report, we study the evolution of the bubble structure within the self-consistent Skyrme-Hartree-Fock mean field (HF) plus pairing correlation. The latter is included in two ways: within the Bardeen-Cooper-Schrieffer theory (BCS) and within the exact pairing solution (EP)<sup>1)</sup> at finite temperature, which are referred to as the FTBCS and FTEP, respectively. The bubble candidates are the neutron-rich  $^{22}\text{O}$  ( $N = 14$ ,  $Z = 8$ ) and doubly-magic  $^{34}\text{Si}$  ( $N = 20$ ,  $Z = 14$ ) nuclei. The calculations are performed with the Skyrme-type interaction MSk3. The binding energies ( $BE$ ) and two proton/neutron separation energies ( $S_{2p/2n}$ ) of these candidate nuclei are fitted to the experimental data by adjusting the parameters  $G_N$  and  $G_Z$  of the neutron and proton pairing interactions, respectively. The finite-temperature HF (FTHF), whose single-particle occupation numbers follow the Fermi-Dirac distribution, is also used to make a comparison with the FTBCS and FTEP. The bubble structure is evaluated by the depletion factor  $F = (\rho_{max} - \rho_{cent})/\rho_{max}$ , where  $\rho_{max}$  and  $\rho_{cent}$  are the maximum and central nucleon densities, respectively.

The numerical calculations are performed within the FTHF, FTBCS and FTEP for  $^{22}\text{O}$  and  $^{34}\text{Si}$ . The pairing effect is known to be dominant in the region around Fermi surface so that a truncated space with the level  $1d_{5/2}$  located below Fermi surface and six levels  $2s_{1/2}$ ,  $1d_{3/2}$ ,  $1f_{7/2}$ ,  $2p_{3/2}$ ,  $1f_{5/2}$ , and  $2p_{1/2}$  above it is taken into account for the neutron shell of  $^{22}\text{O}$  and proton shell of  $^{34}\text{Si}$ . As for the proton shell of  $^{22}\text{O}$  and neutron shell of  $^{34}\text{Si}$ , they are closed and therefore are not affected by pairing. For  $^{34}\text{Si}$ , the experimental value for the occupation number of the  $2s_{1/2}$  level has been measured and reported by Mutschler *et al.*<sup>2)</sup> The pairing interaction parameter  $G$  is adjusted to reproduce this value, which is used as the initial input. For  $^{22}\text{O}$ , because the occupation number of the  $2s_{1/2}$  level is not known, the calculations are based on reproducing its

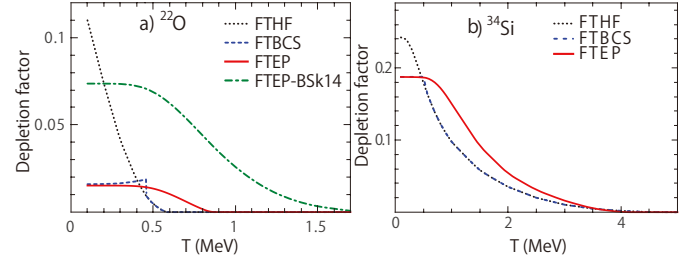


Fig. 1. The depletion factors of  $^{22}\text{O}$  and  $^{34}\text{Si}$  obtained within the FTHF, FTBCS and FTEP at different temperatures.

$BE$  and  $S_{2n}$  values.

The results obtained show that, at  $T \simeq 0$ , the depletion factors  $F$  within the FTBCS and FTEP reach 19% for proton density in  $^{34}\text{Si}$  and 2% for neutron density in  $^{22}\text{O}$ , whereas the FTHF without pairing produces the value of  $F$  at around 24% and 11% for  $^{34}\text{Si}$  and  $^{22}\text{O}$ , respectively (at  $T = 0.1$  MeV). These results indicate that the effect of pairing correlation on the bubble structure is strong in the neutron-rich nucleus  $^{22}\text{O}$ , and weak in the doubly-magic nucleus  $^{34}\text{Si}$ . With increasing  $T$ , the bubbles in these nuclei become less pronounced and completely disappear when  $T$  reaches the critical value  $T_F$ . The value of  $T_F$  in  $^{34}\text{Si}$  is around 4 MeV within the FTBCS and FTEP, whereas, for  $^{22}\text{O}$ , it is 0.57 MeV within the FTBCS and 0.85 MeV within the FTEP (Fig. 1). This difference can be explained by the fact that the BCS pairing gap  $\Delta$  collapses when  $T$  reaches a critical value  $T_c = 0.57\Delta$  ( $T = 0$ ), which makes the depletion factor coincide with that predicted by the FTHF, whereas the EP pairing gap is always finite with increasing  $T$ . This phenomenon causes a significant difference in  $T_F$  for the neutron-rich nucleus  $^{22}\text{O}$ , where the pairing correlation is dominant. On the other hand, this phenomenon does not seem to take place in the doubly-magic nucleus  $^{34}\text{Si}$ . The BSk14 interaction, which is also used in predicting the neutron bubble in  $^{22}\text{O}$ , shows a small pairing in this nucleus instead of strong pairing obtained by using the MSk3 interaction. This indicates that the MSk3 is more suitable than the BSk14 in our study.

## References

- 1) A. Volya, B. A. Brown, V. Zelevinsky, Phys. Lett. B **509**, 37 (2001).
- 2) A. Mutschler *et al.*, Nature **13**, 152 (2017).

<sup>†</sup> Condensed from the article in Phys. Rev. C **97**, 024331 (2018)

<sup>\*1</sup> Duy Tan University, Ho Chi Minh City, Vietnam

<sup>\*2</sup> University of Science - Vietnam National University, Ho Chi Minh City, Vietnam

<sup>\*3</sup> RIKEN Nishina Center

# Dineutron correlation and large quadrupole collectivity in deformed Mg isotopes near neutron drip line

M. Yamagami\*<sup>1</sup>

Dineutron correlation is one of the exotic features in nuclei near the neutron drip line. The pair excitation into continuum states plays a key role in creating the strong spatial correlation between two neutrons. Dineutron correlation is considered to be a universal phenomenon around the drip line but the experimental evidence is still under intense debate except for light mass nuclei. In this study, we discuss low-lying quadruple excitations in deformed Mg isotopes to clarify the continuum effects in pairing correlation, which could suggest the presence of dineutron correlation.

First, we solve the Hartree-Fock-Bogoliubov (HFB) equation with Skyrme energy density functional (EDF) equation with Skyrme energy density functional (EDF). We demonstrate the result using the SkM\* EDF but the UNEDF0 EDF draws the same conclusion. The pairing correlation is active for single-particle states whose energy  $\varepsilon$  satisfies  $\varepsilon < \lambda + E_{\text{pair}}^{(+)}$ . Here,  $\lambda$  is the chemical potential and  $E_{\text{pair}}^{(+)} = 10$  MeV is used. The predicted neutron drip line nucleus is  $^{44}\text{Mg}$  with neutron chemical potential  $\lambda_n = -0.15$  MeV. The quadrupole deformations of  $^{34,36,38,40,42,44}\text{Mg}$  are  $\beta_2 = 0.35, 0.30, 0.28, 0.28, 0.21,$  and  $0.15,$  and the neutron pairing gaps are  $\Delta_n = 1.21, 1.20, 1.17, 0.98, 1.05,$  and  $1.00$  MeV respectively.

On top of the HFB states, we solve the quasiparticle random phase approximation (QRPA) equation in the matrix form.<sup>1)</sup> Figure 1 shows the  $K^\pi = 0^+$  isoscalar quadrupole transition strength  $B(Q^{\text{IS}2}; E_\nu) = |\langle \nu | r^2 Y_{20} | 0 \rangle|^2$  to the excited state  $|\nu\rangle$  at excitation energy  $E_\nu$  in  $^{40,42,44}\text{Mg}$ . The QRPA excitation is generated by the coherent superposition of excitations of both particle-hole and particle-particle types. The transition strengths without the dynamical pairing effects, *i.e.*, QRPA calculation ignoring the residual pairing interactions, are also shown.

It should be noted that the transition strength of low-lying states significantly reduces when the dynamical pairing effect is ignored. This excitation mode is induced by the fluctuation of neutron-pair occupation in Nilsson orbits with different spatial shapes. For example, the prolate-type orbits  $[310]1/2$  and  $[301]1/2$ , and the oblate-type orbit  $[303]7/2$  are the main contributors around  $^{40}\text{Mg}$ .

Figure 2 shows the summation of strength  $S_{\text{IS}2}(6 \text{ MeV}) = \sum_{0 < E_\nu < 6 \text{ MeV}} B(Q^{\text{IS}2}; E_\nu)$ . In  $^{34,36}\text{Mg}$ , the typical model size for stable nuclei,  $E_{\text{pair}}^{(+)} = 4$  MeV, gives reasonable results. The effect of continuum states above  $E_{\text{pair}}^{(+)} = 4$  MeV becomes gradually sizable as it approaches the drip line.  $S_{\text{IS}2}(6 \text{ MeV})$  converges with

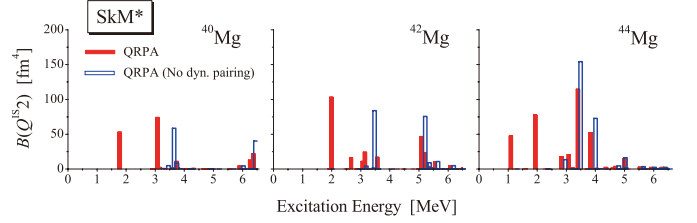


Fig. 1.  $K^\pi = 0^+$  isoscalar quadrupole transition strengths with  $E_{\text{pair}}^{(+)} = 10$  MeV in  $^{40,42,44}\text{Mg}$ . QRPA strengths ignoring the dynamical pairing effect are compared.

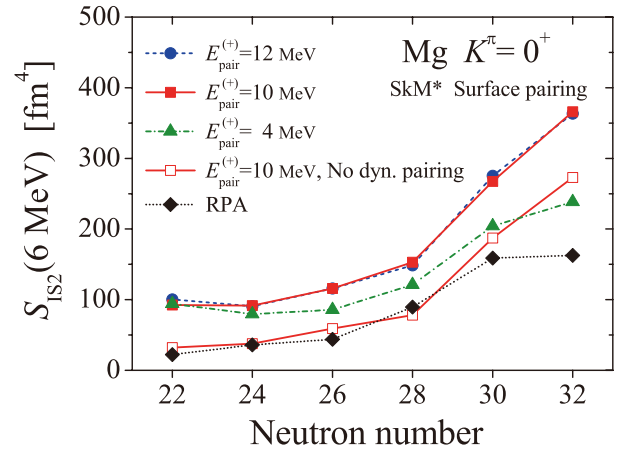


Fig. 2. Summation of strength  $S_{\text{IS}2}(6 \text{ MeV})$  in neutron-rich Mg isotopes are shown. Effects of continuum states and pairing correlation are investigated.

$E_{\text{pair}}^{(+)} = 10$  MeV. It should be noted that the single-particle state with  $\varepsilon \approx 10$  MeV has a wave number  $k \approx 0.27 \text{ fm}^{-1}$  and the spatial size  $\Delta x \approx 1/k \approx 3.7 \text{ fm}$  corresponds to the diameter of a dineutron predicted around  $^{40}\text{Mg}$ .<sup>2)</sup>

Figure 2 also shows the  $S_{\text{IS}2}(6 \text{ MeV})$  of RPA and QRPA ignoring the dynamical pairing correlation. These two results coincide with each other except for  $^{44}\text{Mg}$ .  $S_{\text{IS}2}(6 \text{ MeV})$  increases by 38.9% when static pairing correlation is added in  $^{44}\text{Mg}$ . This is due to an additional particle-hole configuration from the resonant state  $[321]1/2$  to resonant state  $[301]1/2$ .

In conclusion, the coupling to continuum states in pairing correlation enhances the low-lying transition strengths of  $K^\pi = 0^+$  isoscalar quadruple excitations in Mg isotopes near the neutron drip line. This suggests the presence of dineutron correlations.

## References

- 1) M. Yamagami *et al.*, RIKEN Accel. Prog. Rep. **50**, 92 (2017).
- 2) M. Yamagami *et al.*, *Phy. Rev. C* **77**, 064319 (2008).

\*<sup>1</sup> Department of Computer Science and Engineering, University of Aizu

# Isoscalar and isovector spin responses in $sd$ -shell nuclei<sup>†</sup>

H. Sagawa<sup>\*1</sup> and T. Suzuki<sup>\*2</sup>

The spin-isospin response and spin-isospin dependent interactions in nuclei are important fundamental problems in nuclear physics and astrophysics. Recently, isoscalar (IS) and isovector (IV) spin M1 transitions have been investigated by high-resolution proton inelastic scattering measurements at  $E_p = 295$  MeV.<sup>1)</sup> In this study, the spin magnetic dipole transitions and neutron-proton spin-spin correlations in  $sd$ -shell even-even nuclei with  $N = Z$ ,  $^{20}\text{Ne}$ ,  $^{24}\text{Mg}$ ,  $^{28}\text{Si}$ ,  $^{32}\text{S}$ , and  $^{36}\text{Ar}$  along with a  $p$ -shell nucleus  $^{12}\text{C}$  are investigated using shell model wave functions considering the enhanced IS spin-triplet pairing with effective spin operators. In general, the calculated results show good agreement with the experimental energy spectra in  $N = Z$  nuclei as far as the excitation energies are concerned. In comparison with the experimental M1 results, the accumulated IS spin strengths up to 16 MeV show small quenching effect, corresponding to the effective quenched operator  $f^{IS}(\text{eff}) \sim 0.9$ , while a large quenching  $f^{IV}(\text{eff}) \sim 0.7$  is extracted for the IV channel. Similar quenching on the IS spin M1 transitions is obtained by the 20% enhanced IS spin-triplet pairing correlations with the bare spin operator. However, the enhanced IS pairing does not change much the excitation energy spectra. The Towner's effective spin operators efficiently reproduce the accumulated experimental IV spin strength, while the quenching of effective operators is much larger than that observed in the IS spin channel. Consequently, an enhanced IS spin-triplet pairing interaction enlarges the proton-neutron spin-spin correlation deduced from the difference between the IS and IV sum rule strengths. The beta-decay rates and the IS magnetic moments of  $sd$ -shell are also studied in terms of IS pairing and the effective spin operators. Previously, a large quenching of IS magnetic transition strength was suggested in the literature. However, the  $(p, p')$  data in Ref. 1) do not exhibit the large quenching effect on the IS spin transitions. This should further be studied experimentally with possible IS probes such as  $(d, d')$  reactions with comprehensive theoretical calculations.

## References

- 1) H. Matsubara *et al.*, Phys. Rev. Lett. **115**, 102501 (2015) and private communications.
- 2) I. Towner, Phys. Rep. **155**, 263 (1987).

<sup>†</sup> Condensed from the article in Phys. Rev. C **97**, 054333 (2018)

<sup>\*1</sup> RIKEN Nishina Center and Center for Mathematics and Physics, University of Aizu

<sup>\*2</sup> Department of Physics, College of Humanities and Science, Nihon University and National Astronomical Observatory of Japan

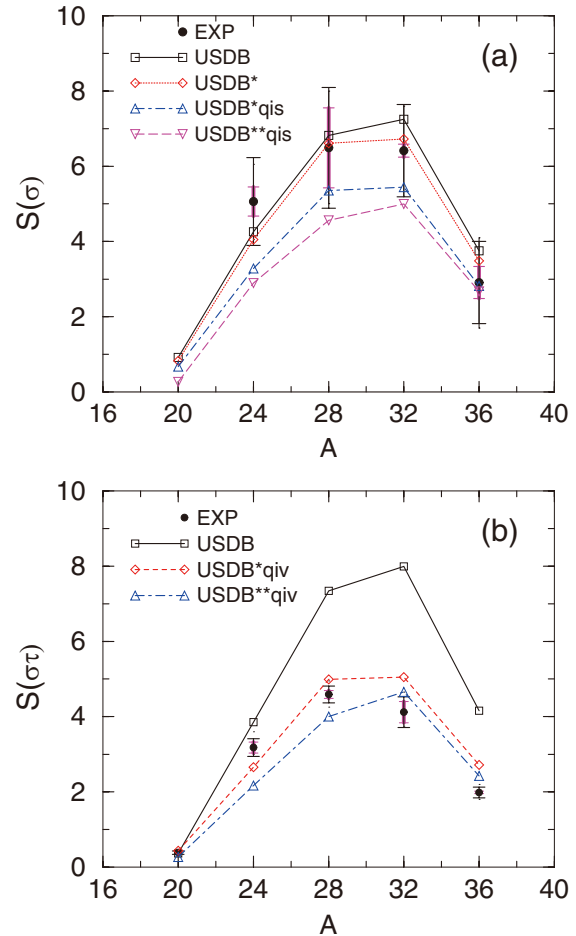


Fig. 1. (Color online) Accumulated spin-M1 transition strengths of (a) IS channel and (b) IV channel. Experimental and theoretical data are summed up to  $E_x = 16$  MeV. Shell model calculations are performed with USDB effective interaction: (a) in the results of USDB\* and USDB\*qis, the IS spin-triplet pairing interaction is enhanced by multiplying the relevant matrix elements with a factor of 1.1 compared to the original USDB interactions, and the quenching factor  $f_s^{IS} = 1.0$  and  $0.9$  for IS spin operator, respectively. For USDB\*\*qis, the IS pairing interaction is enhanced by a factor of 1.2 and a quenching factor  $f_s^{IS} = 0.9$  is introduced for the IS spin operator. Experimental data are taken from Ref. 1). Long thin error bars indicate total experimental uncertainty, while short thick error bars denote the partial uncertainty from the spin assignment. (b) Effective IV operators<sup>2)</sup> are adopted for spin, orbital and spin-tensor operators for USDB\*qiv and USDB\*\*qiv. For the results of USDB\*qiv and USDB\*\*qiv, the IS pairing interaction is enhanced by a factor of 1.1 and 1.2, respectively, using the effective operators.

# Self-consistent constrained HFB in odd-A nuclei<sup>†</sup>

K. Sugawara-Tanabe<sup>\*1,\*2</sup> and K. Tanabe<sup>\*3</sup>

All existing constrained Hartree-Fock-Bogoliubov (CHFB) calculations neglect the Fock or the exchange terms. Here, the constraint conditions are applicable to the proton number  $Z$ , neutron number  $N$ , and the angular momentum along the chosen  $x$ -axis  $\langle I_x \rangle = \sqrt{I(I+1)}$ . The numerical calculations start from the spherical single-particle basis and include the residual quadrupole-quadrupole (Q-Q), monopole-pairing (MP), and quadruple-pairing (QP) interactions.<sup>1)</sup> In the approximation without the exchange terms, only the terms  $Y_0^2$  and  $Y_2^2 + Y_{-2}^2$  in the Q-Q interaction are considered but the terms  $Y_1^2 \pm Y_{-1}^2$  and  $Y_2^2 - Y_{-2}^2$  are not. We have developed the code to include all exchange terms in the residual interactions. The exchange terms of Q-Q contribute to the self-energy  $\Gamma$  and the gap  $\Delta$ , and those of MP and QP to  $\Gamma$ . Then, the constraint on angular momentum  $\langle I_x \rangle$  becomes  $\sqrt{I(I+1) - \langle I_z^2 \rangle}$ . We chose the signature invariant base that reduces the diagonalization space to half<sup>2)</sup> because the total Hamiltonian with three constraints  $H'$  is invariant under the operator  $R_x = \exp(-i\pi I_x)$ . All input matrix elements are rewritten in this base and the spherical single-particle operator in this base  $C_k$  is transformed to quasiparticle operators  $\alpha_i^\dagger = \sum_{k>0} (C_k^\dagger A_{ki} + C_{\hat{k}} B_{ki})$  and  $\alpha_i = \sum_{k>0} (C_{\hat{k}}^\dagger \hat{A}_{ki} + C_k \hat{B}_{ki})$ , where the notation  $\hat{k}$  is the time reversal of  $k$ . Then, the CHFB equation becomes:

$$\begin{pmatrix} h^1 - \omega j_x & \Delta^T \\ \Delta^* & -h^{2*} - \omega j_x \end{pmatrix} \begin{pmatrix} \hat{B}^* & A \\ \hat{A}^* & B \end{pmatrix} = \begin{pmatrix} \hat{B}^* & A \\ \hat{A}^* & B \end{pmatrix} \begin{pmatrix} -\hat{\Lambda} & 0 \\ 0 & \Lambda \end{pmatrix}, \quad (1)$$

where  $h^1$  ( $h^2$ ) includes the spherical single-particle energy and self-energy  $\Gamma$  and  $\omega$  is the Lagrange multiplier for  $I_x = \sum_{k,l>0} (j_x)_{k,l} (C_k^\dagger C_l - C_{\hat{k}}^\dagger C_{\hat{l}})$ . When there is no  $\omega j_x$ , *i.e.*, without constraint on  $\langle I_x \rangle$ ,  $h^2$ ,  $\hat{\Lambda}$ ,  $\hat{A}$ , and  $\hat{B}$  are reduced to  $h^1$ ,  $\Lambda$ ,  $A$ , and  $B$ , respectively. The iteration procedure in the numerical analysis is based on the gradient method.<sup>3)</sup>

Figure 1 compares  $I$  versus transition energy  $\Delta E = E(I) - E(I-2)$ . The parameters are the same spherical single-particle energy as listed in Table 1 in Ref. 1). The strength of MP is  $G_{\pi+\pi+}^{(0)} = G_{\pi-\pi-}^{(0)} = G_{\pi+\pi-}^{(0)} = -0.22$  MeV and  $G_{\nu+\nu+}^{(0)} = G_{\nu-\nu-}^{(0)} = G_{\nu+\nu-}^{(0)} =$

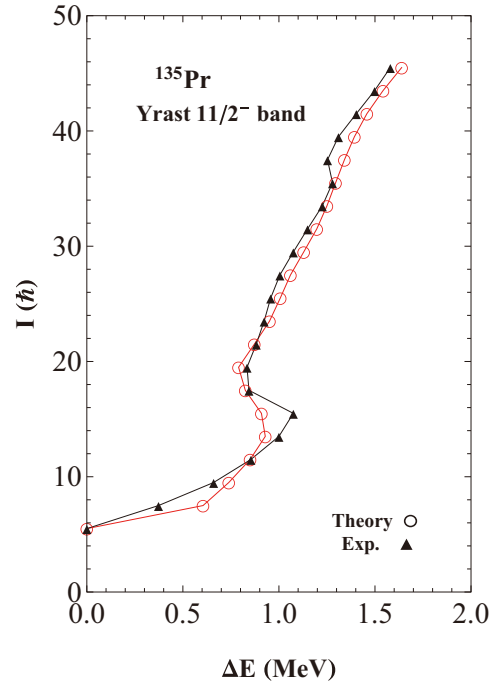


Fig. 1. Backbending plot for  $I$  as a function of energy difference  $\Delta E = E(I) - E(I-2)$ . Experimental data is taken from Ref. 4).

$-0.23$  MeV. The strength of QP is 10% of MP, expressed in terms of  $\text{MeV}/b^4$  and the strength of QQ is  $\chi_{\pi\pi} = -0.030$   $\text{MeV}/b^4$ ,  $\chi_{\nu\nu} = -0.032$   $\text{MeV}/b^4$ , and  $\chi_{\pi\nu} = -0.100$   $\text{MeV}/b^4$  with an oscillator length  $b$ . These numerical results are consistent with the experimental data except for the  $I = 15/2^-$  state. The constraint on the proton number  $Z$  is effective but the value of  $Z$  for + and - parity states is mixed owing to  $G_{\pi+\pi-}^{(0)}$ . For example,  $Z_+ = 13.58$  and  $Z_- = 17.42$  at  $I = 15/2^-$ , while  $Z_+ = 13.99$  and  $Z_- = 17.01$  at  $I = 55/2^-$ , where  $Z = Z_+ + Z_-$  is the proton number outside the magic number 28. For better results, another constraint on  $Z-$  should be included or the MP and QP interactions between the + and - parity states should be dropped. This calculation is preliminary and there is room for finding better parameter sets.

## References

- 1) K. Tanabe, K. Sugawara-Tanabe, Prog. Theor. Phys. **83**, 1148 (1990).
- 2) A. L. Goodman, Nucl. Phys. **86**, 5866 (2001).
- 3) H. J. Mang, B. Samadi, P. Ring, Z. Physik A **279**, 325 (1976).
- 4) C. S. Paul *et al.*, Phys. Rev. C **84**, 047302 (2011).

<sup>†</sup> Condensed from the talk in Int. Symp. on "Simplicity, Symmetry and Beauty," Sept. 26-28, Shanghai (2018)

<sup>\*1</sup> RIKEN Nishina Center

<sup>\*2</sup> Department of Information Design, Otsuma Women's University

<sup>\*3</sup> Department of Physics, Saitama University

# Nuclear symmetry energy and the breaking of the isospin symmetry: how do they reconcile with each other ?<sup>†</sup>

X. Roca-Maza,<sup>\*1</sup> G. Colò,<sup>\*1</sup> and H. Sagawa<sup>\*2</sup>

The density dependence of symmetry energy is still not understood well enough. A deeper understanding is highly needed, because an accurate characterization of the symmetry energy entails profound consequences for the study of neutron distributions in nuclei along the entire nuclear chart, as well of other properties of neutron-rich nuclei.<sup>1)</sup> The symmetry energy is also of paramount importance for understanding the properties of compact objects like neutron stars; it directly affects the determination of the radius of a low-mass neutron star.<sup>2)</sup>

The isobaric analog state (IAS) is one of the well-established properties of nuclei that is measured accurately, and it is dominantly sensitive to the isospin symmetry breaking (ISB) in the nuclear medium due to Coulomb interaction.<sup>3)</sup> If there is an inconsistency between the properties of the symmetry energy and our knowledge of the IAS and ISB forces, it is a serious issue. As discussed often, the neutron skin is strongly correlated with the density dependence of the symmetry energy. Therefore, we cannot accept that the values of the neutron skin do not match our understanding of the isospin symmetry, which is one of the basic symmetries of nature, and its breaking.

Starting from the prototype SAMi functional, a systematically varied family was generated, by keeping a similar quality of the original fit and varying the values of J and L. In addition, a family based on the systematic variation of J and L with respect to a relativistic mean field (RMF) model with density-dependent meson-nucleon vertices (DD-ME) was also introduced. These functionals provide the values of the neutron skin through the Hartree-Fock (HF) or Hartree solution for the ground-state; in addition, they provide, self-consistently, the IAS energy via the charge-exchange random phase approximation (RPA). The results for the IAS energy,  $E_{IAS}$ , as a function of  $\Delta R_{np}$  are plotted in Fig. 1. The results associated with other Skyrme interactions are also plotted. We found a serious discrepancy of (0.5~1) MeV between the calculated and experimental  $E_{IAS}$  for all EDFs in Fig. 1.

To solve this puzzle, we reconsidered all possible contributions to the IAS energy that have not been considered with sufficient care in self-consistent calcula-

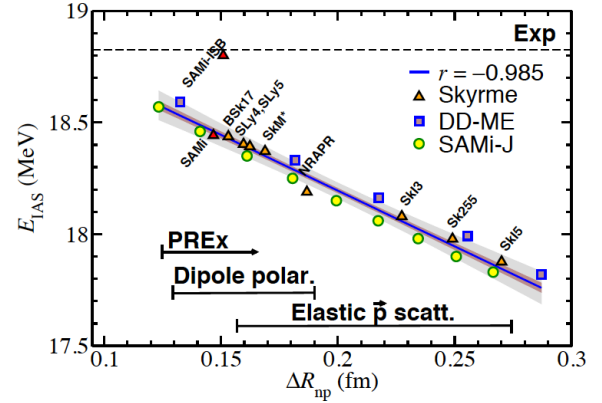


Fig. 1. Energy of the IAS as a function of  $\Delta R_{np}$  with various EDFs. The arrows indicate the experimental results; PREx is obtained from the polarized electron parity violation experiment, Dipole polarizability is the value obtained from the measurement of giant dipole resonances, and elastic  $p$  scattering is the data obtained from the polarized proton scattering cross section analysis.

tions so far. Then, we proposed a new parametrization SAMi-ISB for Skyrme-like EDF, which reconciles standard nuclear properties (saturation density, binding energy, and charge radii of finite nuclei) with both our current understanding of the density behavior of the symmetry energy and the reproduction of the IAS energy of  $^{208}\text{Pb}$ . We have self-consistently included for the first time within the HF+RPA framework, all known contributions that break the isospin symmetry. All of these contributions have been calculated in a model-independent way. We have fixed only two free parameters in the charge symmetry breaking (CSB) and charge independence breaking (CIB) terms, and we have shown that this allows for a good reproduction of the IAS energy of  $^{208}\text{Pb}$  without compromising the other properties of nuclear matter and finite nuclei. The calculated results show a fine agreement with the experimental excitation energy of IAS in  $^{208}\text{Pb}$  reconciling realistic symmetry energy parameters and the neutron skin as shown in Fig. 1. The energies of IAS in Sn isotopes are also improved by SAMi-ISB.

## References

- 1) Bao-An Li *et al.*, Eur. Phys. J. A **50**, 9 (2014).
- 2) C. J. Horowitz *et al.*, J. Phys. G **41**, 093001 (2014).
- 3) N. Auerbach *et al.*, Phys. Rev. Lett. **23**, 484 (1969).

<sup>†</sup> Condensed from the article in Phys. Rev. Lett. **120**, 202501 (2018)

<sup>\*1</sup> Dipartimento di Fisica, Università degli Studi di Milano and INFN, Sezione di Milano

<sup>\*2</sup> RIKEN Nishina Center and Center for Mathematics and Physics, University of Aizu

# Neutron-proton pairing correlations and deformation for $N = Z$ nuclei in $pf$ -shell using deformed BCS and HFB approach<sup>†</sup>

E. Ha,<sup>\*1</sup> M. -K. Cheoun,<sup>\*1</sup> and H. Sagawa<sup>\*2</sup>

Shell evolution by deformation is an important concept to understand the structure of neutron-rich nuclei, whose deformation can be confirmed by rotational energy spectra and the E2 transition probability extracted from the experiments. The shell evolution plays a crucial role in understanding the beta-decays in nucleosynthesis. Such features may also appear in neutron-deficient deformed nuclei, for example,  $N = Z$   $pf$ -shell nuclei. In particular, in RMF calculations, <sup>68</sup>Se and <sup>72</sup>Kr are claimed to have oblate deformations while <sup>48</sup>Cr, <sup>52</sup>Fe, and <sup>64</sup>Ge may have prolate deformations, as presented in Table 1.

In this work, we determine the most stable deformation by investigating the evolution of ground state energies along with the deformation within a framework of the deformed BCS (DBCS) and deformed HFB (DHFB) models. Specifically, <sup>64</sup>Ge is known to cause a bottle-neck on  $p$ - or  $\alpha$ -nucleosynthesis. Then, the neutrino-proton ( $\nu p$ )-process,  $\bar{\nu}_e + p \rightarrow n + e^+$ , produces lots of neutrons which make it possible to escape the bottle-neck by <sup>64</sup>Ge ( $n, p$ ) <sup>64</sup>Ga ( $p, \gamma$ ) <sup>65</sup>Ge reaction and subsequently, bridge the waiting points. Therefore, the nuclear structure of <sup>64</sup>Ge becomes the key to understand the mechanism of these reaction.

First, we studied the evolution of single particle state (SPS) energies for  $N = Z$   $pf$ -shell nuclei by exploiting a deformed Woods-Saxon potential. Second, taking these SPS, we calculated the ground state energies of the nuclei including the pairing interactions of like- ( $nn$  and  $pp$ ) and unlike-pairs ( $np$ ) by the deformed BCS (or HFB) approach. The pairing correlations were found to be sensitive to the deformation parameter  $\beta_2$  and the evolved Fermi energies  $\epsilon_f$ .

The pairing effects of like-pairs bound the nucleus more strongly, but did not significantly change the evolution of ground state energies. In contrast, the  $np$  pairings contributed to the formation of more bound nuclei and significantly affected the  $pf$ -shell deformation. To determine the importance of  $T = 0$  pairing, we introduced an enhanced  $T = 0$  pairing interaction, where the  $T = 0$  pairing matrices obtained by the Bruckner HF calculations were enlarged by a factor of 1.5. We found that the enhanced  $T = 0$  pairing correlations, which played vital roles in the determination of nuclear deformations of  $sd$ -shell nuclei,<sup>1)</sup> are important in the evolution of nuclear deformation. Specifically,

Table 1. Deformation parameter from the experimental E2 transition data<sup>2)</sup> and theoretical deformation parameters by Relativistic Mean Field (RMF),<sup>3)</sup> FRDM model,<sup>4)</sup> and the present results with the enhanced  $T = 0$  pairing for  $N = Z$   $pf$ -shell nuclei. Empirical pairing gaps deduced from the five-point mass formula<sup>5)</sup> are also shown.

$A$	$\beta_2^{E2}$	$\beta_2^{RMF}$	$\beta_2^{FRDM}$	$\beta_2^{ours}$	$\Delta_p^{emp}$	$\delta_{np}^{emp}$
<sup>44</sup> Ti	0.277	0.000	0.011	0.2	2.631	2.068
<sup>48</sup> Cr	0.340	0.225	0.226	0.2	2.128	1.442
<sup>52</sup> Fe	0.230	0.186	-0.011	0.2	1.991	1.122
<sup>64</sup> Ge	0.259	0.217	0.207	0.1	1.807	1.435
<sup>68</sup> Se	0.239	-0.285	0.233	-0.2	1.909	1.522
<sup>72</sup> Kr	0.330	-0.358	-0.366	-0.1	2.001	1.353
<sup>76</sup> Sr	0.443	0.410	0.402	0.1	1.626	0.715

the oblate deformations of <sup>68</sup>Se and <sup>72</sup>Kr and prolate deformations of <sup>52</sup>Fe and <sup>64</sup>Ge could not be explained without the enhanced  $T = 0$  pairing correlations in the present model. Finally, the HFB approach including pairings between different states does not provide any new effects on the nuclear structure but contributes to a more reasonable renormalization of the strength parameter for the nuclear interaction in the nuclear medium.

In conclusion, the evolution of ground state energies is determined by the evolution of the outermost shell. The  $np$  pairing interactions significantly change the evolution of deformation. In particular, the enhanced isoscalar spin-triplet pairing is shown to play an important role in changing the shape of the  $pf$ -shell  $N = Z$  nuclei such as <sup>68</sup>Se and <sup>72</sup>Kr. It is also suggested by the study of pairing gaps that the IS condensation by the enhanced  $T = 0$  pairing may happen in both  $sd$ -shell and  $pf$ -shell nuclei. The state dependent pairing correlations induced by HFB model are found to rarely affect the nuclear structures as compared to the conventional BCS approach.

## References

- 1) E. Ha, M. K. Cheoun, H. Sagawa, Phys. Rev. C **97**, 024320 (2018).
- 2) B. Pritychenko *et al.*, Atomic Data Nucl. Data Tables **107**, 1 (2016).
- 3) G. A. Lalazissis, S. Raman, P. Ring, Atomic Data and Nucl. Data Tables **71**, 1 (1999).
- 4) P. Möller, J. R. Nix, W. D. Myers, W. J. Swiatecki, Atomic Data and Nucl. Data Tables **59**, 185 (1995).
- 5) M. K. Cheoun *et al.*, Nucl. Phys. A **561**, 74 (1993); A **564**, 329 (1993); M. K. Cheoun *et al.*, *ibid.* A **587**, 301 (1995).

<sup>†</sup> Condensed from the article in Phys. Rev. C **97**, 064322 (2018)

<sup>\*1</sup> Department of Physics and Origin of Matter and Evolution of Galaxy (OMEG) Institute, Soongsil University

<sup>\*2</sup> RIKEN, Nishina Center and Center for Mathematics and Physics, University of Aizu

# Spin-singlet and spin-triplet pairing correlations on shape evolution in $sd$ -shell $N = Z$ Nuclei<sup>†</sup>

E. Ha,<sup>\*1</sup> M. -K. Cheoun,<sup>\*1</sup> and H. Sagawa<sup>\*2,\*3</sup>

Pairing correlations play an important role in nuclear structure, and have an important effect on nuclear electro-magnetic (EM) and weak transitions. The pairing correlations are classified into like-pairing (neutron-neutron ( $nn$ ) and proton-proton ( $pp$ )) and unlike-pairing (neutron-proton ( $np$ )) correlations. In particular, for  $N = Z$  nuclei, the  $np$  pairing may become significant because protons and neutrons occupy the same orbital and have the maximum configuration overlap, which is important especially for the  $T = 0$  pairing. The  $nn$  and  $pp$  pairings have isovector (IV) spin-singlet ( $T = 1, J = 0$ ) mode, while the  $np$  pairing correlations have peculiar isoscalar (IS) spin-triplet ( $T = 0, J = 1$ ) as well as IV spin-singlet mode. Over the last few decades, there have been many discussions regarding the  $np$  pairing correlations, in particular, the coexistence of IS and IV correlations and their competitions in some specific nuclear observables.

Recently, interesting experimental data have been reported, which show more quenching in the IV M1 spin transition data for the  $N = Z$   $sd$ -shell nuclei<sup>1)</sup> than the IS data. These features are not expected according to former theoretical discussions.<sup>2,3)</sup> It was pointed out in Ref. 4) that the  $T = 0$  pairing plays a significant role to cause these features in the spin dependent observables.

We studied the shape evolution of  $N = Z$  nuclei,  $^{24}\text{Mg}$ ,  $^{28}\text{Si}$ , and  $^{32}\text{S}$  in the deformed Woods-Saxon (DWS) and deformed BCS (DBCS) approximations taking into account both  $T = 0$  and  $T = 1$  pairing correlations. In the filling approximation for the DWS potential, it is shown that the shape evolution strongly correlates with the shell structure of s.p. energies near the last occupied orbit (Fermi energy). The effect of two types of pairing correlations with isospin  $T = 0$  and  $T = 1$  are studied by the DBCS model with G-matrix-based pairing interactions. We adopted an enhanced  $T = 0$  pairing interaction to clarify the effect of  $T = 0$  pairing on the ground state energy. In Fig. 1, we used a stronger  $T = 0$  interaction (50% stronger than the G-matrix results<sup>4)</sup>), which makes the pairing correlations more transparent, especially at the large prolate deformation and leads to the deep prolate deformation minimum in  $^{24}\text{Mg}$ . A drastic change in the pairing correlation energy is induced by the active  $T = 0$  pairing channel on top of the usual  $T = 1$  channel, implying

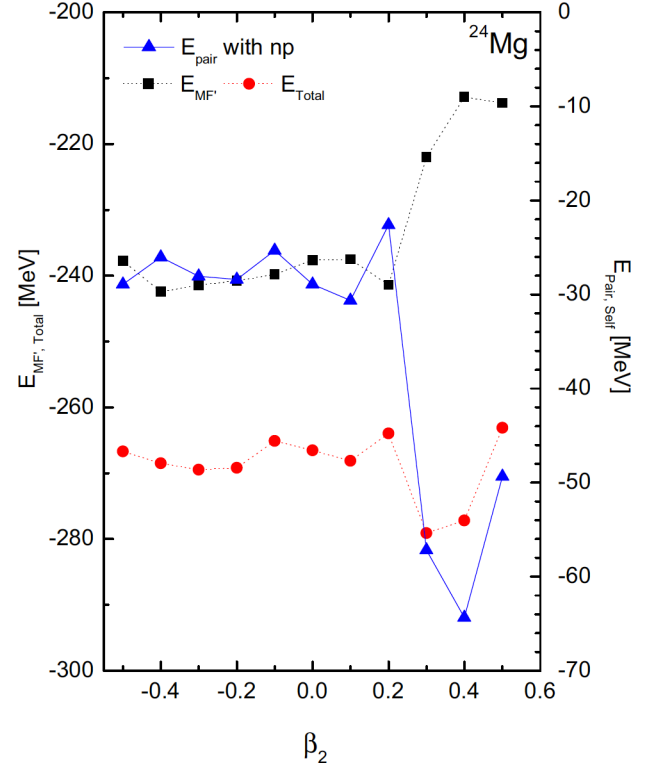


Fig. 1. The ground state energy ( $E_{\text{total}} = E_{\text{MF}'} + E_{\text{pair}}$ ) for  $^{24}\text{Mg}$  by the DBCS model with Woods-Saxon potential. Mean field energy by the DBCS is denoted as  $E_{\text{MF}'}$ .  $E_{\text{pair}}$  is the pairing energy in the right y-axis. The pairing energies are estimated with enhanced  $T = 0$  pairing in  $np$  channel.

that the two pairing channels co-exist in the large deformation region.

In summary, we found a coexistent phase of two types of superconductors in the large deformation region  $|\beta_2| > 0.3$  in  $^{24}\text{Mg}$ ,  $^{28}\text{Si}$  and  $^{32}\text{S}$  with the enhanced  $T = 0$  pairing. The competition between  $T = 0$  and  $T = 1$  pairing channels substantially affect the energy minima of  $^{24}\text{Mg}$ ,  $^{28}\text{Si}$  and  $^{32}\text{S}$ . Our model gives a reasonable deformation minima for these nuclei, *i.e.*, prolate for  $^{24}\text{Mg}$  and  $^{32}\text{S}$  and oblate for  $^{28}\text{Si}$ .

## References

- 1) H. Matsubara *et. al.*, Phys. Rev. Lett. **115**, 102501 (2015).
- 2) A. Arima, K. Shimizu, W. Bentz, H. Hyuga, Adv. Nucl. Phys. **18**, 1 (1987).
- 3) I. S. Towner, Phys. Rep. **155**, 263 (1987).
- 4) H. Sagawa, C. L. Bai, G. Colo, Phys. Scr. **91**, 083011 (2016).

<sup>†</sup> Condensed from the article in Phys. Rev. C **97**, 024320 (2018)

<sup>\*1</sup> Department of Physics and Origin of Matter and Evolution of Galaxy (OMEG) Institute, Soongsil University

<sup>\*2</sup> RIKEN Nishina Center

<sup>\*3</sup> Center for Mathematics and Physics, University of Aizu

# Low-lying collective excited states in non-integrable pairing models based on stationary phase approximation to the path integral<sup>†</sup>

F. Ni,<sup>\*1</sup> N. Hinohara,<sup>\*1,\*2</sup> and T. Nakatsukasa<sup>\*1,\*2,\*3</sup>

The time-dependent mean-field (TDMF) theory is a standard theory to describe the dynamics of nuclei from the microscopic degrees of freedom.<sup>1)</sup> Inclusion of the pairing dynamics leads to the time-dependent Hartree-Fock-Bogoliubov (TDHFB) theory, which has been utilized for a number of studies of nuclear reaction and structure. The small-amplitude approximation of TDHFB with modern energy density functionals, namely quasiparticle random phase approximation (QRPA), has successfully reproduced the properties of giant resonances in nuclei. In contrast, the QRPA description of low-lying quadrupole vibrations is not as good as that of the giant resonances. A large-amplitude nature of the quantum shape fluctuation is supposed to be important for these low-lying collective states.

The TDMF (TDHFB) theory corresponds to an SPA solution in the path integral formulation. It lacks a part of quantum fluctuation, which is important in large amplitude dynamics. To introduce the quantum fluctuation based on the TDHFB theory, requantization is necessary. A simple and straightforward way of requantization is canonical quantization. This is extensively utilized for collective models in nuclear physics.

In our previous work,<sup>2)</sup> we studied various requantization methods for the two-level pair model, in order to investigate the low-lying excited  $0^+$  states. Since the collectivity is rather low in the pairing motion in nuclei, the canonical quantization often fails to produce an approximate answer to the exact solution. In contrast, the stationary phase approximation (SPA) to the path integral can give quantitative results not only for the excitation energies but also for the wave functions and two-particle-transfer strengths. The quantized states obtained in the SPA has two advantages: First, the wave functions are given directly in terms of the microscopic degrees of freedom. Second, the restoration of broken symmetries are automatic. However, the applications of SPA have been limited to integrable systems. This is because we need to find separable periodic trajectories on a classical torus. Since nuclear systems, of course, correspond to non-integrable systems, a straightforward application of the SPA is not possible.

In this paper, we propose a new approach of SPA applicable to non-integrable systems, which is based on the extraction of the one-dimensional (1D) collective coordinate using the adiabatic self-consistent col-

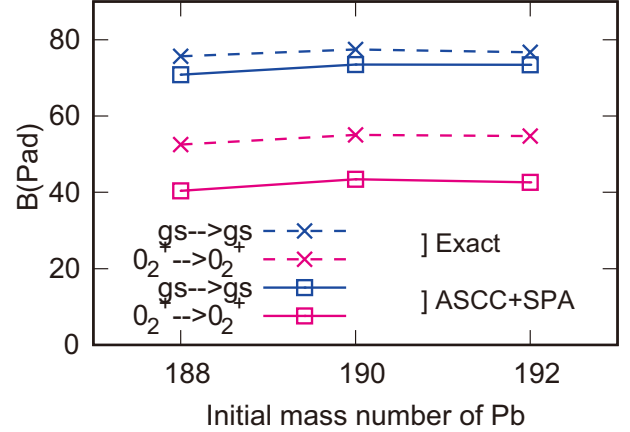


Fig. 1. Calculated two-neutron transfer matrix elements for Pb isotopes.

lective coordinate (ASCC) method.<sup>1)</sup> Since the 1D system is integrable, the collective subspace can be quantized with the SPA. The optimal degree of freedom associated with a slow collective motion is determined self-consistently inside the TDHFB space, without any assumption. Thus, our approach of ASCC+SPA basically consists of two steps: (1) Find a decoupled 1D collective coordinate of the collective motion of interest. (2) Apply the SPA to the collective mode.

On the decoupled collective subspace, which is derived by the ASCC, we apply the Einstein-Brillouin-Keller (EBK) quantization rule,

$$\oint_{C_k} p_1 dq^1 = 2\pi k, \quad (1)$$

where  $k$  is an integer with a unit of  $\hbar = 1$ . Then, on this trajectory  $C_k$ , the  $k$ -th stationary state is given as a superposition of the (generalized) Slater determinants:

$$|\psi_k\rangle = \oint_{C_k} \rho(q, p) dt |q, p\rangle e^{i\mathcal{T}[q, p]}, \quad (2)$$

where  $\mathcal{T}[q, p]$  is the classical action integral. This method is applied to the neutron pairing model for Pb isotopes. We calculate the two-neutron-transfer strengths from the ground to the ground and from the excited to the excited states (Fig. 1). A reasonable agreement is found between the ASCC+SPA and the exact calculations.

## References

- 1) T. Nakatsukasa, K. Matsuyanagi, M. Matsuo, K. Yabana, Rev. Mod. Phys. **88**, 045004 (2016).
- 2) F. Ni, T. Nakatsukasa, Phys. Rev. C **97**, 044310 (2018).

<sup>†</sup> Condensed from the article in Phy. Rev. C **98**, 064327 (2018)

<sup>\*1</sup> Faculty of Pure and Applied Sciences, University of Tsukuba

<sup>\*2</sup> Center for Computational Sciences, University of Tsukuba

<sup>\*3</sup> RIKEN Nishina Center

# Study of giant dipole resonance in hot rotating light mass nucleus $^{31}\text{P}^\dagger$

D. Mondal,<sup>\*1</sup> D. Pandit,<sup>\*1</sup> S. Mukhopadhyay,<sup>\*1,2</sup> S. Pal,<sup>\*1</sup> S. Bhattacharya,<sup>\*3</sup> A. De,<sup>\*4</sup> N. D. Dang,<sup>\*5</sup> N. Q. Hung,<sup>\*6</sup> S. Bhattacharya,<sup>\*1,2</sup> S. Bhattacharyya,<sup>\*1,2</sup> B. Dey,<sup>\*7</sup> P. Roy,<sup>\*1</sup> K. Banerjee,<sup>\*1,2,\*8</sup> and S. R. Banerjee<sup>\*9</sup>

The Isovector Giant Dipole Resonance (GDR) is observed in all nuclei and is characterized by the resonance energy ( $E_G$ ), width ( $\Gamma_G$ ) and strength ( $S_G$ ).<sup>1)</sup> Macroscopically, it is described as out-of-phase oscillation of proton and neutron fluids, while microscopically, it is a coherent excitations of one particle-one hole ( $1p-1h$ ) configurations across one major shell. It can be built on the ground state as well as every excited states of atomic nucleus. The GDR built on the nuclear excited states is experimentally studied by two complementary methods, namely inelastic scattering reactions and fusion evaporation reactions.

In this report, a systematic study of the GDR parameters is presented in a very light mass nucleus  $^{31}\text{P}$  by using fusion evaporation reactions. The compound nucleus (CN)  $^{31}\text{P}$  was populated at three different excitation energies by using the  $\alpha$  beam ( $E_{\text{beam}} = 28, 35, 42$  MeV) from K-130 cyclotron at the Variable Energy Cyclotron Centre, Kolkata. The GDR and nuclear level density (NLD) parameters have been determined by simultaneous statistical model analysis of the high-energy  $\gamma$  ray and neutron spectra measured with the LAMBDA array<sup>2)</sup> and neutron time of flight detectors,<sup>3)</sup> respectively. The angular momentum ( $J$ ) of the multiplicities with a multiplicity filter.<sup>4)</sup> The angular distribution of the high-energy  $\gamma$  rays has been performed to determine the bremsstrahlung component which is observed for the beam energies above  $\sim 10$  MeV/nucleon. The estimation of the bremsstrahlung contribution is crucial for precise determination of the GDR parameters.

It was observed that the GDR remains very much collective in this light mass nucleus and the  $E_G$  remains roughly constant at around 17.5 MeV as the nuclear temperature ( $T$ ) changes. In Fig. 1, the measured GDR widths are compared with the results of calculations within different models and plotted as a function of  $T$ . Panels (a) and (b) show that the thermal shape fluctuation model (TSFM)<sup>5)</sup> and the phenomenological thermal shape fluctuation model (pTSFM)<sup>6)</sup> (phenomenological version of TSFM) overpredict the measured

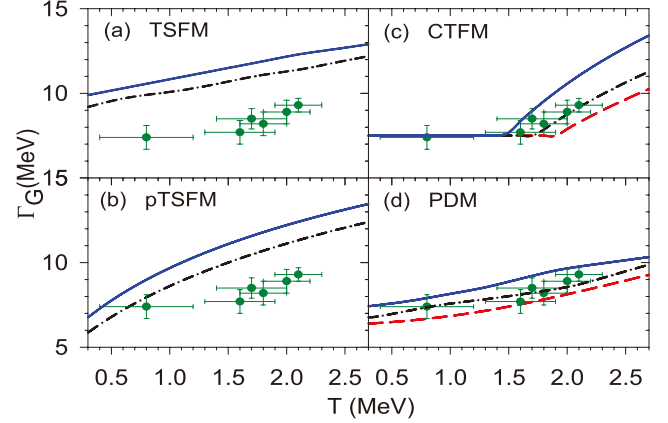


Fig. 1. Comparison of measured GDR width with the results of various model calculations as a function of  $T$  at  $J = 11.5 \hbar$  (black dot-dashed line) and  $J = 15.5 \hbar$  (blue solid line). The red long-dashed lines in panels (c) and (d) are the predictions at  $J = 0 \hbar$ .

widths. In panel (c) the calculations within the critical temperature included fluctuation model (CTFM)<sup>7)</sup> is presented. Within this model, the GDR width remains constant at the ground-state value up to a critical temperature due to the GDR induced fluctuation and increases thereafter. Interestingly, this model nicely reproduced the measured widths. The widths were also described quite well [panel (d)] by the results of calculations based on microscopic phonon damping model (PDM),<sup>8)</sup> according to which the GDR width arises owing to the coupling of the GDR state with the noncollective  $p-h$ ,  $p-p$  and  $h-h$  configurations. The thermal pairing gaps are found to vanish in the ranges of  $T$  and  $J$  considered in this experiment, therefore, have no effect on the measured GDR width in this light mass system. The present results establish the universality of CTFM and PDM in describing the GDR width as a function of temperature and angular momentum.

## References

- 1) M. N. Harakeh, A. van der Woude, *Giant Resonances: Fundamental high-Frequency mode of nuclear excitation* (Clarendon Press, Oxford, 2001).
- 2) S. Mukhopadhyay, *et al.*, Nucl. Instrum. Methods Phys. Res. A **582**, 603 (2007).
- 3) K. Banerjee, *et al.*, Nucl. Instrum. Methods Phys. Res. A **608**, 440 (2009).
- 4) Deepak Pandit, *et al.*, Nucl. Instrum. Methods Phys. Res. A **624**, 148 (2010).
- 5) Y. Alhassid, *et al.*, Phys. Rev. Lett. **61**, 1926 (1988).
- 6) Dimitri Kusnezov, *et al.*, Phys. Rev. Lett. **81**, 542 (1998).
- 7) Deepak Pandit, *et al.*, Phys. Lett. B **713**, 434 (2012).
- 8) N. Dinh Dang, *et al.*, Phys. Rev. Lett. **80**, 4145 (1998).

<sup>†</sup> Condensed from the article in Phys. Lett. B **784**, 423 (2018)

<sup>\*1</sup> Variable Energy Cyclotron Centre

<sup>\*2</sup> Homi Bhabha National Institute

<sup>\*3</sup> Department of Physics, Barasat Govt. College

<sup>\*4</sup> Department of Physics, Ramiganj Girls' College

<sup>\*5</sup> RIKEN Nishina Center

<sup>\*6</sup> Institute of Fundamental and Applied Sciences, Duy Tan University

<sup>\*7</sup> Saha Institute of Nuclear Physics

<sup>\*8</sup> Department of Nuclear Physics, Australian National University

<sup>\*9</sup> (Ex) Variable Energy Cyclotron Centre

### **3. Nuclear Data**



## Verification test of $^{107}\text{Pd}$ transmutation<sup>†</sup>

Y. Miyake,<sup>\*1</sup> N. Ikoma,<sup>\*1</sup> K. Takahashi,<sup>\*1</sup> Y. V. Sahoo,<sup>\*1</sup> and H. Okuno<sup>\*1</sup>

In a previous study, we reported the construction of an implantation beam line for  $^{107}\text{Pd}$  transmutation.<sup>1)</sup> After that,  $^{107}\text{Pd}$  was implanted into a carbon foil and irradiated by a deuteron beam. In this study, a verification test for the  $^{107}\text{Pd}$  transmutation is reported.

$^{107}\text{Pd}$  ions were implanted into a carbon foil as  $^{107}\text{PdO}^-$  with an energy of 20 keV. This foil is a multi-layer graphene sheet with a thickness of  $360\ \mu\text{g}/\text{cm}^2$  developed by KANEKA.<sup>2)</sup> The amount of implanted  $^{107}\text{Pd}$  was analyzed by inductively coupled plasma mass spectrometry (ICP-MS) to be approximately 270 ng in a carbon foil. The  $^{107}\text{Pd}$ -implanted sample was irradiated by deuteron at 12 MeV/nucleon with a current of 1–2 particle  $\mu\text{A}$ . The cumulative irradiation current was 1.09 C, which corresponds the irradiation with a beam current of 1 particle  $\mu\text{A}$  for 12.6 days.

After cooling,  $\gamma$ -ray measurements were conducted. The  $\gamma$ -ray spectrum of the irradiated sample is shown in Fig. 1.  $\gamma$ -ray emitting from radionuclides of  $^7\text{Be}$ ,  $^{105}\text{Ag}$ , and  $^{106m}\text{Ag}$  were detected.  $^7\text{Be}$  is produced from carbon, while  $^{105}\text{Ag}$  and  $^{106m}\text{Ag}$  are generated from the transmutation of  $^{107}\text{Pd}$ . The activities of  $^{105}\text{Ag}$  and  $^{106m}\text{Ag}$  were calculated from the  $\gamma$ -ray spectrum of 345 keV and 450 keV, respectively. The activity was determined using the total net count of  $\gamma$ -ray peaks. The radioactivity was decay-corrected from the day when the deuteron irradiation finished. Considering the  $\gamma$ -ray abundance of 0.41 at 345 keV and 0.28 at 450 keV, the activity was calculated to be  $8.38 \times 10^2$  Bq and  $4.98 \times 10^4$  Bq, which correspond with 0.8 pg of  $^{105}\text{Ag}$  and 9.0 pg of  $^{106m}\text{Ag}$ , respectively.<sup>3)</sup>

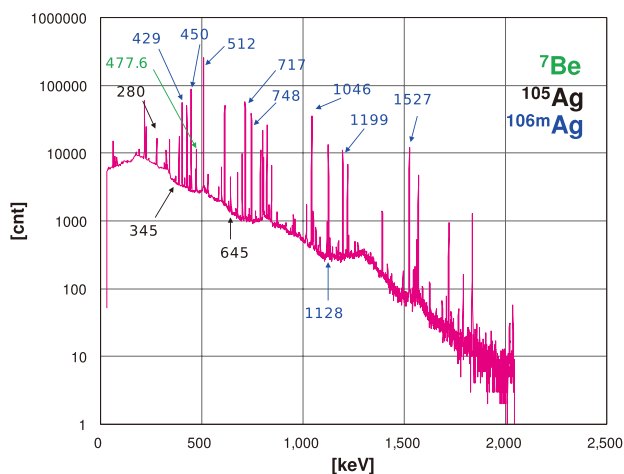


Fig. 1.  $\gamma$ -ray spectrum of irradiated sample.

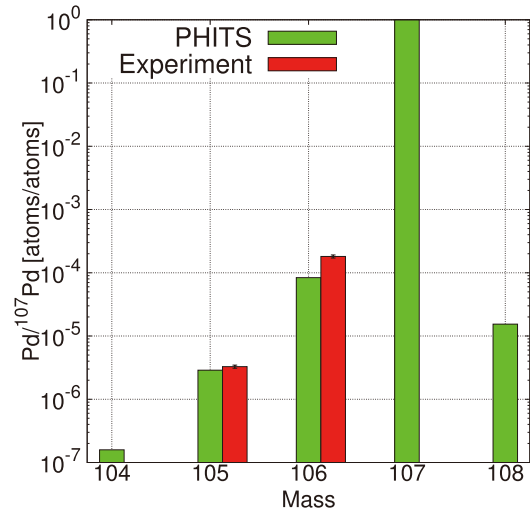


Fig. 2. Isotopic ratio of  $\text{Pd}/^{107}\text{Pd}$  of irradiated sample.

The production yield of nuclides per deuteron was calculated using the Particle and Heavy Ion Transport code System (PHITS) to estimate the amount of  $^{105}\text{Pd}$  and  $^{106}\text{Pd}$  generated by the experiment.<sup>4)</sup> Assuming that all  $^{105}\text{Ag}$  and  $^{106m}\text{Ag}$  detected by the  $\gamma$ -ray measurements will be converted into  $^{105}\text{Pd}$  and  $^{106}\text{Pd}$ , respectively, they amount to 92% for  $^{105}\text{Pd}$  and 25% for  $^{106}\text{Pd}$  generated from the  $^{107}\text{Pd}$  transmutation. Therefore, the total amount of  $^{105}\text{Pd}$  and  $^{106}\text{Pd}$  was estimated to be 0.9 pg for  $^{105}\text{Pd}$  and 40 pg for  $^{106}\text{Pd}$ . Considering that the amount of implanted  $^{107}\text{Pd}$  was estimated to be 270 ng, the isotopic ratios were calculated to be  $3.29 \times 10^{-6}$  for  $^{105}\text{Pd}/^{107}\text{Pd}$  and  $1.49 \times 10^{-4}$  for  $^{106}\text{Pd}/^{107}\text{Pd}$ .

The isotopic ratio normalized by the number of  $^{107}\text{Pd}$  nuclei ( $\text{Pd}/^{107}\text{Pd}$ ) was also evaluated by a simulation using PHITS. Considering the production yield of each nuclide, the change in the isotopic ratios were estimated to be  $2.90 \times 10^{-6}$  for  $^{105}\text{Pd}/^{107}\text{Pd}$  and  $8.43 \times 10^{-5}$  for  $^{106}\text{Pd}/^{107}\text{Pd}$  for deuteron irradiation performed with a beam current of 1 particle  $\mu\text{A}$  for 12.6 d. This estimation is consistent with the experimental results, thereby preliminarily verifying the  $^{107}\text{Pd}$  transmutation (Fig. 2).

This work was funded by the ImPACT Program of the Council for Science, Technology and Innovation (Cabinet Office, Government of Japan).

### References

- 1) Y. Miyake *et al.*, RIKEN Accel. Prog. Rep. **51**, 102 (2018).
- 2) A. Tatami *et al.*, AIP Conference Proceedings, 1962, 030005 (2018).
- 3) R. L. Heath, Gamma-ray spectrum catalogue: Ge(Li) and Si(Li) spectrometry, Fourth edition, Aerojet Nuclear Co., Idaho Falls, Idaho (1974).
- 4) T. Saito *et al.*, J. Nucl. Sci. Technol. **55**, 684–690 (2018).

<sup>†</sup> Condensed from the article in Y. Miyake *et al.*, OECD/NEA (2018) Proceedings of the Fifteens Information Exchange Meetings on Actinide and Fission Product Partitioning and Transmutation, Manchester, UK, 1-3 October 2018.

<sup>\*1</sup> RIKEN Nishina Center

## Measurement of neutron production from 7 MeV/nucleon $\alpha$ incidence on a Bi target

K. Sugihara,<sup>\*1,\*2</sup> E. Lee,<sup>\*1,\*2</sup> N. Shigyo,<sup>\*1,\*2</sup> K. Tanaka,<sup>\*1</sup> A. Akashio,<sup>\*1</sup> and T. Sanami<sup>\*1,\*3</sup>

RIKEN has a plan of installing a new beam line for producing  $^{211}\text{At}$  by  $\alpha$  particle incidence on a  $^{209}\text{Bi}$  target. It is assumed that an  $\alpha$  beam should have an energy of 7.16 MeV/nucleon to reduce undesired byproducts. Validation of Monte Carlo simulation codes on radiation shielding is required for the design of a beam line. The neutron energy spectrum of the  $^{209}\text{Bi}(\alpha, 2n)^{211}\text{At}$  reaction has not been measured. Experimental data of double-differential neutron thick target yields (TTY) are desired as a neutron source term in the radiation shielding design. We measured the neutron energy spectra by the time-of-flight (TOF) method.

The experiment was carried out at the E7B course of AVF cyclotron. The experimental arrangement is illustrated in Fig. 1.

The 7.16 MeV/nucleon  $\alpha$  beam irradiated a  $^{209}\text{Bi}$  target. The repetition rate of the beam was about 16 MHz. The integrated beam current was obtained from the counts of a neutron survey meter set near the target chamber. The thickness of the target was 2 mm, which was longer than the range of the  $\alpha$  particle.

Neutrons from the target were measured with EJ301 liquid organic scintillators that were 2 inch in diameter and thickness. A 2 mm thick plastic scintillator was set as a veto detector. The neutron kinetic energy was determined by the TOF method in which the start and stop signals came from the neutron scintillator and the RF signal of the AVF cyclotron, respectively. The flight path lengths from the target to the detectors were from 1 to 1.2 m as shown in Fig. 1. The background neutrons were estimated from the measurement data with an iron shadow bar of 60 cm thickness between the target and each neutron detector.

Figure 2 shows the TOF spectrum at  $0^\circ$ . The horizontal axis represents the time difference between the

RF signal and the neutron detector. The TDC resolution was about 0.012 ns/ch. The peak at 3650 ch was the prompt  $\gamma$ -ray from the  $\alpha$  incident reactions. Low-energy neutrons from the preceding beam bunch were overlapped in the TOF spectrum. These events were excluded because their small signals were lower than the threshold level of the electronics. The neutron events were extracted by using the difference in the decay part of the signal between neutrons and  $\gamma$ -rays.<sup>1)</sup>

The measured neutron TTY and the calculation results by INCL<sup>2)</sup> and JQMD<sup>3)</sup> models in PHITS<sup>4)</sup> code are shown in Fig. 3. The results of INCL show better agreement with the experimental results than those of JQMD.

The measured data will be applied to the shielding design of the new beam line.

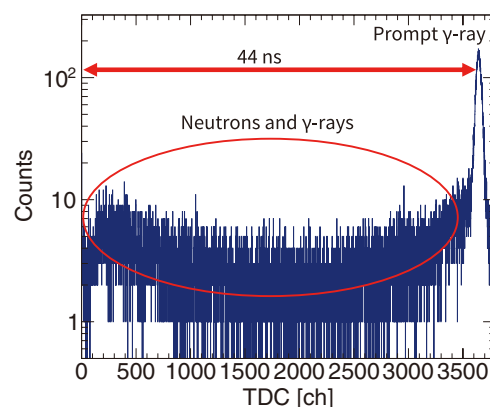


Fig. 2. TOF spectrum at  $0^\circ$ .

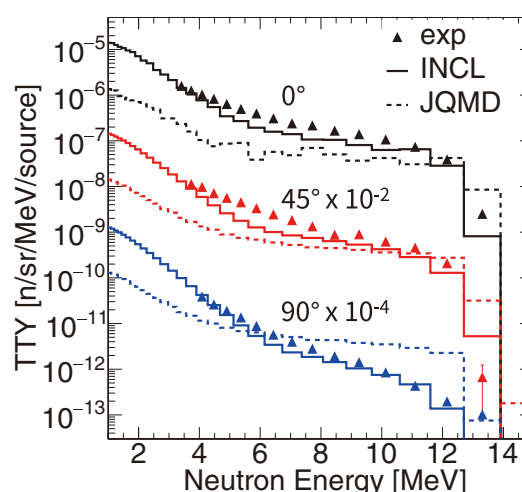


Fig. 3. Neutron TTY and the calculation results by INCL and JQMD implemented in PHITS.

### References

- 1) T. Nakamoto *et al.*, J. Nucl. Sci. Technol. **32**, 827 (1995).
- 2) A. Boudard *et al.*, Phys. Rev. C **87**, 014606 (2013).
- 3) K. Niita *et al.*, Phys. Rev. C **52**, 2620 (1995).
- 4) T. Sato *et al.*, J. Nucl. Sci. Technol. **55** (2018).

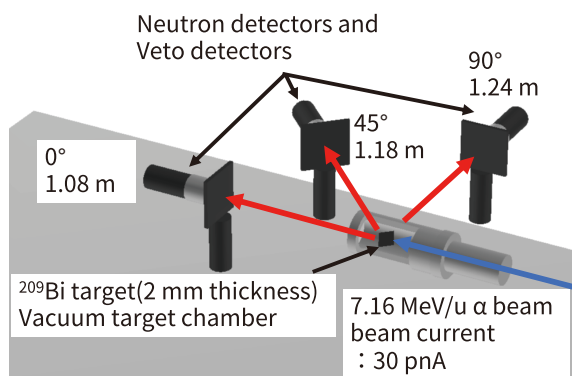


Fig. 1. Experimental arrangement.

\*1 RIKEN Nishina Center

\*2 Department of Applied Quantum Physics and Nuclear Engineering, Kyushu University

\*3 KEK

## EXFOR compilation of RIBF data in 2018

S. Jagjit,<sup>\*1</sup> T. Tada,<sup>\*1</sup> M. Aikawa,<sup>\*1,\*2</sup> D. Ichinkhorloo,<sup>\*1</sup> S. Imai,<sup>\*3</sup> M. Kimura,<sup>\*1</sup> and N. Otuka<sup>\*2,\*4</sup>

Nuclear reaction data is the central cohesive source of support for the new advancements in nuclear technology (*e.g.*, nuclear power, fuel cycles, environmental monitoring, dosimetry, radiation safety, radioisotope production, radiotherapy, and medical diagnostics) and science (*e.g.*, nuclear physics, nuclear chemistry, geophysics, and astrophysics). A nuclear database plays a vital role in providing the best estimated nuclear reaction data to a wide range of data users working in various fields of science and related areas. One such database open to the public is the EXchange FORmat (EXFOR) library for experimental nuclear reaction data.<sup>1)</sup> The EXFOR database is the universally common repository for nuclear reactions, which was established in 1967, and is maintained by the International Network of Nuclear Reaction Data Centres (NRDC) under the auspices of the International Atomic Energy Agency (IAEA).<sup>2)</sup> The scope of EXFOR covers a wide range of nuclear reactions such as neutron-induced, charged-particle, and photon-induced reactions.

The Hokkaido University Nuclear Reaction Data Centre (JCPRG)<sup>3)</sup> was founded in 1973 and has been a member of NRDC since 1975. JCPRG is responsible for the compilation of charged-particle and photon-induced nuclear reactions measured at the facilities located in Japan.<sup>4)</sup> The contribution of JCPRG to the EXFOR database amounts to  $\sim 5\%$  of the total entries.

Our compilation process involves the scanning of peer-reviewed journals for the published papers that meet the scope of EXFOR. A unique entry number is assigned to each selected paper to be compiled for the EXFOR library to track progress in compilation. The compilers extract the bibliographic information, experimental set up, measured physical quantities, measured numerical data, and error information that are given as input to a single entry of EXFOR. During this process, we contact the corresponding authors for questions on the content of the papers and requests for numerical data.

JCPRG has cooperated with the RIKEN Nishina Center for the compilation of data obtained in RIBF since 2010. The purpose of this cooperation is to increase the availability of nuclear reaction data obtained at RIBF. In this article, we report our activities related to the RIBF data. In 2018, we compiled 53 new papers reporting the experiments performed at Japanese

Table 1. Entry numbers with references compiled from RIBF data in 2018.

Enteries	E2516 <sup>5)</sup>	E2542 <sup>6)</sup>	E2543 <sup>7)</sup>
	E2549 <sup>8)</sup>	E2553 <sup>9)</sup>	E2554 <sup>10)</sup>
	E2557 <sup>11)</sup>	E2561 <sup>12)</sup>	E2562 <sup>13)</sup>
	E2574 <sup>14)</sup>	E2575 <sup>15)</sup>	E2576 <sup>16)</sup>
	E2578 <sup>17)</sup>	E2580 <sup>18)</sup>	
Total	14		

facilities and out of these, 14 papers were based on RIBF data. All authors of these 14 entries had kindly provided us the numerical data. The compiled data is accessible by the entry numbers listed in Table 1.

We have established an effective procedure to compile all new publications during the last eight-year collaboration with the RIKEN Nishina Center. Therefore, most of the recent experimental nuclear reaction data is provided by the corresponding authors. This cooperation is valuable and effective, and essential for continuing rapid and reliable compilation.

We would like to take this opportunity to express our gratitude to the authors of these papers for their kind cooperation with the EXFOR compilation process.

### References

- 1) N. Otuka *et al.*, Nucl. Data Sheets **120**, 272 (2014).
- 2) <https://www-nds.iaea.org/>
- 3) Hokkaido University Nuclear Reaction Data Centre: <http://www.jcprg.org/>.
- 4) M. Kimura, AAPS Bulletin **28**, No. 5, 24 (2018).
- 5) S. Hayakawa *et al.*, Phys. Rev. C **93**, 065802 (2016).
- 6) D. Kaji *et al.*, J. Phys. Soc. Jpn. **86**, 085001 (2017).
- 7) J. W. Hwang *et al.*, Phys. Lett. B **769**, 503 (2017).
- 8) T. Sumikama *et al.*, Phys. Rev. C **95**, 051601 (2017).
- 9) S. Momiyama *et al.*, Phys. Rev. C **96**, 034328 (2017).
- 10) H. Suzuki *et al.*, Phys. Rev. C **96**, 034604 (2017).
- 11) V. Vaquero *et al.*, Phys. Rev. Lett. **118**, 202502 (2017).
- 12) N. Fukuda *et al.*, J. Phys. Soc. Jpn. **87**, 014202 (2018).
- 13) Y. Shimizu *et al.*, J. Phys. Soc. Jpn. **87**, 014203 (2018).
- 14) M. Aikawa *et al.*, Nucl. Instrum. Methods Phys. Res. B **426**, 18 (2018).
- 15) N. Ukon *et al.*, Nucl. Instrum. Methods Phys. Res. B **426**, 13 (2018).
- 16) T. Nishi *et al.*, Phys. Rev. Lett. **120**, 152505 (2018).
- 17) M. Aikawa *et al.*, Nucl. Instrum. Methods Phys. Res. B **427**, 91 (2018).
- 18) S. Chebotaryov *et al.*, Prog. Theor. Exp. Phys. **2018**, 053D01 (2018).

<sup>\*1</sup> Faculty of Science, Hokkaido University

<sup>\*2</sup> RIKEN Nishina Center

<sup>\*3</sup> Institute for the Advancement of Higher Education, Hokkaido University

<sup>\*4</sup> NDS, IAEA



## **4. Hadron Physics**



# Preliminary result of the transverse single spin asymmetry in very forward $\pi^0$ production in 510 GeV $p^\uparrow + p$ collisions

M. H. Kim<sup>\*1,\*2</sup> for the RHICf collaboration

The RHICf experiment<sup>1)</sup> measured the transverse single spin asymmetry,  $A_N$ , which is defined as the left-right cross section asymmetry of beam polarization, of very forward  $\pi^0$  in June, 2017. The spin-related interactions between protons and the production mechanism of a particle can be deeply understood by  $A_N$  measurement. To date, the non-zero  $A_N$  of forward  $\pi^0$  has been measured by many experiments, and the parton-level interaction between protons has generally been considered to be the origin of the  $\pi^0$  production. However, recently, larger  $A_N$  was observed for more diffractive-like events than the events driven by hard scattering;<sup>2)</sup> therefore, the measurement of  $A_N$  in very forward  $\pi^0$  production by the RHICf experiment will provide a new input to unveil the origin of the non-zero  $A_N$  of  $\pi^0$ , especially from the viewpoint of diffractive and non-diffractive interactions.

To measure the very forward  $\pi^0$ , we moved an electromagnetic calorimeter (RHICf detector), which was originally developed for the LHCf experiment,<sup>3)</sup> from CERN to BNL, and installed it at the zero-degree area of the STAR experiment, which was 18 m away from the beam collision point. The RHICf detector consists of two sampling calorimeters; smaller one has a lateral dimension of 20 mm  $\times$  20 mm and the larger one has a lateral dimension of 40 mm  $\times$  40 mm. Each tower is composed of 16 GSO plates for energy measurement and 4 layers of GSO bars for position measurement.  $\pi^0$  can be identified and reconstructed by measuring two decayed photons with two towers or even one tower because the position resolution for photons is of the level of a few hundred  $\mu\text{m}$ . We measured very forward  $\pi^0$  with a wide transverse momentum ( $p_T$ ) coverage of  $0 < p_T < 1$  GeV/c and a longitudinal momentum fraction ( $x_F$ ) range of  $0.2 < x_F < 1$ . For the correlation study with other STAR detectors, we took the data using the STAR data acquisition system.

Experimentally,  $A_N$  is calculated by following equation:

$$A_N = \frac{1}{P} \frac{1}{D_\phi} \left( \frac{N^\uparrow - RN^\downarrow}{N^\uparrow + RN^\downarrow} \right), \quad (1)$$

where  $N^{\uparrow(\downarrow)}$  is the number of detected  $\pi^0$  in  $p^{\uparrow(\downarrow)} + p$  collision and  $R$  is the luminosity ratio between two collision types of spin up ( $\uparrow$ ) and down ( $\downarrow$ ).  $P$  represents the average polarization of the proton beam and  $D_\phi$  is a correction factor for  $\pi^0$  azimuthal angle distribution because  $A_N$  usually depends on the particle's azimuthal angle by  $A_N \propto \sin(\phi - \phi_0)$  where  $\phi_0$  is an

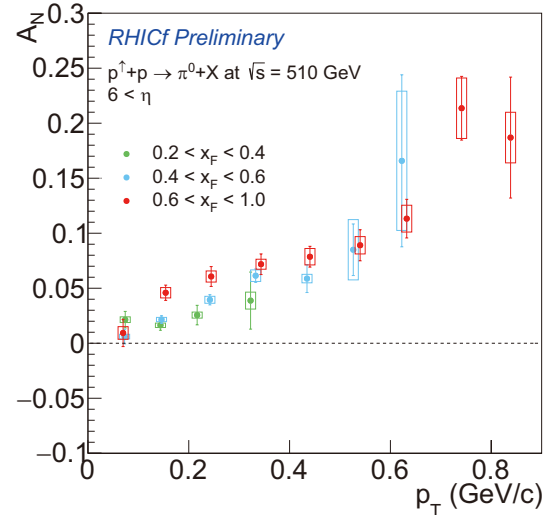


Fig. 1. Preliminary result of the  $A_N$  of very forward  $\pi^0$  production as a function  $p_T$ . The three different colors correspond with different  $x_F$  ranges.

offset angle. Typical values of  $P$  and  $D_\phi$  is around 0.6 and 0.96 respectively.

Figure 1 presents our first result for the  $A_N$  of very forward inclusive  $\pi^0$  production. Surprisingly, non-zero  $A_N$  of  $\pi^0$  was observed even in very forward  $\pi^0$  production.  $A_N$  increases as a function of both  $x_F$  and  $p_T$ . Because the non-zero  $A_N$  in Fig. 1 was driven by the  $\pi^0$  produced in the very forward region where the diffractive process is dominant, the diffraction can be considered to be a possible contributor of this finite  $A_N$  as expected by a recent study.<sup>2)</sup> In order to further study the role of diffraction in the forward  $\pi^0$  production, we are now analyzing the correlation between RHICf and STAR detectors. STAR forward detectors and Roman pot<sup>4)</sup> can identify diffractive events by observing the rapidity gap or a recoil proton. Therefore, we will be able to understand the relation between diffraction and  $A_N$  of (very) forward  $\pi^0$  with a combined RHICf-STAR analysis.

## References

- 1) RHICf Collaboration, LOI, arXiv: 1409.4860v1.
- 2) S. Heppelmann (STAR Collaboration), Proc. Sci. **DIS2013**, 240 (2013).
- 3) O. Adriani *et al.* (LHCf Collaboration), J. Instrum. **3**, S08006 (2008).
- 4) S. Bültmann *et al.*, Nucl. Instrum. Methods Phys. Res. A **535**, 415 (2004).

\*1 RIKEN Nishina Center

\*2 Department of Physics, Korea University

# The stability of energy scale for RHICf photon measurement during the 2017 operation

K. Sato<sup>\*1,\*2</sup> and H. Menjo<sup>\*1,\*2</sup> for the RHICf collaboration

The RHIC forward (RHICf) experiment<sup>1)</sup> aims to verify hadronic interaction models<sup>2-4)</sup> by measuring the production cross-sections of forward neutral particles (photons, neutrons, and  $\pi^0$ ) emitted during proton-proton collisions with a center-of-mass collision energy of  $\sqrt{s} = 510$  GeV at BNL-RHIC, which is important to understand the development of air showers for cosmic-ray physics. The RHICf operation was successfully completed in 2017.

The RHICf detector is located 18 m from the interaction point where the STAR detector is installed. The RHICf detector has two compact sampling and positioning calorimeters. Each calorimeter is composed of 16 layers of GSO scintillators, 4 X-Y hodoscope layers of GSO bar bundles, and tungsten absorber layers. The energy of an incident photon is reconstructed from the summation of the energy deposits in the scintillator layers. The energy calibration of the calorimeters was performed using 50–200 GeV/c electron beams at CERN-SPS before the operation at RHIC, and the systematic uncertainty was found to be about 3%.<sup>5)</sup>

The energy scale can be verified and monitored using  $\pi^0$  events recorded in the proton-proton collision data. The  $\pi^0$  events are identified by measuring the photon pairs produced from  $\pi^0$  decays. The invariant mass of a photon pair,  $M_{\gamma\gamma}$ , is calculated as

$$M_{\gamma\gamma} = \theta \sqrt{E_{\gamma_1} E_{\gamma_2}}, \quad (1)$$

where  $\theta$  is the opening angle of a photon pair, and  $E_{\gamma_1}$  and  $E_{\gamma_2}$  are the photon energies. Figure 1 shows the reconstructed mass distribution of photon pair events obtained in RHICf-Run 2625, which contains  $3.5 \times 10^4$  events. The peak in the distribution corresponds to the  $\pi^0$  events. The distribution is fit with the Gaussian function combined with the Chebyshev polynomial function for the background event. The variation of the invariant-mass peak measured in each RHICf-run is shown in Fig. 2. The horizontal and vertical axes show the run number of the RHICf experiment and the relative peak position of the invariant mass measured in each run to the one in Run 2625, respectively. The red dotted lines show the variations at  $\pm 1.5\%$ . From the result, we conclude that the energy scale of the calorimeters was stable within  $\pm 1.5\%$ , which is less than the uncertainty of the absolute energy scale estimated from the beam test. The small variation may be due to the temperature dependency of the PMTs used in the detector. The detailed investigation is in progress.

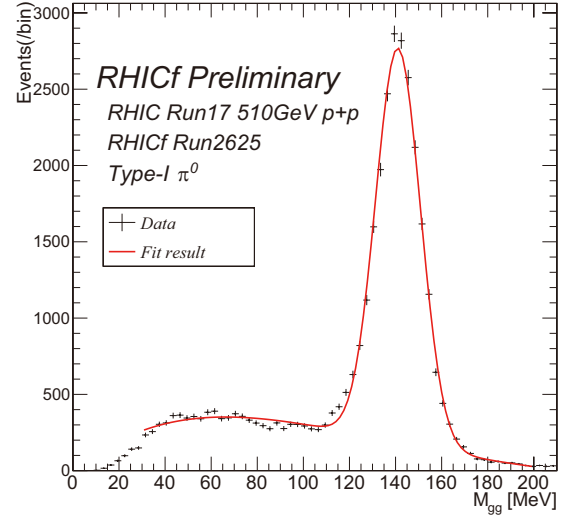


Fig. 1. The invariant mass distribution of photon pair events. Red line shows the composite function of the Gaussian function and the Chebyshev polynomial function.

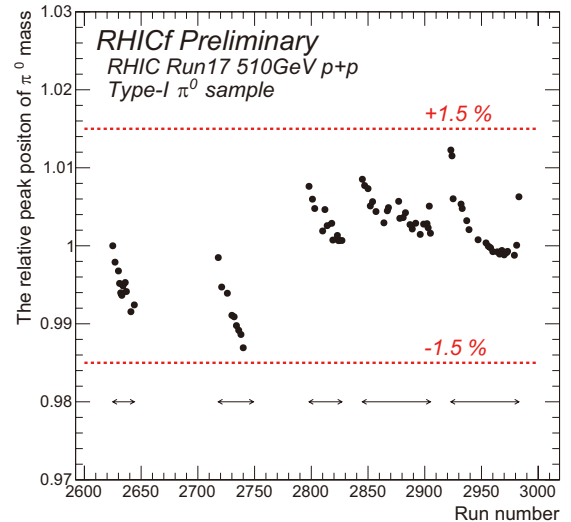


Fig. 2. The relative peak position of the reconstructed  $\pi^0$  mass in each run, which is compared with the one in RHICf-Run 2625. The red dotted lines show  $\pm 1.5\%$ . The lower arrows indicate the physics operation periods with collisions.

## References

- 1) RHICf Collaboration, Letter of Intent, arXiv:1401.1004; RHICf proposal, arXiv:1409.4860.
- 2) T. Pierog, Iu. Karpenko, J. M. Katzy, E. Yatsenko, K. Werner, Phys. Rev. C **92**, 034906 (2015).
- 3) S. Ostapchenko, Phys. Rev. D **83**, 014018 (2011).
- 4) E. -J. Ahn, R. Engel, T. K. Gaisser, P. Lipari, T. Stanev, Phys. Rev. D **80**, 094003 (2009).
- 5) Y. Makino *et al.*, J. Instrum **12**, P03023 (2017).

<sup>\*1</sup> RIKEN Nishina Center

<sup>\*2</sup> Institute for Space-Earth Environmental Research, Nagoya University

# Cross section and longitudinal single-spin asymmetry $A_L$ for forward $W^\pm \rightarrow \mu^\pm \nu$ production in polarized $p + p$ collisions at $\sqrt{s} = 510$ GeV<sup>†</sup>

R. Seidl\*<sup>1</sup> for the PHENIX collaboration

Understanding the spin of the proton and its decomposition is essential to explaining how the strong interaction, described by quantum chromodynamics QCD, creates the basic building blocks of the visible matter in our universe, protons and neutrons. Sea quarks are found to be asymmetric at small to intermediate Bjorken  $x < 0.2$ , where  $x$  is the parton momentum fraction. While several models can describe the measured unpolarized light sea, these models differ significantly in their predictions for the polarized case. Valence quark helicity contributions to the total spin of the nucleon are already relatively well known, but sea quark helicities are still poorly understood. An elegant way to access sea quark helicities is via the weak interaction as possible at the Relativistic Heavy Ion Collider (RHIC).<sup>1)</sup> In  $p + p$  collisions, real  $W$ 's can be produced in the annihilation of predominantly up(down) and anti-down(up) quark pairs for  $W^{+(-)}$  production. Furthermore, the helicity of participating quarks and anti-quarks is fixed to be left-handed and right-handed, respectively, due to the parity violating nature of the weak interaction. If one of the two proton beams is longitudinally polarized, the helicity of the proton beam therefore selects quarks that are polarized parallel or anti-parallel with it and vice versa for anti-quarks.

In this analysis, we rely on the reconstruction of forward-going muons impinging the muon-spectrometer of the PHENIX detector. The data sets used in this analysis were recorded at RHIC during the 2012 and 2013 polarized proton running periods at a center-of-mass energy  $\sqrt{s} = 510$  GeV with a luminosity of approximately

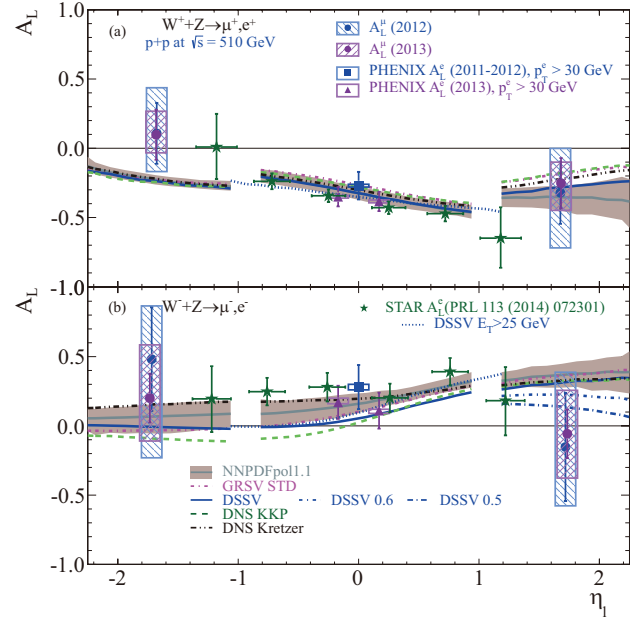


Fig. 2. Longitudinal single spin asymmetry,  $A_L$  for (a)  $W^+ + Z \rightarrow \mu^+, e^+$  and (b)  $W^- + Z \rightarrow \mu^-, e^-$  for PHENIX for 2012 (closed [blue] circles) and 2013 (closed [purple] circles) and previously published data and parameterizations.

53 and 285  $\text{pb}^{-1}$ . The average beam polarizations were between 54% and 58% for the two beams and running periods. For each event a combined probability distribution,  $W_{\text{ness}}$  is formed from all variables. Tracks with high  $W_{\text{ness}}$  ( $> 0.92$ ) are used for further analysis. An unbinned maximum likelihood fit approach is used to determine the final number of  $W$ s and remaining backgrounds. Figure 1 shows the extracted total cross sections for inclusive  $W^\pm \rightarrow \mu^\pm$  production in  $p + p$  collisions at a center-of-mass energy of 510 GeV. The cross sections are consistent within uncertainties with previous measurements at this energy from central  $W \rightarrow e$  decay channels and with the expected NLO predictions. The longitudinal single-spin asymmetries,  $A_L$  are shown in Fig. 2 for positive and negative  $W + Z$  decay muon candidates. They show the first muon single spin asymmetry results from  $W + Z$  decays at pseudorapidities  $|\eta| > 1$  of the decay lepton. They help determine the valence and sea quark helicities at different momentum fractions than at central rapidities. The behavior of the asymmetries is generally consistent with the parameterizations.

### Reference

- 1) C. Bourrely and J. Soffer, Phys. Lett. B **314**, 132 (1993).

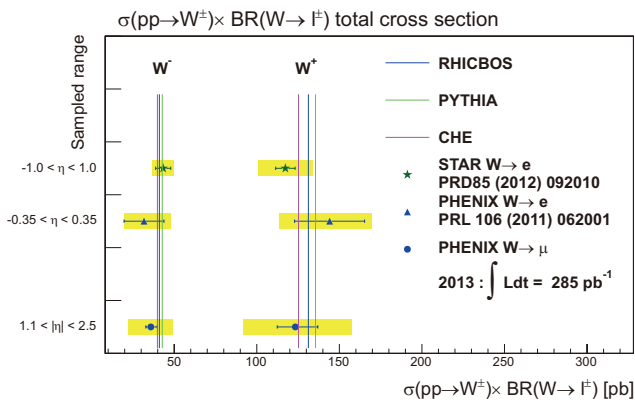


Fig. 1. The  $W^\pm \rightarrow \mu^\pm \nu$  cross section measured at forward and backward rapidity  $1.1 < |\eta| < 2.5$  (closed [blue] circles) and previously published results at central rapidity.

<sup>†</sup> Condensed from the article Phys. Rev. D **98**, 032007 (2018)

\*<sup>1</sup> RIKEN Nishina Center

## Progress in analysis technique for extracting light-antiquark flavor asymmetry by SeaQuest at Fermilab

K. Nagai,<sup>\*1</sup> Y. Goto,<sup>\*2</sup> Y. Miyachi,<sup>\*3</sup> K. Nakano,<sup>\*2,\*4</sup> S. Sawada,<sup>\*2,\*5</sup> T. -A. Shibata,<sup>\*2,\*6</sup> for the E906/SeaQuest Collaboration

The amounts of  $\bar{d}$  and  $\bar{u}$  in a proton were expected to be the same based on the flavor independence of gluon splitting. However, the NMC experiment at CERN showed that the total amount of  $\bar{d}$  exceeds that of  $\bar{u}$ .<sup>1,2)</sup> The NA51 experiment at CERN and the E866 experiment at Fermilab measured the Bjorken  $x$  dependence of the light-antiquark flavor asymmetry  $\bar{d}/\bar{u}$ ,<sup>3,4)</sup> where Bjorken  $x$  is the momentum fraction of a parton to a proton. They found that  $\bar{d}/\bar{u} > 1.0$  at  $x < 0.25$  and  $\bar{d}/\bar{u} < 1.0$  at  $x \sim 0.3$ , although the results at  $x \sim 0.3$  is consistent with 1.0 due to the large statistical uncertainty. It is very important to measure  $\bar{d}/\bar{u}$  in this unclear region in order to understand the proton structure.

The SeaQuest experiment is a Drell–Yan experiment performed at the Fermi National Accelerator Laboratory (Fermilab) in Illinois, US. The main purpose of this experiment is to measure the light-antiquark flavor asymmetry in a proton in  $0.1 < x < 0.45$ , which includes the unclear region in the previous experiments.

As shown in Fig. 1, the Drell–Yan process is a reaction in which an antiquark in a hadron and a quark in another hadron annihilate and decay into a lepton pair via a virtual photon:  $q + \bar{q} \rightarrow \gamma^* \rightarrow \mu^+ + \mu^-$ .<sup>5)</sup> The cross section of the proton–proton Drell–Yan process at the leading order is expressed as

$$\frac{d^2\sigma}{dx_1 dx_2} = \frac{4\pi\alpha^2}{9x_1 x_2} \frac{1}{s} \sum_{i=u,d,s,\dots} e_i^2 [q_i(x_1)\bar{q}_i(x_2) + \bar{q}_i(x_1)q_i(x_2)], \quad (1)$$

where  $x$  is the Bjorken  $x$ , the subscripts (1, 2) denote the beam and the target, respectively, and  $q(x)$  is the parton distribution function. In the SeaQuest acceptance ( $x_1 \gg x_2$ ), the last term of Eq. (1) vanishes because the PDFs of antiquarks are small enough at the high  $x$  region. Therefore, an antiquark of the target proton is always involved in the process and is thus accessible easily.

The SeaQuest experiment measures the muon pairs in the final state of the Drell–Yan process, which is produced with the 120 GeV proton beam provided by the Fermilab Main Injector and the liquid hydrogen and deuterium targets. The details of the SeaQuest spectrometer have been reported in the past.<sup>6)</sup> SeaQuest

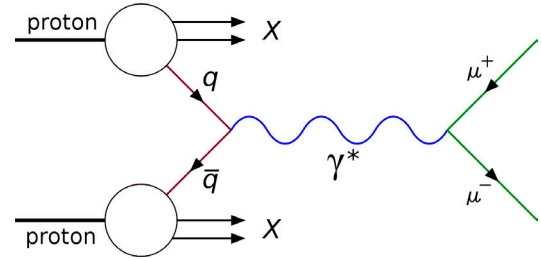


Fig. 1. Diagram of the Drell–Yan process.

took the physics data from 2013 through 2017. The recorded number of beam protons on targets is  $1.4 \times 10^{18}$ . At this moment, about 40% of the data are being analyzed.

The preliminary result of the light-quark flavor asymmetry was reported.<sup>7)</sup> The analysis toward the final result is currently in progress.

There are two difficulties that need to be resolved in the current analysis: the estimation of the beam-intensity dependence of the reconstruction efficiency and that of the random background. We are now testing a new method for resolving them based on real data instead of simulation, namely the so-called extrapolation method.

In this method, we evaluate the cross section ratio first as a function of the beam intensity. Here, we do not apply any corrections. Then it is fitted with a function and extrapolated to the zero beam intensity. The extrapolated value is considered to be the “correct” cross section ratio. Through the simulation, we confirmed that the extrapolation method removes the beam-intensity dependence of the reconstruction efficiency correctly. The investigation to confirm whether this method can handle the random background is in progress.

### References

- 1) P. Amaudruz *et al.*, Phys. Rev. Lett. **66**, 2712 (1991).
- 2) M. Arneodo *et al.*, Phys. Rev. D **50**, R1 (1994).
- 3) A. Baldit *et al.*, Phys. Lett. B **332**, 244 (1994).
- 4) E. A. Hawker *et al.*, Phys. Rev. Lett. **80**, 3715 (1998).
- 5) S. D. Drell, T. M. Yan, Phys. Rev. Lett. **25**, 316 (1970).
- 6) K. Nagai *et al.*, RIKEN Accel. Prog. Rep. **49**, 114 (2016).
- 7) K. Nakano *et al.*, RIKEN Accel. Prog. Rep. **50**, 118 (2017).

<sup>\*1</sup> Institute of Physics, Academia Sinica, Taiwan

<sup>\*2</sup> RIKEN Nishina Center

<sup>\*3</sup> Department of Physics, Yamagata University

<sup>\*4</sup> Department of Physics, Tokyo Institute of Technology

<sup>\*5</sup> Institute of Particle and Nuclear Studies, KEK

<sup>\*6</sup> College of Science and Technology, Nihon University

## Forward hadron calorimeter R&D

Y. Goto,<sup>\*1</sup> H. Matsuda,<sup>\*2</sup> Y. Miyachi,<sup>\*3</sup> I. Nakagawa,<sup>\*1</sup> K. Nakano,<sup>\*1,\*4</sup> R. Seidl,<sup>\*1</sup> T. -A. Shibata,<sup>\*1,\*4,\*5</sup>  
K. Tanida,<sup>\*1,\*6</sup> and Y. Yamazaki<sup>\*7</sup>

High energy polarized proton collision experiments at RHIC in Brookhaven National Laboratory have shown that the perturbative QCD describes experimental data accurately, and have largely developed an understanding of the internal structure of the proton. We will refine it much further and explore how the properties of the proton emerge from internal quark and gluon interactions by measuring the 3D structure of the proton with high precision measurements in the sPHENIX experiment at RHIC and the Electron-Ion Collider (EIC) in the future. The 3D understanding of the proton structure will enable us to understand the origin of the proton spin including the orbital motion of quarks and gluons (or collectively called partons).

We have proposed to construct a forward apparatus of the sPHENIX detector that will expand the kinematic coverage of the measurements of the 3D structure of the proton.<sup>1)</sup> In the forward rapidity region, a large single-spin asymmetry (SSA) or azimuthal modulation is known to exist, which will enable us to study the orbital motion of quarks and gluons. Theoretically, this phenomenon has been explained by the transverse-momentum dependent parton distribution function and correlations of partons in the proton. Based on these theoretical framework, we measure the SSAs of forward jets, hadrons, electrons, photons, etc. systematically in polarized proton collisions with high precision at sPHENIX.

The forward hadron calorimeter is essential for the forward jet reconstruction and hadron energy measurements, along with triggering. Designing and developing this calorimeter is a joint project with the EIC generic detector R&D group eRD1 and the STAR upgrade project.<sup>2)</sup> In addition to being a viable sPHENIX forward calorimeter, the system is designed to fulfill the requirements of a forward hadron calorimeter of an EIC detector.

The forward hadron calorimeter is located outside the flux return yoke of the superconducting solenoid magnet of the sPHENIX barrel detector system, with a front face 3.5 m away from the interaction point. The presence of the flux return yoke only has a minor effect on the calorimeter performance. The forward hadron calorimeter consists of 2,044 towers measuring 10 cm × 10 cm × 81 cm with an expected energy resolution of

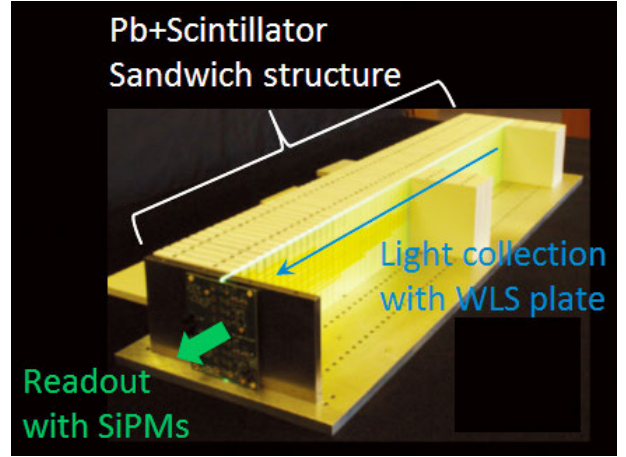


Fig. 1. An image of a tower of the hadron calorimeter.

approximately  $70\%/\sqrt{E(\text{GeV})}$  for single hadrons. It covers a pseudorapidity range of  $1.2 < \eta < 4.0$ .

The design of the calorimeter follows the design of the STAR upgrade project. A prototype calorimeter tower has been made by STAR and it has been tested at the FNAL test beam facility to validate the construction technique. It is scalable and re-configurable with a minimal number of mechanical components. Therefore, it minimizes the resources required for construction and operation. Figure 1 shows an image of the prototype calorimeter tower. It consists of 38 layers of 20 mm iron absorbers and 3 mm plastic scintillator plates, which correspond to a total depth of approximately 4.5 nuclear interaction lengths. A wavelength-shifting (WLS) plate provides uniform and efficient light collection from all scintillation tiles along the depth of the tower. The light from the WLS plate is measured with SiPMs similar to the sPHENIX barrel calorimeters. This allows for the use of common readout electronics for all sPHENIX calorimeter systems. Factors that limit the energy resolution are alignment and non-uniformity.

### References

- 1) E. C. Aschenauer *et al.*, arXiv:1602.03922 [nucl-ex].
- 2) O. D. Tsai *et al.*, J. Phys. Conf. Ser. **587**, no. 1, 012053 (2015).

<sup>\*1</sup> RIKEN Nishina Center

<sup>\*2</sup> J-PARC Center, Japan Atomic Energy Agency

<sup>\*3</sup> Department of Physics, Yamagata University

<sup>\*4</sup> Department of Physics, Tokyo Institute of Technology

<sup>\*5</sup> College of Science and Technology, Nihon University

<sup>\*6</sup> Advanced Science Research Center, Japan Atomic Energy Agency

<sup>\*7</sup> Graduate School of Science, Kobe University

## Development of the intermediate silicon tracker for sPHENIX experiment at RHIC

I. Nakagawa,<sup>\*1</sup> Y. Akiba,<sup>\*1</sup> H. Aso,<sup>\*1,\*2</sup> D. Cacace,<sup>\*3</sup> E. Desmond,<sup>\*3</sup> T. Hachiya,<sup>\*1,\*4</sup> T. Ichino,<sup>\*1,\*2</sup> M. Isshiki,<sup>\*4</sup> T. Kondo,<sup>\*5</sup> H. Kureha,<sup>\*4</sup> E. Mannel,<sup>\*3</sup> G. Mitsuka,<sup>\*1</sup> R. Nouicer,<sup>\*3</sup> R. Pisani,<sup>\*3</sup> K. Sugino,<sup>\*4</sup> A. Suzuki,<sup>\*4</sup> M. Tsuruta,<sup>\*1</sup> T. Todoroki,<sup>\*1</sup> and Y. Yamaguchi<sup>\*1</sup>

The development of the next generation experiment, called sPHENIX,<sup>1)</sup> at RHIC has been firmly proceeded and have passed the critical decision 1 and 3a approval in August 2018. The R&D of the intermediate silicon tracker for sPHENIX is almost in the final stage of the development. The silicon strip sensor design and the high density interconnect (HDI)<sup>2)</sup> had been finalized by the 2nd generation prototyping in early 2018. The 3 layers of INTT telescope ladder modules based on these 2nd generation prototypes were assembled for the beam test at Fermi Laboratory. Shown in the Fig. 1 is the telescope array used for the beam test in March 2018.

The resulting spectra of the 120 GeV primary proton beam measured by a corresponding cell of each ladder layer are shown in Fig. 2. The observed position and the width of the Gaussian shapes are well consistent between the three layers and matches with the expected beam profile which is also measured by the beam profile monitor originally implemented at the test beam facility of Fermi Lab. The noise performance was also quite satisfactory.

The next round beam tests is scheduled in May, 2019 with a full readout chain including a 1.2 meter bus extender<sup>3,4)</sup> and the air cooling stave support structure, which were substituted by temporary solutions in the last beam test because they were still in the middle of development stages and not ready for the beam test. The stave (Fig. 3 is the support structure of the INTT module which consisted of silicon sensors and HDI as

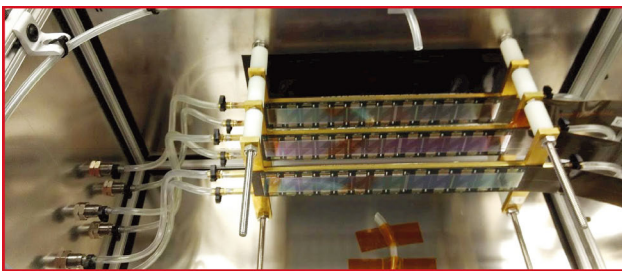


Fig. 1. The telescope of the INTT half ladder detectors assembled for the beam test at Fermi Lab.

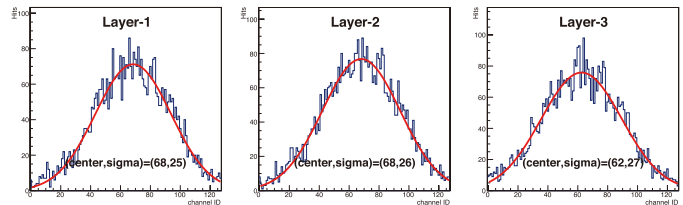


Fig. 2. The telescope of the INTT half ladder detectors assembled for the beam test at Fermi Lab.



Fig. 3. The auto-CAD drawing of the stave support structure with the air cooling tubes.

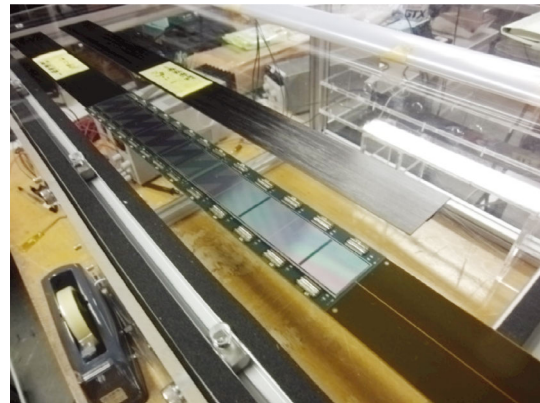


Fig. 4. The HDI module mounted on the prototype stave.

shown in the Fig. 4. It requires not only the stiffness, but also high thermal conductivity in order to remove heat generated from the read out chips mounted on the HDI. The stave is made of a carbon fiber reinforced plastic (CFRP) and its prototyping has been in progress both in Asuka Co. in Japan and Lawrence Berkley National Laboratory in parallel. As well as the measurement of thermal conductivity performance of the prototype staves, the stiffness is also tested before the finalization.

<sup>\*1</sup> RIKEN Nishina Center  
<sup>\*2</sup> Department of Physics, Rikkyo University  
<sup>\*3</sup> Brookhaven National Laboratory  
<sup>\*4</sup> Nara Women's University  
<sup>\*5</sup> Tokyo Metropolitan Industrial Technology Research Institute

### References

- 1) Conceptual Design Report of sPHENIX (2018).
- 2) I. Nakagawa, RIKEN Accel. Prog. Rep. **50**, (2017).
- 3) T. Hachiya *et al.*, in this report.
- 4) M. Tsuruta *et al.*, in this report.

## Tracking performance simulation for INTT at sPHENIX

T. Todoroki,<sup>\*1</sup> Y. Akiba,<sup>\*1</sup> H. Aso,<sup>\*1,\*2</sup> D. Cacace,<sup>\*3</sup> E. Desmond,<sup>\*3</sup> T. Hachiya,<sup>\*1,\*4</sup> T. Ichino,<sup>\*1</sup> M. Isshiki,<sup>\*4</sup> T. Kondo,<sup>\*5</sup> H. Kureha,<sup>\*4</sup> E. Mannel,<sup>\*3</sup> G. Mitsuka,<sup>\*1</sup> I. Nakagawa,<sup>\*1</sup> R. Nouicer,<sup>\*3</sup> R. Pisani,<sup>\*3</sup> K. Sugino,<sup>\*4</sup> A. Suzuki,<sup>\*4</sup> M. Tsuruta,<sup>\*1</sup> and Y. Yamaguchi<sup>\*1</sup>

The sPHENIX tracking system comprises, from the inside to outside, i) the Monolithic-Active-Pixel-Sensor-based Vertex Detector (MVTX),<sup>1)</sup> ii) the Intermediate Silicon Strip Tracker (INTT),<sup>2)</sup> and iii) the Time Projection Chamber (TPC).<sup>2)</sup> MVTX measures the distance of closest approach for heavy-flavour physics. TPC aims at a momentum resolution of 1.2% for different  $\Upsilon$  state separations. INTT has a narrow timing window of 100 ns, which is orders smaller than those of MVTX (4000 ns) and TPC (26400 ns), which provides rejection powers on pile-up events and tracks.

The INTT tracking performance and its optimal layer configuration are evaluated via 1) pile-up event rejections, 2) pile-up track rejections, and 3) MVTX cluster association efficiency to TPC track seeds. For these studies, GEANT4 simulations with PYTHIA8 p+p events at  $\sqrt{s} = 200$  GeV, embedded at realistic collision rates at sPHENIX, are employed. Tracks are reconstructed only with MVTX hit triplets and a cluster in one of the INTT layers for the (1), while tracks are seeded in TPC and interpolated to INTT and MVTX hits with the Hough transformation for the (2) and (3).

Figure 1 Left (Right) shows the event vertex tagging (rejection) efficiency in (out of) the INTT time window as a function of PYTHIA event multiplicity at the collision rate of 12 MHz. The integrated in-time vertex tagging efficiency is  $98.4 \pm 0.3\%$ , and the integrated out-of-time, *i.e.* pile-up, vertex rejection efficiency is 99%. This indicates 1 INTT cluster provides a good rejection of pile-up tracks.

Figure 2 shows the numbers of tracks per  $p_T$  bin width from in-time and pile-up events as a function of  $p_T$  at the collision rate of 10 MHz. The blue and red lines are the generated tracks in in-time and pile-up events.

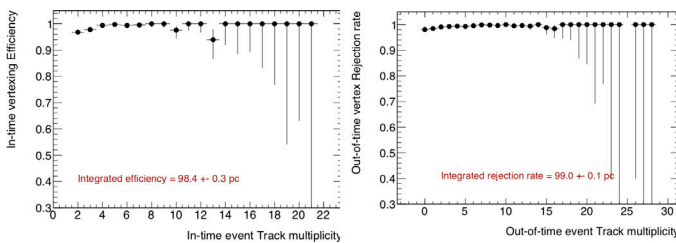


Fig. 1. (Left) In-time vertex tagging and (Right) out-of-time vertex tagging efficiency versus event multiplicity.

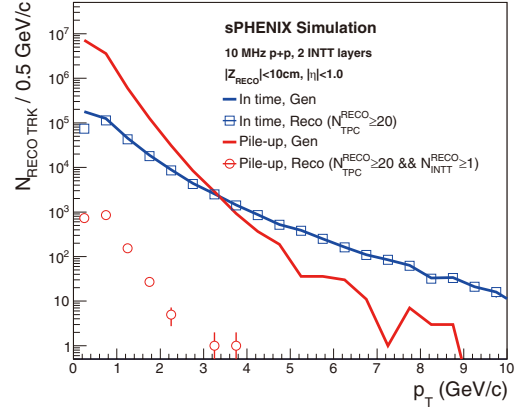


Fig. 2. Number of tracks from in-time and pile-up events as a function of  $p_T$  with different tracking requirements.

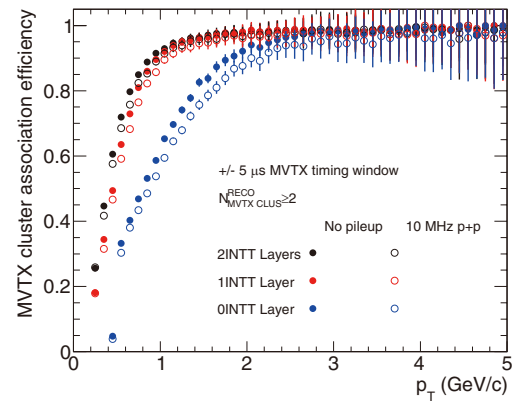


Fig. 3. MVTX cluster association efficiency to TPC track seeds as a function of  $p_T$  with different number of INTT layers.

The red circles show that the pile-up contribution in the reconstructed tracks becomes two orders smaller than that from the in-time events (blue squares) by requiring 1 INTT cluster in addition to 20 TPC clusters in tracking. This also indicates 1 INTT cluster provides a good rejection of pile-up tracks.

Figure 3 shows MVTX cluster association efficiency to TPC track seeds as a function of  $p_T$  at no pile-up (0 Hz) and 10 MHz collision rates. The worst efficiency is obtained without INTT (0INTT Layer) because of the large distance between MVTX and TPC. INTT hits in the association reduce the uncertainty in searching MVTX hits, resulting in better efficiency. The efficiency is the best with 2 INTT layers. These studies show that a two-layer INTT detector is optimal for obtaining the best tracking performance at sPHENIX.

### References

- 1) MVTX proposal submitted to the DOE Office of Science
- 2) sPHENIX proposal, arXiv:1501.06197

<sup>\*1</sup> RIKEN Nishina Center  
<sup>\*2</sup> Department of Physics, Rikkyo University  
<sup>\*3</sup> Brookhaven National Laboratory  
<sup>\*4</sup> Nara Women's University  
<sup>\*5</sup> Tokyo Metropolitan Industrial Technology Research Institute

# Preparation status of the J-PARC E16 experiment in 2018

S. Yokkaichi\*<sup>1</sup> for the J-PARC E16 Collaboration

We have proposed the experiment E16<sup>1)</sup> to measure the vector meson decays in nuclei in order to investigate the chiral symmetry restoration in dense nuclear matter. The experiment will be performed at the J-PARC Hadron Experimental Facility. Scientific (“stage-1”) approval was granted to the experiment E16 by PAC in March 2007. For the full (“stage-2”) approval, the demonstration of experimental feasibility and the prospects of acquiring sufficient funds and beam-line construction are necessary. Therefore a technical design report was submitted to PAC in May 2014, which was revised twice according to the requirements of PAC. The most recent revision was submitted to PAC in Jan. 2017.

In the PAC held in Jul. 2017, stage-2 approval for the 40 shifts (320 hours) of a commissioning run was granted. In this run, the background measurement at the new beamline should be performed. The high-momentum beam line, where the experiment will be conducted is being constructed by KEK. As of Jan. 2019, the target date of the first beam and our commissioning run is between Jan. and Apr. in 2020, depending on the budgetary status of KEK.

This experiment aims to systematically study the spectral modification of vector mesons in nuclei, particularly the  $\phi$  meson, using the  $e^+e^-$  decay channel with statistics that are two orders larger in magnitude than those of the precedent E325<sup>2)</sup> experiment performed at KEK-PS. In other words, it aims to accumulate  $1 \times 10^5$  to  $2 \times 10^5$  events for each nuclear target (H, C, Cu, and Pb) and deduce the dependence of modification the size of matter and meson momentum. The  $e^+e^-$  decays of the  $\rho$ ,  $\omega$ , and  $J/\psi$  mesons can be measured simultaneously. Their yields depend on the trigger condition required to suppress the background  $e^+e^-$  pairs.

In order to increase the statistics by a factor of 100, we plan to use a 30-GeV primary proton beam with an intensity of  $1 \times 10^{10}$  protons per beam pulse of 2-sec duration and 5.52-sec cycle, in the high-momentum beam line. We also use 0.2%-interaction targets that produce an interaction rate of 10 MHz at the targets.

Our spectrometer has 26 modules. Owing to budget limitations, our first goal of the staged construction plan is to construct eight modules, which approximately covers one third of the full acceptance. With the eight-module configuration, we proposed Run-1 with 160 shifts (1280 hours) of physics run after the commissioning run. In the Run-1, we will be able to accumulate the statistics as six times as that of E325 and obtain the velocity dependence of spectral modification in the Cu target, as shown in Fig. 1.

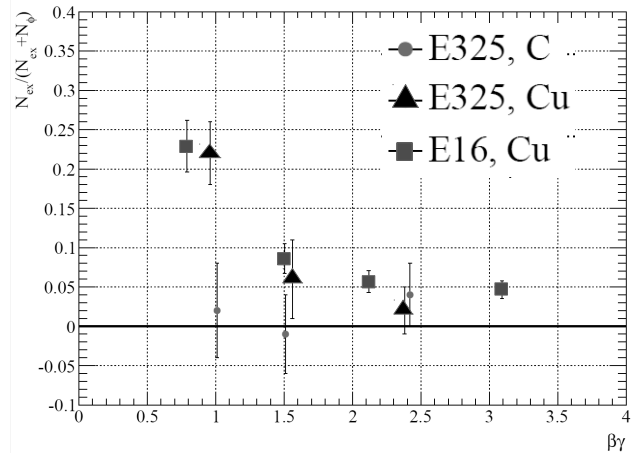


Fig. 1. Expected signal of the spectral modification of  $\phi$  in Run-1. As the measure of the modification, the ratio of excess amount to the amount of mesons in  $\phi$ -peak is examined and plotted as a function of  $\beta\gamma$  of the mesons.

The development of detectors and front-end modules has been completed. We have proceeded the production of detectors such as GEM Tracker (GTR) for tracking,<sup>3)</sup> Hadron Blind Čerenkov detector (HBD),<sup>4)</sup> and Lead-Glass calorimeter (LG) for electron identification. We joined the RD51<sup>5)</sup> collaboration in CERN that aims to develop multi-pixel gas detectors including GEM. We use SRS, which is a readout-system developed by RD51, for GEM readout. For LG readout, a front-end module that uses the DRS4 chip<sup>6)</sup> has been developed by ourselves.

The development of trigger electronics is still underway.<sup>7)</sup> Test of the amp-shaper-discriminator boards to generate the trigger signal at GTR and HBD are in progress toward the production planned in Apr. 2019. The firmwares on the trigger logic and distribution modules are also under construction toward the integrated test planned in May 2019.

## References

- 1) S. Yokkaichi *et al.*, J-PARC proposal No. 16, ([http://j-parc.jp/researcher/Hadron/en/pac\\_0606/pdf/p16-Yokkaichi\\_2.pdf](http://j-parc.jp/researcher/Hadron/en/pac_0606/pdf/p16-Yokkaichi_2.pdf)), Y. Morino *et al.*, JPS Conf. Proc. **8**, 022009 (2015). Y. Komatsu *et al.*, JPS Conf. Proc. **12**, 020005 (2017).
- 2) R. Muto *et al.*, Phys. Rev. Lett. **98**, 042501 (2007).
- 3) W. Nakai *et al.*, RIKEN Accel. Prog. Rep. **49**, 195 (2015).
- 4) K. Kanno *et al.*, Nucl. Instrum. Methods Phys. Res. A **819**, 20 (2016).
- 5) <http://rd51-public.web.cern.ch/RD51-Public/>.
- 6) <https://www.psi.ch/drs/drs-chip/>.
- 7) T. N. Takahashi *et al.*, J. Phys. Conf. Ser. **664**, 082053 (2015).

\*<sup>1</sup> RIKEN Nishina Center

# Spectroscopy of pionic atoms in $^{122}\text{Sn}(d, {}^3\text{He})$ reaction and angular dependence of the formation cross sections<sup>†</sup>

T. Nishi,<sup>\*1,\*2</sup> K. Itahashi,<sup>\*2</sup> G. P. A. Berg,<sup>\*3</sup> H. Fujioka,<sup>\*4</sup> N. Fukuda,<sup>\*2</sup> N. Fukunishi,<sup>\*2</sup> H. Geissel,<sup>\*5</sup> R. S. Hayano,<sup>\*1</sup> S. Hirenzaki,<sup>\*6</sup> K. Ichikawa,<sup>\*1</sup> N. Ikeno,<sup>\*7</sup> N. Inabe,<sup>\*2</sup> S. Itoh,<sup>\*1</sup> M. Iwasaki,<sup>\*2</sup> D. Kameda,<sup>\*2</sup> S. Kawase,<sup>\*8</sup> T. Kubo,<sup>\*2</sup> K. Kusaka,<sup>\*2</sup> H. Matsubara,<sup>\*8</sup> S. Michimasa,<sup>\*8</sup> K. Miki,<sup>\*1</sup> G. Mishima,<sup>\*1</sup> H. Miya,<sup>\*2</sup> H. Nagahiro,<sup>\*6</sup> M. Nakamura,<sup>\*2</sup> S. Noji,<sup>\*1</sup> K. Okochi,<sup>\*1</sup> S. Ota,<sup>\*8</sup> N. Sakamoto,<sup>\*2</sup> K. Suzuki,<sup>\*9</sup> H. Takeda,<sup>\*2</sup> Y. K. Tanaka,<sup>\*1</sup> K. Todoroki,<sup>\*1</sup> K. Tsukada,<sup>\*2</sup> T. Uesaka,<sup>\*2</sup> Y. N. Watanabe,<sup>\*1</sup> H. Weick,<sup>\*5</sup> H. Yamakami,<sup>\*4</sup> and K. Yoshida<sup>\*2</sup>  
(piAF Collaboration)

Spectroscopy of deeply bound pionic atoms has been contributing to understanding of non-perturbative low-energy region of the QCD.<sup>1)</sup> We have started an experimental spectroscopy of pionic atoms at RIBF and conducted our first experiment in 2010 by measuring  $^{122}\text{Sn}(d, {}^3\text{He})$  reactions near the  $\pi^-$  emission threshold for about 15h. We employed deuteron beam with the energy of  $498.9 \pm 0.2$  MeV and a typical intensity of  $2 \times 10^{11}/\text{s}$  accelerated by SRC. Such a high intensity deuteron beam may serve as an irreplaceable basis for high statistical and systematic precision in the spectroscopy and let us achieve opportunities to reach understanding of the the low-energy QCD with unprecedented accuracy.

During the experiment, the deuteron beam impinged on a thin  $^{122}\text{Sn}$  target located at a nominal target position of BigRIPS. We used BigRIPS as a spectrometer to momentum-analyze the emitted  ${}^3\text{He}$  and measured the Q-value of the reaction in the missing-mass measurement. We reconstructed the tracks of the  ${}^3\text{He}$  by a set of tracking detectors placed near the F5 dispersive focal plane. We installed a set of scintillation counters at F5 and F7 focal planes and identified the particles. After applying detailed optical aberration corrections, we achieved excitation spectra of the target Sn nucleus with the best resolution of 0.42 MeV (FWHM). The absolute excitation energy is calibrated by using a polyethylene target to observe two-body reactions of  $\text{H}(d, {}^3\text{He})\pi^0$ .

In the measured excitation spectrum of the target Sn nucleus, we observe three prominent peak structures near the  $\pi^-$  emission threshold as depicted in Fig. 1 of our original paper Ref. 2). The left most peak in the smaller-mass side is assigned to the  $1s$  pionic state mainly coupling with a neutron hole state of  $(3s_{1/2})_n^{-1}$ .

The central peak is assigned mainly to formation of the  $2p$  pionic state. The right most peak in the larger-mass side is contributed from higher pionic orbitals. The pionic states in  $^{121}\text{Sn}$  are observed for the first time. We made an elaborate fitting of the observed spectrum and deduced the  $1s$  and  $2p$  binding energies and the  $1s$  width. The deduced binding energies and the width agree with theoretical calculations.

In the measurement, a large angular acceptance of BigRIPS provided a very unique opportunity. As shown in Fig. 2 of Ref. 2), we observe reaction-angle dependence of the pionic atom formation spectra for the first time. The dependence of both  $1s$  and  $2p$  states are determined experimentally. Comparing the measured dependence with a theoretical prediction,<sup>3)</sup> they are qualitatively agreeing well, and the observed dependence directly confirms the assignment of the angular momenta of the structures in the spectrum.

Quantitatively comparing the measured absolute formation cross sections with the theoretical predictions, we find that the measured  $2p$  cross section fairly well agrees with the theory and that the  $1s$  cross section is smaller by a factor of about 20%. Since a ratio of the measured cross sections of the  $1s$  to  $2p$  state is attributed with relatively small errors, the deviation from the theory invokes important questions in understanding of the pionic atom formation reactions.

In conclusion, we conducted first pionic atom spectroscopy at RIBF and measured pionic  $^{121}\text{Sn}$  as peak structures in the missing-mass spectrum for the first time. Reaction angle dependence of the pionic  $1s$  and  $2p$  formation cross sections are observed and compared with theoretical calculations. The measured dependence qualitatively agree with the theory confirming the correct assignment of the observed structures in the spectrum. Measured absolute  $2p$  cross section well agrees with the theory but the theory overestimates the  $1s$  cross section by a factor of about 5. The measurement firmly proves potential of the RIBF for future high precision spectroscopy of pionic atoms.

## References

- 1) K. Suzuki *et al.*, Phys. Rev. Lett. **92**, 072302 (2004).
- 2) T. Nishi *et al.*, Phys. Rev. Lett. **120**, 152505 (2018).
- 3) N. Ikeno *et al.*, PTEP **2015**, 033D01 (2015).

<sup>†</sup> Condensed from the article in Phys. Rev. Lett. **125**, 152505 (2018)

\*1 University of Tokyo

\*2 RIKEN Nishina Center

\*3 University of Notre Dame

\*4 Kyoto University

\*5 GSI Helmholtzzentrum für Schwerionenforschung GmbH

\*6 Nara Women's University

\*7 Tottori University

\*8 CNS, University of Tokyo

\*9 Stefan Meyer Institute for Subatomic Physics

# Isotope identification in nuclear emulsion plate for double-hypernuclear study<sup>†</sup>

S. Kinbara,<sup>\*1</sup> H. Ekawa,<sup>\*2</sup> T. Fujita,<sup>\*3</sup> S. Hayakawa,<sup>\*4</sup> S. H. Hwang,<sup>\*5</sup> Y. Ichikawa,<sup>\*3</sup> K. Imamura,<sup>\*3</sup> R. Murai,<sup>\*1</sup> M. K. Soe,<sup>\*1</sup> M. Sweet,<sup>\*1</sup> A. Takamine,<sup>\*3</sup> A. M. M. Theint,<sup>\*1</sup> H. Ueno,<sup>\*3</sup> J. Yoshida,<sup>\*6</sup> M. Yoshimoto,<sup>\*1</sup> and K. Nakazawa<sup>\*1</sup>

Double hypernuclei such as double- $\Lambda$  and  $\Xi$  hypernuclei provide information about  $\Lambda$ - $\Lambda$  and  $\Xi$ - $N$  interactions, which are important to understand the inner structure of a neutron star. We have only two reliable information from the NAGARA<sup>1,2)</sup> and KISO<sup>3,4)</sup> events in the E373 experiment. Other events are not uniquely identified for the production and decay processes owing to the remaining possible interpretations. The charge identification method is a key technique to understand the multi-strangeness system.

To develop the method, we exposed eight nuclides ( $^1\text{H}$ ,  $^2\text{H}$ ,  $^3\text{H}$ ,  $^3\text{He}$ ,  $^4\text{He}$ ,  $^7\text{Li}$ ,  $^9\text{Be}$ , and  $^{11}\text{B}$ ) to a nuclear emulsion at RIPS. To study the halo effect in the finite focal depth of objective lens, the exposed angle  $\theta$  perpendicular to the emulsion surface was set to be  $\theta \approx 25^\circ$ ,  $50^\circ$ , and  $75^\circ$ .

To recognize the charge of the particle, we measured the track width and estimated the track volume that reflect the energy-losses. Raw images were taken by microscope with a  $100\times$  objective lens and an 8 bits CCD camera. A focused image, as shown in Fig. 1(a), consists of the most focused layers of raw images. Figure 1(b) is illustrated according to the following equation,  $B_{\text{out}} = 255 \times (B_{\text{in}} - B_{\text{min}})/(B_{\text{max}} - B_{\text{min}})$ , where  $B_{\text{in}}$ ,  $B_{\text{max}}$ , and  $B_{\text{min}}$  are the brightness of each pixel, maximum, and minimum brightness in Fig. 1(a), respectively.  $B_{\text{in}}$  was enhanced to  $B_{\text{out}}$ . Figure 1(c) was illustrated by applying an algorithm called ‘‘difference of Gaussian’’ to Fig. 1(b). Then, a uniform background image was obtained by subtracting Fig. 1(b) from 1(c), as shown in Fig. 1(d). We measured the brightness perpendicular to the track in the Fig. 1(d) and de-

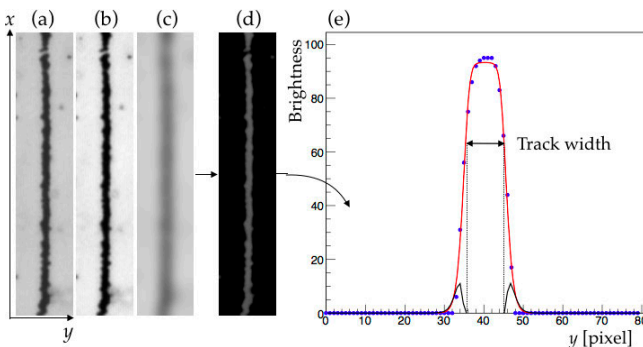


Fig. 1. Image processing method to obtain track width.

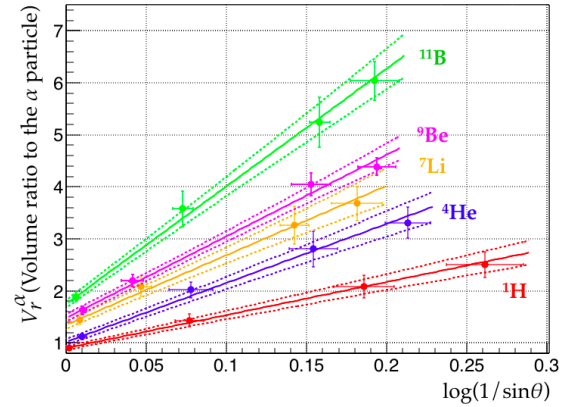


Fig. 2.  $V_r^\alpha$  of each nucleus to  $\alpha$  particle as a function of  $\log(1/\sin\theta)$ .

finned the track width as a distance between two inflection points, which were obtained by applying a fitting function,  $f = a \times \tanh(\text{gauss}(x, \mu, \sigma))$ , to the data in Fig. 1(e).

The track width depends on the photographic development. As a calibration source, we used  $\alpha$  particles which have monochromatic kinetic energy emitted from natural isotope  $^{212}\text{Po}$  in the emulsion. We obtained the calibration function of  $v^\alpha(d)$  with 68  $\alpha$ -particles, where  $v^\alpha$  is the average track volume of an  $\alpha$ -particle at depth  $d$  from the emulsion surface.

The widths were measured for every  $1 \mu\text{m}$  cell along the track. Because the depths of the measured cells changed along the track, a volume ratio  $V_r^\alpha$  to normalize the  $\alpha$ -particle for each nucleus was obtained for measured volume  $V_i$  in  $i$ th cell as  $V_r^\alpha = \sum_{i=1}^{90} V_i / \sum_{i=1}^{90} v^\alpha(d_i)$ , where  $d_i$  is the depth of the  $i$ th cell. We put 200 tracks together at four areas for each nucleus in the exposed emulsion and fitted them according to  $\log(1/\sin\theta)$ , where we set  $\log(1/\sin\theta)$  to be  $\xi$ , as angle dependence of the volume ratio,  $V_r^\alpha(\xi)$ , to the volume of the  $\alpha$  particle, as shown in Fig. 2.

To confirm the utility of the above method, it was applied to one track of a  $\Xi$  hypernucleus candidate detected in the E373 experiment. The nucleus of this track is known as  $^3\text{H}$  or  $^6\text{He}$  by kinematical analysis. Their  $V_r^\alpha$  can be estimated by the data points of  $^1\text{H}$  and  $^4\text{He}$ . Thus, we concluded that the nucleus would be a  $^6\text{He}$  nucleus with a likelihood ratio of 0.9.

<sup>†</sup> Condensed from the article in Prog. Theor. Exp. Phys. **2019**, 011H01 (2019).

<sup>\*1</sup> Physics Department, Gifu University

<sup>\*2</sup> Department of Physics, Kyoto University

<sup>\*3</sup> RIKEN Nishina Center

<sup>\*4</sup> Department of Physics, Osaka University

<sup>\*5</sup> Korea Research Institute of Standards and Science

<sup>\*6</sup> Japan Atomic Energy Agency

## References

- 1) H. Takahashi *et al.*, Phys. Rev. Lett. **87**, 212502 (2001).
- 2) J. K. Ahn *et al.*, Phys. Rev. C **88**, 014003 (2013).
- 3) K. Nakazawa *et al.*, Prog. Theor. Exp. Phys. **2015**, 033D02 (2015).
- 4) E. Hiyama, K. Nakazawa, Annu. Rev. Nucl. Part. Sci. **68**, 131 (2018).

## **5. Hadron Physics (Theory)**



## Short range $\pi J/\psi - D\bar{D}^*$ interaction<sup>†</sup>

Y. Yamaguchi,<sup>\*1</sup> Y. Abe,<sup>\*2</sup> K. Fukukawa,<sup>\*3</sup> and A. Hosaka,<sup>\*4</sup>

Exotic hadrons such as  $XYZ$  states reported in the heavy flavor sector have been one of the interesting topics in hadron and nuclear physics.<sup>1)</sup> Especially, for the exotic mesons near the thresholds, those states could be realized as a hadronic molecule, which is a loosely bound or resonant state of multi-mesons.

$Z_c(3900)$  is an exotic state that has been reported by BESIII,<sup>2)</sup> Belle,<sup>3)</sup> and other facilities.<sup>4,5)</sup> This state has a nonzero electric charge that cannot be possessed by the standard  $c\bar{c}$  state. There have been various studies of  $Z_c(3900)$ , where multiquark states and hadronic molecules have been discussed (see Ref. 1)). On the other hand, the non bound state explanation has also been studied. Recent Lattice QCD simulation by HALQCD<sup>6)</sup> indicates that  $Z_c(3900)$  is a virtual state induced by the strong  $\pi J/\psi - D\bar{D}^*$  potential.

For the exotic state near the threshold, heavy hadron interaction is important to understand the structure. We study the short range  $\pi J/\psi - D\bar{D}^*$  interaction described by (i) the meson exchange model, and (ii) quark exchange model, and compare the results obtained by these models.

In the meson exchange model, the  $D^{(*)}$  meson exchange is introduced, which is given as the Born term of the  $t$ -channel scattering amplitude. The amplitude is obtained by the effective Lagrangians with respect to the heavy quark and chiral symmetries,<sup>7,8)</sup> which are given by

$$\mathcal{L}_{\pi HH} = -\frac{g_\pi}{2f_\pi} \text{Tr} [H_1 \gamma_\mu \gamma_5 \partial^\mu \hat{\pi} \bar{H}_1], \quad (1)$$

$$\mathcal{L}_{\psi HH} = g' \text{Tr} [J \bar{H}_2 \leftrightarrow \partial_\mu \gamma^\mu \bar{H}_1] + \text{H.c.}, \quad (2)$$

where  $g_\pi = 0.59$ ,  $g' = 4/\sqrt{m_\psi m_D^2}$ , and the pion decay constant  $f_\pi = 93$  MeV.

In the quark exchange model, the  $\pi J/\psi - D\bar{D}^*$  interaction is described by the constituent quark model Hamiltonian<sup>9,10)</sup>

$$H_{ij}^q = K_q + \left( -\frac{3}{4}br + \frac{\alpha_s}{r} - C \right) \vec{F}_i \cdot \vec{F}_j - \frac{8\pi\alpha_h}{3m_i m_j} \left( \frac{\sigma^3}{\pi^{3/2}} e^{-\sigma^2 r_{ij}^2} \right) \vec{S}_i \cdot \vec{S}_j \vec{F}_i \cdot \vec{F}_j. \quad (3)$$

In Fig. 1, the cross sections of the  $\pi J/\psi - D\bar{D}^*$  transition obtained using the two models are compared. The cross section obtained using quark exchange is dominated by the spin-spin term, which is contributed by the light quark dynamics instead of the charm quark

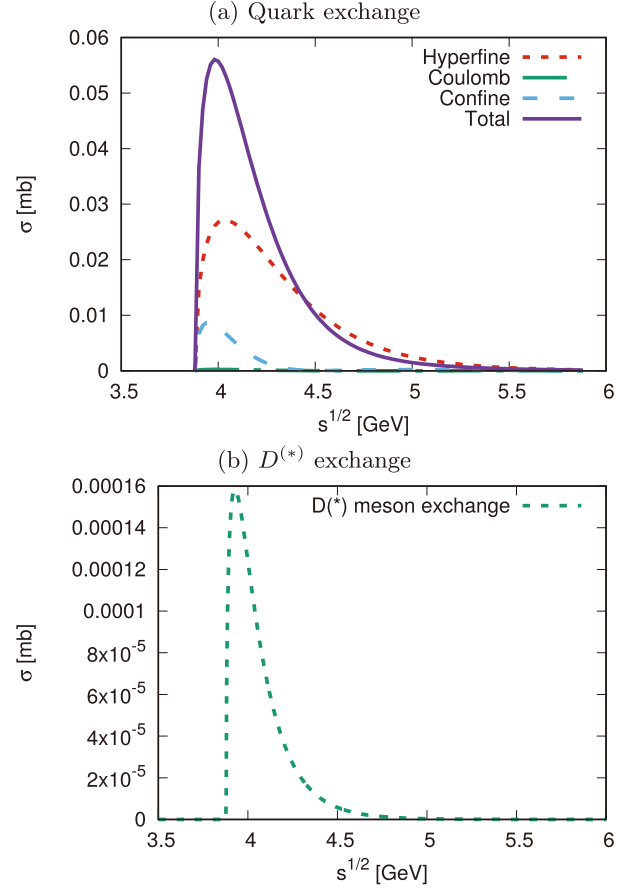


Fig. 1.  $\pi J/\psi - D\bar{D}^*$  cross sections obtained by (a) quark exchange model, and (b)  $D^{(*)}$  exchange model.

dynamics. In comparison with that of quark exchange, the cross section obtained by meson exchange is very small. A large difference is obtained between the two models, and it would be useful to understand the short range interaction in the  $\pi J/\psi - D\bar{D}^*$  channel.

### References

- 1) A. Hosaka, T. Iijima, K. Miyabayashi, Y. Sakai, S. Yasui, Prog. Theor. Exp. Phys. **2016**, 062C01 (2016).
- 2) M. Ablikim *et al.* [BESIII Collaboration], Phys. Rev. Lett. **110**, 252001 (2013).
- 3) Z. Q. Liu *et al.* [Belle Collaboration], Phys. Rev. Lett. **110**, 252002 (2013).
- 4) T. Xiao, S. Dobbs, A. Tomaradze, K. K. Seth, Phys. Lett. B **727**, 366 (2013).
- 5) V. M. Abazov *et al.* [D0 Collaboration], Phys. Rev. D **98**, 052010 (2018).
- 6) Y. Ikeda *et al.* [HAL QCD Collaboration], Phys. Rev. Lett. **117**, 242001 (2016).
- 7) R. Casalbuoni *et al.*, Phys. Rep. **281**, 145 (1997).
- 8) A. V. Manohar, M. B. Wise, *Heavy Quark Physics*, (Cambridge University Press, Cambridge, England, 2000).
- 9) T. Barnes, E. S. Swanson, Phys. Rev. D **46**, 131 (1992).
- 10) E. S. Swanson, Annals Phys. **220**, 73 (1992).

<sup>†</sup> Condensed from the article in EPJ Web Conf. **204**, 01007 (2019)

<sup>\*1</sup> RIKEN Nishina Center

<sup>\*2</sup> NEC

<sup>\*3</sup> Suma Gakuen

<sup>\*4</sup> RCNP, Osaka University

# Proton decay matrix elements at physical quark mass

Y. Aoki,<sup>\*1,\*2 (current:\*3)</sup> Y. Kuramashi,<sup>\*4</sup> and E. Shintani<sup>\*3</sup>

Proton decay is a smoking-gun signal of the physics beyond the standard model (BSM). Grand unified theory (GUT) is the most natural origin of such an event if observed. Despite no clear signal of the supersymmetry or any BSM phenomena at LHC, the idea of unifying the known fundamental interactions is still attractive. Estimate of the QCD contribution of the proton decay matrix element is needed to test GUTs against the proton lifetime bound obtained in the experiment. Also a reliable estimate of the matrix elements is desirable for planning the future generation proton decay detectors.

The proton decay matrix elements are obtained by numerical computation using lattice QCD. So far, the  $2+1$  flavor computations have provided the matrix elements with extrapolation to the physical  $ud$  quark mass from the results at unphysically large masses. This procedure yields one of the largest systematic uncertainties. Settling this systematics is important<sup>1)</sup> and possible using current lattice gauge field ensembles generated at the physical point.

We use gauge field configurations of  $2+1$  flavor QCD generated with non-perturbatively  $O(a)$ -improved Wilson fermions by the PACS collaboration.<sup>2)</sup> As pointed in the previous works (see *e.g.*<sup>3)</sup>), computations using the three-point functions are mandatory to obtain the matrix elements of a proton decaying into a pseudoscalar (and an anti lepton). Last year we reported on the optimization of the parameters of smearing function of the quarks for interpolating operators of proton and mesons. Using this we are extending the computation for the three-point functions. Figure 1 shows the ratio of the three and two-point functions for proton decay form factor  $W_0$  for  $p \rightarrow \pi^0$  via  $LL$  operator ( $\epsilon_{ijk}(u_i^T C P_L d_j) P_L u_k$ ), for three different momentum values  $\vec{p} = 2\pi/64 * \vec{n}_p$ . From the plateau we will obtain the form factor that we are after. Comparison of the two different source-sink separation  $t_s$  is performed, and they show consistent results in the middle. In this study we use  $64^4$  lattice at the physical point mass. Last year we present a result of low energy constant  $\alpha$  computed on  $64^4$  and  $96^4$  volumes. As the results from two volumes are consistent, we expect  $64^4$  is also good for the form factors.

We need several further steps to obtain the form factors in the physical unit ( $\text{GeV}^2$ ) and renormalized in a convenient renormalization scheme for phenomenological use. For the renormalization one needs to solve the operator mixing due to an explicit chiral symmetry

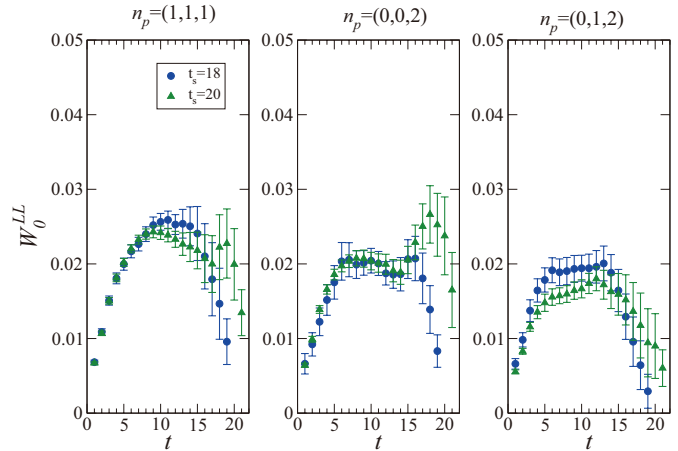


Fig. 1. Time dependence of the ratio of three and two-point functions for proton decay form factor  $W_0$  for  $p \rightarrow \pi^0$  via  $LL$  operator ( $\epsilon_{ijk}(u_i^T C P_L d_j) P_L u_k$ ). The middle points should converge to the form factor in the asymptotic limit of large source-sink separation  $t_s$ , thus develops a plateau.

breaking of the Wilson fermion formulation. The non-perturbative renormalization<sup>4)</sup> can be applied to solve the mixing and at the same time to obtain the totally renormalized operator in the  $\overline{\text{MS}}$  scheme. The use of RI/SMOM schemes<sup>5)</sup> are under investigation. Finally the lattice cutoff squared  $1/a^2$  needs to be multiplied.

This study has shown that we have reasonably a good signal for the form factors and the low energy constants (last year) at the physical quark masses. With a full statistics and a supplemental mass dependence analysis, as well as with a completion of the operator renormalization, this work provides results of proton decay matrix elements with no systematic error from chiral extrapolation for the first time. There is another on-going project<sup>6)</sup> to calculate the same matrix elements with domain-wall fermions with very coarse lattice but with a better control of chiral symmetry. These two studies are complementary to each other and together will bring us to the final goal of estimating the proton decay matrix elements for pseudo-scalar final states with direct simulation at the physical point.

## References

- 1) A. Martin, G. Stavenga, Phys. Rev. D **85**, 095010 (2012).
- 2) Y. Kuramashi, talk given at Lattice 2017.
- 3) Y. Aoki, T. Izubuchi, E. Shintani, A. Soni, Phys. Rev. D **96**, 014506 (2017).
- 4) Y. Aoki, C. Dawson, J. Noaki, Soni, Phys. Rev. D **75**, 014507 (2007).
- 5) C. Sturm, Y. Aoki, N. Christ, T. Izubuchi, C. Sachrajda, A. Soni, Phys. Rev. D **80**, 014501 (2009).
- 6) J. Yoo, Y. Aoki, T. Izubuchi, S. Syritsyn, arXiv:1812.09326.

\*1 KEK Theory Center

\*2 RIKEN Nishina Center

\*3 RIKEN R-CCS

\*4 CCS, University of Tsukuba

# The $\pi\gamma \rightarrow \pi\pi$ transition and the $\rho$ radiative decay width from lattice QCD<sup>†</sup>

C. Alexandrou,<sup>\*1,\*2</sup> L. Leskovec,<sup>\*3</sup> S. Meinel,<sup>\*3,\*4</sup> J. Negele,<sup>\*5</sup> S. Paul,<sup>\*2</sup> M. Petschlies,<sup>\*6</sup> A. Pochinsky,<sup>\*5</sup> G. Rendon,<sup>\*3</sup> and S. Syritsyn<sup>\*7,\*4</sup>

Lattice QCD calculations of hadronic matrix elements of external currents are straightforward as long as the initial and final states contain no more than a single, stable hadron. For multi-hadron states, however, the relation between the finite-volume matrix elements computed on the lattice and the physical infinite-volume matrix elements of interest is quite nontrivial, and is known only for certain cases. The formalism for  $1 \rightarrow 2$  transition matrix elements was pioneered by Lellouch and Lüscher in 2000,<sup>4)</sup> and was later generalized by other authors to more complicated systems.<sup>5–10)</sup>

Our collaboration is using this formalism to compute several  $1 \rightarrow 2$  transition matrix elements of interest in high-energy and nuclear physics, including semileptonic weak decays such as  $B \rightarrow \pi\pi\ell\bar{\nu}$ . The present work considers the electromagnetic process  $\pi\gamma \rightarrow \pi\pi$ , where we take the  $\pi\pi$  system in a  $P$  wave and isospin 1, and allow the photon to be virtual. The hadronic matrix element for this process can be written as

$$\langle \pi\pi | J^\mu | \pi \rangle = \frac{2i\mathcal{V}(q^2, s)}{m_\pi} \epsilon^{\nu\mu\alpha\beta} \epsilon_\nu(P, m)(p_\pi)_\alpha P_\beta, \quad (1)$$

where  $P$  and  $\epsilon$  are the four-momentum and polarization of the two-pion final state,  $p_\pi$  is the four-momentum of the single-pion initial state, and the amplitude  $\mathcal{V}(q^2, s)$  depends on the two scalar variables  $q^2 = (p_\pi - P)^2$  and  $s = P^2$ . Our calculation was performed with  $2 + 1$  flavors of clover fermions, at a pion mass of approximately 320 MeV. Our results for  $\mathcal{V}(q^2, s)$  are shown in Fig. 1. This amplitude shows the expected enhancement associated with the  $\rho$  resonance, which corresponds to a pole at  $s_{\text{pole}} \approx m_\rho^2 + im_\rho\Gamma_\rho$ . One very interesting result, seen for the first time, is the following: for large  $s$ ,  $\mathcal{V}(q^2, s)$  falls off significantly slower compared to what one would expect for purely resonant behavior.

The residue of  $\mathcal{V}(0, s)$  at  $s = s_{\text{pole}}$  is equal to the product of the  $\rho\text{-}\pi\pi$  and  $\rho\text{-}\pi\gamma$  couplings. Our result for the photocoupling is  $|G_{\rho\pi\gamma}| = 0.0802(32)(20)$ ,

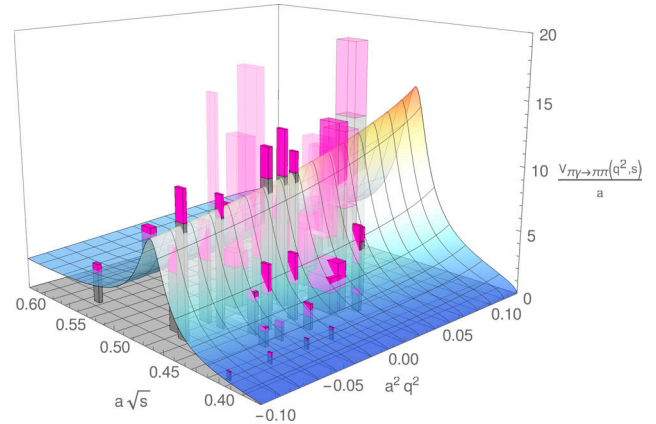


Fig. 1. Our results for the  $\pi\gamma \rightarrow \pi\pi$  transition amplitude as a function of the  $\pi\pi$  invariant mass and the photon virtuality. The magenta boxes show the  $1\sigma$  uncertainties in  $a\sqrt{s}$ ,  $a^2 q^2$ , and  $\mathcal{V}/a$ .

where the first uncertainty originates from the two-point and three-point function fits, while the second uncertainty is an estimate of the parametrization dependence in the analytic continuation. Despite the heavier-than-physical light-quark masses, the lattice result for  $|G_{\rho\pi\gamma}|$  is already close to the value extracted from the measured  $\rho$  radiative decay width.<sup>11)</sup>

## References

- 1) M. Lüscher, Nucl. Phys. B **354**, 531 (1991).
- 2) R. A. Briceño, J. J. Dudek, R. D. Young, Rev. Mod. Phys. **90**, 025001 (2018).
- 3) C. Alexandrou *et al.*, Phys. Rev. D **96**, 034525 (2017).
- 4) L. Lellouch, M. Lüscher, Commun. Math. Phys. **219**, 31 (2001).
- 5) C. J. D. Lin, G. Martinelli, C. T. Sachrajda, M. Testa, Nucl. Phys. B **619**, 467 (2001).
- 6) N. H. Christ, C. Kim, T. Yamazaki, Phys. Rev. D **72**, 114506 (2005).
- 7) M. T. Hansen, S. R. Sharpe, Phys. Rev. D **86**, 016007 (2012).
- 8) R. A. Briceño, Z. Davoudi, Phys. Rev. D **88**, 094507 (2013).
- 9) R. A. Briceño, M. T. Hansen, A. Walker-Loud, Phys. Rev. D **91**, 034501 (2015).
- 10) R. A. Briceño, M. T. Hansen, Phys. Rev. D **92**, 7, 074509 (2015).
- 11) C. Patrignani *et al.* (Particle Data Group), Chin. Phys. C **40**, 100001 (2016).

<sup>†</sup> Condensed from the article in Phys. Rev. D **98**, 074502 (2018)

<sup>\*1</sup> Department of Physics, University of Cyprus

<sup>\*2</sup> Computation-based Science and Technology Research Center, Cyprus Institute

<sup>\*3</sup> Department of Physics, University of Arizona

<sup>\*4</sup> RIKEN Nishina Center

<sup>\*5</sup> Center for Theoretical Physics, Massachusetts Institute of Technology

<sup>\*6</sup> Helmholtz-Institut für Strahlen- und Kernphysik, University of Bonn

<sup>\*7</sup> Department of Physics and Astronomy, Stony Brook University

# Neutron stars from an effective quark theory of QCD<sup>†</sup>

T. Tanimoto,<sup>\*1</sup> W. Bentz,<sup>\*1,\*2</sup> and I. C. Cloët<sup>\*3</sup>

The study of neutron star matter has attracted increased attention recently because of the observation of massive neutron stars exceeding two solar masses<sup>1)</sup> and gravitational wave measurements of a binary neutron star merger event.<sup>2)</sup> In this work, we investigate whether a single effective quark theory of QCD which can describe both the structure of free and in-medium hadrons as well as nuclear systems,<sup>3)</sup> can also produce properties for neutron stars which agree with data. For this purpose, we use the two-flavor Nambu-Jona-Lasinio (NJL) model<sup>4)</sup> with the proper-time regularization scheme, which incorporates important aspects of confinement.<sup>3)</sup>

We calculate the effective potentials of nuclear matter (NM) and quark matter (QM) in the mean field approximation as functions of two independent chemical potentials for baryon number and isospin. The Fermi gas of electrons is also included so as to achieve  $\beta$  equilibrium and charge neutrality. Besides the vacuum (Mexican hat shaped) part, the effective potentials contain pieces which describe the Fermi motion of composite nucleons (case of NM) or constituent quarks (case of QM) in scalar and vector mean fields. The description of the nucleon is based on the Faddeev method in the quark-diquark approximation, taking into account both the scalar and axial vector diquark channels. In the QM sector we also take into account the pairing of quarks in the scalar diquark channel, which gives rise to a gap (color superconductivity). We use the Gibbs equilibrium conditions to describe the phase transition from NM to QM with an intermediate mixed phase. The constituent quark mass (scalar mean field), the gap, and the isoscalar- and isovector-vector mean fields are determined self consistently by minimization of the effective potential for fixed chemical potentials.

The model parameters in the single nucleon and NM sector are the same as in Ref. 3). In order to realize a phase transition to QM at reasonable transition densities (between  $2\rho_0$  and  $4\rho_0$ , where  $\rho_0 = 0.16 \text{ fm}^{-3}$ ) with a stable QM component, we found that it is possible to use the same value for the pairing strength in QM as for the scalar diquark interaction in the single nucleon sector, but the vector couplings must be smaller than in NM by a factor of 0.5–0.68. In the results below we use a reduction factor of 0.68 for both isoscalar- and isovector vector couplings in QM.

By using our equation of state as an input to solve the Tolman-Oppenheimer-Volkoff equations, we can calcu-

late the properties of neutron stars. From our results, shown in Figs. 1 and 2, we can conclude that our NJL model description, which has been very successful for single hadrons and nuclear systems, leads to a satisfying scenario also for the phase transition to QM and the resulting properties of neutron stars.

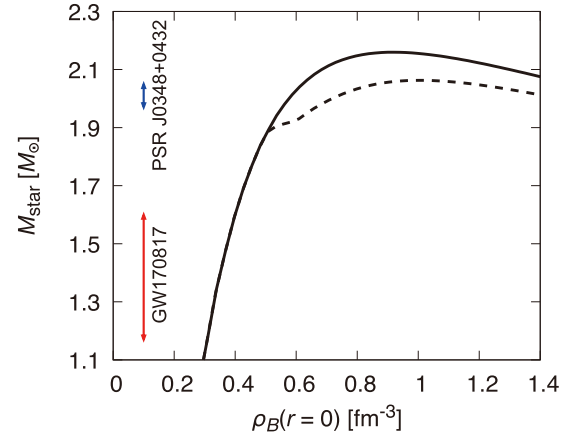


Fig. 1. Neutron star mass vs. central baryon density. The solid line shows the pure NM case, and the dashed line shows a phase transition to QM at about  $3\rho_0$ . PSR J0348 + 0432 and GW170817 indicate the observed values of star masses of Refs. 1–2), respectively.

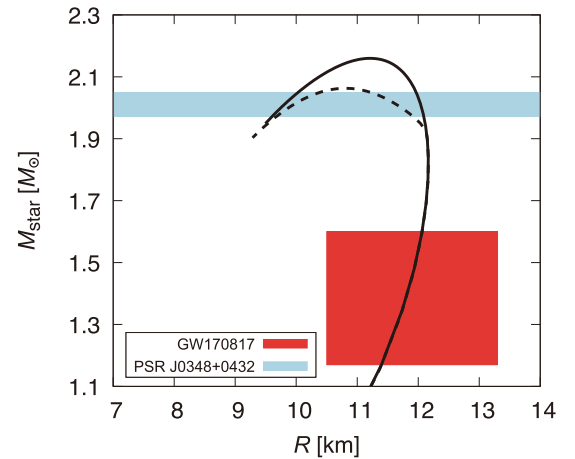


Fig. 2. Mass-radius relation for neutron stars. For explanation of lines and symbols, see the caption to Fig. 1.

## References

- 1) J. Antoniadis *et al.*, *Science* **340**, 6131 (2013).
- 2) B. Abbott *et al.*, (LIGO Scientific, Virgo), *Phys. Rev. Lett.* **119**, 161101 (2017).
- 3) I. C. Cloët, W. Bentz, A. W. Thomas, *Phys. Rev. Lett.* **109**, 182301 (2012).
- 4) Y. Nambu, G. Jona-Lasinio, *Phys. Rev.* **122**, 345 (1961); **124**, 246 (1961).

<sup>†</sup> Condensed from an article by T. Tanimoto *et al.*, to be published in *Phys. Rev. C* (2019).

<sup>\*1</sup> Department of Physics, Tokai University

<sup>\*2</sup> RIKEN Nishina Center

<sup>\*3</sup> Physics Division, Argonne National Laboratory

## **6. Particle Physics**



# Baryon spectrum of an SU(4) composite Higgs theory<sup>†</sup>

E. T. Neil<sup>\*1,\*2</sup> [for the Tel Aviv-Colorado Collaboration]

The possibility that the Higgs boson is not a fundamental scalar, but rather a composite bound state of some new strongly-coupled sector, provides an intriguing scenario for new physics beyond the Standard Model. Current measurements of the properties of the Higgs boson provide only weak constraints on the possible scale of compositeness for the Higgs. If the Higgs is indeed a composite bound state, then there will be an associated spectrum of other new composite particles which may be within discovery reach of the Large Hadron Collider (LHC) or other future colliders. The overall pattern of the spectrum is directly related to the underlying fundamental structure, just as the spectrum of QCD is predicted by the quark masses and the gauge symmetry group SU(3).

The full spectrum of a strongly-coupled gauge theory cannot be predicted by traditional perturbative methods. Instead, lattice simulations can be used to obtain numerical but systematically controlled results for the spectrum of a particular theory. In this work, we chose to study an SU(4) gauge theory proposed as a composite Higgs model by Ferretti.<sup>1)</sup> This model includes two types of fermions, charged under the fundamental **4** and “sextet” two-index antisymmetric **6** representations of SU(4). We have developed a lattice code capable of dealing with fermions in multiple representations, with previous results on the “meson” spectrum<sup>2)</sup> and thermodynamic properties of this theory.<sup>3)</sup>

Composite bound states can be enumerated by classifying all SU(4)-singlet combinations of fermions. Writing the **4** fermions as  $q$  and the **6** fermions as  $Q$ , we can identify bound states such as  $qqqq$  which are direct analogues of the familiar QCD baryons. However, there is an additional baryon-like bound state composed of  $qqQ$  fermions. This “chimera baryon” is especially interesting in the context of the composite Higgs model, in which it has the same quantum numbers as the fundamental top quark. Mixing between the top quark and this top-partner chimera is responsible for the generation of the observed top mass.

Using standard lattice spectroscopy techniques, we compute the mass of the chimera and the other baryon-like states for a range of input fermion masses. The physical limit for the composite Higgs model requires taking the massless limit for the sextet fermions  $m_6 \rightarrow 0$ , but the other fermion mass  $m_4$  remains a free parameter of the model. Figure 1 shows our results for the spectrum versus  $m_4$  with  $1\sigma$  error bands. The units are set in terms of  $F_6$ , the sextet NGB decay constant,

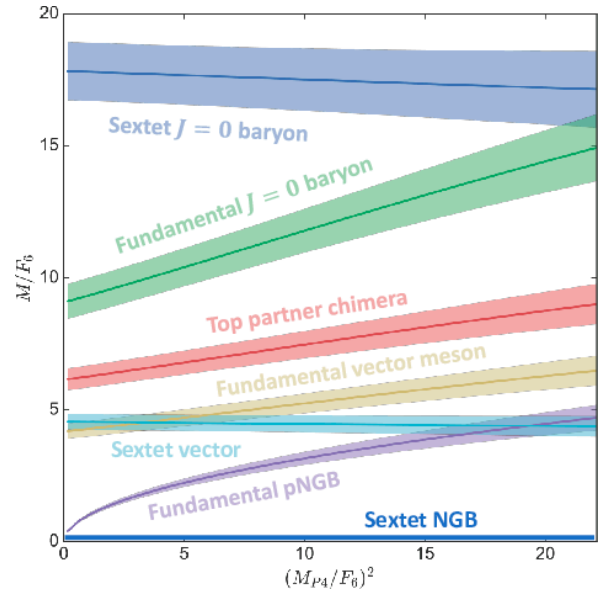


Fig. 1. Spectrum of bound states computed from lattice simulation for SU(4) gauge theory with two Dirac fermions in the **4** and **6** (“sextet”) gauge representations. Bound-state masses (vertical axis) are shown versus the squared fundamental Nambu-Goldstone boson (NGB) mass  $M_{P,4}^2$ , which is proportional to the input fermion mass  $m_4$ , treated as a free parameter. In the context of the composite Higgs model,  $F_6$  is bounded by experiment to be  $F_6 \gtrsim 1$  TeV, so the plot can be read in TeV units. Most bound states are seen to be heavier than 5 TeV for the entire parameter space.

which is related to the Higgs vacuum expectation value; experimental constraints require  $F_6 \gtrsim 1$  TeV, so the plot units are equivalent to TeV scale.

We see that for the full parameter space, all bound states are found to be quite heavy, with masses of order 5 TeV or larger, and thus likely out of the reach of the LHC. However, the fundamental pseudo-Nambu-Goldstone boson (NGB, purple curve) may be within reach for at least part of the parameter space. Future lattice studies will focus on non-perturbative contributions to the Higgs potential in this model, which should greatly constrain the allowed parameters of the model.

## References

- 1) G. Ferretti, JHEP **1406**, 142 (2014).
- 2) V. Ayyar, T. DeGrand, D. C. Hackett, W. I. Jay, E. T. Neil, Y. Shamir, B. Svetitsky, Phys. Rev. D **97**, no. 7, 074505 (2018).
- 3) V. Ayyar, T. DeGrand, D. C. Hackett, W. I. Jay, E. T. Neil, Y. Shamir, B. Svetitsky, Phys. Rev. D **97**, no. 11, 114502 (2018).

<sup>†</sup> Condensed from the article in Phys. Rev. D **97**, no. 11, 114505 (2018)

<sup>\*1</sup> RIKEN Nishina Center

<sup>\*2</sup> Department of Physics, University of Colorado, Boulder

# Updated empirical formulae of the masses of elementary particles

Y. Akiba,\*<sup>1</sup>

	formula	calculated( <i>c</i> )	measured( <i>m</i> )	$ c/m - 1 $
<i>e</i>	$1/(12\pi^2)\epsilon_0^{1/3}(1+(1/4)(1/(6\pi)^2))^{-1}M_{pl}$	0.511002 MeV	$0.510998946 \pm 0.0000000031$ MeV	$5.9 \times 10^{-6}$
$\mu$	$3/2\epsilon_0^{1/3}(1-1/(2\pi)+3/(4\pi)^2)^{-1}M_{pl}$	105.6594 MeV	$105.6583745 \pm 0.0000024$ MeV	$9.6 \times 10^{-6}$
$\tau$	$9\pi\epsilon_0^{1/3}(1-1/(8\pi)+(5/4)(1/(6\pi)^2))^{-1}M_{pl}$	1.77684 GeV	$1.77686 \pm 0.12$ GeV	$1.3 \times 10^{-5}$
<i>t</i>	$8 \times (6\pi)^2\epsilon_0^{1/3}M_{pl}$	172.1 GeV	$173.4 \pm 0.75$ GeV	$7.5 \times 10^{-3}$
<i>c</i>	$12\epsilon_0^{1/3}M_{pl}$	1.24 GeV	$1.28 \pm 0.025$ GeV ( $\overline{\text{MS}}$ at $m_c$ )	$3.4 \times 10^{-2}$
<i>u</i>	$8 \times (6\pi)^{-2}\epsilon_0^{1/3}M_{pl}$	2.07 MeV	$2.15 \pm 0.15$ MeV ( $\overline{\text{MS}}$ at 2 GeV)	$3.8 \times 10^{-2}$
<i>b</i>	$3 \times (6\pi)\epsilon_0^{1/3}(1+1/4\pi+3/(4\pi)^2)^{-1}M_{pl}$	4.18 GeV	$4.18 \pm 0.03$ GeV ( $\overline{\text{MS}}$ at $m_b$ )	$\leq 2 \times 10^{-3}$
<i>s</i>	$\epsilon_0^{1/3}M_{pl}$	91.8 MeV	$93.8 \pm 2.4$ MeV ( $\overline{\text{MS}}$ at 2 GeV)	$2.1 \times 10^{-2}$
<i>d</i>	$(6\pi)^{-1}\epsilon_0^{1/3}(1+1/6\pi)^{-1}M_{pl}$	4.63 MeV	$4.7 \pm 0.2$ MeV ( $\overline{\text{MS}}$ at 2 GeV)	$1.5 \times 10^{-2}$
<i>Z</i>	$1/(8\pi^2)\epsilon_0^{1/4}(1+1/12(1/(6\pi))+1/12(1/(6\pi)^2))^{-1/2}M_{pl}$	91.1862 GeV	$91.1876 \pm 0.0021$ GeV	$1.5 \times 10^{-5}$
<i>W</i>	$2^{-1/4}/(8\pi^2)\epsilon_0^{1/4}(1-1/(4\pi)-2/(4\pi)^2)^{-1/2}M_{pl}$	80.387 GeV	$80.385 \pm 0.015$ GeV	$2.5 \times 10^{-5}$
<i>H</i>	$2^{1/2}/(8\pi^2)\epsilon_0^{1/4}(1+1/(4\pi)+1/(4\pi)^2)^{-1/2}M_{pl}$	125.14 GeV	$125.1 \pm 0.2$ GeV	$3.8 \times 10^{-4}$

In my article in APR2017<sup>1)</sup> I reported empirical formulae of the masses of charged leptons (*e*,  $\mu$ ,  $\tau$ ), quarks (*t*, *c*, *u*, *b*, *s*, *d*), gauge bosons (*Z*, *W*), and Higgs boson (*H*). The formulae yield the masses in terms of the Planck mass  $M_{pl}$  and a dimensionless constant  $\epsilon_0 = 2 \times (6\pi)^{-48}$ . There is no adjustable parameter in the formulae. Note that the value of  $\epsilon_0$  is consistent with the product of the Hubble constant  $H_0$  and the Planck time  $t_{pl} = 1/M_{pl}$ :

$$H_0 \times t_{pl} = (1.211 \pm 0.014) \times 10^{-61},$$

$$\epsilon_0 \equiv 2 \times (6\pi)^{-48} = 1.220608 \times 10^{-61}.$$

Here, the WMAP nine-year value of  $H_0$  is used. This suggests that the masses of elementary particles are related to the expansion of space-time.

Here, I report a small update of the formulae for *b* and *d* quarks and *Z*, *W*, *H* bosons. The revised formulae have better agreement with the data.

The mass values calculated using the formulae are compared with the measured ones. For the calculation, the value of Planck mass from CODATA<sup>2)</sup> is used:

$$M_{pl} = 1.220910 \pm 0.000029 \times 10^{19} \text{ GeV}.$$

The measured values of the particle masses are taken from PDG2016.<sup>3)</sup> In QCD, the mass of a quark is dependent on the scale and the scheme. In the PDG review, the mass of quarks other than the *t* quark are given in the  $\overline{\text{MS}}$  scheme at  $\mu = 2$  GeV for the *u*, *d*, *s* quarks and at  $\mu = m_q$  for the *b* and *c* quarks. For the *t* quark, the measured mass is considered to be the pole mass. The formula for a quark is assumed to yield the  $\overline{\text{MS}}$  mass at the *Z* boson mass  $m_Z$ . The first-order renormalization group equation (RGE) given below is used to correct for the mass value at the scale  $m_Z$  to the mass at the scale the PDG uses:

$$\frac{m(t)}{m_0} = \exp\left(-\int \frac{\alpha_s(t)}{\pi} dt\right),$$

where  $t = \log \mu^2$  and  $\alpha_s(t)$  is the running QCD coupling constant at the scale  $\mu$ . The value of  $\alpha_s(t)$  in the PDG2016 review is used for the calculation.

The formulae, calculated values (*c*) using the formulae, measured values (*m*), and difference  $|c/m - 1|$  are summarized in the table above. The calculations reproduce the measured mass values well.

The agreement is within the uncertainty of the measured mass or the Planck mass ( $2.4 \times 10^{-5}$ ). There is a pattern in the formulae. The formulae can be summarized as

$$m_f = \frac{1}{2}N_f(6\pi)^{n_f}\epsilon_0^{1/3}(1+\delta_l)^{-1}M_{pl},$$

$$m_B = \frac{2^{c_B}}{8\pi^2}\epsilon_0^{1/4}(1+\delta_B)^{-1}M_{pl},$$

where  $m_f$  and  $m_B$  are the masses of charged fermions (leptons and quarks) and bosons, respectively.  $N_f$  are small positive integers,  $n_f$  are integers ranging from  $-2$  to  $2$ , and  $\delta_l$  and  $\delta_B$  are small real numbers.  $c_Z = 0$ ,  $c_W = -1/4$ , and  $c_H = 1/2$ . The pattern suggests the existence of a rule that determines the formulae. Note that all fermion masses are of order of  $(6\pi)^{n_f}\epsilon_0^{1/3}$  with  $-2 \leq n_f \leq 2$  and the boson masses are of the order of  $1/8\pi^2\epsilon_0^{1/4}$ . Presumably, this part is the main part of the mass, and  $(1+\delta_l)$  and  $(1+\delta_B)$  are the correction factors due to interactions.

A model to explain these formulae is reported in a separate article.<sup>4)</sup>

## References

- 1) Y. Akiba, RIKEN Accel. Prog. Rep. **51** (2017).
- 2) P. J. Mohr *et al.*, Rev. Mod. Phys. **88**, 035009 (2016).
- 3) C. Patrignani *et al.* (Particle Data Group), Chin. Phys. C **40**, 100001 (2016).
- 4) Y. Akiba, RIKEN Accel. Prog. Rep. **52** (2018).

\*<sup>1</sup> RIKEN Nishina Center

# A model of the empirical mass formulae of elementary particles

Y. Akiba\*1

In the preceding article<sup>1)</sup> empirical formulae of the masses of charged leptons ( $e, \mu, \tau$ ), quarks ( $t, c, u, b, s, d$ ), and gauge and Higgs bosons ( $Z, W, H$ ) are presented. Here I report a model that can produce these mass formulae.

In the model, there is the minimum duration of time, which is the Planck time  $\tau_{pl} = 1/M_{pl} = 5.3912 \times 10^{-44}$  sec. A term of the action (integral of Lagrangian) of a particle is a wedge product of 48 ‘‘primordial actions’’ (PAs) that are selected from the following 64 PAs:

$$S_{PA} = \left\{ \frac{1}{6\pi} I^\mu \sigma^\nu \tau^a, \frac{1}{6\pi} \varepsilon i, \frac{1}{6\pi} \varepsilon \tau^3, \frac{1}{6\pi} \varepsilon I^c \tau^3, \right. \\ \left. -\frac{1}{2\pi} I^c, -\frac{1}{2\pi} \varepsilon i, i, I^c, -\varepsilon, \varepsilon, 1 \right\}.$$

The wedge product operator  $\wedge$  and orientation operator (sign operator)  $\varepsilon$  have the following reduction rules:

$$\hat{\alpha} \wedge \hat{\beta} = \begin{cases} \hat{\alpha}\hat{\beta} & (\hat{\alpha}\hat{\beta} = -\hat{\beta}\hat{\alpha}) \\ 0 & (\hat{\alpha}\hat{\beta} = \hat{\beta}\hat{\alpha}), \end{cases}$$

$$\hat{\alpha}\hat{\beta}\hat{\gamma} \wedge \hat{\gamma} = \begin{cases} \hat{\alpha}\hat{\beta}\hat{\gamma} & (\hat{\alpha}\hat{\beta} = -\hat{\beta}\hat{\alpha}, \hat{\beta}\hat{\gamma} = -\hat{\gamma}\hat{\beta}, \hat{\gamma}\hat{\alpha} = -\hat{\alpha}\hat{\gamma}) \\ 0 & (\text{otherwise}), \end{cases}$$

$$s \wedge \hat{\alpha} = s\hat{\alpha}, s_1 \wedge s_2 = 0, \hat{\alpha} \wedge s \wedge \hat{\beta} = s\hat{\alpha}\hat{\beta},$$

$$(\varepsilon \wedge)^n = 2^n.$$

Here,  $s$  is scalar. Following these rules, a 48 wedge product of PAs,  $dS = \hat{s}_{i_1} \wedge \cdots \wedge \hat{s}_{i_{48}}$ , is reduced to

a reduced value in the form of  $\pm m(6\pi)^n i^s (\tau^3)^{s'} \epsilon_0$ , where  $\epsilon_0 = 2 \times (6\pi)^{-48}$ ,  $s \in \{0, 1\}$ ,  $s' \in \{0, 1\}$ , and  $m, n (0 \leq n \leq 4)$  are integers. The values of  $s, s', n$ , and  $m$  are determined by the selection of the subset  $\{\hat{s}_1, \cdots, \hat{s}_{48}\}$  from  $S_{PA}$ . The reduced values of 48 wedge products of PAs that correspond to the actions of charged leptons ( $e, \mu, \tau$ ), neutrinos ( $\nu_1, \nu_2, \nu_3$ ), quarks ( $u, c, t, d, s, b$ ), and bosons ( $Z, W, H$ ) are summarized in Table 1. In the table,  $U$  and  $D$  stand for  $U$ -type and  $D$ -type quarks, respectively, when their mass is ignored.

The mass of particles can be obtained from this table. In the below, I shows how the mass formula of the electron can be obtained from the table as an example.

The action of the electron is

$$dS_e = 4(6\pi)^2 i \epsilon_0 \tau^3 + i \epsilon_0 i \tau^3 + 3\epsilon_0.$$

Each term of the action can then be written as a product of the following ‘‘operators’’:

$$\hat{d}_{16} = \epsilon_0^{1/3} (1 + i\sigma^1 + i\sigma^2 + i\sigma^3), \\ \hat{\psi}_{15} = |\psi_{15}| \tau^2 (u_1^2 \sigma^1 + u_2^2 \sigma^2 + u_3^2 \sigma^3), \\ \hat{\psi}_{15}^\dagger = |\psi_{15}| \tau^1 (u_1^1 \sigma^1 + u_2^1 \sigma^2 + u_3^1 \sigma^3), \\ \hat{A}_{18} = (6\pi)^{-2} \epsilon_0^{1/3} (1 + i\sigma^1 + i\sigma^2 + i\sigma^3).$$

Here,  $|\psi_{15}| = (6\pi)\epsilon_0^{1/3}$  and the vectors  $u^1 = (u_1^1, u_2^1, u_3^1)$  and  $u^2 = (u_1^2, u_2^2, u_3^2)$  satisfy  $u^1 \times u^2 = (-1, -1, -1)$  and  $u^1 \cdot u^2 = 1$ . The operators  $i\hat{d}_{16}$  and  $\hat{\psi}_{15}$  correspond to the differential operator  $i\sigma^\mu \partial_\mu$  and the electron field operator, and  $\hat{\psi}_{15}^\dagger$  corresponds to its conjugate. One can show that

$$i\hat{d}_{16} \hat{\psi}_{15}^\dagger \hat{\psi}_{15} = 4(6\pi)^2 \epsilon_0 i \tau^3, \\ \hat{A}_{18} \wedge \hat{\psi}_{15}^\dagger \hat{\psi}_{15} = \epsilon_0 i \tau^3, \\ \mu_e^0 |\psi_{15}|^2 = 3\epsilon_0.$$

Here,  $\mu_e^0 = (12\pi^2)^{-1} \epsilon_0^{1/3}$ . The terms  $4(6\pi)^2 \epsilon_0 i \tau^3$ ,  $\epsilon_0 i \tau^3$ , and  $3\epsilon_0$  correspond to the kinetic, the EM interaction, and the mass term, respectively. From these relations, the mass formula of the electron can be determined.

$$dS_e = \left( 1 + \frac{1}{4} \frac{1}{(6\pi)^2} \right) \left( i\hat{d}_{16} \hat{\psi}_{15}^\dagger \hat{\psi}_{15} + \mu_e |\psi_{15}|^2 \right), \\ \mu_e = \left( 1 + \frac{1}{4} \frac{1}{(6\pi)^2} \right)^{-1} \frac{1}{12\pi^2} \epsilon_0^{1/3}.$$

Similarly, the mass formulae of  $\mu, \tau, \nu_1, \nu_2, \nu_3, u, d, s, c, b, t, Z, W$ , and  $H$  can be obtained from each row in the Table 1.

Reference

1) Y. Akiba, RIKEN Accel. Prog. Rep. **52** (2018).

Table 1. The action of particles per Planck Time.

	$(6\pi)^2 \epsilon_0$		$(6\pi) \epsilon_0$		$\epsilon_0$	
	$i\tau^3$	$i\tau^3$	$i$	$\tau^3$	$i\tau^3$	$i$
$e$	4				1	3
$\mu$	4	-12			27	3
$\tau$	4	-3	3		1+4	
$\nu_1$	-12	-12				-2
$\nu_2$	4		-4			2
$\nu_3$	-12	-12		$\pm 2$		
$U$	-12				$\pm 2$	
$u$	-4					$\pm 8$
$c$	-4					$\pm 24$
$t$	-4					$\pm 8$
$D$	-12				1	
$d$	-12	-12	3			
$s$	-12					3
$b$	4	6	3		27	18
$Z$	12	1			1	18
$H$	4	6				$\pm 18$
$W$	12		18		27	18

\*1 RIKEN Nishina Center



## **7. Astrophysics and Astro-Glaciology**



# High-sensitivity sulfur isotopic measurements for Antarctic ice core analyses<sup>†</sup>

K. Takahashi,<sup>\*1</sup> Y. Motizuki,<sup>\*1</sup> and Y. Nakai<sup>\*1</sup>

Sulfur isotopic measurements have been widely applied in earth sciences to investigate the origin and behavior of sulfur compounds in the lithosphere, hydrosphere, and atmosphere. Recently, sulfur isotopic analyses have also been utilized to elucidate the origin and circulation of various materials in nature in order to develop various scientific research fields, such as environmental, biological, archaeological, and so on.<sup>1,2)</sup> Sulfur isotopic compositions are reported as per mil (‰) variations relative to a standard material (typically Vienna Canyon Diablo Troilite, VCDT) as follows:

$$\delta^{34}\text{S} = \left( \frac{{}^{34}\text{S}}{{}^{32}\text{S}} \right)_{\text{sample}} / \left( \frac{{}^{34}\text{S}}{{}^{32}\text{S}} \right)_{\text{standard}} - 1$$

In Antarctic ice and snow samples, it is considered that the sulfur isotopic ratios reflect the origin and pathway of sulfur compounds from their precursor materials, thus indicating the Antarctic environmental (hydrospheric and atmospheric) conditions. Sulfate and methane-sulfonic acids are the main sulfur components in ice and snow samples, and the sulfate ion is particularly dominant among those species. Several studies have examined the origins and geochemical implications of sulfates based on the sulfur isotopic composition of Antarctic ice and snow samples. Several studies<sup>3,4)</sup> have analyzed the sulfur isotopic compositions of surface snow to investigate the origin of sulfate aerosols and their alteration during transport from coastal areas to the Antarctic interior. Sulfur isotopic compositions in ice cores elucidate the paleo-climatic changes: Cole-Dai *et al.*<sup>5)</sup> and Baroni *et al.*<sup>6)</sup> measured the sulfur isotopic compositions of ice core samples influenced by large volcanic eruptions (*e.g.* Pinatubo, Tambora) to investigate the origin and isotopic fractionation of sulfates during their transport through the stratosphere. In those studies, more than 200 g (containing more than 150 nmol sulfate) samples were required to obtain sulfur isotopic ( $\delta^{34}\text{S}$ ) data.

We developed a high-sensitivity sulfur isotopic ( $\delta^{34}\text{S}$ ) analytical system equipped with an elemental analyzer, a cryo-flow device, and an isotope ratio mass spectrometer, and established a measurement and calibration procedure. Using this system, we precisely measured the sulfur isotopic ratio ( $\delta^{34}\text{S}$ ) of samples containing 5–40 nmol sulfate. Test runs were performed on samples from the Antarctic shallow ice core DF01. Figure 1 shows the depth profiles of the sulfate concentration and the sulfur isotopic ratio ( $\delta^{34}\text{S}$ ) for the samples taken from DF01 at a depth of 8.49 to 9.39 m. The sample taken from a depth of 8.79 m depth is regarded as

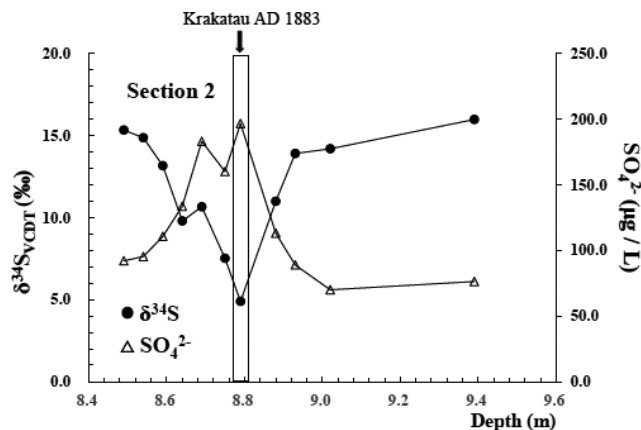


Fig. 1.  $\delta^{34}\text{S}$  (solid circles) and sulfate concentration (open triangles) depth profiles for the two analyzed sections from ice core DF01. The minimum  $\delta^{34}\text{S}$  value and the peak sulfate concentration at 8.79 m depth in section 2 are considered to be due to the AD 1883 eruption of the Krakatau volcano.

corresponding in time to the AD 1883 eruption of the Krakatau volcano. As shown in Fig. 1, it showed a peak sulfate concentration in its depth profile, which is considered to have resulted from a large volcanic eruption. The  $\delta^{34}\text{S}$  value obtained at that depth in the sample was distinct from the values at other depths and consistent with the reported values for volcanic sulfates. The analytical system developed herein is a powerful tool for trace sulfur isotopic analyses. The results obtained from the DF01 ice core samples are the first step towards elucidating high-time-resolution (less than one year) paleo-environmental changes through sulfur isotopic analyses. Furthermore, the other analyses method shown in this study can be applied not only to the analyses of ice core samples, but also to other analyses, such as the analysis of tree rings,<sup>2)</sup> which require small-scale analyses. Therefore, this measurement system is expected to be widely applicable to sulfur isotopic analyses in environmental and geochemical sciences.

## References

- 1) F. Fourrel *et al.*, Proc. Earth Planetary Science **13**, 232 (2015).
- 2) P. M. Wynn *et al.*, Biochemistry **114**, 255 (2013).
- 3) R. Uemura *et al.*, Geophys. Res. Lett. **43**, (11), 5878 (2016).
- 4) N. Akata *et al.*, Seppyo **73**, (5), 339 (2011).
- 5) J. Cole-Dai *et al.*, Geophys. Res. Lett. **36**, (22), L22703 (2009).
- 6) M. Baroni *et al.*, Science **315**, 84 (2007).

<sup>†</sup> Condensed from the article in Rapid. Comm. Mass. **32**, 1911 (2018)

<sup>\*1</sup> RIKEN Nishina Center

# Mass Measurements with the Rare-RI Ring for the $A = 130$ r-process Abundance Peak

S. Naimi,<sup>\*1</sup> H. F. Li,<sup>\*1,\*2</sup> Y. Abe,<sup>\*1</sup> Y. Yamaguchi,<sup>\*1</sup> D. Nagae,<sup>\*1</sup> F. Suzaki,<sup>\*1</sup> M. Wakasugi,<sup>\*1</sup> H. Arakawa,<sup>\*3</sup> W. B. Dou,<sup>\*3</sup> D. Hamakawa,<sup>\*3</sup> S. Hosoi,<sup>\*3</sup> Y. Inada,<sup>\*3</sup> K. Inomata,<sup>\*3</sup> D. Kajiki,<sup>\*3</sup> T. Kobayashi,<sup>\*3</sup> M. Sakaue,<sup>\*3</sup> K. Yokoya,<sup>\*3</sup> T. Yamaguchi,<sup>\*3</sup> R. Kagesawa,<sup>\*4</sup> D. Kamioka,<sup>\*4</sup> T. Moriguchi,<sup>\*4</sup> M. Mukai,<sup>\*4</sup> A. Ozawa,<sup>\*4</sup> S. Ota,<sup>\*5</sup> N. Kitamura,<sup>\*5</sup> S. Masuaoka,<sup>\*5</sup> S. Michimasa,<sup>\*5</sup> D. S. Ahn,<sup>\*1</sup> H. Baba,<sup>\*1</sup> N. Fukuda,<sup>\*1</sup> Y. Shimizu,<sup>\*1</sup> H. Suzuki,<sup>\*1</sup> H. Takeda,<sup>\*1</sup> C. Y. Fu,<sup>\*2</sup> Z. Ge,<sup>\*1,\*2</sup> S. Suzuki,<sup>\*2</sup> Q. Wang,<sup>\*2</sup> M. Wang,<sup>\*2</sup> Yu. A. Litvinov,<sup>\*6</sup> G. Lorusso,<sup>\*7</sup> and T. Uesaka<sup>\*1</sup>

In the fall of 2018, we have conducted an experiment at the Rare-RI Ring (R3) to measure masses of nuclei in the south-west region of  $^{132}\text{Sn}$ . As it has been shown from sensitivity studies<sup>1)</sup> masses of nuclei in the region around  $N = 82$  has the most significant impact on the  $A = 130$  r-process abundance peak. We have measured masses of the most exotic nuclei approaching  $N = 82$ , namely  $^{122}\text{Rh}$ ,  $^{123,124}\text{Pd}$  and  $^{125}\text{Ag}$  isotopes.

Particles of interest were produced at RIBF by impinging a 40-pnA Uranium beam on a 5-mm thick Be target. Particles were identified at BigRIPS by energy loss in an Ionization Chamber (IC) placed at F3 and their Time-of-Flight (ToF) from F3 to F5. After injection into the R3 and storage for about 1 ms, equivalent to almost 2000 turns, the particles were extracted. Figure 1 shows the PID at F3 of all events a BigRIPS in yellow and extracted events after R3 shown in pink.

The mass will be determined from the total time-of-flight in the storage ring and a velocity correction. The mass determination of a particle with  $m_1/q_1$  requires also a reference particle with known mass  $m_0/q_0$

$$\frac{m_1}{q_1} = \frac{m_0}{q_0} \frac{T_1}{T_0} \sqrt{\frac{1 - \beta_1^2}{1 - (\frac{T_1}{T_0} \beta_1)^2}}, \quad (1)$$

with  $\beta_1$  being the particle of interest velocity that is measured along the beamline before injection. The time-of-flight of the reference particle  $T_0$  and particle of interest  $T_1$  inside the ring are determined by a procedure detailed elsewhere.<sup>2)</sup>

Table 1. Preliminary total events extracted after the ring.

Isotope	Events	Isotope	Events
$^{127}\text{Sn}$	104	$^{128}\text{Sn}$	178
$^{126}\text{In}$	287	$^{127}\text{In}$	157
$^{125}\text{Cd}$	140	$^{126}\text{Cd}$	4965
$^{124}\text{Ag}$	1261	$^{125}\text{Ag}$	406
$^{123}\text{Pd}$	122	$^{124}\text{Pd}$	11
$^{122}\text{Rh}$	2		

<sup>\*1</sup> RIKEN Nishina Center

<sup>\*2</sup> IMP, CAS, China

<sup>\*3</sup> Department of Physics, Saitama University

<sup>\*4</sup> Department of Physics, University of Tsukuba

<sup>\*5</sup> CNS, University of Tokyo

<sup>\*6</sup> GSI Helmholtz Center, Darmstadt, Germany

<sup>\*7</sup> NPL, University of Surrey

In Table 1, we show the number of extracted events preliminarily confirmed with the PID. The overall extraction efficiency was lower than expected and was less than 1% for the reference particle. The data analysis is being carried out.

In the future we aim at studying even more exotic, relevant nuclides in this region.

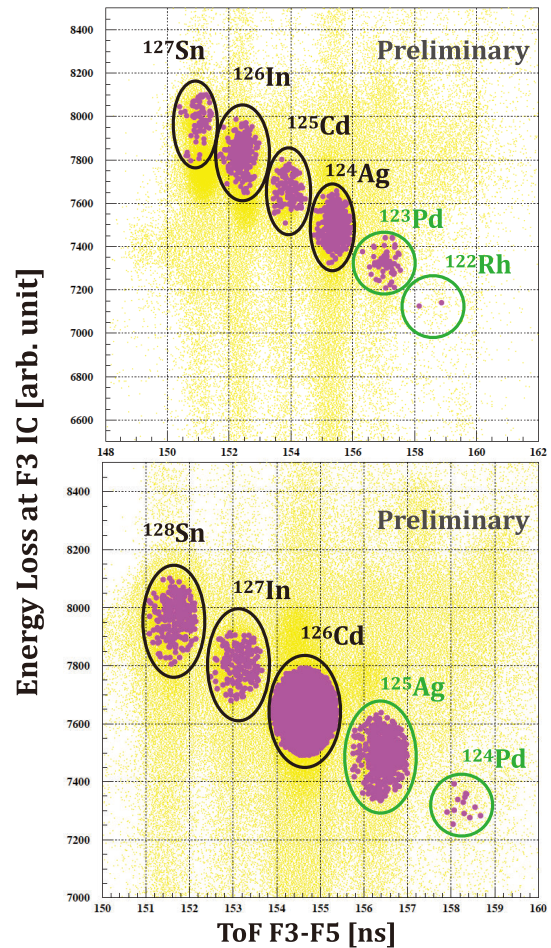


Fig. 1. Particle Identification (PID) showing the energy loss in the Ionization Chamber (IC) at F3 and ToF from F3 to F5. In yellow are shown events at BigRIPS and in pink are shown extracted events after R3. Particles of interested are labeled in green, while reference particles are labeled in black.

## References

- 1) M. Mumpower *et al.*, J. Phys. G **42**, 034027, (2015).
- 2) H. Li *et al.*, in this report.

## **8. Accelerator**



## Construction of New 28-GHz ECR ion source for RILAC

T. Nagatomo,<sup>\*1</sup> Y. Higurashi,<sup>\*1</sup> J. Ohnishi,<sup>\*1</sup> A. Uchiyama,<sup>\*1</sup> K. Kumagai,<sup>\*1</sup> M. Fujimaki,<sup>\*1</sup> T. Nakagawa,<sup>\*1</sup>  
T. Ohki,<sup>\*2</sup> M. Tamura,<sup>\*2</sup> K. Kaneko,<sup>\*2</sup> K. Oyamada,<sup>\*2</sup> A. Yusa,<sup>\*2</sup> H. Yamauchi,<sup>\*2</sup> and O. Kamigaito<sup>\*1</sup>

Since 2017, we have been upgrading the RIKEN linear accelerator RILAC for the RIBF project<sup>1)</sup> and to synthesize new super-heavy elements (SHEs) with atomic number  $Z \geq 119$ . In the upgrade,<sup>2)</sup> some of the latter acceleration cavities of RILAC were planned to be replaced with superconducting quarter-wavelength resonators (SC-QWRs) to increase the energy of the beam with  $M/Q = 6$  from 5 MeV/nucleon to 6 MeV/nucleon for the synthesis of SHEs. In the SHE project, the high intense metallic ion beams, such as Va and Cr ( $> 10$  particle  $\mu\text{A}$ ), are required from the ion source. In addition, because the SC-QWRs are driven by the fixed frequency, these SC-QWRs are skipped in the variable frequency operation especially for the RIBF project. Thus, high-intensity ion beams with a higher charge than before. For example,  $\text{Ca}^{16+}$  beam of  $\sim 100$  electric  $\mu\text{A}$  is required to achieve enough energy without the SC-QWRs to meet the variable frequency acceleration scheme of RIBF. To meet these requirements, we decided to construct a new electron cyclotron resonance ion source that consists of fully superconducting mirror magnets (SC-ECRIS) with a high-power 28 GHz gyrotron microwave generator.

Figure 1 shows the current status of the new 28 GHz SC-ECRIS and gyrotron microwave generator with low energy beam transport (LEBT) constructed in the injection room of the RILAC accelerator building. The SC-ECRIS and microwave generator are the same models as the uranium ion source of RILAC II, which is predominantly used for RIBF project (for details, please see the references).<sup>3-5)</sup> The new SC-ECRIS is designed to be operated with 18 and 28 GHz microwaves. In Fig. 1, the LEBT following the ECRIS consists of a solenoidal lens, an analyzing magnet sandwiched by two steering magnets, a diagnostics chamber, and another solenoidal lens. In the diagnostics chamber, a Faraday cup and a pepper-pot type emittance meter (PPEM) were installed. The  $^{40}\text{Ar}^{11+}$  beam of  $\sim 90$  electric  $\mu\text{A}$  was successfully extracted from the new SC-ECRIS as the first beam with the 18 GHz microwave because the 28 GHz microwave generator was not ready at that time. Figure 2 shows the beam profile ( $x$ - $y$  plot) and horizontal emittance ( $x$ - $x'$  plot) of  $^{40}\text{Ar}^{11+}$  beam with the 18 GHz microwave of 700 W using the PPEM. In Fig. 2, the beam has a characteristic triangular hollow shape with widely spread emittance along the horizontal. The triangular shape is formed by the hexapolar magnetic field of the mirror field of ECRIS and the ions are localized into three peripheral regions in the beam. By selecting one of the three intense regions in the  $x$ -

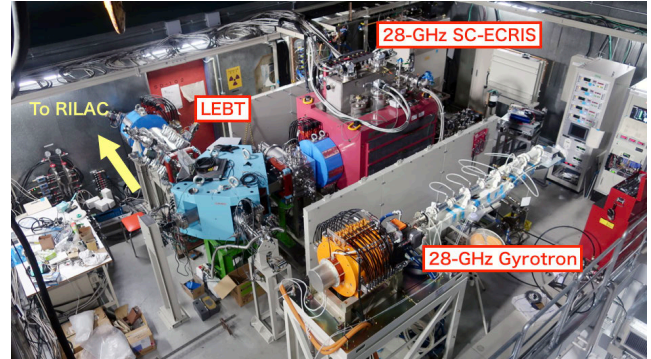


Fig. 1. New 28 GHz SC-ECRIS and LEBT.

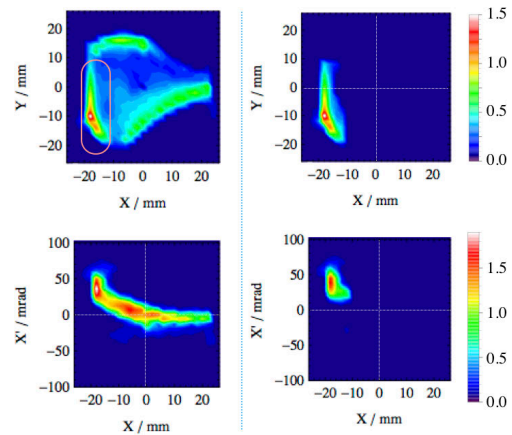


Fig. 2. Obtained beam profile (upper) and horizontal emittance (lower) of  $^{40}\text{Ar}^{11+}$  beam using PPEM. Color indicates the beam intensity in the arbitrary unit.

$y$  space as a red rectangle in the left of Fig. 2, it is found that the localization in the emittance space also appears as shown in the right of Fig. 2. From the result, we can effectively increase the beam brightness, which is defined as the beam intensity per unit emittance, by suitable spatial selection of the localized beam using a combination of slits and steering magnets.

We plan to finish the preparations for the 28 GHz microwave generator and high temperature oven to generate metallic vapor in the first half of 2019.

### References

- 1) Y. Yano, Nucl. Instrum. Methods Phys. Res. B **261**, 1009 (2007).
- 2) O. Kamigaito *et al.*, Proceedings of IPAC2016, Busan, Korea, 1281 (2016).
- 3) T. Nakagawa *et al.*, Rev. Sci. Instrum. **81**, 02A320 (2010).
- 4) Y. Higurashi *et al.*, Rev. Sci. Instrum. **85**, 02A953 (2014).
- 5) G. D. Alton *et al.*, Rev. Sci. Instrum. **65**, 775 (1994).

<sup>\*1</sup> RIKEN Nishina Center

<sup>\*2</sup> SHI Accelerator Service Ltd.

## Development of prototype superconducting linac for low-beta ions

N. Sakamoto,<sup>\*1</sup> O. Kamigaito,<sup>\*1</sup> K. Ozeki,<sup>\*1</sup> K. Suda,<sup>\*1</sup> Y. Watanabe,<sup>\*1</sup> and K. Yamada<sup>\*1</sup>

Since 2015, the accelerator group of Nishina Center has joined the ImPACT program, led by Dr. Fujita, to develop a system for processing the so-called long-lived fission products (LLFPs) via nuclear reactions and transmutations induced by ion beams provided by a particle accelerator.<sup>1)</sup> As a part of this program, a prototype superconducting (SC) linac has been developed. The main purpose of this prototype is to realize a high acceleration field gradient  $E_{acc}$  with a high performance SC-cavity (high- $Q_0$ ) and a spatially efficient cryomodule. The cryomodule is the main component of SC-linac, which comprises 4 K SC-cavities. Finally, we tried to evaluate its stability and reliability using the prototype cryomodule.

The prototype cryomodule (Fig. 1) consists of one SC-cavity, one dummy cavity and a vacuum vessel equipped with a thermal shield. The length of the cryomodule was designed as 1.34 m. The SC-cavity, whose beam ports are connected with bellow pipes and are equipped with a power coupler, is supported by four hollow pillars made of GFRP. To minimize heat conduction from the room temperature part to the 4 K cold part, a thermal shield is installed between the room temperature part and the 4 K cold part. The thermal shield provides thermal anchors to the beam pipes, the power couplers, and the cavity supports.

The developed SC-cavity was based on the structure of a quarter-wave resonator (QWR) (See Fig. 1) with optimum  $\beta$  as low as 0.08 and a resonant frequency of 75.5 MHz, which can be changed up to 5 kHz with a mechanical tuner. The planned operating  $E_{acc}$  is 4.5 MV/m with a  $Q_0$  of  $8.9 \times 10^8$ , which is estimated by using the 3D simulation package Micro Wave Studio (MWS).<sup>2)</sup> Note that  $Q_0$  is defined as the ratio of its stored energy to the

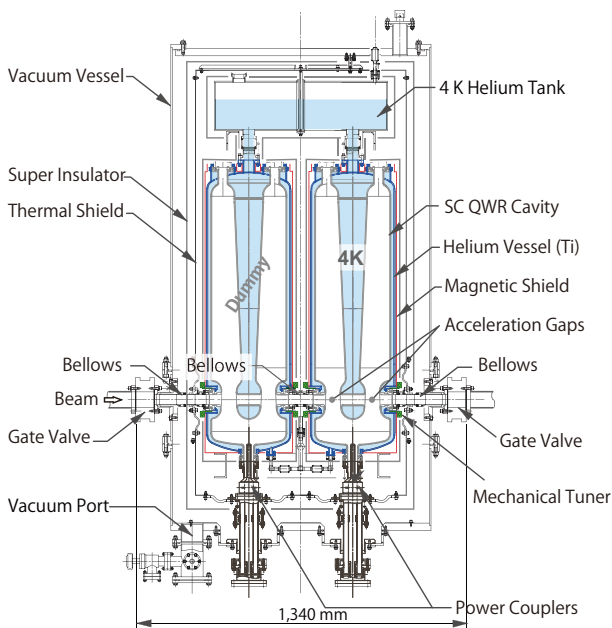


Fig. 1. Schematic of the prototype cryomodule.

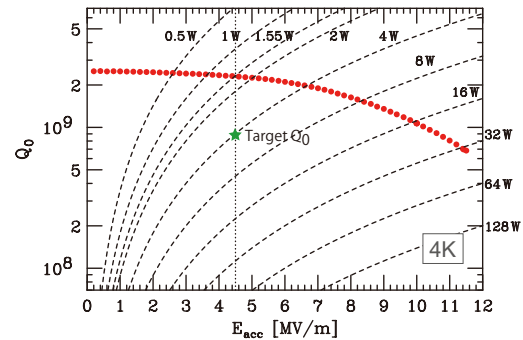


Fig. 2. Measured  $Q_0$  plotted as a function of  $E_{acc}$ . The dashed lines indicate contours of the wall loss.

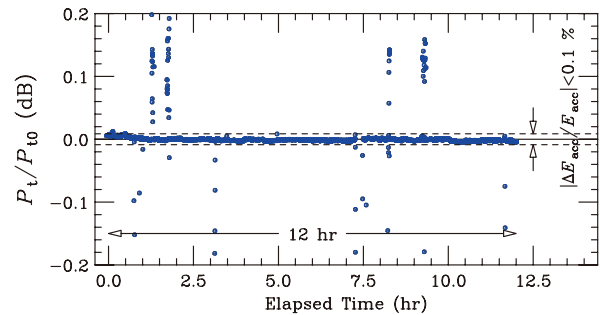


Fig. 3. Power level of the pickup signal ( $P_t/P_{t0}$ ) from the SC-cavity during the long-term operation test.

wall loss of the cavity. The SC-QWR cavity was fabricated using pure niobium sheets.  $Q_0$  was measured by an RF (radio frequency) test, cooling the bulk SC-cavity to 4 K with liquid helium. Extensive study of surface treatment was performed<sup>3)</sup> and a  $Q_0$  of  $2.3 \times 10^9$  was achieved at an  $E_{acc}$  of 4.5 MV/m (Fig. 2).

After integration of the SC-cavity to the prototype cryomodule, a long-term operation test was successfully performed. A solid state amplifier with a maximum output power of 4.5 kW and a digital feedback module have been developed, which excite the SC-cavity with an external  $Q$  of  $1 \times 10^6$ . In the feedback loop, the amplitude of  $E_{acc}$  was limited by an RF limiter and its phase was locked to the reference signal provided by the external signal generator. The amplitude and phase errors were 0.1% and 1 degree, respectively. In Fig. 3, the deviation of the power level of the pickup signal ( $P_t/P_{t0}$ ) was plotted as a function of the elapsed time during the 12 hr operation test at an  $E_{acc}$  of 4.75 MV/m. The reliability with a criteria of  $|\Delta E_{acc}/E_{acc}| \leq 0.1\%$ , was evaluated as 95%. This can be improved by tuning the tuner control.

This research work was funded by the ImPACT Program of the Japan Council for Science, Technology and Innovation (Cabinet Office, Government of Japan).

### References

- 1) <http://www.jst.go.jp/impact/en/program/08.html>.
- 2) <http://www.cst.com>.
- 3) N. Sakamoto *et al.*, SRF2017, WEYA01; K. Yamada *et al.*, PASJ 14th Annual Meeting, TUOL02.

<sup>\*1</sup> RIKEN Nishina Center

# Performance test of bulk-niobium cavities for new superconducting linear accelerators

K. Yamada,<sup>\*1</sup> K. Ozeki,<sup>\*1</sup> N. Sakamoto,<sup>\*1</sup> K. Suda,<sup>\*1</sup> and O. Kamigaito<sup>\*1</sup>

In order to upgrade the beam intensity and energy of the RIKEN Linear Accelerator (RILAC),<sup>1)</sup> an upgrade project of the RILAC is now ongoing. The beam intensity is increased by the newly built 28 GHz superconducting (SC) ECR ion source,<sup>2)</sup> and the beam energy is boosted over 6.5 MeV/nucleon for ions with mass to charge ratio of 6 by the new SC linear accelerator (SRILAC).<sup>3)</sup> The SRILAC consists of three cryomodules including ten SC quarter-wavelength resonators (QWRs) with a resonant frequency of 73 MHz. The SC-QWRs are made of bulk niobium and kept at 4.2 K by using a large liquid-helium refrigerator.

In order to test the performance of SC-QWRs in the SC state, a test stand was prepared at RIKEN based on the test stand at KEK.<sup>4)</sup> We drilled a hole in the floor and installed a cryostat with an inner diameter of 700 mm and a depth of 3240 mm. A magnetic shield was put into the cryostat to prevent the penetration of geomagnetism and achieved a value of less than 10 mGauss. The SC-QWR to be tested is suspended from a flange and stored in the cryostat as shown in Fig. 1. Liquid helium is poured into the cryostat until the cavity is submerged, and the SC-QWR is tested by applying RF power. X-rays may be generated at high voltage by factors such as field emission of electrons, and the test stand is structured to be covered with an iron shield. The validity of the new test stand was confirmed by comparing the test result of a 73 MHz prototype SC-QWR carried out in the RIKEN and the KEK.

The performance test of actual SC-QWRs took place from June 2018. When the assembly of an SC-QWR was completed, the performance test was carried out sequen-

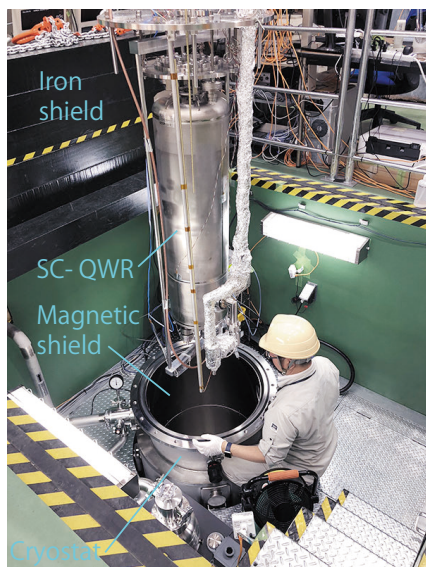


Fig. 1. Installation of a test assembly by suspending a SC-QWR into the cryostat.

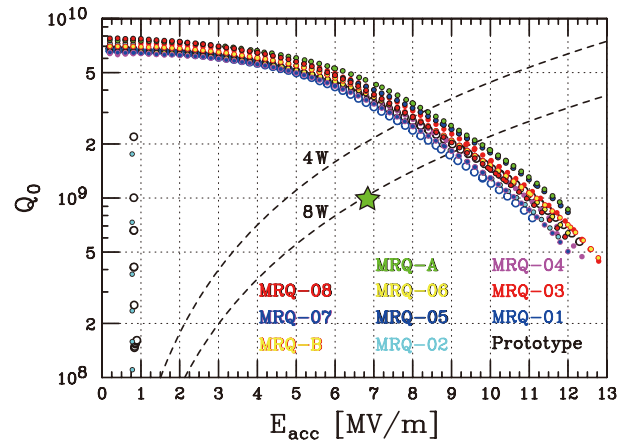


Fig. 2.  $Q_0$  vs  $E_{acc}$  plot of the bulk SC-QWRs. The green star represents the criteria of the SRILAC.

tially and it was confirmed whether or not acceptable performance was obtained. In the early days, there was a problem of vacuum leak of the SC-QWR, but it was stopped by tightening the flange bolts again. All the SC-QWRs were fabricated until November 2018 and tested immediately. The details of the test procedure are the same as that given in Ref. 4).

Figure 2 shows the quality factor  $Q_0$  plotted against acceleration voltage  $E_{acc}$  for all SC-QWRs. Although multipacting was observed at 0.9 MV/m for each SC-QWR as indicated in the figure, it could be processed within a few hours. The test results indicate very high values of  $Q_0$  and  $E_{acc}$  for all SC-QWRs; thus, all the SC-QWRs passed the acceptance test successfully. The maximum  $E_{acc}$  is significantly higher than the required value, and the exponential deterioration of  $Q_0$  has not yet been observed for all SC-QWRs. Note that the resonant frequency of all SC-QWRs is in the range of the frequency tuner as expected.

The SC-QWR with which the performance was confirmed was slowly leaked in an ISO class 1 clean room immediately, the test coupler and vacuum exhaust pipe were removed, and blank flanges were attached to send back to the factory for the post-process of installing the titanium jacket. Currently the SC-QWRs are being installed in the SRILAC cryomodules. The three cryomodules will be completed and allocated in the beginning of March 2019.

## References

- 1) M. Odera *et al.*, Nucl. Instrum. Methods Phys. Res. A **227**, 187 (1984).
- 2) T. Nagatomo *et al.*, in this report.
- 3) N. Sakamoto *et al.*, Proc. of LINAC18, WE2A03, 620 (2018).
- 4) K. Yamada *et al.*, Proc. of LINAC16, THPLR040, 939 (2016).

<sup>\*1</sup> RIKEN Nishina Center

## Input power coupler for SRILAC

K. Ozeki,<sup>\*1</sup> O. Kamigaito,<sup>\*1</sup> N. Sakamoto,<sup>\*1</sup> K. Suda,<sup>\*1</sup> and K. Yamada<sup>\*1</sup>

As an upgrade project of the RIKEN Linear Accelerator (RILAC), the construction of a superconducting heavy ion linear accelerator (Superconducting RILAC, denoted as SRILAC hereinafter) is now in progress.<sup>1,2)</sup> In this report, the progress in the implementation of input power couplers to feed RF power to the resonator is reported.

For the construction of a prototype accelerator system based on the superconducting quarter-wavelength resonator (QWR),<sup>3-9)</sup> which was carried out prior to this project, the couplers were designed to have double disk-type ceramic vacuum windows to ensure the vacuum of QWR as well as to avoid the long antenna design.<sup>10,11)</sup> On the other hand, the couplers for the SRILAC were designed to have single disk-type ceramic vacuum window, in order to simplify the structure and reduce the production cost. The geometry around the vacuum window was designed to have a characteristic impedance of  $50 \Omega$  using CST Microwave Studio.<sup>12)</sup>

The couplers were produced by Mitsubishi Heavy Industries Machinery Systems Ltd. A total of ten couplers were delivered in sequence. A photograph of the couplers is shown in Fig. 1.

The couplers must be kept completely clean and degassed in advance in order to prevent contamination of the QWR. All the operations described below were performed in an ISO class-1 clean room.

At the beginning, the following rinsing operations were performed: deconstruction of the coupler, rinsing of each part using ultrapure water, drying, and re-

construction.

After the rinsing operations, a pair of couplers was mounted on an RF test stand chamber (see Fig. 2), and the RF test stand chamber and the two couplers were baked at  $120^\circ\text{C}$ .

Then, the ceramic vacuum window was processed with RF power (RF process). Figure 2 shows the setup of the RF process. While feeding RF power to the system, the interlocks were set for an emergence of arc light due to a discharge in the coupler, and a loss of vacuum. The RF process was performed five times (the two couplers were processed once), and every time the RF power was successfully fed up to about 5 kW without any difficulty.

After the RF processes were finished, the couplers were attached to the QWRs in the ISO class-1 clean room. The fabrication of the cryomodules is now in progress.

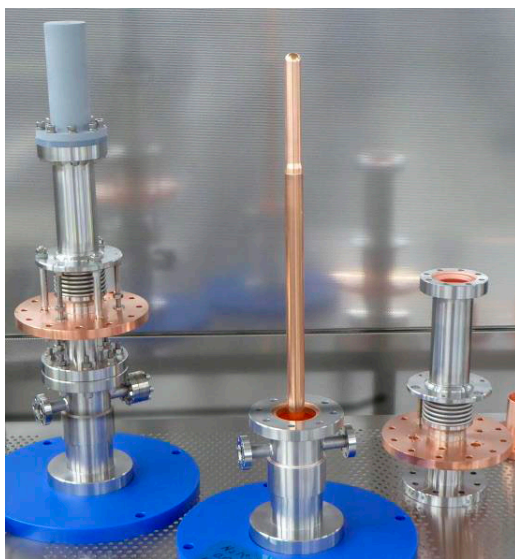


Fig. 1. Two sets of input power couplers. Constructed (left) and deconstructed (center and right) parts.

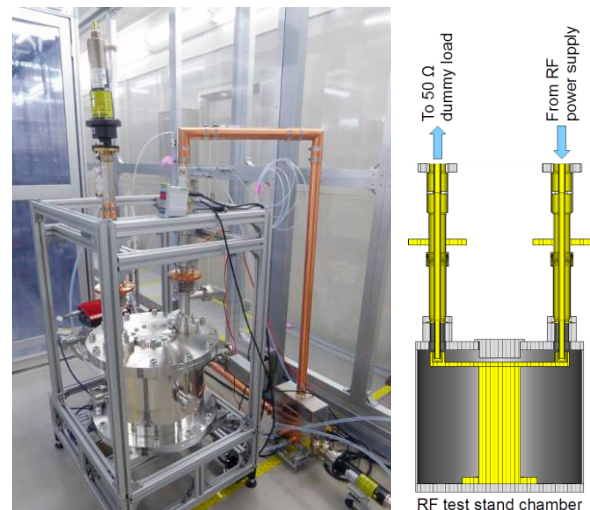


Fig. 2. Photograph (left) and schematic (right) of the RF process. The RF power was fed from the right-side coupler and transmitted to left-side coupler. The left-side coupler was terminated with a dummy load. The input, reflected, and transmitted RF powers were measured.

### References

- 1) N. Sakamoto *et al.*, in this report.
- 2) K. Yamada *et al.*, in this report.
- 3) K. Ozeki *et al.*, Proc. 12th Ann. Meet. PASJ, 1116 (2015).
- 4) N. Sakamoto *et al.*, Proc. SRF2015, 976 (2015).
- 5) K. Ozeki *et al.*, Proc. LINAC16, 598 (2016).
- 6) K. Yamada *et al.*, Proc. LINAC16, 939 (2016).
- 7) K. Yamada *et al.*, Proc. 14th Ann. Meet. PASJ, 17 (2017).
- 8) K. Ozeki *et al.*, RIKEN Accel. Prog. Rep. **51**, 131 (2018).
- 9) N. Sakamoto *et al.*, in this report.
- 10) K. Ozeki *et al.*, Proc. SRF2015, 1335 (2015).
- 11) K. Ozeki *et al.*, RIKEN Accel. Prog. Rep. **49**, 139 (2016).
- 12) <https://www.cst.com/products/cstmws>.

\*1 RIKEN Nishina Center

# Development of RIKEN 28 GHz SC-ECRIS for the production of intense metal ion beam<sup>†</sup>

Y. Higurashi,<sup>\*1</sup> T. Nagatomo,<sup>\*1</sup> J. Ohnishi,<sup>\*1</sup> and T. Nakagawa<sup>\*1</sup>

At RIKEN, we planned to synthesize new elements with atomic number ( $Z$ ) higher than 118, after the experiments for synthesizing the super-heavy element ( $Z = 113$ ).<sup>1)</sup> For this purpose, the production of intense and stable highly charged metallic ion beams, such as  $Ti^{12+,13+}$ ,  $V^{12+,13+}$ , and  $Cr^{13+}$  ions, are required. In particular, there is a strong demand for an intense beam of  $V^{13+}$  ions to synthesize the new element with  $Z = 119$ . Therefore, we conducted test experiments to produce these beams and studied the effect of magnetic field distribution to maximize the beam intensity of these heavy ions for several years.

It is well-known that the “scaling law”<sup>2,3)</sup> and the “high B mode” operation<sup>4-6)</sup> provide some important guidelines to optimize the magnetic mirror ratio of ion sources for the production of various charge states of heavy ions. As a first step to improve the ion source performance for the production of these metallic ion beams, we conducted a systematic study to optimize the magnetic field distribution using the RIKEN 28 GHz SC-ECRIS<sup>7,8)</sup> and the liquid He-free SC-ECRIS<sup>9)</sup> on the basis of these laws. In the systematic studies, it was concluded that the optimum magnetic mirror ratio ( $B_{ext}/B_{min}$ ) is 2.2–2.7 for the production of  $V^{13+}$  ion beam. If we choose  $B_{min} \sim 0.6$  T, which is the optimum value for the 28 GHz microwave operation to maximize the beam intensity, the optimum  $B_{ext}$  is predicted to be 1.3–1.6 T. Therefore, we chose  $B_{ext}$  of 1.4 T for the production of  $V^{13+}$  ion beam.

We used a high-temperature oven<sup>10)</sup> for the production of the V vapor. For long-term operation of the high-

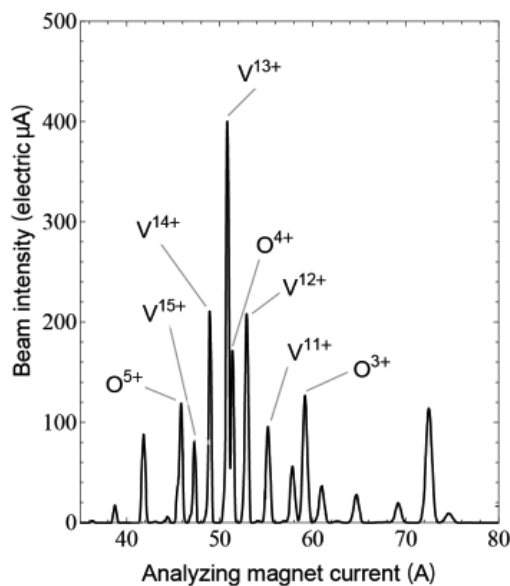


Fig. 1. Charge state distribution of highly charged V ions.

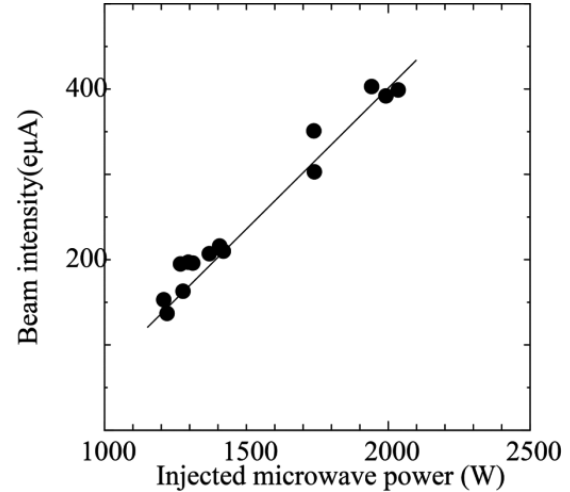


Fig. 2. Beam intensity of  $V^{13+}$  ions as a function of injected microwave power.

temperature oven, we fabricated a new crucible, whose volume is almost two times larger than that of the old one.<sup>11)</sup> To obtain sufficient temperature for evaporating the materials, detailed simulation for optimizing the crucible structure was carefully performed and sufficiently high temperature was obtained to produce the vapor. The detailed results are presented in Ref. 10).

Figure 1 shows the typical charge state distribution of a highly charged V ion beam at the injected microwave power of  $\sim 2$  kW. The extraction voltage was 12.6 kV. The ion source was tuned to produce a  $V^{13+}$  ion beam. The beam intensity increased linearly with increase in the injected microwave power, as shown in Fig. 2, and obtained  $\sim 400$  electric  $\mu A$  of  $V^{13+}$  ion beam with  $\sim 2$  kW. For long term operation (longer than one month), we successfully produced  $\sim 120$  electric  $\mu A$  of  $V^{13+}$  ion beam without break.

## References

- 1) K. Morita, Proceedings of the 14th International Symposium on Nuclei in the Cosmos (NIC2016), JPS Conf. Proc. 14, 010004 (2017).
- 2) R. Geller *et al.*, Proc. 8th Int. Conference on ECR ion sources and their applications, NSCL report MSUCP-47 (MSU, Dec. 1987), p. 1.
- 3) R. Geller, *Electron Cyclotron Resonance Ion Sources and ECR Plasmas*, Institute of Physics, (CRC Press, Bristol, 1996).
- 4) T. Antaya, S. Gammino, Rev. Sci. Instrum. **65**, 1723 (1994).
- 5) S. Gammino *et al.*, Rev. Sci. Instrum. **67**, 4109 (1996).
- 6) D. Hitz *et al.*, Rev. Sci. Instrum. **73**, 509 (2002).
- 7) Y. Higurashi *et al.*, Rev. Sci. Instrum. **85**, 02A953 (2014).
- 8) G. Alton, D. N. Smithe, Rev. Sci. Instrum. **65**, 775 (1994).
- 9) T. Kurita *et al.*, Nucl. Instrum. Methods Phys. Res. B **192**, 429 (2002).
- 10) J. Ohnishi *et al.*, Proceedings of ECRIS 2018.
- 11) J. Ohnishi *et al.*, Rev. Sci. Instrum. **87**, 02A709 (2016).

<sup>†</sup> Condensed from proceedings of ECRIS2018

<sup>\*1</sup> RIKEN Nishina Center

# Beam energy adjuster for super-heavy element synthesis at RIKEN Ring Cyclotron

K. Yamada,<sup>\*1</sup> T. Ohki,<sup>\*2</sup> H. Yamauchi,<sup>\*2</sup> K. Oyamada,<sup>\*2</sup> M. Tamura,<sup>\*2</sup> A. Yusa,<sup>\*2</sup> K. Kaneko,<sup>\*2</sup> T. Maie,<sup>\*1</sup> Y. Watanabe,<sup>\*1</sup> and O. Kamigaito<sup>\*1</sup>

A new experiment on the synthesis of super-heavy element (SHE) is on going in the RIKEN Nishina Center using a vanadium beam<sup>1)</sup> accelerated by the combination of RIKEN Linear Accelerator 2 (RILAC2)<sup>2,3)</sup> and RIKEN Ring Cyclotron (RRC).<sup>4)</sup> For the SHE experiment, the beam energy has to be adjusted to the pinpoint value that continuously irradiates to a target over a long period. However, it is difficult to flexibly change the beam energy by the cyclotron. Therefore, we introduced a beam energy adjuster (BEA) using an acceleration cavity into the beam line from the RRC to the target to ensure that the beam energy can be finely adjusted to approximately  $\pm 3\%$ .

We decided to divert the final-stage acceleration cavity, RF power amplifier, and the control system used as RILAC booster<sup>5)</sup> to the BEA system. This acceleration cavity is a 6 gap quarter-wavelength resonator. Although the cell length does not perfectly match with the velocity of the beam from the RRC, the original layout of the drift tubes was applicable to the fine adjustment of the beam energy. Because the original resonant frequency of the cavity was 75.5 MHz, it was remodeled to 73.0 MHz, which was compatible with the operation frequency of the RRC. To lower the resonant frequency, the outer and inner cylinders were extended by inserting an outer spacer ring and an inner spacer ring, respectively. Both spacer rings were made of oxygen-free copper. The height of both rings was 36 mm, as determined by 3D electromagnetic calculation using Microwave Studio (MWS). Figure 1 shows the calculation model of MWS with the spacers.

The original cavity was transferred to the beam-distribution corridor (D-corridor) in the Nishina Memorial building in the summer of 2017.<sup>6)</sup> After the spacer rings were attached to the cavity, a low-power RF test was performed in October. Figure 2 shows the inner components of the BEA cavity after inserting the spacer ring. The test result indicated that it was successfully remodeled to have a resonant frequency of 73.0 MHz with a quality factor  $Q_0$  of 22500, which was almost equivalent to the original cavity. The control system, vacuum system, cooling water, and control cables were installed simultaneously. Finally, the supply and control cables were wired from a high-voltage power supply located at a power supply building north of the Nishina Memorial building to a tetrode RF amplifier installed at the D-corridor in December. The high-power RF test was also successfully completed

without any serious problems and the BEA system began operations for the SHE experiment from December 2017.

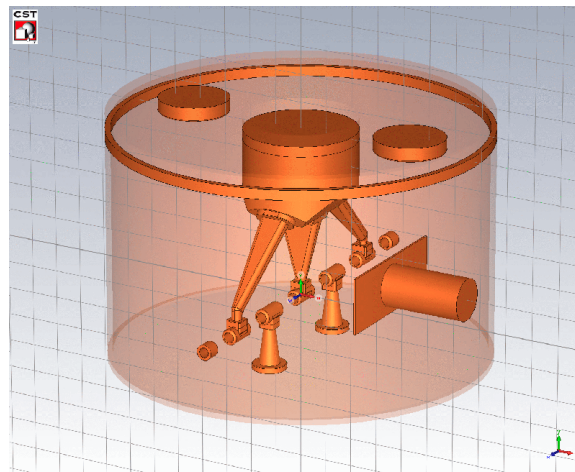


Fig. 1. A model with spacer rings used in the MWS calculation.

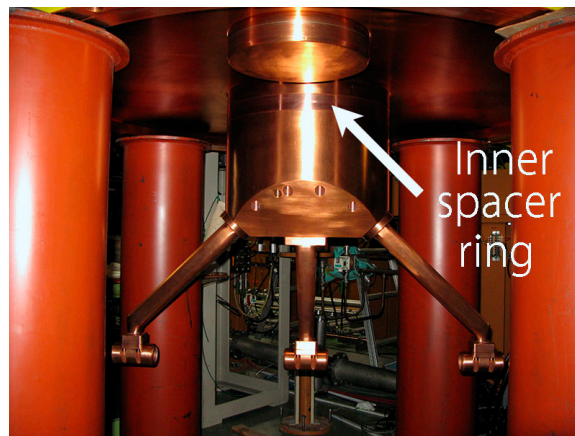


Fig. 2. Inner components of the remodeled cavity.

## References

- 1) Y. Higurashi *et al.*, RIKEN Accel. Prog. Rep. **51**, 17 (2018).
- 2) K. Yamada *et al.*, Proc. of IPAC12, TUOBA02, 1071 (2012).
- 3) K. Suda *et al.*, Nucl. Instrum. Methods Phys. Res. A **722**, 55 (2013).
- 4) Y. Yano, Proc. 13th Int. Cyclo. Conf., 102 (1992).
- 5) O. Kamigaito *et al.*, Rev. Sci. Instrum. **76**, 013306 (2005).
- 6) Y. Watanabe *et al.*, RIKEN Accel. Prog. Rep. **51**, 132 (2018).

<sup>\*1</sup> RIKEN Nishina Center

<sup>\*2</sup> SHI Accelerator Service, Ltd.

# Operation of high-temperature oven for 28-GHz superconducting ECR ion source

J. Ohnishi,\*<sup>1</sup> Y. Higurashi,\*<sup>1</sup> and T. Nakagawa\*<sup>1</sup>

Uranium beams, which are accelerated at the RI-beam Factory (RIBF), are extracted from a 28-GHz superconducting ECR ion source (SC-ECRIS)<sup>1)</sup> by using a high-temperature oven (HTO). Our HTO uses a tungsten crucible, which is joule-heated with a DC current of 600–700 A. Figure 1 shows the dimensions of two types of crucibles. The crucible is heated to approximately 2000°C in order to achieve a UO<sub>2</sub> vapor pressure of 0.1–1 Pa. The HTO, which has been under development since 2013,<sup>2)</sup> was first used to operate the ion source for the RIBF experiments in the autumn of 2016.

The HTO was also used to produce high-intensity vanadium beams in the 28-GHz SC-ECRIS. V<sup>13+</sup> beams with a current of 100  $\mu$ A or more were supplied to the beam time for experiments on super heavy element synthesis from 2018. For the production of vanadium beams, we placed a yttria crucible into a tungsten crucible and filled it with metal vanadium (vapor pressure: 1 Pa at 1827°C) because the metal vanadium should be electrically insulated from the crucible.

Table 1 lists a summary of the machine-time (MT), whose beams were supplied from the 28-GHz SC-ECRIS using the HTO. Four uranium-MT (U-MT) and three vanadium-MT have been performed so far. During normal operation, the average currents of U<sup>35+</sup> and V<sup>13+</sup> were both approximately 100–120  $\mu$ A. The HTO can be operated continuously for at least three weeks because the fillable amount of the R692 type, which was used for these MTs, was approximately 2 and 4 g for vanadium and UO<sub>2</sub>, respectively.

Figure 2 shows the trend of the beam current of U<sup>35+</sup>, the electric current, and the power of heat generation of the crucible during the U-MT in the autumn of 2018. The beam current of U<sup>35+</sup> was measured with a Faraday cup positioned down-stream of the analyzing magnet. The beam current can only be measured when the

Table 1. Summary of MT using HTO.

ion	period	beam current ( $\mu$ A)	operation time (d)	material	consumption rate (mg/h)
U <sup>35+</sup>	10–11/2016	100–120	34	UO <sub>2</sub>	2.4
U <sup>35+</sup>	5–6/2017	60–120	35	UO <sub>2</sub>	3.2
U <sup>35+</sup>	10–11/2017	80–120	7 + 27 + 10	UO <sub>2</sub>	4.0, 4.2, 12
U <sup>35+</sup>	10–12/2018	110–140	27.5 + 30	UO <sub>2</sub>	2.4, 2.4
V <sup>13+</sup>	1–2/2018	100–210	20 + 13	metal V	2.2, 4.1
V <sup>13+</sup>	6–7/2018	100–230	23 + 9	metal V	2.0, 3.8
V <sup>13+</sup>	9/2018	90–110	10	metal V	2.4

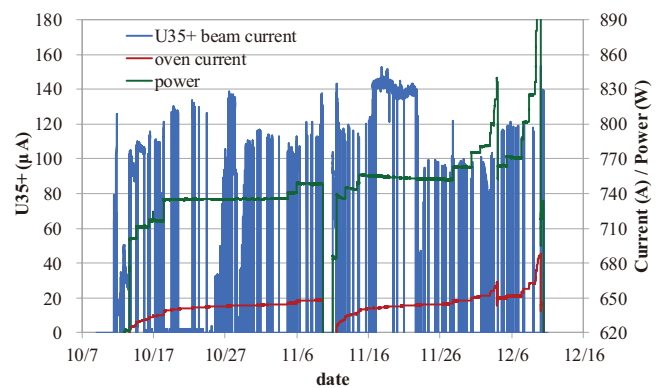


Fig. 2. Operational trend of HTO in U-MT of 2018.

beams are not supplied to the accelerators and change according to the width of the slits located upstream. This trend shows that uranium beams of 120  $\mu$ A or more could be supplied stably except during the last two weeks mentioned below. The power of heat generation of the crucible was obtained by subtracting the Joule loss on the support pipes from the total electric power. The operation of the ion source was interrupted because the crucible was changed to a new one for replenishment of UO<sub>2</sub> on Nov. 9. Although stable operation was performed, we had to increase the current and power of the HTO after the end of November, as can be seen in the figure. The reason was because a vapor-ejection hole of the crucible was blocked by a pileup of UO<sub>2</sub> and the beam intensity decreased. The first blockage that happened on December 6 was resolved naturally and the MT ended as scheduled even though the second blockage occurred. It was found that blockage tends to occur when the amount of vapor is large. This problem is serious, but it has not been solved yet. Details of this article are shown in Ref. 3).

## References

- 1) Y. Higurashi *et al.*, Rev. Sci. Instrum. **85**, 02A953 (2014).
- 2) J. Ohnishi *et al.*, Rev. Sci. Instrum. **87**, 02A709 (2016).
- 3) J. Ohnishi *et al.*, Proc. 23rd Int. Workshop on ECR ion sources, Catania Italy, Sep. 2018, to be published in JACOW Web site.

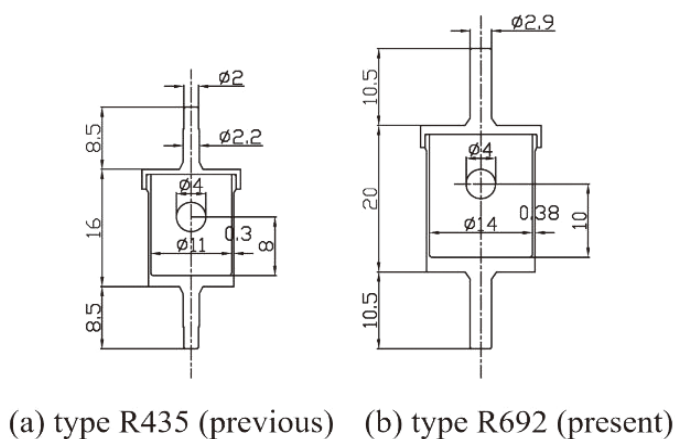


Fig. 1. Schematic of the tungsten crucibles.

\*<sup>1</sup> RIKEN Nishina Center

# Laser Energy Dependence of Plasma Instability by Solenoid Magnetic Field<sup>†</sup>

T. Karino,<sup>\*1,\*3</sup> M. Okamura,<sup>\*1,\*2</sup> T. Kanesue,<sup>\*2</sup> S. Ikeda,<sup>\*2</sup> and S. Kawata<sup>\*3</sup>

A very high current beam is required for heavy-ion inertial fusion (HIF), and therefore the use of a laser ion source using a solenoid is proposed. By using a solenoid magnetic field, the spread of plasma can be suppressed. However, it has been found that a certain range of field strength triggers unstable plasma condition.<sup>1)</sup>

Figure 1 shows the experimental setup. The plasma generated by the laser on the target is measured by a Faraday cup after it is transported through a 3000 mm long solenoid coil located 315 mm from the target. Nd:YAG laser was used with an incident angle of 20°.

Figure 2 shows the example of Au target when the laser energy is 411 mJ. The vertical axis and horizontal axis show the beam current and time of flight, respectively. In the figure, waveforms of the beam current for 40 shots are overlaid on each other. Figure 2 (a) shows the case without the solenoid. Figure 2 (b) shows the case when the solenoid magnetic field is 28.6 G. It is found that the waveform of Fig. 2 (b) is more unstable than the waveform of Fig. 2 (a).

Figure 3 shows the experiment result of the Au target. The vertical axis represents the instability of the plasma, and the horizontal axis represents the solenoid magnetic field. In this experiment, the plasma instability was evaluated based on the standard deviation of the half width over peak current. By using this method, it is possible to know the degree of collapse of the waveform. In Fig. 3, the larger the value on the vertical axis is, the more unstable the plasma is. The energy of the Nd: YAG laser was 312 to 411 mJ. The laser spot size was 3.84 mm. From Fig. 3, it can

be seen that the range of the magnetic field where the beam current becomes unstable varies depending on the laser energy.

Moreover, it was found that the unstable range changes also when the target is changed from another experiment. For example, in the case of Fe, the magnitude of the solenoid magnetic field where the plasma became unstable became smaller than that of Au. From these experimental results, it can be said that the unstable range of plasma varies with the speed and type of plasma.

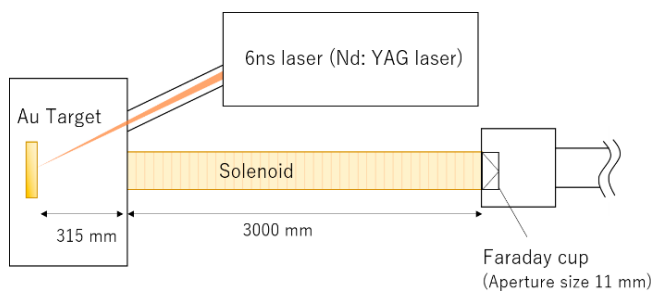


Fig. 1. Experimental equipment.

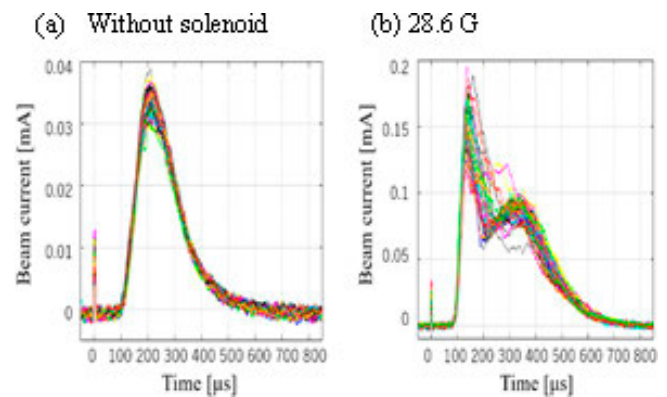


Fig. 2. Waveform of current beam (Laser energy is 411 mJ).

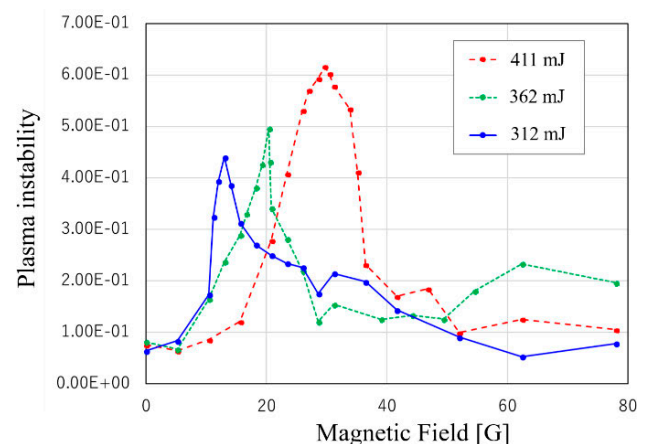


Fig. 3. Experiment result of gold target.

<sup>†</sup> Condensed from the proceedings HIF 2018

<sup>\*1</sup> RIKEN Nishina Center

<sup>\*2</sup> Collider-Accelerator Department, Brookhaven National Laboratory

<sup>\*3</sup> Graduate School of Engineering, Utsunomiya University

## Reference

- 1) K. Takahashi *et al.*, AIP Conf. Proc. **1525**, 241 (2013).

# Evaluation of beam orbit calculation method for the injection line of AVF cyclotron and performance evaluation of pepper-pot emittance monitor

Y. Kotaka,<sup>\*1</sup> Y. Ohshiro,<sup>\*1</sup> H. Yamaguchi,<sup>\*1</sup> N. Imai,<sup>\*1</sup> Y. Sakemi,<sup>\*1</sup> T. Nagatomo,<sup>\*2</sup> M. Kase,<sup>\*2</sup> J. Ohnishi,<sup>\*2</sup> A. Goto,<sup>\*2</sup> K. Hatanaka,<sup>\*3</sup> H. Muto,<sup>\*4</sup> and S. Shimoura<sup>\*1</sup>

We finished developing a calculation method for the beam orbit from the Hyper ECR ion source to the center of the AVF cyclotron using the 4D emittance measured with a pepper-pot emittance monitor<sup>1)</sup> (PEM\_IH10).<sup>2,3)</sup> We attempted to numerically evaluate our calculations of 15 types of beams by comparing other diagnostics.

To evaluate our beam orbit, we compared it to the 2D emittance measured by the 2D emittance monitor<sup>4)</sup> (EM\_I36) installed 6.2 m away from PEM\_IH10 using  $\chi^2$  test. However, it should be noted that the 1D distribution projected from the 2D distribution was used for the comparison.  $\chi^2$  is defined as the sum of squared differences of each position or each angle between the measurement and the calculation divided by an assumed dispersion. However, this value itself is not significant because this experiment was conducted to observe the relative variations in the results. This value was estimated so that  $\chi^2/\text{DOF}$  becomes approximately 1 when the calculation may conform to the measurement by visual judgement.

4D emittance was measured using a standard (x, y) coordinate system perpendicular to the beam direction, where x and y denote the horizontal and vertical directions, respectively. The coordinate system of EM\_I36 (u, w) was rotated by 45 degree against the (x, y) coordinate system, and u' and w' were the angles of u-axis and w-axis, respectively. The left part of Fig. 1 indicates the scatter plot of  $\chi^2/\text{DOFs}$  of u and u'. The  $\chi^2/\text{DOFs}$  of w and w' is indicated in the right part of Fig. 1. The displacements in the position or angle between the measurement and calculation were determined but they were canceled to determine the distribution conformity in this comparison. All values of  $\chi^2/\text{DOF}$  were found to be scattered up to 6. The reasons of this variation are being

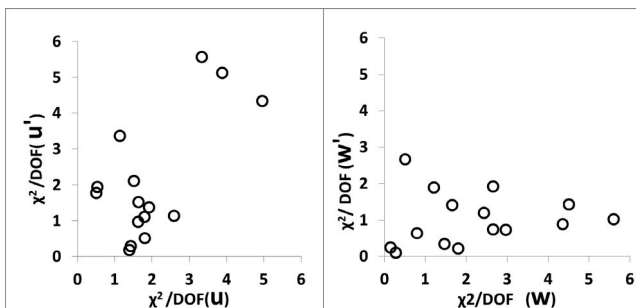


Fig. 1. (left) Scatter plot shows  $\chi^2/\text{DOFs}$  of u and u'. (right) Scatter plot shows  $\chi^2/\text{DOFs}$  of w and w'. Fifteen beams ( $\text{H}^+$ ,  $\text{D}^+$ ,  $^4\text{He}^{2+}$ ,  $^7\text{Li}^{2+}$ ,  $^{11}\text{B}^{4+}$ , and  $^{18}\text{O}^{6+}$ ) are tested.

<sup>\*1</sup> Center for Nuclear Study, University of Tokyo

<sup>\*2</sup> RIKEN Nishina Center

<sup>\*3</sup> RCNP, Osaka University

<sup>\*4</sup> Center of General Education, Tokyo University of Science, Suwa

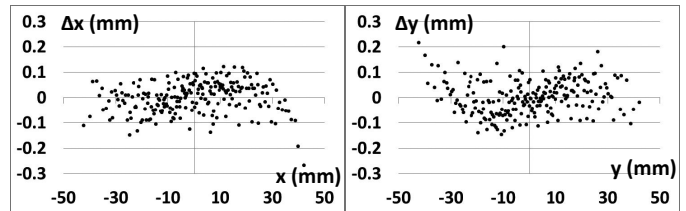


Fig. 2. Differences in distribution between fiducial points and measured position on pixel coordinate: x-axis (left) and y-axis (right).

examined singly.

The above-mentioned displacements for positions and angles were approximately 10 mm and 10 mrad, respectively. One of the considerable reasons is the magnetic hysteresis of the vertical deflection dipole magnet (DMI23). We measured the magnetic hysteresis and found the magnetic difference to be 1.7% when the commonly-used excitation current varied from 10 to 20 A. For example, 1.0% magnetic field difference is estimated to cause 10 mm difference at 300 mm from DMI23 when the excitation current is 25 A. Because we used a setting excited current for the beam orbit calculation without knowing this, these displacements in positions and angles occurred. Therefore, the magnetic field of DMI23 needs to be measured.

After the beam orbit calculation, we started the performance evaluation of PEM\_IH10 for improvement and focused on the position error of the fluorescent plate. As its view was recorded by the digital camera, it transformed to real space by the relationship between the fiducial points on the fluorescent plate and their measured positions on the pixel coordinate. The position error was estimated from the differences between the fiducial points and their transformed positions. Previously, there were 15 fiducial points with a diameter of 1 or 2 mm. The standard deviations (SD) of the differences of x direction and y direction were 0.12 and 0.19 mm, respectively. For improvement, we used a graph paper pasted on the fluorescent plate and selected 225 fiducial points at 5 mm interval in the area of 70 mm square. The differences in the distributions of x and y are shown in the left and the right parts of Fig. 2, respectively. The SD of differences of x and y were improved to 0.06 and 0.07 mm, respectively. Other performance evaluation will be conducted.

## References

- 1) T. Hoffmann *et al.*, AIP Conf. Proc. **546**, 432 (2000).
- 2) Y. Kotaka *et al.*, Proc. 14th Annual Meeting of PASJ, (2017), pp. 1118–1122.
- 3) Y. Kotaka *et al.*, RIKEN Accel. Prog. Rep. **51**, 138 (2018).
- 4) Y. Kotaka *et al.*, RIKEN Accel. Prog. Rep. **41**, 96 (2008).

## Updating control units around the AVF cyclotron

M. Komiyama,<sup>\*1</sup> M. Fujimaki,<sup>\*1</sup> N. Fukunishi,<sup>\*1</sup> R. Koyama,<sup>\*2</sup> M. Hamanaka,<sup>\*2</sup> H. Mukai,<sup>\*3</sup> T. Nakamura,<sup>\*2</sup> and A. Uchiyama<sup>\*1</sup>

We report on the update of the control units around the AVF cyclotron to reduce the difficulties caused by radiation and implement a new beam interlock system under construction (hereafter, AVF-BIS). The beam diagnostic equipment like a beam profile monitor or a Faraday cup on the AVF cyclotron and its beam transport line has been controlled by DIM<sup>1)</sup> since 1989, and the equipment on the beam transport line around RILAC2 has been controlled by N-DIM<sup>2)</sup> since 2012. They were installed in 19-inch racks (hereafter, rack) at two places: the floor on which the AVF cyclotron is placed (hereafter, AVF floor) and the floor that is one level below (hereafter, AVF-M2 floor). Recently, as the performance of the AVF cyclotron has been improved and the beam intensity accelerated by the AVF cyclotron has been increased, there have been frequent issues such as the control unit becoming unresponsive toward the remote control suddenly. In the most frequent case, it occurred three times in 4 h while accelerating a 12 MeV/nucleon deuteron beam with an intensity of 4  $\mu\text{A}$  at the C03 target. Because this frequently occurs during accelerating a deuteron in the AVF cyclotron, we speculate that the cause of the trouble is the influence of radiation, especially the neutrons coming out from the AVF cyclotron and its beam transport line during beam transport. Therefore, we measured the dose of neutron around the installation location of the control unit using the TL badge. Figure 1 shows the measurement locations and results of the two measurements. At the AVF-M2 floor, several racks are placed along the south wall for the control unit. Among them, the control unit where this issue frequently occurs is located at No. 1 in Fig. 1. The results clearly show that the neutron dose at this point is higher than other places. This might be occurring because No. 1 is close to the open hole under the AVF cyclotron (No. 9). However, it has not been specified yet. As the best measure at present, we moved the control unit to a place where the neutron dose was low based on the results.

Simultaneously, we updated the control unit from old DIM to N-DIM. This update was made because the DIM in use was old and the DIM-based existing beam interlock system for the AVF cyclotron needed to be renewed along with its low-energy experimental facility to AVF-BIS.<sup>3)</sup> AVF-BIS stops a beam by outputting signals to a beam chopper and Faraday cup for various interlock signal inputs. In this system, the Faraday cup needs to be controlled by N-DIM.

The updating work was conducted during the summer maintenance period in 2018 as follows:

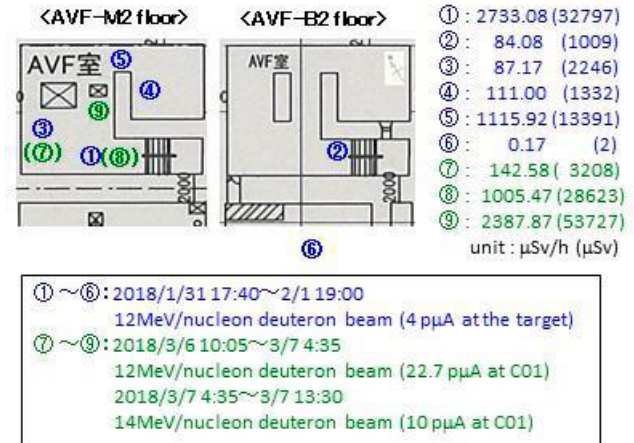


Fig. 1. Neutron dose measurement. The AVF-B2 floor is one floor below the AVF-M2 floor. The data written on the right side shows the average dose (integrated dose).

- (1) To move one of the racks from No. 1 to No. 3 with the N-DIM inside.
- (2) To move some N-DIMs mounted on the rack next to the rack to be relocated to the gap between the existing racks near No. 3.
- (3) To set up some new N-DIMs on the existing racks near No. 3. Remove the signal and control cable from the DIM at No. 3 and AVF floor, and reconnect them to the newly set up N-DIMs.

Consequently, we moved and set up 28 N-DIMs in total. Currently, they control the beam diagnostic equipment on the beam transport line around RILAC2, and the beam diagnostic equipment and vacuum system on the beam transport line downstream of AVF cyclotron. This indicates that approximately 60% of the DIMs under operation at the AVF and AVF-M2 floors have been updated. Because DIM still controls the various equipment attached to the AVF cyclotron and the beam diagnostic equipment of the beam transport line in E7 experimental vault, we are planning to sequentially update the control to N-DIM.

After the summer maintenance, the occurrence of this issue in the control unit was reduced to 0% while accelerating the 12 MeV/nucleon deuteron beam with an intensity of 1.5  $\mu\text{A}$  at the C03 target for more than one month. Thus, it is evident that this maintenance has had certain effect.

### References

- 1) K. Shimizu *et al.*, Proc. Cyclotrons'84, pp. 392–395.
- 2) M. Fujimaki *et al.*, RIKEN Accel. Prog. Rep. **37**, 279 (2004).
- 3) M. Komiyama *et al.*, Proc. ICALEPCS2017, (2017), pp. 427–430.

<sup>\*1</sup> RIKEN Nishina Center

<sup>\*2</sup> SHI Accelerator Service Ltd.

<sup>\*3</sup> Japan Environment Research Corporation

## Reconstruction of RF system controller for RIKEN Ring Cyclotron

K. Yamada,<sup>\*1</sup> S. Fukuzawa,<sup>\*2</sup> M. Hamanaka,<sup>\*2</sup> S. Ishikawa,<sup>\*2</sup> K. Kobayashi,<sup>\*2</sup> R. Koyama,<sup>\*2</sup> T. Nakamura,<sup>\*2</sup> M. Nishida,<sup>\*2</sup> M. Nishimura,<sup>\*2</sup> J. Shibata,<sup>\*2</sup> N. Tsukiori,<sup>\*2</sup> K. Yadomi,<sup>\*2</sup> K. Suda,<sup>\*1</sup> and N. Sakamoto<sup>\*1</sup>

The RIKEN Ring Cyclotron (RRC) has been supplying beams for various experiments as the key accelerator of RIKEN Nishina Center for over 30 years. The RRC has two sets of acceleration cavities and RF power amplifiers,<sup>1)</sup> and each set is controlled by an independent controller system. Most controllers of the RRC's RF system consist of hardware logic using relays and analog transmission to/from low-level circuits and analog meter. Equipment for RF voltage setting, RF phase setting, drivers of frequency tuners and RF power coupler, and drivers of RF matching circuits for amplifier were controlled by independent control boxes for each device. A programmable logic controller (PLC) was used for the indicator control and remote operation interface, and it was replaced in 2004 without changing the system configuration. By updating the low-level circuits in 2007, the analog voltage outputs from the RF voltage and phase setting boxes were converted to digital signals by additional converters and connected to the new low-level circuits. The data logging system did not work because it was old and outdated. The previous hardware type control system could not freely set operation parameters like the frequency tuning system, which caused significant interruption in the machine time. To solve such inconveniences, we decided to update the system that can be integrated and controlled by a PLC.

The new system is controlled by the Mitsubishi Electric MELSEC-Q series PLC and a touch panel for human-machine interface. Figure 1 shows images of the main part of the original control rack and updated control rack. The low-level circuits were transferred from the RRC room to the underground passage and integrated into the PLC control rack, as shown in the right panel of Fig. 1, and controlled directly by the PLC. Power supplies for the tetrodes in the RF amplifier were also controlled directly by the PLC. We replaced the all old signal transducers of the filament and plate power supplies as well as the power supplies for grid electrodes. The old two-phase stepping motors for the two movable boxes, trimmer, and RF power coupler were replaced with a new five-phase stepping motor, SANYO DENKI FSF893S, which can set parameters such as the driving speed. The remote operation of the system was integrated into the operation terminal of RILAC2<sup>2)</sup> through Ethernet using the SCADA software of Wanderware InTouch. The operations of RF voltage and phase were also integrated into the operational interface<sup>3)</sup> using rotary encoders through

the CC-Link slave interface, Anywire AFCS02.

The control system for RRC's RF was successfully updated in March 2016. Owing to these modifications, several improvements were obtained. The time of RF re-excitation when discharged was curtailed from 30 min to a few minutes. The RF voltage was enhanced by more than 10% by the assured automatic re-excitation function. The amplifier damage at the RF voltage trip was significantly reduced by the voltage rump-up function. The resolutions of RF voltage and phase set points were improved from 1/10000 to 1/30000 and 1/36000, respectively. The control system upgrade contributed to the stabilization of beam operation during the RIBF experiment and further performance improvement is expected in combination with the cavity upgrade of RRC reported in Ref. 4).

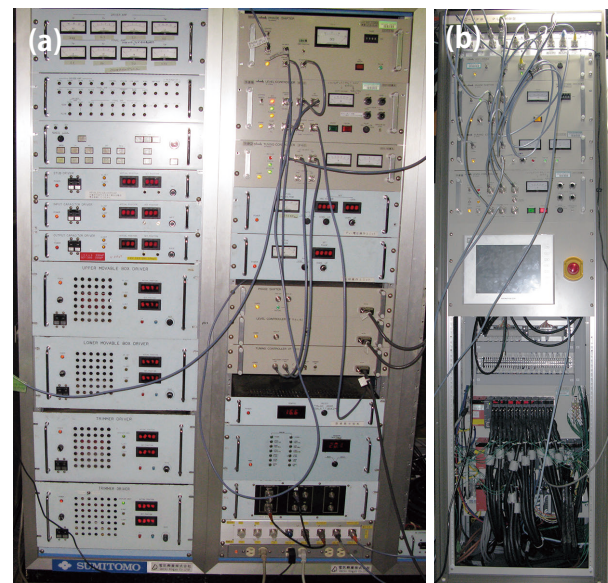


Fig. 1. Main part of control system before (left panel) and after (right panel) the upgrade.

### References

- 1) T. Fujisawa *et al.*, Nucl. Instrum. Methods Phys. Res. A **292**, 1 (1990).
- 2) K. Yamada *et al.*, Proc. of IPAC12, TUOBA02, 1071 (2012).; K. Suda *et al.*, Nucl. Instrum. Methods Phys. Res. A **722**, 55 (2013).
- 3) K. Yamada *et al.*, RIKEN Accel. Prog. Rep. **49**, 150 (2016).
- 4) K. Yamada *et al.*, in this report.

<sup>\*1</sup> RIKEN Nishina Center

<sup>\*2</sup> SHI Accelerator Service Ltd.

## Radiation monitoring for cycrotrons in RIBF

M. Nakamura,<sup>\*1</sup> K. Yamada,<sup>\*1</sup> A. Uchiyama,<sup>\*1</sup> H. Okuno,<sup>\*1</sup> and M. Kase<sup>\*1</sup>

Recently, we attempted to monitor the radiation due to beam loss in the RIBF using ionization chambers (ICs).<sup>1)</sup> Usually, we investigate the radiation from the electrostatic deflection channels (EDC) at RRC and SRC. We input the alarm signal from these ICs to the beam interlock system (BIS).<sup>2,3)</sup> However, four ring cyclotrons RRC, fRC, IRC, and SRC are used in the case of  $^{238}\text{U}^{86+}$  beam acceleration. Hence, we installed the ICs near the EDC of fRC and IRC. Last year, we conducted tests by inputting the alarm signal from the IC signal near the EDC of the IRC. In this report, we attempted to input the alarm signal from the IC near the EDC of fRC to BIS.

We considered the alarm levels of the ICs by comparing the signals from the ICs with those from the thermocouples (TCs) set at the septum of RRC, IRC, and SRC.<sup>2,3)</sup> Suppose that a beam deposits a 600 W heat at the septum electrode of the EDC. The temperature rise at the beam loss point is estimated to be 800°C based on a thermal analysis using the finite element method. At this moment, the temperature difference between the TC set at the nearest part where the beam was irradiated and the cooling water of the septum becomes 10°C. In contrast, the septum is made of Cu and its melting point is 1080°C. Therefore, the septum cannot be melted at these conditions. However, to protect against the risks of damage caused to the septum, the alarm level of the temperature difference of TCs was set to 10°C. Hence, we compared the temperature difference on the septum with the IC signal near the EDC of fRC in the user time (UT) of the  $^{238}\text{U}^{86+}$  beam. The result is shown in Fig. 1. The data demonstrated little dispersion and we can obtain a calibration curve (red line), as shown in Fig. 1. From this curve, we can recognize that the voltage of the IC became approximately 0.55 V when the temperature difference became 10°C.

From October 16 to December 16, the  $^{238}\text{U}^{86+}$  ion beam was accelerated to 345 MeV/nucleon. Usually, we collected the data of TCs and IC within 7–10 days from the beginning of the UT of RIBF. Based on this observation, we determined the alarm level of IC and set it to BIS, which is the time available between this experiment and the next. However, in this term, we could not find any vacant time to input the alarm signal to BIS. Thus, we compared the data when the BIS acted on the signal from the TCs set at EDC of fRC with the data of IC set near the EDC of fRC. We can then consider the propriety of the alarm level of the IC signal.

The IC signal from 0:00 to 5:00 on 12/3/2018 is shown in Fig. 2 as typical example data. From 2:08 to 2:50, BIS acted 20 times by the sudden temperature rising of EDC for the instability of electric field of fRC.

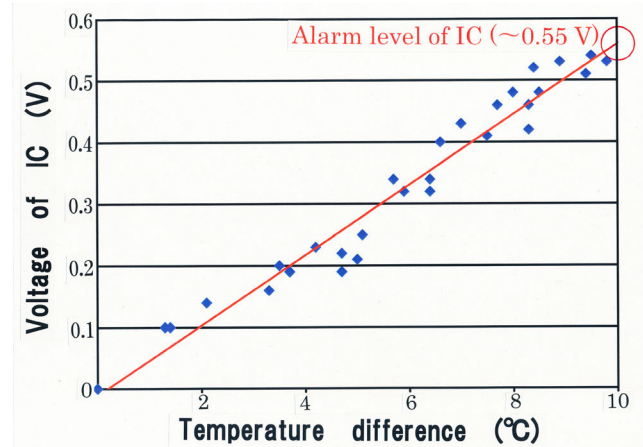


Fig. 1. Correlation of IC voltage and the temperature difference on the septum.

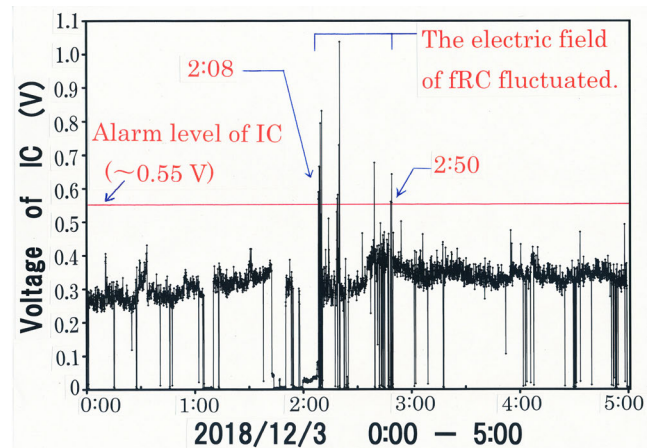


Fig. 2. Signals from the IC installed near the EDC of fRC.

During this term, the value of IC set near the EDC distributed from 0.56 to 1.05 V. Such phenomena were frequently observed on other days of this UT. On observing the IC signals when the BIS from TCs signals acted in this UT, the alarm level of IC described above is found to be reasonable.

We performed investigations by inputting the alarm signal to the BIS during the machine time of the  $^{238}\text{U}^{86+}$  ion beam. However, we could not input the signal from the IC set near the EDC of fRC. Hence, we will investigate the alarm signal from fRC to BIS next time.

### References

- 1) M. Nakamura *et al.*, RIKEN Accel. Prog. Rep. **50**, 152 (2017).
- 2) M. Nakamura *et al.*, RIKEN Accel. Prog. Rep. **49**, 146 (2016).
- 3) M. Nakamura *et al.*, RIKEN Accel. Prog. Rep. **48**, 237 (2015).

<sup>\*1</sup> RIKEN Nishina Center



# Design of reliable control with star-topology fieldbus communication for an electron cyclotron resonance ion source at RIBF<sup>†</sup>

A. Uchiyama,<sup>\*1</sup> T. Nagatomo,<sup>\*1</sup> Y. Higurashi,<sup>\*1</sup> J. Ohnishi,<sup>\*1</sup> T. Nakagawa,<sup>\*1</sup> M. Komiyama,<sup>\*1</sup> N. Fukunishi,<sup>\*1</sup>  
H. Yamauchi,<sup>\*2</sup> M. Tamura,<sup>\*2</sup> and K. Kaneko<sup>\*2</sup>

A new superconducting electron cyclotron resonance ion source (SC-ECRIS) was installed at RILAC in the RIKEN project to increase the beam intensity.<sup>1)</sup> Considering the new SC-ECRIS, the control system should follow the current RIKEN 28-GHz SC-ECRIS control system for RILAC2, because the RIKEN 28-GHz SC-ECRIS control system based on Experimental Physics and Industrial Control System (EPICS) has proven to be successful.<sup>2)</sup> Thus, in the new SC-ECRIS control system, we adopted a programmable logic controller (PLC) of the Yokogawa FA-M3V series.

However, the RIKEN 28-GHz SC-ECRIS control system is less reliable because it uses TCP/IP communication between the PLC controllers for interlock signal. In general, a network I/O-based interlock system is not highly reliable owing to the failure of network switch in the network route and slow signal transmission speed as compared to the bus access. Therefore, the reliability of a signal through TCP/IP is lower than that of an electric signal, which results in a less reliable interlock.

Accordingly, to overcome this disadvantage, a new SC-ECRIS control system has been designed by implementing two different types of CPUs in the main PLC station. Essentially, the sequence PLC CPU (F3SP71) in the first slot and Linux PLC CPU (F3RP61) in the second slot have been implemented in the same PLC base module. In the sequence PLC CPU, the sequential program called ladder program runs for the interlock system and the Linux CPU runs the EPICS input/output controller (IOC) and provides operation services to users via the EPICS Channel Access protocol. In the Yokogawa FA-M3V series, the fieldbus is called the FA bus. The controllers on the main station manage four substations connected through FA bus communication, electrically isolated by optical fibers. Because the heavy ions generated by an ion source are extracted to the low-energy beam transport by high voltage, substations also need to be implemented at the high-voltage stage in some cases. The new SC-ECRIS control system consists of a main PLC station and five PLC substations with star-topology fieldbus communication using optical FA bus modules (see Fig. 1). At present, this control system does not include the control for superconducting electromagnet power supplies. The system has been implemented by another

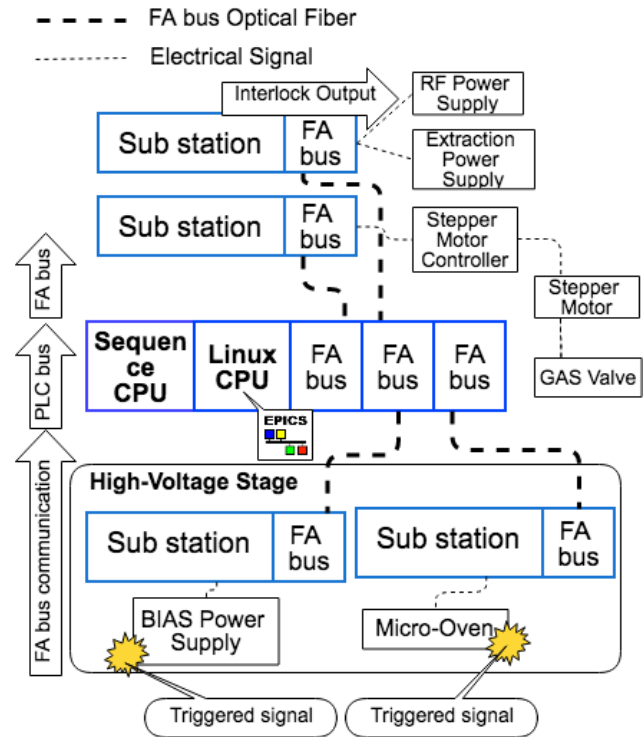


Fig. 1. System chart of new SC-ECRIS control system. Interlock signal is delivered by bus communications.

PLC with EPICS.

This new SC-ECRIS control system was successfully used in the test operation of the new SC-ECRIS performed in August 2018 without any serious problem. Because two CPUs were mounted in one base unit, the trigger signal could be exchanged for interlocking with the sequence PLC CPU from the Linux PLC CPU via the FA bus on the PLC base module. Therefore, it is possible to share the interlock signal of the high-voltage stage with the Linux PLC CPU and sequence PLC CPU without going through the TCP/IP network, which improves the system reliability of the interlock feature successfully without lowering the conventional system usability.

## References

- 1) T. Nagatomo *et al.*, in these proceedings.
- 2) M. Komiyama *et al.*, Proc. ICALEPCS 2009, (2009), pp. 275–277.

<sup>†</sup> Condensed from the article in Proc. PCaPAC2018, No. WEP30

<sup>\*1</sup> RIKEN Nishina Center

<sup>\*2</sup> SHI Accelerator Service Ltd.

## Operation report for Nishina and RIBF water-cooling systems

T. Maie,<sup>\*1</sup> K. Kusaka,<sup>\*1</sup> M. Ohtake,<sup>\*1</sup> Y. Watanabe,<sup>\*1</sup> E. Ikezawa,<sup>\*1</sup> M. Oshima,<sup>\*2</sup> H. Hirai,<sup>\*2</sup> K. Kobayashi,<sup>\*3</sup>  
A. Yusa,<sup>\*3</sup> and J. Shibata<sup>\*3</sup>

### Operation condition

In FY 2018, the cooling systems in Nishina and RIBF were operated for approximately same periods as the accelerators. As the experiments of GARIS II in E6 room had begun, RIBF's cooling systems were operated for approximately two-and-a-half months, which was slightly shorter [than usual]. Nishina's cooling systems' which consisted of AVF-stand alone and AVF + RRC were operated for approximately seven months. There was no significant issue to cause interruption of accelerator operation' and the cooling systems were operated almost steadily except some of minor problems.

### Trouble report

The problems of the cooling systems as follows; Burst of frozen cooling piping in the cooling tower in February 2018 due to the decrease of outside temperature, Malfunctioning of the inverter used for the water-cooling pump caused by aging degradation, Malfunctioning of the control valve.

### Periodic maintenance

- (1) Cleaning of the cooling towers
- (2) Inspection and overhauling of the water-cooling pumps
- (3) Inspection of the inverter for the RIBF water-cooling pumps
- (4) Inspection and overhauling of the air compressor
- (5) Replacement of some superannuated hoses, joints' and valves used in the system
- (6) Cleaning of the strainers and filters used in the deionized water production system
- (7) Extension of the sensing wires of the water leakage alarm to floors of new areas
- (8) Switching electricity during planned power failure as well as restoration of each device
- (9) Securing of minimum power at low load operator of CGS (cogeneration system)

### Establishment and improvement

In this fiscal year, it has been planned that four systems of the RIBF cooling tower' whose performances were degraded by aging' are to be overhauled on a



Fig. 1. Photographs of the four systems of RIBF cooling tower overhaul and new cooling systems for RILAC's superconductive.

large scale, new cooling systems are to be installed along with RILAC's superconductive, and construction of RRC cooling systems for reinforcement of cooling capacity and for stabilization of cooling water temperature. The construction of the RRC cooling systems mentioned above is aimed at elimination of the fluctuation of the magnetic field of an RRC electromagnet due to the inconstancy of the cooling water.

### References

- 1) T. Maie *et al.*, RIKEN Accel. Prog. Rep. **51**, (2017).
- 2) T. Maie *et al.*, RIKEN Accel. Prog. Rep. **50**, (2016).

<sup>\*1</sup> RIKEN Nishina Center

<sup>\*2</sup> Nippon Kucho Service Co., Ltd

<sup>\*3</sup> SHI Accelerator Service Co., Ltd

## Pressure measurement of plasma window with large diameter

N. Ikoma,<sup>\*1,\*2</sup> Y. Miyake,<sup>\*1</sup> M. Takahashi,<sup>\*1</sup> H. Okuno,<sup>\*1</sup> S. Namba,<sup>\*3</sup> and T. Kikuchi<sup>\*4</sup>

The plasma window (PW),<sup>1)</sup> which separates a vacuum from an atmosphere by an arc plasma filling the discharge channel, is a novel beam window technology. It has several applications in an accelerator system such as a gas charge stripper<sup>2,3)</sup> for a heavy ion accelerator or a beam window for an accelerator-driven subcritical reactor (ADS).<sup>4)</sup> In addition, a target system using PW has been proposed in the ImpACT Fujita program<sup>5)</sup> for the transmutation of long-lived fission products (LLFP) into a stable or short-lived nuclei. However, the small diameter of PW is a crucial problem for these applications. The first PW invented by Hershcovitch,<sup>1)</sup> with an aperture of 2.36 mm, aimed at electron beam welding in an atmosphere. However, the beam spot size in our intended case is several tens of millimeters or more. Therefore, to implement the PW in the accelerator system, its diameter needs to be enlarged. Furthermore, an investigation of the relation between confinement pressure and diameter is also important to predict the performance of PW for various purposes. Therefore, we have developed a PW with large diameter in reference to a PW designed by Namba *et al.*<sup>6)</sup> In a previous study,<sup>7)</sup> we reported the performance of a PW with a diameter of 10 mm. After that, we systematically measured the pressure by varying the diameter from 6 to 20 mm. In this study, the preliminary results of pressure measurement have been reported.

The experimental setup is shown in Fig. 1. Argon gas was introduced from the upstream of the PW. It was then exhausted by two mechanical booster pumps (Edwards, EH 500, the exhaust speed of each pump was approximately 100 L/s). Three DC power sup-

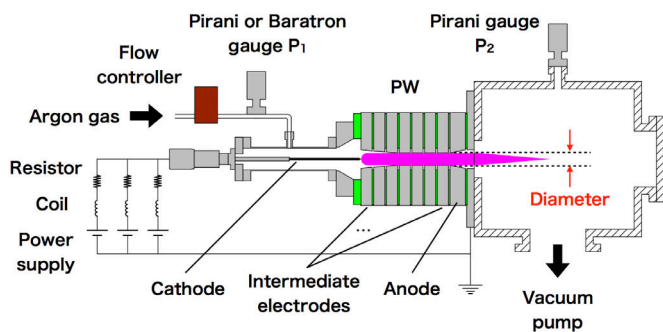


Fig. 1. Experimental setup.

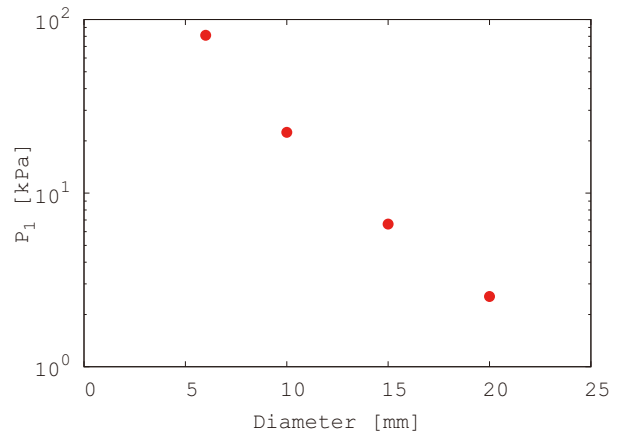


Fig. 2. Dependence of  $P_1$  on the diameter of PW.

plies (TDK Lambda, ESS-400-37-2-D) were connected in parallel between the cathode and anode, and an arc current of 100 A was supplied. The discharge voltage was monitored by a data logger (KEYENCE, NR-600). The gas flow rate was maintained at 20 L/min by the mass flow controller (MKS Instruments, 1579 A) and both upstream and downstream pressures,  $P_1$  and  $P_2$ , were measured.

Figure 2 shows the upstream pressure  $P_1$  on each diameter, which decreased with an increase in the diameter of PW.  $P_2$  was maintained at approximately 200 Pa in each condition. These results will be compared with those of an existing theoretical model ( $P_1 \propto 1/r^2$ ) based on viscous laminar flow.<sup>8,9)</sup> We will determine a prediction model that can describe the confinement pressure in the PW with a large diameter.

This work was supported by RIKEN Junior Research Associate Program and funded by ImpACT Program of Council for Science, Technology and Innovation (Cabinet Office, Government of Japan).

### References

- 1) A. Hershcovitch, J. Appl. Phys. **78**, 5283 (1995).
- 2) H. Okuno *et al.*, Phys. Rev. Accel. Beams **14**, 033503 (2011).
- 3) H. Kuboki *et al.*, J. Radioanal. Nucl. Chem. **299**, 1029 (2014).
- 4) S. Ben-Liang *et al.*, Chin. Phys. C **38**, 018201 (2014).
- 5) Impulsing Paradigm Change through Disruptive Technologies Program ImpACT, <http://www.jst.go.jp/impact/en/index.html>, accessed: January 21, 2019.
- 6) S. Namba *et al.*, Rev. Sci. Instrum. **87**, 083503 (2016).
- 7) N. Ikoma *et al.*, RIKEN Accel. Prog. Rep. **51**, 144 (2018).
- 8) W. A. J. Vijvers *et al.*, Phys. Plasmas **15**, 093507 (2008).
- 9) S. Huang *et al.*, Phys. Plasmas **21**, 123511 (2014).

<sup>\*1</sup> RIKEN Nishina Center

<sup>\*2</sup> Department of Energy and Environment Science, Nagaoka University of Technology

<sup>\*3</sup> Graduate School of Engineering, Hiroshima University

<sup>\*4</sup> Department of Nuclear System Safety Engineering, Nagaoka University of Technology

## Maintenance of vacuum conditions of RILAC

S. Watanabe,<sup>\*1</sup> Y. Watanabe,<sup>\*1</sup> E. Ikezawa,<sup>\*1</sup> K. Yamada,<sup>\*1</sup> N. Sakamoto,<sup>\*1</sup> M. Kase,<sup>\*1</sup> O. Kamigaito,<sup>\*1</sup> M. Nishida,<sup>\*2</sup> K. Yadomi,<sup>\*2</sup> J. Shibata,<sup>\*2</sup> K. Oyamada,<sup>\*2</sup> A. Yusa,<sup>\*2</sup> N. Tsukiori,<sup>\*2</sup> K. Kobayashi,<sup>\*2</sup> S. Fukuzawa,<sup>\*2</sup> T. Nakamura,<sup>\*2</sup> R. Koyama,<sup>\*2</sup> S. Ishikawa,<sup>\*2</sup> M. Hamanaka,<sup>\*2</sup> M. Nishimura,<sup>\*2</sup> T. Ohki,<sup>\*2</sup> H. Yamamoto,<sup>\*2</sup> M. Tamura,<sup>\*2</sup> and K. Kaneko<sup>\*2</sup>

Maintenances of vacuum condition in RILAC are described. There had been two big problems of vacuum conditions at RILAC. One was a vacuum leak at a cavity No. 5, the other was a leak of vacuum at a cavity A1. The cavity No. 5 had a vacuum leak, the pressure of its vacuum was higher than  $1 \times 10^{-4}$  Pa. As for a problem of cavity No. 5, it was difficult to handle it because of its heavy weight, large scale and complicated structure. As shown in Fig. 1, the cavity No. 5 has a large vacuum chamber of which the inner wall was used as an electrode called “outer conductor.” Inside of the outer conductor, there were several electrodes to accelerate an ion beam. Some of the acceleration electrodes were connected to a large cavity called “center conductor.” Junction area between the electrode and the center conductor was sealed using an O-ring. The opposite side of the wall of the center conductor opposite side of the wall was exposed to atmosphere. Flanges were sealed using O-rings. All O-rings of the vacuum-sealing flanges on the outer conductor were exchanged with new ones, however the pressure was not improved, higher than  $1 \times 10^{-4}$  Pa. We found another air-leak point by using a helium leak detector when we shot helium gas from an atmosphere side of the center conductor. The cavity No. 5 was repaired in from September to November. Another vacuum leak point was sealed face between electrodes and the cavity. When helium gas was shot from the atmosphere side of the center conductor to sealed area. A helium leak detector was reacted. To access the O-ring on the center conductor, a large flange of the outer conductor was opened using a crane. To fix the leak, the elec-

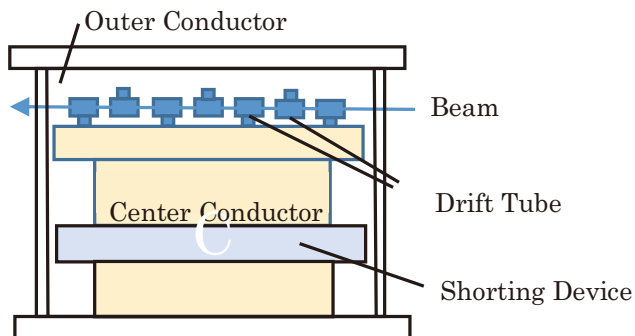


Fig. 1. Schematic diagram of cavity No. 5.

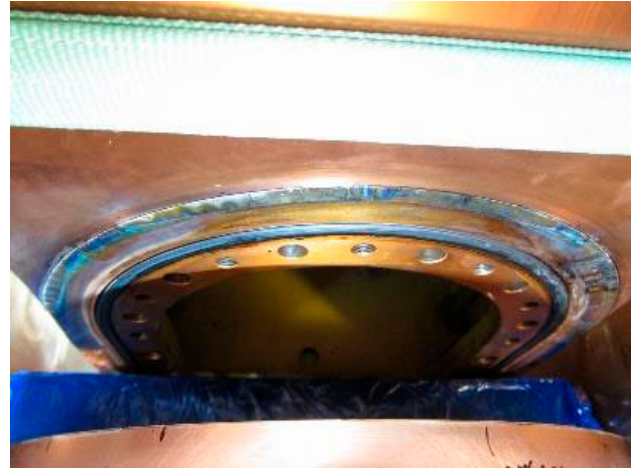


Fig. 2. Sealing face with a degenerate O-ring on center conductor of cavity No. 5.

trode was removed from the center conductor. A deteriorating O-ring across the ages was found as shown in Fig. 2 and the O-ring was replaced with new one. When the electrodes were assembled, thin silver plates were stacked on the joint area to place the electrodes on the level. The leak of the tank was fixed and the pressure of the tank was improved to  $9 \times 10^{-6}$  Pa.

The cavity, A1, had vacuum leak on the bottom flange, however, a location of the leak point was not identified precisely. We presumed that the air-leak point was under the paint covering the vacuum-sealing flanges because of the delayed response of the helium detection. Thus, in October, after removing the paint, we hunted the air-leak once more. The surface of the flange was masked by plastic tape except the checking area to block the ingress of helium gas. The tape was re-covered every time the checking area changing. At last, we found the air-leak point on an area of the cooling pipe on the flange. The vacuum leak area was found and was applied by sealing agent (VACSEAL). The pressure of A1 was improved to  $3 \times 10^{-6}$  Pa.

<sup>\*1</sup> RIKEN Nishina Center

<sup>\*2</sup> SHI Accelerator Service Ltd.



## **9. Instrumentation**



# Application of the Generic Electronics for Time Projection Chamber (GET) readout system for heavy radioactive isotope collision experiments<sup>†</sup>

T. Isobe,<sup>\*1</sup> G. Jhang,<sup>1\*,\*3</sup> H. Baba,<sup>\*1</sup> J. Barney,<sup>\*1,\*3</sup> P. Baron,<sup>\*7</sup> G. Cerizza,<sup>\*1,\*3</sup> J. Estee,<sup>\*1,\*3</sup> M. Kaneko,<sup>\*1,\*2</sup> M. Kurata-Nishimura,<sup>\*1</sup> J. W. Lee,<sup>\*1,\*4</sup> W. G. Lynch,<sup>\*3</sup> T. Murakami,<sup>\*1,\*2</sup> N. Nakatsuka,<sup>\*2</sup> E. C. Pollacco,<sup>\*7</sup> W. Powell,<sup>\*5</sup> H. Sakurai,<sup>\*1</sup> C. Santamaria,<sup>\*1,\*3</sup> D. Suzuki,<sup>\*1</sup> S. Tangwancharoen,<sup>\*3</sup> and M. B. Tsang<sup>\*3</sup>

The S $\pi$ RIT time projection chamber (TPC) is one of the main devices for the S $\pi$ RIT project at RIKEN-RIBF.<sup>1)</sup> The S $\pi$ RIT project aims to study the density-dependent term of the symmetry energy using heavy RI collision through the measurement of charged pions and light nuclei. We have implemented the Generic Electronics for Time Projection Chamber (GET) in S $\pi$ RIT-TPC readout system. The operation of the GET electronics during the last experiment in 2016 went well at DAQ a rate of 60 Hz.

It was hard to identify Li isotopes clearly due to the limitation of the ADC dynamic range. We have developed a method to measure energy loss by using the slope value of each signal instead of the pulse height. Here, the slope is the gradient of the leading signal shape. A cocktail beam of proton, deuteron, triton, <sup>3</sup>He, <sup>4</sup>He, <sup>6</sup>Li, and <sup>7</sup>Li particles with a beam momentum of  $p/Q \sim 1.6$  GeV/ $c$  is made with the BigRIPS fragment separator. Figure 1 shows the energy loss distribution of each projectile. In the case of the high-gain configuration used for the pion measurement, the deposited energy from the  $Z \geq 3$  particles is too high to identify Li isotopes by using signal height information. Due to the saturation of several pads along the Li trajectory, the energy loss resolution of the Li trajectory is worse than that of other light particle trajectories. By using the slope value instead of signal height, it is possible to increase the dynamic range of signal measurement so that the distribution of <sup>6</sup>Li and <sup>7</sup>Li can be separated by  $4\sigma$ .

Figure 2 shows the calibration curves obtained by injecting a long rectangular pulse to the ground wire of TPC: the maximum slope and ADC value as a function of input charge. Although the maximum ADC value is saturated around an input charge of 120 fC, the maximum slope value still shows linearity beyond 120 fC. According to the SPICE simulation, the linearity of the slope value extends up to 200 fC charge input, *i.e.* the dynamic range is increased by 65%.

This work is supported by the Japanese MEXT KAKENHI Grant No. 24105004, the U.S. DOE un-

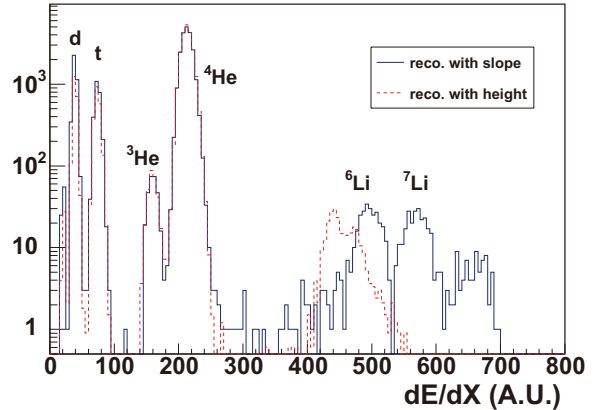


Fig. 1. Energy loss distribution of each particle passing through TPC. Trajectories of  $1.6 \leq p/Q \leq 1.7$  GeV/ $c$  are selected. The spectrum of energy loss reconstructed with the signal height is shown as a dotted line while the spectrum of energy loss reconstructed with the signal slope is shown as a solid line.

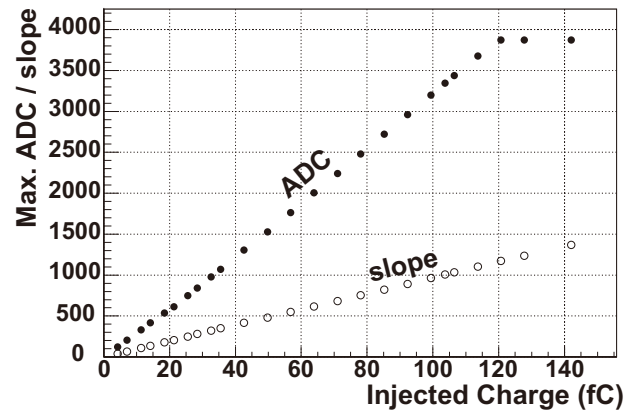


Fig. 2. Pad response induced by a long rectangular pulse injected to the ground plane wire. The induced ADC response is saturated for an injected charge above 120 fC.

der Grant Nos. DE-SC0004835, DE-SC0014530, DE-NA0002923, the U.S. NSF Grant No. PHY-1565546, and the Polish NSC Grant Nos. UMO-2013/09/B/ST2/04064 and UMO-2013/10/M/ST2/00624. The computing resources for analyzing data were provided by the HOKUSAI system at RIKEN.

## References

- 1) S. Rebecca *et al.*, Nucl. Instrum. Methods Phys. Res. A **784**, 513 (2015).
- 2) E. Pollacco *et al.*, Phys. Procedia **37**, 1799 (2012).
- 3) T. Isobe *et al.*, RIKEN Accel. Prog. Rep. **48**, 204 (2015).

<sup>†</sup> Condensed from the article in Nucl. Instrum. Methods Phys. Res. A **899**, 43–48 (2018)

<sup>\*1</sup> RIKEN Nishina Center

<sup>\*2</sup> Department of Physics, Kyoto University

<sup>\*3</sup> National Superconducting Cyclotron Laboratory, Michigan State University

<sup>\*4</sup> Department of Physics, Korea University

<sup>\*5</sup> Department of Physics, University of Liverpool

<sup>\*7</sup> CEA Saclay IRFU/SPhN

# PANDORA, a large volume low-energy neutron detector with real-time neutron-gamma discrimination<sup>†</sup>

L. Stuhl,<sup>\*1,\*2</sup> M. Sasano,<sup>\*2</sup> K. Yako,<sup>\*1</sup> J. Yasuda,<sup>\*3</sup> H. Baba,<sup>\*2</sup> S. Ota,<sup>\*1</sup> and T. Uesaka<sup>\*2</sup>

Recent nuclear physics studies are increasingly focused on the region far from the valley of stability. The increase in the intensity of available exotic isotopes enables the investigation of phenomena with low cross-sections, such as inelastic scattering and charge-exchange (CE) reactions. Because the cross-sections of the CE reactions are very low, it is crucial to efficiently tag these reaction channels and minimize the contaminant events from other reaction channels with larger cross-sections (*e.g.*, elastic scattering, knockout reactions). The  $(p, n)$  CE reactions at intermediate energies (150–300 MeV/nucleon) are a powerful tool to study the spin-isospin excitations in nuclei. The inverse kinematics<sup>1,2)</sup> enables the  $(p, n)$  reactions on exotic nuclei with a high luminosity. In this technique, neutron detectors are used to measure the time-of-flight (ToF) of low-energy recoil neutrons from a few hundred keV to a few MeV produced from the  $(p, n)$  reaction. This methodology has been successfully applied to study the Gamow-Teller strength distribution from  $^{56}\text{Ni}$ <sup>2)</sup> and  $^{132}\text{Sn}$ <sup>3)</sup> isotopes. We also started a program at RIBF aiming to study the spin-isospin responses of  $^{11}\text{Li}$  and  $^{14}\text{Be}$  light drip line nuclei.

The first generation of neutron detectors designed for these measurements, such as LENDA,<sup>4)</sup> WINDS,<sup>5)</sup> and ELENS<sup>6)</sup> cannot distinguish between neutrons and gamma rays. The random gamma background, which mainly arises from the environment, cannot be removed from the neutron spectra. We developed the PANDORA (Particle Analyzer Neutron Detector Of Real-time Acquisition) system as an upgrade of the WINDS detector. PANDORA is based on a plastic scintillator, sensitive to the differences between neutrons and gamma rays. Neutrons and gamma rays can be distinguished by their pulse shapes because their signals in the tail region differ (larger tail for neutrons). PANDORA employs a digital data acquisition system. The signals are read-out with CAEN V1730 digitizer.

We presented the first results on the pulse shape discrimination capabilities of the new large volume plastic scintillator EJ-299-34-based device PANDORA coupled to a digital data acquisition system. The PSD performance was compared to that of the well-established EJ-299-33 scintillator.<sup>7)</sup> We introduced the PSD<sub>mean</sub> offline value as the arithmetic mean of online PSD values of two single-end read-outs (PSD<sub>left</sub> and PSD<sub>right</sub>). The ToF distributions acquired using a  $^{252}\text{Cf}$  fission source

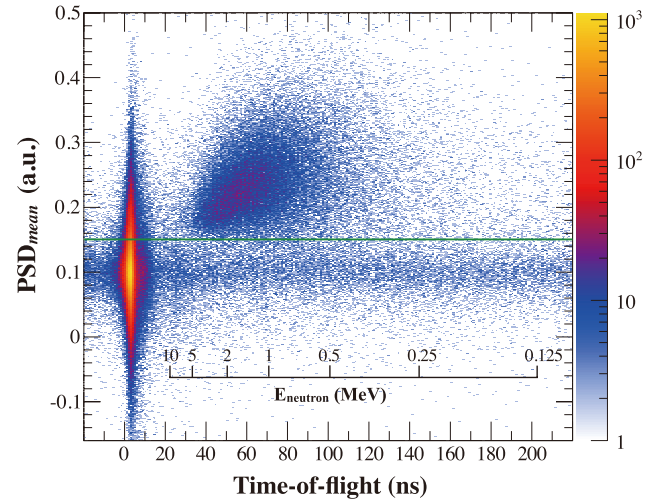


Fig. 1. PSD<sub>mean</sub> vs. ToF spectrum shows a good separation of neutron and gamma-like events. The sharp peak below 10 ns corresponds to events identified as gamma rays, while the distribution in the higher ToF region and PSD<sub>mean</sub> > 0.15 represents neutron-like events. The inner scale corresponds to the kinetic energy of the detected neutrons obtained using the ToF method. A large random gamma background can also be observed.

show that with PANDORA, 91±1% of all detected neutrons can be identified online and 91±1% of the detected gamma rays can be excluded. This online gamma rejection (individual threshold conditions on the left and right PSDs) reduces the background by one order of magnitude.

Our goal of particle-based real-time triggering was successfully attained. This development allows  $(p, n)$  reactions on exotic nuclei to be measured with a secondary beam intensity up to 10<sup>6</sup> particle/sec. Furthermore, this new setup provides opportunity for reaction studies that involve emission of low-energy neutrons. The PANDORA system is capable to provide a filtered data package of energy, timing, PSD information, and digitized pulse shape, which can be used for further improvements offline.

## References

- 1) G. Perdikakis *et al.*, IEEE Trans. Nucl. Sci. **56**, 3 (2009).
- 2) M. Sasano *et al.*, Phys. Rev. Lett. **107**, 202501 (2011).
- 3) M. Sasano *et al.*, EPJ Web of Conf. **107**, 06003 (2016).
- 4) G. Perdikakis *et al.*, Nucl. Instrum. Methods Phys. Res. A **686**, 117 (2012).
- 5) K. Yako *et al.*, RIKEN Accel. Prog. Rep. **45**, V, (2012).
- 6) L. Stuhl *et al.*, Nucl. Instrum. Methods Phys. Res. A **736**, 1 (2014).
- 7) P. Blanc *et al.*, Nucl. Instrum. Methods Phys. Res. A **750**, 1 (2014).

<sup>†</sup> Condensed from the article in Nuclear Instruments and Methods in Phys. Res. A **866**, 164 (2017)

<sup>\*1</sup> Center for Nuclear Study, University of Tokyo

<sup>\*2</sup> RIKEN Nishina Center

<sup>\*3</sup> Department of Physics, Kyushu University

## Measurement of total kinetic energy using LaBr<sub>3</sub>(Ce) crystal in ZeroDegree spectrometer for two-step experiment

H. Suzuki,<sup>\*1</sup> D. S. Ahn,<sup>\*1</sup> N. Fukuda,<sup>\*1</sup> H. Takeda,<sup>\*1</sup> Y. Shimizu,<sup>\*1</sup> R. Taniuchi,<sup>\*1</sup> H. Wang,<sup>\*1</sup> S. Takeuchi,<sup>\*2,\*1</sup> and K. Yoshida<sup>\*1</sup>

A LaBr<sub>3</sub>(Ce) crystal was used as the total-kinetic-energy (TKE) counter for particle identification (PID) in the ZeroDegree spectrometer in the two-step experiment.<sup>1)</sup> In this experiment, events of partially-stripped radioactive isotopes (RI) were not negligible, because the mass numbers,  $A$ , of RIs produced at the target at the entrance of ZeroDegree were over 100 and their kinetic energies were 200 MeV/nucleon. For the PID, the atomic number,  $Z$ , and the mass-to-charge ratio,  $A/Q$ , were deduced based on a TOF- $B\rho\text{-}\Delta E$  method. However, the  $A/Q$  resolution in ZeroDegree with Medium-Resolution-Achromatic mode<sup>2)</sup> was 0.061% in RMS and inadequate to separate fully-stripped RIs from the partially-stripped ones. Thus, the value of  $A$  was deduced from the velocity ( $\beta$ ) and TKE of each RI and was used for the separation.

The LaBr<sub>3</sub>(Ce) crystal<sup>3,4)</sup> was mounted at the end of ZeroDegree. It is cylindrical in shape with 3-inch diameter and length, covered with a 0.5-mm thick Al housing. Nine PIN-photodiodes were attached to the back of the crystal through a light-guide made of Lucite. Five diodes with effective areas of 18 mm<sup>2</sup> (S3204-08; Hamamatsu Photonics K.K.) were arranged in the shape of a cross and other four diodes of 10 mm<sup>2</sup> (S3590-18; Hamamatsu) were placed at the four corners. The signal from each diode was amplified by a pre-amplifier (MSI-8; mesytec GmbH & Co. KG) whose dynamic range was set to be 1 GeV in Si energy-loss equivalent and a shaping amplifier (MSCF-16; mesytec) whose shaping time was set to be 2  $\mu$ s.

The energy of the crystal was calibrated by comparing

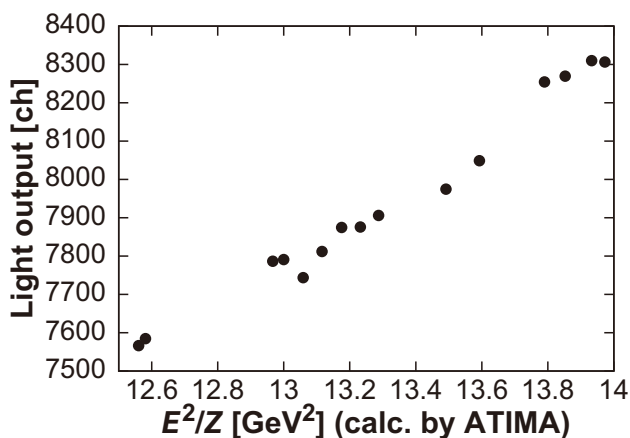


Fig. 1. Relation between light output from LaBr<sub>3</sub>(Ce) crystal and calculated  $\frac{E^2}{Z}$  by ATIMA.<sup>5)</sup>

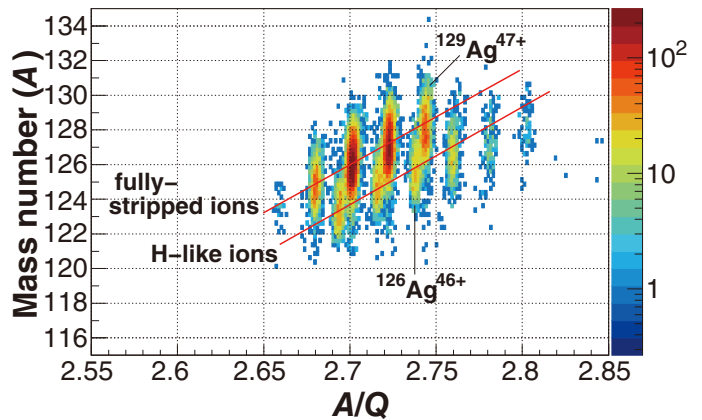


Fig. 2. Separation of Ag isotopes in  $A$  versus  $A/Q$ .  $4.6\sigma$  separation was achieved between  $^{129}\text{Ag}^{47+}$  and  $^{126}\text{Ag}^{46+}$ .

the light output and calculated energy-loss of RIs using an energy-loss code ATIMA.<sup>5)</sup> Owing to the quenching effect, the light output was not proportional to the energy loss. In this experiment,  $\frac{E^2}{Z}$  ( $E$ ; energy loss in the crystal) was found to be proportional to the light output, as shown in Fig. 1. In previous studies by Kobayashi<sup>4)</sup> and Taniuchi *et al.*,<sup>6)</sup>  $\frac{E^2}{Z^2}$  and  $\frac{E}{\sqrt{Z}}$  respectively, were proposed as the proportional variables. It is unclear why the quenching effects are different in these three cases. It may be caused by the width of the  $Z$  range, which was 41–50 in our case, 28–52 in Ref. 4), and 8–50 in Ref. 6).

The distribution of  $A$  in the two-step experiment was 0.95 in RMS around  $^{129}\text{Ag}^{47+}$ . Thus, the resolution of  $A$  was 0.8% and  $3\sigma$  separation was achieved between the fully-stripped  $^{129}\text{Ag}^{47+}$  and H-like  $^{126}\text{Ag}^{46+}$  in mass. In  $A/Q$  axis,  $3.5\sigma$  separation was obtained between these two isotopes. Thus,  $4.6\sigma$  separation was achieved using both  $A/Q$  and  $A$  separations. Figure 2 shows the separation of Ag isotopes in the two-step experiment in  $A$  versus  $A/Q$  plot. The fully-stripped RIs are well separated from the H-like RIs. The charge number,  $Q$ , was deduced from  $A/Q$  and  $A$ .  $2.5\sigma$  separation was achieved in the  $Q$  separation.

### References

- 1) H. Suzuki *et al.*, RIKEN Accel. Prog. Rep. **52**, (2019).
- 2) T. Kubo *et al.*, Prog. Theor. Exp. Phys. **2012**, 03C003 (2012).
- 3) R. Kambayashi, Master's thesis, Rikkyo Univ. (2011).
- 4) K. Kobayashi, Master's thesis, Rikkyo Univ. (2012).
- 5) ATIMA web page, <https://web-docs.gsi.de/~weick/atima>.
- 6) R. Taniuchi *et al.*, RIKEN Accel. Prog. Rep. **48**, 210 (2015).

<sup>\*1</sup> RIKEN Nishina Center

<sup>\*2</sup> Center for Nuclear Study, University of Tokyo

# Prototype of new delay line with chip inductors for the PPAC

H. Sato,<sup>\*1</sup> H. Baba,<sup>\*1</sup> and K. Yoshida<sup>\*1</sup>

In Parallel Plate Avalanche Counter (PPAC), which is used at the BigRIPS, the XY position is deduced by using the delay line readout method.<sup>1)</sup> The X and Y electrode strips are connected to multi-tapped delay lines (DLs). The inductance of the DL is formed by a coil made by winding a  $\phi 0.3$  wire wound around a  $\phi 2.0$  Bakelite rod. Additionally  $\phi 0.12$  lead wires are soldered onto the coil wire every eight turns. Thus, the fabrication and maintenance of this DL is a difficult work that requires an expert for soldering. To simplify the DL fabrication, prototyping of new DL consisting of chip inductors and capacitors has been started.

The new DL is fabricated by the reflow soldering method. A soldering paste is put on the pads of the G10 board via a  $200\ \mu\text{m}$ -thick mask. The chips are placed on the pads and then the board is heated up to around  $160^\circ\text{C}$  on a hot plate to melt the solder. Images of the ordinary DL and the new DL are shown in Fig. 1.

Several new DLs were fabricated and tested. In this report, the properties of the X DL named CLDLX#02 are described. The chip inductors are Murata LQW2BAN91NG00L, whose inductance  $L$  is  $91\ \text{nH} \pm 2\%$ . The chip capacitors are Murata GRM2162C1H390JZ01D, whose capacitance  $C$  is  $39\ \text{pF} \pm 5\%$ , and chips having the same  $C$  within one decimal place were used to realize the same delay time of one pitch ( $T_{dt} = 1.07\sqrt{LC}$ ). The measured average  $T_{dt}$  was  $2.02\ \text{ns}$  with  $1.0\%$  of the standard deviation.

The performance of the  $240\ \text{mm} \times 150\ \text{mm}$  PPAC with new DLs was evaluated with an  $\alpha$  source. Figure 2 (a) shows the X-axis position spectrum of the  $\alpha$ -rays that are uniformly irradiated on the PPAC. The uniformity of the detection sensitivity from  $-108\ \text{mm}$

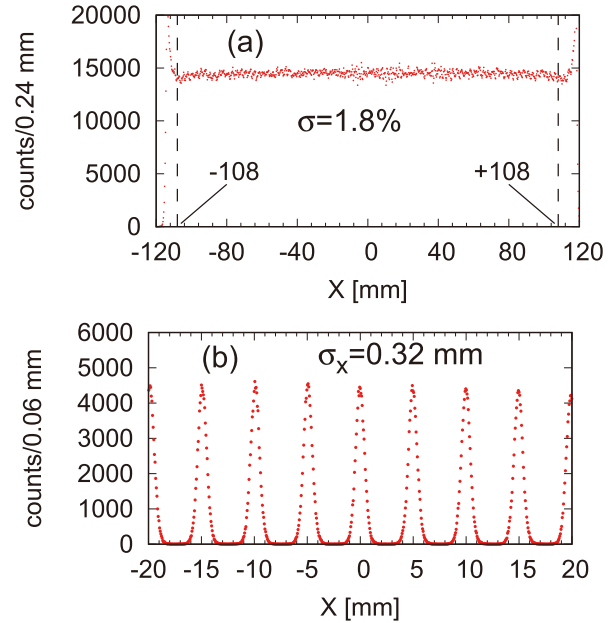


Fig. 2. X-axis position spectrum: (a) uniformly irradiated, (b) with a position calibration mask.

Table 1. Characteristics of CLDLX#02 and 25X#34.

	CLDLX#02	25X#34
inductance [nH]	91	90
capacitance [pF]	39.1	38.4
total delay time [ns]	193	192
delay time of one pitch [ns]	2.02	2.02
signal speed [mm/ns]	1.265	1.261
attenuation rate [%]	65	68
uniformity of sensitivity [%]	1.8	1.4
position resolution [mm]	0.32	0.25

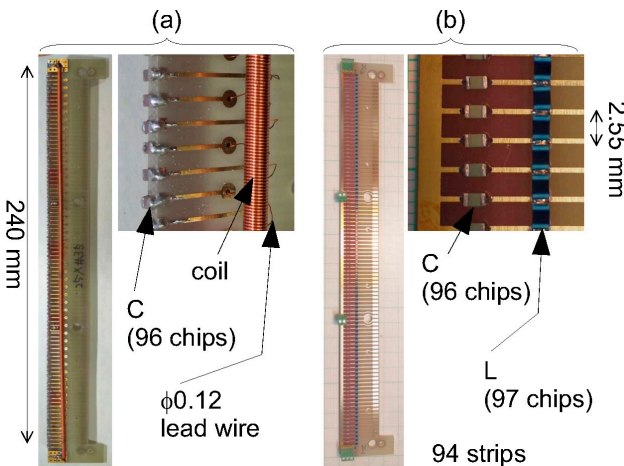


Fig. 1. Images of the DL boards for X. (a) ordinary multi-tapped DL. (b) new DL.

to  $+108\ \text{mm}$  (90% of the full range of X) excluding the statistical fluctuation was  $1.8\%$ . Figure 2 (b) is the spectrum measured with a position calibration mask, which has a slit interval and width of  $5$  and  $0.5\ \text{mm}$ , respectively. The position resolution was measured to be  $0.32\ \text{mm}$  in  $\sigma$ . The characteristics of CLDLX#02 are summarized in Table 1 with those of an ordinary multi-tapped DL (25X#34) for comparison. As presented, the position resolution of CLDLX#02 is slightly wider than that of the 25X#34. Thus, with further modification to obtain better performance, the new DL can be used for the PPAC instead of the ordinary DL. In addition, we are also considering another type of DL whose coil is directly patterned on the G10 board.

## Reference

- 1) H. Kumagai *et al.*, Nucl. Instrum. Methods Phys. Res. B **317**, 717 (2013).

<sup>\*1</sup> RIKEN Nishina Center

# Development of electronics to allow vertex determination in the KISS MSPGC

P. Schury,<sup>\*1</sup> Y. Hirayama,<sup>\*1</sup> H. Choi,<sup>\*1,\*2</sup> H. Miyatake,<sup>\*1</sup> Y. X. Watanabe,<sup>\*1</sup> and M. Mukai<sup>\*1,\*3</sup>

The goal for the KEK Isotope Separation System (KISS)<sup>1)</sup> is to provide precise nuclear data of neutron-rich nuclei near  $N = 126$ . Such nuclei, which play an important role in the r-process, are difficult to produce by traditional means (*e.g.* in-flight fission/fragmentation, fusion, ISOL) and therefore KISS uses multi-nucleon transfer reactions to produce them. The rates of interesting nuclei are typically less than  $1 \text{ s}^{-1}$ .

For understanding the nature of the  $N = 126$  bottleneck presumed to be responsible for the  $3^{\text{rd}}$  peak of the r-process requires precise atomic masses and decay half-lives. In order to provide the nuclear astrophysics community with the necessary precise half-life data, a multi-segmented proportional gas counter (MSPGC)<sup>2)</sup> was developed for KISS. The system as initially envisioned utilized two concentric rings of proportional gas counter (PGC) tubes (16 in each ring), thereby allowing the use of “hit pattern” analysis to discriminate background events such as *e.g.* cosmic rays. This proved to be a successful strategy which allowed meaningfully precise half-life determination from species delivered with rates down to  $0.1 \text{ s}^{-1}$ .

In order to push the half-life measurements to  $N = 126$ , however, will require use of the MSPGC with rates an order of magnitude lower. To accomplish this, the PGC tubes have been upgraded to utilize a resistive wire. By detecting the charge deposited on each end of the wire, it is possible to extract the position of the decay detection along the length of the detector. The 3D decay vertex made possible by this added information should allow half-life determination from yields on the order of  $0.01 \text{ s}^{-1}$ .

This requires a charge-sensitive pre-amplifier, shaping amplifier, and trigger generator for both ends of each PGC tube –64 sets in total. Noise considerations require the pre-amplifier to be located as close to the PGC as possible, while space constraints make it infeasible to pack everything into the area near the MSPGC. A small circuit board with power conditioners, a Cremat CR-110 charge-sensitive amplifier (CSA) ( $g = 1.6 \text{ V/pC}$ ), and an AD8138 differential line driver is installed close to each end of every PGC tube. The differential signals are immune to environmental noise.

An array of receivers, as well as power supplies, is installed within a 3U 19” crate installed in a rack  $\approx 3 \text{ m}$  from the MSPGC. The power for the CSA circuit boards is supplied via a long ribbon cable. The differential line drivers following the CSA allow the signal from each detector to be sent to the receiver crate via

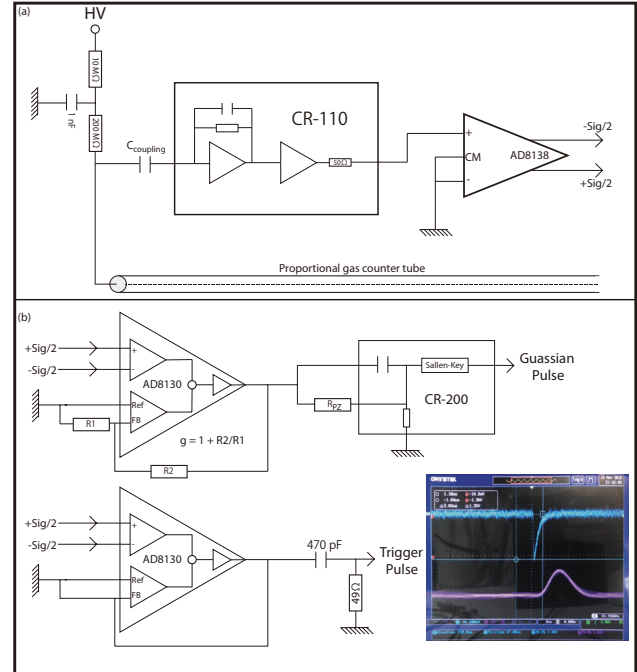


Fig. 1. Sketch of circuitry installed (a) near to and (b) at a distance from the MSPGC. The signal from the CSA is converted to a differential signal to allow noise-free transmission, via long ribbon cable, prior to application of a shaping amplifier. In the inset the trigger pulse is light blue and the Gaussian pulse is purple. The ADC is triggered by the falling edge of the trigger pulse,  $2.5 \mu\text{s}$  prior to the peak of the Gaussian pulse.

the long flat ribbon cable as well. The receiver boards use a pair of AD8130 differential receiver amplifiers to provide a decoupled pair of signals, one to be processed by a CR-200 shaping amplifier and the other to trigger the 14-bit Hoshin C008 analog-to-digital converter (ADC) used to measure the pulse-height of the CR-200 output and determine the detection position along the PGC. Details are given in Fig. 1.

In the initial testing with  $C_{\text{coupling}} = 1 \text{ nF}$ , large  $\sim 100 \text{ kHz}$  oscillations were observed in the CSA output. After consultation with Cremat, it was determined that the each CSA saw the coupling capacitor on the opposite end of the PGC as a heavy load. Reducing  $C_{\text{coupling}}$  to  $100 \text{ pF}$  gave clean, stable signals. Development is ongoing.

## References

- 1) Y. Hirayama *et al.*, Nucl. Instrum. Methods Phys. Res. B **412**, 11 (2017).
- 2) M. Mukai *et al.*, Nucl. Instrum. Methods Phys. Res. A **884**, 1 (2018).

<sup>\*1</sup> KEK Wako Nuclear Science Center

<sup>\*2</sup> Seoul National University

<sup>\*3</sup> Institute of Physics, University of Tsukuba

## Development of Plastic Scintillator Barrel for WASA at GSI

R. Sekiya,<sup>\*1</sup> V. Drozd,<sup>\*2</sup> H. Fujioka,<sup>\*3</sup> K. Itahashi,<sup>\*4</sup> S. Y. Matsumoto,<sup>\*1,\*4</sup> T. R. Saito,<sup>\*2,\*5,\*6</sup> K. Suzuki,<sup>\*7</sup> and Y. K. Tanaka<sup>\*2,\*8</sup>

We plan to conduct new experiments for hypernuclear spectroscopy<sup>1)</sup> and  $\eta'$ -mesic nuclei exploration<sup>2)</sup> using the WASA central detector<sup>3,4)</sup> and the fragment separator (FRS) at GSI. The WASA central detector consists of a superconducting solenoid magnet, a plastic scintillator barrel (PSB), and a cylindrical drift chamber for charged particle measurement and CsI calorimeters for gamma-ray measurement.

We are upgrading the cylindrical part of PSB to achieve 100 ps in time resolution based on the experimental requirement. In the old configuration, we had only one photomultiplier tube with a light guide for each scintillator slat of PSB. We improved the time resolution by detecting photons on both sides using multipixel-photon counters (MPPCs). Since the PSB will be located inside the superconducting solenoid magnet, we chose detectors that can be operated under a magnetic field. MPPC satisfies this requirement.

We made a single slat of PSB as schematically shown in Fig. 1. The size of the plastic scintillator is  $550 \times 38 \times 8 \text{ mm}^3$ . We adopted Eljen EJ-230, which has an attenuation length of 120 cm. We attached four MPPCs (Hamamatsu Photonics S13360-6050CS) on each side of the plastic scintillator and electrically connected them in series. The effective area of the MPPC is  $6 \times 6 \text{ mm}^2$ . The MPPCs were then connected to amplifiers developed in Ref. 5). The amplified signals were recorded by a waveform digitizer (CAEN V1742) with a sampling frequency of 2.5 GHz.

In order to evaluate the time resolution, we irradiated the plastic scintillator with electrons from a  $^{90}\text{Sr}$  source with an endpoint energy of 2.28 MeV. A slit with a gap of 2 mm was inserted between the plastic scintil-

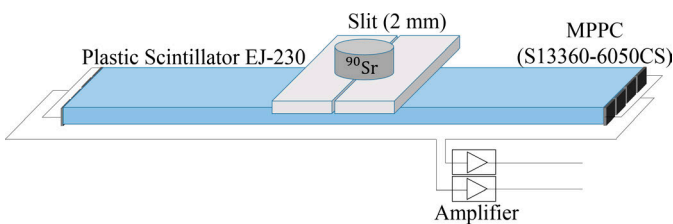


Fig. 1. Schematic configuration of a single slat of PSB.

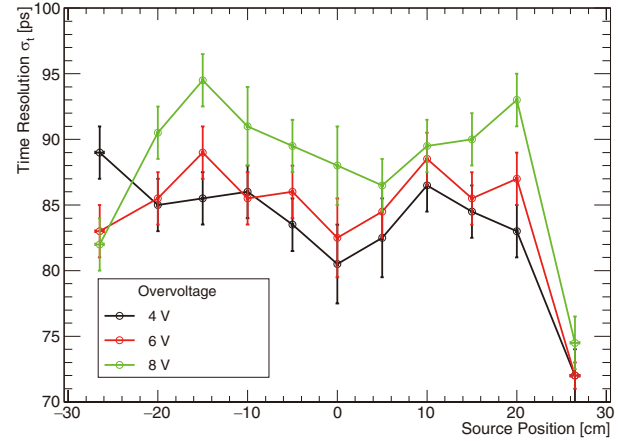


Fig. 2. The dependence of the time resolution  $\sigma_t$  on source positions and applied bias voltages.

lator and the  $^{90}\text{Sr}$  source. We performed measurements by changing the position of the source to investigate the hit position dependence. The overvoltage was also changed to 4, 6, and 8 V.

We evaluated the time resolution of the plastic scintillator by analyzing the waveform data. In the analysis, we simulated a function of constant fraction discriminators by using a software to obtain the precision arrival time of signals at the right and left ends of the plastic scintillator ( $T^R$  and  $T^L$ ). The time resolution of this single slat of PSB ( $\sigma_t$ ) can be estimated by fitting a  $(T^R - T^L)/2$  histogram with a Gaussian function and taking its standard deviation, neglecting the hit position distribution of the electrons.

Figure 2 shows the time resolution  $\sigma_t$  as a function of the source positions. Different colors correspond to different bias voltages. We achieved a time resolution better than 100 ps for all the tested conditions. We also found that the time resolutions become better as the overvoltage is decreased.

Based on the measurements described above, we confirmed that a single slat of PSB achieves the required time resolution. We are planning a more systematic evaluation of the PSB performance by using mono-energetic proton beams.

### References

- 1) T. R. Saito *et al.*, proposal GSI-SIS S447 (2017).
- 2) K. Itahashi *et al.*, proposal GSI-SIS S457 (2017).
- 3) C. Bargholtz *et al.*, Nucl. Instrum. Methods Phys. Res. A **594**, 339 (2008).
- 4) H.-H. Adam *et al.* (WASA-at-COSY Collaboration), arXiv:nucl-ex/0411038 (2004).
- 5) P. W. Cattaneo *et al.*, IEEE Trans. Nucl. Sci. **61**, 2657 (2014).

\*1 Department of Physics, Kyoto University

\*2 GSI Helmholtz Center for Heavy Ion Research

\*3 Department of Physics, Tokyo Institute of Technology

\*4 RIKEN Nishina Center

\*5 High Energy Nuclear Physics Laboratory, Cluster for Pioneering Research, RIKEN

\*6 Helmholtz Institute Mainz

\*7 SMI

\*8 II. Physikalisches Institut, Giessen University

## Energy dependence study of cylindrical drift chamber used for the MTV experiment

F. Goto,<sup>\*1,\*2</sup> H. Baba,<sup>\*2</sup> J. A. Behr,<sup>\*3</sup> T. Kajihara,<sup>\*4</sup> H. Kawamura,<sup>\*5</sup> M. Kitaguchi,<sup>\*1</sup> C. D. P. Levy,<sup>\*3</sup> H. Masuda,<sup>\*4</sup> Y. Nakaya,<sup>\*4</sup> K. Ninomiya,<sup>\*4</sup> J. Onishi,<sup>\*4</sup> R. Openshaw,<sup>\*3</sup> S. Ozaki,<sup>\*4</sup> M. Pearson,<sup>\*3</sup> Y. Sakamoto,<sup>\*4</sup> H. Shibaguchi,<sup>\*4</sup> H. M. Shimizu,<sup>\*1</sup> Y. Shimizu,<sup>\*4</sup> R. Takenaka,<sup>\*4</sup> K. Tamura,<sup>\*4</sup> S. Tanaka,<sup>\*4</sup> R. Tanuma,<sup>\*4</sup> Y. Totsuka,<sup>\*4</sup> E. Watanabe,<sup>\*4</sup> Y. Yamamoto,<sup>\*4</sup> Y. Yamawaki,<sup>\*4</sup> M. Yokohashi,<sup>\*1</sup> and J. Murata<sup>\*4</sup>

The purpose of the MTV (Mott polarimetry for T-violation) experiment is to find a large time reversal symmetry violation (T-violation) in polarized  $^8\text{Li}$   $\beta^-$  decay. T-violation may arise in triple vector correlation ( $R$ -correlation) in beta decay.  $R$ -correlation causes electron transverse polarization and it can be measured by detecting electron Mott scattering asymmetry. In the MTV experiment, which has been running at TRIUMF-ISAC (Isotope Separator and Accelerator), cylindrical drift chamber (CDC) is used as a tracking detector to measure angles of the electron emission and backward scattering per event.<sup>1)</sup> The physics data were collected in 2017.

In 2018, we studied  $\beta^-$  ray energy dependence of CDC to predict Mott asymmetry measured in our system. The electron emission distribution of  $\beta^-$  decay,  $\omega$ , is expressed as:<sup>2)</sup>

$$\omega dE_e d\Omega_e \propto 1 + R\vec{\sigma} \cdot \left[ \frac{\langle \vec{J} \rangle}{J} \times \frac{\vec{p}_e}{E_e} \right] + \dots \quad (1)$$

The definition of  $R$ -correlation can be found in this function, where  $\vec{J}$  is the spin polarization of the parent nuclei, and  $\vec{\sigma}$ ,  $\vec{p}_e$ , and  $E_e$  are the spin polarization, momentum, and energy of electron, respectively. Coefficient  $R$  is predicted from the final state interaction (FSI) between the electron and daughter nucleus. In the standard model, coefficient  $R$  of FSI in  $^8\text{Li}$   $\beta^-$  decay is predicted as

$$R_{\text{FSI}}(^8\text{Li}) = \frac{\alpha Z m_e}{3p_e}. \quad (2)$$

Where  $\alpha$  is the fine structure constant,  $Z$  is the atomic number of daughter nucleus, and  $m_e$  is the electron mass.  $R_{\text{FSI}}$  is a non-zero value but it doesn't violate time reversal symmetry. If a significant difference exists between theoretical  $R_{\text{FSI}}$  and measured  $R$ , it may imply the existence of T-violation. These formulae show that  $\beta^-$

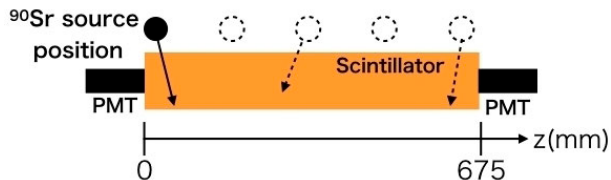


Fig. 1. Setup of the measurement to study the source position dependence.

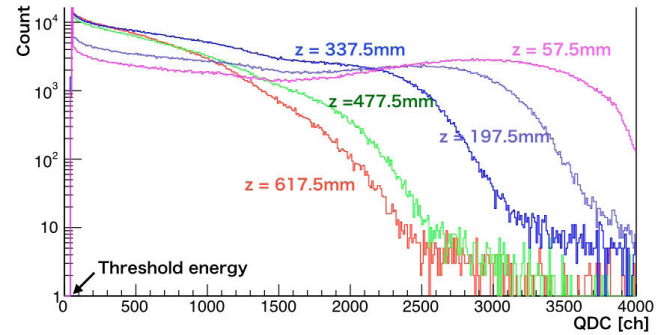


Fig. 2. Energy spectra using  $^{90}\text{Sr}$  radiation source at five different positions from the PMT.

emission distribution depends on  $\beta^-$  ray energy. In our experiment in 2017, we measured  $\beta^-$  emission distribution (Eq. (1)) in its integrated form with  $E_e$ . The prediction of expected asymmetry in our detector system requires the determination of the minimum detectable electron energy. In the 2018 experiment, we measured energy spectra detected by CDC using  $^{90}\text{Sr}$  radiation source and its energy threshold was deduced.

The measurement setup consists of stopping scintillation counters (SCs: used as trigger scintillator of CDC) and two PMT attached on both sides of SC. The most significant ambiguity of CDC energy threshold is due to SC whose length is 675 mm. When an electron hits a different point of SC, the amount of photons reaching PMTs also vary. We placed the radiation source on the SC with a collimator at five different positions to measure the ambiguity of energy threshold (Fig. 1). Figure 2 shows the energy spectra using  $^{90}\text{Sr}$  radiation source at five different positions from the PMT. The end point energy and threshold are defined by fitting on these data with the intrinsic response function of  $^{90}\text{Y}$   $\beta^-$  ray. The cutoff channels of the spectra correspond to the threshold. From these analyses, we determined the average energy threshold as

$$E_{\text{th}} = (6.5 \pm 2.2) \times 10^{-1} \text{ MeV}. \quad (3)$$

The energy threshold that was obtained in 2018 is necessary to calculate the asymmetry expected in our detector. In contrast, we need more analyses on the physics data to set final results  $R$ . In addition, the development of track detection method by machine learning is in progress to reduce systematic errors.

### References

- 1) J. Murata *et al.*, *Hyperfine Interact.* **237**, 125 (2016).
- 2) J. D. Jackson, S. B. Treiman, H. W. Wyld Jr., *Phys. Rev.* **106**, 517 (1957).

\*1 Department of Physics, Nagoya University

\*2 RIKEN Nishina Center

\*3 TRIUMF

\*4 Department of Physics, Rikkyo University

\*5 Cyclotron and Radioisotope Center, Tohoku University

## Development of long and high-density data bus for sPHENIX INTT detector

T. Hachiya,<sup>\*1,\*2</sup> Y. Akiba,<sup>\*1</sup> H. Aso,<sup>\*1,\*3</sup> D. Cacace,<sup>\*4</sup> E. Desmond,<sup>\*4</sup> T. Ichino,<sup>\*1,\*3</sup> M. Isshiki,<sup>\*2</sup> T. Kondo,<sup>\*5</sup> H. Kureha,<sup>\*2</sup> E. Mannel,<sup>\*4</sup> G. Mitsuka,<sup>\*1</sup> I. Nakagawa,<sup>\*1</sup> R. Nouicer,<sup>\*4</sup> R. Pisani,<sup>\*4</sup> K. Sugino,<sup>\*2</sup> A. Suzuki,<sup>\*2</sup> M. Tsuruta,<sup>\*1</sup> T. Todoroki,<sup>\*1</sup> and Y. Yamaguchi<sup>\*1</sup>

The intermediate tracker (INTT) is a silicon strip barrel detector for the sPHENIX experiment.<sup>1)</sup> INTT is implemented in a tight space between an inner silicon detector (MVTX) and the outer TPC, and the readout electronics are placed 120 cm away from the detector. The data bus of INTT must satisfy the following requirements:<sup>2)</sup> (1) flexibility, (2) length of at least 120 cm, (3) high-density signal line (128 lines/5 cm), and (4) high-speed signal transfer (by LVDS). It is challenging to meet all the requirements because high-speed signal transfer and a long data bus are contradictory.

To investigate the technical feasibility of the data bus, we made a prototype of the long and high-density data bus using flexible printed circuit (FPC), which is a film based PC board. A liquid crystal polymer (LCP) was chosen as the film material to reduce signal loss due to the small dielectric tangent. The prototype is a three layer structure in which the middle signal layer is sandwiched by the top and bottom ground layers for a differential impedance ( $Z_{diff}$ ) of 100  $\Omega$ . Figure 1 shows an FPC sheet containing five sets of the signal layer before laminating the top and bottom layers.

We evaluated the electrical and mechanical characteristics of the prototype. As a result, we found that the signal attenuation and return loss are  $-3$  dB and  $-20$  dB, respectively, and  $Z_{diff}$  is 90  $\Omega$ . The thinner line is preferable for 100  $\Omega$ , but more difficult to produce without troubles. The signal distortion was visually tested using the eye diagram. The eye is clearly open as shown in Fig. 2 (left). We also found that the accuracy of the width of the signal lines is  $\pm 3$   $\mu\text{m}$  from the measurement of the line widths for 40 lines on the FPC as shown in Fig. 2 (right). These results show that the prototype meets the requirements within the scope of the specification.

However, two issues are found in the prototype FPC. One is that the peel strength of the laminated layers is weak, and the other is that it is difficult to produce the through holes for long FPC. We studied several ways

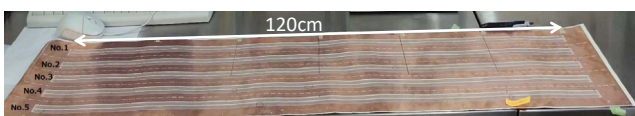


Fig. 1. LCP sheet of the signal layer for the prototype.

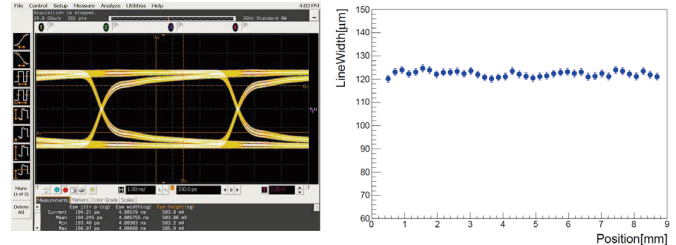


Fig. 2. Characteristics of the prototype FPC. (Left) Clear opening of eye diagram (Right) small variation of the line widths.

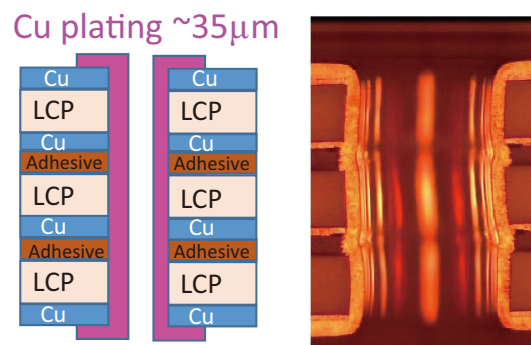


Fig. 3. Result of the Cu-plating for the four layer FPC. (Left) Schematic view of the laminated structure of FPC with Cu-plating. (Right) Result of Cu-plating.

to improve the peel strength. The current status is reported in Ref. 3).

The through hole is produced by drilling a hole on the FPC and Cu-plating the surface of the hole through an electro-chemical process. This requires a big chemical bath to soak the entire FPC. We looked for a company that has a bath big enough for INTT data bus. Along with the company, we tested the Cu-plating on the through hole for the 4 layer FPC. Figure 3 shows the Cu-plating result, which was successful. We will investigate the reliability of the through hole with a thermal shock test as a next step.

We evaluated the feasibility of the long and high-density data bus using FPC. Most of the issues were solved, and some technical issues found in the study are under further investigation. Based on the knowledge from the prototype, we are making the production version of the data bus for INTT. The production version will be tested in 2019.

### References

- 1) I. Nakagawa *et al.*, in this article.
- 2) T. Hachiya *et al.*, RIKEN Accel. Prog. Rep. **51**, 162 (2017).
- 3) M. Tsuruta *et al.*, in this article.

\*1 RIKEN Nishina Center  
 \*2 Department of Physics, Nara Women's University  
 \*3 Department of Physics, Rikkyo University  
 \*4 Brookhaven National Laboratory  
 \*5 Tokyo Metropolitan Industrial Technology Research Institute

## Performance evaluation of sensor module for INTT at sPHENIX

A. Suzuki,<sup>\*1,\*2</sup> Y. Akiba,<sup>\*1</sup> H. Aso,<sup>\*1,\*3</sup> D. Cacace,<sup>\*4</sup> E. Desmond,<sup>\*4</sup> T. Hachiya,<sup>\*1,\*2</sup> T. Ichino,<sup>\*1,\*3</sup> M. Isshiki,<sup>\*2</sup> T. Kondo,<sup>\*5</sup> H. Kureha,<sup>\*2</sup> E. Mannel,<sup>\*4</sup> G. Mitsuka,<sup>\*1</sup> I. Nakagawa,<sup>\*1</sup> R. Nouicer,<sup>\*4</sup> R. Pisani,<sup>\*4</sup> K. Sugino,<sup>\*2</sup> M. Tsuruta,<sup>\*1</sup> T. Todoroki,<sup>\*1</sup> and Y. Yamaguchi<sup>\*1</sup>

Intermediate silicon strip tracker (INTT) is one of the tracking detectors of sPHENIX.<sup>1)</sup> As shown in Fig. 1, INTT ladder consists of high-density interconnect (HDI) FVTX chips for PHENIX (FPHX) and silicon strip sensor.<sup>2)</sup> HDI is a flexible PC board to provide input and output for FPHX. The power to FPHX and silicon strip sensor are supplied through HDI. FPHX is a readout LSI chip used for PHENIX. 26 FPHX are implemented into the INTT ladder. One FPHX readouts 128 strip channels. Each channel is equipped with a shaping amplifier and 3-bit ADC. There are two different sizes of the silicon strip sensor. One of them is  $78 \times 16$  mm for A (20 mm for B). It is sensitive in  $\phi$  direction.

We built a test bench to evaluate the sensor module performance at Nara Women's University as shown in Fig. 2. The read-out system of the bench is described below. First, the hit data is sent from FPHX to read-out card (ROC) through a flexible cable, and are read-out at ROC. Data are sent from ROC to the front-end module (FEM) through an optical fiber and to be formatted. Finally the data from the FEM in the PC is recorded. Figure 3 shows the schematic drawing of the read-out system.

To check the functionality of the read-out system, we input a test pulse from ROC to FPHX with changing

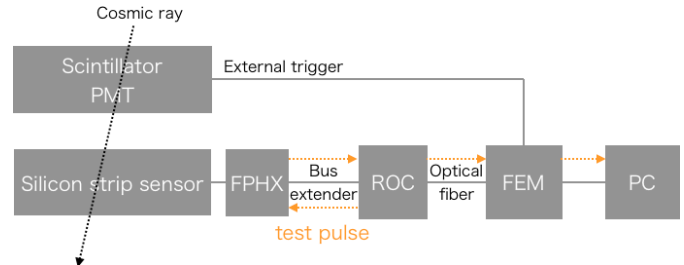


Fig. 3. The schematic drawing of the readout system.

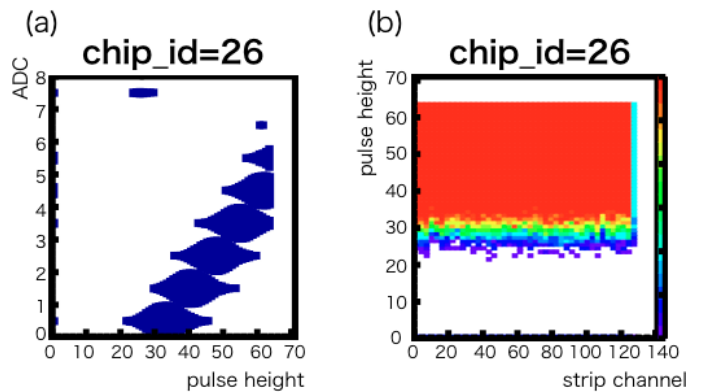


Fig. 4. (a) ADC vs pulse height (b) Pulse height vs strip channel.



Fig. 1. INTT ladder.

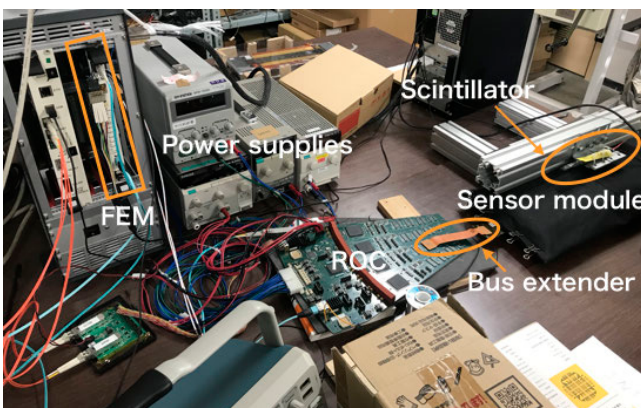


Fig. 2. Test bench setup.

pulse height and measure ADC. Figure 4 (a) shows the correlation between input pulse height and output ADC in a chip. Every chip responded linearly as expected. There were some strange signals in ADC 7 of a chip. Figure 4 (b) shows the number of hits (z-axis) as a function of pulse height (y-axis) in different strip channels (x-axis). All channels responded correctly and the hit efficiency improved at the threshold (pulse heights are near 30). The read-out system operated properly.

We measured the cosmic ray with an external trigger to study the response of minimum ionizing particle (MIP). As shown in Fig. 3, the sensor module and external trigger overlap each other, and the coincidence of both sensor module and external trigger decreases the noise. We are in the progress of accumulating data.

In the next step we will qualitatively evaluate the noise and efficiency by measuring the radiation source and cosmic ray. We plan to conduct the beam test at Fermi lab. in 2019 to evaluate the sensor modules.

### References

- 1) I. Nakagawa *et al.*, in this report.
- 2) C. Aidata *et al.*, Nucl. Instrum. Methods Phys. Res. A **755**, 44–61 (2014).

<sup>\*1</sup> RIKEN Nishina Center  
<sup>\*2</sup> High Energy Physics Department, Nara Women's University  
<sup>\*3</sup> Department of Physics, Rikkyo University  
<sup>\*4</sup> Brookhaven National Laboratory  
<sup>\*5</sup> Management and Planning Department, Tokyo Metropolitan Industrial Technology Research Institute

## Slit system between the foci F2 and F3 of the BigRIPS separator

K. Yoshida,<sup>\*1</sup> M. Ohtake,<sup>\*1</sup> and Y. Yanagisawa<sup>\*1</sup>

A new slit system has been installed between the second and third foci (F2, F3) of the BigRIPS separator, as shown in Fig. 1. The slit system is used to select the angles of RI beams produced at the target (F0) because it is placed at the point-to-parallel spot where the beam angles focusing at F2 are converted to positions by beam-line magnets.

The inset of Fig. 1 shows the structure of the slit system. It consists of horizontal and vertical slits and has a similar structure as the F2 or F7 slit system.<sup>1)</sup> It was installed in a vacuum chamber whose inner dimensions were  $750 \times 360 \times 875 \text{ mm}^3$ . Slit-blades were made by tungsten alloys (HAC2, Nippon Tungsten Co. Ltd.) with dimensions  $150 \times 150 \times 80 \text{ mm}^3$  (horizontal) and  $240 \times 120 \times 80 \text{ mm}^3$  (vertical) and weights 38 and 44 kg, respectively. They were connected to the linear actuators mounted on the wall of the vacuum chamber through the vacuum feedthroughs. The

slit-blade positions were remotely controlled using the stepping motors of the linear actuators. A position accuracy of  $\pm 0.1 \text{ mm}$  was achieved. To support the heavy slit-blades, a rail and cam followers were used for the horizontal slits, whereas Conston springs were used for the vertical slits. A detector stage for the position sensitive detector was also installed at the upstream of the slits in the vacuum chamber.

The hardware of the slit system was installed in March 2018 and its control software was modified in April 2018. The slit system became operational at the beginning of May 2018. Since then, the slit system is used as the standard device to select RI beam angles in the BigRIPS separator.

### Reference

- 1) K. Yoshida *et al.*, RIKEN Accel. Prog. Rep. **38**, 293 (2005).

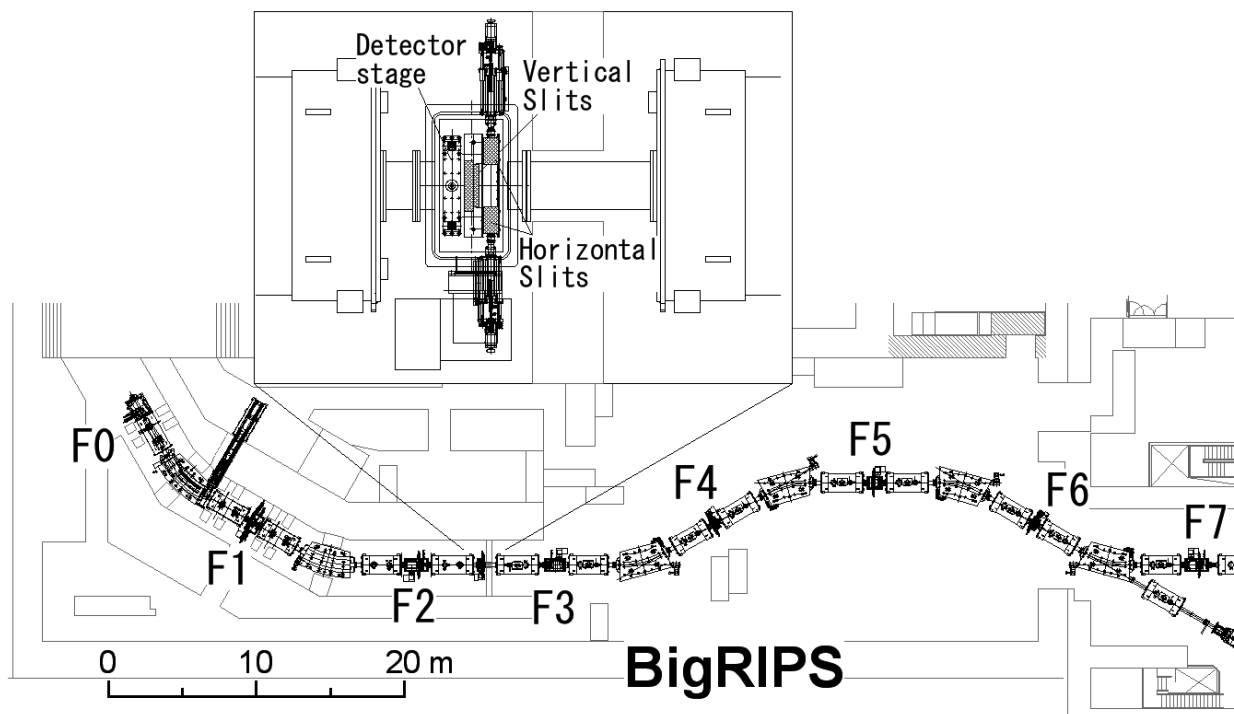


Fig. 1. Layout of the BigRIPS separator. The target (F0) and seven foci (F1-F7) of BigRIPS are indicated in the figure. Inset is the enlarged drawing of the newly installed slit system.

<sup>\*1</sup> RIKEN Nishina Center

## Fast beam interlock system for BigRIPS separator

K. Yoshida\*<sup>1</sup>

The fast beam interlock system for the BigRIPS separator<sup>1)</sup> was designed and constructed in 2014 and has been in operation since then to protect the beam line equipment from hitting the misaligned intensive primary beams due to magnet failure. The interlock system utilizes four compact RIO systems (cRIO) of National Instrument Co. Ltd. as the processing modules and continuously monitors the power supplies of 34 magnets placed at the primary beam line and BigRIPS, where a primary beam is transported. The current monitor signals from the power supplies are digitized by ADCs in cRIO every 2  $\mu$ s and compared with the pre-defined upper and lower limits. A fault signal is generated if the digitized values are beyond these limits. The fault signals are merged into other fault signals and fed to the beam chopper system to cut off the beam. The total response time, which is defined as the time between an analog signal drift and a beam stopping at the third focus (F3) of BigRIPS, was  $\sim 200$   $\mu$ s for a <sup>48</sup>Ca 345 MeV/nucleon beam.

During the operation of fast interlock system, the original system was found to be weak for the fluctuation of input noises. The noise of current monitor signals is not always stable. If the noise suddenly increases, the interlock system detects it as the drift of the current output and generates the fault signal. The beam is then stopped by the beam chopper. This happens a few times per day during the beam time.

The inspection of the current monitor signal using a digital storage type oscilloscope revealed the existence of two types of noise: a bi-polar ringing-like noise with high frequency (more than 2 MHz), a short unipolar pulse whose duration is approximately 20  $\mu$ s. The latter was created with the discharge of electrostatic deflector EDC of the SRC. To prevent the detection of these noises, noise filters are inserted in the analog input lines.

One such noise filter is a passive low-pass filter. EMI filtering capacitor EMIFIL DDS1 0.022  $\mu$ F of Murata was installed at the current monitor outputs of magnet power supplies. The moving average method was also implemented after the ADC of cRIO system, considering the average of 2 to 16 successive digital values from the ADC. Because ADC provides the converted value every 2  $\mu$ s, the averaging takes place between 4 and 32  $\mu$ s. By installing the EMI filter and taking the average of 16 successive AD values, the ringing like noise was completely eliminated from the system. However, the short pulse noise could still be detected because the pulse was slower than the EMI filter and unipolar pulses were not eliminated by averaging.

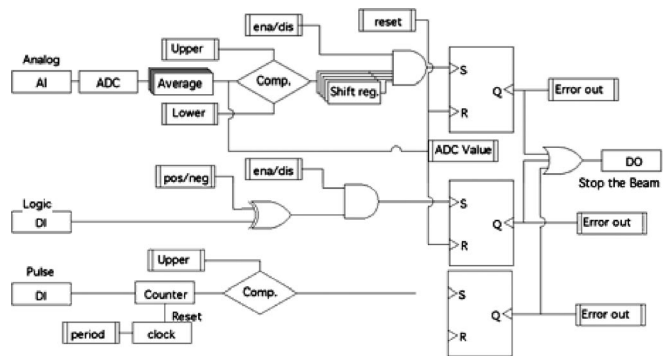


Fig. 1. Logic diagram of upgraded fast interlock system.

To eliminate the short pulse noise, a time-over-limit detection mechanism was further added to the interlock logic. This was accomplished by installing a bit-shift register on the output of the comparator, which compared the digitized signal and pre-defined limits. Each output of the comparator was stored in the first bit of the bit-shift register. The remaining bits of the register were pre-shifted by one bit before storing the first bit. Thus, the 16 bit register stored 16 successive comparison results. A failure signal was generated when all 16 bits were in the “on” state. With this algorithm, the failure signals were only generated for the input signals whose amplitudes exceeded the limit by 32  $\mu$ s. Therefore, the deviation of input signals shorter than 32  $\mu$ s was completely ignored.

The interlock logic was modified as shown in Fig. 1 by modifying the FPGA program code in the cRIO system and no hardware modification was required. The actual modification was performed in April 2018 and since then, the fast beam interlock system has been operated with no noise.

### Reference

- 1) K. Yoshida *et al.*, RIKEN Accel. Prog. Rep. **47**, 169 (2014).

\*<sup>1</sup> RIKEN Nishina Center

# Thermal model simulation of high-power rotating target for BigRIPS separator

Z. Korkulu,<sup>\*1</sup> K. Yoshida,<sup>\*1</sup> Y. Yanagisawa,<sup>\*1</sup> and T. Kubo<sup>\*1,\*2</sup>

Since 2007, a water-cooled high-power rotating disk target made of beryllium or tungsten has been used as the production target at the in-flight radioactive-isotope (RI) beam separator BigRIPS.<sup>1,2)</sup> The diameter of the rotational disk is 30 cm while the thickness can be optimized according to the atomic number and the energy of the selected projectile. To obtain a variety in thickness, the circumference edge of each disk has two steps to realize less thicknesses. The rotational disk target system was designed to withstand the maximum beam intensity of  $^{238}\text{U}$  at 345 MeV/nucleon and 1 particle  $\mu\text{A}$ . Although only about 20% of the goal beam intensity of 82 kW has been achieved, the high-power rotating target system has been successfully operated with various beams. Because the present primary beam intensity is much lower than the goal value, the requirement that Be could withstand the goal intensity cannot be experimentally commissioned. Therefore, we started to develop simulations based on ANSYS Parametric Design Language (APDL)<sup>3)</sup> to calculate the beam spot temperature at various conditions. Earlier, a prototype target system was designed and constructed using the same simulation code.<sup>4,5)</sup>

In the analysis, a complete model built by APDL was used. The primary beam was focused at a diameter of 1 mm (FWHM) with Gaussian beam distribution. The power deposition in beryllium material was calculated with the LISE++ simulation code.<sup>6)</sup> To include the effect of radiation cooling, the emissivity of 0.57 was used for the surface of the Be disk.<sup>5)</sup> The target disk was tightly fixed with screws on the water-cooled aluminum plate (see Fig. 1) and the boundary temperature for the

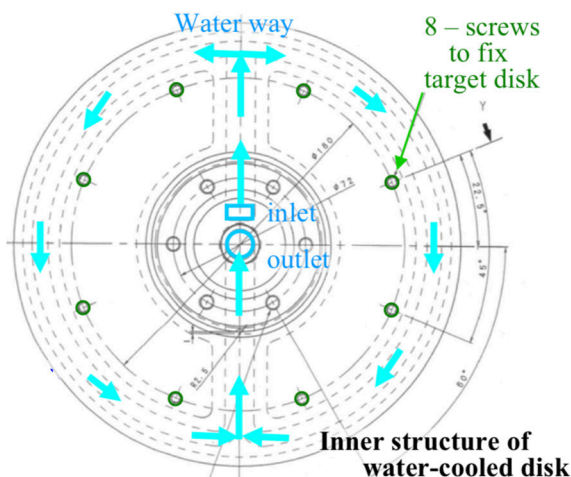


Fig. 1. Cooling-water is introduced to the aluminum disk through a double-piped shaft.

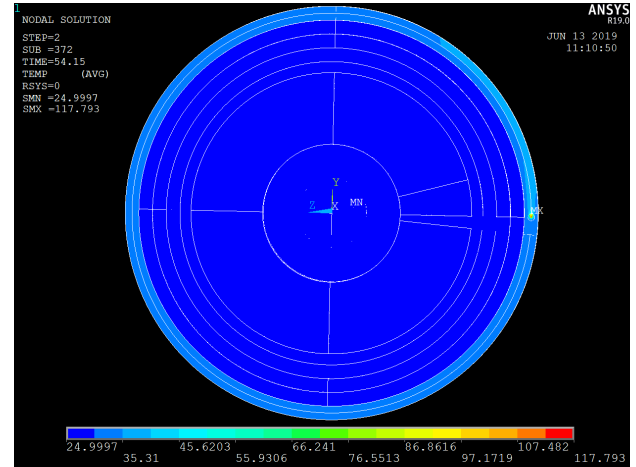


Fig. 2. A  $^{48}\text{Ca}$  primary beam at 345 MeV/nucleon with 470 pA (7.8 kW in beam power) onto the beryllium target of 10 mm thickness. The heat deposited in the target was 0.96 kW for a beam spot size with a diameter and rotation speed of 1 mm and 10 rpm, respectively. The maximum beam spot temperature is approximately 118°C.

cooling water was fixed at 25°C. The heat transfer coefficient, calculated by JAERI formula,<sup>7)</sup> was found to be 10.5 kW/m<sup>2</sup> K at 25°C. Because the beam spot temperature varied with time, the temperature-dependent thermal conductivity of Be and Al was used for temperatures between 25 and 1200°C and 25 and 700°C, respectively.

In our simulations, the heat source was fixed and the target model moved across it based on the mass transport option of ANSYS. To capture the effect of temperature variation occurring in the model, the applied mesh size must be small enough. Although the beam spot temperature became constant after several rotations, this complex model required a few hours of the CPU time. The initial analysis was performed with low rotational speed, from 1 to 10 rotations per minute (rpm), in several steps to confirm the reliability of our simulation code.

The present status of simulated heat distribution with 10 rpm is reported in Fig. 2. Further simulation studies are under way to optimize a small mesh size that can increase the rotation speed of the disk target up to the required velocity of 100 to 1000 rpm.

## References

- 1) A. Yoshida *et al.*, Nucl. Instrum. Methods Phys. Res. A **521**, 65 (2004).
- 2) A. Yoshida *et al.*, Nucl. Instrum. Methods Phys. Res. A **590**, 204 (2008).
- 3) ANSYS, Inc. Product Release 19.0, USA.
- 4) A. Yoshida *et al.*, RIKEN Accel. Prog. Rep. **35**, 152 (2002).
- 5) A. Yoshida *et al.*, RIKEN Accel. Prog. Rep. **37**, 295 (2004).
- 6) O. Tarasov *et al.*, Nucl. Instrum. Methods Phys. Res. B **266**, 4657 (2008).
- 7) J. Boscary *et al.*, Fusion Eng. Des. **43**, 147 (1998).

<sup>\*1</sup> RIKEN Nishina Center

<sup>\*2</sup> Facility for Rare Isotope Beams, Michigan State University

# Primary beam intensity calibration method using charge-states distribution

D. S. Ahn,<sup>\*1</sup> H. Suzuki,<sup>\*1</sup> N. Fukuda,<sup>\*1</sup> Y. Shimizu,<sup>\*1</sup> H. Takeda,<sup>\*1</sup> K. Yoshida,<sup>\*1</sup> Y. Yanagisawa,<sup>\*1</sup> N. Inabe,<sup>\*1</sup> and T. Kubo<sup>\*2,\*1</sup>

The primary beam intensity is an important quantity for experiments to obtain the production cross-sections and rates of radioactive isotopes and monitoring the stability of beam during the experiment. The primary beam intensity is determined using a triple coincidence (3-coin) monitor<sup>1)</sup> by detecting light charged particles recoiling out of the production target in the BigRIPS, as shown in Fig. 1. The advantage of this system is the non-destructive method and its availability at all times during the experiment but the calibration for 3-coin monitor is needed and depends on the combination of beams, targets, and beam energy.

The direct measurement of Faraday cup (FC) read-out is used for the calibration of the 3-coin monitor. The size of FC at the BigRIPS is small owing to the space limitation in the production target chamber, causing escape of the secondary electrons from the FC, even if the electric suppressor is applied. Consequentially, the read-out of FC gives a larger current in cases of heavy-ion primary beams. Therefore, the determination of FC calibration factor (FCF) is quite important to obtain absolute primary beam intensity. In this report, the calibration method of the primary beam intensity for FC using a charge-states distribution of the primary beam is reported.

Figure 2 shows the flow chart for the calibration method of the primary beam intensity for a  $^{238}\text{U}^{86+}$  beam case. In principle, the beam current can be determined by counting the number of incident ions. The primary beam is irradiated to the target and measures the charge-states distribution after the target. The total number of incident ions is obtained from the number of one arbitrary charge-state and its ratio to the total. A 1 mm Be target is used to measure the charge-states distribution of  $^{238}\text{U}$  at 345 MeV/nucleon (such a thin target is preferable to reduce the possible backgrounds of fission fragments). In the experiment, each charge-state was set to the central axis in each time. The relative yield

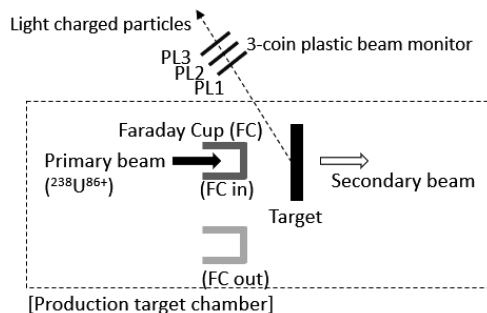


Fig. 1. Schematic view of the primary beam monitoring system at the production target chamber.

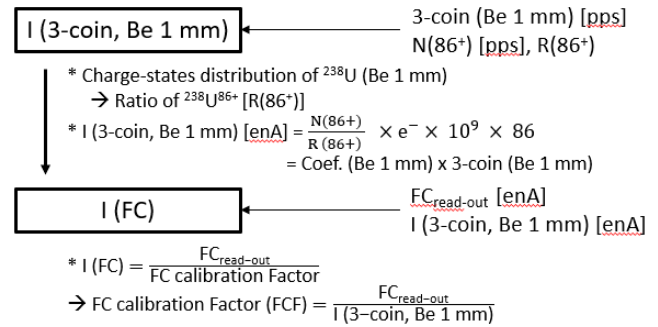


Fig. 2. Flow chart for the calibration method of the primary beam intensity.

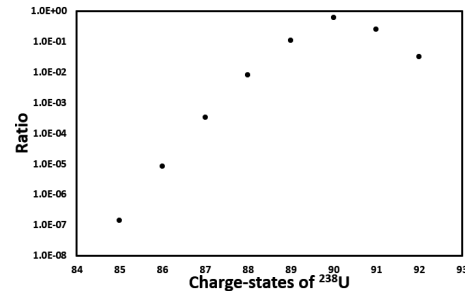


Fig. 3. Experimental charge-states distribution of  $^{238}\text{U}$  after 1 mm Be target.

for the neighboring ionic charge-state was obtained with PPACs at F1 or plastic scintillator at F2 and it as normalized with the total number of counts. Figure 3 shows the charge-state distribution of  $^{238}\text{U}$  after 1 mm Be target in the range from  $92^+$  to  $85^+$ . The number of  $86^+$  charge-states,  $N(86^+)$ , and its ratio,  $R(86^+)$ , after the 1 mm Be target were deduced and the sum of ratio was normalized with 1. The intensity of the primary beam cannot be measured directly with the BigRIPS detectors because it has a significantly higher rate. The countable count rate of  $N(86^+)$  was used to deduce the primary beam intensity whose ratio  $R(86^+)$  was  $8.2 \times 10^{-6}$ . The number of  $86^+$  charge-state was  $\sim 10^{4\sim 5}$  Hz with the full beam intensity (50~100 pA in a U beam case). Thus, we obtained the beam intensity by the 3-coin monitor,  $I(3\text{-coin, Be } 1 \text{ mm})$ .

Consequentially, the FC calibration factor [FCF] was deduced by comparing the read-out of FC [ $\text{FC}_{\text{read-out}}$ ] and  $I(3\text{-coin, Be } 1 \text{ mm})$ , the average value of FCF is 3.2 in the  $^{238}\text{U}^{86+}$  beam case. Similar types of calibration were performed in different primary beam cases. The average values of FCF are 1.7, 1.55, and 1.3 for a  $^{124}\text{Xe}^{54+}$ ,  $^{78}\text{Kr}^{36+}$ , and  $^{70}\text{Zn}^{30+}$  beam at 345 MeV/nucleon, respectively. The FCF is assumed to be 1.0 in the  $^{48}\text{Ca}^{20+}$  and  $^{18}\text{O}^{8+}$  beam cases.

## Reference

- 1) Y. Yamaguchi *et al.*, RIKEN Accel. Prog. Rep. **42**, 161 (2009).

<sup>\*1</sup> RIKEN Nishina Center

<sup>\*2</sup> FRIB/NSCL, Michigan State University

## Angle-tunable degrader system for OEDO

J. W. Hwang,<sup>\*1</sup> S. Michimasa,<sup>\*1</sup> S. Ota,<sup>\*1</sup> M. Dozono,<sup>\*1</sup> N. Imai,<sup>\*1</sup> K. Yoshida,<sup>\*2</sup> Y. Yanagisawa,<sup>\*2</sup> K. Kusaka,<sup>\*2</sup> M. Ohtake,<sup>\*2</sup> D. S. Ahn,<sup>\*2</sup> O. Beliuskina,<sup>\*1</sup> N. Fukuda,<sup>\*2</sup> C. Iwamoto,<sup>\*1</sup> S. Kawase,<sup>\*3</sup> K. Kawata,<sup>\*1</sup> N. Kitamura,<sup>\*1</sup> S. Masuoka,<sup>\*1</sup> H. Otsu,<sup>\*2</sup> H. Sakurai,<sup>\*2</sup> P. Schrock,<sup>\*1</sup> T. Sumikama,<sup>\*2</sup> H. Suzuki,<sup>\*2</sup> M. Takaki,<sup>\*1</sup> H. Takeda,<sup>\*2</sup> R. Tsunoda,<sup>\*1</sup> K. Wimmer,<sup>\*4</sup> K. Yako,<sup>\*1</sup> and S. Shimoura<sup>\*1</sup>

An angle-tunable degrader system was developed for the OEDO beamline,<sup>1)</sup> which slows down a beam separated by BigRIPS<sup>2)</sup> to produce a beam of 10–50 MeV/nucleon. This system is used as a monoenergetic degrader to reduce the beam energy and its spread. Since the system was designed to adjust its wedge angle and thickness, it has high versatility to deal with various experimental conditions. In this report, we present the structure and experimental verification of the system.

The degrader part consists of a pair of Al sheets with quadratic cross sections, and their quadratic coefficients for thickness differ only in their signs. Their overlap, therefore, functions as the wedge degrader, and the wedge angle is changed according to their relative position. The thickness can be also adjusted by introducing an additional plate. The overall system was constructed as shown in Fig. 1, which has a fixed central thickness of 3 mm and a wedge angle from 0 mrad to 40 mrad. The effective area is  $\pm 30$  mm(H)  $\times$   $\pm 50$  mm(V). The averages of thickness deviations from the machining precision for each Al sheet are 33 and 58  $\mu$ m, respectively. The uncertainty of the angle originating from these deviations is 2 mrad.

The commissioning experiment of this system was carried out at the OEDO beamline.<sup>1)</sup> <sup>79</sup>Se of 171 MeV/nucleon, separated by BigRIPS,<sup>2)</sup> was delivered to the degrader system installed at the dispersive FE9 focus. The central thickness of the system was set to 6 mm to slow down the beam to about 40 MeV/nucleon.

The spread of the outgoing energy distribution for the monoenergetic-beam case with an optimized wedge angle was compared with that for the case using the homogeneous degrader, where the wedge angle is 0 mrad, to evaluate the performance of the degrader system. As shown in Fig. 2, while the energy spread in the homogeneous case was measured to be 12.6 MeV/nucleon in full width at half maximum, the spread was reduced to 5.4 MeV/nucleon in the case of the optimized monoenergetic degrader, which is consistent with the estimation by a simulation.

In summary, we developed an angle-tunable degrader system for the OEDO beamline for a low-energy

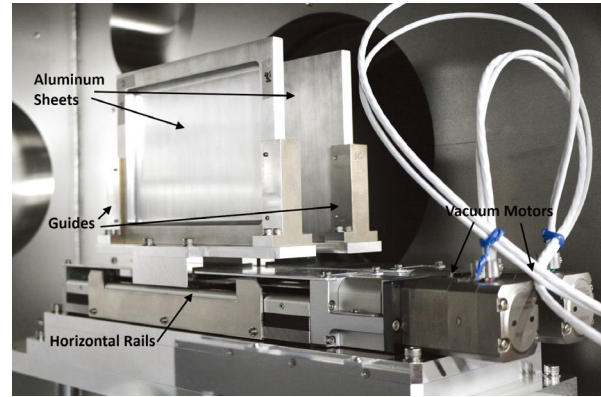


Fig. 1. Picture of the angle-tunable degrader system.

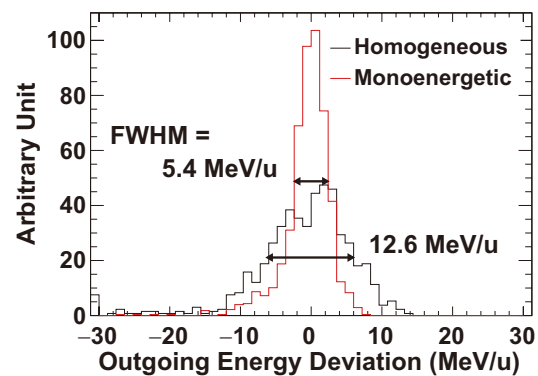


Fig. 2. Distributions of the outgoing energy deviation using a homogeneous degrader (black) and an optimized monoenergetic degrader (red). All the distributions were normalized to have the same number of events.

RI beam. The performance of the system was experimentally verified using <sup>79</sup>Se beam at 171 MeV/nucleon, and we successfully obtained a low-energy beam at  $42 \pm 2.7$  MeV/nucleon with the suppressed spread. We expect that this system can be used for various purposes and conditions thanks to its flexible wedge angle.

This work was funded by ImPACT (Impulsing Paradigm Change through Disruptive Technologies) Program of Council for Science, Technology and Innovation (Cabinet Office, Government of Japan).

### References

- 1) S. Michimasa, *et al.*, Prog. Theor. Exp. Phys., *accepted*.
- 2) T. Kubo, Nucl. Instrum. Methods Phys. Res. B **204**, 97 (2003).

<sup>\*1</sup> Center for Nuclear Study, University of Tokyo

<sup>\*2</sup> RIKEN Nishina Center

<sup>\*3</sup> Department of Advanced Energy Engineering Science, Kyushu University

<sup>\*4</sup> Department of Physics, University of Tokyo

## Development of dispersion-matching optics of primary beam for SRC-BigRIPS system

S. Y. Matsumoto,<sup>\*1,\*2</sup> D. S. Ahn,<sup>\*1</sup> N. Fukuda,<sup>\*1</sup> N. Fukunishi,<sup>\*1</sup> H. Geissel,<sup>\*3</sup> N. Inabe,<sup>\*1</sup> K. Itahashi,<sup>\*1</sup> K. Kusaka,<sup>\*1</sup> T. Nishi,<sup>\*1</sup> Y. Shimizu,<sup>\*1</sup> T. Sumikama,<sup>\*1</sup> H. Suzuki,<sup>\*1</sup> M. Takaki,<sup>\*4</sup> H. Takeda,<sup>\*1</sup> Y. K. Tanaka,<sup>\*1,\*3</sup> T. Uesaka,<sup>\*1</sup> Y. Yanagisawa,<sup>\*1</sup> and K. Yoshida<sup>\*1</sup>

We are working toward the development of a new optics<sup>1)</sup> for SRC-BigRIPS system that can be used for two types of experiments based on missing-mass spectroscopy: search double Gamow-Teller giant resonance and systematic high-precision spectroscopy of pionic atoms (piAF). In these experiments, the largest contribution to the missing-mass resolution is the momentum spread of the primary beam. Therefore, we applied a technique for dispersion matching<sup>2,3)</sup> to suppress the contribution from the momentum spread. The dispersion-matching condition is fulfilled when the dispersions of the BigRIPS spectrometer and its upstream beam-transfer lines are properly adjusted to eliminate the contribution factor as follows:

$$(x_{F5}|\delta_{F0}) + (x_{F5}|x_{F0})(x_{F0}|\delta_{SRC}) = 0.$$

Here,  $x$  is the horizontal position and  $\delta$  is the relative momentum deviation from a reference particle.

In constructing the dispersion-matching optics, we investigated phase distributions of beam transfer-line, *i.e.*, the upstream section between SRC and F0. In the preceding piAF experiment,<sup>4)</sup> the dispersion in SRC-F0 was not properly controlled owing to insufficient information regarding SRC. In addition, we require momentum compaction (ideally achromatic-focus) condition at the intermediate point (T11), thereby isolating the uncertainties in the optical properties of the in-coming beam and de-

Table 1. Measured and designed matrix elements.

Matrix element	Measured value	Designed value
$(x_{F5} \delta_{F0})$	$62.3 \pm 0.5$ mm/%	62.0 mm/%
$(x_{F5} x_{F0})$	$-1.67 \pm 0.03$	-1.82
$(x_{F0} \delta_{SRC})$	$29.1 \pm 0.3$ mm/%	33.4 mm/%

sign T11-F0 by realizing flexible designs at F0.

To deduce the phase distributions at T11 and F0, we used particle trajectories measured by detectors in BigRIPS and traced them back to the upstreams. The matrix elements in T11-F0 and BigRIPS required for the trace-back method are measured by decoupling the corresponding sections by inserting thick degraders at the entrances.

We performed an experiment to examine the beam-transfer line in June 2018. The goal of this experiment is to achieve the dispersion-matching condition by tuning the optics in the beam-transfer line. A primary beam of  $^{18}\text{O}^{8+}$  with an energy of 230 MeV/nucleon was utilized up to F7 to measure the optical matrices. The beam was detected by PPACs at F3, F5, and F7. According to the measurements, we optimized optics in the beam-transfer line to ensure that T11 and F0 have momentum compaction and dispersion, respectively.

We evaluated the resolving power of the dispersion-matching optics by simulating the reaction  $Q$ -value by the energy loss at F0. Figure 1 shows a comparison of position distributions at F5 measured with an Al (75  $\mu\text{m}$  thickness) target represented by red curves and a through-hole represented by blue curves for the standard optics (left panel) and the dispersion-matching optics (right panel). The right panel seemed to exhibit better separation with difference in energy loss of 4.2 MeV. Table 1 presents the measured and designed values of matrix elements related to the dispersion-matching condition. Consequently, we succeeded in separating  $\delta = 0.056\%$  of momentum deviations in  $3.6\sigma$ . The corresponding resolving power is estimated to be 7300.

In summary, we constructed a new optical system to improve the missing-mass resolution by dispersion matching. A precise analysis is in progress.

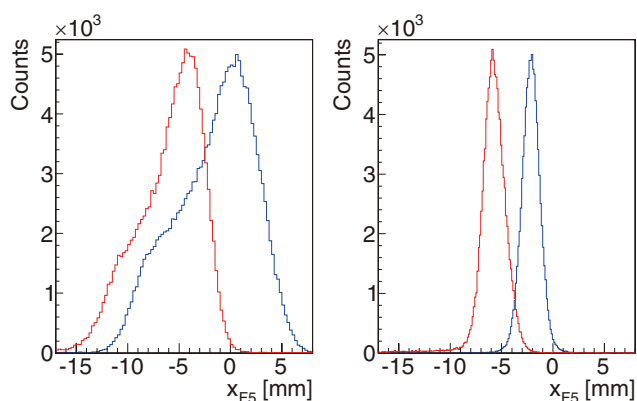


Fig. 1. Position distribution at F5 with the standard (left) and dispersion-matching (right) optics. Red and blue lines represent data with or without target at F0, respectively.

\*1 RIKEN Nishina Center

\*2 Department of Physics, Kyoto University

\*3 GSI Helmholtzzentrum für Schwerionenforschung GmbH

\*4 Center for Nuclear Study, University of Tokyo

### References

- 1) T. Nishi *et al.*, in this report.
- 2) B. L. Cohen, Rev. Sci. Instrum. **30**, 415 (1959).
- 3) T. Wakasa *et al.*, Nucl. Instrum. Methods Phys. Res. A **482**, 79 (2002) and references therein.
- 4) T. Nishi *et al.*, RIKEN Accel. Prog. Rep. **48**, 235 (2015).

## SHE-Mass-II: an MRTOF-MS for Super Heavy Nuclei

M. Wada,<sup>\*1</sup> P. Schury,<sup>\*1</sup> S. Kimura,<sup>\*2</sup> S. Ishizawa,<sup>\*2,\*5</sup> T. Niwase,<sup>\*2,\*3</sup> Y. Ito,<sup>\*4</sup> M. Rosenbusch,<sup>\*2</sup> D. Kaji,<sup>\*2</sup> K. Morimoto,<sup>\*2</sup> H. Haba,<sup>\*2</sup> H. Miyatake,<sup>\*1</sup> X. Y. Watanabe,<sup>\*1</sup> H. Hirayama,<sup>\*1</sup> J. Y. Moon,<sup>\*7,\*1</sup> A. Takamine,<sup>\*2</sup> T. Tanaka,<sup>\*3,\*2</sup> K. Morita,<sup>\*3,\*2</sup> H. Ishiyama,<sup>\*2</sup> and H. Wollnik<sup>\*6</sup>

The SHE-Mass facility was a system with a multi-reflection time-of-flight mass spectrograph (MRTOF-MS)<sup>1)</sup> and a cryogenic gas catcher coupled with the GARIS-II at RILAC. With this setup, we have measured the masses of more than 80 fusion-evaporated products including several trans-fermium nuclides.<sup>2-5)</sup> After the shutdown of GARIS-II at RILAC, we rebuilt a similar setup, *i.e.*, the SHE-Mass-II, at the new GARIS-II in the E6 experimental room.

The new setup has a single stage triplet ion trap system, which directly connects the gas catcher to the MRTOF to achieve high efficiency. The whole setup including vacuum pumps, a gas cylinder, and electric circuits is mounted on a single base plate and the plate is movable on rails to ensure quick coupling and decoupling to the GARIS-II. The gas catcher and ion trap chambers are mounted on a two-dimensional rail system that enables easy maintenance of the internal structures of the setup.

A drawback of the new setup is that more contaminant ions could be expected owing to a difficulty of intermediate mass selection. In the previous setup, we had a 5 m-long beam line between the two ion traps where we could place a Bradbury-Nielsen (BN) ion gate<sup>6)</sup> to select a single mass number. However, the new setup has only a 50 cm distance between the trap and MRTOF where a BN gate can be installed. We developed a 10 times finer gate device made of 13  $\mu$ -thick wires with 130  $\mu$  intervals, which can deflect a 1 keV/ $q$  ion beam by 65 mrad with a  $\pm 100$  V pulse. Such fine structure makes sharp cut on the ion beam. In a preliminary test, a resolution of 2 mass units was achieved.

Another improvement in the new setup is the replacement of a sextuple ion beam guide (SPIG) made of rigid molybdenum rods with a segmented micro quadrupole ion beam guide (S $\mu$ QPIG) made of 2 mm-wide, four-layer printed circuit boards. These devices interface the gas catcher with the triplet ion trap through differential pumping sections. In the previous setup, we needed to run an ion source in the gas catcher to have a ‘space-charge cloud’ which pushed the ions in the SPIG, while in the new setup, a DC gradient potential in the S $\mu$ QPIG carries the rare ions without

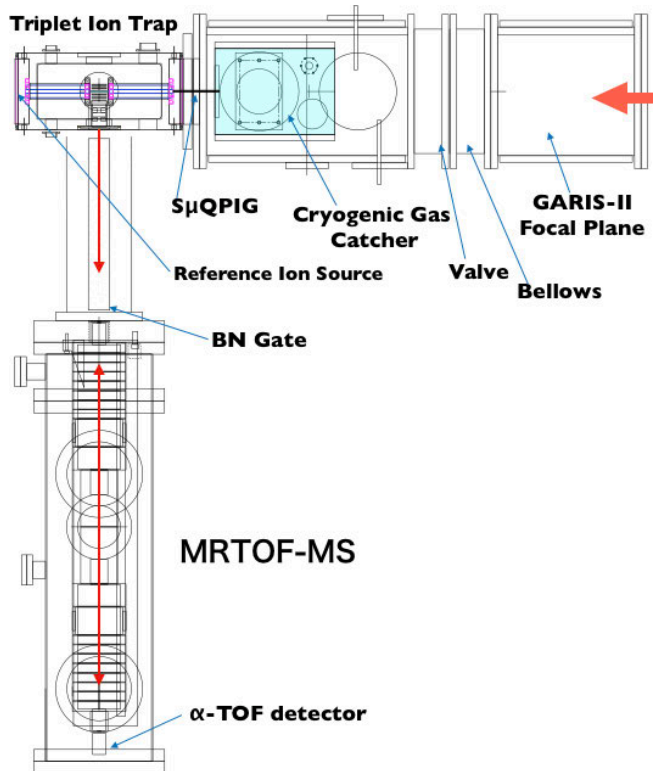


Fig. 1. SHE-Mass-II setup.

support from the space-charge cloud. The new scheme provides cleaner ion beams to the MRTOF.

We also replaced the time-of-flight detector with a newly developed  $\alpha$ -TOF detector, which records the time-of-flight signal and the successive  $\alpha$ -decay, simultaneously. The first online commissioning of the SHE-Mass-II setup was performed in December 2018 and we found that the  $\alpha$ -TOF detector significantly reduced the background level.<sup>7)</sup> An offline experiment using <sup>252</sup>Cf fission source is also in progress.

We are ready to start the direct mass measurement of hot-fusion super heavy elements, <sup>288</sup>Mc and <sup>284</sup>Nh, with the SHE-Mass-II setup.

### References

- 1) P. Schury *et al.*, Nucl. Instrum. Methods Phys. Res. B **335** 39, (2014).
- 2) P. Schury *et al.*, Phys. Rev. C **95**, 011305(R) (2017).
- 3) S. Kimura *et al.*, Int. J. Mass Spectrom. **430**, 134 (2018).
- 4) M. Rosenbusch *et al.*, Phys. Rev. C **97**, 064306 (2018).
- 5) Y. Ito *et al.*, Phys. Rev. Lett. **120**, 152501 (2018).
- 6) N. E. Bradbury, R. A. Nielsen, Phys. Rev. **49**, 388 (1936).
- 7) T. Niwase *et al.*, RIKEN Accel. Prog. Rep. **51**, 157 (2018).

<sup>\*1</sup> KEK, Wako Nuclear Science Center

<sup>\*2</sup> RIKEN Nishina Center

<sup>\*3</sup> Department of Physics, Kyushu University

<sup>\*4</sup> JAEA

<sup>\*5</sup> Department of Physics, Yamagata University

<sup>\*6</sup> Department of Chemistry and Biochemistry, New Mexico State University

<sup>\*7</sup> Institute for Basic Science, Rare Isotope Science Project

## Status and future plans of the MRTOF MS constructed at the SLOWRI facility

M. Rosenbusch,<sup>\*1</sup> M. Wada,<sup>\*1,\*2</sup> H. Ishiyama,<sup>\*1</sup> P. Schury,<sup>\*2</sup> Y. Ito,<sup>\*3</sup> H. Haba,<sup>\*1</sup> S. Ishizawa,<sup>\*1</sup> D. Kaji,<sup>\*1</sup> S. Kimura,<sup>\*1</sup> H. Miyatake,<sup>\*2</sup> J. Y. Moon,<sup>\*4</sup> K. Morimoto,<sup>\*1</sup> K. Morita,<sup>\*1,\*5</sup> T. Niwase,<sup>\*1,\*5</sup> A. Takamine,<sup>\*1</sup> T. Tanaka,<sup>\*1,\*5</sup> and H. Wollnik<sup>\*6</sup>

A new multi-reflection time-of-flight mass spectrograph (MRTOF MS) for the precise measurement of nuclear masses has been assembled at the SLOWRI facility at RIKEN. The device is designed and sized following the successful apparatus<sup>1-4)</sup> presently installed at the gas-filled ion-recoil separator GARIS-II. Two concentric ion mirrors separated by a central drift tube of 26 cm length are facing each other, where each mirror consists of eight electrodes enabling deceleration and reflection of ions and two electrostatic lenses enabling radial confinement (length of each mirror: 35 cm, total length of MRTOF MS: 96 cm). For mass resolving powers in the order of  $m/\delta m > 10^5$  ( $m$  as the mass and  $\delta m$  as measured FWHM of the mass according to the TOF signal), ion-optical aberrations must be reduced accordingly to allow for a narrow time-of-flight focus. Several measures have been undertaken: As radial aberration coefficients from initial angles and diameters of the beam decrease rapidly with the diameter of the ion optics, the electrode diameter has been chosen as large as 10 cm, while the beam diameter is expected to be at the order of a millimeter for the major part of the trajectory. All electrodes consist of precision-machined stainless steel (providing high stability), and have been coated with gold to ensure an excellent electric-field distribution in the absence of chemical compounds bound to the surfaces. The electrodes are further mounted on a precision-machined single solid piece of alumina, where the position of the electrodes (concentric on the outer side as well) is defined by a V-shape of the ceramic support (see photo). One of the technical goals of this setup is the acceptance and storage of ions with kinetic energies of 5 keV or above present at the position of the drift tube. In presently well-known and successful configurations of the electric fields (for positive ions), this requires negative voltages of up to  $-15$  kV at the electrostatic lenses (the broad electrodes at each mirror). Thus, special attention has been given to the choice of the electric feedthroughs, distances of cables, and vacuum compatible insulation of the wires. The wires inside the vacuum allow for biases of more than 10 kV at zero distance between each two cables. The vacuum system of the MRTOF MS device is presently operational, and ion traps for guidance and preparation of radioactive ions are existing and to

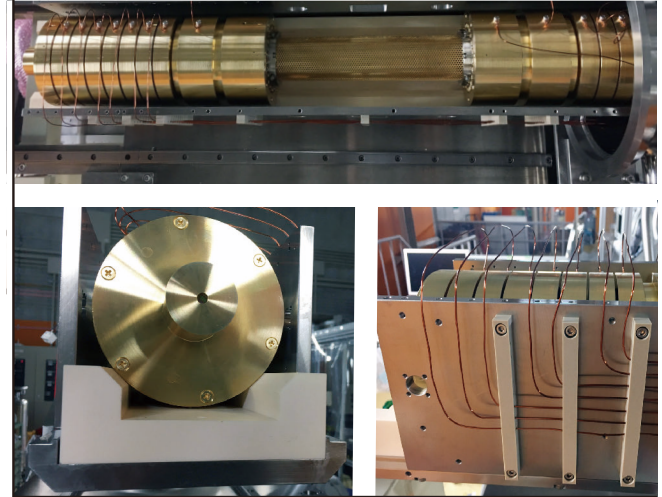


Fig. 1. Top: Photo from the top showing the assembly with gold-coated electrodes. Bottom left: Precision machined ceramic support with V-shape to define the electrode position. Bottom right: Cabling of the electrodes for the suppression of electric discharges.

be installed in near future.

The new MRTOF device has been constructed for two major purposes, which is a coupling to the gas cell presently developed for SLOWRI<sup>5)</sup> to operate in symbiosis with other BigRIPS experiments, and the development and test of novel technologies for MRTOF mass spectrometry. In collaboration with experimental groups operating at BigRIPS, a new project of the SLOWRI facility aims at the installation of a cryogenic helium gas cell at the end of the BigRIPS beam line to accept unused reaction products measured at various in-beam experiments, which are guided to beam dumps otherwise. Application of state-of-the-art technologies as using the in-trap lift technology<sup>6)</sup> and an in-trap deflector<sup>7)</sup> are further planned for the MRTOF MS operation at SLOWRI in future.

### References

- 1) P. Schury *et al.*, Nucl. Instrum. Methods Phys. Res. B **376**, 425 (2015).
- 2) P. Schury *et al.*, Int. J. Mass Spectrom. **359**, 19 (2014).
- 3) Y. Ito *et al.*, Phys. Rev. Lett. **120**, 152501 (2018).
- 4) M. Rosenbusch *et al.*, Phys. Rev. C **97**, 064306 (2018).
- 5) A. Takamine *et al.*, in this report.
- 6) R. N. Wolf *et al.*, Int. J. Mass Spectrom. **313**, 8 (2012).
- 7) P. Fischer *et al.*, Int. J. Mass Spectrom. **435**, 305 (2012).

<sup>\*1</sup> RIKEN Nishina Center

<sup>\*2</sup> Wako Nuclear Science Center (WNSC), IPNS, KEK

<sup>\*3</sup> Advanced Science Research Center, JAEA

<sup>\*4</sup> Institute for Basic Science

<sup>\*5</sup> Department of Physics, Kyushu University

<sup>\*6</sup> Department of Chemistry and Biochemistry, New Mexico State University

# Development of multiple reflection time of flight mass spectrograph at KISS

J. Y. Moon,<sup>\*1</sup> S. C. Jeong,<sup>\*1</sup> M. Wada,<sup>\*2</sup> P. Schury,<sup>\*2</sup> Y. X. Watanabe,<sup>\*2</sup> Y. Hirayama,<sup>\*2</sup> Y. Ito,<sup>\*6</sup> M. Rosenbusch,<sup>\*3</sup> S. Kimura,<sup>\*3</sup> S. Ishizawa,<sup>\*5</sup> T. Niwase,<sup>\*4</sup> H. Wollnik,<sup>\*7</sup> and H. Miyatake<sup>\*2</sup>

KEK Isotope Separation System (KISS) dedicated to the study of the third peak around  $A \sim 195$  in the solar abundance can produce pure low-energy beams of neutron-rich isotopes around  $N = 126$  using multi-nucleon transfer reaction and in-gas cell laser ionization and spectroscopy technique.<sup>1)</sup>

The KISS facility mainly performing beta-decay lifetime study and beta-delayed  $\gamma$ -ray spectroscopy so far, by a multi-reflection time-of-flight (MRTOF-MS), will be able to measure masses of RIs by steering the beam direction toward the MRTOF-MS system while the beta-decay curve is being measured at the decay station. The MRTOF-MS, competitive to the state-of-art Penning trap, features a high mass resolving power of  $>100000$  even in the short measurement time ( $\sim 30$  ms). Together with its lower yield requirement, remarkable strengths the device has are suitable for the short-lived RIs of low production yield.<sup>2)</sup>

Recently, construction of a new MRTOF-MS has been completed (Fig. 1), and presently in the performance test. It consists of a gas cell to cool down the injected ions, a trap system, and a MRTOF chamber. The trap system thermalizes the ions, and converts a continuous

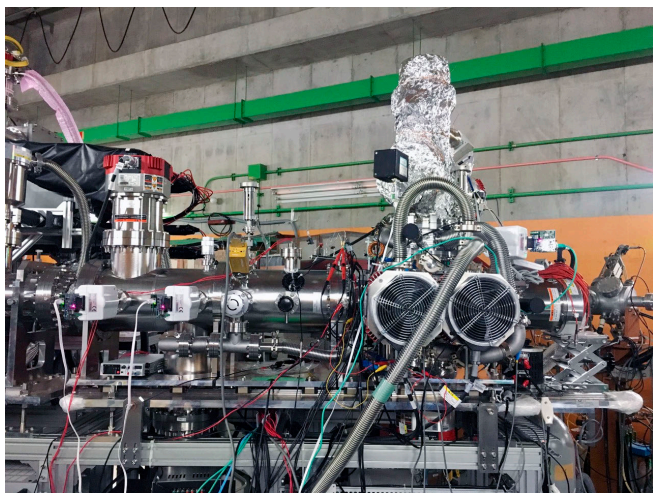


Fig. 1. MRTOF-MS system, constructed and coupled to the KISS beam line.

<sup>\*1</sup> Institute for Basic Science, Rare Isotope Science Project

<sup>\*2</sup> Wako Nuclear Science Center (WNSC), Institute of Particle and Nuclear Studies (IPNS), High Energy Accelerator Research Organization (KEK)

<sup>\*3</sup> RIKEN Nishina Center

<sup>\*4</sup> Department of physics, University of Kyushu

<sup>\*5</sup> Department of physics, University of Yamagata

<sup>\*6</sup> JAEA

<sup>\*7</sup> Department of Chem. & Bio.chem. New Mexico state university

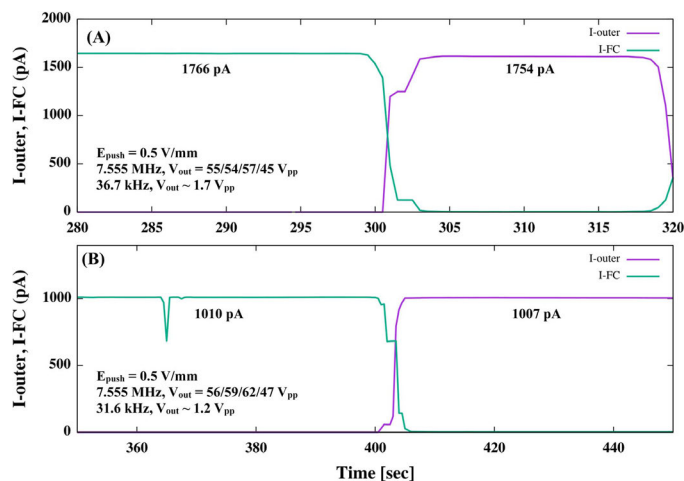


Fig. 2. Ion currents measured at the outer-ring and the faraday cup, respectively for the different pressures – (A)  $P_{\text{He}} = 100$  Pa, (B)  $P_{\text{He}} = 174$  Pa.

beam into a pulsed beam for further MRTOF operation.

In this report, for the gas cell filled with the helium buffer gas, its ion extraction efficiency experimentally measured has been briefed. The investigation has been performed at two different pressures of  $P_{\text{He}} = 100$  and  $174$  Pa. Using a radio frequency (RF) carpet ( $\phi 190$  mm) with a pitch of  $0.64$  mm, an exit hole with  $\phi 1.28$  mm and a thermal  $\text{K}^+$  ion source. The “ion surfing” mode developed by the combination of a repelling RF potential, a DC potential gradient, and a 4-phase audio frequency (AF) potential has been implemented, by which the ions stopped in the gas cell are quickly transported.<sup>3)</sup> When the ion surfing mode with ion drift direction opposite to the exit hole applied, the current measured at the outermost ring of RF carpet ( $I_{\text{outer}}$ ) showed only small difference of around 1%, compared to that at the carpet surface of no RF applied. A faraday cup was installed near the exit, whose current is  $I_{\text{FC}}$ . Figure 2 shows the evidence of the ion surfing mode created, in which the relative phase of AF voltages was changed by time from  $+90^\circ$  (to exit hole) to  $-90^\circ$  (to outer-ring). It has been achieved that most of ions arrived on the carpet were extracted by the “ion surfing” mode, *i.e.* the ratio of the extracted ions to the collected (“extraction efficiency”) close to 100%.

## References

- 1) Y. Hirayama *et al.*, Nucl. Instrum. Methods Phys. Res. B **353**, 4 (2015).
- 2) P. Schury *et al.*, Nucl. Instrum. Methods Phys. Res. B **335**, 39 (2014).
- 3) G. Bollen, Int. J. Mass Spectrom. **335**, 131 (2011).

# Offline test for RF carpet transportation in RF ion guide gas cell at the SLOWRI facility

A. Takamine,<sup>\*1</sup> M. Rosenbusch,<sup>\*1</sup> M. Wada,<sup>\*1,\*3</sup> P. Schury,<sup>\*3</sup> J. Y. Moon,<sup>\*4</sup> T. Sonoda,<sup>\*1</sup> T. M. Kojima,<sup>\*1</sup>  
I. Katayama,<sup>\*1</sup> Y. X. Watanabe,<sup>\*3</sup> H. Ueno,<sup>\*1</sup> and H. Ishiyama<sup>\*1</sup>

We are developing an RF ion guide<sup>1)</sup> gas catcher cell (RFGC) at the SLOWRI facility. Instead of the previously-used cylindrically shaped gas cell, we recently introduced a newly-designed cuboid-shaped gas cell to improve the heat conduction between the cell and a cryocooler. At the same time, we redesigned an RF carpet (RFCP) configuration consisting of two stages of RF-transport electrodes, which is one stage less than that in the previous version<sup>3)</sup> (see Fig. 1). Although the 1st RFCP has been unchanged, the 2nd RFCP now has concentric electrodes to collect ions to the exit hole at the center of the RFCP (Fig. 1(b)). Since the RFCPs are mounted onto the lid (an aluminum plate) of the gas cell, the thermal conductance has been improved and the RFCPs are efficiently cooled down.

We tested the transport performance of the RFGC using a surface ionization Cs ion source placed at the inner wall of the gas cell. The 1st RFCP carries ions to the 2nd RFCP, and the ions are guided to the exit hole by the 2nd RFCP. Firstly, we measured the ion currents collected onto the 1st RFCP by using the 1st RFCP as a Faraday cup, and then transported the ions through the 1st RFCP. After that, the ions were transported to the

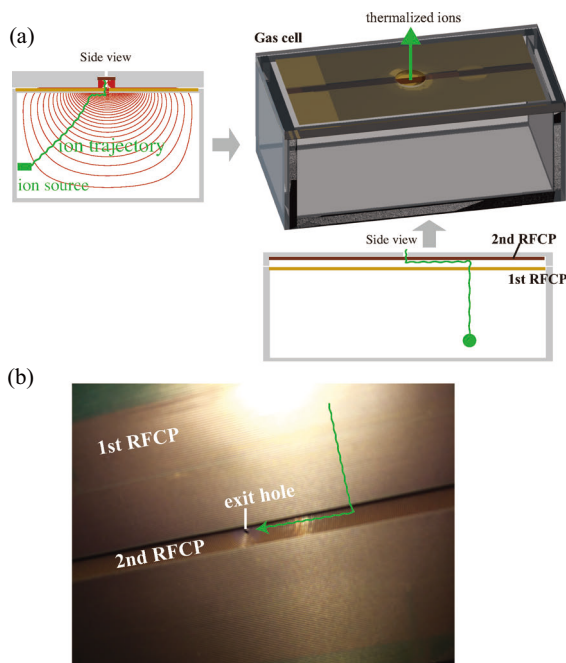


Fig. 1. (a) Sketch of the RFGC with an ion trajectory (green line). Red lines depict equipotential surfaces. (b) Photo of the center region of the RFCPs.

<sup>\*1</sup> RIKEN Nishina Center  
<sup>\*2</sup> Quantum Metrology Laboratory, RIKEN  
<sup>\*3</sup> Wako Nuclear Science Center (WNSC), IPNS, KEK  
<sup>\*4</sup> Institute for Basic Science

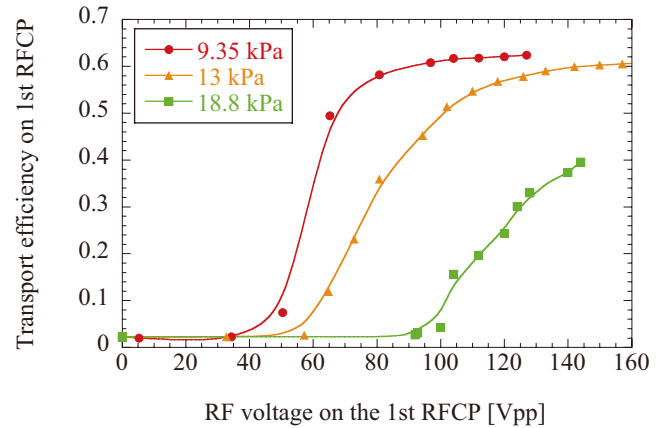


Fig. 2. 1st RFCP transportation test results for three different He gas pressures, namely 9.35 kPa, 13 kPa, and 18.8 kPa. In this test, the drag dc field on the 1st RFCP was 11.7 V/cm and the extraction DC field between the 1st and 2nd RFCPs was 20 V/cm.

2nd RFCP by applying the RF and DC fields to the 1st RFCP. The efficiency was defined by the current measured at the 2nd RFCP divided by that measured at the 1st RFCP. The test was typically performed with currents in the order of a few nA at the 1st RFCP. Figure 2 shows one example of the obtained transport efficiency as a function of the RF voltages applied to the 1st RFCP for three different helium gas pressures. The results show a transport efficiency of  $\approx 60\%$  at pressures of 13 kPa and less.

We subsequently extracted the ions from the exit hole using an ion surfing technique<sup>4)</sup> on the 2nd RFCP, and the extracted ions were detected by a Faraday cup behind the 2nd RFCP. The extraction efficiency was measured to be  $\approx 80\%$ . Therefore, the total efficiency in the present RFCP configuration was obtained to be  $\approx 50\%$ .

We will continue the test for an RFCP with finer pitch, and will try to use an ion surfing type RFCP as the 1st RFCP instead of the DC+RF type used in this measurement. We are now preparing the ion-guide system to be placed behind the 2nd RFCP; it consists of a quadrupole ion beam guide and an ion trapping system. This low-energy RI beam provider will be connected to a multi-reflection time-of-flight mass spectrograph (MRTOF-MS). We plan to start online commissioning of the RFGC in FY2019 at the end of the ZeroDegree beam line.

## References

- 1) M. Wada *et al.*, Nucl. Instrum. Methods Phys. Res. B **204**, 570 (2003).
- 2) A. Takamine *et al.*, RIKEN Accel. Prog. Rep. **50**, 194 (2017).
- 3) A. Takamine *et al.*, RIKEN Accel. Prog. Rep. **50**, 193 (2017).
- 4) G. Bollen, Int. J. Mass Spectrom. **299**, 131 (2011).

## Study of extraction yield of multi-nucleon transfer reaction products by using cooled argon gas cell

Y. Hirayama,<sup>\*1</sup> Y. X. Watanabe,<sup>\*1</sup> M. Oyaizu,<sup>\*1</sup> M. Ahmed,<sup>\*1,\*2</sup> H. Choi,<sup>\*3</sup> S. Iimura,<sup>\*4</sup> H. Ishiyama,<sup>\*5</sup> S. C. Jeong,<sup>\*6</sup> Y. Kakiguchi,<sup>\*1</sup> J. Y. Moon,<sup>\*6</sup> M. Mukai,<sup>\*2</sup> P. Schury,<sup>\*1</sup> M. Wada,<sup>\*1</sup> and H. Miyatake<sup>\*1</sup>

We have developed the KEK Isotope Separation System (KISS) to study the  $\beta$ -decay properties of neutron-rich isotopes with neutron numbers around  $N = 126$  for astrophysics research.<sup>1)</sup> KISS uses a laser ion source to produce pure low-energy ion beams of the isotopes, which are produced as target-like-fragments (TLFs) in multi-nucleon transfer reactions by impinging a stable  $^{136}\text{Xe}$  beam with an energy of approximately 10 MeV/nucleon on a  $^{198}\text{Pt}$  target. The extraction efficiency from the laser ion source, which is based on an argon gas cell, was as low as 0.1%.<sup>2)</sup> We assume that the low extraction efficiency stems from the formation of molecule ions between TLF ions and impurities in the gas cell. The molecule ions would be neutralized in the argon gas cell, and, therefore, we cannot confirm the formation of neutral molecules by detecting and identifying them using usual electromagnetic methods.

To study this assumption, we developed a cooling system for the argon gas cell to freeze out the impurities in the argon gas and gas cell for suppressing the formation probability. Figure 1 shows a schematic view of the gas cell system with a cooling system that consists of a He cryo-module and liquid nitrogen cooling circuit. The gas cell is on the module to be cooled effectively, and liquid nitrogen is flowed along a wall of the gas cell. Two thermometers (Pt100) were installed to monitor the temperatures at the center and the argon gas inlet part of the gas cell. The cooling system enabled the argon gas and the gas cell to be cooled down to approximately 120 K in an off-line cooling test.

To study whether the extraction yield could be increased by suppressing the formation probability of molecules using the cooling system, we performed an on-line experiment using a  $^{136}\text{Xe}^{20+}$  beam with 10.75 MeV/nucleon and an intensity of 20 pA. Figure 2 shows the measured extraction yield of  $^{198}\text{Pt}^+$  (top) and the temperatures (bottom) as a function of time, respectively. The red and blue lines in the bottom figure show the temperatures at the center and the gas inlet part of the gas cell, respectively. The extraction yield decreased with decrease in the temperature, and became almost saturated at 60 min with temperatures of 170 K and 130 K at the center and the gas inlet part of the gas cell, respectively. The origin of bumps measured at approximately 26 and 36 min in the top figure was

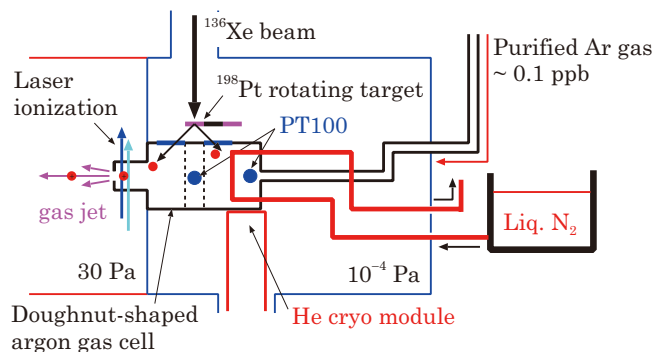


Fig. 1. Schematic view of the gas cell system with a cooling system. The details of the gas cell system were reported in Ref. 2).

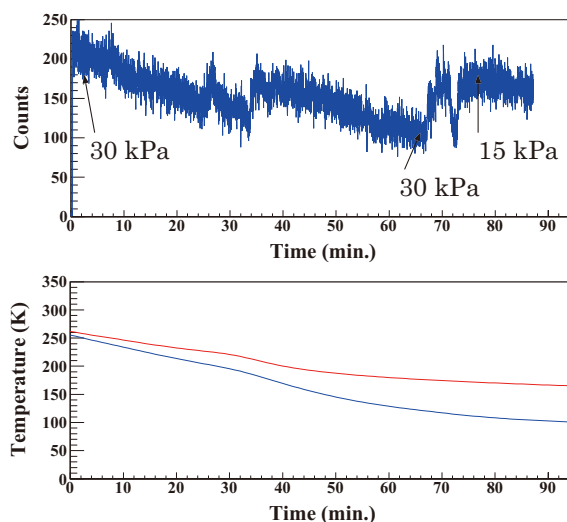


Fig. 2. Measured extraction yield of  $^{198}\text{Pt}^+$  (top) and the temperatures (bottom) as a function of time.

unclear. After saturation, we decreased the argon gas pressure down to 15 kPa from 30 kPa to keep the gas density constant according to the change in temperature. After that, we found a recovery of the extraction yield.

However, we did not find any increase in the extraction yield by cooling the gas cell system. This indicates that the formation of molecules is not the dominant cause for the low extraction yield. The extraction yield of unstable  $^{199}\text{Pt}$  at 170 K was also the same as that measured at room temperature.

### References

- 1) S. C. Jeong *et al.*, KEK Report 2010-2, (2010).
- 2) Y. Hirayama *et al.*, Nucl. Instrum. Methods Phys. Res. B **412**, 11 (2017).

<sup>\*1</sup> Wako Nuclear Science Center (WNSC), Institute of Particle and Nuclear Studies (IPNS), High Energy Accelerator Research Organization (KEK)

<sup>\*2</sup> Department of Physics, University of Tsukuba

<sup>\*3</sup> Seoul National University

<sup>\*4</sup> Osaka University

<sup>\*5</sup> RIKEN Nishina Center

<sup>\*6</sup> Institute for Basic Science, Rare Isotope Science Project

## Yield analysis using target sliding system at KISS

Y. X. Watanabe,<sup>\*1</sup> Y. Hirayama,<sup>\*1</sup> M. Mukai,<sup>\*2</sup> H. S. Choi,<sup>\*3</sup> S. Imura,<sup>\*4</sup> Y. Kakiguchi,<sup>\*1</sup> H. Miyatake,<sup>\*1</sup> M. Oyaizu,<sup>\*1</sup> P. Schury,<sup>\*1</sup> M. Wada,<sup>\*1</sup> A. Taniguchi,<sup>\*5</sup> S. C. Jeong,<sup>\*6</sup> N. Ishiyama,<sup>\*7</sup> M. Ahmed,<sup>\*2</sup> and J. Y. Moon<sup>\*6</sup>

We are developing KEK Isotope Separation System (KISS)<sup>1)</sup> to perform the  $\beta$ - $\gamma$  spectroscopy of neutron-rich nuclei around the neutron-closed shell  $N = 126$ , relevant to the r-process nucleosynthesis. The neutron-rich nuclei are produced by multinucleon transfer (MNT) reactions between the  $^{136}\text{Xe}$  beam and  $^{198}\text{Pt}$  target,<sup>2)</sup> and collected by a gas cell filled with argon placed at the downstream of the target. Because the dense plasma in the argon gas induced by the primary beam would reduce the extraction efficiency for the ions of interest, the gas cell has a beam pipe through which the primary beam passes without entering the gas cell.<sup>3)</sup> Thus the target-like fragments (TLFs) ejected from the target at finite angles can enter the gas cell through the doughnut-shaped 5  $\mu\text{m}$  Kapton window with the inner and outer diameters of 20 and 90 mm, respectively. To optimize the distance between the target and window, which is important for the efficient collection of TLFs, a target sliding system was introduced that can move the target along the beam axis and extraction yields were studied by changing the distance.

In this work, the TLFs of interest were  $^{199}\text{Pt}$  isotopes, which were produced in the MNT reactions of  $^{136}\text{Xe}$  and  $^{198}\text{Pt}$ . The beam was provided by RILAC2 + RRC with an energy of 9.4 MeV/nucleon on the target and the target thickness was 12.5 mg/cm<sup>2</sup>.  $^{199}\text{Pt}$  isotopes entering the gas cell were thermalized and neutralized in the argon gas and transported to the exit of the gas cell by a laminar gas flow. They were irradiated by lasers to be element-selectively ionized and accelerated by a high voltage of 20 kV. After mass-separated by an dipole magnet, they were implanted into an aluminized Mylar tape, where their  $\beta$ -rays were detected to evaluate the implantation rate by fitting the decay curves.

The dots in Fig. 1 show the measured extraction yields by changing the distance between the target and the window. Figure 2 shows the correlation between energies and angles of the  $^{199}\text{Pt}$  TLFs by the GRAZING calculations.<sup>4)</sup> The yields show a wide distribution with a maximum at the energy around zero and angle around 70°. The red line in Fig. 1 indicates the  $^{199}\text{Pt}$  yields considering the calculated correlation in Fig. 2

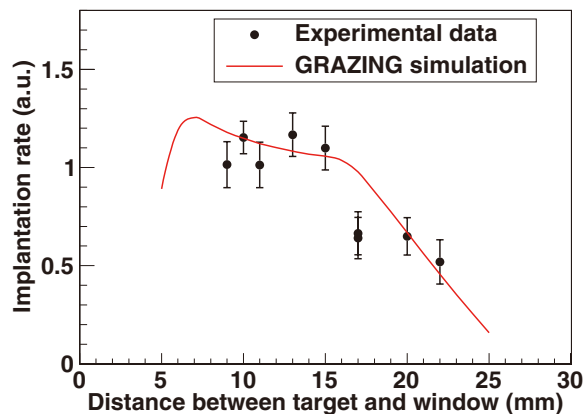


Fig. 1. Yields of  $^{199}\text{Pt}$  by changing the distance between the target and the window.

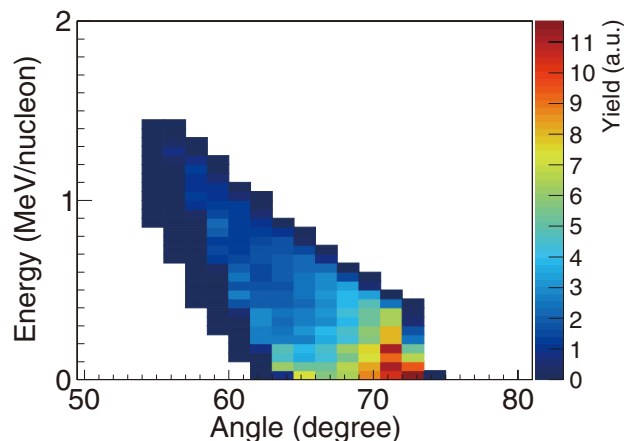


Fig. 2. Correlation between energies and angles of  $^{199}\text{Pt}$  nuclei ejected from the target in MNT reactions of  $^{136}\text{Xe}$  (9.4 MeV/nucleon) +  $^{198}\text{Pt}$  (12.5 mg/cm<sup>2</sup>) by GRAZING calculations.

with the beam spot size ( $\phi 6$  mm) on the target. It is normalized in the experimental data at a distance of 10 mm. These calculations were found to be significantly consistent with the experimental data and they provide a good reference for the optimization of target position.

### References

- 1) Y. Hirayama *et al.*, Nucl. Instrum. Methods Phys. Res. B **376**, 52 (2016).
- 2) Y. X. Watanabe *et al.*, Phys. Rev. Lett. **115**, 172503 (2015).
- 3) Y. Hirayama *et al.*, Nucl. Instrum. Methods Phys. Res. B **412**, 11 (2017).
- 4) A. Winther, Nucl. Phys. A **572**, 191 (1994); **594**, 203 (1995).

<sup>\*1</sup> Wako Nuclear Science Center (WNSC), Institute of Particle and Nuclear Studies (IPNS), High Energy Accelerator Research Organization (KEK)

<sup>\*2</sup> Department of Physics, University of Tsukuba

<sup>\*3</sup> Seoul National University

<sup>\*4</sup> Department of Physics, Osaka University

<sup>\*5</sup> Institute for Integrated Radiation and Nuclear Science, Kyoto University (KURNS)

<sup>\*6</sup> Institute for Basic Science (IBS)

<sup>\*7</sup> RIKEN Nishina Center

# Present status of ERIS at the SCRIT electron scattering facility

T. Ohnishi,<sup>\*1</sup> S. Ichikawa,<sup>\*1</sup> M. Nakano,<sup>\*2</sup> K. Kurita,<sup>\*2</sup> and M. Wakasugi<sup>\*1</sup>

The electron-beam-driven RI separator for SCRIT (ERIS)<sup>1)</sup> at the SCRIT electron scattering facility<sup>2)</sup> is an online isotope separator system used to produce low-energy RI beams for electron scattering experiments of unstable nuclei. Recently, we developed ion-stacking and pulse-extraction systems to improve the DC-to-pulse conversion efficiency using an RFQ cooler buncher named FRAC (fringing-RF-field activated DC-to-pulse converter).<sup>3)</sup> The results were reported in Ref. 4). In the present year, we have adopted the ion-stacking and pulse-extraction systems to the surface-ionization ion source to extend the variety of ion beams. In this paper, we report the results and present the status of ERIS.

Figure 1 shows the schematic of the surface-ionization ion source at ERIS and its electrical potential. The ionization chamber is made of tantalum, which is 25 mm long, contains a hole with a diameter of 1.5 mm, and has inner and outer diameters of 7 and 9 mm, respectively. The exit grid contains a hole with a diameter of 3 mm which is attached to a meshed electrode, and it is 3 mm away from the exit hole of the ionization chamber to avoid thermal deformation. Most of the neutral atoms remain inside the ionization chamber and transfer tube, except those that escape through the small exit hole. The neutral atoms are ionized at the inner wall of the ionization chamber. A large electric current is applied to the ionization chamber through the transfer tube and the inner wall is heated to 1000–2000°C.

The commissioning test was performed using a  $^{133}\text{Cs}$  ion beam of 10 keV. The voltage of the exit grid at the stacking and extraction were 10 and  $-60$  V, respectively. An electric current of 120 A was applied to the ionization chamber. The extracted ions were transported to FRAC and measured by the monitoring system.<sup>5)</sup> Figure 2(a) shows the pulse shape with a stacking time of

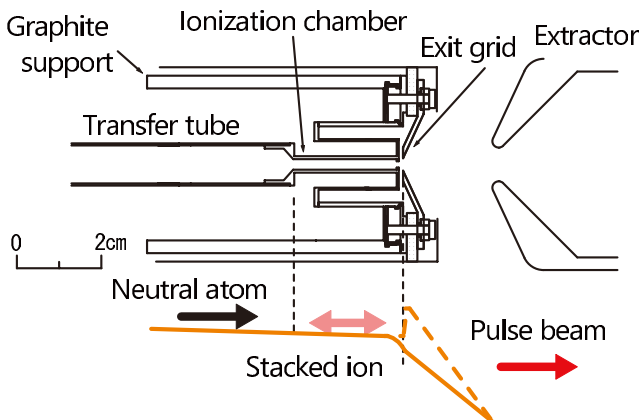


Fig. 1. Schematic of the surface-ionization ion source at ERIS and the electrical potential.

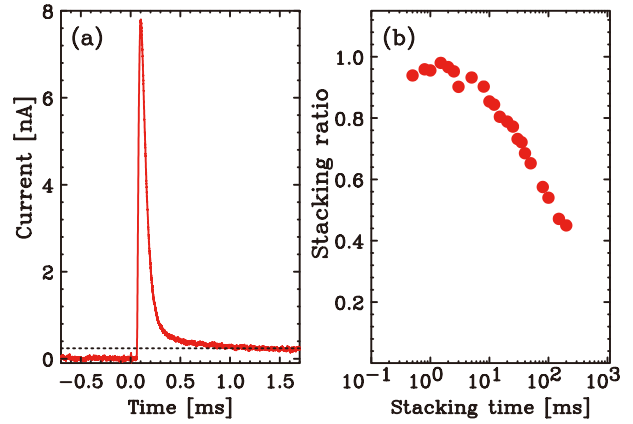


Fig. 2. (a) Pulse shape after 10-ms of stacking; the dotted line shows the current of the continuous beam. (b) Stacking-time dependence of stacking ratio.

10 ms. The extraction period was set to 2 ms to measure the pulse shape. With a stacking time of 10 ms, the pulse height was roughly 34 times of that with a continuous beam. The stacking time dependence of stacking ratio is shown Fig. 2(b). The stacking ratio is the ratio of the charge calculated by subtracting the contribution of the continuous beam from the total charge within a extracted pulse width to the total charge obtained by integrating the continuous beam over the stacking time. A stacking ratio of almost 0.9 was obtained at a stacking of 10 ms. In comparison to previous results<sup>4)</sup> (approximately 0.2 with a 10 ms stacking), the obtained stacking ratio is much larger. We reason that the number of neutral atoms escaped from the ionization chamber during the stacking time is small owing to the high ionization efficiency.

The DC-to-pulse conversion efficiency of FRAC was measured and it exceeded 50% with a longer stacking time of approximately 50 ms. This longer stacking time was enough to cool the ions with a relatively small amount of buffer gas ( $\sim 10^{-3}$  Pa) inside FRAC. This operation condition is needed to connect with the SCRIT device installed inside the electron storage ring. The results at FRAC were reported in Ref. 6).

More detailed study and improvement of the ion stacking inside ERIS is in progress.

## References

- 1) T. Ohnishi *et al.*, Nucl. Instrum. Methods Phys. Res. B **317**, 357 (2013).
- 2) M. Wakasugi *et al.*, Nucl. Instrum. Methods Phys. Res. B **317**, 668 (2013).
- 3) M. Wakasugi *et al.*, Rev. Sci. Instrum. **89**, 095107 (2018).
- 4) T. Ohnishi *et al.*, RIKEN Accel. Prog. Rep. **50**, 192 (2017).
- 5) M. Togasaki *et al.*, RIKEN Accel. Prog. Rep. **44**, 173 (2013).
- 6) S. Sato *et al.*, in this report.

<sup>\*1</sup> RIKEN Nishina Center

<sup>\*2</sup> Department of Physics, Rikkyo University

## Electron-beam-current control at RTM injector

M. Watanabe,<sup>\*1</sup> A. Enokizono,<sup>\*1</sup> and M. Wakasugi<sup>\*1</sup>

SCRIT facility<sup>1)</sup> is a unique facility to measure electron scattering off from short-lived nuclei. In the SCRIT facility, a racetrack microtron (RTM<sup>2)</sup>) is used as the electron injector of the energy of 150 MeV for the electron storage ring (SR2) and ISOL-type nuclei source which is the electron-beam-driven RI separator for SCRIT (ERIS<sup>3)</sup>). We have been working toward upgrading<sup>4)</sup> the RTM to operate ERIS for efficient photo fission and run SR2 in a stable condition. Especially for ERIS, a higher electron beam current is desired for higher ion yield of short-lived nuclei.

RTM is equipped with a cathode-type electron source with the energy of 60 keV. Before adjusting and upgrading the RTM accelerator, it is important to know the specifications of the 60 keV cathode-type electron source of RTM.

It is evident that the electron beam current depends on the temperature of the cathode, which is controlled by the cathode heater power  $P_h$  and the electric field around the cathode to extract thermal electrons from the surface of the cathode. In this study, we examined these relationships.

The commercially available NJK2305, provided by New Japan Radio Co., Ltd., is used as the cathode-type electron source. The maximum electron beam current is 4.25 A at a heater voltage of 6.3 V. It has a grid mesh in front of the cathode surface to make electric field for the extraction of thermal electrons. The beam current ranges from 20 to 70 mA with a grid voltage of 20 V.

Figure 1 shows the cathode-heater-power  $P_h$  dependence of the electron beam current  $I_e$ . Unfortunately, we do not have information about the temperature of the cathode; however, it is considered that temperature is nearly proportional to  $P_h$ . The two lines in the figure represent the grid voltage ( $V_g$ ) of 50 and 200 V. The

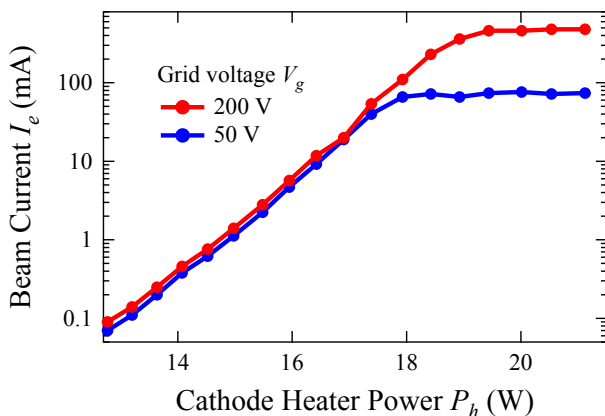


Fig. 1. Electron beam current depending on cathode heater power. It saturates around the heater power of 20 W.

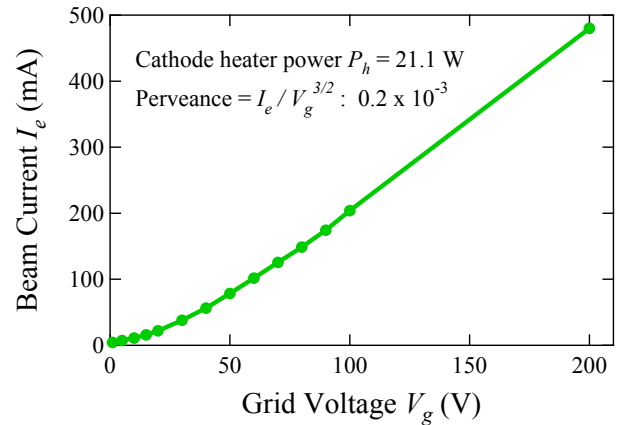


Fig. 2. Electron beam current depending on the grid voltage. The figure shows the case of cathode heater power of 21.1 W, which is saturated.

graph forms straight lines in the logarithmic y-axis up to  $P_h = 18$  W. This is a common behavior of cathode-type electron source. In this range, it should be noted that the electric field by  $V_g$  does not significantly affect the beam current, indicating that the electric field used to extract the electrons does not have a dominant effect on extraction. However temperature plays a significant role in the extraction of thermal electrons. This is consistent with the exponential functions that produce straight lines in the logarithmic scale because the Fermi function is composed of an exponential function.

In contrast,  $I_e$  is saturated above  $P_h = 19$  W. This is interpreted as the space charge between the cathode and grid manages the maximum beam current because the space charge suppresses the electron extraction by screening the electric field.

Figure 2 shows the dependence of electron beam current  $I_e$  on the grid voltage  $V_g$ . It seems that it is easy to extrapolate the line toward the higher  $V_g$  range to produce a higher beam current  $I_e$ . The original design of RTM has a maximum  $V_g$  of 200 V. However, we have already installed a grid voltage power supply of 500 V for this purpose.

According to these results, the heater power  $P_h > 19$  W for the cathode-type electron source NJK2305 is a better option to obtain a controllable beam current with  $V_g < 200$  V.

### References

- 1) M. Wakasugi *et al.*, Nucl. Instrum. Methods Phys. Res. B **17**, 668 (2013).
- 2) T. Hori, Doctoral Thesis, the Graduate University for Advanced Studies (SOKENDAI), 2002.
- 3) T. Ohnishi *et al.*, Nucl. Instrum. Methods Phys. Res. B **317**, 357 (2013).
- 4) M. Watanabe *et al.*, RIKEN Accel. Prog. Rep. **49**, 188 (2015), **50**, 190 (2016), and **51**, 177 (2017).

<sup>\*1</sup> RIKEN Nishina Center

## Modification of dc-to-pulse converter FRAC

S. Sato,<sup>\*1,\*2</sup> M. Wakasugi,<sup>\*2</sup> T. Ohnishi,<sup>\*2</sup> M. Watanabe,<sup>\*2</sup> A. Enokizono,<sup>\*2</sup> K. Kurita,<sup>\*1</sup> and M. Nakano<sup>\*1,\*2</sup>

At the SCRIT electron scattering facility,<sup>1)</sup> we aim at realizing world's first electron scattering experiment for unstable nuclei, after succeeding in the principle verification experiment using stable nuclei  $^{132}\text{Xe}$ .<sup>2)</sup> In order to perform electron scattering with an unstable nuclei with a small production rate, it is important to accumulate and inject ions efficiently into the SCRIT device. For this purpose, it is necessary to convert a continuous ion beam from the ISOL-type ion separator, ERIS (Electron-beam-driven RI separator for SCRIT),<sup>3)</sup> to a pulsed beam with a pulse duration of 300–500  $\mu\text{s}$ . We developed a dc-to-pulse converter, FRAC (Fringing-Rf-field-Activated dc-to-pulse Converter),<sup>4)</sup> based on an RFQ linear ion trap, with a conversion efficiency of 5.6%. In this article, we report about the modification applied to further improve the efficiency and the latest performance of the FRAC.

The first modification is to enable cooling of the accumulated ions with a buffer gas. Ions lose their kinetic energy by collision with the buffer gas and accumulate in a longitudinal potential well created by the DC potential applied to the RFQ rod and a barrier electrode at both ends of the rods. The ions are injected for several seconds, stacked, and consequently ejected as a high-intensity pulsed beam. Ion beam cooler-buncher technology with a buffer gas of  $\sim 1$  Pa is widely used in the world. However, since the SCRIT device operates under a high vacuum of  $\sim 10^{-8}$  Pa, it cannot be used in our beam line. Therefore, we tried to maintain the pressure inside the FRAC as high as possible while keeping the beam line vacuum at  $\sim 10^{-5}$  Pa by differential pumping between the FRAC and beam line. As a result, the vacuum of the FRAC was achieved as  $\sim 10^{-3}$  Pa. Cooling with low-pressure buffer gas requires a long cooling time of several tens of milliseconds, which causes a decrease in efficiency, however, that can be prevented by operating the FRAC in the SPI (Synchronous Pulse Injection) mode,<sup>4)</sup> in which the injection barrier potential is switched open and close synchronously with the arrival of the pre-pulsed beam from ERIS.

The second modification is to enable the application of an electric field gradient in the longitudinal direction of the FRAC. When the potential of the cooling region is uniform, it takes several milliseconds to extract all the cooled ions because they are widely distributed in the entire cooling area with low velocity. Therefore, the RFQ was physically divided into six segments, and descending DC potentials were applied and the potential dropped toward the exit. Consequently, the cooled

Table 1. Conversion efficiency.

$V_d$ \ $f_{\text{inj}}$	5 Hz	10 Hz	20 Hz	50 Hz	100 Hz
0 V	92.2%	88.1%	76.4%	66.7%	60.9%
5 V	92.4%	87.2%	81.8%	74.1%	69.8%
10 V	85.4%	79.1%	73.3%	63.4%	64.2%
15 V	-	-	-	-	53.5%

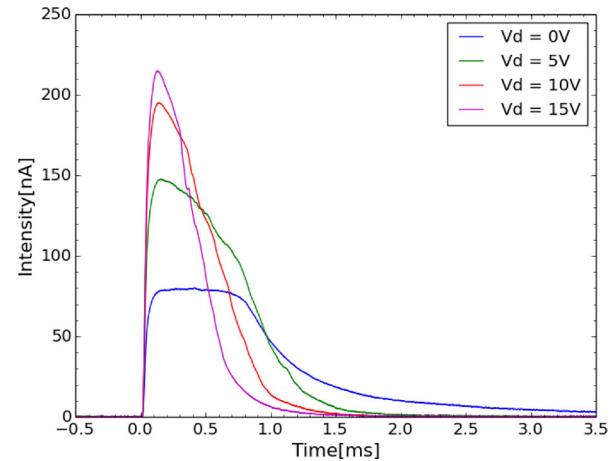


Fig. 1. Waveforms of the output pulsed beam obtained at different  $V_d$ .

ions were locally accumulated in the vicinity of the exit, and as a result, it is possible to extract as a narrow pulse beam.

In the measurement, the electric field gradient was set to be linear. The potential difference between the entrance and the exit,  $V_d$ , and the injection frequency of the pre-pulsed beam,  $f_{\text{inj}}$ , were used as measurement parameters. The conversion efficiency was greatly improved by the present modification. Table 1 shows the conversion efficiency with each measurement parameter. Figure 1 shows the waveform of the extracted pulsed beam when the pre-pulsed beam is injected at 100 Hz, with an ejection cycle of 0.5 Hz. As can be seen in Fig. 1, the pulse width narrows as  $V_d$  increases, and the FWHM is reduced to 418.5  $\mu\text{s}$  at  $V_d = 15$  V. At the same time, however, the conversion efficiency is relatively small. Methods to solve this problems are currently under development.

### References

- 1) M. Wakasugi *et al.*, Nucl. Instrum. Methods Phys. Res. B **317**, 668 (2013).
- 2) K. Tsukada *et al.*, Phys. Rev. Lett. **118**, 262501 (2017).
- 3) T. Ohnishi *et al.*, Nucl. Instrum. Methods Phys. Res. B **317**, 357 (2013).
- 4) M. Wakasugi *et al.*, Rev. Sci. Instrum. **89**, 095107 (2018).

<sup>\*1</sup> Department of Physics, Rikkyo University  
<sup>\*2</sup> RIKEN Nishina Center

## Precise magnetic field measurement of WiSES

H. Wauke,<sup>\*1,\*2</sup> A. Enokizono,<sup>\*1</sup> Y. Honda,<sup>\*1,\*2</sup> K. Kasama,<sup>\*1,\*2</sup> T. Ohnishi,<sup>\*1</sup> T. Suda,<sup>\*1,\*2</sup> S. Takayama,<sup>\*1,\*2</sup>  
T. Tamae,<sup>\*1,\*2</sup> K. Tsukada,<sup>\*1,\*2</sup> M. Wakasugi,<sup>\*1</sup> and M. Watanabe<sup>\*1</sup>

WiSES<sup>1)</sup> (Window-frame Spectrometer for Electron Scattering) is an electron spectrometer for the SCRIT (Self-Confining RI Ion Target) experiment.<sup>2,3)</sup> The dipole magnet<sup>4)</sup> of WiSES has a large aperture for the measurement of scattered electrons in a wide scattering angle at once. The gap volume of the magnet is 140 cm (width), 29 cm (height), 170 cm (depth). In elastic electron scattering experiments, a typical momentum resolution of  $\delta p/p \sim 10^{-3}$  for 150–300 MeV electron energy is required to separate elastic and inelastic scattering events. The momentum resolution measured by elastic scattering for <sup>12</sup>C and <sup>208</sup>Pb is found to not reach the design value. To improve further momentum resolution, we will measure the precise 3D magnetic fields of the WiSES magnet with a precision of  $\delta B/B \sim 10^{-3}$ .

We will use three Hole probes to measure  $B_x$ ,  $B_y$ , and  $B_z$  at the same time. The Hall probe has a Hall sensor inside and reacts to the component of the magnetic field with respect to the normal direction of the sensor surface. However, the Hall probe also detects the magnetic field with respect to the tangent of the sensor, namely the Planar Hall effect.<sup>5)</sup>  $B_{\text{probe}}$  detected by the Hall probe is expressed as follows:

$$B_{\text{probe}} = B \cos \theta + p_H (B \sin \theta)^2 \sin 2\phi, \quad (1)$$

where  $\theta$  is the angle between the normal direction of the sensor and the magnetic field, and  $\phi$  is the rotation angle of the sensor. The first term in Eq. (1) is the Hall effect. The second term in Eq. (1) corresponds to the Planar Hall effect. To determine the value of the Planar Hall coefficient  $p_H$  of the second term, we measured the  $2\phi$  dependence of each probe in a uniform magnetic field.

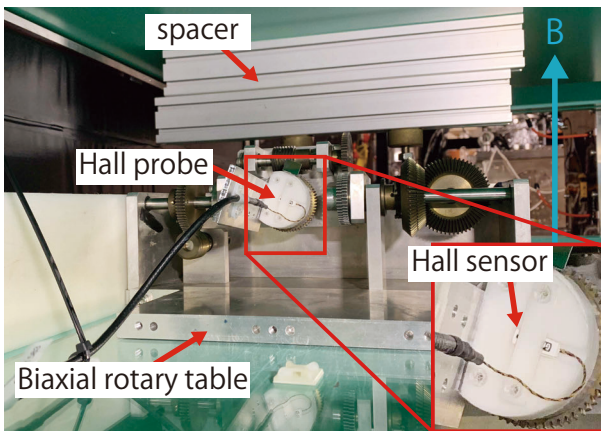


Fig. 1. Setup of Planar Hall effect measurement in WiSES.

<sup>\*1</sup> RIKEN Nishina Center

<sup>\*2</sup> ELPH, Tohoku University

<sup>\*3</sup> Department of Rikkyo University

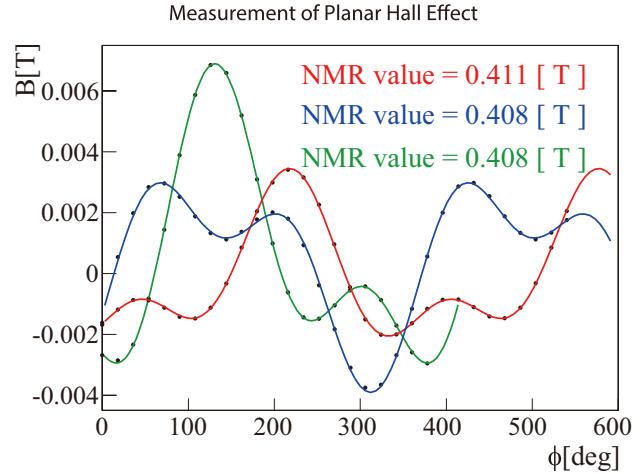


Fig. 2. Result of  $2\phi$  dependent magnetic field by the Planar Hall effect. Each color corresponds to the fitting for each probe.

The setup is shown in Fig. 1. The probe was mounted on a rotating stage in the homogeneous field region of the WiSES magnet. The absolute value of the field was measured by NMR, which was also located in the homogeneous region. The stage could rotate around two axes corresponding to  $\theta$  and  $\phi$  of Eq. (1), with resolutions of 0.3 mrad. In this measurement,  $\theta$  was set to be  $90^\circ$  to suppress the influence of the first term of Eq. (1). The results for the three probes are shown in Fig. 2. By adding some mis-alignment angles of our system as fitting parameters into Eq. (1), our data are well reproduced. In the present fitting, the followings points are included:

- the contribution from the first term of Eq. (1) owing to a small deviation from the  $90^\circ$ ,
- the angle between the probe and the rotary axis of the stage, etc.

Consequently, the  $p_H$ s are evaluated to be 0.008, 0.01, and 0.015. These values are consistent with a previous study ( $p_H = 0.0148$ ).<sup>6)</sup> NMR values for each probe are shown in Fig. 2. Although, the evaluation of systematic errors are ongoing. We will mount three probes on a system to make a triaxial probe, and create a precise map of the magnetic field of the WiSES magnet at the next stage.

### References

- 1) T. Adachi *et al.*, RIKEN Accel. Prog. Rep. **45**, 144 (2012).
- 2) M. Wakasugi *et al.*, Phys. Rev. Lett. **100**, 164801 (2008).
- 3) T. Suda *et al.*, RIKEN Accel. Prog. Rep. **45**, 184 (2013).
- 4) T. Tamae *et al.*, RIKEN Accel. Prog. Rep. **47**, 196 (2014).
- 5) C. Goldberg, R. E. Davis, Phys. Rev. **94**, 1121 (1954).
- 6) S. Tomita, Master Thesis, Tohoku Univ., (2017).

## MPV – Parallel Readout Extension of VME

H. Baba,<sup>\*1</sup> T. Ichihara,<sup>\*1</sup> T. Isobe,<sup>\*1</sup> T. Ohnishi,<sup>\*1</sup> K. Yoshida,<sup>\*1</sup> Y. Watanabe,<sup>\*1</sup> S. Ota,<sup>\*2</sup> S. Shimoura,<sup>\*2</sup> and S. Takeuchi<sup>\*2</sup>

We have been developing a data acquisition (DAQ) system at RIBF. The parallel readout VME DAQ system<sup>1)</sup> was successfully operated in 2016. In this system, the data readout of all VME modules were completely parallelized by a mountable controller (MOCO).<sup>2)</sup> The DAQ performance was significantly improved; however, the usability and robustness of the system was rather problematic. To solve these problems, we developed a new MPV system (MOCO with parallelized VME), which is a type of parallel readout extension of the VME. When we set up the MOCO system, several unwanted features were found: 1) MOCO was installed between the VME module and VME backplane; consequently, the VME module protruded from the VME shelf by 7 cm. Some circuit components on the VME module were exposed, which caused a short-circuit. 2) MOCO had USB connectivity. A single PC can handle multiple MOCOs. However, owing to the congestion in the USB, the data transfer speed fatally degrades. To obtain a good performance, same number of PCs and MOCOs should be installed. 3) To synchronize events between MOCOs and other DAQ devices, trigger and busy signals have to be exchanged. For this purpose, four additional pairs of differential cables were connected to the MOCO located inside the VME shelf, which creates a mess of cables.

In this study, we developed circuit boards known as the MPV controller (Fig. 1) and MPV backplane (Fig. 2). All DAQ communications (*e.g.* trigger and data) for MOCO are done through this controller. Avnet PicoZed 7010<sup>3)</sup> (red board in Fig. 1), which contains Xilinx Zynq-7000 All Programmable System-on-Chip, is adopted as the main circuit of the controller. Logic cir-

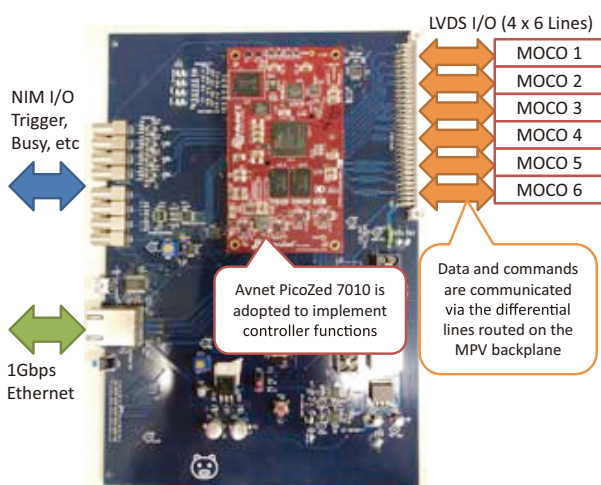


Fig. 1. Image of MPV controller. This controller can simultaneously handle up to 6 modules of MOCO.

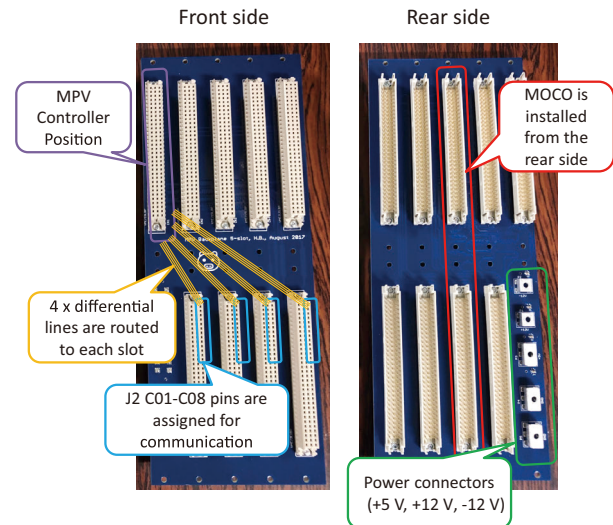


Fig. 2. Image of the MPV backplane (5-slot). 7-slot type is also available. Dimension and mounting holes are compatible with Schroff/NVENT Monolithic Backplane (23001-065 for 5 slot, 23001-067 for 7 slot).

cuits to handle the MOCO are implemented on PicoZed. The MPV controller accesses the MOCO through the differential lines on the backplane. Four pairs of differential lines (LVDS) are routed to each slot from the controller position, *i.e.*, there are 24 pairs of differential lines on the MPV backplane. In the previous MOCO-based system, additional cables and PCs were required. However, this MPV system does not require any extra cables and devices. As shown in Fig. 2, the MPV controller is installed at the left-most slot of the backplane. VME modules are installed at the front, similar to the standard VME system. Simultaneously, MOCOs are inserted from the rear side of the backplane. A MOCO can access the VME module through the DIN41612 connectors. In the standard VME backplane, all slots shared the VME bus lines. In contrast, the MPV backplane has an isolated architecture except for power lines. Data are independently acquired by FPGA on the controller, which can be read-out from the 1 Gbps ethernet port. The maximum possible data rate for the six MOCOs is 960 Mbps, which is within the range of theoretical throughput of 1 Gbps ethernet with a jumbo frame. These features enable the complete parallel read-out of the VME-based DAQ system.

In conclusion, the hardware of the MPV has been successfully produced. The firmware for the MPV controller is under development. This system will be ready in 2019.

### References

- 1) H. Baba *et al.*, RIKEN Accel. Prog. Rep. **50**, 224 (2017).
- 2) H. Baba *et al.*, RIKEN Accel. Prog. Rep. **45**, 9 (2012).
- 3) <http://zedboard.org/product/picozed>

<sup>\*1</sup> RIKEN Nishina Center

<sup>\*2</sup> Center for Nuclear Study, University of Tokyo

## Validation method to merge digital data acquisition with analog data-acquisition system in SAMURAI30 experiment

J. Gao,<sup>\*1,\*3</sup> L. Stuhl,<sup>\*2</sup> M. Sasano,<sup>\*1</sup> K. Yako,<sup>\*2</sup> H. Baba,<sup>\*1</sup> SAMURAI 30 Experiment Collaboration

In this paper, the method to combine the digital data acquisition system (DDAQ) of our low-energy neutron detector PANDORA<sup>1)</sup> and the analog data acquisition system (DAQ) of standard detectors of SAMURAI spectrometer<sup>2)</sup> during the SAMURAI30 experiment<sup>3,4)</sup> is reported.

PANDORA was optimized to detect neutrons with a kinetic energy of 0.1–5 MeV by measuring the related Time-of-Flight (ToF) in the range of 50–300 ns. Data from PANDORA bars (each with a signal from both ends) were read out with duplicated readout. CAEN V1730 modules were used for the charge and pulse shape discrimination information while an analog circuit (discriminators and CAEN V1290 TDC modules) was used for timing and triggering.

For the DDAQ, we daisy chained six CAEN V1730B (16-channel modules) and one CAEN V1730D (8-channel module) waveform digitizers using an optical connection. The unpublished software of digiTES based on Digital Pulse Processing for the Pulse Shape Discrimination (DPP-PSD) firmware<sup>5)</sup> was used to manage different modules in the daisy chain condition and control the digitizers. A LUPO (Logic Unit for Programmable Operation) module<sup>6,7)</sup> was used to generate a 62.5 MHz signal to synchronize timestamps of the seven modules and share the clock with another LUPO in the DAQ system.

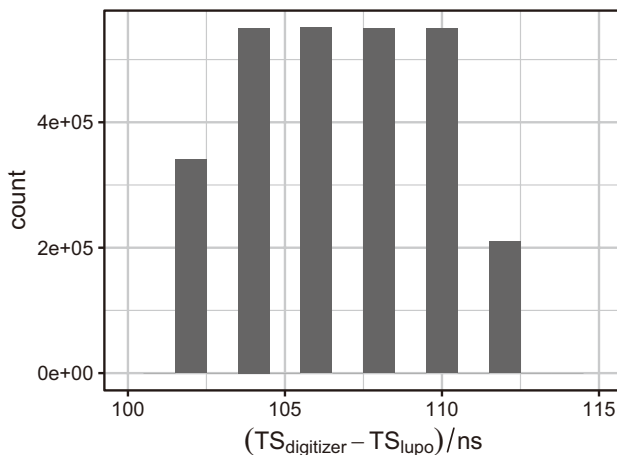


Fig. 1. Time stamp difference between DDAQ and DAQ. V1730B/D has 2 ns timestamp resolution while LUPO has 10 ns resolution.

The acquisition in the digitizers was not based on the self-triggering of each channel. The local triggering option of the two-two coupled channels (in V1730, two neighboring channels were paired) was used to ensure the coincidence between photomultipliers of both sides of PANDORA. The digitizers were configured to ensure that the validation of the local triggers came from an external trigger based on the customer configured software criteria. To manage the coincidence requirements between the two separate acquisition systems, the first channel (ch 0) of each digitizer was dedicated to a logic signal. This external trigger validated the PANDORA self-triggers in a time window of approximately 1  $\mu$ s.

The validation signal originated from the accepted trigger of analog DAQ based on the triple coincidence of “BEAM” (from SBT detectors), analog “PANDORA” (recoil neutron) and “HODOSCOPE” (reaction residues at hodoscopes). This typical trigger rate was  $1.3 \times 10^3$  Hz.

Consistent with our expectation, six different values were observed in Fig. 1. In comparison with the typical dead time of SAMURAI DAQ (approximately 100  $\mu$ s), this method is enough for us to align the two data sets.

We express our gratitude to the RIKEN and CNS staff for the stable operation of the accelerators during the measurement. This work is funded by the China Scholarship Council, KAKENHI project 16H06716, the Japan Society for the Promotion of Science, and Kurata Grant from the Kurata Memorial Hitachi Science and Technology Foundation.

### References

- 1) L. Stuhl *et al.*, Nucl. Instrum. Methods Phys. Res. A **866**, 164 (2017).
- 2) T. Kobayashi *et al.*, Nucl. Instrum. Methods Phys. Res. B **317**, 294 (2013).
- 3) M. Sasano *et al.*, in this report.
- 4) L. Stuhl *et al.*, in this report.
- 5) <http://www.caen.it/csite/CaenProd.jsp>.
- 6) <https://ribf.riken.jp/RIBFDAQ/index.php?DAQ>.
- 7) H. Baba *et al.*, Nucl. Instrum. Methods Phys. Res. A **777**, 75 (2015).

\*1 RIKEN Nishina Center

\*2 Center for Nuclear Study, University of Tokyo

\*3 School of Physics, Peking University

## Development of 1.5-mm thick liquid hydrogen target

S. Koyama<sup>\*1,\*2</sup> and D. Suzuki<sup>\*2</sup>

We report on the development of a thin liquid hydrogen target using the CRYPTA system.<sup>1)</sup> We aim to perform missing mass experiments on proton-rich nuclei with high statistics and reasonable resolution via one and two neutron transfer ( $(p, d)$  and  $(p, t)$ , respectively) reactions with 50 MeV/nucleon radioactive beams, which generate deuterons and tritons ranging between 10 and 30 MeV/nucleon. Consequently we obtained a 1.5 mm thick liquid hydrogen target.

The system was placed in a vacuum chamber. A target cell was connected to a refrigerator with a copper bar and cooled down below the boiling point. To monitor the temperatures, a thermometer labeled ‘A’ was attached to the connecting end of the cell and ‘B’ was attached to the surface of the window frame, as shown in Fig. 1 (a). A gas pipe was connected to the inside of the cell. The pipe was also connected to a reserver tank placed outside the vacuum chamber, which was filled with hydrogen gas. Hydrogen was introduced from the tank to the cell. The hydrogen gas was liquefied near thermometer A and dropped into the cell. A heater was placed near thermometer A to maintain the temperature above the melting point.

The target cell consisted of one body frame and two window frames, all made of aluminum, as shown in Fig. 1 (b). Each window frame had a hole with a diameter of 20-mm at the center. The window frame of the downstream side was tapered to detect recoil particles at large angles. The side view of the constructed target cell is shown in Fig. 1 (a). The volume was defined by a pair of 6.47- $\mu\text{m}$ -thick HAVAR foils glued to the window frames. The designed distance between the

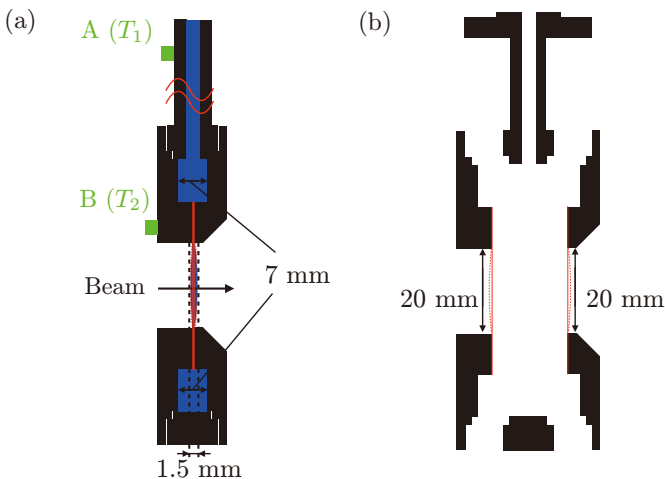


Fig. 1. (a) Side view of the cross-section of target cell. Blue area is filled with liquid hydrogen. Green squares indicate the thermometers. (b) Side view of the cross-section of target cell components.

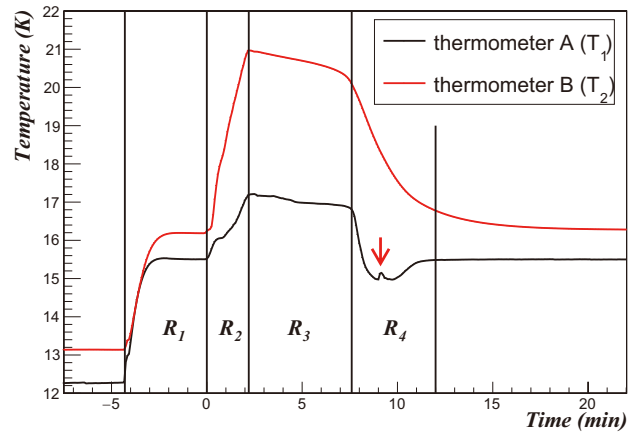


Fig. 2. Variation of temperatures during liquefaction.

foils was 0.5 mm. The liquid hydrogen volume thus defined expanded toward the outside by 0.5 mm at the center of each side due to the 0.8-atm gas pressure. The shape of the expansion was measured with a laser displacement sensor. The total thickness was found to be 1.5 mm at the center. We had no experience of liquefaction of hydrogen in such narrow volume and tested to determine the design of the window frames. Finally, we placed a 7-mm thick volume outside the foils to fully fill the target cell, as shown in Fig. 1 (a).

We performed a test at our test-bench at the RIBF. To visually confirm that the target cell was fully filled with liquid hydrogen, one of the foils was replaced with a 125- $\mu\text{m}$ -thick Kapton foil. Figure 2 shows the variations in the temperature of thermometer A ( $T_1$ ) and thermometer B ( $T_2$ ) during liquefaction. Before introducing the hydrogen gas, the target system was maintained at temperatures above the melting point by the heater ( $R_1$ ). When hydrogen gas was gradually introduced, the temperature of the target became higher because hydrogen gas was cooled ( $R_2$ ). Liquefaction gradually occurred while the temperature was almost constant ( $R_3$ ). During this step, it was observed from outside that only the lower part of the 20-mm diameter hole was filled. While the cell was filled only partially, the full 7-mm thick volume was likely filled at this point. Then, the temperature started to decrease ( $R_4$ ). When  $T_1$  became lower than 15.5 K, the heater turned on and the rate of decrease reduced.  $T_1$  suddenly increased at  $t = 9.5$  min, as indicated by the red arrow. At this point the target was fully filled. This behavior of temperature was observed using HAVAR foils at both sides. Therefore, we consider the target was also fully filled in this condition.

### Reference

- 1) H. Ryuto *et al.*, Nucl. Instrum. Methods Phys. Res. A **555**, 1 (2005).

<sup>\*1</sup> Department of Physics, University of Tokyo

<sup>\*2</sup> RIKEN Nishina Center

## Profile measurement of a large target cell of liquid hydrogen

M. Miwa,<sup>\*1,\*2</sup> M. Sasano,<sup>\*2</sup> X. Sun,<sup>\*3,\*2</sup> L. Stuhl,<sup>\*4</sup> J. Gao,<sup>\*3,\*2</sup> and M. Kurata-Nishimura<sup>\*2</sup>

The  $(p, n)$  reaction in inverse kinematics is a powerful probe for studying nuclear isovector responses in unstable nuclei. In May 2018, the SAMURAI 30 experiment was performed using PANDORA<sup>1)</sup> and SAMURAI<sup>2)</sup> setup with a liquid hydrogen target<sup>3)</sup> to study the GT transitions, including their resonances, in the  $^{11}\text{Li}$  and  $^{14}\text{Be}$  neutron drip line nuclei.<sup>4,5)</sup>

In general, the target thickness along the beam direction is required to obtain the cross sections. However, in the case of a liquid hydrogen target that contains with thin membranes, the target thickness strongly depends on the inflation of the membranes due to the differential pressure between liquid hydrogen and the vacuum in the target chamber.

In the SAMURAI 30 experiment, the target cell was tilted at  $45^\circ$  with respect to the beam direction, so that the recoil neutrons of interest, which were emitted around  $90^\circ$ , did not penetrate the target frame structures. Because the inflated target cell was tilted with respect to the beam line, the evaluation of the target thickness required three-dimensional analysis of the target shape. In this work, we measured the profile of a large target cell of liquid hydrogen by using a laser displacement meter and obtained the effective target thickness along the beam direction by analyzing the profile data.

Figure 1 schematically shows the setup for the target profile measurement. The target cell was filled with  $\text{N}_2$  gas, instead of liquid  $\text{H}_2$ , at 1719 Pa, which corresponds

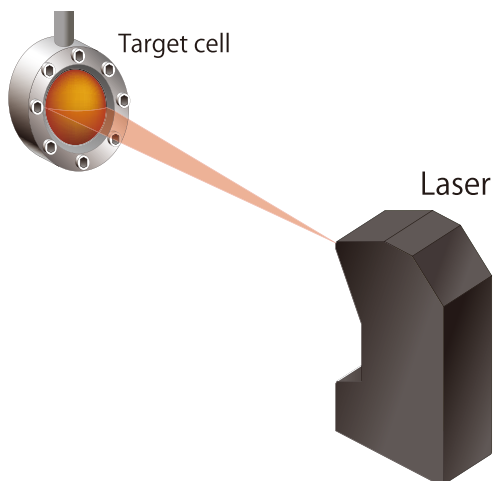


Fig. 1. Schematic of the setup for the two-dimensional profile measurement of the target thickness. The membranes of both sides are irradiated with a laser in the beam direction.

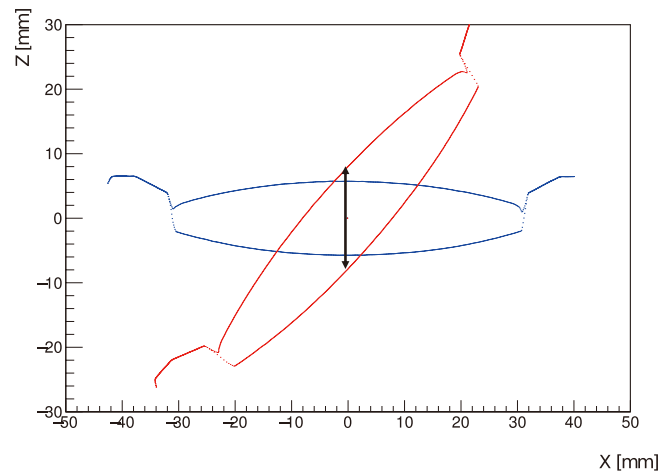


Fig. 2. Profile result of the target shape. The vertical axis indicates the spatial coordinate along the beam direction. The blue and red plots are the original data after the calibration and the data at an angle of  $45^\circ$  respectively.

to the differential pressure of 0.72 kPa. A laser displacement meter (KEYENCE LJ-G5000) was used to measure the target profile. The laser vertically irradiated the target cell surface. The configuration of the laser intensity was automatic, and the sampling time was 2 ms. The measurement can decide the absolute value only in the beam direction, while the position information in the horizontal direction can be just obtained as relative values. The scale of the horizontal position was calibrated by adjusting the inner diameter of the target frame to be the designed value, 50 mm. Here, we note that a typical beam spot of an RI beam at the SAMURAI F13 focal plane has a width of  $\pm 10$  mm and a height of  $\pm 20$  mm.

As a result of the profile measurement, we obtained the target shape data shown in Fig. 2. The blue plots represent original data while the red plots are tilted at an angle of  $45^\circ$ . The profile analysis provided the target thickness after 45-degree rotation as 15.8 mm at the center, 14.3 mm at  $x = \pm 10$  mm, and 7.40 mm at  $y = \pm 20$  mm.

In summary, we evaluated the target profile in the SAMURAI 30 experiment, taking into account the target tilting with respect to the beam direction through the three-dimensional analysis of the target cell.

### References

- 1) L. Stuhl *et al.*, Nucl. Instrum. Methods Phys. Res. A **866**, 164 (2017).
- 2) T. Kobayashi *et al.*, Nucl. Instrum. Methods Phys. Res. B **317**, 304 (2013).
- 3) H. Ryuto *et al.*, Nucl. Instrum. Methods Phys. Res. A **555**, 1 (2005).
- 4) L. Stuhl *et al.*, in this report.
- 5) J. Gao *et al.*, in this report.

\*1 Department of Physics, Saitama University

\*2 RIKEN Nishina Center

\*3 School of Physics, Peking University

\*4 Center for Nuclear Study, University of Tokyo

## The stability of the liquid hydrogen target system during the SAMURAI 30 experiment

X. Sun,<sup>\*1,\*2</sup> M. Sasano,<sup>\*2</sup> M. Miwa,<sup>\*3,\*2</sup> L. Stuhl,<sup>\*4</sup> and J. Gao<sup>\*1,\*2</sup>

The charge-exchange ( $p, n$ ) reactions in inverse kinematics are powerful tools to study the spin-isospin response of light nuclei. In general, Polyethylene ( $\text{CH}_2$ ) is used as the hydrogen target to induce the ( $p, n$ ) reactions, because it is easy to handle and has uniform thickness. However, the background generated from the carbon in  $\text{CH}_2$  is serious.

In the SAMURAI 30 experiment, a thick liquid hydrogen target (LHT)<sup>1)</sup> was used to perform the measurements of the ( $p, n$ ) reactions with a high reaction rate and lower background from carbon. It was required to keep the temperature of the target cell below the boiling point of hydrogen during the measurement. In this report, the stability of the temperature and pressure of the LHT system during the SAMURAI 30 beam time is reported.

The setup of the LHT system is described in Ref. 1). A Gifford-McMahon cycle (GM) refrigerator was used to keep the target cell at a low temperature in order to liquefy the hydrogen. A heat shield covered by aluminum foil was installed around the target cell to prevent heat inflow from the room temperature environment. A Cu tube was used to connect the target cell to the GM refrigerator, to which a heater was attached to control the temperature.

The temperatures of the target cell and the Cu tube were measured using a Si diode thermometer. In the SAMURAI 30 experiment, hydrogen gas with a pressure of 812 hPa was filled into the cell after cooling down the system. The pressure decreased to around 500 hPa when the hydrogen gas was liquefied. Under such conditions, the temperature of the target cell should be kept lower than 18 K during the measurement in order to keep the hydrogen in liquid form.

Figure 1 shows the variations of the temperature and gas pressure with time after the hydrogen gas was liquefied. The temperature was found to be instable during the first 8 hours. The temperatures of the target cell and the Cu tube increased steadily. In order to lower the temperature, the temperature of the water in the chiller was decreased from 22°C to 8°C. However, it was found that this operation had almost no influence on the temperature of the LHT system. The temperature increased gradually, as shown in Fig. 1, but the liquid phase was maintained at just below the boiling point. The temperature of the target cell stabilized at 18.3 K after the pressure of the hydrogen

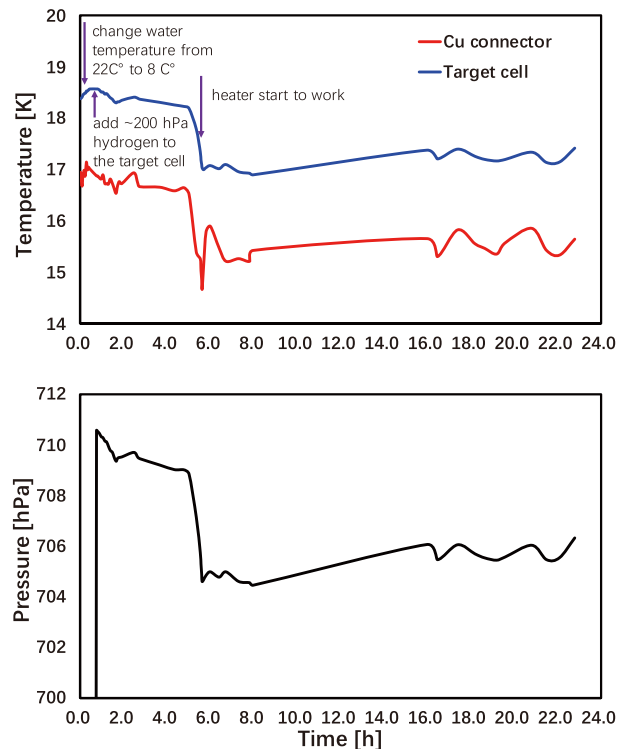


Fig. 1. Variations of the temperature (top panel) and gas pressure (bottom panel) with time. The temperature was measured for both the target cell (blue line) and the Cu connector (red line).

was added to 710 hPa. However, for some reason, a rapid decrease in temperature and pressure was observed 4 hours later. When the temperature of the Cu tube decreased to 14.7 K, the heater started working. The temperature of the target cell was kept at about 15 K and the gas pressure was stable at 705 hPa. The LHT system was maintained at a stable temperature and pressure for more than 8 hours.

In summary, in the SAMURAI 30 experiment, the instability of the LHT system was observed during the first 8 hours of the beam time. During the rest of the beam time, the fluctuation of the temperature and pressure of the LHT system were less than 1.5% and 1%, respectively. Further investigation is necessary to achieve stable control of the system temperature and pressure for a long time.

### Reference

- 1) H. Ryuto *et al.*, Nucl. Instrum. Methods Phys. Res. A **555**, 1 (2005).

<sup>\*1</sup> School of Physics, Peking University

<sup>\*2</sup> RIKEN Nishina Center

<sup>\*3</sup> Department of Physics, Saitama University

<sup>\*4</sup> Center for Nuclear Study, University of Tokyo

# Design of an Ion Source for the eSHE project Toward Pioneering Electron Scattering on Superheavy Elements

S. Naimi,<sup>\*1</sup> T. K. Sato,<sup>\*2</sup> K. Tsukada,<sup>\*3</sup> P. Schury,<sup>\*4</sup> Y. Ito,<sup>\*3</sup> H. Haba,<sup>\*1</sup> Y. Komori,<sup>\*1</sup> T. Ohnishi,<sup>\*1</sup>  
and T. Uesaka<sup>\*1</sup>

Theoretical study shows that the central depression in the nucleonic density is enhanced in superheavy nuclei and is correlated with the symmetry energy.<sup>1)</sup> Electron scattering is a very reliable technique to probe the charge density in heavy nuclei.

The electron scattering on SuperHeavy Elements project, or eSHE project for short, aims at pioneering electron scattering on heavy and superheavy nuclei by creating a missing link between two powerful facilities at RIKEN, the AVF cyclotron and the SCRIT facility. The AVF facility can produce heavy and superheavy nuclei. The SCRIT facility is dedicated for electron scattering on Rare Isotopes (RIs).<sup>2)</sup> The eSHE project mission consists in bringing RIs produced at AVF to the SCRIT facility to perform electron scattering. For this purpose, we prepare a target from RIs produced at AVF, which is then transported to SCRIT facility where the target could be inserted into the oven of ion source designed for this purpose. Since the preparation and transport of the target will take time, only RIs with long lifetime (at least few hours) are considered. Figure 1 shows nuclei heavier than  $^{208}\text{Pb}$  that could be reached by this method. However, the feasibility of SHEs will be limited by the production yield even for long-lived nuclei and a more efficient method is needed. To test the feasibility of this method, we plan to conduct a pilot experiment with  $^{225}\text{Ac}$  with a half-life of 10 days. This isotope can be produced with high intensity at AVF via the reaction  $^{226}\text{Ra}(d, 3n)^{225}\text{Ac}$ , with 24 MeV and 10  $\mu\text{A}$  deuterium beam. To perform electron scattering experiment for 10 hours, a target of 0.3–3 GBq  $^{225}\text{Ac}$  is needed. Due to the low ionisation potential of Ac element, it is possible to achieve high ionisation efficiency with a surface ion source type.<sup>3)</sup> Design of such ion source is shown in Fig. 2, where a double valve system is used to allow insertion of RIs target into the oven of the ion source without breaking the vacuum. The ion source is now under construction and it will be commissioned firstly offline with Lanthanum, which is available commercially as  $\text{La}_2\text{O}_3$  powder. The online commissioning will be performed with  $^{225}\text{Ac}$  produced at the AVF. The aim is to estimate the total efficiency and production, which will determine the feasibility of electron scattering at SCRIT. To achieve the necessary accuracy for electron scattering study, a beam of  $10^6 - 10^7$  ions per second is needed for a period of one month.

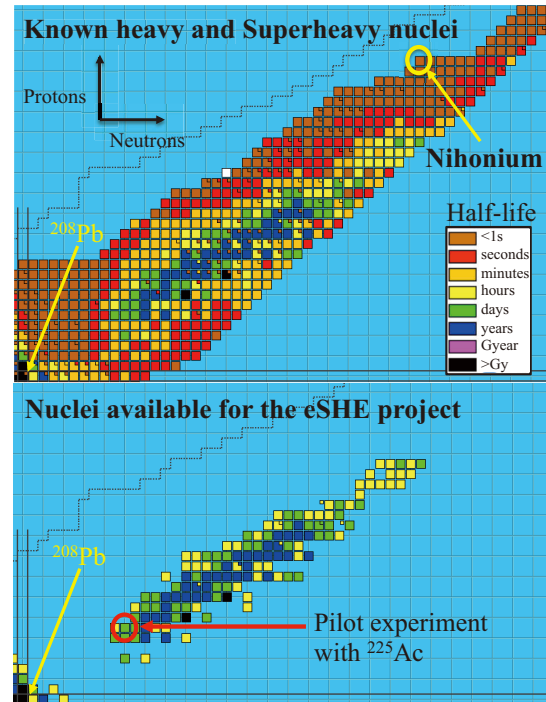


Fig. 1. (Top) All known nuclei heavier than  $^{208}\text{Pb}$  isotope (Bottom) Nuclei with long enough lifetimes that would be available for the eSHE project. A pilot experiment will be conducted with  $^{225}\text{Ac}$ .

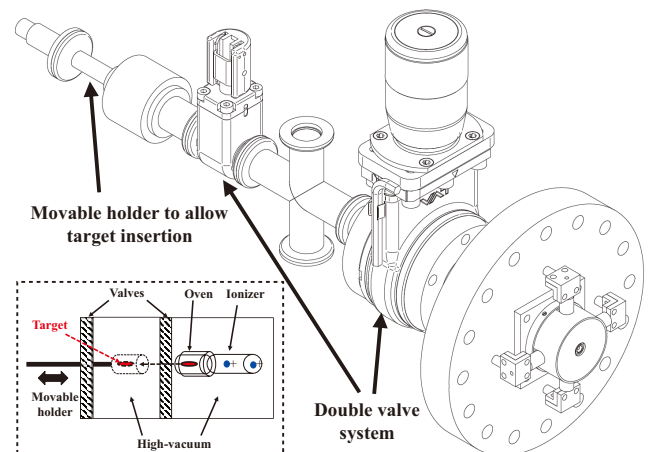


Fig. 2. Design of an ion source for Ac ionization. In the lower left side is shown the schematic of insertion of RIs target into the oven without breaking the vacuum.

<sup>\*1</sup> RIKEN Nishina Center

<sup>\*2</sup> Research group for Heavy Element Nuclear Science, JAEA

<sup>\*3</sup> Research Center for Electron Photon Science, Tohoku University

<sup>\*4</sup> WNSC, IPNS, KEK

## References

- 1) B. Schuetrumpf *et al.*, Phys. Rev. C **96** (2017).
- 2) K. Tsukada *et al.*, Phys. Rev. Lett. **118** (2017).
- 3) T. K. Sato *et al.*, Nature **520** (2015).

# Absolute optical absorption cross-section of Rb atoms injected into superfluid helium using energetic ion beams<sup>†</sup>

K. Imamura,<sup>\*1,\*2</sup> Y. Matsuo,<sup>\*2,\*3</sup> W. Kobayashi,<sup>\*2,\*3</sup> T. Egami,<sup>\*2,\*3</sup> M. Sanjo,<sup>\*2,\*3</sup> A. Takamine,<sup>\*2</sup> T. Fujita,<sup>\*2,\*4</sup> D. Tominaga,<sup>\*2,\*3</sup> Y. Nakamura,<sup>\*1,\*2</sup> T. Furukawa,<sup>\*5</sup> T. Wakui,<sup>\*6</sup> Y. Ichikawa,<sup>\*2</sup> H. Nishibata,<sup>\*2</sup> T. Sato,<sup>\*2</sup> A. Gladkov,<sup>\*2,\*6</sup> L. C. Tao,<sup>\*2,\*8</sup> T. Kawaguchi,<sup>\*2,\*3</sup> Y. Baba,<sup>\*3</sup> M. Iijima,<sup>\*3</sup> H. Gonda,<sup>\*3</sup> Y. Takeuchi,<sup>\*3</sup> R. Nakazato,<sup>\*3</sup> H. Odashima,<sup>\*1</sup> and H. Ueno<sup>\*2</sup>

An in-situ laser spectroscopy method utilizing atomic impurity in superfluid helium (He II) has been developed for the application of nuclear structure study of rare-isotopes. The method is named Optical RI-atom Observation in Condensed Helium as Ion-catcher (OROCHI). The key feature of the technique is that the center wavelengths of the absorption spectra of atoms in He II are largely blue-shifted from those of emission spectra. The feature is significantly advantageous for the detection of fluorescence signals from atoms in He II with ultra-low background. Moreover, He II works as an effective stopper for highly energetic ion beams. The stopping efficiency of He II reaches nearly 100% for the beam energy of several tens of MeV/nucleon. Considering the above reasons, OROCHI has proven to be an efficient method for the study of nuclear structure of low production yield rare-isotopes. We have demonstrated the feasibility of OROCHI using <sup>84-87</sup>Rb ion beams with up to 66 MeV/nucleon energy and 10<sup>4</sup> pps intensity, so far.<sup>1)</sup> However, unexpected laser stray light limits the signal detection sensitivity. To efficiently separate the signal from background, we developed a new fluorescence detection system (FDS) that realizes low background signal detection using double monochromator. The first demonstration of the new FDS was performed using <sup>85</sup>Rb<sup>31+</sup> ion beam delivered from RIPS. We deduced the optical absorption cross-section from the result of fluorescence intensity dependence on beam intensity and applied laser power.

The experimental setup was the same as that in Ref. 2). A 66 MeV/nucleon <sup>85</sup>Rb ion beam was passed through two aluminum energy degraders to adjust the stopping position in He II. During beam stopping position adjustment using various degraders thickness, we confirmed that the injected ions were stopped within 1 mm injection depth. The energy degraded ion beam was introduced into He II. Rubidiums that were diffused from the observation region with approximately several hundred milliseconds after stopping in He II were subjected to a laser light from the Titanium sapphire laser (780 nm,  $\phi \approx 2$  mm). The laser induced fluorescence (LIF) from Rb atoms was focused on the optical fiber

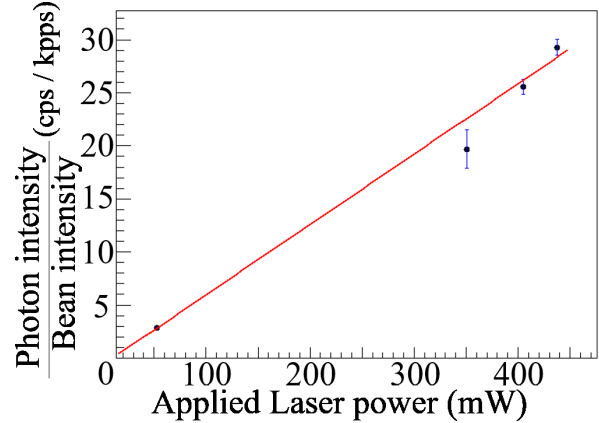


Fig. 1. Measured fluorescence intensity dependence normalized by injected beam intensity.

bundle with an entrance of  $5 \times 2$  mm<sup>2</sup> using the lens unit of the FDS. The LIF guided using the optical fiber bundle was introduced into the double monochromator. Rb D1 emission light (793 nm in He II) was selected using the double monochromator and detected using a photo-multiplier tube.

The measured LIF dependence on beam intensity and applied laser power is shown in Fig. 1. The vertical axis was normalized by the beam intensity and the horizontal axis shows the applied laser power. The observed LIF intensity  $I_{\text{LIF}}$  was obtained using the equation  $I_{\text{LIF}} = N_{\text{obs}} \sigma \Phi_{\text{Laser}} \epsilon_{\text{det}}$ , where  $N_{\text{obs}}$ ,  $\sigma$ ,  $\Phi_{\text{Laser}}$  and  $\epsilon_{\text{det}}$ , denote the number of atoms in the observation region, optical absorption cross-section, photon flux of the laser, and detection efficiency of FDS, respectively.  $N_{\text{obs}}$  was estimated from the beam intensity  $I_{\text{beam}}$  and diffusion time of Rb atom.  $\Phi_{\text{Laser}}$  was proportional to the applied laser power  $P_{\text{Laser}}$ . Thus, the equation for normalized LIF intensity  $I_{\text{LIF}}/I_{\text{beam}}$  can be written as a function of  $P_{\text{Laser}}$ . The value of  $\epsilon_{\text{det}} \approx 10^{-7}$  obtained from the result of experiment using Rb enclosed gas cell was used for the deduction of  $\sigma$ . As a result of our analysis, we deduced  $\sigma = 3.59(16) \times 10^{-15}$  cm<sup>2</sup> as the optical absorption cross-section of Rb in He II. The successful derivation of the quantitative value attributes to the improvement of detection efficiency by two orders of magnitude using the new FDS, as compared to previous work.<sup>1)</sup> We conclude that 200 pps is a sufficient ion beam intensity to detect LIF from Rb atoms in He II in accordance with our experimental result.

## References

- 1) X. F. Yang *et al.*, Phys. Rev. A **90**, 052516 (2014).
- 2) K. Imamura *et al.*, RIKEN Accel. Prog. Rep. **50**, 197 (2017).

<sup>†</sup> Condensed from the article in Appl. Phys. Exp. **12**, 016502 (2019)

\*1 Department of Physics, Meiji University

\*2 RIKEN Nishina Center

\*3 Department of Advanced Sciences, Hosei University

\*4 Department of Physics, Osaka University

\*5 Department of Physics, Tokyo Metropolitan University

\*6 National Institute for Radiological Science

\*7 Department of Physics, Kyungpook National University

\*8 School of Physics, Peking University

# Baseline correction system of laser-microwave double resonance spectrum for atoms injected into superfluid helium by laser sputtering

M. Sanjo,<sup>\*1,\*2</sup> K. Imamura,<sup>\*2,\*3</sup> W. Kobayashi,<sup>\*1,\*2</sup> Y. Takeuchi,<sup>\*1,\*2</sup> A. Takamine,<sup>\*2</sup> T. Furukawa,<sup>\*2,\*4</sup>  
H. Ueno,<sup>\*2</sup> and Y. Matsuo<sup>\*1,\*2</sup>

We have been developing a laser spectroscopic method for the atoms injected into superfluid helium (He II) to measure the hyperfine structure and Zeeman splitting of unstable nuclei with low production yields and short lifetimes. In this method, highly energetic ion beams are efficiently caught as neutralized atoms in superfluid helium owing to its high density. In addition, the absorption wavelength of atoms in He II is largely blue-shifted due to the effect of surrounding He atoms while the emission wavelength is almost the same as that in vacuum. This enables us to detect photons emitted from the atoms with low background by removing the excitation-laser stray light.

So far, in the offline experiment, we succeeded in the measurement of the hyperfine structure constant for  $^{133}\text{Cs}$  atoms with accuracy of  $10^{-5}$  via laser-microwave (MW) double resonance method.<sup>1)</sup> In order to discuss hyperfine anomaly of atoms in He II, it is required to measure hyperfine structure splitting using more than two isotopes. To show the feasibility for deducing hyperfine anomaly parameter using the method, we have performed a series of experiment to measure hyperfine splitting with an accuracy and a precision of  $10^{-6}$  using Rb which has two stable isotopes. It has been difficult to realize sufficient measurement accuracy and precision due to fluctuation of the number of observed photons when we use two-step laser sputtering method to supply atoms in He II.<sup>2)</sup> We here report the development of a baseline correction system to cancel the fluctuation of the number of atoms injected into He II and a preliminary experiment performed using this system.

We need to irradiate a circularly polarized laser light and apply a magnetic field to the atoms to generate spin polarization. We can observe fluorescence from atoms when MW frequency is resonant to the hyperfine structure splitting by scanning MW frequency irradiated to spin polarized atoms. On the other hand, when the excitation laser light is linearly polarized light, we observe photons proportional to the number of atoms in the observation region, because spin polarization does not occur. We can correct the fluctuation of the number of observed photons by using the difference in the observed photons for both polarizations.

The correction system consists of an Electrooptic Modulator (EOM) to quickly switch the polarization of the excitation-laser and a Multi Channel Scaler (MCS) equipped with multi-channel inputs to count photons at the circularly and linearly polarization. In the case that we apply a square wave voltage at 1 kHz to the EOM,

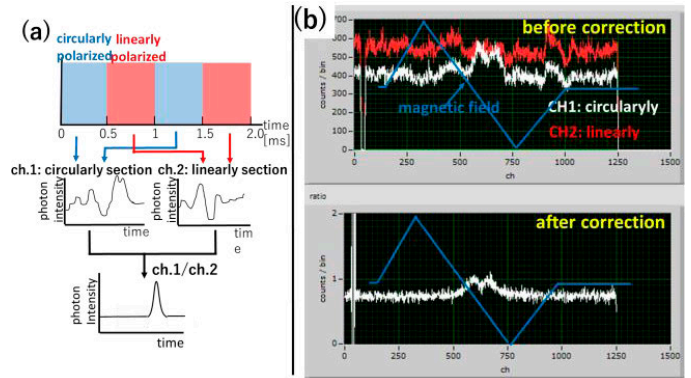


Fig. 1. (a) Scheme of observed photon number calibration via switching of the polarization of excitation-laser with an EOM. (b) Cancellation of the fluctuation of the number of observed photons using Rb in He II.

the polarization is switched as shown in the upper of Fig. 1(a). Next, we detect photons emitted from the atoms at the circularly polarized section (ch. 1) and the linearly polarized section (ch. 2) alternately using coincidence with the signal to EOM as shown in the lower of Fig. 1(a). In ch. 1, hyperfine structure resonance peak superimposed with the base fluctuation caused by the number of atoms variation is observed. In ch. 2, photons proportional to the number of atoms in the observation region is observed. Consequently, it is expected that we can realize measurement free from the fluctuation of number of observed photons by correcting ch. 1 signal counts with ch. 2 ones.

We performed a preliminary experiment for Rb atoms injected into He II by laser sputtering. Atoms are irradiated with a Ti:Sa laser of 100 mW (wavelength: 780 nm) either with circular or linear polarization. Fig. 1(b) shows the spectrum obtained when we swept the magnetic field. We attempted to observe the fluorescence twin peaks when the spin polarization is collapsed at the 0 magnetic field. Channel 1 (white line) in the upper part of Fig. 1(b) shows spectrum in the circularly polarized section, and ch. 2 (red line) shows the spectrum in the linearly polarized section. The lower part of Fig. 1(b) shows the number-of-atoms corrected spectrum. It was confirmed that the baseline fluctuation is clearly canceled. From the result, we concluded that we succeeded in the baseline correction. Future outlook on research is the measurement of hyperfine structure for  $^{85,87}\text{Rb}$  in He II with using this system to evaluate hyperfine anomaly for Rb isotopes in He II.

## References

- 1) K. Imamura, *et al.*, *Hyperfine Interact.* **230**, 73 (2015).
- 2) T. Furukawa, *Phys. Rev. Lett.* **96**, 095301 (2006).

\*1 Department of Advanced Science, Hosei University

\*2 RIKEN Nishina Center

\*3 RIIS, Okayama University

\*4 Department of Physics, Toho University

## Attempt to measure relaxation time of atomic bubble surrounding alkaline atoms in superfluid helium

Y. Takeuchi,<sup>\*1,\*2</sup> M. Sanjo,<sup>\*1,\*2</sup> W. Kobayashi,<sup>\*1,\*2</sup> H. Kuramochi,<sup>\*3</sup> A. Takamine,<sup>\*2</sup> Y. Matsuo,<sup>\*1,\*2</sup> Y. Zempo,<sup>\*4</sup> T. Tahara,<sup>\*3</sup> and H. Ueno<sup>\*2</sup>

Our research group has been developing a new type of nuclear laser spectroscopy method named OROCHI, which is based on laser spectroscopy of atoms in superfluid helium (He II). In this method, the presence of the interaction between injected atoms and surrounding helium atoms plays an important role to prepare a unique spectroscopic environment. In this study, we focus on the structure of the atoms surrounded by He.

When the atoms are introduced into He II, the surrounding helium atoms are pushed out by the exchange (Pauli) repulsion force.<sup>1)</sup> The resulting vacuum region is called “atomic bubble.” For the electronic ground state of the introduced atom, the bubble typically has a radius of 5 ~ 10 Å. When the shape of the electron orbit of the atom changes owing to a state transition such as excitation and absorption, it is considered that atomic bubble is also deformed in He II as the shape of the orbital deforms.

Figure 1 shows the deformation process of the atomic bubble. Because the Franck-Condon principle holds true in the process of absorbing and releasing photons, the radius of the bubble is kept constant before and after the transitions. Therefore, after these short time transitions, the bubble is affected by the electron orbit of the introduced atom and deforms (relaxes) over a certain time. It is known that the wavelengths of atoms in He II shift between absorption and emission owing to this process.<sup>2)</sup> It is estimated that it takes an order of a few picoseconds to deform the bubble but so far the relaxation time has not been measured in the time domain. To clarify the dynamics of the atomic bubble system, we will combine the laser spectroscopic technique in He II and the ultrafast laser spectroscopic technique.<sup>3)</sup>

In this research, we decided to start with Rb as the target atom of this experiment because its characteristics in He II is well studied.<sup>2,4)</sup> We plan to perform experiments using a detection system with a high time resolution for the relaxation time in the excited state.

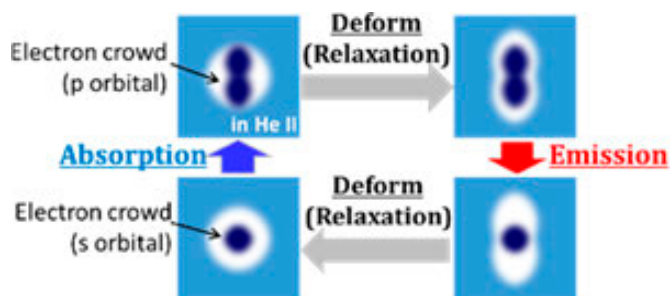


Fig. 1. Deformation cycle of an atomic bubble.

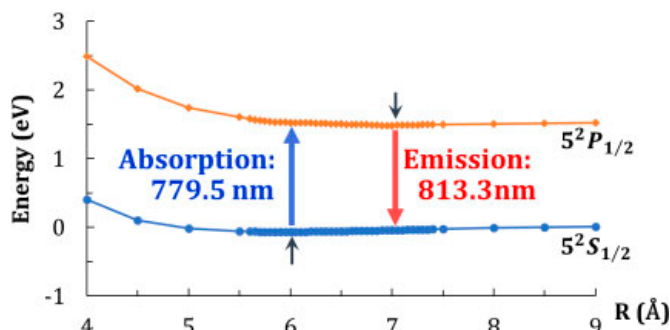


Fig. 2. Energy calculated value of Rb atomic bubble system. (18 helium, Hybrid density functional APF with the basis set Def2TZVPP was used.)

The experiment will be conducted in an offline environment using laser ablation for the introduction of atoms.<sup>4)</sup> In the cryostat used for offline experiments, the atoms are supplied by laser ablation and laser dissociation into He II in a quartz cell installed in the upper part of the helium tank. Then, a pumping laser irradiates to Rb atoms in the observation region and fluorescence is observed using the Time-Correlated Single Photon Counting (TCSPC) system. We plan to obtain the time dependence of the intensity of fluorescence using this system that records the time difference between the irradiation of the excitation laser signal and the detection of the fluorescent photon.<sup>5)</sup> The time resolution of the system is approximately 80 ps. It is considered that emission also occurs during the deformation process of the bubble to the energy minimum of the excited state. Therefore, if we can observe the intensity changes of fluorescence up to several tens of ns, which is the spontaneous emission lifetime, we can estimate the time required for bubble deformation. Currently, performance evaluation of picosecond pulsed Ti: sapphire laser for excitation is ongoing.

Additionally, in parallel with the preparation of the experiment, we calculated atomic energy levels using Gaussian 09 to estimate the amount of wavelength change due to the relaxation of atomic bubbles. The calculation of the energy of the atomic bubble formed by 18 helium atoms resulted in the confirmation of the broadening of the bubble radius and shifts in the atomic transition energy (Fig. 2). Besides, we will derive the influence due to the increase of the number of He atoms for bubble formation and simulate the case for other atoms such as Cs.

### References

- 1) H. Bauer *et al.*, Phys. Lett. A **146**, 134 (1990).
- 2) Y. Takahashi *et al.*, Phys. Rev. Lett. **71**, 1035 (1993).
- 3) D. Mandal *et al.*, Chem. Phys. Lett. **359**, 77 (2002).
- 4) T. Furukawa *et al.*, Hyperfine Interact **196**, 191 (2010).
- 5) W. Becker, *Advanced Time-Correlated Single Photon Counting Techniques*, (Springer, Berlin, Heidelberg, 2005).

\*1 Department of Advanced Sciences, Hosei University

\*2 RIKEN Nishina Center

\*3 Molecular Spectroscopy Laboratory, RIKEN

\*4 Department of Digital Media, Hosei University

# Development of offline ion source for collinear laser spectroscopy of RI beams

M. Tajima,<sup>\*1</sup> A. Takamine,<sup>\*1</sup> T. Asakawa,<sup>\*2</sup> M. Wada,<sup>\*3</sup> Y. Sasaki,<sup>\*2</sup> Y. Nakamura,<sup>\*4</sup> H. Imura,<sup>\*5,\*1</sup>  
K. Okada,<sup>\*6</sup> T. Sonoda,<sup>\*1</sup> H. A. Schuessler,<sup>\*7,\*1</sup> H. Odashima,<sup>\*4</sup> Y. Matsuo,<sup>\*2,\*1</sup> and H. Ueno<sup>\*1</sup>

Collinear laser spectroscopy of RI beams is a powerful probe to directly measure the nuclear properties of ground or isomeric states. We designed and constructed an offline ion source for the planned optical spectroscopy of RI ion beams of refractory elements at a rate of 100 pps. Because it is difficult to obtain ions of refractory elements by the widely-used surface ionization method, we adopted laser ablation of a solid target in He gas and the RF ion guide system<sup>1)</sup> for ion beams with low emittance.

Figure 1(a) shows a sketch of the setup. The RF ion guide system is composed of cylindrical DC electrodes, RF carpet (RFCP), a quadrupole ion guide (QPIG), and RFQ. There are 54 electrodes and an exit hole at the center of RFCP. QPIG is composed of 4 thin plates with 28 electrodes on each plate assembled as an azimuthally four-segmented square tube. RFQ is composed of three segments of four SUS rods and an endcap. A solid target for laser ablation is fixed on the surface of the cylindrical electrode. An aluminosilicate Cs<sup>+</sup> emitter is also prepared for the performance test. Helium gas is introduced constantly and the typical pressure is approximately 22 mbar at the most upstream chamber. This ion source system is floated at 10 kV and connected to a test beamline as shown in Fig. 1(b).

The target is irradiated by an Nd:YAG laser pulse (532 nm, 10 ns width). First, the produced energetic ions are stopped via collisions with He gas and guided to RFCP by a DC electric field. Then, the ions are subsequently guided to the downstream by RFCP, QPIG, and RFQ with applied RF and DC electric fields. After the ions are focused through the Einzel lens and four quadrupoles, they are separated depending on  $m/q$  using a dipole magnet and collected onto a Faraday cup (FC). Figures 1(c)–(e) show the relative beam intensity as a function of the applied RF amplitudes for RFCP, QPIG, and RFQ, respectively, when Ag metal target was used for laser ablation and the Cs<sup>+</sup> emitter was used as a reference. Typical beam intensity at FC is  $10^7$ – $10^8$  ions per laser pulse, which is sufficient for the demonstration of the planned spectroscopy of RI beams.

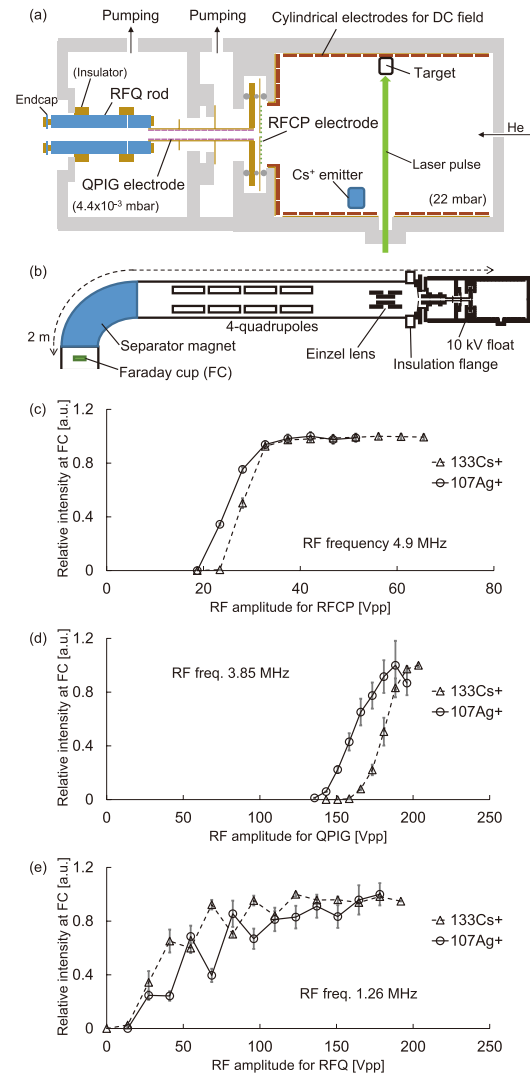


Fig. 1. Sketch of the ion-source system (a) and test beamline (b). Dependence of beam intensity at the Faraday cup as a function of applied RF amplitude for RFCP (c), QPIG (d), and RFQ (e).

As the next step, laser ablation for different targets such as BaF<sub>2</sub> and Zr will be conducted. In addition, we will work toward the development of on-line spectroscopy for low-intensity beams with coincidence method.<sup>2)</sup>

## References

- 1) M. Wada *et al.*, Nucl. Instrum. Methods Phys. Res. B **204**, 570 (2003).
- 2) D. A. Eastham *et al.*, Opt. Commun. **82**, 23 (1991).

\*1 RIKEN Nishina Center

\*2 Department of Advanced Sciences, Hosei University

\*3 Wako Nuclear Science Center, KEK

\*4 Department of Physics, Meiji University

\*5 Nuclear Science and Engineering Research Center, JAEA

\*6 Department of Physics, Sophia University

\*7 Department of Physics and Astronomy, Texas A&M University

## Development of active nuclear spin maser with time-separated feedback scheme for Xe-EDM search

T. Sato,<sup>\*1</sup> Y. Ichikawa,<sup>\*1</sup> A. Takamine,<sup>\*1</sup> A. Gladkov,<sup>\*1</sup> T. Inoue,<sup>\*2,\*3</sup> A. Uchiyama,<sup>\*3,\*1</sup> S. Kojima,<sup>\*4</sup>  
C. Funayama,<sup>\*4</sup> S. Tanaka,<sup>\*4</sup> Y. Sakamoto,<sup>\*4</sup> Y. Ohtomo,<sup>\*4</sup> C. Hirao,<sup>\*4</sup> M. Chikamori,<sup>\*4</sup> E. Hikota,<sup>\*4</sup> T. Suzuki,<sup>\*4</sup>  
M. Tsuchiya,<sup>\*4</sup> T. Furukawa,<sup>\*5</sup> A. Yoshimi,<sup>\*6,\*1</sup> C. P. Bidinosti,<sup>\*7</sup> T. Ino,<sup>\*8</sup> H. Ueno,<sup>\*1</sup> Y. Matsuo,<sup>\*9,\*1</sup>  
T. Fukuyama,<sup>\*10</sup> N. Yoshinaga,<sup>\*11</sup> Y. Sakemi,<sup>\*12,\*4</sup> and K. Asahi<sup>\*1,\*4</sup>

CP violation is one of the critical requirements for generating matter-antimatter asymmetry in the Universe. It is known that the magnitude of CP violation in the Standard Model (SM) of particle physics is insufficient to explain the observed matter dominance in the Universe, and therefore the discovery of extra CP violations originating from new physics beyond the SM is much awaited. A finite permanent electric dipole moment (EDM) of a particle or a system implies the violation of time reversal and CP symmetry. The value of EDMs that are predicted by theories beyond the SM are typically many orders of magnitude larger than those predicted by the SM, and therefore the EDM is one of the most promising probes to search for new physics.

In the current study, we focus on the atomic EDM of Xe, which is sensitive to T, P-odd nucleon-nucleon and nucleon-electron interaction. The EDM is detected by measuring the Larmor frequency of a nuclear spin under the static magnetic and electric field applied at the same time. In order to improve the upper limit of the current for the Xe atomic EDM,  $4.1 \times 10^{-27} e \cdot \text{cm}$ ,<sup>1)</sup> which corresponds to a  $\sim 40$ -nHz frequency precision under a 10-kV/cm electric field, we are developing a nuclear spin maser with an active feedback scheme,<sup>2-4)</sup> which allows observation of a continuous spin oscillation avoiding decay of the signal. In addition, to reduce systematic uncertainties in the spin precession frequency, we are developing co-existing masers of  $^{129}\text{Xe}$  and  $^{131}\text{Xe}$ .<sup>5)</sup> By comparing the frequencies of two masers, the systematic uncertainty, which is caused by drifts in the magnetic field and in the effective field due to the Fermi-contact interaction between Xe and polarized Rb, can be reduced.

We recently found that systematic errors can be further eliminated by reducing the phase deviation between the observed signal and the actual Xe precession caused by the feedback field for masing. The spin precession of Xe is detected through the motion of Rb spins, which adiabatically follow the rotating field produced by the

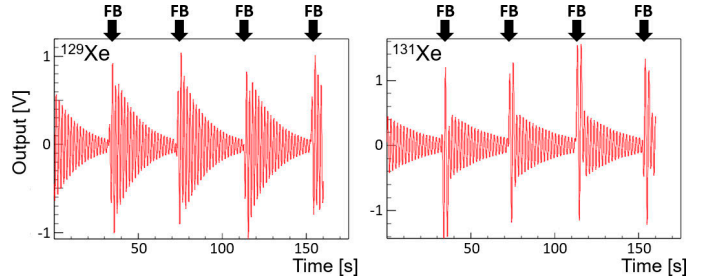


Fig. 1. Maser signals obtained for  $^{129}\text{Xe}$  (left) and  $^{131}\text{Xe}$  (right) with the TSFB scheme. The observation-feedback cycle is repeated every 40 s. After observation for 30 s and a margin of 2 s, a 3 s FB signal was applied to maintain the oscillation of the masers (black arrows).

Xe spins. When the feedback field is superimposed on the Xe spin field, the Rb spin will follow the resultant Xe plus feedback field, and hence the Rb precession phase will be shifted from the Xe precession. The phase shift causes frequency error due to the frequency pulling effect.<sup>2)</sup> To eliminate the pulling effect, we adopt a new scheme for masing, the time-separated feedback (TSFB) scheme. In this scheme, the observation of spin precession and application of the feedback field are separated in time and repeated alternately. The feedback field is generated according to the precession signal, which is acquired during the period without the feedback field, so that the maser operation becomes free from the frequency pulling effect. Note that the spin precession is observed continuously, unlike the repeated free-induction-decay measurements.

A typical signal obtained from the co-existing masers of  $^{129}\text{Xe}$  and  $^{131}\text{Xe}$  with the TSFB scheme is shown in Fig. 1. The frequency error due to the drift in the power of the pumping light for Xe polarization was the dominant source of errors in the conventional active maser. Using the TSFB scheme, we have succeeded in reducing this error from  $\sim 1.6 \mu\text{Hz}$  to below 60 nHz. A detailed study on the frequency characteristics and stability of the TSFB maser is in progress.

### References

- 1) M. A. Rosenberry, T. E. Chupp, Phys. Rev. Lett. **86**, 22 (2001).
- 2) A. Yoshimi *et al.*, Phys. Lett. A **304**, 13 (2002).
- 3) A. Yoshimi *et al.*, Phys. Lett. A **376**, 1924 (2012).
- 4) T. Inoue *et al.*, Eur. Phys. J. D **70**, 129 (2016).
- 5) T. Sato *et al.*, Phys. Lett. A **382**, 588 (2018).

<sup>\*1</sup> RIKEN Nishina Center  
<sup>\*2</sup> FRIS, Tohoku University  
<sup>\*3</sup> CYRIC, Tohoku University  
<sup>\*4</sup> Department of Physics, Tokyo Institute of Technology  
<sup>\*5</sup> Department of Physics, Toho University  
<sup>\*6</sup> RIIS, Okayama University  
<sup>\*7</sup> Department of Physics, University of Winnipeg  
<sup>\*8</sup> Institute of Material Structure Science, KEK  
<sup>\*9</sup> Department of Advanced Sciences, Hosei University  
<sup>\*10</sup> RCNP, Osaka University  
<sup>\*11</sup> Department of Physics, Saitama University  
<sup>\*12</sup> CNS, University of Tokyo

# Epithermal neutron spin filter with dynamic nuclear polarization using photo-excited triplet electron

S. Takada,<sup>\*1,\*2</sup> K. Tateishi,<sup>\*1</sup> T. Inoue,<sup>\*1</sup> Y. Wakabayashi,<sup>\*3</sup> Y. Ikeda,<sup>\*3</sup> Y. Otake,<sup>\*3</sup> T. Yoshioka,<sup>\*2</sup> and T. Uesaka<sup>\*1</sup>

A neutron spin filter using polarized  $^1\text{H}$  media can polarize the neutron beam passing through it because the cross-sections have a large helicity dependence.  $^1\text{H}$  has a flat cross-section of 20 barn in the wide energy range. Therefore, the spin filter of  $^1\text{H}$  media is suitable for epithermal neutrons. A polarized epithermal neutron beam is available, for example, in the  $T$ -violation search in a compound nucleus.<sup>1)</sup> The solid state of  $^1\text{H}$  doped media is often polarized by Dynamic Nuclear Polarization (DNP). DNP is a technique of transferring spin polarization from electrons to nuclei by microwave irradiation. We applied DNP with photo-excited triplet electron spin (Triplet-DNP)<sup>2)</sup> because it can be used at a higher temperature ( $>77$  K) and in a lower magnetic field ( $<1$  T) compared to the conventional DNP method. The neutron spin filter with Triplet-DNP was first developed at the Paul Scherrer Institut (PSI) in Switzerland. They achieved  $^1\text{H}$  polarization of 70% using a naphthalene crystal with a size of  $5 \times 5 \times 5$  mm<sup>3</sup> in 0.36 T and at 25 K,<sup>3,4)</sup> and evaluated its performance using a polarized neutron beam in a meV region. We plan to prepare a 1-cm-thick sample because a thick sample is suitable for the polarization of epithermal neutrons. In addition, we need a large acceptance of the spin filter in order to obtain high statistics. Therefore, we prepared a setup of the neutron spin filter with Triplet-DNP to polarize such a huge sample, and it is shown in Fig. 1. The system is installed in the target chamber made of stainless steel, and the chamber is cooled with cold  $\text{N}_2$  gas.

Triplet-DNP is carried out at 0.3 T and 100 K. A sin-

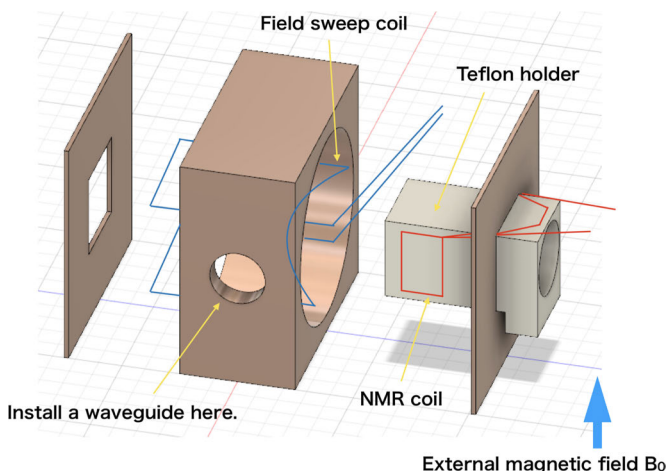


Fig. 1. Setup of the neutron polarization system using Triplet-DNP.

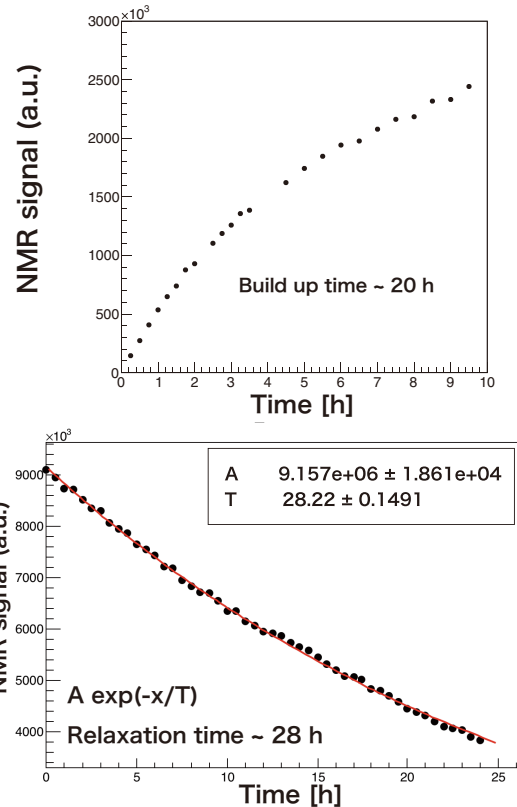


Fig. 2. Polarization build up time (upper) and relaxation time (lower) of the sample.

gle crystal of naphthalene doped with pentacene is used as a filter. To polarize a huge crystal, a high-power laser was implemented into the target chamber. We measured the polarization build up time and relaxation time of the single crystal with a size of  $\phi 15 \times 6$  mm<sup>3</sup> (Fig. 2). The values are longer than assumed. As the next step, we are planning to optimize the strength of the laser and microwave, and the filter thickness. Then, we will check the performance of the neutron spin filter at RIKEN Accelerator-driven compact Neutron source (RANS) in March this year.

## References

- 1) T. Okudaira, 2018, PhD Thesis, Nagoya University, Aichi, Japan.
- 2) A. Henstra, P. Dirksen, W. Th. Wenckebach, Phys. Lett. A **134**, 134 (1988).
- 3) M. Haag, B. van den Brandt, T. R. Eichhorn, P. Hautle, W. Th. Wenckebach, Nucl. Instrum. Methods Phys. Res. A **678**, 91 (2012).
- 4) T. R. Eichhorn, N. Niketic, B. van den Brandt, U. Filges, T. Panzner, E. Rantsiou, W. Th. Wenckebach, P. Hautle, Nucl. Instrum. Methods Phys. Res. A **754**, 10 (2014).

\*1 RIKEN Nishina Center

\*2 Department of Physics, Kyushu University

\*3 RIKEN Center for Advanced Photonics

# Measurement of impurity nuclides in 10.75 MeV/nucleon $^{136}\text{Xe}$ beam in the atmosphere

T. Kambara\*<sup>1</sup> and A. Yoshida\*<sup>1</sup>

On the basis of a fee-based facility sharing program,<sup>1)</sup> private companies in Japan use 95 MeV/nucleon Ar and 70 MeV/nucleon Kr beams from the RIKEN Ring Cyclotron (RRC) to simulate single event effects (SEE) of semiconductor devices by high-LET components of the cosmic rays.<sup>2)</sup> Recently, the demand for heavier ions with higher LET for the SEE test has significantly increased, which has led us to prepare for fee-based Xe-ion irradiations. Because the samples are irradiated in the atmosphere at RIBF, the beam passes through various materials before the sample and fast secondary nuclides produced by nuclear reactions in the materials may contaminate the beam. We study the beam impurities with radiochemical measurements and previously reported results for the Kr beam.<sup>3)</sup>

During a machine-study beamtime in February 2018, we measured the beam impurities of a 10.75 MeV/nucleon  $^{136}\text{Xe}$  beam from RILAC2 and RRC. The setup at the E5A beamline is shown in Fig. 1. The beam spot was spread with a pair of wobbler magnets on the beam line. The beam passed through a Kapton window with a thickness of 25  $\mu\text{m}$  and diameter of 50 mm into the atmosphere, followed by an ionization chamber (IC), AE-1341S, which was produced by Applied Engineering Inc.,<sup>4)</sup> to measure the beam intensity.

In the IC, the beam passed four 6  $\mu\text{m}$  thick mylar foils and a 15  $\mu\text{m}$  thick Al-foil electrode. A test sample of a Si wafer (100 mm diameter and 0.5 mm thick) was attached directly to the exit of the IC to simulate semiconductor devices of clients. The total length of the beam path in the atmosphere was approximately 39 mm. No energy-degrader plates were used in these irradiations. From the output-current measurement of the IC, the total number of primary Xe ions was estimated to be approximately  $1.17 \times 10^{10}$  for a 10 minutes irradiation. According to SRIM calculation,<sup>5)</sup> the energy of the primary Xe ions was approximately 2.3 MeV/nucleon at the surface of the sample in which the ions stopped.

We measured the  $\gamma$  rays from the irradiated sample with a Ge detector 12 times from 7 min to 17.2 days after the irradiation. We analyzed the observed  $\gamma$ -ray peaks according to the tabulated transition energies, lifetimes, and branching ratios,<sup>6)</sup> and identified 15 radionuclides from  $^{135}\text{Xe}$  to  $^{159}\text{Ho}$ . Then, we extrapolated the decay curves of the radioactivity to the end of the irradiation time to obtain the production probabilities of the radionuclides normalized to one incident  $^{136}\text{Xe}$  ion.

Figure 2 shows the obtained nuclide-production prob-

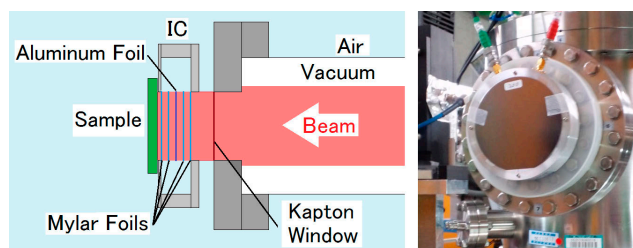


Fig. 1. Schematic diagram (left) and photograph (right) of the setup of irradiation.

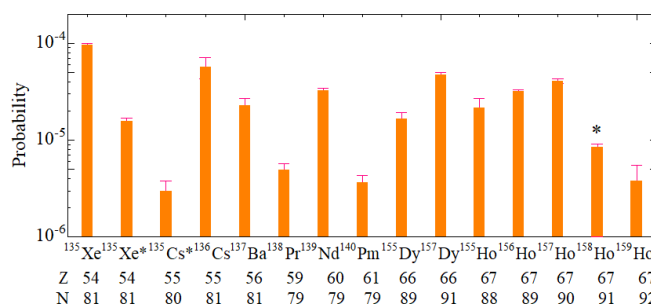


Fig. 2. Measured production probabilities of radionuclides.

Because the tabulated  $\gamma$ -emission probabilities of  $^{158}\text{Ho}$  are in the relative values, the maximum probability is assumed to be 100% of the parent decay.

abilities. Because the Xe ions in the sample had much lower energy than the Coulomb barrier, all the observed radionuclides were produced in the upstream materials and implanted in the sample. The ratios of the observed radionuclides in the beam were below  $10^{-4}$  and the total impurity would be below 1%.

Dy ( $Z = 66$ ) and Ho ( $Z = 67$ ) can be produced only in the Al electrode of the ionization chamber. We suppose that the Ho-isotopes were produced through the complete nuclear fusion reactions followed by multiple neutron emissions, and the observed  $^{155}\text{Dy}$  and  $^{157}\text{Dy}$  were mostly the daughters of  $^{155}\text{Ho}$  and  $^{157}\text{Ho}$ , respectively.

## References

- 1) <http://ribf.riken.jp/sisetu-kyoyo/> (in Japanese text).
- 2) T. Kambara, A. Yoshida, RIKEN Accel. Prog. Rep. **48**, 239 (2015).
- 3) T. Kambara, A. Yoshida, Record of 2018 IEEE Radiation Effects Data Workshop (REDW), p. 94.
- 4) <http://www.o-yo-giken.co.jp/>.
- 5) J. F. Ziegler, <http://www.srim.org/>.
- 6) R. B. Firestone, *Table of Isotopes* (Wiley Interscience, 1998).

\*<sup>1</sup> RIKEN Nishina Center

# Computing and network environment at the RIKEN Nishina Center

T. Ichihara,\*<sup>1</sup> Y. Watanabe,\*<sup>1</sup> and H. Baba\*<sup>1</sup>

We are operating Linux cluster systems<sup>1)</sup> at the RIKEN Nishina Center (RNC).

Figure 1 shows the current configuration of the Linux servers at the RNC. The host *RIBF.RIKEN.JP* is used as the mail server, the NFS server of the user home directory, and the NIS master server. This is the core server for the RIBF Linux cluster.

The hosts *RIBFSMTP1/2* are the mail gateways, which are used for tagging spam mails and isolating virus-infected mails. The latest version of Sophos Email Protection-Advanced (PMX) has been installed. Figure 2 shows the mail trends in 2018. Approximately 50% of the incoming mails were blocked by the PMX ip-blocker.

In order to improve the reliability of mails, we have installed OpenDKIM and OpenDMARK software in the mail server and mail gateway. DomainKeys Identified Mail (DKIM)<sup>2)</sup> is an email authentication method designed to detect forged sender addresses in emails

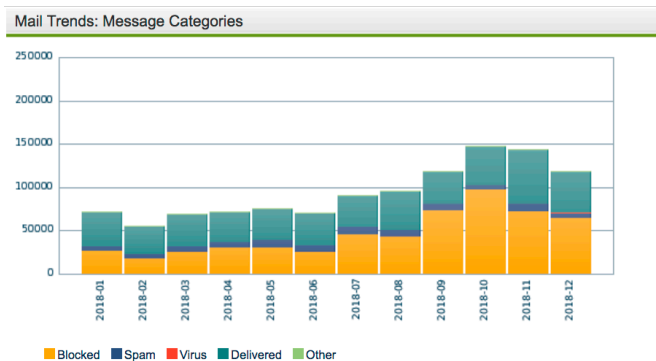


Fig. 2. Mail trends:message categories in 2018.

(email spoofing), a technique often used in phishing and email spam. DMARC (Domain-based Message Authentication, Reporting and Conformance)<sup>3)</sup> is an email-validation system designed to detect and prevent email spoofing, the use of forged sender addresses often used in phishing and email spam. It is expected that combining DKIM and DMARC will reduce phishing and email spam.

The Integrated Digital Conference (INDICO) software<sup>4)</sup> has been operated at *INDICO2.RIKEN.JP* since 2007. We replaced the hardware and software of this server in March 2018. HP DL-320G8 was installed for the new indico server. The indico software was updated from indico 0.99 to 2.1.5. The new indico software uses PostgreSQL database, while the previous indico used Zope Object DataBase (ZODB) written in Python. The migration of the database from ZODB to PostgreSQL has been carried out.

Electric Log (ELOG)<sup>5)</sup> and MoinMoin Wiki<sup>6)</sup> for the RIBF experiments were installed in the server *RIBF-EXP.RIKEN.JP* in 2007. We have updated the ELOG software from elog 2.1.4 to elog 3.1.4 and Wiki software from MoinMoin 1.5.7 to MoinMoin 1.9.10 in January 2019. HP ProLiant DL-20G9 was installed for the new ELOG and Wiki server.

An anonymous ftp server, *FTP.RIKEN.JP*, is managed and operated at the RNC. Major Linux distributions, including Scientific Linux, Ubuntu, and CentOS, are mirrored daily for the convenience of their users and for facilitating high-speed access.

## References

- 1) T. Ichihara *et al.*, RIKEN Accel. Prog. Rep. **51**, 287 (2018).
- 2) <https://en.wikipedia.org/wiki/DKIM> .
- 3) <https://en.wikipedia.org/wiki/DMARC> .
- 4) <https://docs.getindico.io/> .
- 5) <https://elog.psi.ch/elog/> .
- 6) <https://moinmo.in/> .

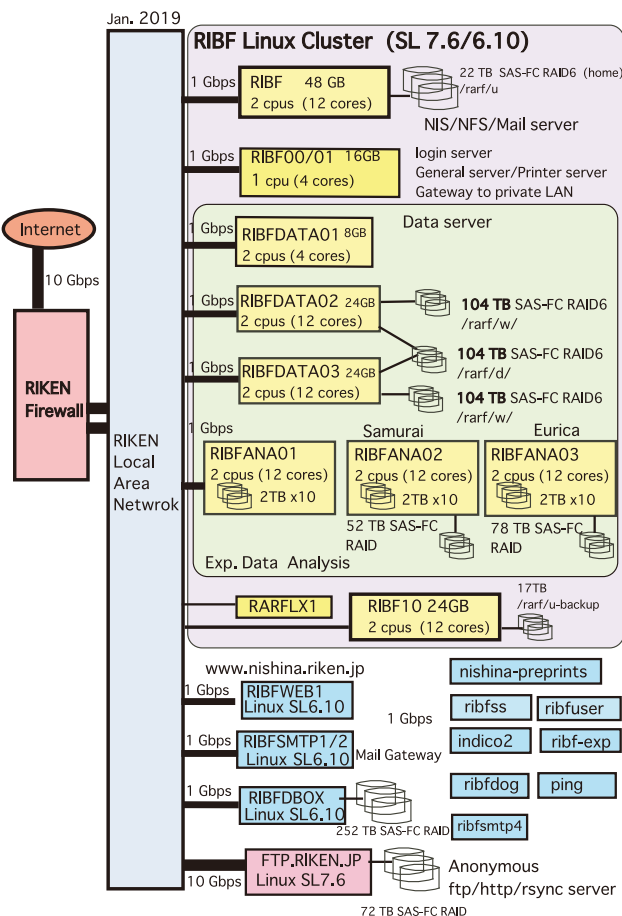


Fig. 1. Configuration of the RIBF Linux cluster.

\*<sup>1</sup> RIKEN Nishina Center

## CCJ operations in 2018

S. Yokkaichi,<sup>\*1</sup> H. En'yo,<sup>\*1</sup> T. Ichihara,<sup>\*1</sup> W. Nakai,<sup>\*1</sup> and Y. Watanabe<sup>\*1</sup>

### Overview

The RIKEN Computing Center in Japan (CCJ)<sup>1)</sup> commenced operations in June 2000 as the largest off-site computing center for the PHENIX<sup>2)</sup> experiment being conducted at RHIC. Since then, CCJ has been providing numerous services as a regional computing center in Asia. We have transferred several hundred TBs of raw data files and nDST<sup>a)</sup> files from the RHIC Computing Facility (RCF)<sup>3)</sup> to CCJ.

Many analysis and simulation projects are being conducted at CCJ, which are listed on the web page <http://ccjsun.riken.go.jp/ccj/proposals/>. As of December 2018, CCJ has contributed to 43 published papers and 43 doctoral theses.

### Computing hardware and software

The network configuration and the computing hardware (nodes) and software (OS, batch queuing systems, database engine, etc.) are almost same as described in the previous APR.<sup>1)</sup> We have two login servers, one main server (users' home directory, NIS, DNS and NTP), and two disk servers whose disk sizes are 13 and 26 TB. The main server has an external SAS RAID (21 TB) for the home and work regions of users, and system usage. Also, the server has a RAID with built-in disks (13 TB) which can be used temporarily by users and the system.

We operate 26 computing nodes, of which 16 nodes were purchased in Mar. 2009 and 10 nodes were purchased in Mar. 2011. Thus, in total, 368 (= 8 × 16 nodes + 24 × 10 nodes) jobs can be processed simultaneously by these computing nodes using a batch queuing system LSF 9.1.3.<sup>4)</sup> Table 1 lists the number of malfunctioning SATA or SAS disks in the HP servers, namely, computing nodes and NFS/AFS servers.

One database (postgreSQL<sup>5)</sup>) server and one AFS<sup>6)</sup> server are operated in order to share the PHENIX computing environment. It should be noted that only the SL5<sup>7)</sup> environment is shared by the computing nodes,

Table 1. Number of malfunctioning HDDs in HP servers during 2011–2018.

Type(Size)	total	2018	'17	'16	'15	'14	'13	'12	'11
SATA(1 TB)	192	16	18	8	14	11	16	20	9
SATA(2 TB)	120	2	10	2	10	0	2	5	4
SATA(4 TB)	10	0	-	-	-	-	-	-	-
SAS(146 GB)	38	3	1	5	3	2	0	1	1
SAS(300 GB)	26	0	1	0	1	1	0	0	1

<sup>\*1</sup> RIKEN Nishina Center

<sup>a)</sup> term for a type of summary data files in PHENIX

which have approximately 0.9 TB of library files. We have two data-transfer servers, on which the grid environment<sup>8)</sup> is installed for data transfer to/from RCF. Two new data-transfer servers will be in operation in early 2019 and replace two servers being currently used. Data transfer of the order of 100 TB from J-PARC and BNL will be performed in the future. In addition, we operate a dedicated server for the RHICf group<sup>9)</sup> and two servers for the J-PARC E16 group,<sup>10)</sup> in order to keep their dedicated compilation and library environments along with some data.

A 10-KVA UPS (supplied by NTT Facilities) was discarded without battery exchange owing to its high cost of exchange. The power wiring was relocated in Nov. 2018. Subsequently, a total power in our UPS system is 30 KVA and a typical average load factor is 51% without jobs and 59% with maximum number of jobs in the calculation nodes.

### Joint operation with ACCC/HOKUSAI

CCJ and the RIKEN Integrated Cluster of Clusters (RICC) have been jointly operated since July 2009. In April 2015, a new system named “HOKUSAI Greatwave” was launched by RIKEN ACCC<sup>11)</sup> and the joint operation with CCJ continued, including a new hierarchical archive system in which approximately 900 TB of CCJ data are stored. Subsequently, the “HOKUSAI BigWaterFall” IA cluster, which has 840 nodes/33600 CPU cores, was launched in 2017 by ACCC. Then a dedicated usage of legacy RICC 10 nodes by CCJ was ended and the direct connection between CCJ and HOKUSAI with the two 10G Ethernet links was also ended. CCJ has not started to use the cluster because it does not support the NFS to share the computing environment of PHENIX unlike RICC. Instead, we are in preparation to use one of the “container technologies” (such as “Docker”<sup>12)</sup>) to share the environment.

### References

- 1) S. Yokkaichi *et al.*, RIKEN Accel. Prog. Rep. **51**, 188 (2018).
- 2) <http://www.phenix.bnl.gov/>.
- 3) <https://www.racf.bnl.gov/>.
- 4) [https://www.ibm.com/support/knowledgecenter/en/SSETD4\\_9.1.3/lsf\\_welcome.html](https://www.ibm.com/support/knowledgecenter/en/SSETD4_9.1.3/lsf_welcome.html).
- 5) <http://www.postgresql.org/>.
- 6) <http://www.openafs.org/>.
- 7) <http://www.scientificlinux.org/>.
- 8) <http://www.globus.org/toolkit/docs/latest-stable/gridftp/>.
- 9) Y. Itow *et al.*, arXiv:1409.4860 (Proposal).
- 10) S. Yokkaichi, RIKEN Accel. Prog. Rep., in this report.
- 11) <http://accr.riken.jp/>
- 12) <https://www.docker.com/>

### **III. RESEARCH ACTIVITIES II**

#### **(Material Science and Biology)**



# **1. Atomic and Solid State Physics (Ion)**



# Effects of asymmetrically-introduced splayed columnar defects on the peak effect in (Ba, K)Fe<sub>2</sub>As<sub>2</sub>

T. Tamegai,<sup>\*1</sup> S. Pyon,<sup>\*1</sup> A. Takahashi,<sup>\*1</sup> A. Yoshida,<sup>\*2</sup> and T. Kambara<sup>\*2</sup>

Iron-based superconductors (IBSs) are intensively studied from both fundamental and applied aspects. In particular, to make these materials practically appealing, the enhancement of critical current density,  $J_c$ , is indispensable. Columnar defects (CDs) introduced by heavy-ion irradiation are known to be very effective to enhance  $J_c$ .<sup>1)</sup> The effects of heavy-ion irradiation have been demonstrated in 122-type IBSs.<sup>2-4)</sup> Compared with heavy-ion irradiated Ba(Fe, Co)<sub>2</sub>As<sub>2</sub>, the  $J_c$  in heavy-ion irradiated (Ba, K)Fe<sub>2</sub>As<sub>2</sub> has been enhanced up to  $\sim 15$  MA/cm<sup>2</sup>. To further enhance  $J_c$  in (Ba, K)Fe<sub>2</sub>As<sub>2</sub>, we have introduced heavy ions in a splayed manner, where CDs are introduced symmetrically from two directions ( $\pm \theta_{CD}$ ) from the  $c$ -axis with the same dose (Fig. 1(a)). We confirmed that  $J_c$  in (Ba, K)Fe<sub>2</sub>As<sub>2</sub> can be enhanced by  $\sim 30\%$  by choosing  $|\theta_{CD}| = 5^\circ$ .<sup>5)</sup> In the course of these studies, we discovered an anomalous peak effect in (Ba, K)Fe<sub>2</sub>As<sub>2</sub> when the CDs are introduced at angles of  $|\theta_{CD}| > 15^\circ$ .<sup>5)</sup> The anomalous peak of  $J_c$  as a function of magnetic field appeared near  $1/3B_\Phi$  ( $B_\Phi = n\Phi_0$ ,  $n$ : density of CDs,  $\Phi_0$ : flux quantum).

As described above, all splayed CDs have been introduced symmetrically with respect to the  $c$ -axis. Therefore, in this study, we introduced asymmetries to the splayed CDs and measured its effect on the anomalous peak. All irradiations were done using a 2.6 GeV U beam at the RI Beam Factory at RIKEN Nishina Center at a total dose of  $B_\Phi = 8$  T ( $n = 4 \times 10^{11}$  cm<sup>-2</sup>). Three types of asymmetries were introduced. (1) We changed the average direction of two the types of CDs from the  $c$ -axis,  $\theta_{CD} = 20^\circ \pm 15^\circ$  (Fig. 1(b)). (2) Instead of changing the direction of two types of CDs, we made different doses for the two directions while maintaining the total dose,

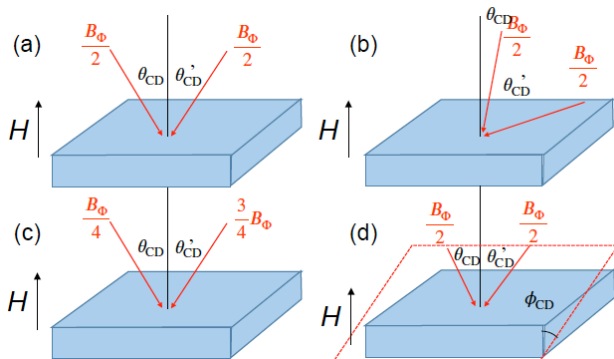


Fig. 1. (a) Standard splayed CDs. (b) Asymmetric splayed CDs with the average direction away from the  $c$ -axis. (c) Splayed CDs with asymmetry in doses. (d) Asymmetric splayed CDs with splay plane tilted away from the  $ac$ -plane.

$B_\Phi = 2$  T and 6 T for  $\theta_{CD} = -15^\circ$  and  $+15^\circ$ , respectively (Fig. 1(c)). (3) The splay plane is tilted, so that it will have an angle  $\phi_{CD}$  from the  $ac$  plane (Fig. 1(d)).  $J_c$ - $H$  at 20 K with various configurations of splayed CDs are compared with the symmetric splayed CDs. It is obvious that the introduction of asymmetry strongly suppresses the anomalous peak effect near  $1/3B_\Phi$ .

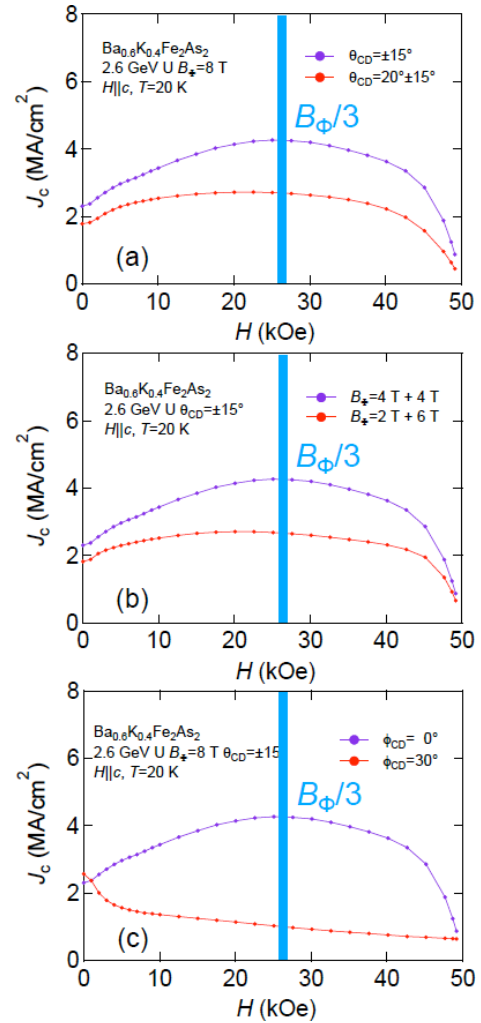


Fig. 2.  $J_c$ - $H$  at 20 K with various configurations of splayed CDs; (a) Comparison of (a) and (b) in Fig. 1, (b) Comparison of (a) and (c) in Fig. 1, and (c) Comparison of (a) and (d) in Fig. 1.

## References

- 1) L. Civale *et al.*, Phys. Rev. Lett. **81**, 45 (1991).
- 2) Y. Nakajima *et al.*, Phys. Rev. B **80**, 012510 (2009).
- 3) F. Ohtake *et al.*, Physica C **518**, 47 (2015).
- 4) T. Tamegai *et al.*, Supercond. Sci. Technol. **25**, 084008 (2012).
- 5) A. Park *et al.*, Phys. Rev. B **97**, 064516 (2018).

<sup>\*1</sup> Department of Applied Physics, The University of Tokyo

<sup>\*2</sup> RIKEN Nishina Center

# Control of the electrical conductivity in diamond by ion implantation

H. Yamazaki,<sup>\*1</sup> T. Minamidate,<sup>\*2</sup> M. Kidera,<sup>\*1</sup> H. M. Yamamoto,<sup>\*3</sup> R. Kato,<sup>\*2</sup> and H. Ueno<sup>\*1</sup>

Although diamond is an insulator with a large band-gap of 5.5 eV, it becomes a semiconductor when doped with a small amount of boron (for *p*-type) or phosphorus (for *n*-type). Doped diamonds hold promise as the material for next-generation devices in place of the existing Si- and GaAs-based semiconductors. In line with this research trend, Ekimov *et al.* reported that B-doped diamond, when doped beyond the metal-to-insulator transition at  $n_B \sim 3 \times 10^{20} \text{ cm}^{-3}$ , shows superconductivity in the samples grown by high-pressure—high-temperature synthesis.<sup>1)</sup> Using inelastic X-ray scattering from a CVD (chemical vapor deposition) grown sample, strong softening of the optical-phonon modes was admittedly observed in superconducting B-doped diamond near the Brillouin-zone center.<sup>2)</sup> Theoretically, the superconducting critical temperature  $T_c$  can be raised substantially by reducing the effects of disorder in the B-doping processes.<sup>3)</sup> For a higher  $T_c$ , more subtle control of doping using CVD and/or MBE (molecular beam epitaxy) methods is highly required, whereas a different method based on ion implantation is also worth investigating since it enables selective ion-doping in a controlled manner.

In this study, we try to control the electrical conductivity in diamond by means of the ion implantation technique, utilizing the beam facilities in RIKEN. For *n*- and *p*-type semiconductors (and possibly superconductors), nitrogen and boron ions are implanted into diamond, respectively. To create an *n*-type semiconductor by N-doping is a challenging work, since nitrogen behaves as a deep donor in diamond and does not contribute to conductivity.<sup>4)</sup> By changing the beam intensity and irradiation time, the concentration of the dopants in diamond was controlled. The electrical conductivity of the doped diamonds was measured using a four-probe configuration. Magnetization measurements were carried out to

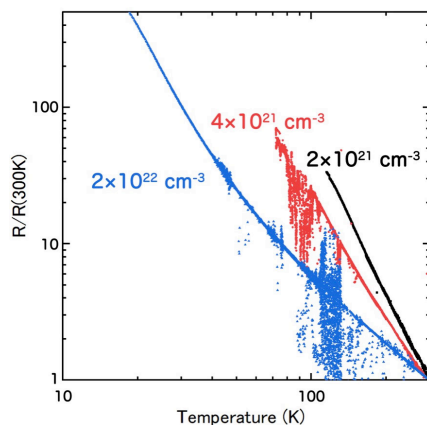


Fig. 1. Temperature dependence of the electrical resistance  $R$  normalized to  $R(300 \text{ K})$  for B-doped diamonds.

<sup>\*1</sup> RIKEN Nishina Center

<sup>\*2</sup> Condensed Molecular Materials Laboratory, RIKEN

<sup>\*3</sup> Institute for Molecular Science

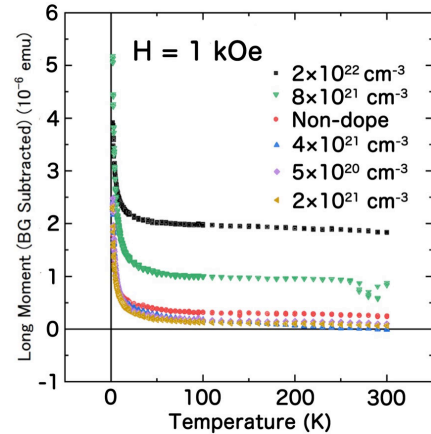


Fig. 2. Temperature dependence of the magnetization for B-doped diamonds.

elucidate the effect of paramagnetic moments (due to lattice defects) and the emergence of superconductivity. Raman spectroscopy and X-ray diffraction (XRD) studies were also performed.

Figure 1 shows the temperature dependence of the electrical resistance  $R$  normalized to  $R(300 \text{ K})$  for B-doped diamonds. Their doping concentrations are indicated in the figure. The fairly high dispersion of data is supposedly due to bad electrical contact between the conductive paste and the diamond surface. A model of thermally-assisted hopping can provide a good fit to the experimental data. We are currently examining the physical significance of the fitting parameters. The results of the magnetization measurements (Fig. 2) show that our B-doped diamonds do not exhibit superconducting transitions at low temperatures, even though the doping concentrations are nominally beyond the metal-to-insulator transition at  $n_B \sim 3 \times 10^{20} \text{ cm}^{-3}$ . Annealing treatment after the irradiation may be necessary for the samples to show superconductivity. The temperature dependence of the magnetization can be represented as the sum of the Curie and temperature-independent components. The correlation between each component and the doping concentration will be clarified by preparing the samples at higher concentrations.

As for the N-doped diamonds (*e.g.* at  $n_N \sim 7.5 \times 10^{21} \text{ cm}^{-3}$ ), the results obtained by Raman spectroscopy and XRD show that they were fully converted into amorphous carbon in the as-implanted state as well as after annealing at 1000 K, likely due to radiation damage. We have to further consider the implantation/annealing process in order to minimize the lattice damage in diamonds.

## References

- 1) E. A. Ekimov *et al.*, *Nature* **428**, 542 (2004).
- 2) M. Hoesch *et al.*, *Phys. Rev. B* **75**, 140508(R) (2007).
- 3) T. Shirakawa *et al.*, *J. Phys. Soc. Jpn.* **76**, 014711 (2007).
- 4) S. J. Sque *et al.*, *Phys. Rev. Lett.* **92**, 017402 (2004).

# Investigation of single event effects observed in SiC-SBDs

Y. Nakada,\*<sup>1</sup> E. Mizuta,\*<sup>1</sup> S. Kuboyama,\*<sup>1</sup> and H. Shindou\*<sup>1</sup>

Wide bandgap semiconductor devices such as GaN and SiC are attractive for next-generation satellites to reduce the energy losses in high-power and high-frequency systems. Although Si remains the dominant material used in space systems, there is now a strong demand for new and more efficient devices. However, there are few reports about power-handling applications. For such use in satellite power applications, the mechanisms of single event effects (SEEs) must be resolved at first with some appropriate steps.

In this study, we report the results of evaluating SEEs on SiC-Schottky barrier diodes (SiC-SBDs) for power-handling applications. The ion species we used in the experiment was <sup>86</sup>Kr, 1242 MeV. The ion range was 113 μm; LET was 27 MeV/(mg/cm<sup>2</sup>) at the device surface. Figure 1 shows the device structure. The SiC-SBD in this study was a type of commercial off-the-shelf (COTS) 1200 V device.

It is known that the failure modes of SiC-SBDs are separated into three regions as shown in Fig. 2.<sup>1)</sup> Region 1 is the non-destructive region where the collected charge is reproducibly measured with no damage. Region 2 is where there is a permanent increase in leakage current and thus, we define “Region 2” as the permanent damage region. Region 3 is defined as the catastrophic failure region where an SEE occurs. However, the cause of the transition from Region 1 to Region 2, and then to Region 3 has yet to be clarified. We therefore focus on the area of transition and discuss Region 1 and 2, particularly in terms of experiments and simulation.

Figure 3 (left) shows the transition of the leakage current (I<sub>r</sub>) at reverse bias condition after irradiation. In Fig. 3 (left), I<sub>r</sub> was shown not to increase up to 220 V but increased above 240 V. We assume that the threshold between 220 V and 240 V is the area of transition from Region 1 to Region 2. Figure 3 (right) shows the I<sub>r</sub> values at 220 V and 240 V during irradiation. I<sub>r</sub> was shown not to increase with Kr fluence at 220 V but does increase at 240 V.

Figure 4 shows the TCAD (technology computer-aided design) simulation results of one particle traversing in SiC-SBD by ECORCE.<sup>2)</sup> The parameters of SiC-SBDs that we used were obtained by measuring the electrical characteristics. A calculated point in Fig. 4 was an in-

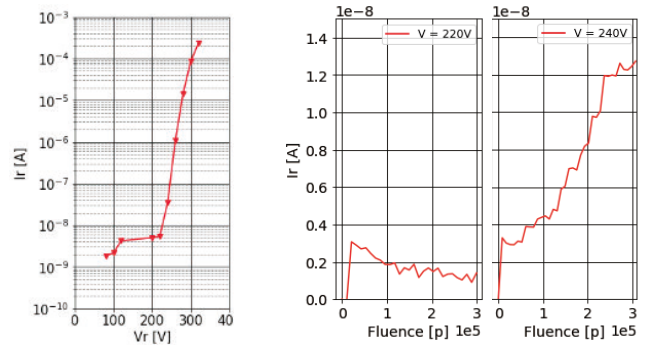


Fig. 3. I<sub>r</sub> values at each voltage after irradiation (left) and increase of I<sub>r</sub> during irradiation at 220 V and 240 V (right).

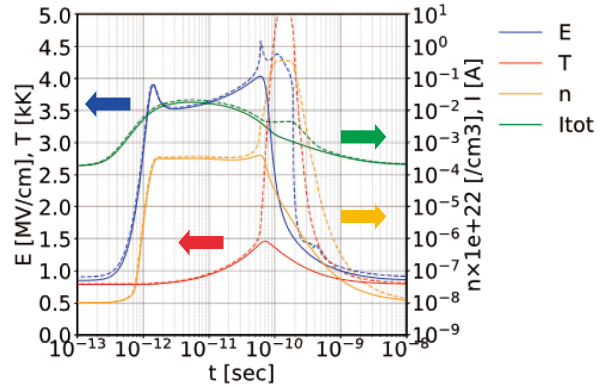


Fig. 4. TCAD simulation results of one particle traversing in SiC-SBD. (V<sub>r</sub> = 220 V; solid line/V<sub>r</sub> = 240 V; dashed line).

cident point of particles, directly below the electrode. In Fig. 4, at first, a particle traverses in a device with electron-hole pairs being generated and thus, the electric field was enhanced further. Second, the total current (I<sub>tot</sub>) was increased. Finally, the increase in current causes the temperature of the calculated point to rise. Compared to V<sub>r</sub> = 220 V, the temperature value at V<sub>r</sub> = 240 V was remarkably high and above the melting point (3000 K) of the SiC crystal. Thus, the temperature exceeding the melting point is assumed to be one owing to device deterioration.

In these experiments, we evaluated the area of transition between the three regions. To assess the experimental data, we conducted TCAD simulation of single event effects. This simulation was available to observe the electron behavior inside SiC-SBDs when one particle makes an incident on a device. On comparing the before and after data, we found a significant difference regarding temperature at the incident point of particles. Although certain issues regarding the simulation parameters remain to be resolved, the ability to simulate the causes of SEE deterioration for power devices is necessary. To resolve these effects, additional experiments are required.

## References

- 1) S. Kuboyama *et al.*, IEEE Trans. **53**, 6 (2006).
- 2) A. Michez *et al.*, IEEE Trans. **62**, 4 (2015).

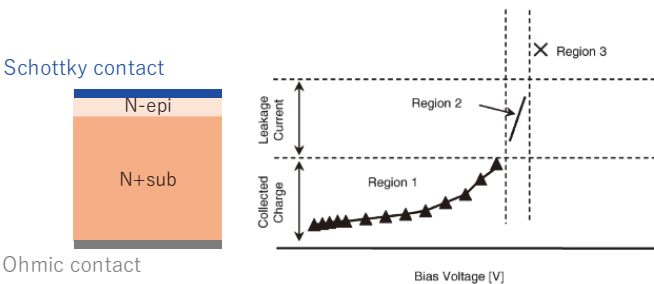


Fig. 1. Device structure. Fig. 2. Characteristic regions observed by heavy ion irradiations on SiC-SBDs.

\*<sup>1</sup> Research and Development Directorate, Japan Aerospace Exploration Agency

# Energy dependence of MeV-ion microbeam size extracted from tapered glass capillary optics

M. Ikekame,<sup>\*1,\*2</sup> T. Ikeda,<sup>\*1,\*2</sup> Y. Hikima,<sup>\*1,\*2</sup> M. Mori,<sup>\*1,\*2</sup> S. Kawamura,<sup>\*1,\*2</sup> T. Minowa,<sup>\*2</sup> and W. -G. Jin<sup>\*2</sup>

Tapered glass capillary optics, which is known as the cell injection needle in life sciences, is capable of producing micrometer-sized MeV ion beams. One of the advantages of this microbeam optics is that the target can either be in vacuum, air, or liquid because the end-window at the capillary outlet keeps the vacuum level inside the capillary. The end-window is fabricated to be thin enough to enable the passage of ions. It also contributes in the close approach of the capillary outlet to the target even in air/liquid so that the broadening of the microbeam size due to multiple-scattering is minimized. An irradiation experiment on a small organ such as an insect's skin using a few MeV energy H/He ions provided by the RIKEN Pelletron accelerator is scheduled to investigate the gene functions relevant to the development of the organ. The combination of MeV ions and the capillary realizes the damage confinement in depth as well as the pin-point lateral damage in the order of  $\mu\text{m}$  to ensure that microscopic observation can be performed to find any change in the shape of the organ after the ion irradiation. We aim at a spot size of several tens of  $\mu\text{m}$  at an irradiation distance of 1 mm or beam divergence of  $1^\circ$ . This report introduces the measurements of the spot sizes and their positions.

Figure 1 shows the plastic end-window of the used capillary whose inlet/outlet sizes were 1.8 mm/9.9  $\mu\text{m}$ , respectively. A 2.8 MeV  $\text{H}^+$  beam entered the capillary mounted at the beam port of BL-W30 line (Fig. 2(a)). The port has a  $\theta$ - $\phi$  (horizontal and vertical) tilting system. The microbeam size and position were measured by the knife-edge method with a step of 75  $\mu\text{m}$ , assuming Gaussian shape. The extracted ions were counted by a PIN photodiode, connected to the pre- and main-amplifiers, discriminator and visual scaler.

Capillary optics is known to have a beam guiding effect. For keV ions, the ion transmission was observed even when the capillary was tilted by up to 80 mrad.<sup>1)</sup> The effect for 2.8 MeV  $\text{H}^+$  was tested for the first time in this energy region. The measured bending angle re-

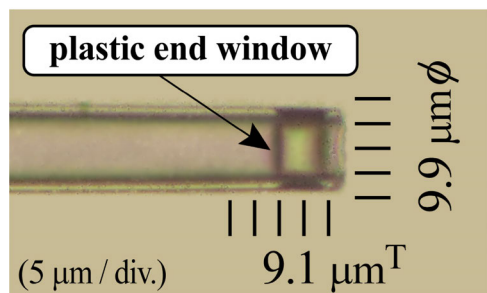


Fig. 1. Outlet of the capillary. The inner diameter and the thickness of the end-window are 9.9  $\mu\text{m}$  and 9.1  $\mu\text{m}$ , respectively. Inner diameter looks larger owing to the refraction index of borosilicate (1.473) for  $\lambda = 587.6 \text{ nm}$ .

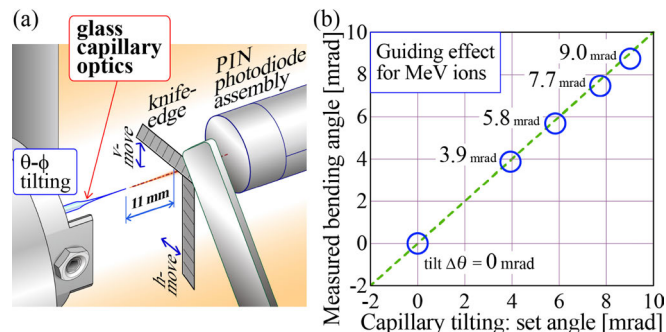


Fig. 2. (a) Measurements of the size and position with knife-edge method. (b) The blue circles show the bending angles as a function of the horizontal tilt angle.

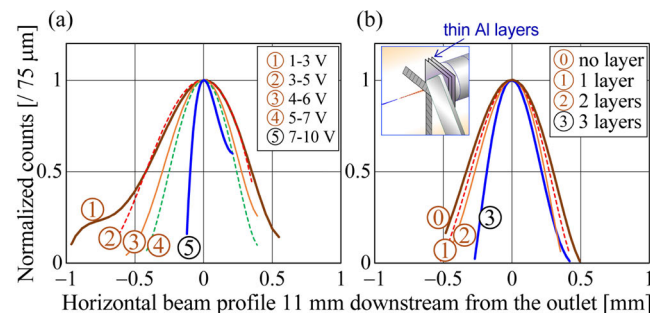


Fig. 3. Microbeam profiles according to (a) ion energy and (b) number of thin Al layers.

constructed from the spot position in Fig. 2(b) shows the guiding for up to 9.0 mrad. However, the measured angles for a larger tilting exhibited degradation due to the asymmetric tails of the spots.

The measured spot sizes according to the ion energy are shown as lines named 1–5 in Fig. 3(a). The ion energy was selected by the pulse height of the main-amplifier output between the low-energy (1–3 V) and high-energy (7–10 V). Line 5 that represents the minimized energy-loss events is the narrowest peak. The peak becomes wider for lower energy events. To obtain narrower microbeams by cutting the low-energy events, a stack of Al-degrader foils was introduced behind the knife-edge. Figure 3(b) shows the beam profiles changing the number of foils of 11  $\mu\text{m}$  thickness each. No ion was counted for more than three layers. The narrowest peak (398  $\mu\text{m}$  in FWHM) was obtained by three layers. The corresponding beam divergence is approximately  $1^\circ$  for each side, which is comparable to that of  $3^\circ$  of the laser microbeam extracted from the same capillary for the laser sight system.<sup>2)</sup> The average energy and standard deviation of the ions at the PIN photodiode are 1.08 MeV and 51.7 keV, respectively, estimated by SRIM code.<sup>3)</sup>

## References

- 1) T. Ikeda *et al.*, Appl. Phys. Lett. **89**, 163502 (2006).
- 2) K. Hirose *et al.*, RIKEN Accel. Prog. Rep. **51**, 193 (2018).
- 3) SRIM-2003, <http://www.srim.org/>.

\*1 RIKEN Nishina Center

\*2 Department of Physics, Toho University

# Development of UV microbeam irradiation system by glass capillary optics

S. Kawamura,<sup>\*1,\*2</sup> T. Ikeda,<sup>\*1,\*2</sup> M. Mori,<sup>\*1,\*2</sup> M. Ikekame,<sup>\*1,\*2</sup> Y. Hikima,<sup>\*1,\*2</sup> T. Minowa,<sup>\*1</sup> and W. G. Jin<sup>\*1</sup>

The tapered glass capillary is known to be a powerful tool for producing ion microbeams. Many studies on ion microbeam produced by the glass capillaries as well as its application of irradiation to a living cell have been reported.<sup>1)</sup> Several years ago, a group from Toho university and RIKEN started studies on the visible-light microbeams by glass capillaries.<sup>2)</sup> Recently, we have developed an ion microbeam irradiation system with a visible-laser microbeam.<sup>3-5)</sup> Another irradiation setup based on UV-laser microbeams will be newly introduced to a beam line of RIKEN Pelletron accelerator so that the ion and UV-laser microbeam irradiations can be switched quickly without any changing around the sample stage. This time, we will report the details on the UV-laser microbeam profiles and the estimation of the beam energy per pulse ([J]) by the glass capillary optics.

The glass capillary was fabricated from a straight glass tube made of borosilicate, whose inner and outer diameters are 1.8 mm and 3.0 mm, respectively. The glass capillaries were made using a puller (Narishige PE-22) by heating a straight glass tube and pulling both ends with a constant force. The outlet diameter  $a$  of the capillary was determined using a microforge (Narishige MF-900).

Figure 1 shows the experimental setup for beam profile measurement. In this measurement, we used a diode laser with wavelength ( $\lambda$ ) of 375 nm. A fluorescent screen was used to obtain the spot shape at the distance  $L$ , called irradiation distance, from the capillary outlet. The spot pictures were taken by a digital camera that is installed behind a fluorescent screen. Generally, the spot shapes for  $L > 1$  mm and  $L < 100 \mu\text{m}$  are like a Fraunhofer diffraction pattern and a Fresnel pattern, respectively, which are known as spot images for a parallel beam entered a small circular aperture. In previous study, the spot pictures with  $\text{Ar}^+$  laser with  $\lambda = 488$  nm were analyzed for  $L > 1$  mm and  $L < 100 \mu\text{m}$ .<sup>4)</sup> We will support the pin-point irradiation to the nucleus in a living cell. Therefore, we defined the irradiation distance ( $L = 17 \mu\text{m}$ ) and obtained spot diameters  $D$ (FWHM) for the microbeam. Figure 2 shows the results of  $D$  as

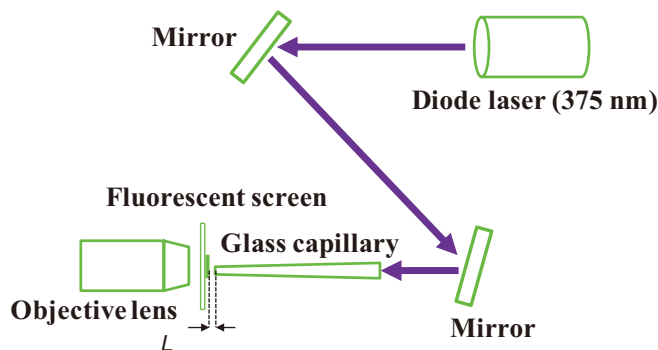


Fig. 1. Experimental setup for beam profile measurement.

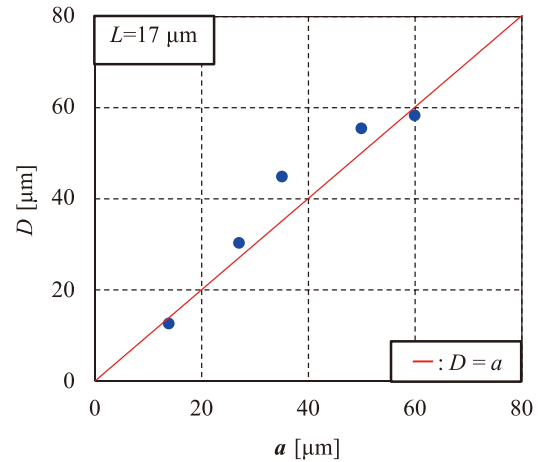


Fig. 2. Spot diameters  $D$ (FWHM) for glass capillaries with different outlet diameters  $a$ . The input laser wavelength was 375 nm.  $L$  is the irradiation distance.

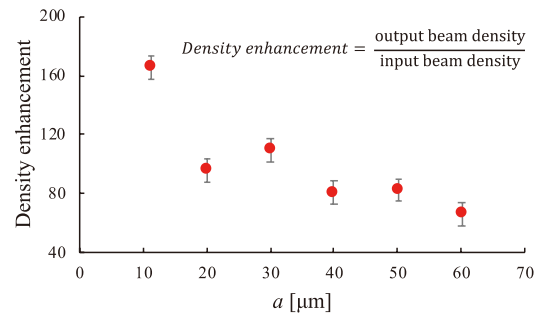


Fig. 3. Density enhancement of the extracted laser beam for  $\lambda = 375$  nm with different outlet diameters  $a$ .

a function of  $a$  at  $L = 17 \mu\text{m}$ . In this experiment, we obtained smaller spots for smaller outlet capillaries without high-order rings like a Fraunhofer diffraction pattern. The spot shapes are good for irradiating a small target like the nucleus in a living cell.

Using a power sensor (Ophir PD-300) and photodiode (HAMAMATSU S2281), we measured the beam power for different glass capillaries, and estimated the focusing ability. To estimate the focusing ability of the capillaries, we introduced density enhancement, which is the ratio between the output beam density at the outlet and the input beam density at the inlet.

Figure 3 shows the density enhancement for glass capillaries that have different outlet diameters. This result means that the tapered glass capillary has a strong focusing ability even for UV-laser beam ( $\lambda = 375$  nm). In the near future, we will install this system to the beam line of the Pelletron accelerator and for biological irradiation.

## References

- 1) T. Ikeda *et al.*, Appl. Phys. Lett. **89**, 163502 (2016).
- 2) W. G. Jin *et al.*, J. Phys. Soc. Jpn. **84**, 114301 (2015).
- 3) M. Koushima *et al.*, J. Phys. Conf. Ser. **875**, 112004 (2017).
- 4) K. Sato *et al.*, RIKEN Accel. Prog. Rep. **51**, 21 (2018).
- 5) K. Hirose *et al.*, RIKEN Accel. Prog. Rep. **51**, 193 (2018).

\*1 Toho University

\*2 RIKEN Nishina Center



## **2. Atomic and Solid State Physics (Muon)**



# Magnetic ordered states of hole-doped pyrochlore iridates ( $Y_{1-x-y}Cu_xCa_y$ ) $_2$ Ir $_2$ O $_7$ investigated by $\mu$ SR

J. Angel,<sup>\*1,\*2</sup> K. Matsuhira,<sup>\*3</sup> and I. Watanabe<sup>\*1,\*2</sup>

The interplay between electron-electron correlation and spin-orbit coupling interaction leads to various exotic states in iridates such as Mott insulator, spin liquid, and Weyl semimetal.<sup>1)</sup> Pyrochlore iridates,  $R_2$ Ir $_2$ O $_7$  ( $R = Y$  and lanthanides) exhibit a largely systematic metal-insulator transition (MIT) among pyrochlore systems and is observed with accompanying magnetic transition by changing  $R$  ion. The Ir atom is expected to play a critical role because Ir has the large spin-orbit coupling effect, which is predicted to cause exotic magnetic properties in  $R_2$ Ir $_2$ O $_7$ . Among  $R_2$ Ir $_2$ O $_7$ , Mott insulator  $Y_2$ Ir $_2$ O $_7$  ( $Y^{3+}$ : non-magnetic;  $Ir^{4+}$ :  $5d^5$ ) is an ideal system for the investigation of the magnetic properties of the Ir atom to clarify its origin. This is because the Y atom does not possess any localized magnetic moments and exhibits the all-in all-out magnetic ground state below the MIT temperature of approximately 170 K.<sup>2-4)</sup> Further, the mechanism of MIT should also be studied by doping holes to the system.<sup>5-7)</sup> A key issue on the Mott insulator is the hole-doping effect; therefore, we investigated the changes in the magnetic properties of  $(Y_{1-x-y}Cu_xCa_y)_2$ Ir $_2$ O $_7$  ( $x = 0.05$ ) in which the hole concentration can be controlled by substituting Ca for Y.

The  $\mu$ SR measurement in the zero-field condition (ZF- $\mu$ SR) was carried out at the RIKEN-RAL Muon Facility, Rutherford-Appleton Laboratory, in the UK using a pulsed positive muon beam. We measured the ZF- $\mu$ SR time spectra of polycrystalline samples,  $(Y_{1-x-y}Cu_xCa_y)_2$ Ir $_2$ O $_7$  ( $x = 0.05$ ) and analyzed them using the following analysis function.

$$A(t) = A_0 e^{-\lambda t} \quad (1)$$

In Eq. (1),  $A(t)$  is the asymmetry of the muon-spin polarization at  $t$ ,  $A_0$  is the initial asymmetry at  $t = 0$ , and  $\lambda$  is the depolarization rate of the asymmetry parameter.

Figure 1 shows the temperature dependence of  $A_0$  measured on  $(Y_{1-x-y}Cu_xCa_y)_2$ Ir $_2$ O $_7$  ( $x = 0.05$ ) at various values of  $y$ . Sudden decreases in  $A_0$  were observed with a decrease in the temperature of the samples up to  $y = 0.10$ . This decrease in  $A_0$  was not observed for  $y = 0.20$  in the metallic state. The decrease implies the appearance of the fast depolarizing component caused by the slowing down of the fluctuations of Ir spins. The dashed lines in Fig. 1 indicate the onset temperatures

of the appearance of the magnetically ordered state in  $(Y_{1-x-y}Cu_xCa_y)_2$ Ir $_2$ O $_7$  ( $x = 0.05$ ). It is clear that the magnetically changes in the electronic state from insulating to metallic. This study will be soon published.

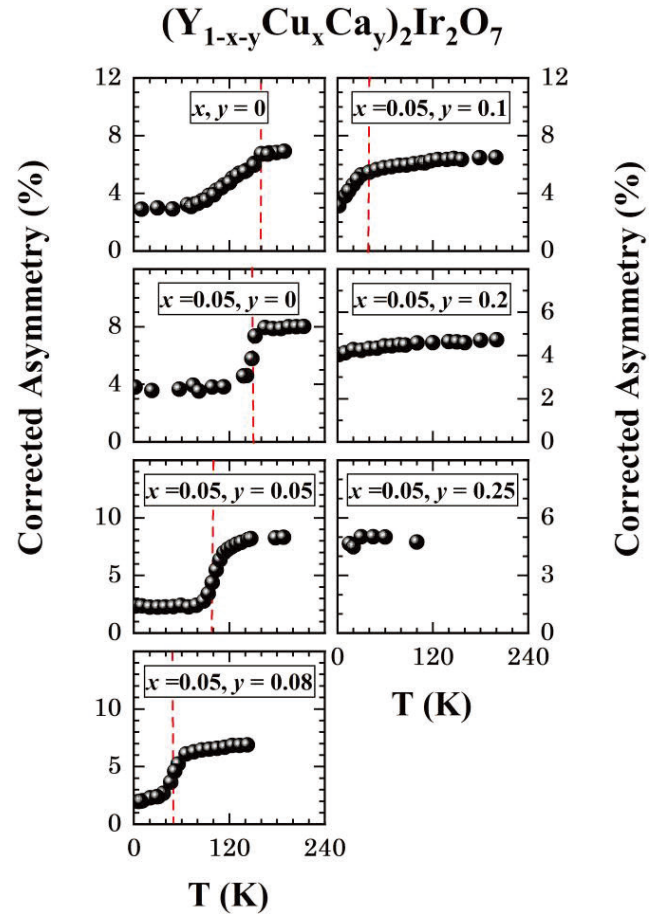


Fig. 1. Temperature dependence of initial asymmetry,  $A_0$  for  $(Y_{1-x-y}Cu_xCa_y)_2$ Ir $_2$ O $_7$  obtained from zero-field  $\mu$ SR measurements.

## References

- 1) W. Witczak-Krempa *et al.*, Annu. Rev. Condens. Matter Phys. **5**, 57 (2014).
- 2) S. M. Disseler *et al.*, Phys. Rev. B **86**, 014428 (2012).
- 3) D. Yanagishima, Y. Maeno, J. Phys. Soc. Jpn. **70**, 2880 (2001).
- 4) N. Taira, M. Wakeshima, Y. Hinatsu, J. Phys. Condens. Matt. **13**, 5527 (2001).
- 5) H. Fukazawa, Y. Maeno, J. Phys. Soc. Jpn. **71**, 2578 (2002).
- 6) L. Savary *et al.*, Phys. Rev. X **4**, 041027 (2014).
- 7) W. K. Zhu *et al.*, Phys. Rev. B **90**, 054419 (2014).

<sup>\*1</sup> RIKEN Nishina Center

<sup>\*2</sup> Department of Condensed Matter Physics, Hokkaido University

<sup>\*3</sup> Graduate School of Engineering, Kyushu Institute of Technology

# Generalization of muon spin relaxation function to study the pseudogap state of the underdoped $\text{La}_{2-x}\text{Sr}_x\text{CuO}_4$

M. D. Umar<sup>\*1,\*2</sup> and I. Watanabe<sup>\*1,\*2</sup>

The origin of the partial gap in the charge and spin sectors at the normal state of cuprate-based superconductors called, pseudogap state, and its interplay with the superconducting state are still elusive. One study proposed that the pseudogap state is a precursor of the superconducting state, while another study argued that the state is a competing order such as spin or charge density waves, stripes, and other exotic orders, for instance, d-density wave and circular current models.<sup>1)</sup>

The  $\mu\text{SR}$  technique is a sensitive tool to investigate the static and dynamic behaviors of the internal magnetic fields. The previous  $\mu\text{SR}$  time spectra of the underdoped regime of  $\text{La}_{2-x}\text{Sr}_x\text{CuO}_4$  showed that the initial line shapes change from the Gaussian-shape depending on the temperature and doping concentration.<sup>2,3)</sup> At a low temperature range, the characteristic temperatures due to the changes in the Gaussian-shape are related to the formation of a spin glass system<sup>2)</sup>, and at a low temperature range and, at a higher temperature range, they are correlated with a minimum resistivity from the metal-insulator crossover experiments.<sup>3)</sup> A product of the Lorentzian and Gaussian functions can approach the changes from the Gaussian-shape in the two previous studies.<sup>2,3)</sup> In a fast fluctuation limit, the longitudinal field dependence of the relaxation rate is described by Redfield formula.<sup>4)</sup> However, the relaxation rate of the Lorentzian function may represent static or dynamic internal fields on the muon site.<sup>5)</sup> Replacing the Gaussian or Lorentzian exponentials of the Kubo-Toyabe functions with a stretched exponential<sup>6)</sup> and convoluting the Gaussian and Lorentzian probability density functions (PDFs)<sup>7)</sup> are two static scenarios that have been pro-

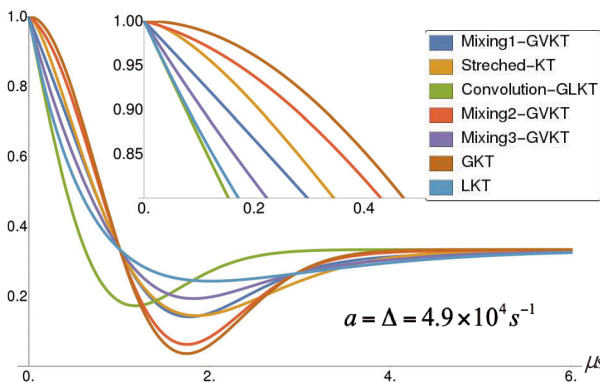


Fig. 1. The line shapes of the mixture of the Gaussian and Lorentzian PDFs in the ZF conditions with three different ratios of weight factors ( $n$ ) compared to the convolution of the Gaussian and Lorentzian PDFs and the stretched exponential scenarios plotted with the same width of the Gaussian ( $\Delta$ ) and Lorentzian ( $a$ ) distributions.

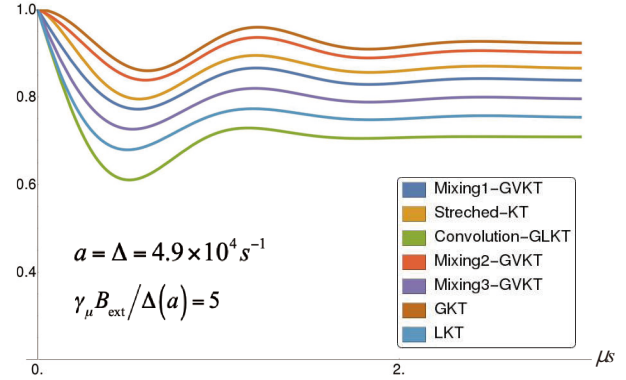


Fig. 2. Calculated time spectra in the LF experiment for all cases in Fig. 1, plotted for the same ratio of the applied longitudinal field ( $\gamma_\mu B_{\text{exp}}$ ) to the width distributions ( $\Delta, a$ ).

posed earlier to fit the intermediate state of the line shape between the Gaussian- and Lorentzian-shapes.

As an alternative for the static scenario due to the tiny changes in the Gaussian-shape, we propose a mixture of Gaussian and Lorentzian PDFs. In general, mixing two or more PDFs is interpreted in terms of either the non-normal behavior of the PDF or the presence of two or more subpopulations.<sup>8)</sup> Moreover, the mixing of the Gaussian and Lorentzian PDFs can approach a convolution of the Gaussian and Lorentzian PDFs.<sup>9)</sup> We apply the Kubo Golden Rule (KGR) formula to derive the muon spin relaxation functions resulting from the mixing of the Gaussian and Lorentzian PDFs for both zero- (ZF) and longitudinal-field (LF) experiments. Our result shows that the mixture of the Gaussian and Lorentzian PDFs can approach the convolution and stretched exponential scenarios. Our derivation also confirmed that the KGR formula for the LF condition can analytically produce the Lorentzian part, which is contrary to a previous claim.<sup>10)</sup> The analysis function of the mixture of the two PDFs exhibits initial slopes between the Gaussian and Lorentzian shapes in both the ZF and LF conditions, whereas the depth and position of a dip in the ZF lineshape change with the ratio of the Gaussian and Lorentzian weighting factors.

## References

- 1) T. Kirzhner, G. Koren, *Sci. Rep.* **4**, 6244 (2014).
- 2) C. Panagopoulos *et al.*, *Phys. Rev. B* **66**, 064501 (2002).
- 3) I. Watabe *et al.*, *J. Phys. Soc. Jpn.* **73**, 2232 (2008).
- 4) R. S. Hayano *et al.*, *Phys. Rev. B* **20**, 850 (1979).
- 5) K. M. Kojima, *Appl. Magn. Reson.* **13**, 111 (1997).
- 6) M. R. Crook *et al.*, *J. Phys. Condens. Matt.* **9**, 1149 (1997).
- 7) M. I. Larkin *et al.*, *Phys. Rev. Lett.* **85**, 1982 (2000).
- 8) G. McLachlan, D. Peel, *Finite Mixture Model* (John Wiley & Son, Canada, 2000).
- 9) T. Ida *et al.*, *J. Appl. Cryst.* **33**, 1311 (2000).
- 10) M. I. Larkin *et al.*, *Physica B* **289–290**, 153 (2000).

\*1 RIKEN Nishina Center

\*2 Department of Physics, Hokkaido University

# Magnetic order in defective reduced graphene oxides (rGO) investigated using $\mu$ SR

R. Asih,<sup>\*1,\*2</sup> M. A. Baqiya,<sup>\*1</sup> D. P. Sari,<sup>\*3,\*2</sup> Darminto,<sup>\*1</sup> and I. Watanabe<sup>\*2</sup>

Several studies have investigated graphene-based materials with a focus on molecular-based magnets. In particular, reduced graphene oxide (rGO) is a fascinating system that has numerous defects and functional group on its sheets; hence, it is ideal to generate the magnetism of intrinsically nonmagnetic graphene. rGO have been reported to exhibit various magnetic states including paramagnetic,<sup>1)</sup> weak super-paramagnetic,<sup>2)</sup> and room temperature ferromagnetic.<sup>3-5)</sup> These magnetic features are believed to be related to the defect states in the rGO sheet.<sup>3,4,6)</sup> A sufficient number of defects, especially in the form of vacancies and chemisorbed hydrogen, can lead to the onset of magnetic ordering. Therefore, we intend to further investigate a possible magnetic ordering in rGO prepared by the green synthesis method.<sup>7)</sup>

The presence of significant number of defects and different types of oxygen functionality in the obtained rGO have been confirmed by Raman, Fourier-transform infrared (FTIR), and photoemission spectroscopies. The defect concentration increases, while that of the oxygen functional group decreases when rGO is thermally reduced at 1000°C (rGO-1000). Furthermore, an enhancement in magnetization was observed when the number of defect increases, confirming defect-induced-magnetism in rGO. It was verified that the magnetic impurities did not contribute toward enhancement of the magnetization. Thus, muon spectroscopy ( $\mu$ SR) could help investigate the possible onset of magnetism in rGO.

$\mu$ SR measurements were performed on the obtained samples, rGO and rGO-1000, under zero-field (ZF) and longitudinal-field (LF) conditions. Figure 1 (a) shows the ZF time spectra of rGO and rGO-1000 at 2 K. No clear muon-spin precession was observed. Muon spin depolarization is prominent up to 4  $\mu$ s, then it is considerably slower in the range of 5–7  $\mu$ s. Further, spin depolarization is observed after 8  $\mu$ s. These features denote the appearance of the oscillation component on the decaying signal; it is a typical feature of graphene-based compounds.<sup>8,9)</sup> Instead of magnetic ordering, the oscillation possibly indicates the nuclear dipolar interaction between muon and proton.<sup>8)</sup> The changes in the initial asymmetry and background along with a small increase in the relaxing amplitude for rGO-1000 compared with that of rGO could be caused by

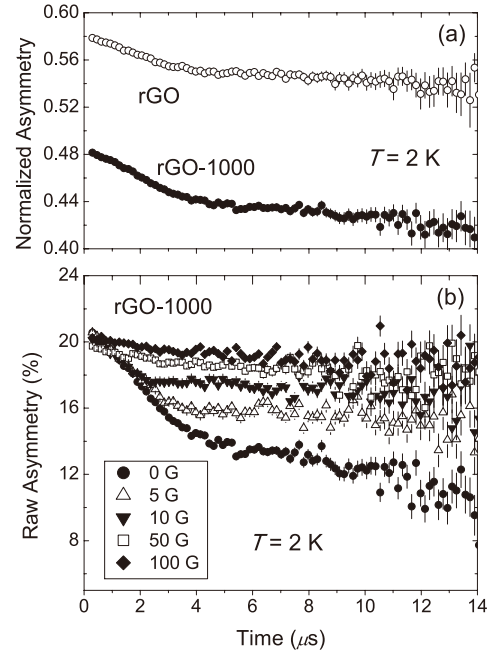


Fig. 1. (a) Zero-field (ZF) time spectra of rGO and rGO-1000 at 2 K. (b) Longitudinal-field (LF) time spectra of rGO-1000 at 2 K.

the increase in defect concentration. A missing fraction can occur in the samples when the positive muon strongly interacts with an electron (hyperfine interaction) either due to the formation of muonium or after the adduction reaction of muonium to form a radical. To confirm the cause, LF- $\mu$ SR measurements were performed to decouple muon spin from the electron spin. Figure 1 (b) displays the LF spectra of rGO-1000. The decoupling is likely to occur owing to the applied field of 100 G, which is much smaller than the field required to recover the free muonium signal (1580 G). This low value demonstrates the formation of a radical complex that was not detected in bare graphene.<sup>9)</sup> Further fitting analysis concomitant with calculation work are required to verify these suggestions.

## References

- 1) Sepioni *et al.*, Phys. Rev. Lett. **105**, 207205 (2010).
- 2) Sarkar *et al.*, Phys. E Low-Dimensional Syst. Nanostruct. **64**, 78–82 (2014).
- 3) Qin *et al.*, Carbon **78**, 559–565 (2014).
- 4) Khurana *et al.*, Nanoscale **5**, 3346–3351 (2013).
- 5) Sun *et al.*, Nano Res. **7**, 1507–1518 (2014).
- 6) Tücek *et al.*, Chem. Soc. Rev. **47**, 3899–3990 (2018).
- 7) Darminto *et al.*, IEEE Trans. Mag. **54**, 1–5 (2018).
- 8) Riccò *et al.*, Nano Lett. **11**, 4919–4922 (2011).
- 9) Gaboardi *et al.*, J. Mater. Chem. A **2**, 1039–1046 (2014).

\*1 Department of Physics, Institut Teknologi Sepuluh Nopember, Indonesia

\*2 RIKEN Nishina Center

\*3 Department of Regional Environment Systems, Shibaura Institute of Technology

# Ground state of quasi-one dimensional competing spin chain $\text{Cs}_2\text{Cu}_2\text{Mo}_3\text{O}_{12}$

T. Goto,<sup>\*1</sup> K. Matsui,<sup>\*1,\*2</sup> J. Angel,<sup>\*3</sup> I. Watanabe,<sup>\*3</sup> T. Sasaki,<sup>\*4</sup> and M. Hase<sup>\*5</sup>

The ground state of the competing-spin chain  $\text{R}_2\text{Cu}_2\text{Mo}_3\text{O}_{12}$ <sup>1,2)</sup> has attracted much interest, not only for the possibility of spin nematic state,<sup>3-7)</sup> but also because the two isomorphous compounds with  $\text{R} = \text{Cs}$  and  $\text{Rb}$  show different ground states.<sup>8-11)</sup> While the former shows a magnetic order at  $T_N = 1.8$  K, the latter shows a small spin gap of  $\Delta/k_B = 1.6$  K. Within a classical spin model, the competing spin chain with the ferromagnetic  $J_1$  for nearest neighboring spins and the antiferromagnetic  $J_2$  for next nearest spins, the helical order is expected for  $|J_2/J_1| > 1/4$ . For both the two compounds satisfy this condition, that is  $J_1 = -93$  and  $J_2 = +33$  K for Cs, and  $-138$  and  $+51$  K for Rb, the difference in their ground states may come from the quantum effect or a tiny inter-chain interaction. As for the Cs-system, the existence of magnetic order has so far been confirmed by the specific heat<sup>7)</sup> and  $\mu\text{SR}$ <sup>8-11)</sup> at zero field, and by NMR<sup>8-11)</sup> under finite fields. However, the observed increase in NMR line width below  $T_N$  becomes quite small when the applied field is lower than 2 T. That is, the increase in FWHM of NMR spectrum below  $T_N$  is decreased from 400 Oe for the measurements above 3 T to only 120 Oe for below 2 T. In order to investigate the spin state under low fields, we have performed LF- $\mu\text{SR}$  experiments on this compound.

Zero (ZF) and longitudinal (LF) field- $\mu\text{SR}$  measurements in the  $^3\text{He}$  temperature range were performed on a powder sample at Riken-RAL Muon facility using a spin-polarized pulsed surface-muon ( $\mu^+$ ) beam with a momentum of 27 MeV/c. The zero-field muon spin depolarization data were analyzed with the function  $G_{\text{KT}}(\tau; \sigma)e^{-\lambda\tau}$ , where  $G_{\text{KT}}$  is Kubo-Toyabe function,  $\sigma \approx 0.068 \mu\text{sec}^{-1}$ , the temperature independent quasi-static field distribution contributed from nuclear moments and  $\lambda$ , the depolarization rate due to the dynamical spin fluctuation.

With decreasing temperature, ZF- $\lambda$  showed an abrupt increase below  $T_N = 1.8$  K, supporting the results of specific heat and NMR.<sup>7,8)</sup> Under finite LF's, the depolarization curves obeyed  $G_{\text{KT}}(\tau; \sigma)e^{-\lambda\tau} + P(\infty)$ , where the constant  $P(\infty)$  is the asymptotic value of muon spin polarization at  $\tau \rightarrow \infty$ .  $P(\infty)$  was dependent on  $H_{\text{LF}}$ , and for example, at 0.3 K,  $P(\infty)$  increased monotonically from zero with increasing  $H_{\text{LF}}$  and reached 0.8 above 3 kOe.<sup>12)</sup> There observed no initial drop in the depolarization function even at the lowest temperature, indicating that the relaxing amplitude was decreased under higher  $H_{\text{LF}}$ .

The temperature dependence of  $\lambda$  under various  $H_{\text{LF}}$  is shown in Fig. 1. Note here that  $\lambda(H_{\text{LF}})$  is a measure of frequency component of  $\gamma H_{\text{LF}}$  in the electron spin fluctuation spectrum. One can see that in higher tem-

perature region above  $T_N$ ,  $\lambda$  is small and nearly independent of  $H_{\text{LF}}$ , indicating that the spin fluctuation has a white spectrum.<sup>13)</sup> With decreasing temperatures, the weight of low frequency part of the spectrum increases significantly, showing the freezing of spin fluctuation due to the magnetic order. This is just analogous to our previous report where the slow down toward the Bose-glass is shown.<sup>13)</sup> However, in the present case, the dynamical spin fluctuation persists even at lower temperatures far below  $T_N$ . At this stage we can only speculate that the spins are in the quasi static ordered state, where only a small static hyperfine field is observed by NMR, and are gradually stabilized with increasing applied field. The latter is in accordance with the increase in  $P(\infty)$  and in the hyperfine field at higher field.<sup>11)</sup> In order to confirm this speculation,  $\mu\text{SR}$  and NMR measurements under the widerange of applied field are necessary, and it is now on the progress.

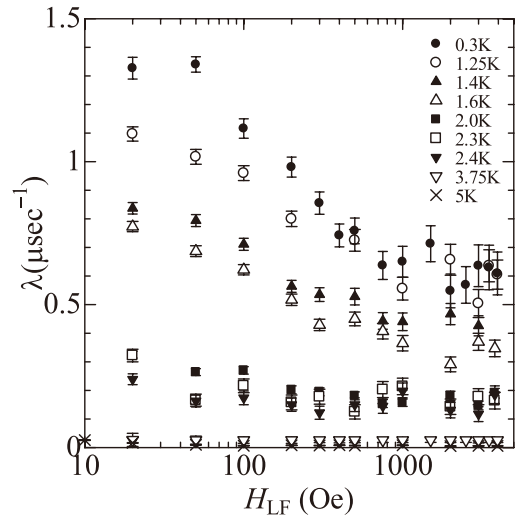


Fig. 1. Temperature dependence of dynamical component of relaxation rate  $\lambda$  under various longitudinal fields  $H_{\text{LF}}$ .

## References

- 1) M. Hase *et al.*, J. Appl. Phys. **97**, 10B303 (2005).
- 2) M. Hase *et al.*, Phys. Rev. B **70**, 104426 (2004).
- 3) M. Hagiwara *et al.*, J. Phys. Conf. Ser. **320**, 012049 (2011).
- 4) H. Tsunetsugu *et al.*, J. Phys. Soc. Jpn. **75**, 083701 (2006).
- 5) T. Hikihara *et al.*, Phys. Rev. B **78**, 144404 (2008).
- 6) M. Sato *et al.*, Phys. Rev. Lett. **110**, 077206 (2013); Phys. Rev. B **83** (2011) 064405, B **79** (2009) 060406(R)
- 7) A. Fujimura *et al.*, IEEE Trans. on Mag. **99**, 1100503 (2016).
- 8) Y. Hoshino *et al.*, JPS Conf. Proc. **3**, 014012 (2014).
- 9) T. Goto *et al.*, J. Phys. Conf. Ser. **828**, 012017 (2017).
- 10) A. Yagi *et al.*, J. Phys. Conf. Ser. **828**, 012016 (2017).
- 11) K. Matsui *et al.*, Phys. Rev. B **96**, 22402(R) (2017).
- 12) K. Matsui *et al.*, JPS Conf. Proc. **21**, 011008 (2018).
- 13) T. Goto *et al.*, Phys. Rev. B **78**, 054422 (2008).

<sup>\*1</sup> Sophia University

<sup>\*2</sup> ISSP, University of Tokyo

<sup>\*3</sup> RIKEN Nishina Center

<sup>\*4</sup> IMR, Tohoku University

<sup>\*5</sup> National Institute for Material Science

# Superconductivity in single crystals of $\lambda$ -(BETS)<sub>2</sub>GaCl<sub>4</sub> studied by transverse-field $\mu$ SR

D. P. Sari,<sup>\*1,\*2</sup> K. Hiraki,<sup>\*3</sup> R. Asih,<sup>\*4,\*2</sup> I. Watanabe,<sup>\*2</sup> and Y. Ishii<sup>\*1</sup>

The superconducting gap structure in  $\lambda$ -(BETS)<sub>2</sub>GaCl<sub>4</sub> is intriguing and has been consistently studied using  $\mu$ SR. We performed transverse field (TF)  $\mu$ SR at fields of 150 Oe down to 0.3 K using a 120 mg randomly oriented sample, at the ISIS Muon Facility in the UK. The temperature dependence of the superfluid density deduced from that experiment is best described by the  $s + d$ -wave with a dominant  $s$ -wave component.<sup>1)</sup> In order to get clearer and more direct evidence in terms of the superconducting gap structure determination, we performed similar measurements using a 75 mg well-aligned sample by applying the external field perpendicular to the conducting  $ac$ -plane. Here, we report the TF dependence of the London penetration depth, which leads to the upper critical field  $H_{c2}$  estimation, in order to check the quality of the experimental setup in aligned single crystals of  $\lambda$ -(BETS)<sub>2</sub>GaCl<sub>4</sub>.

Figure 1 shows a typical TF- $\mu$ SR spectra with a field of 150 Oe in the aligned single crystals at  $T = 0.3$  K and 10 K after being cooled through critical temperature  $T_c \sim 5.3$  K.

The time spectra were fitted by using Eq. (1),

$$A(t) = 0.3438 \times e^{-(\sigma t)^2} \cos(\gamma_\mu H_{int1(sample)} t + \phi) + 0.652 \cos(\gamma_\mu H_{int2(Ag\ foil)} t + \phi) \quad (1)$$

The two oscillation components represent about 35% signal from the sample and 65% signal from the silver package. The damping rate  $\sigma$  becomes prominent once the system enters the superconducting state. The superconducting component of the damping rate  $\sigma_{SC}$  is then given by  $\sigma_{SC}^2 = \sigma^2 - \sigma_{NM}^2$ , where  $\sigma_{NM}^2$  is the signal  $\sigma_{T=10K}$  in the normal state due to the nuclear moments. Furthermore, the TF dependence of  $\sigma_{SC}$  can be used to determine the London penetration depth  $\lambda$  and to give an estimate for the  $H_{c2}$ , following Eq. (2),

$$\sqrt{2}\sigma_{SC}(H) = 4.83 \times 10^4 \times (1 - H_{app}/H_{c2}) \times \left[ 1 + 1.21 \left( 1 - \sqrt{H_{app}/H_{c2}} \right)^3 \right] \lambda^{-2} \quad (2)$$

where  $H_{app} = 150$  Oe and  $\lambda$  is in nm.<sup>2)</sup>

Figure 2 shows the estimation of  $H_{c2\perp}$  from the measurements of the aligned crystals. The resulting  $H_{c2\perp}$ , which is parallel to the  $b$ -axis, is  $41 \pm 19$  kOe, and the absolute value of the London penetration depth at 0 K,  $\lambda(0) = 710 \pm 12$  nm. The estimation of  $H_{c2}$  from the previous TF- $\mu$ SR measurement on a randomly oriented sample was  $43 \pm 25$  kOe.<sup>1)</sup> From magnetoresistance measurements, the  $H_{c2}$  of  $\lambda$ -(BETS)<sub>2</sub>GaCl<sub>4</sub> was reported to

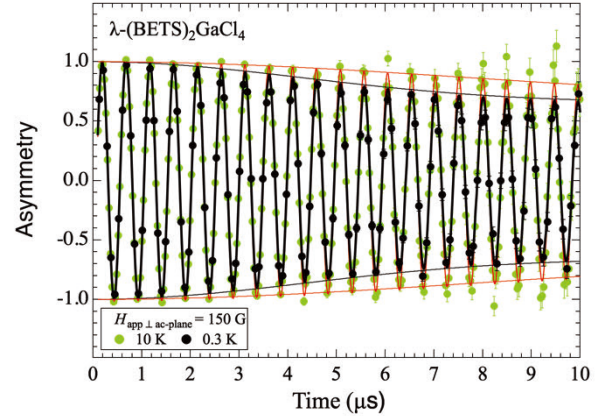


Fig. 1. The normalized TF time spectra in the applied field of 150 Oe measured at  $T = 0.3$  K (black) and 10 K (green). The red and black solid lines are the best-fit results obtained by using Eq. (1). The trace of the envelope of the cosine curve represents the damping rate  $\sigma$  of Eq. (1).

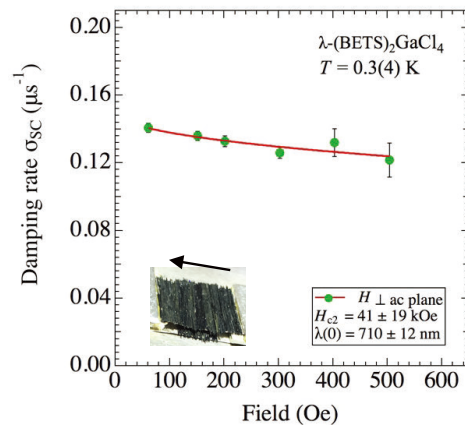


Fig. 2. Transverse-field dependence of damping rate of the muon-spin precession in the superconducting state,  $\sigma_{SC}$ , of  $\lambda$ -(BETS)<sub>2</sub>GaCl<sub>4</sub> taken at 0.3 K. The red and green circles indicate the data for randomly oriented and well-oriented crystals, respectively. The inset figure shows the aligned crystal mounted in a silver foil. The black arrow indicates the direction of the applied field.

have a high anisotropy. The  $H_{c2}$  parallel to  $a$ ,  $b$ , and  $c$ -axes were 150 kOe, 30 kOe, and  $\sim 130$  kOe, respectively.<sup>3)</sup> In comparison with the  $H_{c2}$  in the randomly oriented crystals, the estimation of  $H_{c2\perp}$  is closer to the reference of the magnetoresistance measurement, although the signal we obtained from the sample was smaller than that of the background from silver. It implies that the sample alignment was good enough. Taking into account the low sample mass, we will increase it up to  $\sim 120$  mg in order to obtain a stronger signal and solid results.

## References

- 1) D. P. Sari, *et al.*, to be submitted.
- 2) E. H. Brandt, Phys. Rev. B, **68**, 054506 (2003).
- 3) M. A. Tanatar, *et al.*, Supercond. **12**, 511 (1999).

<sup>\*1</sup> Graduate School of Engineering and Science, Shibaura Inst. of Tech.

<sup>\*2</sup> RIKEN Nishina Center

<sup>\*3</sup> Department of Physics, Fukushima Medical University

<sup>\*4</sup> Institut Teknologi Sepuluh Nopember

## $\mu$ SR study on ferrimagnetism of Na-K alloy clusters incorporated into zeolite LSX under high-pressure helium gas

T. Nakano,<sup>\*1</sup> L. M. Kien,<sup>\*2</sup> I. Watanabe,<sup>\*3</sup> R. Asih,<sup>\*4,\*3</sup> Y. Ishii,<sup>\*5</sup> M. Kibble,<sup>\*6</sup> C. Goodway,<sup>\*6</sup> C. Offer,<sup>\*6</sup> and R. Done<sup>\*6</sup>

Various types of magnetic orderings such as ferromagnetism, antiferromagnetism, and ferrimagnetism have been found in three dimensionally arrayed alkali-metal nanoclusters in zeolite crystals.<sup>1)</sup> The magnetic properties depend on the structure of the zeolite, species of the alkali element, and electron density of the clusters. They are a new class of magnetic materials because their magnetic orderings are realized by the mutual interactions between the s-electrons and they contain no magnetic elements.

In zeolite LSX (low-silica X),  $\beta$ -cages with an inner diameter of 7 Å are arrayed in a diamond structure. A supercage with an inner diameter of 13 Å is formed between the  $\beta$ -cages. The supercages are also arrayed in a diamond structure. It is known that an N-type ferrimagnetism appears when Na-K alloy clusters are incorporated into zeolite LSX ( $\text{Na}_4\text{K}_8\text{Al}_{12}\text{Si}_{12}\text{O}_{48}$  per supercage) by loading K atoms for a certain range of the loading density. The highest Curie temperature  $T_C$  is approximately 20 K. Recently, we found that a new ferromagnetic phase with  $T_C$  as high as 60 K is formed on applying pressure using helium gas. Because the formation of the new magnetic phase has a slow time dependence and is irreversible, it is speculated that the helium atoms are loaded into the pores of the zeolite crystal by pressure and directly change the electronic states of the clusters resulting in the enhancement of the magnetism. In this work, we performed  $\mu$ SR measurements on this system under a high-pressure helium gas to investigate the new magnetic phase.

A high pressure cell newly made of Ti alloy was loaded with a powder sample of K-loaded LSX. This sample shows a ferrimagnetic ordering below 20 K at ambient pressure.  $\mu$ SR measurements were performed at the RIKEN-RAL Muon Facility in the U.K. The pressure cell was loaded into the VARIOX cryostat and connected to a high-pressure He gas handling system which allowed us to control the pressure at any temperatures.<sup>2)</sup> We used a double-pulsed decay muon beam with a momentum of 64.3 MeV/c. Zero-field  $\mu$ SR spectra were obtained by utilizing the ARGUS spectrometer.

The obtained spectra showed slow relaxations. At 50 MPa, the initial asymmetry  $A_0$  of the spectrum

gradually decreased below  $\simeq 90$  K and quickly below  $\simeq 20$  K, as shown in Fig. 1. The decrease in  $A_0$  indicates that the muon spin is depolarized within the time resolution of the measurement,  $\simeq 0.4 \mu\text{s}$ , owing to the appearance of a strong internal magnetic field. After reducing the pressure, the decrease in  $A_0$  below  $\simeq 90$  K disappeared, as seen in Fig. 1. Therefore, the gradual decrease in  $A_0$  at 50 MPa can be attributed to the high  $T_C$  magnetic phase. The phase transition is not sharp. This may be due to a distribution of  $T_C$  originating from a certain inhomogeneity of the He atom loading. At 50 MPa, the ambient pressure phase with  $T_C \simeq 20$  K still remained, thereby indicating a phase separation. A part of the crystal may be loaded with He atoms by pressure. The amplitude of the decrease in  $A_0$  for the high  $T_C$  magnetic phase is approximately half of that in the 20-K phase at an ambient pressure. This result indicates that although there are some inhomogeneities, the high  $T_C$  magnetic phase has sufficient volume and can be regarded as bulk magnetism, which does not originate owing to any impurities.

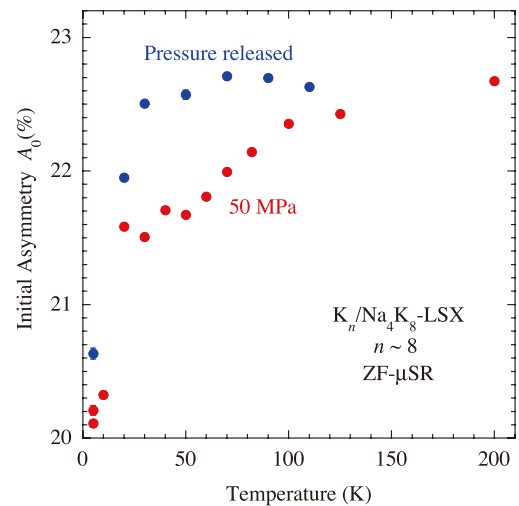


Fig. 1. Initial asymmetry of the  $\mu$ SR spectra of Na-K alloy clusters in zeolite LSX as a function of temperature. The red circles are data taken at 50 MPa and the blue circles are those after reducing the pressure.

<sup>\*1</sup> Institute of Quantum Beam Science, Ibaraki University  
<sup>\*2</sup> Hanoi University of Science, Vietnam National University  
<sup>\*3</sup> RIKEN Nishina Center  
<sup>\*4</sup> Department of Physics, Institut Teknologi Sepuluh Nopember  
<sup>\*5</sup> Department of Physics, Shibaura Institute of Technology  
<sup>\*6</sup> ISIS, Rutherford Appleton Laboratory

### References

- 1) T. Nakano, Y. Nozue, *Adv. Phys. X* **2**, 254 (2017).
- 2) I. Watanabe, Y. Ishii, T. Kawamata, T. Suzuki, F. L. Pratt, R. Done, M. Chowdhury, C. Goodway, J. Dreyer, C. Smith, M. Southern, *Physica B* **404**, 993 (2009).

# Quantum effects of muon on the electronic state of $\text{La}_2\text{CuO}_4$

M. R. Ramadhan,<sup>\*1,\*3</sup> M. I. Mohamed-Ibrahim,<sup>\*2</sup> S. Sulaiman,<sup>\*2</sup> and I. Watanabe<sup>\*1,\*2,\*3</sup>

Muon spin relaxation ( $\mu\text{SR}$ ) studies on  $\text{La}_2\text{CuO}_4$  (LCO) prove the appearance of the antiferromagnetic (AF) long-range ordering as previously observed by powder neutron diffraction experiments.<sup>1)</sup> The appearance of coherent muon-spin precession was observed and the internal field at the muon site was determined to be approximately 410 G.<sup>2)</sup> Neutron diffraction experiments determined the AF spin structure, where the Cu spin had the magnetic moment of  $0.5 \mu_B$  aligning to the  $b$ -axis in the  $\text{CuO}_2$  plane. Recent  $\mu\text{SR}$  studies on the thin film reported the observation of another muon-spin precession component, which experienced less internal field at the muon site of approximately 100–120 G.<sup>3)</sup> Although both  $\mu\text{SR}$  and neutron diffraction experiments sense the same Cu spin in LCO, it is not yet possible to explain the internal fields at the muon site by using the AF spin structure as proposed by neutron diffraction experiments because the position of the implanted muon has not been precisely determined to explain the electronic state.

To deduce more detailed information and knowledge from the  $\mu\text{SR}$  results, we are developing techniques to more precisely estimate the muon position in LCO using the density functional theory (DFT) calculations. The Hubbard parameter  $U$  and exchange parameter  $J$  were set to be 8 and 0.8 eV, respectively. The AF spin structure proposed by Vaknin *et al.* was considered in our non-collinear calculations. To obtain a realistic behavior of muon, we utilized a large 32-unit supercell with a single muon implanted in the lowest position as shown by the electron potential map as reported in the previous study,<sup>4)</sup> resulting in the perturbed system. We also consider the unperturbed system, which is the same supercell with no implanted muon to capture the essential differences between the perturbed and unperturbed systems. The ground state of the supercell was achieved by setting the convergence criterion to be  $1 \times 10^{-5}$  eV and relaxing all atoms until the magnitude of the force on each atom became less than  $0.05 \text{ eV}/\text{\AA}$ . The dipole field value perceived by muon was evaluated using the spin-density grids acquired from our DFT calculations, given by the following equation:

$$H_{dip}(\vec{r}) = \sum_i \frac{1}{|\vec{r} - \vec{r}_i|} \left[ 3(\vec{\rho}_i^S \cdot (\vec{r} - \vec{r}_i)) \frac{(\vec{r} - \vec{r}_i)}{|\vec{r} - \vec{r}_i|^2} - \vec{\rho}_i^S \right] \quad (1)$$

Where  $\vec{\rho}_i^S$  is the magnetic moment of the Cu spin and  $|\vec{r} - \vec{r}_i|$  is the relative distance between the muon and Cu spins. The total internal field at the muon site,  $H_{dip}(\vec{r})$ , is obtained from the summation of all dipole fields due

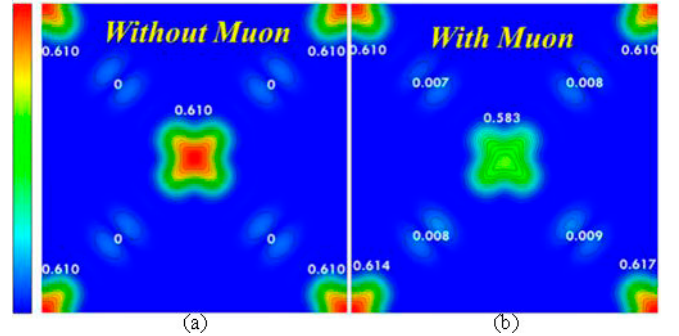


Fig. 1. Comparison of spin density map of LCO for (a) unperturbed system and (b) perturbed system.

to the surrounding Cu spins. For our calculations, we set the spherical region centered by the muon with a radius of  $50 \text{ \AA}$ . This spherical region is sufficient for the convergence of the calculated internal fields.

Figure 1 shows the spin density contour map between the unperturbed (a) and perturbed (b) systems. Our calculations indicate that the unperturbed system is an AF insulator with  $0.61 \mu_B$  and an insulating gap  $\sim 2 \text{ eV}$ , which significantly corresponds with the experimental data.<sup>5)</sup> The perturbed system, however, shows a local deformation in both crystal and spin structure owing to the implanted muon. The nearest Cu spins are affected by the presence of the muon, thereby slightly reducing the value of Cu magnetic moment to  $0.58 \mu_B$ . These local deformations do not affect the electronic structure in general as the muon only affects the surrounding atom, making a large supercell necessary in our studies. Using Eq. (1), we evaluated the dipole field value of the muon inside our perturbed system and obtained a value of 498 G, which is close to the experimental value of 410 G. The difference of  $\sim 80 \text{ G}$  can be attributed to two possible issues. The first issue is the consideration of the zero-point vibrational motion for the implanted muon. The second is the utilization of a more optimized supercell structure to get a better description on how the implanted positive muons affect the crystal and spin structure. We believe that these two key points are mandatory to obtain more information from the muon's position inside the system.

## References

- 1) D. Vaknin *et al.*, Phys. Rev. Lett. **58**, 2802 (1987).
- 2) J. I. Budnick *et al.*, Phys. Lett. A **124**, 103 (1987).
- 3) E. Stilp *et al.*, Phys. Rev. B **88**, 064419 (2013).
- 4) M. R. Ramadhan *et al.*, RIKEN Accel. Prog. Rep. **51**, 197 (2017).
- 5) J. M. Grinder *et al.*, Phys. Rev. B **37**, 7506 (1988).

\*1 Department of Physics, Universitas Indonesia

\*2 School of Distance Education, Universiti Sains Malaysia

\*3 RIKEN Nishina Center

# *Ab-initio* calculation and $\mu$ SR study of the covalency effect in $\text{YBa}_2\text{Cu}_3\text{O}_6$

I. Ramli,<sup>\*1,\*2</sup> S. S. Mohd-Tajudin,<sup>\*3</sup> S. Sulaiman,<sup>\*3</sup> M. I. Mohamed-Ibrahim,<sup>\*3</sup> and I. Watanabe<sup>\*1,\*2</sup>

Since the first discovery of high- $T_c$  in cuprates over three decades ago, extensive studies of their magnetic properties have been carried out in order to explain the mechanism of superconductivity.  $\text{YBa}_2\text{Cu}_3\text{O}_6$  (YBCO<sub>6</sub>), which is the mother compound of the high- $T_c$  cuprate  $\text{YBa}_2\text{Cu}_3\text{O}_{6+x}$ , shows long-range antiferromagnetic (AF) ordering with the Néel temperature  $T_N = 420$  K. The AF ordering in this system arises from the strong on-site coulomb repulsion between electrons, and it is destroyed by changing the oxygen content, which results in superconductivity. A detailed understanding of the electronic structures and magnetic states regarding the mother compound and its chemical derivatives is the key to understand the nature of superconductivity.<sup>1)</sup>

We studied the covalency effect on the magnetic properties of YBCO<sub>6</sub> by *ab-initio* calculations through the density functional theory (DFT) and the muon-spin resonance ( $\mu$ SR) technique. The  $\mu$ SR experiment involves the implantation of muons into the system, and this provides information on the internal field at the muon site, which is very important when discussing the electronic and spin states of the system.

We have carried out  $\mu$ SR experiments on single crystals of YBCO<sub>6</sub> and detected three distinct muon-spin precession components. This result suggests that three different muon sites exist in YBCO<sub>6</sub> with internal fields of 117.7 G, 295.5 G, and 220.4 G. In order to get a deeper understanding of this result, we tried to estimate the muon-sites by *ab-initio* calculations and calculate the internal fields at these muon sites. Since DFT fails to consider the strong correlation effect in a system such as YBCO<sub>6</sub>, an additional Hubbard parameter,  $U$ , was incorporated into our *ab-initio* calculations (DFT+ $U$ ).<sup>2)</sup> The DFT+ $U$  calculations found three local minima in the potential, which can be regarded as initial muon sites in the system since muon has a positive charge. These positions, marked as M1, M2, and M3, are shown in Fig. 1.

The muon perturbation to the host system was calculated by placing one muon at each initial muon site in a large  $4 \times 4 \times 2$  supercell and allowing all ions in the supercell to relax. The large supercell is required to accommodate the behaviour of the muon as an ultra dilute impurity in the host system. In the last step, we calculated the internal field at each relaxed muon position on the basis of dipolar interaction between the muon and the magnetic ions. The calculated internal fields at the muon sites on the basis of ionic picture of magnetism, where spins reside in particular ions, are larger

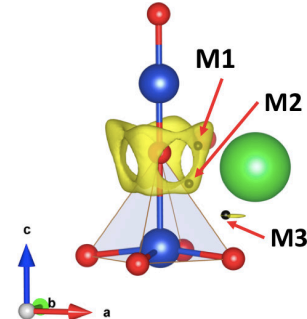


Fig. 1. The muon site positions from DFT+ $U$  calculations.

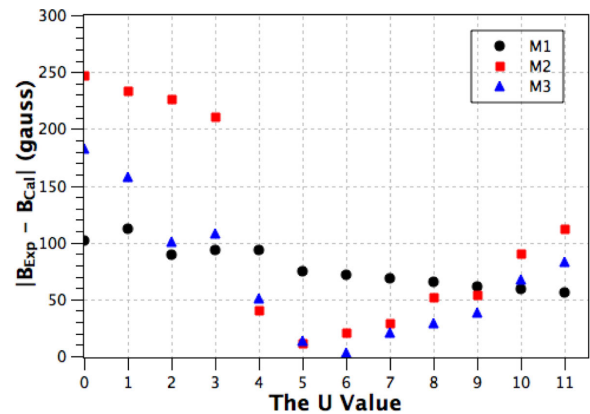


Fig. 2. The differences between the calculated and experimental values of the internal fields as functions of the  $U$  value.

than those deduced from the experiments, although the zero point vibration energy of muons was carefully considered.

The covalency effect, which arises from the strong hybridization between the Cu  $3d$  and the O  $2p$  orbitals, is thought to play a crucial role in this discrepancy. This effect causes the extension of spin density in the real space, although it is contradictory to the ionic picture of magnetism. The DFT+ $U$  calculations have the capability to provide the spin density and have successfully explained the ambiguous missing intensity in copper oxide compounds.<sup>3)</sup> Finally, we examined the internal fields at the muon sites on the basis of the spin density criterion. The internal field at each site has a strong dependence on the  $U$  value. Careful tuning of the  $U$  value was required. The differences between the calculated and experimental values of the internal fields are shown as functions of the  $U$  value in Fig. 2.

## References

- 1) B. Keimer *et al.*, Nature **518**, 179–186 (2015).
- 2) J. Orenstein, A. J. Millis., Science **228**, 468–474 (2000).
- 3) A. C. Walters *et al.*, Nature **5**, 867–872 (2009).

<sup>\*1</sup> RIKEN Nishina Center

<sup>\*2</sup> Department of Condensed Matter Physics, Hokkaido University

<sup>\*3</sup> School of Distance Education, Universiti Sains Malaysia

## Studies of electrical conductivity in 12-mer single-stranded DNA by using scanning tunneling microscope

H. Rozak,<sup>\*1,\*2</sup> W. N. Zaharim,<sup>\*2</sup> I. Miyazaki,<sup>\*3</sup> K. Ichimura,<sup>\*3</sup> M. I. Mohamed-Ibrahim,<sup>\*2</sup> M. R. Samian,<sup>\*4</sup> S. Sulaiman,<sup>\*2</sup> and I. Watanabe<sup>\*1,\*2,\*3</sup>

DNA is a molecule that stores genetic instruction in living things for making other large molecules. The main structure of DNA consists of sugar phosphates and bases. There are four kinds of bases in DNA, namely adenine (A), guanine (G), cytosine (C), and thymine (T).<sup>1)</sup> These bases contain a ring of atoms known as an aromatic group, and they are electron-rich in nature. If their electron clouds overlap within the bases,  $\pi$ - $\pi$  interactions are created and become a medium of electron transport.<sup>2)</sup>

Electron transport in DNA is important in biological processes, especially for understanding the DNA damage and repair mechanisms. According to previous studies,<sup>3,4)</sup> electrons travel through the DNA to scan the damaged area and repair it by using repair protein. Therefore, the main question here is whether DNA is an electrical conductor or not? If DNA is conductive, how do the electrons move along the DNA strand?

In order to answer this question, we carried out scanning tunneling microscope (STM) measurements on a simple sequence DNA. Our samples were composed of 12-mer single stranded synthetic DNA (12-mer ssDNA), and each strand had only one type of base (12mer-ssG, 12mer-ssC, 12mer-ssA or 12mer-ssT). In this report, however, we only show the results of cytosine.

We prepared our 12mer-ssC sample for STM measurements by dissolving of 0.1 mg of powder sample in 2 ml pure water. This solution was shaken by using

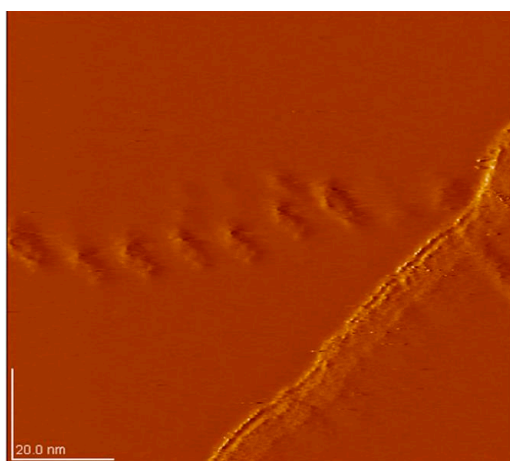


Fig. 1. STM image of 12 mer single stranded cytosine molecule aligned in a one-dimensional chain structure.

\*1 RIKEN Nishina Center

\*2 School of Distance Education, Universiti Sains Malaysia

\*3 Department of Engineering, Hokaido University

\*4 School of Biological Sciences, Universiti Sains Malaysia

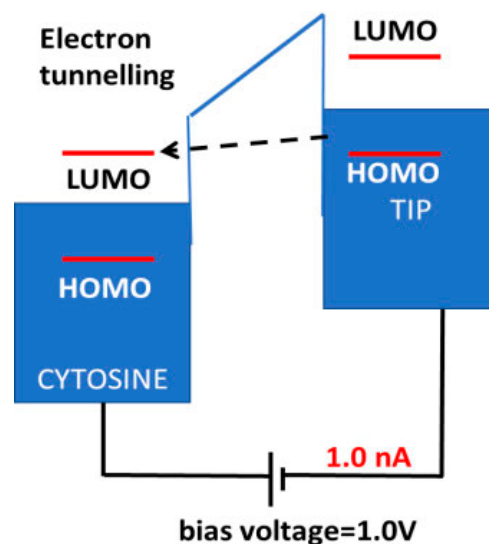


Fig. 2. Schematic picture of the electron tunnelling from the highest molecular orbital (HOMO) of the tip to the lowest molecular orbital (LUMO) of the sample.

an ultrasonic vibrator for about 60 min. Then, we deposited a droplet of the sample on a graphite stage and dried it in a space lined with silica gels for about 2 h. The values of the bias voltage and current we used in our STM measurement were 1.0 V and 0.1 nA, respectively.

From our STM measurements, we successfully observed the molecule image of 12mer-ssC as shown in Fig. 1. This means that the sample is conductive. We understood that electron tunneling occurs from the highest molecular orbital (HOMO) of the tip to the lowest molecular orbital (LUMO) of the sample. Besides, we also observed that the sample molecules are aligned parallel to each other forming a one-dimensional chain structure. Figure 1 shows the STM image of sample in a one-dimensional chain structure. This structure might cause electron transfer in a one-dimensional pass across the edges of the molecules, due to the overlapping of  $\pi$  orbitals between the strands of molecules. This result agrees well with the results of muon spin relaxation: electron transport occurs in the quasi one-dimensionality at room temperature.

### References

- 1) L. Pray, Nature Education **1**, 100 (2008).
- 2) D. M Eley, D. I. Spivey, Trans. Faraday Soc. **58**, 411 (1962).
- 3) E. O'brien *et al.*, Science **355**, eaag1789 (2017).
- 4) Grodick *et al.*, Biochemistry **54**, 962–973(2015).

# Magnetic ordering of $(\text{Eu}_{1-x}\text{Ca}_x)_2\text{Ir}_2\text{O}_7$ studied using muon spin relaxation ( $\mu\text{SR}$ )

U. Widyaiswari,<sup>\*1,\*2</sup> J. Angel,<sup>\*1,\*3</sup> H. Nomura,<sup>\*4</sup> T. Taniguchi,<sup>\*4</sup> K. Matsuhira,<sup>\*4</sup> B. Kurniawan,<sup>\*2</sup> and I. Watanabe<sup>\*1,\*2,\*3</sup>

Pyrochlore oxides have been studied extensively because they show various physical properties such as superconductivity,<sup>1)</sup> spin-glass-like transition,<sup>2)</sup> possibility of a spin liquid state,<sup>3)</sup> and metal-insulator transition (MIT).<sup>4,5)</sup> Pyrochlore lattices have a network of corner-sharing tetrahedra, which makes these systems geometrically frustrated. Pyrochlore iridate series is one of those frustrated systems. In pyrochlore iridates,  $R_2\text{Ir}_2\text{O}_7$  ( $R$  is the  $4f$  rare element), the electronic properties vary with the changing value of  $R$ . Previous study showed MIT at  $T_{\text{MI}}$  accompanied by a magnetic transition in  $\text{Ir}^{4+}$ . The  $T_{\text{MI}}$  decreases with an increase in the  $R^{3+}$  ionic radius and MIT disappears between  $R = \text{Nd}$  and  $\text{Pr}$ .<sup>5)</sup> In  $\text{Eu}_2\text{Ir}_2\text{O}_7$  ( $T_{\text{MI}} = 120$  K),  $\text{Eu}^{3+}$  is a non-magnetic ion ( $J = 0$ ;  $4f^6$ ).<sup>5)</sup> Accordingly, the ordered state of  $\text{Ir}^{4+}$  magnetic moment can be directly examined. This study aims to investigate the hole-doped effect on the magnetic properties in  $(\text{Eu}_{1-x}\text{Ca}_x)_2\text{Ir}_2\text{O}_7$ .

Polycrystalline samples were synthesized using the solid-state reaction and characterized by measuring the muon spin relaxation ( $\mu\text{SR}$ ). The measurement was conducted at the RIKEN-RAL Muon Facility in the United Kingdom using a single pulsed muon beam. The samples were measured in zero-field condition in a temperature range between 1.6 and 200 K.

The results of  $\mu\text{SR}$  measurement were plotted in the zero-field  $\mu\text{SR}$  (ZF- $\mu\text{SR}$ ) time spectra, which can be analyzed and fit using the Lorentzian relaxation function, as shown in Eq. (1).

$$A(t) = A_0 \exp(-\lambda t) \quad (1)$$

This function expresses the muon spin relaxation.  $A_0$  is the initial asymmetry at  $t = 0$  and  $\lambda$  is the relaxation rate of the muon. Figure 1 shows the ZF- $\mu\text{SR}$  time spectra, where the solid line represents the best-fit results. The corrected asymmetry is obtained by subtracting the background components from its asymmetry. It decreases with a decrease in temperature, thereby indicating the existence of an ordered state. The temperature dependence of normalized asymmetry for various  $x$  is shown in Fig. 2. It can be seen for  $x = 0.035$  and  $0.07$ , the ordered states appear in the samples with onset temperature around 100 K. However, for  $x = 0.13$ , there is no ordered state. The result indicates that the magnetic volume fraction decreases with an increase in the concentration of Ca.

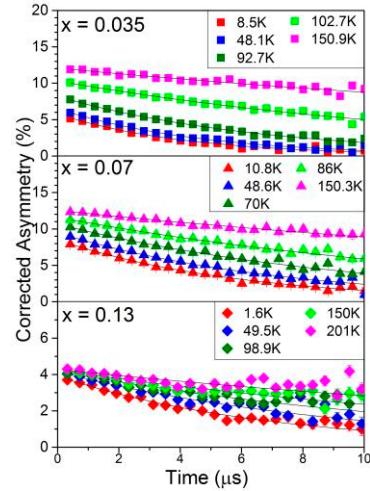


Fig. 1. Zero-field  $\mu\text{SR}$  time spectra of  $(\text{Eu}_{1-x}\text{Ca}_x)_2\text{Ir}_2\text{O}_7$  measured at several temperatures.

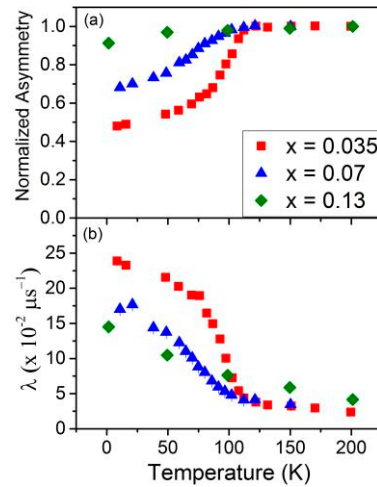


Fig. 2. Temperature dependence of (a) normalized asymmetry and (b) muon relaxation rate obtained from the analysis of ZF- $\mu\text{SR}$  time spectra of  $(\text{Eu}_{1-x}\text{Ca}_x)_2\text{Ir}_2\text{O}_7$ .

From the result of  $\mu\text{SR}$ , it can be concluded that hole doping diminishes the magnetic ordered state of the sample. The effect of hole doping on magnetic ordered states and the physical properties of this system must be investigated by comparing the result of  $\mu\text{SR}$  obtained here with those obtained in other macroscopic studies.

## References

- 1) M. Hanawa *et al.*, Phys. Rev. Lett. **87**, 187001 (2001).
- 2) Y. Ito *et al.*, J. Phys. Chem. Solids **62**, 337 (2001).
- 3) L. Balents, Nature **464**, 199 (2010).
- 4) K. Matsuhira *et al.*, J. Phys. Soc. Jpn. **76**, 043706 (2007).
- 5) K. Matsuhira *et al.*, J. Phys. Soc. Jpn. **80**, 094701 (2011).

<sup>\*1</sup> RIKEN Nishina Center

<sup>\*2</sup> Department of Physics, Universitas Indonesia

<sup>\*3</sup> Department of Condensed Matter Physics, Hokkaido University

<sup>\*4</sup> Faculty of Engineering, Kyushu Institute of Technology

## $\mu$ SR study of the Cu-spin correlation in the electron-underdoped $\text{Pr}_{1.3-x}\text{La}_{0.7}\text{Ce}_x\text{CuO}_{4+\delta}$ ( $x = 0.05$ ) single crystals

T. Adachi,<sup>\*1,\*2</sup> K. Kawabata,<sup>\*2</sup> S. Onishi,<sup>\*2</sup> A. Takahashi,<sup>\*3</sup> Y. Koike,<sup>\*3</sup> and I. Watanabe<sup>\*1</sup>

It has widely been believed in electron-doped high- $T_c$  cuprates with the so-called T'-structure that an antiferromagnetic (AF) order is formed in a parent compound and underdoped samples. Formerly, however, it has been reported that the superconductivity appears even in the parent compound and underdoped samples through the appropriate reduction of excess oxygen from as-grown thin films<sup>1)</sup> and polycrystals,<sup>2)</sup> resulting in a completely different phase diagram from that formerly obtained. These suggest that the superconductivity in the electron-doped cuprates cannot be understood in terms of carrier doping into Mott insulators as in the case of the hole-doped cuprates. Moreover, a raising question is whether or not the Cu-spin correlation is developed in superconducting (SC) samples.

Recently, through improved reduction annealing, we have prepared SC single crystals of the underdoped  $\text{Pr}_{1.3-x}\text{La}_{0.7}\text{Ce}_x\text{CuO}_{4+\delta}$  (PLCCO) with  $x = 0.05 - 0.10$  whose ground states had been believed to be AF.<sup>3,4)</sup> Our recent zero-field (ZF)  $\mu$ SR measurements of PLCCO with  $x = 0.10$ <sup>4,5)</sup> have revealed that, through the reduction annealing, a long-range AF order changes to a short-range one coexisting with the superconductivity. Moreover, it has been found that the further reduction brings about the destruction of the short-range AF order and the increase in the SC transition temperature  $T_c$ . However, in samples with high  $T_c$  values, the Cu-spin correlation has been found to be developed at low temperatures, suggesting the intimate relation between the developed Cu-spin correlation and superconductivity.

In order to investigate the doping dependence of the Cu-spin correlation, we have performed ZF- $\mu$ SR measurements of lightly electron-doped PLCCO with  $x = 0.05$  using a MiniCryo at RIKEN-RAL.

For the as-grown sample of  $x = 0.05$ , it has been found that a long-range AF order is formed below the Neel temperature  $T_N \sim 250$  K and  $T_N$  decreases down to  $\sim 110$  K for the moderately reduced sample. Figure 1 shows ZF- $\mu$ SR time spectra of the further reduced sample of PLCCO ( $x = 0.05$ ) with  $T_c \sim 27$  K. It is found that the spectrum at 200 K shows slow depolarization of muon spins due to nuclear dipole fields at the muon site. With decreasing temperature, the depolarization of muon spins becomes fast gradually and the muon spin precession is observed below  $\sim 100$  K,

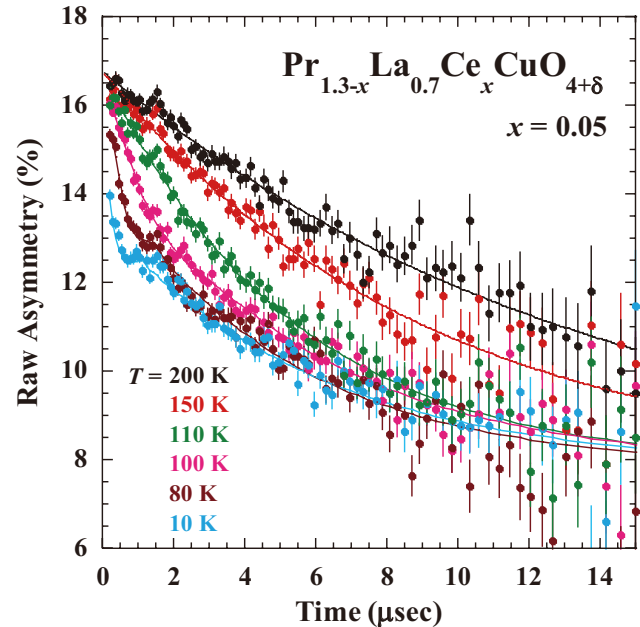


Fig. 1. Zero-field  $\mu$ SR time spectra of the further reduced  $\text{Pr}_{1.3-x}\text{La}_{0.7}\text{Ce}_x\text{CuO}_{4+\delta}$  ( $x = 0.05$ ) with  $T_c \sim 27$  K.

indicating the formation of a long-range AF order. At the lowest temperature of 10 K, however, it is found that the slow depolarization is still observed in a long-time region and the amplitude of the muon-spin precession is small, suggesting that the long-range AF ordered region is not 100% in the further reduced sample but coexists with the slowly fluctuating region of Cu spins. From the analysis of the spectra, it has been estimated that the volume fraction of a magnetically ordered region is  $\sim 25\%$  and the slowly fluctuating region exhibiting the superconductivity is  $\sim 75\%$ . These results suggest that the long-range AF order and superconductivity with a high  $T_c$  value coexist with each other in the further reduced sample of PLCCO with  $x = 0.05$ . In the ideally reduced sample of  $x = 0.05$ , the AF order would disappear and the superconductivity would appear homogeneously under the development of the Cu-spin correlation, which is probably the characteristic of the electron-doped high- $T_c$  cuprates.

### References

- 1) O. Matsumoto *et al.*, *Physica C* **469**, 924 (2009).
- 2) T. Takamatsu *et al.*, *Appl. Phys. Express.* **5**, 073101 (2012).
- 3) T. Adachi *et al.*, *J. Phys. Soc. Jpn.* **82**, 063713 (2013).
- 4) T. Adachi *et al.*, *Condens. Matter* **2**, 23 (2017).
- 5) T. Adachi *et al.*, *J. Phys. Soc. Jpn.* **85**, 114716 (2016).

<sup>\*1</sup> RIKEN Nishina Center

<sup>\*2</sup> Department of Engineering and Applied Sciences, Sophia University

<sup>\*3</sup> Department of Applied Physics, Tohoku University

## Reduction in Néel Temperature of $\text{La}_2\text{CuO}_4$ Nanoparticles

S. Winarsih,<sup>\*1,\*2</sup> F. Budiman,<sup>\*3,\*4</sup> H. Tanaka,<sup>\*3</sup> T. Goto,<sup>\*5</sup> T. Adachi,<sup>\*5</sup> B. Kurniawan,<sup>\*2</sup> B. Soegijono,<sup>\*2</sup> and I. Watanabe<sup>\*1,\*2</sup>

Recent reports on antiferromagnetic nanoparticles focus on the reduction in Néel temperature ( $T_N$ ), the emergence of superparamagnetic behavior, and the increase in the band gap value.<sup>1-3</sup> However, there is no unified research on their magnetically ordered state. The cause of  $T_N$  reduction has also not been investigated. In order to overcome this situation, a study on the magnetic properties of  $\text{La}_2\text{CuO}_4$  nanoparticles (LCO NPs) using muon spin relaxation ( $\mu\text{SR}$ ) and NMR is suggested.  $\text{La}_2\text{CuO}_4$  is a mother compound of high- $T_c$  cuprate oxides that has been well established by experiments and theoretical methods; thus, a probing nano-sized effect in this LCO system can be achieved.<sup>4</sup>

LCO NPs used in the present study were successfully obtained through the sol-gel method. A detailed explanation about sample preparation has been reported in our previous paper.<sup>5</sup> Zero-field (ZF)  $\mu\text{SR}$  on LCO NPs was carried out at RIKEN-RAL Muon Facility in the UK, using a single pulse positive surface muon beam.

ZF- $\mu\text{SR}$  time spectra of LCO NPs with a particle size of 96 nm are shown in Fig. 1. The time spectra were analyzed by using Eq. (1). The first component represents muon spin precession and the second component represents the slow relaxation behavior beyond 1  $\mu\text{s}$ . It is shown that muon spin precession does exist in LCO NPs and it disappears at 100 K. Muon spin precession indicates the formation of the long-range ordered (LRO)

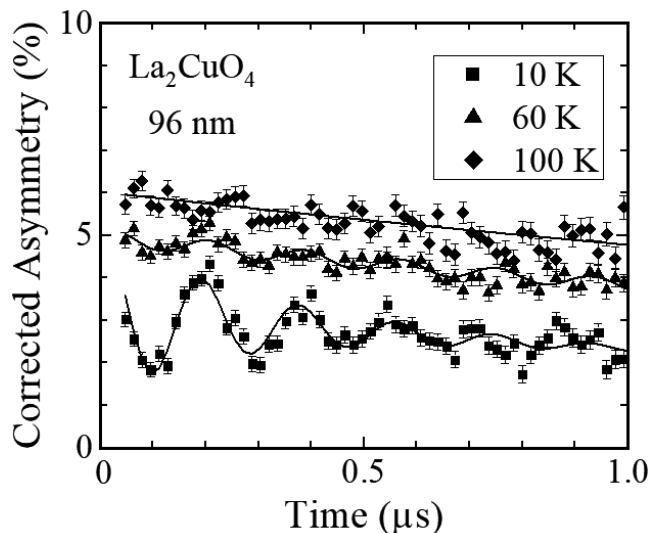


Fig. 1. ZF- $\mu\text{SR}$  time spectra of  $\text{La}_2\text{CuO}_4$  NPs with a particle size of 96 nm.

<sup>\*1</sup> RIKEN Nishina Center

<sup>\*2</sup> Department of Physics, Universitas Indonesia

<sup>\*3</sup> Department of Human Intelligence Systems, Kyushu Institute of Technology

<sup>\*4</sup> School of Electrical Engineering, Telkom University

<sup>\*5</sup> Department of Physics, Sophia University

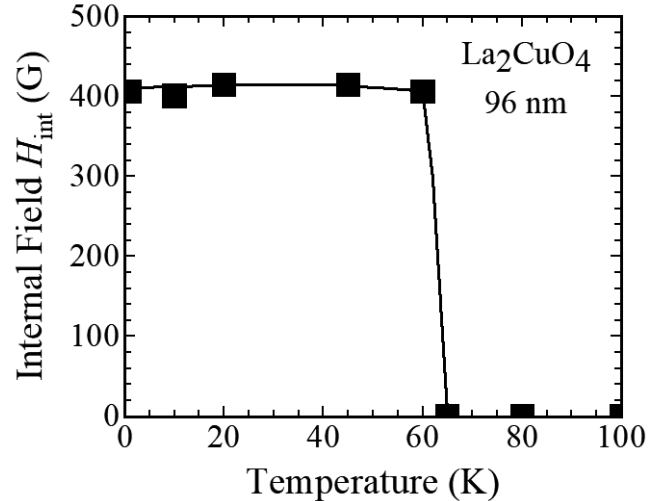


Fig. 2. Temperature dependence of the internal field at the muon site in LCO NPs with a particle size of 96 nm.

state.

$$A(t) = A_1 e^{-\lambda_1 t} \cos(\omega t + \phi) + A_2 e^{-\lambda_2 t} \quad (1)$$

Figure 2 depicts the temperature dependence of the internal field at the muon site,  $H_{\text{int}}$ , of LCO NPs with a particle size of 96 nm. It is shown that  $H_{\text{int}}$  starts to increase below  $\sim 60$  K, indicating that the  $T_N$  of this sample is  $\sim 60$  K; this is strongly suppressed compared to the bulk LCO, which has a  $T_N$  of  $\sim 320$  K.<sup>4</sup>  $H_{\text{int}}$  reaches a saturated value  $\approx 420$  G at low temperatures. This means that LCO NPs have almost the same saturated internal field value as that observed in bulk LCO.<sup>4</sup> It is concluded that the nano-sized effect causes the reduction in  $T_N$  but does not affect the internal field at the muon site. These two phenomena are also observed in a hole-doped  $\text{La}_{2-x}\text{Sr}_x\text{CuO}_4$  bulk system.<sup>6</sup> However, the resistivity of LCO NPs does not show indication of superconducting behavior. The reduction in the  $T_N$  of LCO NPs may be owing to the phase separation into fully antiferromagnetic and paramagnetic regions. Our  $^{139}\text{La}$  NMR results also show that phase separation does exist in LCO NPs. Further analysis is required to describe this phase separation so that the cause of the reduction in  $T_N$  of LCO NPs can be clearly explained.

### References

- 1) X. G. Zheng *et al.*, Phys. Rev. B **72**, 014464 (2005).
- 2) D. Caruntu *et al.*, J. Phys. D, Appl. Phys. **40**, 5801 (2007).
- 3) M. Enhessari *et al.*, Mater. Sci. Semicond. Process **16**, 1517 (2013).
- 4) J. I. Budnick *et al.*, Phys. Lett. A **124**, 1 (1987).
- 5) S. Winarsih *et al.*, Key. Eng. Mater (2019). [in press].
- 6) E. Stilp *et al.*, Phys. Rev. B **88**, 064419 (2013).

## Muon spin relaxation after hydrogen absorption-desorption process in Pd

M. Mihara,<sup>\*1,\*2</sup> H. Araki,<sup>\*3</sup> K. Shimomura,<sup>\*2,\*4</sup> W. Higemoto,<sup>\*2,\*5</sup> M. Mizuno,<sup>\*3</sup> K. Sugita,<sup>\*3</sup> Y. Tanaka,<sup>\*3</sup> Y. Kitayama,<sup>\*3</sup> D. Tomono,<sup>\*2,\*6</sup> E. Torikai,<sup>\*2,\*7</sup> W. Sato,<sup>\*8</sup> K. Ohkubo,<sup>\*3</sup> R. Murakami,<sup>\*3</sup> N. Matsuoka,<sup>\*3</sup> I. Watanabe,<sup>\*2</sup> T. Matsuzaki,<sup>\*2</sup> and R. Kadono<sup>\*2,\*4</sup>

Palladium has a unique property as a hydrogen storage material, by which it can absorb large amounts of hydrogen under ambient hydrogen gas pressure or by electrochemical charging at around room temperature.<sup>1)</sup> By using positron annihilation lifetime spectroscopy, we have found that an anomalously large amount of vacancies are formed in Pd after a hydrogen absorption-desorption process at room temperature.<sup>2,3)</sup> In addition, our recent  $\mu$ SR study on Pd has shown that in electrochemically charged Pd with hydrogen, a  $\beta$  hydride phase ( $\text{PdH}_x$ ) remains even after hydrogen desorption by degassing at room temperature.<sup>4)</sup> These results suggest that residual hydrogen atoms are possibly trapped after the desorption process due to the formation of vacancies. Although some models have been suggested, such as the formation of vacancies in a hydride phase<sup>2,3)</sup> or a vacancy-hydrogen (V-H) cluster<sup>5)</sup> in metal-hydrogen systems, no direct evidence to judge those models have been presented yet. In this report, we present the result of ZF- $\mu$ SR measurements on post-annealed  $\text{PdH}_x$  at various temperatures to clarify the microscopic property of residual hydrogen atoms in Pd.

The  $\mu$ SR experiment was performed at the RIKEN-RAL muon facility and J-PARC. The  $\text{PdH}_x$  samples were prepared by means of electrolytic charging in which a voltage was applied between Pd and Pt plates immersed in NaCl solutions. In order to minimize the time between the post-annealing and the  $\mu$ SR measurement, an equipment consisting of an electric furnace and a glass tube connected to a vacuum pump was prepared beside the  $\mu$ SR experimental port. The post-annealing was done for 1 h just before the  $\mu$ SR measurement, and the amount of removed hydrogen by the post-annealing process was deduced from the weight difference.

The ZF- $\mu$ SR spectra for each sample were well explained by a combination of a dynamic Gaussian Kubo-Toyabe (DKT) function and a nearly non-relaxing component.<sup>4)</sup> Figure 1 shows a typical result of the asymmetry of the relaxing DKT component and the

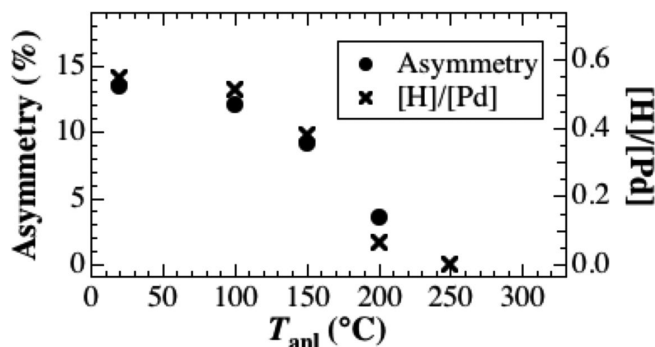


Fig. 1. Post-annealing temperature dependence of asymmetry for ZF- $\mu$ SR in  $\text{PdH}_x$  and hydrogen content.

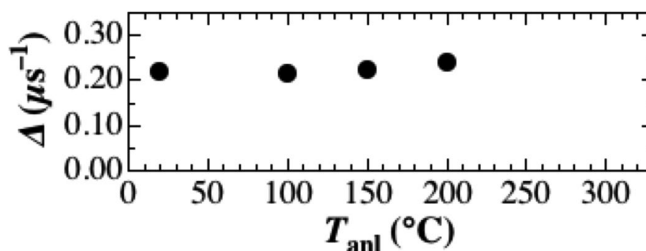


Fig. 2. Post-annealing temperature dependence of field distribution width for ZF- $\mu$ SR in  $\text{PdH}_x$ .

amount of hydrogen content in Pd as a function of the post-annealing temperature. This shows that hydrogen in  $\text{PdH}_x$  is stable up to about 100°C and is mostly removed at around 200°C, and the asymmetry follows almost the same annealing temperature dependence with the hydrogen content. The values of field distribution width  $\Delta$  for the DKT function are nearly constant and independent of the annealing temperature, as shown in Fig. 2. The present result suggests that the residual hydrogen keeps a  $\beta$  hydride phase in which hydrogen atoms stay closely together like a cluster at a trap site and are released from Pd once such a hydrogen cluster is dissociated.

\*1 Department of Physics, Osaka University

\*2 RIKEN Nishina Center

\*3 Division of Materials and Manufacturing Science, Osaka University

\*4 IMSS, KEK

\*5 JAEA

\*6 RCNP, Osaka University

\*7 University of Yamanashi

\*8 Kanazawa University

### References

- 1) B. D. Adams, A. Cheni, *Materialstoday* **14**, 282 (2011).
- 2) K. Sakaki *et al.*, *Mat. Trans.* **43**, 2652 (2002).
- 3) K. Sakaki *et al.*, *J. Alloys Comp.* **414**, 204 (2006).
- 4) M. Mihara *et al.*, *JPS Conf. Proc.* **21**, 011031 (2018).
- 5) Y. Fukai, H. Sugimoto, *J. Phys. Condens. Matt.* **19**, 436201 (2007).

# Negative muon spin rotation with low-density gas target under transverse magnetic field to solve the proton radius puzzle

S. Kanda,<sup>\*1</sup> K. Ishida,<sup>\*2</sup> M. Iwasaki,<sup>\*1,\*2</sup> Y. Ma,<sup>\*1,\*2</sup> S. Okada,<sup>\*1</sup> and M. Sato<sup>\*3</sup>

When a negative muon is captured by a nuclear Coulomb potential, an electron around the nuclei is kicked out and the muon forms an exotic bound state called muonic atom. Muonic atom provides a unique opportunity to study the nuclear structure such as the charge radius of the nuclei. In particular, the proton charge radius attracts renewed interest since the measurement of the Lamb shift in muonic hydrogen.<sup>1)</sup> The experiment derived a significantly discrepant result compared to the results of electron-proton scattering and hydrogen spectroscopy. This discrepancy has been an important unsolved problem in sub-atomic physics.

To obtain a new insight into the puzzle, a new measurement of the ground-state hyperfine splitting (HFS) in muonic hydrogen is planned. The experiment aims to determine the proton Zemach radius, which is defined as a convolution of the electric charge and magnetic moment distributions. As a preliminary experiment toward the spectroscopy of HFS, a muon spin rotation ( $\mu$ SR) measurement with a gaseous hydrogen target was proposed.<sup>2)</sup> The objective of the experiment was to understand the spin depolarization process involving the muonic hydrogen atom.

In a magnetic field, muon spin rotates with the Larmor frequency, which depends on the hyperfine state of muonic atom. Therefore, we can quantify the population of the hyperfine states and the depolarization effect by measuring the angular asymmetry of decay electrons.

Figure 1 illustrates the experimental setup at Port4

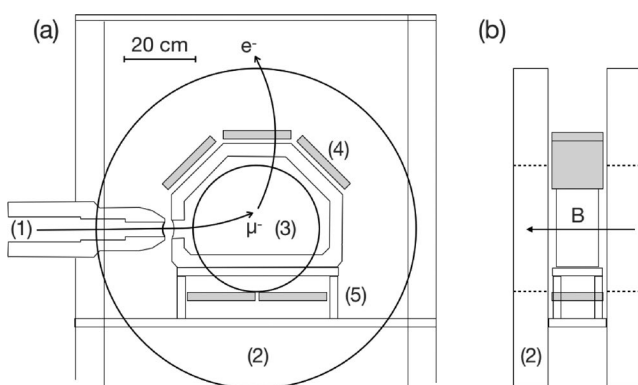


Fig. 1. Experimental setup: (a) cross-sectional view; (b) view from downstream. The numbers in the parentheses denote: (1) negative pulsed muon beam, (2) Helmholtz coils, (3) aluminium gas chamber, (4) top electron detectors, and (5) bottom electron detectors.

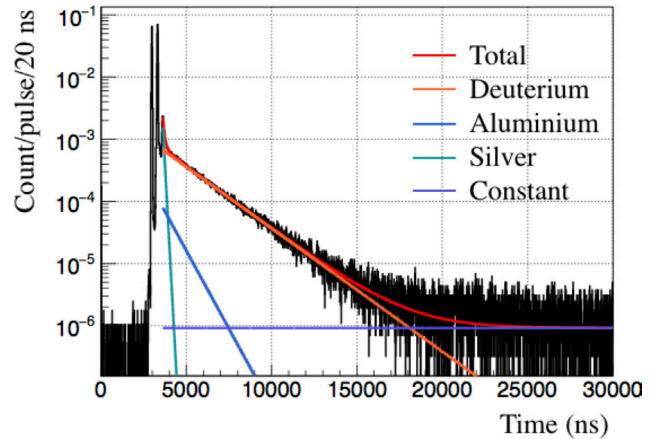


Fig. 2. Decay electron time spectrum with deuterium gas target at 1 atm. No magnetic field was applied. Each line corresponds to the respective fitting result.

in RIKEN-RAL muon facility. A transverse magnetic field was applied using the coils, which are parts of the CHRONUS spectrometer. Decay electrons from the muonic atoms were detected by the segmented scintillation counters with silicon photomultiplier (SiPM) readout. The detectors were originally developed for the muonium production experiment at Port3.<sup>3)</sup> A study conducted in 2016<sup>4)</sup> revealed that a countermeasure for the background arising from the duct-streaming neutrons is essential for sufficient signal-to-noise ratio. Accordingly, the detectors were placed away from the beam axis. The inner walls of the target chamber were covered with silver plates to reduce the lifetime of wall-stopped muons via nuclear capture.

The experiment was conducted in 2018 with a gaseous deuterium target to establish the measurement procedure. Deuterium was selected owing to its longer-lifetime of polarization instead of protium. Figure 2 shows a measured time spectrum of electrons from the muon decays. The spectrum was analyzed using a fitting function containing three exponential components and a constant background. Each exponential component corresponded to the muon lifetime in silver (87 ns), aluminium (864 ns), and deuterium (2195 ns). The beam momentum was optimized at several target densities considering the muonic hydrogen yield. The analysis for the  $\mu$ SR measurement under the transverse magnetic field is in progress.

## References

- 1) R. Pohl *et al.*, *Nature* **466**, 213 (2010).
- 2) S. Kanda *et al.*, *J. Phys. Conf. Ser.* **1138**, 012009 (2018).
- 3) S. Okada *et al.*, *RIKEN Accel. Prog. Rep.* **50**, 244 (2016).
- 4) M. Sato *et al.*, *RIKEN Accel. Prog. Rep.* **51**, 228 (2017).

<sup>\*1</sup> RIKEN Cluster for Pioneering Research

<sup>\*2</sup> RIKEN Nishina Center

<sup>\*3</sup> High Energy Accelerator Research Organization (KEK)

# Measurement of total muonium emission yield from silica aerogel using $\mu$ SR method

K. Ishida,<sup>\*1</sup> K. Suzuki,<sup>\*2</sup> M. Iwasaki,<sup>\*1,\*3</sup> S. Kanda,<sup>\*3</sup> S. Okada,<sup>\*4</sup> T. Mibe,<sup>\*5</sup> Y. Oishi,<sup>\*6</sup> A. Olin,<sup>\*7</sup> S. Kamal,<sup>\*8</sup> and J. Brewer<sup>\*8</sup>

We are working towards the development of producing slow muon beams, as a source of the accelerated cold muon beam, to be used for the muon g-2/EDM measurement planned at J-PARC.<sup>1)</sup> We observed at TRIUMF that the muonium ( $\text{Mu} = \mu^+e^-$ ) emission rate from silica aerogel to vacuum is enhanced by surface ablation.<sup>2,3)</sup> By ionizing the muonium with an intense laser, high intensity slow muon source can be obtained. However, the present muonium yield measurement by tracking of the muon decay positron is limited to a region away ( $\sim 5$  mm) away from the surface owing to the large background from the muoniums decaying in aerogel, whereas we plan to ionize muoniums in the vacuum region less than 5 mm from the surface because most of the muoniums emitted are expected to stay there. Although we can extrapolate the measured muonium yield to the region closer to the surface with modeling, it is much preferable if we can get the information directly.

We performed a new measurement using a completely different method, muonium spin rotation (MuSR) under applied magnetic field ( $\sim 0.22$  mT). The muonium precession is kept during its diffusion in aerogel and even after its emission to vacuum. Here, if we put a metallic foil such as gold attached to the aerogel surface, the muonium entering the metal will become diamagnetic and the muonium precession will stop. This will decrease the precession amplitude with the time after muon beam injection and can be observed as the relaxation in  $\mu$ SR spectra. For example, if 10% of the formed muonium has reached the foil by a given time, the precession amplitude should decrease to 90%. Thus, the precession spectrum gives us information on the timing distribution of the muoniums reaching the foil.

We set an aerogel sample with a gold foil stacked at the downstream surface in the ARGUS  $\mu$ SR spectrometer at the RIKEN-RAL Muon Facility. First, we set the muon beam momentum to stop the muons in the middle of the aerogel and measured the intrinsic muonium spin relaxation. The relaxation ( $0.0389$  ( $11$ )  $\mu\text{s}^{-1}$ ) was subtracted as the background in all the following measurements. Then, we set the momentum

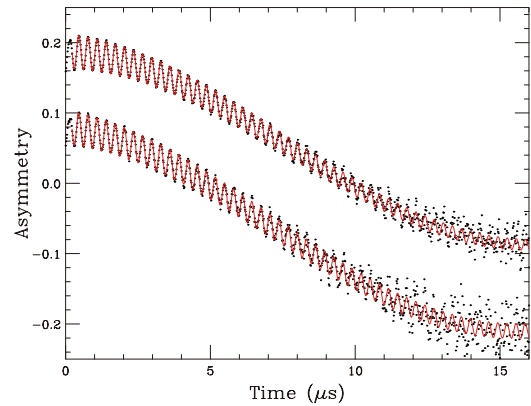


Fig. 1. MuSR spectra under 0.22 mT with muons stopping near the downstream surface of silica aerogel with the gold foil placed at 0 mm (above) and 20 mm (bottom) from the surface. The precession signal with approximately 100 times the period of muonium is due to the diamagnetic muons that did not form muonium.

to ensure that the muon stopping distribution peaked at the downstream surface edge of the aerogel, thereby contributing to the largest muonium emission probability. In this half stopping condition, it is evident that the muonium precession relaxes faster, indicating the gradual loss of muoniums due to transfer to the gold foil. MuSR measurement was also performed for different foil distances (10 and 20 mm) to obtain detailed timing and space information on muonium distribution in vacuum.

The MuSR spectra with the gold foil at 0 mm and 20 mm are compared in Fig. 1. The initial muonium precession amplitude was approximately 2.5% in both cases and the relaxation rates after subtracting the background rate were  $0.0355$  ( $20$ )  $\mu\text{s}^{-1}$  and  $0.0146$  ( $31$ )  $\mu\text{s}^{-1}$ , respectively. The result can be understood by considering the different timing distribution of the muoniums reaching the foil. A detailed analysis to extract the muonium emission rate and timing from the relaxation spectra is in progress.

## References

- 1) M. Abe *et al.*, Prog. Theor. Exp. Phys. **2019**, 053C02 (2019).
- 2) P. Bakule *et al.*, Prog. Theor. Exp. Phys. **2013**, 103C01 (2013).
- 3) G. A. Beer *et al.*, Prog. Theor. Exp. Phys. **2014**, 091C01 (2014).

\*1 RIKEN Nishina Center

\*2 Department of Physics, Nagoya University

\*3 Meson Science Laboratory, RIKEN

\*4 Atomic, Molecular and Optical Physics Laboratory, RIKEN

\*5 IPNS, KEK

\*6 IMSS, KEK

\*7 TRIUMF

\*8 University of British Columbia



### **3. Radiochemistry and Nuclear Chemistry**



## Extraction behavior of rutherfordium as a cationic fluoride complex with a TTA chelate extractant from HF/HNO<sub>3</sub> acidic solutions<sup>†</sup>

A. Yokoyama,<sup>\*1</sup> Y. Kitayama,<sup>\*2</sup> Y. Fukuda,<sup>\*2</sup> H. Kikunaga,<sup>\*3</sup> M. Murakami,<sup>\*4</sup> Y. Komori,<sup>\*4</sup> S. Yanou,<sup>\*4</sup> H. Haba,<sup>\*4</sup> K. Tsukada,<sup>\*5</sup> and A. Toyoshima<sup>\*5</sup>

Rutherfordium (Rf) has atomic number 104 and is the lightest among the transactinide, or superheavy, elements. The element is positioned as a homologue in group 4 of the Periodic Table of elements, which is predicted to be in the 6d transition series. The chemical properties of such elements have attracted much attention because of possible deviations from those of their homologs as a result of enhancement of the relativistic effect for heavy elements. It was found difficult that the characterization is performed based on one-atom-at-a-time chemistry for their low production rates and short half-lives.

In the present study, we used reversed-phase chromatography with 2-thenoyltrifluoroacetone (TTA) as a chelating extractant to clarify the chemical properties of the cationic fluoride complexes of the superheavy element Rf. Unlike previous studies with cation-exchange resins, the use of TTA enables preferential extraction of metal ions in group 4, therefore the specific complex formation constant of Rf can be determined. The experiments were performed at various HF/0.01 M HNO<sub>3</sub> concentrations, with a newly developed resin containing a solution of TTA in n-octanol. Fluoride complexation with Rf was investigated by extraction with TTA, which is sensitive to the valence of the metal complex. The Rf behavior was compared with those of Zr and Hf.

In the chromatography experiments with TTA, 222  $\alpha$ -events, including formation of 29 time-correlated  $\alpha$ -particle pairs (8.00–8.40 MeV) from <sup>261</sup>Rf and its daughter nuclide <sup>257</sup>No, were observed in 1771 cycles. The %ads values for Rf were constant at around 60% in the [F<sup>-</sup>]<sub>eq</sub> range up to 5 × 10<sup>-4</sup> M and then steeply decreased at [F<sup>-</sup>]<sub>eq</sub> = 9 × 10<sup>-4</sup> M. In contrast, the value for Hf decreased significantly from 100% to a few percent at around [F<sup>-</sup>]<sub>eq</sub> = 1 × 10<sup>-4</sup> M. This is in good agreement with the results of the Zr and Hf experiments. This suggests that the cationic fluoride complexes of Rf are more stable than those of Hf at [F<sup>-</sup>]<sub>eq</sub> > 1 × 10<sup>-4</sup> M. Differences among fluoride species formation with Rf and its homologs are

therefore clearly observed in these [F<sup>-</sup>]<sub>eq</sub> ranges.

Decay of No was taken into account in correction of the %ads values. The %ads values for <sup>255</sup>No as a function of [F<sup>-</sup>]<sub>eq</sub> in the range 1.93 × 10<sup>-5</sup> to 1.66 × 10<sup>-3</sup> M were obtained in the study. In the Rf experiments, the %ads values for <sup>261</sup>Rf were constant, at around 60%, in the [F<sup>-</sup>]<sub>eq</sub> range up to 5 × 10<sup>-4</sup> M and then steeply decreased at [F<sup>-</sup>]<sub>eq</sub> = 9 × 10<sup>-4</sup> M. In contrast, in the No experiments, the %ads values for <sup>255</sup>No were less than 10% across the entire range of [F<sup>-</sup>]<sub>eq</sub>. The results of the present work confirm that No is adsorbed on TTA to a small extent and the effect on the %ads values of <sup>261</sup>Rf is negligible.

The obtained *K<sub>d</sub>* values for Rf are compared with those for Zr and Hf from the independent experiments in the present study. The result shows significant differences between the behavior of Rf and those of its homologs. The *K<sub>d</sub>* values for Rf appear at higher F<sup>-</sup> concentrations than those for Zr and Hf. Assuming that during extraction Rf forms species with TTA, similarly to the other elements in group 4, the decrease in extraction may be caused by additional cationic fluoride complexation. The *K<sub>d</sub>* results show that the cationic complex of Rf, [RfF]<sup>3+</sup>, is more stable than those of the other elements at high fluoride concentrations. This stability means that fluoride complexation with the extracted Rf species is weaker than in the cases of the other elements. This conclusion is consistent with the experimental results obtained with a cation-exchange resin.

In conclusion, the adsorption behaviors of Rf, Zr, and Hf with a TTA extractant were observed in dilute solutions of HF and HNO<sub>3</sub>. The behaviors of the No atoms produced in the decay of Rf were determined with <sup>255</sup>No nuclides produced in runs other than the Rf experiments to assess the precise behavior of Rf, without the effects of its daughters. The results of the present study suggest that the chemical species involved in TTA extraction may be [RfF]<sup>3+</sup>, based on comparisons with the results for Zr and Hf. It was concluded that fluoride complexation with Rf cations is weaker than that with either Zr or Hf, which are group 4 homologs. The observed behavior of Rf is supported by theoretical calculations and agrees with the results of previous experiment on cation exchange. This study is the first comparison of complexation data for Rf cations with those for Zr and Hf, other than those based on cation-exchange experiments.

<sup>†</sup> Condensed from *Radiochim. Acta* **107** (1), 27 (2019)

<sup>\*1</sup> Institute and College of Science and Engineering, Kanazawa University

<sup>\*2</sup> Graduate School of Natural Science and Technology, Kanazawa University

<sup>\*3</sup> Research Center for Electron Photon Science, Tohoku University

<sup>\*4</sup> RIKEN Nishina Center

<sup>\*5</sup> Advanced Science Research Center, Japan Atomic Energy Agency

## Coprecipitation experiment of element 102, No, with $\text{Sm}(\text{OH})_3$ using $\text{NH}_3$ and $\text{NaOH}$ solution

H. Ninomiya,<sup>\*1</sup> Y. Kasamatsu,<sup>\*1</sup> S. Hayami,<sup>\*2</sup> M. Nagase,<sup>\*2</sup> Y. Shigekawa,<sup>\*1</sup> N. Kondo,<sup>\*1</sup> E. Watanabe,<sup>\*1</sup> H. Haba,<sup>\*3</sup> T. Yokokita,<sup>\*3</sup> Y. Komori,<sup>\*3</sup> D. Mori,<sup>\*3</sup> Y. Wang,<sup>\*3</sup> K. Ghosh,<sup>\*3</sup> N. Sato,<sup>\*3</sup> and A. Shinohara<sup>\*1</sup>

Heavy elements are expected to have the characteristic chemical properties in the periodic table owing to significant relativistic effects on their orbital electrons. From the previous cation-exchange studies on element 102, nobelium (No) in HCl, the most stable ion valency of No in aqueous solution is reported to be +2, although that of other heavy actinide elements is +3.<sup>1,2)</sup> However, it is difficult to investigate the chemical behavior of heavy elements. Heavy elements with  $Z \geq 101$  are synthesized by heavy-ion-induced nuclear reactions with very low production rates and their half-lives are short.<sup>3)</sup> Thus, the chemical experiments of these elements must be rapidly conducted on one-atom-at-a-time basis using nuclear reaction products transported from the target chamber by a He/KCl gas-jet system. Additionally, for unambiguous identification of a single atom, detection of  $\alpha$  particle is required. Owing to these difficulties, there are a few reports on solution chemical experiments of No. In the tri-n-octylamine chloride extraction system and cation-exchange experiment in HCl, the elution behavior of No was reported to be similar to that of alkaline earth metals.<sup>4)</sup> To deepen the understanding of the chemical properties of No, we aim at investigating a precipitation of nobelium hydroxide.

In previous studies, we newly developed coprecipitation method with samarium hydroxide to investigate the hydroxide and ammine complexation properties of heavy elements.<sup>5)</sup> Then, we succeeded in conducting the coprecipitation experiment of element 104, Rf, in  $\text{NH}_3$  and  $\text{NaOH}$  solutions using the developed suction filtration apparatus. In this study, by applying the coprecipitation method, we performed online coprecipitation experiment of  $^{255}\text{No}$  to investigate the precipitation behavior of nobelium hydroxide.

We produced  $^{255}\text{No}$  ( $T_{1/2} = 186$  s) and  $^{162}\text{Yb}$  ( $T_{1/2} = 18.9$  min) by  $^{248}\text{Cm}(^{12}\text{C}, 5n)^{255}\text{No}$  and  $^{\text{nat}}\text{Gd}(^{12}\text{C}, xn)^{162}\text{Yb}$  reactions with AVF cyclotron at RIKEN. The reaction products were transported by the He/KCl gas-jet system to the chemistry room and dissolved in dilute HCl solution. In the case of making precipitated sample, 20  $\mu\text{g}$  of Sm and 2 mL of the basic solution (dilute or concentrated aqueous  $\text{NH}_3$  or 0.10 or 1.0 M  $\text{NaOH}$  solution) was added into the dissolved solution in the PP beaker and stirred for 5 min at room temperature. Then, the solution containing the precipitate was filtrated using the suction filtration appara-

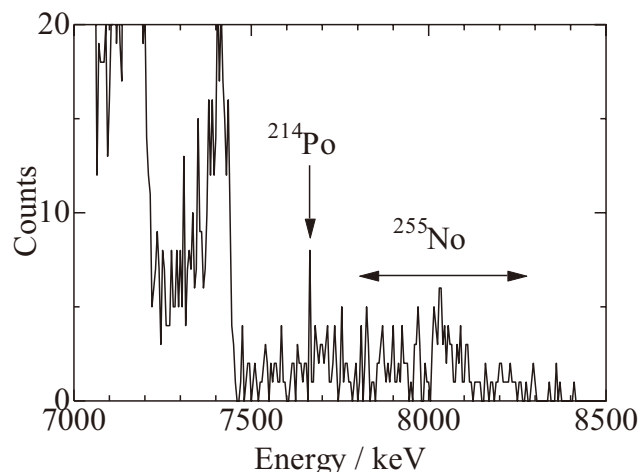


Fig. 1.  $\alpha$ -spectra for  $^{255}\text{No}$  standard samples.

tus controlled by PC. In the case of making standard sample, the reaction products were dissolved in dilute HCl solution and the solution was put on a Ta plate. Then, these precipitated and standard samples were dried and subjected to alpha particle measurement by the automated rapid  $\alpha/\text{SF}$  detection system. After alpha particle measurement,  $\gamma$ -ray activities of  $^{162}\text{Yb}$  in the samples were measured with Ge detectors.

We successfully prepared 51 coprecipitated samples and 48 standard samples. In the alpha-particle measurement (Fig. 1), we detected 243 events for  $^{255}\text{No}$ . The cross-section of  $^{255}\text{No}$  was estimated to be approximately 450 nb and the value was consistent with that obtained in the previous report.<sup>6)</sup> High precipitation yields of No were obtained and the detailed evaluation is now under analysis.

In future, we will discuss the hydroxide complexation properties of  $^{255}\text{No}$  based on the comparison of the coprecipitation behavior of  $^{255}\text{No}$  with those of alkaline earth metal elements.

### References

- 1) J. Maly, T. Sikkeland, R. Silva, A. Ghiorso, *Science* **160**, 1114–1115 (1963).
- 2) G. T. Seaborg, in *The Transuranium Elements*, (McGraw-Hill, New York, 1949).
- 3) M. Schädel, *Radiochim. Acta* **100**, 579 (2012).
- 4) R. J. Silva, W. J. Mcdowell, O. L. Keller, *et al.*, *J. Inorg. Nucl. Chem.* **38**, 1207–1210 (1976).
- 5) Y. Kasamatsu, *et al.*, *Appl. Radiat. Isot.* **118**, 105–116 (2016).
- 6) T. Sikkeland, A. Ghirso, M. J. Nurmi, *Phy. Rev.* **172**, 1232–1238 (1968).

\*1 Graduate School of Science, Osaka University

\*2 Faculty of Science, Osaka University

\*3 RIKEN Nishina Center

## Complex formation of Fr with crown ethers

Y. Komori,<sup>\*1</sup> H. Haba,<sup>\*1</sup> T. Yokokita,<sup>\*1</sup> S. Yano,<sup>\*1</sup> N. Sato,<sup>\*1</sup> K. Ghosh,<sup>\*1</sup> Y. Sakemi,<sup>\*2</sup> and H. Kawamura<sup>\*3</sup>

Francium (Fr) is the heaviest known alkali metal with atomic number 87. It is one of the least-studied elements among the naturally occurring elements because all its isotopes are short-lived. The half-life of its longest-lived isotope,  $^{223}\text{Fr}$ , is only  $T_{1/2} = 21.8$  min. Owing to experimental difficulties, the chemical properties of Fr have not been studied in detail so far. We aim to clarify the chemical bonding nature of Fr, which is influenced by relativistic effects, through complex formation studies of Fr. Recently, Haverlock *et al.* examined the complex formation of  $\text{Fr}^+$  with calix[4]arene-bis(benzocrown-6) (BC6B).<sup>1)</sup> They reported that  $\text{Fr}^+$  is more effectively extracted with BC6B than  $\text{Cs}^+$ . However, the reason for the selectivity is still unclear. In this work, we studied the complex formation of Fr using seven types of crown ethers: 18-crown 6-ether (18C6), dicyclohexano-18-crown 6-ether (DC18C6), dibenzo-18-crown 6-ether (DB18C6), 24-crown 8-ether (24C8), dibenzo-24-crown 8-ether (DB24C8), 21-crown 7-ether (21C7), and dibenzo-21-crown 7-ether (DB21C7). Complex formation stability and selectivity of alkali metals with the crown ethers depend on the ring cavity size and substituent groups of the crown ethers. Therefore, in this work, we will investigate the effects of the cavity size and substituent groups of the crown ethers on the stability and selectivity of the complex formation of Fr.

We produced the second longest-lived isotope of Fr,  $^{212}\text{Fr}$  ( $T_{1/2} = 20$  min), in the  $^{206}\text{Pb}(^{11}\text{B}, 5n)^{212}\text{Fr}$  reaction. Four sets of an  $864\text{-}\mu\text{g}/\text{cm}^2$   $^{206}\text{Pb}$  target on a  $10\text{ }\mu\text{m}$  Be foil were placed in a 12 mm spacing in 129-kPa He. They were irradiated with a  $^{11}\text{B}$  beam at an energy of 86 MeV. The beam energies on the four  $^{206}\text{Pb}$  targets are calculated to be in the range of 70–79 MeV, which covers the peak region of the excitation function of the  $^{206}\text{Pb}(^{11}\text{B}, 5n)^{212}\text{Fr}$  reaction.<sup>2)</sup> The  $^{212}\text{Fr}$  atoms that recoiled out of the  $^{206}\text{Pb}$  target were thermalized in He gas, attached to KCl aerosol particles, and transported through a Teflon capillary to a chemistry laboratory. In the chemistry laboratory, the aerosols were collected on a piece of Naflon sheet for 20 s. The aerosols were dissolved with  $100\text{ }\mu\text{L}$  of 1 M nitric acid and transferred into a polypropylene (PP) tube. Another  $600\text{ }\mu\text{L}$  of 1 M  $\text{HNO}_3$  and  $700\text{ }\mu\text{L}$  of nitrobenzene containing each of the crown ethers were then added into the PP tube. The PP tube was shaken for a certain time for extraction. After centrifuging the PP tube for 2 min,  $500\text{ }\mu\text{L}$  of each phase was subjected to  $\gamma$ -ray spectrometry to determine the distribution ratios ( $D$ ) of Fr. The  $D$  values were measured as functions of the shaking time and the concentration of each crown ether. These results were compared with those of RIs of lighter alkali metals such as  $^{24}\text{Na}$ ,  $^{43}\text{K}$ , and  $^{137}\text{Cs}$ .

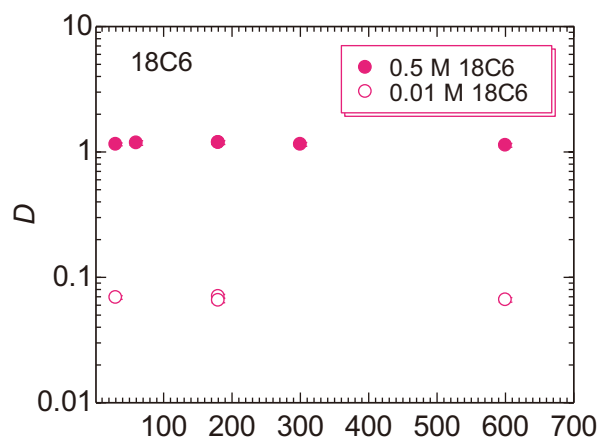


Fig. 1. Variations of  $D$  values of  $\text{Fr}^+$  as a function of shaking time in solvent extraction with 0.01 and 0.5 M 18C6.

Figure 1 shows the variation of the  $D$  values of  $\text{Fr}^+$  as a function of the shaking time in the solvent extraction with 0.01 and 0.5 M 18C6. We found that the extraction equilibrium time of  $\text{Fr}^+$  is as fast as within 30 s. Therefore, we fixed the shaking time to be 3 min. The 18-membered rings, with a cavity diameter of  $2.6\text{--}3.2\text{ }\text{\AA}$ ,<sup>3)</sup> show the highest affinity for  $\text{K}^+$  because their cavity sizes fit the size of  $\text{K}^+$  ion (ionic diameter:  $2.66\text{ }\text{\AA}$ ).<sup>4)</sup> The cavity diameter of the 24-membered crowns is in the range of  $4.5\text{--}5.0\text{ }\text{\AA}$ ,<sup>5)</sup> which is larger than all alkali metal ions. Thus, they show affinity for larger alkali metal ions such as  $\text{Cs}^+$  ( $3.34\text{ }\text{\AA}$ )<sup>4)</sup> and  $\text{Fr}^+$  ( $3.46\text{ }\text{\AA}$ ).<sup>6)</sup> The cavity diameter of 21-membered crowns is in the range of  $3.4\text{--}4.3\text{ }\text{\AA}$ .<sup>3)</sup> When using DB21C7, the  $D$  values of  $\text{Cs}^+$  are slightly larger than those of  $\text{Fr}^+$ , while the  $D$  values of  $\text{Cs}^+$  and  $\text{Fr}^+$  are almost the same when using 21C7. Two benzene rings of DB21C7 may affect the selectivity between  $\text{Cs}^+$  and  $\text{Fr}^+$ .

In this work, the  $D$  values of  $\text{Fr}^+$  with several types of crown ethers are almost the same as those of  $\text{Cs}^+$ , which can be qualitatively understood by the relation between the size of the alkali metal ions and the ring cavity diameter of the crown ethers. However, in the previous study using calixarene, the  $D$  values of  $\text{Fr}^+$  are almost one order of magnitude higher than those of  $\text{Cs}^+$ .<sup>1)</sup> To interpret these results and elucidate the reason of complex formation selectivity between  $\text{Fr}^+$  and  $\text{Cs}^+$ , we will perform further investigations, for example, XAFS studies of the  $\text{Cs}^+$ -crown ether and  $\text{Cs}^+$ -calixarene complexes, and quantum chemistry calculations for  $\text{Fr}^+$  as well as  $\text{Cs}^+$ .

### References

- 1) T. J. Haverlock *et al.*, *J. Am. Chem. Soc.* **125**, 1126 (2003).
- 2) Y. Komori *et al.*, *RIKEN Accel. Prog. Rep.* **51**, 224 (2018).
- 3) C. J. Pedersen, *J. Am. Chem. Soc.* **92**, 386 (1970).
- 4) L. H. Ahrens, *Geochim. Cosmochim. Acta* **2**, 155 (1952).
- 5) M. Chamsaz, *Russ. J. Inorg. Chem.* **50**, 413 (2005).
- 6) L. H. Delmau *et al.*, *J. Phys. Chem. B* **117**, 9258 (2013).

<sup>\*1</sup> RIKEN Nishina Center

<sup>\*2</sup> Center for Nuclear Study, the University of Tokyo

<sup>\*3</sup> Frontier Research Institute for Interdisciplinary Sciences, Tohoku University

## Anion and cation exchange of Pa in HF/HCl mixture solution for Db chemistry

T. Yokokita\*<sup>1</sup> and H. Haba\*<sup>1</sup>

Clarifying the chemical properties of superheavy elements with atomic number  $Z \geq 104$  is an intriguing and important subject. These elements are produced at accelerators using heavy-ion-induced nuclear reactions. The production rates of these elements are low, and their half-lives are short ( $T_{1/2} \leq 1$  min). Thus, chemical studies on these elements are conducted on a single-atom basis.<sup>1)</sup>

$F^-$  ion is a very strong complexing agent for the group-5 elements (Nb and Ta). The fluoride complex species of the heaviest group-5 element, dubnium (Db), is very interesting (Db forms  $[DbOF_x]^{n-}$  or  $[DbF_x]^{n-}$ ) because Nb and Ta form different fluoride complexes (Nb:  $[NbOF_5]^{2-}$ ; Ta:  $[TaF_7]^{2-}$ ) in 0.1–10 M HF ( $[F^-] = 8.9 \times 10^{-3} - 1.9 \times 10^{-2}$  M).<sup>2)</sup> To determine the fluoride complex species of Db, we plan to perform an ion-exchange study of Db. In this study, we performed anion- and cation-exchange experiments of Pa (pseudo homologue of Db) in HF/HCl mixture solution to determine the suitable experimental condition of Db and obtain comparable data for Db.

<sup>233</sup>Pa was obtained as an  $\alpha$ -decay daughter of <sup>237</sup>Np in the following procedure. First, <sup>237</sup>Np in 9 M HCl containing <sup>233</sup>Pa was fed onto the TK400 resin's (TRISKEM) column. <sup>237</sup>Np was then eluted with 9 M HCl and <sup>233</sup>Pa was adsorbed on the resin. The adsorbed <sup>233</sup>Pa species was eluted with 1 M HCl. The eluent containing the Pa tracers was evaporated and dissolved in 9 M HCl. Then, Pa nuclide was purified by anion-exchange column chromatography using a procedure found in Ref. 3).

In the anion-exchange experiments, the anion-exchange resin (MCI GEL CA08Y) was added in 0.25 mL of HF/HCl mixture solution containing <sup>233</sup>Pa in a PP tube and the mixture was shaken using a mixer. Next, the resin was removed by centrifugation. Subsequently, the filtrate was pipetted into another tube, weighed, and subjected to  $\gamma$ -ray spectrometry using a Ge detector. The concentration of HF and HCl was determined by titration with standardized NaOH solution before the experiments. In all anion-exchange experiments, control exper-

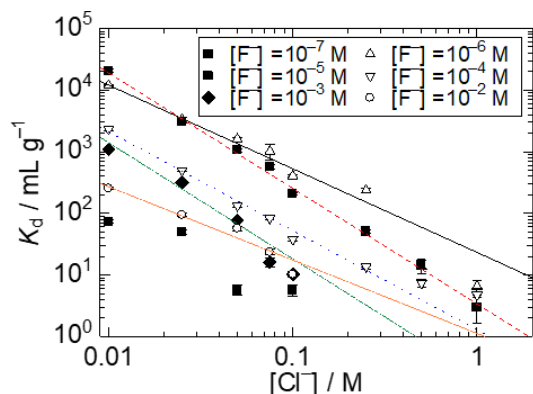


Fig. 1.  $K_d$  values of Pa in anion exchange as a function of  $Cl^-$  concentration.

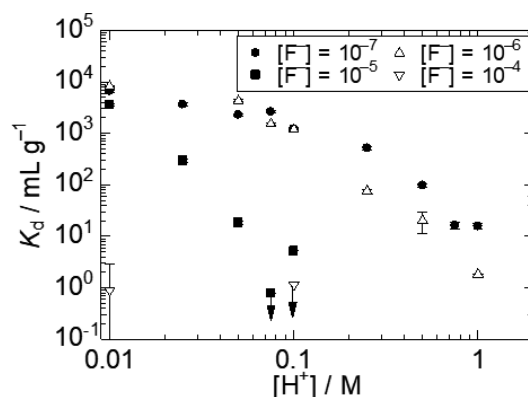


Fig. 2.  $K_d$  values of Pa in cation exchange as a function of  $H^+$  concentration.

iments without the resin were performed. We also performed cation-exchange experiments of Pa using a cation-exchange resin (MCI GEL CK08Y). The experimental procedures were the same as the anion-exchange experiments. The  $K_d$  values were determined from the following equation:

$$K_d = A_r V_s / A_s w_r = (A_c - A_s) V_s / A_s w_r \quad (1)$$

where  $A_r$  and  $A_s$  are the radioactivities on the resin and in the solution, respectively,  $V_s$  is the volume (mL) of the solution, and  $w_r$  is the mass (g) of the dry resin.  $A_c$  denotes the radioactivity of the control solution.

The  $K_d$  values of Pa as a function of  $Cl^-$  concentration in the anion-exchange experiment are shown in Fig. 1. In anion exchange, the  $K_d$  values of Pa linearly decrease with increasing concentration of  $Cl^-$  in  $[F^-] = 10^{-6} - 10^{-2}$  M. These results indicate that Pa forms anionic complexes in the studied conditions. The slope values between  $\log K_d$  and  $\log [Cl^-]$  are  $-1.4$ ,  $-1.9$ ,  $-1.6$ ,  $-1.9$ , and  $-1.2$  in  $[F^-] = 10^{-6}$ ,  $10^{-5}$ ,  $10^{-4}$ ,  $10^{-3}$ , and  $10^{-2}$  M, respectively. These results indicated that the net charge of the adsorbed Pa species are  $-2$  and  $-1$ .

The  $K_d$  values of Pa as a function of  $H^+$  concentration in the cation-exchange experiment are shown in Fig. 2. The  $K_d$  values of Pa were  $> 10^3$  mL  $g^{-1}$  and Pa was adsorbed on the resin in  $[F^-] = 10^{-7} - 10^{-5}$  M and  $[H^+] = 0.01$  M. These results indicate that Pa forms cationic species in these  $F^-$  concentrations. The linear relation between  $\log K_d$  and  $\log [H^+]$  is not obtained. It is suggested that some cationic Pa species coexist and/or Pa forms chloride complexes.

Recently, we produced <sup>95</sup>Nb and <sup>179</sup>Ta (homologues of Db) in the  $^{nat}Zr(d, xn)^{95}Nb$  and  $^{nat}Hf(d, xn)^{179}Ta$  reactions, respectively. We plan to study anion- and cation-exchange behavior of Nb and Ta in HF/HCl using these tracers for Db chemistry.

### References

- 1) A. Türler, V. Pershina, Chem. Rev. **113**, 1273 (2013).
- 2) Y. Kasamatsu *et al.*, J. Radioanal. Nucl. Chem. **279**, 371 (2009).
- 3) Y. Kasamatsu *et al.*, J. Nucl. Radiochem. Sci. **8**, 69 (2007).

\*<sup>1</sup> RIKEN Nishina Center

## Study of anion exchange equilibrium of Zr and Hf in H<sub>2</sub>SO<sub>4</sub> for Rf experiment

T. Yokokita,<sup>\*1</sup> Y. Kasamatsu,<sup>\*2</sup> Y. Komori,<sup>\*1</sup> E. Watanabe,<sup>\*2</sup> K. Ghosh,<sup>\*1</sup> Y. Wang,<sup>\*1</sup> D. Mori,<sup>\*1</sup> A. Shinohara,<sup>\*2</sup> and H. Haba<sup>\*1</sup>

Clarifying the chemical properties of superheavy elements with atomic number  $Z \geq 104$  is an intriguing and important subject. These elements are produced by accelerators using heavy-ion-induced nuclear reactions. The production rates of these elements are low, and their half-lives are short ( $T_{1/2} \leq 1$  min). Therefore, chemical studies on these elements are conducted on a single-atom basis.<sup>1)</sup>

The chemical properties of superheavy elements have been discussed by comparing their chemical behavior with that of lighter homologous elements. The solution chemistry of superheavy elements has been studied mainly for element 104, Rf. In these studies, experiments on Rf and homologous elements was carried out under the same conditions, but even for homologous elements, equilibrated data were obtained only under a few conditions. In particular, it was reported that the chemical reaction kinetics between Zr and Hf are different in H<sub>2</sub>SO<sub>4</sub>.<sup>2)</sup> Equilibrated data are necessary to discuss chemical properties such as complex formation. Therefore, the observation of equilibration and the equilibrated distribution data are very important to characterize the sulfate complex formation of Rf. In our previous study, we performed anion-exchange experiment with <sup>88</sup>Zr, <sup>175</sup>Hf, and <sup>234</sup>Th and determined the suitable experimental condition for Rf.<sup>3)</sup> In this work, we performed online anion-exchange experiments with Zr and Hf by using AMBER<sup>4)</sup> as the model experiment of Rf.

<sup>85</sup>Zr and <sup>169</sup>Hf were produced in the <sup>nat</sup>Ge(<sup>18</sup>O, xn)<sup>85</sup>Zr and <sup>nat</sup>Gd(<sup>18</sup>O, xn)<sup>169</sup>Hf reactions, respectively, using the K70 AVF cyclotron at RIKEN. The nuclear reaction products were transported using a gas-jet system to the chemistry laboratory and deposited on the collection site of AMBER for 60 s. Then, the deposited sample was dissolved in 0.21–0.27 mL of 0.16–0.72 M H<sub>2</sub>SO<sub>4</sub>. The solution sample entered the chemical reaction container containing the anion-exchange resin (MCI GEL CA08Y). After shaking the container with a vortex mixer for 10–600 s, only the solution phase was pushed out of the container by using compressed air, and was assayed by  $\gamma$ -ray spectroscopy. The residual Zr and Hf species adsorbed on the resin were stripped by washing the resin five times with 0.25 mL of 1 M H<sub>2</sub>SO<sub>4</sub>. Subsequently, the resin was conditioned with H<sub>2</sub>SO<sub>4</sub> for the next anion exchange. A control experiment was also performed without the resin to determine the radioactivity of the control solution. The  $Q_d$  values were determined from the following equation:

$$Q_d = A_r V_s / A_s w_r = (A_c - A_s) V_s / A_s w_r \quad (1)$$

where  $A_r$ ,  $A_s$ , and  $A_c$  are radioactivities of the resin, the solution, and the control solution, respectively;  $V_s$  is the volume (mL) of the solution; and  $w_r$  is the mass of the dry resin (g).

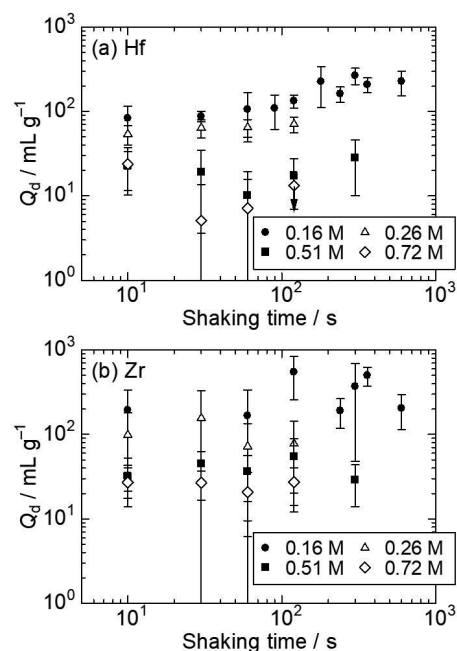


Fig. 1. The  $Q_d$  values of (a) Hf and (b) Zr in anion exchange as a function of shaking time.

The activity of <sup>85</sup>Zr was very low, and the  $Q_d$  values of Zr had large errors. Figures 1(a) and 1(b) show the time dependence of the  $Q_d$  values of Hf and Zr, respectively. The  $Q_d$  values of Hf are constant within the errors in the entire time range studied in 0.26–0.72 M H<sub>2</sub>SO<sub>4</sub>. In 0.16 M H<sub>2</sub>SO<sub>4</sub>, the  $Q_d$  values of Hf become constant within the errors after 180 s. From the time when the  $Q_d$  values became constant within error, the anion-exchange reaction reaches equilibrium within 180 and 10 s in 0.16 and  $\geq 0.26$  M H<sub>2</sub>SO<sub>4</sub>, respectively. From these results, it is seen that the anion-exchange reaction kinetics is slow in low concentration of H<sub>2</sub>SO<sub>4</sub>. It is suggested that the anion-exchange kinetics of Rf may be slow in low concentration of H<sub>2</sub>SO<sub>4</sub>. In the case of Zr, the  $Q_d$  values are constant within the error in the entire time range studied in 0.16–0.72 M H<sub>2</sub>SO<sub>4</sub>. However, from this result, the discussion of anion-exchange reaction equilibrium for Zr is difficult, because the obtained  $Q_d$  values have large error.

In any case, we need to perform experiments with Zr again using enough activity of Zr isotopes. To obtain the small variations'  $Q_d$  values of small variations, we need to suitably adjust the ratio of  $W_r$  and  $V_s$ , when we perform the control experiment. For Hf, the  $Q_d$  values in 0.51 and 0.72 M H<sub>2</sub>SO<sub>4</sub> have large errors; therefore, we plan to perform experiments under this condition again using increased resin weight.

### References

- 1) A. Türlér, V. Pershina, Chem. Rev. **113**, 1273 (2013).
- 2) Z. J. Li *et al.*, Radiochim. Acta **100**, 157 (2012).
- 3) Y. Kasamatsu *et al.*, Radiochim. Acta **103**, 513 (2015).
- 4) T. Yokokita *et al.*, RIKEN Accel. Prog. Rep. **51**, 217 (2018).

\*1 RIKEN Nishina Center

\*2 Graduate School of Science, Osaka University

## Development of $^{211}\text{At}$ -labeled antibody for targeted alpha therapy

Y. Kanayama,<sup>\*1</sup> K. Sakamoto,<sup>\*2</sup> E. Ebisui,<sup>\*3</sup> Y. Wang,<sup>\*4</sup> T. Yokokita,<sup>\*4</sup> Y. Komori,<sup>\*4</sup> D. Mori,<sup>\*4</sup> H. Haba,<sup>\*4</sup> and Y. Watanabe<sup>\*1</sup>

Radiotherapeutic agents labeled with various  $\alpha$ -emitting nuclides have been developed for targeted alpha therapy.  $^{211}\text{At}$  has a simple decay scheme and can avoid the risk of side effects caused by daughter nuclides; it is thus considered a useful  $\alpha$ -emitter for this therapy. Given the requirements for  $^{211}\text{At}$ -labeled pharmaceuticals in the future, RIKEN Nishina Center for Accelerator-Based Science aims to increase the  $^{211}\text{At}$  production scale a global maximum; this prompted us to develop  $^{211}\text{At}$ -labeled drugs and labeling methods.

For the attachment of  $^{211}\text{At}$ , organotin compounds are the most widely used precursor owing to the weakness of the carbon-tin bond, which enables the use of a tin group as a leaving group.<sup>1)</sup> In this study, we used an organotin compound, *N*-succinimidyl-3-(trimethylstannyl)benzoate (m-MeATE), for  $^{211}\text{At}$  labeling. According to the direct astatination procedure reported by Lindegren *et al.*,<sup>2)</sup> m-MeATE was first conjugated with a monoclonal IgG. Then, m-MeATE and IgG were mixed at a molar ratio of 20:1 and incubated for 30 min at 25°C in a pH-8.5 NaCO<sub>3</sub> buffer. The attachment of  $^{211}\text{At}$  was carried out by a modified protocol of the method of Li *et al.*<sup>3)</sup> An oxidizing agent *N*-chlorosuccinimide (NCS) (0.2 mg/ml) was added to the  $^{211}\text{At}$  solution in 1% acetic acid MeOH. Then an IgG/m-MeATE conjugate in a 0.2 M sodium acetate buffer was mixed with the activated  $^{211}\text{At}$  solution, with the final MeOH and NCS concentrations being 11% and 3.6  $\mu\text{g}/\text{ml}$ , respectively. The incubation was performed for 3 min. *N*-iodosuccinimide (0.2 mg/ml) was then added at a final concentration of 5.4  $\mu\text{g}/\text{ml}$ , and the reaction mixture was incubated for another 1 min. For purification, an Amicon Ultra 50 kDa column (Merck) was used in ultrafiltration.

Finally, 5.6 MBq of  $^{211}\text{At}$ -labeled IgG was obtained using 40 MBq of  $^{211}\text{At}$ -MeOH (shown in Table 1). In this experiment, we did not reach the labeling yield that Li *et al.* reported previously ( $40.2 \pm 6.9\%$ ).<sup>3)</sup> Further, we examined the use of a PD Spintrap G-25 gel filtration column for purification, only to reduce the yield.

To demonstrate the usefulness of the  $^{211}\text{At}$ -labeled IgG, we performed a biodistribution study using the mice with xenografted tumors specific to IgG. Three and 24 h after the  $^{211}\text{At}$ -labeled IgG i.v. injections, the mice were dissected to measure tissue radioactivity. As a control group, free  $^{211}\text{At}$  was also administered. The results are shown in Fig. 1. Unexpectedly, the distribution of  $^{211}\text{At}$ -labeled IgG was almost the same as that of

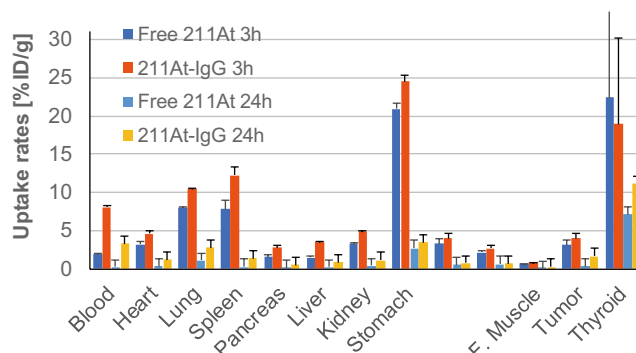


Fig. 1. Biodistribution of free  $^{211}\text{At}$  and  $^{211}\text{At}$ -labeled antibody 3 and 24 h after i.v. injection in the tumor-bearing mice.

Table 1. Labeling results of  $^{211}\text{At}$ -labeled IgG purified by ultrafiltration or gel filtration.

Purification method	Radioactivity yield [%]	Protein yield [%]	Specific activity [kBq/ $\mu\text{g}$ ]
Ultrafiltration	13.9	75.0	12.9
Gel filtration	5.0	69.5	14.9

Table 2. Labeling results of  $^{211}\text{At}$ -labeled IgG or IgG/m-MeATE purified by reduced nonspecific binding gel.

Precursor	Radioactivity yield [%]	Protein yield [%]	Specific Activity [kBq/ $\mu\text{g}$ ]
IgG/m-MeATE	43.9	85.6	31.6
Intact IgG	12.9	79.3	12.5

free  $^{211}\text{At}$ . The high accumulation rates in the stomach and thyroid indicated the physiological accumulation of  $^{211}\text{At}$  detached from IgG.

From these results, we speculated that the increased hydrophobicity by astatination may have caused the nonspecific binding of  $^{211}\text{At}$ -labeled IgG to column filters or gels in the purification step, resulting in a low radioactivity yield despite a high protein yield. To overcome this problem, we used a specialized gel to alleviate nonspecific binding. As shown in Table 2, the radioactivity yields were significantly improved.

In the next step, we will examine a labeling method using decaborane, which is expected to have a higher stability in bonding with  $^{211}\text{At}$  in the body.

### References

- 1) F. Guerard *et al.*, *Cancer Biother. Radiopharm.* **28**, 1 (2013).
- 2) S. Lindegren *et al.*, *J. Nucl. Med.* **49**, 1537 (2008).
- 3) H. K. Li *et al.*, *Cancer Sci.* **108**, 1648 (2017).

<sup>\*1</sup> Laboratory for Pathophysiological and Health Science, RIKEN

<sup>\*2</sup> Laboratory for Nonnatural Amino Acid Technology, RIKEN

<sup>\*3</sup> Liver Cancer Prevention Research Unit, RIKEN

<sup>\*4</sup> RIKEN Nishina Center

## RI imaging tracers for $\text{Na}^+/\text{K}^+$ dynamics in a living body

S. Motomura,\*<sup>1</sup> I. Kii,\*<sup>2</sup> H. Haba,\*<sup>3</sup> H. Yakushiji,\*<sup>1</sup> Y. Watanabe,\*<sup>1</sup> and S. Enomoto\*<sup>4</sup>

Sodium (Na) and potassium (K) are essential metal elements that play important roles in our body. Both metal elements exist as ions in the body and each constitutes approximately 0.2% of the body weight. Although they both are alkali metals located in group 1 of the periodic table of elements, the ions  $\text{Na}^+$  and  $\text{K}^+$  behave very differently in a living body. For example, the concentration of  $\text{Na}^+$  is higher in the extracellular fluid than that in the intracellular fluid, while the concentration of  $\text{K}^+$  is conversely higher in the cell than that in the extracellular fluid.

The different behaviors of  $\text{Na}^+$  and  $\text{K}^+$  are caused by certain functions of some biomolecules that can significantly distinguish the ions. An example of such molecule is  $\text{Na}^+/\text{K}^+$ -ATPase, which takes in two  $\text{K}^+$  ions into a cell and takes out three  $\text{Na}^+$  ions out of a cell in one cycle. This mechanism is used to form the membrane potential in neurons, reabsorption of  $\text{Na}^+$  ions in kidneys, etc.

The idea of the MetalloDiagnosis is to obtain the diagnostic information of molecular functions by observing the behavior of associated metal elements (Fig. 1). Various metal elements are controlled by some biomolecules in a living body. Thus, the behavior of the metal elements can be altered corresponding to whether the molecule is functioning normally or not. If we can non-invasively visualize the different behavior of the associated metal elements, we can make non-invasive imaging diagnosis of the molecular functions.

We are trying to use our imaging apparatus called GREI<sup>1)</sup> to realize the MetalloDiagnosis. The GREI is a kind of gamma-ray imaging camera with an imaging principle called the Compton camera made of germanium semiconductor radiation detectors. The GREI can take three-dimensional images of radio-tracers injected into living animals even by using a single GREI imaging head without any rotation or movement.<sup>2)</sup> Furthermore, the GREI can identify each radioisotope injected simultaneously into an animal by distinguishing the gamma-ray energy in the energy range from 100 keV to 2 MeV, owing to the excellent energy resolution of the semiconductor detectors.

To realize the MetalloDiagnosis by GREI, we need to prepare radioisotopes of each metal element that we are going to take images of the behavior in a living body. For the MetalloDiagnosis of Na and K, we chose  $^{24}\text{Na}$ ,  $^{42}\text{K}$ , and  $^{43}\text{K}$  that have the half-lives of 15-, 12-, and 22-hours, respectively (Table 1). We es-

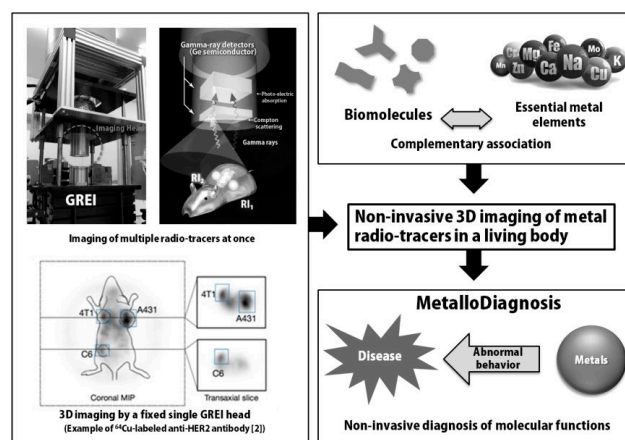


Fig. 1. Concept of MetalloDiagnosis by GREI. Diagnostic information is obtained by observing the associated metals.

Table 1. Radioisotopes of Na and K for GREI imaging.

Nuclide	Half life	Gamma-ray energy (keV)
$^{24}\text{Na}$	15.0 h	1368.6, 2754.0
$^{42}\text{K}$	12.4 h	1524.7
$^{43}\text{K}$	22.3 h	372.8, 617.5

tablished the preparation schemes for these radioisotopes utilizing the nuclear reactions of  $^{\text{nat}}\text{Mg}(d, x)^{24}\text{Na}$  and  $^{\text{nat}}\text{Ca}(d, x)^{42, 43}\text{K}$ . We have also established a delivery scheme for these radioisotopes from Wako to the molecular imaging facility in the RIKEN Kobe campus. It should be noted that we have made delivery of  $^{24}\text{Na}$ ,  $^{42}\text{K}$ , and  $^{43}\text{K}$  radioisotopes 6 times in FY2018.

In the RIKEN Kobe campus, it was the first time that we have used the radioisotopes of  $^{24}\text{Na}$ ,  $^{42}\text{K}$ , and  $^{43}\text{K}$  for experiment. We have started GREI imaging experiment of living mice injected the Na and K radioisotopes simultaneously. For each GREI experiment, approximately 1 MBq and 100 kBq of  $^{24}\text{Na}$  and  $^{43}\text{K}$ , respectively, were used for the time-course imaging of  $\text{Na}^+/\text{K}^+$  dynamics in a living mouse, and it was possible to visualize the different behavior of  $\text{Na}^+$  and  $\text{K}^+$ . This study is ongoing and the results are being prepared to consider for publication.

### References

- 1) S. Motomura *et al.*, J. Anal. At. Spectrom. **28**, 934 (2013).
- 2) T. Ida, S. Motomura *et al.*, Jpn. J. Appl. Phys. **58**, 016002 (2019).

\*<sup>1</sup> RIKEN Center for Biosystems Dynamics Research

\*<sup>2</sup> Compass to Healthy Life Research Complex Program, RIKEN

\*<sup>3</sup> RIKEN Nishina Center

\*<sup>4</sup> RIKEN Center for Life Science Technologies

# Measurement of activation cross sections of alpha particle induced reactions on iridium up to an energy of 50 MeV<sup>†</sup>

S. Takács,<sup>\*1</sup> F. Ditrói,<sup>\*1</sup> Z. Szücs,<sup>\*1</sup> M. Aikawa,<sup>\*2</sup> H. Haba,<sup>\*3</sup> Y. Komori,<sup>\*3</sup> and M. Saito<sup>\*4</sup>

<sup>195m</sup>Pt has proper decay characteristics for internal therapy investigations ( $T_{1/2} = 4.03$  d, IT = 100%,  $E_\gamma = 98.9$  keV, and  $I_\gamma = 11.4\%$ ). This isomeric state transfers its energy by internal transition and emits low energy gamma photons, conversion electrons, and Auger electrons with high intensity. Owing to the low energy of the emitted conversion and Auger electrons, their energy is deposited in a very short range and then, most parts of the deposited energy get concentrated in a small volume, preferably in a single targeted cell. In addition, its low energy gamma photons can be used for imaging. <sup>195m</sup>Pt can be attached to platinum complexes, which are used for chemotherapy, and thus, it can be applied as an effective anti-tumor agent in radiotherapy.

The <sup>195m</sup>Pt for medical applications is produced in reactors in the <sup>194</sup>Pt(n,  $\gamma$ )<sup>195m</sup>Pt reaction with a moderate yield and low specific activity. Charged particle induced reactions may provide high specific activity isotopes. Several production routes to produce <sup>195m</sup>Pt were investigated previously but the <sup>nat</sup>Ir( $\alpha$ , x)<sup>195m</sup>Pt reaction was not studied. The high spin isomeric state (13/2<sup>+</sup>) of <sup>195</sup>Pt can be formed in a reaction with particles capable to transfer high angular momentum. Thus alpha particle bombardment is one of the best ways to produce this radionuclide.

We measured the cross sections of alpha particle induced nuclear reactions on natural iridium using a 51.2-MeV alpha particle beam. The standard stacked-foil target technique and activation method were applied. The activity of the reaction products was assessed without chemical separation using high resolution gamma spectrometry based on a HPGe detector (ORTEC GEM-25185-P).

Two stacks containing Ir target and Ti monitor foils were irradiated at the AVF cyclotron in the RIKEN RI Beam Factory, Wako, Japan, in a Faraday-cup-like vacuum chamber equipped with a long collimator, assuring a small solid angle for the escaping secondary electrons. The initial beam energy was confirmed by the measurement of time of flight before and after the irradiation.<sup>1)</sup> The beam current was kept constant during the irradiation. The beam parameters were also monitored by the <sup>nat</sup>Ti( $\alpha$ , x)<sup>51</sup>Cr monitor reaction.

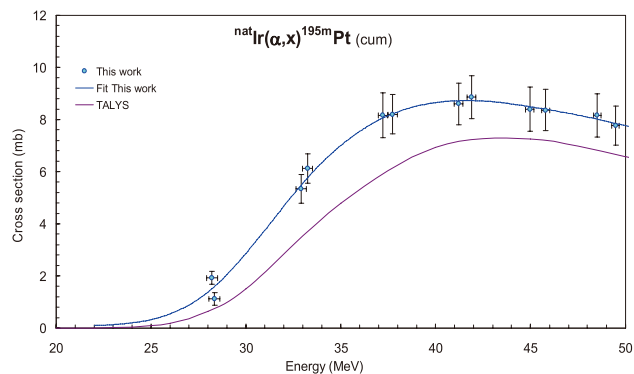


Fig. 1. Cross sections of <sup>nat</sup>Ir( $\alpha$ , x)<sup>195m</sup>Pt reaction in comparison with the predicted data calculated by the TALYS nuclear model code system.<sup>2)</sup>

Excitation functions for the production of <sup>196m2</sup>Au, <sup>196m,g</sup>Au, <sup>195m,g</sup>Au, <sup>194</sup>Au, <sup>193m,g</sup>Au, <sup>192</sup>Au, <sup>191m,g</sup>Au, <sup>191</sup>Pt, <sup>195m</sup>Pt, <sup>194g</sup>Ir, <sup>194m</sup>Ir, <sup>192g</sup>Ir, <sup>190g</sup>Ir, and <sup>189</sup>Ir isotopes were determined up to 50 MeV alpha particle energy on natural iridium target. The measured data were compared to the available experimental data and results of theoretical calculations.<sup>2)</sup> Figure 1 shows the excitation function for the <sup>nat</sup>Ir( $\alpha$ , x)<sup>195m</sup>Pt reaction.

The <sup>nat</sup>Ir( $\alpha$ , x)<sup>195m</sup>Pt production route utilizes the natural iridium target and provides high specific activity of <sup>195m</sup>Pt. The radio-purity of <sup>195m</sup>Pt produced by cyclotrons on iridium targets is somewhat lower than the reactor produced <sup>195m</sup>Pt due to the unavoidable co-produced <sup>193</sup>Pt and <sup>191</sup>Pt radionuclides but the amount of these two isotopes can be reduced by using the enriched <sup>193</sup>Ir target material, and at the same time, the amount of <sup>195m</sup>Pt can be increased. Irradiating an <sup>193</sup>Ir target enriched to 95% with alpha particles of an energy of 50 MeV and beam intensity of 200  $\mu$ A for 24 h, activity of about 1 GBq of <sup>195m</sup>Pt can be achieved at the end of the bombardment.

Besides the excitation function of the <sup>nat</sup>Ir( $\alpha$ , x)<sup>195m</sup>Pt reaction, we measured the cross-section data for the production of <sup>196m2</sup>Au, <sup>196m,g</sup>Au, <sup>191</sup>Pt, <sup>194g</sup>Ir, <sup>194m</sup>Ir, <sup>190g</sup>Ir, and <sup>189</sup>Ir isotopes for the first time. The measured cross sections may also contribute to the improvement of theoretical model codes.

## References

- 1) T. Watanabe, *et al.*, Proc. 5<sup>th</sup> Int. Part. Accel. Conf. (IPAC2014), 3566, (2014).
- 2) A. J. Koning, D. Rochman, Nucl. Data Sheets **113**, 2841 (2012).

<sup>†</sup> Condensed from the article in Appl. Radiat. Isot. **136**, 133 (2018)

<sup>\*1</sup> Institute for Nuclear Research, Hungarian Academy of Sciences

<sup>\*2</sup> Faculty of Science, Hokkaido University

<sup>\*3</sup> RIKEN Nishina Center

<sup>\*4</sup> Graduate School of Biomedical Science and Engineering, Hokkaido University

# Cross-section measurement of $\alpha$ -induced reactions on $^{nat}\text{Er}$ for $^{169}\text{Yb}$ production

M. Saito,<sup>\*1,\*2</sup> M. Aikawa,<sup>\*1,\*2,\*3</sup> M. Sakaguchi,<sup>\*4,\*2</sup> N. Ukon,<sup>\*5,\*2</sup> Y. Komori,<sup>\*2</sup> and H. Haba<sup>\*2</sup>

Radioisotopes (RIs) are widely used in the medical fields such as therapy and diagnosis. To develop such medical treatments, the candidates of medical RIs need to be studied further. Ytterbium-169 ( $^{169}\text{Yb}$ ) is a type of RI that has a half-life of 32.018 days and emits Auger electrons, X and  $\gamma$  rays. The Auger electrons and X rays can be used in brachytherapy as an alternative RI to  $^{125}\text{I}$  and  $^{192}\text{Ir}$ .<sup>1)</sup> The  $\gamma$  rays at 177.21 keV ( $I_\gamma = 22.28\%$ ) and 197.96 keV ( $I_\gamma = 35.93\%$ ) provide the opportunity for diagnosis.<sup>2)</sup> Therefore, owing to these characteristics,  $^{169}\text{Yb}$  can be used in theranostics.

Various reactions can be used to produce  $^{169}\text{Yb}$  such as the neutron-capture reaction on  $^{168}\text{Yb}$  and charged-particle induced reactions on  $^{169}\text{Tm}$  and  $^{nat}\text{Er}$ . Among these, the best production route has not been determined yet. Therefore, we performed systematic studies on the charged-particle induced reactions to produce  $^{169}\text{Yb}$  such as deuteron- and alpha-induced reactions on  $^{169}\text{Tm}$  and alpha-induced reactions on  $^{nat}\text{Er}$ . In this report, we focus on the  $\alpha$ -induced reaction on  $^{nat}\text{Er}$ . The cross-sections for these reactions have already been experimentally measured and reported.<sup>3-6)</sup> However, these cross-sections are different. Therefore, we again measured them to ensure a higher accuracy.

The experiment was performed at the AVF cyclotron of the RIKEN RI Beam Factory using the activation-stacked-foil method. Metallic foils of  $^{nat}\text{Er}$  (purity: 99%, Goodfellow Co., Ltd., UK) and  $^{nat}\text{Ti}$  (purity: 99.6%, Nilaco Corp., Japan) were stacked as the target. The Ti foils were inserted for the  $^{nat}\text{Ti}(\alpha, x)^{51}\text{Cr}$  monitor reaction to assess the target thicknesses and beam parameters. Their average thicknesses were 20.26 and 2.24 mg/cm<sup>2</sup>, which were derived from their measured weights and areas. The stacked target was irradiated for 1 h by a 50-MeV  $\alpha$  beam with an intensity of 100.1 pA measured with a Faraday cup. The initial beam energy was determined by the time of flight measurement.<sup>8)</sup> The energy degradation in the stacked target was calculated by the SRIM code.<sup>9)</sup> The irradiated foils were separated and subjected to the  $\gamma$ -ray spectrometry using a HPGe detector. The nuclear decay data were taken from the NuDat 2.7 database.<sup>10)</sup>

The cross-sections of  $^{nat}\text{Ti}(\alpha, x)^{51}\text{Cr}$  monitor reaction were derived from the measurement of  $\gamma$  line at 320.08 keV ( $I_\gamma = 9.910\%$ ). The result was compared

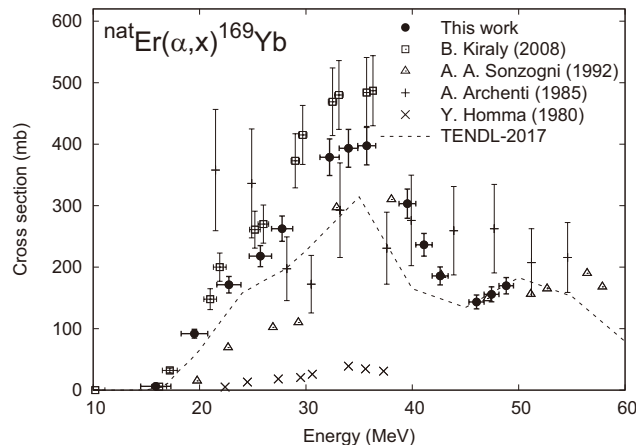


Fig. 1. Preliminary result of  $^{nat}\text{Er}(\alpha, x)^{169}\text{Yb}$  compared with previous data<sup>3-6)</sup> and TENDL-2017.<sup>7)</sup>

with the recommended values of IAEA and we confirmed the accuracy of the foil thicknesses and beam parameters within the uncertainties.

The  $\gamma$  line at 177.21 keV ( $I_\gamma = 22.28\%$ ) was used to derive the cross-sections of  $^{169}\text{Yb}$ . The comparison between our preliminary result, former experimental data, and the TENDL-2017 data is shown in Fig. 1. The peak position of our result is consistent with the data obtained by B. Király *et al.* (2008).<sup>3)</sup> However, the amplitude of their data is larger than our result. Other experimental data<sup>4-6)</sup> are very different from our result. The TENDL-2017 data show a peak at the same energy as ours, although the amplitude of the peak is lower.

## References

- 1) Neil S. Patel *et al.*, *Cardiovasc. Radiat. Med.* **2**, 173 (2001).
- 2) F. H. DeLand *et al.*, *J. Nucl. Med.* **12**, 683 (1971).
- 3) B. Király *et al.*, *Nucl. Instrum. Methods Phys. Res. B* **266**, 549 (2008).
- 4) A. A. Sonzogni *et al.*, *J. Radioanal. Nucl. Chem., Lett.* **165**, 295 (1992).
- 5) A. Aechenti *et al.*, *Radiochimica Acta* **38**, 65 (1985).
- 6) Y. Homma *et al.*, *Int. J. Appl. Radiat. Isot.* **31**, 505 (1980).
- 7) A. J. Koning *et al.*, *Nucl. Data Sheets* **113**, 2841 (2012).
- 8) T. Watanabe *et al.*, *Proc. 5th Int. Part. Accel. Conf. (IPAC2014)*, 3566 (2014).
- 9) J. F. Ziegler *et al.*, *SRIM: the Stopping and Range of Ions in Matter*, <http://www.srim.org/>.
- 10) National Nuclear Data Center, The NuDat 2 database, <http://www.nndc.bnl.gov/nudat2/>.

\*1 Graduate School of Biomedical Science and engineering, Hokkaido University

\*2 RIKEN Nishina Center

\*3 Faculty of Science, Hokkaido University

\*4 School of Science, Hokkaido University

\*5 Advanced Clinical Research Center, Fukushima Medical University

# Activation cross sections of alpha-induced reactions on $^{nat}\text{In}$ for $^{117m}\text{Sn}$ production<sup>†</sup>

M. Aikawa,<sup>\*1,\*2</sup> M. Saito,<sup>\*3,\*2</sup> N. Ukon,<sup>\*4,\*2</sup> Y. Komori,<sup>\*2</sup> and H. Haba<sup>\*2</sup>

The radioisotope  $^{117m}\text{Sn}$  ( $T_{1/2} = 13.76$  d) can be used as a theranostic radioisotope for both medical therapy and imaging. The production of  $^{117m}\text{Sn}$  is of much concern, and the possible production reactions are studied. We focused on one of the reactions, namely the  $^{115}\text{In}(\alpha, x)^{117m}\text{Sn}$  reaction, in this paper. Three experimental literature<sup>1-3)</sup> could be found in the EXFOR library.<sup>4)</sup> The literature data, however, show a large discrepancy from each other. More reliable and accurate data are required for practical use. Therefore, we performed a new experiment to measure the cross sections of the  $^{115}\text{In}(\alpha, x)^{117m}\text{Sn}$  reaction. In addition, the cross sections of the by-products,  $^{113}\text{Sn}$  and  $^{116m}, ^{117}, ^{118m}\text{Sb}$ , were measured.

The experiment was performed at the AVF cyclotron of the RIKEN RI Beam Factory. The stacked foil technique, activation method, and high resolution  $\gamma$ -ray spectrometry were used to derive the activation cross sections. Metallic foils of  $^{nat}\text{In}$  (4.29%  $^{113}\text{In}$  and 95.71%  $^{115}\text{In}$ ) and  $^{nat}\text{Ti}$  were stacked as a target. The target was irradiated by a 51.6-MeV  $\alpha$  beam for 2 h. The incident beam energy was determined using the time-of-flight method.<sup>5)</sup> The beam energy degradation in the stacked target was calculated using the SRIM code.<sup>6)</sup> The average intensity of the beam was 202.1 nA, which was measured by a Faraday cup. The irradiated foils were separated and subjected to  $\gamma$ -ray spectrometry with an HPGe detector.

The excitation function of the  $^{nat}\text{Ti}(\alpha, x)^{51}\text{Cr}$  monitor reaction was used to assess the beam parameters and the target thicknesses. The excitation function could be derived from measurements of the  $\gamma$  line at 320.08 keV ( $I_\gamma = 9.91\%$ ) from the decay of  $^{51}\text{Cr}$  ( $T_{1/2} = 27.7025$  d). The result is in good agreement with the recommended values.<sup>7)</sup> Therefore, we adopted the measured beam parameters and target thicknesses without any adjustments.

The measurement of the 156.02-keV  $\gamma$  line ( $I_\gamma = 2.113\%$ ) from the  $^{117m}\text{Sn}$  decay was performed for the cross sections of the  $^{115}\text{In}(\alpha, x)^{117m}\text{Sn}$  reaction. The cooling time was longer than 45 h for the complete decay of the parent nuclei,  $^{117g}\text{In}$  ( $T_{1/2} = 43.2$  min),  $^{117m}\text{In}$  ( $T_{1/2} = 116.2$  min), and  $^{117}\text{Sb}$  ( $T_{1/2} = 2.80$  h). The cumulative cross sections of  $^{117m}\text{Sn}$  for  $^{nat}\text{In}$  targets were obtained from the measurement. The cross

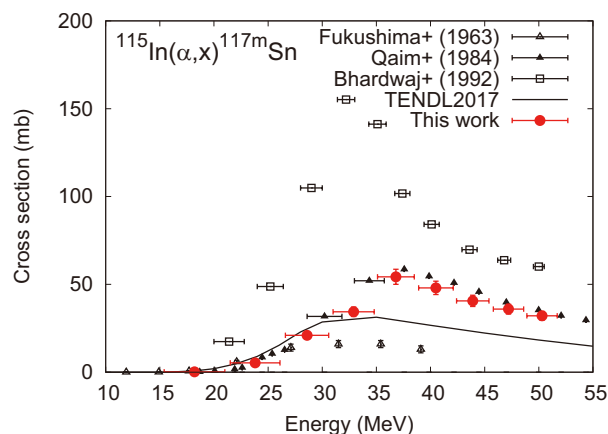


Fig. 1. Excitation function of the  $^{115}\text{In}(\alpha, x)^{117m}\text{Sn}$  reaction.

sections were normalized to those for  $^{115}\text{In}$  enriched targets, taking into account the negligibly small contribution of the  $\alpha$ -capture reaction on  $^{113}\text{In}$ . The result is shown in Fig. 1 in comparison with the previous experimental data<sup>1-3)</sup> and the TENDL-2017 data.<sup>8)</sup> The present result is almost consistent with the data obtained by Qaim and Döhler (1984).<sup>2)</sup> The data obtained by Fukushima *et al.* (1963)<sup>1)</sup> and TENDL-2017 show smaller amplitudes than the others. On the contrary, the data obtained by Bhardwaj *et al.* (1992)<sup>3)</sup> are much larger than that obtained by the others.

In this work, the cross sections of the  $^{115}\text{In}(\alpha, x)^{117m}\text{Sn}$  reaction up to 50 MeV were measured using the stacked foil activation technique and high resolution  $\gamma$ -ray spectrometry. The measured cross sections were compared with the earlier experimental data and the TENDL data. One of the three experimental datasets is in good agreement with our result. Our result can contribute to the estimation of  $^{117m}\text{Sn}$  production.

## References

- 1) S. Fukushimai *et al.*, Bull. Chem. Soc. Jpn. **36**, 1225 (1963).
- 2) S. M. Qaim *et al.*, Int. J. Appl. Radiat. Isot. **35**, 645 (1984).
- 3) M. K. Bhardwaj *et al.*, Int. J. Mod. Phys. E **1**, 389 (1992).
- 4) N. Otuka *et al.*, Nucl. Data Sheets **120**, 272 (2014).
- 5) T. Watanabe *et al.*, Proc. 5th Int. Part. Accel. Conf. (IPAC2014), 3566 (2014).
- 6) SRIM: the Stopping and Range of Ions in Matter, <http://www.srim.org/>.
- 7) A. Hermanne *et al.*, Nucl. Data Sheets **148**, 338 (2017).
- 8) A. J. Koning, D. Rochman, Nucl. Data Sheets **113**, 2841 (2012).

<sup>†</sup> Condensed from the article in Nucl. Instrum. Methods Phys. Res. B **426**, 18 (2018)

\*1 Faculty of Science, Hokkaido University

\*2 RIKEN Nishina Center

\*3 Graduate School of Biomedical Science, Hokkaido University

\*4 Fukushima Global Medical Science Center, Fukushima Medical University

# Investigation of alpha particle induced reactions on natural silver in the 40–50 MeV energy range<sup>†</sup>

F. Ditrói,<sup>\*1</sup> S. Takács,<sup>\*1</sup> H. Haba,<sup>\*2</sup> Y. Komori,<sup>\*2</sup> M. Aikawa,<sup>\*3</sup> M. Saito,<sup>\*4</sup> and T. Murata<sup>\*5</sup>

Natural silver targets were irradiated using a 50 MeV alpha-particle beam in order to measure the activation cross sections of radioisotopes in the 40–50 MeV energy range. Among the radio-products, there are medically important isotopes such as  $^{110m}\text{In}$  and  $^{111}\text{In}$ .<sup>1)</sup> For optimizing the production of these radioisotopes and their purity and specific activity, the cross section data for every produced radioisotope are important. New data were measured in this energy range and the results of some previous measurements were confirmed. Physical yield curves were calculated using the new cross section data completed with the results from the literature.

The irradiation was performed on a dedicated beam line of the K70-MeV AVF cyclotron of the RIKEN RI Beam Factory by using an  $E_\alpha = 50.7 \pm 0.3$  MeV beam. The  $^{nat}\text{Ti}(\alpha, x)^{51}\text{Cr}$  reaction on titanium foils (Ti: 10.9  $\mu\text{m}$ ) was used as a monitor reaction to check and correct the beam intensity and energy degradation through the whole stack. The foils were ordered in groups in such a way that we could compensate or avoid the activity loss or excess activity due to the recoil effect of the radioisotope in question. The first 10 foils of the stack were silver. The Ag foils were arranged in one block, *i.e.* one after other, because for silver, we were

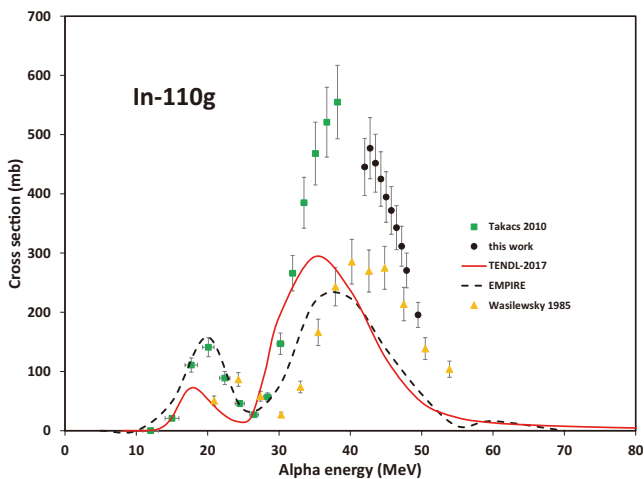


Fig. 1. Excitation function of the  $^{nat}\text{Ag}(\alpha, x)^{110g}\text{In}$  reaction compared with the previous results and the results of the theoretical model code calculations.

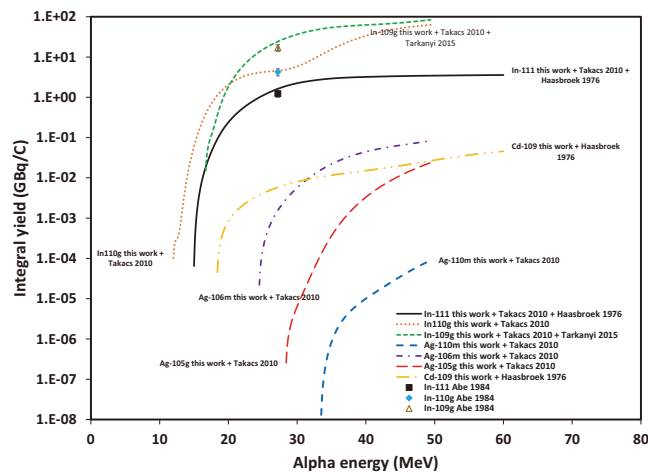


Fig. 2. Calculated physical yields from selected  $\alpha$ -particle induced nuclear reactions on Ag compared with the literature data.

interested in the high energy part (40–50 MeV range).

The excitation functions for  $^{nat}\text{Ag}(\alpha, x)^{111,110m,110g,109g,108g}\text{In}$ ,  $^{111,110m,106m,105g}\text{Ag}$  and  $^{109}\text{Cd}$  were measured in the energy range of 40–50 MeV (*e.g.*  $^{110g}\text{In}$  in Fig. 1). The newly determined cross section data helped clarify the problems between the previous literature results. The cross section deduced for the production of  $^{110g}\text{In}$ ,  $^{109g}\text{In}$ ,  $^{108g}\text{In}$ ,  $^{111}\text{Ag}$ , and  $^{110g}\text{Ag}$  in most cases show a good continuation of the eventually existing literature data in a lower energy region. In the case of  $^{111}\text{In}$  and  $^{109}\text{Cd}$ , the agreement with the previous literature data is excellent. The results of the theoretical nuclear reaction model codes are not systematic and give only partly good estimations for several reactions. There are reactions, for which both (EMPIRE and TENDL) fail completely. Thick target physical yield curves were calculated from the measured cross sections (Fig. 2). The excitation functions for these calculations were constructed by using our new results combined with data from the literature. The literature values agree well with our results.

Among the possible industrial applications, the TLA<sup>2)</sup> method was demonstrated by using  $^{106m}\text{Ag}$ , which is the best radioisotope for this purpose. It has been proved that by using  $^{106m}\text{Ag}$  as a tracer, the wear measurement can be performed with actual parameters.

## References

- 1) F. Tárkányi *et al.*, Nucl. Instrum. Methods Phys. Res. B **351**, 6 (2015).
- 2) F. Ditrói *et al.*, IAEA TECDOC-924, 1997.

<sup>†</sup> Condensed from the article in Nucl. Instrum. Methods Phys. Res. B **436**, 119 (2018)

<sup>\*1</sup> Institute for Nuclear Research, HAS

<sup>\*2</sup> RIKEN Nishina Center

<sup>\*3</sup> Faculty of Science, Hokkaido University

<sup>\*4</sup> Graduate School of Biomed. Sci. and Eng., Hokkaido Univ.

<sup>\*5</sup> School of Science, Hokkaido University

# Production cross sections of deuteron-induced reactions on natural palladium for Ag isotopes<sup>†</sup>

N. Ukon,<sup>\*1,\*2,\*3</sup> M. Aikawa,<sup>\*3,\*4</sup> Y. Komori,<sup>\*3</sup> and H. Haba<sup>\*3</sup>

Radioisotopes (RI) are available for medical therapy and diagnostics.<sup>1)</sup>  $^{103}\text{Pd}$  with a half-life of  $T_{1/2} = 16.991$  d decays (100% electron capture (EC)) into  $^{103\text{m}}\text{Rh}$ , which successively decays (100% isomeric transition) into  $^{103}\text{Rh}$  with a 39.5-keV  $\gamma$ -ray emission.  $^{103}\text{Pd}$  is a medical radioisotope and is available for brachytherapy.<sup>2)</sup> For the effective production of  $^{103}\text{Pd}$ , a variety of reactions should be investigated for comparison, including reactions to produce  $^{103}\text{Ag}$  ( $T_{1/2} = 65.7$  min), which is a parent of  $^{103}\text{Pd}$ . One of the processes used for producing  $^{103}\text{Ag}$  is deuteron-induced reactions on natural palladium, which has only been studied up to 20.3 MeV in previous studies.<sup>3-5)</sup>

In addition to  $^{103}\text{Pd}$ , the radionuclide  $^{104\text{g}}\text{Ag}$  which has a short  $\beta^+$  decay half-life ( $T_{1/2} = 69.2$  min) can be used for diagnostic imaging in positron emission tomography (PET).  $^{111}\text{Ag}$  has significant potential as a therapeutic  $\beta^-$  radionuclide decaying (92%  $\beta^-$ ,  $E_{\beta\text{max}} = 1037$  keV) directly to the ground state of  $^{111}\text{Cd}$ . The PET using  $^{104}\text{Ag}$  has the possible combination of diagnostic studies to investigate the uptake of  $^{111}\text{Ag}$  labelled compounds of the therapeutic radionuclide before treatment.<sup>6)</sup>  $^{104\text{g}}\text{Ag}$ ,  $^{104\text{m}}\text{Ag}$ , and  $^{111}\text{Ag}$  can be obtained by charged particle reactions on  $^{\text{nat}}\text{Pd}$ . Therefore, we investigated the activation cross sections of deuteron-induced reactions on metallic foils of natural palladium ( $^{102}\text{Pd}$  1.02%;  $^{104}\text{Pd}$  11.14%;  $^{105}\text{Pd}$  22.33%;  $^{106}\text{Pd}$  27.33%;  $^{108}\text{Pd}$  26.46%;  $^{110}\text{Pd}$  11.72%) in connection with the production of medically relevant radioisotopes.

The excitation functions of the  $^{\text{nat}}\text{Pd}(d,x)$  reactions were measured by the stacked-foil method, activation method and high-resolution  $\gamma$ -ray spectroscopy.  $^{\text{nat}}\text{Pd}$  foils (purity: 99.95%, Nilaco Corp., Japan) were stacked with  $^{\text{nat}}\text{Ti}$  (purity: 99.6%, Nilaco Corp., Japan) and  $^{\text{nat}}\text{Zn}$  foils (purity: 99.95%, Nilaco Corp., Japan) for monitoring the beam parameters and degrading the beam energy. The thicknesses of the Pd, Ti, and Zn foils were 8.15, 4.93, and 25.14 mg/cm<sup>2</sup>, respectively. The irradiation was performed at the RIKEN AVF cyclotron. A 24-MeV deuteron beam with an average intensity of about 174 nA was irradiated on the target for 20 min. The incident beam energy was measured by the time-of-flight method using plastic scintillator monitors. The beam energy degraded in the stacked target was calculated using the polynomial approximation of stopping-power data.<sup>7)</sup> The  $\gamma$ -ray spectra of the acti-

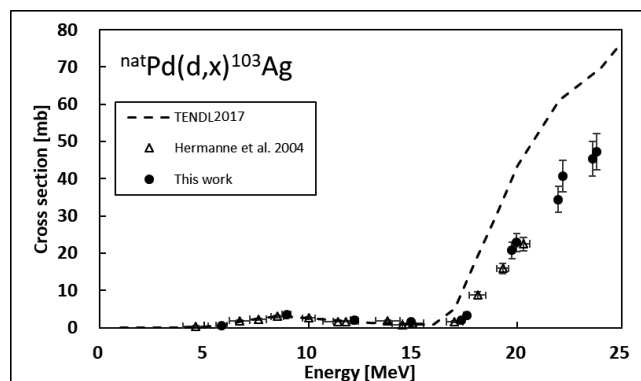


Fig. 1. Excitation function of the  $^{\text{nat}}\text{Pd}(d,x)^{103}\text{Ag}$  reaction. The result is compared with a previous study<sup>4)</sup> and TENDL-2017.<sup>9)</sup>

vated foils were measured using HPGe detectors. The nuclear decay data were taken from the online NuDat 2.6 database.<sup>8)</sup>

We found that our result is in good agreement with the previous data obtained by Hermanne *et al.*<sup>4)</sup> up to 20.3 MeV. On the other hand, the theoretical calculation reproduces well the experimental cross sections up to 15 MeV; however at higher energies, the calculation overestimates the experimental cross sections. We performed an experiment of the deuteron-induced reactions on natural palladium to produce Ag isotopes by using the stacked foil activation technique. The excitation functions of the  $^{\text{nat}}\text{Pd}(d,x)^{103}\text{Ag}$  reaction from 20.3 MeV to 24 MeV,  $^{\text{nat}}\text{Pd}(d,x)^{104\text{g}}\text{Ag}$ , and  $^{\text{nat}}\text{Pd}(d,x)^{104\text{m}}\text{Ag}$  were measured for the first time. The production cross sections of  $^{105}\text{Ag}$ ,  $^{106\text{m}}\text{Ag}$ ,  $^{110\text{m}}\text{Ag}$ , and  $^{111}\text{Ag}$  are in good agreement with the previous experimental data. Above 20.3 MeV, all excitation functions in this work continued smoothly to the data in the previous study.

## References

- 1) J. F. Chatal, C. A. Hoefnagel, *Lancet* **354**, 931 (1999).
- 2) A. S. Meigooni, R. Nath, *Int. J. Radiat. Oncol. Biol. Phys.* **22**, 1125 (1992).
- 3) F. Ditrói, *et al.*, *Nucl. Instrum. Methods Phys. Res. B* **270**, 61 (2012).
- 4) A. Hermanne *et al.*, *Radiochim. Acta* **92**, 215 (2004).
- 5) F. Ditrói *et al.*, *Appl. Radiat. Isot.* **128**, 297 (2017).
- 6) A. Hermanne *et al.*, *Nucl. Instrum. Methods Phys. Res. B* **217**, 193 (2004).
- 7) H. H. Andersen, J. F. Ziegler, *Hydrogen Stopping Powers and Ranges in All Elements*, Vol. 3 (Pergamon, Oxford, 1997).
- 8) National Nuclear Data Center: the NuDat 2 database, <http://www.nndc.bnl.gov/nudat2/>.
- 9) A. J. Koning *et al.*, TENDL-2017: TALYS-based evaluated nuclear data library.

<sup>†</sup> Condensed from the article in *Nucl. Instrum. Methods Phys. Res. B* **426**, 13 (2018)

<sup>\*1</sup> Nuclear Reaction Data Center (JCPRG), Hokkaido University

<sup>\*2</sup> Advanced Clinical Research Center, Fukushima Medical University

<sup>\*3</sup> RIKEN Nishina Center

<sup>\*4</sup> Faculty of Science, Hokkaido University

## Production cross sections of $^{111}\text{Ag}$ in deuteron-induced nuclear reactions on natural palladium

K. Ooe,<sup>\*1</sup> T. Watabe,<sup>\*1</sup> Y. Shirakami,<sup>\*1</sup> D. Mori,<sup>\*2</sup> T. Yokokita,<sup>\*2</sup> Y. Komori,<sup>\*2</sup> H. Haba,<sup>\*2</sup> and J. Hatazawa<sup>\*1</sup>

Several radionuclides such as  $^{90}\text{Y}$  and  $^{131}\text{I}$  are currently used for nuclear medicine therapy of tumors. These radionuclides are produced using nuclear reactors. In Japan, all therapeutic radionuclides are now imported from other countries. Therefore, domestic production using accelerators is desirable for a stable supply of therapeutic radionuclides.

Silver-111 ( $^{111}\text{Ag}$ ) is a  $\beta^-$  emitter, which can be applied to the therapy of tumors. It has a half-life of 7.45 d and can be produced in  $^{110}\text{Pd}(d, x)^{111}\text{Ag}$  reactions using accelerators. This radionuclide also emits  $\gamma$  rays with energies of 342 and 245 keV, which can be used for imaging by single photon emission computed tomography (SPECT). These nuclear properties of  $^{111}\text{Ag}$  are expected to be suitable for theranostics (therapeutics + diagnosis). However,  $^{111}\text{Ag}$  has been rarely applied to the nuclear medicine field. In this study, production cross sections for  $^{\text{nat}}\text{Pd}(d, x)^{111}\text{Ag}$  reactions are investigated for future nuclear medical application of  $^{111}\text{Ag}$ .

The cross sections of  $^{\text{nat}}\text{Pd}(d, x)^{111}\text{Ag}$  reactions were measured by the stacked-foil method. Metallic foils of natural isotopic Pd (purity: 99.95% and thickness: 0.0125 mm, Nilaco Corp., Japan) were used as the target. Metallic foils of  $^{\text{nat}}\text{Ta}$  (purity: 99.95% and thickness: 0.10 mm, Nilaco Corp., Japan) and  $^{\text{nat}}\text{Ni}$  (purity: 99.95% and thickness: 0.001 mm, Nilaco Corp., Japan) were also used as a beam energy degrader and beam intensity monitor with the  $^{\text{nat}}\text{Ni}(d, x)^{61}\text{Cu}$  reactions, respectively. Twenty five Pd and 10 Ni foils were stacked together with 2 Ta foils which were placed on the top of the stack. The irradiation of the stack with the 24 MeV deuteron beam was conducted using the RIKEN K70 AVF Cyclotron. The stack covered the beam energy range of 4–17 MeV for the measurement of cross sections of  $^{\text{nat}}\text{Pd}(d, x)^{111}\text{Ag}$  reactions. The average beam intensity was approximately 180 nA and the irradiation time was 2 h. After the irradiation of the stack, each foil was subjected to  $\gamma$ -ray spectrometry using a HPGe detector. The 245-keV  $\gamma$  peak of  $^{111}\text{Ag}$  was used to calculate the cross sections.

Because  $^{110\text{m}}\text{Ag}$  would be produced simultaneously with  $^{111}\text{Ag}$  and remain in the body for a long time owing to its very long half-life (249.79 d) during radiotherapy, the cross sections of  $^{\text{nat}}\text{Pd}(d, x)^{110\text{m}}\text{Ag}$  reactions were also investigated. The preliminary results of the cross sections of the  $^{\text{nat}}\text{Pd}(d, x)^{111}\text{Ag}$  and

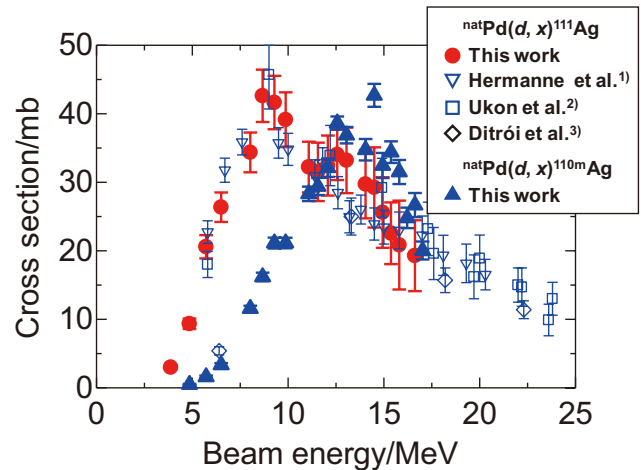


Fig. 1. Excitation functions of  $^{\text{nat}}\text{Pd}(d, x)^{111}\text{Ag}$  and  $^{\text{nat}}\text{Pd}(d, x)^{110\text{m}}\text{Ag}$  reactions.

$^{\text{nat}}\text{Pd}(d, x)^{110\text{m}}\text{Ag}$  reactions are shown in Fig. 1.  $^{111}\text{Ag}$  is produced not only in the direct nuclear reaction but also from the decay of by-products  $^{111\text{m}}\text{Ag}$  ( $T_{1/2} = 64.8$  s) and  $^{111\text{m}}\text{Pd}$  ( $T_{1/2} = 5.5$  h). Therefore, cumulative cross sections for  $^{111}\text{Ag}$  are shown in Fig. 1. The energy at the peak of the excitation function of  $^{\text{nat}}\text{Pd}(d, x)^{111}\text{Ag}$  reactions was approximately 9 MeV with a cross section of approximately 40 mb, which is consistent with the previous results.<sup>1–3)</sup> The excitation function of  $^{\text{nat}}\text{Pd}(d, x)^{110\text{m}}\text{Ag}$  reactions has a maximum of approximately 40 mb at around 14 MeV and almost half amplitude of that of the  $^{\text{nat}}\text{Pd}(d, x)^{111}\text{Ag}$  reactions at around 9 MeV. Although  $^{110\text{m}}\text{Ag}$  is simultaneously produced with  $^{111}\text{Ag}$ , the radioactivity of  $^{110\text{m}}\text{Ag}$  produced with 9-MeV deuteron beam would be approximately 1% of the  $^{111}\text{Ag}$  activity owing to the difference in cross sections and half-lives between  $^{111}\text{Ag}$  and  $^{110\text{m}}\text{Ag}$ .

As the next step for the medical application of  $^{111}\text{Ag}$ , chemical purification of  $^{111}\text{Ag}$  from a Pd target will be performed by ion exchange chromatography.

### References

- 1) A. Hermanne *et al.*, Nucl. Instrum. Methods Phys. Res. B **217**, 193 (2004).
- 2) N. Ukon *et al.*, Nucl. Instrum. Methods Phys. Res. B **426**, 13 (2018).
- 3) F. Ditrói *et al.*, Nucl. Instrum. Methods Phys. Res. B **270**, 61 (2012).

<sup>\*1</sup> Department of Nuclear Medicine and Tracer Kinetics, Osaka University Graduate School of Medicine

<sup>\*2</sup> RIKEN Nishina Center

## Production cross sections of Mo, Nb and Zr radioisotopes from $\alpha$ -induced reaction on $^{nat}\text{Zr}^\dagger$

T. Murata,<sup>\*1,\*2,\*3</sup> M. Aikawa,<sup>\*3,\*2</sup> M. Saito,<sup>\*3,\*2</sup> N. Ukon,<sup>\*4,\*2</sup> Y. Komori,<sup>\*2</sup> H. Haba,<sup>\*2</sup> and S. Takács<sup>\*5</sup>

The most important medical radioisotopes at present are  $^{99m}\text{Tc}$  ( $T_{1/2} = 6.0$  h) and its generator  $^{99}\text{Mo}$  ( $T_{1/2} = 66.0$  h). Nuclear reactions to produce  $^{99}\text{Mo}$  using accelerators are energetically investigated worldwide. One of the charged-particle reactions used to create  $^{99}\text{Mo}$  is the  $^{96}\text{Zr}(\alpha, x)^{99}\text{Mo}$  reaction. Three experimental data<sup>1-3)</sup> were found in a literature survey. The three datasets, however, show quite different shapes from each other. Therefore, we performed two experiments to measure the cross sections of the  $^{96}\text{Zr}(\alpha, x)^{99}\text{Mo}$  reaction. In addition, the cross sections for the production of  $^{93m}\text{Mo}$ ,  $^{90g, 92m, 95g, 95m, 96}\text{Nb}$ , and  $^{88, 89g, 95}\text{Zr}$  isotopes were measured.

Two independent irradiations using different targets and  $\alpha$ -beam energies were performed at the RIKEN AVF cyclotron. The stacked-foil technique, activation method, and high-resolution  $\gamma$ -ray spectrometry were used. Two stacked targets consisted of  $^{nat}\text{Zr}$  foils of different thicknesses (6.75 and 13.22 mg/cm<sup>2</sup>) and  $^{nat}\text{Ti}$  foils (2.43 and 2.40 mg/cm<sup>2</sup>). The targets were respectively irradiated for 2 h by  $\alpha$  beams of two different energies, namely 29 and 50 MeV. The incident beam energies were determined by using the time-of-flight method.<sup>4)</sup> The energy degradation in the targets was calculated using the SRIM code.<sup>5)</sup> The average intensity measured by a Faraday cup was about 400 nA in both cases. The  $\gamma$  lines from the decay of the radioisotopes for each irradiated foil were measured using an HPGe detector.

The excitation function of the  $^{nat}\text{Zr}(\alpha, x)^{99}\text{Mo}$  reaction was derived from measurements of the  $\gamma$  line at 739.500 keV ( $I_\gamma = 12.20\%$ ). The parent nuclei of  $^{99}\text{Mo}$ ,  $^{99g}\text{Nb}$  ( $T_{1/2} = 15.0$  s), and  $^{99m}\text{Nb}$  ( $T_{1/2} = 2.5$  min), decayed during cooling times longer than 47 h. The cross sections of  $^{96}\text{Zr}$  were deduced by taking into account the isotopic composition of natural zirconium. The results are shown in Fig. 1 and compared with previous experimental data<sup>1-3)</sup> and the TENDL-2017 data.<sup>6)</sup> Our results are in complete agreement with the recent experimental data,<sup>3)</sup> but very different from the others. Based on our measured excitation function, the end of bombardment activity of  $^{99}\text{Mo}$  was deduced with the

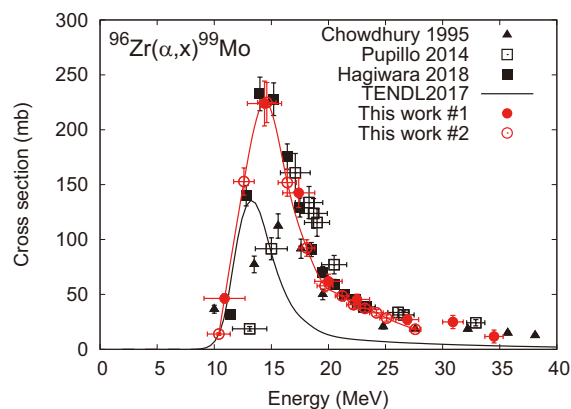


Fig. 1. Excitation function of the  $^{96}\text{Zr}(\alpha, x)^{99}\text{Mo}$  reaction.

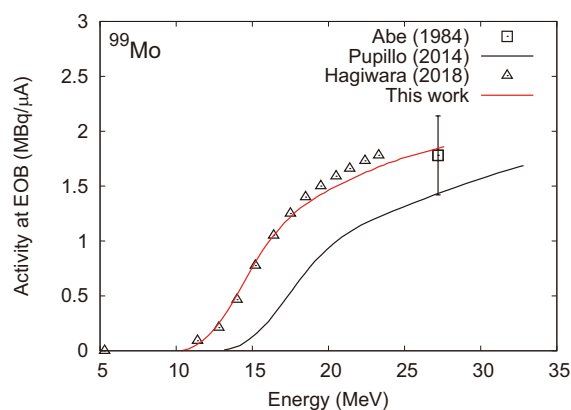


Fig. 2. End of bombardment activity of  $^{99}\text{Mo}$  for 1 h irradiation.

stopping powers obtained using the SRIM code.<sup>5)</sup> Our result shown in Fig. 2 is almost consistent with the two datasets,<sup>3,7)</sup> but larger than one dataset.<sup>2)</sup>

### References

- 1) D. P. Chowdhury *et al.*, Nucl. Instrum. Methods Phys. Res. B **103**, 261 (1995).
- 2) G. Pupillo *et al.*, J. Radioanal. Nucl. Chem. **302**, 911 (2014).
- 3) M. Hagiwara *et al.*, J. Radioanal. Nucl. Chem. **318**, 569 (2018).
- 4) T. Watanabe *et al.*, Proc. 5th Int. Part. Accel. Conf. (IPAC2014), 3566 (2014).
- 5) SRIM: the Stopping and Range of Ions in Matter, <http://www.srim.org/>.
- 6) A. J. Koning *et al.*, Nucl. Data Sheets **113**, 2841 (2012).
- 7) K. Abe *et al.*, J. Nucl. Mater. **123**, 972 (1984).

<sup>†</sup> Condensed from the article in Appl. Radiat. Isot. **144**, 47 (2019)

<sup>\*1</sup> School of Science, Hokkaido University

<sup>\*2</sup> RIKEN Nishina Center

<sup>\*3</sup> Graduate School of Biomedical Science and Engineering, Hokkaido University

<sup>\*4</sup> Advanced Clinical Research Center, Fukushima Medical University

<sup>\*5</sup> Institute for Nuclear Research, Hungarian Academy of Sciences (ATOMKI)

# Activation cross sections of deuteron-induced reactions on niobium up to 24 MeV<sup>†</sup>

M. Aikawa,<sup>\*1,\*2</sup> Y. Komori,<sup>\*2</sup> and H. Haba<sup>\*2</sup>

One of the potential radioisotopes for nuclear medicine is  $^{93m}\text{Mo}$ .<sup>1)</sup> Several reactions to produce  $^{93m}\text{Mo}$  were studied, for example, proton- and deuteron-induced reactions on Nb,  $\alpha$ -induced reactions on Zr, and  $^7\text{Li}$ -induced reactions on Y. In this paper, we focus on the deuteron-induced reactions on Nb because the cross sections of these reactions are about four times larger than those of the proton-induced reactions.<sup>2)</sup> Four experimental data sets up to 50 MeV<sup>2-5)</sup> were found in a literature survey, and they were scattered over several tens of mb at a peak of around 17 MeV. Therefore, we performed an experiment to measure the cross sections of the  $^{93}\text{Nb}(d, 2n)^{93m}\text{Mo}$  reaction.

We used standard methods such as the stacked-foil activation method and off-line  $\gamma$ -ray spectrometry. The stacked target of the experiment was composed of thin metallic foils of  $^{93}\text{Nb}$  (27.11 mg/cm<sup>2</sup>, 99.9% purity, Nilaco Corp., Japan) and  $^{\text{nat}}\text{Ti}$  (9.13 mg/cm<sup>2</sup>, 99.6% purity, Nilaco Corp., Japan). The  $^{\text{nat}}\text{Ti}$  foils were used to monitor the beam parameters. The target was irradiated by a 23.6-MeV deuteron beam at the AVF cyclotron of the RIKEN RI Beam Factory. The incident beam energy was measured by the time-of-flight method using a plastic scintillator monitor.<sup>6)</sup> The irradiation lasted for 30 min with an average intensity of 200.3 nA, which was measured using a Faraday cup. The energy degradation of the beam in the stacked target was calculated using the SRIM code.<sup>7)</sup> The beam parameters and the target thicknesses were assessed by the  $^{\text{nat}}\text{Ti}(d, x)^{48}\text{V}$  monitor reaction. The  $\gamma$  lines from the foils were measured by using a high-resolution HPGe detector.

The 263.049-keV  $\gamma$  line ( $I_\gamma = 57.4\%$ ) from the  $^{93m}\text{Mo}$  IT decay ( $T_{1/2} = 6.85$  h) was measured after a cooling time of about 10 h. The excitation function of the  $^{93}\text{Nb}(d, 2n)^{93m}\text{Mo}$  reaction was derived from the measurement. The result is shown in Fig. 1 together with the earlier experimental data<sup>3-5)</sup> and the TENDL-2017 data.<sup>8)</sup> Our result shows good agreement with the other experimental data in the entire energy region. The theoretical calculation overestimates the experimental data.

The physical yield of  $^{93m}\text{Mo}$  from the  $^{93}\text{Nb}(d, 2n)^{93m}\text{Mo}$  reaction was calculated from the excitation function using the spline fitting shown in Fig. 1 and the stopping power calculated by the SRIM code.<sup>7)</sup> The re-

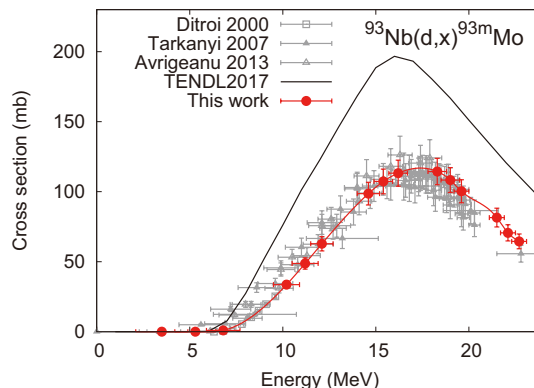


Fig. 1. Excitation function of the  $^{93}\text{Nb}(d, 2n)^{93m}\text{Mo}$  reaction.

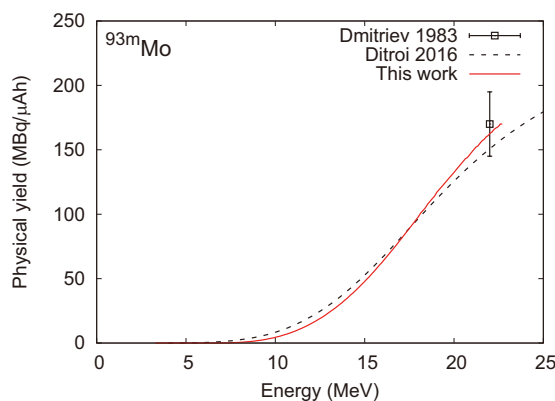


Fig. 2. Physical yield of  $^{93m}\text{Mo}$ .

sult, together with the other experimental data,<sup>2,9)</sup> is shown in Fig. 2. Our result is consistent with the two data studied earlier.<sup>2,9)</sup>

## References

- 1) M. Sadeghi *et al.*, J. Radioanal. Nucl. Chem. **286**, 141 (2010).
- 2) F. Ditrói *et al.*, Nucl. Instrum. Methods Phys. Res. B **373**, 17 (2016).
- 3) F. Ditrói *et al.*, Nucl. Instrum. Methods Phys. Res. B **161–163**, 172 (2000).
- 4) F. Tárkányi *et al.*, Nucl. Instrum. Methods Phys. Res. B **255**, 297 (2007).
- 5) M. Avrigeanu *et al.*, Phys. Rev. C **88**, 014612 (2013).
- 6) T. Watanabe *et al.*, Proc. 5th Int. Part. Accel. Conf. (IPAC2014), 3566 (2014).
- 7) SRIM: The Stopping and Range of Ions in Matter, <http://www.srim.org/>.
- 8) A. J. Koning *et al.*, Nucl. Data Sheets **155**, 1 (2019).
- 9) P. P. Dmitriev *et al.*, INDC(CCP)-210, 1 (1983).

<sup>†</sup> Condensed from the article in Nucl. Instrum. Methods Phys. Res. B **436**, 217 (2018)

<sup>\*1</sup> Faculty of Science, Hokkaido University

<sup>\*2</sup> RIKEN Nishina Center

## New cross section data for production of zirconium-89 by alpha-induced reaction on yttrium target

T. Murata,<sup>\*1,2</sup> M. Aikawa,<sup>\*1,2</sup> M. Saito,<sup>\*1,2</sup> N. Ukon,<sup>\*2,3</sup> Y. Komori,<sup>\*2</sup> H. Haba,<sup>\*2</sup> S. Takács,<sup>\*4</sup> and F. Ditrói<sup>\*4</sup>

Zirconium-89 is considered a good candidate for immuno-PET investigations owing to its decay properties.<sup>1)</sup> Even though it is possible to produce <sup>89</sup>Zr with a low incident beam energy (approximately 12 MeV) and high specific activities by using proton beams (470–1195 mCi/mmol),<sup>1)</sup> it is worthwhile to consider its production using heavier particles. Co-production of <sup>90</sup>Nb, another expectable radionuclide for medicine,<sup>2)</sup> is possible in the same irradiation with alpha particles.

The alpha-induced reaction on natural yttrium is one of the ways to produce <sup>89</sup>Zr and <sup>90</sup>Nb. There are, however, only two earlier studies on the <sup>89</sup>Y( $\alpha$ , x)<sup>89</sup>Zr reaction and no data for the high energy region is available, where higher cross sections seem to be achieved. In this work, a new experiment to measure the cross sections for the <sup>89</sup>Y( $\alpha$ , x)<sup>89</sup>Zr reaction was performed to investigate the optional route for <sup>89</sup>Zr production.

The well known stacked-foil technique and activation method were used to measure the cross sections for the alpha-induced reactions on natural yttrium. The stacked-foil target consisted of yttrium (25  $\mu$ m, Nilaco), titanium (5  $\mu$ m, Nilaco), and aluminum (5  $\mu$ m, Nilaco) foils. The thicknesses were verified within 0.6% by measuring the sizes and weights of the foils. The stacked-foil target was attached to a target holder, which also served as a Faraday-cup, and was irradiated with a 50-MeV alpha beam with an intensity of 200 pA for 1 h using the AVF cyclotron at the RIKEN beam factory. The energy of the alpha beam in each foil was calculated using stopping powers that were obtained from the SRIM software.<sup>3)</sup> The intensity was assumed to be constant in the target. The correctness of the beam parameters and foil thicknesses was checked by monitoring the reactions on aluminum and titanium foils by comparing their cross sections with the IAEA recommended values.

After the irradiation, a cooling time of over 40 min was taken to reduce the background radiation, which is an obstacle for the measurement. A high purity germanium detector was used to collect the gamma-ray spectra from the foils. To derive the cross sections of the monitored reactions, the 1274.5 keV ( $I_\gamma = 99.94\%$ ) and 320.08 keV ( $I_\gamma = 9.91\%$ ) gamma-lines were used for <sup>nat</sup>Al( $\alpha$ , x)<sup>22</sup>Na and <sup>nat</sup>Ti( $\alpha$ , x)<sup>51</sup>Cr reactions, respectively. The data obtained from the monitored re-

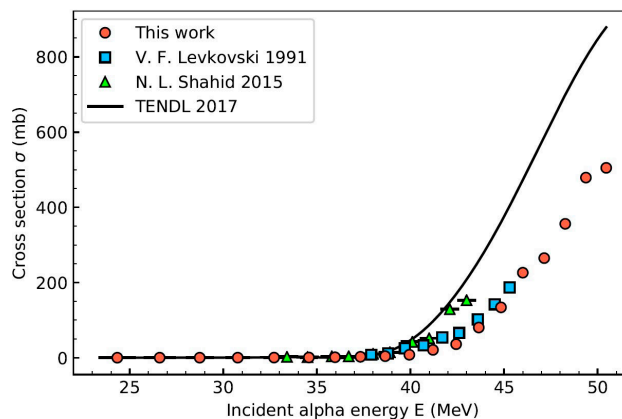


Fig. 1. Experimental cross sections of <sup>89</sup>Y( $\alpha$ , x)<sup>89</sup>Zr reaction with earlier experimental data and TENDL data.

actions was significantly consistent with the IAEA recommended values.

A specific gamma-line of 909.15 keV ( $I_\gamma = 99.04\%$ ) from <sup>89</sup>Zr was used to derive the cross sections of the <sup>89</sup>Y( $\alpha$ , x)<sup>89</sup>Zr reaction. Owing to the short half-life of <sup>89</sup>Nb ( $T_{1/2} = 2.03$  h) as compared to <sup>89</sup>Zr ( $T_{1/2} = 78.41$  h), the derived cross sections were cumulative. The cross sections of <sup>89</sup>Zr are shown in Fig. 1 in comparison with earlier two experiments<sup>4,5)</sup> and TENDL data.<sup>6)</sup> Our result is consistent with Levkovski's result and indicates that the TENDL values are overestimated at higher energy.

In this work, the peak position of the cross sections of <sup>89</sup>Y( $\alpha$ , x)<sup>89</sup>Zr reaction could not be obtained. To find the most efficient energy for <sup>89</sup>Zr production by alpha particles, another experiment using a higher energy alpha beam is needed. In addition to the peak position of the excitation function, the evaluation of specific activity and yields of other co-produced nuclei is needed for the practical application of <sup>89</sup>Y( $\alpha$ , x)<sup>89</sup>Zr reaction.

### References

- 1) M. A. Deri *et al.*, Nucl. Med. Biol. **40**, 3(2013).
- 2) V. Radchenko *et al.*, Nucl. Med. Biol. **41**, 721(2014).
- 3) J. F. Ziegler *et al.*, Nucl. Instrum. Methods Phys. Res. B **268**, 1818 (2010).
- 4) V. N. Levkovski, *Cross Sections of Medium Mass Nuclide Activation (A = 40–100) by Medium Energy Protons and Alpha Particles (E = 10–50 MeV)* (Inter-Vesi, Moscow, 1991).
- 5) M. Shahid *et al.*, Nucl. Instrum. Methods Phys. Res. B **42**, 158(2015).
- 6) A. J. Koning *et al.*, Nucl. Data Sheets **113**, 2841 (2012).

<sup>\*1</sup> Graduate School of Biomedical Science and Engineering, Hokkaido University

<sup>\*3</sup> Advanced Clinical Research Center, Fukushima Medical University

<sup>\*2</sup> Nishina Center for Accelerator-Based Science, RIKEN

<sup>\*4</sup> Institute for Nuclear Research, Hungarian Academy of Sciences (ATOMKI)

# Cross section measurement of the deuteron-induced reaction on $^{89}\text{Y}$ to produce $^{89}\text{Zr}$

M. Sakaguchi,<sup>\*1,\*2</sup> M. Aikawa,<sup>\*2,\*3</sup> M. Saito,<sup>\*2,\*3</sup> N. Ukon,<sup>\*2,\*4</sup> Y. Komori,<sup>\*2</sup> and H. Haba<sup>\*2</sup>

Zirconium-89 ( $T_{1/2} = 78.41$  h) is a positron emitter, which can be used for the diagnostic imaging of Positron Emission Tomography (PET). There are many routes to produce  $^{89}\text{Zr}$ . The  $^{89}\text{Y}(p, n)^{89}\text{Zr}$  reaction and the  $^{89}\text{Y}(d, 2n)^{89}\text{Zr}$  reaction can be quoted as their examples. The former is better known, as many experiments have been performed on this reaction during the last several decades. In contrast, only seven experiments with the latter<sup>1-7</sup> could be found in the literature. The behaviors of the excitation functions of the latter disagree with each other and there are only a few previous experiments that show cross sections over 20 MeV. These facts are obstacles to deciding the most efficient way to obtain this radionuclide. Therefore, we performed an experiment on the  $^{89}\text{Y}(d, 2n)^{89}\text{Zr}$  reaction and measured the cross sections up to 24 MeV.

We adopted the standard stacked-foil activation method for this experiment. The target consisted of  $^{89}\text{Y}$  foils (purity: 99.0%, thickness: 28.6  $\mu\text{m}$ ; Goodfellow Co., Ltd., UK) and  $^{nat}\text{Ti}$  foils (purity: 99.6%, thickness: 20.3  $\mu\text{m}$ ; Nilaco Corp., Japan), which were used for the  $^{nat}\text{Ti}(d, x)^{48}\text{V}$  monitor reaction. This stacked target was positioned in a target holder served as a Faraday cup and irradiated by a 23.6-MeV deuteron beam for 1 h at the RIKEN AVF cyclotron. The average beam intensity was 102.3 nA, which was measured by using the Faraday cup. The energies of the projectile going through each foil and their uncertainties were calculated by using the SRIM<sup>8</sup> code.

After a cooling time of approximately 1 h, we disassembled the stacked foils and measured the  $\gamma$ -ray spectra on each foil by using an HPGe detector. The 909.15-keV  $\gamma$ -line ( $I_\gamma = 99.04\%$ ) following the decay of  $^{89}\text{Zr}$  and the 983.525-keV  $\gamma$ -line ( $I_\gamma = 99.98\%$ ) following the decay of  $^{48}\text{V}$  were measured to derive the cross sections of the  $^{89}\text{Y}(d, 2n)^{89}\text{Zr}$  and  $^{nat}\text{Ti}(d, x)^{48}\text{V}$  reactions, respectively. Keeping the dead time less than 5%, the distance between the measured foils and the HPGe detector was adjusted in every  $\gamma$ -ray measurement.

The cross sections of the  $^{nat}\text{Ti}(d, x)^{48}\text{V}$  reaction were derived, and it was confirmed that their values agree with the IAEA recommended values, which indicates the correctness of the thicknesses and beam parameters within the uncertainties.

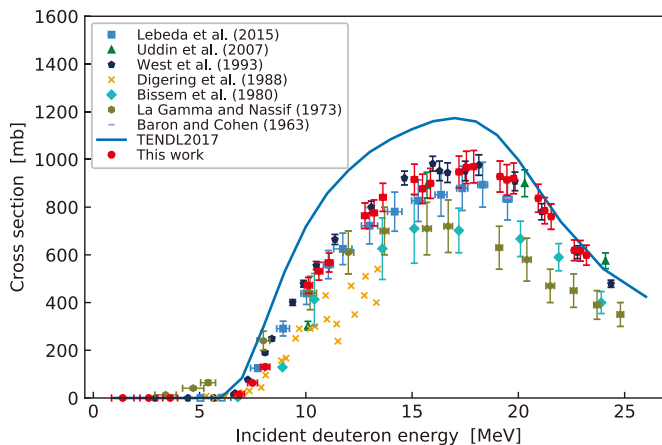


Fig. 1. Excitation function for the  $^{89}\text{Y}(d, 2n)^{89}\text{Zr}$  reaction compared with the previous experimental data and the TENDL data.

Figure 1 shows the excitation function of the  $^{89}\text{Y}(d, 2n)^{89}\text{Zr}$  reaction in this work in comparison with the previous data and the TENDL<sup>9</sup> data. Our result indicates that the peak of the excitation function is located at around 17.9 MeV and the corresponding cross section value is approximately 970 mb. These values are almost the same as that of some of the previous data. On the other hand, the cross section values of the TENDL data are higher than those of all the experimental data in the range between 10 and 20 MeV.

In this work, we performed an experiment on the  $^{89}\text{Y}(d, 2n)^{89}\text{Zr}$  reaction at the RIKEN AVF cyclotron. The stacked foil activation method and  $\gamma$ -ray spectrometry were used for this experiment. The cross sections of this reaction were measured up to 24 MeV. Our result is consistent with some of the previous data. The production yield of  $^{89}\text{Zr}$  in this reaction will be derived and compared with that in other reactions.

## References

- 1) O. Lebeda *et al.*, Nucl. Instrum. Methods Phys. Res. B **360**, 118 (2015).
- 2) M. S. Uddin *et al.*, Radiochim. Acta **95**, 187 (2007).
- 3) H. I. West *et al.*, UCRL-ID-115738, 1 (1993).
- 4) D. Digering *et al.*, J. Radioanal. Nucl. Chem. Lett. **127**, 7 (1988).
- 5) H. H. Bissem *et al.*, Phys. Rev. C **22**, (4), 1468 (1980).
- 6) A. M. La Gamma, S. J. Nassif, Radiochim. Acta **19**, 161 (1973).
- 7) N. Baron, B. L. Cohen, Phys. Rev. **129**, 2636 (1963).
- 8) J. F. Ziegler *et al.*, Nucl. Instrum. Methods Phys. Res. B **268**, 1818 (2010).
- 9) A. J. Koning *et al.*, Nucl. Data Sheets, **113**, 2841 (2012).

<sup>\*1</sup> School of Science, Hokkaido University

<sup>\*2</sup> RIKEN Nishina Center

<sup>\*3</sup> Graduate School of Biomedical Science and Engineering, Hokkaido University

<sup>\*4</sup> Advanced Clinical Research Center, Fukushima Medical University

## Activation cross sections of alpha particle induced reactions on natural nickel up to 50 MeV

S. Takács,<sup>\*1</sup> F. Ditrói,<sup>\*1</sup> H. Haba,<sup>\*2</sup> Y. Komori,<sup>\*2</sup> M. Aikawa,<sup>\*3,\*2</sup> M. Saito,<sup>\*4,\*2</sup> and T. Murata<sup>\*5,\*2</sup>

$^{67}\text{Cu}$  is a medium-energy  $\beta^-$  emitter radionuclide, which is similar to  $^{177}\text{Lu}$ , but offers the advantage of radiation suitable for diagnostics along with a therapy effect. We investigated the  $^{64}\text{Ni}(\alpha, p)^{67}\text{Cu}$  reaction by irradiating natural nickel targets. Cross sections of alpha particle-induced reactions, resulting in the production of  $^{61,64,67}\text{Cu}$ ,  $^{55,56,57,58,60}\text{Co}$ ,  $^{56,57,66}\text{Ni}$ , and  $^{62,63,65}\text{Zn}$  were determined, and the results were compared with data available in the literature.

The stacked target technique and activation method were used, followed by high-resolution gamma spectrometry of the activated target foils. Two independent irradiation experiments using different target foils and irradiation parameters were performed at the AVF cyclotron of the RIKEN RI Beam Factory. The stacked targets consisted of  $^{\text{nat}}\text{Ni}$  target foils (4.11 mg/cm<sup>2</sup> and 4.45 mg/cm<sup>2</sup>) and  $^{\text{nat}}\text{Ti}$  monitor foils to monitor the beam parameters (2.40 and 4.95 mg/cm<sup>2</sup>) of different thicknesses. The targets were irradiated for 1 and 2 h with alpha beams of 186 and 400 nA and energies of  $E_\alpha = 41.6 \pm 0.35$  MeV and  $E_\alpha = 50.73 \pm 0.30$  MeV, respectively. The primary beam energies were determined by the time-of-flight method.<sup>1)</sup> The energy degradation in the targets was calculated by the semiempirical polynomial method of Ziegler *et al.*<sup>2)</sup> The beam intensity was measured by a Faraday cup and was recorded every minute to check its stability in both cases.

The activity of the foils was measured by a HPGe spectrometer to identify the isotopes and to determine their intensity. The  $^{\text{nat}}\text{Ti}(\alpha, x)^{51}\text{Cr}$  reaction was used to monitor the beam intensity and energy degradation through the whole stack. It was not necessary to correct the beam parameters obtained from primary measurements. The foils were placed in pairs in the stack and activity of the lower energy foil of each pair was measured supposing compensation of the activity loss due to the recoil effect.

The newly determined cross section data from the two irradiations correspond well in the overlapping energy region and can be used as one dataset. Because only the  $^{64}\text{Ni}(\alpha, p)$  reaction contributes to the production of  $^{67}\text{Cu}$ , the measured data were normalized to the 100%  $^{64}\text{Ni}$  target composition and were compared to the experimental data measured earlier as well as to

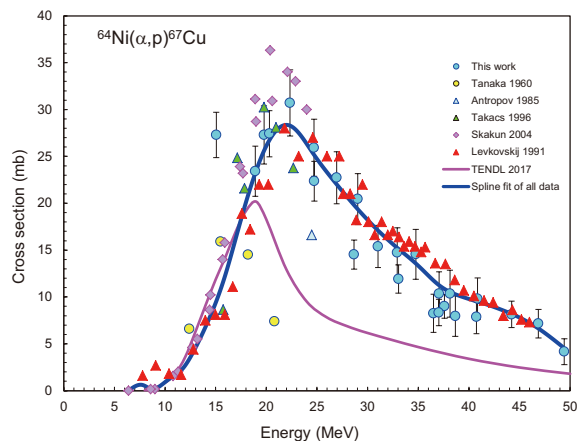


Fig. 1. Excitation function of the  $^{64}\text{Ni}(\alpha, p)^{67}\text{Cu}$  compared with the previous results and with the results of theoretical model codes.

the results of the theoretical nuclear reaction model code TALYS (Fig. 1) taken from the TENDL-2017 data library available online.<sup>3)</sup>

From the measured cross sections, yield curves were calculated and compared with the available experimental yield data. Our results agree well with most values in the literature except for the data of Tanaka (1960)<sup>4)</sup> and Antropov (1985).<sup>5)</sup>

Our preliminary data are, in general, in agreement with data in the literature, however, an additional experiment is required to cover the 20 MeV-to-threshold energy region of the excitation function. Owing to the high energy degradation of the alpha particles the usual stacked target technique cannot be used effectively below 20 MeV. Therefore, a new rotating irradiation setup is designed for measurements in this energy region.

### References

- 1) T. Watanabe *et al.*, Proc. 5<sup>th</sup> Int. Part. Accel. Conf. (IPAC2014), 3566 (2014).
- 2) J. F. Ziegler, Helium stopping powers and ranges in all elements, (Pergamon Press, New York, 1978).
- 3) A. J. Koning *et al.*, Nucl. Data Sheets **155**, 1 (2019). TENDL-2017: Database available from: [https://tendl.web.psi.ch/tendl\\_2017/tendl2017.html](https://tendl.web.psi.ch/tendl_2017/tendl2017.html)
- 4) Tanaka *et al.*, J. Phys. Soc. Jpn. **15**, 2159 (1960).
- 5) Antropov *et al.*, 35. Conf. Nucl. Spectr. and Nucl. Struct., Leningrad (1985).

<sup>\*1</sup> Institute for Nuclear Research, Hungarian Academy of Sciences

<sup>\*2</sup> RIKEN Nishina Center

<sup>\*3</sup> Faculty of Science, Hokkaido University

<sup>\*4</sup> Graduate School of Biomed. Sci. and Eng., Hokkaido University

<sup>\*5</sup> School of Science, Hokkaido University

# Measurement of half-lives of $^{181}, ^{182a}, ^{182b}, ^{183}, ^{184m}\text{Re}$ and $^{187}\text{W}$

Y. Komori\*<sup>1</sup> and H. Haba\*<sup>1</sup>

Chemical characterization of superheavy elements is one of the most important and challenging subjects in nuclear chemistry. We plan to conduct model experiments for the chemical studies of element 107, Bh, using radiotracers of its homologs, Tc and Re. Long-lived  $^{95m}\text{Tc}$  ( $T_{1/2} = 61$  d),  $^{183}\text{Re}$  ( $T_{1/2} = 70$  d), and  $^{184m,g}\text{Re}$  (m:  $T_{1/2} = 169$  d; g:  $T_{1/2} = 35.4$  d) are useful for the model experiments. These isotopes are producible in the deuteron-induced reactions on  $^{\text{nat}}\text{Mo}$  and  $^{\text{nat}}\text{W}$  (nat: natural isotopic abundance) using the RIKEN AVF cyclotron. Previously, we measured the production cross-sections of the Re isotopes in the  $^{\text{nat}}\text{W}(d, x)$  reactions for the quantitative production of  $^{183}, ^{184m,g}\text{Re}$ .<sup>1)</sup> In the course of measurements, we noticed that the half-lives of some Re isotopes such as  $^{181}, ^{183}\text{Re}$  was slightly shorter than those adopted in literatures. Furthermore, recently, the half-life of  $^{182a}\text{Re}$  has been revised from  $12.7 \pm 0.2$  h<sup>2)</sup> to  $14.14 \pm 0.45$  h<sup>3)</sup> because Bonardi *et al.* and Manenti *et al.* suggested that the half-life of  $^{182a}\text{Re}$  is  $13.74 \pm 0.48$  h<sup>4)</sup> and  $14.50 \pm 0.45$  h,<sup>5)</sup> respectively. Therefore, it is worth reinvestigating the half-lives of these Re isotopes. In this work, we measured the half-lives of  $^{181}, ^{182a}, ^{182b}, ^{183}, ^{184m}\text{Re}$  and  $^{187}\text{W}$  and compared them with the half-life values adopted in the Nudat 2.7 database.<sup>6)</sup>

We determined the half-lives of  $^{181}, ^{182a}, ^{182b}\text{Re}$  and  $^{187}\text{W}$  using a reference source method. Four  $^{\text{nat}}\text{W}$  foils with a thickness of  $20 \mu\text{m}$  were irradiated for 5 min with 24 MeV deuteron beam supplied from the RIKEN AVF cyclotron. The average beam current evaluated with the Faraday cup was 425 nA. After the irradiation, three of the  $^{\text{nat}}\text{W}$  foils were repetitively measured with three Ge detectors every 4 h or 6 h with  $^{88}\text{Y}$  ( $T_{1/2} = 106.626 \pm 0.021$  d<sup>7)</sup>).  $^{88}\text{Y}$  was used as the reference source to correct the dead time during the radioactivity measurement.<sup>8)</sup> The cooling time and dead time were  $\geq 1.6$  h after the end of bombardment (EOB) and  $\leq 12.8\%$ . The internal clock time of the computer for data acquisition was synchronized with the Internet time server in RIKEN every 1 h.

As for the long-lived isotopes,  $^{183}, ^{184m}\text{Re}$ , we determined their half-lives by following their interference-free  $\gamma$  lines under low dead time condition of  $\leq 3.0\%$ . A  $^{\text{nat}}\text{W}$  foil with a thickness of  $100 \mu\text{m}$  irradiated with the 24 MeV deuteron beam for 125 min with a beam current of  $5 \text{ p}\mu\text{A}$ , was repetitively measured every 12 h with the Ge detector at the cooling time of 474 d after the EOB.

The half-lives of  $^{181}, ^{182a}, ^{182b}, ^{183}, ^{184m}\text{Re}$  and  $^{187}\text{W}$  determined in this work are listed in Table 1 along with those adopted in the Nudat 2.7 database.<sup>6)</sup> We found

Table 1. Half-lives adopted in Nudat 2.7<sup>6)</sup> for  $^{181}, ^{182a}, ^{182b}, ^{183}, ^{184m}\text{Re}$  and  $^{187}\text{W}$  and those determined in this work. Gamma energy ( $E_\gamma$ ) used for analysis in this work is also listed.

Nuclide	Half-life	$E_\gamma$ [keV]	Half-life
	(Nudat 2.7 <sup>6)</sup> )		(this work)
$^{181}\text{Re}$	$19.9 \pm 0.7$ h <sup>9)</sup>	953.6	$18.94 \pm 0.05$ h
$^{182a}\text{Re}$	$14.14 \pm 0.45$ h <sup>3)</sup>	470.26	$14.33 \pm 0.03$ h
$^{182b}\text{Re}$	$64.2 \pm 0.5$ h <sup>3)</sup>	1427.3	$62.6 \pm 0.5$ h
$^{187}\text{W}$	$24.000 \pm 0.004$ h <sup>10)</sup>	685.81	$23.92 \pm 0.04$ h
$^{183}\text{Re}$	$70.0 \pm 1.4$ d <sup>11)</sup>	291.723	$66.5 \pm 0.1$ d
$^{184m}\text{Re}$	$169 \pm 8$ d <sup>12)</sup>	318.008	$178.7 \pm 0.4$ d
		920.933	$178.5 \pm 0.4$ d

that the half-life of  $^{181}\text{Re}$  is  $18.94 \pm 0.05$  h, which is 0.96-h shorter than the literature data of  $19.9 \pm 0.7$  h.<sup>9)</sup> The half-life of  $^{182a}\text{Re}$  is  $14.33 \pm 0.03$  h, which is consistent with the value of  $14.50 \pm 0.45$  h reported by Manenti *et al.*<sup>5)</sup> and the recently revised value of  $14.14 \pm 0.45$  h by Singh.<sup>3)</sup> The half-life of  $^{182b}\text{Re}$  is  $62.6 \pm 0.5$  h, which is 1.6-h shorter than the literature value of  $64.2 \pm 0.5$  h.<sup>3)</sup> The half-life of  $^{187}\text{W}$  is  $23.92 \pm 0.04$  h, which is slightly shorter than the literature value of  $24.000 \pm 0.004$  h.<sup>10)</sup> The half-life of  $^{183}\text{Re}$  is  $66.5 \pm 0.1$  d, which is 3.5-d shorter than the literature data of  $70.0 \pm 1.4$  d.<sup>11)</sup> The half-lives of  $^{184m}\text{Re}$  determined by the decays of 318-keV and 921-keV  $\gamma$  lines are  $178.5 \pm 0.4$  and  $178.7 \pm 0.4$  d, respectively. The average half-life of  $^{184m}\text{Re}$  is  $178.6 \pm 0.3$  d, which is 9.6-d longer than the literature data of  $169 \pm 8$  d.<sup>12)</sup> For further discussion, we will compare our newly determined half-lives of these isotopes with the previously reported values.

## References

- 1) Y. Komori *et al.*, RIKEN Accel. Prog. Rep. **49**, 245 (2016).
- 2) B. Singh, J. C. Roediger, Nucl. Data Sheets **111**, 2081 (2010).
- 3) B. Singh, Nucl. Data Sheets **130**, 21 (2015).
- 4) M. Bonardi *et al.*, Radiochim. Acta **99**, 1 (2011).
- 5) S. Manenti *et al.*, Radiochim. Acta **102**, 669 (2014).
- 6) Nudat 2.7, Nat. Nucl. Data Center, Brookhaven National Laboratory. (<http://www.nndc.bnl.gov/nudat2/>).
- 7) E. A. McCutchan, A. A. Sonzogni, Nucl. Data Sheets **115**, 135 (2014).
- 8) H. Kikunaga *et al.*, Proc. Radiochim. Acta **1**, 113 (2011).
- 9) S.-c. Wu, Nucl. Data Sheets **106**, 367 (2005).
- 10) M. S. Basunia, Nucl. Data Sheets **110**, 999 (2009).
- 11) C. M. Baglin, Nucl. Data Sheets **134**, 149 (2016).
- 12) C. M. Baglin, Nucl. Data Sheets **111**, 275 (2010).

\*<sup>1</sup> RIKEN Nishina Center

## Production of Np isotopes in nuclear reactions for standard material in accelerator mass spectrometry

Y. Hayakawa,<sup>\*1</sup> A. Yokoyama,<sup>\*2</sup> A. Sakaguchi,<sup>\*3</sup> K. Yamamori,<sup>\*1</sup> K. Sekiguchi,<sup>\*3</sup> S. Yanou,<sup>\*4</sup> Y. Komori,<sup>\*4</sup>  
T. Yokokita,<sup>\*4</sup> and H. Haba<sup>\*4</sup>

The techniques for highly sensitive mass spectrometry, such as ICP-MS and AMS, are rapidly being developed currently. Several elements or nuclides that were not supposed to be applicable in those techniques several decades ago are now quantitatively analyzed. Especially, for long-lived actinides elements, the techniques are becoming more important as a promising alternative to radioactivity measurements. The tracer nuclide for target elements, which is non-existent in nature and absent in target samples, is necessary to establish a standard in the new techniques. Tracers for several elements are available now but the tracer for neptunium has not been developed yet. We aim to devise an efficient method for the production of Np-236 in the ground state of half life  $1.54 \times 10^5$  y as a candidate for tracer nuclide.

In this study, the Np tracer production was implemented in the reactions of  $^{232}\text{Th} + ^7\text{Li}$  and  $^{238}\text{U} + \text{p}$  to measure Np-237 in environmental samples.

For irradiation, target stacks of Th metal foils of two types of thickness were prepared: a thin target for the excitation function measurement and a thick target for tracer production of Np. A silver foil was irradiated at the same time to monitor the beam intensity from the radioactivity of  $^{111}\text{In}$  generated during the irradiation with current integration using a beam course equipped with Faraday cup.

We irradiated the targets with 42 MeV  $^7\text{Li}$  ions from the RIKEN AVF cyclotron. Chemical procedures were performed to isolate Np atoms from the target. As an example of the procedure, the target material was dissolved in 3 M  $\text{HNO}_3$  with Np-239 tracer to check chemical recoveries and the sample was dried by heating. The residue was then dissolved in conc. HCl, repeatedly dried three times, and finally adjusted to 3 M  $\text{HNO}_3$  solution of 4 ml. This solution was introduced into a TEVA resin column, subsequently treated with 3 M  $\text{HNO}_3$  and 10 M HCl for purification, and finally treated with 0.1 M HCl for the elution of Np. To remove Pa, another process with a TK 400 column was performed. To determine the yields of Np isotopes and by-products,  $\gamma$ -ray spectrometry was conducted for the effluents with a Ge detector.

As an example of the result, a measured  $\gamma$  spec-

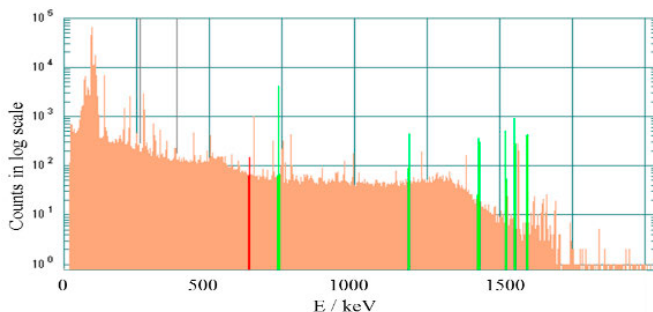


Fig. 1. Example of  $\gamma$  spectrum of isolated Np. (Red: Np-236m, Green: Np-234)

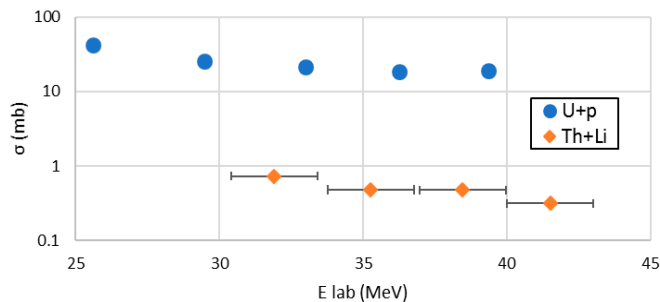


Fig. 2. Exciting functions of  $^{236\text{m}}\text{Np}$  in reactions of  $^{238}\text{U} + \text{p}$  and  $^{232}\text{Th} + ^7\text{Li}$ .

trum is shown in Fig. 1, where many photopeaks of Np isotopes including Np-236m are observed. Figure 2 compares the excitation function of Np-236m obtained from this study to that obtained from the 39 MeV  $\text{p} + \text{U}$  experiment conducted in RCNP of Osaka University. Although the cross section of  $\text{Th} + \text{Li}$  is nearly two orders of magnitude lower than that of  $\text{U} + \text{p}$ , it is predicted that the isomeric ratio of Np-236g to Np-236m for the products of the former reaction is larger than that for the latter, which had been measured to be around 0.5.<sup>1)</sup> The analysis of the result is still in progress and additional experiments including mass spectrometry are in the planning stage at present.

### Reference

- 1) J. Aaltonen, M. Brenner, S. A. Egorov, A. M. Fridkin, V. B. Funschtein, E. A. Gromova, P. Manngård, V. A. Rubchen'a, Yu. A. Selitsky, V. A. Yakovlev, V. S. Zenkevich, *Phys. Rev. C* **41**, 513 (1990).

<sup>\*1</sup> Graduate School of Natural Science and Technology, Kanazawa University

<sup>\*2</sup> Institute and College of Science and Engineering, Kanazawa University

<sup>\*3</sup> Center for Research in Isotopes and Environmental Dynamics, University of Tsukuba

<sup>\*4</sup> RIKEN Nishina Center

## Column chromatography of astatine using weak base anion exchange resin

H. Ikeda,<sup>\*1,\*2,\*3</sup> H. Kikunaga,<sup>\*2,\*3</sup> Y. Komori,<sup>\*3</sup> T. Yokokita,<sup>\*3</sup> D. Mori,<sup>\*3</sup> H. Haba,<sup>\*3</sup> and H. Watabe<sup>\*1</sup>

Astatine (At) is one of the nuclides expected to be applied for targeted  $\alpha$ -particle therapy (TAT). Several methods for At separation are known. Two methods (dry distillation<sup>1)</sup> and wet extraction<sup>2,3)</sup> are used mainly. Dry distillation can obtain a pure solution of At without impurities; however, it requires the construction of a complicated apparatus.<sup>1)</sup> On the other hand, although wet extraction is a simple method, the aqueous solution is contaminated with the organic solvent after back extraction. To solve these problems, we tried At separation using column chromatography.<sup>4)</sup> However, the eluent was too alkaline for biological studies. Therefore, we need to find a solution with mild conditions. In the general wet separation of At, it is necessary to dissolve bismuth metal or bismuth oxide ( $\text{Bi}_2\text{O}_3$ ) into nitric acid. We examined the dissolution method using hydrochloric acid (4 M HCl).<sup>4)</sup> However, large amounts of anions other than astatide anion ( $\text{At}^-$ ) existed in the solution, which was used to dissolve the  $\text{Bi}_2\text{O}_3$  target in our study. This influenced the behavior of At in column chromatography, and we could not achieve a high yield of At tracer. In this work, we reconsidered the chemical operation. Improvement of the dissolution method of the  $\text{Bi}_2\text{O}_3$  target and the conditions of column chromatography were investigated. The radioactivity was measured with a high-purity germanium detector. The quantitation of  $^{211}\text{At}$  was carried out with  $\gamma$ -ray at 687 keV ( $I_\gamma = 0.261\%$ ).

We produced  $^{211}\text{At}$  at the RIKEN Nishina Center using the  $^{209}\text{Bi}(\alpha, 2n)^{211}\text{At}$  reaction (29 MeV, 250 particle nA, 30 min). A  $\text{Bi}_2\text{O}_3$  pellet was used as the target. The irradiated target was added to 12 mL of 0.25 M EDTA  $\cdot$  2Na solution and 0.01 M L-ascorbic acid solution in a 50 mL tube. By shaking this mixture for 60 min, the  $\text{Bi}_2\text{O}_3$  target was completely dissolved.

This solution was used for column chromatography studies. 3-Aminopropyl Silica Gel (Tokyo Chemical Industry Co., Ltd.) was used as the weak anion exchange resin, and 1 mL ( $7\text{ mm}\phi \times 26\text{ mm}$ ) of the resin was filled into the Muromac<sup>®</sup> Mini-column (M size). This was flushed with 25 mL of EtOH, 10 mL of  $\text{H}_2\text{O}$ , and 10 mL of 1 M L-Ascorbic acid in this order (conditioning).

On dissolving the  $\text{Bi}_2\text{O}_3$  target, 71% of  $^{211}\text{At}$  was adsorbed to the 50 mL tube. Column chromatography was carried out using the  $^{211}\text{At}$  remaining in the solution. The operations and results are shown in Fig. 1. We found that  $^{211}\text{At}$  could be separated with a 50% yield

at a more mild condition (0.3–1 M NaOH). However, 7–25% and 1–7% of  $^{211}\text{At}$  were lost at the charge and washing processes, respectively. The column residue of  $^{211}\text{At}$  was 15–22%. The separation method of At in our study is still unstable and has to be improved.

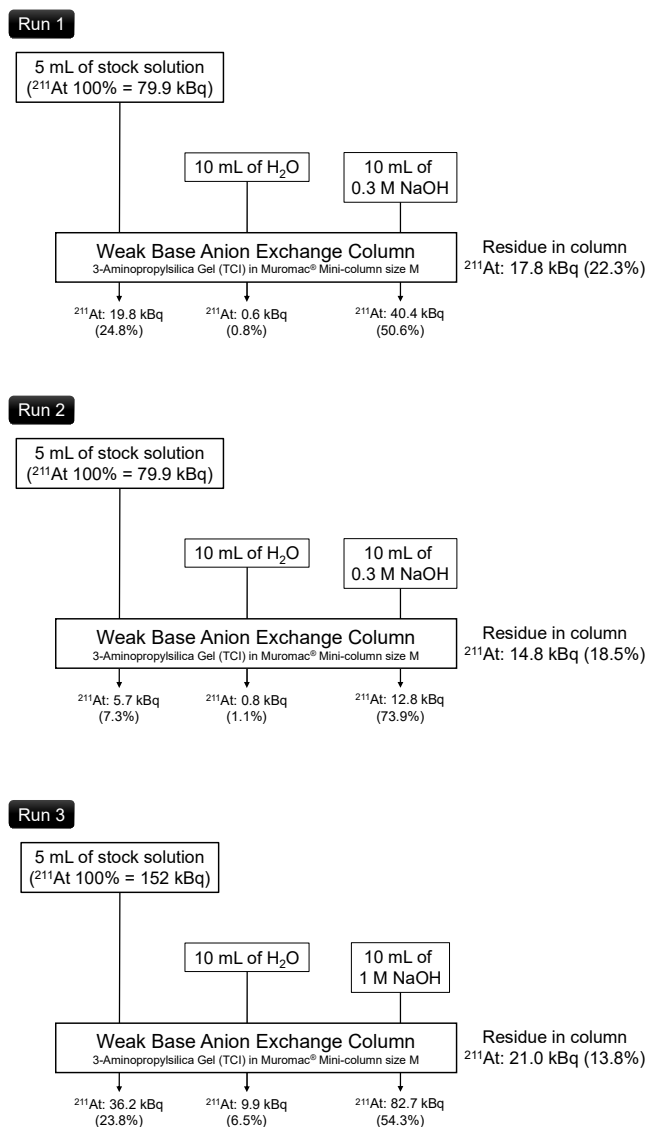


Fig. 1. Methods and results of column chromatography. Run 1 and Run2 had the same conditions; however, the results did not show the same behavior.

### References

- 1) S. Lindegren *et al.*, Appl. Radiat. Isot. **55**, 157 (2001).
- 2) M. S. Sultana *et al.*, J. Radioanal. Nucl. Chem. **243**, 631 (2000).
- 3) C. Zona *et al.*, J. Radioanal. Nucl. Chem. **276**, 819 (2008).
- 4) H. Ikeda *et al.*, RIKEN Accel. Prog. Rep. **51**, 227 (2017).

\*1 Cyclotron and Radioisotope Center, Tohoku University

\*2 Research Center for Electron Photon Science, Tohoku University

\*3 RIKEN Nishina Center

## Speciation analysis of oxidation states of astatine extracted into ethanol-water solutions

Y. Shin,<sup>\*1</sup> K. Kawasaki,<sup>\*1</sup> K. Aoi,<sup>\*2</sup> K. Washiyama,<sup>\*3</sup> A. Yokoyama,<sup>\*2</sup> I. Nishinaka,<sup>\*4</sup> S. Yanou,<sup>\*5</sup> and H. Haba<sup>\*5</sup>

The short-path length and high linear energy transfer of  $\alpha$  particles are expected to enable targeted alpha therapy for the treatment of tumor. A promising nuclide among various  $\alpha$  emitters is  $^{211}\text{At}$  with a half-life of 7.21 h, which has gained popularity owing to its appropriate life and possible compounds as a halogen element. This has been the motivation behind several preclinical studies on At-chemistry<sup>1)</sup> However, the successive chemical processes for the general use of At-chemistry has not been well studied. We aim to study the wet chemistry processes of At that may form a prevailing technology.

In previous studies,<sup>2,3)</sup> the At-211 radioactivity was recovered efficiently from an irradiated Bi target in the chemical systems of dodecane and ethanol solution with oxidizing agents such as N-bromosuccinimide (NBS) and bromine water, which supply  $\text{Br}_2$ . However, the mechanism of solvent extraction was not clarified in the study. Here, we performed a thin layer chromatography (TLC) experiment to investigate the oxidation states of At species extracted into the system with NBS as well as bromine water, in reference to a TLC study on At species.<sup>4)</sup>

The At-211 radioactivity was produced via  $^{209}\text{Bi}(\alpha, 2n)$  reaction at the RIKEN AVF cyclotron and delivered to Kanazawa University. The irradiated Bi target was dissolved in 2 mL of 6 M  $\text{HNO}_3$  and diluted with 10 mL of  $\text{H}_2\text{O}$  to prepare a 1 M  $\text{HNO}_3$  solution, from which the  $^{211}\text{At}$  nuclide was extracted into the dodecane solvent. Aliquots of the solution were subjected to back extractions into 90% ethanol solution with NBS or  $\text{Br}_2$  water after 15 min of its addition or without an oxidizing agent. 10  $\mu\text{L}$  from each sample of  $^{211}\text{At}$  (ca. 15 to 50 Bq) obtained in the back extractions was spotted on a TLC plate (Merck Silica gel 60 F254 aluminum sheet,  $10 \times 2$  cm) and developed with 50% ethanol solution for 90 min (7 cm in flow distance). After drying, the plate was exposed to an imaging plate for 10 to 20 min to perform an image analysis of its radioactivity.

The images of TLC demonstrated in Fig. 1 suggest that three different species were separated. The results of the analysis exhibit that the oxidizing agents of  $\text{Br}_2$  water and NBS significantly increase the oxidized species of  $\text{AtO}_4^-$  instead of decreasing the others' as

compared to the case without an oxidizing agent. This indicates that such oxidation due to the agents causes distribution among the species and enhance the distribution ratio of At during extraction. Therefore, the back-extraction favors the oxidized species instead of  $\text{At}^-$ .

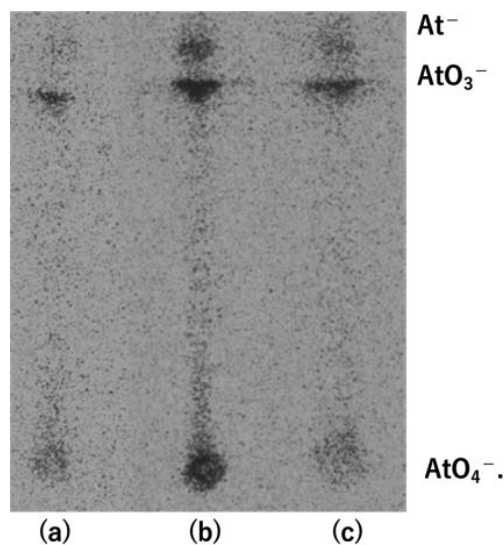


Fig. 1. Imaging of  $^{211}\text{At}$  radioactivity on thin-layer chromatography for (a)  $\text{Br}_2$  water, (b) NBS, and (c) no oxidizing agent (see text for detail).

Table 1. Distributions of At chemical species in extracted solutions.

Chemical species	$\text{Br}_2$ water	NBS	No addition
$\text{At}^-$	12 %	13 %	23 %
$\text{AtO}_3^-$	47 %	45 %	57 %
$\text{AtO}_4^-$	41 %	42 %	20 %

### References

- 1) F. Guérard, J-F. Gestin, M. W. Brechbiel, *Cancer Biother. Radiopharm.*, **28**, 1 (2013).
- 2) E. Maeda, A. Yokoyama, T. Taniguchi, K. Washiyama, I. Nishinaka, *J. Radioanal. Nucl. Chem.* **303** (2), 1465 (2015).
- 3) Y. Shin, K. Kawasaki, N. Yamada, K. Washiyama, A. Yokoyama, I. Nishinaka, S. Yanou, H. Haba, *RIKEN Accel. Prog. Rep.* **51**, 228 (2018).
- 4) I. Nishinaka, K. Hashimoto, H. Suzuki, *J. Radioanal. Nucl. Chem.* **318**, 897 (2018).

<sup>\*1</sup> Institute and College of Science and Engineering, Kanazawa University

<sup>\*2</sup> Graduate School of Natural Science and Technology, Kanazawa University

<sup>\*3</sup> Fukushima Global Medical Science Center, Fukushima Medical University

<sup>\*4</sup> Quantum Beam Science Research Directorate, National Institutes for Quantum and Radiological Science and Technology

<sup>\*5</sup> RIKEN Nishina Center

## Purification of $^{121m}\text{Te}$ by anion exchange chromatography

T. Kubota,<sup>\*1,\*2</sup> K. Iwata,<sup>\*1</sup> S. Fukutani,<sup>\*1</sup> T. Takahashi,<sup>\*1</sup> H. Haba,<sup>\*2</sup> D. Mori,<sup>\*2</sup> and S. Takahashi<sup>\*1</sup>

Radioactive tellurium nuclides, such as  $^{129}\text{Te}$ ,  $^{131}\text{Te}$ , and  $^{132}\text{Te}$ , were released into the environment by the Fukushima accident. These are the parent nuclide of radioactive iodine,  $^{129}\text{I}$ ,  $^{131}\text{I}$ , and  $^{132}\text{I}$ , respectively, regarded as critical for internal exposure, and their fission yield is relatively high. The data on the environmental behavior of tellurium are required to estimate the radiation doses after the accidents. To obtain such data, tracer experiments using radioactive tellurium are essential. This report describes the purification of  $^{121m}\text{Te}$  to prepare an adequate tracer for plant and animal experiments.

Tellurium-121m was produced by the bombardment of  $\text{Sb}_2\text{O}_3$  pellets with 24 MeV deuterons at the RIKEN AVF cyclotron.<sup>1)</sup>  $\text{Sb}_2\text{O}_3$  powder with a purity of 99.999% was pressed to form a pellet with a diameter of 15 mm. The irradiated pellets were transported to the Institute for Integrated Radiation and Nuclear Science, Kyoto University for further treatment.

Tellurium was purified from antimony by anion chromatography where two methods were applied, namely, Downs's method<sup>2)</sup> and its modification. Downs *et al.* reported that the irradiated sample dissolved in HCl was diluted to 2 M HCl and then added with hypochlorite, thereby separating tellurium and antimony by anion chromatography.<sup>2)</sup> In the other method, the mixture of antimony dissolved in conc. HCl and NaClO was poured into an anion exchange column and then tellurium was recovered in eluant.

Figure 1 shows the result of an attempt to purify tellurium by the Downs's method where only antimony is expected to be eluted with 2 M HCl. Both elements

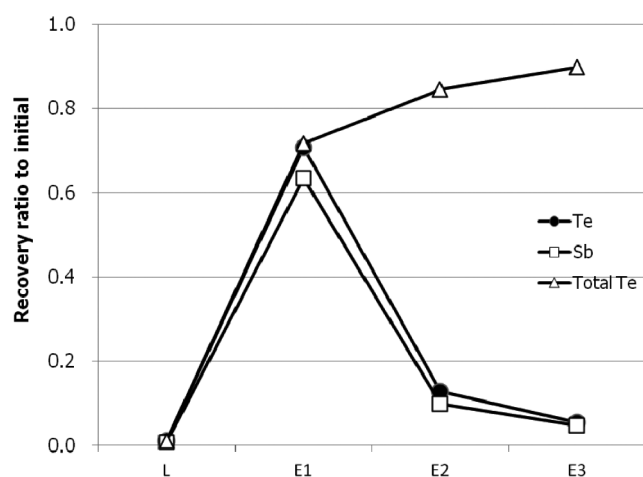


Fig. 1. Recovery of tellurium and antimony in each eluate. L denotes the loading solution of 1 mL and E1, E2, and E3 denote the eluent of 2 mL of 2 M HCl.

<sup>\*1</sup> Institute for Integrated Radiation and Nuclear Science, Kyoto University

<sup>\*2</sup> RIKEN Nishina Center

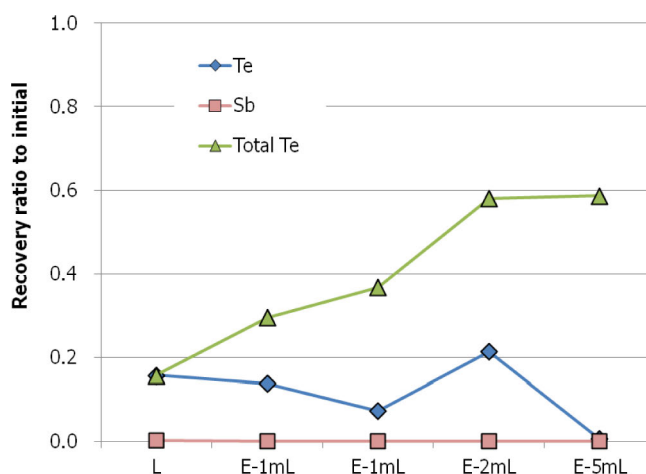


Fig. 2. Recovery of tellurium and antimony in each eluate. L denotes the loading solution of 1.4 mL and E denotes the eluent of a mixture of conc. HCl and 5% NaClO in the ratio of 10:1 (v/v).

were, however, similarly eluted; hence, tellurium cannot be purified.

Figure 2 shows the purification of tellurium by the modification method. Tellurium was eluted first in the reverse elution order described in Downs's method and was consequently separated from antimony with a recovery of 60%.

Antimony forms  $\text{Sb(V)-chloro}$  complex ion in oxidizing  $\text{HCl}^{3)}$  to be strongly adsorbed onto anion exchange resin. Thus, the concentration of antimony in the eluate can be ignored for the loading solution in both methods. The fate of antimony depended on the following eluents, whose redox potential and chloride concentration are critical for the separation where tellurium can be obtained without antimony when both values are high.

Because  $\text{Te(VI)}$  is not adsorbed onto the anion exchange resin at any concentration of HCl,<sup>4)</sup> the valency of tellurium in the eluate is 6 and that of remaining would be 4. The rate of redox reaction with NaClO is considered to affect the elution property. Therefore, an appropriate regulation of redox potential would yield a higher tellurium recovery with high purity. In addition, the disadvantage of the purification method used here naturally causes to evolve toxic chlorine gas.

The purification method was established to provide a tracer of carrier free radioactive tellurium without antimony. Further investigations are still required from the perspective of safety as well as recovery.

### References

- 1) T. Kubota *et al.*, RIKEN Accel. Prog. Rep. **50**, 254 (2017).
- 2) D. Downs, D. A. Miller, J. Rad. Nucl. Chem. **262**, 241 (2004).
- 3) C. Yoshimura *et al.*, Japan Analyst **13**, 1249 (1964).
- 4) K. Kimura *et al.*, Japan Analyst **7**, 174 (1958).

## Production of arsenic RI tracer from gallium oxide target by alpha beam irradiation

H. Ikeda,<sup>\*1,\*2,\*3</sup> H. Kikunaga,<sup>\*2,\*3</sup> Y. Komori,<sup>\*3</sup> T. Yokokita,<sup>\*3</sup> D. Mori,<sup>\*3</sup> H. Haba,<sup>\*3</sup> and H. Watabe<sup>\*1</sup>

Arsenic (As) is toxic to living beings. Therefore, it is considered one of the most important environmental pollutants. Contamination of soil by As significantly influences the living environment and agriculture. Phytoextraction is an effective method to remove As from the contaminated soil.<sup>1)</sup> Thus it is necessary to determine the plant species that can efficiently extract As to achieve effective As removal. We need to investigate which plant species more efficiently extract arsenic to achieve effective arsenic removal. We believe that plant imaging using radioisotope (RI) is effective for that purpose. Arsenic is known to be stable in the trivalent and pentavalent oxidation states. However, it is suggested that the pentavalent arsenic species are predominant in soil due to the biological activity of transforming microorganisms.<sup>2)</sup> Therefore, the arsenic species in the same oxidation state as in soil are preferred for our present purpose. It was recently reported<sup>3,4)</sup> that the  $^{72}\text{Se}(T_{1/2} = 8.5 \text{ d})/^{72}\text{As}(T_{1/2} = 26.0 \text{ h})$  generator was prepared from a germanium target irradiated with protons. The tracer from the method, however, includes beta emitters useless for the positron imaging. In this study, we aim to develop a method for the tracer preparation of  $^{74}\text{As}$  ( $T_{1/2} = 17.77 \text{ d}$ ), a positron emitter using the reaction system of a gallium (Ga) target with alpha particles for less contamination of beta emitters in the tracer. The  $^{74}\text{As}$  radioactivity was measured by gamma-ray spectrometry with a high-purity germanium detector.

0.1 g of  $\text{Ga}_2\text{O}_3$  powder was formed into pellets (10 mm $\phi$ ). Each pellet was covered with an aluminum foil (10  $\mu\text{m}$  thickness) and used as a target. The target was irradiated with an alpha beam (29 MeV, 1.5  $\mu\text{A}$ ) for 30 min. Following processes for tracer preparation were started after the byproducts such as  $^{71}\text{As}$  ( $T_{1/2} = 65 \text{ h}$ ) and  $^{72}\text{As}$  decayed out at least 4 weeks after the irradiation. The irradiated  $\text{Ga}_2\text{O}_3$  was dissolved in 1 mL of 12 M NaOH by heating up to 80°C. 917 mg of non-irradiated  $\text{Ga}_2\text{O}_3$  was dissolved in 9 mL of 12 M NaOH and added to the target solution, which was neutralized into a pH of 4 to 5 with ca. 2 mL of 6 M HCl and changed into the suspending solution. The suspension was subjected to solvent extraction with 5 mL of 1 M Di-(2-ethylhexyl)phosphoric acid (HDEHP) organic solution with either of benzene, toluene, and 1-octanol by shaking for ca. 1 h. The aqueous phase from solvent extraction with toluene or benzene was processed into the following chemical treatment after precipitation of

Table 1. Arsenic yields extracted into aqueous phase.

solvent	benzene	toluene	1-octanol
yield (%)	$66.5 \pm 0.8$	$65.8 \pm 0.9$	$40.2 \pm 0.5$

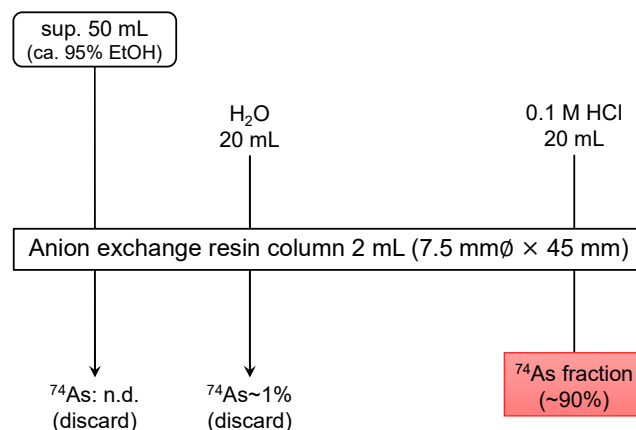


Fig. 1. A part of the scheme for As tracer preparation.

NaCl by adding ethanol.

The supernatant collected from the aqueous solution was treated after measuring its radioactivity, as depicted in Fig. 1, where a chromatography column of 2 mL anion exchange resin of Muromac<sup>®</sup> 1  $\times$  8 100–200 mesh ( $\text{Cl}^-$  form) filled into the 30 Muromac<sup>®</sup> Mini-column M (7.5 mm $\phi$   $\times$  45 mm) was used. This column was flushed with 20 mL of  $\text{H}_2\text{O}$ , 20 mL of 1 M NaOH, and 20 mL of  $\text{H}_2\text{O}$  in a sequential order. The ion form of the resin was changed from  $\text{Cl}^-$  to  $\text{OH}^-$  in the preparative conditioning. The supernatant was charged into the column, which was flushed with 20 mL of  $\text{H}_2\text{O}$  to remove ethanol and undesired species. After that,  $^{74}\text{As}$  was eluted with 20 mL of 0.1 M HCl.

Table 1 presents the results of solvent extraction. The recoveries of  $^{74}\text{As}$  isotope are nearly the same for benzene and toluene except for 1-octanol. The loss of  $^{74}\text{As}$  in coprecipitation with NaCl was ca. 1.7%. The column chromatographic process in Fig. 1 lost ca. 10% of the charged  $^{74}\text{As}$  onto the column. We successfully prepared an  $^{74}\text{As}$  tracer solution including 60% of the produced radioactivity in a  $\text{Ga}_2\text{O}_3$  target combining solvent extraction and anion exchange column chromatography.

### References

- 1) M. Lei *et al.*, *Env. Sci. and Poll. Res.* **25**, 124 (2018).
- 2) R. E. Macur *et al.*, *Env. Sci. and Tech.* **38**, 104 (2004).
- 3) M. Jahn *et al.*, *Radiochim. Acta* **98**, 807 (2010).
- 4) D. E. Wycoff *et al.*, *J. Chromatogr. A* **1340**, 109 (2014).

\*1 Cyclotron and Radioisotope Center, Tohoku University

\*2 Research Center for Electron Photon Science, Tohoku University

\*3 RIKEN Nishina Center

## Production of $^{44\text{m}}\text{Sc}$ for multiple-isotope PET

T. Fukuchi,<sup>\*1</sup> S. Yano,<sup>\*2</sup> H. Haba,<sup>\*1</sup> and Y. Watanabe<sup>\*1</sup>

We have been working toward the development of a next-generation positron emission tomography (PET) system, known as multiple-isotope PET (MI-PET). MI-PET is designed to coincide with  $\gamma$ -ray using additional detectors and identify the tracer by detecting the prompt  $\gamma$ -ray, which is emitted after positron emission from positron- $\gamma$  emitter. Figure 1 shows an image and schematic illustration of the developed MI-PET system. The system is composed of a PET system and additional  $\gamma$ -ray detectors. The PET system consists of pixelized gadolinium orthosilicate (GSO) scintillation detectors and has a ring geometry with an inner diameter and width of 95 mm and 37.5 mm, respectively. Eight bismuth germanium oxide (BGO) scintillation detectors constitute the additional eight detectors, each with a dimension of  $50 \times 50 \times 30 \text{ mm}^3$ , arranged in two rings mounted on each side of the PET ring.<sup>1)</sup>

For multiple-isotope imaging using MI-PET, at least one positron- $\gamma$  emitter is necessary as a tracer. Scandium-44 is one of the candidates for the specific radioactive tracer for MI-PET owing to its large positron and  $\gamma$ -ray emission ratio and moderate half-life ( $^{44}\text{Sc}$ : 3.97 h,  $^{44\text{m}}\text{Sc}$ : 58.61 h). Therefore, we studied the production of  $^{44\text{m}}\text{Sc}$  and its imaging using MI-PET.

For  $^{44\text{m}}\text{Sc}$  production, we used  $^{\text{nat}}\text{CaO}$  powder as the target material, which was pressed into a disk with an inner diameter and thickness of 10-mm and  $376\text{-mg/cm}^2$ , respectively. The target was irradiated for 3 h with a 24-MeV deuteron beam having an intensity of  $3.0 \mu\text{A}$  at the RIKEN AVF cyclotron. The irradiated CaO target was dissolved in 6 M HCl and evaporated to become dry. Subsequently, the residue was dissolved in 5 mL of 2 M HCl. The solution was passed through an anion exchange resin column (DGA resin, particle size: 50–100  $\mu\text{m}$ ) filled in a Muromac column.<sup>2)</sup> The resin was then washed with 5 mL of 2 M HCl and  $^{44\text{m}}\text{Sc}$  was eluted from the resin with 10 mL of 0.1 M HCl. Finally, approximately 2.0 MBq of  $^{44\text{m}}\text{Sc}$  with 90% radiochemical

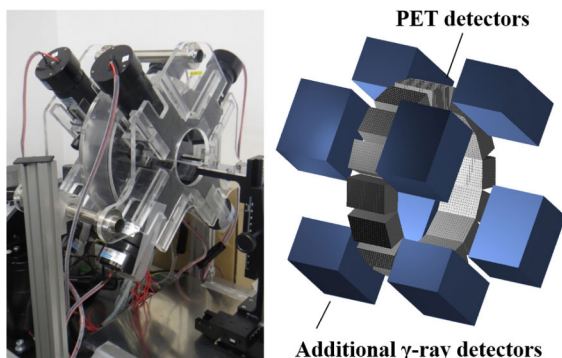


Fig. 1. Image (left) and schematic illustration (right) of the developed PET system.

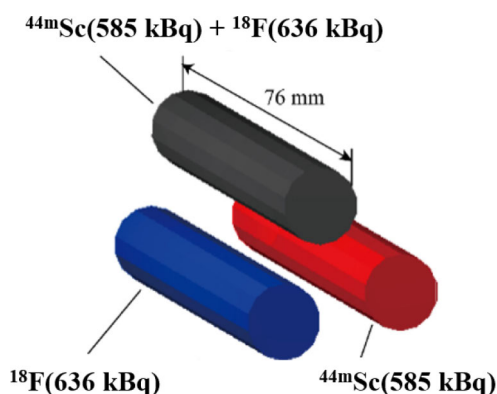


Fig. 2. Illustration of rod phantom configuration.

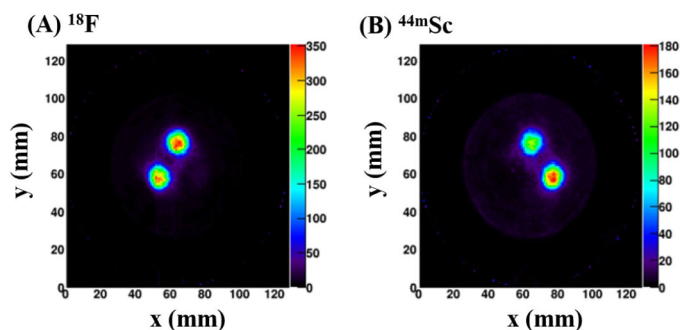


Fig. 3. The x-y plane projection images of rod phantom. Images were reconstructed with (A) absence or (B) presence of  $\gamma$ -ray detection.

yield was obtained.

To test the imaging ability of the MI-PET system for  $^{44\text{m}}\text{Sc}$ , we scanned a dual radionuclide rod phantom that comprised three cylindrical rods with a diameter and length of 10 mm and 76 mm, respectively. Scandium-44m and  $^{18}\text{F}$  (pure positron emitter) dissolved in water were poured into the rods. The first rod had  $^{44\text{m}}\text{Sc}$  (585 kBq) and  $^{18}\text{F}$  (636 kBq) activities. The second and third rods had  $^{44\text{m}}\text{Sc}$  (585 kBq) and  $^{18}\text{F}$  (636 kBq) activities, respectively. The configuration of this rod phantom is illustrated in Fig. 2. The rods were positioned parallel to the scanner's axial direction and a 30-min scan was performed.

Figure 3 shows the reconstructed phantom images as the x-y plane projection images of the rod phantom with the absence (A) or presence (B) of  $\gamma$ -ray detection. From these images, the distribution of  $^{44\text{m}}\text{Sc}$  and  $^{18}\text{F}$  is evident.

This study demonstrates the feasibility of  $^{44\text{m}}\text{Sc}$  imaging using MI-PET. In future, we will conduct multiple isotope animal experiments using  $^{44\text{m}}\text{Sc}$  and the other PET tracer. We will also synthesize useful MI-PET drug labeled with  $^{44\text{m}}\text{Sc}$ .

### References

- 1) T. Fukuchi *et al.*, *Med. Phys.* **40**, 6, 2257 (2017).
- 2) C. Alliot *et al.*, *Nucl. Med. Bio.* **42**, 524 (2015).

<sup>\*1</sup> RIKEN Center for Biosystems Dynamics Research

<sup>\*2</sup> RIKEN Nishina Center

## Adsorption experiments of $^{88}\text{Y}$ and $^{143}\text{Pm}$ on in $\text{HNO}_3$

T. Yokokita,<sup>\*1</sup> S. Yano,<sup>\*1</sup> Y. Komori,<sup>\*1</sup> and H. Haba<sup>\*1</sup>

Seventeen elements of Sc, Y, and 15 lanthanides are called as rare earth elements (REEs). REEs are used in a wide range of applications such as semiconductors, catalysis, lasers, magnets, and neutron absorbers.<sup>1)</sup> It is difficult to purify them due to their very similar chemical properties. Therefore, simple and effective mutual separation methods are needed to obtain pure materials for the industry.

So far, many extractants have been developed, and some extractants are commercially available. However, the adsorption behavior of REEs on those resins were only reported for some elements in some inorganic solutions. A systematic study of the adsorption behavior of many elements will be useful for the development of separation and purification technology. In this work, to develop the separation methods of REEs, we studied the adsorption behavior of Y and Pm using 18 commercially available resins.

$^{88}\text{Y}$  and  $^{143}\text{Pm}$  were produced in the  $^{\text{nat}}\text{Sr}(d, xn)^{88}\text{Y}$  and  $^{\text{nat}}\text{Pr}(\alpha, xn)^{143}\text{Pm}$  reactions using the K70 AVF cyclotron at RIKEN and were separated from the target materials using LN resin. In the adsorption experiments, the resins (Actinide, CU, DGA (normal), DGA (branched), LN, LN2, Muromac 1 × 8, Muromac 50 W × 8, Pb, RE, Sr, TBP, TK 100, TK 101, TK 400, TRU, UTEVA, and ZR resins) were added in 1 mL of  $\text{HNO}_3$  containing  $^{88}\text{Y}$  or  $^{143}\text{Pm}$  in a PP tube, and the mixture was shaken for 4 h using a mixer. After that, the resin was removed by centrifugation. Subsequently, the filtrate was pipetted into another tube and weighed and then subjected to  $\gamma$ -ray spectrometry using a Ge detector. Finally, the  $\text{HNO}_3$  concentrations of the aqueous phases were determined by titration with a standardized NaOH solution. In all the adsorption experiments, control experiments without the resin were performed. The  $K_d$  values were determined from the following equation:

$$K_d = A_r V_s / A_s w_r = (A_c - A_s) V_s / A_s w_a \quad (1)$$

where  $A_r$ ,  $A_s$ , and  $A_c$  are the radioactivities of the resin, the solution, and the control solution, respectively.  $V_s$  is

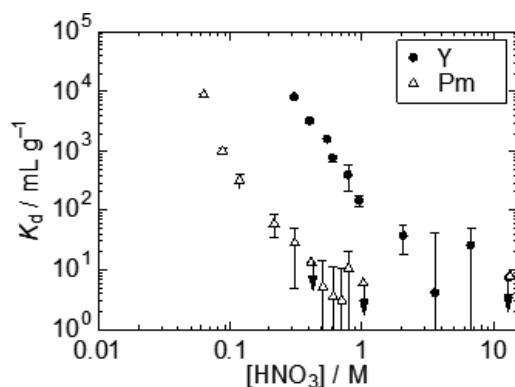


Fig. 1. The  $K_d$  values of Y and Pm with LN resin as a function of  $\text{HNO}_3$  concentration.

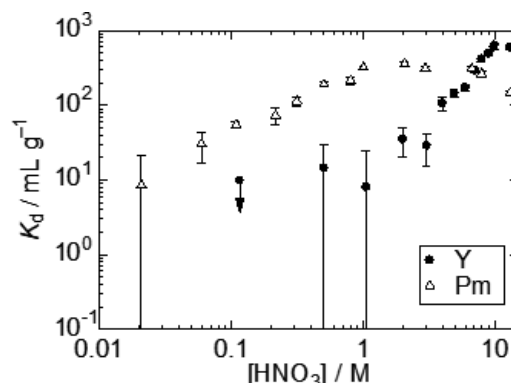


Fig. 2. The  $K_d$  values of Y and Pm with TRU resin as a function of  $\text{HNO}_3$  concentration.

the volume (mL) of the solution, and  $w_a$  is the mass (g) of the dry resin.

We investigated the  $K_d$  values of Y and Pm as functions of  $\text{HNO}_3$  concentration. The  $K_d$  values of Y and Pm were low ( $\leq 20 \text{ mL g}^{-1}$ ) and constant when we used CU, Muromac 1 × 8, Pb, Sr, TBP, TK 101, TK 400, UTEVA, and ZR resins in 0.1–13 M  $\text{HNO}_3$ . It was found that these resins are not suitable for the separation of Y and Pm in  $\text{HNO}_3$ .

Using DGA (branched) and Muromac 50 W × 8 resins, Y and Pm were adsorbed on the resins in some  $\text{HNO}_3$  concentrations, and the  $K_d$  values of Y agreed with those of Pm. Therefore, these resins are not useful for the separation of Y and Pm from each other.

When Actinide and DGA (normal) resins were used, the  $K_d$  values of Y and Pm were  $\geq 10^2 \text{ mL g}^{-1}$ , and the values were different from each other. Y and Pm can be separated using these resins. However, those  $K_d$  values were  $\geq 10^2 \text{ mL g}^{-1}$  in 0.1–13 M  $\text{HNO}_3$ , and both Y and Pm were adsorbed on the resins. The Y and Pm species adsorbed on these resins can be stripped by using a large volume of eluents, and this separation method requires a long time. It is concluded that Actinide and DGA (normal) resins are not suitable for the separation of Y and Pm.

Figure 1 shows the dependences of the  $K_d$  values of Y and Pm on the  $\text{HNO}_3$  concentration in the adsorption experiment using LN resin. When LN resin is used, the  $K_d$  values of Y are higher than those of Pm in a high  $\text{HNO}_3$  concentration range. The same behavior was observed using LN2 and TK 100 resins. Figure 2 shows the  $\text{HNO}_3$  concentration dependences of the  $K_d$  values of Y and Pm on the TRU resin. The  $K_d$  values of Y are lower than those of Pm when TRU resin is used. The same behavior was obtained with RE resin. It is suggested that these resins are useful for the separation of Y and Pm.

In the future, we will perform adsorption experiments using other REE elements and discuss about good separation conditions for REEs.

### Reference

- 1) B. Swain, E. O. Otu, Sep. Purif. Technol. **83**, 82 (2011).

<sup>\*1</sup> RIKEN Nishina Center

## **4. Radiation Chemistry and Biology**



## Development of new cultivar of Hibiscus by C-ion beam irradiation

S. Ochiai,<sup>\*1</sup> M. Ochiai,<sup>\*1</sup> Y. Ochiai,<sup>\*1</sup> Y. Hayashi,<sup>\*2</sup> and T. Abe<sup>\*2</sup>

Hibiscus is a well-known flowering shrub that belongs to the mallow family (Malvaceae). There are a lot of cultivated varieties over the world with wide variations in flower color and shape. It is popular in Japan as an ornamental plant. We, Hanakongou Co. Ltd., have developed original cultivars of Hibiscus and nine of them are currently in the market. In this study, we attempted mutation induction by heavy-ion beam irradiation to increase the variations in flower colors of our original cultivars. Consequently, we successfully developed a new color cultivar from ‘mother-pink’ (Fig. 1).

Two kinds of cultivars (‘mother-pink,’ ‘moon-light’) and a strain called dark-red of hibiscus were used for the irradiation treatment in 2014. The cuttings were irradiated with C-ion beams (LET 23 keV/ $\mu\text{m}$ ) at doses of 10, 20, 30, and 40 Gy. The irradiated cuttings were planted in the soil and the rooted cutting was cultivated in a greenhouse. The number of survived plants were counted after seven months. Table 1 lists the number of survived plants. There was no decrease in the survival at 20 Gy in ‘mother-pink’ and ‘moon-light.’ However, the survival rate at 20 Gy was lesser than 50% in dark-red. We multiplied cuttage from ‘mother-pink’ irradiated with 20 Gy. The growth of irradiated cuttings varied individually even with high survival rate. No mutation in the color of flowers or leaves were observed in the survived 35 plants. We selected the plants with well rooting from the 35 plants and produced 500 cuttings in 2015. Some plants grown from these cuttings had leaves with a lighter color and no mutation in the color of the flower was observed. Propagation by cutting was repeated in 2016 and we cultivated 1,300 plants. We isolated three mutated plants with orange flowers from the 1,300 plants. A stability in the flower color mutation was confirmed by cultivating 60 cuttings from three plants in 2017. Although the flower size, intensity of flower color, and length of internode were different, all plants bloomed with orange flowers. The percentage of

plants that had deep orange colored flowers and suitable internode length for potted flowers was approximately 90%. We used these plants for propagation. The traits of the mutant were evaluated in 2018 using 500 cuttings from the selected plant. The characteristics of mutant flower are listed in Table 2. These traits were almost stable. ‘Mother-Pink’ has a characteristic of continuously blooming, even in the hot summer season. We confirmed that the selected mutant maintained this excellent characteristic. This mutant is named ‘mother-orange’ and it is under application for variety registration.



Fig. 1. Flower of mutant. Original ‘mother-pink’ (left) and new cultivar ‘mother-orange’ (right).

Table 1. Effect of C-ion beam irradiation on survival in Hibiscus.

	Dose (Gy)	Number of cuttings		
		Irradiated	Planted	Survived
Mother-pink	20	44	35	35
	30	40	23	9
	40	35	4	0
Moon-light	10	41	41	41
	20	40	40	39
	30	40	36	8
Dark-red	10	29	29	28
	20	30	30	14
	30	25	25	1

Table 2. Comparison of flower characteristics between original cultivar (‘mother-pink’) and mutant.

	Shape			Color*				
	Shape	Direction	Diameter	Bud	Petal (Banded type)		Staminal column	Filament
					Band 1	Band 2		
Original	Trumpet-shaped	Horizontal	14 cm	45A	155B	52C	20D	White
Mutant	Horizontal	Upward	12 cm	53B	5A	N30A	15D	Pale red

\*: Definition of color groups from RHS (The Royal Horticultural Society) color chart. 45A: Vivid red, 53B: Strong red, 155B: Yellowish white, 5A: Brilliant Greenish Yellow, 52C: Deep Pink, N30A: Vivid Reddish Orange, 20D: Pale yellow, 15D: Light yellow

<sup>\*1</sup> Hanakongou Co., Ltd.

<sup>\*2</sup> RIKEN Nishina Center

## Effect of heavy ion beam irradiation on germination and mutation rate in local Toraja rice

R. Sjahril,<sup>\*1</sup> M. Riadi,<sup>\*1</sup> Rafiuddin,<sup>\*1</sup> T. Sato,<sup>\*2,\*3</sup> K. Toriyama,<sup>\*2</sup> Y. Hayashi,<sup>\*3</sup> T. Abe,<sup>\*3</sup> and A. R. Trisnawaty<sup>\*1</sup>

Tana Toraja is one of the areas in South Sulawesi that has wide local rice germplasm diversity. Based on the results of a survey of local rice in the Tana Toraja district, Suhardi *et al.* found approximately 29 local varieties of Toraja rice, each of which has exotic characteristics such as brown rice, red, aromatic and glutinous.<sup>1)</sup> The local rice cultivars have many unique traits, for example black and red rice. These colored rice cultivars are in the spotlight as food with health-promoting benefits because these pigments found in them have an antioxidative effect.<sup>2)</sup> However, improved rice cultivars are expanded in this area. Most farmers grow no native rice cultivar because the yield of these cultivars is lower than the improved cultivars and have long maturity during 5–6 months (Fig. 1). It is feared this will result in a lack of local rice cultivars as germplasm materials. Our research aims to improve the productivity of local cultivars with unique trait by heavy-ion beam irradiation. In this study, we evaluated seed germination as a result of irradiation using ion beam in two varieties of Toraja local rice.

Pare Ambo and Pare Lea are black and red rice cultivar (*Oryza sativa* L.) in Tana Toraja, respectively (Fig. 2). Dry seeds packed in a plastic case were irradiated with Ar (309 keV/ $\mu\text{m}$ ) and C (30 keV/ $\mu\text{m}$ ) in RI-beam factory, RIKEN Nishina Center, Japan. The doses of Argon-ion and Carbon-ion were 10 and 150 Gy, respectively.<sup>3,4)</sup>

Each grain from one panicle for each M<sub>1</sub> plant was germinated in one line method on a 15 cm Petri dish and transplanted into small plastic bags. The germination



Fig. 1. Local red rice “Pare Lea” has a long culm tending to lodge.



Fig. 2. Pre Ambo (Black rice) and Pare Lea (red rice).

<sup>\*1</sup> Hasanuddin University, Makassar, Indonesia

<sup>\*2</sup> Tohoku University, Sendai, Japan

<sup>\*3</sup> RIKEN Nishina Center

Table 1. Germination rate (%) on M<sub>1</sub> and M<sub>2</sub> seeds in Tana Toraja rice cultivars Pare Ambo and Pare Lea.

Cultivar	Before Irradiation	M <sub>1</sub>		M <sub>2</sub>	
		Irradiation Ion		Irradiation Ion	
		Carbon	Argon	Carbon	Argon
Pare Ambo	85	54	55	85	90
Pare Lea	98	97	98	93	94

Table 2. Number of plants undergoing albino mutation in Tana Toraja rice cultivars Pare Ambo and Pare Lea.

Ion	Cultivar	M <sub>2</sub> plants	Albino	Mutation Rate
		(No.)	(No.)	(%)
Carbon	Pare Ambo	414	8	1.9
	Pare Lea	1619	46	2.8
Argon	Pare Ambo	90	1	1.1
	Pare Lea	1034	22	2.1

percentages of seeds used before being irradiated are 85% and 98% in Pare Ambo and Pare Lea, respectively (Table 1). Ion beam irradiation reduced the germination percentage of Pare Ambo by approximately 30%. However, the germination percentage of Pare Lea after irradiation was approximately the same as before irradiation. M<sub>1</sub> seeds of Pare Ambo and Pare Lea irradiated with Argon-ion produced better seedling growths than Carbon-ion.

Further M<sub>2</sub> seed germination shows uniqueness in some seedlings, such as lighter leaf color, albinism and wrinkled leaf, which could prove to be potential mutant lines in tested M<sub>2</sub> lines seed. Chlorophyll mutation in M<sub>2</sub> plant was observed through the color of the leaves ten days after sowing until the plant was transplanted into the rice field. The irradiation treatment with ion beam also gives rise to chlorophyll mutations as seen in M<sub>2</sub> of Pare Ambo and Pare Lea (Table 2). A higher albino mutation rate was found in M<sub>2</sub> population irradiated by carbon ion instead of argon ion in both cultivars. The occurrence chlorophyll mutation occurring is a mutagenic effect of carbon-ion beam, which indicates that the treatment is effective in the creation of genetic diversity in the M<sub>2</sub> population.

### References

- 1) Sahardi *et al.*, Proc. of Nat. Sem. on Gen. Res. of Agr. (2013), pp. 34–43.
- 2) Rahim *et al.*, Int. J. Pharma. Phytochem. Res. **8**, 771–776, (2016).
- 3) Y. Hayashi *et al.*, RIKEN Accel. Prog. Rep. **51**, 238 (2018).
- 4) Y. Hayashi *et al.*, RIKEN Accel. Prog. Rep. **50**, 27 (2017).

## Isolation of the chalky grain mutant 13–45 in rice (*Oryza sativa L.*)

T. Katsube-Tanaka,<sup>\*1</sup> R. Tabassum,<sup>\*1</sup> T. Dosaka,<sup>\*1</sup> C. Masuoka,<sup>\*1</sup> M. Tsuyama,<sup>\*1</sup> Y. Mukai,<sup>\*1</sup> C. Nukigi,<sup>\*1</sup>  
H. Ichida,<sup>\*2</sup> R. Morita,<sup>\*2</sup> and T. Abe<sup>\*2</sup>

High temperature during the grain filling of rice diminishes the grain quality as well as productivity. Chalk values and peak head rice yields were quadratically increased and linearly decreased, respectively, against an increase in the nighttime air temperature during the R8 stage where one brown hull appeared on the main stem panicle.<sup>1)</sup> Chalky grains have several air spaces between the starch granules in amyloplast,<sup>2)</sup> resulting in lowered palatability<sup>3)</sup> as well as substantial yield loss due to reduced polishing efficiency.<sup>4)</sup> The molecular mechanism underlying the rice grain chalkiness is supposed to be complicated and largely unknown.

In this study, a novel chalky rice mutant was isolated from heavy ion beam (Carbon, 20 Gy, LET: 22.6–60.3 keV/ $\mu\text{m}$ )-irradiated rice (*O. sativa* ssp. *japonica* cultivar Nipponbare) of 1,116 lines. The mutant tentatively named 13–45 showed significantly higher chalky ratio (0.4–0.6), which was defined by the averaged ratio of chalky area to grain area of all brown rice grains within a panicle than the wild type (<0.1) at 28°C (Fig. 1). Meanwhile, the chalky ratio of both the wild type and the mutant became low (<0.06) and similar to each other at 24°C. These results suggested that the rice grain of the mutant 13–45 is very sensitive to high temperature and is useful for the analysis of the mechanism underlying the chalkiness caused by high temperature during grain filling.

Prolamin, the second most abundant and hydrophobic seed storage protein in rice, is composed of 13 kDa and 10 kDa polypeptides. Prolamin is often demonstrated to decrease under heat stress. When the total seed proteins were compared by western blotting with anti-10 kDa prolamin antibody, a band around 70 kDa clearly disappeared in the mutant 13–45. The 70 kDa polypeptide of the wild type was insoluble and purified by 2D-PAGE for Peptide mass fingerprinting, resulting in the identification of chloroplastic 70 kDa heat shock-related protein: cpHsp70.

Rice genome contains two *cpHsp70* genes: *cpHsp70-1* and *cpHsp70-2*. The transcription levels for the two genes were not different between the mutant 13–45 and the wild type. Thus, the coding region and promoter region (~2 kbp) of the two genes in the mutant 13–45 were cloned and sequenced, demonstrating that a single nucleotide polymorphism (SNP) was exclusively detected at the 3' region of the second exon of *cpHsp70-2*. The SNP resulted in amino acid substitution of the 259th aspartic acid with valine (D259 V) in an ATPase domain. The whole exome sequencing analysis of the mutant 13–45 confirmed that only three homozygous mutations including the SNP in *cpHsp70-2* caused non-synonymous



Fig. 1. External appearance of brown rice for the wild type (Nipponbare) and mutant 13–45 grown under conventional field condition (high, 28°C) and cool temperature condition (low, 24°C).

substitutions and frameshifts in the coding sequences.

Transgenic plants of the mutant 13–45 expressing wild type *cpHsp70-2* were produced and the chalky ratio averaged by six panicles was compared with those of the mutant 13–45 and the wild type. The chalky ratio of the transgenic line 7(6/12) was significantly lower (0.08) than that of the mutant (0.15–0.23) and comparable to that of the wild type (0.07). The results indicated that *cpHsp70-2* is a causal gene for the chalkiness of the mutant 13–45.

The intrinsic ATPase activity of recombinant cpHsp70-2 was compared between the mutant 13–45 and the wild type. The results showed that the  $K_m$  of the mutant 13–45 type was slightly lower (higher in affinity) than that of the wild type and  $V_{max}$  of the mutant 13–45 type was significantly lower by 23% than that of the wild type. Besides, the growth of DnaK (Hsp70 homologue)-defective *Escherichia coli* (*E. coli*) cells complemented with DnaK with D201 V mutation (equivalent to the rice D259 V mutation) was significantly reduced at 37°C. The growth of DnaK-defective *E. coli* cells complemented with wild type DnaK was not different from that of the non-complemented DnaK-defective *E. coli* cells at 37°C. Taken together, these results suggest that the lowered function of *cpHsp70-2* is involved with the chalkiness of the mutant 13–45.

### References

- 1) S. B. Lanning *et al.*, *Field Crops Res.* **124**, 132 (2011).
- 2) T. Tashiro, I. F. Wardlaw, *Aust. J. Agric. Res.* **42**, 485 (1991).
- 3) S. S. Kim *et al.*, *Cereal Chem.* **77**, 376 (2000).
- 4) N. Sreenivasulu *et al.*, *J. Exp. Bot.* **66**, 1737 (2015).

<sup>\*1</sup> Graduate School of Agriculture, Kyoto University

<sup>\*2</sup> RIKEN Nishina Center

# Molecular analysis of the stay-green mutant *dye1* induced by carbon ion beams in rice<sup>†</sup>

H. Yamatani,<sup>\*1</sup> M. Nakano,<sup>\*1</sup> Y. Hayashi,<sup>\*2</sup> Y. Masuda,<sup>\*1</sup> T. Abe,<sup>\*2</sup> and M. Kusaba<sup>\*1</sup>

Chlorophyll synthesis and degradation are carefully regulated in plants not only because chlorophyll is an essential photosynthetic molecule, but also because in its free form it can damage cells photo-oxidatively.<sup>1)</sup> Mutants that retain the green of leaves under senescence-inducing conditions are known as stay-green mutants. We isolated a stay-green mutant from a rice M<sub>2</sub> population (*Oryza sativa* L.) irradiated with carbon ion beams (1.6 GeV, 23 keV/μm, 20 Gy). It exhibited delayed yellowing during natural senescence in the paddy field. This recessive mutant, named *delayed yellowing1-1* (*dye1-1*), was greener than the wild-type cultivar, Nipponbare, five weeks after heading, when most leaves are senescent (Fig. 1).

We performed map-based cloning of *DYE1*. An analysis of the F<sub>2</sub> population and its progeny revealed that *DYE1* is located on chromosome 8. Fine mapping of *DYE1* delimited the candidate region within 43.1 kb, which contained seven predicted genes (Fig. 2). A next-generation sequence analysis revealed that *dye1-1* has a G-to-A substitution at the second exon of *Lhca4*, causing amino acid substitution from glutamic acid to lysine (E146K). *Lhca4* is a subunit of the light-harvesting complex for photosystem I (PSI). This residue corresponds to E154 in Arabidopsis *Lhca4*, which is a pigment-binding site conserved not only among *Lhca* subunits but also among *Lhcb* subunits (light-harvesting complex for photosystem II) of different species.<sup>2)</sup>

A blue native-PAGE analysis revealed a significant change in the conformation of PSI-LHCI supercomplex in *dye1-1* (Fig. 3). Nevertheless, the biomass of *dye1-1* was comparable to that of the wild-type. Interestingly,

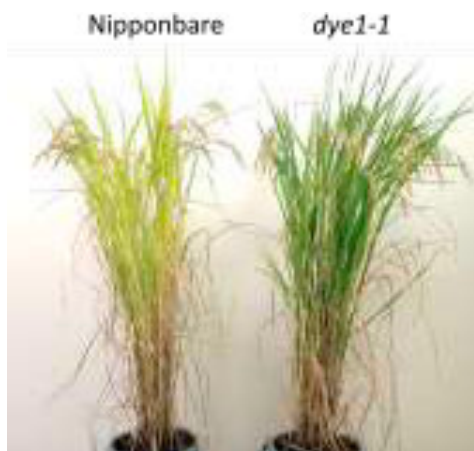


Fig. 1. *dye1* exhibits a stay-green phenotype during natural senescence (five weeks after heading).

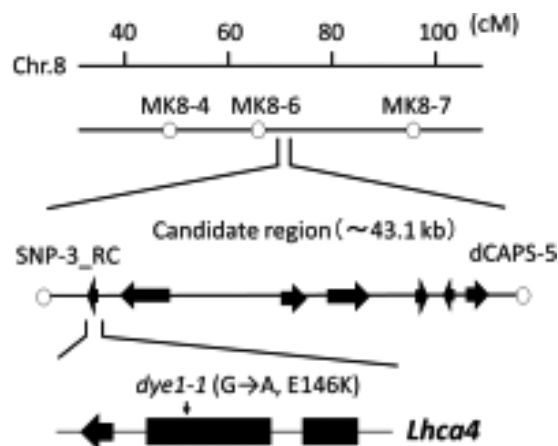


Fig. 2. *DYE1* encodes *Lhca4*, a subunit of the PSI antenna complex LHCI.

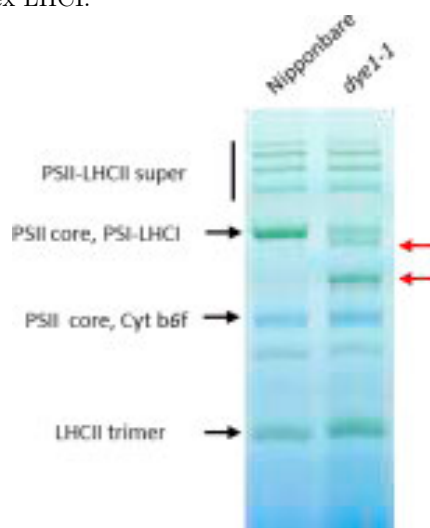


Fig. 3. Blue native-PAGE analysis of photosystems. Arrows indicate newly merged bands in *dye1-1*.

*Lhcb1*, a subunit of the trimeric LHCII, was highly accumulated in *dye1-1*. The high accumulation of LHCII in the LHCI mutant *dye1-1* may compensate the reduced PSI activity by the impairment of LHCI antenna (*Lhca4*), suggesting a novel functional interaction between LHCI and LHCII.

Higher chlorophyll content in leaves is observed before and during senescence in *dye1-1*, indicating that the impairment of *Lhca4* influences chlorophyll synthesis and/or degradation during the development and senescence of leaves in rice. It will be of great interest to examine whether mutants of other LHCI subunits show a high chlorophyll content/stay-green phenotype.

## References

- 1) Tanaka *et al.*, The Arabidopsis Book 9, e0145, (2011).
- 2) A. N. Melkozernov, R. E. Blankenship, J. Biol. Chem. **278**, 44542–44551, (2003).

<sup>†</sup> Condensed from the article in J. Exp. Bot. **69**, 1027–1035 (2018)

<sup>\*1</sup> Graduate School of Science, Hiroshima University

<sup>\*2</sup> RIKEN Nishina Center

# An early-flowering einkorn wheat mutant with deletions of *PHYTOCLOCK 1/LUX ARRHYTHMO* and *VERNALIZATION 2* exhibits a high level of *VERNALIZATION 1* expression induced by vernalization†

A. Nishiura,\*<sup>1</sup> S. Kitagawa,\*<sup>1</sup> M. Matsumura,\*<sup>1</sup> Y. Kazama,\*<sup>2</sup> T. Abe,\*<sup>2</sup> N. Mizuno,\*<sup>3</sup> S. Nasuda,\*<sup>3</sup> and K. Murai\*<sup>1</sup>

The early-flowering or early-heading phenotype in bread wheat (*Triticum aestivum*) cultivars is important as it can produce an early harvest. This characteristic is particularly beneficial in East Asia as it allows harvesting to before the onset of the rainy season. To understand the molecular mechanism of flowering in wheat, we developed a large-scale mutant panel in diploid einkorn wheat (*T. monococcum*) using a heavy-ion beam.<sup>1)</sup> Einkorn wheat seeds were exposed to a heavy-ion beam and then sown in the field. Selfed seeds from each spike of M<sub>1</sub> plants were used to generate M<sub>2</sub> lines. Every year over the past 15 years, we have obtained approximately 1,000 M<sub>2</sub> lines and built up a mutant panel with 10,000 M<sub>2</sub> lines. This mutant panel is being systematically screened for mutations affecting reproductive growth, especially for the flowering-time mutants. From the large scale mutant panel, we have identified four extra early-flowering mutants, named *extra early-flowering1* (*exe1*), *exe2*, *exe3*, and *exe4*.<sup>2)</sup> The four *exe* mutants fall into two groups namely Type I (moderately extra early-flowering type: *exe1* and *exe3*) and Type II (extremely extra early-flowering type: *exe2* and *exe4*). An analysis of *VERNALIZATION 1* (*VRN1*), a flowering promoter gene, shows that it is more highly expressed in seedlings at early developmental stages in both Type I and II mutants than wild-type (WT). These findings indicate that the difference in earliness between Type I and II mutants is associated to the level of *VRN1* expression.

The differences between the diurnal gene expression patterns in the field were examined for four clock-related genes and three clock downstream genes in WT and *exe3* mutant plants grown in the field, respectively. The biggest difference was found for a clock-related gene, *PHYTOCLOCK 1/LUX ARRHYTHMO*, which is abbreviated to *Wheat PCL1* (*WPCL1*). The *WPCL1* was not expressed in the *exe3* mutant plants, whereas it was highly expressed during sunset in WT plants. PCR analysis of DNA markers indicated that the *exe3* mutant had a deletion of *WPCL1* in the genome, which was co-segregated with the mutant phenotype in the segregation line.

We confirmed that the original strain KU104-1 carried a mutation that produced a null allele of a flowering repressor gene *VERNALIZATION 2* (*VRN2*). As

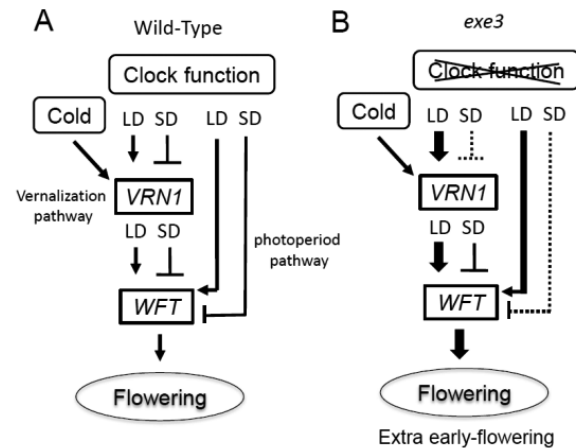


Fig. 1. Model for the extra early-flowering phenotype in the *exe3* mutants compared with wild-type. (A) Wild-type, (B) *exe3* mutant

a result, the *exe3* mutant has both *WPCL1* and *VRN2* loss-of-function mutations. The analysis of plant development in a growth chamber showed that vernalization treatment accelerated flowering time in the *exe3* mutant under short day (SD) as well as long day (LD) conditions and the early-flowering phenotype was correlated with the earlier up-regulation of *VRN1*. The deletion of *WPCL1* affects the SD-specific expression patterns of some clock-related genes, clock downstream genes, and photoperiod pathway genes, suggesting that the *exe3* mutant causes a disordered SD response. The present study indicates that *VRN1* expression is associated with the biological clock and the *VRN1* up-regulation is not influenced by the presence or absence of *VRN2*.

A model for the extra early-flowering phenotype of *exe3* mutant is shown in Fig. 1. The disruption of clock function also affects the expression of the florigen gene *WFT* through the *VRN1* expression. A high level of *WFT* expression was observed in the *exe3* mutant under LD conditions, suggesting that the disrupted clock somehow induces *WFT* expression. Under SD conditions, another florigen gene could be up-regulated by the disrupted clock function and accelerate flowering in the *exe3* mutant. The up-regulation of *VRN1* is controlled by the vernalization pathway and clock function. It is not related to *VRN2* and determines the earliness in wheat.

† Condensed from the article in J. Plant Physiol. **222**, 28 (2018)

\*<sup>1</sup> Faculty of Bioscience and Biotechnology, Fukui Prefectural University

\*<sup>2</sup> RIKEN Nishina Center

\*<sup>3</sup> Graduate School of Agriculture, Kyoto University

## References

- 1) K. Murai *et al.*, Nucl. Instrum. Methods Phys. Res. B **314**, 59 (2013).
- 2) A. Nishiura *et al.*, Breed. Sci. **64**, 213 (2014).

## Effects of carbon-ion irradiation to male gametes on double fertilization in *Cyrtanthus mackenii*

T. Hirano,<sup>\*1,\*2</sup> Y. Watarikawa,<sup>\*1,\*3</sup> Y. Hayashi,<sup>\*2</sup> T. Abe,<sup>\*2</sup> and H. Kunitake<sup>\*1</sup>

Heavy-ion-beam mutagenesis has been applied for various plant materials, and many mutants have been successfully obtained through the screening process. As one of the plant materials for the irradiation, pollen was used for mutant induction.<sup>1,2)</sup> When pollen grains of *Cyrtanthus mackenii* (Amaryllidaceae) were irradiated with a carbon-ion beam, inhibitory effects on pollen tube growth were not observed.<sup>3)</sup> It is reported that generative cells in the irradiated pollen grains can recognize and manage genomic lesions using DNA damage response pathways during pollen tube growth. However, with high-dose irradiation (40 Gy), sperm cell formation is prevented and the generative cells are not divided into two sperm cells; however, the cell cycle progresses. The male gametes are called generative-cell-like sperm cells (GC-like SCs). In this study, we analyzed the reproduction process involved in the irradiated pollen grains to reveal the behavior of male gametes during double fertilization.

Anthers of *C. mackenii* in 0.2-mL tubes were irradiated with C ions (22.5 keV/ $\mu\text{m}$ ) at a dose of 10 or 40 Gy and then stored at  $-20^{\circ}\text{C}$ . The pollen grains with or without carbon ion beam irradiation were crossed with unirradiated female organs. The ovules were fixed with an FAA solution (formaldehyde, acetic acid, and ethanol) for 3 days after the crossing (DAC), and we observed the developmental states of the ovules by using the paraffin section method.

In the embryo sacs at 3 DAC with the unirradiated pollen grains, a degenerated synergid cell, an undivided egg, and central cells were observed. In the sexual reproduction process of higher plants, one of the synergid cells, which succeed in interacting with the pollen tube, is degenerated. Therefore, it is indicated that the pollen tubes reached one of the synergid cells until 3DAC, and the embryo sacs were considered immediately before or after fertilization. In addition to the embryo sacs at the fertilization phase, we observed abnormal embryo sacs without the egg apparatus and central cell (Fig. 1). The proportions of the embryo sacs in the fertilization phase, abnormal development, and unfertilization were 79%, 9%, and 12%, respectively.

In the pollen grains irradiated at 10 Gy, pollen tubes also arrived at the embryo sacs until 3 DAC. The proportions of the embryo sacs in the fertilization phase, abnormal development, and unfertilization were 79%,

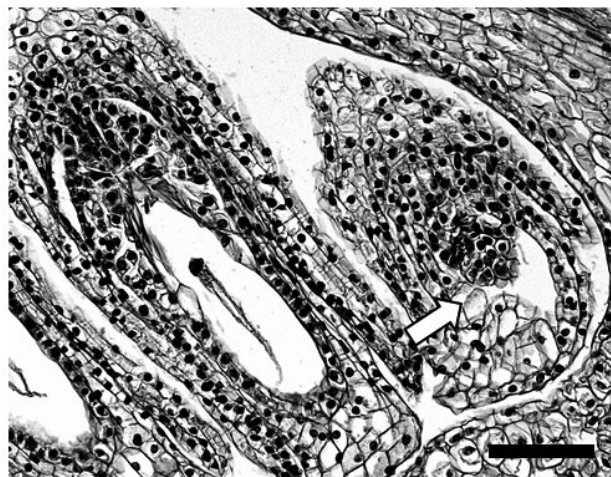


Fig. 1. Abnormal embryo sac formed 3 days after the crossing with unirradiated pollen grains. The arrow indicates the abnormal embryo sac. The embryo sac on the left side has a central cell. Bar = 50  $\mu\text{m}$ .

6%, and 15%, respectively, and were the same as that in the case of unirradiated pollen grains. After 40 Gy irradiation, the proportion of embryo sacs in the fertilization phase was 58% and that in the abnormal development was 28%. These results indicated that pollen tubes from the irradiated pollen grains also arrived at the embryo sacs until 3 DAC.

Since the abnormal embryo sacs were commonly observed with or without carbon-ion irradiation, the abnormal development is interpreted to be affected by environmental factors or the plant status. Based on the interpretation, the proportion of embryo sacs at the fertilization phase is thought not to be drastically decreased in the pollen grains irradiated at 40 Gy. It is also suggested that inhibitory effects on pollen tube growth would not be observed *in vivo*. However, there is a possibility that under high-dose irradiation, pollen tubes or male gametes promote abnormal embryo sac formation.

We are now observing embryo sacs after 14 DAC. Those data are expected to reveal double fertilization and the embryogenesis process involved in the irradiated male gametes and will be useful for understanding abnormal embryo sac formation.

### References

- 1) K. Naito *et al.*, Genet. **169**, 881 (2005).
- 2) Y. Kazama *et al.*, Sci. Rep. **6**, 18917 (2016).
- 3) T. Hirano *et al.*, AoB Plants **5**, plt004 (2011).

\*1 Faculty of Agriculture, University of Miyazaki

\*2 RIKEN Nishina Center

\*3 present affiliation: Agriculture and Forestry Technical Development Center, Nagasaki Prefectural Government

## Death of pollen tetrads caused by chromosomal rearrangement

Y. Kazama,<sup>\*1</sup> H. Abe,<sup>\*1</sup> K. Ishii,<sup>\*1</sup> M. Sato,<sup>\*2</sup> T. Hirano,<sup>\*3</sup> K. Toyooka,<sup>\*2</sup> and T. Abe<sup>\*1</sup>

Chromosomal rearrangements can be induced with high efficiency by using high-LET irradiation.<sup>1)</sup> They are considered one of the important mutations during evolution, because chromosomal rearrangements can affect the gene expression patterns.<sup>2)</sup> On the other hand, they sometimes cause a defect in the inheritance of chromosomes, because of the loss of a large set of essential genes (Fig. 1).

To observe such a defect of chromosome inheritance, we used an *Arabidopsis* T-DNA tagging mutant (SALK\_123114), which was provided by the Arabidop-

sis Bio-Resource Center (ABRC). A whole genome analysis followed by the mutation detection with AMAP<sup>3)</sup> revealed a reciprocal translocation between chromosome 1 and 2 in this mutant (Fig. 1). The T-DNA was inserted in the junction region. We crossed this mutant with another mutant (SALK\_056345) to trace the inheritance of the chromosome by inserting T-DNA in chromosome 2 of SALK\_056345. In the F2 generation, we detected only three types of chromosomes, namely wild type, F1 type, and SALK\_123114 type (Fig. 1), and no double mutant had both T-DNA. This result indicates that half of the zygote would be dead in the F1 plants. Indeed, about half of the pollens in the anthers of F1 plants were dead (data not shown), and about half of the seeds in siliques could not mature in the F1 plants (data not shown), indicating that cell death occurred in both pollen and egg developments.

From the whole genome mutation analysis, cells having pairs of a non-translocated chromosome and a translocated chromosome were expected to be dead during the development of pollens and eggs due to the loss of large sets of genes. One pair lacked a part of chromosome 2, which contains 1,734,820 bp. The other pair lacked a part of chromosome 1, which contains 5,804,110 bp. To determine the timing of the cell death, we observed the pollen development in the F1 plants. When TUNEL assay<sup>1</sup>, which can detect fragmentation of the DNA generated during cell death, was performed, positive signals were detected in some of the tetrad cells in the F1 plants. This result indicates that the death of the pollen cells occurred just after meiosis.

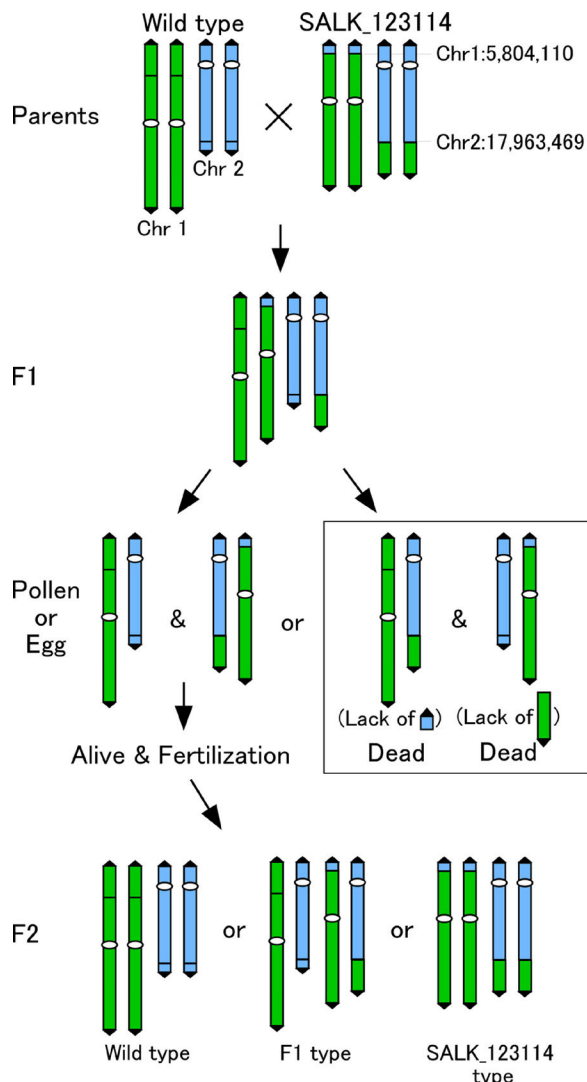


Fig. 1. Ideogram of cell death occurring due to the genetic cross of the rearrangement mutant.

<sup>\*1</sup> RIKEN Nishina Center

<sup>\*2</sup> RIKEN Center for Sustainable Resource Science

<sup>\*3</sup> Department of Agriculture, Miyazaki University

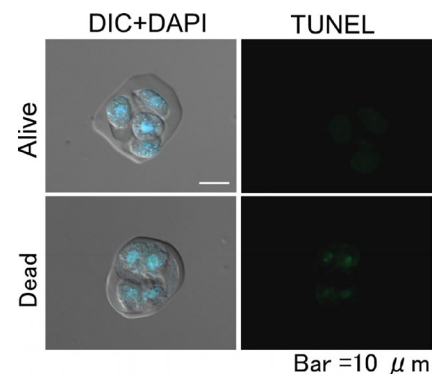


Fig. 2. Images of TUNEL assay in pollen tetrads.

### References

- 1) Y. Kazama *et al.*, *Plant J.* **92**, 1020 (2017).
- 2) Y. Kazama *et al.*, *Cytologia* **83**, 125 (2018).
- 3) K. Ishii *et al.*, *Genes Genet. Syst.* **91**, 229 (2016).

## Estimation of efficient dose for heavy-ion beam mutagenesis by whole-genome mutational analysis in *Arabidopsis thaliana*

K. Ishii,<sup>\*1</sup> H. Ichida,<sup>\*1</sup> S. Ohbu,<sup>\*1</sup> and T. Abe<sup>\*1</sup>

Heavy-ion beams are used as an effective mutagen that induces localized mutations due to its higher linear energy transfer (LET). The observation of the occurrence ratio of albino mutants as the mutation frequency in the M2 generation after carbon-ion beam irradiation (30 keV/ $\mu\text{m}$ ) at doses of 50–500 Gy showed that the mutation frequency increased with increasing dose between 50–350 Gy and plateaued at 400 Gy.<sup>1)</sup> However, the measurement of mutation frequency by visual screening of mutants from a large number of irradiated plants is time-consuming. In this study, we tried to estimate an efficient dose for heavy-ion beam mutagenesis by performing whole-genome mutational analysis on relatively small numbers of irradiated plants.

Dry seeds of *Arabidopsis thaliana* (the Col-0 strain) were irradiated with  $^{12}\text{C}^{6+}$  (135 MeV/nucleon) ions, at doses of 0–350 Gy. The LET of C ion beams was controlled to 30 keV/ $\mu\text{m}$ . M<sub>2</sub> seeds were harvested from self-pollinated M<sub>1</sub> plants, and ten M<sub>3</sub> plants were harvested from one self-pollinated M<sub>2</sub> plant. Genomic DNA was extracted from the mixture of leaves of the ten M<sub>3</sub> plants. Five DNA pools were sequenced for each dose using HiSeq X-Ten sequencing systems (Illumina Inc.). The read sequences obtained were input into the mutational analysis pipeline AMAP, as described previously, with some modifications.<sup>2)</sup> In short, after mapping the read sequences to the reference genome sequence (TAIR10) with BWA (BWA-MEM) software, the mutation candidates were detected with GATK (HaplotypeCaller), PINDEL, and BREAKDANCER software. Then, the AMAP filtered out the false-positives by using its own algorithm.

In spite of the process of filtering out false-positives, confirmation of the mutation candidates in one DNA pool (350-Gy irradiation) by using INTEGRATIVE GENOMICS VIEWER (IGV) software revealed that 81% of the candidates were still false-positives (data not shown). We configured additional criteria for the determination of false-positives. Among the mutation candidates output from GATK, those with the ‘QUAL’ value (calculated by GATK) less than 150 or ‘MAPPING\_QUAL’ value (calculated by BWA) less than 60 were treated as false-positives. Among the mutation candidates output from PINDEL, those with the ratio of the number of read sequences supporting the mutation to that of mapped read sequences less than 0.2 or with the number of reads supporting the mutation less than 5 were treated as false-positives. Among the mutation candidates output from BREAKDANCER, those with the ratio of the number of read sequences supporting the mutation to that of mapped read sequences less than 0.15 were treated as false-positives. Also, among the mutation candidates

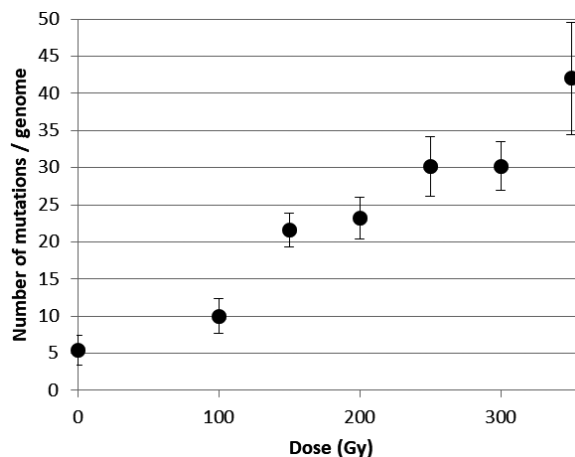


Fig. 1. Average number of mutations. Five DNA pools were analyzed at each dose.

output from PINDEL or BREAKDANCER, two candidates from different DNA pools overlapping one another by more than 80% of their regions were treated as false-positives. By using IGV software, it was revealed that 21% of the candidates in the DNA pool (350-Gy) were false-positives after these additional filtrations and that 9% of the positive mutations were filtered out by the additional filtrations. The mutation candidates in all DNA pools were tested with the additional filtrations and checked using IGV software.

The number of mutations per genome increased monotonically as the irradiation dose increased and did not plateau until 350 Gy (Fig. 1). In this study, it was suggested that irradiation at 350 Gy is efficient in the range of 0–350 Gy. Although the means for evaluating the mutation frequency in this study was different from that in the previous study,<sup>1)</sup> the tendency of increase in the mutation frequency in proportion to the irradiation dose was similar. The mutation analysis method in this study covered all mutations in the whole genome while the mutation analysis by visual screening covered only those in genes related to the development of chloroplasts. Because this method can determine the type (single nucleotide substitution, deletion, insertion, inversion, or chromosomal rearrangement) and the size of each mutation, the previous study revealed the LET-dependent effect for mutation induction: heavy-ion beams with higher LET can induce chromosomal rearrangements or large deletions more frequently than those with lower LET.<sup>3)</sup> In this study, it was also revealed that this method can be applied to the dose-dependent effect for mutation induction.

### References

- 1) Y. Kazama *et al.*, BMC Plant Biol. **11**, 161 (2011).
- 2) K. Ishii *et al.*, Genes Genet. Syst. **91**, 4, 229–233 (2016).
- 3) Y. Kazama *et al.*, Plant J. **92**, 6, 1020–1030 (2017).

<sup>\*1</sup> RIKEN Nishina Center

# Characterization of L-cysteine requiring mutants derived from heavy-ion-beam irradiated cells in the unicellular green alga *Parachlorella kessleri*

T. Yamazaki,<sup>\*1,\*2</sup> E. Kounosu,<sup>\*1</sup> T. Takeshita,<sup>\*1,\*2,\*3</sup> A. Hirata,<sup>\*1,\*3,\*4</sup> S. Ota,<sup>\*1,\*2</sup> Y. Kazama,<sup>\*5</sup> T. Abe,<sup>\*5</sup> and S. Kawano<sup>\*1,\*2,\*3</sup>

Many microalgae show accumulation of neutral lipids, such as triacylglycerols (TAGs), in oil bodies under conditions in which there is a lack of nutrients, including nitrogen, phosphorus and sulfur, in their environment. Although sulfur starvation in microalgae induces lipid accumulation, little is known about the underlying mechanism. Interest in this phenomenon is divided into two aspects: 1) the connection between recognition of sulfur starvation and lipid synthesis and 2) whether the mechanism of lipid induction under sulfur-starvation conditions is shared with those of other nutrient-starvation conditions. To answer these questions, we obtained heavy-ion-beam irradiated algal mutants that require L-cysteine, which is an amino acid with sulfur.<sup>1)</sup>

Sulfate is the most highly oxidized sulfur compound, is widespread in nature and is the most important supplier of sulfur for green plants, including microalgae (Fig. 1A). Plants incorporate sulfate intracellularly as a sulfur source. In green algae and land plants, sulfate is taken up by the sulfate transporter (SULTR) across the plasma membrane. Sulfate in the cytosol is transported into chloroplasts by chloroplast localized SULTR. In chloroplasts, sulfate is bound to ATP by sulfate adenylyltransferase (ATS) and deoxidized to sulfite by adenylyl-sulfate kinase (APSK) and adenylyl sulfate reductase (APR). Sulfite is reduced by sulfite reductase (SiR) and finally assimilated into L-cysteine by exchanging sulfide with the acetyl group of O-acetyl-L-serine (OAS) in a reaction catalyzed by O-acetylserine (thiol) lyase (OAS TL). L-cysteine is metabolized to L-methionine through L-homocysteine in chloroplasts and mitochondria.<sup>2)</sup> Although knowledge of the microalgal sulfate-assimilation pathway is limited, the homologous genes that function in sulfate assimilation in land plants have been identified in *Chlamydomonas*.

*Chlorella* and *Parachlorella* species are unicellular immotile green microalgae classified in the Trebouxiophyceae, which have spherical cells less than  $\sim 10 \mu\text{m}$  in diameter containing a chloroplast. *Parachlorella kessleri* accumulates TAG under sulfate-limited conditions.<sup>3)</sup> Therefore, this species can be used as a model for investigation of the response to nutrient starvation. We reported an investigation of the regulatory system of lipid and starch synthesis under sulfate-starvation con-

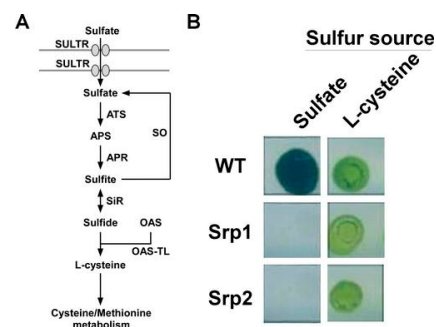


Fig. 1. Sulfur-assimilation pathway and isolated Srp mutants of *P. kessleri*. (A) Schematic of the sulfate assimilation pathway. WT, wild type (B) Phenotype of Srp mutants.

ditions,<sup>1)</sup> and summarize it in this report.

Mutagenesis of *P. kessleri* was performed according to our previous method. For isolation of cysteine requiring *P. kessleri* mutants using Fe-ion treatments, 200  $\mu\text{L}$  aliquots of a 2-day-old *P. kessleri* culture were transferred into tubes. The samples were stored at 4°C prior to being subjected to heavy-ion-beam irradiation. Cells were irradiated in the RIKEN RI-beam factory (Wako, Saitama, Japan) at doses of 25 and 50 Gy. The linear energy transfer value was 790  $\text{keV}\mu\text{m}^{-1}$ . The irradiated cells were spread onto L-cysteine medium 1.5% agar plates for isolation of single colonies. Approximately 13,000 colonies were picked as isolates and inoculated onto both L-cysteine medium 1.5% agar plates and sulfate medium 1.5% agar plates. Isolates that grew only in L-cysteine were identified as sulfate repressed proliferation (Srp) mutants (Fig. 1B). The strains were deposited in the National Institute of Technology and Evaluation, Tokyo, Japan, under accession numbers FERM BP-22268 (for Srp 1) and FERM BP-22288 (for Srp 2).

A phenotype of these mutants under sulfate replete conditions exhibited that cell proliferation was suppressed like the phenotype of wild type under sulfur deplete conditions, but starch was highly accumulated. The effects of sulfate and L-cysteine on lipid and starch accumulation in the wild type and mutants were compared in media containing different sulfur compounds as sulfur sources. Our results suggest that a shortage of L-cysteine, which is a metabolite of sulfate, induces lipid accumulation and that sulfate ions promote starch accumulation in chloroplasts. This study was supported by JST, CREST and START (to SK).

## References

- 1) Condensed from the article in Yamazaki *et al.*, *Algal Res.* **36**, 37–47 (2018).
- 2) Ravel *et al.*, *J. Biol. Chem.* **279**, 22548–22557 (2004).
- 3) Takeshita *et al.*, *Bioresource Technol.* **158**, 127–134 (2014).

<sup>\*1</sup> Department of Integrated Biosciences, Graduate School of Frontier Sciences, University of Tokyo

<sup>\*2</sup> JST, CREST

<sup>\*3</sup> Future Center Initiative, University of Tokyo

<sup>\*4</sup> Bioimaging Center, Graduate School of Frontier Sciences, University of Tokyo

<sup>\*5</sup> RIKEN Nishina Center

# Increase of lipid production upon outdoor cultivation of heavy-ion beam irradiation mutant *Parachlorella kessleri* PK4 and identification of its genetic variations<sup>†</sup>

T. Takeshita,<sup>\*1</sup> K. Oshima,<sup>\*2,\*3</sup> K. Ishii,<sup>\*4</sup> H. Kawamoto,<sup>\*1</sup> S. Ota,<sup>\*1,\*3</sup> T. Yamazaki,<sup>\*1,\*3</sup> A. Hirata,<sup>\*5</sup> Y. Kazama,<sup>\*4</sup> T. Abe,<sup>\*5</sup> M. Hattori,<sup>\*2,\*3</sup> and S. Kawano<sup>\*1,\*3</sup>

In recent years, microalgae have gained significant attention as a promising feedstock for the biofuel industry. Some microalgae such as *Parachlorella kessleri*, a species separated from the genus *Chlorella*, can accumulate high levels of starch and lipids that can be used for the production of bioethanol and biodiesel, respectively.<sup>1,2)</sup> Irradiation of *P. kessleri* with heavy-ion beams with varying doses and ion species resulted in the generation of phenotypes with potential economic relevance in terms of lipid production.<sup>3)</sup> One such mutant, PK4, exhibited high lipid accumulation under nitrogen starvation conditions.<sup>3)</sup>

In this study, the lipid accumulation of PK4 was analyzed using two experimental systems: a laboratory-based small-scale culture and thin-layer photobioreactor (T-PBR) mass cultivation in a culture volume of 150 l. Nutrient dilution was adopted to maximize the lipid productivity by exploiting the PK4 response to nutrient limitation. We also determined its genetic variation by whole genome re-sequencing.

TAP and UP media were compared to maximize the lipid productivity of PK4 at a laboratory scale (80 ml). The growth of wild type (WT) and PK4 stopped in the complete TAP media on day 6 post-inoculation, but both WT and PK4 continued to proliferate in the UP media even on day 8 post-inoculation. In the complete UP media, only a small amount of lipid accumulated in either WT or PK4 cultures. The culture on day 4 post-inoculation was collected and diluted with sterilized distilled water and individual cultivations were continued. PK4 accumulated more lipids and at an earlier stage than WT in UP medium after nutrient dilution.

The nutrient dilution experiment was performed in a 150 l thin layer- photobioreactor (T-PBR) (Fig. 1). The culture was diluted with water four times to induce nutrient limitation on day 7 post-inoculation. Lipids began to increase from day 9 post-inoculation (2 days after dilution) and continued to increase until the last day of cultivation (38% DW,  $2.0 \text{ g} \cdot \text{L}^{-1}$ ). The maximum lipid content was 66% per dry weight (Day13,  $2.9 \text{ g} \cdot \text{L}^{-1}$ ) and the maximum lipid productivity after dilution was  $0.59 \text{ g} \cdot \text{L}^{-1} \cdot \text{day}^{-1}$ .

The locations of genetic variation in PK4 were inves-

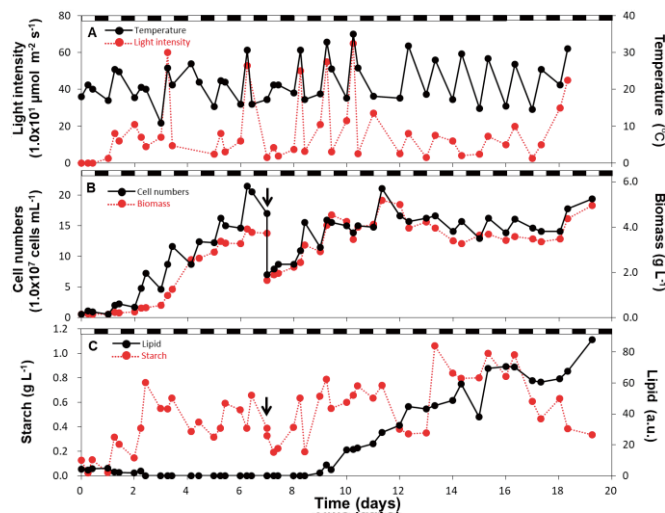


Fig. 1. Time-series data in T-PBR. (A) water temperature and light intensity, (B) cell numbers and biomass, and (C) content of starch and lipids. The culture was diluted with water four times on day 7 post-inoculation.

tigated by next-generation sequencing (Illumina MiSeq and HiSeq). In total, we identified three loci, which probably caused the observed phenotype in the automated mutation analysis pipeline (AMAP) with some modifications.<sup>4)</sup> They correspond to putative homologs of elicitor-responsive protein (9934\_t), ATP/ADP transporter (9067\_t) and endo-1,4- $\beta$ -mannanase (8741\_t). There are three copies of the 9067\_t gene in the genome. One of the three homologs is ATP and ADP transporter localized in the chloroplast envelope. However the relationship of this transporter with membrane lipids has been discussed.<sup>5)</sup> The 8741\_t gene has 13 genetic copies. Mannan is one of the polysaccharides present in the cell wall of algae.<sup>6)</sup> 1,4- $\beta$ -mannanase hydrolyzes  $\beta$ -1,4-mannosidic linkages of D-mannan, as well as galacto- and glucomannans at random site.<sup>7)</sup> A study of metabolites or genetics including complementation of the affected genes would be required to determine the gene(s) whose mutation is responsible for the PK4 phenotype.

## References

- 1) B. Fernandes *et al.*, *Bioresour Technol.* **144**, 268–274 (2013).
- 2) X. Li, *et al.*, *Biotechnol Bioeng.* **110**, 97–107 (2013).
- 3) S. Ota *et al.*, *Bioresour Technol.* **149**, 432–438 (2013).
- 4) K. Ishii *et al.*, *Syst.* **91**, 229–233 (2017).
- 5) A. G. Navarro *et al.*, *J. Cell. Physiol.* **229**, 2126–2136 (2014).
- 6) H. Takeda *et al.*, *Phytochemistry* **34**, 1053–1055 (1993)
- 7) Do Bien-Cuong *et al.*, *Factories* **8**, 59 (2009).

<sup>†</sup> Condensed from the article in *Algal Res.* **35**, 416–426 (2018)

<sup>\*1</sup> Department of Integrated Biosciences, Graduate School of Frontier Sciences, University of Tokyo

<sup>\*2</sup> Center for Omics and Bioinformatics, Graduate School of Frontier Sciences, University of Tokyo

<sup>\*3</sup> Japan Science and Technology Agency (JST), CREST

<sup>\*4</sup> RIKEN Nishina Center

<sup>\*5</sup> Bioimaging Center, Graduate School of Frontier Sciences, University of Tokyo

## Pleiotropic mutant of plant-symbiotic edible mushroom *Tricholoma matsutake* induced by argon-ion beam<sup>†</sup>

H. Murata,<sup>\*1</sup> T. Abe,<sup>\*2</sup> H. Ichida,<sup>\*2</sup> Y. Hayashi,<sup>\*2</sup> T. Yamanaka,<sup>\*1</sup> T. Shimokawa,<sup>\*1</sup> and K. Tahara<sup>\*1</sup>

*Tricholoma matsutake* is an ectomycorrhizal fungus that produces prized mushrooms “matsutake” in association with conifers.<sup>1)</sup> Currently, there are no fungal strains as useful in cultivating fruits as commercial saprophytic edible mushrooms. Developing the strains that are suitable for spawn cultivation will greatly contribute to the artificial cultivation of mycorrhizal mushrooms. Previously, we reported that an argon-ion beam (<sup>40</sup>Ar<sup>17+</sup>, 95 MeV/nucleon) efficiently killed *T. matsutake* strains on agar plates at a dose of over 100 Gy and generated some mutants whose mycelial morphology was different from that of the wild-type.<sup>2)</sup> In this study, we document that the irradiation of argon-ion beam on *T. matsutake* induces a mutant that has pleiotropically altered phenotypes in mycelial morphology and degrading enzymatic activities.

The mutant Ar 59 was obtained by irradiating the mycelia of *T. matsutake* NBRC 33136 on modified Melin-Norkrans agar containing 1.5% V8 juice with an argon-ion beam at a dose of 500 Gy. Next, the mycelial colony was separated into pieces and transferred onto fresh agars.<sup>2)</sup> The Ar 59 strain formed a hedgehog-like colony on the potato dextrose agar (PDA) containing 0.1% azurin-crosslinked (AZCL)-amylose and 0.1% AZCL-hydroxyethyl (HE)-cellulose substrates, unlike the wild-type strain that had a flat mycelial mat with flower-like areal hyphae on the inoculation plug (Figs. 1 (a–d)). The Ar 59 strain exhibited a significantly higher amylose- and cellulose-degrading activities than the wild-type strain. In addition, clear halo zones, resulting from the conversion of water-insoluble dye-linked substrates into water soluble substances, were formed around the colonies during the incubation period of 21 days. These clear halo zones extended for seven additional days (Figs. 1 (e–h)).

The phenotype of strain Ar 59 differed substantially from those of *T. matsutake* NBRC 33136, which raises a concern whether Ar 59 is a contaminant. Therefore, the relationship between the NBRC33136 and Ar 59 strains was clarified by analyzing the sequences of their rRNA gene ITS (867 bp) and IGS1 (361 bp) regions, and the phylum-specific mobile DNA *megB1* (479 bp). The results showed that the strain sequences were identical. Therefore, strain Ar 59 was proven to be a mutant of *T. matsutake* NBRC33136.

We have isolated a pleiotropic mutant whose colony morphology differs from that of the wild-type *T. mat-*

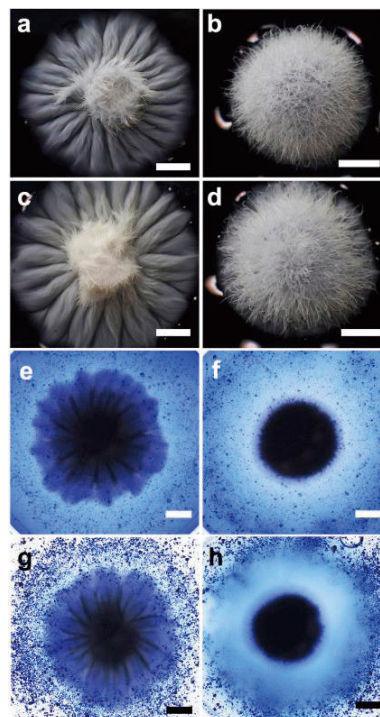


Fig. 1. Traits of *T. matsutake* mutant Ar 59 on PDA containing AZCL-amylose and AZCL-HE-cellulose. (a–d) Colony morphology. (a, c) NBRC 33136 on PDA containing AZCL-amylose and AZCL-HE-cellulose, respectively. (b, d) Strain Ar 59 on PDA containing AZCL-amylose and AZCL-HE-cellulose, respectively. (e–h) Depolymerizing activities. (e, g) NBRC 33136 on PDA containing AZCL-amylose and AZCL-HE-cellulose. (f, h) Strain Ar 59 on PDA containing AZCL-amylose and AZCL-HE-cellulose, respectively. Clear halo zones around the colonies were scored as enzymatic activities (e–h).

*sutake* strain NBRC33136 and has acquired high levels of amylose- and cellulose-degrading activities. Its pleiotropic feature indicates that argon-ion beams may have deleted a part of negative regulatory region that controls various traits. Whether heavy-ion beams that break double-stranded regions of DNA ranging in size from a few bp to over 1 kilobase positively influence the life cycle of fungus, rendering fruiting in spawn cultivation, remains to be clarified. However, irradiation with heavy-ion beams may be useful to create new traits in *T. matsutake*.

### References

- 1) A. Yamada *et al.*, *Mycoscience* **55**, 27 (2014).
- 2) H. Murata *et al.*, *RIKEN Accel. Prog. Rep.* **51**, 244 (2018).

<sup>†</sup> Condensed from the article in *Mycorrhiza* **28**, 171 (2018)

<sup>\*1</sup> Forestry and Forest Products Research Institute

<sup>\*2</sup> RIKEN Nishina Center

# Comparison of biological effect between low- and high-LET irradiation on DSB repair in the filamentous fungus *Neurospora crassa*<sup>†</sup>

L. Ma,<sup>\*1,\*2,\*3</sup> Y. Kazama,<sup>\*2</sup> T. Hirano,<sup>\*2,\*4</sup> R. Morita,<sup>\*2</sup> S. Tanaka,<sup>\*1</sup> T. Abe,<sup>\*2</sup> and S. Hatakeyama<sup>\*1</sup>

Ionizing radiations induce various cellular injuries, especially DNA double-strand breaks (DSBs). To obtain insights on the biological effects on several forms of ionizing radiations causing DSBs, we examined the cell killing effect, mutation frequency, and mutation type profile using the model filamentous fungus *Neurospora crassa*.<sup>1)</sup>

Two repair pathways, homologous recombination (HR) repair and non-homologous end-joining (NHEJ), recognizes and processes DSBs to maintain the integrity of genetic information. Asexual spores of wild-type *Neurospora crassa* and two DSB repair-deficient mutants (NHEJ-related *mus-52* knockout strain and HR-related *mei-3* nonsense mutant) were irradiated with X-ray (200 kVp, 2–5 keV/μm) as a low-linear energy transfer (LET) beam, and C- (135 MeV/nucleon, 30 keV/μm), Ar- (95 MeV/nucleon, 287 keV/μm), and Fe- (90 MeV/nucleon, 641 keV/μm) ion beams as high-LET beams. The survival rates were examined by a colony formation assay. Mutagenesis frequencies at *ad-3* loci were calculated as a ratio of visual purple colonies to total colonies. Mutation spectra at the *ad-3B* gene of collected mutants were examined by DNA sequencing. The experimental schema is shown in Fig. 1.

To determine the relative biological effectiveness (RBE) values on the killing effect, the doses with 50% survival in each ion-beam irradiation were compared with those obtained after X-ray irradiation as the reference radiation. RBEs of C-, Ar-, and Fe-ion beams were calculated to be 3.0, 7.4, and 5.8, respectively. Therefore, the Ar-ion displayed the greatest lethal effect on *Neurospora crassa*, which was found to be 2.5 times more effective than the C-ion. The rank order of RBE was Ar > Fe > C-ion > X-ray.

The killing effect profile of the X-ray irradiation was quite similar to the C-ion beam. The *mus-52* strain exhibited sensitivity to X-ray similar to that observed in the *mei-3* strain at 100 Gy. However, little additional cell death was observed at 200, 300, and 400 Gy. The survival rate in response to the high-LET ion-beam irradiation progressively decreased with the absorbed dose for all irradiated strains. In the case of C-ion beam irradiation, the sensitivity of the *mus-52* strain was higher than that of the wild-type and *mei-3* strains at low doses. In the case of Ar-ion beam irradiation, the *mei-3* strain exhibited the highest sensitivity at all doses. In the case of Fe-ion beam irradiation, the survival curves

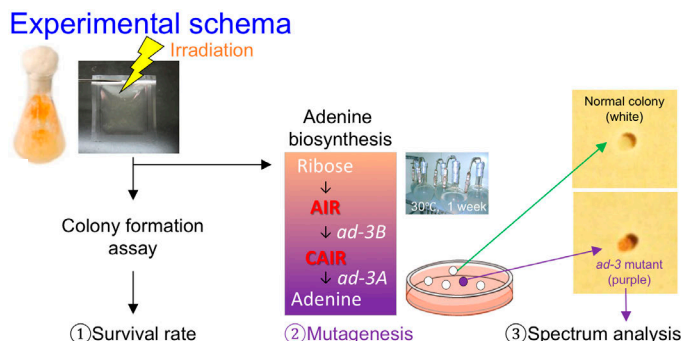


Fig. 1. Experimental schema of biological effect evaluation.

of three strains did not differ at lower doses, whereas obvious differences in sensitivity (*mei-3* > *mus-52* > WT) were observed at higher doses.

The mutation frequency in the *ad-3* loci indicated that *mei-3* > wild type > *mus-52* in all irradiated beams. The Ar-ion beam demonstrated a higher mutagenic capability than the Fe-ion beam in both the wild-type and *mei-3* strains. The mutation frequency of the wild-type strain was lower in response to Fe-ion beams than the X-rays. The deletion mutations were the most frequent but the deletion size increased with the increasing value of LET. The high-LET ion beams tended to induce larger deletions, with Fe-ion beams inducing deletions > 100 bp and Ar-ion beams causing deletions that ranged from 2 to 100 bp. Alternatively, low-LET X-ray induced deletions of 1 bp.

Our results indicated that high-LET ion beams exhibit higher cell killing and increased deletion size than low-LET X-ray in *Neurospora crassa*. These different LET-dependent phenomena may be due to the physical properties of each radiation and repair mechanism of the damage induced in *Neurospora crassa*. Our results may be useful in selecting the appropriate beam source to mutagenize fungi for further research and agricultural applications. For example, C-ion beams, which predominantly cause single-nucleotide deletions and base exchanges but few large deletions compared with higher-LET Ar- and Fe-ion beams, may be useful in generating novel fungal strains harboring mutation in essential genes without destroying the neighboring genes.

## Reference

- 1) L. Ma *et al.*, Fungal Biol. **117**, 227–38 (2013).

<sup>†</sup> Condensed from the article in Int. J. Radiat. Biol. **94**, 1125–1133 (2018)

<sup>\*1</sup> Laboratory of Genetics, Faculty of Science, Saitama University

<sup>\*2</sup> RIKEN Nishina Center

<sup>\*3</sup> Gunma University Heavy Ion Medical Center

<sup>\*4</sup> Faculty of Agriculture, University of Miyazaki

## Effect of different conditions of the mutant isolation system on rotifers by using heavy-ion beam irradiation

K. Tsuneizumi,\*<sup>1</sup> M. Yamada,\*<sup>1</sup> K. Ichinose,\*<sup>1</sup> H. Ichida,\*<sup>1</sup> and T. Abe\*<sup>1</sup>

Heavy-ion beam mutagenesis is generally recognized as an effective method for mutation breeding.<sup>1,2)</sup> Although this method has been greatly successful with plants, its application to animals is limited. Therefore, we plan to acquire more basic data to set up the optimal conditions for a heavy-ion beam irradiation system by using *Brachionus plicatilis sensu stricto* (rotifer) as the model.<sup>3)</sup>

In aquaculture, rotifers are used as the live bait for larval fishes that have just been born. As larval fishes grow, they select food based on the mouth size.<sup>4)</sup> Rotifers are used for larval fishes at first, and later on the brown shrimp *Artemia* is used. Rotifers average around 300  $\mu\text{m}$  in length, while *Artemia* is between 400  $\mu\text{m}$  and 1 cm in length. When switching food from rotifer to *Artemia*, a live bait of a suitable size (300–400  $\mu\text{m}$ ) has not been found yet. During this gap time, larval fishes die of starvation or cannibalize each other, and these problems result in a significant decrease in the number of larval fishes. It is known to be a common bottleneck in aquaculture.

In this study, to overcome the problem of starvation and cannibalization, we plan to establish large rotifers required during the gap time. Using heavy-ion beams accelerated by the RIBF accelerator at RIKEN, we measured the biological effect of heavy-ion beam

irradiation on rotifers under different conditions. After irradiation, each rotifer was separated to a plastic culture dish and cultivated at 20°C at a salinity of 1.8%. Nonirradiated rotifers almost survived through the experiment. On the contrary, the survival rate of rotifers irradiated by 600 Gy of carbon-ion beam was decreased to 41.7% by the 16th day after irradiation (Fig. 1). The survival rate of rotifers irradiated by 200 Gy of argon-ion beam was decreased to 15.0% by the 15th day after irradiation (Fig. 2). The survival rate decreased gradually depending on the degree of irradiation dose (Figs. 1, 2). These data will be helpful for the establishment of the mutant isolation system by heavy-ion beam irradiation on rotifers.

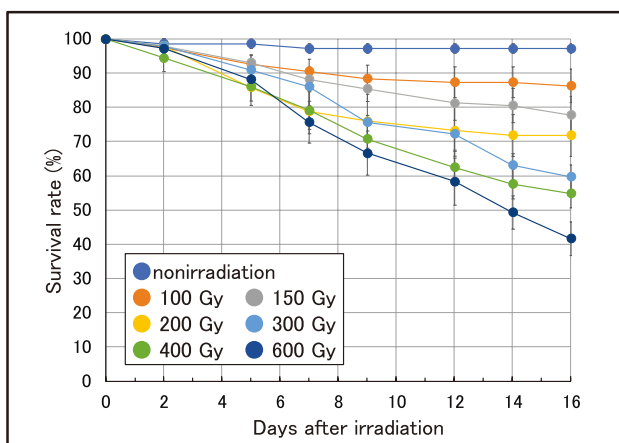


Fig. 1. Effects of different carbon irradiation conditions on survival rate of rotifers. The rotifers were irradiated with carbon-ion beams at different dose levels (100, 150, 200, 300, 400, and 600 Gy). The survival rates were measured every two or three days under each condition after irradiation. The data includes mean  $\pm$  SE of six independent experiments. The bars represent the SE of data.

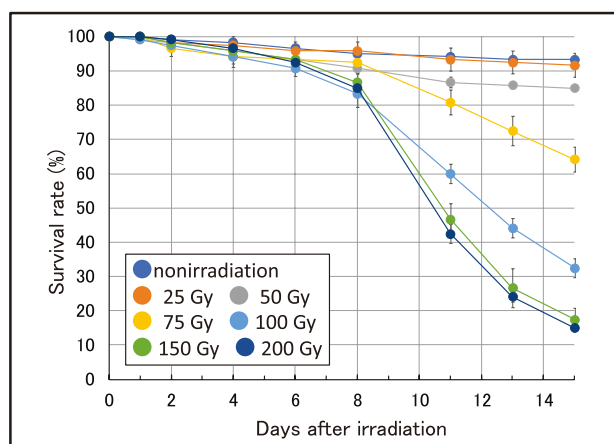


Fig. 2. Effects of different argon irradiation conditions on survival rate of rotifers. The rotifers were irradiated with argon-ion beams at different dose levels (25, 50, 75, 100, 150, and 200 Gy). The survival rates were measured every two or three days under each condition after irradiation. The data includes mean  $\pm$  SE of six independent experiments. The bars represent the SE of data.

### References

- 1) T. Abe *et al.*, in *Plant Mutation Breeding and Biotechnology*, edited by Q. Y. Shu *et al.*, (CABI, Oxfordshire, 2012).
- 2) A. Tanaka *et al.*, *J. Radiat. Res.* **51**, 223 (2010).
- 3) S. Mills *et al.*, *Hydrobiologia* **796**, 39 (2017).
- 4) Y. Sawada *et al.*, *Bull. Fish. Lab. Kinki Univ.* **7**, 1 (2000).

\*<sup>1</sup> RIKEN Nishina Center

## The inhibitor of DNA-PK suppressed DNA repair after heavy-ion irradiation in quiescent mammalian cells

M. Izumi\*<sup>1</sup> and T. Abe\*<sup>1</sup>

Accelerated heavy-ion particles with high linear energy transfer (LET) induce complex clustered DNA damage, which is an obstacle to efficient repair. DNA double-strand breaks (DSBs) are most lethal damage among them and are repaired primarily by non-homologous end joining (NHEJ) or homologous recombination (HR) in mammalian cells, whereas alternative NHEJ (alt-NHEJ) and/or single strand annealing (SSA) work only when both NHEJ and HR are impaired.

Several published studies using the Chinese hamster ovary (CHO) cells and two CHO mutant lines deficient in HR or NHEJ suggest that NHEJ does not efficiently repair DNA damages and that HR is essential for survival after heavy-ion irradiation.<sup>1,2)</sup> On the other hand, a study using inhibitors against NHEJ and HR in human lung cancer cell line suggests that NHEJ is a major DNA repair pathway after heavy-ion irradiation.<sup>3)</sup> Therefore, the DNA repair mechanism is still controversial in higher eukaryotes.

In this study, we investigated the repair mechanism in quiescent mammalian cells, where HR does not work. To estimate the secondary carcinogenesis in radiation therapy, it is important to know whether DNA damages are repaired by NHEJ or highly mutagenic alt-NHEJ and/or SSA, because the majority of the cells in the body exist in a quiescent state. First, we investigated the foci formation of phosphorylated histone H2AX, which reflects the presence of DSBs after irradiation (Fig. 1). The number of histone H2AX foci reached maximum immediately after X-ray or carbon ion irradiation and decreased similarly as time proceeded in both logarithmically growing cells and quiescent cells. These results suggest that NHEJ is a major repair pathway in both logarithmically growing cells and quiescent cells since HR does not work in quiescent cells and requires a much longer time (> 8 h) than NHEJ.

To confirm that NHEJ is a major pathway in quiescent cells, we investigated the effect of NU7441, a potent specific inhibitor of DNA-PK, which is involved in NHEJ (Fig. 2). NU7441 increased the number of phosphorylated histone H2AX 16 h after carbon ion irradiation, suggesting that NHEJ is the dominant DNA repair pathway. It is also suggested that alt-NHEJ or SSA does not work efficiently in quiescent cells.

In the previous report, we have shown that the cell survival of CHO cells is dependent on HR<sup>4)</sup> as several groups have already reported.<sup>1,2)</sup> HR may play a major role in DNA repair in CHO cells because CHO cells are not arrested in the G1 phase and accumulate in the S-G2 phase after irradiation due to the lack of p53

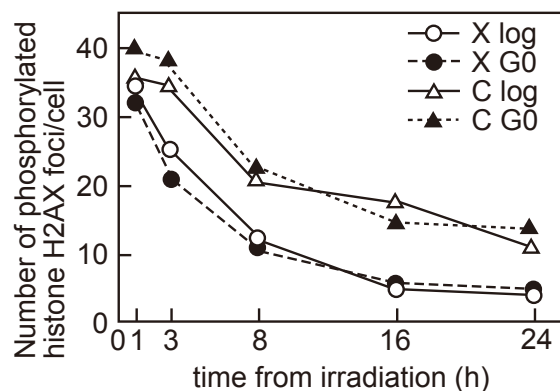


Fig. 1. The number of phosphorylated histone H2AX foci after irradiation. NB1RGB cells were synchronized in the quiescent state by serum starvation for 48 h. Cells in the proliferating state (○ △) or quiescent state (●) were irradiated with 5 Gy of X-ray or carbon ions (LET = 80 keV/μm), and the phosphorylated histone H2AX was detected by immunostaining 1–24 h post irradiation.

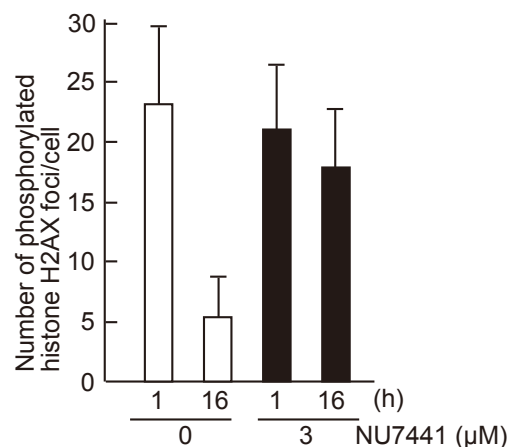


Fig. 2. The effect of NU7441 on DNA repair. The quiescent NB1RGB cells were treated with 3 μM NU7441 and irradiated with 2 Gy of carbon ions, and the phosphorylated histone H2AX was detected 16 h post irradiation.

(data not shown). On the contrary, the majority of logarithmically growing NB1RGB cells (60–70%) are in the G1 phase and stay in the G1 phase until DSB repair is completed. Therefore, NHEJ may play a major role in DNA repair in NB1RGB cells. Currently, we are examining the effect of drugs on several cell lines to investigate whether the genetic background can explain the selection of repair pathways.

### References

- 1) H. Wang *et al.*, DNA repair **7**, 725 (2008).
- 2) S. C. Genet *et al.*, Oncology Rep. **28**, 1591 (2012).
- 3) H. Ma *et al.*, Radiat. Oncol. **10**, 225 (2015).
- 4) M. Izumi, T. Abe, RIKEN Accel. Prog. Rep. **47**, 253 (2014).

\*<sup>1</sup> RIKEN Nishina Center

## Phosphorylation and accumulation of low-dose high-LET heavy ion-induced bystander signaling molecules

M. Tomita,<sup>\*1,\*2</sup> T. Tsukada,<sup>\*2</sup> and M. Izumi<sup>\*2</sup>

Radiation-induced bystander response (RIBR) is a cellular response induced in non-irradiated cells that received bystander signals from directly irradiated cells.<sup>1)</sup> RIBR induced by low doses of high-linear energy transfer (LET) radiation is an important issue for the health of astronauts and in hadrontherapy. Here, we investigated the underlying molecular mechanisms and biological implications of high-LET RIBR.

We found that normal human fibroblast WI-38, cultured confluent, irradiated with high-LET (1000 keV/ $\mu\text{m}$ ) iron (Fe) ions showed the bystander cell killing effect at low doses ( $\leq 0.2$  Gy).<sup>2)</sup> In addition, we reported that gap-junction intercellular communication (GJIC), cyclooxygenase-2 (COX-2), and nitric oxide (NO) were involved in its signal transfer.<sup>3)</sup>

Figure 1 shows the phosphorylation and accumulation of bystander signaling related molecules in WI-38 cells irradiated with 0.1 Gy of Fe ions. Cells were pretreated with or without c-PTIO (a scavenger of NO) or lindane (an inhibitor of GJIC). Left panels were previously reported.<sup>4)</sup> The phosphorylation of Akt at Ser473 and NF- $\kappa$ B p65 at Ser536 and accumulation of COX-2 were observed in the cell 3 h after irradiation. They were efficiently inhibited by c-PTIO. Phosphorylated histone H2AX at Ser139 ( $\gamma$ -H2AX) is widely used as a surrogate marker of DNA double-strand breaks (DSBs).  $\gamma$ -H2AX was observed 3 and 6 h after irradiation

and the one at 6 h was inhibited by c-PTIO. These results suggest that phosphorylation of NF- $\kappa$ B, Akt, and histone H2AX and accumulation of COX-2 were mainly mediated by NO. Meanwhile, phosphorylation of Akt at 3 h after irradiation was also inhibited by lindane but that of NF- $\kappa$ B and  $\gamma$ -H2AX was not (right panels). Surprisingly, COX-2 was overexpressed in the cells pretreated with lindane irrelevantly to irradiation. It is well known that COX-2 overexpressed cancer cells are resistant to the induction of apoptosis.<sup>5)</sup> The ability of lindane to inhibit GJIC is apparent,<sup>1)</sup> whereas COX-2 overexpression in addition to inhibition of Akt may also contribute to the inhibition of bystander cell killing, even if DSBs are induced in the bystander cells.

Continued studies must elucidate the role of GJIC. The obtained results suggested that NF- $\kappa$ B, Akt, and COX-2 were involved in the low-dose of high-LET heavy-ion-induced bystander signaling.

### References

- 1) M. Tomita, M. Maeda, J. Radiat. Res. **56**, 205 (2015).
- 2) M. Tomita *et al.*, RIKEN Accel. Prog. Rep. **48**, 302 (2015).
- 3) M. Tomita *et al.*, RIKEN Accel. Prog. Rep. **50**, 266 (2017).
- 4) M. Tomita *et al.*, RIKEN Accel. Prog. Rep. **51**, 234 (2018).
- 5) M Tsujii, R. N. DuBois, Cell **83**, 493 (1995).

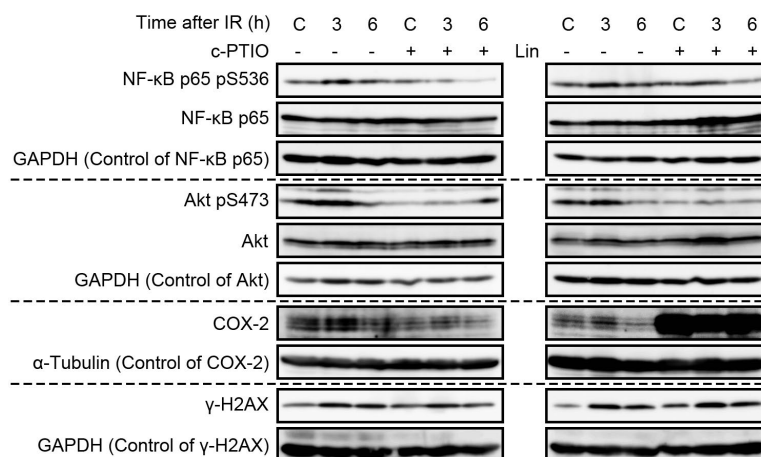


Fig. 1. Phosphorylation and accumulation of bystander signaling related molecules. WI-38 cells were pretreated with or without c-PTIO (20  $\mu\text{M}$ ) or lindane (Lin, 50  $\mu\text{M}$ ) 2 h before irradiation with 0.1 Gy of 90 MeV/nucleon Fe ions (1000 keV/ $\mu\text{m}$ ). Cells were harvested 3 and 6 h after irradiation followed by immunoblotting.

\*1 Radiation Safety Research Center, Central Research Institute of Electric Power Industry

\*2 RIKEN Nishina Center

## CR-39 imaging method to estimate microbeam profiles produced by tapered glass capillary optics

Y. Hikima,<sup>\*1,\*2</sup> T. Ikeda,<sup>\*1,\*2</sup> M. Ikekame,<sup>\*1,\*2</sup> M. Mori,<sup>\*1,\*2</sup> S. Kawamura,<sup>\*1,\*2</sup> T. Minowa,<sup>\*2</sup> and W. -G. Jin<sup>\*2</sup>

To perform accurate ion microbeam irradiation on biological targets, such as the nucleus of a mammalian cell, bacterium, and a small organ of an insect, the beam profiles should be quantitatively estimated to obtain the narrowest beam spot. We employed tapered glass capillary optics with an end-window at the thin outlet to produce microbeams of MeV ions. This optics realizes the irradiation whose target is even in air or liquid. The beam structure produced by the capillary optics was already reported to have core and halo components.<sup>1)</sup> The ions without any scattering on the inner glass wall maintain their initial directions and generate a sharp spot known as the core. The other ions suffering from the scattering may form a broad spot, which is called a halo component. The halo component should be suppressed to obtain narrower beam size, thereby resulting in good position resolution for irradiation experiments.

A plastic tracking detector CR-39 is available for the observation of microbeam profiles, where the ion hitting point appears as a pit with a diameter of a few  $\mu\text{m}$  after etching with, for example, 7N-NaOH for 2 h. However, the standard CR-39 detector is not suitable for H ions owing to low linear energy transfer (LET). In this study, a CR-39 with higher sensitivity, whose product name is HARZLAS, was employed. Although it is generally difficult to implement the analysis of pit distribution created by microbeam because the pits in the spot overlap each other, the parametrization of the halo component can be free from overlapping. Here, we report an analysis of the microbeam profiles of H ion with an energy of 2.8 MeV to aim at a small-sized spot (several tens of  $\mu\text{m}$ ) at an irradiation distance of 1 mm or divergence of  $1^\circ$ .

We have started the trial of using the brightness (darkness) information of each unit area in a microscopic photo of a piece of CR-39 as the density of the pits, assuming that all pits are separated and are approximately

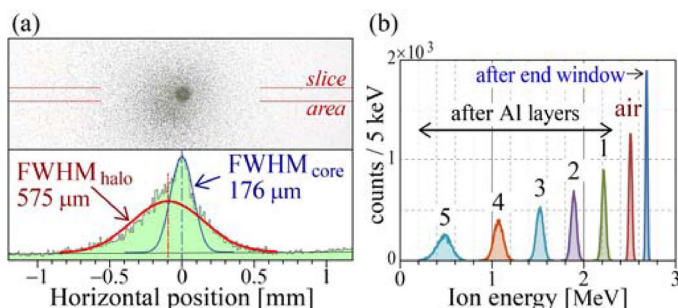


Fig. 1. (a) 2.8 MeV  $\text{H}^+$  microbeam spot on CR-39 and the histogram along with slice area. (b) Ion energies after transmitting the materials estimated by SRIM simulation. No ions were transmitted through more than five layers.

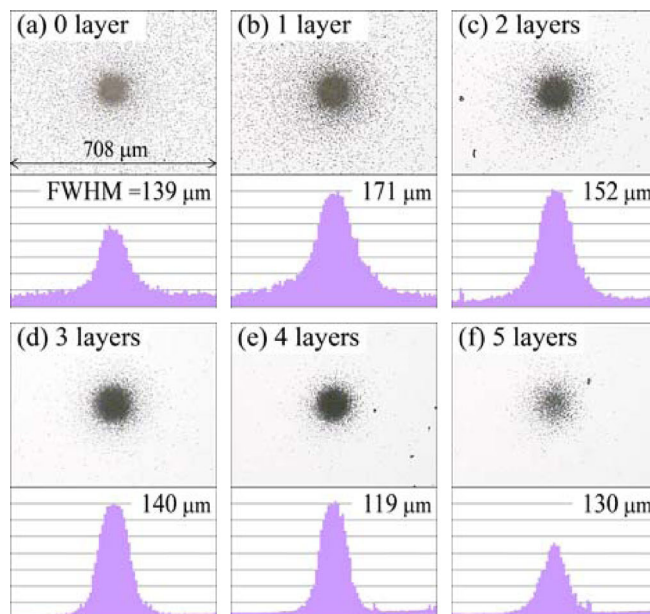


Fig. 2. Spot sizes according to the number of Al layers with thickness of  $11 \mu\text{m}$ . Panel (e) shows the narrowest spot.

of the same size. This method cannot be implemented to the center of the core. However, it can be possibly applied to the halo component and the region outlining the core. An  $\text{H}^+$  beam accelerated by the RIKEN Pelletron accelerator was transmitted through a capillary with an outlet of  $9.9 \mu\text{m}$ . Then, a spot was formed on a piece of CR-39 at an irradiation distance of 1 mm, which is shown in the upper panel of Fig. 1 (a). The green histogram in the lower panel expresses the sum of darkness along with a horizontal thin zone shown as the slice area in the upper panel. The histogram was analyzed to have two Gaussian peaks with 176 and  $575 \mu\text{m}$  in FWHM corresponding to the core and halo component, respectively. However, the core size is not used in further analysis because the darkness density at the center is already saturated. The ions in the halo component had relatively lower energies, which can be stopped if Al layers with a thickness of  $11 \mu\text{m}$  are inserted. Figure 1 (b) shows the decline of ion energy as the layers were added according to the SRIM simulation.<sup>2)</sup> Figure 2 shows the beam spots and the histograms showing the spot sizes. As shown in Fig. 2 (e), the narrowest spot was obtained with four layers. The energy of ions was estimated to be 1.08 MeV with a standard deviation of 52 keV regarding the simulation. This method can determine the accurate number of Al layers to obtain the narrowest spot.

### References

- 1) J. Hasegawa *et al.*, J. Appl. Phys. **110**, 044913 (2011).
- 2) Simulation code, SRIM-2003, <http://www.srim.org/>.

\*1 RIKEN Nishina Center

\*2 Department of Physics, Toho University

## Stability test of ion microbeams produced by tapered glass capillary optics for biological use

T. Ikeda,<sup>\*1</sup> M. Hamagaki,<sup>\*1</sup> M. Ikekame,<sup>\*1,\*2</sup> Y. Hikima,<sup>\*1,\*2</sup> and H. Sato<sup>\*1</sup>

Ion beam irradiation to cell nucleus has played an important role in the induction of artificial damage in DNA. The extent or type of DNA damage depends on the stopping power of the ion, which is a function of ion mass and velocity. For example, heavy ion cancer therapy employs carbon ions. Ion beam breeding to produce mutants of plants uses C, Ar, and Fe ions and so on. Both cases use fast heavy-ions in the order of 10 to 100 MeV/nucleon to obtain a range varying between a few mm and a few tens of cm and maintain a stopping power large enough to induce double-strand breaks (DSB) in DNA. To investigate a similar effect in single cells, slow light-ions (H or He) with energy of a few MeV are available. A  $\text{He}^{2+}$  ion with 4 MeV energy has the range of approximately 20  $\mu\text{m}$  in water, which is larger than the thickness of cells, and a stopping power greater than 200 keV/ $\mu\text{m}$ , which is strong enough to create DSB.

Employing such H or He ions with energies of a few MeV provided by the Pelletron tandem accelerator (1.7 MV max.) in Nishina R&D Building, we developed a microbeam irradiation system based on single tapered glass capillary optics with a plastic end-window at the thin outlet. Figure 1 (a) shows an image of an approximately 7-cm-long glass capillary mounted at the beam port of BL-W30. The capillary inlet/outlet diameters were 1.8 mm/10  $\mu\text{m}$ , respectively, and the thickness of the end-window at the outlet was 9  $\mu\text{m}$ . The cylindrical object just downstream of the capillary was a PIN photodiode assembly to count the ions.

Because we plan to perform single-ion irradiation to a cell nucleus, the stopping power of the ions and the dose (number of ions in the target area) are critical factors. A cell irradiation system, in particular, requires accurate irradiation time and highly stable microbeam intensity. However, the stability of Pelletron terminal (acceleration) voltage is not better than 0.5% and consequently, the microbeam intensity was really unstable until the beginning of 2018. The accelerated ions go through a series of quadrupole magnets (QM), a vertical steerer, and a switching magnet (SM), and enter the capillary optics after travelling 5–6 m. The unstable terminal voltage results in the fluctuation of the spot position. To stabilize the number of ions entering the capillary, the beam was defocused by QM. The beam profile was monitored by an  $\text{Al}_2\text{O}_3$  fluorescent plate with a 5 mm interval grid connected to a pico-ammeter shown in Fig. 1 (b). The profile monitor was installed at BL-W15, which is a beam line next to BL-W30. The monitor and the capillary optics were at a similar distance from SM. Figure 1 (c)

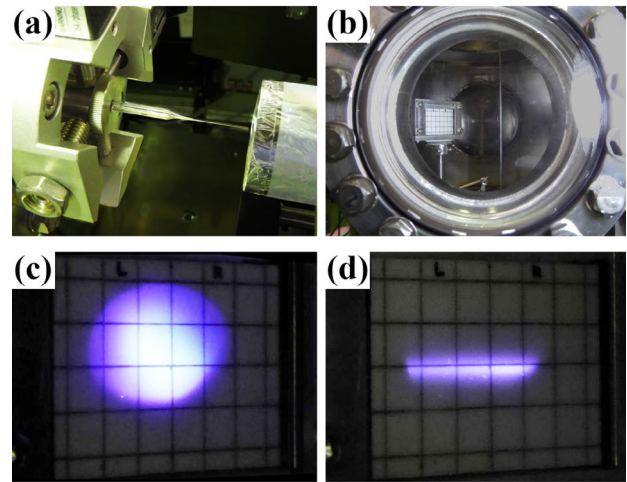


Fig. 1. (a) Tapered glass capillary optics mounted at a beam port of BL-W30. (b)  $\text{Al}_2\text{O}_3$  fluorescent plate with 5-mm interval grid in BL-W15. (c) Round-shaped beam spot. (d) A spot defocused horizontally but focused vertically.

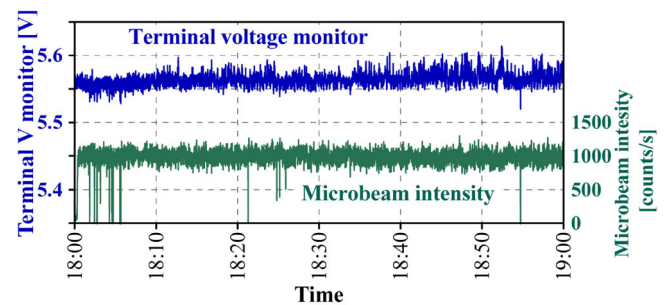


Fig. 2. Pelletron terminal voltage monitor (blue) and microbeam intensity (green) as a function of time.

shows a round shaped beam spot. Because the position fluctuation was mainly in the horizontal direction, the beam was defocused horizontally but focused vertically as shown in Fig. 1 (d).

After profile tuning, the beam was switched to BL-W30. The upper curve in Fig. 2 shows the time evolution of the Pelletron terminal voltage monitor ( $\sim 5.56$  V) proportional to the terminal voltage setting to 1.400 MV. The standard deviation ( $\sigma$ ) was 2.372 kV (0.169%), which corresponds to  $\sim 5$  mm fluctuation at the capillary entrance. However, the modified shape as shown in Fig. 1 (d) realized the stable rate of the microbeam around 1000 ions per second even when the terminal voltage became more unstable within 0.9% peak-to-peak. The fluctuation  $\sigma$  of ion-count rate (microbeam intensity) in Fig. 2 was 8.10%, which became successfully stable. Before this method, the ion-count rate had fluctuated between 0 and 1000 counts/s randomly.

<sup>\*1</sup> RIKEN Nishina Center

<sup>\*2</sup> Department of Physics, Toho University



## **IV. OPERATION RECORDS**



## Program Advisory Committee meetings for nuclear physics and for materials and life experiments

K. Yoneda,<sup>\*1</sup> K. Ishida,<sup>\*1</sup> H. Yamazaki,<sup>\*1</sup> N. Imai,<sup>\*2</sup> Y. X. Watanabe,<sup>\*3</sup> K. Yako,<sup>\*2</sup> H. Miyatake,<sup>\*3</sup>  
M. Iwasaki,<sup>\*1</sup> and H. Ueno <sup>\*1</sup>

The Program Advisory Committees (PAC) are in charge of reviewing the scientific proposals submitted for the use of the accelerator facility of RIKEN Nishina Center (RNC). Three PAC meetings were held in fiscal year 2018; one for the proposals of nuclear physics (NP-PAC), and two for the proposals of materials and life experiments (ML-PAC). The NP-PAC reviewed experimental proposals at RIBF, whereas the ML-PAC reviewed proposals at Rutherford Appleton Laboratory (RAL) and RIBF.

### NP-PAC

The 19th NP-PAC meeting was held from November 29 through December 1, 2018,<sup>1)</sup> with attendance of 16 PAC members. 33 proposals including 3 construction proposals were reviewed, and 14 proposals were approved as grade A. The outcome of the NP-PAC meeting is summarized in Table 1.

The 19th NP-PAC members are as follows:

A. Bracco (INFN, the chair), D. Ackermann (GANIL), A. Andreyev (University of York), I. Hamamoto (University of Lund/RNC), R.V.F. Janssens (University of North Carolina at Chapel Hill), A.O. Macchiavelli (LBNL), D.J. Morrissey (MSU), T. Nagae (Kyoto University), H. Nakada (Chiba University), K. Ogata (RCNP, Osaka University), T. Rauscher (University of Hertfordshire), K. Sekiguchi (Tohoku Univer-

Table 1. Summary of the outcome of the 19th NP-PAC meeting. The proposals ranked as A are treated as “approved” proposals.

19th NP-PAC (November 29–December 1, 2018)		
	requested proposals (days)	approved proposals (days)
GARIS	2 (31.5)	1 (17)
CRIB (AVF)	5 (44.5)	3 (35)
RIPS	0 (0)	0 (0)
KISS	0 (0)	0 (0)
BigRIPS/ZD	10 (71)	3 (13.5)
SHARAQ/OEDO	6 (53.5)	2 (16)
Rare RI Ring	1 (13.5)	1 (9)
SAMURAI	9 (74.5)	4 (20)
Total	33 (288.5)	14 (110.5)

<sup>\*1</sup> RIKEN Nishina Center

<sup>\*2</sup> Center for Nuclear Study, the University of Tokyo

<sup>\*3</sup> Wako Nuclear Science Center, Institute of Particle and Nuclear Studies, KEK

sity), H. Simon (GSI), P. Van Duppen (KU Leuven), Y.-H. Zhang (IMP).

### ML-PAC

The 16th and 17th ML-PACs were held on July 20, 2018, and in January, 2019, respectively.<sup>2)</sup> The PAC meeting was held for the 16th ML-PAC, and the proposals were reviewed with only submitted documents, as was done from in the 13th ML-PAC meeting. The 17th ML-PAC review was done only by mail review, as the number of proposals to review was relatively small. The outcome of the meeting is summarized in Table 2.

The 16th and 17th ML-PAC members are as follows: A. Hiller (ISIS, RAL, the chair), T. Azuma (RIKEN), R. Kadono (KEK), A. Kawamoto (Hokkaido University), S. Kawano (University of Tokyo), K. Kubo (ICU), P. Mendels (University of Paris), Z. Qin (Chinese Academy of Sciences), H. Yamase (NIMS), and X.G. Zheng (Saga University).

Table 2. Summary of the outcome of the 16th and 17th ML-PAC meetings. The RIBF proposals ranked as A are treated as “approved” proposals.

16th ML-PAC (July 20, 2018)		
	requested proposals (days)	approved proposals (days)
RAL	14 (68)	9 (25)
RIBF	2 (8)	2 (8)
Total	16 (76)	11 (33)
17th ML-PAC (January 2019)		
	requested proposals (days)	approved proposals (days)
RAL	7 (39)	6 (19)
RIBF	1 (1)	1 (1)
Total	8 (40)	7 (20)

### References

- 1) <http://www.nishina.riken.jp/RIBF/NP-PAC/index.html>.
- 2) <http://www.nishina.riken.jp/RIBF/ML-PAC/index.html>.

## Beam-time statistics of RIBF experiments

K. Yoneda<sup>\*1</sup> and H. Ueno<sup>\*1</sup>

This report describes the statistics of the beam times (BTs) at the RIBF facility in fiscal year (FY) 2018. The BTs are categorized into the following two groups: high-energy-mode and low-energy-mode BTs. In the former mode, the beams are delivered in the acceleration scheme of AVF, RILAC, or RILAC2  $\rightarrow$  RRC  $\rightarrow$  (fRC  $\rightarrow$  IRC  $\rightarrow$ ) SRC, where the accelerators in parentheses can be skipped in cascade acceleration depending on the beam species used. In the latter mode, the acceleration scheme is AVF or RILAC ( $\rightarrow$  RRC).

The BTs in the high-energy mode were scheduled from May to June and from October to December 2018, considering the restriction of utility-power use, budgetary constraints, the maintenance schedule of the accelerator system and co-generation system, etc. In the series of experiments performed in spring, the primary beam of  $^{18}\text{O}$  was provided to users, and the  $^{238}\text{U}$  primary beam was provided in autumn. Ten experiments approved by the RIBF Program Advisory Committees (PAC)<sup>1)</sup> with an approved BT of 59 days were conducted. The facility development programs used 3.5 days of BT; these are defined as machine study (MS) experiments. Two PAC-approved experiments had to be canceled due to sudden schedule change caused by accelerator troubles.

The summary of the high-energy-mode BTs in FY2018 is given in Fig. 1 as a bar chart. User time decreased compared to the BT in FY2017; this is mainly due to the startup tuning of the newly-introduced RRC-RF cavities, and troubles of water leakage from the new RF cavities. The total length of the MS is almost as short as the length in FY2017. Even though there remain only few newly-introduced facility device requiring beam tests, the opportunities of machine studies should be promoted as an investment for expanding the potential capability and availability of the facility.

The summary of the low-energy mode is shown in Fig. 2. Here, the BTs are classified based on the accelerator operation modes, i.e., AVF standalone, RILAC standalone, and RRC. In FY2018, the total BT length of the low-energy mode increased compare to that in FY2017 regardless of the RILAC shutdown started in the middle of June 2017 for accelerator upgrade. The relatively longer AVF-standalone time and RRC time are due to the long runs for the transmutation experiment and superheavy element search. It is anticipated that RRC will be mostly used for the superheavy element search experiments until RILAC becomes available again in FY2019.

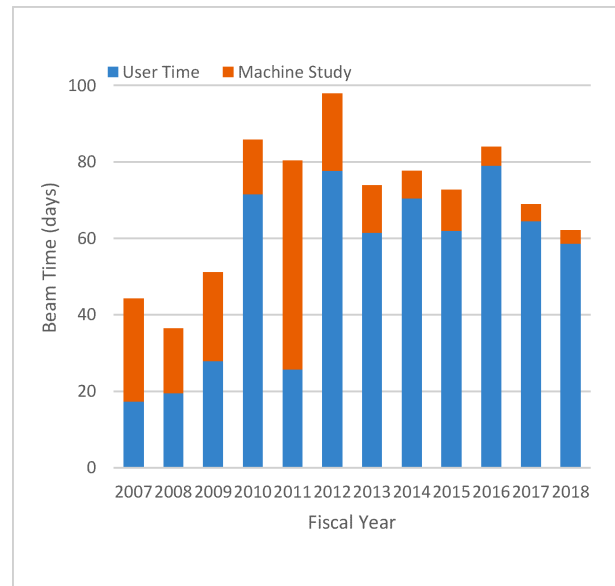


Fig. 1. Bar chart showing the BT statistics for high-energy-mode experiments from FY2007 to FY2018. The accelerator tuning time and Nishina Center mission time are not included.

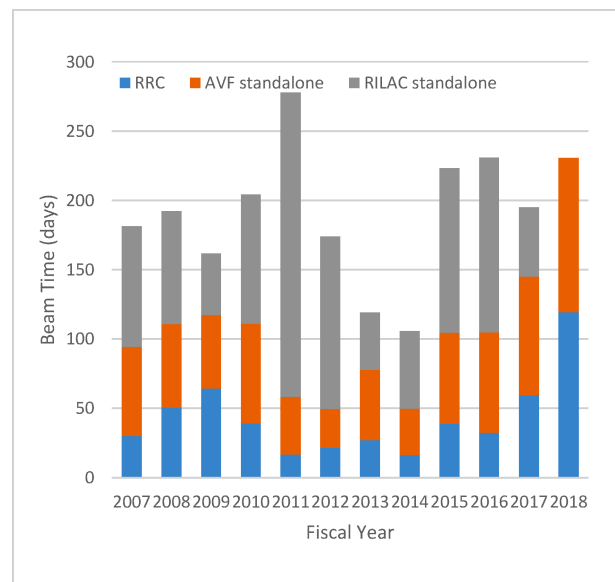


Fig. 2. Bar chart showing the BT statistics for low-energy-mode experiments from FY2007 to FY2018.

### Reference

- 1) K. Yoneda, K. Ishida, H. Yamazaki, N. Imai, Y. Watanabe, K. Yako, H. Miyatake, H. Ueno, in this report.

<sup>\*1</sup> RIKEN Nishina Center

## Electric power consumption of RIKEN Nishina Center in 2018

E. Ikezawa,<sup>\*1</sup> Y. Watanabe,<sup>\*1</sup> H. Yamasawa,<sup>\*1</sup> and O. Kamigaito<sup>\*1</sup>

The average hourly electrical power consumption for each day in the RIKEN Nishina Center (RNC) in 2018 is shown in Fig. 1. The total electrical power consumption by RNC in 2018 was 54,200 MWh, which was 26% lower than that in 2017. When RI Beam Factory (RIBF) experiments using an uranium ( $^{238}\text{U}$ ) beam were conducted, the maximum electrical power supply to the RIKEN Wako campus from the commercial power reached 19.2 MW with a CGS output of 5.0 MW on November 15, 2018, and the maximum electrical power consumption of RNC reached 15.4 MW on November 12, 2018.

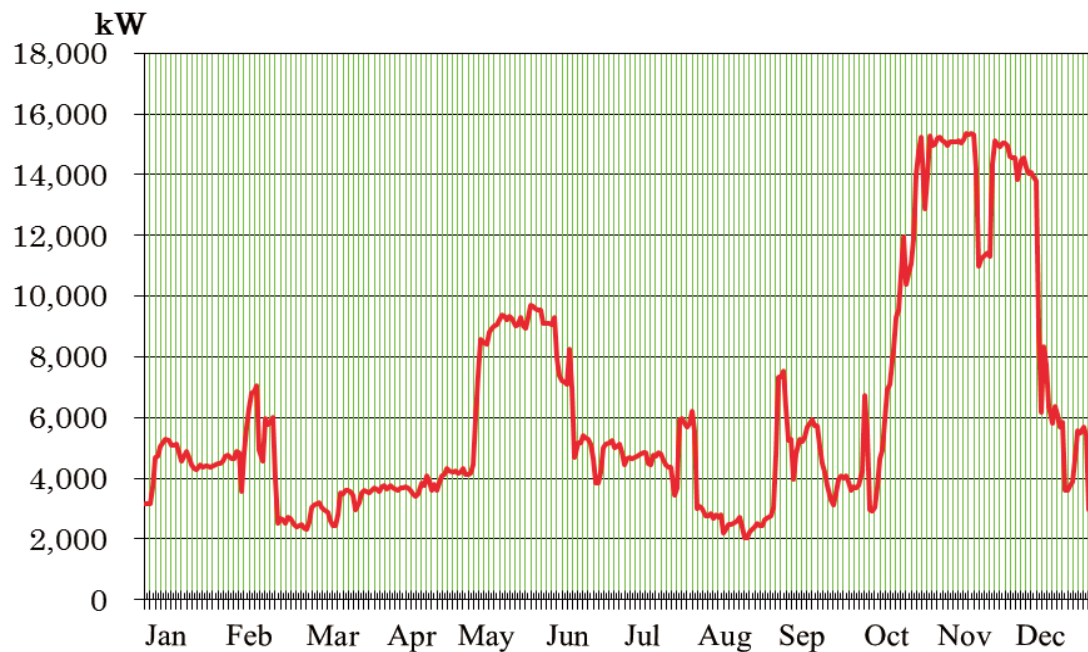


Fig. 1. Average hourly electrical power consumption for each day in RNC in 2018.

<sup>\*1</sup> RIKEN Nishina Center

# Operation report of the ring cyclotrons in the RIBF accelerator complex

J. Shibata,<sup>\*1</sup> K. Suda,<sup>\*2</sup> T. Dantsuka,<sup>\*2</sup> M. Fujimaki,<sup>\*2</sup> T. Fujinawa,<sup>\*2</sup> N. Fukunishi,<sup>\*2</sup> S. Fukuzawa,<sup>\*1</sup> M. Hamanaka,<sup>\*1</sup> H. Hasebe,<sup>\*2</sup> Y. Higurashi,<sup>\*2</sup> E. Ikezawa,<sup>\*2</sup> H. Imao,<sup>\*2</sup> S. Ishikawa,<sup>\*1</sup> O. Kamigaito,<sup>\*2</sup> Y. Kanai,<sup>\*2</sup> M. Kase,<sup>\*2</sup> M. Kidera,<sup>\*2</sup> K. Kobayashi,<sup>\*1</sup> M. Komiyama,<sup>\*2</sup> R. Koyama,<sup>\*1</sup> K. Kumagai,<sup>\*2</sup> T. Maie,<sup>\*2</sup> M. Nagase,<sup>\*2</sup> T. Nagatomo,<sup>\*2</sup> T. Nakagawa,<sup>\*2</sup> M. Nakamura,<sup>\*2</sup> T. Nakamura,<sup>\*1</sup> M. Nishida,<sup>\*1</sup> M. Nishimura,<sup>\*1</sup> J. Ohnishi,<sup>\*2</sup> H. Okuno,<sup>\*2</sup> K. Ozeki,<sup>\*2</sup> N. Sakamoto,<sup>\*2</sup> N. Tsukiori,<sup>\*1</sup> A. Uchiyama,<sup>\*2</sup> S. Watanabe,<sup>\*2</sup> T. Watanabe,<sup>\*2</sup> Y. Watanabe,<sup>\*2</sup> K. Yadomi,<sup>\*1</sup> K. Yamada,<sup>\*2</sup> and H. Yamasawa<sup>\*2</sup>

The operation report of the ring cyclotrons in the RIBF accelerator complex from Jan. to Dec. 2018 is presented. Table 1 presents a summary of the beams accelerated by these cyclotrons. The availability is defined as the ratio of the actual beam service time to the scheduled beam service time, which is an index of the stable operation of accelerators. Multiple experiments supplying identical beams are shown as a block, whereas the experiments with the <sup>51</sup>V beam are not shown, because the new element search experiments are conducted as the closed beam time under the Nishina Center Director. The total beam supply time was 1719.4 h excluding the V beam supply. The service of RRC was not available due to the upgrade of the resonators<sup>1)</sup> during the period of two months from February. In the old facility (RARF), the actual beam service time was 477.0 h, and the availability was 108.5%. Stable beams were supplied as usual. In the new facility (RIBF), two beam services were carried out. The total beam supply time was 1242.4 h, and the availability was 84.2%.

For the synthesis of the 119th element, three beam services were carried out. The <sup>51</sup>V beams were supplied with the availability of 73.5%. The availability was low due to the vacuum leakages caused by cooling water leakage at the new resonators of RRC and had to be aborted for repairs.

For the beam supply of <sup>18</sup>O, the maximum beam intensity was 600 particle nA, and the availability was 100.6% for seven experiments. There were failures in the RRC, namely in the plate and filament power supplies for an intermediate amplifier of RF No.1 and in a vacuum control system, which seemed to be caused mainly by radiation.

A <sup>238</sup>U beam at 345 MeV/nucleon was supplied for eight experiments, and the maximum beam intensity of 72 particle nA was the highest ever. The availability decreased to 67.8% owing to several troubles. The beam supply was started 7.5 d later than scheduled due to the failures and repairs of the SRC-EIC and -EDC, abnormal termination of the rotating charge stripper, and a severe beam tuning to reduce beam losses. The rotation-stops of the charge stripper occurred frequently even during the beam supply. Finally, a ferrofluidic seal was exchanged to recover stable operation. Furthermore, a vacuum leakage happened again at the RRC resonator No.1 in November, and the repair was performed. It took 8 d for the repair and beam tuning to resume the beam supply.

## Reference

- 1) K. Yamada *et al.*, “Remodeling of acceleration cavity resonators for RIKEN Ring Cyclotron”, in this report.

Table 1. Summary of the accelerated beams in 2018.

Beam particle	Energy (MeV/nucleon)	Acceleration mode	Beam course	Beam intensity (particle nA)		Beam service time (h)		Availability (%)
				Requested	Actual	Scheduled	Actual	
RARF								
<sup>12</sup> C	135	AVF-RRC	E5B (Biology)	1	467	36.0	17.9	87.0
<sup>14</sup> N	135		E3B (RI production)	500	600	76.0	74.2	97.6
<sup>40</sup> Ar	95		E5A (Industry)	1	8.8	20.0	35.0	174.8
<sup>56</sup> Fe	90		E5B (Biology)	1	0.6	6.0	5.2	100.0
<sup>84</sup> Kr	70		E3A (JAXA) / E5A (Industry)	1	6.6	154.0	174.4	113.2
<sup>86</sup> Kr	66		E3A (JAXA / Industry)	1	1.6	26.0	25.0	99.6
<sup>136</sup> Xe	10.75		RILAC2-RRC	E2B (KEK/KISS)	250	340	48.0	47.7
<sup>136</sup> Xe	10.75	E3A (JAXA) / E5A (Industry)		1	330	57.0	55.5	110.1
<sup>238</sup> U	10.75	E5A (Material)		2	2.2	24.0	24.9	103.6
<sup>40</sup> Ar	160	AVF-RRC-IRC	E5B (Biology)	1	23	25.0	17.2	100.0
RIBF								
<sup>18</sup> O	230	AVF-RRC-SRC	BigRIPS/SAMURAI	> 700	600.0	540.0	543.0	100.6
<sup>238</sup> U	345	RILAC2-RRC-fRC-IRC-SRC	BigRIPS/BigRIPS-F12/ZDS/Rare RI Ring	> 60	72.0	1032.0	699.4	67.8
Total						2044.0	1719.4	89.8

\*1 SHI Accelerator Service Ltd.

\*2 RIKEN Nishina Center

## RILAC operation

E. Ikezawa,<sup>\*1</sup> T. Ohki,<sup>\*2</sup> M. Kase,<sup>\*1</sup> T. Nakagawa,<sup>\*1</sup> N. Sakamoto,<sup>\*1</sup> H. Okuno,<sup>\*1</sup> N. Fukunishi,<sup>\*1</sup> Y. Watanabe,<sup>\*1</sup> M. Komiyama,<sup>\*1</sup> A. Uchiyama,<sup>\*1</sup> T. Maie,<sup>\*1</sup> M. Nagase,<sup>\*1</sup> M. Fujimaki,<sup>\*1</sup> T. Watanabe,<sup>\*1</sup> H. Hasebe,<sup>\*1</sup> H. Imao,<sup>\*1</sup> K. Ozeki,<sup>\*1</sup> K. Suda,<sup>\*1</sup> Y. Higurashi,<sup>\*1</sup> K. Yamada,<sup>\*1</sup> S. Watanabe,<sup>\*1</sup> M. Kidera,<sup>\*1</sup> T. Nagatomo,<sup>\*1</sup> H. Yamauchi,<sup>\*2</sup> K. Oyamada,<sup>\*2</sup> M. Tamura,<sup>\*2</sup> A. Yusa,<sup>\*2</sup> K. Kaneko,<sup>\*2</sup> and O. Kamigaito<sup>\*1</sup>

For the upgrade of RILAC, the following works have been in progress at the LINAC building during the reporting period. The details are described elsewhere in this progress report.

- (1) The new 28 GHz superconducting electron cyclotron resonance ion source and the low energy beam transport (LEBT) were installed. The necessary preparation for the test was conducted.
- (2) The section after the A2 cavity reconstituted. The necessary preparation for the installation of a superconducting RILAC (sRILAC), middle energy beam transport (MEBT), high energy beam transport (HEBT), and helium refrigerator was conducted.
- (3) The GARIS3 was installed in the e2 beam courses in target room no. 1.
- (4) The air cooling fan coil units in the radiation-controlled area were replaced.

We performed the following maintenances during the reporting period.

- (1) In the radio frequency systems, DC high-voltage power supplies were subjected to annual inspection. The major components with mechanical parts were subjected to simple inspection.

- (2) The water pumps were subjected to simple inspection. All cooling towers were subjected to monthly inspection.
- (3) All turbomolecular pumps were subjected to simple inspection. Cryogenic pumps used for the No. 5 cavity, A1 cavity, and standby units were overhauled.

We performed the following repairs during the reporting period. The details are described elsewhere in this progress report.

- (1) The No. 5 cavity had a serious vacuum leak due to a deteriorated vacuum gasket of the center conductor in the cavity. The external dimensions of the gasket are  $10 \pm 0.1$  mm height,  $8 \pm 0.1$  mm width, and  $4273 \pm 13.5$  mm length in the radial direction. We replaced it with a new one. In addition, silver plates for the electrical contact of the center conductor were replaced with new ones.
- (2) The bottom plate of the A1 cavity had a vacuum leak. We repaired the plate with a repair material.

---

<sup>\*1</sup> RIKEN Nishina Center

<sup>\*2</sup> SHI Accelerator Service Ltd.

## Operation report on the RIKEN AVF cyclotron for 2018

K. Kobayashi,<sup>\*1</sup> K. Ozeki,<sup>\*2</sup> M. Fujimaki,<sup>\*2</sup> N. Fukunishi,<sup>\*2</sup> S. Fukuzawa,<sup>\*1</sup> A. Goto,<sup>\*2</sup> M. Hamanaka,<sup>\*1</sup> H. Hasebe,<sup>\*2</sup> Y. Higurashi,<sup>\*2</sup> E. Ikezawa,<sup>\*2</sup> H. Imao,<sup>\*2</sup> S. Ishikawa,<sup>\*1</sup> O. Kamigaito,<sup>\*2</sup> K. Kaneko,<sup>\*1</sup> M. Kase,<sup>\*2</sup> M. Kidera,<sup>\*2</sup> M. Komiyama,<sup>\*2</sup> Y. Kotaka,<sup>\*3</sup> R. Koyama,<sup>\*1</sup> K. Kumagai,<sup>\*2</sup> T. Maie,<sup>\*2</sup> M. Nagase,<sup>\*2</sup> T. Nagatomo,<sup>\*2</sup> T. Nakagawa,<sup>\*2</sup> T. Nakamura,<sup>\*1</sup> M. Nishida,<sup>\*1</sup> M. Nishimura,<sup>\*1</sup> J. Ohnishi,<sup>\*2</sup> H. Okuno,<sup>\*2</sup> Y. Oshiro,<sup>\*3</sup> K. Oyamada,<sup>\*1</sup> N. Sakamoto,<sup>\*2</sup> J. Shibata,<sup>\*1</sup> K. Suda,<sup>\*2</sup> M. Tamura,<sup>\*1</sup> N. Tsukiori,<sup>\*1</sup> A. Uchiyama,<sup>\*2</sup> S. Watanabe,<sup>\*2</sup> T. Watanabe,<sup>\*2</sup> Y. Watanabe,<sup>\*2</sup> K. Yadomi,<sup>\*1</sup> K. Yamada,<sup>\*2</sup> and A. Yusa<sup>\*1</sup>

The yearly report on the operation of the RIKEN AVF cyclotron (denoted as AVF hereafter) for the period January–December 2018, is presented. AVF has four beam courses of various ion beams used for stand-alone operations: C01 (machine study), C03 (RI production), E7A (CRIB), and E7B (student experiment). In addition, AVF is used as an injector of RRC. In this mode, beams are delivered to three courses: RRC-RARF, RRC-IRC E5, and RRC-IRC-SRC. The beam courses are shown schematically in Fig. 1.

The yearly operation statistics and beams accelerated using AVF are summarized in Table 1 and 2, respectively. Remarkable operations achieved this year include a development test of C-foil and a demonstration experiment of nuclear transmutation. For C-foil development, an endurance test was performed for 150 h at C03. The experiment to demonstrate nuclear transmutation was carried out at C03. Most of the delivered time to C03 (2067 h, twice as long as that in the usual year) was spent on this experiment. In the RIBF experiment (RRC-IRC-SRC course), the beam was continuously delivered without any break for 600 h, out of a total delivered time of 820 h. In a total operation time of 5042 h, only 7 h was spent for AVF repairs. In the

last experiment in July, a cooling water pipe of PHASE SLIT leaked inside the AVF vacuum. Therefore, the RARF experiment was canceled.

Table 1. Comparison of AVF operation statistics with that of the previous year.

Particle	Energy [MeV/u]	Course
<b>Stand-alone operation</b>		
<i>d</i>	11.00	E7B
<i>d</i>	12.00	C03, E7B
<i>d</i>	14.00	C03
$\alpha$	6.50	E7B
$\alpha$	7.16	E7B
$\alpha$	7.25	C03
$\alpha$	12.50	C03, E7B
${}^7\text{Li}$	5.60	E7A
${}^7\text{Li}$	6.00	C03, E7A
${}^{11}\text{B}$	7.82	C03
${}^{12}\text{C}$	7.30	C03
${}^{18}\text{O}$	6.08	C03
${}^{18}\text{O}$	7.00	E7A
${}^{40}\text{Ar}$	3.78	C03
<b>Operation as injector of RRC</b>		
${}^{12}\text{C}$	7.00	RRC - RARF
${}^{14}\text{N}$	3.97	RRC - RARF
${}^{18}\text{O}$	4.51	RRC - RIBF
${}^{40}\text{Ar}$	5.19	RRC - RIBF
${}^{40}\text{Ar}$	5.20	RRC - RARF
${}^{56}\text{Fe}$	5.00	RRC - RARF
${}^{84}\text{Kr}$	3.97	RRC - RARF
${}^{86}\text{Kr}$	3.78	RRC - RARF

Table 2. AVF beam list in 2018.

AVF stand-alone operation	2017	2018
Tuning of AVF [h]	742	886
Trouble of AVF [h]	4	6
C01 M.S. [h]	32	0
C03 exp. [h]	1113	2067
E7A exp. [h]	245	262
E7B exp. [h]	597	274
Sub total [h]	2697	3489
AVF operation as injector of RRC	2017	2018
Tuning of AVF [h]	141	132
Trouble of AVF [h]	9	1
RRC-RARF exp. [h]	564	600
RRC-RIBF exp. [h]	549	820
Sub total [h]	1254	1551
<b>Total [h]</b>	<b>3951</b>	<b>5042</b>

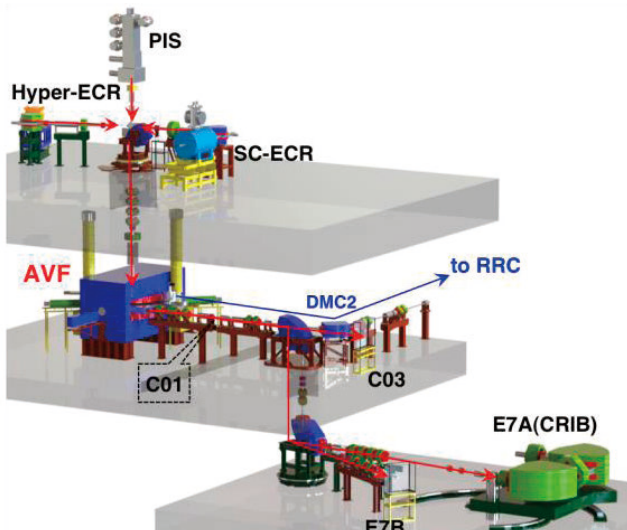


Fig. 1. Overview of AVF cyclotron with ion sources, experimental courses, and beam transport line to RRC.

\*1 SHI Accelerator Service Ltd.

\*2 RIKEN Nishina Center

\*3 Center for Nuclear Study, the University of Tokyo

## Present status of the liquid-helium supply and recovery system

T. Dantsuka,<sup>\*1</sup> H. Okuno,<sup>\*1</sup> M. Nakamura,<sup>\*1</sup> M. Kase,<sup>\*1</sup> S. Tsuruma,<sup>\*1</sup> M. Ohshima,<sup>\*2</sup> H. Miura,<sup>\*2</sup>  
H. Shiraki,<sup>\*2</sup> H. Hirai,<sup>\*2</sup> and H. Hazama<sup>\*2</sup>

The liquid-helium supply and recovery system,<sup>1)</sup> which can produce liquid helium at a liquefaction rate of 200 L/h from pure helium gas, had been under stable operation since the beginning of April 2001. As operation failure due to deterioration over time has increased in recent years, duplication of liquefier was conducted in 2017. The new liquefier can produce liquid helium at a liquefaction rate of 220 L/h from pure helium gas. Consequently, even when the liquefier breaks down, it can be repaired without stopping the supply of liquid helium.

The volumes of liquid helium supplied each year from 2001 to 2017 are shown in Fig. 1. From 2001 to 2013, there was a gradual increase in the supplied volume, with two declines in 2009 and 2011. In 2014, the supplied volume decreased owing to a malfunction in the system. However, in 2015, the supplied volume returned to its original value. In 2016, the supplied volume decreased but slightly increased in 2017.

The purity of helium gas recovered from the laboratories gradually improved after the new system was constructed. At present, the impurity concentration in the recovered gas rarely exceeds 200 ppm. The volume of helium gas recovered from each building in the Wako campus as well as the volume transported to the liquid helium supply and recovery system were measured. The recovery efficiency, which is defined as the ratio of the amount of recovered helium gas to the amount of supplied liquid helium, was calculated. The recovery efficiency for the buildings on the south side of the Wako campus, namely the Cooperation Center building of the Advanced Device Laboratory, Chemistry and Material Physics building, and Nanoscience Joint Laboratory building, increased to more than 85%.

### Reference

- 1) K. Ikegami *et al.*, RIKEN Accel. Prog. Rep. **34**, 349 (2001).

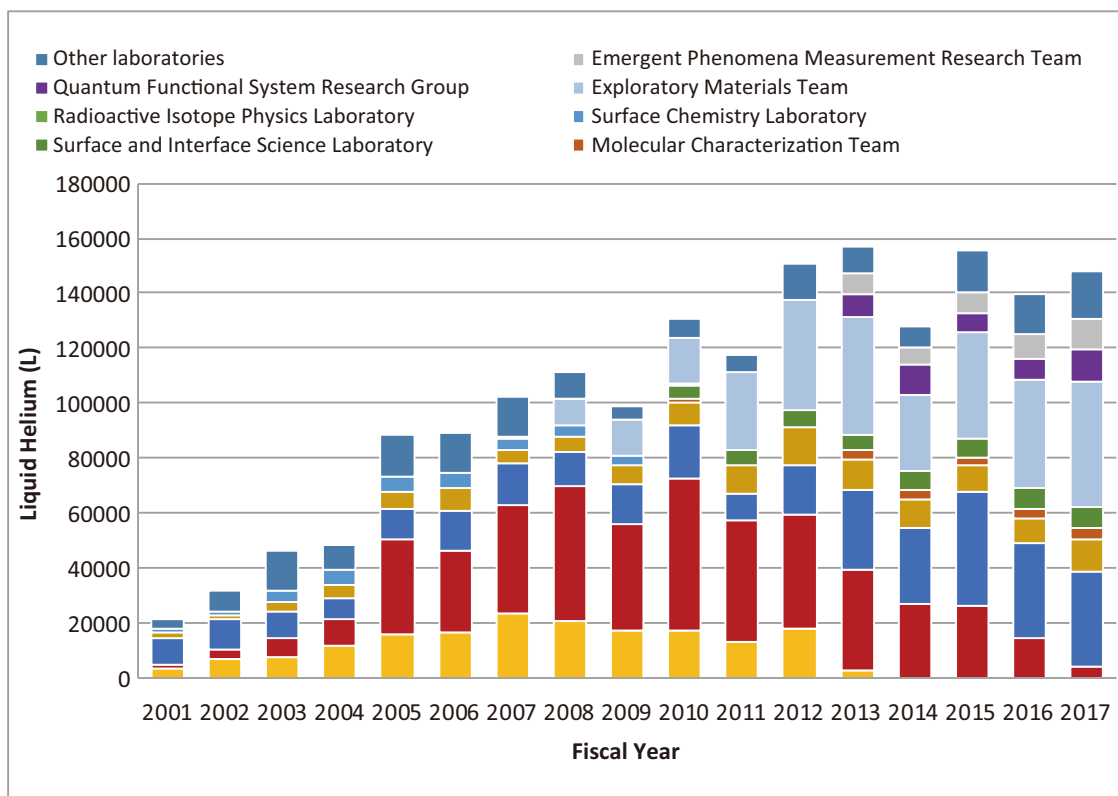


Fig. 1. Volumes of liquid helium supplied to the various laboratories for each fiscal year from 2001 to 2017.

<sup>\*1</sup> RIKEN Nishina Center

<sup>\*2</sup> Nippon Air Conditioning Service K.K

## Present status of the BigRIPS cryogenic plant

K. Kusaka,<sup>\*1</sup> M. Ohtake,<sup>\*1</sup> K. Yoshida,<sup>\*1</sup> M. Ohshima,<sup>\*2</sup> A. Mikami,<sup>\*2</sup> H. Hazama,<sup>\*2</sup> H. Miura,<sup>\*2</sup> H. Shiraki,<sup>\*2</sup> H. Hirai,<sup>\*2</sup> M. Haneda,<sup>\*2</sup> R. Sasaki,<sup>\*2</sup> K. Kimura,<sup>\*2</sup> M. Noguchi,<sup>\*3</sup> and N. Suzuki<sup>\*3</sup>

After the September 2017 incident wherein water pipelines for the refrigerator system were severely blocked by muddy impurities, we replaced the entire piping of the cooling water system for the BigRIPS cryogenic plant in March 2018. Figure 1 shows the new cooling water pipelines for the compressor unit and refrigerator. We changed the cooling water system for the refrigerator from the cool-water system using cooling towers to the chilled-water system using RIBF absorption chillers. The cooling efficiency of the turbine system has greatly improved.

Based on the RIBF beam-time schedule, we performed two continuous operations at the BigRIPS cryogenic plant in 2018. The first operation lasted from Apr. 17 to June 18 and the second from Sept. 28 to Dec. 17. We operated the cryogenic system without any trouble in both periods. We measured the vibrations of the compressor unit and observed the low oil contamination in helium gas during operations. The total operation time of the compressor unit was 68,291 h.

Figure 2 shows the vibration acceleration in the vertical and horizontal directions as a function of the total operation time. We measured the vibrations of the compressor at the high-pressure and low-pressure sides since 2015. Except the rapid increase of the vibration acceleration at the operation time of 59,000 h, which indicates the damage in the bearing unit that occurred in Dec. 2016,<sup>1)</sup> the vibration acceleration stayed less than  $8 \text{ m/s}^2$  during the operation period.

Figure 3 shows an estimate of the oil contamination level at the entrance of the third coalescer vessel as a function of the coalescer filter operation time. By mea-



Fig. 1. New cooling water piping for the compressor and refrigerator.

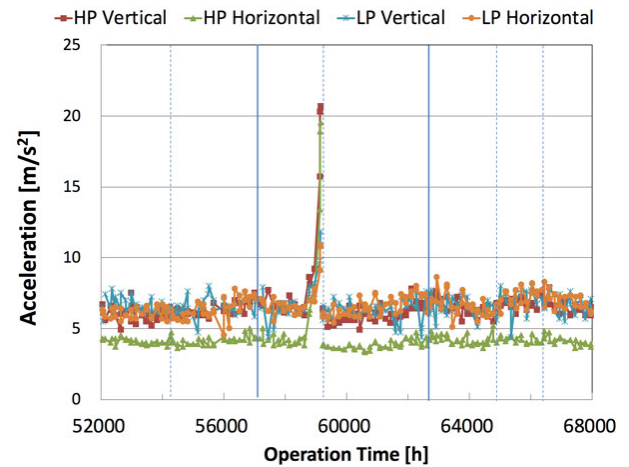


Fig. 2. Vibration acceleration of the compressor unit.

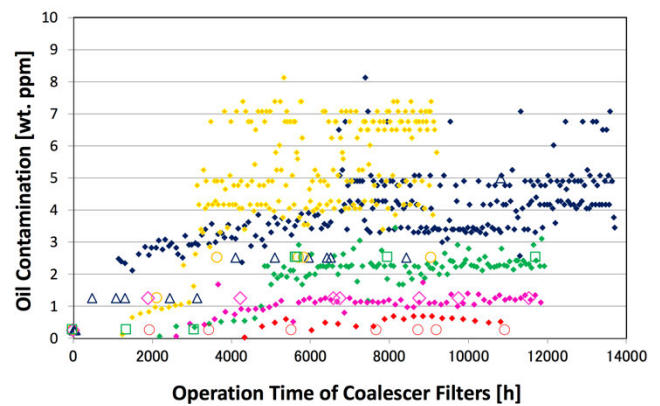


Fig. 3. Oil contamination at the entrance of the third coalescer vessel.

suring the operation interval of the drain valves of the coalescer vessels in the compressor unit, the oil contamination level was evaluated.<sup>2)</sup> The navy blue, green, and yellow diamonds represent the estimates for the 2008–2009, 2010–2011, and 2012–2013 operations, respectively. The estimate for the 2014–2015 and 2016–2018 operations are shown with pink and red diamonds, respectively. The oil contamination values measured using the oil check kit are also shown. The open triangles, squares, and circles represent the results for the 2008–2009, 2010–2011, and 2012–2013 operations. The results for the 2014–2015 and 2016–2018 operations are indicated by the open diamonds and circles, respectively. Both estimations of the oil contamination level are consistent with each other and the performance efficiency of the latest filter elements seems to be better than that of the others.

### References

- 1) K. Kusaka *et al.*, RIKEN Accel. Prog. Rep. **50**, 285 (2017).
- 2) K. Kusaka *et al.*, RIKEN Accel. Prog. Rep. **41**, 309 (2010).

<sup>\*1</sup> RIKEN Nishina Center

<sup>\*2</sup> Nippon Kucho Service Co., Ltd.

<sup>\*3</sup> Mayekawa Mfg. Co., Ltd.

## Radiation safety management at RIBF

K. Tanaka,<sup>\*1</sup> Y. Uwamino,<sup>\*1</sup> H. Sakamoto,<sup>\*1</sup> R. Hirunuma-Higurashi,<sup>\*1</sup> H. Mukai,<sup>\*2</sup> A. Akashio,<sup>\*1</sup> T. Okayasu,<sup>\*1</sup> R. Suzuki,<sup>\*3</sup> M. Takekoshi,<sup>\*3</sup> Y. Yamauchi,<sup>\*3</sup> K. Igarashi,<sup>\*1</sup> S. Iizuka,<sup>\*1</sup> N. Usudate,<sup>\*1</sup> and Y. Shioda<sup>\*1</sup>

In this paper, the results of radiation monitoring at RIBF, conducted at the border of the facility and the radiation-controlled area are reported. In addition, the residual doses along the accelerator setups are presented. In 2018, a  $^{238}\text{U}$  beam of approximately 345 MeV/nucleon was provided at an intensity of 70 particle nA during October to December. A  $^{18}\text{O}$  beam of approximately 230 MeV/nucleon of 700 particle nA was used in May and June.

The dose rates at the boundary of the radiation-controlled area were monitored. Neutron and  $\gamma$ -ray monitors were used at three locations: the roofs of the RRC, IRC, and BigRIPS. Figure 1 shows the annual neutron dose at these positions. In 2018, even the highest annual dose of  $51 \mu\text{Sv/y}$  at the IRC roof was lower than the legal limit of  $5.2 \text{ mSv/y}$ .

The dose rates at the site boundary, where the legal limit is  $1 \text{ mSv/y}$ , were monitored. Neutron and  $\gamma$ -ray monitors were used, and the annual dose in 2018 was found to be lower than the detection limit after background correction. The detection limit of the neutron monitor is  $2 \mu\text{Sv/y}$  and that of the  $\gamma$ -ray monitor is  $8 \mu\text{Sv/y}$ . Therefore, it was inferred that the annual dose at the boundary was less than  $10 \mu\text{Sv/y}$ , which is considerably lower than the legal limit.

The residual radioactivity at the deflectors of the cyclotrons was measured just before the maintenance work. The residual dose depends on factors such as

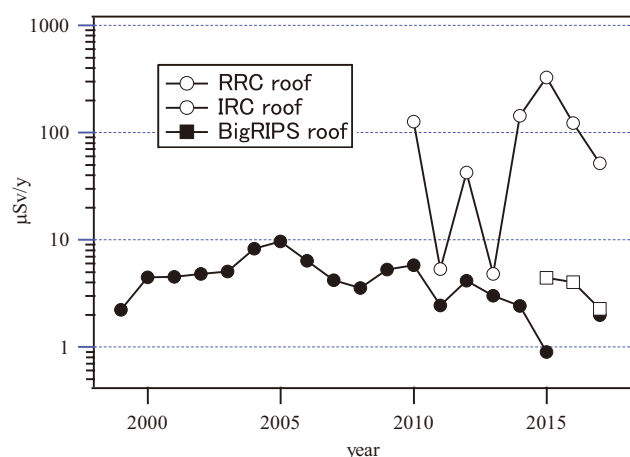


Fig. 1. Radiation dose at the boundary of radiation-controlled area.

\*1 RIKEN Nishina Center

\*2 Japan Environment Research Corporation

\*3 Daiwa Atomic Engineering Corporation

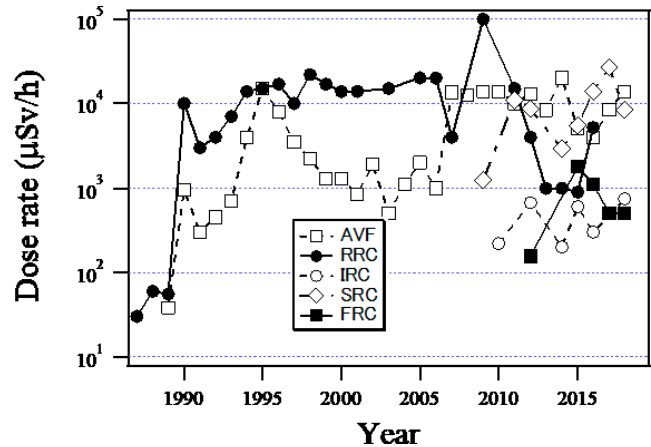


Fig. 2. Dose rates of residual radioactivity at the deflectors of five cyclotrons.

beam intensity, accelerator operation time, and cooling time. The dose rates from 1986 are shown in Fig. 2. The dose rates for FRC, IRC, and SRC are shown for years after 2006, when the RIBF started its operation. For AVF, the dose rate increased in 2006 because the radioisotope production was started in that year and thus, the beam intensity increased.

The residual radioactivity along the beam lines was measured after every experiment. Figure 3 shows the locations of measurement points where high residual doses were observed. Table 1 lists the dose rates, beam conditions, and cooling time at the measurement points. The maximum dose was  $17.8 \text{ mSv/h}$  at point 19, which is in the vicinity of beam dump of BigRIPS.

The radioactivity in the closed cooling system at BigRIPS was measured. The water for the F0 target, exit beam dump, and side-wall dump were sampled in June. The water in the closed cooling systems for the F0 target and exit beam dump was replaced in May 2018. Therefore, the detected radioisotopes in the F0 target and exit beam dump were generated during one month of operation in RIBF. For the side-wall beam dump, part of the water was replaced in January 2018, but all the water was replaced in March 2015; the results are presented in Table 2. A liquid scintillation counter (LSC-7400, Hitachi Co. Ltd.) was used for the low energy  $\beta$  ray of 18 keV from H-3 nuclide. A Ge detector (GC2019, Canberra Co. Ltd.) was also used for the  $\gamma$  rays emitted from other radionuclides. The radionuclides, except H-3, were already filtered by an ion exchange resin in the closed cooling systems.

Although the overall value of contamination was less than the legal limit for drain water, as presented in Table 2, the water from the closed cooling system will be dumped into the drain tank before the next operation to prevent contamination in the room in case of a water leakage.

The e-learning module, which can be accessed anytime from anywhere (even from outside RIKEN), has been used to re-train the radiation workers at RIBF. Approximately 630 radiation workers have completed the training in 2018.

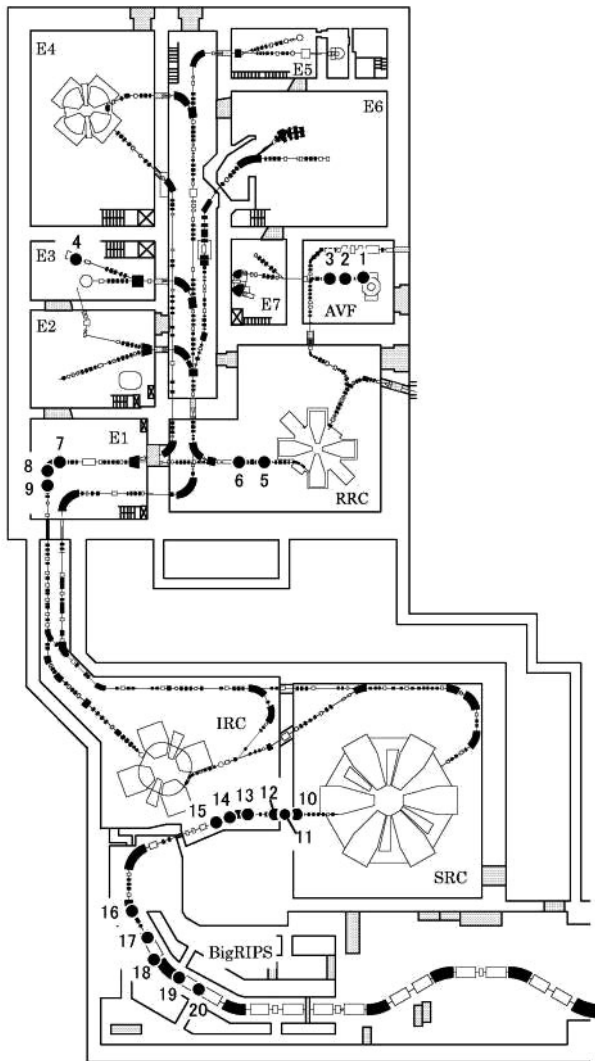


Fig. 3. Layout of the beam lines at RIBF. The measurement locations listed in Table 1 are indicated.

Table 1. Dose rates measured at beam lines in 2017.

Points 1–24 indicate the locations where measurements were taken as shown in Fig. 3.

Point	Dose rate ( $\mu\text{Sv/h}$ )	Date (M/D)	Particle	Energy (MeV/u)	Intensity (pnA)	Cooling time (h)
1	200	8/24	Ar-40	5.2	40	573
2	400	8/24	Ar-40	5.2	40	573
3	170	8/24	Ar-40	5.2	40	573
4	1000	10/10	N-14	135	357	120
5	250	8/24	Ar-40	95	1	571
6	150	8/24	Ar-40	95	1	571
7	5500	12/17	U-238	50	342	159
8	1800	12/17	U-238	50	342	159
9	700	12/17	U-238	50	342	159
10	100	12/20	U-238	345	72	231
11	9600	12/20	U-238	345	72	231
12	140	12/20	U-238	345	72	231
13	350	12/20	U-238	345	72	231
14	1600	7/25	Ar-40	160	1	983
15	400	7/25	Ar-40	160	1	983
16	200	7/25	O-18	230	600	1133
17	1430	12/20	U-238	345	72	231
18	3450	12/20	U-238	345	72	231
19	17800	12/20	U-238	345	72	231
20	241	12/20	U-238	345	72	589

Table 2. Concentrations of radionuclide in the cooling water at BigRIPS, the allowable legal limits for drain water, and the ratios of concentration to the allowable limit.

Cooling water	Nuclide	Concentration[a] ( $\text{Bq/cm}^3$ )	Limit[b] ( $\text{Bq/cm}^3$ )	Ratio to limit [a/b]
BigRIPS F0 target	H-3	3.4	60	$5.8\text{e-}2$
			summation	$5.8\text{e-}2$
BigRIPS exit beam dump	H-3	3.8	60	$6.4\text{e-}2$
	Mn-54	$1.3\text{e-}3^{1)}$	1	$1.3\text{e-}3$
			summation	$6.4\text{e-}2$
BigRIPS side-wall beam dump	H-3	53.	60	0.89
	Be-7	$8.6\text{e-}2$	30	$2.9\text{e-}3$
	Mn-54	$1.2\text{e-}3$	1	$1.2\text{e-}3$
			summation	0.89

1) read as  $1.3 \times 10^{-3}$

## Operation of the Pelletron tandem accelerator

T. Ikeda,\*<sup>1</sup> M. Hamagaki,\*<sup>1</sup> and H. Sato\*<sup>1</sup>

The tandem accelerator (Pelletron 5SDH-2, 1.7 MV max.) in the Nishina R&D Building, which is managed by the Detector Team of RNC, is a joint-use equipment at the Wako campus. Figure 1 shows the configuration of the beam elements. Two ion sources are located in the upstream of the accelerator. One is the RF charge-exchange ion source called Alphasross, which is mainly used for the extraction of He<sup>-</sup> ions. The negative charge state of He ions is realized by transmission through Rb vapor. The other one is the Source of Negative Ions by Cesium Sputtering (SNICS). Almost all other ions can be extracted from SNICS as negative ions, *e.g.*, H<sup>-</sup> and C<sup>-</sup>. These ions are installed as a solid cathode, *e.g.*, TiH<sub>2</sub> for H<sup>-</sup>, to be sputtered by Cs ions.<sup>1)</sup> Thus far, the ion species of H, He, Li, B, C, N, O, Si, Ti, Ni, Cu, and Au have been accelerated by 0.5–1.7 MV.

The accelerator has four beam lines named BL-E/*Wnn* (*nn* stands for the bending angle). BL-E45 is used for surface modification. BL-E15 is reserved for the analysis of Rutherford backscattering (RBS) spectrometry/elastic recoil detection analysis (ERDA). The microbeam port is BL-W30, which employs tapered glass capillary

Table 1. Beam conditions and experiments conducted in the tandem accelerator.

Ion	Energy [MeV]	Beam current [pnA]	Experiment	Operation time [days]
<sup>1</sup> H <sup>+</sup>	1.0–3.0	0.008–420	Irradiation	25
<sup>4</sup> He <sup>+,2+</sup>	2.0–4.8	0.2–300	Irradiation	4

with an end-window to irradiate biological sample in solution.

The range of the ion beams is several 10 μm at most for water (density = 1 g/cm<sup>3</sup>). Only H<sup>+</sup> can have ranges greater than 100 μm for water. All the experiments except for microbeam irradiation with the glass capillaries should be performed in vacuum chambers, where heavy ions of several MeV, such as Au ions, can provide stopping powers greater than 200 keV/μm at only the surface layer of samples or detector-sensitive areas.

This year, BL-W15 (Fig. 2) started to be used again after the renewal of the beam diagnostic system consisting of two Al<sub>2</sub>O<sub>3</sub> fluorescent plates with current monitors. This system helps to focus the beams down to a few cm in diameter at the end of the line by tuning a quadrupole magnet as shown in Fig. 1. The beam line was used for the experiments of detector calibration and Nishina School.

During the annual reporting period from Jan. 1 to Dec. 31, 2018, the total machine time including a machine study was 29 days, where the condition test of the ion sources is not counted. The ion species accelerated in 2018 were only light ions H<sup>+</sup>, He<sup>+</sup>, He<sup>2+</sup> with energies ranging from 1.0 to 4.8 MeV, as summarized in Table 1. Experimental studies were performed on the following subjects.

- (1) Machine study of a proton microbeam using tapered glass capillaries (1 day)
- (2) Test of microbeam irradiation on single cells at BL-W30 (24 days)
- (3) ERDA experiments using carbon ions (0 day)
- (4) Educational experiment of proton capture by a carbon nucleus for Nishina School (1 day)
- (5) Development of charged particle/gamma ray detector to be used for RIBF experiments (2 days)
- (6) Other development using protons (1 day)

Since the experimental area is approved as a second-class radiation-controlled area, the users of all measurements can access their setup even during the beam irradiation time. The users are free from any setup for remote control utilities. These points are the advantages of using the RIKEN Pelletron accelerator.

### Reference

- 1) R. Middleton, *A Negative-Ion Cookbook* (Univ. Pennsylvania, Philadelphia, PA 19104, 1990).

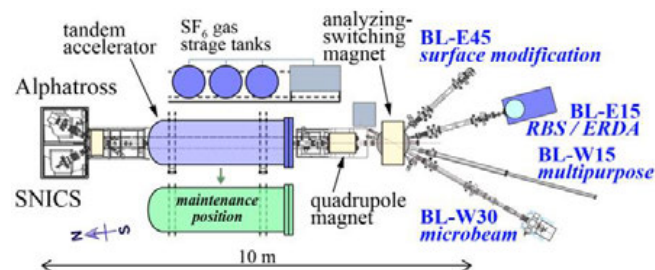


Fig. 1. Pelletron tandem accelerator and beamlines in the Nishina R&D Building.



Fig. 2. BL-W15 started to be used again as a multipurpose beam line after the renewal of the beam diagnostic system. The degree of vacuum level for the user setup is required to be better than 10<sup>-4</sup> Pa. (Left). A setup for calibration of gamma ray detectors using a resonance reaction with a carbon target bombarded by 1 or 2 MeV proton beams (Right).

\*<sup>1</sup> RIKEN Nishina Center

## Fee-based activities by the industrial application research team

A. Yoshida,<sup>\*1</sup> T. Kambara,<sup>\*1</sup> H. Haba,<sup>\*1</sup> and D. Mori<sup>\*1</sup>

Fee-based activities conducted by the Industrial Application Research Team (former Industrial Cooperation Team) in 2018, which include the utilization of heavy-ion beams in the industry and distribution of radioisotopes, are summarized below.

RIKEN Nishina Center allows the use of the AVF cyclotron, RILAC, and RIKEN Ring Cyclotron (RRC) by private companies in Japan for a fee.<sup>1)</sup> In 2018, four fee-based beamtimes were successfully performed for the irradiation test of space-use semiconductor devices: an 80-hour beamtime with a 70-MeV/nucleon  $^{84}\text{Kr}$  beam in February, 40-hour beamtime with a 70-MeV/nucleon  $^{84}\text{Kr}$  and 20-hour beamtime with a 95-MeV/nucleon  $^{40}\text{Ar}$  in July, and 8-hour beamtime with a 70-MeV/nucleon  $^{84}\text{Kr}$  beam in December. The former three beamtimes were at the E5A and the last one was at the E3A beamline, where the clients irradiated their samples in the atmosphere. In addition, we performed a three-hour machine-study beamtime in February with a 10.75-MeV/nucleon  $^{136}\text{Xe}$  beam, in which we studied the properties of beam to prepare future fee-based utilizations.

Since 2007, RIKEN has distributed radioisotopes (RIs) to users in Japan for a fee in collaboration with the Japan Radioisotope Association<sup>2)</sup> (JRIA). The nuclides are  $^{65}\text{Zn}$  ( $T_{1/2} = 244$  days),  $^{109}\text{Cd}$  ( $T_{1/2} = 463$  days),  $^{88}\text{Y}$  ( $T_{1/2} = 107$  days), and  $^{85}\text{Sr}$  ( $T_{1/2} = 65$  days), produced by the Nuclear Chemistry Research Team (former RI Applications Team) at the AVF cyclotron. According to a material transfer agreement (MTA) drawn between JRIA and RIKEN, JRIA mediates the transaction of RIs and distributes them to users.  $^{65}\text{Zn}$  and  $^{109}\text{Cd}$  are delivered approximately two weeks after the acceptance of an order.  $^{85}\text{Sr}$  and  $^{88}\text{Y}$ , which have shorter half-lives, are not stocked like  $^{65}\text{Zn}$  and  $^{109}\text{Cd}$  but are produced in a scheduled beamtime after an order is accepted. Therefore, they are delivered two months or more after the order is placed. These details can be found on the online ordering system J-RAM<sup>3)</sup> of JRIA.

In 2018, we delivered three shipments of  $^{65}\text{Zn}$  with a total activity of 9.7 MBq, two shipments of  $^{88}\text{Y}$  with a total activity of 2 MBq, and no shipments of  $^{109}\text{Cd}$ . The final recipients of RIs were a university, a research institute, and a medical research center.

Figure 1 shows the yearly trends in the number of orders and the amount of distributed RIs. Compared with 2017, the amount of distributed  $^{65}\text{Zn}$  increased by a factor of 2.6 and that of  $^{88}\text{Y}$  remained the same.

We anticipate that the demand for short-lifetime RIs would increase in future and are considering to add

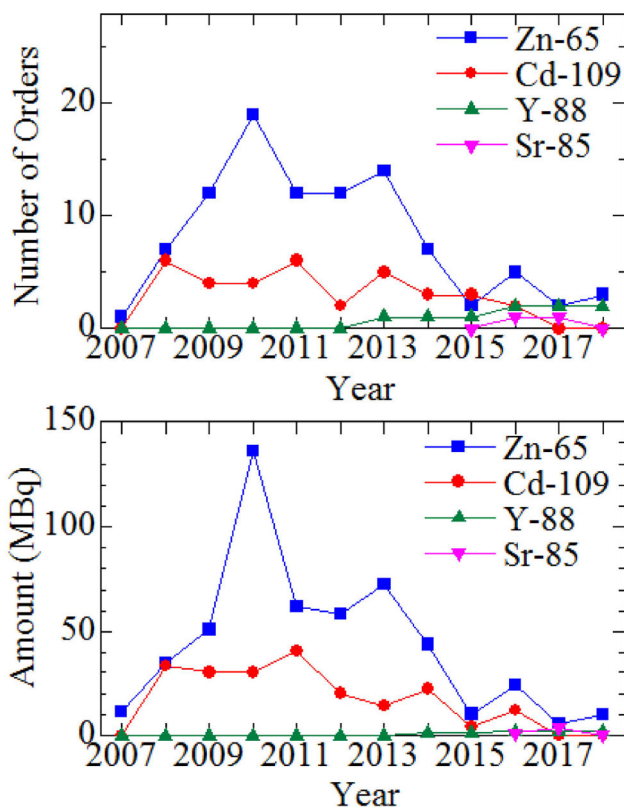


Fig. 1. Number of orders (upper) and amount (lower) of the RIs distributed yearly from 2007 to 2017. The distribution of  $^{88}\text{Y}$  started in 2010 and that of  $^{85}\text{Sr}$  in 2015.

such RIs to the fee-based distribution. As the first step, we announced the distribution of the new RI  $^{67}\text{Cu}$  ( $T_{1/2} = 61.8$  h) in August. It will be produced in a scheduled beamtime after an order is accepted.

### References

- 1) <http://ribf.riken.jp/sisetu-kyoyo/> (Japanese).
- 2) <http://www.jrias.or.jp/> (Japanese), <http://www.jrias.or.jp/e/> (English).
- 3) <https://www.j-ram.net/jram/DispatchTopPage.do> (Japanese).

<sup>\*1</sup> RIKEN Nishina Center

## **V. EVENTS**



## DIS2018 International Workshop

Y. Goto\*<sup>1</sup> for the DIS2018 Local Organizing Committee

DIS2018 International Workshop was held from April 16th to 20th at Port Island, Kobe. It was the 26th in an annual series of International Workshops on Deep Inelastic Scattering (DIS) and Related Subjects covering an eclectic mixture of material related to quantum chromodynamics (QCD) and DIS as well as a general survey of the hottest current topics in high energy physics. The majority of the program was devoted to the most recent results from experiments at BNL, CERN, Fermilab, Jefferson Lab, and KEK. Relevant theoretical advances were also covered in detail.

On the first day, topics of this year were overviewed both theoretically and experimentally through plenary talks. This year, experimental reviews were presented for each topics of physics instead of each facility owing to the expansion of the community, which was dominated by LHC. The Electron Ion Collider (EIC) became more realistic and the nuclear physics community showed more interest in this future facility. First, the nucleon structure with unpolarized, polarized, and neutrino scatterings in various energies were reviewed. Next, hadron final states, hadron scatterings with perturbative QCD and jet, precision measurements, and the search of physics beyond the standard model (BSM) were reviewed and theoretical ideas were presented. In the last session, soft scatterings, fragmentation and exotic hadrons, three-dimensional (3D) hadron structure, and hadron structure with lattice QCD were discussed as non-perturbative QCD physics with emphasis on Japanese activities.

From the second to the fourth day, parallel sessions were held for the following working groups (WGs):

- WG1: structure functions and parton densities
- WG2: low  $x$  and diffractive physics
- WG3: Higgs and BSM physics in hadron collisions
- WG4: hadronic and electroweak observables
- WG5: physics with heavy flavors
- WG6: spin and 3D structure
- WG7: future of DIS

A special topic for this year's workshop was the discussion of the future projects of DIS regarding the submission of a document to the European Strategy Update for Particle Physics (ESUPP) led by the International Advisory Committee of the workshop. A special joint session for all working groups was held after the regular parallel sessions in the second day. Panelists from EIC, LHeC ( $e+p$  collider at LHC), VHEp ( $e+p$  collider with a plasma accelerator), and  $e+p$  option of FCC (Future Circular Collider) presented their new accelerator facilities, theorists reviewed QCD and heavy-



Fig. 1. Group photo of the DIS2018 workshop.

ion theories motivating these projects with broad perspective, and participants discussed the involvement of these projects in the document.

On the last day (fifth day), summaries from each WG were given by the conveners of the WG in the morning session. Two future projects, EIC and LHeC, and related physics topics were reviewed to discuss important points from their point of view in the afternoon.

The workshop was organized by the Graduate School of Science, Kobe University, RIKEN Nishina Center, and KEK with support from Grant-in-Aid Scientific Research on Innovative Areas, MEXT, Japan: “New expansion of particle physics of post-Higgs era by LHC: revealing the vacuum and space-time structure,” and sponsored by DESY, CERN, Kobe Tourism Bureau & Kobe Convention Bureau, and Tsutomu Nakauchi Foundation for Promoting Conventions.

The workshop was held in two meeting locations: the Convention Hall of Kobe University for the plenary sessions and the Kobe International Convention Centre for the parallel sessions. A total of 254 participants demonstrated 256 presentations. A group photo is shown in Fig. 1. Slides shown in the workshop are available at <https://indico.cern.ch/event/656250/> and the proceedings of the workshop are published online at <https://pos.sissa.it/316>.

\*<sup>1</sup> RIKEN Nishina Center

# RIKEN Open Day 2018

K. Yoshida,\*<sup>1</sup> and T. Uesaka\*<sup>1</sup>

RIKEN Open Day, where several laboratories showcased their experimental devices and research activity to the public in RIKEN Wako campus, was held on April 21, 2018. In the Nishina Center, 17 research groups, comprising 276 researchers participated in the event, as listed in Table 1. The leaflet that introduced the exhibition content in the Nishina Center is shown in Fig. 1. It was handed out to the visitors at RIBF. The radiation controlled area in the RIBF building was opened for visitors to display the superconducting cyclotron SRC and other experimental devices along with the exhibition of laboratories. Dr. Wakasugi, the group director of the Instrumentation Development Group, gave a scientific lecture titled “What we can see and do with the Storage Ring” at the Ohkochi Memorial Hall.

A total of 2533 and 7935 visitors came to RIBF and RIKEN, respectively.



Fig. 1. Leaflet for RIKEN Open Day provided by Nishina Center.

Table 1. List of exhibitions.

Laboratory/Group/Team	Exhibition theme	Participants
Accelerator Group	The World's Strongest Superconducting Ring Cyclotron	41
SLOWRI Team	Ion Trap and Ultra-Slow RI Production	6
BigRIPS Team	Superconducting RI Beam Separator BigRIPS	10
Rare RI-Ring Team	Precision Measurement of Nuclear Mass	10
Spin Isospin Laboratory.	Microscopes for Unstable Nuclei	22
SAMURAI Team	SAMURAI Magnetic Spectrometer	7
Nuclear Spectroscopy Laboratory	Tiny Magnets in Materials	12
Nishina Center	Nuclear Chart with LEGO Block	4
Nuclear Chemistry Research Team	Environmental Radiation and Useful Radiation	9
Ion Beam Breeding Team	Creating Amazing Plants	13
Superheavy Element Research Group	The Discovery of Nihonium	9
SCRIT Team	Handmade Spectrometer	9
Radioactive Isotope Physics Laboratory	Daruma Dolls Challenge	16
	See Radiation with Diffusion Cloud Chamber	
Radiation Laboratory	Enjoy Spinning a Variety of Tops	13
	Research Activities in the Experimental Hadron Physics	
High-energy Astrophysics Laboratory.	Dawn of Gravitational Wave Astronomy	37
Meson Science Laboratory	Introductory Meson Science	22
	Particle Physics Experience	
Quantum Hadron Physics Laboratory	Elementary Particles, Nuclei and the Universe	9
	Operation and Management	27

\*<sup>1</sup> RIKEN Nishina Center

## Workshop on “The r-process and unstable nuclei in multi-messenger astronomy”

N. Nishimura,<sup>\*1,\*8</sup> T. Abe,<sup>\*2,\*3,\*8</sup> K. Nakazato,<sup>\*4,\*8</sup> H. Sakurai,<sup>\*2,\*5</sup> Y. Sekiguchi,<sup>\*6,\*1</sup> H. Ueno,<sup>\*5</sup> T. Uesaka,<sup>\*5</sup> and K. Yoshida<sup>\*7,\*8</sup>

The workshop on “The r-process and unstable nuclei in multi-messenger astronomy” (研究会「重力波観測時代の r プロセスと不安定核」) was held on 20–22 June 2018 at the RIKEN Nishina center. This workshop was sponsored by the RIKEN Nishina Center and “Priority Issue 9 to be Tackled by Using Post-K Computer” (JICFuS), and was supported by the members of RIBF Theory Forum.

The main scientific goal of the workshop was to summarize the recent progress on the study of the r-process, which is one of the most dominant nucleosynthesis processes for the cosmic origin of heavy elements beyond iron. The workshop was directly motivated by the recent (17 August 2017) successful observations of gravitational waves from a neutron-star merger event (GW170817) and the associated optical transient called *kilonova/macronova*, powered by r-process nucleosynthesis. We discussed several aspects of neutron-star mergers, focusing on nuclear physics, *e.g.*, experiments/theory of unstable nuclei, gravitational wave astronomy, optical observation, and the theoretical models of neutron-star mergers using supercomputers such as the K Computer.

The scientific program consisted of 8 sessions, *i.e.*, “multi-messenger astronomy of neutron-star-mergers,” “high-energy astronomy,” “the cosmic origin and evolution of r-process,” “the nuclear equation of state (EoS),” “nuclear masses,” “ $\beta$ -decay,” “nuclear fission,” and “the studies of unstable-nuclei in large facilities in Japan.” They covered a wide range of research fields in both nuclear-physics and astrophysics, thus reflecting the multi-disciplinary culture of nucleosynthesis studies. More than hundred participants gathered in the RIBF lecture Hall (Fig. 1) to provide recent progress of their studies and to discuss the application to r-process studies. This included 18 invited talks, 17 oral contributions, 7 poster presentations.

The workshop started with a session for reporting the “multi-messenger” observation of GW170817 including the kilonova, which opened a new era of astronomy triggered by gravitational wave detection and a theoretical understanding of the neutron-star merger as the astrophysical site of the r-process. The re-



Fig. 1. Many interesting presentations were given at RIBF Conference Hall in the 3-day workshop.

maining problems relevant to the nuclear-physics properties and aimed toward the complete understanding of kilonovae (and thus GW events) were highlighted. Following the talks on astronomy, the results of unstable-nuclei, *e.g.*, the measurements of  $\beta$ -decay half-lives at RIBF and the plan of experiments targeting the nuclear masses and neutron-capture in RIBF were reported. Although there are still several gaps, it appears that the r-process can connect (terrestrial) nuclear-physics experiments with the transients in the sky.

GW170817 also imposes strict restrictions on the EoS of neutron stars obtained from the GW signals as well as traditional astronomical observation. Several talks focused on the physics of neutron stars and related astronomical phenomena with an emphasis on the GW observation. The future experimental plans regarding the EoS were given as well as the theoretical progress of the EoS were presented.

The presentation files are available on the workshop website.<sup>1)</sup> The next iteration of this workshop<sup>2)</sup> is planned to be held at Yukawa Institute for Theoretical Physics in Kyoto University in May 2019. We will mostly focus on various topics in theoretical nuclear physics on such as the problems in r-process nucleosynthesis and (future) experiments of neutron-rich nuclei far from stability.

### References

- 1) URL: <https://sites.google.com/view/rp2018/>
- 2) URL: <https://www2.yukawa.kyoto-u.ac.jp/~rp2019/>

<sup>\*1</sup> Center for Gravitational Physics, YITP, Kyoto University

<sup>\*2</sup> Department of Physics, The University of Tokyo

<sup>\*3</sup> Center for Nuclear Study, The University of Tokyo

<sup>\*4</sup> Faculty of Arts and Science, Kyushu University

<sup>\*5</sup> RIKEN Nishina Center

<sup>\*6</sup> Department of Physics, Toho University

<sup>\*7</sup> Department of Physics, Kyoto University

<sup>\*8</sup> RIBF Theory Forum

# TESLA Technology Collaboration Meeting 2019 at RIKEN Nishina Center

N. Sakamoto \*<sup>1</sup>

The mission of the TESLA Technology Collaboration<sup>1)</sup> (TTC) is to advance R&D on the SRF technology and related accelerator studies across diverse scientific applications, and to provide a bridge for the communication and sharing of ideas, developments, and testing across associated projects. The TTC meeting is held once/twice a year changing locations in Europe, Asia, and North America. This time, the TTC meeting (Fig. 1) was held from 26 June to 29 June, 2018 at RIKEN Nishina Center (RNC).<sup>2)</sup>

The TTC meeting covers subjects related to superconducting RF technology extensively. The timetable of this meeting is shown in Fig. 2. In each session, a specific subject chosen by the technical board members was discussed intensively, and the information obtained from experimental and theoretical studies at various laboratories and companies was exchanged (see Table 1). In this meeting, there were four working group sessions and one hot topic session as follows:

- WG1: What are the performance limits for low-beta resonators?
- WG2: How to improve the present specification for bulk Niobium?
- WG3: High Q and high gradient performance.
- WG4: Special applications of SRF cavities.
- Hot Topic: Warm vacuum sections between low beta cryomodules.

Note that since the meeting was hosted by RNC, subjects related to the low-beta ion accelerator were chosen for the WG1 and Hot Topic sessions. Eight plenary talks were conducted on these subjects: Overview on fabrication and treatment problems with Quarter- and Half-Wave Resonator (QWR, HWR), Spoke (Z. Conway, ANL), Overview talks for niobium material and specification (A. Palczewski, JLab), RIKEN overview and SRF activities (O. Kamigaito, RNC), Lessons learned



Fig. 1. Group photo taken during the meeting.

Time	Date	June, 26 (Tue)	June, 27 (Wed)	June, 28 (Thu)	June, 29 (Fri)
8:30 - 9:00		Registration			
9:00 - 9:30		Welcome/Introduction	Plenary talk 3	WG3 / WG4	Summary WG1/WG2
9:30 - 10:00		Plenary talk 1	Plenary talk 4	(parallel)	Summary WG3/WG4
10:00 - 10:30		Plenary talk 2	Plenary talk 5		TB/CB report
10:30 - 11:00		Coffee Break			
11:00 - 11:30		WG1 / WG2	WG1 / WG2	WG3 / WG4	Special Seminar 1
11:30 - 12:00		(parallel)	(parallel)	(parallel)	Special Seminar 2
12:00 - 12:30					Closing
12:30 - 14:00	Lunch				
14:00 - 14:30		WG1 / WG2	WG3 / WG4	Plenary talk 6	
14:30 - 15:00		(parallel)	(parallel)	Plenary talk 7	
15:00 - 15:30				Plenary talk 8	
15:30 - 16:00		Coffee Break			Lab. Tour
16:00 - 16:30		WG1 / WG2	WG3 / WG4	Hot Topics	
16:30 - 17:00		(parallel)	(parallel)		
17:00 - 17:30					
17:30 - 18:00					
18:00 - 18:30		CB meeting	TB meeting	Dinner	
18:30 - 19:00				at RIKEN-Cafeteria	
19:00 - 19:30					
19:30 - 20:00					

Fig. 2. Timetable of the sessions for the TTC meeting at RNC.

Table 1. Statistics of registrants of TTC2018 at RNC.

Country	#	Labs and Companies
Brazil	1	CBMM
Canada	2	TRIUMF
China	19	IHEP, Peking U., IMP, NINGXIA
France	2	CEA-Saclay, CEA-Gif-sur-Yvette
Germany	14	DESY, HIM, HZB
Italy	3	INFN-LNL, SAES
Japan	55	KEK, RNC, JAEA, QST, MHI-MS, Tokyo Denka, SAES, TOSHIBA, ULVAC Miyoshi-Gokin, NEURON Japan, R-DEC, ScandiNova, Sojitz
Korea	4	Korea U., IBS
Sweden	4	ESS-ERIC, Uppsala U.
Switzerland	4	CERN
UK	1	STFC Daresbury
USA	34	Fermilab, JLab, SLAC, FRIB/MSU, BNL, ANL, NW U. Cornell U., OD U., Stony Brook U., ATI, II-VI, ISOHIM

during module assembly and first cool-down test in FRIB (T. Xu, MSU), Recent theoretical and experimental progress in N<sub>2</sub> doping and infusion (M. Checchin, Fermilab), Overview talks for Nb<sub>3</sub>Sn and other thin film technology (G. Ereemeev, JLab), SC CH structure in Mainz/Frankfurt/Darmstadt (F. Dziuba, GSI), and Technical progress of crab cavity in fabrication and tests at CERN (M. Garlasche, CERN). Two special seminars were presented by H. Kawata from KEK and K. Sakamoto from QST, introducing the industrial applications in compact-ERL at KEK and the high intensity neutron source project at QST-Rokkasho.

The meeting was conducted successfully, and it had more than 120 participants. The next meeting will be held at TRIUMF (Vancouver, Canada) in February 2019.

## References

- 1) <https://tesla-new.desy.de>.
- 2) <https://indico.desy.de/indico/event/20010/program>.

\*<sup>1</sup> RIKEN Nishina Center

## Participation in Hokkaido Science Festival

N. Miyauchi\*<sup>1</sup>

The year 2018 marked the 150th anniversary of the naming of “Hokkaido.” As part of a series of events commemorating the 150th anniversary, an event called “Hokkaido Science Festival” was hosted by the Hokkaido government.<sup>1)</sup> The purpose of the event was to evoke the challenging spirit of, in particular, young people in Hokkaido and to foster the youth into becoming globally competitive human resources. The event was held at the Hokkaido Prefectural Sports Center (also called “Hokkai Kitayell”) on August 6–7, 2018 in Sapporo, and persons of considerable prominence attended lectures that encouraged audience participation. Also, companies, universities, and research institutes participated and conducted various explanation exhibitions and experience-based programs. Figure 1 shows a venue in the Hokkaido Prefectural Sports Center.

The Nishina Center (more precisely, User Liaison Group) participated in the event, together with the Public Relations Office, and conducted a workshop for children and an exhibition. The Public Relations Office conducted an exhibition on “Kagakudo 100 books.<sup>2)</sup>”

We introduced the RIBF facility through the following three exhibitions. The first one was a participatory exhibition (i.e., workshop) entitled “Let’s make a nihonium nucleus with ironing beads.” In this workshop, using ironing beads, which are children’s toys, the participants constructed a three-dimensional nihonium pixel craft, after being explained about nuclear structures and how nihonium was discovered at the Nishina Center. The scene of the workshop is shown in Fig. 2.

The second one was a panel exhibition. Here, in addition to panels on the research at the RIBF facility, an oversized panel on SRC was also displayed. This extra-large SRC panel was aimed at getting the people to realize its scale while staying in Sapporo. Thus, by taking pictures in front of it, the visitors were able to



Fig. 1. A photograph taken at an exhibition hall in the Hokkaido Prefectural Sports Center

take pictures as if they had actually come to the RIBF facility. This panel was particularly well-received by children and their parents.

The third one is the 3D nuclear chart made of Lego Blocks (Fig. 3). This 3D nuclear chart drew considerable attention, probably due to the familiarity of Lego Blocks and the rarity of the nuclear chart created with it. The 3D nuclear chart was a good exhibit, because it could generate interest owing to its interesting structure, and also because it allows researchers to make intuitive explanations using the actual nuclear chart. This display was also well received by the visitors.

Unfortunately, the location of our exhibition inside the venue was not good, and hence the exhibit that attracted the most participants was not ours. However, the visitors were able to thoroughly discuss the contents of the exhibition and enjoyed the display.



Fig. 2. A photograph taken at the workshop for making a nihonium nucleus with ironing beads.



Fig. 3. A photograph taken at the exhibition of a 3D nuclear chart made of Lego Blocks.

### References

- 1) <http://www.pref.hokkaido.lg.jp/ss/tsk/hokkaido-sciencefestival.htm> .
- 2) <https://kagakudo100.jp/> .

\*<sup>1</sup> RIKEN Nishina Center

## QNP2018 International Conference

Y. Goto<sup>\*1</sup> for the QNP2018 Local Organizing Committee

QNP2018 International Conference was held from November 13th to 17th in Tsukuba. It was the 8th one in a series of International Conference on Quarks and Nuclear Physics. The conference was held at the Tsukuba International Congress Center (EPOCHAL TSUKUBA). Experimentalists and theorists discussed recent developments in the field of hadron and nuclear physics.

The conference began with plenary talks on neutron stars and hadron physics. Recent progress in gravitational waves and dense baryonic matter, and the strangeness in neutron stars were discussed. In the plenary sessions, experimental reviews on quark and gluon structure of hadrons, hadron spectroscopy, hadron interactions and nuclear structure, and hot and dense matter were presented. Theoretical reviews were given for these subjects including reviews from lattice QCD. There were also plenary talks on experimental facilities, GSI-FAIR project, Jefferson Lab 12 GeV program, Belle-II project, J-PARC hadron project, and EIC project.

In four parallel sessions, following topics were covered:

Quark and gluon structure of hadrons  
parton distribution functions, generalized parton distributions, transverse momentum distributions, and high-energy hadron reactions, among others.

Hadron spectroscopy  
heavy quark physics, exotics, and  $N^*$ , among others.

Hadron interactions and nuclear structure  
hypernuclear physics, kaonic nuclei, and baryon interactions, among others.

Hot and cold dense matter  
quark-gluon plasma, color glass condensate, dense stars, strong magnetic field, mesons in nuclear medium, and hadronization, among others.

One of the highlights of the conference was the results from J-PARC on their first major project on strange nuclear physics. They obtained a large charge symmetry breaking effect in the hypernuclei, the first clear  $\Xi$  hypernucleus, and Kaonic nucleus. J-PARC physics covers wide areas of hadron physics, strangeness nuclear physics, exotic hadrons, hadrons in nuclear medium, nucleon structure functions, and quark-hadron matter.

Social events such as excursions to Tsukuba space



Fig. 1. Group photo of the QNP2018 conference.

center of JAXA and Belle-II of KEK, local sake brewery and Mt. Tsukuba, soba noodle cooking, and Kashima-Jingu shrine and historical Edo-taste downtown of Sawara were conducted, which were interactive. Participants also enjoyed good reception at the congress center and conference dinner at the hotel Grand Shinonome.

This conference was held with financial supports by KEK/J-PARC, RCNP, APCTP, JSPS Grant on Innovative Area: “Clustering as a window on the hierarchical structure of quantum systems,” Tsukuba Tourism and Convention Association, and Tsukuba City. We also received support from JAEA, RIKEN, and SOKENDAI.

A total of 216 participants from 25 countries attended the conference. There were 23 plenary talks and 128 parallel talks (including 15 invited keynote talks) in four parallel sessions. A group photo is shown in Fig. 1.

The full program and presentation files are available online at the conference website: <https://conference-indico.kek.jp/indico/event/33/> and the proceedings of the conference will be published online in JPS Conference Proceedings.

A satellite workshop on “hadron structure and interaction in finite density matter” was held from November 11th to 12th at KEK Tokai Campus hosted by KEK and JAEA (<http://j-parc-th.kek.jp/workshops/2018/11-11/>). Another workshop on the “progress on hadron structure functions in 2018” was held from November 18 to 19 at KEK Tsukuba Campus (<http://j-parc-th.kek.jp/workshops/2018/11-18/>).

<sup>\*1</sup> RIKEN Nishina Center

## RIBF “Hodan-kai” meeting on the future of exotic nuclear physics

T. Matsumoto<sup>\*1,\*2</sup> on behalf of the RIBF “Hodan-kai” meeting organizers

The second in the series of the RIBF “Hodan-kai” meeting by young researchers was held at Kobe campus of RIKEN, Integrated Innovation Building, from Feb. 18 to 20, 2019. The venue was in a relatively isolated place, and actually this was one of the key factors for the success of the meeting; the participants were forced to be in the meeting room and concentrate on physics. The RIBF “Hodan-Kai” meeting is organized by members of RIBF Theory Forum and supported by RIKEN Nishina Center, RIKEN iTHEMS, and JIC-FuS. This meeting is aimed at an intensive discussion based purely on curiosity, such as what is interesting and what we want to do in the future in a frank and low-pressure atmosphere. The style of “Hodan-kai” is thus different from a usual workshop.

The first “Hodan-kai” meeting was held at the same place from Jul. 21 to Aug. 2, 2017. In the first meeting, we focused on the latest theoretical research of nuclear physics. The number of presentations was 23, and we engaged in a heated debate. Although we shared recognition for the progress in theoretical research, we wanted more discussions with experimentalists and researchers in various fields in order to definitize a new agenda for the future of nuclear physics. The program and summary of the first “Hodan-kai” meeting can be seen in the web site.<sup>1)</sup>

Based on the direction obtained at the first meeting, we arranged the second meeting as follows: 7 presentations on experimental research in nuclear physics, 6 presentations on theoretical research in nuclear



Fig. 2. Atmosphere of the banquet.

physics, and 12 presentations on some related fields, namely deep learning, quantum computing, computational physics, weak measurement, super-heavy elements, hadron physics, and laser physics. The number of presentations was 14 for invited and 11 for contributed. In the second meeting, there were 42 participants from various fields, and we had a heated discussion beyond the scheduled time. Thus, it was a very meaningful meeting. The program of the second “Hodan-kai” meeting can be seen in the web site.<sup>2)</sup> Following the success of this meeting, we are planning to hold the next meeting in February 2020, and welcome many young researchers to join.

### References

- 1) <https://indico2.riken.jp/event/2509/> .
- 2) <https://indico2.riken.jp/event/2864/> .



Fig. 1. Atmosphere of the 2nd “Hodan-kai” meeting.

<sup>\*1</sup> Department of Physics, Kyushu University

<sup>\*2</sup> RIBF Theory Forum

## Symposium on “Science and Technology Explored with Periodic Table” celebrating the “IYPT2019 in Japan”

H. Sakurai\*<sup>1</sup>

The year 2019 is the 150<sup>th</sup> anniversary of Dmitry Mendeleev’s discovery of the periodic system and has thus been proclaimed to be the “International Year of the Periodic Table of Chemical Elements” (IYPT2019) by the United Nations General Assembly and UNESCO<sup>1)</sup>. As the first official event at the IYPT2019 in Japan, a kick-off symposium titled “Science and Technology Explored with Periodic Table” was organized at the Science Council of Japan (SCJ), Tokyo, on February 23<sup>rd</sup>, 2019.<sup>2)</sup>

The symposium was coupled with an opening ceremony to celebrate the IYPT2019. Prof. Ken Sakai, chairman of the SCJ committees of the IYPT2019 and IUPAC, gave an opening introduction of the event. Celebration addresses were made by representatives of hosting and supporting organizations of the symposium, including SCJ, The Chemical Society of Japan, The Physical Society of Japan, and RIKEN. On behalf of RIKEN, Prof. Shigeo Koyasu, one of the executives, spoke about the history of RIKEN over a 100 years and highlighted the contributions made by RIKEN to the development of the periodic table.

Invited talks related to elements and the periodic table were given by distinguished chemists and physicists: Profs. Kouhei Tamao, Hideo Hosono, Susumu Kitagawa, Yoshiteru Maeno, Hiroko Tokoro, Kousuke Morita, and Kazuyuki Tatsumi. Prof. Morita presented a history of element finding and production and emphasized the role of RIKEN in the production of Element 113, “Nihonium.”



Fig. 1. Photo of the IYPT2019 symposium held at the hall of Science Council of Japan on February 23<sup>rd</sup>, 2019.



Fig. 2. Group photo of representatives of hosting organization with the speakers and organizers of the opening ceremony and symposium.

A discussion session was chaired by Prof. Hiroyoshi Sakurai. Questions about elements were raised by the audience, and answers were provided by speakers and organizers to help the general public understand elements better.

The closing remark was made by Prof. Mihoko Nojiri, vice chairman of the SCJ IYPT2019 committee and chairman of the SCJ IUPAC committee.

The symposium was open for public and the number of total participants was about 200, including media reporters.

The SCJ IYPT2019 committee acknowledges the many people, who supported the organization of the ceremony and symposium, as well as the administration and staff members at RIKEN Nishina Center for their support: Asako Takahashi, Yunike Shimizu, Kazushige Fukushima, Tetsuo Nayuki, Keiko Iwano, Kumiko Sugita, Midori Shishido, Tomomi Okayasu, Midori Yamamoto, and Mitsue Yamamoto. The symposium poster was designed by Narumasa Miyachi. Dr. Ryo Taniuchi was in charge of photography.

### References

- 1) <https://www.iypt2019.org>.
- 2) <https://www.iypt2019.jp>.

\*<sup>1</sup> RIKEN Nishina Center

# **VI. ORGANIZATION AND ACTIVITIES OF RIKEN NISHINA CENTER**

**(Activities, Members, Publications & Presentations)**



# 1. Organization

## 1.1 Organization Chart as of March 31, 2019 (End of FY2018)



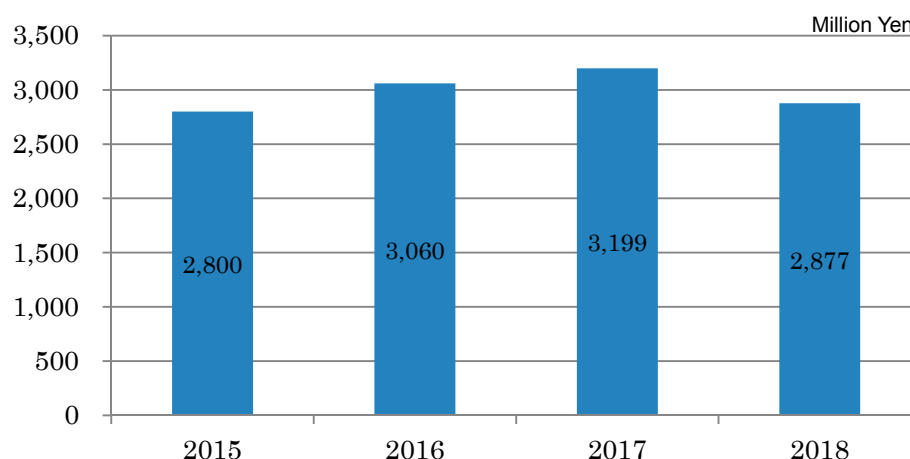
### 1.2 Topics in FY2018

In FY2018, the RNC reorganized the former three division system consisting of the Theory Research Division, the Subnuclear System Research Division and the RIBF Research Division into a four division system.

Year	Date	Topics in Management
2018	Apr. 1	Newly appointed: Team Leader of the SLOWRI Team: Hironobu ISHIYAMA
2018	Apr. 1	Newly appointed: Team Leader of the Computing and Network Team: Hidetada BABA
2018	May. 1	Newly appointed: Team Leader of the Plant Genome Evolution Research Team: Yusuke KAZAMA
2019	Jan. 11	Interim Review of the Chief Scientist, Tomohiro UESAKA

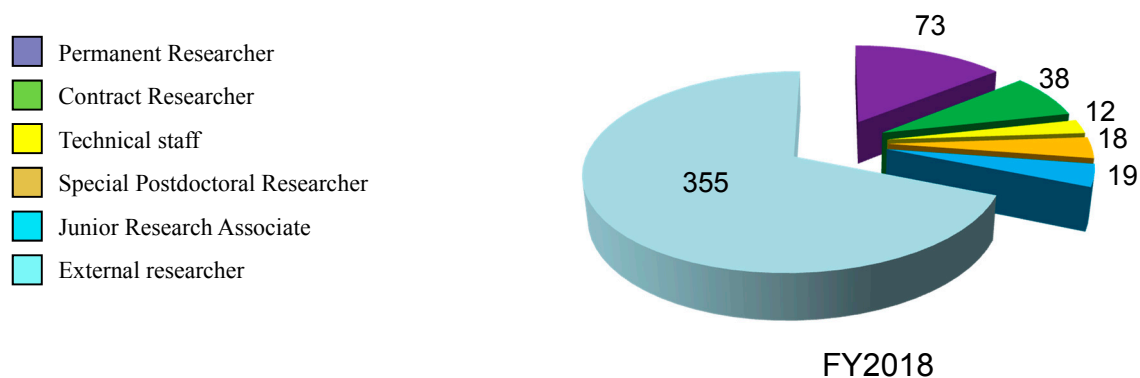
### 2. Finances

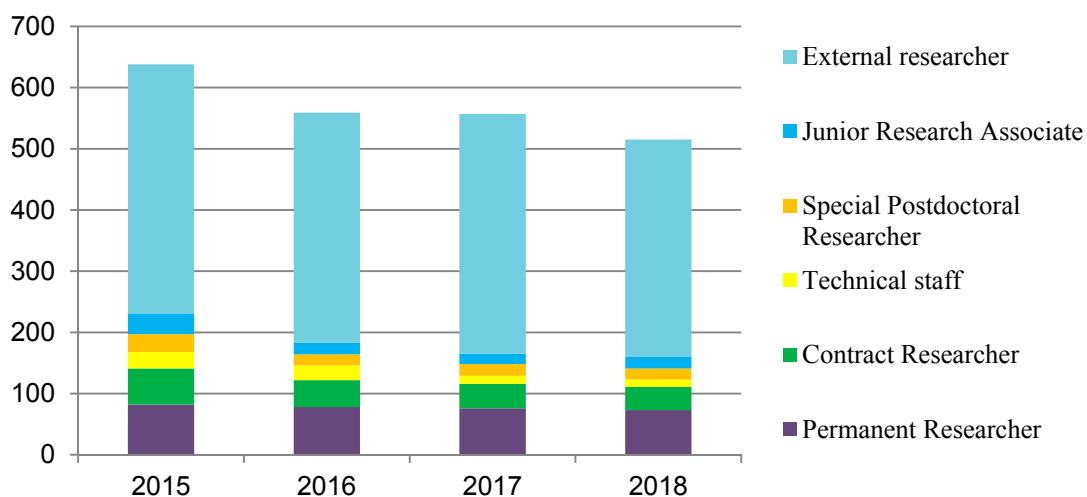
A transition of the RNC budget for the past five years is shown in following graph.



### 3. Staffing

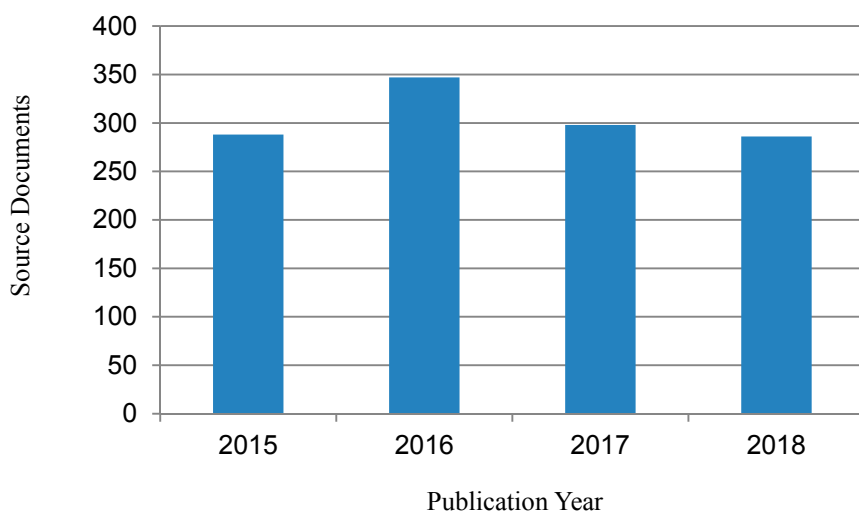
At the start of FY 2018, there were 160 personnel affiliated with RNC and 355 researchers visiting RNC for research purpose. The following graphs show a breakdown of personnel into six categories as of April 1, 2018, and a transition of the number of each category.





#### 4. Research publication

The number of papers published annually from RNC is shown graphically using the data obtained from Clarivate Analytics' Web of Science Documents.



Citation analysis for the past four years

As of March 2019

Indicators	Year			
	2015	2016	2017	2018
Total number of papers	288	347	298	286
Percentage of papers in top 10%	17.01	15.85	16.78	20.63
Percentage of papers in top 1%	1.39	1.44	2.68	4.20

## 5. Management

Headed by the RNC Director Hideto En'yo, the RIKEN Nishina Center for Accelerator-Based Science (RNC) consists of:

- 9 Laboratories
- 10 Groups with 27 Teams
- 2 overseas research centers with 3 Groups

as of the end of FY2018. There are also two 'Partner Institutes' which conduct research in the laboratories set up in RNC. RNC is managed by its Director who takes into consideration the majority decision of the RNC Coordination Committee. The management of RNC is supported by the following committees:

- Program Advisory Committee
- Safety Review Committee
- RIBF Machine Time Committee
- Public Relations Committee

There are also committees to support the President of RIKEN and/or the Director of RNC such as:

- Nishina Center Advisory Council with three subcommittees:
  - RBRC Scientific Review Committee (SRC)
  - International Advisory Committee for the RIKEN-RAL Muon Facility
  - RBRC Management Steering Committee (MSC)

---

### Nishina Center for Accelerator-based Science

---

#### Executive Members (as of March 31, 2019)

Hideto EN'YO	Director RNC, Chief Scientist, Director of Radiation Laboratory
Hiroyoshi SAKURAI	Deputy Director (Nuclear Science and Transmutation Research Division)
Osamu KAMIGAITO	Deputy Director (Research Facility Development Division)
Tomoko ABE	Deputy Director (Accelerator Application Division)
Yasushige YANO	Senior Advisor
Tohru MOTOBAYASHI	Senior Advisor
Hideyuki SAKAI	Senior Advisor

---

### RNC Coordination Committee

---

The following subjects relevant to the RNC management are deliberated under the chairmanship of the RNC Director:

- Establishment of the new organization or reorganization in RNC
- Personnel management of RNC researchers
- Research themes and research budget
- Approval of the Partner Institutes
- Evaluation of the management of RNC and the response to the recommendations by external evaluation

The RNC Coordination Committee is held monthly.

#### Members (as of March 31, 2019)

Hideto EN'YO	Director, RNC, Director, Radiation Laboratory
Hiroyoshi SAKURAI	Deputy Director, RNC; Group Director, Radioactive Isotope Physics Laboratory and Nuclear Transmutation Data Research Group; Team Leader, Muon Date Team
Osamu KAMIGAITO	Deputy Director, RNC; Group Director, Accelerator Group and High-Intensity Accelerator R&D Group; Team Leader, Infrastructure Management Team
Tomoko ABE	Deputy Director, RNC; Group Director, Beam Mutagenesis Group; Team Leader, Ion Beam Breeding Team
Yasushige YANO	Senior Advisor, RNC
Tohru MOTOBAYASHI	Senior Advisor, RNC
Hideyuki SAKAI	Senior Advisor, RNC
Tomohiro UESAKA	Group Director, Spin Isospin Laboratory and Research Instruments Group
Hideki UENO	Group Director, Nuclear Spectroscopy Laboratory and User Liaison Group; Team Leader, Outreach Team
Toru TAMAGAWA	Group Director, High Energy Astrophysics Laboratory
Kosuke MORITA	Group Director, Superheavy Element Research Group
Yuko MOTIZUKI	Group Director, Astro-Glaciology Research Group
Hiroki OKUNO	Deputy Group Director, Accelerator Group; Team Leader, Accelerator R&D Team, Cryogenic Technology Team, and High-Power Target R&D Team
Nobuhisa FUKUNISHI	Deputy Group Director, Accelerator Group; Team Leader, Beam Dynamics & Diagnostics Team
Masanori WAKASUGI	Group Director, Instrumentation Development Group; Team Leader, Rare RI-Ring Team and SCRIT Team
Hiromitsu HABA	Group Director, RI Application Research Group; Team Leader, RI Application Team and Superheavy Element

	Production Team
Tetsuo HATSUDA	Group Director, Quantum Hadron Physics Laboratory
Emiko HIYAMA	Group Director, Strangeness Nuclear Physics Laboratory
Masahiko IWASAKI	Group Director, Meson Science Laboratory
Kanenuobu TANAKA	Group Director, Safety Management Group
Koji MORIMOTO	Team Leader, Superheavy Element Device Development Team
Hideaki OTSU	Team Leader, SAMURAI Team and Fast RI Data Team
Toshiyuki SUMIKAMA	Team Leader, Slow RI Data Team
Naruhiko SAKAMOTO	Team Leader, Cyclotron Team and High-Gradient Cavity R&D Team
Takahide NAKAGAWA	Team Leader, Ion Source Team
Eiji IKEZAWA	Team Leader, RILAC Team
Hironobu ISHIYAMA	Team Leader, SLOWRI Team
Koichi YOSHIDA	Team Leader, BigRIPS Team
Hidetada BABA	Team Leader, Computing and Network Team
Hiromi SATO	Team Leader, Detector Team
Yusuke KAZAMA	Team Leader, Plant Genome Evolution Research Team
Atsushi YOSHIDA	Team Leader, Industrial Application Research Team
Yasuyuki AKIBA	Group Leader, Experimental Group, RIKEN BNL Research Center
Taku IZUBUCHI	Group Leader, Computing Group, RIKEN BNL Research Center
Ken-ichiro YONEDA	Team Leader, RIBF User Liaison Team
Tsukasa TADA	Vice Chief Scientist, Quantum Hadron Physics Laboratory
Yutaka WATANABE	Deputy Team Leader, Infrastructure Management Team
Yasushi WATANABE	Deputy Team Leader, RIBF User Liaison Team
Teruo NAYUKI	Director, Nishina Center and iTHEMS Promotion Office

## Program Advisory Committee

The Program Advisory Committee reviews experimental proposals submitted by researchers and reports the approval/disapproval of the proposals to the RNC Director. The Committee also reports to the RNC Director the available days of operation at RIBF or the Muon Facility at RAL allocated to researchers. The Committee is divided into three categories according to the research field.

- Nuclear Physics Experiments at RIBF (NP-PAC): academic research in nuclear physics
- Materials and Life Science Researches at RNC (ML-PAC): academic research in materials science and life science
- Industrial Program Advisory Committee (In-PAC): non-academic research

### **Program Advisory Committee for Nuclear Physics Experiments at RI Beam Factory (NP-PAC)**

The 19<sup>th</sup> NP-PAC was held on November 29–December 1, 2018 at RIBF.

#### **Members (as of March 31, 2019)**

Angela BRACCO (Chair)	INFN
Dieter ACKERMANN	GANIL
Andrei ANDREYEV	University of York
Ikuko HAMAMOTO	Lund University
Robert V.F. JANSSENS	University of North Carolina at Chapel Hill
Augusto O. MACCHIAVELLI	Lawrence Berkeley National Laboratory
David J. MORRISSEY	Michigan State University
Tomofumi NAGAE	Kyoto University
Hitoshi NAKADA	Chiba University
Alexandre OBERTELLI	Technische Universität Darmstadt
Kazuyuki OGATA	RCNP, Osaka University
Tomas RAUSCHER	University of Basel
Kimiko SEKIGUCHI	Tohoku University
Haik SIMON	GSI
Piet VAN DUPPEN	K.U.Leuven
Yuhu ZHANG	Institute of Modern Physics, CAS

### **Program Advisory Committee for Materials and Life Science Researches at RIKEN Nishina Center (ML-PAC)**

The 16<sup>th</sup> and 17<sup>th</sup> ML-PAC was held on July 20, 2018 and January 2019 at RIBF, respectively.

#### **Members (as of March 31, 2019)**

Adrian HILLIER (Chair)	ISIS, RAL (UK)
Toshiyuki AZUMA	RIKEN Cluster for Pioneering Research
Ryosuke KADONO	Institute of Materials Structure Science (KEK)
Atsushi KAWAMOTO	Hokkaido University
Norimichi KOJIMA	Toyota RIKEN
Kenya KUBO	ICU
Philippe MENDELS	Universite Paris-SUD(France)

Atsushi SHINOHARA	Osaka University
Shukri SULAIMAN	Universiti Sains Malaysia (Malaysia)
Hiroiyuki YAMASE	NIMS
Shigeo YOSHIDA	Thera-Projects
Xu-Guang ZHENG	Saga University

### **Industrial Program Advisory Committee (In-PAC)**

The 8<sup>th</sup> In-PAC was held on June 29, 2018 at RNC.

## **Safety Review Committee**

---

The Safety Review Committee is composed of two sub committees, the Safety Review Committee for Accelerator Experiments and the Hot-Lab Safety Review Committee. These Committees review the safety regarding the usage of radiation generating equipment based on the proposal submitted to the RNC Director from the spokesperson of the approved experiment.

### **Safety Review Committee for Accelerator Experiments**

#### **Members (as of March 31, 2019)**

Hiromi SATO (Chair)	Team Leader, Detector Team
Kouji MORIMOTO	Team Leader, Superheavy Element Device Development Team
Eiji IKEZAWA	Team Leader, RILAC Team
Hiromitsu HABA	Team Leader, RI Application Team
Shinichiro MICHIMASA	Assistant Prof., Center for Nuclear Study, University of Tokyo
Hidetoshi YAMAGUCHI	Lecturer, Center for Nuclear Study, University of Tokyo
Yutaka WATANABE	Associate Professor, High Energy Accelerator Research Organization, KEK
Atsushi YOSHIDA	Team Leader, Industrial Cooperation Team
Koichi YOSHIDA	Team Leader, BigRIPS Team
Naoki FUKUDA	Nishina Center Research Scientist, BigRIPS Team
Naruhiko SAKAMOTO	Team Leader, Cyclotron Team
Daisuke SUZUKI	Research Scientist, Radioactive Isotope Physics Laboratory
Juzo ZENIHIRO	Research Scientist, Spin Isospin Laboratory
Yuichi ICHIKAWA	Research Scientist, Nuclear Spectroscopy Laboratory

#### **Ex officio members**

Kanenobu TANAKA	Group Director, Safety Management Group
Hisao SAKAMOTO	Technical Scientist, Safety Management Group

### **Hot-Lab Safety Review Committee**

#### **Members (as of March 31, 2019)**

Masako IZUMI (Chair)	Senior Research Scientist, Ion Beam Breeding Team
Kanenobu TANAKA	Group Director, Safety Management Group
Hisao SAKAMOTO	Safety Management Group
Hiroki MUKAI	Technical Staff I, Assigned Employee, Safety Management Group
Eriko HIGURASHI	Technical Scientist, Safety Management Group
Hiromitsu HABA	Team Leader, RI Application Team

## **RIBF Machine Time Committee**

---

Upon request of the RNC Director, the RIBF Machine Time Committee deliberates on the machine time schedule of RIBF and reports the results to the Director.

#### **Members (as of March 31, 2019)**

Hideki UENO (Chair)	Group Director, User Liaison and Industrial Cooperation Group and Nuclear Spectroscopy Laboratory
Osamu KAMIGAITO	Group Director, Accelerator Group
Masanori WAKASUGI	Group Director, Instrumentation Development Group
Tomohiro UESAKA	Group Director, Research Instruments Group and Spin Isospin Laboratory
Nobuhisa FUKUNISHI	Deputy Group Director, Accelerator Group
Hiroki OKUNO	Deputy Group Director, Accelerator Group
Hiroiyoshi SAKURAI	Group Director, Radioactive Isotope Physics Laboratory
Tomoko ABE	Group Director, Beam Mutagenesis Group
Hiromitsu HABA	Group Director, RI Application Research Group
Kanenobu TANAKA	Group Director, Safety Management Group
Ken-ichiro YONEDA	Team Leader, RIBF User Liaison Team

Kouji MORIMOTO Team Leader, Superheavy Element Research Device Development Team  
Koichi YOSHIDA Team Leader, BigRIPS Team

**External members**

Kentaro YAKO Associate Professor, Center for Nuclear Study, University of Tokyo  
Hidetoshi YAMAGUCHI Lecturer, Center for Nuclear Study, University of Tokyo  
Michiharu WADA Professor, High Energy Accelerator Research Organization, KEK

**Observers**

Hideto EN'YO Director, RNC  
Susumu SHIMOURA Director, Center for Nuclear Study, University of Tokyo  
Hiroari MIYATAKE Director, KEK Wako Nuclear Science Center

Kosuke MORITA Group Director, Superheavy Element Research Group  
Hideaki OTSU Team Leader, SAMURAI Team  
Atsushi YOSHIDA Team Leader, Industrial Cooperation Team  
Tohru MOTOBAYASHI Senior Advisor, RNC  
Kazushige FUKUSHIMA Manager, Nishina Center and iTHEMS Promotion Office

**Public Relations Committee**

Upon request of the RNC Director, the Public Relations Committee deliberates and coordinates the following matters:

- Creating public relations system for RNC
- Prioritization of the public relations activities for RNC
- Other general and important matters concerning the public relations of RNC

**Members (as of March 31, 2019)**

Teruo NAYUKI Director, Nishina Center and iTHEMS Promotion Office  
Hiroyoshi SAKURAI Deputy Director, RNC; Group Director, Radioactive Isotope Physics Laboratory  
Osamu KAMIGAITO Deputy Director, RNC; Group Director, Accelerator Group  
Tomoko ABE Deputy Director, RNC; Group Director, Beam Mutagenesis Group  
Tetsuo HATSUDA Group Director, Quantum Hadron Physics Laboratory  
Masahiko IWASAKI Group Director, Meson Science Laboratory  
Tomohiro UESAKA Group Director, Spin Isospin Laboratory and Research Instruments Group  
Hideki UENO Group Director, Nuclear Spectroscopy Laboratory and User Liaison Group  
Toru TAMAGAWA Group Director, High Energy Astrophysics Laboratory  
Emiko HIYAMA Group Director, Strangeness Nuclear Physics Laboratory  
Kosuke MORITA Group Director, Superheavy Element Research Group

**RBRC Management Steering Committee (MSC)**

RBRC MSC is set up according to the Memorandum of Understanding between RIKEN and BNL concerning the collaboration on the Spin Physics Program at the Relativistic Heavy Ion Collider (RHIC). The 24<sup>th</sup> MSC was held on June 12, 2018.

**Members (as of June 12, 2018)**

Motoko KOTANI Executive Director, RIKEN  
Shoji NAGAMIYA Senior Visiting Scientist, RNC  
Tetsuo HATSUDA Program Director, RIKEN Interdisciplinary Theoretical and Mathematical Sciences Program  
Robert TRIBBLE Deputy Director for Science and Technology, BNL  
David LISSAUER Deputy Chair, Physics Department, BNL  
Berndt MUELLER Associate Laboratory Director for Nuclear and Particle Physics, BNL

**6. International Collaboration**

Country	Partner Institute	Objects	RNC contact person
China	China Nuclear Physics Society	Creation of the council for China -Japan research collaboration on nuclear physics	Hiroyoshi SAKURAI, Director, Radioactive Isotope Physics Laboratory
	Peking University	Nuclear Science	Hiroyoshi SAKURAI, Director, Radioactive Isotope Physics Laboratory

	Institute of Modern Physics, Chinese Academy of Science	Physics of heavy ions	Hiroyoshi SAKURAI, Director, Radioactive Isotope Physics Laboratory
	School of Nuclear Science and Technology, Lanzhou University	Framework	Masahiko IWASAKI, Director, Meson Science Laboratory
	School of Physics, Nanjing University	Framework	Emiko HIYAMA, Director, Strangeness Nuclear Physics Laboratory
	Department of Physics, Faculty of Science, The University of Hong Kong	Experimental and educational research collaboration in experimental nuclear physics	Hiroyoshi SAKURAI, Director, Radioactive Isotope Physics Laboratory
	School of physics, Nankai University	Framework	Emiko HIYAMA, Director, Strangeness Nuclear Physics Laboratory
Finland	University of Jyväskylä	Basic nuclear physics and related instrumentation	Hironobu ISHIYAMA, Team Leader, SLOWRI Team
France	National Institute of Nuclear Physics and Particle Physics (IN2P3)	Physics of heavy ions	Tohru MOTOBAYASHI, Senior Advisor, RNC
Germany	Technische Universität München	Nuclear physics, hadron physics, nuclear astrophysics	Emiko HIYAMA, Director, Strangeness Nuclear Physics Laboratory
	GSI	Physics of heavy ions and accelerator	Hiroyoshi SAKURAI, Director, Radioactive Isotope Physics Laboratory
	Department of Physics, Technische Universität Darmstadt	Framework	Emiko HIYAMA, Director, Strangeness Nuclear Physics Laboratory
Hungary	The Institute of Nuclear Research of the Hungarian Academy of Sciences (ATOMKI)	Nuclear physics, Atomic Physics	Tomohiro UESAKA, Director, Spin Isospin Laboratory
Indonesia	ITB, UNPAD, ITS, UGM, UI	Material science using muons at the RIKEN-RAL muon facility	Masahiko IWASAKI, Director, Meson Science Laboratory
Italy	Applied Physics Division, National Institute for New Technologies, Energy and Environment (ENEA)	Framework	Tohru MOTOBAYASHI, Senior Advisor, RNC
	European Center for Theoretical Studies in Nuclear Physics and Related Areas (ECT*)	Theoretical physics	Tetsuo HATSUDA, Director, Quantum Hadron Physics Laboratory
	Istituto Nazionale di Fisica Nucleare (INFN)	Physics of heavy ions	Hiroyoshi SAKURAI, Director, Radioactive Isotope Physics Laboratory
<b>Country</b>	<b>Partner Institute</b>	<b>Objects</b>	<b>RNC contact person</b>
Korea	Seoul National University	Nishina School	Hiroyoshi SAKURAI, Director, Radioactive Isotope Physics Laboratory
	College of Natural Science, Ewha Women's University	Framework	Tomohiro UESAKA, Director, Spin Isospin Laboratory
	College of Natural Sciences, INHA University	Framework	Emiko HIYAMA, Director, Strangeness Nuclear Physics Laboratory
Malaysia	Universiti Sains Malaysia	Muon Science	Masahiko IWASAKI, Director, Meson Science Laboratory
Norway	Faculty of Mathematics and Natural Science, University of Oslo (UiO MN)	Framework	Hiroyoshi SAKURAI, Director, Radioactive Isotope Physics Laboratory
Poland	The Henryk Niewodniczanski Institute of Nuclear Physics, Polish Academy of Sciences (IFPAN)	Framework	Hiroyoshi SAKURAI, Director, Radioactive Isotope Physics Laboratory
Romania	"Horia Hulubei" National Institute of Physics and Nuclear Engineering Bucharest-Magurele, Romania	Framework	Tomohiro UESAKA, Director, Spin Isospin Laboratory
Russia	Joint Institute for Nuclear Research (JINR)	Framework	Tomohiro UESAKA, Director, Spin Isospin Laboratory
	Russian Research Center "Kurchatov Institute"	Framework	Hiroyoshi SAKURAI, Director, Radioactive Isotope Physics Laboratory

Switzerland	Paul Scherrer Institute	Improve the performance and reliability of accelerator systems	Osamu KAMIGAITO, Director, Accelerator Group
UK	The Science and Technology Facilities Council	Muon science using the ISIS Facility at the Rutherford Appleton Laboratory	Masahiko IWASAKI, Director, Meson Science Laboratory
USA	BNL	The Spin Physics Program at the Relativistic Heavy Ion Collider (RHIC)	Hideto EN'YO, Director, Radiation Laboratory
	Columbia University	The development of QCDCQ	Hideto EN'YO, Director, Radiation Laboratory
	Michigan State University	Comprehensive The use of TPC (Time Projection Chamber)	Tomohiro UESAKA, Director, Spin Isospin Laboratory
Vietnam	Vietnam Atomic Energy Commission	Framework	Tohru MOTOBAYASHI Senior Advisor, RNC
	Institute of Physics, Vietnam Academy of Science and Technology	Framework	Hiroyoshi SAKURAI, Director, Radioactive Isotope Physics Laboratory
Europe	European Nuclear Science and Application Research2	Framework	Tomohiro UESAKA, Director, Spin Isospin Laboratory

## 7. Awards

Awardee, Laboratory / Team	Award	Organization	Date
Hiroki OKUNO, Deputy Group Director, Accelerator Group Kensuke KUSAKA, Nishina Center Research Scientist, BigRIPS Team	The 22nd Superconductivity Science and Technology Award	Forum of Superconductivity Science and Technology	Apr. 16
Hideaki OTSU, Team Leader, Fast RI Data Team Hiroyoshi SAKURAI, Team Leader, Muon Data Team Teichiro MATSUZAKI, Contract Researcher, Muon Data Team	The 21st Century Invention Prize	Japan Institute Invention and Innovation	Jun. 12
Minjung KIM, Intern, Radiation Laboratory	2018 Gertrude Scharff-Goldhabor Prize	Brookhaven Woman in Science (BWIS)	Jul. 17
Yuya TANIZAKI, Special Postdoctoral Researcher, Theory Group, RIKEN BNL Research Center	The 13th Particle Physics Medal(FY2018): Young Scientist Award in Theoretical Particle Physics	Particle Theory Committee	Sep. 16
Taku IZUBUCHI, Group Leader, Computing Group, RIKEN BNL Research Center	APS Fellow	American Physical Society	Sep. 11
Naoki KIMURA, Student Trainee, SLOWRI Team	The 2018 International Conference Presentation Incentive Award	The Atomic Collision Society of Japan	Jun. 18
Masato NAKAMURA, Senior Technical Scientist, Cryogenic Technology Team	The Saitama prefecture High-pressure Gas Chairman Commendation	The Saitama prefecture High-pressure Gas Committee	Oct. 16
Takahiro NISHI, Postdoctoral Researcher, Spin Isospin Laboratory	The 13th Young Scientist Award of the Physical Society of Japan in the field of experimental physics/The 25th Award for Outstanding Young Physicists-Experimental Nuclear Physics	The Physical Society of Japan	Mar. 15

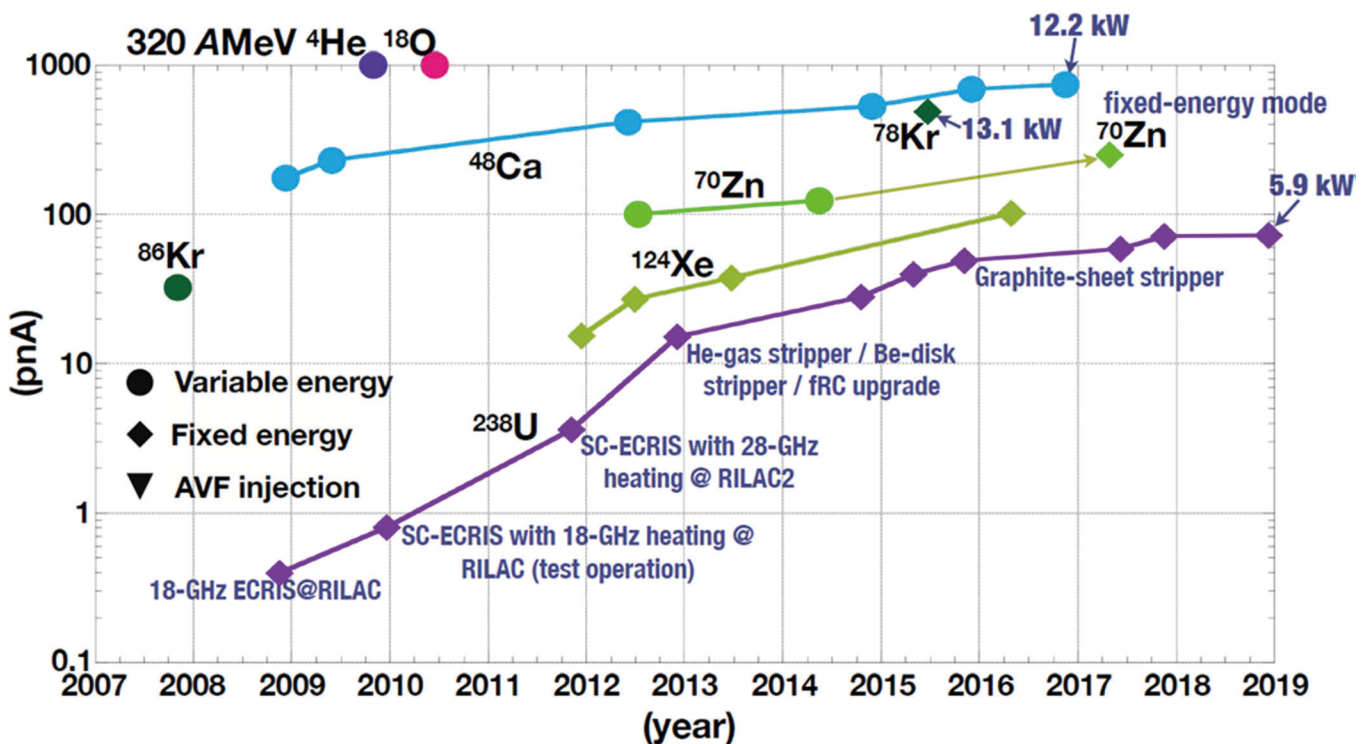
### 8. Brief overview of the RI Beam Factory

#### Intensity of Primary Beams

Achieved beam intensities (as of March 2018)

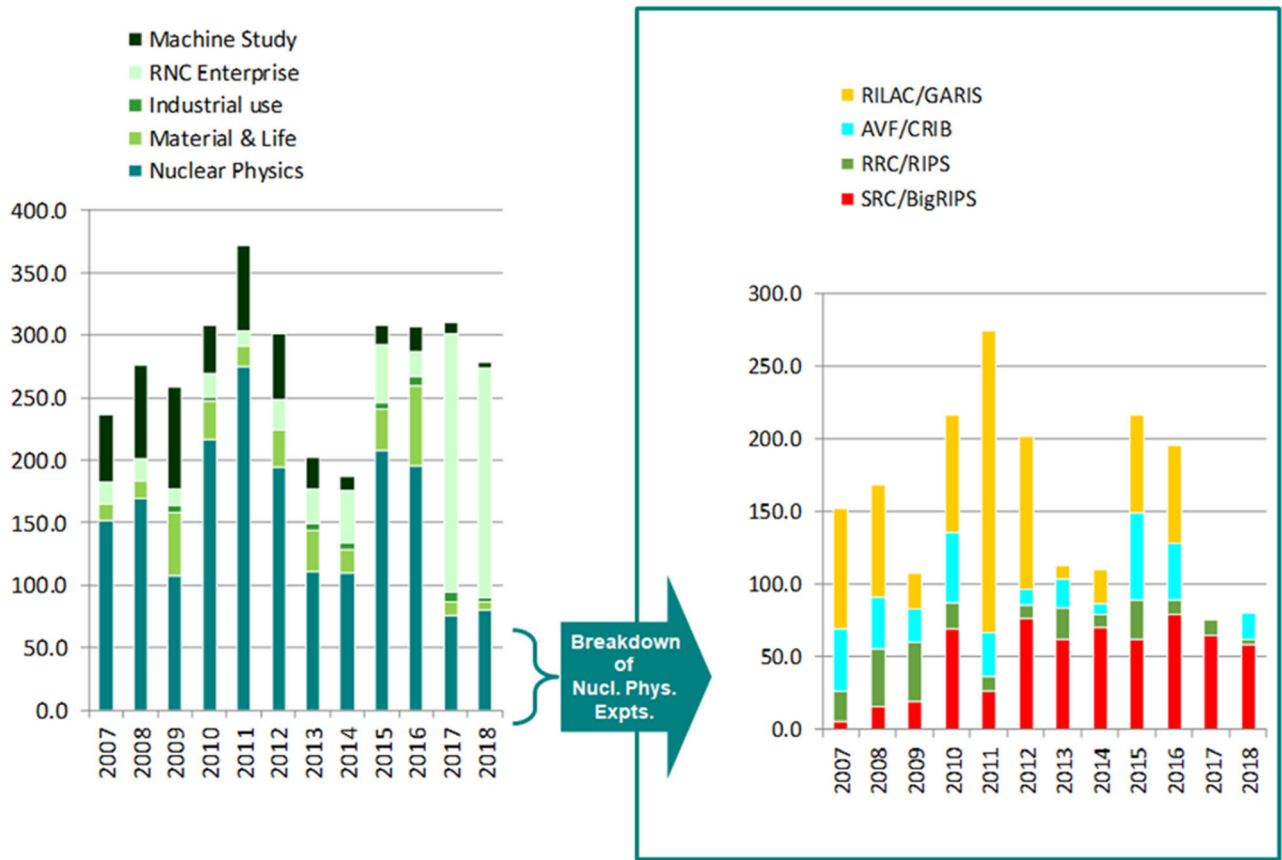
$^{238}\text{U}$	70 pA (345 MeV/nucleon, Nov. 2017)
$^{124}\text{Xe}$	102 pA (345 MeV/nucleon, Apr. 2016)
$^{86}\text{Kr}$	30 pA (345 MeV/nucleon, Nov. 2007)
$^{78}\text{Kr}$	486 pA (345 MeV/nucleon, May. 2015)
$^{70}\text{Zn}$	250 pA (345 MeV/nucleon, May 2017)
$^{48}\text{Ca}$	730 pA (345 MeV/nucleon, Nov. 2016)
$^{18}\text{O}$	1000 pA (345 MeV/nucleon, Jun. 2010)
$^{14}\text{N}$	400 pA (250 MeV/nucleon, Oct. 2010)
$^4\text{He}$	1000 pA (250 MeV/nucleon, Oct. 2009)
d	1000 pA (250 MeV/nucleon, Oct. 2010)
pol. d	120 pA, $P\sim 80\%$ (250 MeV/nucleon, May 2015)

### History of Beam Intensity Upgrade

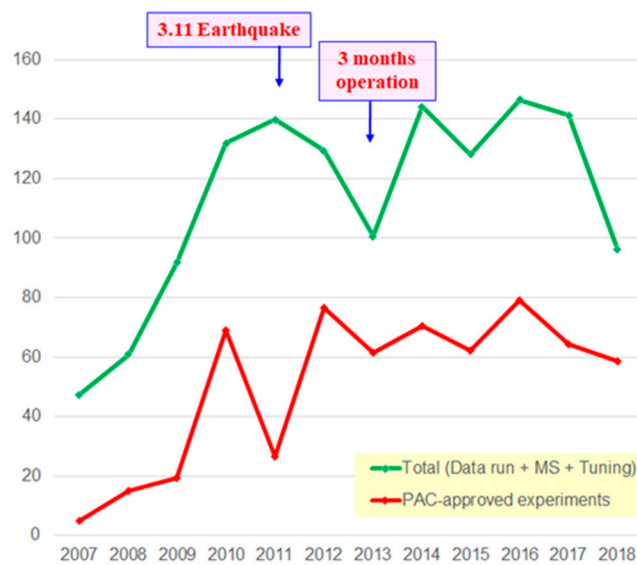


Beam energies of the beams without explicitly indicated are 345 A MeV.

Total beam time for experiments



Total beam time allocated to BigRIPS experiments



## Nuclear Science and Transmutation Research Division Radioactive Isotope Physics Laboratory

### 1. Abstract

This Laboratory works as one of core research groups conducting programs at the world-premiere heavy-ion accelerator facility of RIKEN “RI Beam Factory (RIBF).” The Laboratory explores exotic nuclear structures and dynamics in exotic nuclei that have never been investigated before, such as those with largely imbalanced proton and neutron numbers. Our aim is to develop new experimental techniques utilizing fast radioactive isotope (RI) beams at RIBF, to discover new phenomena and properties in exotic nuclei. The Laboratory is focusing three major subjects; shell evolution of very neutron-rich nuclei, the r-process path and equation-of-state in asymmetric nuclear matter. The Laboratory has initiated international collaborations for in-beam gamma spectroscopy, decay spectroscopy and heavy-ion induced reactions, and has formed a discussion forum for next generation gamma detectors.

### 2. Major Research Subjects

- (1) Study of structure and dynamics of exotic nuclei through developments of new tools in terms of reaction- and technique-based methodology
- (2) Research on EOS in asymmetric nuclear matter via heavy-ion induced reactions
- (3) Detector developments for spectroscopy and reaction studies

### 3. Summary of Research Activity

#### (1) In-beam gamma spectroscopy

In the medium and heavy mass region explored at RIBF, collective natures of nuclei are one of important subjects, which are obtained through production and observation of high excited and high spin states. To populate such states, heavy-ion induced reactions such as fragmentation, fission are useful. So far, we have developed two-step fragmentation method as an efficient method to identify and populate excited states, and lifetime measurements to deduce transition strength.

Devices utilized for the in-beam gamma spectroscopy are ZeroDegree Spectrometer (ZDS) and a NaI array DALI2. Since the end of 2008, the first spectroscopy on nuclei island-of-inversion region was performed, we have explored step-by-step new and unknown regions in the nuclear chart. The second campaign in 2009 was organized to study background components originating from atomic processes in a heavy target. Neutron-rich nuclei at  $N = 20$  to 28 were studied in 2010. In 2011–2013, we conducted experiment programs for Ca-54, Ni-78, neutron-rich nuclei at  $N = 82$  and neutron-deficient nuclei at  $Z = 50$ .

A multitude of data obtained with inelastic, nucleon knock-out, fragmentation channels have been analyzed and published. In 2011–2013, collective natures of Mg-36, 38 and Si-42 were both published in PRL. Excited states firstly observed in Ca-54 were reported in Nature to demonstrate a new nuclear magic number of 34. Fragmentation reaction has been found efficient for nuclei with  $A > 100$  and low-lying excited state in Pd-126 has been successfully observed and reported in PRC.

To further strengthen the in-beam gamma spectroscopy at RIBF, we have proposed a new setup of MINOS + DALI2 to search for the 1st excited states in even-even neutron-rich nuclei with  $Z \sim 20$  to 40. The program was submitted to the PAC 2013 as a new category of proposal, “proposal for scientific program” and was S-ranked. A dedicated collaboration “SEASTAR” has been established as a subset of in-beam gamma collaboration “SUNFLOWER.” The three campaigns were organized in 2014, 2015 and 2017 to study very neutron-rich isotopes, and were very productive to access very neutron-rich nuclei such as Ar-52, Ca-56, Ni-78, Kr-100, Zr-110.

A new project of high resolution gamma spectroscopy with fast beams has been proposed at PAC 2018 and the campaign programs are scheduled in 2020. MINIBALL and several Ge tracking detectors from Japan, Europe and the USA are being combined to form an array of germanium detectors. The new setup aims to accelerate researches of the nuclear structure by observing gamma-lines in even-odd nuclei and measuring lifetimes of excited states. The first workshop will be organized in April, 2019, and having 55 participants.

Concerning a next generation detector, a discussion forum has been established to write up a white paper on tracking germanium detectors and high-efficient crystal detectors such as LaBr<sub>3</sub> and GAGG.

#### (2) Decay spectroscopy

Beta- and isomer-spectroscopy is an efficient method for studying nuclear structure, especially for non-yrast levels. We had accumulated experimental techniques at the RIPS facility to investigate nuclear structure in light mass region via beta-gamma and beta-p coincidence. Concerning the medium and heavy mass region available at RIBF, we have developed two position-sensitive active-stoppers, strip-silicon detectors and a cylindrical active stopper called CAITEN, to achieve a low-background measurement by taking correlation between heavy ion stop position and beta-ray emission position. A site of decay-spectroscopy at the new facility of RIBF is the final focal plane of ZDS, where high precision of TOF in particle identification is obtained due to a long flight path from BigRIPS to ZDS.

At the end of 2009, the first decay spectroscopy was organized with a minimum setup of four clover gamma detectors and silicon strip detectors, to study neutron-rich nuclei with  $A \sim 110$ . The first campaign was found successful and efficient to publish four letter articles in 2011, two PRL’s and two PLB’s. One of the PRL papers is associated to the r-process path where half-lives for 18 neutron-rich nuclei were determined for the first time. The other PRL paper reported a finding of deformed magic number 64 in the Zr isotopes.

The success of the first decay-spectroscopy campaign stimulated to form a new large-scale collaboration “EURICA,” where a twelve Euroball cluster array is coupled with the silicon-strip detectors to enhance gamma efficiency by a factor of 10. A construction proposal of “EURICA” was approved in the PAC 2011, and the commissioning was successfully organized in spring 2012. Since then, physics runs have been conducted for programs approved to survey nuclei of interest as many as possible, such as Ni-78, Pd-128, Sn-100. So far, 44 papers including 12 PRL’s and 10 PLB’s were published. One of the highlights is discovery of a seniority isomer in Pd-128, of which cascade gamma decay gives the energy of first excited state and robustness of  $N = 82$  magic number, and the other is a half-life measurement for 110 neutron-rich nuclei across the  $N = 82$  shell gap, which shows implications for the mechanism and universality of the r-process path. The EURICA collaboration finished its physics programs in summer 2016.

Beta-delayed neutron emission probability of medium and heavy neutron-rich nuclei is important to understand nuclear structure and the r-process path. In 2013, a new collaboration “BRIKEN” has been established to form a He-3 detector array. A present design of the array has neutron efficiency as high as 70% up to 3 MeV. The array was coupled with the AIDA silicon strip system. A construction proposal was approved at the PAC 2013 and three physics proposals have been approved. The commissioning run was conducted in autumn 2016. The major physics runs were conducted in 2017 and 2018.

The CAITEN detector was successfully tested with fragments produced with a Ca-48 beam in 2010.

### (3) Equation-of-state via heavy-ion central collisions

Equation-of-state in asymmetric nuclear matter is one of major subjects in physics of exotic nuclei. Pi-plus and pi-minus yields in central heavy ion collisions at the RIBF energy are considered as one of EOS sensitive observables at the RIBF energy. To observe charged pions, a TPC for the SAMURAI spectrometer is being constructed under an international collaboration “S $\pi$ RIT;” Construction proposal was submitted at the PAC 2012, and physics proposals were approved at the PAC 2012 and 2013. The physics runs were successfully conducted in spring 2016. The data analysis is in progress to produce the first physics results.

An international symposium “NuSYM” on nuclear symmetry energy was organized at RIKEN July 2010 to invite researchers in three sub-fields, nuclear structure, nuclear reaction and nuclear astrophysics, and to discuss nuclear symmetry energy together. Since then, the symposium series have been held every year and been useful to encourage theoretical works and to strengthen the collaboration.

### (4) Nucleon correlation and cluster in nuclei

Nucleon correlation and cluster in nuclei are matters of central focus in a “beyond mean-field” picture. The relevant programs with in-beam gamma and missing-mass techniques are to depict nucleon condensations and correlations in nuclear media as a function of density as well as temperature. Neutron-halo and  $\alpha$ -skin nuclei are objects to study dilute neutron matter at the surface. By changing excitation energies in neutron-rich nuclei, clustering phenomena and role of neutrons are to be investigated.

In 2013, two programs were conducted at the SAMURAI spectrometer. One is related to proton-neutron correlation in the C-12 nucleus via p-n knockout reaction with a carbon target. The other is to search for a cluster state in C-16, which was populated via inelastic alpha scattering. The data is being analyzed. In 2018 a program to find out proton-cluster states was organized by utilizing low-energy radioactive isotope beams at GANIL-LISE, where the RIKEN liquid hydrogen target was installed.

A new project based on missing mass spectroscopy was launched to investigate an exotic cluster state in a very proton-rich nucleus. The experiment will be organized at GANIL with combination of RIKEN liquid hydrogen target CRYPTA and the MUST2 detector array in 2018.

## Members

### Group Director

Hiroyoshi SAKURAI (Deputy Director, RNC)

### Special Temporary Research Scientist

Takashi ICHIHARA

### Research/Technical Scientists

Yoichi NAKAI (Senior Research Scientist)

Tadaaki ISOBE (Senior Research Scientist)

Akihisa KOHAMA (Senior Research Scientist)

Pieter Christiaan DOORNENBAL (Senior Research Scientist)

Shunji NISHIMURA (Senior Research Scientist)

Daisuke SUZUKI (Research Scientist)

### Contract Researcher

Mizuki NISHIMURA

### Research Consultants

Masayasu ISHIHARA

Hiroyuki MURAKAMI

Akitsu IKEDA

Kenichi MATSUYANAGI

Kenji TANABE

**Special Postdoctoral Researcher**

Browne FRANK

Shintaro GO

**Foreign Postdoctoral Researcher**

He WANG

**Research Associate**

Ryo TANIUCHI

**Junior Research Associates**

Masanori KANEKO (Kyoto Univ.)

Hideki SHIMIZU (Univ. of Tokyo)

**International Program Associates**

Xiaohui SUN (Peking Univ.)

Phong VI (VNU of Science)

**Visiting Researcher**

Benoit Jean-Pacal Camille MAUSS (JSPS Fellow)

**Senior Visiting Scientists**

Kengo OGAWA (Chiba Univ.)

Koichiro ASAHU (Tokyo Tech)

Shigeru KUBONO (Univ. of Tokyo)

**Visiting Scientists**

Hooi Jing ONG (RCNP)

Alan MCINTOSH (Texas A &amp; M Univ.)

Akira ONO (Tohoku Univ.)

Jin WU (ANL)

Megumi NIKURA (Univ. of Tokyo)

Kathrin WIMMER (Univ. of Tokyo)

Kazuhiro OYAMATSU (Aichi Shukutoku University)

Jin-hee CHANG (MSU)

Silvio CHERUBINI (Univ. of Catania)

Tetsuya MURAKAMI (Kyoto Univ.)

Clementine SANTAMARIA (Berkeley Lab.)

Yoshiharu MORI (Kyoto Univ.)

Daiki NISHIMURA (Tokyo Univ. of Sci.)

Kazuo IEKI (Rikkyo Univ.)

Kei IIDA (Kochi University)

Rensheng WANG (Soochow Univ.)

Takashi KISHIDA (Aoyama Univ.)

Mitsunori FUKUDA (Osaka Univ.)

Gabor KISS (MTA Atomki)

Takuji IZUMIKAWA (Niigata Univ.)

Naohiko OTSUKA (Intl. Atomic Energy Agency, Austria)

Nori AOI (RCNP)

Natsumi IKENO (Tottori Univ.)

Takashi OHTSUBO (Niigata Univ.)

Giuseppe LORUSSO (National Physics Lab., UK)

Khiem Hong LE (Vietnam Academy of Sci. and Tech.)

Giordano CERIZZA (NSCL)

Maya TAKECHI (Niigata Univ.)

Hui Ching LEE (Univ. of Hong Kong)

Evgueni NIKOLSKI (RRC Kurchatov Inst.)

Satoshi TAKEUCHI (Tokyo Tech)

Martha Liliana CORTES SUA (INFN)

Byungsik HONG (Korea Univ.)

Hiroshi WATANABE (Beihang Univ.)

Paer-Anders SOEDERSTROEM (T. U. Darmstadt)

Alexey OGLOBLIN (Kurchatov Institute)

**Visiting Technicians**

Ivan KOJOUHAROV (GSI)

Jorge AGRAMUNT ROS (Valencia City Hall)

**Student Trainees**

Akira HOMMA (Niigata Univ.)

Noritsugu NAKATSUKA (Kyoto Univ.)

Tomohito AMANO (Univ. of Tokyo)

Takeshi SAITO (Univ. of Tokyo)

Satoru MOMIYAMA (Univ. of Tokyo)

Ayumi YAGI (Osaka Univ.)

Natsumi OGAWA (Univ. of Tokyo)

Takuma KOIWAI (Univ. of Tokyo)

Justin ESTEE (Michigan State University)

Kosuke ONISHI (Osaka Univ.)

Naoya YOSHIDA (Univ. of Tokyo)

Yusuke FUJINO (Rikkyo Univ.)

JungWoo LEE (Korea University)

Takanobu SUGIHARA (Osaka Univ.)

Rento YAMADA (Univ. of Tokyo)

Phong VI (VNU of Science)

Shunpei KOYAMA (Univ. of Tokyo)

Naoto KANDA (Niigata Univ.)

Jun TSUTSUMI (Univ. of Tokyo)

Linh BUI (Vietnam Atomic Energy Institute)

Jonathan BARNEY (Michigan State University)

So SATO (Rikkyo Univ.)

Zhuljeta TONEVA (University of Sofia St. Kl. Ohridski)

Takamichi AOKI (Univ. of Tokyo)

Shinnosuke KANAYA (Osaka Univ.)

Moe NAKANO (Rikkyo Univ.)

**Part-time Worker**

Keishi MATSUI (Univ. of Tokyo)

## List of Publications & Presentations

### Publications

#### [Journal]

#### (Original Papers) \*Subject to Peer Review

- H. L. Crawford, P. Fallon, A. O. Macchiavelli, P. Doornenbal, N. Aoi, F. Browne, C. M. Campbell, S. Chen, R. M. Clark, M. L. Cortes, M. Cromaz, E. Ideguchi, M. D. Jones, R. Kanungo, M. MacCormick, S. Momiyama, I. Murray, M. Niikura, S. Paschalis, M. Petri, H. Sakurai, M. Salathe, P. Schrock, D. Steppenbeck, S. Takeuchi, Y. K. Tanaka, R. Taniuchi, H. Wang, K. Wimmer, "First spectroscopy of the near drip-line nucleus  $^{40}\text{Mg}$ ," *Phys. Rev. Lett.* **122**, 052501 (2019).
- P. J. Davies, J. Park, H. Grawe, R. Wadsworth, R. Gernhauser, R. Krucken, F. Nowacki, D. S. Ahn, F. Ameil, H. Baba, T. Back, B. Blank, A. Blazhev, P. Boutachkov, F. Browne, I. Celikovic, M. Dewald, P. Doornenbal, T. Faestermann, Y. Fang, G. de France, N. Fukuda, A. Gengelbach, J. Gerl, J. Giovinazzo, S. Go, N. Goel, M. Gorska, E. Gregor, H. Hotaka, S. Ilieva, N. Inabe, T. Isobe, D. G. Jenkins, J. Jolie, H. S. Jung, A. Jungclaus, D. Kameda, G. D. Kim, Y. -K. Kim, I. Kojouharov, T. Kubo, N. Kurz, M. Lewitowicz, G. Lorusso, D. Lubos, L. Maier, E. Merchan, K. Moschner, D. Murai, F. Naqvi, H. Nishibata, D. Nishimura, S. Nishimura, I. Nishizuka, Z. Patel, N. Pietralla, M. M. Rajabali, S. Rice, H. Sakurai, H. Schaffner, Y. Shimizu, L. F. Sinclair, P. -A. Soderstrom, K. Steiger, T. Sumikama, H. Suzuki, H. Takeda, J. Taprogge, P. Thole, S. Valder, Z. Wang, N. Warr, H. Watanabe, V. Werner, J. Wu, Z. Y. Xu, A. Yagi, K. Yoshinaga, Y. Zhu, "Toward the limit of nuclear binding on the  $N = Z$  line: Spectroscopy of  $^{96}\text{Cd}$ ," *Phys. Rev. C* **99**, 021302 (2019).
- Z. Elekes, Á. Kriepkó, D. Sohler, K. Sieja, K. Ogata, K. Yoshida, P. Doornenbal, A. Obertelli, G. Authelet, H. Baba, D. Calvet, F. Château, A. Corsi, A. Delbart, J.-M. Gheller, A. Gillibert, T. Isobe, V. Lapoux, M. Matsushita, S. Momiyama, T. Motobayashi, H. Otsu, C. Péron, A. Peyaud, E. C. Pollacco, J.-Y. Rousse, H. Sakurai, C. Santamaria, Y. Shiga, S. Takeuchi, R. Taniuchi, T. Uesaka, H. Wang, K. Yoneda, F. Browne, L. X. Chung, Zs. Dombrádi, F. Flavigny, S. Franchoo, F. Giacoppo, A. Gottardo, K. Hadyńska-Klęk, Z. Korkulu, S. Koyama, Y. Kubota, J. Lee, M. Lettmann, C. Louchart, R. Lozeva, K. Matsui, T. Miyazaki, M. Niikura, S. Nishimura, L. Olivier, S. Ota, Z. Patel, E. Sahin, C. Shand, P.-A. Söderström, I. Stefan, D. Steppenbeck, T. Sumikama, D. Suzuki, Zs. Vajta, V. Werner, J. Wu, Z. Xu, "Nuclear structure of  $^{76}\text{Ni}$  from the (p, 2p) reaction," *Phys. Rev. C* **99**, 014312 (2019).
- H. N. Liu, A. Obertelli, P. Doornenbal, C. A. Bertulani, G. Hagen, J. D. Holt, G. R. Jansen, T. D. Morris, A. Schwenk, R. Stroberg, N. Achouri, H. Baba, F. Browne, D. Calvet, F. Chateau, S. Chen, N. Chiga, A. Corsi, M. L. Cortes, A. Delbart, J. -M. Gheller, A. Giganon, A. Gillibert, C. Hilaire, T. Isobe, T. Kobayashi, Y. Kubota, V. Lapoux, T. Motobayashi, I. Murray, H. Otsu, V. Panin, N. Paul, W. Rodriguez, H. Sakurai, M. Sasano, D. Steppenbeck, L. Stuhl, Y. L. Sun, Y. Togano, T. Uesaka, K. Wimmer, K. Yoneda, O. Aktas, T. Aumann, L. X. Chung, F. Flavigny, S. Franchoo, I. Gasparic, R. -B. Gerst, J. Gibelin, K. I. Hahn, D. Kim, T. Koiwai, Y. Kondo, P. Koseoglou, J. Lee, C. Lehr, B. D. Linh, T. Lokotko, M. MacCormick, K. Moschner, T. Nakamura, S. Y. Park, D. Rossi, E. Sahin, D. Sohler, P. -A. Soderstrom, S. Takeuchi, H. Tornqvist, V. Vaquero, V. Wagner, S. Wang, V. Werner, X. Xu, H. Yamada, D. Yan, Z. Yang, M. Yasuda, L. Zanetti, "How robust is the  $N = 34$  subshell closure? First spectroscopy of  $^{52}\text{Ar}$ ," *Phys. Rev. Lett.* **122**, 072502 (2019).
- I. Murray, M. MacCormick, D. Bazin, P. Doornenbal, N. Aoi, H. Baba, H. Crawford, P. Fallon, K. Li, J. Lee, M. Matsushita, T. Motobayashi, T. Otsuka, H. Sakurai, H. Scheit, D. Steppenbeck, S. Takeuchi, J. A. Tostevin, N. Tsunoda, Y. Utsuno, H. Wang, K. Yoneda, "Spectroscopy of strongly deformed  $^{32}\text{Ne}$  by proton knockout reactions," *Phys. Rev. C* **99**, 011302 (2019).
- J. Park, R. Krucken, D. Lubos, R. Gernhauser, M. Lewitowicz, S. Nishimura, D. S. Ahn, H. Baba, B. Blank, A. Blazhev, P. Boutachkov, F. Browne, I. Celikovic, G. de France, P. Doornenbal, T. Faestermann, Y. Fang, N. Fukuda, J. Giovinazzo, N. Goel, M. Gorska, H. Grawe, S. Ilieva, N. Inabe, T. Isobe, A. Jungclaus, D. Kameda, G. D. Kim, Y. -K. Kim, I. Kojouharov, T. Kubo, N. Kurz, Y. K. Kwon, G. Lorusso, K. Moschner, D. Murai, I. Nishizuka, Z. Patel, M. M. Rajabali, S. Rice, H. Sakurai, H. Schaffner, Y. Shimizu, L. Sinclair, P. -A. Soderstrom, K. Steiger, T. Sumikama, H. Suzuki, H. Takeda, Z. Wang, H. Watanabe, J. Wu, Z. Y. Xu, "New and comprehensive beta- and betap-decay spectroscopy results in the vicinity of  $^{100}\text{Sn}$ ," *Phys. Rev. C* **99**, 034313 (2019).
- V. Vaquero, A. Jungclaus, P. Doornenbal, K. Wimmer, A. M. Moro, K. Ogata, T. Furumoto, S. Chen, E. Nacher, E. Sahin, Y. Shiga, D. Steppenbeck, R. Taniuchi, Z. Y. Xu, T. Ando, H. Baba, F. L. Bello Garrote, S. Franchoo, K. Hadyńska-Klek, A. Kusoglu, J. Liu, T. Lokotko, S. Momiyama, T. Motobayashi, S. Nagamine, N. Nakatsuka, M. Niikura, R. Orlandi, T. Y. Saito, H. Sakurai, P. A. Soderstrom, G. M. Tveten, Zs. Vajta, M. Yalcinkaya, "In-beam gamma-ray spectroscopy of  $^{136}\text{Te}$  at relativistic energies," *Phys. Rev. C* **99**, 034306 (2019).
- K. Wimmer, F. Recchia, S. M. Lenzi, S. Riccetto, T. Davinson, A. Estrade, C. J. Griffin, S. Nishimura, F. Nowacki, V. Phong, A. Poves, P. -A. Soderstrom, O. Aktas, M. Al-Aqeel, T. Ando, H. Baba, S. Bae, S. Choi, P. Doornenbal, J. Ha, L. Harkness-Brennan, T. Isobe, P. R. John, D. Kahl, G. Kiss, I. Kojouharov, N. Kurz, M. Labiche, K. Matsui, S. Momiyama, D. R. Napoli, M. Niikura, C. Nita, Y. Saito, H. Sakurai, H. Schaffner, P. Schrock, C. Stahl, T. Sumikama, V. Werner, W. Witt, P. J. Woods, "First spectroscopy of  $^{61}\text{Ti}$  and the transition to the island of inversion at  $N = 40$ ," *Phys. Lett. B* **792**, 16 (2019).
- H. Sakurai, "Nuclear physics with RI Beam Factory," *Front. Phys.* **13**, 132111 (2018).
- M. L. Cortes, P. Doornenbal, M. Dupuis, S. M. Lenzi, F. Nowacki, A. Obertelli, S. Peru, N. Pietralla, V. Werner, K. Wimmer, G. Authelet, H. Baba, D. Calvet, F. Chateau, A. Corsi, A. Delbart, J.-M. Gheller, A. Gillibert, T. Isobe, V. Lapoux, C. Louchart, M. Matsushita, S. Momiyama, T. Motobayashi, M. Niikura, H. Otsu, C. Peron, A. Peyaud, E. C. Pollacco, J.-Y. Rousse, H. Sakurai, C. Santamaria, M. Sasano, Y. Shiga, S. Takeuchi, R. Taniuchi, T. Uesaka, H. Wang, K. Yoneda, F. Browne, L. X. Chung, Zs. Dombradi, S. Franchoo, F. Giacoppo, A. Gottardo, K. Hadyńska-Klek, Z. Korkulu, S. Koyama, Y. Kubota, J. Lee, M. Lettmann, R. Lozeva, K. Matsui, T. Miyazaki, S. Nishimura, L. Olivier, S. Ota, Z. Patel, E. Sahin, C. M. Shand, P.-A. Soderstrom, I. Stefan, D. Steppenbeck, T. Sumikama, D. Suzuki, Zs. Vajta, J. Wu, Z. Xu, "Inelastic scattering of neutron-rich Ni and Zn isotopes off a proton target," *Phys. Rev. C* **97**, 044315 (2018).
- A. Corsi, A. Obertelli, P. Doornenbal, F. Nowacki, H. Sagawa, Y. Tanimura, N. Aoi, H. Baba, P. Bednarczyk, S. Boissinot, M. Ciemala, A. Gillibert, T. Isobe, A. Jungclaus, V. Lapoux, J. Lee, K. Matsui, M. Matsushita, T. Motobayashi, D. Nishimura, S. Ota, E. Pollacco,

- H. Sakurai, C. Santamaria, Y. Shiga, D. Sohler, D. Steppenbeck, S. Takeuchi, R. Taniuchi, H. Wang, "Spectroscopy of nuclei around  $^{100}\text{Sn}$  populated via two-neutron knockout reactions," *Phys. Rev. C* **97**, 044321 (2018).
- X. Y. Liu, Z. Liu, B. Ding, P. Doornenbal, A. Obertelli, S. M. Lenzi, P. M. Walker, L. X. Chung, B. D. Linh, G. Authelet, H. Baba, D. Calvet, F. Chateau, A. Corsi, A. Delbart, J. -M. Gheller, A. Gillibert, T. Isobe, V. Lapoux, M. Matsushita, S. Momiyama, T. Motobayashi, M. Niikura, F. Nowacki, H. Otsu, C. Peron, A. Peyaud, E. C. Pollacco, J. -Y. Rousse, H. Sakurai, M. Sasano, Y. Shiga, S. Takeuchi, R. Taniuchi, T. Uesaka, H. Wang, K. Yoneda, Y. H. Lam, T. H. Huang, M. D. Sun, W. Q. Zhang, H. Y. Lu, D. S. Hou, F. Browne, Zs. Dombradi, S. Franchoo, F. Giacoppo, A. Gottardo, K. Hadynska-Klek, Z. Korkulu, S. Koyama, Y. Kubota, J. Lee, M. Lettmann, R. Lozeva, K. Matsui, T. Miyazaki, S. Nishimura, C. Louchart, L. Olivier, S. Ota, Z. Patel, E. Sahin, C. Santamaria, C. Shand, P.-A. Soderstrom, G. L. Stefan, D. Steppenbeck, T. Sumikama, D. Suzuki, Zs. Vajta, V. Werner, J. Wu, Z. Xu, X. H. Zhou, Y. H. Zhang, H. S. Xu, F. S. Zhang, "Spectroscopy of  $^{65,67-25}\text{Mn}$ : Strong coupling in the  $N = 40$  'island of inversion'," *Phys. Lett. B* **784**, 392 (2018).
- J. Park, R. Krucken, D. Lubos, R. Gernhauser, M. Lewitowicz, S. Nishimura, D. S. Ahn, H. Baba, B. Blank, A. Blazhev, P. Boutachkov, F. Browne, I. Celikovic, G. de France, P. Doornenbal, T. Faestermann, Y. Fang, N. Fukuda, J. Giovinazzo, N. Goel, M. Gorska, H. Grawe, S. Ilieva, N. Inabe, T. Isobe, A. Jungclaus, D. Kameda, G. D. Kim, Y. -K. Kim, I. Kojouharov, T. Kubo, N. Kurz, G. Lorusso, K. Moschner, D. Murai, I. Nishizuka, Z. Patel, M. M. Rajabali, S. Rice, H. Sakurai, H. Schaffner, Y. Shimizu, L. Sinclair, P.-A. Soderstrom, K. Steiger, T. Sumikama, H. Suzuki, H. Takeda, Z. Wang, H. Watanabe, J. Wu, Z. Y. Xu, "beta decays of the heaviest  $N = Z - 1$  nuclei and proton instability of  $^{97}\text{In}$ ," *Phys. Rev. C* **97**, 051301R (2018).
- O. B. Tarasov, D. S. Ahn, D. Bazin, N. Fukuda, A. Gade, M. Hausmann, N. Inabe, S. Ishikawa, N. Iwasa, K. Kawata, T. Komatsubara, T. Kubo, K. Kusaka, D. J. Morrissey, M. Ohtake, H. Otsu, M. Portillo, T. Sakakibara, H. Sakurai, H. Sato, B. M. Sherrill, Y. Shimizu, A. Stolz, T. Sumikama, H. Suzuki, H. Takeda, M. Thoennessen, H. Ueno, Y. Yanagisawa, K. Yoshida, "Discovery of  $^{60}\text{Ca}$  and implications for the stability of  $^{70}\text{Ca}$ ," *Phys. Rev. Lett.* **121**, 022501 (2018).
- Zs. Vajta, D. Sohler, Y. Shiga, K. Yoneda, K. Sieja, D. Steppenbeck, Zs. Dombradi, N. Aoi, P. Doornenbal, J. Lee, H. Liu, M. Matsushita, S. Takeuchi, H. Wang, H. Baba, P. Bednarczyk, Zs. Fulop, S. Go, T. Hashimoto, E. Ideguchi, K. Ieki, K. Kobayashi, Y. Kondo, R. Minakata, T. Motobayashi, D. Nishimura, H. Otsu, H. Sakurai, Y. Sun, A. Tamai, R. Tanaka, Z. Tian, T. Yamamoto, X. Yang, Z. Yang, Y. Ye, R. Yokoyama, J. Zenihiro, "Proton single particle energies next to  $^{78}\text{Ni}$ : Spectroscopy of  $^{77}\text{Cu}$  via single proton knock-out reaction," *Phys. Lett. B* **782**, 99 (2018).
- K. Wimmer, W. Korten, T. Arici, P. Doornenbal, P. Aguilera, A. Algora, T. Ando, H. Baba, B. Blank, A. Boso, S. Chen, A. Corsi, P. Davies, G. de Angelis, G. de France, D. T. Doherty, J. Gerl, R. Gernhauser, D. Jenkins, S. Koyama, T. Motobayashi, S. Nagamine, M. Niikura, A. Obertelli, D. Lubos, B. Rubio, E. Sahin, T. Y. Saito, H. Sakurai, L. Sinclair, D. Steppenbeck, R. Taniuchi, R. Wadsworth, M. Zielinska, "Shape coexistence and isospin symmetry in  $A = 70$  nuclei: Spectroscopy of the  $T - Z = 1$  nucleus  $^{70}\text{Kr}$ ," *Phys. Lett. B* **785**, 441 (2018).
- O. Wieland, A. Bracco, F. Camera, R. Avigo, H. Baba, N. Nakatsuka, T. Aumann, S. R. Banerjee, G. Benzoni, K. Boretzky, C. Caesar, S. Ceruti, S. Chen, F. C. L. Crespi, V. Derya, P. Doornenbal, N. Fukuda, A. Giaz, K. Ieki, N. Kobayashi, Y. Kondo, S. Koyama, T. Kubo, M. Matsushita, B. Million, T. Motobayashi, T. Nakamura, M. Nishimura, H. Otsu, T. Ozaki, A. T. Saito, H. Sakurai, H. Scheit, F. Schindler, P. Schrock, Y. Shiga, M. Shikata, S. Shimoura, D. Steppenbeck, T. Sumikama, S. Takeuchi, R. Taniuchi, Y. Togano, J. Tscheuschner, J. Tsubota, H. Wang, K. Wimmer, K. Yoneda, "Low-lying dipole response in the unstable  $^{70}\text{Ni}$  nucleus," *Phys. Rev. C* **98**, 064313 (2018).
- R. Yokoyama, E. Ideguchi, G. S. Simpson, M. Tanaka, S. Nishimura, P. Doornenbal, G. Lorusso, P. -A. Soderstrom, T. Sumikama, J. Wu, Z. Y. Xu, N. Aoi, H. Baba, F. L. Bello Garrote, G. Benzoni, F. Browne, R. Daido, Y. Fang, N. Fukuda, A. Gottardo, G. Gey, S. Go, N. Inabe, T. Isobe, D. Kameda, K. Kobayashi, M. Kobayashi, I. Kojouharov, T. Komatsubara, T. Kubo, N. Kurz, I. Kuti, Z. Li, M. Matsushita, S. Michimasa, C. B. Moon, H. Nishibata, I. Nishizuka, A. Odahara, Z. Patel, S. Rice, E. Sahin, H. Sakurai, H. Schaffner, L. Sinclair, H. Suzuki, H. Takeda, J. Taprogge, Zs. Vajta, H. Watanabe, A. Yagi, T. Inakura, "Beta-gamma spectroscopy of the neutron-rich  $^{150}\text{Ba}$ ," *Prog. Theor. Exp. Phys.* **2018**, 041D02 (2018).
- S. Hatakeyama, W. Horiuchi, A. Kohama, "Nuclear surface diffuseness revealed in nucleon-nucleus diffraction," *Phys. Rev. C* **97**, 054607 (2018).
- B. C. Rasco, N. T. Brewer, R. Yokoyama, R. Grzywacz, K. P. Rykaczewki, A. Tolosa-Delgado, J. Agramunt, J. L. Taín, A. Algora, O. Hall, C. Griffin, T. Davinson, V. H. Phong, J. Liu, S. Nishimura, G. G. Kiss, N. Nepal, A. Estrade, "The ORNL analysis technique for extracting  $\beta$ -delayed multi-neutron branching ratios with BRIKEN," *Nucl. Instrum. Methods Phys. Res. A* **911**, 79 (2018).
- A. I. Morales, G. Benzoni, H. Watanabe, G. de Angelis, S. Nishimura, L. Coraggio, A. Gargano, N. Itaco, T. Otsuka, Y. Tsunoda, P. Van Isacker, F. Browne, R. Daido, P. Doornenbal, Y. Fang, G. Lorusso, Z. Patel, S. Rice, L. Sinclair, P. Söderström, T. Sumikama, J. J. Valiente-Dobón, J. Wu, Z. Y. Xu, A. Yagi, R. Yokoyama, H. Baba, R. Avigo, F. L. Bello Garrote, N. Blasi, A. Bracco, A. M. Bruce, F. Camera, S. Ceruti, F. C. L. Crespi, M. -C. Delattre, Zs. Dombradi, A. Gottardo, T. Isobe, I. Kojouharov, N. Kurz, I. Kuti, S. Lalkovski, K. Matsui, B. Melon, D. Mengoni, T. Miyazaki, V. Modamio-Hoybjor, S. Momiyama, D. R. Napoli, M. Niikura, R. Orlandi, Zs. Podolyák, P. H. Regan, H. Sakurai, E. Sahin, D. Sohler, H. Schaffner, R. Taniuchi, J. Taprogge, Zs. Vajta, O. Wieland, M. Yalcinkay, "Is seniority a partial dynamic symmetry in the first  $\nu g_{9/2}$  shell?," *Phys. Lett. B* **781**, 706 (2018).
- VI Ho Phong, S. Nishimura, Le Hong Khiem, "Evaluation of simultaneous fitting method for  $\beta$ -decay half-lives and  $\beta$ -delayed multi-neutron emission probabilities developed for the BRIKEN experiment," *Commun. Phys.* **28**, 311 (2018).
- T. Isobe, G. Jhang, H. Baba, J. Barney, P. Baron, G. Cerizza, J. Estee, M. Kaneko, M. Kurata-Nishimura, J. W. Lee, W. G. Lynch, T. Murakami, N. Nakatsuka, E. C. Pollacco, W. Powell, H. Sakurai, C. Santamaria, D. Suzuki, S. Tangwanchaoen, M. B. Tsang, "Application of the Generic Electronics for Time Projection Chamber (GET) readout system for heavy radioactive isotope collision experiments," *Nucl. Instrum. Methods Phys. Res. A* **899**, 43 (2018).
- E. C. Pollacco, G. F. Grinyer, F. Abu-Nimeh, T. Ahn, S. Anvar, A. Arokiaraj, Y. Ayyad, H. Baba, M. Babo, P. Baron, D. Bazin, S. Beceiro-Novo, C. Belkhiria, M. Blaizot, B. Blank, J. Bradt, G. Cardella, L. Carpenter, S. Ceruti, E. De Filippo, E. Delagnes, S. De Luca,

- H. De Witte, F. Druillole, B. Duclos, F. Favela, A. Fritsch, J. Giovinozzo, C. Gueye, T. Isobe, P. Hellmuth, C. Huss, B. Lachacinski, A. T. Laffoley, G. Lebertre, L. Legeard, W. G. Lynch, T. Marchi, L. Martina, C. Maugeais, W. Mittig, L. Nalpas, E. V. Pagano, J. Pancin, O. Poleschuk, J. L. Pedroza, J. Pibernat, S. Primault, R. Raabe, B. Raine, A. Rebi, M. Renaud, T. Roger, P. Roussel-Chomaz, P. Russotto, G. Saccà, F. Saillant, P. Sizun, D. Suzuki, J. A. Swartz, A. Tizon, N. Usher, G. Wittwer, J. C. Yang, "GET: A generic electronics system for TPCs and nuclear physics instrumentation," *Nucl. Instrum. Methods Phys. Res. A* **887**, 81–93 (2018).
- D. Kahl, H. Yamaguchi, S. Kubono, A. A. Chen, A. Parikh, D. N. Binh, J. Chen, S. Cherubini, N. N. Duy, T. Hashimoto, S. Hayakawa, N. Iwasa, H. S. Jung, S. Kato, Y. K. Kwon, S. Nishimura, S. Ota, K. Setoodehnia, T. Teranishi, H. Tokieda, T. Yamada, C. C. Yun, L. Y. Zhang, "First measurement of  $^{30}\text{S} + \alpha$  resonant elastic scattering for the  $^{30}\text{S}(\alpha, p)$  reaction rate," *Phys. Rev. C* **97**, 015802 (2018).
- H. Muto, Y. Ohshiro, Y. Kotaka, H. Yamaguchi, Y. Sakemi, K. Kobayashi, M. Nishimura, M. Oyaizu, S. Kubono, M. Kase, T. Hattori, S. Shimoura, "Note: An innovative method for  $^{12}\text{C}^{4+}$  suppression in  $^{18}\text{O}^{6+}$  beam production in an electron cyclotron resonance ion source (selected as the editor's pick)," *Rev. Sci. Instrum.* **89**, 016103 (2018).
- Y. M. Xing, K. A. Li, Y. H. Zhang, X. H. Zhou, M. Wang, Yu. A. Litvinov, K. Blaum, S. Wanajo, S. Kubono, G. Martínez-Pinedo, A. Sieverding, R. J. Chen, P. Shuai, C. Y. Fu, X. L. Yan, W. J. Huang, X. Xu, X. D. Tang, H. S. Xu, T. Bao, X. C. Chen, B. S. Gao, J. J. He, Y. H. Lam, H. F. Li, J. H. Liu, X. W. Ma, R. S. Mao, M. Si, M. Z. Sun, X. L. Tu, Q. Wang, J. C. Yang, Y. J. Yuan, Q. Zeng, P. Zhang, X. Zhou, W. L. Zhan, S. Litvinov, G. Audi, T. Uesaka, Y. Yamaguchi, T. Yamaguchi, A. Ozawa, C. Fröhlich, T. Rauscher, F.-K. Thielemann, B. H. Sun, Y. Sun, A. C. Dai, F. R. Xu, "Mass Measurements of neutron-deficient Y, Zr, and Nb isotopes and their impact on  $rp$  and  $\nu p$  nucleosynthesis processes," *Phys. Lett. B* **781**, 358–363 (2018).
- C. Y. Fu, Y. H. Zhang, X. H. Zhou, M. Wang, Yu. A. Litvinov, K. Blaum, H. S. Xu, X. Xu, P. Shuai, Y. H. Lam, R. J. Chen, X. L. Yan, T. Bao, X. C. Chen, H. Chen, J. J. He, S. Kubono, D. W. Liu, R. S. Mao, X. W. Ma, M. Z. Sun, X. L. Tu, Y. M. Xing, P. Zhang, Q. Zeng, X. Zhou, W. L. Zhan, S. Litvinov, G. Audi, T. Uesaka, Y. Yamaguchi, T. Yamaguchi, A. Ozawa, B. H. Sun, Y. Sun, F. R. Xu, "Masses of the  $T_z = -3/2$  nuclei  $^{27}\text{P}$  and  $^{29}\text{S}$ ," *Phys. Rev. C* **98**, 014315 (2018).
- D. Kim, G. W. Kim, S. Y. Park, A. Kim, K. I. Hahn, K. Abe, O. Beliuskina, S. Hayakawa, N. Imai, N. Kitamura, Y. Sakaguchi, H. Yamaguchi, S. M. Cha, K. Y. Chae, M. S. Kwag, S. W. Hong, E. J. Lee, J. H. Lee, E. K. Lee, J. Y. Moon, S. H. Bae, S. H. Choi, S. Kubono, V. Panin, Y. Wakabayashi, N. Iwasa, D. Kahl, A. A. Chen, "Study of  $^{19}\text{F}$  levels with  $E_x = 6.7\text{--}7.7$  MeV by the  $^{15}\text{N} + \alpha$  scattering experiment," *J. Korean Phys. Soc.* **73**, 265–270 (2018).
- Y. P. Xu, D. Y. Pang, X. Y. Yun, S. Kubono, C. A. Bertulani, C. X. Yuan, "Possible determination of high-lying single-particle components with  $(p, d)$  reactions," *Phys. Rev. C* **98**, 044622 (2018).
- L. Y. Zhang, J. J. He, S. Wanajo, D. Dell'Aquila, S. Kubono, G. Zhao, "New thermonuclear  $^{10}\text{B}(\alpha, p)^{13}\text{C}$  rate and its astrophysical implication in the  $\nu p$ -process," *Astrophys. J.* **868**, 24 (2018).
- S. Takeuchi, T. Nakamura, M. Shikata, Y. Togano, Y. Kondo, J. Tsubota, T. Ozaki, A. Saito, H. Otsu, He Wang, H. Sakurai, Y. Watanabe, S. Kawase, D. S. Ahn, M. Aikawa, T. Ando, S. Araki, Sidong Chen, N. Chiga, P. Doornenbal, S. Ebata, N. Fukuda, T. Isobe, S. Kawakami, T. Kin, S. Koyama, S. Kubono, Y. Maeda, A. Makinaga, M. Matsushita, T. Matsuzaki, S. Michimasa, S. Momiyama, S. Nagamine, K. Nakano, M. Niikura, K. Ogata, T. Saito, Y. Shiga, Y. Shimizu, S. Shimoura, T. Sumikama, P. A. Söderström, H. Suzuki, H. Takeda, R. Taniuchi, M. Uesaka, Y. Watanabe, K. Wimmer, T. Yamamoto, K. Yoshida, "Coulomb breakup reactions of  $^{93,94}\text{Zr}$  in inverse kinematics," *Prog. Theor. Exp. Phys.* **2019**, 013D02 (2019).
- Z. Y. Xu, H. Heylen, K. Asahi, F. Boulay, J. M. Daugas, R. P. de Groote, W. Gins, O. Kamalou, Á. Koszorús, M. Lykiardopoulou, T. J. Mertzimekis, G. Neyens, H. Nishibata, T. Otsuka, R. Orset, A. Poves, T. Sato, C. Stodel, "Nuclear moments of the low-lying isomeric  $1^+$  state of  $^{34}\text{Al}$ : Investigation on the neutron  $1p_{1h}$  excitation across  $N = 20$  in the island of inversion," *Phys. Lett. B* **782**, 619–626 (2018).
- Y. Ichikawa, Y. Ichikawa, H. Nishibata, A. Takamine, K. Imamura, T. Fujita, T. Sato, Y. Shimizu, D. S. Ahn, K. Asahi, H. Baba, D. L. Balabanski, F. Boulay, J. M. Daugas, N. Fukuda, A. Gladkov, N. Inabe, Y. Ishibashi, Y. Ohtomo, T. Otsuka, T. Sumikama, H. Suzuki, H. Takeda, L. C. Tao, H. Ueno, H. Yamazaki, "Interplay between nuclear shell evolution and shape deformation revealed by the magnetic moment of  $^{75}\text{Cu}$ ," *Nat. Phys.* **15**, 321–325 (2019).
- P. Sarriguren, A. Algora, G. G. Kiss, " $\beta$ -Decay properties of neutron-rich Ca, Ti, and Cr isotopes," *Phys. Rev. C* **98**, 024311 (2018).
- M. L. Cortés, M. Reese, S. Doublet, S. Saha, H. Schaffner, F. Ameil, P. Bednarczyk, J. Gerl, M. Gorska, N. Pietralla, J. Vesic, "Silicon photomultipliers as readout for a segmented time-of-flight plastic detector," *Nucl. Instrum. Methods Phys. Res. A* **899**, 101–105 (2018).
- [Proceedings]**
- H. Wang, N. Aoi, S. Takeuchi, M. Matsushita, P. Doornenbal, T. Motobayashi, D. Steppenbeck, K. Yoneda, H. Baba, Zs. Dombrádi, K. Kobayashi, Y. Kondo, J. Lee, H. Liu, R. Minakata, D. Nishimura, H. Otsu, H. Sakurai, D. Sohler, Y. Sun, Z. Tian, R. Tanaka, Y. Yogan, Zs. Vajta, Z. Yang, T. Yamamoto, Y. Ye, R. Yokoyama, "Nuclear structure study for the neutron-rich nuclei beyond  $^{132}\text{Sn}$ : In-beam gamma-ray spectroscopy of  $^{136}\text{Sn}$  and  $^{132}\text{Cd}$ ," *EPJ Web Conf.* **178**, 02019 (2018).
- G. X. Zhang, H. Watanabe, F. G. Kondev, G. J. Lane, P. H. Regan, P.-A. Söderström, P. M. Walker, H. Kanaoka, Z. Korkulu, P. S. Lee, J. J. Liu, S. Nishimura, J. Wu, A. Yagi, D. S. Ahn, T. Alharbi, H. Baba, F. Browne, A. M. Bruce, R. J. Carroll, K. Y. Chae, Zs. Dombrádi, P. Doornenbal, A. Estrade, N. Fukuda, C. Griffin, E. Ideguchi, N. Inabe, T. Isobe, S. Kanaya, I. Kojouharov, T. Kubo, S. Kubono, N. Kurz, I. Kuti, S. Lalkovski, C. S. Lee, E. J. Lee, G. Lorusso, G. Lotay, C.-B. Moon, I. Nishizuka, C. R. Nita, A. Odahara, Z. Patel, V. H. Phong, Zs. Podolyák, O. J. Roberts, H. Sakurai, H. Schaffner, C. M. Shand, Y. Shimizu, T. Sumikama, H. Suzuki, H. Takeda, S. Terashima, Zs. Vajta, J. J. Valiente-Dóbon, Z. Y. Xu, " $\beta$ - $\gamma$  and isomeric decay spectroscopy of  $^{168}\text{Dy}$ ," *EPJ Web Conf.* **178**, 02023 (2018).
- X. Sun, H. Wang, H. Otsu, H. Sakurai, D. S. Ahn, M. Aikawa, P. Doornenbal, N. Fukuda, T. Isobe, S. Kawakami, S. Koyama, T. Kubo, S. Kubono, G. Lorusso, Y. Maeda, A. Makinaga, S. Momiyama, K. Nakano, M. Niikura, Y. Shiga, P.-A. Söderström, H. Suzuki, "Reaction study of  $^{136}\text{Xe}$  on proton, deuteron and carbon at 168 A MeV," *Proceedings of the 15th International Conference on Nuclear Reaction Mechanisms*, edited by F. Cerutti, A. Ferrari, T. Kawano, F. Salva-Pujol, P. Talou, CERN-Proceedings-2019-001, 153–157

(CERN, Geneva, 2019).

- T. Yamamoto, H. M. Shimizu, M. Kitaguchi, K. Hirota, T. Okudaira, C. C. Haddock, N. Oi, I. Ito, S. Endo, S. Takada, J. Koga, T. Yoshioka, T. Ino, K. Asahi, T. Momose, T. Iwata, K. Sakai, T. Oku, A. Kimura, M. Hino, T. Shima, Y. Yamagata, “Development of a neutron spin filter for a  $T$  violation search in compound nuclei,” JPS Conf. Proc. **22**, 011018 (2018).
- M. Kitaguchi, K. Asahi, S. Endo, Christopher C. Haddock, M. Hino, K. Hirota, T. Ino, I. Ito, T. Iwata, J. Koga, Y. Miyachi, T. Momose, N. Oi, T. Okudaira, K. Sakai, T. Shima, H. M. Shimizu, S. Takada, Y. Yamagata, T. Yamamoto, T. Yoshioka, “Fundamental physics using high-performance optics,” JPS Conf. Proc. **22**, 011034 (2018).
- J. Koga, S. Takada, T. Yoshioka, H. M. Shimizu, K. Hirota, T. Okudaira, N. Oi, I. Ito, T. Yamamoto, S. Endo, C. C. Haddock, M. Kitaguchi, A. Kimura, K. Sakai, T. Ino, K. Asahi, T. Momose, T. Iwata, M. Hino, T. Shima, Y. Yamagata, “Measurement of  $(n, \gamma)$  reaction of  $^{117}\text{Sn}$  for  $T$ -violation search by using compound nucleus,” JPS Conf. Proc. **22**, 011035 (2018).
- T. Okudaira, H. M. Shimizu, M. Kitaguchi, K. Hirota, C. C. Haddock, N. Oi, I. Ito, T. Yamamoto, S. Endo, S. Takada, J. Koga, T. Yoshioka, T. Ino, K. Asahi, T. Momose, T. Iwata, K. Sakai, T. Oku, A. Kimura, M. Hino, T. Shima, Y. Yamagata, “Measurement of angular distributions in  $^{139}\text{La}(n, \gamma)$  reaction for  $T$  violation search,” JPS Conf. Proc. **22**, 011041 (2018).

#### [Others]

- 中井陽一, 「大気微粒子と銀河宇宙線」, 加速器ハンドブック第 20.3.2 節, 2018 年, 丸善出版.
- 西村俊二, 「放射性核種の短寿命半減期測定—エキソチックな不安定核の崩壊と元素合成—」, 原子力学会誌 ATOMOS **60**, No. 10, 35–39 (2018).
- 小濱洋央, 「くろたま模型 in PHITS」, 『核データニュース』, No.122 (通巻 158 号), p. 44, 2019 年 2 月.
- 山中長閑, 吉永尚孝, 旭耕一郎, 「反磁性原子の電気双極子モーメントで探る新物理」, 日本物理学会誌 **73**, 382–387 (2018).

### Oral Presentations

#### [International Conference etc.]

- H. Sakurai (invited), “Facility-upgrade of RIBF for diversity enhancement in nuclear physics,” 13th International Conference on Nucleus-Nucleus Collisions NN2018, Omiya, Japan, December 4–8, 2018.
- H. Sakurai (invited), “Recent highlights and future programs at RIBF,” The 10th China-Japan Joint Nuclear Physics Symposium, Huizhou, China, November, 2018.
- H. Sakurai (invited), “Recent activities and highlights at the RIBF,” International Conference on Simplicity, Symmetry and Beauty of Atomic Nuclei, Shanghai, China, September, 2018.
- H. Sakurai (invited), “The RIBF Facility and Its Future,” 20th Northeastern Asian Symposium-2018 on Nuclear Physics in the 21st Century, Nagoya, September, 2018.
- H. Sakurai (invited), “Recent activities and perspectives,” 1st Symposium on Intermediate-energy Heavy Ion Collisions (iHIC2018), Beijing, China, April, 2018.
- S. Nishimura (invited), “Experimental challenges relevant to the  $r$ -process,” EMMI Rapid Reaction Task Force: The physics of neutron star mergers at GSI/FAIR Symposium GSI, Darmstadt, Germany, June 4–15, 2018.
- S. Nishimura (invited), “Decay spectroscopy of exotic nuclei at RIBF,” International workshop on Physics at HIAF High-Energy Beam Lines and Nuclear Astrophysics, Beihang Univ., China, December 13–15, 2018.
- S. Nishimura (invited), “Experiments Relevant to  $r$ -Process Nucleosynthesis at RIBF,” 5th Joint Meeting of the APS Division of Nuclear Physics and the Physical Society of Japan, Hawaii, USA, October 23, 2018.
- S. Nishimura (invited), “Experiments related to  $r$ -process nucleosynthesis at RIBF,” Nuclear Physics in Stellar Explosions, Debrecen, Hungary, September 12–14, 2018.
- S. Nishimura (invited), “Experiments related to astrophysical nucleosynthesis,” 20th Northeastern Asian Symposium-2018 on Nuclear Physics in the 21st Century, Nagoya, September, 2018.
- T. Isobe (invited), “The  $S\pi$ RIT and pion detectors in RIKEN for the experimental study of symmetry energy with heavy ion collisions,” International Workshop on Multi facets of Eos and Clustering, Catania, Italy, May 22–25, 2018.
- T. Isobe (invited), “Implementation of GET readout system for heavy RI collision experiment with  $S\pi$ RIT-TPC at RIBF,” GET Workshop: General Electronic for Physics, Haut Carre, France, October 10–12, 2018.
- T. Isobe (invited), “Study of density dependent asymmetric nuclear EOS by using heavy RI collisions at RIKEN-RIBF,” 52nd Reimei Workshop “Experimental and Theoretical Hadron Physics: Recent Exciting Developments,” Tokai, Japan, January 9–11, 2019.
- T. Isobe (invited), “Experimental study of density dependent symmetry energy at RIBF- $S\pi$ RIT experiment,” 5th Joint Meeting of the APS Division of Nuclear Physics and the Physical Society of Japan, Hawaii, USA, October 23–27, 2018.
- P. Doornenbal (invited), “Spectroscopy of neutron-rich Ca and Ni isotopes,” Nuclear Structure 2018 (NS2018), East Lansing, USA, August 6–10, 2018.
- D. Suzuki (invited), “Transfer reaction experiments using deuterated isobutene gas in active targets,” Workshop on Gas-filled Detectors and Systems (GDS): Rare-gas target handling and recycling systems, Institute de Physique Nucléaire d’Orsay, France, January 23–25, 2019.
- S. Kubono (invited), “Possible programs at HUS pelletron in nuclear astrophysics—Approach to core-collapse supernovae—,” International Workshop on research opportunity at HUS Pelletron Facility, Hanoi University of Science, Hanoi, Vietnam, April 12, 2018.
- S. Kubono (invited), “Experimental challenge to the cosmological Li problem,” Int. Conf. on Nuclei in the Cosmos (NIC 2018), Gran Sasso, Italy, June 25–29, 2018.

- S. Kubono (invited), “Heavy element synthesis under explosive burning on neutron stars,” ASRC International Workshop, Tokai, Japan, March 25–27, 2019.
- H. Wang *et al.*, “Nuclear reaction study for long-lived fission products in high-level radioactive waste: Cross section measurements for proton- and deuteron-induced spallation reactions,” 13th International Conference on Nucleus-Nucleus Collisions (NN2018), Omiya, Saitama, Japan, December 4–8, 2018.
- H. Wang *et al.*, “Spallation reaction study for fission products in nuclear waste: Cross section measurements for  $^{107}\text{Pd}$ ,  $^{137}\text{Cs}$ ,  $^{136}\text{Xe}$ , and  $^{90}\text{Sr}$  on proton and deuteron at different reaction energies,” Fifteenth NEA Information Exchange Meeting on Actinide and Fission Product Partitioning and Transmutation, Manchester Hall, Manchester, UK, September 30–October 3, 2018.
- H. Wang *et al.*, “Nuclear reaction study for high-level radioactive waste: Cross section measurements for proton- and deuteron-induced spallation reactions of long-lived fission products,” The 15th edition of the Varenna Conference on Nuclear Reaction Mechanisms (NRM), Varenna, Italy, June 11–15, 2018.
- H. Wang *et al.*, “Nuclear structure study for the neutron-rich cadmium nuclei beyond  $^{132}\text{Sn}$ ,” The 10th international conference on Direct Reactions with Exotic Beams (DREB2018), Matsue, Japan, June 5–8, 2018.
- M. L. Cortes (invited), “Development of a new scintillation detector based spectrometer at the RIBF,” 3rd Workshop of the Nuclear Spectroscopy Instrumentation Network of ENSAR2 (NuSpln), Valencia, Spain, June 25–29, 2018.
- M. L. Cortes (invited), “Recent results from in-beam gamma experiments at the RIBF,” NUSTAR Annual meeting 2019, GSI, Darmstadt, Germany, February 25–March 1, 2019.
- M. L. Cortes *et al.*, “First Spectroscopy of  $^{62}\text{Ti}$ : Shell Evolution Towards  $^{60}\text{Ca}$ ,” Nuclear Structure 2018 (NS2018), East Lansing, USA, August 5–10, 2018.
- M. Kurata-Nishimura *et al.*, “Collective flow at neutron rich Sn+Sn collisions with 270 MeV/u,” 8th International Symposium on Nuclear Symmetry Energy (NuSYM2018), Busan, South Korea, September 10–13, 2018.
- M. Kurata-Nishimura *et al.*, “Collective flow at neutron rich Sn+Sn collisions with 270 MeV/u,” 13th International Conference on Nucleus-Nucleus Collisions NN2018, Omiya, Japan, December 4–8, 2018.
- M. Kurata-Nishimura *et al.*, “ $\pi\text{RIT}$ -TPC experiment with neutron rich Sn + Sn collisions in RIKEN-RIBF,” 5th Joint Meeting of the APS Division of Nuclear Physics and the Physical Society of Japan, Hawaii, USA, October 23–27, 2018.
- M. Kaneko *et al.*, “Study of light cluster production in intermediate energetic heavy-RI collision at RIBF,” 13th International Conference on Nucleus-Nucleus Collisions NN2018, Omiya, Japan, December 4–8, 2018.
- M. Kaneko *et al.*, “Study of light cluster production in intermediate energetic heavy-RI collision at RIBF,” 8th International Symposium on Nuclear Symmetry Energy (NuSYM2018), Busan, South Korea, September 10–13, 2018.
- M. Kaneko *et al.*, “Study of light cluster production in intermediate energetic heavy-RI collision at RIBF,” 5th Joint Meeting of the APS Division of Nuclear Physics and the Physical Society of Japan, Hawaii, USA, October 23–27, 2018.
- X. Sun *et al.*, “Reaction study of  $^{136}\text{Xe}$  on proton, deuteron and carbon at 168 MeV/u,” 15th Varenna Conference on Nuclear Reaction Mechanism, Varenna, Italy, June 11–15, 2018.

#### [Domestic Conference]

- 櫻井博儀 (招待講演), 「元素の進化, 合成と変換」, 学術会議 公開シンポジウム, 「基礎科学研究の意義と社会 (物理分野から)」, 東京, 2018 年 12 月 17 日.
- 櫻井博儀 (招待講演), 「元素変換の基礎研究と将来」, 学術会議 公開シンポジウム, 「素粒子物理・原子核物理分野の大型施設計画・大規模研究計画マスタープラン」, 東京, 2019 年 2 月 19 日.
- 西村俊二 (招待講演), 「ZDS における重元素合成」, 研究会, 「重力は観測時代の r プロセスと不安定核」, 理研, 2018 年 6 月 20–22 日 (20 日).
- S. Nishimura (invited), “Study on r-process at RIKEN RIBF,” 日本物理学会: “Korea-Japan Symposium on Unstable Nuclei and Nuclear Astrophysics,” 九州大学, 2019 年 3 月 14 日.
- 西村俊二 (招待講演), 「崩壊から探る重元素合成」, 研究会「超重元素研究の新展開」, 九州大学, 2018 年 7 月 30–31 日.
- 西村俊二 (招待講演), 「CERN-NA44 実験 (初期)」, 記念研究会「広島大学におけるハドロン・クォーク物理学の歩み」, 広島大学, 2019 年 3 月 11 日.
- 磯部忠昭, 「理研 RIBF における重 RI 衝突実験用タイムプロジェクトチャンバーの性能評価」, 日本物理学会年次大会, 福岡市, 2019 年 3 月.
- 富田成夫, 山本直樹, 中井陽一, 「静電リングを用いた  $\text{Li@C}_{60}^+ + e^-$  実験」, 日本物理学会第 74 回年次大会, 福岡市, 2019 年 3 月 15 日.
- P. Doornenbal (invited), “SUNFLOWER status report,” RIBF UEC Meeting, Wako, Japan, September 5–6, 2018.
- D. Suzuki (invited), “Study of rp-process at OEDO,” OEDO workshop, Riken Wako Campus, Japan, June 11, 2018.
- H. Wang, “Spallation reaction study for fission products in high-level radioactive waste: Towards a new invention of nuclear transmutation,” the All RIKEN workshop 2018, Wako, Japan, December 14, 2018.
- M. L. Cortes, “First spectroscopy of  $^{62}\text{Ti}$ ,” RIBF Week 2018, Wako, Japan, September 3–7, 2018.
- M. L. Cortes, “Recent developments towards a new scintillator array at RIBF using GAGG detector,” RIBF Week 2018, Wako, Japan, September 3–7, 2018.
- M. L. Cortes, “Fall 2018 beam time overview,” RIBF Week 2018, Wako, Japan, September 3–7, 2018.
- F. Browne, “Asymmetric dynamics around the magic octupole numbers  $Z = 34$  and  $N = 54$ ,” RIBF Week 2018, RIKEN, Wako, Japan, September 3–7, 2018.

**Posters Presentations****[International Conference etc.]**

- Y. Nakai, N. Watanabe, Y. Oba, "Laboratory experiment for hydrogenation of C<sub>60</sub> fullerenes deposited on a solid surface under low temperature conditions," The Olympian Symposium 2018 on "Gas and stars from milli- to mega- parsecs," Paralia Katerini, May 31, 2018.
- X. Sun *et al.*, "Isotopic cross sections of proton-, deuteron- and carbon-induced reactions on <sup>136</sup>Xe," 13th International Conference on Nucleus-Nucleus Collisions, Omiya, Japan, December 4–8, 2018.
- H. Shimizu *et al.*, "Isomeric RIB Production of Aluminum-26," XV International Symposium on Nuclei in the Cosmos, Assergi, Italy, June 24–29, 2018.

**[Domestic Conference]**

- 中井陽一, 渡部直樹, "低温薄膜状 C<sub>60</sub> 固体にトラップされた水素分子の振動回転励起の赤外吸収スペクトル," 原子衝突学会第 43 回年会, 宇治, 2018 年 10 月 13 日.

**Seminars/Lectures**

- S. Nishimura, "Introduction of RIKEN," "Studying nuclear structure using RI beams," "Possibility using pelletron for nuclear physics experiment," International Training Course on the Possibilities for Studying Nuclear Physics using the Pelletron Accelerator, Hanoi, Vietnam, December 17–20, 2018.
- H. Wang, "Reaction study for fission products in high-level radioactive waste for nuclear transmutation," The 411th PKU Lecture on Nuclear Science, Peking University, Beijing, China, January 9, 2019.

## Nuclear Science and Transmutation Research Division

### Spin isospin Laboratory

#### 1. Abstract

The Spin Isospin Laboratory pursues research activities putting primary focus on interplay of spin and isospin in exotic nuclei. Understanding nucleosyntheses in the universe, especially those in *r*- and *rp*-processes is another big goal of our laboratory.

Investigations on isospin dependences of nuclear equation of state, spin-isospin responses of exotic nuclei, occurrence of various correlations at low-densities, evolution of spin-orbit coupling are main subjects along the line. We are leading a mass measurement project with the Rare RI Ring project, too. Through the experimental studies, we will be able to elucidate a variety of nuclear phenomena in terms of interplay of spin and isospin, which will in turn, lead us to better understanding of our universe.

#### 2. Major Research Subjects

- (1) Direct reaction studies of neutron-matter equation of state
- (2) Study of spin-isospin responses with RI-beams
- (3) *R*-process nucleosynthesis study with heavy-ion storage ring
- (4) Application of spin-polarization technique to RI-beam experiments and other fields
- (5) Development of special targets for RI-beam experiments

#### 3. Summary of Research Activity

##### (1) Direct reaction studies of neutron matter equation of state

Direct reactions induced by light-ions serve as powerful tools to investigate various aspects of nuclei. We are advancing experimental programs to explore equation of state of neutron matter, via light-ion induced reactions with RI-beams.

##### (1-1) Determination of a neutron skin thickness by proton elastic scattering

A neutron skin thickness is known to have strong relevance to asymmetry terms of nuclear equation of state, especially to a term proportional to density. The ESPRI project aims at determining density distributions in exotic nuclei precisely by proton elastic scattering at 200–300 MeV/nucleon. An experiment for  $^{132}\text{Sn}$  that is a flagship in this project has been successfully performed.

##### (1-2) Asymmetry terms in nuclear incompressibility

Nuclear incompressibility represents stiffness of nuclear matter. Incompressibility of symmetric nuclear matter is determined to be  $230 \pm 20$  MeV, but its isospin dependence still has a large uncertainty at present. A direct approach to the incompressibility of asymmetric nuclear matter is an experimental determination of energies of isoscalar giant monopole resonances (GMR) in heavy nuclei. We have developed, in close collaboration with Center for Nuclear Study (CNS) of University of Tokyo, an active gas target for deuteron inelastic scattering experiments to determine GMR energies. The active gas target has been already tested with oxygen and xenon beams at HIMAC and finally has been applied to a  $^{132}\text{Sn}$  experiment at RIBF.

##### (1-3) Multi-neutron and $\alpha$ -cluster correlations at low densities

Occurrences of multi-neutron and  $\alpha$ -cluster correlations are other interesting aspects of nuclear matter and define its low-density behavior. The multi-neutron and  $\alpha$ -cluster correlations can be investigated with the large-acceptance SAMURAI spectrometer. The SAMURAI has been already applied to experiments to explore light neutron-rich nuclei close to the dripline. We plan to reinforce experimental capabilities of the SAMURAI by introducing advanced devices such as MINOS (Saclay) and NeuLAND (GSI).

##### (1-4) Fission barrier heights in neutron-rich heavy nuclei

The symmetry energy has a strong influence on fission barrier heights in neutron-rich nuclei. Knowledge on the fission barrier heights, which is quite poor at present, is quite important for our proper understanding on termination of the *r*-process. We are planning to perform, in collaboration with the TU Munich group, (*p*, 2*p*)-delayed fission experiments at the SAMURAI to determine the fission barrier heights in neutron-rich nuclei in Pb region.

##### (2) Study of spin-isospin responses with RI-beams

The study of spin-isospin responses in nuclei forms one of the important cores of nuclear physics. A variety of collective states, for example isovector giant dipole resonances, isobaric analogue states, Gamow-Teller resonances, have been extensively studied by use of electromagnetic and hadronic reactions from stable targets.

The research opportunities can be largely enhanced with light of availabilities of radioactive isotope (RI) beams and of physics of unstable nuclei. There are three possible directions to proceed. The first direction is studies of spin-isospin responses of unstable nuclei via inverse-kinematics charge exchange reactions. A neutron-detector array WINDS has been constructed, under a collaboration of CNS, Tokyo and RIKEN, for inverse kinematics (*p*, *n*) experiments at the RI Beam Factory. We have already applied WINDS to the (*p*, *n*) experiments for  $^{12}\text{Be}$ ,  $^{132}\text{Sn}$  and plan to extend this kind of study to other exotic nuclei.

The second direction is studies with RI-beam induced charge exchange reaction. RI-beam induced reactions have unique properties which are missing in stable-beam induced reactions and can be used to reach the yet-to-be-discovered states. We have constructed the SHARAQ spectrometer and the high-resolution beam-line at the RI Beam Factory to pursue the capabilities of RI-beam induced reactions as new probes to nuclei. One of the highlights is an observation of  $\beta^+$  type isovector spin monopole resonances (IVSMR) in  $^{208}\text{Pb}$  and  $^{90}\text{Zr}$  via the (*t*,  $^3\text{He}$ ) reaction at 300 MeV/nucleon.

The third direction is studies of neutron- and proton-rich nuclei via stable-beam induced charge exchange reactions, which is conducted under collaboration with Research Center for Nuclear Physics (RCNP), Osaka University. We have performed the double charge exchange  $^{12}\text{C}(^{18}\text{O}, ^{18}\text{Ne})^{12}\text{Be}$  reaction at 80 MeV/nucleon to investigate structure of a neutron-rich  $^{12}\text{Be}$  nucleus. Peaks corresponding to ground and excited levels in  $^{12}\text{Be}$  have been clearly observed. Another double charge exchange reaction, ( $^{12}\text{C}, ^{12}\text{Be}(0_2^+)$ ) are being used to search for double Gamow-Teller resonances.

**(3) R-process nucleosynthesis study with heavy-ion storage ring**

Most of the r-process nuclei become within reach of experimental studies for the first time at RI Beam Factory at RIKEN. The Rare RI Ring at RIBF is the unique facility with which we can perform mass measurements of r-process nuclei. Construction of the Rare RI Ring started in FY2012 in collaboration with Tsukuba and Saitama Universities. A major part of the ring has been completed and the commissioning run is planned in FY2014.

We are planning to start precise mass measurements of r-process nuclei soon. A series of experiments will start with nuclei in the  $A = 80$  region and will be extended to heavier region.

**(4) Application of spin-polarization technique to RI-beam experiments and other fields**

A technique to produce nuclear polarization by means of electron polarization in photo-excited triplet states of aromatic molecules can open new applications. The technique is called "Triplet-DNP." A distinguished feature of Triplet-DNP is that it works under a low magnetic field of 0.1–0.7 T and temperature higher than 100 K, which exhibits a striking contrast to standard dynamic nuclear polarization (DNP) techniques working in extreme conditions of several Tesla and sub-Kelvin.

We have constructed a polarized proton target system for use in RI-beam experiments. Recent experimental and theoretical studies have revealed that spin degrees of freedom play a vital role in exotic nuclei. Tensor force effects on the evolution of shell and possible occurrence of  $p$ - $n$  pairing in the proton-rich region are good examples of manifestations of spin degrees of freedom. Experiments with the target system allow us to explore the spin effects in exotic nuclei. It should be noted that we have recently achieved a proton polarization of 40% at room temperature in a pentacene- $d_{14}$  doped p-terphenyl crystal.

Another interesting application of Triplet-DNP is sensitivity enhancement in NMR spectroscopy of biomolecules. We started a new project to apply the Triplet-DNP technique to study protein-protein interaction via two-dimensional NMR spectroscopy, in close collaboration with biologists and chemists.

**(5) Development of special targets for RI-beam experiments**

For the research activities shown above, we are developing and hosting special targets for RI-beam experiments listed below:

- (1) Polarized proton target (described in (4))
- (2) Thin solid hydrogen target
- (3) MINOS (developed at Saclay and hosted by the Spin Isospin Laboratory)

**Members****Group Director**

Tomohiro UESAKA

**Research/Technical Scientists**

Masaki SASANO (Research Scientist)  
Juzo ZENIHIRO (Research Scientist)

Sarah NAIMI (Research Scientist)  
Kenichiro YONEDA (Senior Research Scientist)

**Contract Researchers**

Daisuke NAGAE  
Takeshi INOUE

Kenichiro TATEISHI

**Special Postdoctoral Researchers**

Kenichiro TATEISHI

Yuki KUBOTA

**Postdoctoral Researchers**

Fumi SUZAKI

Takahiro NISHI

**Research Associate**

Masami SAKO

**Junior Research Associates**

Shunichiro OMIKA (Saitama Univ.)  
Shoichiro MASUOKA (Univ. of Tokyo)

Shusuke TAKADA (Kyushu Univ.)

**International Program Associates**

Jian GAO (Peking Univ.)  
Siwei HUANG (Peking Univ.)  
Jian GAO (Peking Univ.)

Siwei HUANG (Peking Univ.)  
Hongfu LI (Institute of Modern Physics, Chinese Academic of Science)

**Short International Program Associate**

Dana TUDOR (Univ. of Bucharest)

**Research Consultants**

Harutaka SAKAGUCHI

Kazuko TANABE

**Senior Visiting Scientist**

Hiroyuki SAGAWA (Aizu Univ.)

**Visiting Scientists**

Didier BEAUMEL (IPN)  
 Panin VALELII (CEA Saclay)  
 Yasuyuki SUZUKI (Niigata Univ.)  
 Yang ZAIHONG (Osaka Univ.)  
 Yosuke KONDO (Tokyo Tech.)  
 Junki TANAKA (TU darmstadt.)  
 Zoltan ELEKES (ATOMKI)  
 Dorottya KUNNE SOHLER (Institute of Nuclear Research  
 Hungarian Academy of Sciences (ATOMKI))  
 Hidetoshi AKIMUNE (Konan Univ.)  
 Yohei MATSUDA (Osaka Univ.)  
 Satoru TERASHIMA (Beihang University)  
 Yasuhiro TOGANO (Tokyo Tech.)  
 Valdir GUIMARAES (Instituto de Fisica da Universidade de  
 Sao Paulo)  
 Satoshi SAKAGUCHI (Kyusyu Univ.)  
 Kenjiro MIKI (TU Darmstadt)  
 Yasutaka TANIGUCHI (Nihon Institute of Medical Science)  
 Valerie LAPOUX (CEA Saclay)  
 Tetsuaki MORIGUCHI (Univ. of Tsukuba)  
 Alexandre OBERTELLI (CEA Saclay)  
 Kazuyuki OGATA (Osaka Univ.)  
 Alain GILLIBERT (CEA Saclay)  
 Shinji SUZUKI (Univ. of Tsukuba)  
 Emanuel POLLACCO (CEA Saclay)  
 Zsolt VAJTA (Institute of Nuclear Research Hungarian  
 Academy of Sciences (ATOMKI))  
 Anna CORSI (CEA Saclay)  
 Yuma KIKUCHI (Osaka City Univ.)  
 Istvan KUTI (Institute of Nuclear Research Hungarian  
 Academy of Sciences (ATOMKI))

Yury LITVINOV (GSI)  
 Yuhu ZHANG (CAS)  
 Makoto NEGORO (Osaka Univ.)  
 Igor GASPARIC (Ruder Boskovic Inst. Zagreb Croatia)  
 Konstanze BORETZKY (GSI)  
 Hans Toshihide TOERNQVIST (TU Darmstadt)  
 Zsolt FULOP (Institute of Nuclear Research Hungarian  
 Academy of Sciences (ATOMKI))  
 Christoph CAESAR (GSI)  
 Haik SIMON (GSI)  
 Zsolt DOMBRADI (Institute of Nuclear Research Hungarian  
 Academy of Sciences (ATOMKI))  
 Matthias HOLL (TU Darmstadt)  
 Takayuki YAMAGUCHI (Saitama Univ.)  
 Akinori KAGAWA (Osaka Univ.)  
 Takashi NAKAMURA (Tokyo Tech.)  
 Baohua SUN (Beihang Univ.)  
 Atsushi TAMII (Osaka Univ.)  
 Leyla ATAR (TU Darmstadt)  
 Attila KRASZNAHORKAY (ATOMKI)  
 Zoltan HALASZ (ATOMKI)  
 Takashi WAKUI (Tohoku Univ.)  
 Li-Gang CAO (North China Electric Power Univ.)  
 Kimiko SEKIGUCHI (Tohoku Univ.)  
 Kaori KAKI (Shizuoka Univ.)  
 Wang HE (Tokyo Tech.)  
 Zhuang GE (Institute of Modern Physics Chinese Academy of  
 Sciences)  
 Momo MUKAI (Tsukuba Univ.)  
 Yelei SUN (CEA Saclay)

**Visiting Technicians**

Gilles AUTHELET (CEA Saclay)  
 Alain DELBART (CEA Saclay)  
 Jean-Marc GHELLER (CEA Saclay)  
 Arnaud GIGANON (CEA Saclay)  
 Cedric PERON (CEA Saclay)

Daniel KOERPER (GSI)  
 Jean-Yves ROUSSE (CEA Saclay)  
 Clement HILAIRE (CEA Saclay)  
 Denis CALVET (CEA Saclay)

**Student Trainees**

Tatsuya FURUNO (Kyoto Univ.)  
 Takuma NISHIMURA (Saitama Univ.)  
 Mizuki SHIKATA (Tokyo Tech.)  
 Motoki MURATA (Kyoto Univ.)  
 Junichi TSUBOTA (Tokyo Tech.)  
 Sebastian Benedikt REICHERT (TU Munchen)  
 Yuuki TAKEUCHI (Saitama Univ.)  
 Atsumi SAITO (Tokyo Tech.)  
 Syunichirou OHMIKA (Saitama Univ.)  
 Atomu WATANABE (Tohoku Univ.)  
 Hiroshi MIURA (Saitama Univ.)  
 Julian KAHLBOW (TU Darmstadt)  
 Taras LOKOTKO (Univ. of Hong Kong)  
 Vadim WAGNER (TU Darmstadt)  
 Dahee KIM (Ewha Womans Univ.)  
 Tetsuro SHIMADA (Tokyo Tech.)  
 Tomoyuki MUKAI (Tohoku Univ.)  
 Hareru MIKI (Tokyo Tech.)  
 Shinnosuke NAKAI (Tohoku Univ.)  
 Kohei SHIMATANI (Tohoku Univ.)  
 Takato TOMAI (Tokyo Tech.)  
 Su-yeon PARK (Ewha Womans Univ.)

Akihiro HIRAYAMA (Tokyo Tech.)  
 Takaaki KOBAYASHI (Saitama Univ.)  
 Simon LINDBERG (Chalmers University of Technology)  
 Masanori HOSOYAMADA (Kyushu Univ.)  
 Masamichi AMANO (Univ. of Tsukuba)  
 Yusuke KAWASHIMA (Kyushu Univ.)  
 Daisuke SAKAE (Kyushu Univ.)  
 Saiya FUJIWARA (Kyushu Univ.)  
 Kiyoshi WAKAYAMA (Saitama Univ.)  
 Mamoru SAKAUE (Saitama Univ.)  
 Sergey CHEBOTARYOV (Kyungpook National Univ.)  
 Kenjiro YOKOTA (Saitama Univ.)  
 Alexandra-Ionela CHILUG (Univ. of Bucharest)  
 Shun HOSOI (Saitama Univ.)  
 Tomoya HARADA (Toho Univ.)  
 Yasuhito INADA (Saitama Univ.)  
 Kosei TANIUE (Univ. of Miyazaki)  
 Li PENJIE (The Univ. of Hong Kong)  
 Masahiro YASUDA (Tokyo Tech.)  
 Shuhei GOTO (Kyushu Univ.)  
 Hiroki YAMADA (Tokyo Tech.)  
 Jianwei ZHAO (Beihang Univ.)

Jun OKAMOTO (Tohoku Univ.)  
 Hisanori OSHIRO (Kyushu Univ.)  
 Yu NASU (Tohoku Univ.)  
 Daiki INOMOTO (Kyushu Univ.)  
 Shota MATSUMOTO (Kyoto Univ.)  
 Shunya ISHIDA (Tohoku Univ.)  
 Simon GIRAUD (Université de Nantes)  
 Yuma HIRAI (Kyushu Univ.)  
 Yu ANDO (Kyungpook National Univ.)  
 Dora SZALKAI (Eotvos Larand Univ.)  
 Mayuko MATSUMOTO (Tokyo Tech.)  
 Shinji MITSUMOTO (Kyushu Univ.)  
 Daiki KAMIOKA (Univ. of Tsukuba)  
 Hina KASAHARA (Kyushu Univ.)  
 Christopher LEHR (TU Darmstadt)  
 Akira YASUDA (Tokyo Tech.)  
 Tomoya FUJII (Saitama Univ.)  
 Yuuki FUJII (Tokyo Tech.)  
 Kunimitsu NISHIMURO (Saitama Univ.)  
 Yuuki YOSHITOME (Tokyo Tech.)  
 Kumi INOMATA (Saitama Univ.)

Leo KAGESAWA (Tsukuba Univ.)  
 Hiroki ARAKAWA (Saitama Univ.)  
 Daiki HAMAKAWA (Saitama Univ.)  
 Kento INABA (Kyoto Univ.)  
 Yu TAKAHASHI (Kyoto Univ.)  
 Wenbo DOU (Saitama Univ.)  
 Toshiya KAWAMURA (Toho Univ.)  
 Daisuke KAJIKI (Saitama Univ.)  
 Midori MIWA (Saitama Univ.)  
 Yuta UTSUGI (Tohoku Univ.)  
 Evgeniy MILMAN (Kyungpook National Univ.)  
 Minami INOUE (Tohoku Univ.)  
 Nancy Anne HUPIN (University of Paris-Saclay)  
 Yuya HAMANO (Kyushu Univ.)  
 Yang LIU (Peking Univ.)  
 Shigehito SAKAKI (Kyushu Univ.)  
 Jun FENG (Peking Univ.)  
 Taishi KUBO (Kyushu Univ.)  
 Biao YANG (Peking Univ.)  
 Riku MATSUMURA (Toho Univ.)  
 Zanetti LORENZO (TU Darmstadt)

### Intern

Richard CRANE

### Part-time Worker

Kotaro YAMADA

### Assistants

Emiko ISOGAI

Yuri TSUBURAI

## List of Publications & Presentations

### Publications

#### [Journal]

#### (Original Papers) \*Subject to Peer Review

- S. Adachi, T. Kawabata, K. Minomo, T. Kadoya, N. Yokota, H. Akimune, T. Baba, H. Fujimura, M. Fujiwara, Y. Funaki, T. Furuno, T. Hashimoto, K. Hatanaka, K. Inaba, Y. Ishii, M. Itoh, C. Iwamoto, K. Kawase, Y. Maeda, H. Matsubara, Y. Matsuda, H. Matsuno, T. Morimoto, H. Morita, M. Murata, T. Nanamura, I. Ou, S. Sakaguchi, Y. Sasamoto, R. Sawada, Y. Shimizu, K. Suda, A. Tamii, Y. Tameshige, M. Tsumura, M. Uchida, T. Uesaka, H. P. Yoshida, S. Yoshida, "Systematic analysis of inelastic  $\alpha$  scattering off self-conjugate  $A = 4n$  nuclei," *Phys. Rev. C* **97**, 014601 (2018).
- S. Chebotaryov, S. Sakaguchi, T. Uesaka, T. Akieda, Y. Ando, M. Assie, D. Beaumel, N. Chiga, M. Dozono, A. Galindo-Uribarri, B. Heffron, A. Hirayama, T. Isobe, K. Kaki, S. Kawase, W. Kim, T. Kobayashi, H. Kon, Y. Kondo, Y. Kubota, S. Leblond, H. Lee, T. Lokotko, Y. Maeda, Y. Matsuda, K. Miki, E. Milman, T. Motobayashi, T. Mukai, S. Nakai, T. Nakamura, A. Ni, T. Noro, S. Ota, H. Otsu, T. Ozaki, V. Panin, S. Park, A. Saito, H. Sakai, M. Sasano, H. Sato, K. Sekiguchi, Y. Shimizu, I. Stefan, L. Stuhl, M. Takaki, K. Taniue, K. Tateishi, S. Terashima, Y. Togano, T. Tomai, Y. Wada, T. Wakasa, T. Wakui, A. Watanabe, H. Yamada, Z. Yang, M. Yasuda, J. Yasuda, K. Yoneda, J. Zenihiro, "Proton elastic scattering at 200 A MeV and high momentum transfers of 1.7–2.7 fm<sup>-1</sup> as a probe of the nuclear matter density of <sup>6</sup>He," *Prog. Theor. Exp. Phys.* **2018**, 053D01 (2018).
- A. Corsi, A. Obertelli, P. Doornenbal, F. Nowacki, H. Sagawa, Y. Tanimura, N. Aoi, H. Baba, P. Bednarczyk, S. Boissinot, M. Ciemala, A. Gillibert, T. Isobe, A. Jungclaus, V. Lapoux, J. Lee, K. Matsui, M. Matsushita, T. Motobayashi, D. Nishimura, S. Ota, E. Pollacco, H. Sakurai, C. Santamaria, Y. Shiga, D. Sohler, D. Steppenbeck, S. Takeuchi, R. Taniuchi, H. Wang, "Spectroscopy of nuclei around <sup>100</sup>Sn populated via two-neutron knockout reactions," *Phys. Rev. C* **97**, 044321 (2018).
- M. L. Cortés, P. Doornenbal, M. Dupuis, S. M. Lenzi, F. Nowacki, A. Obertelli, S. Péru, N. Pietralla, V. Werner, K. Wimmer, G. Authalet, H. Baba, D. Calvet, F. Château, A. Corsi, A. Delbart, J. M. Gheller, A. Gillibert, T. Isobe, V. Lapoux, C. Louchart, M. Matsushita, S. Momiyama, T. Motobayashi, M. Niikura, H. Otsu, C. Péron, A. Peyaud, E. C. Pollacco, J. Y. Roussé, H. Sakurai, C. Santamaria, M. Sasano, Y. Shiga, S. Takeuchi, R. Taniuchi, T. Uesaka, H. Wang, K. Yoneda, F. Browne, L. X. Chung, Z. Dombradi, S. Franchoo, F. Giaccoppo, A. Gottardo, K. Hadynska-Klek, Z. Korkulu, S. Koyama, Y. Kubota, J. Lee, M. Lettmann, R. Lozeva, K. Matsui, T. Miyazaki, S. Nishimura, L. Olivier, S. Ota, Z. Patel, E. Sahin, C. M. Shand, P. A. Söderström, I. Stefan, D. Steppenbeck, T. Sumikama, D. Suzuki, Z. Vajta, J. Wu, Z. Xu, "Inelastic scattering of neutron-rich Ni and Zn isotopes off a proton target," *Phys. Rev. C* **97**, 44315 (2018).
- C. Y. Fu, Y. H. Zhang, X. H. Zhou, M. Wang, Y. A. Litvinov, K. Blaum, H. S. Xu, X. Xu, P. Shuai, Y. H. Lam, R. J. Chen, X. L. Yan, T. Bao, X. C. Chen, H. Chen, J. J. He, S. Kubono, D. W. Liu, R. S. Mao, X. W. Ma, M. Z. Sun, X. L. Tu, Y. M. Xing, P. Zhang, Q. Zeng, X. Zhou, W. L. Zhan, S. Litvinov, G. Audi, T. Uesaka, Y. Yamaguchi, T. Yamaguchi, A. Ozawa, B. H. Sun, Y. Sun, F. R. Xu, "Masses of the  $T_z = 3/2$  nuclei <sup>27</sup>P and <sup>29</sup>S," *Phys. Rev. C* **98**, 014315 (2018).

- E. Ha, M. K. Cheoun, H. Sagawa, "Spin singlet and spin triplet pairing correlations on shape evolution in  $sd$ -shell  $N = Z$  nuclei," *Phys. Rev. C* **97**, 24320 (2018).
- E. Ha, M. K. Cheoun, H. Sagawa, W. Y. So, "Neutron-proton pairing correlations and deformation for  $N = Z$  nuclei in the  $pf$  shell within the deformed BCS and Hartree-Fock-Bogoliubov approach," *Phys. Rev. C* **97**, 64322 (2018).
- S. Kawase, T. Uesaka, T. L. Tang, D. Beaumel, M. Dozono, T. Fukunaga, T. Fujii, N. Fukuda, A. Galindo-Uribarri, S. Hwang, N. Inabe, T. Kawabata, T. Kawahara, W. Kim, K. Kisamori, M. Kobayashi, T. Kubo, Y. Kubota, K. Kusaka, C. Lee, Y. Maeda, H. Matsubara, S. Michimasa, H. Miya, T. Noro, Y. Nozawa, A. Obertelli, K. Ogata, S. Ota, E. Padilla-Rodal, S. Sakaguchi, H. Sakai, M. Sasano, S. Shimoura, S. Stepanyan, H. Suzuki, T. Suzuki, M. Takaki, H. Takeda, A. Tamii, H. Tokieda, T. Wakasa, T. Wakui, K. Yako, J. Yasuda, Y. Yanagisawa, R. Yokoyama, K. Yoshida, K. Yoshida, J. Zenihiro, "Exclusive quasi-free proton knockout from oxygen isotopes at intermediate energies," *Prog. Theor. Exp. Phys.* **2018**, 021D01 (2018).
- H. Z. Liang, H. Sagawa, M. Sasano, T. Suzuki, M. Honma, "Gamow-Teller transitions from high-spin isomers in  $N = Z$  nuclei," *Phys. Rev. C* **98**, 14311 (2018).
- X. Y. Liu, Z. Liu, B. Ding, P. Doornenbal, A. Obertelli, S. M. Lenzi, P. M. Walker, L. X. Chung, B. D. Linh, G. Authelet, H. Baba, D. Calvet, F. Château, A. Corsi, A. Delbart, J. M. Gheller, A. Gillibert, T. Isobe, V. Lapoux, M. Matsushita, S. Momiyama, T. Motobayashi, M. Niikura, F. Nowacki, H. Otsu, C. Péron, A. Peyaud, E. C. Pollacco, J. Y. Rousse, H. Sakurai, M. Sasano, Y. Shiga, S. Takeuchi, R. Taniuchi, T. Uesaka, H. Wang, K. Yoneda, Y. H. Lam, T. H. Huang, M. D. Sun, W. Q. Zhang, H. Y. Lu, D. S. Hou, F. Browne, Z. Dombradi, S. Franchoo, F. Giacoppo, A. Gottardo, K. Hadynska-Klek, Z. Korkulu, S. Koyama, Y. Kubota, J. Lee, M. Lettmann, R. Lozeva, K. Matsui, T. Miyazaki, S. Nishimura, C. Louchart, L. Olivier, S. Ota, Z. Patel, E. Sahin, C. Santamaria, C. Shand, P. A. Söderström, G. L. Stefan, D. Steppenbeck, T. Sumikama, D. Suzuki, Z. Vajta, V. Werner, J. Wu, Z. Xu, X. H. Zhou, Y. H. Zhang, H. S. Xu, F. S. Zhang, "Spectroscopy of  $^{65,67}\text{Mn}$ : Strong coupling in the  $N = 40$  island of inversion," *Phys. Lett. B* **784**, 392 (2018).
- A. M. Long, T. Adachi, M. Beard, G. P. A. Berg, M. Couder, R. J. DeBoer, M. Dozono, J. Görres, H. Fujita, Y. Fujita, K. Hatanaka, D. Ishikawa, T. Kubo, H. Matsubara, Y. Namiki, S. O'Brien, Y. Ohkuma, H. Okamura, H. J. Ong, D. Patel, Y. Sakemi, Y. Shimbara, S. Suzuki, R. Talwar, A. Tamii, A. Volya, T. Wakasa, R. Watanabe, M. Wiescher, R. Yamada, J. Zenihiro, " $\alpha$ -unbound levels in  $^{34}\text{Ar}$  from  $^{36}\text{Ar}(p,t)^{34}\text{Ar}$  reaction measurements and implications for the astrophysical  $^{30}\text{S}(\alpha,p)^{33}\text{Cl}$  reaction rate," *Phys. Rev. C* **97**, 054613 (2018).
- Z. -J. Luo, K. Yu, X. -R. Zhou, J. -W. Cui, H. Sagawa, "Effects of deformation, pairing and tensor correlation on the evolution of bubble structure within the Skyrme-Hartree-Fock method," *Eur. Phys. J. A* **54**, 193 (2018).
- S. Michimasa, M. Kobayashi, Y. Kiyokawa, S. Ota, D. S. Ahn, H. Baba, G. P. A. Berg, M. Dozono, N. Fukuda, T. Furuno, E. Ideguchi, N. Inabe, T. Kawabata, S. Kawase, K. Kisamori, K. Kobayashi, T. Kubo, Y. Kubota, C. S. Lee, M. Matsushita, H. Miya, A. Mizukami, H. Nagakura, D. Nishimura, H. Oikawa, H. Sakai, Y. Shimizu, A. Stolz, H. Suzuki, M. Takaki, H. Takeda, S. Takeuchi, H. Tokieda, T. Uesaka, K. Yako, Y. Yamaguchi, Y. Yanagisawa, R. Yokoyama, K. Yoshida, S. Shimoura, "Magic nature of neutrons in  $^{54}\text{Ca}$ : First mass measurements of  $^{55-57}\text{Ca}$ ," *Phys. Rev. Lett.* **121**, 022506 (2018).
- T. Nishi, K. Itahashi, G. P. A. Berg, H. Fujioka, N. Fukuda, N. Fukunishi, H. Geissel, R. S. Hayano, S. Hirenzaki, K. Ichikawa, N. Ikeno, N. Inabe, S. Itoh, M. Iwasaki, D. Kameda, S. Kawase, T. Kubo, K. Kusaka, H. Matsubara, S. Michimasa, K. Miki, G. Mishima, H. Miya, H. Nagahiro, M. Nakamura, S. Noji, K. Okochi, S. Ota, N. Sakamoto, K. Suzuki, H. Takeda, Y. K. Tanaka, K. Todoroki, K. Tsukada, T. Uesaka, Y. N. Watanabe, H. Weick, H. Yamakami, K. Yoshida, "Spectroscopy of pionic atoms in  $^{122}\text{Sn}(d, ^3\text{He})$  reaction and angular dependence of the formation cross sections," *Phys. Rev. Lett.* **120**, 152505 (2018).
- S. Noji, H. Sakai, N. Aoi, H. Baba, G. P. A. Berg, P. Doornenbal, M. Dozono, N. Fukuda, N. Inabe, D. Kameda, T. Kawabata, S. Kawase, Y. Kikuchi, K. Kisamori, T. Kubo, Y. Maeda, H. Matsubara, S. Michimasa, K. Miki, H. Miya, H. Miyasako, S. Sakaguchi, Y. Sasamoto, S. Shimoura, M. Takaki, H. Takeda, S. Takeuchi, H. Tokieda, T. Ohnishi, S. Ota, T. Uesaka, H. Wang, K. Yako, Y. Yanagisawa, N. Yokota, K. Yoshida, R. G. T. Zegers, "Excitation of the isovector spin monopole resonance via the exothermic  $^{90}\text{Zr}(^{12}\text{N}, ^{12}\text{C})$  reaction at 175 MeV/nucleon," *Phys. Rev. Lett.* **120**, 172501 (2018).
- X. Roca-Maza, G. Colò, H. Sagawa, "Nuclear symmetry energy and the breaking of the isospin symmetry: How do they reconcile with each other?," *Phys. Rev. Lett.* **120**, 01002 (2018).
- H. Sagawa, T. Suzuki, "Isoscalar and isovector spin response in  $sd$ -shell nuclei," *Phys. Rev. C* **97**, 054333 (2018).
- C. Santamaria, A. Obertelli, S. Ota, M. Sasano, E. Takada, L. Audirac, H. Baba, D. Calvet, F. Château, A. Corsi, A. Delbart, P. Doornenbal, A. Giganon, A. Gillibert, Y. Kondo, Y. Kubota, C. Lahonde-Hamdoun, V. Lapoux, D. Leboeuf, C. S. Lee, H. N. Liu, M. Matsushita, T. Motobayashi, M. Niikura, M. Kurata-Nishimura, H. Otsu, A. Peyaud, E. C. Pollacco, G. Prono, H. Tokieda, T. Uesaka, J. Zenihiro, "Tracking with the MINOS Time Projection Chamber," *Nucl. Instrum. Methods Phys. Res. A* **905**, 138 (2018).
- Z. Vajta, D. Sohler, Y. Shiga, K. Yoneda, K. Sieja, D. Steppenbeck, Z. Dombrádi, N. Aoi, P. Doornenbal, J. Lee, H. Liu, M. Matsushita, S. Takeuchi, H. Wang, H. Baba, P. Bednarczyk, Z. Fülöp, S. Go, T. Hashimoto, E. Ideguchi, K. Ieki, K. Kobayashi, Y. Kondo, R. Minakata, T. Motobayashi, D. Nishimura, H. Otsu, H. Sakurai, Y. Sun, A. Tamaii, R. Tanaka, Z. Tian, T. Yamamoto, X. Yang, Z. Yang, Y. Ye, R. Yokoyama, J. Zenihiro, "Proton single particle energies next to  $^{78}\text{Ni}$ : Spectroscopy of  $^{77}\text{Cu}$  via single proton knock-out reaction," *Phys. Lett. B* **782**, 99 (2018).
- Y. M. Xing, K. A. Li, Y. H. Zhang, X. H. Zhou, M. Wang, Y. A. Litvinov, K. Blaum, S. Wanajo, S. Kubono, G. Martínez-Pinedo, A. Sieverding, R. J. Chen, P. Shuai, C. Y. Fu, X. L. Yan, W. J. Huang, X. Xu, X. D. Tang, H. S. Xu, T. Bao, X. C. Chen, B. S. Gao, J. J. He, Y. H. Lam, H. F. Li, J. H. Liu, X. W. Ma, R. S. Mao, M. Si, M. Z. Sun, X. L. Tu, Q. Wang, J. C. Yang, Y. J. Yuan, Q. Zeng, P. Zhang, X. Zhou, W. L. Zhan, S. Litvinov, G. Audi, T. Uesaka, Y. Yamaguchi, T. Yamaguchi, A. Ozawa, C. Fröhlich, T. Rauscher, F. K. Thielemann, B. H. Sun, Y. Sun, A. C. Dai, F. R. Xu, "Mass measurements of neutron-deficient Y, Zr, and Nb isotopes and their impact on rp and vp nucleosynthesis processes," *Phys. Lett. B* **781**, 358 (2018).
- Y. H. Zhang, P. Zhang, X. H. Zhou, M. Wang, Y. A. Litvinov, H. S. Xu, X. Xu, P. Shuai, Y. H. Lam, R. J. Chen, X. L. Yan, T. Bao, X. C. Chen, H. Chen, C. Y. Fu, J. J. He, S. Kubono, D. W. Liu, R. S. Mao, X. W. Ma, M. Z. Sun, X. L. Tu, Y. M. Xing, Q. Zeng,

X. Zhou, W. L. Zhan, S. Litvinov, K. Blaum, G. Audi, T. Uesaka, Y. Yamaguchi, T. Yamaguchi, A. Ozawa, B. H. Sun, Y. Sun, F. R. Xu, "Isochronous mass measurements of  $T_z = -1$   $fp$ -shell nuclei from projectile fragmentation of  $^{58}\text{Ni}$ ," *Phys. Rev. C* **98**, 14319 (2018).

### [Proceedings]

- V. P. Ladygin, A. V. Averyanov, E. V. Chernykh, D. Enache, Y. V. Gurchin, A. Y. Isupov, M. Janek, J. T. Karachuk, A. N. Khrenov, D. O. Krivenkov, P. K. Kurilkin, N. B. Ladygina, A. N. Livanov, S. M. Piyadin, S. G. Reznikov, Y. T. Skhomenko, A. A. Terekhin, A. V. Tishevsky, T. Uesaka, "First results on the energy scan of the vector  $A_y$  and tensor  $A_{yy}$  and  $A_{xx}$  analyzing powers in deuteron-proton elastic scattering at nuclotron," in XVII Work. High Energy Spin Phys. "DSPIN-2017," **938**, 12007 (2018).
- M. Lettmann, V. Werner, N. Pietralla, P. Doornenbal, A. Obertelli, T. R. Rodriguez, K. Sieja, G. Authalet, H. Baba, D. Calvet, F. Chateau, S. Chen, A. Corsi, A. Delbart, J. M. Gheller, A. Giganon, A. Gillibert, V. Lapoux, T. Motobayashi, M. Niikura, N. Paul, J. Y. Roussé, H. Sakurai, C. Santamaria, D. Steppenbeck, R. Taniuchi, T. Uesaka, T. Ando, T. Arici, A. Blazhev, F. Browne, A. Bruce, R. J. Carroll, L. X. Chung, M. L. Cortés, M. Dewald, B. Ding, F. Flavigny, S. Franchoo, M. Górska, A. Gottardo, A. Jungclaus, J. Lee, B. D. Linh, J. Liu, Z. Liu, C. Lizarazo, S. Momiyama, K. Moschner, S. Nagamine, N. Nakatsuka, C. Nita, C. R. Nobs, L. Olivier, Z. Patel, Z. Podolyák, M. Rudigier, T. Saito, C. Shand, P. A. Söderström, I. Stefan, V. Vaquero, K. Wimmer, Z. Xu, "Signatures of triaxiality in low-spin spectra of  $^{86}\text{Ge}$ ," in XXII Int. Sch. Nucl. Physics, Neutron Phys. Appl. **1023**, 12023 (2018).
- Y. Niu, G. Colo, E. Vigezzi, C. Bai, Z. Niu, H. Sagawa, "Beyond mean-field description of Gamow-Teller resonances and  $\beta$ -decay," in 12th Int. Spring Semin. Nucl. Phys. Curr. Probl. Prospect. Nucl. Struct. **966**, 12046 (2018).
- H. Sagawa, K. Hagino, "Di-neutron correlations and decay dynamics of nuclei near and beyond drip line," in 12th Int. Spring Semin. Nucl. Phys. Curr. Probl. Prospect. Nucl. Struct. **966**, 12003 (2018).

### Oral Presentations

#### [International Conference etc.]

- T. Uesaka (invited), "Various aspects of nuclear matter studied with direct reactions," International Workshop on New Aspects of Hadron and Nuclear/Astro Physics, Tashkent, Uzbekistan, November 5–10, 2018.
- T. Uesaka (invited), "30-year perspective of experimental nuclear physics at RIBF/RCPN," International Symposium on the paths of nuclear physics from 1950's towards 2020's, Tokyo, Japan, September 23, 2018.
- T. Uesaka (invited), "Congelation of correlated nucleons in nuclei," 20th Northeastern Asian Symposium-2018 on Nuclear Physics in the 21st Century, Nagoya, Japan, September 19–20, 2018.
- T. Uesaka (invited), "Nuclear Double Gamow-Teller Responses—little known aspects of nuclear structure—," 6th Symposium on Neutrinos and Dark Matter in Nuclear Physics 2018, Daejeon, Korea, June 29–July 4, 2018.
- H. Sagawa, "The nuclear symmetry energy and the breaking of the isospin symmetry: How do they reconcile with each other?," 13th International conference on nucleus-nucleus collisions (NN2018), Saitama, Japan, December 4–8, 2018.
- H. Sagawa (invited), "Current topics of spin-isospin response," IVth Topical Workshop on Modern Aspects of in Nuclear Structure, Bormio, Italy, February 2018.
- M. Sasano, "Gamow-Teller Giant Resonance in  $^{132}\text{Sn}$ ," 13th International conference on nucleus-nucleus collisions (NN2018), Saitama, Japan, December 4–8, 2018.
- S. Naimi, "Rare-RI Ring (R3) at RIBF/Riken: Mass measurement of r-process nuclei," Workshop on Nuclear Astrophysics at Rings and Recoil Separators, GSI Darmstadt, Germany, March 2018.
- J. Zenihiro, "Direct determination of neutron skin thickness of  $^{48}\text{Ca}$  via proton elastic scattering," 13th International conference on nucleus-nucleus collisions (NN2018), Saitama, Japan, December 4–8, 2018.
- J. Zenihiro, "Direct determination of neutron skin thickness of  $^{48}\text{Ca}$  from proton elastic scattering and the ESPRI project," Hawaii2018 -Fifth Joint Meeting of the Nuclear Physics Divisions of the APS and JPS, Hawaii, USA, October 2018.
- J. Zenihiro, "New detector design for  $(p, p)$ ,  $(p, pX)$  experiments," SAMURAI Workshop, RIBF week 2018, Saitama, Japan, September 2018.
- J. Zenihiro, "Overview of RIBF," The 17th CNS International Summer School (CNSSS18), Saitama, Japan, August 2018.
- Y. Kubota, "Probing neutron-neutron correlation in  $^{11}\text{Li}$  via the quasi-free  $(p, pn)$  reaction," Hadrons and Nuclear Physics meet ultracold atoms: a French Japanese workshop, Paris, France, January 2018.
- K. Tateishi (invited), "Neutron spin filter based on nuclear polarization technique," Polarised Neutrons for Condensed-Matter Investigations (PNCMI), UK, July 2018.
- J. Gao, "Study of Gamow-Teller transition on  $^{14}\text{Be}$  with PANDORA," 13th International conference on nucleus-nucleus collisions (NN2018), Saitama, Japan, December 4–8, 2018.
- M. Miwa, "Production of n-rich nuclei via 2-proton knockout with deuterium target," 13th International conference on nucleus-nucleus collisions (NN2018), Saitama, Japan, December 4–8, 2018.

#### [Domestic Conference]

- 松田洋平, 「炭素 14 偏極陽子弾性散乱測定の実況」, 日本物理学会第 73 回年次大会, 東京理科大学, 野田, 2018 年 3 月 22–25 日.
- 原田知也, 「大強度イオンビーム用の Xe ガスシンチレーション検出器の開発」, 日本物理学会第 73 回年次大会, 東京理科大学, 野田, 2018 年 3 月 22–25 日.
- 松本翔汰, 「BigRIPS における高精度パイ中間子原子分光・二重 Gamow-Teller 巨大共鳴探索実験に向けた新検出器システムの性能評価 (ii)」, 日本物理学会第 73 回年次大会, 東京理科大学, 野田, 2018 年 3 月 22–25 日.
- 高田秀佐, 「複合核共鳴における時間反転対称性の破れ探索実験のための Triplet-DNP を用いた中性子スピフィルターの開発」, 日本物理学会第 73 回年次大会, 東京理科大学, 野田, 2018 年 3 月 22–25 日.

## Nuclear Science and Transmutation Research Division

### Nuclear Spectroscopy Laboratory

#### 1. Abstract

The research group has conducted nuclear-physics studies utilizing stopped/slowed-down radioactive-isotope (RI) beams mainly at the RIBF facility. These studies are based on the technique of nuclear spectroscopy such as  $\beta$ -ray-detected NMR ( $\beta$ -NMR),  $\gamma$ -PAD (Perturbed Angular Distribution), laser, and Mössbauer among other methods that takes advantage of intrinsic nuclear properties such as nuclear spins, electromagnetic moments, and decay modes. In particular, techniques and devices for the production of spin-controlled RI beams have been developed and combined to the spectroscopic studies, which enable high-sensitivity measurements of spin precessions/resonances through a change in the angular distribution of radiations. Anomalous nuclear structures and properties of far unstable nuclei are investigated from thus determined spin-related observables. The group also aims to apply such techniques to interdisciplinary fields such as fundamental physics and materials science by exploiting nuclear probes.

#### 2. Major Research Subjects

- (1) Nuclear spectroscopy utilizing spin-oriented fast RI beams
- (2) Nuclear/Atomic laser spectroscopy & SLOWRI R&D
- (3) Application of RI probes to materials science
- (4) Fundamental physics: Study of symmetry

#### 3. Summary of Research Activity

##### (1) Nuclear spectroscopy utilizing spin-oriented fast RI beams

Measurements of static electromagnetic nuclear moments over a substantial region of the nuclear chart have been conducted for structure studies on the nuclei far from the  $\beta$ -decay stability. Utilizing nuclear spin orientation phenomena of RIs created in the projectile-fragmentation reaction, ground- and excited-state electromagnetic nuclear moments been determined by means of the  $\beta$ -ray-detected nuclear magnetic resonance ( $\beta$ -NMR) and the  $\gamma$ -ray time differential perturbed angular distribution ( $\gamma$ -TDPAD) methods. In particular, a new method developed for controlling spin in a system of rare RIs, taking advantage of the mechanism of the two-step projectile fragmentation reaction combined with the momentum-dispersion matching technique, has been developed and employed making fully use of world's highest intensity rare RIBs delivered from BigRIPS for rare isotopes.

##### (2) Nuclear/Atomic laser spectroscopy & SLOWRI R&D

The group has been conducting system development for nuclear laser spectroscopy from the following two approaches in order to realize experiments for rare isotopes at RIBF. One is collinear laser spectroscopy for a large variety of elements using slowed-down RI beams produced via a projectile-fragmentation reaction, which can be achieved only by the universal low-energy RI-beam delivery system, SLOWRI, under installation in collaboration with the SLOWRI Team. This slowed-down RI-beam scheme enables to perform high-precision laser spectroscopy even with fast-fragmentation-based RIBs without the elemental limitation problematic in the ISOL-based RIBs.

The other approach is a new method utilizing superfluid helium (He II) as a stopping medium of energetic RI beams, in which the characteristic atomic properties of ions surrounded by superfluid helium enables us to perform unique nuclear laser spectroscopy. RI ions trapped in He II are known to exhibit a characteristic excitation spectrum significantly blue-shifted compared with the emission one. Consequently, the background derived from the excitation-laser stray light, which often causes serious problems in measurements, can be drastically reduced.

##### (3) Application of RI probes to materials science

The application of RI and heavy ion beams as a probe for condensed matter studies is also conducted by the group. The microscopic material dynamics and properties have been investigated through the deduced internal local fields and the spin relaxation of RI probes based on various spectroscopies utilizing RI probes such as  $\beta$ -NMR/NQR spectroscopy, Mössbauer spectroscopy, the  $\gamma$ -ray time differential perturbed angular correlation ( $\gamma$ -TDPAC) spectroscopy. Furthermore, studies on the control of electrical conductivity of diamond by boron and nitrogen implantation are ongoing.

Provided that highly spin-polarized RI probes are produced independently of their element properties and doped into a substance as an impurity, the constituent particle of the substance can be substituted by the same element RI probe without changing the material structure. This scheme provides a new opportunity for materials-science researches, but a key technology, production of element-independent highly spin-polarized RI beams, has not yet been achieved. In this subject, the group has conducted R&D studies to realize an ultra-slow & highly-spin-polarized RI beams, based on the technique of the atomic beam resonance.

##### (4) Fundamental physics: Study of symmetry

The nuclear spins of stable and unstable isotopes sometimes play important roles in fundamental physics research. New experimental methods and devices have been developed for studies of the violation of time reversal symmetry (T-violation) using spin-polarized nuclei. These experiments aim to detect the small frequency shift in the spin precession arising from new mechanisms beyond the Standard Model.

## Members

### Group Director

Hideki UENO

### Research/Technical Scientists

Hiroki YAMAZAKI (Senior Research Scientist)

Yuichi ICHIKAWA (Senior Research Scientist)

Aiko TAKAMINE (Research Scientist)

### Research & Development Scientist

Tetsu SONODA

### Special Postdoctoral Researcher

Tomoya SATO

### Postdoctoral Researcher

Minori TAJIMA

### Junior Research Associate

Keita KAWATA (Univ. of Tokyo)

### International Program Associate

Aleksey GLADKOV (Kyungpook National Univ.)

### Senior Visiting Scientists

Yukari MATSUO (Hosei Univ.)

Hideyuki SAKAI (Univ. of Tokyo)

Takaharu OTSUKA (Univ. of Tokyo)

### Visiting Researcher

Hiroki NISHIBATA (JSPS Fellow)

### Visiting Scientists

Wataru SATO (Kanazawa Univ.)

Kensaku MATSUTA (Osaka Univ.)

Jin NAKAMURA (Univ. of Elec.-Com.)

Satoshi TSUTSUI (JASRI)

Takamasa MOMOSE (Univ. of British Columbia)

Jean-Michel DAUGAS (CEA)

Yoshio KOBAYASHI (Univ. of Elec.-Com.)

Jiro MURATA (Rikkyo Univ.)

Jun MIYAZAKI (Hokuriku Univ.)

Yasuhiro YAMADA (Tokyo Univ. of Science)

Kenya KUBO (International Christian Univ.)

Akihiro YOSHIMI (Okayama Univ.)

Dimiter L. BALABANSKI (IHIN)

Naoki NISHIDA (Tokyo Univ. of Science)

Takeshi INOUE (Tohoku Univ.)

Yoko ISHIBASHI (Tohoku Univ.)

Kei IMAMURA (Okayama Univ.)

Takashi ABE (Univ. of Tokyo)

Deyan T. YORDANOV (IPN Orsay)

Georgi GEORGIEV (CNRS)

Andrew E. STUCHBERY (ANU)

### Student Trainees

Masaomi TANAKA (Osaka Univ.)

Takafumi KAWAGUCHI (Hosei Univ.)

Makoto SANJO (Hosei Univ.)

Wataru KOBAYASHI (Hosei Univ.)

Yasuharu TAKEUCHI (Hosei Univ.)

Tomoaki YADA (Hosei Univ.)

Katsumi TOZUKA (Hosei Univ.)

Takumi ASAKAWA (Hosei Univ.)

Kazuho DOI (Hosei Univ.)

Yusuke SASAKI (Hosei Univ.)

Shota AMAGASA (Tokyo Univ. of Science)

Masanari SEKI (Tokyo Univ. of Science)

Honami ITO (Tokyo Univ. of Science)

Fuminori HATAYAMA (Tokyo Univ. of Science)

Kazuki HAMAZAKI (Tokyo Univ. of Science)

Takumi FUNABASHI (T Tokyo Univ. of Science)

Kenya TAKAHASHI (Univ. of Elec.-Com.)

Yutaro NAKAMURA (Meiji Univ.)

Takatoshi MAEKAWA (International Christian Univ.)

Aiko UCHIYAMA (Tohoku Univ.)

Taichi AKAOKA (Hosei Univ.)

Airi TODA (Hosei Univ.)

Yuika TAKEUCHI (Hosei Univ.)

Ryo TAKEMURA (Tokyo Univ. of Science)

Kyouichi IZUOKA (Tokyo Univ. of Science)

Timothy James GRAY (ANU)

Showen FANG (Univ. of Chicago)

Rafaela GSPONER (ETH Zurich)

### Interns

Dawei GUAN (Peking Univ.)

Yucai MAO (Peking Univ.)

Teng XIANG (Peking Univ.)

Gen LI (Peking Univ.)

Geliang LIU (Peking Univ.)

Seung Hyun PARK (Seoul National Univ.)

Mun Jung JUNG (Seoul National Univ.)

Kyuwon SEO (Seoul National Univ.)

Hyunsoo HA (Seoul National Univ.)  
 Jin NAMKUNG (Seoul National Univ.)  
 Ho Cheong TANG (The Univ. of Hong Kong)  
 Tik Tsun YEUNG (The Univ. of Hong Kong)

Yuen Shan TANG (The Univ. of Hong Kong)  
 Taranjit SINGH (The Univ. of Hong Kong)  
 Qingqing ZHAO (The Univ. of Hong Kong)  
 Kwok Lung FAN (The Univ. of Hong Kong)

### Temporary Staffing

Yuka TAGUCHI

Emiko FUJINO

### Assistant

Izumi YOSHIDA

## List of Publications & Presentations

### Publications

#### [Journal]

#### (Original Papers) \*Subject to Peer Review

- Y. Ito, P. Schury, M. Wada, F. Arai, H. Haba, Y. Hirayama, S. Ishizawa, D. Kaji, S. Kimura, H. Koura, M. MacCormick, H. Miyatake, J. Y. Moon, K. Morimoto, K. Morita, M. Mukai, I. Murray, T. Niwase, K. Okada, A. Ozawa, M. Rosenbusch, A. Takamine, T. Tanaka, Y. X. Watanabe, H. Wollnik, and S. Yamaki, "First mass measurements of nuclides around  $Z = 100$  with a multireflection time-of-flight mass spectrograph," *Phys. Rev. Lett.* **120**, 152501 (2018). \*
- O. B. Tarasov, D. S. Ahn, D. Bazin, N. Fukuda, A. Gade, M. Hausmann, N. Inabe, S. Ishikawa, N. Iwasa, K. Kawata, T. Komatsubara, T. Kubo, K. Kusaka, D. J. Morrissey, M. Ohtake, H. Otsu, M. Portillo, T. Sakakibara, H. Sakurai, H. Sato, B. M. Sherrill, Y. Shimizu, A. Stolz, T. Sumikama, H. Suzuki, H. Takeda, M. Thoennessen, H. Ueno, Y. Yanagisawa, and K. Yoshida, "Discovery of  $^{60}\text{Ca}$  and implications for the stability of  $^{70}\text{Ca}$ ," *Phys. Rev. Lett.* **121**, 022501 (2018). \*
- M. Hase, Y. Ebukuro, H. Kuroe, M. Matsumoto, A. Matsuo, K. Kindo, J. R. Hester, T. J. Sato, and H. Yamazaki, "Erratum: Magnetism of the antiferromagnetic spin-3/2 dimer compound  $\text{CrVMoO}_7$  having an antiferromagnetically ordered state [*Phys. Rev. B* **95**, 144429 (2017)]," *Phys. Rev. B* **98**, 139901 (2018). \*
- B. A. Marsh, T. Day Goodacre, S. Sels, Y. Tsunoda, B. Andel, A. N. Andreyev, N. A. Althubiti, D. Atanasov, A. E. Barzakh, J. Billowes, K. Blaum, T. E. Cocolios, J. G. Cubiss, J. Dobaczewski, G. J. Farooq-Smith, D. V. Fedorov, V. N. Fedosseev, K. T. Flanagan, L. P. Gaffney, L. Ghys, M. Huyse, S. Kreim, D. Lunney, K. M. Lynch, V. Manea, Y. Martinez Palenzuela, P. L. Molkanov, T. Otsuka, A. Pastore, M. Rosenbusch, R. E. Rossel, S. Rothe, L. Schweikhard, M. D. Seliverstov, P. Spagnoletti, C. Van Beveren, P. Van Duppen, M. Veinhard, E. Verstraelen, A. Welker, K. Wendt, F. Wienholtz, R. N. Wolf, A. Zadornaya, K. Zuber, "Characterization of shape-staggering effect in mercury nuclei," *Nat. Phys.* **14**, 1163 (2018). \*
- S. Kimura, Y. Ito, D. Kaji, P. Schury, M. Wada, H. Haba, T. Hashimoto, Y. Hirayama, M. MacCormick, H. Miyatake, J. Y. Moon, K. Morimoto, M. Mukai, I. Murray, A. Ozawa, M. Rosenbusch, H. Schatz, A. Takamine, T. Tanaka, Y. X. Watanabe, H. Wollnik, "Atomic masses of intermediate-mass neutron-deficient nuclei with relative uncertainty down to 35-ppb via multireflection time-of-flight mass spectrograph," *Int. J. Mass Spectrom.* **430**, 134 (2018). \*
- Z. Y. Xu, H. Heylen, K. Asahi, F. Boulay, J. M. Daugas, R. P. de Groote, W. Gins, O. Kamalou, Á. Koszorús, M. Lykiardopoulou, T. J. Mertzimekis, G. Neyens, H. Nishibata, T. Otsuka, R. Orset, A. Poves, T. Sato, C. Stodel, J. C. Thomas, N. Tsunoda, Y. Utsuno, M. Vandebrouck, X. F. Yang, "Nuclear moments of the low-lying isomeric  $1^+$  state of  $^{34}\text{Al}$ : Investigation on the neutron  $1p_{1h}$  excitation across  $N = 20$  in the island of inversion," *Phys. Lett. B* **782**, 619–626 (2018). \*
- K. Imamura, Y. Matsuo, W. Kobayashi, T. Egami, M. Sanjo, A. Takamine, T. Fujita, D. Tominaga, Y. Nakamura, T. Furukawa, T. Wakui, Y. Ichikawa, H. Nishibata, T. Sato, A. Gladkov, L. C. Tao, T. Kawaguchi, Y. Baba, M. Iijima, H. Gonda, Y. Takeuchi, R. Nakazato, H. Odashima, and H. Ueno, "Absolute optical absorption cross-section measurement of Rb atoms injected into superfluid helium using energetic ion beams," *App. Phys. Exp.* **12**, 016502 (2019). \*
- S. Kinbara, H. Ekawa, T. Fujita, S. Hayakawa, S.H. Hwang, Y. Ichikawa, K. Imamura, H. Itoh, H. Kobayashi, R. Murai, K. Nakazawa, M.K. Soe, A. Takamine, A.M.M. Theint, H. Ueno, J. Yoshida, "Charge identification of low-energy particles for double-strangeness nuclei in nuclear emulsion," *Prog. Theor. Exp. Phys.* **2019**, 011H01 (2019). \*
- Y. Ichikawa, H. Nishibata, Y. Tsunoda, A. Takamine, K. Imamura, T. Fujita, T. Sato, S. Momiyama, Y. Shimizu, D. S. Ahn, K. Asahi, H. Baba, D. L. Balabanski, F. Boulay, J. M. Daugas, T. Egami, N. Fukuda, C. Funayama, T. Furukawa, G. Georgiev, A. Gladkov, N. Inabe, Y. Ishibashi, Y. Kobayashi, S. Kojima, A. Kusoglu, T. Kawaguchi, T. Kawamura, I. Mukul, M. Niikura, T. Nishizaka, A. Odahara, Y. Ohtomo, T. Otsuka, D. Ralet, G. S. Simpson, T. Sumikama, H. Suzuki, H. Takeda, L. C. Tao, Y. Togano, D. Tomonaga, H. Ueno, H. Yamazaki and X. F. Yang, "Measurement of the magnetic moment of  $^{75}\text{Cu}$  reveals the interplay between nuclear shell evolution and shape deformation," *Nat. Phys.* **15**, 321–325 (2019). \*
- H. Nishibata, S. Kanaya, T. Shimoda, A. Odahara, S. Morimoto, A. Yagi, H. Kanaoka, M. R. Pearson, C. D. P. Levy, M. Kimura, N. Tsunoda, and T. Otsuka, "Structure of  $^{31}\text{Mg}$ : Shape coexistence revealed by  $\beta$ - $\gamma$  spectroscopy with spin-polarized  $^{31}\text{Na}$ ," *Phys. Rev. C* **99**, 024322 (2019). \*

### Oral Presentations

#### [International Conference etc.]

- Y. Ichikawa, H. Nishibata, Y. Tsunoda, A. Takamine, K. Imamura, T. Fujita, T. Sato, S. Momiyama, Y. Shimizu, D. S. Ahn, K. Asahi, H. Baba, D. L. Balabanski, F. Boulay, J. M. Daugas, T. Egami, N. Fukuda, C. Funayama, T. Furukawa, G. Georgiev, A. Gladkov,

- N. Inabe, Y. Ishibashi, Y. Kobayashi, S. Kojima, A. Kusoglu, T. Kawaguchi, T. Kawamura, I. Mukul, M. Niikura, T. Nishizaka, A. Odahara, Y. Ohtomo, T. Otsuka, D. Ralet, G. S. Simpson, T. Sumikama, H. Suzuki, H. Takeda, L. C. Tao, Y. Togano, D. Tomonaga, H. Ueno, H. Yamazaki and X. F. Yang, “Single-particle states and collective modes: results from magnetic moment measurement of  $^{75\text{m}}\text{Cu}$ ,” 10th International Conference on Direct Reactions with Exotic Beams (DREB2018), Matsue, Japan, June 4–8, 2018.
- H. Nishibata (Invited), T. Shimoda, A. Odahara, S. Morimoto, S. Kanaya, A. Yagi, H. Kanaoka, M. R. Pearson, C. D. P. Levy, M. Kimura, Shape coexistence in  $^{31}\text{Mg}$  revealed by  $\beta$ - and  $\beta$ - $\gamma$  spectroscopy with spin-polarize  $^{31}\text{Na}$ ,” The IX International Symposium on Exotic Nuclei (EXON2018), Petrozavodsk, Russia, September 1–15 (2018).
- A. Takamine (Invited), “Laser spectroscopy project at the SLOWRI facility in RIKEN,” 20th Northeastern Asian Symposium-2018 on Nuclear Physics in the 21st Century, Naogya, Japan, September 18–19 (2018).
- Y. Ichikawa, H. Nishibata, Y. Tsunoda, A. Takamine, K. Imamura, T. Fujita, T. Sato, S. Momiyama, Y. Shimizu, D. S. Ahn, K. Asahi, H. Baba, D. L. Balabanski, F. Boulay, J. M. Daugas, T. Egami, N. Fukuda, C. Funayama, T. Furukawa, G. Georgiev, A. Gladkov, N. Inabe, Y. Ishibashi, Y. Kobayashi, S. Kojima, A. Kusoglu, T. Kawaguchi, T. Kawamura, I. Mukul, M. Niikura, T. Nishizaka, A. Odahara, Y. Ohtomo, T. Otsuka, D. Ralet, G. S. Simpson, T. Sumikama, H. Suzuki, H. Takeda, L. C. Tao, Y. Togano, D. Tomonaga, H. Ueno, H. Yamazaki and X. F. Yang, “Magnetic moment of isomeric state of  $^{75}\text{Cu}$ ,” Fifth Joint Meeting of the Nuclear Physics Divisions of the APS and the JPS (HAWAII2018), Waikoloa, Hawaii, USA, October 23–27 (2018).
- T. Sato (Invited), “Coexisting Xe-129 and Xe-131 masers with active feedback scheme for Xe atomic EDM search,” Fifth Joint Meeting of the Nuclear Physics Divisions of the APS and the JPS (HAWAII2018), Waikoloa, Hawaii, USA, October 23–27 (2018).
- H. Nishibata, S. Kanaya, T. Shimoda, A. Odahara, S. Morimoto, A. Yagi, H. Kanaoka, M. R. Pearson, C. D. P. Levy, M. Kimura, N. Tsunoda, T. Otsuka, “Structure of neutron-rich  $^{31}\text{Mg}$  by  $\beta$ -decay spectroscopy of spin-polarized  $^{31}\text{Na}$ ,” Fifth Joint Meeting of the Nuclear Physics Divisions of the APS and the JPS (HAWAII2018), Waikoloa, Hawaii, USA, October 23–27 (2018).
- A. Gladkov, Y. Ishibashi, H. Yamazaki, Y. Ichikawa, A. Takamine, H. Nishibata, K. Asahi, T. Sato, W. Y. Kim, T. Fujita, L. C. tao, T. Egami, D. Tomonaga, T. Kawaguchi, M. Sanjo, W. Kobayashi, K. Imamura, Y. Nakamura, G. Georgiev, J. M. Daugas, H. Ueno, “ $\beta$ -NMR measurements of the ground-state nuclear moments for  $^{21}\text{O}$ ,” Fifth Joint Meeting of the Nuclear Physics Divisions of the APS and the JPS (HAWAII2018), Waikoloa, Hawaii, USA, October 23–27 (2018).
- K. Kawata, S. Ota, M. Dozono, S. Michimasa, H. Nishibata, C. Iwamoto, N. Kitamura, S. Matsuoka, R. Tsunoda, T. Harada, H. Sakai, N. Imai, K. Yako, T. Sato, “Production of isomers around  $^{52}\text{Fe}$  nucleus via projectile fragmentation,” Fifth Joint Meeting of the Nuclear Physics Divisions of the APS and the JPS (HAWAII2018), Waikoloa, Hawaii, USA, October 23–27 (2018).
- T. Otsuka (Invited), “Quantum self-organization and nuclear collectivity,” Fifth Joint Meeting of the Nuclear Physics Divisions of the APS and the JPS (HAWAII2018), Waikoloa, Hawaii, USA, October 23–27 (2018).
- E. Ideguchi for the CAGRA collaboration, “Study of deformed structure in mass 40 region using CAGRA gamma-ray spectroscopy,” Fifth Joint Meeting of the Nuclear Physics Divisions of the APS and the JPS (HAWAII2018), Waikoloa, Hawaii, USA, October 23–27 (2018).
- S. Iimura, M. Fukutome, M. Hisamitsu, H. Umehara, S. Kanaya, H. Nishibata, A. Odahara, T. Shimoda, T. Hara, M. Kinoshita, T. Nakajima, R. Shudo, R. Wabayashi, “Precision half-life measurement of  $^{18}\text{N}$ ,” Fifth Joint Meeting of the Nuclear Physics Divisions of the APS and the JPS (HAWAII2018), Waikoloa, Hawaii, USA, October 23–27 (2018).
- H. Umehara, S. Iimura, S. Kanaya, H. Nishibata, A. Odahara, T. Shimoda, M. Kinoshita, R. Shudo, R. Nakajima, T. Hara, R. Wakabayashi, “Study of neutron unbound states in  $^{18}\text{O}$  by  $\beta$ -delayed neutron decay of  $^{18}\text{N}$ ,” Fifth Joint Meeting of the Nuclear Physics Divisions of the APS and the JPS (HAWAII2018), Waikoloa, Hawaii, USA, October 23–27 (2018).
- D. Nishimura, M. Fukuda, A. Honma, Y. Ichikawa, A. Kitagawa, K. Matsuta, M. Mihara, T. Ohtsubo, M. Tanaka, S. Sato, “Branching-Ratio Measurements for Superallowed  $\beta$  Emitters at NIRS-HIMAC,” Fifth Joint Meeting of the Nuclear Physics Divisions of the APS and the JPS (HAWAII2018), Waikoloa, Hawaii, USA, October 23–27 (2018).
- M. Rosenbusch, H. Haba, Y. Hirayama, S. Ishizawa, Y. Ito, D. Kaji, S. Kimura, H. Koura, H. Miyatake, J. Y. Moon, K. Morimoto, S. Nishimura, T. Niwase, P. Scurry, A. Takamine, T. Tanaka, H. Ueno, M. Wada, Y. Watanabe, H. Wollnik, “Follow-Ups on Great Achievements: New MRTOF-MS Projects at RIKEN-RIBF,” Fifth Joint Meeting of the Nuclear Physics Divisions of the APS and the JPS (HAWAII2018), Waikoloa, Hawaii, USA, October 23–27 (2018).
- H. Suzuki, K. Yoshida, H. Takeda, Y. Shimizu, D. S. Ahn, T. Sumikama, N. Inabe, T. Kobatsubara, H. Sato, Z. Korkulu, K. Kusaka, Y. Yanagisawa, M. Ohtake, H. Ueno, S. Michimasa, N. Kitamura, K. Kawata, N. Imai, O. B. Tarasov, D. Bazin, T. Kubo, J. Nolen, W. F. Henning, “Production of very neutron-rich Pd isotopes around  $N = 82$  by projectile fragmentation of a RI beam of  $^{132}\text{Sn}$  at 280 MeV/u,” Fifth Joint Meeting of the Nuclear Physics Divisions of the APS and the JPS (HAWAII2018), Waikoloa, Hawaii, USA, October 23–27 (2018).
- S. Kimura, Y. Ito, D. Kaji, P. Schury, M. Wada, H. Haba, T. Hashimoto, Y. Hirayama, M. MacCormick, H. Miyatake, J. Y. Moon, K. Morimoto, M. Mukai, I. Murray, A. Ozawa, M. Rosenbusch, H. Schatz, A. Takamine, T. Tanaka, Y. Watanabe, H. Wollnik, “Atomic masses of intermediate-mass neutron-deficient nuclei with relative uncertainty down to 35-ppb via MRTOF-MS,” Fifth Joint Meeting of the Nuclear Physics Divisions of the APS and the JPS (HAWAII2018), Waikoloa, Hawaii, USA, October 23–27 (2018).
- S. Masuoka, S. Shimoura, M. Takaki, S. Michimasa, S. Ota, M. Dozono, C. Iwamoto, K. Kawata, N. Kitamura, M. Kobayashi, R. Nakajima, H. Tokieda, R. Yokoyama for the SHARAQ 10 collaboration, “Re-measurement of the  $^4\text{He}(^6\text{He}, ^8\text{Be})$  reaction,” Fifth Joint Meeting of the Nuclear Physics Divisions of the APS and the JPS (HAWAII2018), Waikoloa, Hawaii, USA, October 23–27 (2018).
- O. B. Tarasov, D. S. Ahn, D. Bazin, N. Fukuda, A. Gade, M. Hausmann, N. Inabe, S. Ishikawa, N. Iwaza, K. Kawata, T. Komatsubara, T. Kubo, K. Kusaka, D. J. Morrissey, M. Ohtake, H. Otsu, M. Portillo, T. Sakakibara, H. Sakurai, H. Sato, B. M. Sherrill, Y. Shimizu, A. Stolz, T. Sumikama, H. Suzuki, “Discovery of  $^{60}\text{Ca}$ ,” Fifth Joint Meeting of the Nuclear Physics Divisions of the APS and the JPS (HAWAII2018), Waikoloa, Hawaii, USA, October 23–27 (2018).
- T. Abe, P. Maris, T. Miyagi, P. Navratil, T. Otsuka, N. Shimizu, Y. Utsuno, J. P. Vary, T. Yoshida, “Recent results and implications

- of no-core MCSM calculations for nuclear structure,” Fifth Joint Meeting of the Nuclear Physics Divisions of the APS and the JPS (HAWAII2018), Waikoloa, Hawaii, USA, October 23–27 (2018).
- N. Tsunoda, T. Otsuka, N. Shimizu, K. Takayanagi, M. Hjorth-Jense, T. Suzuki, “Study of neutron-rich nuclei via nuclear force and microscopic theory,” Fifth Joint Meeting of the Nuclear Physics Divisions of the APS and the JPS (HAWAII2018), Waikoloa, Hawaii, USA, October 23–27 (2018).
- S. Yoshida, N. Shimizu, T. Togashi, T. Otsuka, “Uncertainty quantification in nuclear shell-model calculations,” Fifth Joint Meeting of the Nuclear Physics Divisions of the APS and the JPS (HAWAII2018), Waikoloa, Hawaii, USA, October 23–27 (2018).
- T. Suzuki, T. Otsuka, N. Tsunoda, “Structure of neutron-rich carbon isotopes: shell evolution and two-neutron-halo at the dripline,” Fifth Joint Meeting of the Nuclear Physics Divisions of the APS and the JPS (HAWAII2018), Waikoloa, Hawaii, USA, October 23–27 (2018).
- A. Takamine (Invited), “Prospects for laser spectroscopy project at the SLOWRI facility in RIKEN RIBF,” 2018 KPS Fall Meeting, Changwon, Korea, October 24–26 (2018).
- T. Sato (Invited), “Atomic EDM searches in RIKEN,” The 10th China-Japan Joint Nuclear Physics Symposium (CJNP2018), Huizhou, China, November 18–23 (2018).
- H. Ueno (Invited), “R&D of spin-controlled RI beams,” The 10th China-Japan Joint Nuclear Physics Symposium (CJNP2018), Huizhou, China, November 18–23 (2018).
- M. Tajima (Invited), “Laser spectroscopy of RI beams at the SLOWRI facility of RIKEN,” The 10th China-Japan Joint Nuclear Physics Symposium (CJNP2018), Huizhou, China, November 18–23 (2018).
- T. Otsuka (Invited), “Messages from nuclear masses on the quantum phase transitions and the quantum self-organization,” The 10th China-Japan Joint Nuclear Physics Symposium (CJNP2018), Huizhou, China, November 18–23 (2018).
- Y. Ichikawa, H. Nishibata, Y. Tsunoda, A. Takamine, K. Imamura, T. Fujita, T. Sato, S. Momiyama, Y. Shimizu, D. S. Ahn, K. Asahi, H. Baba, D. L. Balabanski, F. Boulay, J. M. Daugas, T. Egami, N. Fukuda, C. Funayama, T. Furukawa, G. Georgiev, A. Gladkov, N. Inabe, Y. Ishibashi, Y. Kobayashi, S. Kojima, A. Kusoglu, T. Kawaguchi, T. Kawamura, I. Mukul, M. Niihara, T. Nishizaka, A. Odahara, Y. Ohtomo, T. Otsuka, D. Ralet, G. S. Simpson, T. Sumikama, H. Suzuki, H. Takeda, L. C. Tao, Y. Togano, D. Tomonaga, H. Ueno, H. Yamazaki and X. F. Yang, “Magnetic moment of  $^{75m}\text{Cu}$  measured with highly spin-aligned beam,” 13th International Conference on Nucleus-Nucleus Collisions (NN2018), Omiya, Saitama, Japan, December 4–8 (2018).
- H. Yamazaki, A. Gladkov, Y. Ishibashi, Y. Ichikawa, A. Takamine, H. Nishibata, K. Asahi, T. Sato, W. Y. Kim, T. Fujita, L. C. tao, T. Egami, D. Tominaga, T. Kawaguchi, M. Sanjo, W. Kobayashi, K. Imamura, Y. Nakamura, G. Georgiev, J. M. Daugas, H. Ueno, “ $\beta$ -NMR/NQR spectroscopy as a local probe of condensed matter,” Technical Meeting on Novel Multidisciplinary Applications with Unstable Ion Beams and Complementary Techniques, Vienna, Austria, December 10–14 (2018).
- Y. Ichikawa (Invited), “Nuclear magnetic dipole moments measured with spin-oriented RI beams at RIKEN RIBF,” The International Conference on HYPERFINE Interactions and Applications (HYPERFINE 2019), Goa, India, February 10–15 (2019).
- T. Sato (Invited), “ $^{129}\text{Xe}/^{131}\text{Xe}$  double-species spin maser for Xe-EDM search,” The 11th International Workshop on Fundamental Physics Using Atoms (FPUA2019), Okinawa, Japan, March 1–4 (2019).

#### [Domestic Conference]

- 高峰愛子 (招待講演), 「高偏極 RI ビームの生成と核・物質科学研究への応用」, 新学術領域研究「宇宙観測検出器と量子ビームの出会い。新たな応用への架け橋。」キックオフシンポジウム, 仙台, 2018年12月17–18日。
- 高峰愛子, Marco Rosenbusch, 和田道治, Peter Schury, Jun-young Moon, 園田哲, 小島隆夫, 渡邊裕, 片山一郎, 上野秀樹, 石山博恒, 「理研 RIBF SLOWRI 施設における RF イオンガイドガスセル開発」, 日本物理学会第 74 回年次大会, 福岡, 2019年3月14–17日。
- 小林航, 今村慧, 三條真, 藤田朋美, 高峰愛子, 古川武, 上野秀樹, 松尾由賀利, 「超流動ヘリウム中 Ag 原子に対する二重共鳴分光実験」, 日本物理学会第 74 回年次大会, 福岡, 2019年3月14–17日。
- 三條真, 今村慧, 小林航, 竹内由衣花, 高峰愛子, 古川武, 上野秀樹, 松尾由賀利, 「超流動ヘリウム中 Rb 原子の超微細構造間隔測定のための観測原子数補正システム」, 日本物理学会第 74 回年次大会, 福岡, 2019年3月14–17日。
- 西畑洸希 (招待講演), 「偏極 Na ビームで探る中性子過剰原子核  $^{30}\text{Mg}$ ,  $^{31}\text{Mg}$  の多様な原子核構造」, 日本物理学会第 74 回年次大会, 福岡, 2019年3月14–17日。
- 大塚孝治 (招待講演), 「計算核物理の展望」, 日本物理学会第 74 回年次大会, 福岡, 2019年3月14–17日。
- 田島美典, 「Development of offline ion source for collinear laser spectroscopy of RI beams」, 第 10 回停止・低速 RI ビームを用いた核分光研究会 (10th SSRI), 福岡, 2019年3月18–19日。
- 市川雄一, 「不安定核の核スピン偏極・整列生成について」, 第 10 回停止・低速 RI ビームを用いた核分光研究会 (10th SSRI), 福岡, 2019年3月18–19日。
- 川田敬太, 「Production of isomer around  $^{52}\text{Fe}$  nucleus via projectile fragmentation」, 第 10 回停止・低速 RI ビームを用いた核分光研究会 (10th SSRI), 福岡, 2019年3月18–19日。
- 西畑洸希, 「スピン整列ビームを用いた核モーメント測定と核分光研究への応用」, 第 10 回停止・低速 RI ビームを用いた核分光研究会 (10th SSRI), 福岡, 2019年3月18–19日。

## Nuclear Science and Transmutation Research Division High Energy Astrophysics Laboratory

### 1. Abstract

In the immediate aftermath of the Big Bang, the beginning of our universe, only hydrogen and helium existed. However, nuclear fusion in the interior of stars and the explosion of supernovae in the universe over 13.8 billion years led to the evolution of a world brimming with the many different elements we have today. By using scientific satellites or balloons to observe X-rays and gamma-rays emitted from celestial objects, we are observing the synthesis of the elements at their actual source. Our goal is to comprehensively elucidate the scenarios for the formation of the elements in the universe, together with our research on sub-atomic physics through the use of an accelerator.

### 2. Major Research Subjects

- (1) Nucleosynthesis in stars, supernovae, and neutron star mergers
- (2) Plasma and vacuum in extremely strong magnetism and gravity
- (3) Research and development of innovative X-ray and gamma-ray detectors

### 3. Summary of Research Activity

High Energy Astrophysics Laboratory started in April 2010. The goal of our research is to reveal the mechanism of nucleosynthesis and the evolution of elements in the universe, and to observe/discover exotic physical phenomena in extremely strong magnetic and/or gravitational fields. We have observed supernova remnants, strongly magnetized neutron stars, pulsars, black holes and galaxies with X-ray astronomical satellites, balloons and ground-based telescopes.

#### (1) Nucleosynthesis in the universe

##### (1-1) ASTRO-H/Hitomi

The 6th Japanese X-ray satellite ASTRO-H/Hitomi was launched in February 2016. Hitomi carried four X-ray and gamma-ray detectors covering the 0.3–600 keV energy range. We, in collaboration with JAXA (Japan Aerospace Exploration Agency), Tokyo Metropolitan University, Kanazawa University, Saitama University, NASA/GSFC etc., contributed to the soft X-ray spectrometer (SXS), which achieves unprecedented energy resolution ( $<7$  eV) in the 0.3–12 keV energy band with a low temperature micro calorimeter. Although we were supposed to discover many previously-unknown elemental lines in universe and measured abundance of those elements with SXS, Hitomi was unfortunately lost by an accident in March 2016. A recovery mission of Hitomi (named XRISM) was started in 2017 and is now under construction for launch in 2021.

##### (1-2) MAXI

From April 2018, High Energy Astrophysics Laboratory hosts MAXI (Monitor of All-sky X-ray Image) onboard International Space Station (ISS), which was attached on ISS in 2009. MAXI is a RIKEN-lead project collaborating with JAXA and other universities. Since MAXI scans X-ray all-sky in 90 minutes, many transient objects including neutron star or blackhole binaries are found. All of the data are going to public soon after they are taken, and almost all of the groups in high-energy phenomena rely on the MAXI data. In 2018, we issued 34 alerts as ATEL (Astronomer's Telegram) and 5 new blackhole candidates were found. To detect counterparts of neutron star merger events (*i.e.* gravitational wave events), we have prepared an automatic searching system and keep watching all-sky.

##### (1-3) Astrophysical Data Analysis

In parallel with the mission development/operations, we performed data analysis.

- We proved that the abundance ratios of the iron-peak elements in the Perseus cluster were consistent with the solar abundance. In previous studies, overabundance of Cr, Mn, and Ni are reported, but Hitomi's high spectroscopic data denied the overabundance. The inter-galactic medium of the nearby cluster has similar abundance pattern of our galaxy.
- We have detected a mysterious hump in the spectrum of the neutronstar low-mass X-ray binary, Aquila X-1. The hump can be interpreted as a recombination-edge of heavy elements (Cd) which were possibly produced by rp-process in X-ray bursts on the neutron star surface.

#### (2) Extremely strong magnetism and gravity

We have contributed to the NASA's world-first X-ray polarimeter mission IXPE (Imaging X-ray Polarimeter Explorer). High Energy Astrophysics Laboratory is responsible for providing the gas electron multipliers (GEMs) to the IXPE mission: the GEM is a key device of the X-ray polarimeter and produced based on our patent for space use. The IXPE satellite will be launched in 2021, and we have already provided the flight qualified GEMs to the project in FY2018.

By using the IXPE mission, we aim to proof the strong magnetism of Magnetars, which are one of the species of neutron stars which have ultra-strong magnetic field  $B > 10^{11}$  T. In such ultra-strong magnetic field, higher-order diagrams,  $O(eB/m^2)$ ,  $O(eB/m^2)^2$  etc., never eliminated in the QED perturbation theory. As the results, we observe newly-emerging phenomenon such as vacuum polarization, vacuum birefringence, etc. If such exotic phenomena are detected, we sure that Magnetars have really ultra-strong magnetic field.

**(3) Innovative X-ray and gamma-ray detectors**

In collaboration with NASA Goddard Space Flight Center, we have developed and tested a hard X-ray polarimeter with a Time Projection Chamber technique. This TPC polarimeter is one of candidates of the future satellite XPP (X-ray polarimeter Probe mission) planned with an international consortium.

**Members****Group Director**

Toru TAMAGAWA

**Research/Technical Scientist**

Tatehiro MIHARA (Senior Research Scientist)

**Contract Researcher**

Takao KITAGUCHI

**Special Postdoctoral Researchers**

Toshio NAKANO

Shin'ya Nakashima

Liyi GU

**Junior Research Associate**

Ryo SASAKI (Chuo Univeristy)

**Visiting Researcher**

Asami HAYATO (JSPS Fellow)

**Visiting Scientists**

Tomoki KIMURA (Tohoku University)

Hirokazu ODAKA (Univeristy of Tokyo)

Yukikatsu TERADA (Saitama Univeristy)

Motohide KOKUBUN (ISAS/JAXA)

Masaki WAKABAYASHI (Jakulin Commercial Company LC)

Aya BAMBA (University of Tokyo)

Naohisa INADA (National Institute of Tech., Nara College)

Rohta TAKAHASHI (Tomakomai Nat'l College of Tech.)

Toru MISAWA (Shinshu Univeristy)

Yoko TAKEUCHI (TIRI)

Satoru KATSUDA (Saitama Univeristy)

Shin'ya YAMADA (Tokyo Metropolitan University)

Yujin NAKAGAWA (JAMSTEC)

Teruaki ENOTO (Kyoto University)

Kazuki KOMIYA (TIRI)

Hirofumi NODA (Tohoku Univeristy)

Yuki OKURA (NAOJ)

Yuzuru TAWARA (Nagoya Univeristy)

Ikuyuki MITSUISHI (Nagoya Univeristy)

Harufumi TSUCHIYA (JAEA)

**Student Trainees**

Megu KUBOTA (Tokyo University of Science)

Yuuki WADA (University of Tokyo)

Naoto MURATA (Tokyo University of Science)

Sonoe ODA (Tokyo University of Science)

Yuanhui ZHOU (Tokyo University of Science)

Miho OKUBO (Tokyo University of Science)

Takaya WAKAMATSU (Tokyo University of Science)

Marina TSUTSUMI (Tokyo University of Science)

Keisuke UCHIYAMA (Tokyo University of Science)

Kento ADACHI (Tokyo University of Science)

**List of Publications & Presentations****Publications****[Journal]****(Original Papers) \*Subject to Peer Review**

M. Kubota, T. Tamagawa, K. Makishima, T. Nakano, W. Iwakiri, M. Sugizaki, K. Ono, "An enigmatic hump around 30 keV in Suzaku spectra of Aquila X-1 in the hard state," *Publ. Astron. Soc. Jpn.* **71**, 148 (2019). \*

The Hitomi collaboration, "Detection of polarized gamma-ray emission from the Crab nebula with the Hitomi Soft Gamma-ray Detector," *Publ. Astron. Soc. Jpn.* **70**, 118 (2018). \*

M. Kubota, H. Odaka, T. Tamagawa, T. Nakano, "Discovery of redshifted He-like iron absorption line from luminous accreting neutron star SMC X-1," *Astrophys. J. Lett.* **868**, L26 (2018). \*

O' Dell, L. Stephen *et al.*, "The imaging X-ray polarimetry explorer (IXPE): technical overview," *Proceedings of the SPIE* **106991**, 106991X (2018).

M. Tashiro *et al.*, "Concept of the X-ray astronomy recovery mission," *Proceedings of the SPIE* **10699**, 1069922 (2018).

The Hitomi collaboration, "Hitomi X-ray observation of the pulsar wind nebula G21.5-0.9," *Publ. Astron. Soc. Jpn.* **70**, 027 (2018). \*

Y. Wada, G. S. Bowers, T. Enoto, M. Kamogawa, Y. Nakamura, T. Morimoto, D. M. Smith, Y. Furuta, K. Nakazawa, T. Yuasa, A. Matsuki, M. Kubo, T. Tamagawa, K. Makishima, H. Tsuchiya, "Termination of electron acceleration in thundercloud by intracloud/intercloud discharge," *Geophys. Res. Lett.* **45**, 5700–5707 (2018). \*

- T. Takahashi *et al.*, “Hitomi (ASTRO-H) X-ray Astronomy Satellite,” *J. Astron. Telesc. Instrum. Syst.* **4**, 21402 (2018). \*
- M. Tsujimoto, K. Morihana, T. Hayashi, T. Kitaguchi, “Suzaku and NuSTAR X-ray spectroscopy of  $\gamma$  Cassiopeiae and HD 110432,” *Publ. Astron. Soc. Jpn.* **70**, 109 (2018). \*
- B. W. Grefenstette, W. R. Cook, F. A. Harrison, T. Kitaguchi, K. K. Madsen, H. Miyasaka, S. N. Pike, “Pushing the limits of NuSTAR detectors,” *Proceedings of the SPIE* **10709**, 107092 V (2018).
- H. Tajima *et al.*, “Design and performance of Soft Gamma-ray Detector onboard the Hitomi (ASTRO-H) satellite,” *J. Astron. Telesc. Instrum. Syst.* **4**, 21411 (2018). \*
- S. Nakahira, M. Shidatsu, K. Makishima, Y. Ueda, K. Yamaoka, T. Mihara, H. Negoro, T. Kawase, N. Kawai, K. Morita, “Discovery and state transitions of the new Galactic black hole candidate MAXI J1535-571,” *Publ. Astron. Soc. Jpn.* **70**, 95 (2018). \*
- F. Yatabe, K. Makishima, T. Mihara, M. Nakajima, M. Sugizaki, S. Kitamoto, Y. Yoshida, T. Takagi, “An application of the Ghosh & Lamb model to the accretion-powered X-ray pulsar X Persei,” *Publ. Astron. Soc. Jpn.* **70**, 89 (2018). \*
- T. Kawamuro, Y. Ueda, M. Shidatsu, T. Hori, M. Morii, S. Nakahira, N. Isobe, N. Kawai, T. Mihara, M. Matsuoka, T. Morita, M. Nakajima, H. Negoro, S. Oda, T. Sakamoto, M. Serino, M. Sugizaki, A. Tanimoto, H. Tomida, Y. Tsuboi, H. Tsunemi, S. Ueno, K. Yamaoka, S. Yamada, A. Yoshida, W. Iwakiri, Y. Kawakubo, Y. Sugawara, S. Sugita, Y. Tachibana, T. Yoshii, “The 7-year MAXI/GSC X-ray source catalog in the high Galactic latitude sky (3MAXI),” *Astrophys. J. Suppl. Ser.* **238**, 32 (2018). \*
- S. Sugita, N. Kawai, S. Nakahira, H. Negoro, M. Serino, T. Mihara, K. Yamaoka, M. Nakajima, “MAXI upper limits of the electromagnetic counterpart of GW170817,” *Publ. Astron. Soc. Jpn.* **70**, 70 (2018). \*
- K. Yoshida, D. Yonetoku, M. Arimoto, T. Sawano, Y. Kagawa, M. Ina, K. Ota, D. Suzuki, K. Miyao, S. Watanabe, T. Mihara, Y. Takao, H. Ikeda, S. Yagitani, Y. Kasahara, T. Imachi, T. Kita, K. Kawagoshi, H. Segawa, T. Nakashima, T. Minamoto, K. Kyutoku, “Kanazawa-SAT3: micro-satellite mission for monitoring x-ray transients coincide with gravitational wave events,” *Proceedings of the SPIE* **10699**, 1069962 (2018).
- M. Takahashi, Y. Inome, S. Yoshii, A. Bamba, S. Gunji, D. Hadasch, M. Hayashida, H. Katagiri, Y. Konno, H. Kubo, J. Kushida, D. Nakajima, T. Nakamori, T. Nagayoshi, K. Nishijima, S. Nozaki, D. Mazin, S. Mashuda, R. Mirzoyan, H. Ohoka, R. Orito, T. Saito, S. Sakurai, J. Takeda, M. Teshima, Y. Terada, F. Tokanai, T. Yamamoto, T. Yoshida, “A technique for estimating the absolute gain of a photomultiplier tube,” *Nucl. Instrum. Methods Phys. Res. A* **894**, 1 (2018). \*
- K. Nakazawa *et al.*, “Hard x-ray imager onboard Hitomi (ASTRO-H),” *J. Astron. Telesc. Instrum. Syst.* **4**, 21410 (2018). \*
- K. Hagino *et al.*, “In-orbit performance and calibration of the Hard X-ray Imager onboard Hitomi (ASTRO-H),” *J. Astron. Telesc. Instrum. Syst.* **4**, 21409 (2018). \*
- A. Simionescu, S. Nakashima, H. Yamaguchi, K. Matsushita, F. Mernier, N. Werner, T. Tamura, K. Nomoto, J. de Plaa, S. -C. Leung, A. Bamba, E. Bulbul, M. E. Eckart, Y. Ezoe, A. C. Fabian, Y. Fukazawa, L. Gu, Y. Ichinohe, M. N. Ishigaki, J. S. Kaastra, C. Kilbourne, T. Kitayama, M. Leutenegger, M. Loewenstein, Y. Maeda, E. D. Miller, R. F. Mushotzky, H. Noda, C. Pinto, F. S. Porter, S. Safi-Harb, K. Sato, T. Takahashi, S. Ueda, S. Zha, “Constraints on the chemical enrichment history of the Perseus Cluster of galaxies from high-resolution X-ray spectroscopy,” *Mon. Not. R. Astron. Soc.* **483**, 1701–1721 (2019). \*
- H. Yamaguchi, T. Tanaka, D. R. Wik, J. Rho, A. Bamba, D. Castro, R. K. Smith, A. R. Foster, H. Uchida, R. Petre, B. J. Williams, “Evidence for rapid adiabatic cooling as an origin of the recombining plasma in the supernova remnant W49B revealed by NuSTAR observations,” *Astrophys. J. Lett.* **868**, L35 (2018). \*
- T. Kasuga, T. Sato, K. Mori, H. Yamaguchi, A. Bamba, “Asymmetric expansion of the Fe ejecta in Kepler’s supernova remnant,” *Publ. Astron. Soc. Jpn.* **70**, 88 (2018). \*
- S. Nakashima, Y. Inoue, N. Yamasaki, Y. Sofue, J. Kataoka, K. Sakai, “Spatial distribution of the Milky Way hot gaseous halo constrained by Suzaku X-ray observations,” *Astrophys. J.* **862**, 34 (2018). \*
- M. Akita, J. Kataoka, M. Arimoto, Y. Sofue, T. Totani, Y. Inoue, S. Nakashima, “Diffuse X-ray emission from the northern arc of loop i observed with Suzaku,” *Astrophys. J.* **862**, 88 (2018). \*
- M. Katsuragawa, S. Nakashima, H. Matsumura, T. Tanaka, H. Uchida, S. -H. Lee, Y. Uchiyama, M. Arakawa, T. Takahashi, “Suzaku X-ray observations of the mixed-morphology supernova remnant CTB 1,” *Publ. Astron. Soc. Jpn.* **70**, 110 (2018). \*
- F. Fraschetti, S. Katsuda, T. Sato, J. R. Jokipii, J. Giacalone, “Vortical amplification of the magnetic field at an inward shock of supernova remnant Cassiopeia A,” *Phys. Rev. Lett.* **120**, 251101 (2018). \*
- L. Gu, J. Mao, J. de Plaa, A. J. J. Raassen, C. Shah, J. S. Kaastra, “Charge exchange in galaxy clusters,” *Astronomy & Astrophysics* **611**, A26 (2018). \*
- J. Mao, J. de Plaa, J. S. Kaastra, C. Pinto, L. Gu, F. Mernier, H. -L. Yan, Y. -Y. Zhang, H. Akamatsu, “Nitrogen abundance in the X-ray halos of clusters and groups of galaxies,” *Astronomy & Astrophysics* **621**, A9 (2019). \*
- F. Mernier, N. Werner, J. de Plaa, J. S. Kaastra, A. J. J. Raassen, L. Gu, J. Mao, I. Urdampilleta, A. Simionescu, “Solar chemical composition in the hot gas of cool-core ellipticals, groups, and clusters of galaxies,” *Mon. Not. R. Astron. Soc.* **480**, L95 (2018). \*
- F. Mernier, J. de Plaa, N. Werner, J. S. Kaastra, A. J. J. Raassen, L. Gu, J. Mao, I. Urdampilleta, N. Truong, A. Simionescu, “Mass-invariance of the iron enrichment in the hot haloes of massive ellipticals groups, and clusters of galaxies,” *Mon. Not. R. Astron. Soc.* **478**, L116 (2018). \*
- T. Akahori, Y. Kato, K. Nakazawa, T. Ozawa, L. Gu, M. Takizawa, Y. Fujita, H. Nakanishi, N. Okabe, K. Makishima, “ATCA 16 cm observation of CIZA J1358.9-4750: Implication of merger stage and constraint on non-thermal properties,” *Publ. Astron. Soc. Jpn.* **70**, 53 (2018). \*

## Oral Presentations

### [International Conference etc.]

- T. Tamagawa, (Invited), "Imaging X-ray polarimeter explorer (IXPE)," New Eyes on X-ray Astronomical Objects with Japanese and Chinese Observatories, Sagami-hara, Japan, November 19, 2018.
- S. Nakashima, K. Matsushita, XARM pre-project team, "Status of the XARM mission," The eROSITA Consortium Meeting, Garching, Germany, April 24, 2018.
- S. Nakashima, J. Kataoka, M. Akita, Y. Inoue, Y. Soufe, N. Yamasaki, K. Sakai, "X-ray & Gamma-ray observations of the Fermi bubbles," Frontier Research in Astrophysics-III Mondello Workshop 2018, Palermo, Italy, May 29, 2018.
- S. Nakashima, on behalf of the Hitomi collaboration, "Highlights of the Hitomi X-ray observatory," Frontier Research in Astrophysics-III Mondello Workshop 2018, Palermo, Italy, May 30, 2018.
- T. Sato, "Kinematical asymmetries and their interpretations in Kepler's supernova remnant and Cassiopeia A," Shocking Supernovae: surrounding interactions and unusual events, Stockholm, Sweden, May 28, 2018.
- L. Gu, "Atomic data and plasma code needed for XRISM and Athena," AtomDB Workshop 2018, CfA, Cambridge, USA, November 1, 2018.
- L. Gu, "Results from the Hitomi satellite," X-ray Astronomy workshop 2018, Bonn, Germany, June 24, 2018.
- L. Gu, "Atomic data and plasma code for future X-ray spectroscopy," RIKEN Workshop on Atomic Physics 2018, Wako, Japan, May 30, 2018.

### [Domestic Conference]

- 内田和海, 「南極周回気球による硬 X 線偏光観測ミッション X-Calibur の現状と今後」, 日本天文学会 2018 年秋季年会, 姫路, 2018 年 9 月 19-21 日.
- 三石郁之, 「X 線偏光観測衛星 IXPE への参加現状 (2)」, 日本天文学会 2018 年秋季年会, 姫路, 2018 年 9 月 19-21 日.
- 二村泰介, 「X 線偏光観測衛星 IXPE 搭載 X 線望遠鏡用受動型熱制御素子サーマルシールドの開発 (3)」, 日本天文学会 2018 年秋季年会, 姫路, 2018 年 9 月 19-21 日.
- 小田苑会, 「ブラックホール X 線連星 MAXI J1828-249 の X 線および可視光観測」, 日本天文学会 2018 年秋季年会, 姫路, 2018 年 9 月 19-21 日.
- 窪田恵, 「大質量 X 線連星 SMC X-1 から的高電離鉄吸収線の発見とその起源」, 日本天文学会 2018 年秋季年会, 姫路, 2018 年 9 月 19-21 日.
- 澤野達哉, 「重力波源 X 線対応天体探査計画 Kanazawa-SAT3 フライトモデル製作状況 (2)」, 日本天文学会 2018 年秋季年会, 姫路, 2018 年 9 月 19-21 日.
- 鈴木大智, 「超小型衛星搭載広視野 X 線撮像検出器の撮像性能評価」, 日本天文学会 2018 年秋季年会, 姫路, 2018 年 9 月 19-21 日.
- 渡辺彰汰, 「超小型衛星搭載ガンマ線検出器試作モデルの評価」, 日本天文学会 2018 年秋季年会, 姫路, 2018 年 9 月 19-21 日.
- 根来均, 「X線新星 MAXI J1727-203 の発見と MAXI/GSC が検出した 2018 年度前半の突発現象」, 日本天文学会 2018 年秋季年会, 姫路, 2018 年 9 月 19-21 日.
- 中島基樹, 「MAXI, Swift, RXTE による X 線連星パルサー GS 1843-02 の軌道位相に依存した X 線スペクトル変動」, 日本天文学会 2018 年秋季年会, 姫路, 2018 年 9 月 19-21 日.
- 大枝幹, 「Be/X 線連星パルサー Swift J0243.6+6124 の Eddington 光度近傍における X 線スペクトル, パルス波形の変化」, 日本天文学会 2018 年秋季年会, 姫路, 2018 年 9 月 19-21 日.
- 岩切渉, 「MAXI-NICER 連携 (MANGA) による巨大恒星フレアの軟 X 線観測」, 日本天文学会 2018 年秋季年会, 姫路, 2018 年 9 月 19-21 日.
- 北口貴雄, 「機械学習を用いた飛跡画像処理による光電子追跡型 X 線偏光計の感度向上」, 日本物理学会秋季大会, 松本, 2018 年 9 月 14-17 日.
- 澤野達哉, 「重力波対応 X 線突発天体探査超小型衛星計画 Kanazawa-SAT3 における X 線撮像検出器フライトモデル開発状況」, 日本物理学会秋季大会, 松本, 2018 年 9 月 14-17 日.
- 高尾祐介, 「Kanazawa-SAT3 ガンマ線バースト用ガンマ線検出器」, 日本物理学会秋季大会, 松本, 2018 年 9 月 14-17 日.
- 玉川 徹, 「X 線偏光観測衛星 IXPE」, 第 15 回 MPGD 研究会, 京都, 2018 年 12 月 14-15 日.
- 内山慶祐, 「IXPE 衛星搭載用 GEM の製作と性能評価」, 第 15 回 MPGD 研究会, 京都, 2018 年 12 月 14-15 日.
- 武内陽子, 「LTCC-GEM の加工精度の測定」, 第 15 回 MPGD 研究会, 京都, 2018 年 12 月 14-15 日.
- 石崎欣尚, 「X 線分光撮像衛星 (XRISM) 搭載 Resolve の開発状況」, 宇宙科学シンポジウム, 相模原, 2019 年 1 月 9-10 日.
- 早藤麻美, 「X 線偏光観測衛星 IXPE 搭載に向けた偏光計用ガス電子増幅フォイルの開発」, 宇宙科学シンポジウム, 相模原, 2019 年 1 月 9-10 日.
- 高橋弘充, 「硬 X 線集光偏光計 X-Calibur 気球実験の 2018 年フライトと将来計画」, 宇宙科学シンポジウム, 相模原, 2019 年 1 月 9-10 日.
- 水野恒史, 「X 線偏光観測衛星 IXPE」, 宇宙科学シンポジウム, 相模原, 2019 年 1 月 9-10 日.
- 三石郁之, 「X 線偏光観測衛星 IXPE 搭載に向けた望遠鏡用サーマルシールドの開発」, 宇宙科学シンポジウム, 相模原, 2019 年 1 月 9-10 日.
- 田村啓輔, 「南極周回気球による硬 X 線偏光観測実験 X-Calibur の 2021 年将来フライトへ向けて」, 日本天文学会 2019 年春季年会, 小金井, 2019 年 3 月 14-17 日.
- 高橋弘充, 「硬 X 線偏光観測実験 X-Calibur の 2018-2019 年気球フライトに向けた準備状況」, 日本天文学会 2019 年春季年会,

- 小金井, 2019 年 3 月 14-17 日.
- 三石郁之, 「X 線偏光観測衛星 IXPE への参加現状 (3)」, 日本天文学会 2019 年春季年会, 小金井, 2019 年 3 月 14-17 日.
- 清水貞行, 「X 線偏光観測衛星 IXPE 搭載 X 線望遠鏡用受動型熱制御素子サーマルシールドの開発 (4)」, 日本天文学会 2019 年春季年会, 小金井, 2019 年 3 月 14-17 日.
- 楊冲, 「XMM 衛星データを用いた MCXCJ0157.4-0550 の 2 次元温度密度構造の解析 2」, 日本天文学会 2019 年春季年会, 小金井, 2019 年 3 月 14-17 日.
- 榎戸輝揚, 「さそり座 X-1 の X 線モニタリングに特化した超小型衛星プロジェクト構想」, 日本天文学会 2019 年春季年会, 小金井, 2019 年 3 月 14-17 日.
- 林多佳由, 「強磁場激変星反射 X 線モデルの V1223 Sagittarii への適用」, 日本天文学会 2019 年春季年会, 小金井, 2019 年 3 月 14-17 日.
- 佐々木亮, 「MAXI-NICER 連携 (MANGA) による RS CVn 型星 GT Mus の巨大フレア観測」, 日本天文学会 2019 年春季年会, 小金井, 2019 年 3 月 14-17 日.
- 杉崎睦, 「重力波に対応した X 線放射の監視観測のための MAXI の運用状況」, 日本天文学会 2019 年春季年会, 小金井, 2019 年 3 月 14-17 日.
- 李晋, 「Lobster Eye 光学系の GEANT4 シミュレーション」, 日本天文学会 2019 年春季年会, 小金井, 2019 年 3 月 14-17 日.
- 澤野達哉, 「重力波源 X 線対応天体探査計画 Kanazawa-SAT3 フライトモデル製作状況 (3)」, 日本天文学会 2019 年春季年会, 小金井, 2019 年 3 月 14-17 日.
- 浅井和美, 「中性子星低質量 X 線連星の長期変動について」, 日本天文学会 2019 年春季年会, 小金井, 2019 年 3 月 14-17 日.
- 根来均, 「X 線新星 MAXI J1810-222 の発見と MAXI/GSC が検出した 2018 年度後半の突発現象」, 日本天文学会 2019 年春季年会, 小金井, 2019 年 3 月 14-17 日.
- 河合誠之, 「マグネター XTE J1810-197 の突発 X 線増光の MAXI による発見と NuSTAR によるフォローアップ」, 日本天文学会 2019 年春季年会, 小金井, 2019 年 3 月 14-17 日.
- 岩切渉, 「RXTE 衛星が捉えた X 線バースター EXO 1745-248 のスーパーバースト終了直後の強い輝線構造」, 日本天文学会 2019 年春季年会, 小金井, 2019 年 3 月 14-17 日.
- 和田有希, 「雷活動に由来するガンマ線の観測プロジェクト: 多地点観測の進展と大気電場・電波との協同観測」, 日本物理学会第 74 回年次大会, 伊都, 2019 年 3 月 14-17 日.
- 小高裕和, 「明るい降着型パルサー SMC X-1 から的高電離鉄吸収線の発見とその解釈」, 日本物理学会第 74 回年次大会, 伊都, 2019 年 3 月 14-17 日.
- 玉川徹, 「X 線偏光観測衛星 IXPE: プロジェクト概要と進捗」, 日本物理学会第 74 回年次大会, 伊都, 2019 年 3 月 14-17 日.
- 郡司修一, 「X 線偏光観測衛星 IXPE でのブラックホール観測における解析手法の研究」, 日本物理学会第 74 回年次大会, 伊都, 2019 年 3 月 14-17 日.
- 高橋弘充, 「硬 X 線集光偏光計 X-Calibur 気球実験の 2018 年フライトと将来計画」, 日本物理学会第 74 回年次大会, 伊都, 2019 年 3 月 14-17 日.
- 大久保美穂, 「高エネルギー X 線の偏光を検出する Time Projection Chamber 型偏光計の開発」, 日本物理学会第 74 回年次大会, 伊都, 2019 年 3 月 14-17 日.
- 窪田めぐ, 「Aquila X-1 「すざく」 スペクトルにおける 30 keV 付近の未解明なハンプ構造」, 日本物理学会第 74 回年次大会, 伊都, 2019 年 3 月 14-17 日.

## Nuclear Science and Transmutation Research Division Superheavy Element Research Group

### 1. Abstract

The elements with their atomic number  $Z > 103$  are called as trans-actinide or superheavy elements. This group has been studying the physical and chemical properties of superheavy elements. They must be produced by artificially for the scientific study utilizing the accelerators in RIBF. Two teams lead the study of the superheavy elements. Superheavy Element Production Team studies various methods of efficient production of the superheavy elements and their physical and chemical properties. Superheavy Element Device Development Team develops the main experimental device, *i.e.*, the gas-filled recoil ion separator, GARIS.

The synthesis of elements having atomic numbers over 119 will be attempted with the aim of establishing nuclear synthesis technology that reaches the “island of stability” where the lifetime of atomic nuclei is expected to be prolonged significantly. With the aim of constructing an ultimate nuclear model, maximum utilization will be made of key experimental devices which become fully operational in order to conduct research for the syntheses of element 119 and 120.

### 2. Major Research Subjects

Superheavy Element Production Team

- (1) Searching for new elements
- (2) Spectroscopic study of the nucleus of heavy elements
- (3) Chemistry of superheavy elements
- (4) Study of a reaction mechanism for fusion process

Superheavy Element Device Development Team

- (5) Maintenance of GARIS, GARIS-II and development of new gas-filled recoil ion separator GARIS-III
- (6) Maintenance and development of detector and DAQ system for GARIS, GARIS-II and GARIS-III
- (7) Maintenance and development of target system for GARIS, GARIS-II and GARIS-III

### 3. Summary of Research Activity

#### (1) Searching for new elements

To expand the periodic table of elements and the nuclear chart, we will search for new elements.

#### (2) Spectroscopic study of the nucleus of heavy elements

Using the high sensitivity system for detecting the heaviest element, we plan to perform a spectroscopic study of nuclei of the heavy elements.

#### (3) Chemistry of superheavy elements

Study of chemistry of the trans-actinide (superheavy element) has just started world-wide, making it a new frontier in the field of chemistry. Relativistic effects in chemical property are predicted by many theoretical studies. We will try to develop this new field.

#### (4) Study of a reaction mechanism for fusion process

Superheavy elements have been produced by complete fusion reaction of two heavy nuclei. However, the reaction mechanism of the fusion process is still not well understood theoretically. When we design an experiment to synthesize nuclei of the superheavy elements, we need to determine a beam-target combination and the most appropriate reaction energy. This is when the theory becomes important. We will try to develop a reaction theory useful in designing an experiment by collaborating with the theorists.

#### (5) Research Highlight

The discovery of a new element is one of the exciting topics both for nuclear physicists and nuclear chemists. The elements with their atomic number  $Z > 103$  are called as trans-actinides or superheavy elements. The chemical properties of those elements have not yet been studied in detail. Since those elements do not exist in nature, they must be produced by artificially, by using nuclear reactions for the study of those elements. Because the production rate of atoms of those elements is extremely small, an efficient production and collection are key issues of the superheavy research. In our laboratory, we have been trying to produce new elements, studying the physical and chemical properties of the superheavy elements utilizing the accelerators in RIKEN.

Although the Research Group for Superheavy element has started at April 2013, the Group is a renewal of the Superheavy Element Laboratory started at April 2006, based on a research group which belonged to the RIKEN accelerator research facility (RARF), and had studied the productions of the heaviest elements. The main experimental apparatus is a gas-filled recoil ion separator GARIS. The heaviest elements with their atomic numbers, 107 (Bohrium), 108 (Hassium), 109 (Meitnerium), 110 (Darmstadtium), 111 (Roentgenium), and 112 (Copernicium) were discovered as new elements at Helmholtzzentrum für Schwerionenforschung GmbH (GSI), Germany by using  $^{208}\text{Pb}$  or  $^{209}\text{Bi}$  based complete fusion reactions, so called “cold fusion” reactions. We have made independent confirmations of the productions of isotopes of 108th, 110th, 111th, and 112th elements by using the same reactions performed at GSI. After these work, we observed an isotope of the 113th element,  $^{278}\text{113}$ , in July 2004, in April, 2005, and in August 2012. The isotope,  $^{278}\text{113}$ , has both the largest atomic number, ( $Z = 113$ ) and atomic mass number ( $A = 278$ ) which have determined experimentally among the isotopes which have been produced by cold fusion reactions. We could show the world highest sensitivity for production and detection of the superheavy elements by these observations. Our results that related to  $^{278}\text{113}$  has been recognized as a discovery

of new element by a Joint Working Party of the International Union of Pure and Applied Chemistry (IUPAC) and International Union of Pure and Applied Physics (IUPAP). Finally, we named the 113th element as “Nihonium.”

We decided to make one more recoil separator GARIS-II, which has an acceptance twice as large as existing GARIS, in order to realize higher sensitivity. The design of GARIS-II has finished in 2008. All fabrication of the separator will be finished at the end of fiscal year 2008. It has been ready for operation after some commissioning works.

Preparatory work for the study of the chemical properties of the superheavy elements has started by using the gas-jet transport system coupled to GARIS. The experiment was quite successful. The background radioactivity of unwanted reaction products has been highly suppressed. Without using the recoil separator upstream the gas-jet transport system, large amount of unwanted radioactivity strongly prevents the unique identification of the event of our interest. This new technique makes clean and clear studies of chemistry of the heaviest elements promising.

The spectroscopic study of the heaviest elements has started by using alpha spectrometry. New isotope,  $^{263}\text{Hs}$  ( $Z = 108$ ), which has the smallest atomic mass number ever observed among the Hassium isotopes, had discovered in the study. New spectroscopic information for  $^{264}\text{Hs}$  and its daughters have obtained also. The spectroscopic study of Rutherfordium isotope  $^{261}\text{Rf}$  ( $Z = 104$ ) has done and 1.9-s isomeric state has directly produced for the first time.

Preparatory works for the study of the new superheavy elements with atomic number 119 and 120 have started in 2013. We measured the reaction products of the  $^{248}\text{Cm}(^{48}\text{Ca}, \text{xn})^{296-x}\text{Lv}$  ( $Z = 116$ ) previously studied by Frelöv Laboratory of Nuclear Reaction, Russia, and GSI. We observed 5 isotopes in total which tentatively assigned to  $^{293}\text{Lv}$ , and  $^{292}\text{Lv}$ .

## Members

### Group Director

Kosuke MORITA

### Visiting Scientist

Kunihiro FUJITA (Kyushu Univ.)

## List of Publications & Presentations

### Oral Presentations

#### [International Conference etc.]

K. Morita, “Present Status and Perspectives of SHE Researches at RIKEN,” 13th International Conference on Nucleus-Nucleus Collisions (NN2018), Ohmiya, Saitama, Japan, December 4, 2018.

#### [Others]

森田浩介, 周期表 150 年記念シンポジウム, 「第 113 番新元素ニホニウムの発見」, 学術会議講堂, 2019 年 2 月 23 日.

森田浩介, 「新元素の探索」, 鹿児島中央高等学校 SSH, 鹿児島中央高校体育館, 2018 年 9 月 4 日.

## Nuclear Science and Transmutation Research Division

### Superheavy Element Research Group

### Superheavy Element Production Team

#### 1. Abstract

The elements with atomic number  $Z > 103$  are called as trans-actinide or superheavy elements (SHEs). Superheavy Element Production Team investigates synthesis of SHEs, nuclear properties of SHE nuclei, and chemical properties of SHEs mainly in collaboration with Superheavy Element Devise Development Team and Nuclear Chemistry Research Team of RIKEN Nishina Center.

#### 2. Major Research Subjects

- (1) Search for new superheavy elements
- (2) Decay spectroscopy of the heaviest nuclei
- (3) Study of reaction mechanisms for production of the heaviest nuclei
- (4) Study of chemical properties of the heaviest elements

#### 3. Summary of Research Activity

##### (1) Search for new superheavy elements

In November, 2016, the 7th period of the periodic table was completed with the official approval of four new elements, nihonium (Nh, atomic number  $Z = 113$ ), moscovium (Mc,  $Z = 115$ ), tennessine (Ts,  $Z = 117$ ), and oganesson (Og,  $Z = 118$ ) by IUPAC. We have started to search for new elements to expand the chart of the nuclides toward to the island of stability and the periodic table of the elements toward the 8th period of the periodic table. Since June, 2017, RIKEN heavy-ion Linear ACcelerator (RILAC) has been shut down for its upgrade until the end of 2019. During this long-term break, to continue SHE studies at RIBF, we moved GAs-filled Recoil Ion Separator II (GARIS II) from the irradiation room of RILAC to the E6 room of RIKEN Ring Cyclotron (RRC). In December 2017, the RRC + GARIS II setup became ready for SHE studies. We first conducted the commissioning of the RRC + GARIS II setup in the  $^{nat}\text{La} + ^{51}\text{V}$ ,  $^{159}\text{Tb} + ^{51}\text{V}$ , and  $^{208}\text{Pb} + ^{51}\text{V}$  reactions. Then, we started to search for new element, element 119 in the  $^{248}\text{Cm} + ^{51}\text{V}$  reaction in January, 2018.

##### (2) Decay spectroscopy of the heaviest nuclei

We measured precision masses of  $^{63}\text{Cu}$ ,  $^{64-66}\text{Zn}$ ,  $^{65}\text{Ga}$ ,  $^{65-67}\text{Ge}$ ,  $^{67}\text{As}$ ,  $^{78,81}\text{Br}$ ,  $^{80}\text{Rb}$ ,  $^{79}\text{Sr}$ ,  $^{210-214}\text{Ac}$ ,  $^{210-214}\text{Ra}$ ,  $^{246}\text{Es}$ ,  $^{251}\text{Fm}$ ,  $^{249-252}\text{Md}$ , and  $^{254}\text{No}$  using a multireflection time-of-flight mass spectrograph coupled to GARIS II at RILAC mainly in collaboration with High Energy Accelerator Research Organization.

##### (3) Study of reaction mechanisms for production of the heaviest nuclei

SHE nuclei have been produced by complete fusion reactions of two heavy nuclei. However, the reaction mechanism of the fusion process is still not well understood both theoretically and experimentally. In collaboration with Kyushu Univ., we measured excitation functions for the quasielastic scattering of the  $^{208}\text{Pb} + ^{48}\text{Ca}$ ,  $^{208}\text{Pb} + ^{50}\text{Ti}$ ,  $^{238}\text{U} + ^{48}\text{Ca}$ ,  $^{248}\text{Cm} + ^{22}\text{Ne}$ ,  $^{248}\text{Cm} + ^{26}\text{Mg}$ ,  $^{248}\text{Cm} + ^{30}\text{Si}$ ,  $^{248}\text{Cm} + ^{34}\text{S}$ ,  $^{248}\text{Cm} + ^{40}\text{Ar}$ ,  $^{248}\text{Cm} + ^{48}\text{Ca}$ , and  $^{248}\text{Cm} + ^{50}\text{Ti}$  reactions using GARIS at RILAC. The quasielastic barrier distributions were successfully extracted for these systems, and compared with coupled-channels calculations. It was found that the results can be utilized to locate the optimal energy for the future searches for undiscovered superheavy nuclei.

##### (4) Study of chemical properties of the heaviest elements

Chemical characterization of newly-discovered SHEs ( $Z \geq 104$ ) is an extremely interesting and challenging subject in modern nuclear and radiochemistry. In collaboration with Nuclear Chemistry Research Team of RIKEN Nishina Center, we are developing SHE production systems as well as rapid single-atom chemistry apparatuses for chemistry studies of SHEs. We installed a gas-jet transport system to the focal plane of GARIS at RILAC. This system is a promising approach for exploring new frontiers in SHE chemistry: the background radiations from unwanted products are strongly suppressed, the intense primary heavy-ion beam is absent in the gas-jet chamber, and hence the high gas-jet extraction yield is attained. Furthermore, the beam-free conditions make it possible to investigate new chemical systems. We have been developing an ultra-rapid gas-chromatograph apparatus at the focal plane of GARIS. This apparatus consists of an RF carpet gas cell and a cryo-gas-chromatograph column with Si detector array. For the aqueous chemistry of SHEs, we have been developing a flow solvent extraction apparatus which consists of a continuous dissolution apparatus, a flow extraction apparatus, and a liquid scintillation counter.

#### Members

##### Team Leader

Hiromitsu HABA

**Research/Technical Scientist**

Daiya KAJI

**Junior Research Associate**

Taiki TANAKA

**Visiting Scientists**

Satoshi ADACHI (Kyushu Univ.)

Marc ASFARI (Institut Pluridisciplinaire Hubert Curien)

Olivier DORVAUX (Institut Pluridisciplinaire Hubert Curien)

Satoshi SAKAGUCHI (Kyushu Univ.)

Mirei TAKEYAMA (Yamagata Univ.)

Benoit Jean-Paul GALL (Strasbourg Univ.)

Masaomi TANAKA (Kyushu Univ.)

Zaiguo GAN (Institute of Modern Physics)

Huabin YANG (Institute of Modern Physics)

Shintaro GO (Kyushu Univ.)

Zhiyuan ZHANG (Institute of Modern Physics)

Hiroyuki KOURA (Japan Atomic Energy Agency)

**Student Trainees**

Takeshi HIRANO (Kyushu Univ.)

Natsuki NAITO (Kyushu Univ.)

Takahiro HIRAKAWA (Kyushu Univ.)

Toshitaka NIWASE (Kyushu Univ.)

Kieran KESSACI (Strasbourg Univ.)

Kazuya SHIRASAKA (Kyushu Univ.)

Shun MITSUOKA (Kyushu Univ.)

Yoshihide SUEKAWA (Kyushu Univ.)

Ikuto MURAKAMI (Kyushu Univ.)

**List of Publications & Presentations****Publications****[Journal]****(Original Papers) \*Subject to Peer Review**

- M. Rosenbusch, Y. Ito, P. Schury, M. Wada, D. Kaji, K. Morimoto, H. Haba, S. Kimura, H. Koura, M. MacCormick, H. Miyatake, J. Y. Moon, K. Morita, I. Murray, T. Niwase, A. Ozawa, M. Reponen, A. Takamine, T. Tanaka, H. Wollnik, "New mass anchor points for neutron-deficient heavy nuclei from direct mass measurements of radium and actinium isotopes," *Phys. Rev. C* **97**, 064306 1–8 (2018).\*
- Y. Ito, P. Schury, M. Wada, F. Arai, H. Haba, Y. Hirayama, S. Ishizawa, D. Kaji, S. Kimura, H. Koura, M. MacCormick, H. Miyatake, J. Y. Moon, K. Morimoto, K. Morita, M. Mukai, I. Murray, T. Niwase, K. Okada, A. Ozawa, M. Rosenbusch, A. Takamine, T. Tanaka, Y. X. Watanabe, H. Wollnik, S. Yamaki, "First direct mass measurements of nuclides around  $Z = 100$  with a multireflection time-of-flight mass spectrograph," *Phys. Rev. Lett.* **120**, 152501 1–6 (2018).\*
- S. Kimura, Y. Ito, D. Kaji, P. Schury, M. Wada, H. Haba, T. Hashimoto, Y. Hirayama, M. MacCormicke, H. Miyatake, J. Y. Moon, K. Morimoto, M. Mukai, I. Murray, A. Ozawa, M. Rosenbusch, H. Schatz, A. Takamine, T. Tanaka, Y. X. Watanabe, H. Wollnik, "Atomic masses of intermediate-mass neutron-deficient nuclei with relative uncertainty down to 35-ppb via multireflection time-of-flight mass spectrograph," *Int. J. Mass Spectrom.* **430**, 134–142 (2018).\*
- K. Morita, K. Morimoto, D. Kaji, H. Haba, H. Kudo, "Discovery of new element, nihonium, and perspectives," *Prog. Nucl. Sci. Technol.* **5**, 8–13 (2018).\*
- L. Lens, A. Yakushev, C. E. Düllmann, M. Asai, J. Ballof, M. Block, H. M. David, J. Despotopulos, A. D. Nitto, K. Eberhardt, J. Even, M. Götz, S. Götz, H. Haba, L. Harkness-Brennan, F. P. Heßberger, R. D. Herzberg, J. Hoffmann, A. Hübner, E. Jäger, D. Judson, J. Khuyagbaatar, B. Kindler, Y. Komori, J. Konki, J. V. Kratz, J. Krier, N. Kurz, M. Laatiaoui, S. Lahiri, B. Lommel, M. Maiti, A. K. Mistry, C. Mokry, K. Moody, Y. Nagame, J. P. Omtvedt, P. Papadakis, V. Pershina, J. Runke, M. Schädel, P. Scharrer, T. Sato, D. Shaughnessy, B. Schausten, P. Thörle-Pospiech, N. Trautmann, K. Tsukada, J. Uusitalo, A. Ward, M. Wegrzecki, N. Wiehl, V. Yakusheva, "Online chemical adsorption studies of Hg, Tl, and Pb on SiO<sub>2</sub> and Au surfaces in preparation for chemical investigations on Cn, Nh, and Fl at TASCA," *Radiochim. Acta* **106**, 949–962 (2018).\*
- T. Tanaka, K. Morita, "Optimum incident energy for new element search," *AAPPS (Association of Asia Pacific Physical Societies) Bulletin* **28**, 28–30 (2018).
- H. Haba, "A new period in superheavy-element hunting," *Nat. Chem.* **11**, 10–13 (2019).\*
- A. Yokoyama, Y. Kitayama, Y. Fukuda, H. Kikunaga, M. Murakami, Y. Komori, S. Yano, H. Haba, K. Tsukada, A. Toyoshima, "Extraction behavior of rutherfordium as a cationic fluoride complex with a TTA chelate extractant from HF/HNO<sub>3</sub> acidic solutions," *Radiochim. Acta* **107**, 27–32 (2019).\*
- Y. Wang, S. Cao, J. Zhang, F. Fan, J. Yang, H. Haba, Y. Komori, T. Yokokita, K. Morimoto, D. Kaji, Y. J. Wittwer, R. Eichler, A. Türler, Z. Qin, "The study of rhenium pentacarbonyl complexes using single-atom chemistry in gas phase," *Phys. Chem. Chem. Phys.* **21**, 7147–7154 (2019).\*
- I. Tsekhanovich, A. N. Andreyev, K. Nishio, D. Denis-Petit, K. Hirose, H. Makii, Z. Matheson, K. Morimoto, K. Morita, W. Nazarewicz, R. Orlandi, J. Sadhukhan, T. Tanaka, M. Vermeulen, M. Warda, "Observation of the competing fission modes in <sup>178</sup>Pt," *Phys. Lett. B* **790**, 583–588 (2019).\*
- 羽場宏光, 「GARIS が拓く超重元素の化学—106 番元素シーボーギウムのカルボニル錯体の合成—」, *Radioisotopes* **67**, 527–535 (2018).\*
- 羽場宏光, 「超重元素の合成—原子番号 113 以降の超重元素の合成と発見—」, *Radioisotopes* **67**, 277–289 (2018).\*

- 田中泰貴, 森田浩介, 「新元素探索の最適な入射エネルギー」, 日本物理学会誌 **73**, 234–235 (2018).
- 羽場宏光, 「ニホニウムはいかにして誕生したのか 1. 元素の発見と周期表」, 現代化学 **4**, No. 565, 34–37 (2018).
- 羽場宏光, 「ニホニウムはいかにして誕生したのか 2. 同位体と核図表」, 現代化学 **5**, No. 566, 18–21 (2018).
- 羽場宏光, 「ニホニウムはいかにして誕生したのか 3. 人工元素」, 現代化学 **6**, No. 567, 44–48 (2018).
- 羽場宏光, 「ニホニウムはいかにして誕生したのか 4. 幻の新元素」, 現代化学 **7**, No. 568, 36–39 (2018).
- 羽場宏光, 「ニホニウムはいかにして誕生したのか 5. 超重元素」, 現代化学 **8**, No. 569, 40–43 (2018).
- 羽場宏光, 「ニホニウムはいかにして誕生したのか 6. 理研の新元素探索 (1)」, 現代化学 **9**, No. 570, 24–28 (2018).
- 羽場宏光, 「ニホニウムはいかにして誕生したのか 7. 理研の新元素探索 (2)」, 現代化学 **10**, No. 571, 53–57 (2018).
- 羽場宏光, 「ニホニウムはいかにして誕生したのか 8. 理研の新元素探索 (3)」, 現代化学 **11**, No. 572, 25–28 (2018).
- 羽場宏光, 「ニホニウムはいかにして誕生したのか 9. ロシアと米国による新元素探索」, 現代化学 **12**, No. 573, 52–56 (2018).
- 羽場宏光, 「ニホニウムはいかにして誕生したのか 10. ニホニウム命名」, 現代化学 **1**, No. 574, 44–49 (2019).
- 羽場宏光, 「ニホニウムはいかにして誕生したのか 11. さらなる新元素を求めて」, 現代化学 **2**, No. 575, 42–46 (2019).
- 羽場宏光, 「ニホニウムはいかにして誕生したのか 12. 新元素の化学的性質」, 現代化学 **3**, No. 576, 42–46 (2019).

**(Proceedings)**

- Y. Aritomo, N. Liyana, S. Tanaka, Y. Miyamoto, B. Yanagi, K. Hagino, T. Tanaka, K. Nishio, M. Ohta, “Estimation for synthesis of superheavy elements,” JPS Conf. Proc. **23**, 013001 1–4 (2018).

**[Book]****(Original Paper)**

- 桜井弘, 根矢三郎, 寺嶋孝仁, 笹森貴裕, 羽場宏光, 「元素検定 2」, 化学同人, 2018 年 8 月 20 日.

**Oral Presentations****[International Conference etc.]**

- H. Haba, “Production and applications of radioisotopes at RIKEN RI Beam Factory,” Seminar at Brookhaven National Laboratory, New York, USA, May, 2018.
- H. Haba, “Synthesis and chemistry of superheavy elements at RIKEN,” DAE-BRNS Eighth Biennial Symposium on Emerging Trends in Separation Science and Technology (SESTEC-2018), Goa, India, May, 2018.
- H. Haba, “Production and applications of radioisotopes at RIKEN RI Beam Factory,” Seminar at Inter-University Accelerator Centre, New Delhi, India, May, 2018.
- H. Haba, “Applications with unstable ion beams and complementary techniques at the RIKEN,” Consultancy Meeting on Novel Multidisciplinary Applications with Unstable Ion Beams and Complementary Techniques, Vienna, Austria, July, 2018.
- H. Haba, “Present Status and perspectives of SHE researches at RIKEN,” IX International Symposium on Exotic Nuclei (EXON-2018), Petrozavodsk, Russia, September, 2018.
- Y. Ito, P. Schury, M. Wada, F. Arai, H. Haba, Y. Hirayama, S. Ishizawa, D. Kaji, S. Kimura, H. Koura, M. MacCormick, H. Miyatake, J. Y. Moon, K. Morimoto, K. Morita, M. Mukai, I. Murray, T. Niwase, K. Okada, A. Ozawa, M. Rosenbusch, A. Takamine, T. Tanaka, Y. X. Watanabe, H. Wollnik, S. Yamaki, “Direct mass measurements of heavy/superheavy nuclei with an MRTOF-MS coupled with the GARIS-II,” The International Conference on Electromagnetic Isotope Separators and Related Topics (EMIS) 2018, Geneva, Switzerland, September, 2018.
- M. Rosenbusch, Y. Ito, M. Wada, P. Schury, F. Arai, H. Haba, Y. Hirayama, S. Ishizawa, D. Kaji, S. Kimura, H. Koura, M. MacCormick, H. Miyatake, J. Y. Moon, K. Morimoto, K. Morita, M. Mukai, I. Murray, T. Niwase, K. Okada, A. Ozawa, A. Takamine, T. Tanaka, Y. X. Watanabe, H. Wollnik, S. Yamaki, “Advances and future plans for nuclear mass measurements at RIKEN,” The International Conference on Electromagnetic Isotope Separators and Related Topics (EMIS) 2018, Geneva, Switzerland, September, 2018.
- M. Mukai, Y. Hirayama, Y. X. Watanabe, P. Schury, M. Ahmed, H. Haba, H. Ishiyama, S. C. Jeong, Y. Kakiguchi, S. Kimura, J. Y. Moon, M. Oyaizu, A. Ozawa, J. H. Park, H. Ueno, M. Wada, H. Miyatake, “Development of a multi-segmented proportional gas counter for  $\beta$ -decay spectroscopy at KISS,” The International Conference on Electromagnetic Isotope Separators and Related Topics (EMIS) 2018, Geneva, Switzerland, September, 2018.
- T. Tanaka, K. Morita, K. Morimoto, D. Kaji, H. Haba, R. A. Boll, N. T. Brewer, S. Van Cleve, D. J. Dean, S. Ishizawa, Y. Ito, Y. Komori, K. Nishio, T. Niwase, B. C. Rasco, J. B. Roberto, K. P. Rykaczewski, H. Sakai, D. W. Stracener, K. Hagino, “Fusion dynamics for hot fusion reactions revealed in quasielastic fusion barrier distributions,” JPS-APS Joint meeting on Nuclear Physics Division, Hawaii, U.S.A., October, 2018.
- H. Haba, “Production of radioisotopes for application studies at RIKEN RI Beam Factory,” 4th International Conference on Application of RadiotraCers and Energetic Beams in Sciences (ARCEBS-2018), Kolkata, India, November, 2018.
- Y. Komori, H. Haba, T. Yokokita, S. Yano, N. Sato, K. Ghosh, Y. Sakemi, H. Kawamura, “Measurement of excitation functions of the  $^{206/207/208}\text{Pb}(^{11}\text{B}, \text{X})^{212}\text{Fr}$  reactions and complex formation studies of Fr with crown ethers,” 4th International Conference on Application of RadiotraCers and Energetic Beams in Sciences (ARCEBS-2018), Kolkata, India, November, 2018.
- H. Haba, “Production and application of radioisotopes using He jet transport system at RIKEN RI Beam Factory,” Seminar at Variable Energy Cyclotron Centre, Kolkata, India, November, 2018.
- T. Tanaka, K. Morita, K. Morimoto, D. Kaji, H. Haba, R. A. Boll, N. T. Brewer, S. Van Cleve, D. J. Dean, S. Ishizawa, Y. Ito, Y. Komori, K. Nishio, T. Niwase, B. C. Rasco, J. B. Roberto, K. P. Rykaczewski, H. Sakai, D. W. Stracener, K. Hagino, “Fusion dynamics for hot fusion reactions revealed in quasielastic fusion barrier distributions,” 13th International Conference on Nucleus-Nucleus Collisions,

Omiya, Japan, December, 2018.

- H. Haba, "Production of radioisotopes for application studies at RIKEN RI Beam Factory," Technical Meeting on Novel Multidisciplinary Applications with Unstable Ion Beams and Complementary Techniques, Vienna, Austria, December, 2018.
- Y. Komori, "Activities related to SHE target production and aqueous chemistry of SHEs at RIKEN," NUSPRASEN Workshop on Superheavy element research, target techniques and related topics, GSI, Darmstadt, Germany, February, 2019.
- H. Haba, "Present status and perspectives of SHE researches at RIKEN," NUSPRASEN Workshop on Superheavy element research, target techniques and related topics and NUSTAR Annual Meeting 2019, Darmstadt, Germany, February, 2019.
- T. Tanaka, "Fusion dynamics for hot fusion reactions revealed in quasielastic fusion barrier distributions," 54th ASRC International Workshop Sakura-2019 "Nuclear Fission and Structure of Exotic Nuclei," Tokai, Japan, March, 2019.

#### [Domestic Conference]

- H. Haba, "Present status and perspectives of superheavy element chemistry at RIKEN," 研究会「超重元素研究の新展開」, 福岡市, 2018年7月.
- 田中泰貴, 「超重核領域での系統的な核融合反応の研究」研究会, 「超重元素研究の新展開」, 福岡市, 2018年7月.
- 羽場宏光, 「理研におけるRI製造応用～新元素の化学から核医学の診断・治療まで～」, 大阪大学放射線科基盤機構発足記念シンポジウム, 豊中市, 2018年8月.
- 庭瀬暁隆, 和田道治, P. Schury, 伊藤由太, 加治大哉, M. Rosenbusch, 木村創大, 森本幸司, 羽場宏光, 石澤倫, 森田浩介, 宮武宇也, H. Wollnik, 「MRTOF-MS用の $\alpha$ -ToF検出器の性能評価」, 2018日本放射化学学会年会・第62回放射化学討論会, 京都市, 2018年9月.
- 羽場宏光, 「新元素ニホニウム発見への道のり」, 第5回奇石博物館サイエンスカフェ, 富士宮市, 2018年10月.
- 羽場宏光, 「理研におけるRI製造応用～新元素の探索から核医学の診断・治療まで～」, 放射線科学ワークショップ「文理共創を革新する量子ビーム科学」, 文京区, 2019年2月.
- 羽場宏光, 「理研RIビームファクトリーで製造する応用研究用ラジオアイソトープ」, 理研シンポジウム「精密武装抗体の合成と機能評価」, 千代田区, 2019年3月.
- 早水友洋, 長濱弘季, 小澤直也, 堤惇, 原田健一, 田中香津生, 内山愛子, 青木貴稔, 畠山温, 高橋義朗, 羽場宏光, 大前宣昭, 酒見泰寛, 「電子の永久電気双極子モーメント探索へ向けたフランシウム原子の生成とトラップ」, 日本物理学会第74回年次大会(2019年), 福岡市, 2019年3月.
- 羽場宏光, 「新元素の合成と化学」, 第37回量子系分子科学セミナー, 神戸市, 2019年3月.
- 小森有希子, 羽場宏光, 横北卓也, 矢納慎也, 佐藤望, Ghosh Kaustab, 酒見泰寛, 川村広和, 「 $^{206/207/208}\text{Pb}(^{11}\text{B}, \text{X})^{212}\text{Fr}$ 反応の励起関数測定とクラウンエーテルを用いたFrの錯形成反応」, 日本化学会第99春季年会2019, 神戸市, 2019年3月.
- 横北卓也, 笠松良崇, 小森有希子, 渡邊瑛介, ゴーシュコースタフ, 王洋, 森大輝, 篠原厚, 羽場宏光, 「Rfの硫酸錯体研究に向けたバッチ型固液抽出装置によるZr及びHfの陰イオン交換」, 日本化学会第99春季年会2019, 神戸市, 2019年3月.
- 二宮秀美, 笠松良崇, 速水翔, 永瀬将浩, 重河優大, 近藤成美, 渡邊瑛介, 羽場宏光, 横北卓也, 小森有希子, 森大輝, 王洋, ゴーシュコースタフ, 佐藤望, 篠原厚, 「102番元素Noのアンモニア水及び水酸化ナトリウム水溶液中におけるサマリウム共沈挙動」, 日本化学会第99春季年会2019, 神戸市, 2019年3月.
- 田中泰貴, 「超重元素関連の装置開発」, 新学術領域研究「宇宙観測検出器と量子ビームの出会い。新たな応用への架け橋。」若手ハードウェア研究会, 豊中市, 2019年3月.
- T. Tanaka, "Study of barrier distributions from quasielastic scattering cross sections towards superheavy nuclei synthesis," 10th Stop and Slow Radio Isotope (SSRI) Workshop, 福岡市, 2019年3月.

#### Posters Presentations

##### [International Conference etc.]

- T. Niwase, K. Fujita, Y. Yamano, K. Watanabe, D. Kaji, K. Morimoto, H. Haba, T. Hirano, S. Mitsuoka, K. Morita, "Measurement of fusion barrier distribution in  $^{51}\text{V} + ^{208}\text{Pb}$  system," 13th International Conference on Nucleus-Nucleus Collisions, Omiya, Japan, December 2018.

##### [Domestic Conference]

- 近藤成美, 笠松良崇, 永瀬将浩, 安田勇輝, 重河優大, 大内昂輝, 神田晃亮, 二宮秀美, 渡邊瑛介, 羽場宏光, 久保木祐生, 小森有希子, 横北卓也, 矢納慎也, 佐藤望, 篠原厚, 「Rfの塩酸系での溶媒抽出挙動の有機溶媒依存性」, 2018日本放射化学学会年会・第62回放射化学討論会, 京都市, 2018年9月.
- 村上郁斗, 平川貴啓, 内藤夏樹, 坂口聡志, 藤田訓裕, 郷慎太郎, 足立智, 田中聖臣, 田中泰貴, 庭瀬暁隆, 森本幸司, 羽場宏光, 加治大哉, 馬場秀忠, Pierre Brionnet, 木村創大, 酒井英行, 森田浩介, 「超重元素識別のためのデータ解析手法の開発」, 日本物理学会第74回年次大会, 福岡市, 2019年3月.



**Oral Presentations****[International Conference etc.]**

- K. Morimoto, "Superheavy element research at RIKEN," 13th International Conference on Nucleus-Nucleus Collisions (NN2018), Ohmiya, Saitama, Japan, December 5, 2018.
- S. Kimura, "Atomic masses of intermediate-mass neutron-deficient nuclei with relative uncertainty down to 35-ppb via MRTOF- MS," Fifth joint meeting of the nuclear physics divisions of the APS and the JPS, Hawaii, USA, 2018.
- T. Niwase, M. Wada, P. Schury, Y. Ito, D. Kaji, M. Rosenbusch, S. Kimura, K. Morimoto, H. Haba, S. Ishizawa, K. Morita, H. Miyatake, H. Wollnik, "Development of  $\alpha$ -ToF detector for correlation measurement of atomic masses and decay properties," 5th Joint Meeting of the APS Division of Nuclear Physics and the Physical Society of Japan, October 27, 2018.
- T. Niwase, K. Fujita, Y. Yamano, K. Watanabe, D. Kaji, K. Morimoto, H. Haba, T. Hirano, S. Mitsuoka, K. Morita, "Measurement of fusion barrier distribution in  $^{51}\text{V} + ^{208}\text{Pb}$  system," Nucleus-Nucleus Collisions (NN2018), December 5, 2018.

**[Domestic Conference]**

- D. Kaji, S. Mitsuoka, G. Hirano, T. Niwase, K. Morimoto, 「X線観測による超重核の原子番号直接同定に向けた Si-Ge 検出器アレイの開発」, 日本放射化学会第 62 回討論会, 京都大学, 京都, 2018 年 9 月.
- T. Niwase, 「超重核質量分析へ向けた  $\alpha$ -ToF 検出器の開発」, 超重元素研究の新展開, 九州大学, 福岡, 2018 年 7 月 31 日.
- T. Niwase, M. Wada, P. Schury, Y. Ito, S. Kimura, M. Rosenbusch, D. Kaji, K. Morimoto, H. Haba, S. Yamaki, T. Tanaka, K. Morita, A. Takamine, H. Miyatake, Y. Hirayama, Y. Watanabe, J. Y. Moon, M. Mukai, H. Wollnik, 「MRTOF-MS 用の  $\alpha$ -ToF 検出器の性能評価」, 2018 日本放射化学会年会 第 62 回放射化学討論会, 2018 年 9 月.
- T. Niwase, 「超重核精密分析へ向けた  $\alpha$ -ToF 検出器の開発」, 核データと重元素合成を中心とする宇宙核物理研究会, 北海道大学, 札幌, 2019 年 3 月.
- T. Niwase, D. Kaji, K. Morimoto, nSHE collaboration, 「超重核合成実験のための Si 検出器 box の開発」, 日本物理学会第 74 回年次大会 2019 年 3 月.
- T. Niwase, 「 $\alpha$ -ToF 検出器の開発と  $^{207}\text{Ra}$  の質量-崩壊特性測定」, 第 10 回停止・低速 RI ビームを用いた核分光研究会, 2019 年 3 月.

**[Others]**

- 森本幸司, 「新元素ニホニウムの発見と、さらなる挑戦」, 日本物理学会公開講座, 東京大学本郷キャンパス, 2018 年 11 月 17 日.
- 森本幸司, 「新元素「ニホニウム」の発見と今後の展開」, 甲南大学プレミア 4th 「元素の起源に関する探究プロジェクト」, 甲南大学甲友会館, 2019 年 3 月 21 日.

## Nuclear Science and Transmutation Research Division Astro-Glaciology Research Group

### 1. Summary of Research Activity

Our Astro-Glaciology Research Group promotes both experimental and theoretical studies to open up the new interdisciplinary research field of astro-glaciology, which combines astrophysics, astrochemistry, climate science, and glaciology.

On the experimental side, we analyze ice cores drilled at the Dome Fuji station, in Antarctica, in collaboration with the National Institute of Polar Research (NIPR, Tokyo). These ice cores are time capsules, which preserve atmospheric information of the past. In particular, ice cores obtained around the Dome Fuji station are known to be unique because they contain much more information on conditions in the stratosphere. This means that there are significant advantages in using Dome Fuji ice cores if we wish to study the universe, since gamma-rays and high-energy protons that are emitted in certain astronomical processes affect the chemical and isotopic compositions in the stratosphere. Our principal aim is to acquire and interpret information preserved in ice cores regarding:

- Signatures of past solar cycles and volcanic eruptions;
- Relationships between climate change and solar activity;
- Traces of past supernova explosions in our galaxy, in order to understand better the rate of galactic supernova explosions.

Moreover, we are promoting the projects on:

- Development of precise analytical techniques and instrumentation of high-sensitivity and high-temporal resolution;
- The evolution of molecules in space;
- The application of our high-sensitivity method of isotopic analysis to archaeological artifacts.

On the theoretical side, we are simulating numerically:

- Changes in the chemical composition of the stratosphere induced by gamma-rays and/or high-energy particles emitted from explosive astronomical phenomena, such as galactic supernovae and solar proton events; and
- The explosive nucleosynthesis (including the r-process, the rapid neutron capture process, which creates elements heavier than iron) that arises in the environment of core-collapse supernova explosions.

It is noteworthy that the as yet not fully understood frequency of supernova explosions in our galaxy is crucial to an understanding of the r-process nucleosynthesis. These all will contribute to understanding relationships between the universe and earth, to advance the Astro-Glaciology to Astro-Terrestrial Science.

### Members

#### Group Director

Yuko MOTIZUKI

#### Research/Technical Scientists

Kazuya TAKAHASHI (Senior Research Scientist)

Yoichi NAKAI (Senior Research Scientist)

#### Senior Visiting Scientist

Yasushige YANO

#### Visiting Scientists

Hideharu AKIYOSHI (Nat'l Inst. for Environ. Studies)

Akira HORI (Kitami Inst. of Tech.)

Hideki MADOKORO (Mitsubishi Heavy Ind., Ltd.)

Kenji TANABE (Okayama Univ. of Sci.)

#### Assistant

Keiko SUZUKI

#### Part-time Worker

Satomi NEGISHI

### List of Publications & Presentations

#### Publications

##### [Journal]

##### (Original Papers) \*Subject to Peer Review

C. L. Fryer, F. Timmes, A. L. Hungerford, A. Couture, Y. Motizuki *et al.*, "Catching Element Formation In The Act—The Case for a New MeV Gamma-Ray Mission: Radionuclide Astronomy in the 2020s," A White Paper submitted to the 2020 Decadal Survey, (USA, Feb. 2019).

F. Miyake, K. Horiuchi, Y. Motizuki, Y. Nakai, K. Takahashi, K. Masuda, H. Motoyama, H. Matsuzaki, "<sup>10</sup>Be signature of the cosmic ray event in the 10th century CE in both hemispheres, as confirmed by quasi-annual <sup>10</sup>Be data from the Antarctic Dome Fuji ice core," *Geophys. Res. Lett.* **46**, 11–18 (2019). \*

K. Takahashi, Y. Nakai, Y. Motizuki, T. Ino, S. Ito, S. B. Ohkubo, T. Minami, Y. Takaku, Y. Yamaguchi, M. Tanaka, H. Motoyama, "High-sensitivity sulfur isotopic measurements for Antarctic ice core analyses," *Rapid Communications in Mass Spectrom.* **32**, 1991–1998 (2018). \*

E. Tsantini, T. Minami, K. Takahashi, M. A. C. Ontiveros, "Analysis of sulfur isotopes to identify the origin of cinnabar in the Roman wall paintings from Badalona (Spain)," *J. Archaeol. Sci. Rep.* **18**, 300–307 (2018). \*

#### [Annals]

##### (Original Papers) \*Subject to Peer Review

河野摩耶, 高橋和也, 今津節生, 南武志, 「福岡県安徳台遺跡群における朱の使い分けについて」, *古代*, **142**, 97–103 (2018).\*

#### [Book]

##### (Original Papers) \*Subject to Peer Review

中井陽一, 『加速器ハンドブック』 (共同執筆), 日本加速器学会編, pp. 533–533 (「大気微粒子と銀河宇宙線」), 丸善出版, (2018). \*

### Oral Presentations

#### [International Conference etc.]

Y. Motizuki (Invited talk), "Relationship between temperature proxy and solar activity studied with a Dome Fuji (Antarctica) shallow ice core," PSTEP A04 International Workshop: Impact of solar activity variations on surface climate via several pathways, Kyoto, February 19–20, 2019.

Y. Motizuki, K. Takahashi, Y. Nakai, H. Motoyama, K. Kodera, "New annually-resolved water isotope data of the past 2000 years from a Dome-Fuji shallow ice core," CLIVASH2k workshop, Cambridge, UK, September 4–5, 2018.

Y. Nakai, N. Watanabe, Y. Oba, "Laboratory experiment for hydrogenation of C<sub>60</sub> fullerenes deposited on a solid surface under low temperature conditions," The Olympian Symposium 2018 on "Gas and stars from milli- to mega- parsecs," Paralia Katerini, Greece, May 31, 2018.

#### [Domestic Conference]

望月優子 (招待講演), 「南極の水からひもとく宇宙と地球の歴史」, 仁科記念講演会「アイソトープで探る宇宙」, 公益財団法人仁科記念財団, 西東京, 2018年11月11日.

望月優子 (招待講演), 「テラ・アストロノミー—宇宙と地球を結ぶ物理科学—」, 埼玉大学理学部物理量子力学特別講義, さいたま, 2019年1月7日.

中井陽一, 渡部直樹, 「低温薄膜状 C<sub>60</sub> 固体にトラップされた水素分子の振動回転励起の赤外吸収スペクトル」, 原子衝突学会第43回年会, 京都, 2018年10月13日.

高橋和也, 中井陽一, 望月優子, 井野敏行, 伊藤茂, 大久保智, 高久雄一, 山口義尊, 田中美穂, 本山秀明, 「南極氷床コアの詳細解析を見据えた硫黄同位体比分析の高感度化の試み」, 日本分析化学会第67回年会, 仙台, 2018年9月12–14日.

南武志, 高橋和也, 「超微量硫黄同位体分析法の開発と考古学資料分析の利点」, 日本文化財科学会第35回大会, 奈良, 2018年7月7日.

三宅美沙, 堀内一穂, 櫻井敬久, 増田公明, 本山秀明, 松崎浩之, 望月優子, 高橋和也, 中井陽一, 「ドームふじアイスコアの <sup>10</sup>Be 分析による単年宇宙線イベントの調査 II」, "Research of annual cosmic ray events using <sup>10</sup>Be in the Dome Fuji ice core II," 日本地球惑星科学連合2018年連合大会, 千葉, 2018年5月20–24日.

三宅美沙, 堀内一穂, 望月優子, 中井陽一, 高橋和也, 増田公明, 本山秀明, 松崎浩之, 「ドームふじアイスコアの一年分解能 <sup>10</sup>Be データにみられる AD993/994 宇宙イベント」, 第21回 AMS シンポジウム, 東京, 2018年12月17–18日.

三宅美沙, 堀内一穂, 望月優子, 中井陽一, 高橋和也, 増田公明, 本山秀明, 松崎浩之, 「約単年分解能 <sup>10</sup>Be データを用いた 994 年宇宙線イベントの調査」, ドームふじアイスコアコンソーシアム年次研究集会, 立川, 2019年3月27–28日.

菅澤佳世, 三宅美沙, 堀内一穂, 笹公和, 望月優子, 高橋和也, 中井陽一, 本山秀明, 松崎浩之, 「ドームふじアイスコア中 <sup>10</sup>Be と <sup>36</sup>Cl の高分解能測定による BC5480 年宇宙線イベントの調査」, ドームふじアイスコアコンソーシアム年次研究集会, 立川, 2019年3月27–28日.

### Posters Presentations

#### [International Conference etc.]

Y. Motizuki, K. Takahashi, Y. Nakai, S. Wada, K. Horiuchi, F. Miyake, H. Motoyama, H. Akiyoshi, T. Imamura, K. Kodera, "Terra-Astronomy/multi-disciplinary studies with Antarctic Ice cores and Numerical Simulations," The Ninth International Symposium on Polar Science, Tachikawa, December 4–7, 2018.

Y. Nakai, N. Watanabe, Y. Oba, "Hydrogenation of C<sub>60</sub> deposited on a substrate under low temperature condition," The 30<sup>th</sup> International Conference on Photonic, Electronic and Atomic Collisions, Cairns Australia, August 2017.

K. Takahashi, "New method for comprehensive detection of trace elements in environmental or biochemical materials using an electron-cyclotron-resonance ion-source mass spectrometer," the 4th World Congress on Mass Spectrometry, London, UK, June 2017.

### Press Release

K. Takahashi, Y. Nakai, Y. Motizuki, T. Ino, S. Ito, Satoru B. Ohkubo, T. Minami, Y. Takaku, Y. Yamaguchi, M. Tanaka, H. Motoyama, "Signature of the large volcanic eruption in AD1883 detected by new high-sensitivity sulfur isotopic measurement method applied to an Antarctic ice core," The Japan Society for Analytical Chemistry, Tokyo, Aug. 31, 2018, for a presentation at the 67th annual meeting of the Japan Society for Analytical Chemistry, Sendai, September 12–14, 2018.

Paper information, “High-sensitivity sulfur isotopic measurements for Antarctic ice core analyses,” *Rapid Communications in Mass Spectrometry* **32**, 1991–1998 (2018).

K. Takahashi, “Mass spectrometry tracks tiny amounts of sulfur in Antarctic ice cores—An advanced isotope-measuring system can reveal insights about past environments in shorter time frames,” *Research Highlight, RIKEN RESEARCH, SUMMER*, 2019, 11.

## Nuclear Science and Transmutation Research Division

### Nuclear Transmutation Data Research Group

#### 1. Abstract

The nuclear waste problem is an inevitable subject in nuclear physics and nuclear engineering communities. Since the Chicago Pile was established in 1942, nuclear energy has become one of major sources of energy. However, nowadays the nuclear waste produced at nuclear power plants has caused social problems. Minor actinide components of the waste have been studied well as a fuel in fast breeder reactors or ADS. Long-lived fission products (LLFP) in waste, on the other hand, have not been studied extensively. A deep geological disposal has been a policy of several governments, but it is difficult to find out location of the disposal station in terms of security, sociology and politics. To solve the social problem, a scientific effort is necessary for nuclear physics community to find out efficient methods for reduction of nuclear waste radioactivity. In the world-wide situation above, our Group aims to obtain reaction data of LLFP at RIBF and other muon facilities for muon capture data. These data are necessary to design an accelerator-based system for transmutation, and also may lead to a new discovery and invention for peaceful use of nuclear power and the welfare of humanity.

#### 2. Major Research Subjects

The Group is formed by three research teams. The first two Teams, “Fast RI Data Team” and “Slow RI Data Team,” are in charge of proton- and deuteron-induced reaction data of LLFP in inverse kinematics at RIBF. The third Team “Muon Data Team” is to obtain muon capture data of LLFP at muon facilities. All of the teams are focusing to obtain high-quality data which are essentially necessary to establish reliable reaction models. Each team has its own subjects and promotes LLFP reaction programs based on their large experiences, techniques and skills.

#### 3. Summary of Research Activity

In 2014, all the teams polished up experimental strategies, formed collaboration and prepared experiments. Physics runs for spallation reaction were successfully organized at RIBF in 2015–2017. The muon program started at RCNP, Osaka University in spring 2016 and the data for Pd isotopes were successfully obtained in 2017–2019 via in-beam method with DC beams at RCNP, and via activation method with pulsed beams at J-PARC and ISIS-RAL/RIKEN facilities.

The reaction data obtained with both fast and energy-degraded beams at RIBF encouraged the nuclear data group of JAEA, and a new database called “JENDLE/ImPACT-2018” has been released. The new database has been generated by a newly developed reaction model “DEURACS” which treats deuteron-induced reactions. DEURACS reproduces very well cross section data, and much better than other reaction models. A simulation code “PHITS” has been re-coordinated to use the database information.

In December 2018, the Team leader, Hideaki Otsu, was invited to join Technical Meeting of IAEA, entitled “Novel Multidisciplinary Applications with Unstable Ion Beams and Complementary Techniques.” Our activity has been demonstrated and recognized internationally.

#### Members

##### Group Director

Hiroyoshi SAKURAI (concurrent: Director, RI Physics Lab.)

##### Assistant

Izumi YOSHIDA

Asako TAKAHASHI

#### List of Publications & Presentations

##### Publications

###### [Journal]

###### (Original Papers) \*Subject to Peer Review

S. Takeuchi, T. Nakamura, M. Shikata, Y. Togano, Y. Kondo, J. Tsubota, T. Ozaki, A. Saito, H. Otsu, H. Wang, H. Sakurai, Y. Watanabe, S. Kawase, D. S. Ahn, M. Aikawa, T. Ando, S. Araki, S. Chen, N. Chiga, P. Doornenbal, S. Ebata, N. Fukuda, T. Isobe, S. Kawakami, T. Kin, S. Koyama, S. Kubono, Y. Maeda, A. Makinaga, M. Matsushita, T. Matsuzaki, S. Michimasa, S. Momiyama, S. Nagamine, K. Nakano, M. Niikura, K. Ogata, T. Saito, Y. Shiga, Y. Shimizu, S. Shimoura, T. Sumikama, P. A. Söderstrom, H. Suzuki, H. Takeda, R. Taniuchi, M. Uesaka, Y. Watanabe, K. Wimmer, T. Yamamoto, and K. Yoshida, “Coulomb breakup reactions of  $^{93,94}\text{Zr}$  in inverse kinematics,” *Prog. Theor. Exp. Phys.* **2019**, 013D02 (2019).

###### [Proceedings]

H. Sakurai, H. Okuno, N. Sakamoto, Y. Mori, T. Matsuzaki, M. Fukuda, R. Fujita, M. Kawashima, “Reduction and resource recycling of high-level radioactive wastes through nuclear transmutations—(5) Accelerator transmutation system and related developments for element technologies—,” *Proceedings of Fifteenth NEA Information Exchange Meeting on Actinide and Fission Product Partitioning and Transmutation.*

## Oral Presentations

### [International Conference etc.]

H. Sakurai (invited), “New steps reaching the horizon,” ImPACT International Symposium on “New Horizons of Partitioning and Transmutation Technologies with Accelerator System,” Tokyo, Japan, December, 2018.

H. Sakurai *et al.*, “Nuclear reaction study for high-level radioactive waste: Cross section measurements for proton- and deuteron-induced spallation of long-lived fission products,” The 10th China-Japan Joint Nuclear Physics Symposium, Huizhou, China, November, 2018.

### [Domestic Conference]

櫻井博儀, 「核変換による高レベル放射性廃棄物の大幅な低減・資源化 (6-2) ImPACT 加速器 2017 モデルの進展」, 日本原子力学会, 水戸, 2019 年 3 月 21 日.

櫻井博儀, 「加速器: 核変換を実用化する革新的加速器」, ImPACT 公開成果報告会, 東京, 2019 年 3 月 9 日.

## Posters Presentations

### [International Conference etc.]

H. Sakurai, H. Okuno, N. Sakamoto, Y. Mori, T. Matsuzaki, M. Fukuda, R. Fujita, M. Kawashima, “Reduction and resource recycling of high-level radioactive wastes through nuclear transmutations—(5) Accelerator transmutation system and related developments for element technologies—,” Fifteenth NEA Information Exchange Meeting on Actinide and Fission Product Partitioning and Transmutation, OECE/NEA, 1<sup>st</sup>, Manchester, UK, October, 2018.

### [Domestic Conference]

櫻井博儀, 「システム評価」, ImPACT 公開成果報告会, 東京, 2019 年 3 月 9 日.

## Awards

大津秀暁, 藤田玲子, 松崎禎市郎, 櫻井博儀, 下浦享, 水口浩司, 大井川宏之, 小澤正基, 仁井田浩二, 21 世紀発明賞, 公益社団法人発明協会, 2018 年 6 月 12 日.

## Press Release

日経新聞, 核廃棄物「変換」に活路, 先端技術, 2018 年 7 月 29 日, 日刊 30 面.

読売新聞, 「核のこみ」から希少金属, 2019 年 2 月 17 日, 日刊 31 面.

## Outreach Activities

櫻井博儀, 「核変換—放射性物質を高効率で短寿命・無害化する」, 第 34 回「西宮サイエンス談話会」, 甲南大学西宮キャンパス・西宮サイエンス談話会 (甲南大学マネジメント創造学部), 2018 年 7 月 28 日.

## Nuclear Science and Transmutation Research Division

### Nuclear Transmutation Data Research Group

#### Fast RI Data Team

### 1. Abstract

Fast RI team aims at obtaining and accumulating the cross section data for long lived fission products (LLFPs) in order to explore the possibility of using accelerator for nuclear transmutation.

LLFPs as nuclear waste have been generated continuously in nuclear power plants for wealth for human lives, while people noticed the way of disposal has not necessarily been established, especially after the Fukushima Daiichi power plant disaster. One of the ways to reduce the amount of LLFP or to recover them as recycled resources is nuclear transmutation technique.

RIBF facility has a property to generate such LLFP as a secondary beam and the beam species are identified by event by event. Utilizing the property, absolute values of the cross section of various reactions on LLFPs are measured and accumulated as database.

### 2. Major Research Subjects

- (1) Measurement of reaction products by the interaction of LLFPs with proton, deuteron, and photon to explore candidate reactions for transmutation of LLFPs.
- (2) Evaluation of the cross section data for the neutron induced reactions from the obtained data.

### 3. Summary of Research Activity

- (1) Acting as collaboration hub on many groups which plan to take data using fast RI beam in RIBF facility.
- (2) Concentrating on take data for proton and deuteron induced spallation reactions with inverse kinematics.
- (3) Accumulating the cross section data and evaluating them as evaluated nuclear data.
- (4) Evaluating cross section of neutron induced reaction on LLFP by collaborating with the nuclear model calculation and evaluation group.

## Members

### Team Leader

Hideaki OTSU (Concurrent: Team Leader, SAMURAI Team)

### Technical Staff I

Nobuyuki CHIGA

### Contract Researcher

He WANG

### Visiting Scientists

Takashi TERANISHI (Kyushu Univ.)

Satoshi TAKEUCHI (Tokyo Tech)

### Student Trainees

Keita NAKANO (Kyushu Univ.)

Kazuya CHIKAATO (Niigata Univ.)

Kenji NISHIZUKA (Niigata Univ.)

Kotaro IRIBE (Kyushu Univ.)

Ayaka IKEDA (Niigata Univ.)

Hiroya YOSHIDA (Kyushu Univ.)

Junki SUWA (Kyushu Univ.)

## List of Publications & Presentations

### Publications

#### [Proceedings]

X. Sun, H. Wang, H. Otsu, H. Sakurai *et al.*, "Reaction study of  $^{136}\text{Xe}$  on proton, deuteron and carbon at 168A MeV," Proceedings of the 15th International Conference on Nuclear Reaction Mechanisms, CERN-Proceedings-2019-001 (CERN, Geneva, 2019), pp. 153–157.

### Oral Presentations

#### [International Conference etc.]

H. Otsu, "Direct measurement of proton and deuteron induced reaction cross sections on long lived fission products using inverse kinematics," Technical Meeting on Novel Multidisciplinary Applications with Unstable Ion Beams and Complementary Techniques, IAEA Headquarters, Vienna, Austria, December, 2018.

H. Wang *et al.*, "Nuclear reaction study for long-lived fission products in high-level radioactive waste: Cross section measurements for proton- and deuteron-induced spallation reactions," 13th International Conference on Nucleus-Nucleus Collisions (NN2018), Omiya, Saitama, Japan, December 4–8, 2018.

- H. Sakurai, H. Wang *et al.*, “Spallation reaction study for fission products in nuclear waste: Cross section measurements for  $^{107}\text{Pd}$ ,  $^{137}\text{Cs}$ ,  $^{136}\text{Xe}$ , and  $^{90}\text{Sr}$  on proton and deuteron at different reaction energies,” the 10th China-Japan Joint Nuclear Physics Symposium, Huizhou, China, November 18–23, 2018.
- H. Wang *et al.*, “Spallation reaction study for fission products in nuclear waste: Cross section measurements for  $^{107}\text{Pd}$ ,  $^{137}\text{Cs}$ ,  $^{136}\text{Xe}$ , and  $^{90}\text{Sr}$  on proton and deuteron at different reaction energies,” Fifteenth NEA Information Exchange Meeting on Actinide and Fission Product Partitioning and Transmutation, Manchester Hall, Manchester, UK, September 30–October 3, 2018.
- H. Wang *et al.*, “Nuclear reaction study for high-level radioactive waste: Cross section measurements for proton- and deuteron-induced spallation reactions of long-lived fission products,” The 15th edition of the Varenna Conference on Nuclear Reaction Mechanisms (NRM), Varenna, Italy, June 11–15, 2018.

#### [Domestic Conference]

- 武内聡 他 6 名, ImPACT-RIBF Collaboration, 「クーロン分解反応による  $^{79,80}\text{Se}$  および  $^{93,94}\text{Zr}$  の光吸収断面積導出」, 日本物理学会第 73 回年次大会, 野田, 2018 年 3 月.
- 道正新一郎 他 8 名, ImPACT-RIBF Collaboration, 「OEDO ビームラインの開発および 2017 年度実験」, 日本原子力学会年会, 大阪, 2018 年 3 月.
- 堂園昌伯 他 8 名, ImPACT-RIBF Collaboration, 「低速 RI ビームを用いた  $^{107}\text{Pd}$ ,  $^{93}\text{Zr}$  の陽子および重陽子誘起反応測定」, 日本原子力学会年会, 大阪, 2018 年 3 月.
- 武内聡 他 5 名, 「 $^{79,80}\text{Se}$  および  $^{93,94}\text{Zr}$  のクーロン分解反応断面積の統計崩壊モデルを使った解析」, 日本原子力学会年会, 大阪, 2018 年 3 月.
- 諏訪純貴 他 9 名, 「Y, Zr, Nb 同位体に対する 100 MeV/nucleon 陽子・重陽子入射反応の同位体生成断面積測定」, 日本原子力学会年会, 大阪, 2018 年 3 月.
- 千賀信幸, 「低エネルギー中重核用イオンチェンバーの設計・製作」, 平成 29 年度核融合科学研究所技術研究会, 岐阜, 2018 年 3 月.

#### Posters Presentations

##### [International Conference etc.]

- X. Sun *et al.*, “Isotopic cross sections of proton-, deuteron- and carbon-induced reactions on  $^{136}\text{Xe}$ ,” 13<sup>th</sup> International Conference on Nucleus-Nucleus Collisions, Omiya, Japan, December 4–8, 2018.

##### [Domestic Conference]

- 三木晴瑠, 「 $^{238}\text{U}$  の飛行核分裂反応における低速  $^{107}\text{Pd}$  および  $^{77}\text{Se}$  のアイソマー比の測定」, 日本物理学会第 73 回年次大会, 野田, 2018 年 3 月.

#### Awards

- 中野敬太, 「長寿命核分裂生成物 Zr-93 の短寿命化・再資源化に向けた核反応データ測定」, 九州大学エネルギーウィーク 2018 優秀賞

#### Press Release

- H. Otsu, T. Matsuzaki, H. Sakurai, Jointly awarded “the 21st Century Invention Prize” for their research on Radioactive waste processing method, Joint PR released with Toshiba Co, Toshiba Energy Systems & Solutions Corporation, JAEA, JST, Director General for Science and Technology and Innovation on the research, May 17, 2018.

#### Outreach Activities

- Lecture of contents related to the 21st Century Invention Prize in the presense of Prince Hitachinomiya Masahito, Prince Hitachi House, Aoyama, Tokyo June 1, 2018.

## Nuclear Science and Transmutation Research Division

### Nuclear Transmutation Data Research Group

#### Slow RI Data Team

### 1. Abstract

This team is in charge of the development of low-energy RI beams of long-lived fission fragments (LLFP) from the  $^{238}\text{U}$  by means of degrading the energy of beams produced by the BigRIPS fragment separator.

### 2. Major Research Subjects

Studies of the slowing down and purification of RI beams are the main subjects of the team. Developments of devices used for the slowing down of RI beams are also an important subject.

- (1) Study and development of the slowed-down methods for LLFP.
- (2) Development of the devices used for the slowing down.
- (3) Operation of the BigRIPS separator and supply the low energy LLFP beam to the experiment in which the cross sections of LLFP are measured at the low energy.
- (4) Development of the framework to seamlessly handle device, detector, DAQ, and analysis for the easy control of the complicated slowed-down RI beam production and its development.

### 3. Summary of Research Activity

A new OEDO beam line, designed for the slowed-down RI beams, was constructed under the collaboration with CNS, the University of Tokyo. Our group was responsible for the construction of the infrastructure such as the cooling water and the electrical equipment, and the movement and alignment of existing vacuum chambers, quadrupole magnets. The power supply for the Superconducting Triplet Quadrupoles (STQ) was made, which had a stability also under the low current condition.

Slowed-down  $^{93}\text{Zr}$  beams with 20 or 50 MeV/nucleon were successfully developed at June 2016 for the first time. The methods to obtain the narrow energy, position, and angle distribution were developed. The methods of the energy adjustment and the particle identification at 50 MeV/nucleon were developed. The  $^{93}\text{Zr}$  and  $^{107}\text{Pd}$  beams with 50 MeV/nucleon were produced for the nuclear-transmutation experiments using proton or deuteron targets at October 2016. The commissioning experiment of the OEDO beam line was successfully performed at June 2017. The first transmutation experiments using OEDO beam line were performed with  $^{93}\text{Zr}$ ,  $^{107}\text{Pd}$ , and  $^{79}\text{Se}$  around 20 MeV/nucleon.

With our developments, the slowed-down RI beams became ready for the transmutation experiments. On the other hand, the procedure to make the slowed-down RI beams became highly specialized. In order to easily produce the slowed-down RI beam, the framework is under the development to seamlessly handle the device, detector, DAQ, and analysis.

### Member

#### Team Leader

Toshiyuki SUMIKAMA

### List of Publications & Presentations

#### Oral Presentations

##### [International Conference etc.]

- T. Sumikama *et al.*, "New control method of slowed-down RI beam and new PID method of secondary-reaction fragments at RIKEN RI beam factory," International Conference on Electromagnetic Isotope Separators and Related Topics (EMIS XVIII), Geneva, Switzerland, September 16–21, 2018.

## Nuclear Science and Transmutation Research Division

### Nuclear Transmutation Data Research Group

#### Muon Data Team

### 1. Abstract

Dr. Yoshio Nishina observed muons in cosmic rays in 1937. The muon is an elementary particle similar to electron and classified to lepton group. The muon has positive or negative electric charge, and the lifetime is 2.2  $\mu\text{sec}$ . The negative muon ( $\mu^-$ ) is 207 times heavier than the electron and behaves as a “heavy electron” in materials. The negative muon is captured by atomic orbits of nuclei to form a muonic atom and cascades down to the 1 s orbit to make muon nuclear capture. The muon is combined with a proton in the nucleus to convert to a neutron and a neutrino. The muon nuclear capture reaction on a nucleus ( ${}^A_ZN$ ) with the atomic number  $Z$  and mass number  $A$  generates the isotopes of  ${}^{A-x}_{Z-1}N$  ( $x = 0, 1, 2, 3, 4$ ) by emitting some neutrons in the reaction. The phenomenon is called “muon nuclear transmutation.” The reaction branching ratio of  ${}^A_ZN(\mu^-, xn\nu)_{Z-1}^{A-x}N$  reactions ( $x = 0, 1, 2, 3, 4$ ) is one of important factors toward various applications with nuclear transmutation technique. From a viewpoint of the nuclear physic, the muon nuclear capture reaction is very unique and interesting. A high-energy compound nuclear state is suddenly generated in the nuclei associated with a weak conversion process of proton to neutron and neutrino. Many experimental results have been so far reported, however, the reaction mechanism itself is not well clarified. The research team aims at obtaining the experimental data to investigate the reaction mechanism of muon nuclear capture, and also at theoretical understanding on the nuclear capture reaction.

### 2. Major Research Subjects

- (1) Experimental clarification on the mechanism of nuclear muon capture reaction
- (2) Theoretical understanding on the nuclear muon capture reaction
- (3) Interdisciplinary applications with the nuclear transmutation technique

### 3. Summary of Research Activity

There are two experimental methods to study the muon nuclear capture reaction. The first one is “muon in-beam spectroscopy method.” The neutron and  $\gamma$ -ray emissions from the excited states of  ${}^{A-x}_{Z-1}N$  nuclei are prompt events and are observed by the “muon in-beam spectroscopy method” with a DC muon beam. The reaction branching ratio is directly determined by measuring the neutron multiplicity in the reaction. The DC muon beam is available at the MuSIC (Muon Science Innovative Channel) muon facility in the Research Center for Nuclear Physics (RCNP) at Osaka University. The second one is “muon activation method” with the pulsed muon beam. The produced unstable nuclei  ${}^{A-x}_{Z-1}N$  make  $\beta^{+/-}$  decays. The  $\gamma$ -rays associated with  $\beta^{+/-}$  decays to the daughter nuclei are observed in the experiment. The build-up curve of  $\gamma$ -ray yield at muon beam-on and the decay curve at beam-off are measured. Since the half-lives and decay branching ratios of  $\beta^{+/-}$ - $\gamma$  decays are known, the reaction branching ratios to the  ${}^{A-x}_{Z-1}N$  nuclei are determined by the  $\gamma$ -ray yield curves. The pulsed muon beam is available at the RIKEN-RAL Muon Facility in the UK and J-PARC muon facility.

Muon nuclear capture reactions are studied on five isotope-enriched palladium targets ( ${}^{104,105,106,108,110}\text{Pd}$ ) and five isotope-enriched zirconium targets ( ${}^{90,91,92,94,96}\text{Zr}$ ) employing two experimental methods. By obtaining the experimental data on the Pd and Zr targets, the reaction mechanism is investigated experimentally, and the results are compared with appropriate theoretical calculations. The  ${}^{107}\text{Pd}$  is classified to a long-lived fission product (LLFP) and is contained in a spent nuclear fuel. The study of muon nuclear capture on the Pd and Zr targets is aiming at exploring a possible reaction path to make the nuclear transmutation of the Pd and Zr metal extracted from the spent nuclear fuel without an isotope separation process. This research was funded by the ImpACT Program of Council for Science, Technology and Innovation (Cabinet Office, Government of Japan).

#### (1) Experiments with “muon in-beam spectroscopy method”

Muon nuclear capture reactions were investigated on five palladium targets ( ${}^{104,105,106,108,110}\text{Pd}$ ) by employing the DC muon beam at MuSIC. The  $\gamma$ -ray and neutron in the muon nuclear capture reaction were measured with the time information relative to muon beam arrival. The measured neutron multiplicity gives the reaction branching ratio of  ${}^A_{46}\text{Pd}(\mu^-, xn\nu)_{45}^{A-x}\text{Rh}$  reactions, where  $A = 104, 105, 106, 108, 110$  and  $x = 0, 1, 2, 3, 4$ .

Employing a newly built neutron spectrometer, the neutron was measured to obtain the reaction branching ratios of muon capture reactions on the Pd targets. We have constructed a neutron spectrometer named “Seamine”: Scintillator Enclosure Array for Muon Induced Neutron Emission. The spectrometer consists of 21 liquid scintillation counters, 2 Ge  $\gamma$ -ray detectors, 7 BaF<sub>2</sub> counters. The Pd target, muon beam counters and muon degraders are placed at the center of spectrometer. The neutron counter is a BC-501A liquid scintillation counter with 20 cm diameter and 5 cm depth and is connected to a 5” photo multiplication tube (H4144-01). The total neutron detection efficiency is estimated 5%, where the distance is 4 cm from the target to neutron counters. The Ge  $\gamma$ -ray detectors are placed at 10 cm from the target, and the typical detection efficiency is 0.5% for 200 keV  $\gamma$ -ray. The BaF<sub>2</sub> counters are located beneath the target to detect fast  $\gamma$ -rays emitted from the compound nucleus formed in the reactions. Signals from the liquid scintillation counters are processed in a CAEN V1730B waveform digitizer (16 channel, 14 bit, 500 M samplings/sec.). The neutron- $\gamma$  discrimination is performed on-line during the experiment, and the detailed data analysis is conducted off-line after the experiment. The neutron energy spectrum is constructed in the digitizer. Signals from Ge detectors are also processed in the digitizer to obtain the energy and time spectrum of  $\gamma$ -rays associated with the reaction. Signals from the BaF<sub>2</sub> counters and muon beam counters are sent to the digitizer to make the fast timing signals.

We have established the muon in-beam spectroscopy method employing the “Seamine” spectrometer. The neutron data analysis

is in progress to obtain the multiplicity, the energy and the TOF spectrum using start signals given by  $\gamma$ -rays detected in the BaF<sub>2</sub> counters. The  $\gamma$ -ray data gives the energy spectrum of prompt  $\gamma$ -rays and muonic X-rays originated from the <sup>104,105,106,108,110</sup>Pd targets.

### (2) Experiments with “muon activation method” at the RIKEN-RAL Muon Facility

We conducted the experiments on the muon nuclear capture employing the muon activation method at the RIKEN-RAL Muon Facility in the UK. The pulsed muon beam was irradiated on the <sup>104,105,106,108,110</sup>Pd targets. The  $\gamma$ -rays were detected by a Ge detector located at the downstream of the Pd targets to maximize the detection efficiency. The build-up and decay curves of  $\gamma$ -ray intensities were measured associated with  $\beta^{+/-}$  decays of produced unstable nuclei to daughter nuclei. The  $\gamma$ -ray-yield curves give the absolute radiation activity produced by the reaction, and the reaction branching ratios are determined for <sup>A</sup>Pd( $\mu^-$ ,  $x\nu$ )<sup>A-x</sup>Rh reactions. The decay curves of  $\gamma$ -rays from the produced nuclei with long half-lives were measured under low  $\gamma$ -ray background at an experimental apparatus built in a separated room. The detailed off-line data analysis is in progress.

### (3) Experiments with “muon activation method” at J-PARC muon facility

The experiments employing the muon activation method were performed at J-PARC muon facility. The five isotope-enriched Pd targets (<sup>104,105,106,108,110</sup>Pd) were irradiated by the pulsed muon beam, and the build-up and decay curves of  $\gamma$ -ray intensities were measured.

In addition to the Pd targets, the experiments on five isotope-enriched Zr target (<sup>90,91,92,94,96</sup>Zr) were conducted to obtain the reaction branching ratios of <sup>A</sup>Zr( $\mu^-$ ,  $x\nu$ )<sup>A-x</sup>Y reactions, where A = 90, 91, 92, 94, 96. The obtained reaction branching ratios on the Pd and Zr targets are important to understand the reaction mechanism of muon nuclear capture. The <sup>93</sup>Zr is one of the LLFP and is contained in a spent nuclear fuel. The experiment on the Zr targets is to explore a possibility to realize the nuclear transmutation of the Zr metal extracted from the spent nuclear fuel.

In order to obtain the reaction branching ratio of <sup>107</sup>Pd( $\mu^-$ ,  $x\nu$ )<sup>107-x</sup>Rh reactions, the muon activation experiment was performed employing a Pd target containing <sup>107</sup>Pd of 15.3%. The  $\gamma$ -ray intensities associated with  $\beta^{+/-}$  decays of produced unstable nuclei were measured to obtain the build-up and decay curves. Once the branching ratios of the reactions on the <sup>104,105,106,108,110</sup>Pd targets are obtained, these contributions are extracted from the branching-ratio data obtained for the Pd target with <sup>107</sup>Pd. The reaction branching ratio of <sup>107</sup>Pd( $\mu^-$ ,  $x\nu$ )<sup>107-x</sup>Rh reactions is finally determined. The detailed off-line data analysis is in progress.

### (4) Comparison with theory

The muon activation method gives the reaction branching ratios. The muon in-beam spectroscopy method gives the neutron multiplicity and the neutron energy spectrum. These experimental results are important to understand the compound nuclear state and neutron emission mechanism. The reaction branching ratios obtained by the muon activation method are compared with the results of neutron multiplicity measurements. The neutron energy spectrum is considered to be reflected by the energy distribution of compound nuclear state and neutron emission mechanism. The experimental results are compared with the appropriate calculations employing the neutron emission mechanisms due to an evaporation, a cascade and a direct emission processes with assuming the energy distribution at compound nuclear state.

## Members

### Team Leader

Hiroyoshi SAKURAI

### Contract Researcher

Teiichiro MATSUZAKI

## List of Publications & Presentations

### Publications

#### [Journal]

#### (Original Papers) \*Subject to Peer Review

D. Hatakeyama, K. Nishimura, K. Matsuda, T. Namiki, Seungwon Lee, N. Nunomura, T. Aida, T. Matsuzaki, R. Holmestad, S. Wenner, C. D. Marioara, “Effect of copper addition on the cluster formation behavior of Al-Mg-Si, Al-Zn-Mg, and Al-Mg-Ge in the natural aging,” METALLURGICAL AND MATERIALS TRANSACTIONS A V49A, (2018) p. 5871.

### Oral Presentations

#### [International Conference etc.]

T. Matsuzaki, H. Sakurai, “A new production method of <sup>99</sup>Mo by muon nuclear transmutation,” International Symposium on Technetium and Rhenium, Science and Utilization, Moscow, Russia, October 2018.

#### [Domestic Conference]

斎藤岳志, 新倉潤, 櫻井博儀, 松崎禎市郎, 他, 「ミューオン原子 X 線を用いた Pd 同位体の核荷電半径の測定」, 日本物理学会 73 回 年次大会, 東京理科大学野田キャンパス, 野田, 2018 年 3 月.

斎藤岳志, 新倉潤, 松崎禎市郎, 櫻井博儀, 他, “Study for the muon capture on palladium isotopes via neutron measurement,” 第 5 回日米物理学会 合同核物理分科会, ハワイ 米国, 2018 年 10 月.

新倉潤, 斎藤岳志, 松崎禎市郎, 櫻井博儀, 他, 「ミューオン捕獲による Pd 同位体の核変換」, 日本物理学会 74 回年次大会, 九州大学, 福岡, 2019 年 3 月.

斎藤岳志, 新倉潤, 松崎禎市郎, 櫻井博儀, 他, 「パラジウムのミューオン捕獲に伴う放出中性子の直接測定」, 日本物理学会 74 回年次大会, 九州大学, 福岡, 2019 年 3 月.

三木謙二郎, 酒井大輔, 上坂友洋, 宇津城雄大, 酒井英行, 笹野匡紀, 関口仁子, 松崎禎市郎, 「RIBF における  ${}^3\text{H}(t, {}^3\text{He})3\text{n}$  反応測定の為の三重水素標的の開発」, 日本物理学会 74 回年次大会, 九州大学, 福岡, 2019 年 3 月.

新倉潤, 斎藤岳志, 松崎禎市郎, 櫻井博儀, 「ミューオン原子核捕獲反応による核変換」, 日本原子力学会春の年会, 茨城大学, 水戸, 2019 年 3 月.

### Award

大津秀暁, 藤田玲子, 松崎禎市郎, 櫻井博儀, 下浦享, 水口浩司, 大井川宏之, 小澤正基, 仁井田浩二, 平成 30 年度全国発明表彰「21 世紀発明賞」, 「放射性廃棄物の処理方法の発明」, (特許第 6106892 号), 2018 年 6 月.

### Patent

松崎禎市郎, 櫻井博儀, 「ミューオン照射による放射性物質の製造方法およびその製造物質」, 特許 PCT 出願 (日本, アメリカ, カナダ, ヨーロッパ), (国際出願番号 PCT/JP2017/003226), (2018 年 8 月).

## Nuclear Science and Transmutation Research Division High-Intensity Accelerator R&D Group

### 1. Abstract

The R&D group, consisting of two teams, develops elemental technology of high-power accelerators and high-power targets, aiming at future applications to nuclear transmutations of long-lived fission product into short-lived nuclides. The research subjects are superconducting rf cavities for low-velocity ions, design of high-power accelerators, high-power target systems and related technologies.

Nuclear transmutation with high-intensity accelerators is expected to reduce the high-level radioactive wastes and to recycle the precious resources such as rare-earth materials in future. This method is one of the important applications of the ion-accelerator technologies that have been developed at RIKEN for a long time. Under the framework of ImPACT Fujita Program, we have conducted R&D of elemental technology related to the high-power accelerators and high-power targets.

We gained a lot of experiences in these R&Ds. Among them, the development of a superconducting rf cavity has become the basis of the upgrade program of the RILAC facility which started in 2016.

### 2. Major Research Subjects

- (1) R&D of elemental technology of high-power accelerators and high-power targets

### 3. Summary of Research Activity

- (1) A high-gradient rf cavity has been constructed and tested based on the superconducting rf technology.
- (2) Several candidates for the high-power target have been proposed and their prototypes have been tested.
- (3) A high-current deuteron RFQ has been designed.

### Member

#### Group Director

Osamu KAMIGAITO (concurrent: Group Director, Accelerator Group)

## Nuclear Science and Transmutation Research Division

### High-Intensity Accelerator R&D Group

### High-Gradient Cavity R&D Team

#### 1. Abstract

We develop new components for accelerators dedicated for low-beta-ions with very high intensity. Specifically, we are designing and constructing a cryomodule for superconducting linac efficient for acceleration of low-beta-ions. In parallel, we try to optimize an rf acceleration system by making computer simulations for acceleration of very high intensity beams.

#### 2. Major Research Subjects

- (1) Development of high-gradient cavities for low beta ions
- (2) Development of power saving cryomodules

#### 3. Summary of Research Activity

- Development of highly efficient superconducting accelerator modules

#### Members

##### Team Leader

Naruhiko SAKAMOTO (concurrent: Cyclotron Team)

##### Research/Technical Scientists

Kazunari YAMADA (concurrent: Senior Technical Scientist, Beam Dynamics & Diagnostics Team)

Yutaka WATANABE (concurrent: Senior Technical Scientist, RILAC team)

Kazutaka OZEKI (concurrent: Technical Scientist, Cyclotron Team)

Kenji SUDA (concurrent: Technical Scientist, Cyclotron Team)

##### Postdoctoral Researcher

Xingguang LIU

#### List of Publications & Presentations

##### Publications

##### Oral Presentations

###### [Domestic Conference]

N. Sakamoto, K. Yamada, K. Suda, K. Ozeki, Y. Watanabe, O. Kamigaito, H. Okuno, "Reduction and resource recycling of high-level radioactive wastes through nuclear transmutation (6-1) development of prototype superconducting-linac for intense low-beta ion beams," Annual Meeting of Atomic Energy Society Japan, Mito, March 20–22, 2019.

N. Sakamoto, K. Yamada, K. Suda, K. Ozeki, Y. Watanabe, O. Kamigaito, H. Okuno, "Advances of accelerator technology development for nuclear transmutation in the ImPACT program-2 prototype of superconducting linear accelerator for intense deuteron beam," Meeting of Atomic Energy Society Japan, Okayama, September 5–7, 2018.

**Nuclear Science and Transmutation Research Division**  
**High-Intensity Accelerator R&D Group**  
**High-Power Target R&D Team**

**1. Abstract**

The subjects of this team cover R&D studies with respect to target technology for the transmutation of the LLFPs. Furthermore this team works for the demonstration test of the transmutation of  $^{107}\text{Pd}$ .

**2. Major Research Subjects**

- (1) Liquid lithium target for production of neutron or muon
- (2) Beam window without solid structure
- (3) Ion implantation and TIMS for the demonstration of the transmutation of  $^{107}\text{Pd}$

**3. Summary of Research Activity**

- (1) Liquid lithium target for production of neutron or muon  
(H. Okuno, N. Furutachi)
- (2) Beam window with solid structure  
(H. Okuno)
- (3) Ion implantation and TIMS of  $^{107}\text{Pd}$   
(Y. Miyake, Y. Sahoo, M. Takahashi)

**Members****Team Leader**

Hiroki OKUNO (concurrent: Deputy Group Director, Accelerator Gr.)

**Postdoctoral Researcher**

Yasuto MIYAKE

**Contract Researcher**

Naoya FURUTACHI

**Part-time Workers**

Mamoru TAKAHASHI  
Akira TAKAGI

YuVin SAHOO

## Research Facility Development Division Accelerator Group

### 1. Abstract

The Accelerator Group, consisting of seven teams, pursues various upgrade programs of the world-leading heavy-ion accelerator facility, RI Beam Factory (RIBF), to enhance the accelerator performance and operation efficiency. The programs include the R&D of superconducting ECR ion source, charge stripping systems, beam diagnostic devices, radiofrequency systems, control systems, and beam simulation studies. We are also maintaining the large infrastructure to realize effective operation of the RIBF. Moreover, we are actively promoting the applications of the facility to a variety of research fields.

Our primary mission is to supply intense, stable heavy-ion beams for the users through effective operation, maintenance, and upgrade of the RIBF accelerators and related infrastructure. The director members shown above govern the development programs that are not dealt with by a single group, such as intensity upgrade and effective operation. We also discuss the future plans of RIBF along with other laboratories belonging to the RIBF research division.

Various improvements and developments have been carried out for the RIBF accelerators in order to upgrade the beam intensities and stability. Owing to the efforts, for example, the intensity of the uranium beam has increased by 40% in the last three years, resulting in the intensity of 72 pA (5.9 kW) at the exit of the superconducting ring cyclotron. We also started providing intense vanadium beams for the synthesis of a new element [119] at GARIS II, which was recently moved to the cyclotron facility.

In 2016, a supplemental budget was approved for the upgrade of RIBF aiming at synthesizing heavier new elements. A superconducting linac booster has been constructed at the RILAC facility with this budget under the collaboration with KEK researchers. We also constructed a new superconducting ECR ion source at RILAC, and started the test operation in 2018. The beam commissioning with the upgraded RILAC facility is scheduled in this fiscal year. The accelerating cavities of the ring cyclotron, which has been suffered from the low accelerating voltage, were also modified with this budget. It is expected that the uranium beam intensity will be increased significantly in near future for the BigRIPS experiments as well as the metallic ion beams for GARIS II experiments for the synthesis of super heavy elements.

On the other hand, we have started a new project with RCNP, Osaka university, for the promotion of application research using short-lived radioisotopes since 2017. A high-power target for production of At-211 is under development with RI Application Research Group of RNC in the framework of this project. It will be installed and tested in the upgraded RILAC facility in near future. An upgrade plan of RIBF for further increasing heavy-ion beams, especially the uranium beam, has been continuously discussed. The plan proposed recently is based on a new idea of “charge-stripper ring,” which is used to improve the overall stripping efficiency of the uranium beam. This device recirculates and re-injects the uranium ions into the charge stripper until the ions become the charge state required for the succeeding acceleration, while the bunch structure is kept with its isometric orbit lengths for all the charge states. A preliminary design of the magnets is under progress after intensive optical study of the device. The final goal of this plan is to increase the uranium beam intensity by 30 times of the present value, namely up to 2000 pA, at the exit of SRC.

### 2. Major Research Subjects

- (1) Intensity upgrade of RIBF accelerators (Okuno)
- (2) Effective and stable operation of RIBF accelerators (Fukunishi)
- (3) Construction of the superconducting linac booster at the RILAC facility
- (4) Promotion of the future plan

### 3. Summary of Research Activity

- (1) The maximum intensity of the calcium beam reached 740 pA at 345 MeV/nucleon, which corresponds to 12.3 kW. That of the krypton beam reached 486 pA, corresponding to 13.4 kW.
- (2) The maximum intensities of the uranium and xenon beams reached 72 and 102 pA, respectively, at 345 MeV/nucleon.
- (3) The overall beam availability for the RIBF experiments averaged for 5 years from 2013 to 2017 was 92%. It fell down to 79% in 2018 because of several hardware troubles. Efforts to restore the availability to more than 90% are ongoing.
- (4) The large infrastructure was properly maintained based on a well-organized cooperation among the related sections.
- (5) A major upgrade of the accelerator facility has been conducted aiming at synthesizing heavier new elements. It includes construction of a superconducting linac booster of RILAC, construction of a new superconducting ECR ion source, and modification of the accelerating cavities of the ring cyclotron (RRC).
- (6) An intensity-upgrade plan of the RIBF has been further investigated. Design study of the charge-stripper ring has been started.

### Members

#### Group Director

Osamu KAMIGAITO

**Deputy Group Directors**

Hiroki OKUNO (for intensity upgrade)

Nobuhisa FUKUNISHI (for stable and efficient operation)

**Junior Research Associate**

Takahiro KARINO (Utsunomiya Univ.)

**Research Part-time Worker I**

Akira GOTO

**Research Consultants**

Masayuki KASE  
Tadashi FUJINAWA

Robert JAMESON  
Toshiyuki HATTORI

**Visiting Scientists**

Eiji KAKO (KEK)  
Hirotaka NAKAI (KEK)  
Kensei UMEMORI (KEK)

Taro KONOMI (KEK)  
Noboru SASAO (Okayama Univ.)  
Yasutaka IMAI (Okayama Univ.)

**Student Trainees**

Akira FUJIEDA (Okayama Univ.)

Hiroyuki KAINO (Okayama Univ.)

**Assistant**

Karen SAKUMA

**Administrative Part-time Worker II**

Ryoko UMEZAKI

**Research Facility Development Division  
Accelerator Group  
Accelerator R&D Team**

### 1. Abstract

We are developing the key hardware in upgrading the RIBF accelerator complex. Our primary focus and research is charge stripper which plays an essential role in the RIBF accelerator complex. Charge strippers remove many electrons in ions and realize efficient acceleration of heavy ions by greatly enhancing charge state. The intensity of uranium beams is limited by the lifetime of the carbon foil stripper conventionally installed in the acceleration chain. The improvement of stripper lifetimes is essential to increase beam power towards the final goal of RIBF in the future. We are developing the low-Z gas stripper. In general gas stripper is free from the lifetime related problems but gives low equilibrium charge state because of the lack of density effect. Low-Z gas stripper, however, can give as high equilibrium charge state as that in carbon foil because of the suppression of the electron capture process. Another our focus is the upgrade of the world's first superconducting ring cyclotron.

### 2. Major Research Subjects

- (1) Development of charge strippers for high power beams (foil, low-Z gas)
- (2) Upgrade of the superconducting ring cyclotron
- (3) Maintenance and R&D of the electrostatic deflection/inflexion channels for the beam extraction/injection

### 3. Summary of Research Activity

#### (1) Development of charge strippers for high power beams (foil, low-Z gas)

(H. Hasebe, H. Imao, H. Okuno)

We are developing the charge strippers for high intensity heavy ion beams. We are focusing on the developments on carbon or berrilium foils and gas strippers including He gas stripper.

#### (2) Upgrade of the superconducting ring cyclotron

(J. Ohnishi, H. Okuno)

We are focusing on the upgrade of the superconducting ring cyclotron.

#### (3) Maintenance and R&D of the electrostatic deflection/inflexion channels for the beam extraction/injection

(J. Ohnishi, H. Okuno)

We are developing high-performance electrostatic channels for high power beam injection and extraction.

## Members

### Team Leader

Hiroki OKUNO (concurrent: Deputy Group Director, Accelerator Group)

### Research/Technical Scientists

Hiroshi IMAO (Senior Research Scientist)

Jun-ichi OHNISHI (Senior Technical Scientist)

### Technical Scientist

Hiroo HASEBE

### Visiting Scientists

Andreas ADELMANN (Paul Scherrer Institute)

Hironori KUBOKI (KEK)

Noriyosu HAYASHIZAKI (Tokyo Institute of Technology)

### Junior Research Associate

Naoya IKOMA (Nagaoka Univ. of Technology)

### Student Trainees

Taishi SASAKI (Nagaoka Univ. of Technology)

Yoshiki SHIKUMA (Nagaoka Univ. of Technology)

## List of Publications & Presentations

### Publications

#### [Proceedings]

H. Imao, "Development of Gas stripper at RIBF," Proceeding of IPAC2018, MOZGBE1, Vancouver, BC, Canada, 2018.

**Oral Presentations**

**[International Conference etc.]**

H. Imao, "Development of Gas stripper at RIBF," Proceeding of IPAC2018, MOZGBE1, Vancouver, BC, Canada, 2018.

H. Okuno, "Present status of and recent developments at RIKEN RIBF," 14th International Conference on Heavy Ion Accelerator Technology (HIAT'18), Lanzhou, China, October, 2018.

## Research Facility Development Division

### Accelerator Group

### Ion Source Team

#### 1. Abstract

Our aim is to operate and develop the ECR ion sources for the accelerator-complex system of the RI Beam Factory. We focus on further upgrading the performance of the RI Beam Factory through the design and fabrication of a superconducting ECR ion source for production of high-intensity heavy ions.

#### 2. Major Research Subjects

- (1) Operation and development of the ECR ion sources
- (2) Development of a superconducting ECR heavy-ion source for production of high-intensity heavy ion beams

#### 3. Summary of Research Activity

##### (1) Operation and development of ECR ion sources

(T. Nakagawa, M. Kidera, Y. Higurashi, T. Nagatomo, Y. Kanai, and H. Haba)

We routinely produce and supply various kinds of heavy ions such as zinc and calcium ions for the super-heavy element search experiment as well as uranium ions for RIBF experiments. We also perform R&D's to meet the requirements for stable supply of high-intensity heavy ion beams.

##### (2) Development of a superconducting ECR ion source for use in production of a high-intensity heavy ion beam

(T. Nakagawa, J. Ohnishi, M. Kidera, Y. Higurashi, and T. Nagatomo)

The RIBF is required to supply heavy ion beams with very high intensity so as to produce RI's and for super-heavy element search experiment. We have designed and are fabricating an ECR ion source with high magnetic field and high microwave-frequency, since the existing ECR ion sources have their limits in beam intensity. The coils of this ion source are designed to be superconducting for the production of high magnetic field. We are also designing the low-energy beam transport line of the superconducting ECR ion source.

#### Members

##### Team Leader

Takahide NAKAGAWA

##### Research/Technical Scientists

Takashi NAGATOMO (Technical Scientist)  
Masanori KIDERA (Technical Scientist)

Yoshihide HIGURASHI (Technical Scientist)

##### Special temporal employee

Yasuyuki KANAI

#### List of Publications & Presentations

##### Publications

###### [Proceedings]

###### (Original Papers) \*Subject to Peer Review

- T. Nagatomo *et al.*, "Residual gas effect in LEBT on transverse emittance of multiply charged heavy ion beams extracted from ECR ion source," IOP Conf. Proc. 2011, 080004(2018)\*
- Y. Higurashi *et al.*, "Development of RIKEN 28 GHz SC-ECRIS for production of intense metal ion beam," Proc. of ECRIS2018, doi:10.18429/JACoW-ECRIS2018-TUA1
- T. Nagatomo *et al.*, "New 28-GHz superconducting electron cyclotron resonance ion source for synthesizing super-heavy elements with  $Z > 118$ ," Proc. of ECRIS2018, doi:10.18429/JACoW-ECRIS2018-TUA3

##### Oral Presentations

###### [International Conference etc.]

- T. Nakagawa, "Developments of RIKEN 28 GHz SC-ECRIS for synthesizing the super-heavy elements," 14th International Conference on Heavy Ion Accelerator Technology (HIAT2018), Lanzhou, China, October 22–26, 2018.
- T. Nakagawa, "Development of RIKEN 28 GHz SC-ECRIS for production of intense metal ion beam," International Workshop on ECR Ion Sources (ECRIS2018), Catania, Italy, September 10–14, 2018.
- T. Nagatomo, "New 28-GHz superconducting electron cyclotron resonance ion source for synthesizing super-heavy elements with  $Z > 118$ ," Catania, Italy, September 10–14, 2018.

## Research Facility Development Division

### Accelerator Group

### RILAC Team

#### 1. Abstract

The operation and maintenance of the RIKEN Heavy-ion Linac (RILAC) have been carried out. There are two operation modes: one is the stand-alone mode operation and the other is the injection mode operation. The RILAC has been used especially as an injector for the RIKEN RI- Beam Factory accelerator complex. The RILAC is composed of the ECR ion source, the frequency-variable RFQ linac, six frequency-variable main linac cavities, and six energy booster cavities (CSM).

#### 2. Major Research Subjects

- (1) The long term high stability of the RILAC operation.
- (2) Improvement of high efficiency of the RILAC operation.

#### 3. Summary of Research Activity

The RILAC was started to supply ion beams for experiments in 1981. Thousands hours are spent in a year for delivering many kinds of heavy-ion beams to various experiments.

The RILAC has two operation modes: one is the stand-alone mode operation delivering low-energy beams directly to experiments and the other is the injection mode operation injecting beams into the RRC. In the first mode, the RILAC supplies a very important beam to the nuclear physics experiment of “the research of super heavy elements.” In the second mode, the RILAC plays a very important role as upstream end of the RIBF accelerator complex.

The maintenance of these devices is extremely important in order to keep the long-term high stability and high efficiency of the RILAC beams. Therefore, improvements are always carried out for the purpose of more stable and more efficient operation.

#### Members

##### Team Leader

Eiji IKEZAWA

##### Research/Technical Scientist

Yutaka WATANABE (Senior Technical Scientist)

#### List of Publications & Presentations

##### Publications

###### [Proceedings]

K. Kaneko, E. Ikezawa, T. Ohki, H. Yamauchi, K. Oyamada, M. Tamura, A. Yusa, Y. Watanabe, O. Kamigaito, “Present status of RILAC,” Proceedings of the 15th Annual Meeting of Particle Accelerator Society of Japan, 1304–1306 (2018).

##### Posters Presentations

###### [Domestic Conference]

K. Kaneko, E. Ikezawa, T. Ohki, H. Yamauchi, K. Oyamada, M. Tamura, A. Yusa, Y. Watanabe, O. Kamigaito, “Present status of RILAC,” The 15th Annual Meeting of Particle Accelerator Society of Japan, Nagaoka, Japan, August 7–10, 2018.

## Research Facility Development Division Accelerator Group Cyclotron Team

### 1. Abstract

Together with other teams of Nishina Center accelerator division, maintaining and improving the RIBF cyclotron complex. The accelerator provides high intensity heavy ions. Our mission is to have stable operation of cyclotrons for high power beam operation. Recently stabilization of the rf system is a key issue to provide 10 kW heavy ion beam.

### 2. Major Research Subjects

- (1) RF technology for Cyclotrons
- (2) Operation of RIBF cyclotron complex
- (3) Maintenance and improvement of RIBF cyclotrons
- (4) Single turn operation for polarized deuteron beams
- (5) Development of superconducting cavity

### 3. Summary of Research Activity

- Development of the rf system for a reliable operation
- Development of highly stabilized low level rf system
- Development of superconducting cavity
- Development of the intermediate-energy polarized deuteron beams.

## Members

### Team Leader

Naruhiko SAKAMOTO

### Research/Technical Scientists

Kazutaka OZEKI (Technical Scientist)

Kenji SUDA (Technical Scientist)

## List of Publications & Presentations

### Publications

#### [Proceedings]

N. Sakamoto, K. Ozeki, O. Kamigaito, A. Miyamaoto, H. Okuno, K. Suda, Y. Watanabe, K. Yamada, H. Hara, K. Sennyu, T. Yanagisawa, E. Kako, H. Nakai, K. Umemori, "Construction status of the superconducting Linac at the RIKEN Radioactive Isotope Facility," Proceedings of the 29th Linear Accelerator Conference, Beijing, China, September 16–21, 2018.

小山亮, 福澤聖児, 濱仲誠, 石川盛, 小林清志, 仲村武志, 西田稔, 西村誠, 柴田順翔, 月居憲俊, 矢富一慎, 須田健嗣, 藤卷正樹, 福西暢尚, 後藤彰, 長谷部裕雄, 日暮祥英, 今尾浩士, 加瀬昌之, 上垣外修一, 木寺正憲, 込山美咲, 熊谷桂子, 真家武士, 長瀬誠, 長友傑, 中川孝秀, 大西純一, 奥野広樹, 大関和貴, 坂本成彦, 内山暁仁, 渡部秀, 渡邊環, 渡邊裕, 山田一成, 小高康熙, 大城幸光, 「理研 AVF サイクロトロン運転の現状報告」, 第 14 回日本加速器学会年会, p.1395, 北海道大学, 札幌市, 2018 年 8 月 1–3 日.

西村誠, 福澤聖児, 濱仲誠, 石川盛, 小林清志, 小山亮, 仲村武志, 西田稔, 柴田順翔, 月居憲俊, 矢富一慎, 須田健嗣, 藤卷正樹, 福西暢尚, 後藤彰, 長谷部裕雄, 日暮祥英, 今尾浩士, 加瀬昌之, 上垣外修一, 木寺正憲, 込山美咲, 熊谷桂子, 真家武士, 長瀬誠, 長友傑, 中川孝秀, 大西純一, 奥野広樹, 大関和貴, 坂本成彦, 内山暁仁, 渡部秀, 渡邊環, 渡邊裕, 山田一成, 山澤秀行, 「理研 RIBF におけるリングサイクロトロン運転の現状報告」, 第 14 回日本加速器学会年会, 北海道大学, 札幌市, 2018 年 8 月 1–3 日.

### Oral Presentations

#### [International Conference etc.]

N. Sakamoto, K. Ozeki, O. Kamigaito, A. Miyamaoto, H. Okuno, K. Suda, Y. Watanabe, K. Yamada, H. Hara, K. Sennyu, T. Yanagisawa, E. Kako, H. Nakai, K. Umemori, "Construction Status of the Superconducting Linac at the RIKEN Radioactive Isotope Facility," 29th Linear Accelerator Conference, Beijing, China, September 16–21, 2018.

### Posters Presentations

#### [Domestic Conference]

小山亮, 福澤聖児, 濱仲誠, 石川盛, 小林清志, 仲村武志, 西田稔, 西村誠, 柴田順翔, 月居憲俊, 矢富一慎, 須田健嗣, 藤卷正樹, 福西暢尚, 後藤彰, 長谷部裕雄, 日暮祥英, 今尾浩士, 加瀬昌之, 上垣外修一, 木寺正憲, 込山美咲, 熊谷桂子, 真家武士, 長瀬誠, 長友傑, 中川孝秀, 大西純一, 奥野広樹, 大関和貴, 坂本成彦, 内山暁仁, 渡部秀, 渡邊環, 渡邊裕, 山田一成, 小高康熙, 大城幸光, 「理研 AVF サイクロトロン運転の現状報告」, 第 14 回日本加速器学会年会, p.1395, 北海道大学, 札幌市, 2018 年 8 月 1–3 日.

西村誠, 福澤聖児, 濱仲誠, 石川盛, 小林清志, 小山亮, 仲村武志, 西田稔, 柴田順翔, 月居憲俊, 矢富一慎, 須田健嗣, 藤卷正樹, 福西暢

尚, 後藤彰, 長谷部裕雄, 日暮祥英, 今尾浩士, 加瀬昌之, 上垣外修一, 木寺正憲, 込山美咲, 熊谷桂子, 真家武士, 長瀬誠, 長友傑, 中川孝秀, 大西純一, 奥野広樹, 大関和貴, 坂本成彦, 内山暁仁, 渡部秀, 渡邊環, 渡邊裕, 山田一成, 山澤秀行, 「理研 RIBF におけるリングサイクロロン運転の現状報告」, 第 14 回日本加速器学会年会, 北海道大学, 札幌市, 2018 年 8 月 1-3 日.

## Research Facility Development Division

### Accelerator Group

### Beam Dynamics & Diagnostics Team

#### 1. Abstract

Aiming at stable and efficient operation of the RIBF cascaded cyclotron system, Beam Dynamics and Diagnostics Team develops power supplies, beam instrumentation, computer control and beam dynamic studies. We have successfully increased the beam availability for user experiments to more than 90%. We have also established small-beam-loss operations. The latter strongly contributes to recent high-power operations at RIBF.

#### 2. Major Research Subjects

- (1) More efficient and stable operations of the RIBF cascaded cyclotron system
- (2) Maintenance and developments of the beam instrumentation
- (3) Developments of computer control system for more intelligent and efficient operations
- (4) Maintenance and improvements of the magnet power supplies for more stable operations
- (5) Upgrade of the existing beam interlock system for high-power beams with few tens of kW

#### 3. Summary of Research Activity

- (1) High-intensity heavy-ion beams such as 72-pnA uranium, 102-pnA xenon, 486-pnA krypton, and 740-pnA calcium beams have been obtained.
- (2) The world-first high-Tc SQUID beam current monitor has been developed.
- (3) The bending power of the fixed-frequency Ring Cyclotron has been upgraded to 700 MeV.
- (4) The world-most-intense V beams are stably supplied to super-heavy-element search experiments.
- (5) The RIBF control system has been operated stably by replacing legacy hardware controllers carried over from our old facility with new ones. Several useful operation tools are also developed.
- (6) The dated power supplies exciting the main coils of RIKEN Ring Cyclotron has been upgrade to a new one having a better long-term stability than the old ones.

#### Members

##### Team Leader

Nobuhisa FUKUNISHI (concurrent; Deputy Group Director,  
Accelerator Gr.)

##### Research/Technical Scientists

Masaki FUJIMAKI (Senior Technical Scientist)  
Kazunari YAMADA (Senior Technical Scientist)  
Keiko KUMAGAI (Senior Technical Scientist)

Akito UCHIYAMA (Technical Scientist)  
Tamaki WATANABE (Senior Technical Scientist)

##### Expert Technician

Misaki KOMIYAMA

##### Part-time Worker

Makoto NAGASE

##### Visiting Scientists

Kenichi ISHIKAWA (Univ. of Tokyo)  
Takuya MAEYAMA (Kitasato Univ.)

Shin-ichiro HAYASHI (Hiroshima Int'l Univ.)

#### List of Publications & Presentations

##### Publications

###### [Journal]

###### (Original Papers) \*Subject to Peer Review

- T. Maeyama, Y. Ishida, Y. Kudo, K. Fukasaku, K. L. Ishikawa, N. Fukunishi, "Polymer gel dosimeter with AQUAJoint as hydrogel matrix," *Radiat. Phys. Chem.* **146**, 121–125, doi:0.10216/j.radphyschem.2018.01.014 (2018).
- T. Nishi, K. Itahashi, G. P. A. Berg, H. Fujioka, N. Fukuda, N. Fukunishi, H. Geissel, R. S. Hayano, S. Hirezaki, K. Ichikawa, N. Ikeno, N. Inabe, S. Itoh, M. Iwasaki, D. Kameda, S. Kawase, T. Kubo, K. Kusaka, H. Matsubara, S. Michimasa, K. Miki, G. Mishima, H. Miya, H. Nagahiro, M. Nakamura, S. Noji, K. Okochi, S. Ota, N. Sakamoto, S. Suzuki, H. Takeda, Y. K. Tanaka, K. Todoroki, K. Tsukada, T. Uesaka, Y. N. Watanabe, H. Weick, H. Yamakami, K. Yoshida, "Spectroscopy of pionic atoms in  $^{122}\text{Sn}(d, ^3\text{He})$  reaction and angular dependence of the formation cross section," *Phys. Rev. Lett.* **120**, 152502 (2018).

**Oral Presentations****[International Conference etc.]**

T. Nagatomo, Y. Higurashi, J. Ohnishi, A. Uchiyama, K. Kumagai, M. Fujimaki, N. Fukunishi, N. Sakamoto, T. Nakagawa, O. Kamigaito, “New 28-GHz superconducting electron cyclotron resonance ion source for synthesizing super-heavy elements with  $Z > 118$ ,” 23th. Int. Workshop on ECR Ion Sources (ECRIS2018), TUA3 (pp. 53–57), Catania, Italy, September 2018.

**[Domestic Conference]**

T. Watanabe, H. Imao, O. Kamigaito, N. Sakamoto, N. Fukunishi, M. Fujimaki, K. Yamada, Y. Watanabe, R. Koyama, T. Toyama, T. Miyao, A. Miura, “Development of beam energy position monitor system for RIKEN superconducting acceleration cavity,” 15th Annual Meeting of Particle Accelerator Society of Japan, pp. 49–54, Nagaoka, Japan, August 2018.

**Posters Presentations****[International Conference etc.]**

A. Uchiyama, T. Nagatomo, Y. Higurashi, J. Ohnishi, T. Nakagawa, M. Komiyama, N. Fukunishi, H. Yamauchi, M. Tamura, “Design of reliable control with star-topology fieldbus communication for an electron cyclotron resonance ion source at RIBF,” 12th International Workshop on Personal Computers and Particle Accelerator Controls (PCaPAC2018), WEP30, Hsinchu, Taiwan, October 2018.

M. Komiyama, M. Fujimaki, N. Fukunishi, K. Kumagai, A. Uchiyama, “Recent development of the RIKEN RI Beam Factory control system,” 12th International Workshop on Personal Computers and Particle Accelerator Controls (PCaPAC2018), WEP15, Hsinchu, Taiwan, October 2018.

**[Domestic Conference]**

T. Watanabe, H. Imao, O. Kamigaito, N. Sakamoto, N. Fukunishi, M. Fujimaki, K. Yamada, Y. Watanabe, R. Koyama, T. Toyama, T. Miyao, A. Miura, “Development of beam energy position monitor system for RIKEN superconducting acceleration cavity,” 15th Annual Meeting of Particle Accelerator Society of Japan, pp. 49–54, Nagaoka, Japan, August 2018.

A. Uchiyama, M. Komiyama, “Current status of server and system infrastructure for RIBF control system,” 15th Annual Meeting of Particle Accelerator Society of Japan, pp. 597–600, Nagaoka, Japan, August 2018.

K. Kobayashi, K. Ozeki, A. Goto, J. Ohnishi, Y. Oshiro, S. Fukuzawa, M. Hamanaka, S. Ishikawa, R. Koyama, T. Nakamura, M. Nishida, M. Nishimura, J. Shibata, N. Tsukiori, K. Yadomi, K. Kaneko, K. Oyamada, M. Tamura, A. Yusa, M. Fujimaki, N. Fukunishi, H. Hasebe, Y. Higurashi, H. Imao, M. Kase, O. Kamigaito, M. Kidera, M. Komiyama, K. Kumagai, T. Maie, M. Nagase, T. Nagatomo, T. Nakagawa, H. Okuno, N. Sakamoto, K. Suda, A. Uchiyama, S. Watanabe, T. Watanabe, Y. Watanabe, K. Yamada, Y. Kotaka, “Status report on operation of RIKEN AVF cyclotron,” 15th Annual Meeting of Particle Accelerator Society of Japan, pp. 1293–1297, Nagaoka, Japan, August 2018.

J. Shibata, K. Suda, S. Fukuzawa, M. Hamanaka, S. Ishikawa, K. Kobayashi, R. Koyama, T. Nakamura, M. Nishida, M. Nishimura, N. Tsukiori, K. Yadomi, T. Dantsuka, M. Fujimaki, T. Fujinawa, N. Fukunishi, H. Hasebe, Y. Higurashi, E. Ikezawa, H. Imao, O. Kamigaito, Y. Kanai, M. Kase, M. Kidera, M. Komiyama, K. Kumagai, T. Maie, M. Nagase, T. Nagatomo, T. Nakagawa, M. Nakamura, J. Ohnishi, H. Okuno, N. Sakamoto, K. Ozeki, A. Uchiyama, S. Watanabe, T. Watanabe, Y. Watanabe, K. Yamada, H. Yamasawa, “Status report of the operation of RIBF Ring cyclotrons,” 15th Annual Meeting of Particle Accelerator Society of Japan, pp. 1298–1303, Nagaoka, Japan, August 2018.

**Research Facility Development Division**  
**Accelerator Group**  
**Cryogenic Technology Team**

### 1. Abstract

We are operating the cryogenic system for the superconducting ring cyclotron in RIBF. We are operating the helium cryogenic system in the south area of RIKEN Wako campus and delivering the liquid helium to users in RIKEN. We are trying to collect efficiently gas helium after usage of liquid helium.

### 2. Major Research Subjects

- (1) Operation of the cryogenic system for the superconducting ring cyclotron in RIBF
- (2) Operation of the helium cryogenic plant in the south area of Wako campus and delivering the liquid helium to users in Wako campus.

### 3. Summary of Research Activity

- (1) Operation of the cryogenic system for the superconducting ring cyclotron in RIBF  
(H. Okuno, T. Dantsuka, M. Nakamura, T. Maie)
- (2) Operation of the helium cryogenic plant in the south area of Wako campus and delivering the liquid helium to users in Wako campus.  
(T. Dantsuka, S. Tsuruma, H. Okuno).

## Members

### Team Leader

Hiroki OKUNO (concurrent: Deputy Group Director, Accelerator Group)

### Research/Technical Scientist

Masato NAKAMURA (Senior Technical Scientist)

### Expert Technicians

Takeshi MAIE

Tomoyuki DANTSUKA

### Part-time Workers

Shizuho TSURUMA

Mayumi KUROIWA

## Research Facility Development Division Accelerator Group Infrastructure Management Team

### 1. Abstract

Our team is in charge of operation, maintenance, and monitoring of research infrastructure of the whole RIBF, such as cooling water system, air conditioner system, building equipment, and so on. It is very important to keep these infrastructures working properly for the effective and efficient operation of RIBF.

We are also involved in the planning of the RIBF beam time, which is conducted by the RIBF User Liaison Team, through the estimation of the utility costs such as the electricity and the gas used for the power generator. Another important mission of our team is to coordinate large-scale repair works carried out by the RIKEN Facility Section so that the beam time can proceed smoothly.

In the last three years, there were big construction works related to the upgrade project of the RILAC facility. We carried out the design of the SRF test facility, took part in the design work of the new building for radioisotope purification, jointly designed the ion source room, and so on. The transfer work of GARIS II and the room-temperature cavities of the RILAC booster was conducted by our team.

### 2. Major Research Subjects

- (1) Operation, maintenance and monitoring of infrastructure of RI Beam Factory.
- (2) Participation in the beam time planning through utility cost estimation.
- (3) Coordination of large construction work and modification related to RI Beam Factory.

### Members

#### Team Leader

Osamu KAMIGAITO (concurrent; Group Director, Accelerator Group)

#### Deputy Team Leader

Yutaka WATANABE (concurrent; Senior Technical Scientist, RILAC Team.)

#### Research/Technical Scientist

Shu WATANABE (Senior Technical Scientist)

#### Special Temporary Employee

Hideyuki YAMASAWA

## Research Facility Development Division Instrumentation Development Group

### 1. Abstract

This group develops core experimental installations at the RI Beam factory. Three projects are currently going on. SLOWRI is an experimental installations under testing and a common element enabling multiple-use. This will stop high-energy RI beams in a gas-catcher system and re-accelerates up to several-tenth keV, and the high-quality cold RI beam will be delivered to the users. SCRIT is the world first facility for an electron scattering off unstable nuclei, and has been constructed independently of the RIBF main facility. The first physic result was demonstrated in 2017, and the facility is now under upgrading of the electron beam power driving the RI beam production. Rare-RI Ring is an event-by-event operated heavy-ion storage ring aiming at the precision mass measurement for extremely rare exotic nuclei. This is now open for an experimental proposal application, and has already performed PAC-approved experiments. All instrumentations were designed to maximize the research potential of the world's most intense RI beams, and the exclusive equipment available at the RI Beam Factory makes experimental challenges possible. Technologies and experiences accumulated in this group will be able to provide opportunities of new experimental challenges and the foundation for future developments of RIBF.

### 2. Major Research Subjects

- (1) SCRIT Project
- (2) SLOWRI Project
- (3) Rear RI Ring Project
- (4) Beam recycling development (in future plan)

### 3. Summary of Research Activity

We are developing beam manipulation technology in carrying out above listed project. They are the high-quality slow RI beam production (SCRIT and SLOWRI), the beam cooling and stopping (SCRIT and SLOWRI), and the beam accumulation technology (Rare RI Ring) in a storage ring. The technological knowhow accumulated in our projects will play a significant role in the next generation RIBF. Status and future plan for each project is described in subsections. The electron scattering from  $^{132}\text{Xe}$  isotopes has been successfully measured and the nuclear charge density distribution has been obtained in SCRIT. We are almost ready for the electrons scattering experiments for unstable nuclei. Rare RI Ring has been commissioned and the performances has been evaluated. We have demonstrated a mass-measurement capability of R3 and successfully started mass-measurements for unknown-mass nuclei in the experiments approved by PAC. SLOWRI is now under test experiments to establish a slow RI beam production using two types of gas cells. PALIS has been commissioned from 2015, and basic functions such as, for instance, the RI-beam stopping in Ar gas cell and the extraction from the gas cell have been evaluated. RF ion-guide gas cell is now under testing and it is planned to be commissioned in next year. Future plans for these projects are described in subsections.

We are going to start a new project from next year. According to the future plan of Nishina center, we are going to start to develop a beam re-cycling technique. A circulation of an RI beam in a storage ring equipped by a thin internal target is maintained until that some nuclear reaction happen at the target. The circulating beam loses a energy and the emittance grows up turn by turn because of existing internal target. In order to establish a beam re-cycling technique, the energy loss and the emittance growth have to be compensated by using a re-acceleration system and a beam-cooling or a fast feedback system. A beam re-cycling technique is supposed to greatly enhance an RI use efficiency in a nuclear physics study. As a first step for the development of these novel technique, we are going to install a testbench consisting of a relatively small size of heavy-ion storage ring that will be connect to our ISOL (ERIS) in SCRIT facility. This ring named sLSR is equipped by acceleration devices and beam-cooling devices necessary in our R&D study, and was originally constructed at the Institute for Chemical Research, Kyoto University more than ten years ago. This will be moved to RIBF in this year, and re-constructed by the SCRIT facility in following year.

### Members

#### Group Director

Masanori WAKASUGI

#### Visiting Scientist

Akira OZAWA (Univ. of Tsukuba)

#### Research Fellow

Mamoru TOGASHI (Rikkyo Univ.)

#### Student Trainees

Mitsuki HORI (Rikkyo Univ.)

So SATO (Rikkyo Univ.)

Nobuaki UCHIDA (Rikkyo Univ.)

Moe NAKANO (Rikkyo Univ.)

Shinnosuke SASAMURA (Rikkyo Univ.)

**Part-time Worker**

Mitsuki HORI

**List of Publications & Presentations**

Publications and presentations for each project team are listed in subsections.

Research Facility Development Division  
Instrumentation Development Group  
SLOWRI Team

## 1. Abstract

SLOWRI is a universal low-energy RI-beam facility at RIBF that provides a wide variety of short-lived nuclei as high-purity and low-emittance ion beams or stored ions in a trap, including a parasitic operation mode. The SLOWRI team develops and manages the facility and performs high-precision spectroscopy experiments. The construction of the SLOWRI facility began in FY2013 and commissioning work is ongoing. High-energy radioactive ion beams from the projectile fragment separator BigRIPS are thermalized in a large He gas catcher cell (RFC cell) or in a small Ar gas catcher cell (PALIS cell). From these gas cells, the low-energy ion beams will be delivered via mass separators and switchyards to various devices: such as an ion trap, a collinear fast beam apparatus, and a multi-reflection time of flight mass spectrograph. A multi-reflection time-of-flight mass spectrograph (MRTOF) has been also developed. Two mass measurement projects using MRTOF mass spectrographs have been started: one is for trans uranium elements at the GARIS facility and the other is for r-process nuclides at SLOWRI facility. At GARIS-II, we installed second prototype SLOWRI combined with MRTOF, which is a medium-sized cryogenic RF-carpet He gas cell. Using second prototype SLOWRI, more than 80 nuclear masses have been measured including first mass measurements of Md and Es isotopes. At SLOWRI facility, third prototype SLOWRI is under construction, which is 50-cm-long RF-carpet-type He gas cell combined with MRTOF. The third prototype will be installed at F11 of BigRIPS, downstream of ZeroDegree spectrometer, which can provide symbiotic measurements with other BigRIPS experiments.

An online commissioning experiment of parasitic low-energy production facility (PALIS) was performed and confirmed that the PALIS setup can coexist with other BigRIPS experiments. Currently, PALIS gas cell is under on- and off-line commissioning.

## 2. Major Research Subjects

- (1) Construction of the stopped and low-energy RI-beam facility, SLOWRI.
- (2) Development of a multi-reflection time-of-flight mass spectrograph for precision mass measurements of short-lived nuclei.
- (3) Development of collinear laser spectroscopy apparatus.
- (4) Development of a parasitic slow RI-beam production method using resonance laser ionization.
- (5) Development of highly charged ion trap for fundamental physics

## 3. Summary of Research Activity

### (1) Construction of stopped and low-energy RI-beam facility (SLOWRI)

SLOWRI consists of two gas catchers (RF carpet gas cell and PALIS gas cell), mass separators a 50-m-long beam transport line, a beam cooler-buncher, an isobar separator, and a laser system. The RF carpet gas cell will be installed at the exit of the D5 dipole magnet of BigRIPS. The gas catcher contains a large cryogenic He gas cell with a large traveling wave rf-carpet. The PALIS gas cell is installed in the vicinity of the second focal plane slit of BigRIPS. It will provide parasitic RI-beams from those ions lost in the slits during other experiments. In this gas catcher, thermalized RI ions quickly become neutral and will be re-ionized by resonant laser radiations. The beam transport line consists of four dipole magnets, two focal plane chambers, 62 electrostatic quadrupole singlets, 11 electrostatic quadrupole quartets and 7 beam profile monitors. Off- and on-line commissioning is underway.

Based on test experiments with the prototype setups, the RF-carpet gas cell contains a three stage rf-carpet structure: a gutter rf carpet (1<sup>st</sup> carpet) for the collection thermal ions in the cell into a small slit, a narrow (about 10 mm) traveling-wave rf-carpet for collection of ions from the gutter carpet and for transporting the ions towards the exit, and a small rf carpet for extraction from the gas cell. In FY2018, ion extraction test at off-line using this carpet has been successfully performed with about 60% extraction efficiency to ions gathered on 1<sup>st</sup> carpet. We will install the RF-carpet gas cell combined with MRTOF at F11 of BigRIPS at first, where the on-line commissioning and systematic mass measurements will be started from FY2019. At F11, symbiotic measurements with other BigRIPS experiments can be performed.

### (2) Development of a multi-reflection TOF mass spectrograph for short-lived nuclei

The atomic mass is one of the most important quantities of a nucleus and has been studied in various methods since the early days of modern physics. From among many methods we have chosen a multi-reflection time-of-flight (MR-TOF) mass spectrometer. Slow RI beams extracted from the RF ion-guide are bunched and injected into the spectrometer with a repetition rate of ~100 Hz. A mass-resolving power of 170,000 has been obtained with a 2 ms flight time for <sup>40</sup>K and <sup>40</sup>Ca isobaric doublet. This mass-resolving power should allow us to determine ion masses with an accuracy of  $\leq 10^{-7}$ .

The MR-TOF mass spectrograph has been placed under the GARIS-II separator aiming at direct mass measurements of trans-uranium elements. A medium-sized cryogenic He gas cell was placed at the focal plane of GARIS-II and a bunched low-energy heavy ion beam was transported to the trap of MR-TOF. Mass measurements of more than 80 nuclides, including short-lived ( $T_{1/2} = 10$  ms) isotopes of Ra and several isotopes of the trans-uranium elements Fm, Es, No and Md were performed in collaboration with Wako Nuclear Science Center (WNSC) of KEK and Super Heavy Element Synthesis team of RIKEN. The highest precisions, achieved for Ga isotopes, reached a level of 0.03 ppm. The masses of four isotopes of Es and Md were measured for the first time, allowing for confirmation of the  $N = 152$  shell closure in Md. Using these new mass data as anchor-points, the masses of seven isotopes of super-heavy elements up to Mt were indirectly determined. For comprehensive mass measurements of all available nuclides, multiple

units of gas catchers and MR-TOF devices will be placed at GARIS-III, KISS as well as the BigRIPS + SLOWRI facilities of RIBF.

### (3) Development of collinear fast beam apparatus for nuclear charge radii measurements

The root-mean-square charge radii of unstable nuclei have been determined exclusively by isotope shift measurements of the optical transitions of singly charged ions or neutral atoms by laser spectroscopy. Many isotopes of alkali, alkali-earth, and noble-gas elements in addition to several other elements have been measured by collinear laser spectroscopy since these ions all have good optical transitions and are available at conventional ISOL facilities. However, isotopes of other elements, especially refractory and short-lived ones, have not been investigated so far.

In SLOWRI, isotopes of all atomic elements will be provided as well collimated, mono-energetic ion beams. This should expand the range of nuclides available for laser spectroscopy. In the first years of the RIBF project, elements in the vicinity of Ni, such as Ni, Co, Fe, Cr, Cu, Ga, and Ge are planned to be investigated. They all have possible optical transitions in the ground states of neutral atoms with presently available laser systems. Some of them have so called recycling transitions, which enhance the detection probabilities noticeably. Furthermore, the multistep resonance ionization (RIS) method can be applied to the isotopes of Ni as well as those of some other elements. The required minimum intensity for this method can be as low as 10 atoms per second.

An off-line mass separator and a collinear fast beam apparatus with a large solid-angle fluorescence detector was built previously. A 617-nm transition of the metastable  $\text{Ar}^+$  ion at 20 keV was measured with both collinear and anti-collinear geometry, which allowed determination of the absolute resonant frequency of the transition at rest with a relative accuracy better than  $10^{-8}$ . A new setup is under preparation at the SLOWRI experiment area in collaboration with the Ueno nuclear spectroscopy laboratory.

### (4) Development of parasitic slow RI-beam production scheme using resonance laser ionization

More than 99.9% of RI ions produced in projectile fission or fragmentation are simply dumped in the first dipole magnet and the slits. A new scheme, named PALIS, meant to rescue such precious RI using a compact gas catcher cell and resonance laser ionization, was proposed as a part of SLOWRI. The thermalized RI ions in a cell filled with Ar gas can be quickly neutralized and transported to the exit of the cell by gas flow. Irradiation of resonance lasers at the exit ionizes neutral RI atoms efficiently and selectively. The resonance ionization scheme itself can also be a useful method to perform hyperfine structure spectroscopy of RI of many elements.

An online setup has been fabricated in FY2013 and the first online commissioning took place in FY2015. It was confirmed that the PALIS gas cell is not deleterious for BigRIPS experiments, and a reasonable amount of radioactive Cu isotopes was extracted from the cell by gas flow. At off-line, using  $\alpha$  rays from Am source, impurities inside the gas cell have been investigated. Thanks to baking the gas cell with gas flow, almost impurities have been successfully suppressed at off-line condition. Technical developments are under progress in on- and off-line commissioning.

### (5) Development of highly charged ion trap for fundamental physics

Some particular transitions in highly charged ions (HCI) are sensitive to the temporal variation of the fine structure constant. High precision spectroscopy of such transitions can be a probe for the verification of fundamental physics. A cryogenic ion trap setup consisting of a micro electron beam ion trap ( $\mu$ EBIT) and a linear RFQ ion trap in a compact cryogenic enclosure is under development in collaboration with Quantum Metrology Laboratory. First candidate HCIs, such as  $\text{Ba}^{7+}$  or  $\text{Ho}^{14+}$  can be produced in the  $\mu$ EBIT and sympathetically cooled by laser cooled  $\text{Be}^+$  ions in the linear RFQ trap, following which the “clock” transition can be measured by electron-shelving spectroscopy. The final target is  $^{249}\text{Cf}^{15+}$ , which is known to have the most sensitive transition to the temporal variation of the fine structure constant.

## Members

### Team Leader

Hironobu ISHIYAMA

### Research/Technical Scientists

Takao KOJIMA (Senior Research Scientist)

Tetsu SONODA (Technical Scientist)

Aiko TAKAMINE (concurrent; Nuclear Spectroscopy Laboratory)

Takeshi MAIE (concurrent; Cryogenic Technology Team)

### Special Postdoctoral Researcher

Marco ROSENBUSCH

### Part-time Worker

Ichiro KATAYAMA

### Visiting Scientists

Hans A SCHUESSLER (Texas A&M Univ.)

Hideki IIMURA (JAEA)

Kunihiro OKADA (Sophia Univ.)

Mikael REPONEN (JYFL)

Hermann WOLLNIK (Univ. of Giessen)

Hideki TOMITA (Nagoya Univ.)

Volker SONNENSCHNEIDER (Nagoya Univ.)

**Student Trainees**

Naoki KIMURA (Sophia Univ.)  
 Masaya OOHASHI (Nagoya Univ.)

Kento SUZUKI (Univ. of Electro-Communications)  
 Ryunosuke KODAMA (Univ. of Electro-Communications)

**List of Publications & Presentations****Publications****[Journal]****(Original Papers) \*Subject to Peer Review**

- M. Rosenbusch, Y. Ito, P. Schiry, M. Wada, D. Kaji, K. Morimoto, H. Haba, S. Kimura, H. Koura, M. MacCorimik, H. Miyatake, J. Y. Moon, K. Morita, I. Murray, T. Niwase, A. Ozawa, M. Reponen, A. Takamine, T. Tanaka, H. Wollnik, "New mass anchor points for neutron-deficient heavy nuclei from direct mass measurements of radium and actinium isotopes," *Phys. Rev. C* **97**, 064306 (2018). \*
- N. Kimura, R. Kodama, K. Suzuki, S. Ohishi, M. Wada, K. Okada, N. Ohmae, H. Katori, N. Nakamura, "Direct wavelength measurement of the visible M1 transition in Ba<sup>7+</sup> with a novel calibration method," *Plasma and Fusion Research* **14**, 1201021 (2019). \*
- Y. Ito, P. Schury, M. Wada, F. Arai, H. Haba, Y. Hirayama, S. Ishizawa, D. Kaji, S. Kimura, H. Koura, M. MacCormick, H. Miyatake, J. Y. Moon, K. Morimoto, K. Morita, M. Mukai, I. Murray, T. Niwase, K. Okada, A. Ozawa, M. Rosenbusch, A. Takamine, T. Tanaka, Y. X. Watanabe, H. Wollnik, S. Yamaki, "First direct mass measurements of nuclides around Z = 100 with a multireflection time-of-flight mass spectrograph," *Phys. Rev. Lett.* **120**, 152501 (2018). \*
- T. Sonoda, H. Iimura, M. Reponen, M. Wada, I. Katayama, V. Sonnenschein, T. Takamatsu, H. Tomita, T. M. Kojima, "The laser and optical system for the RIBF-PALIS experiment," *Nucl. Instrum. Methods Phys. Res. A* **877**, 118–123 (2018). \*
- S. Kimura, Y. Ito, D. Kaji, P. Schury, M. Wada, H. Haba, T. Hashimoto, Y. Hirayama, M. MacCormick, H. Miyatake, J. Y. Moon, K. Morimoto, M. Mukai, I. Murraya, A. Ozawa, M. Rosenbusch, H. Schatz, A. Takamine, T. Tanaka, Y. X. Watanabe, H. Wollnik, "Atomic masses of intermediate-mass neutron-deficient nuclei with relative uncertainty down to 35-ppb via multireflection time-of-flight mass spectrograph," *Int. J. Mass Spectrom.* **430**, 134–142 (2018).
- T. M. Kojima, "Ion guiding in macro-size insulating capillaries: straight, tapered, and curved shapes," *J. Phys. B: At. Mol. Opt. Phys.* **51**, 042001 (2018). \*
- K. Imamura, Y. Matsuo, W. Kobayashi, T. Egami, M. Sanjo, A. Takamine, T. Fujita, D. Tominaga, Y. Nakamura, T. Furukawa, T. Wakui, Y. Ichikawa, H. Nishibata, T. Sato, A. Gladkov, L. C. Tao, T. Kawaguchi, Y. Baba, M. Iijima, H. Gonda, Y. Takeuchi, R. Nakazato, H. Odashima, H. Ueno, "Absolute optical absorption cross-section measurement of Rb atoms injected into superfluid helium using energetic ion beams," *App. Phys. Exp.* **12**, 016502 (2019). \*
- M. Reponen, V. Sonnenschein, T. Sonoda, H. Tomita, M. Oohashi, D. Matsui, M. Wada, "Towards in-jet resonance ionization spectroscopy: An injection-locked Titanium:Sapphire laser system for the PALIS-facility," *Nucl. Instrum. Methods Phys. Res. A* **908**, 236–243 (2018). \*

**Oral Presentations****[International Conference etc.]**

- A. Takamine, "Laser spectroscopy project at the SLOWRI facility in RIKEN," 20th Northeastern Asian Symposium-2018 on Nuclear Physics in the 21st Century, Nagoya, Japan, September 18–19, 2018.
- A. Takamine, "Prospects for laser spectroscopy project at the SLOWRI facility in RIKEN RIBF," 2018 Korea Physics Society Fall Meeting, Changwon, Korea, October 24–26, 2018.
- N. Kimura, R. Kodama, K. Suzuki, S. Ohishi, M. Wada, K. Okada, N. Ohmae, H. Katori, N. Nakamura, "Visible spectroscopy of highly charged barium ions in a compact electron beam ion trap with a buffer gas calibration method," 19th International Conference on the Physics of Highly Charged Ions (HCI2018), Lisboa, Portugal, September, 2018.
- N. Kimura, R. Kodama, K. Suzuki, S. Ohishi, M. Wada, K. Okada, N. Ohmae, H. Katori, N. Nakamura, "Applications of buffer gas in a compact EBIT for reliable spectroscopic calibration," The 13th International Symposium on Electron Beam Ion Sources and Traps (EBIST2018), Shanghai, China, October, 2018.
- M. Rosenbusch, "Status and future plans for MRTOF mass measurements at RIKEN-RIBF," International Conference on Electromagnetic Isotope separator and related topics (EMIS XVIII), CERN (Geneva), Swiss, September 16–21, 2018.
- M. Rosenbusch, "MRTOF mass measurements at RIBF: Recent measurements of heavy isotopes and future plans for the super-heavy region," TASCAs workshop, GSI (Darmstadt), Germany, September 25, 2018.
- M. Rosenbusch, "Recent successes of multi-reflection devices at RIKEN's RIBF facility and some thoughts about highly accurate mass calibration using ion traps," 10th International Conference on Charged Particle Optics (CPO-10), Key West (Florida), USA, October 17–21, 2018.
- M. Rosenbusch, "Follow-ups on great achievements: New MRTOF-MS projects at RIKEN-RIBF," Fifth joint meeting of the Division of Nuclear Physics of the American Physical Society (APS) with the nuclear physicists of the Physical Society of Japan (JPS), Hawaii, USA, October 23–27, 2018.
- H. Ishiyama, "SLOWRI and related topics," RIBF Seminar, Wako, Japan, July 3, 2018.
- H. Ishiyama, "Present status of SLOWRI," RIBF Users Meeting 2018, Wako, Japan, September 5, 2018.
- H. Ishiyama, "Present status of SLOWRI," SSRI-PNS collaboration meeting 2018, Wako, Japan, September 4, 2018.

**[Domestic Conference]**

高峰愛子, 「高偏極 RI ビームの生成と核・物質科学研究への応用」, 新学術領域研究「宇宙観測検出器と量子ビームの出会い. 新たな応用への架け橋.」, キックオフシンポジウム, 仙台, 2018 年 12 月 17-18 日.

## Research Facility Development Division Instrumentation Development Group Rare RI-ring Team

### 1. Abstract

The aim of Rare-RI Ring (R3) is to measure the masses of short-lived unstable nuclei far from the beta-stability line. In particular, a high-precision mass measurement for nuclei located around the r-process pass (rare-RI) is required in nucleosynthesis point of view. The R3 completed the construction at the end of 2014, and has been performed commissioning experiments several times by 2017. Through the commissioning experiments, we confirmed the high ability of R3 as a storage ring capable of handling one event, and demonstrated that it is possible to perform the time-of-flight Isochronous Mass Spectrometry (IMS) in shorter than 1 ms. We have acquired an adequate efficiency to conduct the mass measurement experiments in the end of 2017. In 2018, we have successfully conducted the first mass measurement experiment for  $^{74,76}\text{Ni}$ ,  $^{122}\text{Rh}$ ,  $^{123,124}\text{Pd}$ , and  $^{125}\text{Ag}$ . The analysis is in progress for giving the new experimental mass values of  $^{74,76}\text{Ni}$ ,  $^{122}\text{Rh}$ ,  $^{124}\text{Pd}$ , and for improving the experimental mass values of  $^{123}\text{Pd}$ ,  $^{125}\text{Ag}$ .

### 2. Major Research Subjects

- (1) Developments of heavy-ion storage ring
- (2) Precision mass measurement for rarely produced isotopes related to r-process.

### 3. Summary of Research Activity

In the commissioning experiments up to 2017, we confirmed the unique performances of R3 and demonstrated the time-of-flight isochronous mass measurement method. The ring structure of R3 was designed with a similar concept of a separate-sector ring cyclotron. It consists of six sectors and straight sections, and each sector consists of four rectangular bending magnets. Two magnets at both ends of each sector are additionally equipped with ten trim coils to form a precise isochronous field. We have realized in forming the precise isochronous field of 5 ppm with wide momentum range of  $\Delta p/p = \pm 0.5\%$ . Another performance required for R3 is to efficiently seize hold of an opportunity of the mass measurement for rare-RI produced unpredictably. It was realized by constructing the Isotope-Selectable Self-trigger Injection (ISSI) scheme which pre-identified rare-RI itself triggers the injection kicker magnets. Key device was an ultra-fast response kicker system that has been successfully developed. Full activation of the kicker magnetic field can be completed within the flight time of the rare-RI from an originating point (F3 focal point in BigRIPS) of the trigger signal to the kicker position in R3.

Since R3 accumulates, in principle, only one event, we fabricated high-sensitive beam diagnostic devices in the ring. They should be applicable even for one event circulation. One of them is a cavity type of Schottky pick-up installed in the straight section of R3. The Schottky pick-up successfully monitored a single  $^{78}\text{Kr}^{36+}$  ion circulation with the measurement time of less than 10 ms in the first commissioning experiment. We also confirmed that it is useful for fine tuning of the isochronous field. Another is a timing monitor, which detects secondary electrons emitted from thin carbon foil placed on the circulation orbit. The thickness of the foil is  $50 \mu\text{g}/\text{cm}^2$ . This timing monitor is working well to observe first several tens turns for injected event.

We performed mass measurement in the third commissioning experiment by using unstable nuclei which masses are well-known. The masses of  $^{79}\text{As}$ ,  $^{77}\text{Ga}$ ,  $^{76}\text{Zn}$ , and  $^{75}\text{Cu}$  relative to  $^{78}\text{Ge}$  were derived with the accuracy of  $\sim 10$  ppm. In addition, we have improved the extraction efficiency to 2% by considering the matching condition between the emittance of injection events and the acceptance of R3. This extraction efficiency was sufficient to conduct the accepted two proposals: mass measurements of Ni isotopes and mass measurements of Sn region.

In the beginning of 2018, we examined the feasibility of these two proposals in detail. Consequently, we decided to proceed with two proposals at the same period. In the beginning of November 2018, we have conducted the first experiment using the R3 to measure the masses for  $^{74,76}\text{Ni}$  in 4 days. After that, we also measured the masses for  $^{122}\text{Rh}$ ,  $^{123,124}\text{Pd}$ , and  $^{125}\text{Ag}$  in 4.5 days at the end of November 2018. These nuclei were successfully extracted from R3 with the efficiency of 1–2%. The masses of  $^{74,76}\text{Ni}$ ,  $^{122}\text{Rh}$ , and  $^{124}\text{Pd}$  can be determined experimentally for the first time. On the other hand, the masses of  $^{123}\text{Pd}$  and  $^{125}\text{Ag}$  will be improved the precision compared with previous experimental values. These analyses are still in progress. Since each proposal has a machine time of several days to measure the masses of exotic nuclei, we will plan to conduct the mass measurements of the other Ni isotopes and nuclei of Sn region in 2019.

## Members

### Team Leader

Masanori WAKASUGI (concurrent: Group Director, Instrumentations Development Gr.)

### Research/Technical Scientist

Yoshitaka YAMAGUCHI (Technical Scientist)

**Expert Technician**

Takeshi MAIE (concurrent: Cryogenic Technology Team)

**Postdoctoral Researcher**

Yasushi ABE

**Special Postdoctoral Researcher**

Fumi SUZAKI

**List of Publications & Presentations****Publications****Oral Presentations****[International Conference etc.]**

- S. Naimi, “The Rare-RI Ring ready to conquer Terra Incognita—Mass measurement of r-process nuclei at RIKEN—,” FRIB and the GW170817 kilonova Workshop, East Lansing, USA, July, 2018.
- T. Yamaguchi, “Rare-RI Ring project in RIKEN and a proposal at CSRe,” Symposium on Precision Physics Experiments with Stored Highly Charged Ions at Low Energies, Lanzhou, China, August, 2018.
- D. Nagae, S. Omika, Y. Abe, Y. Yamaguchi, F. Suzaki, K. Wakayama, N. Tadano, R. Igosawa, K. Inomata, H. Arakawa, K. Nishimuro, T. Fujii, T. Mitsui, T. Yamaguchi, T. Suzuki, S. Suzuki, T. Moriguchi, M. Amano, D. Kamioka, A. Ozawa, S. Naimi, Z. Ge, Y. Yanagisawa, H. Baba, S. Michimasa, S. Ota, G. Lorusso, Y. A. Litvinov, M. Wakasugi, T. Uesaka, Y. Yano, “Demonstration of mass measurement using Rare-RI Ring,” The IX International Symposium on EXOTic Nuclei (EXON-2018), Petrozavodsk, Russia, September, 2018.
- Y. Yamaguchi, “Rare-RI Ring in cyclotron facility RIBF,” The International Conference on Electromagnetic Isotope Separators and Related Topics (EMIS2018), Geneva, Switzerland, September, 2018.
- A. Ozawa, “Mass measurements in Rare-RI Ring in RIBF,” Workshop on Physics at HIAF High-Energy Beam Lines, Beijing, China, December, 2018.

**[Domestic Conference]**

- 山口貴之, 「Precision mass spectrometry of stored exotic nuclei」, 重力波観測時代の r プロセスと不安定核, 和光, 2018 年 6 月.
- 向井もも, 「稀少 RI リングにおける中性子過剰 Ni 領域の質量測定」, 核データと重元素合成を中心とする宇宙核物理研究会, 札幌, 2019 年 3 月.
- 山口由高, 阿部康志, 洲崎ふみ, 若杉昌徳, 長江大輔, 大甕舜一朗, 小沢顕, S. Naimi, H. Li, Z. Ge, 上坂友洋, 山口貴之, 荒川裕樹, 稲田康人, 猪股玖美, 小林孝彰, 坂上護, 西室国光, 細井駿, 横田健次郎, 景澤怜央, 上岡大起, 向井もも, 森口哲朗, 鈴木伸司, Q. Wang, 大田晋輔, 北村徳隆, 増岡翔一朗, 道正新一郎, Y. A. Litvinov, 「稀少 RI リングの質量測定」, 日本物理学会第 74 回年次大会, 福岡, 2019 年 3 月.
- 阿部康志, 長江大輔, 山口由高, 上坂友洋, S. Naimi, 洲崎ふみ, 若杉昌徳, 荒川裕樹, 稲田康人, 猪股玖美, 大甕舜一朗, 小林孝彰, 坂上護, 西室国光, 細井駿, 横田健次郎, 山口貴之, 景澤怜央, 上岡大起, 向井もも, 森口哲朗, 小沢顕, 鈴木伸司, Z. Ge, H. Li, Q. Wang, 大田晋輔, 北村徳隆, 増岡翔一朗, 道正新一郎, Y. A. Litvinov, K. Wang, 「稀少 RI リング実験における単一核種選択法の開発」, 日本物理学会第 74 回年次大会, 福岡, 2019 年 3 月.
- 洲崎ふみ, 阿部康志, 若杉昌徳, 山口由高, 天野将道, 荒川裕樹, 馬場秀忠, Z. Ge, 細井駿, 稲田康人, 猪股玖美, 上岡大起, 北村徳隆, 小林孝彰, H. Li, Y. A. Litvinov, 増岡翔一朗, 道正新一郎, 森口哲朗, 長江大輔, S. Naimi, 西室国光, 大甕舜一朗, 大田晋輔, 小沢顕, 鈴木伸司, 上坂友洋, 若山清志, 山口貴之, 「共鳴ショットキービックアップを用いた稀少 RI リングの等時性場調整」, 日本物理学会第 74 回年次大会, 福岡, 2019 年 3 月.

**Posters Presentations****[International Conference etc.]**

- S. Omika, T. Yamaguchi, N. Tadano, Y. Abe, M. Amano, Z. Ge, D. Kamioka, T. Moriguchi, D. Nagae, S. Naimi, A. Ozawa, F. Suzaki, S. Suzuki, T. Suzuki, T. Uesaka, M. Wakasugi, K. Wakayama, Y. Yamaguchi, “Development of a new in-ring beam monitor in the Rare-RI Ring,” The International Conference on Electromagnetic Isotope Separators and Related Topics (EMIS2018), Geneva, Switzerland, September 2018.
- Z. Ge, T. Uesaka, S. Naimi, D. Nagae, Y. Abe, S. Omika, F. Suzaki, H. Li, Y. Yamaguchi, M. Wakasugi, K. Wakayama, T. Yamaguchi, H. Arakawa, K. Inomata, K. Nishimuro, T. Kobayashi, A. Ozawa, S. Suzuki, T. Moriguchi, A. Kitagawa, S. Sato, G. Lorusso, Y. Yano, “High-resolution selection and identification of secondary beams for mass measurements,” The 7th International Conference on Trapped Charged Particles and Fundamental Physics (TCP2018), Michigan, USA, September–October 2018.

## Research Facility Development Division Instrumentation Development Group SCRIT Team

### 1. Abstract

The SCRIT Electron Scattering Facility has been constructed at RIKEN RIBF. This aims at investigation of internal nuclear structure for short-lived unstable nuclei by means of electron scattering. SCRIT (Self-Confining RI Ion Target) is a novel method to form internal targets in an electron storage ring. This is a unique method for making electron scattering experiments for unstable nuclei possible. Construction of the facility has been started in 2009. This facility consists of an electron accelerator (RTM), a SCRIT-equipped electron storage ring (SR2), an electron-beam-driven RI separator (ERIS), and a window-frame spectrometer for electron scattering (WiSES) which consists of a large window-frame dipole magnet, drift chambers and trigger scintillators. Installation of all components in the facility was completed in 2015. After the comprehensive test and tuning, the luminosity was reached to  $3 \times 10^{27}/(\text{cm}^2\text{s})$  with the number of injected ions of  $3 \times 10^8$ . In 2016, we successfully completed a measurement of diffraction of scattered electrons from  $^{132}\text{Xe}$  nuclei and determined the charge density distribution for the first time. The facility is now under setting up to move the first experiment for unstable nuclei.

### 2. Major Research Subjects

Development of SCRIT electron scattering technique and measurement of the nuclear charge density distributions of unstable nuclei.

### 3. Summary of Research Activity

SCRIT is a novel technique to form internal target in an electron storage ring. Positive ions are three dimensionally confined in the electron beam axis by transverse focusing force given by the circulating electron beam and applied electrostatic longitudinal mirror potential. The created ion cloud composed of RI ions injected from outside works as a target for electron scattering. Construction of the SCRIT electron scattering facility has been started in 2009. The electron accelerators RTM and the storage ring SR2 were successfully commissioned in 2010. Typical accumulation current in SR2 is 250–300 mA at the energy range of 100–300 MeV that is required energy range in electron scattering experiment. The SCRIT device was inserted in the straight section of SR2 and connected to an ISOL named ERIS (Electron-beam-driven RI separator for SCRIT) by 20-m long low energy ion transport line. A buncher system based on RFQ linear trap named FRAC (Fringing-RF-field-Activated dc-to-pulse converter) was inserted in the transport line to convert the continuous beam from ERIS to pulsed beam, which is acceptable for SCRIT. The detector system WiSES consisting of a high-resolution magnetic spectrometer, drift chambers and trigger scintillators, was constructed, and it has a solid angle of 100 msr, energy resolution of  $10^{-3}$ , and the scattering angle coverage of 25–55 degrees. A wide range of momentum transfer, 80–300 MeV/c, is covered by changing the electron beam energy from 150 to 300 MeV.

We successfully measured a diffraction pattern in the angular distribution of scattered electron from  $^{132}\text{Xe}$  isotope at the electron beam energy of 150 MeV, 200 MeV, and 300 MeV, and derived the nuclear charge distribution by assuming two-parameters Fermi model for the first time. At this time, luminosity was reached to  $3 \times 10^{27}/(\text{cm}^2\text{s})$  at maximum and the averaged value was  $1.2 \times 10^{27}/(\text{cm}^2\text{s})$  with the number of injected target ions of  $3 \times 10^8$ .

We are now under preparation for going to the experiments for unstable nuclei. There are some key issues for that. They are increasing the intensity of the RI beams from ERIS, efficient DC-to-pulse conversion at FRAC, improving the transmission efficiency from FRAC to SCRIT, and effective suppression of the background in measurement of scattered electrons. RI beam intensity will be improved by upgrading the electron beam power from 10 W to 60 W, increasing the contained amount of U in the target ion source, and some modifications in mechanical structure in the ion source. For upgrading the electron beam power, the RF system of RTM has been maintained intensively, and we will continue the development of RTM. For efficient DC-to-pulse conversion, we established the two-step bunching method, which is time compression at FRAC in combination with pre-bunching at the ion source using grid action. Furthermore, we will improve the conversion efficiency and the transmission efficiency from FRAC to the SCRIT device by cooling the trapped ions using minuscule amounts of a buffer gas. These improvements on FRAC were already confirmed in off-line test. Since one of significant contribution to the background for scattered electron is scattering from massive structural objects around the trapping region originated from halo components of the electron beam, we remodeled the SCRIT electrodes. The vacuum pump system at the SCRIT device has been upgraded to reduce the contribution of residual gases. Luminosity for radioactive Xe isotopes is expected to be more than  $10^{26}/(\text{cm}^2\text{s})$  after these improvements. Then, we will be able to start experiments for unstable nuclei. When further upgrading in the RTM power planed to be 3 kW will be achieved, we can extend the measurements to more exotic nuclei.

In 2018, we have been developing several instruments. One is the introduction of the surface-ionization type ion source at ERIS in order to increase kinds of radioactive beam and to produce high intensity beam. Another development is the upgrading of the drift chamber located in front of the magnetic spectrometer of WiSES to improve the momentum resolution and angular acceptance. These developments help us to realize experiments for unstable nuclei.

## Members

### Team Leader

Masanori WAKASUGI (concurrent: Group Director, Instrumentations Development Gr.)

### Research/Technical Scientists

Masamitsu WATANABE (Senior Research Scientist)

Tetsuya OHNISHI (Senior Technical Scientist)

### Contract Researcher

Akitomo ENOKIZONO

### Expert Technician

Taleshi MAIE (concurrent: Cryogenic Technology Team)

### Research Consultants

Tadaaki TAMAE

Shin-ichi ICHIKAWA

Masahiro HARA

Takashi EMOTO

### Senior Visiting Scientist

Toshitada HORI (Hiroshima University)

### Visiting Scientists

Shuo WANG (Shandong University)

Toshimi SUDA (Tohoku University)

Ryo OGAWARA (National Institute of Radiological Sciences)

Kyo TSUKADA (Tohoku University)

Yuki HONDA (Tohoku University)

### Student Trainees

Keita KASAMA (Tohoku University)

Hikari WAUKE (Tohoku University)

Syota TAKAYAMA (Tohoku University)

Taihei AOYAGI (Tohoku University)

Kazuki NAMBA (Tohoku University)

## List of Publications & Presentations

### Publications

#### [Journal]

#### (Original Papers) \*Subject to Peer Review

M. Wakasugi, M. Togasaki, T. Ohnishi, K. Kurita, R. Toba, M. Watanabe, K. Yamada, "FRAC: Fringing-RF-field-activated dc-to-pulse converter for low-energy ion beams," *Rev. Sci. Instrum.* **89**, 095107 (2018).

A. Enokizono, T. Ohnishi, K. Tsukada, "The SCRIT electron scattering facility at RIKEN: The world's first electron femtoscope for short-lived unstable nuclei," *Nucl. Phys. News* **28**, 18–22 (2018).

#### [Proceedings]

T. Ohnishi, A. Enokizono, M. Hara, M. Hori, S. Ichikawa, M. Wakasugi, M. Watanabe, K. Adachi, T. Fujita, T. Hori, K. Kurita, M. Togasaki, N. Uchida, K. Yamada, T. Suda, T. Tamae, K. Tsukada, "The SCRIT electron scattering facility project at the RIKEN RI Beam Factory," *Acta Phy. Pol. B* **49**, 483–493 (2018).

### Oral Presentations

#### [International Conference etc.]

K. Tsukada, "Present status of the SCRIT electron scattering facility," 5<sup>th</sup> Joint Meeting of the APS Division of Nuclear Physics and the Physical Society of Japan, Waikoloa, Hawaii, USA, October 23–27, 2018.

K. Tsukada (invited), "Electron scattering from <sup>208</sup>Pb and <sup>132</sup>Xe ions at the SCRIT facility," The 7<sup>th</sup> international conference on Trapped Charged Particles and Fundamental Physics (TCP2018), Traverse, Michigan, USA, September 30–October 5, 2018.

K. Tsukada (invited), "Present status of the electron scattering experiments at the SCRIT facility," ECT\* conference, "Probing exotic structure of short-lived nuclei by electron scattering," Trento, Italy, July 16–20, 2018.

#### [Domestic Conference]

塚田暁, 「Present status of the SCRIT electron scattering facility」, ELPH 研究会, 東北大学, 仙台, 2019 年 3 月.

高山祥汰, 青柳泰平, 市川進一, 大西哲哉, 榎園昭智, 笠間桂太, 栗田和好, 佐藤蒼, 須田利美, 玉江忠明, 塚田暁, 中野萌絵, 南波和希, 原雅弘, 堀利匡, 本多佑記, 和宇慶ひかり, 若杉昌徳, 渡邊正満, 「電子・不安定核散乱実験用ドリフトチェンバーの開発と性能評価」, 日本物理学会, 九州大学, 福岡, 2019 年 3 月.

和宇慶ひかり, 青柳泰平, 市川進一, 大西哲哉, 榎園昭智, 笠間桂太, 栗田和好, 佐藤蒼, 須田利美, 高山祥汰, 玉江忠明, 塚田暁, 中野萌絵, 南波和希, 原雅弘, 堀利匡, 本多佑記, 若杉昌徳, 渡邊正満, 「SCRIT 実験に用いる電子スペクトロメーターの精密磁場測定」, 日本物理学会, 九州大学, 福岡, 2019 年 3 月.

塚田暁 (invited), 「The SCRIT electron scattering facility: Toward the world's first study of unstable nuclei by electron scattering」, PRL60 周年シンポジウム, 日本物理学会, 信州大学, 松本, 2018 年 9 月.

内田信昭, 足立江介, 市川進一, 榎園昭智, 大西哲哉, 笠間桂太, 栗田和好, 須田利美, 玉江忠明, 塚田暁, 戸ヶ崎衛, 原雅弘, 藤田峻広, 堀充希, 堀利匡, 山田耕平, 若杉昌徳, 渡邊正満, 「SCRIT 実験における捕獲されたイオンのモジュレーション依存性」, 日本物理学会, 東京理科大学, 千葉, 2018 年 3 月.

堀充希, 榎園昭智, 大西哲哉, 原雅弘, 栗田和好, 若杉昌徳, 渡邊正満, 「電子蓄積リングにおける二光子相関を用いたバンチ長モニター開発」, 日本物理学会, 東京理科大学, 千葉, 2018 年 3 月.

高山祥汰, 須田利美, 塚田暁, 本多佑記, 玉江忠明, 笠間桂太, 青柳泰平, for the SCRIT collaboration, 「SCRIT 電子スペクトロメーター性能向上に向けた飛跡検出器の開発」, 日本物理学会, 東京理科大学, 千葉, 2018 年 3 月.

### Posters Presentations

#### [International Conference etc.]

T. Ohnishi, S. Ichikawa, M. Nakano, K. Kurita, M. Wakasugi, "Present status of electron-beam-driven RI separator for SCRIT at RIKEN RI Beam Factory," 18th International Conference on Electromagnetic Isotope separators and Related Topics (EMIS2018), Geneva, Switzerland, September 16–21, 2018.

## Research Facility Development Division Research Instruments Group

### 1. Abstract

The Research Instruments Group is the driving force at RI Beam Factory (RIBF) for continuous enhancement of activities and competitiveness of experimental research. Consisting of four teams, we are in charge of the operation, maintenance, and improvement of the core research instruments at RIBF, such as the BigRIPS in-flight RI separator, ZeroDegree spectrometer and SAMURAI spectrometer, and the related infrastructure and equipment. We are also in charge of the production and delivery of RI beams using the BigRIPS separator. The group also conducts related experimental research as well as R&D studies on the research instruments.

### 2. Major Research Subjects

Design, construction, operation, maintenance, and improvement of the core research instruments at RIBF and related R&D studies. Experimental studies on exotic nuclei.

### 3. Summary of Research Activity

The current research subjects are summarized as follows:

- (1) Production and delivery of RI beams and related research
- (2) Design, construction, operation, maintenance, and improvement of the core research instruments at RIBF and their related infrastructure and equipment
- (3) R&D studies on the core research instruments and their related equipment at RIBF
- (4) Experimental research on exotic nuclei using the core research instruments at RIBF

### Members

#### Group Director

Hideki UENO (~ 2018.03)

Tomohiro UESAKA (2018.04 ~)

#### Senior Visiting Scientists

Toshio KOBAYASHI (Tohoku University)

Jerry NOLEN (Argonne National Laboratory)

#### Visiting Scientist

Toshiyuki KUBO (Michigan State University)

#### Student Trainee

Fumitaka ENDO (Tohoku University)

## Research Facility Development Division

### Research Instruments Group

### BigRIPS Team

#### 1. Abstract

This team is in charge of design, construction, development and operation of BigRIPS in-flight separator and its related research instruments at RI beam factory (RIBF). They are employed not only for the production of RI beams but also the experimental studies using RI beams.

#### 2. Major Research Subjects

Design, construction, development and operation of BigRIPS in-flight separator, RI-beam transport lines, and their related research instruments

#### 3. Summary of Research Activity

This team is in charge of design, construction, development and operation of BigRIPS in-flight separator, RI-beam transport lines, and their related research instruments such as ZeroDegree spectrometer at RI beam factory (RIBF). They are employed not only for the production of RI beams but also various kinds of experimental studies using RI beams.

The research subjects may be summarized as follows:

- (1) General studies on RI-beam production using in-flight scheme.
- (2) Studies on ion-optics of in-flight separators, including particle identification of RI beams
- (3) Simulation and optimization of RI-beam production.
- (4) Development of beam-line detectors and their data acquisition system.
- (5) Experimental studies on production reactions and unstable nuclei.
- (6) Experimental studies of the limits of nuclear binding.
- (7) Development of superconducting magnets and their helium cryogenic systems.
- (8) Development of a high-power production target system.
- (9) Development of a high-power beam dump system.
- (10) Development of a remote maintenance and remote handling systems.
- (11) Operation, maintenance and improvement of BigRIPS separator system, RI-beam transport lines, and their related research instruments such as ZeroDegree spectrometer and so on.
- (12) Experimental research using RI beams.

#### Members

##### Team Leader

Koichi YOSHIDA

##### Research/Technical Scientists

Yoshiyuki YANAGISAWA (Senior Research Scientist)

Naohito INABE (Senior Technical Scientist)

Masao OHTAKE (Senior Technical Scientist)

Kensuke KUSAKA (Senior Technical Scientist)

Hiroyuki TAKEDA (Technical Scientist)

Naoki FUKUDA (Technical Scientist)

##### Contract Researchers

Yohei SHIMIZU

Deuk Soon AHN

Hiroshi SUZUKI

##### Postdoctoral Researcher

Zeren KORKULU

##### Research Consultant

Hidekazu KUMAGAI

##### Part-time Worker

Tetsuro KOMATSUBARA

##### Visiting Scientists

Daisuke KAMEDA (TOSHIBA Corp.)

Michael Andrew FAMILIANO (Western Michigan University)

Daniel Pierre BAZIN (NSCL, MSU)

Bradley Marc SHERRILL (NSCL, MSU)

Yutaka MIZOI (Osaka Elec.-Com. University)

Naohito IWASA (Tohoku University)

Tuomas Arne Santeri GRAHN (University of Jyväskylä)

Oleg Borisovich TARASOV (NSCL, MSU)

Hans GEISSEL (GSI)

David Joseph MORRISSEY (NSCL, MSU)

Alfredo ESTRADA VAZ (Central Michigan University)  
Mauricio PORTILLO (NSCL, MSU)

Alan Matthew AMTHOR (Bucknell University)  
Kazuo IEKI (Rikkyo University)

### Student Trainees

Junki AMANO (Rikkyo University)  
Ha JEONGSU (Seoul National University)

Takahiro SAKAKIBARA (Tohoku University)  
Shunki ISHIKAWA (Tohoku University)

## List of Publications & Presentations

### Publications

#### [Journal]

#### (Original Papers) \*Subject to Peer Review

- N. Fukuda, T. Kubo, D. Kameda, N. Inabe, H. Suzuki, Y. Shimizu, H. Takeda, K. Kusaka, Y. Yanagisawa, M. Ohtake, K. Tanaka, K. Yoshida, H. Sato, H. Baba, M. Kurokawa, T. Ohnishi, N. Iwasa, A. Chiba, T. Yamada, E. Ideguchi, S. Go, R. Yokoyama, T. Fujii, H. Nishibata, K. Ieki, D. Murai, S. Momota, D. Nishimura, Y. Sato, J. Hwang, S. Kim, O. B. Tarasov, D. J. Morrissey, G. Simpson, "Identification of new neutron-rich isotopes in the rare-earth region produced by 345 MeV/nucleon  $^{238}\text{U}$ ," *J. Phys. Soc. Jpn.* **87**, 014202 (2018).\*
- Y. Shimizu, T. Kubo, N. Fukuda, N. Inabe, D. Kameda, H. Sato, H. Suzuki, H. Takeda, K. Yoshida, G. Lorusso, H. Watanabe, G. S. Simpson, A. Jungclaus, H. Baba, F. Browne, P. Doornenbal, G. Gey, T. Isobe, Z. Li, S. Nishimura, P. Söderström, T. Sumikama, J. Taprogge, Z. Vajta, J. Wu, Z. Xu, A. Odahara, A. Yagi, H. Nishibata, R. Lozeva, C. Moon, H. Jung, "Observation of new neutron-rich isotopes among fission fragments from in-flight fission of 345 MeV/nucleon  $^{238}\text{U}$ : Search for new isotopes conducted concurrently with decay measurement campaigns," *J. Phys. Soc. Jpn.* **87**, 014203 (2018).\*
- S. Noji, H. Sakai, N. Aoi, H. Baba, G. P. A. Berg, P. Doornenbal, M. Dozono, N. Fukuda, N. Inabe, D. Kameda, T. Kawabata, S. Kawase, Y. Kikuchi, K. Kisamori, T. Kubo, Y. Maeda, H. Matsubara, S. Michimasa, K. Miki, H. Miya, H. Miyasako, S. Sakaguchi, Y. Sasamoto, S. Shimoura, M. Takaki, H. Takeda, S. Takeuchi, H. Tokieda, T. Ohnishi, S. Ota, T. Uesaka, H. Wang, K. Yako, Y. Yanagisawa, N. Yokota, K. Yoshida, R. G. T. Zegers, "Excitation of the isovector spin monopole resonance via the exothermic  $^{90}\text{Zr}(^{12}\text{N}, ^{12}\text{C})$  reaction at 175 MeV/nucleon," *Phys. Rev. Lett.* **120**, 172501 (2018).\*
- O. B. Tarasov, D. S. Ahn, D. Bazin, N. Fukuda, A. Gade, M. Hausmann, N. Inabe, S. Ishikawa, N. Iwasa, K. Kawata, T. Komatsubara, T. Kubo, K. Kusaka, D. J. Morrissey, M. Ohtake, H. Otsu, M. Portillo, T. Sakakibara, H. Sakurai, H. Sato, B. M. Sherrill, Y. Shimizu, A. Stolz, T. Sumikama, H. Suzuki, H. Takeda, M. Thoennessen, H. Ueno, Y. Yanagisawa, K. Yoshida, "Discovery of  $^{60}\text{Ca}$  and implications for the stability of  $^{70}\text{Ca}$ ," *Phys. Rev. Lett.* **121**, 022501 (2018).\*
- S. Michimasa, M. Kobayashi, Y. Kiyokawa, S. Ota, D. S. Ahn, H. Baba, G. P. A. Berg, M. Dozono, N. Fukuda, T. Furuno, E. Ideguchi, N. Inabe, T. Kawabata, S. Kawase, K. Kisamori, K. Kobayashi, T. Kubo, Y. Kubota, C. S. Lee, M. Matsushita, H. Miya, A. Mizukami, H. Nagakura, D. Nishimura, H. Oikawa, H. Sakai, Y. Shimizu, A. Stolz, H. Suzuki, M. Takaki, H. Takeda, S. Takeuchi, H. Tokieda, T. Uesaka, K. Yako, Y. Yamaguchi, Y. Yanagisawa, R. Yokoyama, K. Yoshida, S. Shimoura, "Magic nature of neutrons in  $^{54}\text{Ca}$ : First mass measurements of  $^{55-57}\text{Ca}$ ," *Phys. Rev. Lett.* **121**, 022506 (2018).\*
- J. Yasuda, M. Sasano, R. G. T. Zegers, H. Baba, D. Bazin, W. Chao, M. Dozono, N. Fukuda, N. Inabe, T. Isobe, G. Jhang, D. Kameda, M. Kaneko, K. Kisamori, M. Kobayashi, N. Kobayashi, T. Kobayashi, S. Koyama, Y. Kondo, A. J. Krasznahorkay, T. Kubo, Y. Kubota, M. Kurata-Nishimura, C. S. Lee, J. W. Lee, Y. Matsuda, E. Milman, S. Michimasa, T. Motobayashi, D. Muecher, T. Murakami, T. Nakamura, N. Nakatsuka, S. Ota, H. Otsu, V. Panin, W. Powell, S. Reichert, S. Sakaguchi, H. Sakai, M. Sako, H. Sato, Y. Shimizu, M. Shikata, S. Shimoura, L. Stuhl, T. Sumikama, H. Suzuki, S. Tangwanchaoren, M. Takaki, H. Takeda, T. Tako, Y. Togano, H. Tokieda, J. Tsubota, T. Uesaka, T. Wakasa, K. Yako, K. Yoneda, J. Zenihiro, "Extraction of the Landau-Migdal parameter from the Gamow-Teller giant resonance in  $^{132}\text{Sn}$ ," *Phys. Rev. Lett.* **121**, 132501 (2018).\*
- S. Leblond, F. M. Marqués, J. Gibelin, N. A. Orr, Y. Kondo, T. Nakamura, J. Bonnard, N. Michel, N. L. Achouri, T. Aumann, H. Baba, F. Delaunay, Q. Deshayes, P. Doornenbal, N. Fukuda, J. W. Hwang, N. Inabe, T. Isobe, D. Kameda, D. Kanno, S. Kim, N. Kobayashi, T. Kobayashi, T. Kubo, J. Lee, R. Minakata, T. Motobayashi, D. Murai, T. Murakami, K. Muto, T. Nakashima, N. Nakatsuka, A. Navin, S. Nishi, S. Ogoshi, H. Otsu, H. Sato, Y. Satou, Y. Shimizu, H. Suzuki, K. Takahashi, H. Takeda, S. Takeuchi, R. Tanaka, Y. Togano, A. G. Tuff, M. Vandebrouck, K. Yoneda, "First observation of  $^{20}\text{B}$  and  $^{21}\text{B}$ ," *Phys. Rev. Lett.* **121**, 262502 (2018).\*
- J. Park, R. Krucken, D. Lubos, R. Gernhauser, M. Lewitowicz, S. Nishimura, D. S. Ahn, H. Baba, B. Blank, A. Blazhev, P. Boutachkov, F. Browne, I. Celikovic, G. de France, P. Doornenbal, T. Faestermann, Y. Fang, N. Fukuda, J. Giovinazzo, N. Goel, M. Gorska, H. Grawe, S. Ilieva, N. Inabe, T. Isobe, A. Jungclaus, D. Kameda, G. D. Kim, Y. -K. Kim, I. Kojouharov, T. Kubo, N. Kurz, G. Lorusso, K. Moschner, D. Murai, I. Nishizuka, Z. Patel, M. M. Rajabali, S. Rice, H. Sakurai, H. Schaffner, Y. Shimizu, L. Sinclair, P. -A. Soderstrom, K. Steiger, T. Sumikama, H. Suzuki, H. Takeda, Z. Wang, H. Watanabe, J. Wu, Z. Y. Xu, " $\beta$  decays of the heaviest  $N = Z - 1$  nuclei and proton instability of  $^{97}\text{In}$ ," *Phys. Rev. C* **97**, 051301R (2018).\*
- J. L. Tain, J. Agramunt, D. S. Ahn, A. Algora, J. M. Allmond, H. Baba, S. Bae, N. T. Brewer, R. Caballero-Folch, F. Calvino, P. J. Coleman-Smith, G. Cortes, T. Davinson, I. Dillmann, C. Domingo-Pardo, A. Estrade, N. Fukuda, S. Go, C. Griffin, R. Grzywacz, J. Ha, O. Hall, L. Harkness-Brennan, T. Isobe, D. Kahl, M. Karny, G. G. Kiss, M. Kogimtzis, A. Korgul, S. Kubono, M. Labiche, I. Lazarus, J. Lee, J. Liu, G. Lorusso, K. Matsui, K. Miernik, F. Montes, B. Moon, A. I. Morales, N. Nepal, S. Nishimura, R. D. Page, Z. Podolyak, V. F. E. Pucknell, B. C. Rasco, P. H. Regan, A. Riego, B. Rubio, K. P. Rykaczewski, Y. Saito, H. Sakurai, Y. Shimizu, J. Simpson, P. A. Soderstrom, D. W. Stracener, T. Sumikama, R. Surman, H. Suzuki, M. Takechi, H. Takeda, A. Tarifeno-Saldivia, S. L. Thomas, A. Tolosa-Delgado, V. H. Phong, P. Woods, "The BRIKEN project: Extensive measurements of  $\beta$ -delayed neutron emitters for the astrophysical r process," *Acta Phys. Pol. B* **49**, 417 (2018).\*
- O. Wieland, A. Bracco, F. Camera, R. Avigo, H. Baba, N. Nakatsuka, T. Aumann, S. R. Banerjee, G. Benzoni, K. Boretzky, C. Caesar,

S. Ceruti, S. Chen, F. C. L. Crespi, V. Derya, P. Doornenbal, N. Fukuda, A. Giaz, K. Ieki, N. Kobayashi, Y. Kondo, S. Koyama, T. Kubo, M. Matsushita, B. Million, T. Motobayashi, T. Nakamura, M. Nishimura, H. Otsu, T. Ozaki, A. T. Saito, H. Sakurai, H. Scheit, F. Schindler, P. Schrock, Y. Shiga, M. Shikata, S. Shimoura, D. Steppenbeck, T. Sumikama, S. Takeuchi, R. Taniuchi, Y. Togano, J. Tscheuschner, J. Tsubota, H. Wang, K. Wimmer, K. Yoneda, “Low-lying dipole response in the unstable  $^{70}\text{Ni}$  nucleus,” *Phys. Rev. C* **98**, 064313 (2018).\*

R. Yokoyama, E. Ideguchi, G. S. Simpson, Mn.Tanaka, S. Nishimura, P. Doornenbal, G. Lorusso, P. -A. Söderström, T. Sumikama, J. Wu, Z. Y. Xu, N. Aoi, H. Baba, F. L. Bello Garrote, G. Benzoni, F. Browne, R. Daido, Y. Fang, N. Fukuda, A. Gottardo, G. Gey, S. Go, N. Inabe, T. Isobe, D. Kameda, K. Kobayashi, M. Kobayashi, I. Kojouharov, T. Komatsubara, T. Kubo, N. Kurz, I. Kuti, Z. Li, M. Matsushita, S. Michimasa, C. B. Moon, H. Nishibata, I. Nishizuka, A. Odahara, Z. Patel, S. Rice, E. Sahin, H. Sakurai, H. Schaffner, L. Sinclair, H. Suzuki, H. Takeda, J. Taprogge, Zs. Vajta, H. Watanabe, A. Yagi, T. Inakura, “Beta-gamma spectroscopy of the neutron-rich  $^{150}\text{Ba}$ ,” *Prog. Theor. Exp. Phys.* **2018**, 041D02 (2018).\*

### [Proceedings]

#### (Original Papers) \*Subject to Peer Review

K. Kusaka, M. Ohtake, K. Yoshida, K. Tanaka, H. Mukai, Y. Uwamino, T. Kubo, “Radiation effects in superconducting quadrupoles for BigRIPS in-flight separator at RIKEN,” *IEEE Trans. Appl. Supercond.* **28**, 1 (2018).\*

#### [Other]

福田直樹, 「73 種の新 RI を発見—RIBF で加速する未踏の原子核世界の開拓—」, *Isotope News* **759**(2018 年 10 月号), 22 (2018).

## Oral Presentations

### [International Conference etc.]

N. Fukuda, “Present status of RI-beam production at BigRIPS: Search for new isotopes and nuclear drip lines, and measurement of production cross sections,” *EURORIB 2018*, Giens, France, May 27–June 1, 2018.

D. S. Ahn, “Discovery of the  $^{39}\text{Na}$  nuclide, the most neutron-rich Na isotope ( $N = 28$ ) with the BigRIPS in-flight separator,” *Nuclear Structure 2018 Michigan State University*, East Lansing, Michigan, USA, August 5–10, 2018.

K. Kusaka, “Long term operation of the superconducting triplet quadrupoles with cryocoolers for BigRIPS in-flight separator at RIKEN,” *27th International Cryogenics Engineering Conference (ICEC27-ICMC 2018)*, Oxford, UK, September 3–7, 2018.

N. Fukuda, “Production of new isotopes and search for neutron drip line with the BigRIPS separator at RIKEN RI Beam Factory,” *IX International Symposium on Exotic Nuclei (EXON2018)*, Petrozavodsk, Russia, September 10–15, 2018.

H. Takeda, “New ion-optical modes of the BigRIPS and ZeroDegree Spectrometer for the production of high-quality RI beams,” *International Conference on ElectroMagnetic Isotope Separators and Related Topics (EMIS2018)*, CERN, Geneva, Switzerland, September 16–21, 2018.

Y. Yanagisawa, “Operational experience of the high-power production target system for BigRIPS separator,” *The International Nuclear Target Development Society (INTDS) Conference 2018*, MSU/FRIB, East Lansing, Michigan, USA, October 8–12, 2018.

K. Yoshida, “Thermal model simulation of the high power target system for BigRIPS separator,” *The International Nuclear Target Development Society (INTDS) Conference 2018*, MSU/FRIB, East Lansing, Michigan, USA, October 8–12, 2018.

H. Suzuki, “Production of very neutron-rich Pd isotopes around  $N = 82$  by projectile fragmentation of a RI beam of  $^{132}\text{Sn}$  at 280 MeV/u,” *Fifth Joint Meeting of the Nuclear Physics Divisions of the APS and the JPS (HAWAII2018)*, Waikoloa, Hawaii, USA, October 23–27 (2018).

N. Fukuda, “Present status of RI-beam production at BigRIPS separator,” *The 10th China-Japan Joint Nuclear Physics Symposium*, Huizhou, China, November 18–23, 2018.

### [Domestic Conference]

西隆博, D. S. Ahn, G. P. A. Berg, 堂園昌伯, 藤岡宏之, 福田直樹, 福西暢尚, H. Geissel, E. Haettner, 橋本直, 早野龍五, 比連崎悟, 堀井啓志, 池野なつ美, 稲辺尚人, 板橋健太, 伊藤聖, 岩崎雅彦, 亀田大輔, 川瀬頌一郎, 木佐森慶一, 清川裕, 久保敏幸, 日下健祐, 松原礼明, 松下昌史, 道正新一郎, 三木謙二郎, 三嶋剛, 宮裕之, 村井大地, 村上洋平, 永廣秀子, 中村祐喜, 新倉, 野地俊平, 大河内公太, 大田晋輔, 坂本成彦, 関口仁子, 鈴木宏, 鈴木謙, 高木基伸, 竹田浩之, 田中良樹, 轟孔一, 塚田暁, 上坂友洋, 渡辺珠以, Helmut Weick, 山田裕之, 山上大貴, 柳澤善行, 吉田光一, 「理化学研究所における ( $d, ^3\text{He}$ ) 反応を用いたパイ中間子原子の分光実験」, 日本物理学会第 73 回年次大会 (2018 年), 東京理科大学 (野田キャンパス), 千葉, 2018 年 3 月 22–25 日.

福田直樹, 清水陽平, 鈴木宏, A. H. N. DeukSoon, 竹田浩之, 炭竈聡之, 宮武宇也, 渡辺裕, 稲辺尚人, 西村俊二, 大津秀暁, 吉田光一, 上野秀樹, 佐藤広海, 鈴木大介, 笹野匡紀, 磯部忠昭, 平山賀一, 家城和夫, 天野順貴, 「 $^{238}\text{U}$  の入射核破碎反応を用いた  $N = 126$  近傍の中性子過剰核の生成」, 日本物理学会第 73 回年次大会 (2018 年), 東京理科大学 (野田キャンパス), 千葉, 2018 年 3 月 22–25 日.

## Research Facility Development Division

### Research Instruments Group

### SAMURAI Team

#### 1. Abstract

In collaboration with research groups in and outside RIKEN, the team designs, develops and constructs the SAMURAI spectrometer and relevant equipment that are and will be used for reaction experiments using RI beams at RI Beam Factory. The SAMURAI spectrometer consists of a large superconducting dipole magnet and a variety of detectors to measure charged particles and neutrons. After the commissioning experiment in March 2012, the team prepared and conducted, in collaboration with researchers in individual experimental groups, the first series of experiments with SAMURAI in May 2012. Then, several numbers of experiments were well performed until now utilizing the property of SAMURAI. The team also provides basis for research activities by, for example, organizing collaboration workshops by researchers who are interested in studies or plan to perform experiments with the SAMURAI spectrometer.

#### 2. Major Research Subjects

Design, operation, maintenance and improvement of the SAMURAI spectrometer and its related research instruments. Support and management for SAMURAI-based research programs. Generate future plans for next generation instruments for nuclear reaction studies.

#### 3. Summary of Research Activity

The current research subjects are summarized as follows:

- (1) Operation, maintenance and improvement of a large superconducting dipole magnet that is the main component of the SAMURAI spectrometer.
- (2) Design, development and construction of various detectors that are used for nuclear reaction experiments using the SAMURAI spectrometer.
- (3) Preparation for planning experiments using SAMURAI spectrometer.
- (4) Maintenance and improvement of the SAMURAI beam line.
- (5) Formation of a collaboration platform called SAMURAI collaboration.
- (6) Preparation for next generation spectrometer for nuclear reaction studies.

#### Members

##### Team Leader

Hideaki OTSU

#### List of Publications & Presentations

##### Publications

###### [Journal]

###### (Original Papers) \*Subject to Peer Review

- H. N. Liu, A. Obertelli *et al.*, “How robust is the  $N = 34$  subshell closure? First spectroscopy of  $^{52}\text{Ar}$ ,” *Phys. Rev. Lett.* **122**, 072502 (2019).
- S. Takeuchi, T. Nakamura *et al.*, “Coulomb breakup reactions of  $^{93,94}\text{Zr}$  in inverse kinematics,” *Prog. Theor. Exp. Phys.* **2019**, 013D02 (2019).
- S. Leblond, M. Marques *et al.*, “First observation of  $^{20}\text{B}$  and  $^{21}\text{B}$ ,” *Phys. Rev. Lett.* **121**, 262502 (2018).
- S. Chebotaryov *et al.*, “Proton elastic scattering at 200 A MeV and high momentum transfers of  $1.7\text{--}2.7\text{ fm}^{-1}$  as a probe of the nuclear matter density of  $^6\text{He}$ ,” *Prog. Theor. Exp. Phys.* **2018**, 5, 1, 053D01 (2018).
- J. Yasuda, M. Sasano *et al.*, “Extraction of the Landau-Migdal parameter from the Gamow-Teller giant resonance in  $^{132}\text{Sn}$ ,” *Phys. Rev. Lett.* **121**, 132501 (2018).
- T. Isobe *et al.*, “Application of the Generic Electronics for Time Projection Chamber (GET) readout system for heavy Radioactive isotope collision experiments,” *Nucl. Instrum. Methods Phys. Res. A* **899**, 43 (2018).

##### Oral Presentations

###### [International Conference etc.]

- H. Otsu, “Invariant mass spectroscopy of neutron-rich nuclei with large acceptance spectrometer SAMURAI,” Fifth Joint Meeting of the Nuclear Physics Divisions of the APS and the JPS (HAWAII2018), Waikoloa, Hawaii, USA, October 23–27 (2018).
- T. Isobe, “Performance of SPiRIT-TPC with GET readout system for heavy ion collision experiment,” Workshop on Active Targets and Time Projection Chambers for High-intensity and Heavy-ion beams in Nuclear Physics, Santiago de Compostela, Spain, January 17–19, 2018.

- B. Tsang, “Highlights of the SPiRIT Time Projection Chamber, Workshop on Active Targets and Time Projection Chambers for High-intensity and Heavy-ion beams in Nuclear Physics,” Santiago de Compostela, Spain, January 17–19, 2018.
- J. Estee, “Extending Dynamic Range, Calculating and Calibrating  $dE/dx$  in the SPiRIT TPC,” Workshop on Active Targets and Time Projection Chambers for High-intensity and Heavy-ion beams in Nuclear Physics, Santiago de Compostela, Spain, January 17–19, 2018.
- G. Jhang, “An overview of the analysis software for SPiRIT experiments,” Workshop on Active Targets and Time Projection Chambers for High-intensity and Heavy-ion beams in Nuclear Physics, Santiago de Compostela, Spain, January 17–19, 2018.
- T. Isobe, “The SPiRIT and pion detectors in RIKEN for the experimental study of symmetry energy with heavy ion collisions,” International Workshop on Multi facets of Eos and Clustering IWM-EC 2018, Catania, Italy, May 22–25, 2018.
- T. Isobe, “Implementation of GET readout system for heavy RI collision experiment with SPiRIT-TPC at RIBF,” GET WORKSHOP: General Electronic for Physics, Université de Bordeaux, France, October 10–12, 2018.
- T. Isobe, “Experimental study of density dependent symmetry energy at RIBF-SPiRIT experiment,” Fifth Joint Meeting of the Nuclear Physics Divisions of the APS and the JPS (HAWAII2018), Waikoloa, Hawaii, USA, October 23–27 (2018).
- T. Isobe, “Study of density dependent asymmetric nuclear EOS by using heavy RI collisions at RIKEN-RIBF,” 52nd Reimei Workshop, Experimental and Theoretical Hadron Physics: Recent Exciting Developments, Tokai, Japan, Jan 9–11, 2019.
- M. Kurata-Nishimura, “SPiRIT-TPC experiment with neutron rich Sn + Sn collisions in RIKEN-RIBF,” Fifth Joint Meeting of the Nuclear Physics Divisions of the APS and the JPS (HAWAII2018), Waikoloa, Hawaii, USA, October 23–27 (2018).
- M. Kaneko, “Study of light cluster production in intermediate energetic heavy-RI collision at RIBF,” Fifth Joint Meeting of the Nuclear Physics Divisions of the APS and the JPS (HAWAII2018), Waikoloa, Hawaii, USA, October 23–27 (2018).
- W. G. Lynch, “Present and expected constraints on the Nuclear Symmetry Energy,” 8th International Symposium on Nuclear Symmetry Energy (NuSYM2018), Busan, South Korea, September 10–13, 2018.
- M. Kurata-Nishimura, “Collective flow at neutron rich Sn + Sn collisions with 270 MeV/u,” 8th International Symposium on Nuclear Symmetry Energy (NuSYM2018), Busan, South Korea, September 10–13, 2018.
- G. Ghang, “Recent results on pion analysis of Sn + Sn collisions,” 8th International Symposium on Nuclear Symmetry Energy (NuSYM2018), Busan, South Korea, September 10–13, 2018.
- M. Kaneko, “Study of light cluster production in intermediate energetic heavy-RI collision at RIBF,” 8th International Symposium on Nuclear Symmetry Energy (NuSYM2018), Busan, South Korea, September 10–13, 2018.
- R. Wang, “Quality assurance for TPC data analysis of intermediate energy heavy ion collisions,” 8th International Symposium on Nuclear Symmetry Energy (NuSYM2018), Busan, South Korea, September 10–13, 2018.
- J. W. Lee, “Charged particle track reconstruction for heavy ion collision experiments with SPiRIT Time Projection Chamber,” 8th International Symposium on Nuclear Symmetry Energy (NuSYM2018), Busan, South Korea, September 10–13, 2018.
- M. Kaneko, “Study of light cluster production in intermediate energetic heavy-RI collision at RIBF,” 8th International Symposium on Nuclear Symmetry Energy (NuSYM2018), Busan, South Korea, September 10–13, 2018.
- T. Murakami, “Probing Nuclear Symmetry Energy at high densities with SPiRIT-TPC,” The 20th Northeastern Asia Symposium, Nagoya, Japan, September 19–20, 2018.
- T. Murakami, “Experiments Probing Nuclear Symmetry Energy at Supra-Saturation Densities,” Nucleus-Nucleus Collisions (NN2018), Saitama, Japan, December 4–8, 2018.
- W. G. Lynch, “Probing the Equation of State of Neutron-rich Matter,” Nucleus-Nucleus Collisions (NN2018), Saitama, Japan, December 4–8, 2018.
- M. Kaneko, “Study of light cluster production in intermediate energetic heavy-RI collision at RIBF,” Nucleus-Nucleus Collisions (NN2018), Saitama, Japan, December 4–8, 2018.
- M. Kurata-Nishimura, “Collective flow at neutron rich Sn + Sn collisions with 270 MeV/nucleon,” Nucleus-Nucleus Collisions (NN2018), Saitama, Japan, December 4–8, 2018.
- T. Nakamura, “Multi-neutron clusters in neutron-rich nuclei,” Workshop on Clusters in Quantum Systems: from Atoms to Nuclei and Hadrons, Sendai, Japan, January 28–February 1, 2019.
- T. Nakamura, “Exploring towards the neutron-rich limit of nuclei, and beyond,” 57th International Winter Meeting on Nuclear Physics, Bormio Italy, January 21–25, 2019.
- T. Nakamura, “Breakup reactions of neutron-rich nuclei for application to stellar reactions,” ECT\* Workshop on “Indirect Methods in Nuclear Astrophysics,” Trento, Italy, November 5–9, 2018.
- T. Nakamura, “Exploration towards the nuclear limit: neutron drip line and beyond,” Fifth Joint Meeting of the Nuclear Physics Divisions of the APS and the JPS (HAWAII2018), Waikoloa, Hawaii, USA, October 23–27 (2018).
- T. Nakamura, “Exploration around and beyond the limit of nuclear stability: Exotic structure and reactions,” 5th Tokyo Tech-Uppsala University Joint Symposium, Uppsala, Sweden, September 24–25, 2018.
- T. Nakamura, “Clustering as a window on the hierarchical structure of quantum systems,” SAMURAI International Collaboration Workshop, RIKEN, Japan, September 5–6, 2018.
- T. Nakamura, “Recent Experiments and Perspectives of SAMURAI,” RIBF Users meeting 2018, Wako, Japan, September 5–6, 2018.
- T. Nakamura, “Exploration of extremes of nuclei at SAMURAI at RIBF,” SFB1245 Workshop, Mainz, Germany, July 4–6, 2018.
- T. Nakamura, “Search for multi-neutron clusters in unbound excited states of  $^{10}\text{He}$  and  $^{28}\text{O}$ ,” SAMURAI International Collaboration Workshop, RIKEN, Wako, Japan, September 5–6, 2018.
- Y. Kondo, “Experimental study of neutron-rich oxygen isotopes beyond the drip line,” Nucleus-Nucleus Collisions (NN2018), Saitama,

Japan, December 4–8, 2018.

- Y. Kondo, “Recent progress and developments for experimental studies with the SAMURAI spectrometer,” International Conference on Electromagnetic Isotope Separator and Related Topics (EMIS2018), CERN, Geneva, Switzerland, September 16–21, 2018.
- Y. Kondo, “Experimental studies of unbound neutron-rich nuclei,” XXII International Conference on Few-Body Problems in Physics (FB22), Caen, France, July 9–13, 2018.
- Y. Kondo, “Study of the unbound nuclei  $^{27}\text{O}$  and  $^{28}\text{O}$  using proton removal reactions,” 10th International Conference on Direct Reactions with Exotic Beams (DREB2018), Matsue, Japan, June 4–8, 2018.
- T. Tomai, “Breakup reactions of one-neutron halo nucleus  $^{31}\text{Ne}$ ,” 10th International Conference on Direct Reactions with Exotic Beams (DREB2018), Matsue, Japan, June 4–8, 2018.
- T. Tomai, “Coulomb breakup reaction of one neutron halo nucleus  $^{31}\text{Ne}$ ,” Nucleus-Nucleus Collisions (NN2018), Saitama, Japan, December 4–8, 2018.
- M. Yasuda, “In-beam gamma-ray spectroscopy of  $^{28-30}\text{Ne}$ ,” Nucleus-Nucleus Collisions (NN2018), Saitama, Japan, December 4–8, 2018.
- H. Miki, “Structure of  $^{28}\text{F}$  studied by the  $(n, p)$  type charge-exchange reaction of  $^{28}\text{Ne}$ ,” Fifth Joint Meeting of the Nuclear Physics Divisions of the APS and the JPS (HAWAII2018), Waikoloa, Hawaii, USA, October 23–27 (2018).
- T. Tomai, “Coulomb breakup reaction of  $^{31}\text{Ne}$  and its halo structure,” Fifth Joint Meeting of the Nuclear Physics Divisions of the APS and the JPS (HAWAII2018), Waikoloa, Hawaii, USA, October 23–27 (2018).
- M. Yasuda, “In-beam gamma-ray spectroscopy of F and Ne isotopes near the island of inversion,” Fifth Joint Meeting of the Nuclear Physics Divisions of the APS and the JPS (HAWAII2018), Waikoloa, Hawaii, USA, October 23–27 (2018).
- T. Shimada, “Spectroscopy of the unbound neutron-rich nucleus  $^{30}\text{F}$ ,” Fifth Joint Meeting of the Nuclear Physics Divisions of the APS and the JPS (HAWAII2018), Waikoloa, Hawaii, USA, October 23–27 (2018).
- Y. Togano, “Matter radius of two-neutron halo nucleus  $^{22}\text{C}$ ,” NN2018, Saitama Japan, December 4–8, 2018.
- Y. Togano, “New gamma-ray detector CATANA for in-beam gamma-ray spectroscopy with fast RI beams,” EMIS2018, Geneva Switzerland, September 16–21, 2018.
- Y. Togano, “Studies of  $^{22}\text{C}$  and  $^{50,52}\text{Ca}$  at SAMURAI,” EXON2018, Petrozavodsk Russia, September 10–15, 2018.
- Y. Togano, “E1 responses of neutron-rich Ca isotopes  $^{50}\text{Ca}$  and  $^{52}\text{Ca}$ ,” DREB2018, Matsue, Japan, June 4–8, 2018.
- Y. Togano, “Electric dipole response of  $^{50,52}\text{Ca}$ ,” Fifth Joint Meeting of the Nuclear Physics Divisions of the APS and the JPS (HAWAII2018), Waikoloa, Hawaii, USA, October 23–27 (2018).
- Y. Fujino, “Coulomb excitation of  $^{52}\text{Ca}$ ,” Fifth Joint Meeting of the Nuclear Physics Divisions of the APS and the JPS (HAWAII2018), Waikoloa, Hawaii, USA, October 23–27 (2018).
- D. Beumel, “Investigation of nuclear overlaps near the neutron dripline,” International Conference on Recent Issues in Nuclear and Particle Physics 2 Visva-Bharati, India, February 3–5, 2019.
- D. Beumel, “Nuclear overlaps near the neutron dripline,” International Workshop on “Clusters in Quantum Systems: from Atoms to Nuclei and Hadrons,” Sendai, Japan, January 28–February 1, 2019.

#### [Domestic Conference]

- 磯部忠昭, 「理研 RIBF における重 RI 衝突実験用—タイムプロジェクションチャンバーの性能評価」, 日本物理学会第 74 回年次大会, 九州大学, 福岡, 2019 年 3 月.
- 三木晴瑠, 「荷電交換反応を用いた中性子過剰非束縛核  $^{28}\text{F}$  の研究」, 日本物理学会第 74 回年次大会, 九州大学, 福岡, 2019 年 3 月.
- 栗原篤志, 「 $^{22}\text{C}$  のクーロン分解反応」, 日本物理学会第 74 回年次大会, 九州大学, 福岡, 2019 年 3 月.
- 斗米貴人, 「核力分解反応を用いた  $^{31}\text{Ne}$  の励起状態の探索」, 日本物理学会第 74 回年次大会, 九州大学, 福岡, 2019 年 3 月.

#### [Domestic Conference]

- 磯部忠昭, 「理研 RIBF における重 RI 衝突実験用—タイムプロジェクションチャンバーの性能評価」, 日本物理学会第 74 回年次大会, 九州大学, 福岡, 2019 年 3 月.
- 三木晴瑠, 「荷電交換反応を用いた中性子過剰非束縛核  $^{28}\text{F}$  の研究」, 日本物理学会第 74 回年次大会, 九州大学, 福岡, 2019 年 3 月.
- 栗原篤志, 「 $^{22}\text{C}$  のクーロン分解反応」, 日本物理学会第 74 回年次大会, 九州大学, 福岡, 2019 年 3 月.
- 斗米貴人, 「核力分解反応を用いた  $^{31}\text{Ne}$  の励起状態の探索」, 日本物理学会第 74 回年次大会, 九州大学, 福岡, 2019 年 3 月.

#### Master Thesis

- 山田啓貴, 「中性子過剰核  $^{32}\text{Ne}$  のインビーム  $\gamma$  線分光」, 東京工業大学理学院物理学系.
- 安田昌弘, 「逆転の島境界核のスペクトロスコピー」, 東京工業大学理学院物理学系.
- 松本真由子, 「中性子過剰核  $^{32}\text{Ne}$  の非束縛準位の探索」, 東京工業大学理学院物理学系.

#### Bachelor Thesis

- 吉留勇起, 「非束縛中性子過剰核分光のための荷電交換反応の研究」, 東京工業大学.
- 安田聖, 「ダイニュートロン探索のための高精細中性子検出器の開発」, 東京工業大学.

**Research Facility Development Division  
Research Instruments Group  
Computing and Network Team**

### 1. Abstract

This team is in charge of development, management and operation of the computing and network environment, mail and information servers and data acquisition system and management of the information security of the RIKEN Nishina Center.

### 2. Major Research Subjects

- (1) Development, management and operation of the general computing servers
- (2) Development, management and operation of the mail and information servers
- (3) Development, management and operation of the data acquisition system
- (4) Development, management and operation of the network environment
- (5) Management of the information security

### 3. Summary of Research Activity

This team is in charge of development, management and operation of the computing and network environment, mail and information servers and data acquisition system and management of the information security. The details are described elsewhere in this progress report.

#### (1) Development, management and operation of the general computing servers

We are operating Linux/Unix NIS/NFS cluster system for the data analysis of the experiments and general computing. This cluster system consists of eight computing servers with 64 CPU cores and totally 200 TB RAID of highly-reliable Fibre-channel interconnection. Approximately 700 user accounts are registered on this cluster system. We are adopting the latest version of the Scientific Linux (X86\_64) as the primary operating system, which is widely used in the accelerator research facilities, nuclear physics and high-energy physics communities in the world.

#### (2) Development, management and operation of the mail and information servers

We are operating RIBF.RIKEN.JP server as a mail/NFS/NIS server. This server is a core server of RIBF Linux cluster system. Postfix has been used for mail transport software and dovecot has been used for imap and pop services. These software packages enable secure and reliable mail delivery. Sophos Email Security and Control (PMX) installed on the mail front-end servers which tags spam mails and isolates virus-infected mails. The probability to identify the spam is approximately 95–99%. We are operating several information servers such as Web servers, Integrated Digital Conference (INDICO) server, Wiki servers, Groupware servers, Wowza streaming servers. We have been operating approximately 70 units of wireless LAN access points in RNC. Almost the entire radiation-controlled area of the East Area of RIKEN Wako campus is covered by wireless LAN for the convenience of experiments and daily work.

#### (3) Development, management and operation of the data acquisition system

We have developed the standard data-acquisition system named as RIBFDAQ. This system can process up to 40 MB/s data. By using crate-parallel readout from front-end systems such as CAMAC and VME, the dead time could be minimized. To synchronize the independent DAQ systems, the time stamping system has been developed. The resolution and depth of the time stamp are 10 ns and 48 bits, respectively. This time stamping system is very useful for beta decay experiments such as EURICA, BRIKEN and VANDLE projects. One of the important tasks is the DAQ coupling, because detector systems with dedicated DAQ systems are transported to RIBF from foreign facilities. In case of SAMURAI Silicon (NSCL/TUM/WUSTL), the readout system is integrated into RIBFDAQ. The projects of MUST2 (GANIL), MINOS (CEA Saclay), NeuLAND (GSI) and TRB3 (TUM) cases, data from their DAQ systems are transferred to RIBFDAQ and merged online. For SPIRIT (RIKEN/GANIL/CEA Saclay/NSCL), RIBFDAQ is controlled from the NARVAL-GET system that is a large-scale signal processing system for the time projection chamber. EURICA (GSI), BRIKEN (GSI/Univ. Liverpool/IFIC), VANDLE (UTK) and OTPC (U. Warsaw) projects, we adopt the time stamping system to apply individual trigger for each detector system. In this case, data are merged in offline. In addition, we are developing intelligent circuits based on FPGA. General Trigger Operator (GTO) is an intelligent triggering NIM module. Functions of “common trigger management,” “gate and delay generator,” “scaler” are successfully implemented. The trigger system in BigRIPS DAQ has been successfully upgraded by 5 GTO modules. To improve the data readout speed of VME system, we are developing FPGA-based small VME controller named as Mountable-Controller (MOCO). This controller can be attached to each ADC/TDC VME module. Usually, in the VME system, one master controller readout data from all modules in the VME shelf. On the other hand, data readout is carried out in parallel by multiple MOCO boards even ADC/TDC modules are in the same VME shelf. To establish robust MOCO-based VME system, we have developed MOCO with Parallelized VME (MPV) system which is a kind of the parallel readout extension of the VME bus. This MPV system merges data from multiple MOCOs and send it to the DAQ server.

#### (4) Development, management and operation of the network environment

We have been managing the network environment collaborating with Information Systems Division in RIKEN. All the Ethernet ports of the information wall sockets are capable of the Gigabit Ethernet connection (10/100/1000 BT). In addition, a 10 Gbps network

port has been introduced to the RIBF Experimental area in for the high-speed data transfer of RIBF experiment to HOKUSAI. Approximately 70 units of wireless LAN access points have been installed to cover the almost entire area of Nishina Center.

#### (5) Management of the information security

It is essential to take proper information security measures for information assets. We are managing the information security of Nishina Center collaborating with Information Systems Division in RIKEN.

### Members

#### Team Leader

Hidetada BABA

#### Research/Technical Scientist

Yasushi WATANABE (concurrent; Senior Research Scientist,  
Radiation Lab.)

#### Junior Research Associates

Fumiya GOTO (Nagoya Univ.)

#### Special Temporary Employee

Takashi ICHIHARA (concurrent; Special Temporary Em-  
ployee, RI Physics Lab.)

### List of Publications & Presentations

#### Publications

##### [Journal]

##### (Original Papers) \*Subject to Peer Review

- A. Tolosa-Delgado *et al.*, “Commissioning of the BRIKEN detector for the measurement of very exotic  $\beta$ -delayed neutron emitters,” Nucl. Instrum. Methods Phys. Res. A **925**, 133–147 (2019).
- C. Santamaria *et al.*, “Tracking with the MINOS time projection chamber,” Nucl. Instrum. Methods Phys. Res. A **905**, 138–148 (2018).
- T. Isobe *et al.*, “Application of the Generic Electronics for Time Projection Chamber (GET) readout system for heavy radioactive isotope collision experiments,” Nucl. Instrum. Methods Phys. Res. A **899**, 43–48 (2018).
- E. C. Pollacco *et al.*, “GET: A generic electronics system for TPCs and nuclear physics instrumentation,” Nucl. Instrum. Methods Phys. Res. A **887**, 81–93 (2018).

#### Oral Presentations

##### [International Conference etc.]

- H. Baba, “Parallel read-out extension of the VME DAQ system,” 5th Joint Meeting of the APS Division of Nuclear Physics and the Physical Society of Japan, Waikoloa Village, HI, USA, October 23–27, 2018.

#### Posters Presentations

##### [International Conference etc.]

- H. Baba, “Prototype of a multi-host type DAQ front-end system for RI-beam experiments,” 21th IEEE Real Time Conference, Colonial Williamsburg, VA, USA, June 9–15, 2018.

## Research Facility Development Division

### Research Instruments Group

### Detector Team

#### 1. Abstract

This team is in charge of development, fabrication, and operation of various detectors used for nuclear physics experiments at RIBF. Our current main mission is maintenance and improvement of detectors which are used at BigRIPS separator and its succeeding beam lines for beam diagnosis and particle identification of RI beams. We are also engaged in R&D of new detectors that can be used for higher-intensity RI beams. In addition, we are doing the R&D which uses the pelletron accelerator together with other groups.

#### 2. Major Research Subjects

Development, fabrication, and operation of various detectors for nuclear physics experiments, including beam-line detectors which are used for the production and delivery of RI beams (beam diagnosis and particle identification). R&D which uses the pelletron accelerator.

#### 3. Summary of Research Activity

The current research subjects are summarized as follows:

- (1) Maintenance and improvement of the beam-line detectors which are used at BigRIPS separator and its succeeding beam lines.
- (2) Development of new beam-line detectors with radiation hardness and tolerance for higher counting rates
- (3) Management of the pelletron accelerator and R&D which uses the pelletron

#### Members

##### Team Leader

Hiromi SATO

##### Research/Technical Scientist

Tokihiro IKEDA (Senior Research Scientist)

##### Special Temporary Employee

Manabu HAMAGAKI

##### Visiting Scientist

Takeshi KOIKE (Tohoku University)

##### Student Trainees

Shunya KAWAMURA (Toho University)

Masaya SAKAI (University of Tokyo)

Kento TAKEMOTO (University of Tokyo)

Mayuka IKEKAME (Toho University)

Yuka HIKIMA (Toho University)

Mitsumasa MORI (Toho University)

#### List of Publications & Presentations

##### Publications

###### [Journal]

###### (Original Papers) \*Subject to Peer Review

- Y. Hashimoto, H. H. Huang, M. Yoshimura, M. Hara, T. Hara, Y. Hara, M. Hamagaki, "Dependence on treatment ion energy of nitrogen plasma for oxygen reduction reaction of high ordered pyrolytic graphite," *Jpn. J. Appl. Phys.* **57**, 125504 (2018). \*
- O. B. Tarasov, D. S. Ahn, D. Bazin, N. Fukuda, A. Gade, M. Hausmann, N. Inabe, S. Ishikawa, N. Iwasa, K. Kawata, T. Komatsubara, T. Kubo, K. Kusaka, D. J. Morrissey, M. Ohtake, H. Otsu, M. Portillo, T. Sakakibara, H. Sakurai, H. Sato, B. M. Sherrill, Y. Shimizu, A. Stolz, T. Sumikama, H. Suzuki, H. Takeda, M. Thoennessen, H. Ueno, Y. Yanagisawa, K. Yoshida, "Discovery of  $^{60}\text{Ca}$  and Implications For the Stability of  $^{70}\text{Ca}$ ," *Phys. Rev. Lett.* **121**, 022501 (2018). \*
- S. Chebotaryov, S. Sakaguchi, T. Uesaka, T. Akieda, Y. Ando, M. Assie, D. Beaumel, N. Chiga, M. Dozono, A. Galindo-Uribarri, B. Heffron, A. Hirayama, T. Isobe, K. Kaki, S. Kawase, W. Kim, T. Kobayashi, H. Kon, Y. Kondo, Y. Kubota1, S. Leblond, H. Lee, T. Lokotko, Y. Maeda, Y. Matsuda, K. Miki, E. Milman, T. Motobayashi, T. Mukai, S. Nakai, T. Nakamura, A. Ni, T. Noro, S. Ota, H. Otsu, T. Ozaki, V. Panin, S. Park, A. Saito, H. Sakai, M. Sasano, H. Sato, K. Sekiguchi, Y. Shimizu, I. Stefan, L. Stuhl, M. Takaki, K. Taniue, K. Tateishi, S. Terashima, Y. Togano, T. Tomai, Y. Wada, T. Wakasa, T. Wakui, A. Watanabe, H. Yamada, Zh. Yang, M. Yasuda, J. Yasuda, K. Yoneda, J. Zenihiro, "Proton elastic scattering at 200 AMeV and high momentum transfers of 1.7–2.7 fm $^{-1}$  as a probe of the nuclear matter density of  $^6\text{He}$ ," *Prog. Theor. Exp. Phys. Issue 053D01* (2018). \*
- S. Leblond, F. M. Marques, J. Gibelin, N. A. Orr, Y. Kondo, T. Nakamura, J. Bonnard, N. Michel, N. L. Achouri, T. Aumann, H. Baba, F. Delaunay, Q. Deshayes, P. Doornenbal, N. Fukuda, J. W. Hwang, N. Inabe, T. Isobe, D. Kameda, D. Kanno, S. Kim, N. Kobayashi, T. Kobayashi, T. Kubo, J. Lee, R. Minakata, T. Motobayashi, D. Murai, T. Murakami, K. Muto, T. Nakashima, N. Nakatsuka, A. Navin, S. Nishi, S. Ogoshi, H. Otsu, H. Sato, Y. Satou, Y. Shimizu, H. Suzuki, K. Takahashi, H. Takeda, S. Takeuchi, R. Tanaka, Y. Togano, A. G. Tuff, M. Vandebrouck, K. Yoneda, "First observation of  $^{20}\text{B}$  and  $^{21}\text{B}$ ," *Phys. Rev. Lett.* **121**, 262502 (2018). \*

J. Yasuda, M. Sasano, R. G. T. Zegers, H. Baba, D. Bazin, W. Chao, M. Dozono, N. Fukuda, N. Inabe, T. Isobe, G. Jhang, D. Kameda, M. Kaneko, K. Kisamori, M. Kobayashi, N. Kobayashi, T. Kobayashi, S. Koyama, Y. Kondo, A. J. Krasznahorkay, T. Kubo, Y. Kubota, M. Kurata-Nishimura, C. S. Lee, J. W. Lee, Y. Matsuda, E. Milman, S. Michimasa, T. Motobayashi, D. Muecher, T. Murakami, T. Nakamura, N. Nakatsuka, S. Ota, H. Otsu, V. Panin, W. Powell, S. Reichert, S. Sakaguchi, H. Sakai, M. Sako, H. Sato, Y. Shimizu, M. Shikata, S. Shimoura, L. Stuhl, T. Sumikama, H. Suzuki, S. Tangwanchareon, M. Takaki, H. Takeda, T. Tako, Y. Togano, H. Tokieda, J. Tsubota, T. Uesaka, T. Wakasa, K. Yako, K. Yoneda, J. Zenihiro, "Extraction of the Landau-Migdal parameter from the Gamow-Teller giant resonance in  $^{132}\text{Sn}$ ," *Phys. Rev. Lett.* **121**, 132501 (2018). \*

## Oral Presentations

### [International Conference etc.]

T. Ikeda, "Transmission of keV and MeV ions through glass capillary for microbeam engineering," 1st Mini-Workshop for Physics of Ions: Frontiers and Applications/Symposium on Physics and Applications of Ion Beams, (Lanzhou University), Lanzhou, Gansu, China, July 2018.

### [Domestic Conference]

池田時浩, 浜垣学, 佐藤広海, 「理化学研究所におけるタンデム加速器の現状 (2017–2018 年度)」, 第 31 回「タンデム加速器及びその周辺技術の研究会」, (東京都市大学), 東京都世田谷区, 2018 年 7 月.

池田時浩, 廣瀬寛士, 佐藤謙太, 浜垣学, 河村俊哉, 松原充芳, 池亀真由佳, 引間宥花, 森光正, 箕輪達哉, 佐藤広海, 金衛国, 「キャピラリー光学系によるレーザーおよびイオンマイクロビームの同時生成」, 日本物理学会 2018 年秋季大会, (同志社大学), 京田辺市, 2018 年 9 月.

佐藤謙太, 池田時浩, 廣瀬寛士, 幸島美輝子, 松原充芳, 箕輪達哉, 金衛国, 「キャピラリー光学系による可視光レーザーマイクロスポットの構造評価」, 日本物理学会 2018 年秋季大会, (同志社大学), 京田辺市, 2018 年 9 月.

河村俊哉, 池田時浩, 松原充芳, 池亀真由佳, 引間宥花, 森光正, 箕輪達哉, 金衛国, 「キャピラリー光学系による紫外線レーザーマイクロスポットライトの開発」, 日本物理学会 2018 年秋季大会, (同志社大学), 京田辺市, 2018 年 9 月.

池田時浩, 「ガラスキャピラリーによるマイクロビームの生成と応用」, 首都大学東京化学学科第 287 回化学コロキウム, (首都大学東京), 八王子市, 2018 年 9 月.

池田時浩, 引間宥花, 森光正, 池亀真由佳, 河村俊哉, 松原充芳, 箕輪達哉, 金衛国, 「ガラスキャピラリーによるイオンマイクロビーム照射で生じた細胞核内イオントラックの解析」, 第 61 回放射線化学討論会, (大阪市立大学), 大阪市, 2018 年 9 月.

池亀真由佳, 池田時浩, 森光正, 引間宥花, 河村俊哉, 松原充芳, 箕輪達哉, 金衛国, 「ガラスキャピラリーによるマルチ量子マイクロビーム照射に向けたイオンビームプロファイル測定」, 第 61 回放射線化学討論会, (大阪市立大学), 大阪市, 2018 年 9 月.

森光正, 池田時浩, 池亀真由佳, 引間宥花, 河村俊哉, 松原充芳, 箕輪達哉, 金衛国, 「ガラスキャピラリー光学系によるマイクロレーザービームプロファイルの測定: 微小ティルト角依存性」, 第 61 回放射線化学討論会, (大阪市立大学), 大阪市, 2018 年 9 月.

引間宥花, 池田時浩, 森光正, 池亀真由佳, 河村俊哉, 松原充芳, 箕輪達哉, 金衛国, 「ガラスキャピラリー光学系による紫外線マイクロビームの形状測定: フォトクロミックシートを使ったスポット転写」, 第 61 回放射線化学討論会, (大阪市立大学), 大阪市, 2018 年 9 月.

河村俊哉, 池田時浩, 池亀真由佳, 森光正, 引間宥花, 松原充芳, 箕輪達哉, 金衛国, 「紫外線マイクロビーム細胞照射システムの開発: 微小距離でのプロファイル測定とエネルギー評価」, 第 61 回放射線化学討論会, (大阪市立大学), 大阪市, 2018 年 9 月.

櫻井誠, 西田尚史, 堀結喜, 山内亜香音, 池田時浩, 「ガラスキャピラリーを用いた多価イオンの収束手法」, 2018 年日本表面真空学会学術講演会, (神戸国際会議場), 神戸市, 2018 年 11 月.

池田時浩, 池亀真由佳, 引間宥花, 森光正, 河村俊哉, 松原充芳, 箕輪達哉, 金衛国, 「フタ付ガラスキャピラリー光学系で生成された大気中 MeV イオンマイクロビームのプロファイル測定」, 日本物理学会第 74 回年次大会, (九州大学), 福岡市, 2019 年 3 月.

酒井雅哉, 池田時浩, 安井明, 千葉奈津子, 竹本健人, 上坂充, 「 $\alpha$ 線治療のための He イオンマイクロビーム DNA 照射分析の基礎研究」, 日本原子力学会 2019 年春の年会, (茨城大学), 水戸市, 2019 年 3 月.

竹本健人, 「マイクロビームを用いた局所的照射による DNA 損傷の 3 次元位置情報解析」, 日本原子力学会 2019 年春の年会, (茨城大学), 水戸市, 2019 年 3 月.

## Posters Presentations

### [International Conference etc.]

K. Yokokawa, K. Takahashi, J. Matsumoto, H. Shiromaru, T. Ikeda, T. M. Kojima, "Current-dependent ion beam guiding by straight macro capillaries," 10th International Symposium on Swift Heavy Ions in Matter & 28th International Conference on Atomic Collisions in Solids (SHIM-ICACS 2018), (Université Caen Normandie), Caen, France, July 2018.

T. Ikeda, T. Irimatsugawa, Y. Miura, N. Nakada, T. M. Kojima, I. Hakamada, N. Matsufuji, M. Sakama, M. Miwa, M. Ohno, "A transmission experiment of carbon ion beam of 100 MeV/nucleon through tapered glass tubes," 10th International Symposium on Swift Heavy Ions in Matter & 28th International Conference on Atomic Collisions in Solids (SHIM-ICACS 2018), (Université Caen Normandie), Caen, France, July, 2018.

### [Domestic Conference]

河村俊哉, 池田時浩, 佐藤謙太, 松原充芳, 池亀真由佳, 引間宥花, 森光正, 箕輪達哉, 金衛国, 「ガラスキャピラリー光学系によるイオン・レーザーマイクロビーム生成とその応用」, 第 39 回原子衝突若手の会, (奈良ユースホテル), 奈良市, 2018 年 10 月.

池田時浩, 池亀真由佳, 森光正, 引間宥花, 河村俊哉, 松原充芳, 箕輪達哉, 金衛国, 「ガラスキャピラリーで生成された MeV イオンマイクロビーム形状の微小ティルト角依存性」, 原子衝突学会第 43 回年会, (京都大学), 宇治市, 2018 年 10 月.

横川貴一, 高橋航大, 松本淳, 城丸春夫, 池田時浩, 小島 隆夫, 「低速多価イオンビームに対するガラス直管によるガイド効果にお

る素材ごとのビーム電流依存性」, 原子衝突学会第 43 回年会, (京都大学), 宇治市, 2018 年 10 月.

## Accelerator Applications Research Division Beam Mutagenesis Group

### 1. Abstract

This group promotes various applications of ion beams from RI Beam Factory (RIBF). Ion Beam Breeding Team studies various biological effects of fast heavy ions and develops new technology to breed plants and microbes by heavy-ion irradiations. RI Applications Team studies production and application of radioisotopes for various research fields, development of trace element analysis and its application, and development of chemical materials for ECR ion sources of RIBF accelerators.

### 2. Major Research Subjects

Research and development in biology, chemistry and materials science utilizing heavy-ion beams from RI Beam Factory.

### 3. Summary of Research Activity

- (1) Biological effects of fast heavy ions
- (2) Molecular nature of DNA alterations induced by heavy-ion irradiation
- (3) Research and development of heavy-ion breeding
- (4) RI application researches
- (5) Research and development of RI production technology at RIBF
- (6) Developments of trace elements analyses
- (7) Development of chemical materials for ECR ion sources of RIBF accelerators

### Members

#### Group Director

Tomoko ABE

### List of Publications & Presentations

Publications and presentations for each research team are listed in subsections.

## Accelerator Applications Research Division

### Beam Mutagenesis Group

### Ion Beam Breeding Team

#### 1. Abstract

Ion beam breeding team studies various biological effects of fast heavy ions. It also develops new technique to breed plants and microbes by heavy-ion irradiations. Fast heavy ions can produce dense and localized ionizations in matters along their tracks, in contrast to photons (X rays and gamma rays) which produce randomly distributed isolated ionizations. These localized and dense ionization can cause double-strand breaks of DNA which are not easily repaired and result in mutation more effectively than single-strand breaks. A unique feature of our experimental facility at the RIKEN Ring Cyclotron (RRC) is that we can irradiate living tissues in atmosphere since the delivered heavy-ion beams have energies high enough to penetrate deep in matter. This team utilizes a dedicated beam line (E5B) of the RRC to irradiate microbes, plants and animals with beams ranging from carbon to iron. Its research subjects cover physiological study of DNA repair, genome analyses of mutation, and development of mutation breeding of plants by heavy-ion irradiation. Some new cultivars have already been brought to the market.

#### 2. Major Research Subjects

- (1) Study on the biological effects by heavy-ion irradiation
- (2) Study on the molecular nature of DNA alterations induced by heavy-ion irradiation
- (3) Innovative applications of heavy-ion beams

#### 3. Summary of Research Activity

We study biological effects of fast heavy ions from the RRC using 135 A MeV C, N, Ne ions, 95 A MeV Ar ions, 90 A MeV Fe ions and from the IRC using 160 A MeV Ar ions. We also develop breeding technology of microbes and plants. Main subjects are:

##### (1) Study on the biological effects by heavy-ion irradiation

Heavy-ion beam deposits a concentrated amount of dose at just before stop with severely changing the linear energy transfer (LET). The peak of LET is achieved at the stopping point and known as the Bragg peak (BP). It is well known to be good for cancer therapy to adjust the BP to target malignant cells. On the other hand, a uniform dose distribution is a key to the systematic study for heavy-ion mutagenesis, and thus to the improvement of the mutation efficiency. Therefore plants and microbes are treated using ions with stable LET. We investigated the effect of LET ranging from 23 to 640 keV/ $\mu$ m, on mutation induction using dry seeds of the model plants *Arabidopsis thaliana*. The most effective LET (LETmax) was 30 keV/ $\mu$ m. LETmax irradiations showed the same mutation rate as that by chemical mutagens, which typically cause high mutation rate. The LETmax of imbibed rice (*Oryza sativa* L.) seeds, dry rice seeds and dry wheat (*Triticum monococcum*) seeds were shown to be 50–63 keV/ $\mu$ m, 23–30 keV/ $\mu$ m and 50 keV/ $\mu$ m, respectively. In the case of microbe (*Mesorhizobium lotii*), the results showed a higher incidence of deletion mutations for Fe ions at 640 keV/ $\mu$ m than for C ions at 23–40 keV/ $\mu$ m. Thus, the LET is an important factor to be considered in heavy-ion mutagenesis.

##### (2) Study on the molecular nature of DNA alterations induced by heavy-ion irradiation

Detailed analyses on the molecular nature of DNA alterations have been reported as an LET-dependent effect for induced mutation. The most mutations were deletions ranging from a few to several tens of base pairs (bp) in the *Arabidopsis thaliana* mutants induced by irradiation with C ions at 30 keV/ $\mu$ m and rice mutants induced by irradiation with C ions at 50 keV/ $\mu$ m or Ne ions at 63 keV/ $\mu$ m. LETmax is effective for breeding because of its very high mutation frequency. Since most mutations are small deletions, these are sufficient to disrupt a single gene. Thus, irradiation can efficiently generate knockout mutants of a target gene, and can be applied to reverse genetics. On the other hand, irradiation with Ar ions at 290 keV/ $\mu$ m showed a mutation spectrum different from that at LETmax: the proportion of small deletions (<1 kbp) was low, while that of large deletions ranging from several to several tens of kbp, and rearrangements was high. Many genes in the genome (>10%) are composed of tandem duplicated genes that share functions. For knockout of the tandem duplicated genes, large deletions are required, and the appropriate deletion size is estimated to be around 5–10 kbp and 10–20 kbp based on the gene density in *Arabidopsis* and rice, respectively. No method is currently available to efficiently generate deletion mutants of this size. As such, higher LET irradiation is promising as a new mutagen suitable for the functional analysis of tandem duplicated genes.

##### (3) Innovative application of heavy-ion beams

We have formed a consortium for ion-beam breeding. It consisted of 24 groups in 1999, in 2018, it consisted of 180 groups from Japan and 17 from overseas. Breeding was performed previously using mainly flowers and ornamental plants. We have recently put a new sweet-smelling onion cultivar with tearless and non-pungent, 'Smile Balls' on the market. Beneficial variants have been grown for various plant species, such as high yield rice, semi-dwarf early rice, semi-dwarf buckwheat, semi-dwarf barley, hypoallergenic peanut, spineless oranges, non-flowering Eucalyptus and lipids-hyperaccumulating unicellular alga. The target of heavy-ion breeding is extended from flowers to crops so that it will contribute to solve the global problems of food and environment. We collaborate with the National Research and Development Agency, Japan Fisheries Research and Education Agency and Nagasaki University. The monogonont rotifer (*Brachionus* spp.) is a complex species and an essential food source for finfish aquaculture. The *B. plicatilis* is divided into three major clades (small, medium and large (L)) based on body length. Although the body size ranges from 100

to 300  $\mu\text{m}$  in length, a mutation breeding of rotifers with larger size is expected for the purpose of productivity improvement in the aquaculture industry. Therefore, we conducted a large-scale screening to isolate gigantic rotifers by heavy-ion-beam irradiation to L-type rotifers. Then we have established 23 mutant lines that have an average length of over 350  $\mu\text{m}$  (a maximum length reached 404  $\mu\text{m}$ ) through over ten thousand of individual mutagenized lines. These data will be useful to choose the suitable lines that satisfies the request of the aquaculture industry.

## Members

### Team Leader

Tomoko ABE (concurrent: Group Director, Accelerator Applications Research Gr.)

### Research/Technical Scientists

Kazuhide TSUNEIZUMI (Senior Research Scientist)  
Masako IZUMI (Senior Research Scientist)  
Teruyo TSUKADA (Senior Research Scientist)  
Katsunori ICHINOSE (Senior Technical Scientist)

Tokihiro IKEDA (concurrent)  
Hiroshi ABE (Senior Technical Scientist)  
Ryouhei MORITA (Technical Scientist)

### Contract Researchers

Hiroyuki ICHIDA  
Kotaro ISHII

Yusuke KAZAMA

### Technical Staff I

Yoriko HAYASHI

Yuki SHIRAKAWA

### Technical Staff II

Sumie OHBU  
Taeko WAKANA

Mieko YAMADA

### Research Consultants

Masahiro MII

### Part-time Workers

Hideo TOKAIRIN

Sachiko KOGURE

### Visiting Scientists

Makoto FUJIWARA (Univ. of Tokyo)  
Masao WATANABE (Tohoku Univ.)  
Hisashi TSUJIMOTO (Tottori Univ.)  
Yutaka MIYAZAWA (Tohoku Univ.)  
Toshinari GODO (Flower & Garden Bank)  
Masanori TOMITA (CRIEPI)  
Toshikazu MORISHITA (Nat'l. Inst. Agric. Res.)  
Koji MURAI (Fukui Pref. Univ.)  
Hinako TAKEHISA (Nat'l. Inst. Agric. Sci.)  
Akiko HOKURA (Tokyo Denki Univ.)  
Norihiro OHTSUBO (Kyoto Pref. Univ.)

Eitaro FUKATSU (Forestry and Forest Products Res. Inst.)  
Tomonari HIRANO (Univ. of Miyazaki)  
Yoichi SATO (Riken Food Co., Ltd.)  
Ali FERJANI (Tokyo Gakugei Univ.)  
Katsutomo SASAKI (Nat'l Agric. and Food Res. Org.)  
Kunio SUZUKI (Technoflora, Co., Ltd.)  
Kazumitsu MIYOSHI (Chiba. Univ.)  
Tadashi SATO (Tohoku Univ.)  
Takeshi YAMAKI (Riken Vitamin Co., Ltd.)  
Ayumi DEGUCHI (Chiba Univ.)  
Kyosuke NIWA (Tokyo Univ. of Marine Sci. & Tech.)

### Visiting Technicians

Takuji YOSHIDA (Takii Seed Co., Ltd.)  
Daisuke SAITO (Riken Food Co., Ltd.)

Keiji IKEDA (KK SeaAct)  
Yukiko KAWANISHI (Nippon Beet Sugar Mfg. Co., Ltd.)

### Research Fellow

Hironari UCHIDA (Saitama Pref. Res. Inst.)

### Student Trainees

Kazuki TAKANASHI (Tokyo Denki Univ.)  
Yoshihiro TAKAHASHI (Kitazato Univ.)  
Takuya NISHINOBO (Tokyo Denki Univ.)  
Koichi NAMBU (Tokyo Denki Univ.)

Naoko HIROSE (Tokyo Denki Univ.)  
Koya INOUE (Tokyo Denki Univ.)  
Naoki OZEKI (Aichi Pref. Agric. Col.)

## List of Publications & Presentations

### Publications

#### [Journal]

##### (Original Papers) \*Subject to Peer Review

- S. Niwa, Y. Kazama, T. Abe, T. Ban, "Tracking haplotype for QTLs associated with Fusarium head blight resistance in Japanese wheat (*Triticum aestivum* L.) lineage," *Agriculture & Food Security* **7**, Article4 (2018). \*
- A. Nishiura, S. Kitagawa, M. Matsumura, Y. Kazama, T. Abe, N. Mizuno, S. Nasuda, K. Murai, "An early-flowering einkorn wheat mutant with deletions of PHYTOCLOCK 1/LUX ARRHYTHMO and VERNALIZATION 2 exhibits a high level of VERNALIZATION 1 expression induced by vernalization," *J. Plant Physiol.* **222**, 28–38 (2018). \*
- H. Yamatani, K. Kohzuma, M. Nakano, T. Takami, Y. Kato, Y. Hayashi, Y. Monden, Y. Okumoto, T. Abe, T. Kumamaru, A. Tanaka, W. Sakamoto, M. Kusaba, "Impairment of Lhca4, a subunit of LHCI, causes high accumulation of chlorophyll and the stay-green phenotype in rice," *J. Exp. Bot.* **69**, 5, 1027–1035 (2018). \*
- M. T. Fujiwara, M. Yasuzawa, K. H. Kojo, Y. Niwa, T. Abe, S. Yoshida, T. Nakano, R. D. Itoh, "The Arabidopsis *arc5* and *arc6* mutations differentially affect plastid morphology in pavement and guard cells in the leaf epidermis," *PLOS ONE* **13**, 2, e0192380 (2018). \*
- Y. Koide, A. Ogino, T. Yoshikawa, Y. Kitashima, N. Saito, Y. Kanaoka, K. Onishi, Y. Yoshitake, T. Tsukiyama, H. Saito, M. Teraishi, Y. Yamagata, A. Uemura, H. Takagi, Y. Hayashi, T. Abe, Y. Fukuta, Y. Okumoto, A. Kanazawa, "Lineage-specific gene acquisition or loss is involved in interspecific hybrid sterility in rice," *Proc. Natl. Acad. Sci.* **115**, 9, E1955-E1962 (2018). \*
- Y. Kazama, T. Hirano, T. Abe, S. Matsunaga, "Chromosomal rearrangement: From induction by heavy-ion irradiation to in vivo engineering by genome editing," *Cytologia* **83**, 2, 125–128 (2018). \*
- T. Takeshita, N. I. Ivanov, K. Oshima, K. Ishii, H. Kawamoto, S. Ota, T. Yamazaki, A. Hirata, Y. Kazama, T. Abe, M. Hattori, K. Bišová, V. Zachleder, S. Kawano, "Comparison of lipid productivity of *Parachlorella kessleri* heavy-ion beam irradiation mutant PK<sub>4</sub> in laboratory and 150-L mass bioreactor, identification and characterization of its genetic variation," *Algal Res.* **35**, 416–426 (2018). \*
- L. Ma, Y. Kazama, T. Hirano, R. Morita, S. Tanaka, T. Abe, S. Hatakeyama, "LET dependence on killing effect and mutagenicity in the model filamentous fungus *Neurospora crassa*," *Int. J. Radiat. Biol.* **94**, 12, 1125–1133 (2018). \*
- T. Yamazaki, E. Konosu, T. Takeshita, A. Hirata, S. Ota, Y. Kazama, T. Abe, S. Kawano, "Independent regulation of the lipid and starch synthesis pathways by sulfate metabolites in the green microalga *Parachlorella kessleri* under sulfur starvation conditions," *Algal Res.* **36**, 37–47 (2018). \*

#### [Proceedings]

##### (Original Papers) \*Subject to Peer Review

- R. Sjahril, M. Riadi, Rafiuddin, T. Sato, K. Toriyama, T. Abe, R. A. Trisnawaty, "Effect of heavy ion beam irradiation on germination of local Toraja rice seed (M1-M2) mutant generation," *IOP Conf. Ser.: Earth Environ. Sci.* **157**, 012046 (2018[A10]).

### Oral Presentations

#### [International Conference etc.]

- T. Abe, Y. Hayashi, R. Morita, H. Ichida, "Ion-beam mutagenesis —An innovative and effective method for plant breeding and gene discovery," *FAO/IAEA International Symposium on Plant Mutation Breeding and Biotechnology*, Vienna, Austria, August 2018.
- M. Tomita, T. Tsukada, M. Izumi, "Bystander cell killing effects induced by low-fluences of high-LET radiations," *the 64th Annual Radiation Research Society Meeting*, Chicago, USA, September 2018.
- T. Abe, Y. Hayashi, R. Morita, H. Ichida, "An innovative method for plant mutation breeding and gene discovery," *13th International Conference on Nucleus-Nucleus Collisions*, Saitama, Japan, December 2018.

#### [Domestic Conference]

- 風間裕介, 石井公太郎, 平野智也, 若菜妙子, 山田美恵子, 大部澄江, 阿部知子, 「シロイヌナズナ変異体の全ゲノムリシーケンスで明らかにした突然変異誘発への LET の影響」, 日本育種学会第 133 回講演会, 福岡, 2018 年 3 月.
- 市田裕之, 森田竜平, 白川侑希, 林依子, 阿部知子, 「イネ無選抜エキソーム解析による重イオンビーム誘発変異の解析」, 日本育種学会第 133 回講演会, 福岡, 2018 年 3 月.
- 吉田祐樹, 成田典之, 星野里奈, 矢野覚士, 風間裕介, 阿部知子, 堀口吾朗, 塚谷裕一, 「レーザー変位センサ測定によるシロイヌナズナの葉の厚さ変異体の単離と解析」, 第 59 回日本植物生理学会, 札幌, 2018 年 3 月.
- R. Tabassum, T. Tanaka, T. Abe, "Analysis on White Immature Grains of the Rice Mutant Line 13-45 IV. Quantitative comparison among cultivars," *日本作物学会第 245 回講演会*, 宇都宮, 2018 年 3 月.
- 阿部知子, 「加速器施設の突然変異育種利用—重イオンビーム育種技術の開発—九州シンクロトロン光研究センター研究成果報告会 (特集:放射光を中心とした量子ビームの農業・漁業分野への貢献), 佐賀, 2018 年 8 月.
- 田中朋之, R. Tabassum, 道坂怜生, 阿部知子, 「イネ突然変異系統 13-45 における白未熟粒発生機構の解析 第 5 報: 原因候補遺伝子産物の機能解析」, *日本作物学会第 246 回講演会*, 札幌, 2018 年 9 月.
- 阿部知子, 「重イオンビーム育種の現状」, *MIYADAI TAIYO AoiFarm Lab キックオフシンポジウム*, 宮崎, 2018 年 10 月.

### Posters Presentations

#### [International Conference etc.]

- Y. Oono, H. Ichida, R. Morita, S. Nozawa, T. Abe, H. Kato, Y. Hase, "Effect of ion beams on rice genome sequence revealed by exome

analysis,” 16th International Symposium on Rice Functional Genomics, Tokyo, Japan, September 2018.

- Y. Kazama, K. Ishii, T. Hirano, M. Yamada, S. Ohbu, T. Abe, “Highly efficient induction of chromosomal rearrangement by heavy-ion irradiation in the model plant *Arabidopsis thaliana*,” Principles of Chromosome Structure and Function, EMBL Symposium, Heidelberg, Germany, September 2018.
- T. Hirano, Y. Kazama, K. Ishii, N. Vuong, S. Ohbu, H. Kunitake, T. Abe, “Characterization of large flower mutants having chromosomal rearrangements in the model plant *Arabidopsis thaliana*,” Principles of Chromosome Structure and Function, EMBL Symposium, Heidelberg, Germany, September 2018.
- H. Ichida, R. Morita, Y. Shirakawa, Y. Hayashi, T. Abe, “An exome sequencing based characterization of carbon ion beam-induced mutations in an unselected rice population,” The 5th International Rice Congress, Singapore, Singapore, October 2018.

#### [Domestic Conference]

- 佐藤陽一, 萩原亮, 斎藤大輔, 中裕之, 柏谷伸一, 平野智也, 市田裕之, 福西暢尚, 阿部知子, 河野重行, 小野克徳, 「三陸産ワカメ優良系統開発と実用化に向けた取り組み」, 日本藻類学会第 42 回大会, 仙台, 2018 年 3 月.
- 遠藤貴司, 佐藤浩子, 石森裕貴, 中込佑介, 佐藤雅志, 林依子, 市田裕之, 阿部知子, 「重イオンビーム照射によるイネ有用変異体の探索」, 日本育種学会第 133 回講演会, 福岡, 2018 年 3 月.
- 上田純平, 風間裕介, 阿部知子, 村井耕二, 「早生突然変異体コムギ系統における花成遅延復帰変異体 late-heading 1 の同定」, 日本育種学会第 133 回講演会, 福岡, 2018 年 3 月.
- 森田竜平, 市田裕之, 一瀬勝紀, 白川侑希, 林依子, 佐藤雅志, 阿部知子, 「重イオンビーム誘発変異の網羅的検出に向けたプログラムの検討」, 日本育種学会第 133 回講演会, 福岡, 2018 年 3 月.
- 中野絢菜, 相井城太郎, 小森美佳, 阿部知子, 森下敏和, 鈴木達郎, 清水明美, 田中宥司, 「イオンビーム照射由来ダツタンソバ半矮性変異体 sdb における原因遺伝子の同定」, 日本育種学会第 133 回講演会, 福岡, 2018 年 3 月.
- 山谷浩史, 上妻馨梨, 中野道治, 高見常明, 加藤裕介, 林依子, 門田有希, 奥本裕, 阿部知子, 熊丸敏博, 田中歩, 坂本亘, 草場信, 「イネ stay-green 突然変異体 dye1 の分子遺伝学的解析」, 第 59 回日本植物生理学会年会, 札幌, 2018 年 3 月.
- 大野豊, 市田裕之, 野澤樹, 森田竜平, 加藤浩, 阿部知子, 長谷純宏, 「イネ炭素イオンビーム誘発変異体のエキソーム解析」, 第 59 回日本植物生理学会年会, 札幌, 2018 年 3 月.
- 大野豊, 市田裕之, 野澤樹, 森田竜平, 加藤浩, 阿部知子, 長谷純宏, 「イネにおける炭素イオンビーム誘発変異のエキソーム解析」, イネ遺伝学・分子生物学ワークショップ 2018, 三島, 2018 年 7 月.
- Q. N. Vuong, 風間裕介, 石井公太郎, 大部澄江, 國武久登, 阿部知子, 平野智也, 「シロイヌナズナ大輪変異体リソースを用いた花器官サイズ制御機構の解析」, 日本植物学会第 82 回大会, 広島, 2018 年 9 月.
- 風間裕介, 平野智也, 石井公太郎, 若菜妙子, 山田美恵子, 大部澄江, 阿部知子, 「高 LET 重イオンビームは高頻度で染色体再編成を誘発する」, 日本植物学会第 82 回大会, 広島, 2018 年 9 月.
- 風間智彦, 市田裕之, 阿部知子, 佐藤雅志, 鳥山欽哉, 「細胞質雄性不稔性イネへの重イオンビームと EMS 処理による稔性回復変異体の解析」, 第 13 回東北育種研究集会, 弘前, 2018 年 11 月.
- 大野豊, 市田裕之, 野澤樹, 森田竜平, 加藤浩, 阿部知子, 長谷純宏, 「イネにおけるイオンビーム誘発変異のゲノム解析」, 第 41 回日本分子生物学会年会, 横浜, 2018 年 11 月.

**Accelerator Applications Research Division**  
**Beam Mutagenesis Group**  
**Plant Genome Evolution Research Team**

## 1. Abstract

The plant genome evolution research team studies the effect of heavy-ion induced chromosomal rearrangements on plant phenotypes. Chromosome rearrangements including translocation, inversion, and deletion are thought to play an important role in evolution and have a great potential to provide large phenotypic changes. However, this potential has not been fully investigated because of the lack of an effective method to induce rearrangements. We recently found that chromosomal rearrangements are frequently induced after heavy-ion irradiations with high valence numbers such as Fe ions or Ar ions. This frequency is 30 times higher than that of the previous techniques and allows characterization of the effect of chromosomal rearrangements. By analyzing changes of gene expressions and chromatin statuses in mutants having chromosomal rearrangements, we study the effect of the chromosome rearrangements on plant phenotypes of the mutants. In addition, we investigate the developmental process of a plant sex chromosome, which is a representative example of the naturally occurring chromosomal rearrangements involved in adaptation and evolution.

## 2. Major Research Subjects

- (1) Study on the effect of chromosomal rearrangements on plant genomes and phenotypes
- (2) Identification of the plant sex-determining genes and their evolutionary study

## 3. Summary of Research Activity

### (1) Study on the effect of chromosomal rearrangements on plant genomes and phenotypes

In order to investigate the effect of chromosome rearrangements on plant phenotypes, we analysed the *Arabidopsis* mutant Ar55-as1, which were originally induced by Ar-beam irradiation at a dose of 50 Gy with an LET of 290 keV/ $\mu\text{m}$ . This mutant has no homozygous mutation in any genes but has chromosomal rearrangements in the genome. This mutant shows a clear morphological mutant phenotype in which the petiole is shorter than wild-type plants. As a result of the investigation of the trait of each individual and the presence or absence of chromosome rearrangements in the M3 generation of the mutant, we found that the inversion of chromosome 2 is responsible for the phenotype. In addition, this inversion was found to be a dominant mutation. From this finding, we showed that a chromosome rearrangement can dominantly affect the plant phenotype. We are currently investigating the effect of this inversion on gene expression.

We also attempted to induce a chromosome rearrangement at a target position by using genome editing technology, because this technique will be necessary when the functional analysis of chromosomal rearrangements will be performed in the future. There has been no report in which a large chromosomal rearrangement was induced in *A. thaliana* by the genome editing. However, we expected that if it is a proven chromosomal region where chromosome rearrangement has occurred by heavy-ion irradiation, it can be induced even when using genome editing. As a result, 760-kb inversion or deletion was successfully induced by genome editing.

### (2) Identification of the plant sex-determining genes and their evolutionary study

A dioecious plant, *Silene latifolia*, has heteromorphic sex chromosomes (X and Y). We previously identified sex changing mutants of *S. latifolia* by heavy-ion mutagenesis. The sex-changing mutants include hermaphroditic mutants and asexual mutants. The formers have both stamens and gynoecium, while the latter have no reproductive organs. By using the deletion status of these mutant lines, we previously developed *S. latifolia* Y chromosome map, which identified the location of both GSF and SPF on the same chromosome arm. By whole-genome analysis and RNA seq analysis, we are now narrowing down the GSF and SPF regions.

## Members

### Team Leader

Yusuke KAZAMA

### Research Part-time Workers

Sachiko USUDA

Haruka WATANABE

### Visiting Scientist

Tomonari HIRANO (Univ. of Miyazaki)

### Student Trainee

Alvin SANMAYA (Sophia Univ.)

## List of Publications & Presentations

### Publications

#### [Journal]

#### (Original Papers) \*Subject to Peer Review

- N. Fujita, Y. Kazama, N. Yamagishi, K. Watanabe, S. Ando, H. Tsuji, S. Kawano, N. Yoshikawa, K. Komatsu, "Development of the VIGS system in the dioecious plant *Silene latifolia*," *Int. J. Mol. Sci.* **20**, E1031 (2019).\*
- Y. Kazama, T. Hirano, T. Abe, S. Matsunaga, "Chromosomal rearrangement: from induction by heavy-ion irradiation to in vivo engineering by genome editing," *Cytologia* **83**, 125–128 (2018).\*
- L. Ma, Y. Kazama, T. Hirano, R. Morita, S. Tanaka, T. Abe, S. Hatakeyama, "LET dependence on killing effect and mutagenicity in the model filamentous fungus *Neurospora crassa*," *Int. J. Radiation. Biol.* **94**, 1125–1133 (2018).\*
- T. Yamazaki, E. Konosu, T. Takashita, A. Hirata, S. Ota, Y. Kazama, T. Abe, S. Kawano, "Independent regulation of the lipid and starch synthesis pathways by sulfate metabolites in the green microalga *Parachlorella kessleri* under sulfur starvation-conditions," *Algal Res.* **36**, 37–47 (2018).\*
- T. Takeshita, I. N. Ivanov, K. Oshima, K. Ishii, H. Kawamoto, S. Ota, T. Yamazaki, A. Hirata, Y. Kazama, T. Abe, M. Hattori, K. Bisova, V. Zachleder, S. Kawano, "Comparison of lipid productivity of *Parachlorella kessleri* heavy-ion beam irradiation mutant PK4 in laboratory and 150-L mass bioreactor, identification and characterization of its genetic variation," *Algal Res.* **35**, 416–426 (2018).\*

### Oral Presentations

#### [Domestic Conference]

- 風間裕介, 「難しいけど面白い! 植物巨大 Y 染色体の研究」, 第 4 回農学中手の会, 大津, 2018 年 12 月.
- Y. Kazama, "Study of plant sex chromosome by using heavy-ion induced mutants. 1st Symposium on heavy and cluster ions mutagenesis of microorganisms for finding solutions to the issue of hyper-productivity, energy and environment," Tsukuba, January 29, 2019.

### Posters Presentations

#### [International Conference etc.]

- K. Ishii, Y. Kazama, T. Hirano, T. Takeshita, S. Kawano, T. Abe, "Development of a pipeline for whole-genome mutational analysis and Its application on heavy-ion mutagenesis," Plant and Animal Genome XXVII Conference, San Diego, January 2019.
- T. Hirano, Y. Kazama, K. Ishii, V. Q. Nhat, S. Ohbu, H. Kunitake, T. Abe, "Characterization of large flower mutants having chromosomal rearrangements in the model plant *Arabidopsis thaliana*," EMBO|EMBL Symposium: Principles of Chromosome Structure and Function, Heidelberg, Germany, September 2018.
- Y. Kazama, K. Ishii, T. Hirano, M. Yamada, S. Ohbu, T. Abe, "Highly efficient induction of chromosomal rearrangement by heavy-ion irradiation in the model plant *Arabidopsis thaliana*," EMBO|EMBL Symposium: Principles of Chromosome Structure and Function, Heidelberg, Germany, September 2018.

#### [Domestic Conference]

- Q. N. Vuong, 風間裕介, 石井公太郎, 大部澄江, 國武久登, 阿部知子, 平野智也, 「シロイヌナズナ大輪変異体リソースにおける花器官サイズ制御機構の解析」, 日本植物学会第 82 回大会, 広島, 2018 年 9 月.
- 風間裕介, 平野智也, 石井公太郎, 若菜妙子, 山田美恵子, 大部澄江, 阿部知子, 「高 LET 重イオンビームは高頻度で染色体再編成を誘発する」, 日本植物学会第 82 回大会, 広島, 2018 年 9 月.
- 藤田尚子, 風間裕介, 山岸紀子, 安藤咲, 辻寛之, 吉川信幸, 小松健, 「ウイルスベクターを利用したヒロハノマンテマの遺伝子機能解析系の確立」, 日本植物学会第 82 回大会, 広島, 2018 年 9 月.

## Accelerator Applications Research Division

### RI Application Research Group

#### 1. Abstract

RI Application Research Group promotes industrial applications of radioisotopes (RI) and ion beams at RIKEN RI Beam Factory (RIBF). Nuclear Chemistry Research Team develops production technologies of useful RIs for application studies in nuclear and radiochemistry. The team also develops technologies of mass spectrometry for trace-element and isotope analyses and apply them to the research fields such as cosmochemistry, environmental science, archaeology and so on. Industrial Application Research Team promotes industrial applications of the accelerator facility and its related technologies.

#### 2. Major Research Subjects

- (1) Research and development of RI production technologies at RIBF
- (2) RI application researches
- (3) Development of trace element analyses using accelerator techniques and its application to geoscience and archaeological research fields
- (4) Development of chemical materials for ECR ion sources of the RIBF accelerators
- (5) Development of technologies on industrial utilization and novel industrial applications of RIBF
- (6) Support of industrial utilization of the heavy-ion beams at RIBF
- (7) Support of some materials science experiments
- (8) Fee-based distribution of RIs produced at RIBF

#### 3. Summary of Research Activity

See the subsections of Nuclear Chemistry Research Team and Industrial Application Research Team.

#### Members

##### Group Director

Hiromitsu HABA

##### Team Leader

Atsushi YOSHIDA

#### List of Publications & Presentations

See the subsections of Nuclear Chemistry Research Team and Industrial Application Research Team.

## Accelerator Applications Research Division

### RI Application Research Group

### Nuclear Chemistry Research Team

#### 1. Abstract

The Nuclear Chemistry Research Team develops production technologies of radioisotopes (RIs) at RIKEN RI Beam Factory (RIBF) for application studies in the fields of physics, chemistry, biology, engineering, medicine, pharmaceutical and environmental sciences. We use the RIs mainly for nuclear and radiochemical studies such as RI production and superheavy element chemistry. The purified RIs such as  $^{65}\text{Zn}$ ,  $^{67}\text{Cu}$ ,  $^{85}\text{Sr}$ ,  $^{88}\text{Y}$ , and  $^{109}\text{Cd}$  are delivered to universities and institutes through Japan Radioisotope Association. We also develop new technologies of mass spectrometry for the trace-element analyses using accelerator technology and apply them to the research fields such as cosmochemistry, environmental science, archaeology and so on. We perform various isotopic analyses on the elements such as S, Pd, and Pb using ICP-MS, TIMS, IRMS, and so on. We also develop chemical materials for ECR ion sources of the heavy-ion accelerators at RIBF.

#### 2. Major Research Subjects

- (1) Research and development of RI production technologies at RIBF
- (2) RI application researches
- (3) Development of trace element analyses using accelerator techniques and its application to geoscience and archaeological research fields
- (4) Development of chemical materials for ECR ion sources of the heavy-ion accelerators at RIBF

#### 3. Summary of Research Activity

##### (1) Research and development of RI production technologies at RIBF and RI application researches

Due to its high sensitivity, the radioactive tracer technique has been successfully applied for investigations of the behavior of elements in the fields of chemistry, biology, engineering, medicine, pharmaceutical and environmental sciences. We have been developing production technologies of useful radiotracers at RIBF and conducting their application studies in collaboration with many researchers in various fields. With 14-MeV proton, 24-MeV deuteron, and 50-MeV alpha beams from the AVF cyclotron, we presently produce about 50 radiotracers from  $^7\text{Be}$  to  $^{211}\text{At}$ . Among them,  $^{65}\text{Zn}$ ,  $^{67}\text{Cu}$ ,  $^{85}\text{Sr}$ ,  $^{88}\text{Y}$ , and  $^{109}\text{Cd}$  are delivered to Japan Radioisotope Association for fee-based distribution to the general public in Japan. Our RIs are also distributed to researchers under the Supply Platform of Short-lived Radioisotopes for Fundamental Research, supported by MEXT KAKENHI. On the other hand, radionuclides of a large number of elements are simultaneously produced from metallic targets such as  $^{nat}\text{Ti}$ ,  $^{nat}\text{Ag}$ ,  $^{nat}\text{Hf}$ , and  $^{197}\text{Au}$  irradiated with a 135-MeV/nucleon  $^{14}\text{N}$  beam from the RIKEN Ring Cyclotron. These multitracers are also supplied to universities and institutes as collaborative researches.

In 2018, we developed production technologies of radioisotopes such as  $^{24}\text{Na}$ ,  $^{42,43}\text{K}$ ,  $^{44\text{m}}\text{Sc}$ ,  $^{74}\text{As}$ ,  $^{124}\text{Sb}$ ,  $^{111}\text{Ag}$ ,  $^{206}\text{Bi}$ , and  $^{211}\text{At}$  which were strongly demanded but lack supply sources in Japan. We also investigated the excitation functions for the  $^{nat}\text{Zn}(d, x)$ ,  $^{89}\text{Y}(d, x)$ ,  $^{93}\text{Nb}(d, x)$ ,  $^{nat}\text{Pd}(d, x)$ ,  $^{159}\text{Tb}(d, x)$ ,  $^{nat}\text{Er}(d, x)$ ,  $^{nat}\text{Ni}(\alpha, x)$ ,  $^{169}\text{Tm}(\alpha, x)$ , and  $^{nat}\text{W}(\alpha, x)$  reactions to quantitatively produce useful RIs. We used radiotracers of  $^{206}\text{Bi}$  and  $^{211}\text{At}$  for application studies in chemistry,  $^{24}\text{Na}$ ,  $^{42,43}\text{K}$ ,  $^{44\text{m}}\text{Sc}$ ,  $^{67}\text{Cu}$ , and  $^{211}\text{At}$  in nuclear medicine. We also produced  $^{65}\text{Zn}$  and  $^{88}\text{Y}$  for our scientific researches on a regular schedule and supplied the surpluses through Japan Radioisotope Association to the general public. In 2018, we accepted 3 orders of  $^{65}\text{Zn}$  with a total activity of 9.7 MBq and 2 orders of  $^{88}\text{Y}$  with 2 MBq. We also distributed  $^{44\text{m}}\text{Sc}$  (10 MBq  $\times$  1),  $^{88}\text{Zr}$  (1 MBq  $\times$  1 and 2 MBq  $\times$  3),  $^{95}\text{Nb}$  (2 MBq  $\times$  3),  $^{121\text{m}}\text{Te}$  (2 MBq  $\times$  2),  $^{124}\text{Sb}$  (2 MBq  $\times$  1),  $^{175}\text{Hf}$  (1 MBq  $\times$  1 and 2 MBq  $\times$  1),  $^{179}\text{Ta}$  (1 MBq  $\times$  2), and  $^{211}\text{At}$  (5 MBq  $\times$  3, 10 MBq  $\times$  2, 40 MBq  $\times$  1, 50 MBq  $\times$  1, 70 MBq  $\times$  1, 80 MBq  $\times$  5, and 100 MBq  $\times$  4) under the Supply Platform of Short-lived Radioisotopes for Fundamental Research.

##### (2) Superheavy element chemistry

Chemical characterization of newly-discovered superheavy elements (SHEs, atomic numbers  $Z \geq 104$ ) is an extremely interesting and challenging subject in modern nuclear and radiochemistry. We are developing SHE production systems as well as rapid single-atom chemistry apparatuses at RIBF. Using heavy-ion beams from RILAC and AVF,  $^{261}\text{Rf}$  ( $Z = 104$ ),  $^{262}\text{Db}$  ( $Z = 105$ ),  $^{265}\text{Sg}$  ( $Z = 106$ ), and  $^{266}\text{Bh}$  ( $Z = 107$ ) are produced in the  $^{248}\text{Cm}(^{18}\text{O}, 5n)^{261}\text{Rf}$ ,  $^{248}\text{Cm}(^{19}\text{F}, 5n)^{262}\text{Db}$ ,  $^{248}\text{Cm}(^{22}\text{Ne}, 5n)^{265}\text{Sg}$ , and  $^{248}\text{Cm}(^{23}\text{Na}, 5n)^{266}\text{Bh}$  reactions, respectively, and their chemical properties are investigated.

We installed a gas-jet transport system to the focal plane of the gas-filled recoil ion separator GARIS at RILAC. This system is a promising approach for exploring new frontiers in SHE chemistry: the background radiations from unwanted products are strongly suppressed, the intense primary heavy-ion beam is absent in the gas-jet chamber, and hence the high gas-jet extraction yield is attained. Furthermore, the beam-free condition makes it possible to investigate new chemical systems. To realize aqueous chemistry studies of Sg and Bh, we have been developing a continuous and rapid solvent extraction apparatus which consists of a continuous dissolution apparatus Membrane DeGasser (MDG), a Flow Solvent Extractor (FSE), and a liquid scintillation detector for  $\alpha$ /SF-spectrometry. On the other hand, we have a gas-jet coupled target system and a safety system for a radioactive  $^{248}\text{Cm}$  target on the beam line of AVF. In 2018, the distribution coefficients of  $^{261}\text{Rf}$  on the anion-exchange resin in the  $\text{H}_2\text{SO}_4$  system were measured with the AutoMated Batch-type solid-liquid Extraction apparatus for Repetitive experiments of transactinides (AMBER). The co-precipitation behavior of  $^{255}\text{No}$  with Sm hydroxide was also investigated with the computer-controlled suction filtration apparatus for the preparation of precipitated samples of heavy elements (CHIN). In 2018, we also produced radiotracers of  $^{88}\text{Zr}$ ,  $^{95}\text{Nb}$ ,  $^{95\text{m}}\text{Tc}$ ,  $^{175}\text{Hf}$ ,  $^{177,179}\text{Ta}$ , and

$^{183}\text{Re}$  at AVF and conducted model experiments for aqueous chemistry studies on Rf, Db, and Bh.

### (3) Development of trace element analyses using accelerator techniques and its application to geoscience and archaeological research fields

We have been developing the ECR Ion Source Mass Spectrometer (ECRIS-MS) for trace element analyses. In 2018, we renovated the detection system of ECRIS-MS and evaluated its sensitivity and mass resolution power. We equipped a laser-ablation system with an ion source and a pre-concentration system to achieve high-resolution analyses for noble gases such as Kr and Xe.

Using the conventional ICP-MS, TIMS, IRMS, and so on, we analyzed sediments such as a ferro-manganese nodule in the Pacific Ocean to elucidate its growth history concerning the environmental changes in the ocean. We also studied Pb and S isotope ratios on cinnabar and asphalt samples from ancient ruins in Japan to elucidate the distribution of goods in the archaic society and to reveal the establishment of the Yamato dynasty in the period from Jomon to Tumulus. In 2018, we improved the sensitivity in the S isotopic analyses using “trapping and focusing” techniques and analyzed pigments of the Roman ruins. We improved the sampling method for the pigments using a S-free adhesive tape. We applied this method to analyze the red-color substances on the artifacts from Kyoden remains from Izumo to show that they were originated from Hokkaido. We also measured Pd isotopic ratios to investigate the  $^{107}\text{Pd}$  transmutation.

### (4) Development of chemical materials for ECR ion sources of the heavy-ion accelerators at RIBF

In 2018, we prepared metallic  $^{238}\text{U}$  rods and  $^{238}\text{UO}_2$  on a regular schedule for  $^{238}\text{U}$ -ion accelerations with the 28-GHz ECR of RILAC II.

## Members

### Team Leader

Hirimitsu HABA

### Research/Technical Scientist

Kazuya TAKAHASHI

### Postdoctoral Researchers

Kaustab GHOSH

Yang WANG

Yukiko KOMORI

Takuya YOKOKITA

### Technical Staff I

Daiki MORI

### Research Consultants

Hisaaki KUDO

### Part-time Workers

Michiko KITAGAWA

Nozomi SATO

Minako OSANAI

### Visiting Scientists

Masayuki AIKAWA (Hokkaido Univ.)

Aya SAKAGUCHI (Univ. of Tsukuba)

Kazuhiko AKIYAMA (Tokyo Met. Univ.)

Miho SATAKE (Fujifilm Toyama Chem. Co., Ltd.)

Osuke FUJIMOTO (Fujifilm Toyama Chem. Co., Ltd.)

Kenji SHIMAZOE (Univ. of Tokyo)

Hayato IKEDA (Tohoku Univ.)

Keisuke SUEKI (Univ. of Tsukuba)

Noriko ISHIOKA (Takasaki Advanced Rad. Res. Inst., QST)

Kentaro SUZUKI (Fujifilm Toyama Chem. Co., Ltd.)

Masamichi KAJITA (Fujifilm Toyama Chem. Co., Ltd.)

Hiroyuki TAKAHASHI (Univ. of Tokyo)

Hiroshi KATO (Fujifilm Toyama Chem. Co., Ltd.)

Miho TAKAHASHI (Tokyo Univ. Marine Sci. and Tech.)

Hirokazu KAWAMURA (Tohoku Univ.)

Miwako TAKAHASHI (National Inst. of Radiological Sci., QST)

Mayeen Uddin KHANDAKER (Sunway Univ.)

Yuichi TAKAKU (Institute for Environmental Sci.)

Hidetoshi KIKUNAGA (Tohoku Univ.)

Hiroki TAKASHIMA (National Cancer Center Japan)

Yoshikatsu KOGA (National Cancer Center Japan)

Kazuo TANAKA (Tohoku Univ.)

Shoko KUBOTA (Fujifilm Toyama Chem. Co., Ltd.)

Masayoshi TODA (Tokyo Univ. Marine Sci. and Tech.)

Takumi KUBOTA (Kyoto Univ.)

Atsushi TOYOSHIMA (Osaka Univ.)

Susanta Kumar LAHIRI (Saha Institute of Nucl. Phys.)

Takashi UI (Fujifilm Toyama Chem. Co., Ltd.)

Toshimitsu MOMOSE (International Univ. Health Welfare)

Naoyuki UKON (Fukushima Med. Univ.)

Akio NAGANO (Fujifilm Toyama Chem. Co., Ltd.)

Akihiko YOKOYAMA (Kanazawa Univ.)

Eri NAKAMURA (Fujifilm Toyama Chem. Co., Ltd.)

Zenko YOSHIDA (ATOX Co., Ltd.)

Kazuhiro OOE (Osaka Univ.)

Koji YOSHIMURA (Okayama Univ.)

Shinobu OSHIKIRI (Fujifilm Toyama Chem. Co., Ltd.)

Shigeki WATANABE (Takasaki Advanced Rad. Res. Inst., QST)

Yasutaka SAITO (Fujifilm Toyama Chem. Co., Ltd.)

**Visiting Technicians**

Akimitsu KANDA (Japan Radioisotope Association)  
 Yuichirou WAKITANI (Japan Radioisotope Association)  
 Yuki TAKEMURA (ATOX Co., Ltd.)

Mami YUKI (ATOX Co., Ltd.)  
 Shusaku TAZAWA (ATOX Co., Ltd.)

**Student Trainees**

Sadia ADACHI (Univ. of Tsukuba)  
 Masahiro NAGASE (Osaka Univ.)  
 Wei Seng FOONG (Univ. of Tokyo)  
 Yuki NARUSE (Niigata Univ.)  
 Yuta HAYAKAWA (Kanazawa Univ.)  
 Hidemi NINOMIYA (Osaka Univ.)  
 Sho HAYAMI (Osaka Univ.)  
 Sho OKUBO (Okayama Univ.)  
 Xuan HOU (Univ. of Tokyo)  
 Ryota OZAKI (Okayama Univ.)  
 Takumi IKEDA (Osaka Univ.)  
 Moemi SAITOH (Hokkaido Univ.)  
 Junpei INAGAKI (Univ. of Tsukuba)  
 Michiya SAKAGUCHI (Hokkaido Univ.)  
 Saki ITO (Tohoku Univ.)  
 Daisuke SATO (Niigata Univ.)  
 Ayuna KASHIHARA (Univ. of Tsukuba)  
 Keita SEKIGUCHI (Univ. of Tsukuba)

Cheonghun KIM (Univ. of Tokyo)  
 Yudai SHIGEKAWA (Osaka Univ.)  
 Michiko KITAGAWA (Kindai Univ.)  
 Kaori SHIRAI (Niigata Univ.)  
 Mariko KOBAYASHI (Univ. of Tokyo)  
 Kenta SUZUKI (Okayama Univ.)  
 Narumi KONDO (Osaka Univ.)  
 Tomohiro TOMITSUKA (Niigata Univ.)  
 Masaharu KURINO (Univ. of Tokyo)  
 Eisuke WATANABE (Osaka Univ.)  
 Ryoga MORITA (Kanazawa Univ.)  
 Kouhei YAMAMORI (Kanazawa Univ.)  
 Takuya MORIYAMA (Niigata Univ.)  
 Yuki YASUDA (Osaka Univ.)  
 Mayu MURATA (Kanazawa Univ.)  
 Zhihong ZHONG (Univ. of Tokyo)  
 Tomohiro MURATA (Hokkaido Univ.)

**List of Publications & Presentations****Publications****[Journal]****(Original Papers) \*Subject to Peer Review**

- M. Rosenbusch, Y. Ito, P. Schury, M. Wada, D. Kaji, K. Morimoto, H. Haba, S. Kimura, H. Koura, M. MacCormick, H. Miyatake, J. Y. Moon, K. Morita, I. Murray, T. Niwase, A. Ozawa, M. Reponen, A. Takamine, T. Tanaka, H. Wollnik, "New mass anchor points for neutron-deficient heavy nuclei from direct mass measurements of radium and actinium isotopes," *Phys. Rev. C* **97**, 064306 1–8 (2018). \*
- Y. Ito, P. Schury, M. Wada, F. Arai, H. Haba, Y. Hirayama, S. Ishizawa, D. Kaji, S. Kimura, H. Koura, M. MacCormick, H. Miyatake, J. Y. Moon, K. Morimoto, K. Morita, M. Mukai, I. Murray, T. Niwase, K. Okada, A. Ozawa, M. Rosenbusch, A. Takamine, T. Tanaka, Y. X. Watanabe, H. Wollnik, S. Yamaki, "First direct mass measurements of nuclides around  $Z = 100$  with a multireflection time-of-flight mass spectrograph," *Phys. Rev. Lett.* **120**, 152501 1–6 (2018). \*
- N. Ukon, M. Aikawa, Y. Komori, H. Haba, "Production cross sections of deuteron-induced reactions on natural palladium for Ag isotopes," *Nucl. Instrum. Methods Phys. Res. B* **426**, 13–17 (2018). \*
- M. Aikawa, M. Saito, N. Ukon, Y. Komori, H. Haba, "Activation cross sections of alpha-induced reactions on  $^{nat}\text{In}$  for  $^{117\text{m}}\text{Sn}$  production," *Nucl. Instrum. Methods Phys. Res. B* **426**, 18–21 (2018). \*
- M. Aikawa, M. Saito, S. Ebata, Y. Komori, H. Haba, "Activation cross sections of  $\alpha$ -induced reactions on  $^{nat}\text{Zn}$  for Ge and Ga production," *Nucl. Instrum. Methods Phys. Res. B* **427**, 91–94 (2018). \*
- S. Kimura, Y. Ito, D. Kaji, P. Schury, M. Wada, H. Haba, T. Hashimoto, Y. Hirayama, M. MacCormicke, H. Miyatake, J. Y. Moon, K. Morimoto, M. Mukai, I. Murray, A. Ozawa, M. Rosenbusch, H. Schatz, A. Takamine, T. Tanaka, Y. X. Watanabe, H. Wollnik, "Atomic masses of intermediate-mass neutron-deficient nuclei with relative uncertainty down to 35-ppb via multireflection time-of-flight mass spectrograph," *Int. J. Mass Spectrom.* **430**, 134–142 (2018). \*
- K. Morita, K. Morimoto, D. Kaji, H. Haba, H. Kudo, "Discovery of new element, nihonium, and perspectives," *Prog. Nucl. Sci. Technol.* **5**, 8–13 (2018). \*
- F. Ditrói, S. Takács, H. Haba, Y. Komori, M. Aikawa, M. Saito, T. Murata, "Investigation of alpha particle induced reactions on natural silver in the 40–50 MeV energy range," *Nucl. Instrum. Methods Phys. Res. B* **436**, 119–129 (2018). \*
- L. Lens, A. Yakushev, C. E. Düllmann, M. Asai, J. Ballof, M. Block, H. M. David, J. Despotopoulos, A. D. Nitto, K. Eberhardt, J. Even, M. Götz, S. Götz, H. Haba, L. Harkness-Brennan, F. P. Heßberger, R. D. Herzberg, J. Hoffmann, A. Hübner, E. Jäger, D. Judson, J. Khuyagbaatar, B. Kindler, Y. Komori, J. Konki, J. V. Kratz, J. Krier, N. Kurz, M. Laatiaoui, S. Lahiri, B. Lommel, M. Maiti, A. K. Mistry, C. Mokry, K. Moody, Y. Nagame, J. P. Omtvedt, P. Papadakis, V. Pershina, J. Runke, M. Schädel, P. Scharrer, T. Sato, D. Shaughnessy, B. Schausten, P. Thörle-Pospiech, N. Trautmann, K. Tsukada, J. Uusitalo, A. Ward, M. Wegrzecki, N. Wiehl, V. Yakusheva, "Online chemical adsorption studies of Hg, Tl, and Pb on  $\text{SiO}_2$  and Au surfaces in preparation for chemical investigations on Cn, Nh, and Fl at TASCA," *Radiochim. Acta* **106**, 949–962 (2018). \*
- E. Tsantini, T. Minami, K. Takahashi, M. Á. C. Ontiveros, "Analysis of sulphur isotopes to identify the origin of cinnabar in the Roman wall paintings from Badalona (Spain)," *J. Archaeological. Sci. Rep.* **18**, 300–307 (2018). \*

- K. Takahashi, Y. Nakai, Y. Motizuki, T. Ino, S. Ito, S. B. Ohkubo, T. Minami, Y. Takaku, Y. Yamaguchi, M. Tanaka, H. Motoyama, "High-sensitivity sulfur isotopic measurements for Antarctic ice core analyses," *Rapid Commun. Mass Spectrom.* **32**, 1991–1998 (2018). \*
- T. Murata, M. Aikawa, M. Saitoc, N. Ukon, Y. Komori, H. Haba, S. Takács, "Production cross sections of Mo, Nb and Zr radioisotopes from  $\alpha$ -induced reaction on  $^{nat}\text{Zr}$ ," *Appl. Radiat. Isot.* **144**, 47–53 (2019). \*
- H. Haba, "A new period in superheavy-element hunting," *Nat. Chem.* **11**, 10–13 (2019). \*
- A. Yokoyama, Y. Kitayama, Y. Fukuda, H. Kikunaga, M. Murakami, Y. Komori, S. Yano, H. Haba, K. Tsukada, A. Toyoshima, "Extraction behavior of rutherfordium as a cationic fluoride complex with a TTA chelate extractant from HF/HNO<sub>3</sub> acidic solutions," *Radiochim. Acta* **107**, 27–32 (2019). \*
- K. Fujiki, Y. Kanayama, S. Yano, N. Sato, T. Yokokita, P. Ahmadi, Y. Watanabe, H. Haba, K. Tanaka, "<sup>211</sup>At-labeled immunoconjugate via a one-pot three-component double click strategy: practical access to  $\alpha$ -emission cancer radiotherapeutics," *Chem. Sci.* **10**, 1936–1944 (2019). \*
- Y. Wang, S. Cao, J. Zhang, F. Fan, J. Yang, H. Haba, Y. Komori, T. Yokokita, K. Morimoto, D. Kaji, Y. J. Wittwer, R. Eichler, A. Türler, Z. Qin, "The study of rhenium pentacarbonyl complexes using single-atom chemistry in gas phase," *Phys. Chem. Chem. Phys.* **21**, 7147–7154 (2019). \*
- F. Miyake, K. Horiuchi, Y. Motizuki, Y. Nakai, K. Takahashi, K. Masuda, H. Motoyama, H. Matsuzaki, "<sup>10</sup>Be signature of the cosmic ray event in the 10th century CE in both hemispheres, as confirmed by quasi-annual <sup>10</sup>Be data from the Antarctic Dome Fuji ice core," *Geophys. Res. Lett.* **46**, 11–18 (2019). \*
- 羽場宏光, 「GARIS が拓く超重元素の化学—106 番元素シーボーギウムのカルボニル錯体の合成—」, *Radioisotopes* **67**, 527–535 (2018). \*
- 羽場宏光, 「超重元素の合成—原子番号 113 以降の超重元素の合成と発見—」, *Radioisotopes* **67**, 277–289 (2018). \*
- 羽場宏光, 「ニホニウムはいかにして誕生したのか 1. 元素の発見と周期表」, *現代化学* **4**, No. 565, 34–37 (2018).
- 羽場宏光, 「ニホニウムはいかにして誕生したのか 2. 同位体と核図表」, *現代化学* **5**, No. 566, 18–21 (2018).
- 羽場宏光, 「ニホニウムはいかにして誕生したのか 3. 人工元素」, *現代化学* **6**, No. 567, 44–48 (2018).
- 羽場宏光, 「ニホニウムはいかにして誕生したのか 4. 幻の新元素」, *現代化学* **7**, No. 568, 36–39 (2018).
- 羽場宏光, 「ニホニウムはいかにして誕生したのか 5. 超重元素」, *現代化学* **8**, No. 569, 40–43 (2018).
- 羽場宏光, 「ニホニウムはいかにして誕生したのか 6. 理研の新元素探索 (1)」, *現代化学* **9**, No. 570, 24–28 (2018).
- 羽場宏光, 「ニホニウムはいかにして誕生したのか 7. 理研の新元素探索 (2)」, *現代化学* **10**, No. 571, 53–57 (2018).
- 羽場宏光, 「ニホニウムはいかにして誕生したのか 8. 理研の新元素探索 (3)」, *現代化学* **11**, No. 572, 25–28 (2018).
- 羽場宏光, 「ニホニウムはいかにして誕生したのか 9. ロシアと米国による新元素探索」, *現代化学* **12**, No. 573, 52–56 (2018).
- 羽場宏光, 「ニホニウムはいかにして誕生したのか 10. ニホニウム命名」, *現代化学* **1**, No. 574, 44–49 (2019).
- 羽場宏光, 「ニホニウムはいかにして誕生したのか 11. さらに新元素を求めて」, *現代化学* **2**, No. 575, 42–46 (2019).
- 羽場宏光, 「ニホニウムはいかにして誕生したのか 12. 新元素の化学的性質」, *現代化学* **3**, No. 576, 42–46 (2019).
- 鈴木智和, 渡部浩司, 菊永英寿, 羽場宏光, 福田光宏, 「短寿命 RI 供給プラットフォーム実現のための放射線障害防止法上の手続きについて」, *日本放射線安全管理学会誌* 第 17 巻, 2 号, 121–124 (2018). \*
- 河野摩耶, 高橋和也, 今津節生, 南武志, 「福岡県安徳台遺跡群における朱の使い分けについて」, *古代*, 第 142 号, 97–103 (2018). \*

#### [Proceedings]

- T. Karino, M. Okamura, H. Haba, T. Kanetsue, S. Ikeda, S. Kawata, "Characteristic investigation of <sup>96</sup>Zr oxide," *AIP Conf. Proc.* **2011**, 070004 1–3 (2018). \*

#### [Book]

- 桜井弘, 根矢三郎, 寺嶋孝仁, 笹森貴裕, 羽場宏光, 「元素検定 2」, 化学同人, 2018 年 8 月 20 日.
- 高橋和也, 南武志, 「2018 年度京田遺跡発掘調査報告書, 第 5 節 4 区出土遺物付着異物水銀朱の硫黄同位体比分析」, 出雲市文化財課, 2019 年 3 月.

### Oral Presentations

#### [International Conference etc.]

- T. Murata, M. Aikawa, M. Saito, N. Ukon, Y. Komori, H. Haba, S. Takács, "<sup>99</sup>Mo production from  $\alpha$ -induced reaction on <sup>96</sup>Zr," The 18th Radiochemical Conference (RadChem 2018), Mariánské Lázně, Czech Republic, May 2018.
- M. Saito, M. Aikawa, T. Murata, N. Ukon, Y. Komori, H. Haba, S. Takács, "Production cross section measurement of alpha induced reaction on  $^{nat}\text{Yb}$  to produce medical RI <sup>177</sup>Lu," The 18th Radiochemical Conference (RadChem 2018), Mariánské Lázně, Czech Republic, May 2018.
- A. Yokoyama, A. Sakaguchi, K. Yamamori, Y. Hayakawa, K. Sekiguchi, S. Yanou, Y. Komori, T. Yokokita, H. Haba, N. Takahashi, A. Shinohara, "Production of Np isotopes in nuclear reactions for a standard material in accelerator mass spectrometry," The 18th Radiochemical Conference (RadChem 2018), Mariánské Lázně, Czech Republic, May 2018.
- H. Haba, "Production and applications of radioisotopes at RIKEN RI Beam Factory," Seminar at Brookhaven National Laboratory, New York, USA, May 2018.
- H. Haba, "Synthesis and chemistry of superheavy elements at RIKEN," DAE-BRNS Eighth Biennial Symposium on Emerging Trends in Separation Science and Technology (SESTEC-2018), Goa, India, May 2018.
- H. Haba, "Production and applications of radioisotopes at RIKEN RI Beam Factory," Seminar at Inter-University Accelerator Centre,

New Delhi, India, May 2018.

- H. Haba, "Applications with unstable ion beams and complementary techniques at the RIKEN," Consultancy Meeting on Novel Multidisciplinary Applications with Unstable Ion Beams and Complementary Techniques, Vienna, Austria, July 2018.
- K. Takahashi, H. Motoyama, "The isotopic measurements of oxygen and hydrogen in Dome-Fuji (Antarctica) ice core: Annually-resolved temperature reconstructions of the past 2000 years," The 4th International Conference on Water Resource and Environment (WRE 2018), Kaoshiung, Taiwan, July 2018.
- H. Haba, "Present status and perspectives of SHE researches at RIKEN," IX International Symposium on Exotic Nuclei (EXON-2018), Petrozavodsk, Russia, September 2018.
- Y. Ito, P. Schury, M. Wada, F. Arai, H. Haba, Y. Hirayama, S. Ishizawa, D. Kaji, S. Kimura, H. Koura, M. MacCormick, H. Miyatake, J. Y. Moon, K. Morimoto, K. Morita, M. Mukai, I. Murray, T. Niwase, K. Okada, A. Ozawa, M. Rosenbusch, A. Takamine, T. Tanaka, Y. X. Watanabe, H. Wollnik, S. Yamaki, "Direct mass measurements of heavy/superheavy nuclei with an MRTOF-MS coupled with the GARIS-II," The International Conference on Electromagnetic Isotope Separators and Related Topics (EMIS) 2018, Geneva, Switzerland, September 2018.
- M. Rosenbusch, Y. Ito, M. Wada, P. Schury, F. Arai, H. Haba, Y. Hirayama, S. Ishizawa, D. Kaji, S. Kimura, H. Koura, M. MacCormick, H. Miyatake, J. Y. Moon, K. Morimoto, K. Morita, M. Mukai, I. Murray, T. Niwase, K. Okada, A. Ozawa, A. Takamine, T. Tanaka, Y. X. Watanabe, H. Wollnik, S. Yamaki, "Advances and future plans for nuclear mass measurements at RIKEN," The International Conference on Electromagnetic Isotope Separators and Related Topics (EMIS) 2018, Geneva, Switzerland, September 2018.
- M. Mukai, Y. Hirayama, Y. X. Watanabe, P. Schury, M. Ahmed, H. Haba, H. Ishiyama, S. C. Jeong, Y. Kakiguchi, S. Kimura, J. Y. Moon, M. Oyaizu, A. Ozawa, J. H. Park, H. Ueno, M. Wada, H. Miyatake, "Development of a multi-segmented proportional gas counter for  $\beta$ -decay spectroscopy at KISS," The International Conference on Electromagnetic Isotope Separators and Related Topics (EMIS) 2018, Geneva, Switzerland, September 2018.
- H. Haba, "Production of radioisotopes for application studies at RIKEN RI Beam Factory," 4th International Conference on Application of Radiotracers and Energetic Beams in Sciences (ARCEBS-2018), Kolkata, India, November 2018.
- Y. Komori, H. Haba, T. Yokokita, S. Yano, N. Sato, K. Ghosh, Y. Sakemi, H. Kawamura, "Measurement of excitation functions of the  $^{206/207/208}\text{Pb}(^{11}\text{B}, x)^{212}\text{Fr}$  reactions and complex formation studies of Fr with crown ethers," 4th International Conference on Application of Radiotracers and Energetic Beams in Sciences (ARCEBS-2018), Kolkata, India, November 2018.
- H. Haba, "Production and application of radioisotopes using He jet transport system at RIKEN RI Beam Factory," Seminar at Variable Energy Cyclotron Centre, Kolkata, India, November, 2018.
- T. Tanaka, K. Morita, K. Morimoto, D. Kaji, H. Haba, R. A. Boll, N. T. Brewer, S. Van Cleve, D. J. Dean, S. Ishizawa, Y. Ito, Y. Komori, K. Nishio, T. Niwase, B. C. Rasco, J. B. Roberto, K. P. Rykaczewski, H. Sakai, D. W. Stracener, K. Hagino, "Fusion dynamics for hot fusion reactions revealed in quasielastic fusion barrier distributions," 13th International Conference on Nucleus-Nucleus Collisions, Omiya, Japan, December 2018.
- H. Haba, "Production of radioisotopes for gamma-ray imaging at RIKEN RI Beam Factory," Workshop on Multiple Photon Coincidence Imaging, Narita, Japan, December 2018.
- H. Haba, "Production of radioisotopes for application studies at RIKEN RI Beam Factory," Technical Meeting on Novel Multidisciplinary Applications with Unstable Ion Beams and Complementary Techniques, Vienna, Austria, December 2018.
- Y. Komori, "Activities related to SHE target production and aqueous chemistry of SHEs at RIKEN," NUSPRASEN Workshop on Superheavy element research, target techniques and related topics, GSI, Darmstadt, Germany, February 2019.
- H. Haba, "Present status and perspectives of SHE researches at RIKEN," NUSPRASEN Workshop on Superheavy element research, target techniques and related topics and NUSTAR Annual Meeting 2019, Darmstadt, Germany, February 2019.

#### [Domestic Conference]

- H. Haba, "Present status and perspectives of superheavy element chemistry at RIKEN," 研究会「超重元素研究の新展開」, 福岡, 2018年7月.
- 南武志, 高橋和也, 「超微量硫黄同位体分析法の開発と考古学試料分析の利点」, 日本文化財科学会第35回大会, 奈良, 2018年7月.
- 羽場宏光, 「理研におけるRI製造応用～新元素の化学から核医学の診断・治療まで～」, 大阪大学放射線科基盤機構発足記念シンポジウム, 豊中, 2018年8月.
- 小森有希子, 「理研における超重元素化学研究の現状と将来計画」, 第57回化学夏の学校, 長野, 2018年8月.
- 庭瀬暁隆, 和田道治, P. Schury, 伊藤由太, 加治大哉, M. Rosenbusch, 木村創大, 森本幸司, 羽場宏光, 石澤倫, 森田浩介, 宮武宇也, H. Wollnik, 「MRTOF-MS用の $\alpha$ -ToF検出器の性能評価」, 2018日本放射化学会年会・第62回放射化学討論会, 京都, 2018年9月.
- 海老原充, 大浦泰嗣, 白井直樹, 永川栄泰, 櫻井昇, 羽場宏光, 松崎浩之, 鶴田治雄, 森口祐一, 「首都圏に飛来した福島原発事故由来の放射性エアロゾル中の $^{129}\text{I}/^{131}\text{I}$ 比」, 2018日本放射化学会年会・第62回放射化学討論会, 京都, 2018年9月.
- 佐藤望, 羽場宏光, 横北卓也, Ghosh Kaustab, Wang Yang, 小森有希子, 森大輝, 高橋和也, 木村俊夫, 松本幹雄, 「理研におけるAt-211の製造頒布」, 2018日本放射化学会年会・第62回放射化学討論会, 京都, 2018年9月.
- 小森有希子, 「 $^{nat}\text{Mo}(d, x)$  および  $^{nat}\text{W}(d, x)$  反応による Tc, Re 同位体の生成断面積測定」, Chemical Probe 合宿形式セミナー, 千葉, 2018年10月.
- 羽場宏光, 「新元素ニホニウム発見への道のり」, 第5回奇石博物館サイエンスカフェ, 富士宮, 2018年10月.
- 篠原厚, 豊嶋厚史, 吉村崇, 兼田(中島)加珠子, 張子見, 永田光知郎, 渡部直史, 畑澤順, 大江一弘, 山村朝雄, 白崎謙次, 菊永英寿, 羽場宏光, 鷲山幸信, 「短寿命 $\alpha$ 線核種の飛散率等の基礎データ取得と合理的法規制に向けた安全性検証と放射線管理法の開発」, 日本放射線安全管理学会第17回学術大会, 名古屋, 2018年12月.

- 豊嶋厚史, 篠原厚, 吉村崇, 兼田 (中島) 加珠子, 張子見, 永田光知郎, 渡部直史, 大江一弘, 山村朝雄, 白崎謙次, 菊永英寿, 羽場宏光, 鷲山幸信, 「短寿命アルファ線放出核種 At-211 の合理的規制に向けた飛散率測定」, 日本放射線安全管理学会第 17 回学術大会, 名古屋, 2018 年 12 月.
- 羽場宏光, 「理研における RI 製造応用～新元素の探索から核医学の診断・治療まで～」, 放射線科学ワークショップ「文理共創を革新する量子ビーム科学」, 文京区, 2019 年 2 月.
- 羽場宏光, 「理研 RI ビームファクトリーで製造する応用研究用ラジオアイソトープ」, 理研シンポジウム「精密武装抗体の合成と機能評価」, 千代田区, 2019 年 3 月.
- 鎌田圭, 吉野将生, 庄子育宏, 山路晃弘, 黒澤俊介, 横田有為, 大橋雄二, 島添健次, 高橋美和子, 羽場宏光, 百瀬敏光, 高橋浩之, 吉川彰, 「CeBr<sub>3</sub> シンチレータ単結晶の大型化とアッセンブリ技術の開発」, 第 66 回応用物理学会春季学術講演会, 大田区, 2019 年 3 月.
- 羽場宏光, 小森有希子, 横北卓也, 森大輝, 高橋浩之, 島添健次, 鎌田圭, 百瀬敏光, 高橋美和子, 「多光子イメージング用カリウム 43 の製造技術開発」, 第 66 回応用物理学会春季学術講演会, 大田区, 2019 年 3 月.
- 島添健次, 上ノ町水紀, 高橋浩之, 鎌田圭, 高橋美和子, 羽場宏光, 百瀬敏光, 「多光子多分子核医学イメージング技術の研究開発」, 第 66 回応用物理学会春季学術講演会, 大田区, 2019 年 3 月.
- 高橋美和子, 島添健次, 大島佑介, 高橋浩之, 鎌田圭, 羽場宏光, 百瀬敏光, 「多核種同時核医学イメージング技術の開発と検証」, 第 66 回応用物理学会春季学術講演会, 大田区, 2019 年 3 月.
- 鈴木健太, 羽場宏光, 原秀明, 平木貴宏, 藤枝亮, 藤本弘之, 海野弘行, 笠松良崇, 北尾真司, 小無健司, 増田孝彦, 宮本祐樹, 岡井晃一, 笹尾登, 佐藤帯子, Thorsten Schumm, 瀬戸誠, 重河優大, Simon Stellmer, 玉作賢治, 植竹智, 渡部信, 渡部司, 山口敦史, 安田勇輝, 依田芳卓, 吉見彰洋, 吉村浩司, 吉村太彦, 「トリウム 229 の原子核時計遷移分光」, 日本物理学会第 74 回年次大会 (2019 年), 福岡, 2019 年 3 月.
- 早水友洋, 長濱弘季, 小澤直也, 堤惇, 原田健一, 田中香津生, 内山愛子, 青木貴稔, 島山温, 高橋義朗, 羽場宏光, 大前宣昭, 酒見泰寛, 「電子の永久電気双極子モーメント探索へ向けたフランシウム原子の生成とトラップ」, 日本物理学会第 74 回年次大会 (2019 年), 福岡, 2019 年 3 月.
- 海野弘行, 羽場宏光, 原秀明, 平木貴宏, 藤枝亮, 藤本弘之, 鈴木健太, 笠松良崇, 北尾真司, 小無健司, 増田孝彦, 宮本祐樹, 岡井晃一, 笹尾登, 佐藤帯子, Thorsten Schumm, 瀬戸誠, 重河優大, Simon Stellmer, 玉作賢治, 植竹智, 渡部信, 渡部司, 山口敦史, 安田勇輝, 依田芳卓, 吉見彰洋, 吉村浩司, 吉村太彦, 「核共鳴散乱を用いたトリウム 229 アイソマー準位への人工的遷移」, 日本物理学会第 74 回年次大会 (2019 年), 福岡, 2019 年 3 月.
- 羽場宏光, 「新元素の合成と化学」, 第 37 回量子系分子科学セミナー, 神戸, 2019 年 3 月.
- 小森有希子, 羽場宏光, 横北卓也, 矢納慎也, 佐藤望, Ghosh Kaustab, 酒見泰寛, 川村広和, 「<sup>206/207/208</sup>Pb(<sup>11</sup>B, x)<sup>212</sup>Fr 反応の励起関数測定とクラウンエーテルを用いた Fr の錯形成反応」, 日本化学会第 99 春季年会 2019, 神戸, 2019 年 3 月.
- 横北卓也, 笠松良崇, 小森有希子, 渡邊瑛介, ゴーシュコースタフ, 王洋, 森大輝, 篠原厚, 羽場宏光, 「Rf の硫酸錯体研究に向けたバッチ型固液抽出装置による Zr 及び Hf の陰イオン交換」, 日本化学会第 99 春季年会 2019, 神戸, 2019 年 3 月.
- 二宮秀美, 笠松良崇, 速水翔, 永瀬将浩, 重河優大, 近藤成美, 渡邊瑛介, 羽場宏光, 横北卓也, 小森有希子, 森大輝, 王洋, ゴーシュコースタフ, 佐藤望, 篠原厚, 「102 番元素 No のアンモニア水及び水酸化ナトリウム水溶液中におけるサマリウム共沈挙動」, 日本化学会第 99 春季年会 2019, 神戸, 2019 年 3 月.
- 齋藤萌美, 合川正幸, 坂口理哉, 右近直之, 小森有希子, 羽場宏光, 「医療用放射性核種 <sup>169</sup>Yb 生成のための <sup>248</sup>Er への 50 MeV アルファ粒子入射における生成断面積測定」, 日本原子力学会 2019 年春の年会, 水戸, 2019 年 3 月.
- 横北卓也, 「Rf の硫酸錯体に関する研究: 同族元素 Zr, Hf, Th を用いた基礎研究～Rf の陰イオン交換」, 2019 重元素核化学ワークショップ, 和光, 2019 年 3 月.
- 小森有希子, 「Fr の錯形成反応」, 2019 重元素核化学ワークショップ, 和光, 2019 年 3 月.
- 小森有希子, 「Sg と Bh の溶液化学に向けた GARIS ガスジェット直結型迅速溶媒抽出装置の開発」, 2019 重元素核化学ワークショップ, 和光, 2019 年 3 月.
- 横北卓也, 「Db のフッ化物錯体の研究に向けた Nb, Ta, Pa を用いた HF/HCl 系のイオン交換及び今後の研究計画」, 2019 重元素核化学ワークショップ, 和光, 2019 年 3 月.
- W. Yang, “Gas-phase chemistry of technetium and rhenium carbonyl complexes with short-lived isotopes,” 2019 重元素核化学ワークショップ, 和光, 2019 年 3 月.
- W. Yang, “Mass spectrometric speciation of metal-carbonyls in the gas phase,” 2019 重元素核化学ワークショップ, 和光, 2019 年 3 月.

## Posters Presentations

### [International Conference etc.]

- T. Niwase, K. Fujita, Y. Yamano, K. Watanabe, D. Kaji, K. Morimoto, H. Haba, T. Hirano, S. Mitsuoka, K. Morita, “Measurement of fusion barrier distribution in <sup>51</sup>V + <sup>208</sup>Pb system,” 13th International Conference on Nucleus-Nucleus Collisions, Omiya, Japan, December, 2018.

### [Domestic Conference]

- 近藤成美, 笠松良崇, 永瀬将浩, 安田勇輝, 重河優大, 大内昂輝, 神田晃充, 二宮秀美, 渡邊瑛介, 羽場宏光, 久保木祐生, 小森有希子, 横北卓也, 矢納慎也, 佐藤望, 篠原厚, 「Rf の塩酸系での溶媒抽出挙動の有機溶媒依存性」, 2018 日本放射化学会年会・第 62 回放射化学討論会, 京都, 2018 年 9 月.
- 川崎康平, 新裕喜, 青井景都, 鷲山幸信, 西中一郎, 羽場宏光, 矢納慎也, 横山明彦, 「ラドンガス密封シリンジを利用した Rn-At ジェネレーターシステムの開発」, 2018 日本放射化学会年会・第 62 回放射化学討論会, 京都, 2018 年 9 月.
- 新裕喜, 川崎康平, 青井景都, 横山明彦, 鷲山幸信, 西中一郎, 矢納慎也, 羽場宏光, 「<sup>211</sup>Rn-<sup>211</sup>At ジェネレーター開発のためのアスタチン溶媒抽出の研究—<sup>131</sup>I との抽出挙動の比較及び酸化剤の効果の調査—」, 2018 日本放射化学会年会・第 62 回放射化学討論

会, 京都, 2018 年 9 月.

雨倉啓, 秋山和彦, 久富木志郎, 羽場宏光, 「金属内包フラーレン合成実験のための無担体  $^{139}\text{Ce}$  トレーサーの調製」, 2018 日本放射化学会年会・第 62 回放射化学討論会, 京都, 2018 年 9 月.

篠原厚, 吉村崇, 豊嶋厚史, 兼田加珠子, 張子見, 永田光知郎, 渡部直史, 大江一弘, 畑澤順, 山村朝雄, 白崎謙次, 菊永英寿, 羽場宏光, 鷲山幸信, 「短寿命  $\alpha$  線核種の合理的規制のためのデータ取得による安全性検証と安全管理・教育方法の開発」, 2018 日本放射化学会年会・第 62 回放射化学討論会, 京都, 2018 年 9 月.

坂口理哉, 合川正幸, 小森有希子, 羽場宏光, 「 $^{89}\text{Y}$  標的への重陽子入射反応による  $^{89}\text{Zr}$  生成反応断面積」, 2018 年度核データ研究会, 目黒区, 2018 年 11 月.

横北卓也, 「アルファ線核医学治療用核種アスタチン-211 の製造開発」, Chemical Probe 合宿形式セミナー, 千葉, 2018 年 10 月.

兼田 (中島) 加珠子, 篠原厚, 吉村崇, 豊嶋厚史, 張子見, 永田光知郎, 渡部直史, 大江一弘, 山村朝雄, 白崎謙次, 菊永英寿, 羽場宏光, 鷲山幸信, 「動物実験における短寿命アルファ線核種の体内外の分布」, 日本放射線安全管理学会第 17 回学術大会, 名古屋, 2018 年 12 月.

永田光知郎, 吉村崇, 豊嶋厚史, 篠原厚, 兼田 (中島) 加珠子, 張子見, 渡部直史, 大江一弘, 山村朝雄, 白崎謙次, 菊永英寿, 羽場宏光, 鷲山幸信, 「短寿命  $\alpha$  線放出核種の合理的規制のためのラジウム-223 およびその子孫核種の飛散率等の測定」, 日本放射線安全管理学会第 17 回学術大会, 名古屋, 2018 年 12 月.

村上郁斗, 平川貴啓, 内藤夏樹, 坂口聡志, 藤田訓裕, 郷慎太郎, 足立智, 田中聖臣, 田中泰貴, 庭瀬暁隆, 森本幸司, 羽場宏光, 加治大哉, 馬場秀忠, Pierre Brionnet, 木村創大, 酒井英行, 森田浩介, 「超重元素識別のためのデータ解析手法の開発」, 日本物理学会第 74 回年次大会 (2019 年), 福岡, 2019 年 3 月.

## Accelerator Applications Research Division

### RI Application Research Group

### Industrial Application Research Team

#### 1. Abstract

Industrial application research team handles non-academic activities at RIBF corresponding mainly to industries.

#### 2. Major Research Subjects

- (1) Support of industrial utilization of the RIBF accelerator beam.
- (2) Development of technologies related to the industrial utilization and novel industrial applications.
- (3) Fee-based distribution of radioisotopes produced at RIKEN AVF Cyclotron.
- (4) Development of real-time wear diagnostics of industrial material using RI beams.

#### 3. Summary of Research Activity

##### (1) Support of Industrial Utilization of RIBF

RNC promote facility-sharing program “Promotion of applications of high-energy heavy ions and RI beams.” In this program, RNC opens the old part of the RIBF facility, which includes the AVF cyclotron, RILAC, RIKEN Ring Cyclotron and experimental instruments, to non-academic proposals from users including private companies. The proposals are reviewed by a program advisory committee, industrial PAC (IN-PAC). The proposals which have been approved by the IN-PAC are allocated with beam times and the users pay RIKEN the beam time fee. The intellectual properties obtained by the use of RIBF belong to the users. In order to encourage the use of RIBF by those who are not familiar with utilization of ion beams, the first two beam times of each proposal can be assigned to trial uses which are free of beam time fee.

In June 2018, the eighth IN-PAC met and approved one fee-based proposal from a new private company. In January 2019, IN-PAC reviewed by e-mail one fee-based continuing proposal from a private company and approved it. In July 2018, a fee-based beamtime was performed with a Kr-84 (70 MeV/nucleon) and an Ar-40 (95 MeV/nucleon) beam at the E5A beamline. In December 2018, a fee-based beamtime was performed with a Kr-86 (66 MeV/nucleon) beam at the E3A beamline. The clients used the beam to simulate single-event effects of space-use semiconductors by heavy-ion components of cosmic rays.

##### (2) Development of technologies related to the industrial utilization and novel industrial applications

We develop technologies to assess and improve the quality of the beam used for the semiconductor irradiations. Before each beam time, we measure the properties of the beam; the dependence of the beam energy on the degrader thickness, the beam LET-distribution at a certain depth of an irradiated sample calculated with the energy-loss code (SRIM), and the relation between the beam flux and the reading of a transmission-type detectors. Since the beam is extracted to the atmosphere and passes through materials, it can be contaminated with secondary nuclides produced by nuclear reactions in the materials. We study the beam impurity using radiochemical measurements and compared the results with simulations by the PHITS code. In 2018, the results were reported at the IEEE international conference and were shared with the clients.

##### (3) Fee-based distribution of radioisotopes produced at RIKEN AVF Cyclotron

We have been handling fee-based distribution of radioisotopes since 2007. The radionuclides are Zn-65 ( $T_{1/2} = 244$  days), Cd-109 (463 days), Y-88 (107 days) and Sr-85 (65 days) which are produced at the AVF cyclotron by the nuclear chemistry research team. According to a material transfer agreement (MTA) drawn between Japan Radioisotope Association (JRIA) and RIKEN, JRIA mediates the transaction of the RIs and distributes them to users. Details can be found on the online ordering system J-RAM home page of JRIA.

In 2018, we started distribution of new RI Cu-67 (62 hours). We delivered one shipment of Cu-67 with an activity of 5 MBq, 3 shipments of Zn-65 with a total activity of 9 MBq and 3 shipments of Y-88 with an activity of 3 MBq. The final recipients of the RIs are universities, research institutes and medical research centers.

##### (4) Development of real-time wear diagnostics of industrial material using RI beams

We are developing a method to determine the spatial distribution of gamma-ray emitting RIs on periodically-moving objects, named “GIRO” (Gamma-ray Inspection of Rotating Object), that is based on the same principle as the medical PET imaging but is simpler and less expensive. Two pairs of detectors were employed to obtain 3D image data. We also performed single-photon emission computer tomography (SPECT) mode measurement. GIRO can obtain SPECT-mode data together with PET-mode data. This method can be used for real-time inspection of a closed system in a running machine. In 2018, we are developing a portable size GIRO system in order to bring and demonstrate it for private companies.

## Members

### Team Leader

Atsushi YOSHIDA

### Contract Researcher

Tadashi KAMBARA

### Technical Staff I

Daiki MORI (concurrent: RI Application Team)

## List of Publications & Presentations

### Publications

#### [Journal]

#### (Original Papers) \*Subject to Peer Review

- A. Yoshida, 「21.5.1 RI ビームによるリアルタイム摩耗試験」, 日本加速器学会著 加速器ハンドブック 21 章暮らしに役立つ加速器技術 21.5 化学工業・工業技術, 丸善出版 2018 年 4 月, ISBN 978-4-621-08901-9.
- T. Kambara, A. Yoshida, “Facility for Heavy-Ion Irradiation of Semiconductors at RIKEN RI-Beam Factory,” 2018 IEEE Radiation Effects Data Workshop (REDW) Workshop Record, pg.94, DOI: 10.1109/NSREC.2018.8584278.

### Oral Presentations

#### [International Conference etc.]

- A. Yoshida, “Wear diagnostics using low-energy RIBs and their  $\gamma$ -ray imaging,” Technical Meeting on Novel Multidisciplinary Applications with Unstable Ion Beams and Complementary Techniques, International Atomic Energy Agency (IAEA), Wien Austria, December 10–14, 2018.

### Posters Presentations

#### [International Conference etc.]

- T. Kambara, A. Yoshida, “Facility for heavy-ion irradiation of semiconductors at RIKEN RI-Beam Factory,” 2018 IEEE Radiation Effects Data Workshop (REDW) Workshop, July 19, 2018.

### Patents

- A. Yoshida, T. Kambara, R. Uemoto, A. Nagano, H. Uno, N. Takahashi, “Wear diagnostics method and instrument,” 2015-1490 patent applied.
- T. Kambara, A. Yoshida, H. Takeichi, “Gamma-ray measurement method and instrument,” 2014-034417, patent registered.

## Subnuclear System Research Division Quantum Hadron Physics Laboratory

### 1. Abstract

Atomic nuclei are made of protons and neutrons bound by the exchange of pion and other mesons. Also, protons and neutrons are made of quarks bound by the exchange of gluons. These strong interactions are governed by the non-Abelian gauge theory called the quantum chromodynamics (QCD). On the basis of theoretical and numerical analyses of QCD, we study the interactions between the nucleons, properties of the dense quark matter realized at the center of neutron stars, and properties of the hot quark-gluon plasma realized in the early Universe. Strong correlations common in QCD and cold atoms are also studied theoretically to unravel the universal features of the strongly interacting many-body systems. Developing perturbative and non-perturbative techniques in quantum field theory and string theory are of great importance not only to solve gauge theories such as QED and QCD, but also to find the theories beyond the standard model of elementary particles. Various theoretical approaches along this line have been attempted.

### 2. Major Research Subjects

- (1) Perturbative and non-perturbative methods in quantum field theories
- (2) Theory of spontaneous symmetry breaking
- (3) Lattice gauge theory
- (4) QCD under extreme conditions
- (5) Nuclear and atomic many-body problems

### 3. Summary of Research Activity

#### (1) Perturbative and non-perturbative methods in quantum field theories

##### (1-1) 10<sup>th</sup> order QED calculation and the lepton anomalous magnetic moments

First preliminary value of the tenth-order QED contribution to the electron anomalous magnetic moment  $a_e = (g - 2)/2$  was reported by us in 2012. Since then, we have been improving and establishing its accuracy: We reevaluated the most difficult and large set of the Feynman diagrams by using advanced techniques of numerical calculation especially suitable to RIKEN's supercomputer. As a result, we have obtained precise values for the eighth- and tenth-order terms. Assuming the validity of the standard model, it leads to the world-best value of the fine-structure constant  $\alpha^{-1}(a_e) = 137.035\,999\,1570(29)(27)(18)(331)$ , where uncertainties are from the eighth-order term, tenth-order term, hadronic and electroweak terms, and the experimental measurement of  $a_e$ . This is the most precise value of  $\alpha$  available at present in the world and provides a stringent constraint on possible theories beyond the standard model.

##### (1-2) Picard-Lefschetz theory and the sign problem

Understanding strongly-correlated quantum field theories and many-body systems has been one of the ultimate goals in contemporary physics. Exact diagonalization of a Hamiltonian provides us with complete information on the system; however, it usually requires the huge computational cost and is limited to small systems. For large systems, numerical simulation on discretized space-time lattice with quantum Monte Carlo method is a powerful ab initio tool based on the importance sampling. In many quantum systems of great interest, however, it suffers from the so-called sign problem; large cancellation occurs between positive and negative quantities to obtain physical signals, so that the computational time grows exponentially with the system size. So far, many attempts have been proposed overcome the sign problem, which include the two promising candidates, the complex Langevin method and the Lefschetz-thimble method. In particular, the Lefschetz-thimble approach is a generalization of the steepest descent method for multiple oscillatory integrals. In the past few years, we have studied extensively the mathematical basis of the Lefschetz-thimble method as well as its practical applications to quantum systems such as the real-time path integral for quantum tunneling, zero-dimensional bosonic and fermionic models, the one-site Hubbard model, and Polyakov-loop effective models for QCD. We have shown that the interference among multiple Lefschetz thimbles is important to reproduce the general non-analytic behavior of the observables as a function of the external parameter. Such an interference is a key to understand the sign problem of finite-density QCD.

##### (1-3) Functional renormalization group

- BEC-BCS crossover in cold fermionic atoms

We have developed a fermionic functional renormalization group (FRG) and applied this method to describe the superfluid phase transition of the two-component fermionic system with an attractive contact interaction. The connection between the fermionic FRG approach and the conventional Bardeen-Cooper-Schrieffer (BCS) theory with Gorkov and Melik-Barkhudarov (GMB) correction was clarified in the weak coupling region by using the renormalization group flow of the fermionic four-point vertex with particle-particle and particle-hole scatterings. To go beyond the BCS + GMB theory, coupled FRG flow equations of the fermion self-energy and the four-point vertex are studied under an Ansatz concerning their frequency/momentum dependence. We found that the fermion self-energy turns out to be substantial even in the weak coupling regime, and the frequency dependence of the four-point vertex is essential to obtain the correct asymptotic-ultraviolet behavior of the flow for the self-energy. The superfluid transition temperature and the associated chemical potential were evaluated in the region of negative scattering lengths.

- Tricritical point of the superconducting transition

The order of the phase transition in the Abelian Higgs model with complex scalar fields became of interest because of the analyses of the spontaneous symmetry breaking due to radiative corrections in 3 + 1 dimensions, and of a superconductor near the critical point with the dimensionally reduced Ginzburg-Landau theory. Indeed, the fluctuations of the gauge field were of great importance and may even turn the second-order transition to first-order at least for strongly type-I superconductors. We analyzed the order of the

superconducting phase transition via the functional renormalization group approach: We derived for the first time fully analytic expressions for the  $\beta$  functions of the charge and the self-coupling in the Abelian Higgs model with  $N$ -component scalar field in  $d = 3$  dimensions. The result supports the existence of two charged fixed-points: an infrared (IR) stable fixed point describing a second-order phase transition and a tricritical fixed point controlling the region of the parameter space that is attracted by the former one. It was found that the region separating first and second-order transitions can be uniquely characterized by the critical Ginzburg-Landau parameter,  $\kappa_c \approx 0.62/\sqrt{2}$  for  $N = 1$ .

- Chiral dynamics under strong magnetic field

The magnetic field is not only interesting as a theoretical probe to the dynamics of QCD, but also important in cosmology and astrophysics: A class of neutron stars called magnetars has a strong surface magnetic field of order  $10^{10}$  T while the primordial magnetic field in early Universe is estimated to be even as large as  $\sim 10^{19}$  T. In non-central heavy-ion collisions at RHIC and LHC, a magnetic field of the strength  $\sim 10^{15}$  T perpendicular to the reaction plane could be produced and can have impact on the thermodynamics and transport properties of the quark-gluon plasma. We investigated the quark-meson model in a magnetic field using the functional renormalization group equation beyond the local-potential approximation. We considered anisotropic wave function renormalization for mesons in the effective action, which allows us to investigate how the magnetic field distorts the propagation of neutral mesons. We found that the transverse velocity of mesons decreases with the magnetic field at all temperatures. Also, the constituent quark mass is found to increase with magnetic field, resulting in the crossover temperature that increases monotonically with the magnetic field.

#### (1-4) Emergent spacetime

In quantum field theories, symmetry plays an essential and exceptional role. Focusing on some proper symmetry and delving into its meaning have been proven to be one of the most fruitful strategies. A recent example is the  $SO(2, 4)$  symmetry in AdS/CFT correspondence which leads to unexpected connection between gravity and gauge theory defined in different dimensions. We offer another example of quantum field theory where symmetry plays a central role and reveals interesting phenomena: Our focal point is the global conformal symmetry in two dimensional conformal field theory (2d CFT), which is homomorphic to  $SL(2, \mathbb{R})$ . We have shown that 2d CFT admits a novel quantization which we call dipolar quantization. Usually the study of the quantum field theory starts by defining the spacetime where the field is situated. On the other hand, in our case, we first obtain quantum system and then the nature of spacetime emerges. This is in accordance with the general ideas of emergent spacetime such as those discussed in matrix models.

### (2) Theory of spontaneous symmetry breaking

#### (2-1) Dispersion relations of Nambu-Goldstone modes at finite temperature and density

We clarified the dispersion relations of Nambu-Goldstone (NG) modes associated with spontaneous breaking of internal symmetries at finite temperature and/or density. We showed that the dispersion relations of type-A and type-B NG modes are linear and quadratic in momentum, whose imaginary parts are quadratic and quartic, respectively. In both cases, the real parts of the dispersion relations are larger than the imaginary parts when the momentum is small, so that the NG modes can propagate for long distances. We derived the gap formula for NG modes in the presence of explicit symmetry breaking. We also discussed the gapped partners of type-B NG modes, when type-A and type-B NG modes coexist.

#### (2-2) Effective field theory for spacetime symmetry breaking

We studied the effective field theory for spacetime symmetry breaking from the local symmetry point of view. By gauging spacetime symmetries, the identification of Nambu-Goldstone (NG) fields and the construction of the effective action were performed based on the breaking pattern of diffeomorphism, local Lorentz, and isotropic Weyl symmetries as well as the internal symmetries including possible central extensions in nonrelativistic systems. Such a local picture provides a correct identification of the physical NG fields, while the standard coset construction based on global symmetry breaking does not. We also revisited the coset construction for spacetime symmetry breaking: Based on the relation between the Maurer-Cartan one-form and connections for spacetime symmetries, we classified the physical meanings of the inverse Higgs constraints by the coordinate dimension of broken symmetries. Inverse Higgs constraints for spacetime symmetries with a higher dimension remove the redundant NG fields, whereas those for dimensionless symmetries can be further classified by the local symmetry breaking pattern.

#### (2-3) Nambu-Goldstone modes in dissipative systems

Spontaneous symmetry breaking (SSB) in Hamiltonian systems is a universal and widely observed phenomena in nature, *e.g.*, the electroweak and chiral symmetry breakings, superconductors, ferromagnets, solid crystals, and so on. It is also known that the SSB occurs even in dissipative systems such as reaction diffusion system and active matters. The translational symmetry in the reaction diffusion system is spontaneously broken by a spatial pattern formation such as the Turing pattern in biology. The rotational symmetry is spontaneously broken in the active hydrodynamics which describes collective motion of biological organisms. We found that there exist two types of NG modes in dissipative systems corresponding to type-A and type-B NG modes in Hamiltonian systems. By taking the  $O(N)$  scalar model obeying a Fokker-Planck equation as an example, we have shown that the type-A NG modes in the dissipative system are diffusive modes, while they are propagating modes in Hamiltonian systems. We pointed out that this difference is caused by the existence of two types of Noether charges,  $Q^{\alpha_R}$  and  $Q^{\alpha_A}$ :  $Q^{\alpha_R}$  are symmetry generators of Hamiltonian systems, which are not generally conserved in dissipative systems.  $Q^{\alpha_A}$  are symmetry generators of dissipative systems described by the Fokker-Planck equation and are conserved. We found that the NG modes are propagating modes if  $Q^{\alpha_R}$  are conserved, while those are diffusive modes if they are not conserved.

### (3) Lattice gauge theory

#### (3-1) Hadron interactions from lattice QCD

One of the most important goals in nuclear physics is to determine baryon-baryon interactions directly from QCD. To achieve this goal, the HAL QCD Collaboration has been developing a novel lattice QCD formulation (HAL QCD method) and performing first-principles numerical simulations. We have calculated the spin-orbit forces for the first time from QCD by the HAL QCD method, and have observed the attraction in the  $^3P_2$  channel related to the P-wave neutron superfluidity in neutron star cores. Our calculation of the N- $\Omega$  interaction shows that this system is bound in the  $^5S_2$  channel. We have shown that the  $\Omega$ - $\Omega$  interaction in the spin-singlet channel is in the unitary region where the scattering length becomes large. Three-nucleon forces have been calculated for several heavy quark masses. Our lattice calculations was extended to the heavy quark systems, *e.g.* the exotic tetraquark,  $T_{cc}$  and  $T_{cs}$ . Properties of the light and medium-heavy nuclei ( $^4\text{He}$ ,  $^{16}\text{O}$ ,  $^{40}\text{Ca}$ ) have been calculated by combining the nuclear many-body techniques and the nuclear forces obtained from lattice QCD. Also, we have theoretically and numerically shown that the Luscher's method traditionally used in studying the hadron-hadron interactions does not lead to physical results for baryon-baryon interactions unless the lattice volume is unrealistically large, so that the HAL QCD method is the only reliable approach to link QCD to nuclear physics.

As a part of the High Performance Computing Infrastructure (HPCI) Project 5, we have completed the generation of (2 + 1)-flavor full QCD configurations with a large box,  $V = (8 \text{ fm})^3$ , and with nearly physical pion mass, 145 MeV, on the 10 Pflops super computer "K." We are currently in the process of calculations of baryon-baryon interactions using these configurations.

#### (3-2) Momenta and Angular Momenta of Quarks and Gluons inside the Nucleon

Determining the quark and gluon contributions to the spin of the nucleon is one of the most challenging problems in QCD both experimentally and theoretically. Since the quark spin is found to be small ( $\sim 25\%$  of the total proton spin) from the global analysis of deep inelastic scattering data, it is expected that the rest should come from the gluon spin and the orbital angular momenta of quarks and gluons. We made state-of-the-art calculations (with both connected and disconnected insertions) of the momenta and the angular momenta of quarks and gluons inside the proton. The u and d quark momentum/angular momentum fraction extrapolated to the physical point is found to be 0.64(5)/0.70(5), while the strange quark momentum/angular momentum fraction is 0.024(6)/0.023(7), and that of the gluon is 0.33(6)/0.28(8). This implies that the quark spin carries a fraction of 0.25(12) of the proton spin. Also, we found that the quark orbital angular momentum, which turned out to be dominated by the disconnected insertions, constitutes 0.47(13) of the proton spin.

### (4) QCD under extreme conditions

#### (4-1) Production and Elliptic Flow of Dileptons and Photons in the semi-Quark Gluon Plasma

A notable property of peripheral heavy-ion collisions at RHIC and LHC is the elliptic flow which is a measure of the transfer of initial spatial anisotropy to momentum anisotropy. Both the PHENIX experiment at RHIC and the ALICE experiment at LHC have announced a puzzling observation; a large elliptic flow for photons, comparable to that of hadrons. We considered the thermal production of dileptons and photons at temperatures above the QCD critical temperature ( $T_c$ ) on the basis of semi-QGP, a theoretical model for describing the quark-gluon plasma (QGP) near  $T_c$ . With realistic hydrodynamic simulations, we have shown that the strong suppression of photons in semi-QGP due to the inhibition of colored excitations tends to bias the elliptical flow of photons to that generated in the hadronic phase. This increases the total elliptic flow for thermal photons significantly towards the experimental data.

#### (4-2) Deriving relativistic hydrodynamics from quantum field theory

Hydrodynamics describes the spacetime evolution of conserved quantities, such the energy, the momentum, and the particle number. It does not depend on microscopic details of the system, so that it can be applied to many branches of physics from condensed matter to high-energy physics. One of the illuminating examples is the recent success of relativistic hydrodynamics in describing the evolution of QGP created in heavy-ion collisions. Inspired by the phenomenological success of relativistic hydrodynamics in describing QGP, theoretical derivations of the relativistic hydrodynamics have been attempted on the basis of the kinetic theory, the fluid/gravity correspondence, the non-equilibrium thermodynamics, and the projection operator method. In our study, a most microscopic and non-perturbative derivation of the relativistic hydrodynamics from quantum field theory was given on basis of the density operator with local Gibbs distribution at initial time. Performing the path-integral formulation of the local Gibbs distribution, we derived the generating functional for the non-dissipative hydrodynamics microscopically. Moreover, we formulated a procedure to evaluate dissipative corrections.

#### (4-3) Hadron-quark crossover in cold and hot neutron stars

We studied bulk properties of cold and hot neutron stars (NS) on the basis of the hadron-quark crossover picture where a smooth transition from the hadronic phase to the quark phase takes place at finite baryon density. By using a phenomenological equation of state (EOS) "CROver" which interpolates the two phases at around 3 times the nuclear matter density ( $\rho_0$ ), it is found that the cold NSs with the gravitational mass larger than two solar mass can be sustained. This is in sharp contrast to the case of the first-order hadron-quark transition. The radii of the cold NSs with the CROver EOS are in the narrow range ( $12.5 \pm 0.5$ ) km which is insensitive to the NS masses. Due to the stiffening of the EOS induced by the hadron-quark crossover, the central density of the NSs is at most  $4\rho_0$  and the hyperon-mixing barely occurs inside the NS core. This constitutes a solution of the long-standing hyperon puzzle first pointed out by Takatsuka *et al.* The effect of color superconductivity (CSC) on the NS structures was also examined with the hadron-quark crossover picture. For the typical strength of the diquark attraction, a slight softening of the EOS due to two-flavor CSC takes place and the maximum mass is reduced by about 0.2 solar mass. The CROver EOS is generalized to the supernova matter at finite temperature to describe the hot NSs at birth. The hadron-quark crossover was found to decrease the central temperature of the hot NSs under isentropic condition. The gravitational energy release and the spin-up rate during the contraction from the hot NS to the cold NS were also estimated.

**(5) Nuclear and atomic many-body problems****(5-1) Giant dipole resonance in hot nuclei**

Over the last several decades, extensive experimental and theoretical works have been done on the giant dipole resonance (GDR) in excited nuclei covering a wide range of temperature ( $T$ ), angular momentum ( $J$ ) and nuclear mass. A reasonable stability of the GDR centroid energy and an increase of the GDR width with  $T$  (in the range  $\sim 1\text{--}3$  MeV) and  $J$  are the two well-established results. Some experiments have indicated the saturation of the GDR width at high  $T$ : The gradual disappearance of the GDR vibration at much higher  $T$  has been observed. Experiments on the Jacobi transition and the GDR built on superdeformed shapes at high rotational frequencies have been reported in a few cases. We have demonstrated that thermal pairing included in the phonon damping model (PDM) is responsible for the nearly constant width of GDR at low temperature  $T < 1$  MeV. We have also shown that the enhancement observed in the recent experimentally extracted nuclear level densities in  $^{104}\text{Pd}$  at low excitation energy and various angular momenta is the first experimental evidence of the pairing reentrance in finite (hot rotating) nuclei. The results of calculations within the PDM were found in excellent agreement with the latest experimental data of GDR in the compound nucleus  $^{88}\text{Mo}$ .

**(5-2) Hidden pseudospin symmetries and their origins in atomic nuclei**

The quasi-degeneracy between single-particle orbitals,  $(n, l, j = l + 1/2)$  and  $(n - 1, l + 2, j = l + 3/2)$ , indicates a hidden symmetry in atomic nuclei, the so-called pseudospin symmetry (PSS). Since the introduction of the concept of PSS in atomic nuclei, there have been comprehensive efforts to understand its origin. Both splittings of spin doublets and pseudospin doublets play critical roles in the evolution of magic numbers in exotic nuclei discovered by modern spectroscopic studies with radioactive ion beam facilities. Since the PSS was recognized as a relativistic symmetry in 1990s, many special features, including the spin symmetry (SS) for anti-nucleon, and other new concepts have been introduced. We have published a comprehensive review article (Liang *et al.*, Phys. Rept. 2015) on the PSS and SS in various systems, including extensions of the PSS study from stable to exotic nuclei, from non-confining to confining potentials, from local to non-local potentials, from central to tensor potentials, from bound to resonant states, from nucleon to anti-nucleon spectra, from nucleon to hyperon spectra, and from spherical to deformed nuclei. We also summarized open issues in this field, including the perturbative nature, the supersymmetric representation with similarity renormalization group, and the puzzle of intruder states.

**(5-3) Efimov Physics in cold atoms**

For ultra-cold atoms and atomic nuclei, the pairwise interaction can be resonant. Then, universal few-body phenomena such as the Efimov effect may take place. We carried out an exploratory study suggesting that the Efimov effect can induce stable many-body ground states whose building blocks are universal clusters. We identified a range of parameters in a mass and density imbalanced two-species fermionic mixture for which the ground state is a gas of Efimov-related universal trimers. An explicit calculation of the trimer-trimer interaction reveals that the trimer phase is an  $\text{SU}(3)$  Fermi liquid stable against recombination losses. We proposed to experimentally observe this phase in a fermionic mixture of  $^6\text{Li}$ - $^{53}\text{Cr}$  atoms. We have also written a comprehensive review article on theoretical and experimental advances in Efimov physics.

**(5-4) Supersymmetric Bose-Fermi mixtures**

Some special Bose-Fermi mixtures of cold atoms and molecules in optical lattices could be prepared in such a way as they exhibit approximate supersymmetry under the interchange of bosons and fermions. Since supersymmetry is broken at finite temperature and/or density, an analog of the Nambu-Goldstone excitation, dubbed the ‘‘Goldstino,’’ should appear. We evaluated the spectral properties of the Goldstino in a Bose-Fermi mixture of cold atoms and molecules. We derived model independent results from sum rules obeyed by the spectral function. Also, by carrying out specific calculations with random phase approximation, analytic formula for the dispersion relation of Goldstino at small momentum was obtained.

**Members****Group Director**

Tetsuo HATSUDA

**Vice Chief Scientist**

Tsukasa TADA

**Research/Technical Scientists**Takumi DOI (Senior Research Scientist)  
Yoshimasa HIDAKA (Senior Research Scientist)Pascal Raphaël Gabriel NAIDON (Senior Research Scientist)  
Haozhao LIANG (Senior Research Scientist)**Nishina Center Research Scientists**

Makiko NIO

Dang NGUYEN DINH

**Special Postdoctoral Researchers**Shinya GONGYO  
Matthias Wilhelm Georg BERWEINTakahiro DOI  
Tomoya HAYATA

**Postdoctoral Researcher**

Takumi IRITANI

**International Program Associate**

Jie LIU (Nanjing Univ.)

**Visiting Researcher**

Hiroyuki TAJIMA (JSPS Fellow)

**Senior Visiting Scientist**

Koichi YAZAKI (Univ. of Tokyo)

**Visiting Scientists**

Noriyoshi ISHII (Osaka Univ.)  
 Tatsuyuki TAKATSUKA (Iwate Univ.)  
 Motoi TACHIBANA (Saga Univ.)  
 Kanabu NAWA (Univ. of Tokyo Hospital)  
 Masashi HAYAKAWA (Nagoya Univ.)  
 Gergely FEJOS (Keio Univ.)  
 Kenji SASAKI (Kyoto Univ.)  
 Takashi SANO (AIST)  
 Tatsumi AOYAMA (KEK)  
 Takashi INOUE (Nihon Univ.)  
 Shinya AOKI (Kyoto Univ.)  
 Kenji MORITA (QST)  
 Hiroshi SUZUKI (Kyushu Univ.)  
 Sachiko TAKEUCHI (Japan College of Social Work)  
 Kenji FUKUSHIMA (Univ. of Tokyo)  
 Toshifumi NOUMI (Kobe Univ.)  
 Atsushi NAKAMURA (Hiroshima Univ.)  
 Takayuki MATSUKI (Tokyo Kasei Univ.)  
 Takeo INAMI (Sungkyunkwan Univ.)  
 Nodoka YAMANAKA (IPN Orsay)

Hung NGUYEN (Duy Tan University)  
 Rhine Kumar Arayakkandi Keechiprath (Cochin Univ. of Sci.  
 and Tech.)  
 Koji HASHIMOTO (Osaka Univ.)  
 Yoichi KAZAMA (Univ. of Tokyo)  
 Keiko MURANO (Osaka Univ.)  
 Di-Lun YANG (Kyoto Univ.)  
 Daisuke KADOH (Keio Univ.)  
 Yoji OHASHI (Keio Univ.)  
 Minoru ETO (Yamagata Univ.)  
 Takashi NAKATSUKASA (Tsukuba Univ.)  
 Yoichi IKEDA (Osaka Univ.)  
 Hiroshi TOKI (Osaka Univ.)  
 Norisuke SAKAI (Keio Univ.)  
 Tetsuo MATSUI (The Open Univ. of Japan)  
 Masaki MURATA (Univ. of Tokyo Hospital)  
 Kazuo FUJIKAWA (Univ. of Tokyo)  
 Makoto TAKIZAWA (Showa Pharm. Univ.)  
 Shoichi SASAKI (Tohoku Univ.)

**Student Trainees**

Takaya MIYAMOTO (Kyoto Univ.)  
 Hikaru SAKAKIBARA (Univ. of Tokyo)  
 Tan Phuc LE (Univ. of Sci., Vietnam National Univ.)  
 Zhiheng WANG (Tsukuda Univ.)  
 Asahi CHIKAOKA (Univ. of Tokyo)

Yixin GUO (USTC)  
 Daisuke OHASHI (Univ. of Tokyo)  
 Yutaro AKAHOSHI (Kyoto Univ.)  
 Tomoya NAITO (Univ. of Tokyo)

## Subnuclear System Research Division Strangeness Nuclear Physics Laboratory

### 1. Abstract

We proposed accurate calculation method called ‘Gaussian Expansion Method using infinitesimally shifted Gaussian lobe basis function.’ When one proceeds to four-body systems, calculation of the Hamiltonian matrix elements becomes much laborious. In order to make the four-body calculation tractable even for complicated interactions, the infinitesimally-shifted Gaussian lobe basis function has been proposed. The GEM with the technique of infinitesimally-shifted Gaussians has been applied to various three-, four- and five-body calculations in hypernuclei, the four-nucleon systems, and cold-atom systems. As results, we succeeded in extracting new understandings in various fields.

### 2. Major Research Subjects

- (1) Hypernuclear structure from the view point of few-body problem
- (2) Structure of exotic hadron system
- (3) quantum atomic system and ultra cold atomic system
- (4) Equation of state for neutron star

### 3. Summary of Research Activity

- (1) To investigate the effect of  $T = 3/2$  three-body force, we have studied super heavy hydrogen system,  ${}^5\text{H}$  as a five-body system. In this calculation, we employ several realistic forces and calculate resonant state. As a result, without  $T = 3/2$  three-body force, we reproduce the experimental data.
- (2) Motivated by observed data of pentaquark system by LHCb, we studied this system as a five-body system within the framework of non-relativistic constituent quark model. It was difficult to describe the experimental data. It would be indicated that the observed state should be meson-baryon resonant state which we are not able to calculate with the present framework.
- (3) We calculate  ${}^9_{\Lambda}\text{Be}$  within the framework of  $\alpha\alpha\Lambda$  three-body model. We obtain many resonant states above  ${}^5_{\Lambda}\text{He} + \alpha$  threshold. Furthermore, we categorized  ${}^8\text{Be}$  analog, genuine hypernuclear analog, and  ${}^9\text{Be}$  analog which are consistent with past calculation by Motoba *et al.*

## Members

### Group Director

Emiko HIYAMA

### Special Postdoctoral Researchers

Hajime TOGASHI  
Kadir Utku CAN

Yasuhiro YAMAGUCHI

### Postdoctoral Researcher

Dalibor SKOUPIL

### Junior Research Associate

Jehee LEE (Tokyo Tech.)

### Visiting Scientists

Masayuki ASAKAWA (Osaka Univ.)	Toshio MOTOBA (Osaka Elec.-Com. Univ.)
Akinobu DOTE (KEK)	Tetsuo HYODO (Kyoto Univ.)
Yasuro FUNAKI (Kanto Gakuin Univ.)	Masahiro ISAKA (Hosei Univ.)
Kazuma NAKAZAWA (Gifu Univ.)	Daisuke JIDO (Tokyo Tech.)
Takayuki MYO (Osaka Inst. of Tech.)	Shuichi GOJUKI (SGI Japan Ltd.)
Ying ZHANG (Tianjin Univ.)	Soichi ISHIKAWA (Hosei Univ.)
Hidekatsu NEMURA (Osaka Univ.)	Hyun-Chul KIM (Inha Univ.)
Toru SATO (Osaka Univ.)	Thomas Adriaan RIJKEN (Univ. Nijmegen)
Taiichi YAMADA (Kanto Gakuin Univ.)	Xian-Rong ZHOU (East China Normal Univ.)
Shimpei ENDO (Tohoku Univ.)	Atsushi HOSAKA (Osaka Univ.)
Takenori FURUMOTO (Yokohama National Univ.)	Petr VESELY (Academy of Science of Czech Rep.)
Jinniu HU (Nankai Univ.)	Shoji SHINMURA (Gifu Univ.)
Yasuo YAMAMOTO (Tsuru Univ.)	Kei KOTAKE (Fukuoka Univ.)
Philipp GUBLER (JAEA)	Hans-Josef SCHULZE (INFN)
Makoto OKA (JAEA)	Dalibor SKOUPIL (Kyushu Unvi.)
Wolfram WEISE (TUM)	Jean-Marc RICHARD (Lyon Univ.)
Atsushi UMEYA (Nihon Inst. of Tech.)	Masanobu YAHIRO (Kyushu Unvi.)

Tingting SUN (Zhengzhou Univ.)  
 Lorenzo CONTESSI (Hebrew Univ. of Jerusalem)  
 Ulugbek YAKHSHIEV (Inha Univ.)  
 Satoshi NAKAMURA (Tohoku Univ.)  
 Shin WATANABE (National Inst. of Tech., Gifu College)  
 Satoru HIRENZAKI (Nara Women's Univ.)

Jirina STONE (Univ. of Tennessee Knoxville)  
 Tomokazu FUKUDA (Osaka Elec.-Com. Univ.)  
 Jiwei CUI (Xidian Univ.)  
 Kiyomi IKEDA (Niigata Univ.)  
 Chengjun XIA (Zhejiang University)

### Student Trainees

Saori MAEDA (Tokyo Tech.)  
 Jie LIU (Nanjing Univ.)  
 Christiane SCHMICKLER (TU Darmstadt)

Kongyi HU (Nankai Univ.)  
 Qian WU (Nanjing Univ.)  
 Qi MENG (Nanjing Univ.)

### Part-time Worker

Yoko FUJITA

## List of Publications & Presentations

### Publications

#### [Book]

K. U. Can, “*Electromagnetic Form Factors of Charmed Baryons in Lattice QCD, Springer Theses Series*,” (Springer, Singapore, 2018).

#### [Journal]

#### (Original Papers) \*Subject to Peer Review

- E. Hiyama, K. Nakazawa, “Structure of  $S = -2$  hypernuclei and hyperon-hyperon interaction,” *Annual Review of Nuclear and Particle Science and Particle Science* **68** (2018).  
 Y. Shimizu, Y. Yamaguchi, M. Harada, “Heavy quark spin multiplet structure of  $\bar{P}^{(*)}\Sigma_Q^{(*)}$  molecular states,” *Phy. Rev. D* **98**, 014021 (2018).  
 E. Hiyama, M. Kamimura, “Study of various few-body systems using Gaussian expansion method (GEM),” *Frontiers of Physics* **13**, (2018).  
 E. Hiyama, A. Hosaka, M. Oka, J. M. Richard, “Quark model estimate of hidden-charm pentaquark resonances,” *Phy. Rev. C*, **10**, 1103/*Phy. Rev. C* **98**, 045208, 98 (2018).  
 H. Togashi, K. Nakazato, Y. Takehara, S. Yamamuro, H. Suzuki, M. Takano, “Supernova equation of state based on realistic nuclear forces,” *RIKEN Accel. Prog. Rep.* **51** (2018). (Highlights of the year に選出)  
 U. Yakhshiev, H. C. Kim, E. Hiyama, “Instanton effects on charmonium states,” *Phy. Rev. D* **98**, 114036 (2018).  
 H. Bahtiyar, K. U. Can, G. Erkol, M. Oka, T. T. Takahashi, “Radiative transitions of doubly charmed baryons in lattice QCD,” *Phy. Rev. D* **98**, 114505 (2018).  
 H. Nagakura, S. Furusawa, H. Togashi, S. Richers, K. Sumiyoshi, S. Yamada, “Comparing treatments of weak reactions with nuclei in simulations of core-collapse supernovae,” *Astrophys. J. Suppl. Ser.* **240** (2019).  
 Y. Shimizu, Y. Yamaguchi, M. Harada, “Heavy quark spin multiplet structure of  $P_c$ -like pentaquark as P-wave hadronic molecular state,” arXiv:1901.09215 [hep-ph] (2019).  
 J. Lee, N. Yamanaka, E. Hiyama, “Effect of the Pauli exclusion principle in the electric dipole moment of  ${}^9\text{Be}$  with  $|\Delta S| = 1$  interactions,” *Phy. Rev. C* **99**, 055503 (2019).

#### [Proceedings]

Y. Yamaguchi, “Spin degeneracy of Hadronic molecules in the heavy quark region,” *J. Phys. Conf. Ser.* **981**, 012015 (2018).

### Oral Presentations

#### [International Conference etc.]

- E. Hiyama, “Structure of light  $p$ -shell  $\Xi$  hypernuclei,” The 13th International Conference on Hypernuclear and strange particle Physics, Portsmouth, USA, June 2018.  
 E. Hiyama, “Recent progress of few-body problems in Physics,” International Conference on Simplicity, Symmetry and Beauty of Atomic Nuclei, Shanghai, China, September 2018.  
 E. Hiyama, “Recent progress of hypernuclear physics,” 5th Joint Meeting of the APS Division of Nuclear Physics and the Physical Society of Japan, Hawaii, USA, October 2018.  
 E. Hiyama, “Structure of light hypernuclei,” International workshop on Universal Physics In Many-Body Quantum Systems—From Atoms to Quarks—, Tokai, Ibaraki, December 2018.  
 E. Hiyama, “Future Prospect In hypernuclear physics using HIAF,” International workshop on “HIAF High-Energy Beam Line Physics and Nuclear Astrophysics,” Beijing, China, December 2018.  
 E. Hiyama, “Structure of light  $s$ -shell  $\Xi$  hypernuclei,” 57th International Winter meeting on Nuclear physics, Bormio, Italy, January 2019.  
 E. Hiyama, “Five-body structure of pentaquark,” Korea-Japan Joint Workshop on the Present and Future in Hadron Physics at J-PARC, Busan, Korea March, 2019.

- H. Togashi, E. Hiyama, M. Takano, “Hyperon equation of state for core-collapse simulations based on the variational many-body theory,” HYP2018, Norfolk, USA, June 2018.
- H. Togashi, K. Nakazato, Y. Takehara, S. Yamamuro, H. Suzuki, M. Takano, “Supernova equation of state and symmetry energy at sub-nuclear densities,” 8th International Symposium on Nuclear Symmetry Energy (NuSYM2018), Busan, Korea, September 2018. (招待講演)
- H. Togashi, “Systematic study of nuclear equations of state in core-collapse supernovae,” Deciphering Multi-dimensional Nature of Core-collapse Supernovae via Gravitational-wave and Neutrino Signatures (SNeGWv2018), Toyama, Japan, October 2018.
- H. Togashi, “Systematic study of supernova equations of state at sub-nuclear densities with the Thomas-Fermi calculation,” 5th Joint Meeting of the APS Division of Nuclear Physics and the Physical Society of Japan, Hawaii, USA, October 2018.
- H. Togashi, M. Takano, K. Nakazato, Y. Takehara, S. Yamamuro, H. Suzuki, K. Sumiyoshi, E. Hiyama, “Equation of state for hyperonic nuclear matter and its application to compact astrophysical objects,” International workshop on “Hadron structure and interaction in dense matter,” Tokai, Japan, November 2018. (招待講演)
- Y. Yamaguchi, “ $\pi J/\psi-D\bar{D}^*$  potential described by the quark exchange diagram,” XXII International Conference on Few-Body Problems in Physics, Caen, France, July 2018.
- Y. Yamaguchi, “ $\pi J/\psi-D\bar{D}^*$  potential described by the quark exchange diagram,” The XXIVth International Baldin Seminar on High Energy Physics Problems, Dubna, Russia, September 2018.
- Y. Yamaguchi, “Short range  $\pi J/\psi-D\bar{D}^*$  potential by the constituent quark model,” Workshop on Dense Matter from Chiral Effective Theories 2018, Nagoya, Japan, October 2018.
- Y. Yamaguchi, “Short range  $\pi J/\psi-D\bar{D}^*$  interaction by the quark exchange diagram,” 5th Joint Meeting of the APS Division of Nuclear Physics and the Physical Society of Japan, Hawaii, USA, October 2018.
- Y. Yamaguchi, “Short range interaction in  $\pi J/\psi-D\bar{D}^*$  channel,” The international workshop New aspects of the Hadron and Astro/Nuclear Physics, The National University of Uzbekistan, Tashkent, Uzbekistan, November 2018.
- Y. Yamaguchi, “Short range  $\pi J/\psi-D\bar{D}^*$  potential,” International workshop on Hadron structure and interaction in dense matter, Tokai, Ibaraki, November 2018.
- Y. Yamaguchi, “Short-range meson-meson interaction in the hidden-charm sector,” International workshop: Clusters in quantum systems: from atoms to nuclei and hadrons, Sendai, Japan, January, 2019.
- K. U. Can, “Charmed baryon spectrum in 2+1-flavor Lattice QCD,” The 36th Annual International Symposium on Lattice Field Theory, East Lansing, Michigan, USA, July 2018.
- K. U. Can, “Charmed baryon spectrum in Lattice QCD—a work in progress,” XIIIth Quark Confinement and the Hadron Spectrum, Maynooth University, Maynooth, Ireland, July–August 2018.
- K. U. Can, “Spectrum of the charmed baryons in 2+1-flavor Lattice QCD,” The 8th International Conference on Quarks and Nuclear Physics, Tsukuba, Japan, November 2018.

#### [Domestic Conference]

- E. Hiyama, “Gaussian Expansion Method and its application to nuclear physics,” RIKEN-YCU Joint Workshop, Wako, Japan, April 2018.
- H. Togashi, “Microscopic equation of state for supernovae and compact stars,” RIKEN-YCU Joint Workshop, Wako, Japan, April 2018.
- 富樫甫, 肥山詠美子, 鷹野正利, 「バリオン間相互作用に基づく核物質の状態方程式と天体物理への応用」, 研究会「重力波観測時代の r プロセスと不安定核」, 和光市, 2018 年 6 月.
- 富樫甫, 「核物質状態方程式と高密度天体現象」, 理研—九大ワークショップ—素粒子・原子核から宇宙へ—, 神戸, 2018 年 11 月. (招待レビュー講演)
- Y. Yamaguchi, “Heavy exotics near thresholds and Hadron interactions,” RIKEN-YCU Joint Workshop, Wako, Japan, April 2018
- 山口康宏, 「 $\pi J/\psi-D\bar{D}^*$  チャンネルにおける近距離力」, 理研—九大ワークショップ—素粒子・原子核から宇宙へ—, 神戸市, 2018 年 11 月.
- 山口康宏, 安倍幸大, 福川賢治, 保坂淳, 「 $\pi J/\psi-D\bar{D}^*$  チャンネルにおける近距離相互作用」, 日本物理学会第 74 回年次大会, 福岡, 2019 年 3 月.
- K. U. Can, “Hadron physics in Lattice QCD,” RIKEN-YCU Joint Workshop, Wako, Japan, April 2018.
- J. Lee, “Binding energy of Be-9-lambda,” RIKEN-YCU Joint Workshop, Wako, Japan, April 2018.

#### [Others]

- H. Togashi, M. Takano, “Cluster variational method for hyperonic nuclear matter with coupled channels,” 8th International Conference on Quarks and Nuclear Physics (QNP2018), Tsukuba, Japan, November 2018.
- H. Togashi, “Effects of nuclear saturation properties on the supernova equations of state at sub-nuclear densities,” 2nd Annual Symposium of GW-genesis, Kyoto, Japan, November 2018.

#### Awards

- 富樫甫, 平成 30 年度理化学研究所桜舞賞研究奨励賞, 2019 年 3 月.
- 富樫甫, 2018 年度基礎科学・国際特別研究員研究成果発表会ポスター賞 (物理学 I 分野), 2019 年 1 月.

## Subnuclear System Research Division Radiation Laboratory

### 1. Abstract

Nucleons, such as protons and neutrons, are a bound state of constituent quarks glued together with gluons. The detail structure of nucleons, however, is not well understood yet. Especially the mechanism to build up the spin of proton, which is  $1/2$ , is a major problem in physics of the strong force. The research goal of Radiation Laboratory is to solve this fundamental question using the world first polarized-proton collider, realized at RHIC in Brookhaven National Laboratory (BNL) in USA. RHIC stands for Relativistic Heavy Ion Collider, aiming also to create Quark Gluon Plasma, the state of Universe just after the Big Bang, and study its property. RIKEN-BNL Research Center (RBRC) directed by S. Aronson carries our core team at BNL for those exciting researches using the PHENIX detector. We have observed that the proton spin carried by gluons is finite and indeed sizable. We also identified W bosons in the electron/positron decay channel and in the muon decay channel, with which we are about to conclude how much anti-quarks carry the proton spin. Other than the activities at RHIC we are preparing and starting new experiments at J-PARC and Fermilab to study the nature of hadron. We are also performing technical developments such as novel ion sources, fine-pitch silicon pixel detectors and high-performance trigger electronics.

### 2. Major Research Subjects

- (1) Spin physics with relativistic polarized-proton collisions at RHIC
- (2) Study of nuclear matter at high temperature and/or at high density
- (3) Technical developments on radiation detectors and accelerators

### 3. Summary of Research Activity

#### (1) Experimental study of spin structure of proton using RHIC polarized proton collider

[See also RIKEN-BNL Research Center Experimental Group for the activities at BNL]

The previously published central neutral pion double spin asymmetries at the highest collision energies at RHIC of 510 GeV have been augmented with the release of charged pion double spin asymmetries in 2017 by PHENIX and are currently being prepared for publication. The ordering of the three pion asymmetries allows a direct determination of the sign of the gluon polarization which has been found to be nonzero. With the valence quark spin contribution already reasonably well known, the contributions from sea quarks and orbital angular momenta remain to be understood. PHENIX has collected data to access the sea quark polarizations via leptonic decays of W bosons. In 2018, the world's only forward and backward W boson single spin asymmetries have been published, thus completing the publication of all W related measurements of PHENIX.

While orbital angular momentum cannot be directly accessed at RHIC, several transverse spin phenomena have been observed which relate to orbital angular momentum and the three-dimensional structure of the nucleon. These phenomena by themselves have become a major field of research as the dynamics of the strong interaction. During the 2015 RHIC operation, collisions of transversely polarized protons with Au and Al nuclei were provided for the first time. Two rather surprising results have been discovered here. First, the single transverse spin asymmetries for  $J/\psi$  particles which are found to be consistent with zero to even higher precisions, show distinctly nonzero asymmetries in proton-Au collisions at the lowest transverse momenta both if detected at slightly forward or backward regions with respect to the polarized beam. The mechanism for such a behavior is not known and the publication of these results in 2018 has stimulated substantial theoretical discussions to understand these findings. Also charged hadron single spin asymmetries have been observed in all three colliding systems. While a previously known nonzero forward asymmetry for positive hadrons was confirmed, a substantial reduction of these asymmetries for  $p + \text{Al}$  and  $p + \text{Au}$  collisions was observed. Such a reduction was predicted by several theoretical models describing the non-linear effects of high gluon densities in nuclei suggested by the so-called color-glass-condensate. While the kinematic region does not reach into the range where the color-glass-condensate is expected, this reduction in asymmetries has been met with interest by the theory community. The results have been submitted to publication for positive hadrons and a more detailed publication is prepared including the negative hadrons.

In June of 2017, we installed an electro-magnetic calorimeter in the most forward area of the STAR experiment and took polarized proton collision data for neutral particle production (neutron, photon, neutral pion). The cross-section measurement will give us new inputs to develop high-energy particle-collision models which are essential to understand air-shower from ultra-high energy cosmic rays. The asymmetry measurement will enable us to understand the hadron collision mechanism based on QCD. An unexpectedly large neutral pion asymmetry has been found using this data that may connect to the large pion asymmetries at smaller rapidities and higher transverse momenta. The preliminary results are currently being prepared for publication. Some of us are participating in the Fermilab SeaQuest experiment as a pilot measurement of muon pairs from Drell-Yan process using a 120-GeV unpolarized proton at Fermilab. After finishing unpolarized measurements in 2017 to study the quark spin-orbit effect, a new measurement with a polarized proton target will start in 2019 to study the sea-quark orbit effect of the polarized proton in the target.

For many jet related measurements fragmentation functions are necessary to gain spin and or flavor sensitivity. Those are currently extracted by some of us using the Belle data. In addition to using the fragmentation results with RHIC measurements, they will also provide the basis for most of the key measurements to be performed at the electron-ion collider. In 2018, transverse momentum dependent cross sections of pions, kaons and protons were extracted as a function of fractional energy and event topology. These measurements relate to essentially all transverse spin or momentum dependent measurements at RHIC, semi-inclusive DIS and the EIC.

## (2) Experimental study of quark-gluon plasma using RHIC heavy ion collider

[See also RIKEN-BNL Research Center Experimental Group for the activities at BNL]

We have completed several key measurements in the study of quark-gluon plasma at RHIC. As the top of them, we lead the analysis of the first thermal photon measurement in heavy ion collisions. The measurement indicates that the initial temperature reached in the central Au + Au collision at 200 GeV is about 350 MeV, far above the expected transition temperature  $T_c \sim 170$  MeV, from hadronic phase to quark-gluon plasma. This work was rewarded by Nishina Memorial Prize given to Y. Akiba in 2011. We also measured direct photons in  $d + Au$  and direct photon flow strength  $v_2$  and  $v_3$  in Au + Au.

We lead measurement of heavy quark (charm and bottom) using VTX, a 4-layer silicon vertex tracker which we jointly constructed with US DOE. The detector was installed in PHENIX in 2011. PHENIX recorded approximately 10 times more data of Au + Au collisions in the 2014 run than the 2011 run. PHENIX recorded high statistics  $p + p$  and  $p + A$  data in 2015, and the doubled the Au + Au in 2016. PHENIX concluded its data taking in the 2016 run.

The results of the 2011 run was published in Physical Review C (Phy. Rev. C **93**, 034904 (2016)). This is the first publication from VTX. The result showed that the electrons from bottom quark decay is suppressed for  $p_T > 4$  GeV/c, but the suppression factor is smaller than that of charm decay electrons for  $3 < p_T < 4$  GeV/c. This is the first observation of bottom electron suppression in heavy ion collisions, and the first result that shows the bottom and charm suppression is different. The results of  $b \rightarrow e$  and  $c \rightarrow e$  measurement in the 2015  $p + p$  run has been published in Phys. Rev. D **99**, 092003 (2019). The centrality dependence of the suppression  $b \rightarrow e$  and  $c \rightarrow e$  from the 2014 Au+Au data will be published soon. Preliminary results of the flow of  $b \rightarrow e$  and  $c \rightarrow e$  was presented in Quark Matter 2018 conference.

In Wako we are operating a cluster computer system (CCJ) specialized to analyze huge data sets taken with the PHENIX detector. It consists of 28 nodes (18 old nodes and 10 new nodes) each of which has two CPUs and 10 sets of local disks for data repository (old node: quad-core CPU, 1 TB disk, new node: six-core CPU, 2 TB disk). There are 264 CPU cores and 380 TB disks in total. This configuration ensures the fastest disk I/O when each job is assigned to the node where the required data sets are stored. It is also important that this scheme doesn't require an expensive RAID system and network. Through this development we have established a fast and cost-effective solution in analyzing massive data.

The data of 0.9 Pbyte obtained by the PHENIX experiment is stored in a hierarchical storage system which is a part of HOKUSAI GreatWave supercomputer system operated by the Advanced Center for Computing and Communication (ACCC). In addition, we operate a dedicated server for the RHICf group and two servers for the J-PARC E16 group, to keep their dedicated compilation and library environments, and some data.

## (3) Study of properties of mesons and exotic hadrons with domestic accelerators

Preparation of the experiment E16 at J-PARC Hadron experimental facility is underway with several Grant-in-Aids. This experiment aims to perform a systematic study of the spectral modification of low-mass vector mesons in nuclei to explore the physics of chiral symmetry breaking and restoration in dense nuclear matter, namely, the mechanism proposed by Nambu to generate most of hadron masses.

The Gas Electron Multiplier (GEM) technology is adopted for the two key detectors, GEM Tracker (GTR) and Hadron-blind Cherenkov detector (HBD). To improve electron-identification performance, lead-glass calorimeters (LG) are used in combination with HBD. We are in the production phase. The parts for six modules of GTR, four modules of HBD and six modules of LG are delivered, and their assembly processes have started. Read-out electronics and trigger logic modules were also fabricated and delivered. Development of firmware on the trigger logic modules is on-going. We have been a member of the CERN-RD51 collaboration to acquire the read-out technology for GEM. The current MoU for RD51 will be extended for the period of 2019–2023.

Due to the budgetary limitation, we aim to install a part of detectors at the beginning of the experiment, eight modules of GTR/HBD/LG out of 26 modules in the full installation. J-PARC PAC gave us a stage-2 approval on July 2017, to the commissioning run (Run 0), which will be performed when the beam line is completed. Although there is a significant delay from the originally planned date of March 2016, the construction of the beam line by KEK will be completed in the first half of 2020 to perform this experiment with the stage-2 approval. We are preparing the spectrometer toward the Run 0.

## (4) Detector development for PHENIX experiment

The PHENIX experiment proposes substantial detector upgrades to go along the expected accelerator improvements, including the future electron-ion collider "eRHIC." The present PHENIX detector is repurposed to the sPHENIX (super PHENIX) detector which reuses the Babar solenoid magnet at SLAC and is covered by the hadronic calorimeter which was not available in the previous RHIC experiments. The sPHENIX project is now funded by DOE, and RIKEN will participate in the construction of the inner silicon tracker (INTT). The R&D of the INTT has been in progress since 2015 and the 2nd generation prototype successfully demonstrated a designed performance through the beam test executed at Fermilab in March 2018. The pre-production model including a full readout chain will be completed after the examination in the 2<sup>nd</sup> round beam test at Fermilab in June 2019 followed by the final technical review in Summer, 2019.

We have been developing a plan to build a forward spectrometer to be added to the sPHENIX detector. With this addition, the fsPHENIX detector will have both hadronic and electromagnetic calorimetry as well as tracking in the forward rapidity region. This upgrade makes it possible to study forward jets and hadrons in jets which are of vital importance for the cold QCD program in polarized  $p + p$  and  $p + A$  collisions at RHIC. The fsPHENIX detector can be further upgraded to the ePHENIX detector to be used for electron-ion collisions at eRHIC. We are preparing test bench to perform R&D for the forward hadron calorimeter.

**Members****Group Director**

Hideto EN'YO (Director, RNC)

**Vice Chief Scientist**

Yasuyuki AKIBA

**Research/Technical Scientists**

Yasushi WATANABE (Senior Research Scientist)  
 Satoshi YOKKAICHI (Senior Research Scientist)  
 Yuji GOTO (Senior Research Scientist)

Ralf SEIDL (Senior Research Scientist)  
 Itaru NAKAGAWA (Senior Research Scientist)

**Postdoctoral Researcher**

Koki KANNO

**Research Associate**

Wataru NAKAI

**International Program Associates**

Minho KIM (Korea Univ.)

Junsang PARK (Seoul Nat'l Univ.)

**Senior Visiting Scientists**

Toshiaki SHIBATA (Tokyo Tech.)

Takashi NAKANO (Osaka Univ.)

**Visiting Scientists**

Kyoichiro OZAWA (KEK)  
 Kenji FUKUSHIMA (Univ. of Tokyo)  
 Susumu SATO (JAEA)  
 Tomohiro NISHITANI (Nagoya Univ.)  
 Megumi NARUKI (Kyoto Univ.)  
 Tomonori TAKAHASHI (Osaka Univ.)  
 Kiyoshi TANIDA (JAEA)  
 Tsutomu MIBE (KEK)  
 Taku GUNJI (Univ. of Tokyo)  
 Masahiro OKAMURA (BNL)  
 Kazuya AOKI (KEK)

Shunzo KUMANO (KEK)  
 Munehisa OHTANI (Kyorin Univ.)  
 Bentz WOLFGANG (Tokai Univ.)  
 Kenichi NAKANO (Tokyo Tech.)  
 Shin-ya SAWADA (KEK)  
 Maya SHIMOMURA (Nara Women's Univ.)  
 Kenta SHIGAKI (Hiroshima Univ.)  
 Hiroaki MENJO (Nagoya Univ.)  
 Sanghwa PARK (Stony Brook University)  
 Yuhei MORINO (KEK)  
 Tomoya HOSHINO (Yokogawa Electric Co.)

**Student Trainees**

Mana UENO (Nagoya Univ.)  
 Jaehee YOO (Korea University)  
 Qidong Zhou (Nagoya Univ.)  
 Yosuke UEDA (Hiroshima Univ.)  
 Seiya MIYATA (Univ. of Tokyo)  
 Kenta SATO (Nagoya Univ.)  
 Sakiko ASHIKAGA (Kyoto Univ.)  
 Hiromu ASO (Rikkyo Univ.)  
 Yuri ITO (Nara Woman's Univ.)  
 Sakurako ISHIMARU (Nara Woman's Univ.)  
 Tomoko SAKAMOTO (Nara Woman's Univ.)  
 Kaede KAMANO (Nara Woman's Univ.)

Risa NISHITANI (Nara Woman's Univ.)  
 Kazuki SUZUKI (Kyoto Univ.)  
 Hiroki KATO (Tsukuba Univ.)  
 Ryohei FUJII (Kyoto Univ.)  
 Takahiro ICHINO (Rikkyo Univ.)  
 Yoko MINATO (Nara Woman's Univ.)  
 Ayaka SUZUKI (Nara Woman's Univ.)  
 Tomoki MURAKAMI (Univ. of Tokyo)  
 Se Young HAN (Ewha Womans Univ.)  
 Kazuya NAKAGAWA (Tsukuba Univ.)  
 Kazuki SATO (Tsukuba Univ.)

**Interns**

Minjung KIM (Seoul Nat'l Univ.)  
 Kenichiro SHIINA (Rikkyo Univ.)

Masaya ICHIKAWA (Kyoto Univ.)  
 Benard MULILO (Korea University)

**Part-time Workers**

Hidekazu MASUDA (Rikkyo Univ.)  
 Kazuya NAGASHIMA (Hiroshima Univ.)  
 Yorito YAMAGUCHI

Masato TSURUTA (Rikkyo Univ.)  
 Michiko SEKIMOTO

**Assistant**

Keiko SUZUKI

**List of Publications & Presentations****Publications****[Journal]****(Original Papers) \*Subject to Peer Review**

- R. Arnaldi *et al.* (NA60 Collaboration), “Nuclear dependence of light neutral meson production in  $p$ -A collisions at 400 GeV with NA60,” *Eur. Phys. J. C* **79**, no.5, 443 (2019).
- C. Aidala *et al.* (PHENIX Collaboration), “Measurement of charm and bottom production from semileptonic hadron decays in  $p + p$  collisions at  $\sqrt{s_{NN}} = 200$  GeV,” *Phy. Rev. D* **99**, no.9, 092003 (2019).
- C. Aidala *et al.* (PHENIX Collaboration), “Nonperturbative transverse momentum broadening in dihadron angular correlations in  $\sqrt{s_{NN}} = 200$  GeV proton-nucleus collisions,” *Phy. Rev. C* **99**, no.4, 044912 (2019).
- A. Adare *et al.* (PHENIX Collaboration), “Pseudo rapidity dependence of particle production and elliptic flow in asymmetric nuclear collisions of  $p + \text{Al}$ ,  $p + \text{Au}$ ,  $d + \text{Au}$ , and  $^3\text{He} + \text{Au}$  at  $\sqrt{s_{NN}} = 200$  GeV,” *Phys. Rev. Lett.* **121**, no.22, 222301 (2018).
- C. Adare *et al.* (PHENIX Collaboration), “Low-momentum direct photon measurement in Cu + Cu collisions at  $\sqrt{s_{NN}} = 200$  GeV,” *Phy. Rev. C* **98**, no.5, 054902 (2018).
- A. Adare *et al.* (PHENIX Collaboration), “Creation of quark-gluon plasma droplets with three distinct geometries,” *Nature Phys.* **15**, no.3, 214–220 (2019).
- C. Aidala *et al.* (PHENIX Collaboration), “Measurements of  $\mu\mu$  pairs from open heavy flavor and Drell-Yan in  $p + p$  collisions at  $\sqrt{s} = 200$  GeV,” *Phy. Rev. D* **99**, no.7, 072003 (2019).
- C. Aidala *et al.* (PHENIX Collaboration), “Nonperturbative transverse-momentum-dependent effects in dihadron and direct photon-hadron angular correlations in  $p + p$  collisions at  $\sqrt{s} = 200$  GeV,” *Phy. Rev. D* **98**, no.7, 072004 (2018).
- C. Aidala *et al.* (PHENIX Collaboration), “Single-spin asymmetry of  $J/\psi$  production in  $p + p$ ,  $p + \text{Al}$ , and  $p + \text{Au}$  collisions with transversely polarized proton beams at  $\sqrt{s_{NN}} = 200$  GeV,” *Phy. Rev. D* **98**, no.1, 012006 (2018).
- A. Adare *et al.* (PHENIX Collaboration), “Cross section and longitudinal single-spin asymmetry  $A_L$  for forward  $W^\pm \rightarrow \mu \pm \nu$  production in polarized  $p + p$  collisions at  $\sqrt{s} = 510$  GeV,” *Phy. Rev. D* **98**, no.3, 032007 (2018).
- A. Adare *et al.* (PHENIX Collaboration), “Measurement of two-particle correlations with respect to second- and third-order event planes in Au + Au collisions at  $\sqrt{s_{NN}} = 200$ ,” *Phy. Rev. C* **99**, no.5, 054903 (2019).
- A. Adare *et al.* (PHENIX Collaboration), “Measurement of emission angle anisotropy via long-range angular correlations with high  $p_T$  hadrons in  $d + \text{Au}$  and  $p + p$  collisions at  $\sqrt{s_{NN}} = 200$  GeV,” *Phy. Rev. C* **98**, no.1, 014912 (2018).
- A. Adare *et al.* (PHENIX Collaboration), “Measurements of mass-dependent azimuthal anisotropy in central  $p + \text{Au}$ ,  $d + \text{Au}$ , and  $^3\text{He} + \text{Au}$  collisions at  $\sqrt{s_{NN}} = 200$  GeV,” *Phy. Rev. C* **97**, 064904 (2018).
- A. Adare *et al.* (PHENIX Collaboration), “Measurement of  $\phi$ -meson production at forward rapidity in  $p + p$  collisions at  $\sqrt{s} = 510$  GeV and its energy dependence from  $\sqrt{s} = 200$  GeV,” *Phy. Rev. D* **98**, no.9, 092006 (2018).
- C. Aidala *et al.* (PHENIX Collaboration), “Measurements of multiparticle correlations in  $d + \text{Au}$  collisions at 200, 62.4, 39, and 19.6 GeV and  $p + \text{Au}$  collisions at 200 GeV and implications for collective behavior,” *Phys. Rev. Lett.* **120**, no.6, 062302 (2018).
- C. Aidala *et al.* (PHENIX Collaboration), “Nuclear dependence of the transverse-single-spin asymmetry for forward neutron production in polarized  $p + \text{A}$  collisions at  $\sqrt{s_{NN}} = 200$  GeV,” *Phys. Rev. Lett.* **120**, no.2, 022001 (2018).
- Y. Itow *et al.*, “Recent results from the LHCf and RHICf experiments,” *EPJ Web Conf.* **208**, 05004 (2019).

**Oral Presentations****[International Conference etc.]**

- I. Nakagawa, “Medium-energy nuclear physics at RHIC with sPHENIX and an sPHENIX forward upgrade,” XXVI International Workshop on Deep Inelastic Scattering and related Subjects, 17<sup>th</sup>, Kobe, Japan, April 2018.
- Y. Goto, “Asymmetry measurement of very forward neutral particle production in the RHICf experiment,” Diffraction and Low-x 2018, 29<sup>th</sup>, Reggio Calabria, Italy (Invited), August 2018.
- Y. Goto (RHICf collaboration), “Very forward neutral particle measurement in the RHICf experiment,” 5th Joint Meeting of the APS Division of Nuclear Physics and the Physics Society of Japan, Hawaii, USA, October 26, 2018.
- Y. Goto, “Nucleon structure study at RHIC and EIC,” YKIS2018b Symposium on Recent Developments in Quark-Hadron Sciences, 12<sup>th</sup>, Kyoto, Japan (Invited), June 2018.
- Y. Goto, “Electron-Ion Collider project,” Workshop on Progress on Hadron Structure Functions in 2018, 19<sup>th</sup>, Tsukuba, Japan (Invited), November 2018.

**[Domestic Conference]**

- S. Ichikawa, 「J-PARC E16 実験のためのトリガー中継モジュールのファームウェア開発及び性能評価」, 日本物理学会第 73 回年次大会, 野田, 2018 年 3 月 22–25 日.
- K. Suzuki, 「J-PARC E16 実験における Hadron Blind Detector のためのトリガー回路の開発」, 日本物理学会第 73 回年次大会, 野田, 2018 年 3 月 22–25 日.

## Subnuclear System Research Division Meson Science Laboratory

### 1. Abstract

Particles like muons, pions, and kaons have finite life times, so they do not exist in natural nuclei or matters. By implanting these particles into nuclei/matters, exotic phenomena in various objects can be studied from new point of view.

For example, kaon is the second lightest meson, which has strange quark as a constituent quark. It is expected that if one embeds mesons into nuclei, the sizes of the nuclei become smaller and one can form a high-density object beyond the normal nuclear density. Study of this object could lead to better understanding of the origin of the mass of the matter, and may reveal the quark degree of freedom beyond the quark-confinement. The other example is the weak interaction in nuclear matter. It can only be studied by the weak decay of hypernuclei, which have Lambda particle in the nuclei.

Muon provides even wider scope of studies, covering condensed matter physics as well as nuclear and atomic physics, and we are trying to extend the application field further into chemical and biological studies. For instance, stopping positively charged muon in a material, we obtain information on the magnetic properties or the local field at the muon trapped site ( $\mu$ SR). Injecting negatively charged muon to hydrogen gas, muonic hydrogen atom ( $\mu p$ ) is formed. We are planning to measure  $\mu p$  hyperfine splitting energy to measure proton magnetic radius, which is complementary quantity to the proton charge radius and its puzzle. We are also interested in precision measurement of muon property itself, such as muon anomalous magnetic moment ( $g - 2$ ).

In our research, we introduce different kind of impurities into nuclei/matters, and study new states of matter, new phenomena, or the object properties.

### 2. Major Research Subjects

- (1) Study of meson property and interaction in nuclei
- (2) Origin of matter mass/quark degree of freedom in nuclei
- (3) Condensed matter and material studies with muon
- (4) Nuclear and particle physics studies via muonic hydrogen
- (5) Development of ultra cold muon beam, and its application from material science to particle physics

### 3. Summary of Research Activity

#### (1) Hadron physics at J-PARC, RIKEN-RIBF, GSI and Spring-8

Kaon and pion will shed a new insight to the nuclear physics. The recent discovery of deeply bound pionic atom enables us to investigate the properties of mesons in nuclear matter. At RIKEN-RIBF, we are preparing precise experimental study of the pionic atom. Very lately, we succeeded to discover kaonic nuclear bound state, " $K^-pp$ ," at J-PARC. The yield dependence on momentum-transfer shows that observed system is unexpectedly small. We extended our study on  $\Lambda$  (1405) that could be  $K^-p$  bound state. By these experiments, we are studying the  $\bar{K}N$  interaction, and clarify the nature of kaon in nuclei. At Spring-8 and at GSI, we are planning to study omega and eta' nuclei. By these experiments, we aim to be a world-leading scientific research group using these light meta-stable particles.

#### (1-1) Deeply bound kaonic nuclei

J-PARC E15 experiment had been performed to explore the simplest kaonic nuclear bound state, " $K^-pp$ ." Because of the strong attraction between  $\bar{K}N$ , the  $\bar{K}$  in nuclei may attract surrounding nucleons, resulting in forming a deeply bound and extremely dense object. Measurement of the kaon properties at such a high density medium will provide precious information on the origin of hadron masses, if the standard scenario of the hadron-mass-generation mechanism, in which the hadron masses are depends on matter density and energy, is correct. Namely, one may study the chiral symmetry breaking of the universe and its partial restoration in nuclear medium.

The E15 experiment was planned to identify the nature of the " $K^-pp$ " bound state by the in-flight  ${}^3\text{He}(K^-, n)$  reaction, which allows us to investigate such state both in the formation via the missing-mass spectroscopy using the emitted neutron, and in its decay via the invariant-mass spectroscopy by detecting decay particles from " $K^-pp$ ." For the experiment, we constructed a dedicated spectrometer system at the secondary beam-line, K1.8BR, in the hadron hall of J-PARC.

With the  $\Lambda pn$  final states obtained in the first stage experiment, we observed a kinematic anomaly in the  $\Lambda p$  invariant mass near the mass threshold of  $M(K^-pp)$  (total mass of kaon and two protons) at the lower momentum transfer  $q$  region. We conducted a successive experiment to examine the nature of the observed kinematical anomaly in the  $\Lambda pn$  final state, and we confirmed the existence of the bound state below the mass threshold of  $M(K^-pp)$  at as deep as the binding energy of 50 MeV. The momentum transfer  $q$  naturally prefers lower momentum for the bound state formation, but the observed event concentration extended as large as  $\sim 650$  MeV/c. The simplest interpretation based on the PWIA calculation indicates that the observed object could be as small as  $\sim 0.5$  fm. This observation means that *a meson ( $\bar{q}q$ ) forms a quantum state where baryons ( $qqq$ ) exist as nuclear medium, i.e., a highly excited novel form of nucleus with a kaon, in which the mesonic degree-of-freedom still holds*. This is totally new form of nuclear system, which never been observed before.

#### (1-2) Precision X-ray measurement of kaonic atom

To study the  $\bar{K}N$  interaction at zero energy from the atomic state level shift and width of kaon, we have performed an X-ray spectroscopy of atomic  $3d \rightarrow 2p$  transition of negatively charged  $K^-$ -mesons captured by helium atoms. However, our first experiment is insufficient in energy resolution to see the  $K^-$ -nucleus potential. Aiming to provide a breakthrough from atomic level observation,

we introduce a novel X-ray detector, namely superconducting transition-edge-sensor (TES) microcalorimeter offering unprecedented high energy resolution, being more than one order of magnitude better than that achieved in the past experiments using conventional semiconductor detectors. The experiment J-PARC E62 aims to determine  $2p$ -level strong interaction shifts of kaonic  ${}^3\text{He}$  and  ${}^4\text{He}$  atoms by measuring the atomic  $3d \rightarrow 2p$  transition X-rays using TES detector with 240 pixels having about  $23 \text{ mm}^2$  effective area and the average energy resolution of 7 eV (FWHM) at 6 keV. We carried out the experiment at J-PARC in June 2018 and successfully observed distinct X-ray peaks from both atoms. The data analysis is now ongoing.

Another important X-ray measurement of kaonic atom would be  $2p \rightarrow 1s$  transition of kaonic deuteron ( $K^-d$ ). We have measured same transition of kaonic hydrogen ( $K^-p$ ), but the width and shift from electro-magnetic (EM) value reflect only isospin average of the  $K^{\text{bar}}N$  interaction. We can resolve isospin dependence of the strong interaction by the measurements both for  $K^-p$  and  $K^-d$ . The experiment J-PARC E57 aims at pioneering measurement of the X-rays from  $K^-d$  atoms. Prior to full (stage-2) approval of the E57 proposal, we performed a pilot run with hydrogen target in March 2019.

### (1-3) Deeply bound pionic atoms and $\eta'$ mesonic nuclei

We have been working on precision spectroscopy of pionic atoms systematically, which leads to understanding of the non-trivial structure of the vacuum and the origin of hadron masses. The precision data set stringent constraints on the chiral condensate at nuclear medium. We are presently preparing for the precision systematic measurements at RIBF. A pilot experiment performed in 2010 showed a unprecedented results of pionic atom formation spectra with finite reaction angles. The measurement of pionic  ${}^{121}\text{Sn}$  performed in 2014 showed a very good performance of the system. We have been analyzing the data to achieve information on the pion-nucleus interaction based on the pionic atom spectroscopy.

We are also working on spectroscopy of  $\eta'$  mesonic nuclei in GSI/FAIR. Theoretically, peculiarly large mass of  $\eta'$  is attributed to UA(1) symmetry and chiral symmetry breaking. As a result, large binding energy is expected for  $\eta'$  meson bound states in nuclei ( $\eta'$ -mesonic nuclei). From the measurement, we can access information about gluon dynamics in the vacuum via the binding energy and decay width of  $\eta'$ -nuclear bound state.

## (2) Muon science at RIKEN-RAL branch

The research area ranges over particle physics, condensed matter studies, chemistry and life science. Our core activities are based on the RIKEN-RAL Muon Facility located at the Rutherford-Appleton Laboratory (UK), which provides intense pulsed-muon beams. We have variety of important research activities such as particle/nuclear physics studies with muon's spin and condensed matter physics by muon spin rotation/relaxation/resonance ( $\mu\text{SR}$ ).

### (2-1) Condensed matter/materials studies with $\mu\text{SR}$

To improve our two  $\mu\text{SR}$  spectrometers, ARGUS (Port-2) and CHRNU (Port-4), we adjusted the threshold level of the muon-detector system for the zero-field condition. At this condition, we optimized the efficiency of the detector system and the counting rate was improved nearly 50% without any deformation of the time spectrum.

Among our scientific activities on  $\mu\text{SR}$  studies from year 2016 to 2019, following studies are most important subjects of material sciences at the RIKEN-RAL muon facility:

- (1) Novel superconducting state having the steeper nodal gaps in the quasi two-dimensional organic superconductor  $\lambda$ -[BETS] $_2\text{GaCl}_4$
- (2) Tiny magnetic moments and spin structures of  $\text{Ir}^{4+}$  in hole-doped pyrochlore iridates  $\text{Y}_{1.95-y}\text{Cu}_{0.05}\text{Ca}_y\text{Ir}_2\text{O}_7$  and  $\text{Eu}_{2-x}\text{Ca}_x\text{Ir}_2\text{O}_7$
- (3) Magnetism and spin structure in superoxide  $\text{CsO}_2$ ,  $\text{RbO}_2$  and  $\text{NaO}_2$
- (4) Magnetic properties of the nano-cluster gold in the border of macro- and micro-scale
- (5) Novel magnetic properties of nano-size La-based high- $T_c$  superconducting cuprates
- (6) Effects of the spatial distributions of magnetic moments and muon positions estimated from density functional theory (DFT) and dipole-field calculations

### (2-2) Nuclear and particle physics studies via ultra-cold muon beam and muonic atoms

If we can improve muon beam emittance, timing and energy dispersion (so-called "ultra-cold muon"), then the capability of  $\mu\text{SR}$  studies will be drastically improved. The ultra-cold muon beam can stop in a thin foil, multi-layered materials and artificial lattices, so one can apply the  $\mu\text{SR}$  techniques to surface and interface science. The development of ultra-cold muon beam is also very important as the source of pencil-like small emittance muon beam for muon  $g-2$  measurement.

We had been working on the R&D of the "ultra-cold muon" generation based on the following technique, namely, positive muon beam with thermal energy has been produced by laser ionization of muoniums in vacuum (bound system of  $\mu^+$  and electron) emitted from the hot tungsten surface by stopping "surface muon beam" at Port-3. However, the muon yield and obtained emittance was far from satisfactory, and remained to be far from any kind of realistic application.

Therefore, in this mid-term, we are developing two key components, high efficiency muonium generator at room temperature and high intensity ionization laser. The study of muonium generator has been done in collaboration with TRIUMF. In 2013, we demonstrated at least 10 times increase of the muonium emission efficiency by fabricating fine laser drill-holes on the surface of silica aerogel. Further study was done in 2017 with more than 20 aerogel target having different surface conditions. We are analyzing the data to identify which condition most contributed to increasing the muonium emission efficiency. We also developed a high power Lyman- $\alpha$  laser in collaboration with laser group at RIKEN. In this laser development, we succeeded to synthesize novel laser crystal Nd:YAG, which has an ideal wavelength property for laser amplification to generate Lyman- $\alpha$  by four-wave mixing in Kr gas cell. We already achieved 10 times increase of Lyman- $\alpha$  generation than before. While we plan to increase the intensity by one more order, we are suffering from optical inhomogeneity in making a larger size crystal so far. We are developing several schemes to solve this

problem.

Concerning the muonic atom, we are planning a new precise measurement of proton radius. A large discrepancy was found recently in the proton charge radius between the new precise value from muonic hydrogen atom at PSI and those from normal hydrogen spectroscopy and e-p scattering. We propose a precise measurement of Zemach radius (with charge and magnetic distributions combined) using the laser spectroscopy of hyperfine splitting energy in the muonic hydrogen atom. Preparation of the hydrogen target, mid-infrared laser and muon spin polarization detectors is in progress. As a key parameter for designing the experiment, we need the quench rate of the muonic proton polarization due to collision with surrounding protons, for which only theoretical estimations are available. We successfully measured the quench rate of muonic deuterium polarization in deuterium gas, which confirmed the long lifetime consistent with the calculation. Measurement for muonic proton is planned in FY2019.

## Members

### Group Director

Masahiko IWASAKI

### Research/Technical Scientists

Haruhiko OUTA (Senior Research Scientist)

Fuminori SAKUMA (Senior Research Scientist)

Isao WATANABE (Senior Research Scientist)

Yue MA (Senior Research Scientist)

Kenta ITAHASHI (Senior Research Scientist)

### Contract Researcher

Katsuhiko ISHIDA

### Research Consultants

Yoshinori AKAISHI

Masayasu KAMIMURA

Hironari MIYAZAWA

Eiichi YAGI

### Junior Research Associates

Fahmi ASTUTI (Hokkaido Univ.)

Muhamad UMAR (Hokkaido Univ.)

Juila ANGEL (Hokkaido Univ.)

### International Program Associates

Harison Binti ROZAK (UTM)

Redo Muhammad RAMADHAN (Universitas Indonesia)

Suci WINARSIH (Universitas Indonesia)

Utami WIDYAISWARI (Universitas Indonesia)

### Senior Visiting Scientist

Kazuhiro TANAKA (KEK)

### Visiting Scientists

Toshimitsu YAMAZAKI (Univ. of Tokyo)

Atsushi OKAZAWA (Univ. of Tokyo)

Mototsugu MIHARA (Osaka Univ.)

Hiroko ARIGA (Hokkaido Univ.)

Donald George FLEMING (Univ. of British Columbia)

Yoshiki TANAKA(GSI)

Yasuo NOZUE (Osaka Univ.)

Katsuhiko NISHIMURA (Univ. of Toyama)

Takehito NAKANO (Osaka Univ.)

Kenji MATSUDA (Univ. of Toyama)

Tadashi ADACHI (Sophia Univ.)

Mohamed Ismail MOHAMED IBRAHIM (USM)

Zyun Francis EZAWA (Tohoku Univ.)

Shukri SULAIMAN (USM)

Yasuyuki ISHII (Shibaura Inst. of Tech.)

Eberhard WIDMANN (SMI)

Johann ZMESKAL (SMI)

Koichi ICHIMURA (Hokkaido Univ.)

Risdiana (UNPAD)

Youichi IGARASHI (KEK)

Takao SUZUKI (Shibaura Inst. of Tech.)

KwangYong CHOI (Chung-Ang Univ.)

Georg Peter BERG (Univ. of Notre Dame)

Emma HAETTNER (GSI)

Takayuki GOTO (Sophia Univ.)

Andrea VACCHI (INFN)

Masaya ENOMOTO (Tokyo Univ. of Sci.)

Dita PUSPITA SARI (Shibaura Inst. of Tech.)

Hiroyuki FUJIOKA (Tokyo Tech.)

Retno ASIH (Institut Teknologi Sepuluh Nopember)

Takayuki KAWAMATA (Tohoku Univ.)

Lee SEUNGWON (Univ. of Toyama)

Agustinus NUGROHO (ITB)

Takahiro NAMIKI (Univ. of Toyama)

Yuta SADA (Osaka Univ.)

Hiraki KO-ICHI (Fukushima Medical Univ.)

Ichiro SHIRAKI (Univ. of Yamanashi)

Naohito SAITO (KEK)

Kensuke SUZUKI (Tohoku Univ.)

Kouichirou SHIMOMURA (KEK)

Kyosuke ISODA (Kagawa Univ.)

Ryousuke KADONO (KEK)

Ken SUZUKI (SMI)

Wataru HIGEMOTO (JAEA)

Catalina Oana CURCEANU(INFN)

Yoji KOIKE (Tohoku Univ.)

Maryam HASSANVAND(IUT)

Kazuhiko SATOH (Saitama Univ.)

Kazuki UENO (KEK)  
 Masaru YOSOI (Osaka Univ.)  
 Lusy SAFRIANI (UNPAD)  
 Kazuki OHISHI (Comprehensive Res. Org. for Sci. and Soc.)  
 Hiroyuki NOUMI (Osaka Univ.)  
 Yasuhiro MIYAKE (KEK)

Zhuan XU (Zhejiang Univ.)  
 Yu OISHI (KEK)  
 Hiroshi TANIDA (Toyama Prefectural Univ.)  
 Seiko KAWAMURA (JAEA)  
 Satoru HIRENZAKI (Nara women's Univ.)

#### Research Fellow

Yuki NOZAWA (Osaka Univ.)

#### Student Trainees

Yuni WATANABE (Univ. of Tokyo)  
 Sungwon YOON (Catholic Univ. of Korea)  
 Ryo KITAMURA (Univ. of Tokyo)  
 Akane SAKAUE (Kyoto Univ.)

Kazuki MATSUI (Sophia Univ.)  
 Muhamad UMAR (Hokkaido Univ.)  
 Ainul Fauzeeha Binti ROZLAN (Univ. Saints Malaysia)  
 Irwan RAMLI (Hokkaido Univ.)

#### Part-time Worker

Irwan RAMLI (Research Part-time Worker I)

#### Assistants

Mitsue YAMAMOTO  
 Yoko FUJITA

Noriko ASAKAWA

## List of Publications & Presentations

### Publications

#### [Journal]

#### (Original Papers) \*Subject to Peer Review

- Darminto, R. Asih, Kurniasari, M. A. Baqia, S. Mustofa, Suasmoro, T. Kawamata, K. Kato, I. Watanabe, Y. Koike, "Enhanced magnetism by temperature induced defects in reduced graphene oxide prepared from coconut shells," *IEEE Transactions on Magnetics* **54**, 1600105-1-5 (2018).
- W. Liao *et al.*, "Measurement and mechanism investigation of negative and positive muon-induced upsets in 65-nm bulk SRAMS," *IEEE Trans. Nucl. Sci.* **65** (2018) 1734. \*
- E. Mocchiutti *et al.*, (FAMU collaboration), "First FAMU observation of muon transfer from mup atoms to higher-Z elements," *Journal of Instrumentation* **13**, 02019 (2018). \*
- A. Adamczak *et al.*, (FAMU collaboration), "The FAMU experiment at RIKEN-RAL to study the muon transfer rate from hydrogen to other gases," *Journal of Instrumentation* **13**, 12033 (2018). \*
- Y. Sassa, M. Mansson, O. K. Forslund, O. Tjernberg, V. Pomjakushin, O. Ofer, E. J. Ansaldo, J. H. Brewer, I. Umegaki, Y. Higuchi, Y. Ikedo, H. Nozaki, M. Harada, I. Watanabe, H. Sakurai, J. Sugiyama, "The metallic quasi-1D spin-density-wave compound  $\text{NaV}_2\text{O}_4$  studied by angle-resolved photoelectron spectroscopy," *J. Electron. Spectrosc. Relat. Phenom.* **224**, 79-83 (2018).
- R. Asih, N. Adam, S. S. Mohd-Tajudin, D. P. Sari, K. Matsuhira, H. Guo, M. Wakeshima, Y. Hinatsu, T. Nakano, Y. Nozue, S. Slaiman, M. I. Mohamed-Ibrahim, P. K. Biswas, I. Watanabe, "Magnetic moments and ordered states in pyrochlore irridates  $\text{Nd}_2\text{Ir}_2\text{O}_7$  and  $\text{Sm}_2\text{Ir}_2\text{O}_7$  studies by muon-spin relaxation," *J. Phys. Soc. Jpn.* **86**, 240705 (2018).
- M. Miyajima, F. Astuti, T. Kakuto, A. Matsuo, D. P. Sari, R. Asih, K. Okunishi, T. Nakano, Y. Nozue, K. Kindo, I. Watanabe, T. Kambe, "Magnetism and high-magnetic field magnetization in alkali superoxide  $\text{CsO}_2$ ," *J. Phys. Soc. Jpn.* **87**, 063704-1-4 (2018).
- T. Suzuki, K. Katayama, I. Kawasaki, I. Watanabe, H. Tanaka, "Spin fluctuations in the spin-1/2 kagome lattice antiferromagnet  $(\text{Rb}_{1-x}\text{Cs}_x)_2\text{Cu}_3\text{SnF}_{12}$  around the quantum critical point detected by muon-spin relaxation technique," *J. Phys. Soc. Jpn.* **87**, 074708-1-6 (2018).
- T. Kawamata, K. Ohashi, T. Takamatsu, T. Adachi, M. Kato, I. Watanabe, Y. Koike, "Impurity effects on the electronic state in the underdoped (Cu-free) superconductor  $T'-\text{La}_{1.8}\text{Eu}_{0.2}\text{CuO}_4$  studied by muon spin relaxation," *J. Phys. Soc. Jpn.* **87**, 094717 (2018).
- S. N. A. Afmad, S. Sulaiman, L. S. Ang, I. Watanabe, "First-principle studies on magnetic structure and exchange interactions of  $\beta\text{-Et}_n\text{Me}_{4-n}\text{Z}[\text{Pd}(\text{dmit})_2]_2$ ," *J. Phys. Soc. Jpn.* **87**, 124709-1-6 (2018).
- F. Astuti, M. Miyajima, T. Fukuda, M. Kodani, T. Nakano, T. Kambe, I. Watanabe, "Anionomagnetism combined lattice symmetry in alkali-metal superoxide  $\text{RbO}_2$ ," *J. Phys. Soc. Jpn.* **88**, 043701 (2018).
- K. L. Brown, C. P. J. Stockdale, H. Luo, X. Zhao, J.-H. Li, D. Viehland, G. Xu, P. M. Gehring, K. Ishida, A. D. Hillier, C. Stock, "Depth dependent element analysis of  $\text{PbMg}_{1/3}\text{Nb}_{2/3}\text{O}_3$  using muonic X-rays," *Journal of Physics: Condensed Matter* **30**, 125703 (2018). \*
- Kumar, C. N. Cuo, F. Astuti, T. Shang, M. K. Lee, C. S. Lue, I. Watanabe, J. A. T. Baker, T. Shiroka, L. J. Chang, "Nodeless superconductivity in the cage-type superconductor  $\text{Sc}_5\text{Ru}_6\text{Sn}_{18}$  with preserved time-reversal symmetry," *J. Phys. Condens. Matt.* **30**, 315803-1-11 (2018).
- E. Mocchiutti *et al.*, (FAMU collaboration), "FAMU: study of the energy dependent transfer rate  $\Lambda\mu p$  to  $\mu\text{O}$ ," *J. Phys. C* **1138**, 2018. \*
- E. Spurayoga, A. A. Nugroho, D. Onggo, A. O. Polyakov, T. T. M. Palstra, I. Watanabe, "3D long-range magnetic ordering in  $(\text{C}_2\text{H}_5\text{NH}_3)_2\text{CuCl}_4$  compound revealed by internal magnetic field from muon spin rotation and first principal calculation," *Physica B* **545**, 76-79 (2018).

- M. Clemenza *et al.*, “CHNET.TANDEM experiment: Use of negative muons at RIKEN-RAL Port 4 for elemental characterization of Nuragic votive ship samples,” Nucl. Instrum. Methods Phys. Res. A, <https://doi.org/10.1016/j.nima.2018.11.076>. \*
- S. Bae *et al.*, “First muon acceleration using a radio frequency accelerator,” Phys. Rev. Accel. Beams **21**, 050101 (2018). \*
- $\eta$ -PRiME/Super-FRS Collaboration (Y. K. Tanaka (Tokyo U.) *et al.*), “Missing-mass spectroscopy of the  $^{12}\text{C}(p, d)$  reaction near the  $\eta'$ -meson production threshold,” Phys. Rev. C **97**, 015202 (2018), DOI: 10.1103/PhysRevC.97.015202
- J-PARC E15 collaboration (S. Ajimura (Osaka U) *et al.*), “K-ppiAF Collaboration (T. Nishi (Tokyo U. & Nishina Ctr., RIKEN) *et al.*), “Spectroscopy of pionic atoms in  $^{122}\text{Sn}(d, ^3\text{He})$  reaction and angular dependence of the formation cross sections,” Phys. Rev. Lett. **120**, 152505 (2018), DOI: 10.1103/PhysRevLett.120.152505
- K. Kurashima, T. Adachi, Kensuke M. Suzuki, Y. Fukunaga, T. Kawamata, T. Noji, H. Miyasaka, I. Watanabe, M. Miyazaki, A. Koda, R. Kadono, Y. Koike,” “Development of ferromagnetic fluctuations in heavily overdoped  $(\text{Bi, Pd})_2\text{Sr}_2\text{CuO}_{6+\delta}$  copper oxides,” Phys. Rev. Lett. **121**, 057002-1–6 (2018).
- J-PARC E15 collaboration (S. Ajimura (Osaka U) *et al.*), “ $K^-pp$ , a  $\bar{K}$ -meson nuclear bound state, observed in  $^3\text{He}(K^-, \Lambda p)n$  reactions,” Phys. Lett. B **789**, 620–625 (2019). \*
- ppiAF Collaboration (T. Nishi *et al.*), “Spectroscopy of pionic atoms in  $^{122}\text{Sn}(d, ^3\text{He})$  reaction and angular dependence of the formation cross sections,” Phys. Rev. Lett. **120**, 152505 (2018), DOI: 10.1103/PhysRevLett.120.152505.

### [Proceedings]

#### (Original Papers) \*Subject to Peer Review

- P. Strasser *et al.*, “New precise measurements of muonium hyperfine structure at J-PARC MUSE,” EPJ Web Conf. **198** (2019) 00003 (8 pages), <https://doi.org/10.1051/epjconf/201919800003>, Proc. of Quantum Technology International Conference 2018 (QTech 2018)
- B. V. Hampshire, K. Butcher, K. Ishida, G. Green, D. Paul, A. Hillier, “Using negative muons as a probe for depth profiling silver Roman coinage,” Heritage **2**, 400–407 (2019), Proc. of the 8th International Conference on Synchrotron Radiation and Neutrons in Art and Archaeology, doi:10.3390/heritage2010028. \*
- T. Sumura, T. Ishimoto, H. Kuwahara, K. Kurashima, Y. Koike, I. Watanabe, M. Yiyazaki, A. Koda, R. Kadono, T. Adachi, “Reduction effects on Cu-spin fluctuation in the electron-doped  $T'$ -cuprate  $\text{Pr}_{1.3-x}\text{La}_{0.7}\text{Ce}_x\text{CuO}_{4+\delta}$  ( $x = 0.10$ ),” JPS Conf. Proc. **21**, 011027 (2018).
- A. Hillier, K. Ishida, P. Seller, M. C. Veale, M. D. Wilson, “Element specific imaging using muonic x-rays,” JPS Conf. Proc. **21**, 011042 (2018)
- Risdiana, T. Saragi, W. A. Somantri, S. Pratiwi, D. Suhendar, M. Manawan, B. J. Suroto, I. Watanabe, “Zn-induced development of the Cu-spin correlation in electron-doped superconducting cuprates of  $\text{Eu}_{2-x}\text{Ce}_x\text{CuO}_4$ ,” J. Phys. Conf. Ser. **1013**, 012180-1–5 (2018).
- S. Kanda, K. Ishida, M. Iwasaki, Y. Ma, S. Okada, A. Takamine, H. Ueno, K. Midorikawa, N. Saito, S. Wada, M. Yumoto, Y. Oishi, M. Sato, S. Aikawa, K. S. Tanaka, Y. Matsuda, “Measurement of the proton Zemach radius from the hyperfine splitting in muonic hydrogen atom,” J. Phys. Conf. Ser. **1138**, 012008 (2018). 10th Int. Conf. on Precision Physics of Simple Atomic Systems.
- A. D. Hillier, J. S. Lord, K. Ishida, C. Rogers, “Muons at ISIS,” Philosophical Transactions Royal Society A **377**, 20180064 Contribution to a Theo Murphy meeting issue “Cosmic-ray muography”
- S. Kanda, K. Ishida, M. Iwasaki, Y. Ma, A. Takamine, H. Ueno, K. Midorikawa, N. Saito, S. Wada, M. Yumoto, S. Okada, Y. Oishi, M. Sato, S. Aikawa, K. S. Tanaka, Y. Matsuda, “Precision laser spectroscopy of the ground state hyperfine splitting in muonic hydrogen,” Proceeding of Science (NuFact2017) 122.

### Oral Presentations

#### [International Conference etc.]

- S. Kanda, “Precision spectroscopy of muonic systems with high-intensity pulsed muon beam,” Workshop on Lepton Flavor Physics with Most Intense DC Muon Beams, Tokyo, April 2018.
- S. Kanda, “Measurement of the proton Zemach radius from the hyperfine splitting in muonic hydrogen atom,” PSAS2018, Vienna, May 2018.
- F. Sakuma, “Search for the kaonic bound state  $\bar{K}NN$  at J-PARC,” 15th International Workshop on Meson Physics (MESON2018), KRAKOW, POLAND, June 7–12, 2018.
- F. Sakuma, “Search for the Kaonic Bound State  $\bar{K}NN$  via  $^3\text{He}(K^-, \Lambda p \Sigma \pi)n$  reactions,” YKIS2018b Symposium, “Recent developments in quark-hadron sciences,” Yukawa Institute for Theoretical Physics, Kyoto University, Kyoto, Japan, June 11–15, 2018.
- K. Ishida, “Future opportunities in  $\mu$ - $p$  atoms,” FAMU Meeting, Trieste, Italy, June 2018.
- M. Iwasaki, “A quest for the “ $K^-pp$ ” bound state via  $^3\text{He}(K^-, n)$  reaction, J-PARC E15 experiment,” The 13th International Conference on Hypernuclear and Strange Particle Physics (HYP2018), Portsmouth, June 24–29, 2018.
- H. Asano, “Spectroscopic study of the  $\Lambda(1405)$  resonance via the  $d(K^-, n)$  reaction at J-PARC,” The 13th International Conference on Hypernuclear and Strange Particle Physics (HYP2018), Portsmouth, June 24–29, 2018.
- H. Asano, “Spectroscopic study of the  $\Lambda(1405)$  resonance via the  $d(K^-, n)$  reaction at J-PARC,” The 13th International Conference on Hypernuclear and Strange Particle Physics, Virginia, USA, June 2018.
- T. Yamaga, “Studies of the KNN bound state via the exclusive analysis of the in-flight  $(K^-, n)$  reaction at J-PARC,” The 22nd International Conference on Few-Body Problems in Physics (FB22), Caen, France, July 9–13, 2018.
- S. Kanda, “Laser spectroscopy of the hyperfine splitting in muonic hydrogen atom by a measurement of decay electron asymmetry,” Nucleon Spin Structure at Low Q: A Hyperfine View, Trento, July 2018.
- S. Kanda, “Precision spectroscopy of exotic atoms involving muon,” NuFact2018, Virginia, August 2018.

- H. Asano, “High-rate fiber tracker,” Workshop on Physics with General Purpose Spectrometer in the High-momentum Beam Line, Osaka, Japan, August 2018.
- S. Kanda, “Laser spectroscopy of the ground-state hyperfine splitting in muonic hydrogen atom,” Symposium for Muon and Neutrino Physics 2018, Osaka, September 2018.
- H. Noumi, “ $\pi\Sigma$  spectra in the kaon-induced reaction on deuteron,” The fifth joint meeting of the Division of Nuclear Physics of the American Physical Society with the nuclear physicists of the Physical Society of Japan, Waikoloa, USA, October 2018.
- K. Ishida, “Proton Zemach radius measurement by the hyperfine splitting of muonic hydrogen“(invited),” The fifth Joint Meeting of the Nuclear Physics Divisions of the American Physical Society and the Physical Society of Japan, Waikoloa, USA, October 2018.
- S. Okada, “Kaonic atom X-ray spectroscopy with transition edge sensors,” The 2018 Applied Superconductivity Conference (ASC2018), Seattle, USA, October 28–November 2, 2018.
- T. Yamaga, “Results of  $\bar{K}NN$  search via the  $(K^-, n)$  reaction at J-PARC,” The 8th International Conference on Quarks and Nuclear Physics (QNP2018), Tsukuba, Japan, November 13–17, 2018.
- S. Kawasaki, “The E31 spectroscopic experiment of  $\Lambda(1405)$  via in-flight  $d(K^-, n)$  reaction at J-PARC K1.8BR,” The 8th International Conference on Quarks and Nuclear Physics (QNP2018), Tsukuba, Japan, November 13–17, 2018.
- F. Sakuma, “ $\bar{K}$ -nuclear bound state at J-PARC,” 13th International Conference on Nucleus-Nucleus Collisions (NN2018), Omiya, Saitama, Japan, December 4–8, 2018.
- T. Hashimoto, “Kaonic atom experiments at J-PARC,” The 8th International Conference on Quarks and Nuclear Physics (QNP2018), Tsukuba, Japan, November 13–17, 2018.
- T. Yamaga, “Results of experimental search for  $\bar{K}NN$  bound state at J-PARC,” Reimei Workshop on Experimental and Theoretical Hadron Physics: Recent Exciting Developments, Tokai, Japan, January 9–11, 2019.
- H. Asano, “ $\Lambda(1405)$  from  $d(K^-, n)$  reaction,” Reimei Workshop on Experimental and Theoretical Hadron Physics: Recent Exciting Developments, Tokai, Japan, January 9–11, 2019.
- S. Okada, “Kaonic atom x-ray spectroscopy at J-PARC,” Reimei Workshop on Experimental and Theoretical Hadron Physics: Recent Exciting Developments, Tokai, Japan, January 9–11, 2019.
- K. Ishida, “Proton radius measurement with muonic atoms,” International Workshop on the Structure of the Proton, Sagae, Yamagata, February 2019.
- S. Kanda, “Development of instruments for the proton radius measurement at RIKEN,” International Workshop on the Structure of the Proton, Sagae, Yamagata, February 2019.
- K. Itahashi, “Spectroscopy of pionic atoms and deduction of chiral symmetry in nuclear matter,” NN2018, Omiya, Saitama, December 2018.
- K. Itahashi, “Spectroscopy of meson-nucleus bound states,” HIAF Workshop, Beijing, November 2018.

#### [Domestic Conference]

- 石田勝彦, 「ミュオン原子による陽子半径決定」, 大阪大学理学部物理セミナー, 豊中, 2018年8月.
- 佐久間史典, 「New results on the “ $K^-pp$ ” bound state from J-PARC 原子核中におけるハドロンの性質とカイラル対称性の役割」, 東北大学電子光理学研究センター, 仙台, 2018年9月.
- 橋本直, 「J-PARCにおけるK中間子原子X線分光」, 原子核中におけるハドロンの性質とカイラル対称性の役割, 東北大学電子光理学研究センター, 仙台, 2018年9月.
- 神田聡太郎, “Residual polarization and hyperfine transition rate in muonic hydrogen,” 新学術領域研究「宇宙観測検出器と量子ビームの出会い. 新たな応用への架け橋」, キックオフシンポジウム, 東北, 2018年12月.
- 神田聡太郎, “Laser spectroscopy of the hyperfine splitting in muonic hydrogen,” 第9回 Muon 科学と加速器研究研究会, 大阪, 2019年1月.
- 石田勝彦, 「理研 RAL ミュオン施設」, 第9回「Muon 科学と加速器研究」, RCNP, 吹田, 2019年1月.
- 石田勝彦, 「ミュオン水素原子による由志半径測定」, ELPH 研究会 C021 「電子散乱による原子核研究—陽子半径, 不安定核の電荷密度分布を中心に—」, 東北大学電子光理学研究センター, 仙台, 2019年3月.
- 浅野秀光, 「J-PARC E31 実験における  $\Lambda(1405)$  生成の運動量移行依存性」, 日本物理学会第74回年次大会, 九州大学, 福岡, 2019年3月.
- O. Zhadyra, “The physics experiment E31 to search for the  $\Lambda(1405)$  via the  $d(K^-, n)\pi\Sigma$  reaction at J-PARC K1.8BR,” 日本物理学会第74回年次大会, 九州大学, 福岡, 2019年3月.
- 浅野秀光, 「J-PARC E31 実験における  $\Lambda(1405)$  生成の運動量移行性」, 日本物理学会第74回年次大会, 九州大学, 福岡, 2019年3月.
- 川崎新吾, 「 $d(K^-, n)\pi^0\Sigma^0$  反応による  $\Lambda(1405)$  の研究」, 日本物理学会第74回年次大会, 九州大学, 福岡, 2019年3月.
- 神田聡太郎, 「ミュオン水素原子のレーザー分光に向けたスピン回転実験」, 日本物理学会第74回年次大会, 九州大学, 福岡, 2019年3月.

## Subnuclear System Research Division RIKEN BNL Research Center

### 1. Abstract

The RIKEN BNL Research Center was established in April 1997 at Brookhaven National Laboratory with Professor T. D. Lee of Columbia University as its initial Director. It is funded by the Rikagaku Kenkyusho (RIKEN, The Institute of Physical and Chemical Research) of Japan. The Center is dedicated to the study of strong interactions, including spin physics, lattice QCD and RHIC physics through the nurturing of a new generation of young physicists. Professor Lee was succeeded by BNL Distinguished Scientist, N. P. Samios, who served until 2013. Dr. S. H. Aronson led the Center from 2013. After strong and significant leadership for 4 years, S. Aronson stepped down from Director in March 31<sup>st</sup> 2017. Hideto En'yo succeeds from JFY 2017. Support for RBRC was initially for five years and has been renewed four times, and presently extends to 2023. The Center is located in the BNL Physics Department. The RBRC Theory Group activities are closely and intimately related to those of the Nuclear Theory, High Energy Theory, and Lattice Gauge Theory Groups at BNL. The RBRC Experimental Group works closely with Radiation Laboratory at RIKEN, Wako, the RHIC Spin Group at BNL, the RHIC Spin Physics community, and the PHENIX collaboration. BNL provides office space, management, and administrative support. In addition, the Computational Science Initiative (CSI) and Information Technology Division (ITD) at BNL provide support for computing, particularly the operation and technical support for the RBRC 400 Teraflop QCDCQ (QCD Chiral Quark) lattice gauge theory computer. D. Kharzeev (Stony Brook/BNL) is leader of the Theory Group. Y. Akiba (RIKEN) is Experimental Group leader. T. Izubuchi (BNL) is Computing Group leader.

### 2. Major Research Subjects

Major research subjects of the theory group are

- (1) Heavy Ion Collision
- (2) Perturbative QCD
- (3) Phenomenological QCD

Major research subjects of the computing group are

- (1) Search for new law of physics through tests for Standard Model of particle and nuclear physics
- (2) Dynamics of QCD and related theories
- (3) Theoretical and algorithmic development for lattice field theories, QCD machine design

Major research subject of the experimental group are

- (1) Experimental Studies of the Spin Structure of the Nucleon
- (2) Study of Quark-Gluon Plasma at RHIC
- (3) sPHENIX detector construction

### 3. Summary of Research Activity

Summary of Research Activities of the three groups of the Center are given in the sections of each group.

## Members

### Director

Hideto EN'YO (concurrent: Director, Nishina Center for Accelerator-Based Science)

### Administrative Staff

Kazushige FUKUSHIMA (Administration Manager, Nishina Center and iTHEMS Promotion Office)

Pamela ESPOSITO (Administrative Assistant)

Maureen MCNEIL-SHEA (Administrative Assistant)

Hiroshi ITO (Deputy Administration Manager, Nishina Center and iTHEMS Promotion Office)

**Subnuclear System Research Division**  
**RIKEN BNL Research Center**  
**Theory Group**

## 1. Abstract

The efforts of the RBRC theory group are concentrated on the major topics of interest in High Energy Nuclear Physics and strongly interacting Chiral Matter. This includes: understanding of the Quark-Gluon Plasma; the nature of dense quark matter; the initial state in high energy collisions, the Color Glass Condensate; its evolution through a Glasma; spin physics, as is relevant for polarized hadronic collisions; physics relevant to electron-hadron collisions and the Electron-Ion Collider; quantum transport and the Chiral Magnetic Effect.

Theory Group hosted many joint tenure track positions with universities in U.S. and Japan.

## 2. Major Research Subjects

- (1) Heavy Ion Collisions
- (2) Perturbative Quantum Chromo-Dynamics (QCD)
- (3) Phenomenological QCD
- (4) Chiral Matter

## 3. Summary of Research Activity

### (1) Phase diagram of QCD

The heavy ion program at Relativistic Heavy Ion Collider (RHIC) at BNL is focused on the study of the properties of QCD matter at high energy densities and high temperatures. The RBRC Theory group performs research that supports and guides the experimental program at RHIC. In the past year, RBRC researchers had identified the possibility for the higher-order phase transitions in QCD (H. Nishimura, R. Pisarski, V. Skokov) by using the novel approach based on the matrix models.

The first-principle studies of QCD phase diagram at finite baryon density using the lattice Monte Carlo approach are very difficult because of the so-called “sign problem.” The work by H. Nishimura and Y. Tanizaki, in collaboration with J. Verbaarschot of Stony Brook Nuclear Theory group, has proposed a new kind of the gradient flow method that can be used to alleviate this problem.

An important feature of strongly interacting matter at finite baryon density is the liquid-gas phase transition. The paper by H. Nishimura (in collaboration with M. Ogilvie and K. Pangeni) develops a field-theoretic approach to the liquid-gas phase transition based on an effective 3D field theory.

Quantum anomalies play an important role in QCD phase transitions. Y. Tanizaki, Y. Kikuchi (who will join the RBRC Theory group in 2018) and collaborators utilized the method of “anomaly matching” to obtain important constraints on the dynamics of deconfinement and chiral restoration phase transitions in QCD. They also used this method to study the vacuum structure of QCD at finite theta-angle.

### (2) QCD Matter at High Energy Density and at small $x$

The RHIC experimental heavy ion program is designed to study the properties of matter at energy densities much greater than that of atomic nuclei. This includes the initial state of nucleus-nucleus collisions, the Color Glass Condensate, the intermediate state to which it evolves, the Glasma, and lastly the thermal state to which it evolves, the Quark-Gluon Plasma. Theorists at the RBRC have made important contributions to all of these subjects.

During the past year, V. Skokov (in collaboration with A. Kovner, and others) investigated the role of entanglement in gluon fields at small Bjorken  $x$  in generating the azimuthal anisotropy of hadrons produced in AA and pA collisions at RHIC. It has been found that the correlations inside the small  $x$  distributions effectively generate odd azimuthal harmonics in hadron distributions, with a long-range separation in rapidity. In collaboration with A. Kovner and M. Lublinsky, V. Skokov also investigated the possible effect of quark-gluon correlations at small  $x$  on the studies of the Chiral Magnetic Effect in pA collisions at RHIC. D. Kharzeev, in collaboration with W. Li and Z. Tu, investigated the role of fluctuating proton size on the CME studies in pA collisions, and found that these fluctuations induce a significant correlation between the direction of magnetic field and the reaction plane, enabling the observation of CME.

The Isobar run at RHIC (made possible due to the RIKEN scientists working on Zr source) completed in 2018 will establish or rule out the existence of the Chiral Magnetic Effect (originally proposed by RBRC theorists) in the quark-gluon plasma. During the past year, D. Kharzeev and H.-U. Yee, in collaboration with Y. Hirono, M. Mace and others have developed the Chiral Magneto-Hydrodynamics (CMHD) approach to the Chiral Magnetic Effect (CME) in quark-gluon plasma. The first numerical results of CMHD have become available due to the collaboration of RBRC with the ECHO-QGP group. H.-U. Yee and collaborators investigated dynamical instabilities in CMHD. D. Kharzeev and H.-U. Yee, in collaboration with M. Stephanov, solved a long-standing puzzle of the apparent discrepancy between the field theory and the kinetic theory on the magnitude of the CME current at finite frequency. D. Kharzeev, with Y. Hirono and A. Sadofyev, proposed a new “chiral propulsion effect” for the chiral solitons on vortices in chiral media.

The activity of RBRC members described above bridges the gap between fundamental theory and phenomenology of heavy ion collisions. This includes the lattice QCD studies, the analytical work on the dynamics of phase transitions, the development of hydrodynamical and kinetic theory approaches incorporating quantum anomalies, and phenomenology. Much of the current work in the field is based on the ideas originally developed by the RBRC theorists.

**(3) Chiral Matter**

Much of the work done at the RBRC Theory group has broad implications beyond the domain of Nuclear and High Energy physics. One example is the Chiral Magnetic Effect, originally proposed to occur in quark-gluon plasma, but discovered recently in condensed matter systems, so-called Dirac and Weyl semimetals (the original experimental observation of CME was made at BNL in  $ZrTe_5$  in a paper co-authored by D. Kharzeev). It has become clear that RBRC can make a very substantial impact also on condensed matter physics, where the methods developed at RBRC can be applied to a new set of problems. Vice versa, some of the new theoretical developments in condensed matter physics can be utilized for the study of QCD matter. Because of this, the RBRC developed a new initiative on Chiral Matter focusing on the studies of quantum behavior in strongly interacting matter containing chiral fermions—this includes the quark-gluon plasma, electroweak plasma, Dirac and Weyl semimetals, and topological insulators.

In the past year, the RBRC members within this new initiative obtained a number of new results. Some of them, with a direct relevance for the quark-gluon plasma, have been already described above; other results are of direct relevance for condensed matter physics. D. Kharzeev, Y. Tanizaki and Y. Kikuchi (a postdoc who has joined RBRC in 2018), in collaboration with R. Meyer, found that asymmetric Weyl semimetals support a giant photocurrent as a result of chiral anomaly. D. Kharzeev, Y. Kikuchi and R. Meyer also proposed a new kind of dynamical CME in asymmetric Weyl semimetals that does not require an external source of chirality, and proposed an experiment to test their prediction. D. Kharzeev with his Stony Brook student S. Kaushik have identified a new type of quantum oscillations in the CME conductivity at finite doping, and with another student E. Philip have established the existence of the chiral magnetic photocurrent.

The Chiral Matter initiative has already broadened the impact of RBRC beyond the traditional domain of high-energy nuclear physics, and has extended the RBRC research into a new and extremely active area.

**Members****Group Leader**

Dmitri KHARZEEV

**Special Postdoctoral Researchers**

Yuya TANIZAKI

Hiromichi NISHIMURA

**RBRC Researchers**

Yuta KIKUCHI (Postdoctoral Researcher)

Jordy DE VRIES (RHIC Physics Fellow)

Chun SHEN (RHIC Physics Fellow)

Vladimir SKOKOV (RHIC Physics Fellow)

**Subnuclear System Research Division**  
**RIKEN BNL Research Center**  
**Experimental Group**

## 1. Abstract

RIKEN BNL Research Center (RBRC) Experimental Group studies the strong interactions (QCD) using RHIC accelerator at Brookhaven National Laboratory, the world first heavy ion collider and polarized  $p + p$  collider. We have three major activities: Spin Physics at RHIC, Heavy ion physics at RHIC, and detector upgrades of PHENIX experiment at RHIC.

We study the spin structure of the proton using the polarized proton-proton collisions at RHIC. This program has been promoted by RIKEN's leadership. The first focus of the research is to measure the gluon spin contribution to the proton spin. Recent results from PHENIX  $\pi^0$  measurement and STAR jet measurement has shown that gluons in the proton carry about 30% of the proton spin. This is a major milestone of RHIC spin program. The second goal of the spin program is to measure the polarization of anti-quarks in the proton using  $W \rightarrow e$  and  $W \rightarrow \mu$  decays. The results of  $W \rightarrow e$  measurement was published in 2016. The final results of  $W \rightarrow \mu$  was published in 2018.

The aim of Heavy ion physics at RHIC is to re-create Quark Gluon Plasma (QGP), the state of Universe just after the Big Bang. Two important discoveries, jet quenching effect and strong elliptic flows, have established that new state of dense matter is indeed produced in heavy ion collisions at RHIC. We are now studying the property of the matter. Recently, we have measured direct photons in Au + Au collisions for  $1 < p_T < 3$  GeV/c, where thermal radiation from hot QGP is expected to dominate. The comparison between the data and theory calculations indicates that the initial temperature of 300 MeV to 600 MeV is achieved. These values are well above the transition temperature to QGP, which is calculated to be approximately 160 MeV by lattice QCD calculations.

We had major roles in detector upgrades of PHENIX experiment, namely, the silicon vertex tracker (VTX) and muon trigger upgrades. Both of the upgrade is now complete. The VTX is the main device to measure heavy quark (charm and bottom) production and the muon trigger is essential for  $W \rightarrow \mu$  measurement. The results from the first run with VTX detector in 2011 was published. The results show that electrons from bottom quark decay is strongly suppressed at high  $p_T$ , but the suppression is weaker than that of charm decay electron for  $3 < p_T < 4$  GeV/c. We have recorded 10 times as much Au + Au collisions data in each of the 2014 run and 2016 run. The large dataset will produce definitive results on heavy quark production at RHIC.

PHENIX completed its data taking in 2016. We are now working on R&D of intermediate silicon tracker INTT for sPHENIX, a new experiment at RHIC that will be installed in the PHENIX IR.

## 2. Major Research Subjects

- (1) Experimental Studies of the Spin Structure of the Nucleon
- (2) Study of Quark-Gluon Plasma at RHIC
- (3) PHENIX detector upgrades

## 3. Summary of Research Activity

We study the strong interactions (QCD) using the RHIC accelerator at Brookhaven National Laboratory, the world first heavy ion collider and polarized  $p + p$  collider. We have three major activities: Spin Physics at RHIC, Heavy ion physics at RHIC, and detector upgrades of PHENIX experiment. From 2015, Y. Akiba (Experimental Group Leader) is the Spokesperson of PHENIX experiment.

### (1) Experimental study of spin structure of proton using RHIC polarized proton collider

How is the spin of proton formed with 3 quarks and gluons? This is a very fundamental question in Quantum Chromodynamics (QCD), the theory of the strong nuclear forces. The RHIC Spin Project has been established as an international collaboration between RIKEN and Brookhaven National Laboratory (BNL) to solve this problem by colliding two polarized protons for the first time in history. This project also has extended the physics capabilities of RHIC.

The first goal of the Spin Physics program at RHIC is to determine the gluon contribution to proton spin. It is known that the spin of quark accounts for only 25% of proton spin. The remaining 75% should be carried either by the spin of gluons or the orbital angular momentum of quarks and gluons. One of the main goals of the RHIC spin program has been to determine the gluon spin contribution. Before the start of RHIC, there was little experimental constraint on the gluon polarization,  $\Delta G$ .

PHENIX measures the double helicity asymmetry ( $A_{LL}$ ) of  $\pi^0$  production to determine the gluon polarization. Our most recent publication of  $\pi^0 A_{LL}$  measurement at 510 GeV shows non-zero value of  $A_{LL}$ , indicating that gluons in the proton is polarized. Global analysis shows that approximately 30% of proton spin is carried by gluons.

RHIC achieved polarized  $p + p$  collisions at 500 GeV in 2009. The collision energy increased to 510 GeV in 2012 and 2013. The main goal of these high energy  $p + p$  run is to measure anti-quark polarization via single spin asymmetry  $A_L$  of the  $W$  production. We upgraded the muon trigger system to measure  $W \rightarrow \mu$  decays in the forward direction. With the measurement of  $W \rightarrow e$  and  $W \rightarrow \mu$ , we can cover a wide kinematic range in anti-quark polarization measurement. The 2013 run is the main spin run at 510 GeV. PHENIX has recorded more than 150/pb of data in the run. The final results of the  $A_L$  measurement in  $W \rightarrow e$  channel in combined data of 2011 to 2013 was published in 2016. The paper on the final results of  $W \rightarrow \mu$  was published in 2018. These high statistics results give strong constraints on the polarization of anti-quarks in the proton.

RHIC has the first polarized proton nucleus collision run in 2015. In this run, we discovered a surprisingly large nuclear dependence of single spin asymmetry of very forward neutron. The paper of this discovery was published in Physical Review Letters.

**(2) Experimental study of Quark-Gluon Plasma using RHIC heavy-ion collider**

The goal of high energy heavy ion physics at RHIC is study of QCD in extreme conditions *i.e.* at very high temperature and at very high energy density. Experimental results from RHIC have established that dense partonic matter is formed in Au + Au collisions at RHIC. The matter is very dense and opaque, and it has almost no viscosity and behaves like a perfect fluid. These conclusions are

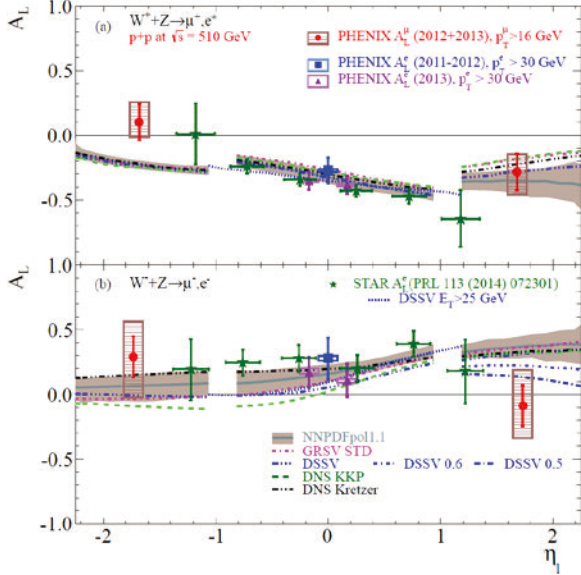


Fig. 1. Single spin asymmetry  $A_L$  of electrons from  $W$  and  $Z$  decays. The  $A_L$  is sensitive to the polarization of anti-quarks in the proton. The curves and the shaded region show theoretical calculations based on various polarized parton distribution (PDF) sets. The mid-rapidity points were published in Phys. Rev. D **93**, 051103(R) (2016). The forward/backward points were published in Phys. Rev. D **98**, 032007 (2018).

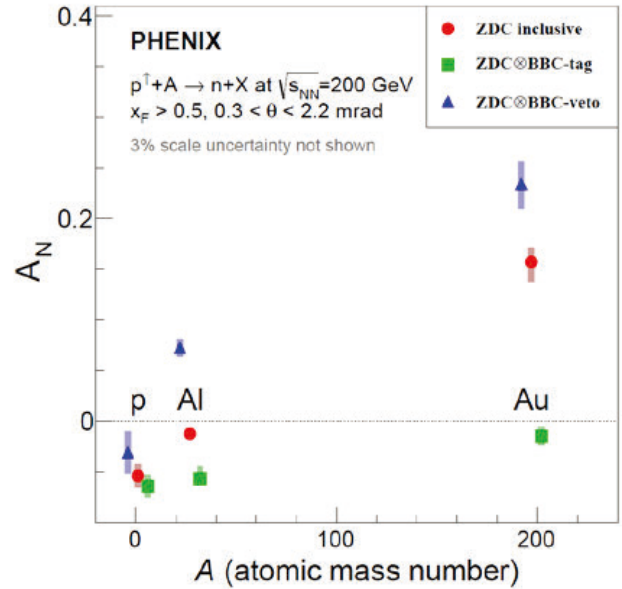


Fig. 2. Single spin asymmetry  $A_N$  of very forward neutron in  $p + p$ ,  $p + \text{Al}$ , and  $p + \text{Au}$  collision. Published in Phys. Rev. Lett. **120**, 022001 (2018).

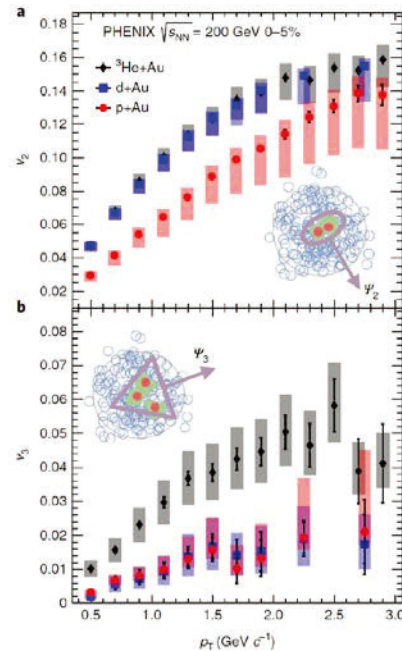
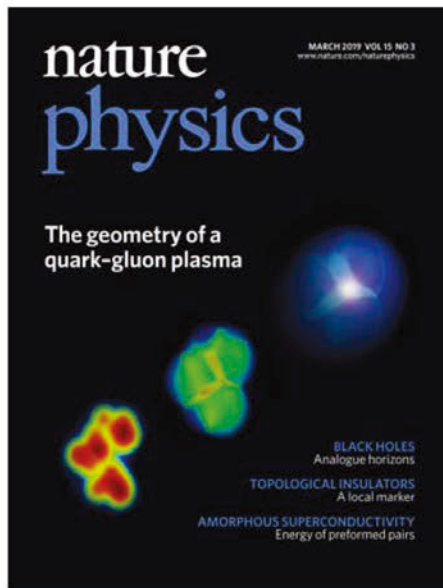


Fig. 3. Left: Cover of Nature Physics March 2019 issue featuring the PEHNIX article reporting strong evidence of small QGP droplet formation. Right: Data of elliptic and triangular flow measured in  $p + \text{Au}$ ,  $d + \text{Au}$  and  $^3\text{He} + \text{Au}$  collisions.

primarily based on the following two discoveries:

- Strong suppression of high transverse momentum hadrons in central Au + Au collisions (jet quenching)
- Strong elliptic flow

These results are summarized in PHENIX White paper, which has approximately 2700 citations to date.

The focus of the research in heavy ion physics at RHIC is now to investigate the properties of the matter. RBRC have played the leading roles in some of the most important results from PHENIX in the study of the matter properties. These include (1) measurements of heavy quark production from the single electrons from heavy flavor decay (2) measurements of  $J/\psi$  production (3) measurements of di-electron continuum and (4) measurements of direct photons.

Our most important result is the measurement of direct photons for  $1 < p_T < 5$  GeV/c in  $p + p$  and Au + Au through their internal conversion to  $e^+e^-$  pairs. If the dense partonic matter formed at RHIC is thermalized, it should emit thermal photons. Observation of thermal photon is direct evidence of early thermalization, and we can determine the initial temperature of the matter. It is predicted that thermal photons from QGP phase is the dominant source of direct photons for  $1 < p_T < 3$  GeV/c at the RHIC energy. We measured the direct photon in this  $p_T$  region from measurements of quasi-real virtual photons that decays into low-mass  $e^+e^-$  pairs. Strong enhancement of direct photon yield in Au + Au over the scaled  $p + p$  data has been observed. Several hydrodynamical models can reproduce the central Au + A data within a factor of two. These models assume formation of a hot system with initial temperature of  $T_{\text{init}} = 300$  MeV to 600 MeV. This is the first measurement of initial temperature of quark gluon plasma formed at RHIC. These results are recently published in Physical Review Letters. Y. Akiba is the leading person of the analysis and the main author of the paper. **He received 2011 Nishina memorial Prize mainly based on this work.**

PHENIX experiment measured the flow in small collision systems ( $p + \text{Au}$ ,  $d + \text{Au}$ , and  $^3\text{He} + \text{Au}$ ), and observed strong flow in all of these systems. Theoretical models that assume formation of small QGP droplets best describe the data. These results are published in Nature Physics in 2019.

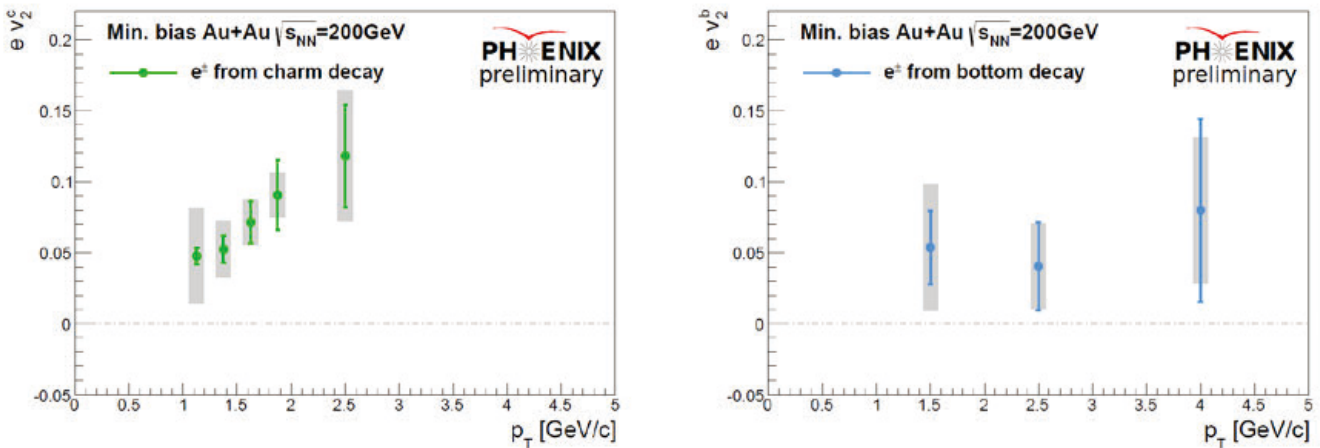


Fig. 4. Preliminary results of the elliptic flow strength  $v_2$  of single electrons from charm and bottom decays.

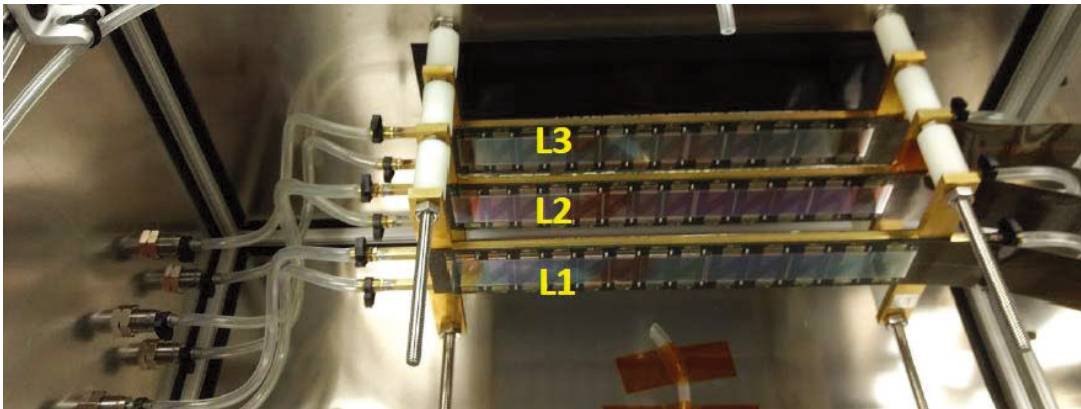


Fig. 5. Three ladder telescope made from INTT silicon tracker prototype. The prototype detector was tested in a beam test at FNAL in February 2018.

**(3) Detector upgrade**

The group had major roles in several PHENIX detector upgrades, namely, the silicon vertex tracker (VTX) and muon trigger upgrades. VTX is a high precision charged particle tracker made of 4 layers of silicon detectors. It is jointly funded by RIKEN and the US DOE. The inner two layers are silicon pixel detectors and the outer two layers are silicon strip detectors. Y. Akiba is the project manager and A. Deshpande is the strip system manager. The VTX detector was completed in November 2010 and subsequently installed in PHENIX. The detector started taking data in the 2011 run. With the new detector, we measure heavy quark (charm and bottom) production in  $p + p$ ,  $A + A$  collisions to study the properties of quark-gluon plasma. The final result of the 2011 run was published. The result show that single electrons from bottom quark decay is suppressed, but not as strong as that from charm decay in low  $p_T$  region ( $3 < p_T < 4 \text{ GeV}/c$ ). This is the first measurement of suppression of bottom decay electrons at RHIC and the first observation that bottom suppression is smaller than charm. We have recorded 10 times as much Au + Au collisions data in each of the 2014 run and 2016 run. The large dataset will produce definitive results on heavy quark production at RHIC. A preliminary results on the elliptic flow strength  $v_2$  of  $b \rightarrow e$  and  $c \rightarrow e$  has been presented in Quark Matter 2018 conference.

PHENIX completed its data taking in 2016. We are now working on R&D of intermediate silicon tracker INTT for sPHENIX, a new experiment at RHIC that will be installed in the PHENIX IR. A three ladder telescope of INTT prototype modules was tested in a beam test at FNAL. The prototype detector worked very well during the test.

**Members****Group Leader**

Yasuyuki AKIBA (Deputy Chief Scientist)

**RBRC Researchers**

Jan BERNAUER (RHIC Physics Fellow)

Itaru NAKAGAWA (RIKEN Spin Program Researcher, concurrent: Radiation Lab.)

Takashi HACHIYA (RIKEN BNL Fellow, Nara Women's University)

Takashi ICHIHARA (RIKEN Spin Program Researcher, concurrent: RI Physics Lab.)

Yorito YAMAGUCHI

Takahito TODOROKI

Atsushi TAKETANI (RIKEN Spin Program Researcher, concurrent: Neutron Beam Technology Team, Advanced Photonics Technology Development Group, RAP)

Megan CONNORS (RHIC Physics Fellow)

Marta VERWEIJ (RHIC Physics Fellow)

Yasushi WATANABE (RIKEN Spin Program Researcher, concurrent: Radiation Lab.)

Satoshi YOKKAICHI (RIKEN Spin Program Researcher, concurrent: Radiation Lab.)

Yuji GOTO (RIKEN Spin Program Researcher, concurrent: Radiation Lab.)

Ralf SEIDL (RIKEN Spin Program Researcher, concurrent: Radiation Lab.)

**Visiting Scientists**

Stefan BATHE (Baruch College University of New York)

Takao SAKAGUCHI (BNL)

Rachid NOUCER (BNL)

Takashi SAKO (University of Tokyo)

Masahiro OKAMURA (BNL)

Hiroaki MENJO (Nagoya University)

Gaku MITSUKA (KEK)

**List of Publications & Presentations****Publications****Oral Presentations****[International Conference etc.]**

T. Hachiya, "Nuclear modification factor and flow of charm and bottom quarks in Au + Au collisions at  $\sqrt{s_{NN}} = 200 \text{ GeV}$  by the PHENIX Experiment," Quark Matter 2018 (QM2018), Venice, Italy, May 13–19, 2018.

T. Hachiya, "Heavy Flavor Physics at RHIC," :Fifth Joint Meeting of the Nuclear Physics Divisions of the APS and the JPS (HAWAII2018), Waikoloa, HI, USA, October 23–27, 2018.

T. Hachiya, "Recent experimental studies on high-energy heavy ion collisions," 13th International Conference on Nucleus-Nucleus Collisions (NN2018), Omiya, Japan, December 4–8, 2018.

## Subnuclear System Research Division RIKEN BNL Research Center Computing Group

### 1. Abstract

The computing group founded in 2011 as a part of the RIKEN BNL Research Center established at Brookhaven National Laboratory in New York, USA, and dedicated to conduct researches and developments for large-scale physics computations important for particle and nuclear physics. The group was forked from the RBRC Theory Group.

The main mission of the group is to provide important numerical information that is indispensable for theoretical interpretation of experimental data from the first principle theories of particle and nuclear physics. Their primary area of research is lattice quantum chromodynamics (QCD), which describes the sub-atomic structures of hadrons, which allow us the ab-initio investigation for strongly interacting quantum field theories beyond perturbative analysis.

The RBRC group and its collaborators have emphasized the necessity and importance of precision calculations, which will precisely check the current understandings of nature, and will have a potential to find a physics beyond the current standard model of fundamental physics. We have therefore adopted techniques that aim to control and reduce any systematic errors. This approach has yielded many reliable results.

The areas of the major activities are R&D for high performance computers, developments for computing algorithms, and researches of particle, nuclear, and lattice theories. Since the inception of RBRC, many breakthroughs and pioneering works has carried out in computational forefronts. These are the use of the domain-wall fermions, which preserve chiral symmetry, a key symmetry for understanding nature of particle nuclear physics, the three generations of QCD devoted supercomputers, pioneering works for QCD calculation for Cabibbo-Kobayashi-Maskawa theory, QCD + QED simulation for isospin breaking, novel algorithm for error reduction in general lattice calculation. Now the chiral quark simulation is performed at the physical up, down quark mass, the precision for many basic quantities reached to accuracy of sub-percent, and the group is aiming for further important and challenging calculations, such as the full and complete calculation of CP violating  $K \rightarrow \pi\pi$  decay and  $\epsilon'/\epsilon$ , or hadronic contributions to muon's anomalous magnetic moment  $g - 2$ . Another focus area is the nucleon's shape, structures, and the motion of quarks and gluon inside nucleon called parton distribution, which provide theoretical guidance to physics for future Electron Ion Collider (EIC), Hyper Kamiokande, DUNE, or the origin of the current matter rich universe (rather than anti-matter). Some of members carry out interesting research on strong gauge dynamics other than QCD to get hints for the true nature of the Higgs particle or the Dark Matter, or even quantum gravity.

### 2. Major Research Subjects

- (1) Search for new law of physics through tests for Standard Model of particle and nuclear physics, especially in the framework of the Cabibbo-Kobayashi-Maskawa (CKM), hadronic contributions to the muon's anomalous magnetic moment ( $g - 2$ ) for FNAL and J-PARC's experiments, as well as B physics at Belle II and LHCb.
- (2) Nuclear Physics and dynamics of QCD or related theories, including study for the structures of nucleons related to physics for Electron Ion Collider (EIC or eRHIC), Hyper Kamiokande, T2K, DUNE.
- (3) Theoretical and algorithmic development for lattice field theories, QCD machine (co-)design and code optimization.

### 3. Summary of Research Activity

In 2011, QCD with Chiral Quarks (QCDCQ), a third-generation lattice QCD computer that is a pre-commercial version of IBM's Blue Gene/Q, was installed as an in-house computing resource at the RBRC. The computer was developed by collaboration among RBRC, Columbia University, the University of Edinburgh, and IBM. Two racks of QCDCQ having a peak computing power of  $2 \times 200$  TFLOPS are in operation at the RBRC. In addition to the RBRC machine, one rack of QCDCQ is owned by BNL for wider use for scientific computing. In 2013, 1/2 rack of Blue Gene/Q is also installed by US-wide lattice QCD collaboration, USQCD. The group has also used the IBM Blue Gene supercomputers located at Argonne National Laboratory and BNL (NY Blue), and Hokusai and RICC, the super computers at RIKEN (Japan), Fermi National Accelerator Laboratory, the Jefferson Lab, and others. From 2016, the group started to use the institutional cluster both GPU and Intel Knight Landing (KNL) clusters installed at BNL and University of Tokyo extensively.

Such computing power enables the group to perform precise calculations using up, down, and strange quark flavors with proper handling of the important symmetry, called chiral symmetry, that quarks have. The group and its collaborators carried out the first calculation for the direct breaking of CP (Charge Parity) symmetry in the hadronic K meson decay ( $K \rightarrow \pi\pi$ ) amplitudes,  $\epsilon'/\epsilon$ , which provide a new information to CKM paradigm and its beyond. They also provide the hadronic contribution in muon's anomalous magnetic moment  $(g - 2)_\mu$ . These calculation for  $\epsilon'/\epsilon$ , hadronic light-by-light of  $(g - 2)_\mu$ , are long waited calculation in theoretical physics delivered for the first time by the group. The  $K \rightarrow \pi\pi$  result in terms of  $\epsilon'/\epsilon$  currently has a large error, and deviates from experimental results by  $2.1 \sigma$ . To collect more information to decide whether this deviation is from the unknown new physics or not, the group continues to improve the calculation in various way to reduce their error. Hadronic light-by-light contribution to  $(g - 2)_\mu$  is improved by more than two order of magnitudes compared to our previous results. As of 2019 summer, their calculation is among the most precise determination for the  $g - 2$  hadronic vacuum polarization (HVP), and only one calculation in the world for the hadronic light-by-light (HLbL) contribution at physical point. These  $(g - 2)_\mu$  calculations provide the first principle theoretical prediction for on-going new experiment at FNAL and also for the planned experiment at J-PARC. Other projects including flavor physics in the framework of the

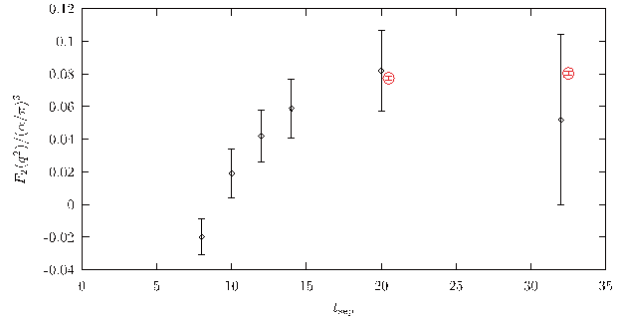
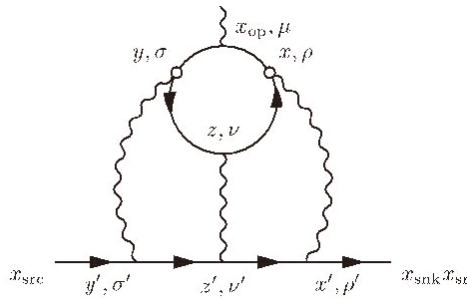


Fig. 1. Muon  $g - 2$  Hadronic Light-by-Ligh contribution. HLBL diagram (left). New sampling method (red) reduce the statistical noise from the previous method (black) by more than a factor of 10 at the same cost.

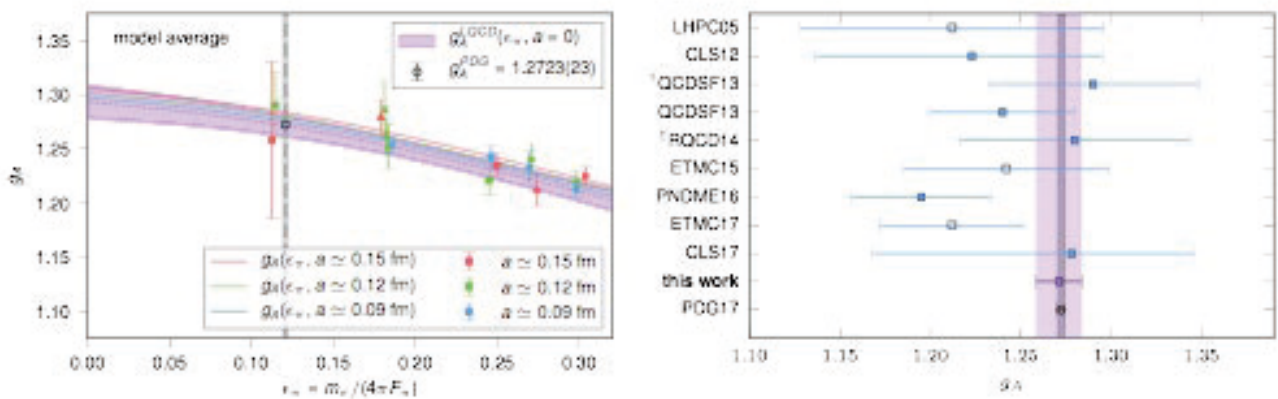


Fig. 2. Physical-point extrapolation for  $g_A$  (left), Summary of LQCD calculations (right) from Nature **558**, 91–94 (2018).

CKM theory for kaons and B mesons that include the new calculation of b-baryon decay,  $\Lambda_b \rightarrow p$ ; the electromagnetic properties of hadrons; the proton's and neutron's form factors and structure function including electric dipole moments; proton decay; nucleon form factors, which are related to the proton spin problem or neutrino-nucleon interaction; Neutron-antineutron oscillations; inclusive hadronic decay of  $\tau$  leptons; nonperturbative studies for beyond standard model such composite Higgs or dark matter models from strong strongly interacting gauge theories; a few-body nuclear physics and their electromagnetic properties; QCD thermodynamics in finite temperature/density systems such as those produced in heavy-ion collisions at the Relativistic Heavy Ion Collider; Quantum Information, Quantum Computing; and applications of machine learning in field theories.

The lifetime of the neutron is determined by its axial charge,  $g_A$ , which also governs pion exchange between nucleons. Member of RBRC (Rinaldi) and collaborators (including C. C. Chang of iTHEMS) carried out 1%-level accurate LQCD calculation of  $g_A$  for the first time by employing several innovative methods (such as unconventional extraction of the QCD matrix element using Feynman-Hellmann theorem, different sea- and valence quark actions, or the computational use of Graphic Processor Units). The paper was published in the Nature journal, was covered by many press releases, and also led to the Gordon Bell Prize finalist.

The RBRC group and its collaborators have emphasized the necessity and importance of precision calculations, which will provide stringent checks for the current understandings of nature, and will have a potential to find physics beyond the current standard model of fundamental physics. We have therefore adopted techniques that aim to control and reduce any systematic errors. This approach has yielded many reliable results, many of basic quantities are now computed within sub-percent accuracies.

The group also delivers several algorithmic breakthroughs, which speed up generic lattice gauge theory computation. These novel technique divides the whole calculation into frequent approximated calculations, and infrequent expensive and accurate calculation using lattice symmetries called All Mode Averaging (AMA), or a compression for memory needs by exploiting the local-coherence of QCD dynamics. Together with another formalism, zMobius fermion, which approximate chiral lattice quark action efficiently, the typical calculation is now improved by a couple of orders of magnitudes, and more than an order of magnitude less memory needs compared to the traditional methods. RBRC group and its collaborators also provide very efficient and generic code optimized to the state-of-arts CPU or GPU, and also improve how to efficiently generate QCD ensemble.

Table 1. Summary of current physics program and their impacts.

Theme	Significant Outcomes	Expected Impacts & Extensions
(a) DWF QCD ensemble generation and measurements of basic quantities	Hadron spectrum, $f_\pi, f_K, K_{I3}, B_K$ , and accurate ChPT Low Energy Constants (LECs)	Basis of physical observables
(b) Operator Renormalization	Precise matrix elements, bag parameters quark masses, and coupling constants	Reduced systematic error in <i>e.g.</i> $K \rightarrow \pi\pi$ amplitudes
(c) Computational Algorithms, Software, and Machines	Fast and Cost-Effective Computing All Mode Averaging (AMA) PhySyHCAI	Unprecedented precision and new physical quantities
(d) $K$ physics	$K_{I3}, \Delta I = 1/2, 3/2, K \rightarrow \pi\pi$ amplitudes, $\epsilon'/\epsilon$	New tests of the SM
(e) $B$ physics	$K_L - K_S$ Mass Difference, $\epsilon_K^{\text{LD}}$	
(f) QED and Isospin breaking effects	Matrix elements for (semi-)leptonic decays and $B^0 - \bar{B}^0$ oscillations	CKM matrix, <i>e.g.</i> , $V_{ub}, V_{ts}, V_{td}$ and R-ratios for LUV tests .
(g) Muon Anomalous Magnetic Moment $(g-2)_\mu$	Better determination of quark masses Proton-Neutron Mass Difference	A step towards sub-% precision groundwork for $(g-2)_\mu$
(h) Nucleon calculations for HEP	Hadronic Vacuum Polarization contribution Light-by-Light contribution	$(g-2)_\mu$ experiments at BNL, FNAL, J-PARC
	Vector/Axial form factors of nucleon Proton decay matrix element Nucleon EDM and $F_3(q^2)$ from vacuum angle $\theta$ and quark's (Chromo) EDM Parton Distribution Function	DUNE, Super-K, T2K GUT EDM experiments incl. ORNL, LANL Origin of matter in Universe LHC, Electron-Ion Colliders

## Members

### Group Leader

Taku IZUBUCHI

### Special Postdoctoral Researchers

Akio TOMIYA

Enrico RINALDI

### RBRC Researchers

Yasumichi AOKI (RIKEN BNL Fellow, KEK)  
Ethan NEIL (RHIC Physics Fellow)  
Stefan MEINEL (RHIC Physics Fellow)

Sergey SYRITSYN (RHIC Physics Fellow)  
Luchang JIN (RHIC Physics Fellow)

### Visiting Scientists

Thomas BLUM (Univ. of Connecticut)  
Chulwoo JUNG (BNL)  
Shigemi OHTA (KEK)  
Tomomi ISHIKAWA (Shanghai Jiao-Tong Univ.)  
Christoph LEHNER (BNL)

Meifeng LIN (BNL)  
Robert MAWHINNEY (Columbia Univ.)  
Hiroshi OKI (Nara Women's Univ.)  
Christopher KELLY (Columbia Univ.)

## List of Publications & Presentations

### Publications

#### [Journal]

#### (Original Papers) \*Subject to Peer Review

- E. Rinaldi, S. Syritsyn, M. L. Wagman, M. I. Buchoff, C. Schroeder, J. Wasem, "Lattice QCD determination of neutron-antineutron matrix elements with physical quark masses," arxiv:1901.07519, submitted to Phys. Rev. D. \*
- A. Nicholson, E. Berkowitz, H. Monge-Camacho, D. Brantley, N. Garron, C. C. Chang, E. Rinaldi, C. Monahan, C. Bouchard, M. A. Clark, B. Joo, T. Kurth, B. Tiburzi, P. Vranas, A. Walker-Loud, "Symmetries and interactions from lattice QCD," arxiv:1812.11127. \*
- E. Berkowitz, M. A. Clark, A. Gambhir, K. McElvain, A. Nicholson, E. Rinaldi, P. Vranas, A. Walker-Loud, C. C. Chang, B. Joo, T. Kurth, K. Orginos, "Simulating the weak death of the neutron in a femtoscale universe with near-Exascale computing," arxiv:1810.01609, Gordon Bell prize finalist \*
- E. Rinaldi, S. Syritsyn, M. L. Wagman, M. I. Buchoff, C. Schroeder, J. Wase, "Neutron-antineutron oscillations from lattice QCD," arxiv:1809.00246. \*

- T. Appelquist, R. C. Brower, G. T. Fleming, A. Gasbarro, A. Hasenfratz, X. -Y. Jin, E. T. Neil, J. C. Osborn, C. Rebbi, E. Rinaldi, D. Schaich, P. Vranas, E. Weinberg, O. Witzel, “Nonperturbative investigations of SU(3) gauge theory with eight dynamical flavors,” *Phys. Rev. D* **99**, 014509 (2019). \*
- C. Alexandrou, L. Leskovec, S. Meinel, J. Negele, S. Paul, M. Petschlies, A. Pochinsky, G. Rendon, S. Syritsyn, “ $\pi\gamma \rightarrow \pi\pi$  transition and the  $\rho$  radiative decay width from lattice QCD,” *Phys. Rev. D* **98**, 7, 074502 (2018). \*
- T. Izubuchi, Y. Kuramashi, C. Lehner, E. Shintani (PACS collaboration), “Finite-volume correction on the hadronic vacuum polarization contribution to muon  $g - 2$  in lattice QCD,” *Phys. Rev. D* **98**, 054505 (2018). \*
- P. Petreczky, T. Izubuchi, L. Jin, C. Kallidonis, N. Karthik, S. Mukherjee, C. Shugert, S. Syritsyn, “Pion structure from lattice QCD,” arXiv:1812.04334 \*
- T. Blum, P. A. Boyle, V. Gülpers, T. Izubuchi, L. Jin, C. Jung, A. Jüttner, C. Lehner, A. Portelli, J. T. Tsang (RBC and UKQCD Collaborations), “Calculation of the hadronic vacuum polarization contribution to the muon anomalous magnetic moment,” *Phys. Rev. Lett.* **121**, 022003 (2018). \* [Editors’ suggestion]
- C. C. Chang, A. Nicholson, E. Rinaldi, E. Berkowitz, N. Garron, D. Brantley, H. Monge-Camacho, C. Monahan, C. Bouchard, M. A. Clark, B. Joo, T. Kurth, K. Orginos, P. Vranas, A. Walker-Loud, “A per-cent-level determination of the nucleon axial coupling from quantum chromodynamics,” *Nature* **558**, 91–94 (2018). \*
- T. Izubuchi, X. Ji, L. Jin, I. W. Stewart, Y. Zhao, “Factorization theorem relating Euclidean and light-cone parton distributions,” *Phys. Rev. D* **98**, 056004 (2018). \*
- T. Appelquist, R. C. Brower, G. T. Fleming, A. Gasbarro, A. Hasenfratz, J. Ingoldby, J. Kiskis, J. C. Osborn, C. Rebbi, E. Rinaldi, D. Schaich, P. Vranas, E. Weinberg, O. Witzel, “Linear sigma EFT for nearly conformal gauge theories,” *Phys. Rev. D* **98**, 114510 (2018). \* [Editors’ suggestion]
- P. Boyle, R. Hudspeth, T. Izubuchi, A. Jüttner, C. Lehner, R. Lewis, K. Maltman, H. Ohki, A. Portelli, M. Spraggs (RBC and UKQCD Collaborations), “Novel  $|V_{us}|$  determination using inclusive strange  $\tau$  decay and lattice hadronic vacuum polarization functions,” *Phys. Rev. Lett.* **121**, 202003 (2018). \*
- A. Carosso, A. Hasenfratz, E. T. Neil, “Nonperturbative renormalization of operators in near-conformal systems using gradient flows,” *Phys. Rev. Lett.* **121**, 201601 (2018). \*
- K. Hashimoto, S. Sugishita, A. Tanaka, A. Tomiya, “Deep learning and holographic QCD,” *Phys. Rev. D* **98**, 106014 (2018). \*
- L. Jin, H-W. Lin *et al.*, “Proton isovector helicity distribution on the lattice at physical pion mass,” *Phys. Rev. Lett.* **121**, 24, 242003 (2018). \*
- X. Feng, L. -C. Jin, X. -Y. Tuo, S. -C. Xia, “Light-neutrino exchange and long-distance contributions to  $0 \nu 2 \beta$  decays: An exploratory study on  $\pi\pi \rightarrow ee$ ,” *Phys. Rev. Lett.* **122**, 022001 (2019). \*
- A. Nicholson, E. Rinaldi *et al.*, “Heavy physics contributions to neutrinoless double beta decay from QCD,” *Phys. Rev. Lett.* **121**, 172501 (2018). \*
- B. Chakraborty, E. Neil *et al.*, “Strong-isospin-breaking correction to the muon anomalous magnetic moment from lattice QCD at the physical point,” *Phys. Rev. Lett.* **120**, 152001 (2018). \*
- V. Ayyar, T. DeGrand, M. Golterman, D. C. Hackett, W. I. Jay, E. T. Neil, Y. Shamir, B. Svetitsky, “Spectroscopy of SU(4) composite Higgs theory with two distinct fermion representations,” *Phys. Rev. D* **97**, 074505 (2018). \*
- A. Bazavov, E. Neil *et al.*, “Short-distance matrix elements for  $D^0$ -meson mixing for  $N_f = 2 + 1$  lattice QCD,” *Phys. Rev. D* **97**, 034513 (2018). \*
- S. Meinel, “ $\Lambda_c \rightarrow N$  form factors from lattice QCD and phenomenology of  $\Lambda_c \rightarrow n\ell^+ \nu_\ell$  and  $\Lambda_c \rightarrow p\mu^+ \mu^-$  decays,” *Phys. Rev. D* **97**, 034511 (2018). \*
- N. Hasan, J. Green, S. Meinel, M. Engelhardt, S. Krieg, J. Negele, A. Pochinsky, S. Syritsyn, “Computing the nucleon charge and axial radii directly at  $Q^2 = 0$  in lattice QCD,” *Phys. Rev. D* **97**, 034504 (2018). \*
- E. Rinaldi, E. Berkowitz, M. Hanada, J. Maltz, P. Vranas, “Toward holographic reconstruction of bulk geometry from lattice simulations,” *J. High Energy Phys.* **1802**, 042 (2018). \*
- J. -W. Chen, L. Jin, H. -W. Lin, Y. -S. Liu, Y. -B. Yang, J. -H. Zhang, Y. Zhao, “Lattice calculation of parton distribution function from LaMET at physical pion mass with large nucleon momentum,” *Phys. Rev. Lett.* **121**, 242003 (2018). \*
- J. -W. Chen, L. Jin *et al.*, “Kaon distribution amplitude from lattice QCD and the flavor SU(3) symmetry,” *Nucl. Phys. B* **939**, 429–446 (2019). \*
- J. -W. Chen, T. Ishikawa, L. Jin, H. -W. Lin, A. Schäfer, Y. -B. Yang, J. -H. Zhang, Y. Zhao, “Gaussian-weighted parton quasi-distribution,” *Sci. China Phys. Mech. Astron.* **62**, 991021 (2019).
- J. -W. Chen, T. Ishikawa, L. Jin, H. -W. Lin, Y. -B. Yang, J. -H. Zhang, Y. Zhao, “Parton distribution function with nonperturbative renormalization from lattice QCD,” *Phys. Rev. D* **97**, 014505 (2018). \*
- K. Hashimoto, S. Sugishita, A. Tanaka, A. Tomiya, “Deep learning and holographic QCD,” *Phys. Rev. D* **98**, 106014 (2018).
- K. Kashiwa, Y. Kikuchi, A. Tomiya, “Phase transition encoded in neural network,” arXiv:1812.01522. \*

### [Proceedings]

#### (Original Papers) \*Subject to Peer Review

USQCD Collaboration (V. Cirigliano, T. Izubuchi, S. Syritsyn *et al.*), “The role of lattice QCD in searches for violations of fundamental symmetries and signals for new physics,” arXiv:1904.09704 [hep-lat].

K. Maltman, T. Izubuchi, H. Ohki *et al.*, “Current status of inclusive hadronic  $\tau$  determinations of  $|V_{us}|$ ,” *SciPost Phys. Proc.* **1**, 006 (2019).

- S. Syritsyn, T. Izubuchi, H. Ohki, “Calculation of nucleon electric dipole moments induced by quark chromo-electric dipole moments and the QCD  $\theta$ -term,” arXiv:1901.05455 [hep-lat].
- J. -S. Yoo, Y. Aoki, T. Izubuchi, S. Syritsyn, “Proton decay matrix element on the lattice with physical pion mass,” PoS LATTICE2018, **187**, (2019).
- M. Bruno, T. Izubuchi, C. Lehner, A. Meyer, “On isospin breaking in  $\tau$  decays for  $(g-2)_\mu$  from lattice QCD,” Proc. Sci. **LATTICE2018**, 135 (2018).
- S. Syritsyn, T. Izubuchi, H. Ohki, “Progress in the nucleon electric dipole moment calculations in lattice QCD,” arXiv:1810.03721.
- P. Boyle, R. J. Hudspith, T. Izubuchi, A. Jüttner, C. Lehner, R. Lewis, K. Maltman, H. Ohki, A. Portelli, M. Spraggs, “ $|V_{us}|$  determination from inclusive strange tau decay and lattice HVP,” EPJ Web Conf. **175**, 13011 (2018).
- S. Hashimoto, B. Colquhoun, T. Izubuchi, T. Kaneko, H. Ohki, “Inclusive  $B$  decay calculations with analytic continuation,” EPJ Web Conf. **175**, 13006 (2018).
- M. Abramczyk, S. Aoki, T. Blum, T. Izubuchi, H. Ohki, S. Syritsyn, “Computing nucleon EDM on a lattice,” EPJ Web Conf. **175**, 06027 (2018).
- T. Izubuchi, Y. Kuramashi, C. Lehner, E. Shintani, “Lattice study of finite volume effect in HVP for muon  $g-2$ ,” EPJ Web Conf. **175**, 06020 (2018).
- S. Syritsyn, “Nucleon EDM on a lattice at the physical point,” LATTICE 2018, July 22–28, 2018; to be published in Proc. Sci. Confinement.
- M. Engelhardt, J. Green, N. Hasan, S. Krieg, S. Meinel, J. Negele, J. Negele, A. Pochinsky, S. Syritsyn, “Quark orbital angular momentum in the proton evaluated using a direct derivative method,” Proc. Sci. **SPIN2018**, 047 (2019).
- S. Paul, G. Silvi, C. Alexandrou, G. Koutsou, S. Krieg, L. Leskovec, S. Meinel, J. Negele, M. Petschlies, A. Pochinsky, G. Rendon, S. Syritsyn, “Towards the P-wave nucleon-pion scattering amplitude in the  $\Delta(1232)$  channel,” Proc. Sci. **LATTICE2018**, 089 (2018).
- G. Rendon, L. Leskovec, S. Meinel, J. Negele, S. Paul, M. Petschlies, A. Pochinsky, G. Silvi, S. Syritsyn, “ $K\pi$  scattering and the  $K^*(892)$  resonance in  $2+1$  flavor QCD,” Proc. Sci. **LATTICE2018**, 073 (2018).
- L. Leskovec, C. Alexandrou, S. Meinel, J. W. Negele, S. Paul, M. Petschlies, A. Pochinsky, G. Rendon, S. Syritsyn, “Calculating the  $\rho$  radiative decay width with lattice QCD,” Proc. Sci. **LATTICE2018**, 065 (2018).
- C. Kallidonis, S. Syritsyn, M. Engelhardt, J. Green, S. Meinel, J. Negele, A. Pochinsky, “Nucleon electromagnetic form factors at high  $Q^2$  from Wilson-clover fermions,” Proc. Sci. **LATTICE2018**, 125 (2018).
- L. Leskovec, C. Alexandrou, S. Meinel, J. W. Negele, S. Paul, M. Petschlies, A. Pochinsky, G. Rendon, S. Syritsyn, “A lattice QCD study of the  $\rho$  resonance,” CIPANP 2018, (2018).
- S. Paul, C. Alexandrou, L. Leskovec, S. Meinel, J. Negele, M. Petschlies, A. Pochinsky, G. Rendon, S. Syritsyn, “ $\pi\pi$  P-wave resonant scattering from lattice QCD,” EPJ Web Conf. **175**, 05022 (2018).
- K Suzuki, S. Aoki, Y. Aoki, G. Cossu, H. Fukaya, S. Hashimoto (JLQCD Collaboration), “Axial  $U(1)$  symmetry at high temperature in 2-flavor lattice QCD,” EPJ Web of Conferences **175**, 07025-1–8 (2018).
- S. Aoki, Y. Aoki, G. Cossu, H. Fukaya, S. Hashimoto, K. Suzuki, “Topological susceptibility in  $N_f = 2$  QCD at finite temperature,” EPJ Web of Conferences **175**, 07024-1–8 (2018).
- C. Rohrhofer, Y. Aoki, G. Cossu, H. Fukaya, L. Ya. Glozman, S. Hashimoto, C. B. Lang, S. Prelovsek, “Degeneracy of vector-channel spatial correlators in high temperature QCD,” EPJ Web of Conferences **175**, 07029-1–8 (2018).
- Y. Aoki, T. Aoyama, E. Bennett, M. Kurachi, T. Maskawa, K. Miura, K. Nagai, H. Ohki, E. Rinaldi, A. Shibata, K. Yamawaki, T. Yamazaki, “Flavor-singlet spectrum in multi-flavor QCD,” EPJ Web Conf. **175**, 01008 (2018).
- E. Berkowitz, A. Nicholson, C. C. Chang, E. Rinaldi, M. A. Clark, B. Joo, T. Kurth, P. Vranas, A. Walker-Loud, “Calm multi-baryon operators,” EPJ Web Conf. **175**, 08023 (2018).
- E. Rinaldi, E. Berkowitz, M. Hanada, J. Maltz, P. Vranas, “Toward holographic reconstruction of bulk geometry from lattice simulations,” EPJ Web Conf. **175**, 05029 (2018).

## Oral Presentations

### [International Conference etc.]

- T. Izubuchi (invited), “Hadronic contributions to muon  $g-2$ ,” Frontiers in Lattice QCD and related topics, Kyoto Univ. Yukawa Institute, April 15–26, 2019.
- T. Izubuchi, “Lattice QCD studies of muon  $g-2$  and tau decay,” 6th KEK Flavor Factory Workshop (KEK-FF 2019), KEK, February 16, 2019.
- T. Izubuchi, “Precise calculation of muon  $g-2$  based on lattice QCD,” Massively parallel programming from Quantum Chemistry and Physics 2019, Kobe, RIKEN AICS, January 16, 2019.
- T. Izubuchi (invited seminar), “ $|V_{us}|$  from  $\tau$ ,” Columbia University, January 28, 2019.
- T. Izubuchi, “ $|V_{us}|$  from taus (LQCD),” invited talk, 10th International Workshop on the CKM Unitarity Triangle CKM2018, September 17–21, 2018.
- T. Izubuchi (invited seminar), “Hadronic contributions to muon  $g-2$ —LQCD confronting the most precise experiments—,” Department of Theoretical Physics (DTP), Tata Institute of Fundamental Research (TIFR), Mumbai, India, April 26, 2018.
- T. Izubuchi, “Nuclear form factor calculation using DWQCD,” 36th International Symposium on Lattice Field Theory (Lattice 2018), at Lansing, MI, July 23–28, 2018.

- S. Meinel (invited), “ $B \rightarrow K^* \ell \ell$  from lattice QCD,” 6th KEK Flavor Factory Workshop, Tsukuba, Japan, February 15, 2019.
- S. Meinel (Invited parallel talk), “Exclusive semileptonic  $b$  baryon decays from lattice QCD,” 10th International Workshop on the CKM Unitarity Triangle (CKM 2018), University of Heidelberg, Germany, September 18, 2018.
- S. Meinel (Invited), “Form factors for  $b$  hadron decays from lattice QCD,” Frontiers in Lattice Quantum Field Theory, IFT, Madrid, Spain, May 28, 2018.
- S. Meinel, “Flavor physics with charm and bottom baryons, Invited seminar,” Cosmology Seminar, Arizona State University, Tempe, AZ, May 2, 2018.
- S. Meinel (invited), “Opportunities for lattice QCD in quark and lepton flavor physics,” USQCD All Hands Meeting, Fermilab, Batavia, IL, April 20, 2018.
- S. Meinel (invited), “ $\Lambda_b \rightarrow \Lambda_c^{(*)}$  form factors from lattice QCD,” Challenges in Semileptonic  $B$  Decays, MITP, Mainz, Germany, April 9, 2018.
- S. Syritsyn, “Nucleon electric dipole moments from Lattice QCD,” Theory Seminar, University of Maryland, October 11, 2018.
- S. Syritsyn (invited), “Progress on the nucleon EDM in lattice QCD,” XIIIth Quark Confinement and Hadron Spectrum, Maynooth University, Ireland, July 31–August 6, 2018.
- Y. Aoki, “QCD phase transition,” (invited), International Workshop on Massively Parallel Programming for Quantum Chemistry and Physics 2019, Kobe, Japan, January 15, 2019.
- Y. Aoki (invited), “Topology and axial  $U(1)$  symmetry in two-flavor hot QCD, lattice and functional techniques for exploration of phase structure and transport properties in quantum chromodynamics,” Dubna, Russia, September 5, 2018.
- Y. Aoki, “Topological susceptibility in  $N_f = 2$  QCD at finite temperature—volume study,” Lattice 2018, East Lansing, MI, USA, July 24, 2018.
- Y. Aoki (invited), “Lattice QCD and hadron structure,” DIS 2018, Kobe, Japan, April 16, 2018.
- L. Jin (plenary), The 36th Annual International Symposium on Lattice Field Theory (LATTICE 2018), July 2018.
- L. Jin (invited), Second Plenary Workshop of the Muon  $g - 2$  Theory Initiative, Mainz, June 2018.
- L. Jin (invited), First Workshop of the Muon  $g - 2$  Theory Initiative, Q Center, June 2017.
- L. Jin (invited), QCD Evolution 2017, Jefferson Lab, May 2017.
- L. Jin (invited), Lattice PDF Workshop, University of Maryland, April 2018.
- E. Neil, “Non-perturbative renormalization in Monte Carlo simulations using gradient flow,” CTQM Seminar, University of Colorado, Boulder, CO, February 2019.
- E. Neil, “Light composite scalar from  $N_f = 8$  lattice gauge theory,” Continuum and Lattice Approaches to the Infrared Behavior of Conformal and Quasi-Conformal Gauge Theories, Simons Center for Geometry and Physics, Stony Brook, NY, January 2018.
- E. Rinaldi (invited seminar), “The neutron lifetime with near-Exascale computing,” Computational Science Initiative, BNL, Upton, NY, January 2019.
- E. Rinaldi (invited seminar), “First- principles lattice QCD calculations of the neutron beta decay: challenges and prospects,” Institut für Kernphysik, Forschungszentrum, Jülich, Germany, December 2018.
- E. Rinaldi (invited), “First-principles lattice QCD calculations of the neutron beta decay: challenges and prospects,” Particle Physics with Neutrons at ESS, Nordita University, Stockholm, Sweden, December 2018.
- E. Rinaldi (invited), “Lattice calculations for neutron-antineutron oscillations,” Particle Physics with Neutrons at ESS, Nordita University, Stockholm, Sweden, December 2018.
- E. Rinaldi (invited seminar), “Illuminating dark matter with supercomputers,” York University, Toronto, Canada, November 2018.
- E. Rinaldi (invited), “First-principles QCD calculation of the neutron lifetime,” Beta Decay as a Probe of New Physics, the Amherst Center for Fundamental Interactions, University of Massachusetts, Amherst, MA, November 2018.
- E. Rinaldi (invited seminar), “New results on strongly-coupled theories near the conformal window,” University of Rome 3, Rome, Italy, October 2018.
- E. Rinaldi (invited seminar), “Beyond the Standard Model physics with lattice simulations,” University of Milan Bicocca, Milan, Italy, October 2018.
- E. Rinaldi (invited), “Lattice composite dark matter,” Interdisciplinary approach to QCD-like composite dark matter, ECT\*, Trento, Italy, October 2018.
- E. Rinaldi, “Ungauging the gauge/gravity duality,” Quantum Gravity meets Lattice QFT, ECT\*, Trento, Italy, September 2018.
- E. Rinaldi, “Neutron-antineutron oscillations,” Lattice 2018, Michigan State University, USA, July 2018.
- E. Rinaldi, “First-principles lattice QCD calculation of the neutron lifetime,” ICHEP2018, Seoul, South Korea, July 2018.
- E. Rinaldi (invited seminar), “New results on strongly-coupled theories near the conformal window,” Tsukuba University, Tsukuba, Japan, June, 2018.
- E. Rinaldi, “Composite Dark Matter,” CIPANP18, Palm Springs, CA, USA, June, 2018.
- E. Rinaldi (invited seminar), “How to test the gauge/gravity duality with lattice simulations,” New York University, New York, NY, USA, May 2018.
- E. Rinaldi (invited), “High-precision tests of the gauge/gravity duality and future applications,” Lattice for Beyond the Standard Model Physics (LBSM18), University of Colorado, Boulder, CO, USA, April 2018.
- T. Akio, “Towards reduction of autocorrelation in HMC by machine learning,” Bielefeld university, October 2018.
- T. Akio, “Detection of phase transition via convolutional neural networks,” Regenceburg university, October 2018.

- T. Akio, “Chiral phase transition of three flavor QCD with nonzero magnetic field using standard HISQ,” Eötvös Loránd University, October 2018.
- T. Akio, “Chiral phase transition of three flavor QCD with nonzero magnetic field using standard HISQ,” Oskaka University, November 2018.
- T. Akio, “Chiral phase transition of three flavor QCD with nonzero magnetic field using standard HISQ,” Tsukuba University, November 2018.

**[Domestic Conference]**

- 青木保道, 「QCD 相転移—現状と解明に向けて」, 素粒子・原子核・宇宙「京からポスト京に向けて」, シンポジウム 2018, 筑波大学東京キャンパス, 東京, 2019 年 1 月 9 日.
- 青木保道, 「QCD の有限温度相転移とトポロジー—サブ課題 A「QCD 相転移」—」, 重点課題 9 研究報告会, 筑波大学 CCS, 茨城, 2018 年 10 月 3 日.
- 青木保道, 「2 フレーバー格子 QCD の高温相におけるディラックスペクトルと軸性 U(1) 対称性」, 日本物理学会 2018 年秋期大会, 信州大学, 長野, 2018 年 9 月 16 日.
- 青木保道, 「有限温度 2 フレーバー QCD のトポロジカル感受率—有限体積効果」, 日本物理学会 2018 年秋期大会, 信州大学, 長野, 2018 年 9 月 16 日.
- 青木保道, 「有限温度 QCD : 相転移, トポロジー, axion」, YITPPPP2018, (招待講演), 京都大学, 京都, 2018 年 8 月 9 日.
- 青木保道, “Topology and axial U(1) symmetry at high temperature in  $N_f = 2$  QCD,” セミナー, 理研 AICS, 兵庫, 2018 年 1 月 15 日.

## Subnuclear System Research Division RIKEN Facility Office at RAL

### 1. Abstract

Our core activities are based on the RIKEN-RAL Muon Facility located at the ISIS Neutron & Muon Source at the Rutherford Appleton Laboratory (UK), which provides intense pulsed-muon beams. The RIKEN-RAL Muon Facility is a significant and long-standing collaboration between RIKEN and RAL in muon science.

Muons have their own spins with 100% polarization, and can detect local magnetic fields and their fluctuations at muon stopping sites very precisely. The method to study the characteristics of materials by observing time dependent changes of muon spin polarization is called “Muon Spin Rotation, Relaxation and Resonance” ( $\mu$ SR method), and is applied to study electro-magnetic properties of insulating, metallic, magnetic and superconducting systems. Muons reveal static and dynamic properties of the electronic state of materials in the zero-field condition, which is the ideal magnetic condition for research into magnetism. For example, we have carried out  $\mu$ SR investigations on a wide range of materials including frustrated pyrochlore systems, which have variety of exotic ground states of magnetic spins, so the magnetism study of this system using muon is quite unique.

The ultra-cold muon beam can be stopped in thin foil, multi-layered materials and artificial lattices, which enables us to apply the  $\mu$ SR techniques to surface and interface science. The development of an ultra-cold muon beam is also very important as a source of pencil-like small emittance muon beam for muon  $g - 2$ /EDM measurement. We have been developing muonium generators to create more muonium atoms in vacuum even at room temperature to improve beam quality compared with the conventional hot-tungsten muonium generator. We have demonstrated a strong increase in the muonium emission efficiency by fabricating fine laser drill-holes on the surface of silica aerogel. We are also developing a high power Lyman-alpha laser in collaboration with the Advanced Photonics group at RIKEN. The new laser will ionize muoniums 100 times more efficiently for slow muon beam generation.

Over the past 2–3 years, a significant development activity in muon elemental analysis has taken place, proton radius experiments have continued and been developed, and chip irradiation experiments have also continued.

### 2. Major Research Subjects

- (1) Materials science by muon-spin-relaxation method and muon site calculation
- (2) Development of elemental analysis using pulsed negative muons
- (3) Nuclear and particle physics studies via muonic atoms and ultra-cold muon beam
- (4) Other muon applications

### 3. Summary of Research Activity

#### (1) Material Science at the RIKEN-RAL Muon Facility

Muons have their own spins with 100% polarization, and can detect local magnetic fields and their fluctuations at muon stopping sites very precisely. The  $\mu$ SR method is applied to studies of newly fabricated materials. Muons enable us to conduct (1) material studies under external zero-field condition, (2) magnetism studies with samples without nuclear spins, and (3) measurements of muon spin relaxation changes at wide temperature range with same detection sensitivity. The detection time range of local field fluctuations by  $\mu$ SR is  $10^{-6}$  to  $10^{-11}$  second, which is an intermediate region between neutron scattering method ( $10^{-10}$ – $10^{-12}$  second) and Nuclear Magnetic Resonance (NMR) (longer than  $10^{-6}$  second). At Port-2 and 4 of the RIKEN-RAL Muon Facility, we have been performing  $\mu$ SR researches on strong correlated-electron systems, organic molecules, energy related materials and biological samples to study electron structures, superconductivity, magnetism, molecular characters and crystal structures.

Among our scientific activities on  $\mu$ SR studies from year 2016 to 2019, following subjects of material sciences are most important achievements at the RIKEN-RAL muon facility:

- (1) Novel superconducting state having the steeper nodal gaps in the quasi two-dimensional organic superconductor  $\lambda$ -[BETS]<sub>2</sub>GaCl<sub>4</sub>
- (2) Tiny magnetic moments and spin structures of Ir<sup>4+</sup> in hole-doped pyrochlore iridates Y<sub>1.95-y</sub>Cu<sub>0.05</sub>Ca<sub>y</sub>Ir<sub>2</sub>O<sub>7</sub> and Eu<sub>2-x</sub>Ca<sub>x</sub>Ir<sub>2</sub>O<sub>7</sub>
- (3) Magnetism and spin structure in superoxide CsO<sub>2</sub>, RbO<sub>2</sub> and NaO<sub>2</sub>
- (4) Magnetic properties of the nano-cluster gold in the border of macro- and micro-scale
- (5) Novel magnetic properties of nano-size La-based high- $T_c$  superconducting cuprates
- (6) Effects of the spatial distributions of magnetic moments and muon positions estimated from density functional theory (DFT) and dipole-field calculations
- (7) Measurement of Li and Na ion diffusion in battery materials
- (8) Muon as a probe of hydrogen behavior in functional and energy materials
- (9) Negative muon SR application to internal field measurement

Result-(1) We developed a novel method to determine the superconducting gap structure in conjunction with the density functional theory calculations. It was concluded that the two-dimensional organic superconductor  $\lambda$ -[BETS]<sub>2</sub>GaCl<sub>4</sub> has a steeper superconducting gap and clear line nodes showing both the  $s$ -wave and  $d$ -wave characters. Result-(2) Doped hole effects on the magnetic properties of corner-shared magnetic moments on pyrochlore systems gave us new interpretations to understand exotic phenomena, like the quantum criticality of magnetic moments and a quasi-magnetic monopole state. Result-(3) In CsO<sub>2</sub>, we confirmed a novel coexisting state of the so-called spin-liquid state and a magnetically ordered state of magnetic moment which are on the  $\pi$ -orbital of oxygen atoms.

We also observed the spin-gap state in  $\text{NaO}_2$ . Those findings open a new scheme of quantum magnetic properties of  $\pi$  electrons on light elements. Result-(4) and (5) The nano-size effect show a new scheme of electronic properties of metallic element. The gold is the most typical example to have a possibility to possess magnetic properties due to the nano-size effect. We confirmed that the nano-gold cluster can have free electronic moment on one nano-cluster. The same nano-size effect was tested on the La-based high- $T_c$  superconducting oxide. The severe restriction on the magnetic interaction is expected to provide novel effects on the magnetic and superconducting properties of the high- $T_c$  superconducting oxide. We confirmed the reduction in the magnetic interaction and the disappearance of the superconducting state by decreasing the size of the particle size. Result-(6) Well known and deeply investigated  $\text{La}_2\text{CuO}_4$  has opened a new scheme of the Cu spin. Taking into account quantum effects to expand the Cu-spin orbital and muon positions, we have succeeded to explain newly found muon sites and hyperfine fields at those sites. Result-(7) Movement of ions is an essential requirement for an efficient battery. The  $\mu\text{SR}$  has been actively used to measure the ion hopping rate in microscopic level in Li- and Na-ion batteries. We also started a study of macroscopic Li movement from its depth dependent concentration using negative muons. Result-(8) Muon shows similar behavior as hydrogen in materials and its behavior can be measured even at very low concentration. Thus  $\mu\text{SR}$  was applied to understand energy and functional materials such as graphene,  $\text{TiO}_2$  catalyst and hydrogen storage materials. Result-(9) Recently a clear Kubo-Toyabe-type relaxation was observed for negative muons captured by Mg. This will open the door to studying the dynamic behavior of light elements in solids with  $\mu^-$ SR from a fixed viewpoint of the nucleus.

We have been developing muon activities in Asian countries. We enhanced international collaborations to organize new  $\mu\text{SR}$  experimental groups and to develop muon-site calculation groups using computational method. We renewed MOU with Universiti Sains Malaysia (USM) in order to develop activities on the muon-site calculation. We are also continuing collaborations in  $\mu\text{SR}$  experiments on strongly correlated systems with researchers from Taiwan and Korea including graduate students. We are starting to collaborate with the new Chinese muon group who are developing the Chinese Muon Facility and trying to develop more muon activities in the Asian area.

## (2) Development of elemental analysis using pulsed negative muons

There has been significant development of elemental analysis using negative muons on Port 4 and Port 1 over the past couple of years. Currently, elemental analysis commonly uses X-ray and electron beams, which accurately measure surfaces. However a significant advantage of muonic X-rays over those of electronic X-rays is their higher energy due to the mass of the muon. These high energy muonic X-rays are emitted from the bulk of the samples without significant photon self-absorption. The penetration depth of the muons can be varied by controlling the muon momentum, providing data from a thin slice of sample at a given depth. This can be over a centimetre in iron, silver and gold or over 4 cm in less dense materials such as carbon.

Some techniques for elemental analysis are destructive or require the material under investigation to undergo significant treatment and some of the techniques are only sensitive to the surface. Therefore, negative muons offer a unique service in which they can measure inside, beyond the surface layer and completely non-destructively.

The areas of science that have used negative muons for elemental analysis have been very diverse. The largest area is the cultural heritage community as the non-destructive ability is particularly important and will become more so. This community have investigated swords from different eras, coins (Roman gold and silver, Islamic silver and from the Tudor Warship Mary Rose), Bronze Age tools and cannon balls. In addition, energy materials (Li composition for hydrogen storage), bio-materials (search for iron to potentially help understand Alzheimer's), engineering alloys (manufacturing processes for new materials for jet engines), and functional materials (surface effects in piezo electrics) have also been investigated.

## (3) Ultra-cold (low energy) Muon Beam Generation and Applications

Positive muon beam with thermal energy has been produced by laser ionization of muonium (bound system of  $\mu^+$  and electron) emitted from a hot tungsten surface with stopping surface muon beam at Port-3. The method generates a positive muon beam with acceleration energy from several 100 eV to several 10 keV, small beam size (a few mm) and good time resolution (less than 8 nsec). By stopping the ultra-cold muon beam in thin foil, multi-layered materials and artificial lattices, we can precisely measure local magnetic field in the materials, and apply the  $\mu\text{SR}$  techniques to surface and interface science. Since there has been no appropriate probe to study magnetism at surface and interface, the ultra-cold muon beam will open a new area of these research fields. In addition, the development of ultra-cold muon beam is very important as the source of ultra-cold (pencil-like small emittance) muon beam for muon  $g - 2/\text{EDM}$  measurement. It is essential to increase the slow muon beam production efficiency by 100 times for these applications. There are three key techniques in ultra-cold muon generation: production of thermal muonium, high intensity Lyman-alpha laser and the ultra-cold muon beam line.

A high-power Lyman-alpha laser was developed in collaboration with the Advanced Photonics group at RIKEN. The new laser system is used at J-PARC U-line and, upon completion, will ionize muoniums 100 times more efficiently for slow muon beam generation. In this development, we succeeded to synthesize novel ceramic-based Nd:YAG crystal, which realized a highly efficient and stable laser system. However, larger size crystal than presently available is needed for full design power, and we are working hard to improve the crystal.

We also succeeded in developing an efficient muonium generator, laser ablated silica aerogel, which emits more muoniums into vacuum even at room temperature. In 2013 at TRIUMF, by utilizing positron tracking method of muon decay position, we demonstrated at least 10 times increase of the muonium emission efficiency by fabricating fine laser drill-holes on the surface of silica aerogel. Further study was carried out in 2017 to find the optimum fabrication that will maximize the muonium emission. An alternative detection method using muonium spin rotation, which will be sensitive even to muoniums near the surface, was tested at RIKEN-RAL in 2018 and was found successful.

In RIKEN-RAL Port 3, the ultra-cold muon beam line, which had been designed with hot tungsten, was completely rebuilt to use advantage of the new room temperature silica aerogel target. The equipment was tested with surface muon beam and basic data such as muon stopping in aerogel were taken. We are waiting the laser crystal development in order to proceed to ultra-cold muon generation. A similar target design will be adopted in the ultimate cold muon source planned for muon  $g - 2$ /EDM at J-PARC.

#### (4) Other Fundamental Physics Studies

A measurement of the proton radius using muonic hydrogen at PSI revealed that the proton charge radius is surprisingly smaller than the radius measured using normal hydrogen spectroscopy and e-p scattering by more than 5 times their experimental precision. In contrast to the conventional measurement by means of electron, the PSI experiment utilized muonic hydrogen atom, and measured two different allowed transitions from one of the 2S levels to one of the 2P levels. The muonic atom has larger sensitivity to the proton radius because the negative muon orbits closer to the proton, although there is no reason why these measurements can yield inconsistent results if there exists no exotic physics or unidentified phenomenon behind. The cause of the discrepancy is not understood yet, thus a new measurement with independent method is much anticipated.

We proposed the measurement of the proton radius by using the hyperfine splitting of the muonic hydrogen ground state. This hyperfine splitting is sensitive to the Zemach radius, which is a convolution of charge and magnetic-dipole distributions inside proton. We are planning to re-polarize the muonic hydrogen by a circularly polarized excitation laser (excites one of the  $F = 1$  states and regenerates the muon spin polarization), and detect the recovery of the muon decay-asymmetry along the laser.

At RIKEN, we are developing dedicated laser system (mid-infrared high-power pulse laser system at around  $6 \mu\text{m}$ ). We have tested the efficiency of our wavelength conversion scheme. We are going to test band-width narrowing using a seed laser of (Quantum Cascade Laser) and the laser reflection cavity. Preparation using muon beam is also in progress. We measured the muon stopping distribution in low-density hydrogen-gas cell, which gave us consistent results with beam simulation. The study of the beam originated background level gives us reasonably small level, in which we can conduct a precision measurement. Another key is the lifetime of the polarized triplet muonic hydrogen state. We successfully observed the muon spin precession of muonic deuterium atom in 2018 for the first time in the world, from which we can set limit on the lifetime. The measurement with muonic protium is planned in 2019.

#### (5) Other topics

RIKEN and ISIS have signed a new collaboration agreement for the period 2018–2023. This is the fourth in a continuous series of agreements, the first being signed in 1990, resulting in a partnership which will have lasted over 30 years. Under the new agreement, ownership and operation of the facility pass to ISIS, a refurbishment programme of the facility will be undertaken, a user programme for Japanese scientists will continue, and the partnership between RIKEN and ISIS will be continued. The RIKEN-RAL collaboration is regularly highlighted as a good example of UK-Japanese science partnership at the UK-Japan Joint Committee on Science and Technology (chaired by the UK Chief Scientific Advisor to Government and a counterpart from Japan) — for example, Dr. King and Dr. Watanabe presented RIKEN-RAL at the November 2016 meeting of the Committee. The RIKEN-RAL collaboration has also enabled the development of collaborative activity between RIKEN and other Asian universities, *e.g.* through several MoUs with Indonesian and Malaysian universities.

## Members

### Director

Philip KING

### Research Scientist

Isao WATANABE (concurrent: Meson Science Lab.)

### Contract Researcher

Katsuhiko ISHIDA (concurrent: Meson Science Lab.)

### Administration Manager

Kazushige FUKUSHIMA (concurrent: Nishina Center and iTHEMS Promotion Office)

## List of Publications & Presentations

### Publications

#### [Journal]

#### (Original Papers) \*Subject to Peer Review

Q. Awan, J. Ahmad, Q. Sun, W. Hub, A. Berlie, Y. Liu, “Structure, dielectric and ferroelectric properties of lead-free (Ba, Ca)(Ti, Zr)O<sub>3-x</sub>BiErO<sub>3</sub> piezoelectric ceramics,” *Ceram. Int.* **44**, 6872–6877 (2018).

Darminto, R. Asih, Kurniasari, M. A. Baqia, S. Mustofa, Suasmoro, T. Kawamata, K. Kato, I. Watanabe, Y. Koike, “Enhanced magnetism by temperature induced defects in reduced graphene oxide prepared from coconut shells,” *IEEE Transactions on Magnetics* **54**, 1600105-1–5 (2018).

- W. Liao *et al.*, “Measurement and mechanism investigation of negative and positive muon-induced upsets in 65-nm bulk SRAMS,” IEEE Trans. Nucl. Sci **65** (2018) 1734. \*
- R. Bethany, McBride, J. Lieschke, A. Berlie, D. L. Cortie, H. Y. Playford, T. Lu, N. Narayanan, R. L. Withers, D. Yu, Y. Liu, “Study of the B-site ion behaviour in the multiferroic perovskite bismuth iron chromium oxide,” J. App. Phys. **123**, 154104 (2018).
- E. Mocchiutti *et al.* (FAMU collaboration), “First FAMU observation of muon transfer from mup atoms to higher-Z elements,” J. Instrum. **13**, 02019 (2018). \*
- A. Adamczak *et al.* (FAMU collaboration), “The FAMU experiment at RIKEN-RAL to study the muon transfer rate from hydrogen to other gases,” J. Instrum. **13**, 12033 (2018). \*
- Y. Sassa, M. Mansson, O. K. Forslund, O. Tjernberg, V. Pomjakushin, O. Ofer, E. J. Ansaldo, J. H. Brewer, I. Umegaki, Y. Higuchi, Y. Ikedo, H. Nozaki, M. Harada, I. Watanabe, H. Sakurai, J. Sugiyama, “The metallic quasi-1D spin-density-wave compound  $\text{NaV}_2\text{O}_4$  studied by angle-resolved photoelectron spectroscopy,” J. Electron Spectrosc. Relat. Phenom. **224**, 79–83 (2018).
- R. Asih, N. Adam, S. S. Mohd-Tajudin, D. P. Sari, K. Matsuhira, H. Guo, M. Wakeshima, Y. Hnatsu, T. Nakano, Y. Nozue, S. Slaiman, M. I. Mohamed-Ibrahim, P. K. Biswas, I. Watanabe, “Magnetic moments and ordered states in pyrochlore irridates  $\text{Nd}_2\text{Ir}_2\text{O}_7$  and  $\text{Sm}_2\text{Ir}_2\text{O}_7$  studies by muon-spin relaxation,” J. Phys. Soc. Jpn. **86**, 240705 (2018).
- M. Miyajima, F. Astuti, T. Kakuto, A. Matsuo, D. P. Sari, R. Asih, K. Okunishi, T. Nakano, Y. Nozue, K. Kindo, I. Watanabe, T. Kambe, “Magnetism and high-magnetic field magnetization in alkali superoxide  $\text{CsO}_2$ ,” J. Phys. Soc. Jpn. **87**, 063704-1–4 (2018).
- T. Suzuki, K. Katayama, I. Kawasaki, I. Watanabe, H. Tanaka, “Spin fluctuations in the spin-1/2 kagome lattice antiferromagnet  $(\text{Rb}_{1-x}\text{Cs}_x)_2\text{Cu}_3\text{SnF}_{12}$  around the quantum critical point detected by muon-spin relaxation technique,” J. Phys. Soc. Jpn. **87**, 074708-1–6 (2018).
- T. Kawamata, K. Ohashi, T. Takamatsu, T. Adachi, M. Kato, I. Watanabe, Y. Koike, “Impurity effects on the electronic state in the underdoped (Cu-free) superconductor  $T'\text{-La}_{1.8}\text{Eu}_{0.2}\text{CuO}_4$  studied by muon spin relaxation,” J. Phys. Soc. Jpn. **87**, 094717 (2018).
- S. N. A. Afmad, S. Sulaiman, L. S. Ang, I. Watanabe, “First-principle studies on magnetic structure and exchange interactions of  $\beta\text{-Et}_n\text{Me}_{4-n}\text{Z}[\text{Pd}(\text{dmit})_2]_2$ ,” J. Phys. Soc. Jpn. **87**, 124709-1–6 (2018).
- F. Astuti, M. Miyajima, T. Fukuda, M. Kodani, T. Nakano, T. Kambe, I. Watanabe, “Anionomagnetism combined lattice symmetry in alkali-metal superoxide  $\text{RbO}_2$ ,” J. Phys. Soc. Jpn. **88**, 043701 (2018).
- K. L. Brown, C. P. J. Stockdale, H. Luo, X. Zhao, J. -H. Li, D. Viehland, G. Xu, P. M. Gehring, K. Ishida, A. D. Hillier, C. Stock, “Depth dependent element analysis of  $\text{PbMg}_{1/3}\text{Nb}_{2/3}\text{O}_3$  using muonic X-rays,” J. Phys. Conds. Matt. **30**, 125703 (2018). \*
- Kumar, C. N. Cuo, F. Astuti, T. Shang, M. K. Lee, C. S. Lue, I. Watanabe, J. A. T. Baker, T. Shiroka, L. J. Chang, “Nodeless Superconductivity in the cage-type superconductor  $\text{Sc}_5\text{Ru}_6\text{Sn}_{18}$  with Preserved time-reversal symmetry,” J. Phys. Conds. Matt. **30**, 315803-1–11 (2018).
- E. Mocchiutti *et al.* (FAMU collaboration), “FAMU: study of the energy dependent transfer rate  $\Lambda\mu p \rightarrow \mu\text{O}$ ,” J. Phys. C **1138**, 2018. \*
- E. Spurayoga, A. A. Nugroho, D. Onggo, A. O. Polyakov, T. T. M. Palstra, I. Watanabe, “3D long-range magnetic ordering in  $(\text{C}_2\text{H}_5\text{NH}_3)_2\text{CuCl}_4$  compound revealed by internal magnetic field from muon spin rotation and first principal calculation,” Physica B **545**, 76–79 (2018).
- M. Clemenza *et al.*, “CHNET\_TANDEM experiment: Use of negative muons at RIKEN-RAL Port 4 for elemental characterization of Nuragic votive ship samples,” Nucl. Instrum. Methods Phys. Res. A, <https://doi.org/10.1016/j.nima.2018.11.076>. \*
- K. Kurashima, T. Adachi, Kensuke M. Suzuki, Y. Fukunaga, T. Kawamata, T. Noji, H. Miyasaka, I. Watanabe, M. Miyazaki, A. Koda, R. Kadono, Y. Koike, “Development of Ferromagnetic fluctuations in heavily overdoped  $(\text{Bi}, \text{Pd})_2\text{Sr}_2\text{CuO}_{6+\delta}$  copper oxides,” Phys. Rev. Lett. **121**, 057002-1–6 (2018).

### [Proceedings]

#### (Original Papers) \*Subject to Peer Review

- B. V. Hampshire, K. Butcher, K. Ishida, G. Green, D. Paul, A. Hillier, “Using negative muons as a probe for depth profiling silver Roman coinage,” Heritage **2**, 400–407 (2019), Proc. of the 8th International Conference on Synchrotron Radiation and Neutrons in Art and Archaeology, doi:10.3390/heritage2010028. \*
- T. Sumura, T. Ishimoto, H. Kuwahara, K. Kurashima, Y. Koike, I. Watanabe, M. Yiyazaki, A. Koda, R. Kadono, T. Adachi, “Reduction Effects on Cu-spin Fluctuation in the electron-doped  $T'$ -cuprate  $\text{Pr}_{1.3-x}\text{La}_{0.7}\text{Ce}_x\text{CuO}_{4+\delta}$  ( $x = 0.10$ ),” JPS Conf. Proc. **21**, 011027 (2018). \*
- A. Hillier, K. Ishida, P. Seller, M. C. Veale, M. D. Wilson, “Element specific imaging using muonic x-rays,” JPS Conf. Proc. **21**, 011042 (2018).
- Risdiana, T. Saragi, W. A. Somantri, S. Pratiwi, D. Suhendar, M. Manawan, B. J. Suroto, I. Watanabe, “Zn-induced development of the Cu-spin Correlation in electron-doped superconducting cuprates of  $\text{Eu}_{2-x}\text{Ce}_x\text{CuO}_4$ ,” J. Phys. Conf. Ser. **1013**, 012180-1–5 (2018). \*
- S. Kanda, K. Ishida, M. Iwasaki, Y. Ma, S. Okada, A. Takamine, H. Ueno, K. Midorikawa, N. Saito, S. Wada, M. Yumoto, Y. Oishi, M. Sato, S. Aikawa, K. S. Tanaka, Y. Matsuda, “Measurement of the proton Zemach radius from the hyperfine splitting in muonic hydrogen atom,” J. Phys. Conf. Ser. **1138**, 012008 (2018). 10th Int. Conf. on Precision Physics of Simple Atomic Systems. \*
- A. D. Hillier, J. S. Lord, K. Ishida, C. Rogers “Muons at ISIS,” Philos. Trans. R. Soc. A **377**, 20180064 Contribution to a Theo Murphy meeting issue “Cosmic-ray muography.” \*
- S. Kanda, K. Ishida, M. Iwasaki, Y. Ma, A. Takamine, H. Ueno, K. Midorikawa, N. Saito, S. Wada, M. Yumoto, S. Okada, Y. Oishi, M. Sato, S. Aikawa, K. S. Tanaka, Y. Matsuda, “Precision laser spectroscopy of the ground state hyperfine splitting in muonic hydrogen,” Proc. Sci. **NuFact2017**, 122 (2018). \*

**Oral Presentations****[International Conference etc.]**

- S. Kanda, "Precision Spectroscopy of muonic systems with high-intensity pulsed muon beam," Workshop on Lepton Flavor Physics with Most Intense DC Muon Beams, Tokyo, April, 2018.
- S. Kanda, "Measurement of the proton Zemach radius from the hyperfine splitting in muonic hydrogen atom," 10th International Conference on Precision Physics of Simple Atomic Systems (PSAS 2018), Vienna, May, 2018.
- K. Ishida, "Future opportunities in mu-p atoms," FAMU meeting, Trieste, Italy, June, 2018.
- S. Kanda, "Laser spectroscopy of the hyperfine splitting in muonic hydrogen atom by a measurement of decay electron asymmetry," Sohtaro Kanda, Nucleon Spin Structure at Low Q: A Hyperfine View, Trento, July, 2018.
- S. Kanda, "Precision spectroscopy of exotic atoms involving muon," The 20th International Workshop on Neutrinos from Accelerators (NuFact2018), Virginia, August, 2018.
- S. Kanda, "Laser spectroscopy of the ground-state hyperfine splitting in muonic hydrogen atom," Symposium for Muon and Neutrino Physics 2018, Osaka, September, 2018.
- K. Ishida, "Proton Zemach radius measurement by the hyperfine splitting of muonic hydrogen (invited)," The Fifth Joint Meeting of the Nuclear Physics Divisions of the American Physical Society and the Physical Society of Japan, Waikoloa, USA, October, 2018.
- K. Ishida, "Proton radius measurement with muonic atoms," International workshop on the structure of the proton, Sagae, Yamagata, February, 2019.
- S. Kanda, "Development of instruments for the proton radius measurement at RIKEN," International workshop on the structure of the proton, Sagae, Yamagata, February, 2019.

**[Domestic Conference]**

- 石田勝彦, 「ミュオン原子による陽子半径決定」, 大阪大学理学部物理セミナー, 豊中, 2018年8月.
- 神田聡太郎, "Residual polarization and hyperfine transition rate in muonic hydrogen," 新学術領域研究「宇宙観測検出器と量子ビームの出会い. 新たな応用への架け橋」, キックオフシンポジウム, 東北, 2018年12月.
- 神田聡太郎, "Laser spectroscopy of the hyperfine splitting in muonic hydrogen," 第9回 Muon 科学と加速器研究研究会, 大阪, 2019年1月.
- 石田勝彦, 「理研 RAL ミュオン施設」, 第9回「Muon 科学と加速器研究」, RCNP, 吹田, 2019年1月.
- 石田勝彦, 「ミュオン水素原子による由志半径測定」, ELPH 研究会 C021 「電子散乱による原子核研究—陽子半径, 不安定核の電荷密度分布を中心に—」, 東北大学電子光理学研究センター, 仙台, 2019年3月.
- 神田聡太郎, ミューオン水素原子のレーザー分光に向けたスピン回転実験, 日本物理学会第74回年次大会, 九州大学, 福岡, 2019年3月.

## Safety Management Group

### 1. Abstract

The RIKEN Nishina Center for Accelerator-Based Science possesses one of the largest accelerator facilities in the world, which consists of two heavy-ion linear accelerators and five cyclotrons. This is the only site in Japan where uranium ions are accelerated. The center also has electron accelerators of microtron and synchrotron storage ring. Our function is to keep the radiation level in and around the facility below the allowable limit and to keep the exposure of workers as low as reasonably achievable. We are also involved in the safety management of the Radioisotope Center, where many types of experiments are performed with sealed and unsealed radioisotopes.

### 2. Major Research Subjects

- (1) Safety management at radiation facilities of Nishina Center for Accelerator-Based Science
- (2) Safety management at Radioisotope Center
- (3) Radiation shielding design and development of accelerator safety systems

### 3. Summary of Research Activity

Our most important task is to keep the personnel exposure as low as reasonably achievable, and to prevent an accident. Therefore, we daily patrol the facility, measure the ambient dose rates, maintain the survey meters, shield doors and facilities of exhaust air and wastewater, replenish the protective supplies, and manage the radioactive waste. Advice, supervision and assistance at major accelerator maintenance works are also our task.

The entrance and exit management system for which is the part of the radiation control system developed for the RILAC upgrade was installed and started to operate. Interlock system will be set in the next year.

Minor improvements of the radiation safety systems were also done. The radiation monitors at the Nishina building has been replaced annually from 2015 because they get older, which were installed in 1986.

## Members

### Group Director

Yoshitomo UWAMINO (–March 31, 2018)

Kanenobu TANAKA (April 1, 2018–)

### Research/Technical Scientists

Rieko HIGURASHI (Technical Scientist)

Hisao SAKAMOTO (Technical Scientist)

### Expert Technician

Atsuko AKASHIO

### Research Consultant

Masaharu OKANO (Japan Radiation Res. Soc.)

### Visiting Scientists

Noriaki NAKAO (Shimizu Corp.)

Nobuhiro SHIGYO (Kyushu Univ.)

Toshiya SANAMI (KEK)

Masayuki HAGIWARA (KEK)

Hiroshi YASHIMA (Kyoto Univ.)

Arim LEE (Pohang Accelerator Laboratory POSTECH)

### Student Trainees

Kenta SUGIHARA (Kyushu Univ.)

Shougo IZUMITANI (Kyushu Univ.)

Eunji LEE (Kyushu Univ.)

### Technical Staff I

Hiroki MUKAI

Tomoyuki DANTSUKA (concurrent: Cryogenic Technology Team)

### Temporary Staffing

Ryuji SUZUKI

### Part-time Workers

Kimie IGARASHI (Administrative Part-time Worker I)

Shin FUJITA (Part-time Worker)

Satomi IIZUKA (Administrative Part-time Worker II)

Hiroko AISO (Part-time Worker)

Naoko USUDATE (Administrative Part-time Worker II)

Hiroshi KATO (Part-time Worker)

Yukiko SHIODA (Administrative Part-time Worker II)

**Assistant**

Tomomi OKAYASU

**List of Publications & Presentations****Publications****Oral Presentations****[Domestic Conference]**

田中鐘信, 「理化学研究所 RIBF 加速器施設の火災時対応と個人線量管理について」, 第 6 回加速器施設安全シンポジウム, 東海村, 2018 年 1 月.

杉原健太, 李恩智, 執行信寛, 田中鐘信, 赤塩敦子, 佐波俊哉, 「Bi に対する 7 MeV/u  $\alpha$  入射による中性子生成量測定」, 日本原子力学会 2019 年春の年会, 水戸, 2019 年 3 月.

## User Liaison Group

### 1. Abstract

The essential mission of the User Liaison Group is to maximize the research activities of RIBF by attracting users in various fields with a wide scope. The Group consists of two teams. The RIBF User Liaison Team provides various supports to visiting RIBF users through the RIBF Users Office. Managing RIBF beam time and organizing the Program Advisory Committee Meetings to review RIBF experimental proposals are also important mission of the Team in order to enhance collaborative-use of the RIBF. The Outreach Team has created various information materials, such as pamphlets, posters, and homepages, to introduce the research activities in the RNC. On the homepage, we provide information on usage of the RIBF facility. The team also participate in science introduction events hosted by public institutions. In addition, the User Liaison Group also takes care of laboratory tours for RIBF visitors from public. The numbers of visitors amounts to 2,300 per year.

### Members

#### Group Director

Hideyuki SAKAI (–March 31, 2018)

Hideki UENO (April 1, 2019–)

#### Senior Visiting Scientists

Ikuko HAMAMOTO (Lund Univ.)

Munetake ICHIMURA (Univ. of Tokyo)

#### Assistants

Tomomi OKAYASU (Concurrent: Safety Management Grp.)

Yu NAYA

Yoko FUJITA

Midori YAMAMOTO

## User Liaison Group

### RIBF User Liaison Team

#### 1. Abstract

To enhance synergetic common use of the world-class accelerator facility, the Radioisotope Beam Factory (RIBF), it is necessary to promote a broad range of applications and to maximize the facility's importance. The facilitation and promotion of the RIBF are important missions charged to the team. Important operational activities of the team include: i) the organization of international Program Advisory Committee (PAC) meetings to review experimental proposals submitted by RIBF users, ii) RIBF beam-time operation management, and iii) promotion of facility use by hosting outside users through the RIBF Independent Users program, which is a new-user registration program begun in FY2010 at the RIKEN Nishina Center (RNC) to enhance the synergetic common use of the RIBF. The team opened the RIBF Users Office in the RIBF building in 2010, which is the main point of contact for Independent Users and provides a wide range of services and information.

#### 2. Major Research Subjects

- (1) Facilitation of the use of the RIBF
- (2) Promotion of the RIBF to interested researchers

#### 3. Summary of Research Activity

##### (1) Facilitation of the use of the RIBF

The RIBF Users Office, formed by the team in 2010, is a point of contact for user registration through the RIBF Independent User program. This activity includes:

- registration of users as RIBF Independent Users,
- registration of radiation workers at the RIKEN Wako Institute,
- provision of an RIBF User Card (a regular entry permit) and an optically stimulated luminescence dosimeter for each RIBF Independent User, and
- provision of safety training for new registrants regarding working around radiation, accelerator use at the RIBF facility, and information security, which must be completed before they begin RIBF research.

The RIBF Users Office is also a point of contact for users regarding RIBF beam-time-related paperwork, which includes:

- contact for beam-time scheduling and safety review of experiments by the In-House Safety Committee,
- preparation of annual Accelerator Progress Reports, and
- maintaining the above information in a beam-time record database.

In addition, the RIBF Users Office assists RIBF Independent Users with matters related to their visit, such as invitation procedures, visa applications, and the reservation of on-campus accommodation.

##### (2) Promotion of the RIBF to interested researchers

- The team has organized an international PAC for RIBF experiments; it consists of leading scientists worldwide and reviews proposals in the field of nuclear physics (NP) purely on the basis of their scientific merit and feasibility. The team also assists another PAC meeting for material and life sciences (ML) organized by the RNC Advanced Meson Laboratory. The NP and ML PAC meetings are organized twice a year.
- The team coordinates beam times for PAC-approved experiments and other development activities. It manages the operating schedule of the RIBF accelerator complex according to the decisions arrived at by the RIBF Machine Time Committee.
- To promote research activities at RIBF, proposals for User Liaison and Industrial Cooperation Group symposia/mini-workshops are solicited broadly both inside and outside of the RNC. The RIBF Users Office assists in the related paperwork.
- The team is the point of contact for the RIBF users' association. It arranges meetings at RNC headquarters for the RIBF User Executive Committee of the users' association.
- The Team conducts publicity activities, such as arranging for RIBF tours, development and improvement of the RNC official web site, and delivery of RNC news via email and the web.

#### Members

##### Team Leader

Ken-ichiro YONEDA

##### Contract Researcher

Tadashi KAMBARA (Concurrent: Industrial Application Research Team)

## User Liaison Group Outreach Team

### 1. Abstract

The Outreach Team has created various information materials to introduce research activities in the RNC. For instance, the team makes brochures introducing the RNC and the RIBF accelerator facility, posters of symposia and the summer school hosted by RNC, the center homepage containing information such as details of RNC and the procedure for the use of the RIBF facility, and images of equipment and facilities available for researchers inside and outside RIKEN, among the others. Furthermore, the team also participates in science introduction events hosted by public institutions.

### 2. Major Work Contents

The major work contents of the Outreach Team is to promote the publicity of RNC, through the creation of various materials such as brochures, websites, posters, and videos, among the others. The arrangement of tours of the RIBF facility and the exhibition and introduction of the RIBF facility at science events are also conducted independently or in cooperation with RIKEN Public Relations Office.

### 3. Summary of Work Activity

The specific work contents performed by the team are as follows:

- [Website] The Team creates/manages the RNC official website (<http://www.nishina.riken.jp>), which introduces the organization and its research activities. This website plays an important role in providing information to researchers who visit RNC to conduct his/her own research.
- [Brochures] The Team has produced various brochures introducing the organization and the studies performed at RNC. The brochures named “Your body is made of star scraps” explaining element synthesis in the universe and “Introduction of RIBF Facility” in a cartoon style for children are among them.
- [Posters] Conference/Symposium posters connected with RNC were prepared on the request of organizers. For general purpose, a special poster featuring the nuclear chart has been prepared for distribution. In commemoration of the discovery of nihonium, brochures and posters dedicated to the ceremony were made.
- [RIBF Cyclopedica] In April 2012, the permanent exhibition hall (RIBF Cyclopedica) located at the entrance hall of the RIBF building was set up in cooperation with RIKEN Public Relations Office. Explanatory illustrations on nuclear science, research at RIBF, RIBF history, a 3D nuclear chart built with LEGO blocks, and a 1/6-size GARIS model are displayed to help understanding through visual means. The Team is also working on updating the exhibits.
- [RIBF facility tour] The Team arranges RIBF facility tour for over 2000 visitors per year. The tour is guided by a researcher.
- [Science event participation] In 2010, 2012, 2013, 2015, and 2016, the sub-team opened an exhibition booth of RNC to introduce the latest research activities on the occasion of the “Science Agora” organized by Japan Science and Technology Agency (JST). From time to time, the sub-team was invited to participate in scientific events by MEXT, Wako city, and Nissan global foundation.

One attraction targeting children is the hands-on work of assembling “Iron-beads” to create a nuclear chart or a shape of nihonium. In addition to the above-noted work contents, the Team conducts a variety of works, such as taking pictures of meetings organized by RNC, cooperation in the production of a 3D video to explain the accelerators and the research at RIBF, among the others.

## Members

### Team Leader

Hideki UENO

### Deputy Team Leader

Yasushi WATANABE (concurrent: Senior Research Scientist,  
Radiation Laboratory)

### Technical Staff I

Narumasa MIYAUCHI (concurrent: Research Administrator,  
Office of the Center Director)

## List of Publications & Presentations

### Outreach Activities

Hokkaido Science Festival 2018, Sapporo, Japan, August 6–7, 2018.

## Partner Institutions

The Nishina Center established the “Research Partnership System” in 2008. This system permits an external institute to develop its own projects at the RIKEN Wako campus in equal partnership with the Nishina Center. At present, two institutes, the Center for Nuclear Study, the University of Tokyo (CNS); and the Wako Nuclear Science Center (WNSC), Institute of Particle and Nuclear Studies (IPNS), High-energy Accelerator Research Organization (KEK) are conducting research activities under the Research Partnership System.

CNS and the Nishina Center signed the partnership agreement in 2008. Until then, CNS had collaborated in joint programs with RIKEN under the “Research Collaboration Agreement on Heavy Ion Physics” (collaboration agreement) signed in 1998. The partnership agreement redefines procedures related to the joint programs while keeping the spirit of the collaboration agreement. The joint programs include experimental nuclear-physics activities using CRIB, SHARAQ, and GRAPE at RIBF, accelerator development, and activities at RHIC PHENIX.

KEK started low-energy nuclear physics activity at RIBF in 2011 under the Research Partnership System. The joint experimental programs are based on KISS (KEK Isotope Separator). After the R&D studies on KISS, it became available for users from 2015.

The experimental proposals that request the use of the above-noted devices of CNS and KEK together with the other RIBF key devices are screened by the Program Advisory Committee for Nuclear Physics experiments at RI Beam Factory (NP-PAC). The NP-PAC meetings are co-hosted together with CNS and KEK.

The activities of CNS and KEK are reported in the following pages.

**Partner Institution**  
**Center for Nuclear Study, Graduate School of Science**  
**The University of Tokyo**

## 1. Abstract

The Center for Nuclear Study (CNS) aims to elucidate the nature of nuclear system by producing the characteristic states where the Isospin, Spin and Quark degrees of freedom play central roles. These researches in CNS lead to the understanding of the matter based on common natures of many-body systems in various phases. We also aim at elucidating the explosion phenomena and the evolution of the universe by the direct measurements simulating nuclear reactions in the universe. In order to advance the nuclear science with heavy-ion reactions, we develop AVF upgrade, CRIB and SHARAQ facilities in the large-scale accelerators laboratories RIBF. The OEDO facility has been developed as an upgrade of the SHARAQ, where a RF deflector system has been introduced to obtain a good quality of low-energy beam. We added a new group for fundamental symmetry by using heavy RIs. We promote collaboration programs at RIBF as well as RHIC-PHENIX and ALICE-LHC with scientists in the world, and host international meetings and conferences. We also provide educational opportunities to young scientists in the heavy-ion science through the graduate course as a member of the department of physics in the University of Tokyo and through hosting the international summer school.

## 2. Major Research Subjects

- (1) Accelerator Physics
- (2) Nuclear Astrophysics
- (3) Nuclear spectroscopy of exotic nuclei
- (4) Quark physics
- (5) Nuclear Theory
- (6) OEDO/SHARAQ project
- (7) Exotic Nuclear Reaction
- (8) Low Energy Nuclear Reaction Group
- (9) Active Target Development
- (10) Fundamental Physics

## 3. Summary of Research Activity

### (1) Accelerator Physics

One of the major tasks of the accelerator group is the AVF upgrade project that includes development of ion sources, upgrading the AVF cyclotron of RIKEN and the beam line to CRIB. In 2017, the operating time of the HyperECR was 2414 hours, which is 61% of the total operating time of the AVF cyclotron. The beam extraction system of the HyperECR is under development to realize a high intensity and low emittance beam. We have succeeded to suppress  $^{12}\text{C}^{4+}$  beam which contaminated  $^{18}\text{O}^{6+}$  beam by measuring the light intensity of the CIV line spectrum. The calculation model of injection beam orbit of the AVF cyclotron was completed and the adjustment of the position and angle deviation between the measured beam orbit and the calculated beam orbit is carried on. The detailed studies on ion optics of the beamline to CRIB from AVF cyclotron were performed with beam diagnosis system and simulation code, and it turned out the loss of the beam intensity is occurred at the entrance of the vertical deflection bending magnet.

### (2) Nuclear Astrophysics

The main activity of the nuclear astrophysics group is to study astrophysical reactions and special nuclear clustering using the low-energy RI beam separator CRIB. Several experimental projects on big-bang nucleosynthesis (BBN) are currently under way. To give a solution to the cosmological  $^7\text{Li}$  abundance problem,  $^7\text{Be}(n, \alpha)/(n, p)$  astrophysical reactions were studied with the Trojan Horse method, and the rate of  $^7\text{Be}(n, p_1)$ , the  $(n, p)$  reaction with  $^7\text{Li}$  excitation, is evaluated at the BBN temperature for the first time.  $^7\text{Be}(d, p)$  measurement with a  $^7\text{Be}$ -implanted target was carried out in 2018, in collaboration with RCNP, Osaka Univ. and JAEA.  $^8\text{Li}(\alpha, n)$  reaction has been considered as responsible to the production of nuclei heavier than boron in some models of the BBN. To solve the discrepancy between the previous measurements of  $^8\text{Li}(\alpha, n)$ , a new experiment with  $\gamma$ -ray measurement was performed at CRIB in Sep. 2018. To confirm the exotic linear-chain cluster structure in  $^{14}\text{C}$  nucleus indicated in the previous  $^{10}\text{Be} + \alpha$  resonant scattering measurement at CRIB, a new measurement was carried out at INFN-LNS, Catania, Italy, under the collaboration of CNS, INFN, Univ. Edinburgh and other institutes, in Oct. 2018. A measurement on  $^{25}\text{Al} + p$  resonant scattering was performed at CRIB in Feb. 2019, to study the resonances relevant for the astrophysical  $^{22}\text{Mg}(\alpha, p)$  reaction in X-ray bursters.

### (3) Nuclear structure of exotic nuclei

The NUSPEQ (NUclear SPectroscopy for Extreme Quantum system) group studies exotic structures in high-isospin and/or high-spin states in nuclei. The CNS GRAPE (Gamma-Ray detector Array with Position and Energy sensitivity) is a major apparatus for high-resolution in-beam gamma-ray spectroscopy. Missing mass spectroscopy using the SHARAQ is used for another approach on exotic nuclei. In 2017, the following progress has been made. Experimental data taken under the EURICA collaboration has been analyzed for studying octupole deformation in neutron-rich Ba isotopes and preparing publication. A new experiment measuring the  $^4\text{He}(^8\text{He}, ^8\text{Be})4n$  reaction was performed for better statistics and better accuracy in order to verify a candidate of the ground state of the tetra neutrons just above the  $4n$  threshold, which is under analysis.

**(4) Quark Physics**

Main goal of the quark physics group is to understand the properties of hot and dense nuclear matter created by colliding heavy nuclei at relativistic energies. The group has been involved in the PHENIX experiment at Relativistic Heavy Ion Collider (RHIC) at Brookhaven National Laboratory, and the ALICE experiment at Large Hadron Collider (LHC) at CERN. As for ALICE, the group has involved in the data analyses, which include the measurement of low-mass lepton pairs in Pb-Pb and  $p$ -Pb collisions,  $J/\psi$  measurements in  $p$ -Pb collisions, long range two particle correlations in  $p$ -Pb collisions, and searches for thermal photons in  $p$ -Pb collisions. The group has involved in the ALICE-TPC upgrade using a Gas Electron Multiplier (GEM). Development of the new data readout system for the upgrade, which aims online data processing by utilizing FPGA and GPU, has been ongoing in 2017.

**(5) Nuclear Theory**

The nuclear theory group participates a project, "Priority Issue 9 to be tackled by using the Post-K Computer" and promotes computational nuclear physics utilizing supercomputers. In FY2017, we performed the Monte Carlo shell model calculations of the Sn isotopes and revealed that the anomalous enhancement of the  $B(E2)$  transition probabilities in the neutron-deficient region is caused by the proton excitation from the  $1g_{9/2}$  orbit, and found that the second-order quantum phase transition occurs around  $N = 66$ . We also investigated the double Gamow-Teller strength distribution of double-beta decay emitters, such as  $^{48}\text{Ca}$ . We theoretically predict a linear relation between the nuclear matrix elements of the double Gamow-Teller transition and the neutrinoless double beta decay. In parallel, we have been promoting the CNS-RIKEN collaboration project on large-scale nuclear structure calculations and performed shell-model calculations under various collaborations with many experimentalists for investigating the exotic structure of neutron-rich nuclei, such as  $^{35}\text{Mg}$ ,  $^{136}\text{Ba}$ ,  $^{138}\text{Ce}$ , and  $^{135}\text{La}$ .

**(6) OEDO/SHARAQ project**

The OEDO/SHARAQ group pursues experimental studies of RI beams by using the high-resolution beamline and the SHARAQ spectrometer. A mass measurement by TOF- $B\rho$  technique for very neutron-rich successfully reaches calcium isotopes beyond  $N = 34$ ,  $^{55,57}\text{Ca}$ , and the preparation of publication is ongoing. The experimental study of  $0^-$  strength in nuclei using the parity-transfer charge exchange ( $^{16}\text{O}$ ,  $^{16}\text{F}$ ) is on progress and the data analysis is on the final stage. The OEDO beamline, which was an upgrade of the high-resolution beamline to produce low-energy RI beams, has started the operation in June and has successfully achieved the designed ion-optical performance. The first and second experiments were performed in October and November, and new data for nuclear transmutation of long lived fission products (LLFPs) were successfully obtained.

**(7) Exotic Nuclear Reaction**

The Exotic Nuclear Reaction group studies various exotic reactions induced by beams of unstable nuclei. One subject is inverse-kinematics ( $p, n$ ) reaction. In 2017 a set of neutron counters PANDORA was used for the first time at HIMAC facility for the study of the  $^6\text{He}(p, n)$  reaction. Candidate nuclei to study are high spin isomers such as  $^{52}\text{Fe}(12^+)$ . Development of isomer beam was carried out.

**(8) Low Energy Nuclear Reaction Group**

A recoil particle detector for missing mass spectroscopy, named TiNA, had been developed under the collaboration with RIKEN and RCNP. TiNA consists of 6 sector telescopes. Each of which as a stripped-type SSD and 2 CsI(Tl) crystals. After the test experiment at the tandem facility of Kyushu Univ., TiNA was employed at the physics experiment with OEDO. Development of the tritium target is still on-going. Several deuterium doped Ti targets were fabricated at the Toyama Univ. They were tested by using  $d(^{12}\text{C}, d)$  reaction at the tandem facility at Kyushu. The amount of deuterium was found to be scattered. The optimum condition to make the target will be sought for. The production cross section  $^{178\text{m}2}\text{Hf}$  was evaluated for the mass production in the future. The digital signal processing devices for the GRAPE have been developed to measure the cascade transitions from the isomeric state. After chemical separation of Hf at the hot laboratory at RIBF. The week cascade decay was successfully measured.

**(9) Active Target Development**

Two types of gaseous active target TPCs called CAT's and GEM-MSTPC are developed and used for the missing mass spectroscopy. The CAT's are employed for the study of equation of state of nuclear matter. The measurement of giant monopole resonance in  $^{132}\text{Sn}$  at RIBF with CAT-S and the data analysis is ongoing. In 2017, we developed a larger active target called CAT-M, which has 10-times larger active volume than that of CAT-S. The CAT-M was commissioned at HIMAC and the excitation energy spectrum of  $^{136}\text{Xe}$  for proton scattering was measured. The GEM-MSTPC is employed for the nuclear astrophysics study. The data analysis of ( $\alpha, p$ ) reaction on  $^{18}\text{Ne}$  and  $^{22}\text{Mg}$  and the  $\beta$ -decay of  $^{16}\text{Ne}$  followed by  $\alpha$  emission are ongoing.

**(10) Fundamental Physics**

Although the Standard Model of particle physics is being steadily and successfully verified, the disappearance of the antimatter in the universe could not be sufficiently explained; a more fundamental framework is required and has to be studied. In order to understand the mechanism of matter-antimatter symmetry violation, we are developing the next generation experiments employing ultracold atoms to search for the electron electric dipole moment (EDM) using heavy element francium (Fr) in an optical lattice at RIBF. The developments of a high intensity surface ionizer to produce Fr and a magneto-optical trap (MOT) are in progress, and Fr-MOT experiments are going on at present at CYRIC.

**Members****Director**

Susumu SHIMOURA

**Scientific Staff**

Susumu SHIMOURA (Professor)  
 Hidetoshi YAMAGUCHI (Lecturer)  
 Yasuhiro SAKEMI (Professor)  
 Shin'ichiro MICHIMASA (Assistant Professor)  
 Kentaro YAKO (Associate Professor)

Taku GUNJI (Associate Professor)  
 Nobuaki IMAI (Associate Professor)  
 Shinsuke OTA (Assistant Professor)  
 Noritaka SHIMIZU (Project Associate Professor)  
 Hiroki NAGAHAMA (Assistant Professor)

**Guest Scientists**

Yutaka UTSUNO (Guest Professor)  
 Yutaka MIZOI (Guest Associate Professor)

Ningtao ZHANG (Guest Post Doctoral Associate)

**Technical Staff**

Yasuteru KOTAKA

**Technical Assistants**

Yukimitsu OHSHIRO  
 Reiko KOJIMA  
 Mamoru KATAYANAGI

Hiroshi KUREI  
 Masayoshi YAGYU

**Project Research Associates**

Tomoaki TOGASHI  
 Olga BELIUSKINA  
 Masanori DOZONO

Seiya HAYAKAWA  
 Takashi ABE  
 Naofumi TSUNODA

**Post Doctoral Associates**

Shinichi HAYASHI  
 Chihiro IWAMOTO  
 Philipp SCHROCK  
 Lei YANG  
 Laszlo STUHL  
 Yusuke TSUNODA

Javier MENENDEZ SANCHEZ  
 Jongwon HWANG  
 Takayuki MIYAGI  
 Satoshi TAKEUCHI  
 Tomohiro HAYAMIZU

**Assistant Teaching Staff**

Hiroshi TOKIEDA  
 Motonobu TAKAKI

Yuko SEKIGUCHI

**Graduate Students**

Ryo NAKAJIMA  
 Soichiro MASUOKA  
 Noritaka KITAMURA  
 Keita KAWATA

Hideki SHIMIZU  
 Rieko TSUNODA  
 Naoya OZAWA

**Administration Staff**

Toshio OSUGI  
 Ikuko YAMAMOTO  
 Mikio OKI

Takako ENDO  
 Yukino KISHI

**List of Publications & Presentations****Publications****[Journal]****(Original Papers) \*Subject to Peer Review**

T. Nishi, K. Itahashi, G. P. A. Berg, H. Fujioka, N. Fukuda, N. Fukunishi, H. Geissel, R. S. Hayano, S. Hirenzaki, K. Ichikawa, N. Ikeno, N. Inabe, S. Itoh, M. Iwasaki, D. Kameda, S. Kawase, T. Kubo, K. Kusaka, H. Matsubara, S. Michimasa, K. Miki, G. Mishima, H. Miya, H. Nagahiro, M. Nakamura, S. Noji, K. Okochi, S. Ota, N. Sakamoto, K. Suzuki, H. Takeda, Y. K. Tanaka, K. Todoroki, K. Tsukada, T. Uesaka, Y. N. Watanabe, H. Weick, H. Yamakami, K. Yoshida, "Spectroscopy of pionic atoms in  $^{122}\text{Sn}(d, ^3\text{He})$  reaction and angular dependence of the formation cross sections," Phys. Rev. Lett. **120**, 152505 (2018). \*

- M. L. Cortes, P. Doornenbal, M. Dupuis, S. M. Lenzi, F. Nowacki, A. Obertelli, S. Peru, N. Pietralla, V. Werner, K. Wimmer, G. Authelet, H. Baba, D. Calvet, F. Chateau, A. Corsi, A. Delbart, J. M. Gheller, A. Gillibert, T. Isobe, V. Lapoux, C. Louchart, M. Matsushita, S. Momiyama, T. Motobayashi, M. Niikura, H. Otsu, C. Peron, A. Peyaud, E. C. Pollacco, J. Y. Rousse, H. Sakurai, C. Santamaria, M. Sasano, Y. Shiga, S. Takeuchi, R. Taniuchi, T. Uesaka, H. Wang, K. Yoneda, F. Browne, L. X. Chung, Z. Dombradi, S. Franchoo, F. Giacoppo, A. Gottardo, K. Hadynska-Klek, Z. Korkulu, S. Koyama, Y. Kubota, J. Lee, M. Lettmann, R. Lozeva, K. Matsui, T. Miyazaki, S. Nishimura, L. Olivier, S. Ota, Z. Patel, E. Sahin, C. M. Shand, P.-A. Söderström, I. Stefan, D. Steppenbeck, T. Sumikama, D. Suzuki, Z. Vajta, J. Wu, Z. Xu, “Inelastic scattering of neutron-rich Ni and Zn isotopes off a proton target,” *Phys. Rev. C* **97**, 044315 (2018). \*
- A. Corsi, A. Obertelli, P. Doornenbal, F. Nowacki, H. Sagawa, Y. Tanimura, N. Aoi, H. Baba, P. Bednarczyk, S. Boissinot, M. Ciemala, A. Gillibert, T. Isobe, A. Jungclaus, V. Lapoux, J. Lee, K. Matsui, M. Matsushita, T. Motobayashi, D. Nishimura, S. Ota, E. Pollacco, H. Sakurai, C. Santamaria, Y. Shiga, D. Sohler, D. Steppenbeck, S. Takeuchi, R. Taniuchi, H. Wang, “Spectroscopy of nuclei around  $^{100}\text{Sn}$  populated via two-neutron knockout reactions,” *Phys. Rev. C* **97**, 044321 (2018). \*
- R. Yokoyama, E. Ideguchi, G. S. Simpson, Mn. Tanaka, S. Nishimura, P. Doornenbal, G. Lorusso, P.-A. Söderström, T. Sumikama, J. Wu, Z. Y. Xu, N. Aoi, H. Baba, F. L. B. Garrote, G. Benzoni, F. Browne, R. Daido, Y. Fang, N. Fukuda, A. Gottardo, G. Gey, S. Go, N. Inabe, T. Isobe, D. Kameda, K. Kobayashi, M. Kobayashi, I. Kojouharov, T. Komatsubara, T. Kubo, N. Kurz, I. Kuti, Z. Li, M. Matsushita, S. Michimasa, C. B. Moon, H. Nishibata, I. Nishizuka, A. Odahara, Z. Patel, S. Rice, E. Sahin, H. Sakurai, H. Schaffner, L. Sinclair, H. Suzuki, H. Takeda, J. Taprogge, Z. Vajta, H. Watanabe, A. Yagi, T. Inakura, “Beta-gamma spectroscopy of the neutron-rich  $^{150}\text{Ba}$ ,” *Prog. Theor. Exp. Phys.* **2018**, 041D02 (2018). \*
- S. Noji, H. Sakai, N. Aoi, H. Baba, G. P. A. Berg, P. Doornenbal, M. Dozono, N. Fukuda, N. Inabe, D. Kameda, T. Kawabata, S. Kawase, Y. Kikuchi, K. Kisanori, T. Kubo, Y. Maeda, H. Matsubara, S. Michimasa, K. Miki, H. Miya, H. Miyasako, S. Sakaguchi, Y. Sasamoto, S. Shimoura, M. Takaki, H. Takeda, S. Takeuchi, H. Tokieda, T. Ohnishi, S. Ota, T. Uesaka, H. Wang, K. Yako, Y. Yanagisawa, N. Yokota, K. Yoshida, R. G. T. Zegers, “Excitation of the isovector spin monopole resonance via the exothermic  $^{90}\text{Zr}(^{12}\text{N}, ^{12}\text{C})$  reaction at 175 MeV/u,” *Phys. Rev. Lett.* **120**, 172501 (2018). \*
- S. Chebotaryov, S. Sakaguchi, T. Uesaka, T. Akieda, Y. Ando, M. Assie, D. Beaumel, N. Chiga, M. Dozono, A. Galindo-Uribarri, B. Heffron, A. Hirayama, T. Isobe, K. Kaki, S. Kawase, W. Kim, T. Kobayashi, H. Kon, Y. Kondo, Y. Kubota, S. Leblond, H. Lee, T. Lokotko, Y. Maeda, Y. Matsuda, K. Miki, E. Milman, T. Motobayashi, T. Mukai, S. Nakai, T. Nakamura, A. Ni, T. Noro, S. Ota, H. Otsu, T. Ozaki, V. Panin, S. Park, A. Saito, H. Sakai, M. Sasano, H. Sato, K. Sekiguchi, Y. Shimizu, I. Stefan, L. Stuhl, M. Takaki, K. Taniue, K. Tateishi, S. Terashima, Y. Togano, T. Tomai, Y. Wada, T. Wakasa, T. Wakui, A. Watanabe, H. Yamada, Z. Yang, M. Yasuda, J. Yasuda, K. Yoneda, J. Zenihiro, “Proton elastic scattering at 200 AMeV and high momentum transfers of  $1.7\text{--}2.7\text{ fm}^{-1}$  as a probe of the nuclear matter density of  $^6\text{He}$ ,” *Prog. Theor. Exp. Phys.* **2018**, 053D01 (2018). \*
- A. M. Long, T. Adachi, M. Beard, G. P. A. Berg, M. Couder, R. J. de Boer, M. Dozono, J. Gorres, H. Fujita, Y. Fujita, K. Hatanaka, D. Ishikawa, T. Kubo, H. Matsubara, Y. Namiki, S. O’Brien, Y. Ohkuma, H. Okamura, H. J. Ong, D. Patel, Y. Sakemi, Y. Shimbara, S. Suzuki, R. Talwar, A. Tamii, A. Volya, T. Wakasa, R. Watanabe, M. Wiescher, R. Yamada, J. Zenihiro, “ $\alpha$ -unbound levels in  $^{34}\text{Ar}$  from  $^{36}\text{Ar}(p, t)^{34}\text{Ar}$  reaction measurements and implications for the astrophysical  $^{30}\text{S}(\alpha, p)^{33}\text{Cl}$  reaction rate,” *Phys. Rev. C* **97**, 054613 (2018). \*
- S. Michimasa, M. Kobayashi, Y. Kiyokawa, S. Ota, D. S. Ahn, H. Baba, G. P. A. Berg, M. Dozono, N. Fukuda, T. Furuno, E. Ideguchi, N. Inabe, T. Kawabata, S. Kawase, K. Kisanori, K. Kobayashi, T. Kubo, Y. Kubota, C. S. Lee, M. Matsushita, H. Miya, A. Mizukami, H. Nagakura, D. Nishimura, H. Oikawa, H. Sakai, Y. Shimizu, A. Stolz, H. Suzuki, M. Takaki, H. Takeda, S. Takeuchi, H. Tokieda, T. Uesaka, K. Yako, Y. Yamaguchi, Y. Yanagisawa, R. Yokoyama, K. Yoshida, S. Shimoura, “Magic nature of neutrons in  $^{54}\text{Ca}$ : First mass measurements of  $^{55,57}\text{Ca}$ ,” *Phys. Rev. Lett.* **121**, 022506 (2018). \*
- X. Y. Liu, Z. Liu, B. Ding, R. Doornenbal, A. Obertelli, S. M. Lenzi, P. M. Walker, L. X. Chung, B. D. Linh, G. Authelet, H. Baba, D. Calvet, F. Chateau, A. Corsi, A. Delbart, J. M. Gheller, A. Gillibert, T. Isobe, V. Lapoux, M. Matsushita, S. Momiyama, T. Motobayashi, M. Niikura, F. Nowacki, H. Otsu, C. Peron, A. Peyaud, E. C. Pollacco, J. Y. Rousse, H. Sakurai, M. Sasano, Y. Shiga, S. Takeuchi, R. Taniuchi, T. Uesaka, H. Wang, K. Yoneda, Y. H. Lam, T. H. Huang, M. D. Sun, W. Q. Zhang, H. Y. Lu, D. S. Hou, E. Browne, Z. Dombradi, S. Franchoo, F. Giacoppo, A. Gottardo, K. Hadynska-Klek, Z. Korkulu, S. Koyama, Y. Kubota, J. Lee, M. Lettmann, R. Lozeva, K. Matsui, T. Miyazaki, S. Nishimura, C. Louchart, L. Olivier, S. Ota, Z. Patel, E. Sahin, C. Santamaria, C. Shand, P.-A. Söderström, G. L. Stefan, D. Steppenbeck, T. Sumikama, D. Suzuki, Z. Vajta, V. Werner, J. Wu, Z. Xu, X. H. Zhou, Y. H. Zhang, H. S. Xu, F. S. Zhang, “Spectroscopy of  $^{65,67}_{25}\text{Mn}$ : Strong coupling in the  $N = 40$  island of inversion,” *Phys. Lett. B* **784**, 392–396 (2018). \*
- J. Yasuda, M. Sasano, R. G. T. Zegers, H. Baba, D. Bazin, W. Chao, M. Dozono, N. Fukuda, N. Inabe, T. Isobe, G. Jhang, D. Kameda, M. Kaneko, K. Kisanori, M. Kobayashi, N. Kobayashi, T. Kobayashi, S. Koyama, Y. Kondo, A. J. Krasznahorkay, T. Kubo, Y. Kubota, M. Kurata-Nishimura, C. S. Lee, J. W. Lee, Y. Matsuda, E. Milman, S. Michimasa, T. Motobayashi, D. Muecher, T. Murakami, T. Nakamura, N. Nakatsuka, S. Ota, H. Otsu, V. Panin, W. Powell, S. Reichert, S. Sakaguchi, H. Sakai, M. Sako, H. Sato, Y. Shimizu, M. Shikata, S. Shimoura, L. Stuhl, T. Sumikama, H. Suzuki, S. Tangwancharoen, M. Takaki, H. Takeda, T. Tako, Y. Togano, H. Tokieda, J. Tsubota, T. Uesaka, T. Wakasa, K. Yako, K. Yoneda, J. Zenihiro, “Extraction of the Landau-Migdal parameter from the Gamow-Teller giant resonance in  $^{132}\text{Sn}$ ,” *Phys. Rev. Lett.* **121**, 132501 (2018). \*
- C. Santamaria, A. Obertelli, S. Ota, M. Sasano, E. Takada, L. Audirac, H. Baba, D. Calvet, F. Chateau, A. Corsi, A. Delbart, P. Doornenbal, A. Giganon, A. Gillibert, Y. Kondo, Y. Kubota, C. Lahonde-Hamdoun, V. Lapoux, D. Leboeuf, C. S. Lee, H. N. Liu, M. Matsushita, T. Motobayashi, M. Niikura, M. Kurata-Nishimura, H. Otsu, A. Peyaud, E. C. Pollacco, G. Prono, H. Tokieda, T. Uesaka, J. Zenihiro, “Tracking with the MINOS Time Projection Chamber,” *Nucl. Instrum. Methods Phys. Res. A* **905**, 138–148 (2018). \*
- S. Shimoura, “Direct reactions as quantum probes for nuclei,” *Eur. Phys. J. Plus* **133**, 463 (2018). \*
- O. Wieland, A. Bracco, F. Camera, R. Avigo, H. Baba, N. Nakatsuka, T. Aumann, S. R. Banerjee, G. Benzoni, K. Boretzky, C. Caesar, S. Ceruti, S. Chen, FCL. Crespi, V. Derya, P. Doornenbal, N. Fukuda, A. Giaz, K. Ieki, N. Kobayashi, Y. Kondo, S. Koyama, T. Kubo, M. Matsushita, B. Million, T. Motobayashi, T. Nakamura, M. Nishimura, H. Otsu, T. Ozaki, A. T. Saito, H. Sakurai, H. Scheit,

- F. Schindler, P. Schrock, Y. Shiga, M. Shikata, S. Shimoura, D. Steppenbeck, T. Sumikama, S. Takeuchi, R. Taniuchi, Y. Togano, J. Tscheuschner, J. Tsubota, H. Wang, K. Wimmer, K. Yoneda, “Low-lying dipole response in the unstable  $^{70}\text{Ni}$  nucleus,” *Phys. Rev. C* **98**, 064313 (2018). \*
- Y. Kubota, M. Sasano, T. Uesaka, M. Dozono, M. Itoh, S. Kawase, M. Kobayashi, C. S. Lee, H. Matsubara, K. Miki, H. Miya, Y. Ono, S. Ota, K. Sekiguchi, T. Shima, T. Taguchi, T. L. Tang, H. Tokieda, T. Wakasa, T. Wakui, J. Yasuda, J. Zenihiro, “Development of a neutron detector with a high position resolution at intermediate energies,” *Nucl. Instrum. Methods Phys. Res. A* **914**, 32–41 (2019). \*
- S. Takeuchi, T. Nakamura, M. Shikata, Y. Togano, Y. Kondo, J. Tsubota, T. Ozaki, A. Saito, H. Otsu, H. Wang, H. Sakurai, Y. Watanabe, S. Kawase, D. Ahn, M. Aikawa, T. Ando, S. Araki, S. Chen, N. Chiga, P. Doornenbal, S. Ebata, N. Fukuda, T. Isobe, S. Kawakami, T. Kin, S. Koyama, S. Kubono, Y. Maeda, A. Makinaga, M. Matsushita, T. Matsuzaki, S. Michimasa, S. Momiyama, S. Nagamine, K. Nakano, M. Niikura, K. Ogata, T. Saito, Y. Shiga, Y. Shimizu, S. Shimoura, T. Sumikama, P. A. Söderström, H. Suzuki, H. Takeda, R. Taniuchi, M. Uesaka, Y. Watanabe, K. Wimmer, T. Yamamoto, K. Yoshida, “Coulomb breakup reactions of  $^{93-94}\text{Zr}$  in inverse kinematics,” *Prog. Theor. Exp. Phys.* **2019**, 013D02 (2019). \*
- Z. Elekes, A. Kripko, D. Sohler, K. Sieja, K. Ogata, K. Yoshida, P. Doornenbal, A. Obertelli, G. Authelet, H. Baba, D. Calvet, F. Chateau, A. Corsi, A. Delbart, J. M. Gheller, A. Gillibert, T. Isobe, V. Lapoux, M. Matsushita, S. Momiyama, T. Motobayashi, H. Otsu, C. Peron, A. Peyaud, E. C. Pollacco, J. Y. Rousse, H. Sakurai, C. Santamaria, Y. Shiga, S. Takeuchi, R. Taniuchi, T. Uesaka, H. Wang, K. Yoneda, F. Browne, L. X. Chung, Z. Dombradi, F. Flavigny, S. Franchoo, F. Giacoppo, A. Gottardo, K. Hadynska-Klek, Z. Korkulu, S. Koyama, Y. Kubota, J. Lee, M. Lettmann, C. Louchart, R. Lozeva, K. Matsui, T. Miyazaki, M. Niikura, S. Nishimura, L. Olivier, S. Ota, Z. Patel, E. Sahin, C. Shand, P. A. Söderström, I. Stefan, D. Steppenbeck, T. Sumikama, D. Suzuki, Z. Vajta, V. Werner, J. Wu, Z. Xu, “Nuclear structure of  $^{76}\text{Ni}$  from the  $(p, 2p)$  reaction,” *Phys. Rev. C* **99**, 014312 (2019). \*
- L. Stuhl *et al.*, “Study of the Gamow-Teller transitions in  $^6\text{He}$  with PANDORA system (17H391),” 2017 Annual Report of the Research Project with Heavy Ions at NIRS-HIMAC, (2018). \*
- S. Acharya *et al.* [ALICE Collaboration], “Longitudinal asymmetry and its effect on pseudorapidity distributions in Pb-Pb collisions at  $\sqrt{s_{NN}} = 2.76$  TeV,” *Phys. Lett. B* **781**, 20 (2018). \*
- S. Acharya *et al.*, [ALICE Collaboration], “First measurement of  $\Xi_c^0$  production in  $pp$  collisions at  $\sqrt{s} = 7$  TeV,” *Phys. Lett. B* **781**, 8 (2018). \*
- S. Acharya *et al.* [ALICE Collaboration], “ $\Lambda_c^+$  production in  $pp$  collisions at  $\sqrt{s} = 7$  TeV and in  $p$ -Pb collisions at  $\sqrt{s_{NN}} = 5.02$  TeV,” *J. High Energy Phys.* **04**, 108 (2018). \*
- S. Acharya *et al.* [ALICE Collaboration], “Prompt and non-prompt  $J/\psi$  production and nuclear modification at mid-rapidity in  $p$ -Pb collisions at  $\sqrt{s_{NN}} = 5.02$  TeV,” *Eur. Phys. J. C* **78**, 466 (2018). \*
- S. Acharya *et al.* [ALICE Collaboration], “Constraints on jet quenching in  $p$ -Pb collisions at  $\sqrt{s_{NN}} = 5.02$  TeV measured by the event-activity dependence of semi-inclusive hadron-jet distributions,” *Phys. Lett. B* **783**, 95 (2018). \*
- S. Acharya *et al.* [ALICE Collaboration], “Measurement of the inclusive  $J/\psi$  polarization at forward rapidity in  $pp$  collisions at  $\sqrt{s} = 8$  TeV,” *Eur. Phys. J. C* **78**, 562 (2018). \*
- S. Acharya *et al.* [ALICE Collaboration], “ $\phi$  meson production at forward rapidity in Pb-Pb collisions at  $\sqrt{s_{NN}} = 2.76$  TeV,” *Eur. Phys. J. C* **78**, 559 (2018). \*
- S. Acharya *et al.* [ALICE Collaboration], “Energy dependence and fluctuations of anisotropic flow in Pb-Pb collisions at  $\sqrt{s_{NN}} = 5.02$  and 2.76 TeV,” *J. High Energy Phys.* **07**, 103 (2018). \*
- S. Acharya *et al.* [ALICE Collaboration], “Inclusive  $J/\psi$  production at forward and backward rapidity in  $p$ -Pb collisions at  $\sqrt{s_{NN}} = 8.16$  TeV,” *J. High Energy Phys.* **07**, 160 (2018). \*
- S. Acharya *et al.* [ALICE Collaboration], “Anisotropic flow in Xe-Xe collisions at  $\sqrt{s_{NN}} = 5.44$  TeV,” *Phys. Lett. B* **784**, 82 (2018). \*
- S. Acharya *et al.* [ALICE Collaboration], “Neutral pion and  $\eta$  meson production in  $p$ -Pb collisions at  $\sqrt{s_{NN}} = 5.02$  TeV,” *Eur. Phys. J. C* **78**, 624 (2018). \*
- S. Acharya *et al.* [ALICE Collaboration], “Inclusive  $J/\psi$  production in Xe-Xe collisions at  $\sqrt{s_{NN}} = 5.44$  TeV,” *Phys. Lett. B* **785**, 419 (2018). \*
- S. Acharya *et al.* [ALICE Collaboration], “Anisotropic flow of identified particles in Pb-Pb collisions at  $\sqrt{s_{NN}} = 5.02$  TeV,” *J. High Energy Phys.* **09**, 006 (2018). \*
- S. Acharya *et al.* [ALICE Collaboration], “Azimuthally-differential pion femtoscopy relative to the third harmonic event plane in Pb-Pb collisions at  $\sqrt{s_{NN}} = 2.76$  TeV,” *Phys. Lett. B* **785**, 320 (2018). \*
- S. Acharya *et al.* [ALICE Collaboration], “Dielectron production in proton-proton collisions at  $\sqrt{s} = 7$  TeV,” *J. High Energy Phys.* **1809**, 064 (2018). \*
- S. Acharya *et al.* [ALICE Collaboration], “Neutral pion and  $\eta$  meson production at midrapidity in Pb-Pb collisions at  $\sqrt{s_{NN}} = 2.76$  TeV,” *Phys. Rev. C* **98**, 044901 (2018). \*
- S. Acharya *et al.* [ALICE Collaboration], “Medium modification of the shape of small-radius jets in central collisions at  $\sqrt{s_{NN}} = 2.76$  TeV,” *J. High Energy Phys.* **1810**, 139 (2018). \*
- S. Acharya *et al.* [ALICE Collaboration], “Transverse momentum spectra and nuclear modification factors of charged particle in  $pp$ ,  $p$ -Pb and Pb-Pb collisions at the LHC,” *J. High Energy Phys.* **1811**, 013 (2018). \*
- S. Acharya *et al.* [ALICE Collaboration], “Transverse momentum spectra and nuclear modification factors of charged particles in Xe-Xe collisions at  $\sqrt{s_{NN}} = 5.44$  TeV,” *Phys. Lett. B* **788**, 166 (2019). \*
- S. Acharya *et al.* [ALICE Collaboration], “Measuring  $K_s^0 K^\pm$  interaction using  $pp$  collisions  $\sqrt{s} = 7$  TeV,” *Phys. Lett. B* **790**, 22 (2019). \*
- S. Acharya *et al.* [ALICE Collaboration], “ $\Upsilon$  suppression at forward rapidity in Pb-Pb collisions at  $\sqrt{s_{NN}} = 5.02$  TeV,” *Phys. Lett. B* **790**, 89 (2019). \*

- S. Acharya *et al.* [ALICE Collaboration], “Direct photon elliptic flow in Pb-Pb collisions at  $\sqrt{s_{NN}} = 2.76$  TeV,” *Phys. Lett. B* **789**, 308 (2019). \*
- S. Acharya *et al.* [ALICE Collaboration], “Charged jet cross section and fragmentation in proton-proton collisions at  $\sqrt{s} = 2.76$  and 8 TeV,” *Phys. Rev. D* **99**, 012016 (2019). \*
- S. Acharya *et al.* [ALICE Collaboration], “Dielectron and heavy-quark production in inelastic and high-multiplicity proton-proton collisions at  $\sqrt{s} = 13$  TeV,” *Phys. Lett. B* **788**, 505 (2019). \*
- S. Acharya *et al.* [ALICE Collaboration], “Suppression of  $\Lambda(1520)$  resonance production in central Pb-Pb collisions at  $\sqrt{s_{NN}} = 2.76$  TeV,” *Phys. Rev. C* **99**, 024905 (2019). \*
- S. Acharya *et al.* [ALICE Collaboration], “ $p$ - $p$ ,  $p$ - $\Lambda$  and  $\Lambda$ - $\Lambda$  correlation studied via femtoscopy in  $pp$  reactions at  $\sqrt{s} = 7$  TeV,” *Phys. Rev. C* **99**, 024001 (2019). \*
- S. Acharya *et al.* [ALICE Collaboration], “Measurement of dielectron production in central Pb-Pb collisions at  $\sqrt{s_{NN}} = 2.76$  TeV,” *Phys. Rev. C* **99**, 024002 (2019). \*
- S. Acharya *et al.* [ALICE Collaboration], “Event-shape engineering for the  $D$ -meson elliptic flow in mid-central Pb-Pb collisions at  $\sqrt{s_{NN}} = 5.02$  TeV,” *J. High Energy Phys.* **02**, 150 (2019). \*
- S. Acharya *et al.* [ALICE Collaboration], “Azimuthal anisotropy of heavy-flavor decay electrons in  $p$ -Pb collisions at  $\sqrt{s_{NN}} = 5.02$  TeV,” *Phys. Rev. Lett.* **122**, 072301 (2019). \*
- S. Acharya *et al.* [ALICE Collaboration], “Centrality and pseudorapidity dependence of charged-particle multiplicity density in Xe-Xe collisions at  $\sqrt{s_{NN}} = 5.02$  TeV,” *Phys. Lett. B* **790**, 35 (2019). \*
- N. N. Duy, K. Y. Chae, S. M. Cha, H. Yamaguchi, K. Abe, S. H. Bae, D. N. Binh, S. H. Choi, K. I. Hahn, S. Hayakawa, B. Hong, N. Iwasa, D. Kahl, L. H. Khiem, A. Kim, D. H. Kim, E. J. Kim, G. W. Kim, M. J. Kim, K. Kwak, M. S. Kwak, E. J. Lee, S. I. Lim, B. Moon, J. Y. Moon, S. Y. Park, V. H. Phong, H. Shimizu, L. Yang, Z. Ge, T. V. N. Hao, “Beam production of  $^{18}\text{Ne}$  with in-flight method for alpha scattering at CRIB,” *Nucl. Instrum. Methods Phys. Res. A* **897**, 8–13 (2018). \*
- D. Kim, G. W. Kim, S. Y. Park, A. Kim, K. I. Hahn, K. Abe, O. Beliuskina, S. Hayakawa, N. Imai, N. Kitamura, Y. Sakaguchi, H. Yamaguchi, S. M. Cha, K. Y. Chae, M. S. Kwag, S. W. Hong, E. J. Lee, J. H. Lee, E. K. Lee, J. Y. Moon, S. H. Bae, S. H. Choi, S. Kubono, V. Panin, Y. Wakabayashi, N. Iwasa, D. Kahl, A. A. Chen, “Study of  $^{19}\text{F}$  levels with  $E_x = 6.7$ – $7.7$  MeV by the  $^{15}\text{N} + \alpha$  scattering experiment,” *Journal of the Korean Physical Society*, **73**, 265–270 (2018). \*
- S. M. Cha, K. Y. Chae, M. J. Kim, M. S. Kwag, E. J. Lee, K. Abe, S. Hayakawa, H. Shimizu, H. Yamaguchi, L. Yang, S. H. Bae, S. H. Choi, D. N. Binh, N. N. Duy, Z. Ge, V. H. Phong, K. I. Hahn, B. Hong, B. Moon, N. Iwasa, D. Kahl, L. H. Khiem, A. Kim, D. H. Kim, G. W. Kim, S. I. Lim, S. Y. Park, E. J. Kim, K. Kwak, J. Y. Moon, “Study of  $\alpha$ -cluster structure in  $^{22}\text{Mg}$  using a radioactive ion beam,” *Journal of the Korean Physical Society*, **73**, 1055–1060 (2018). \*
- A. Uchiyama, K. Harada, K. Sakamoto, U. Dammalapati, T. Inoue, M. Itoh, S. Ito, H. Kawamura, K. S. Tanaka, R. Yoshioka, Y. Sakemi, “Effective multiple sideband generation using an electro-optic modulator for a multiple isotope magneto-optical trap,” *Rev. Sci. Instrum.* **89**, 123111 (2018). \*
- A. Uchiyama, K. Harada, T. Inoue, H. Kawamura, K. S. Tanaka, M. Itoh, T. Aoki, A. Hatakeyama, Y. Takahashi, Y. Sakemi, “Development of a dual isotope co-magnetometer using laser cooled rubidium toward electron electric dipole moment measurement using francium,” *J. Phys. Conf. Ser.* **1206**, 012008 (2019). \*
- 酒見泰寛, 「冷却原子を用いた電子の電気双極子能率の探索」, 光学 (一般社団法人・日本光学会), **47**, 301 (2018). \*
- 長濱弘季, 「反陽子の基礎物理量の高精度測定」, しょうとつ (原子衝突学会誌), 第 15 卷 5 号, 91 (2018). \*
- S. Yoshida, N. Shimizu, T. Togashi, T. Otsuka, “Uncertainty quantification in the nuclear shell model,” *Phys. Rev. C* **98**, 061301(R) (2018). \*
- S. Yoshida, Y. Utsuno, N. Shimizu, T. Otsuka, “Systematic shell-model study of beta-decay properties and Gamow-Teller strength distributions in  $A \sim 40$  neutron-rich nuclei,” *Phys. Rev. C* **97**, 054321 (2018). \*
- Md. S. R. Laskar, N. Shimizu, Y. Utsuno, “ $g$ -Factor measurement of 2738 keV isomer in  $^{135}\text{La}$ ,” *Phys. Rev. C* **99**, 014308 (2019). \*
- N. Shimizu, T. Mizusaki, “Variational Monte Carlo method for shell-model calculations in odd-mass nuclei and restoration of symmetry,” *Phys. Rev. C* **98**, 054309 (2018). \*
- T. Mizusaki, M. Oi, N. Shimizu, “Why does the sign problem occur in evaluating the overlap of HFB wave functions?,” *Phys. Lett. B* **779**, 237 (2018). \*
- J. Menendez, N. Shimizu, K. Yako, “Is it possible to study neutrinoless decay by measuring double Gamow-Teller transitions?,” *J. Phys. Conf. Ser.* **1056**, 012307 (2018). \*
- X. F. Yang, Y. Tsunoda, T. Otsuka, “Investigating the large deformation of the  $5/2^+$  isomeric state in  $^{73}\text{Zn}$ : An indicator for triaxiality,” *Phys. Rev. C* **97**, 044324 (2018). \*
- A. I. Morales, T. Otsuka, Y. Tsunoda, “Is seniority a partial dynamic symmetry in the first  $\nu g_{9/2}$  shell?,” *Phys. Lett. B* **781**, 706 (2018). \*
- T. Togashi, Y. Tsunoda, T. Otsuka, N. Shimizu, M. Honma, “Novel shape evolution in Sn isotopes from magic numbers 50 to 82,” *Phys. Rev. Lett.* **121**, 062501 (2018). \*
- B. A. Marsh, Y. Tsunoda, T. Otsuka, “Characterization of the shape-staggering effect in mercury nuclei,” *Nature Physics* **14**, 1163 (2018). \*
- P. Singh, T. Otsuka, T. Togashi, Y. Tsunoda, “Evidence for coexisting shapes through lifetime measurements in  $^{98}\text{Zr}$ ,” *Phys. Rev. Lett.* **121**, 192501 (2018). \*
- D. Rosiak, Y. Tsunoda, T. Togashi, T. Otsuka, “Enhanced quadrupole and octupole strength in doubly magic  $^{132}\text{Sn}$ ,” *Phys. Rev. Lett.* **121**, 252501 (2018). \*
- M. Stryczyk, Y. Tsunoda, T. Otsuka, “ $\beta$ -decay study of the  $^{66}\text{Mn}$ - $^{66}\text{Fe}$ - $^{66}\text{Co}$ - $^{66}\text{Ni}$  decay chain,” *Phys. Rev. C* **98**, 064326 (2018). \*

- Ł. W. Iskra, . . . , T. Otsuka, T. Togashi, Y. Tsunoda, . . . , “Revised  $B(E3)$  transition rate and structure of the  $3^-$  level in  $^{96}\text{Zr}$ ,” *Phys. Lett. B* **788**, 396 (2018). \*
- Y. Ichikawa, Y. Tsunoda, and T. Otsuka *et al.*, “Interplay between nuclear shell evolution and shape deformation revealed by magnetic moment of  $^{75}\text{Cu}$ ,” *Nat. Phys.* **15**, 321 (2018). \*
- C. Loelius, T. Otsuka, N. Tsunoda, “Enhanced electric dipole strength for the weakly bound states in  $^{27}\text{Ne}$ ,” *Phys. Rev. Lett.* **121**, 262501 (2018). \*
- H. Nishibata, N. Tsunoda, T. Otsuka, “Structure of  $^{31}\text{Mg}$ : Shape coexistence revealed by  $\beta$ - $\gamma$  spectroscopy with spin-polarized  $^{31}\text{Na}$ ,” *Phys. Rev. C* **99**, 024322 (2018). \*

### [Proceedings]

#### (Original Papers) \*Subject to Peer Review

- N. Imai, “Nuclear reaction data of low-energy LLFP produced by OEDO,” Proceedings of the 2017 Symposium on Nuclear Data, JAEA-Conf2018-001, 39–44 (2018). \*
- M. La Commara, M. Mazzocco, A. Boiano, C. Boiano, C. Manea, C. Parascandolo, D. Pierroutsakou, C. Signorini, E. Strano, D. Torresi, H. Yamaguchi, D. Kahl, P. DiMeo, J. Grebosz, N. Imai, Y. Hirayama, H. Ishiyama, N. Iwasa, S. C. Jeong, H. M. Jia, Y. H. Kim, S. Kimura, S. Kubono, C. J. Lin, H. Miyatake, M. Mukai, T. Nakao, M. Nicoletto, Y. Sakaguchi, A. M. Sanchez-Benitez, F. Soramel, T. Teranishi, Y. Wakabayashi, Y. X. Watanabe, L. Yang, Y. Y. Yang, “ $^{8}\text{B} + ^{208}\text{Pb}$  elastic scattering at Coulomb barrier energies,” *IOP Conf. Series: J. Phys. Conf. Ser.* **966**, 012010 (2018). \*
- D. Kahl, H. Shimizu, H. Yamaguchi, K. Abe, O. Beliuskina, S. M. Cha, K. Y. Chae, A. A. Chen, Z. Ge, S. Hayakawa, N. Imai, N. Iwasa, A. Kim, D. H. Kim, M. J. Kim, S. Kubono, M. S. Kwag, J. Liang, J. Y. Moon, S. Nishimura, S. Oka, S. Y. Park, A. Psaltis, T. Teranishi, Y. Ueno, L. Yang, “Impact of the  $^{26}\text{Al}(p, \gamma)$  reaction to galactic  $^{26}\text{Al}$  yield,” *AIP Conf. Proc.* **1947(1)**, 020003 (2018). \*
- S. Hayakawa, K. Abe, O. Beliuskina, S. M. Cha, K. Y. Chae, S. Cherubini, P. Figuera, Z. Ge, M. Gulino, J. Hu, A. Inoue, N. Iwasa, D. Kahl, A. Kim, D. H. Kim, G. Kiss, S. Kubono, M. L. Cognata, M. L. Commara, L. Lamia, M. Lattuada, E. J. Lee, J. Y. Moon, S. Palmerini, C. Parascandolo, S. Y. Park, D. Pierroutsakou, R. G. Pizzone, G. G. Rapisarda, S. Romano, H. Shimizu, C. Spitaleri, X. D. Tang, O. Trippella, A. Tumino, P. Vi, H. Yamaguchi, L. Yang, N. T. Zhang, “Measurements of the neutron-induced reactions on  $^7\text{Be}$  with CRIB by the trojan horse method,” *AIP Conf. Proc.* **1947(1)**, 020011 (2018). \*
- H. Yamaguchi, D. Kahl, S. Hayakawa, L. Yang, H. Shimizu, Y. Sakaguchi, K. Abe, Y. Wakabayashi, T. Hashimoto, T. Nakao, S. Kubono, T. Suhara, N. Iwasa, A. Kim, D. H. Kim, S. M. Cha, M. S. Kwag, J. H. Lee, E. J. Lee, K. Y. Chae, N. Imai, N. Kitamura, P. Lee, J. Y. Moon, K. B. Lee, C. Akers, H. S. Jung, N. N. Duy, L. H. Khiem, C. S. Lee, S. Cherubini, M. Gulino, C. Spitaleri, G. G. Rapisarda, M. L. Cognata, L. Lamia, S. Romano, A. Coc, N. de Sereville, F. Hammache, G. Kiss, S. Bishop, T. Teranishi, T. Kawabata, Y. K. Kwon, D. N. Binh, “Indirect studies on astrophysical reactions at the low-energy RI beam separator CRIB,” *AIP Conf. Proc.* **1947(1)**, 020022 (2018). \*
- H. Yamaguchi, S. Hayakawa, L. Yang, H. Shimizu, D. Kahl, “Direct measurements and detection techniques with low-energy RIBs,” *EPJ Web Conf.*, **184**, 01017 (2018). \*
- A. Inoue, A. Tamii, K. Abe, S. Adachi, N. Aoi, M. Asai, M. Fukuda, G. Gey, T. Hashimoto, E. Ideguchi, J. Isaak, N. Kobayashi, Y. Maeda, H. Makii, K. Matsuta, M. Mihara, M. Miura, T. Shima, H. Shimizu, R. Tang, T. Dinh Trong, H. Yamaguchi, L. Yang, “Study of the contribution of the  $^7\text{Be}(d, p)$  reaction to the  $^7\text{Li}$  problem in the Big-Bang Nucleosynthesis,” *EPJ Web Conf.* **184**, 02007 (2018). \*
- H. Shimizu, D. Kahl, H. Yamaguchi, K. Abe, O. Beliuskina, S. M. Cha, K. Y. Chae, A. A. Chen, Z. Ge, S. Hayakawa, N. Imai, N. Iwasa, A. Kim, D. H. Kim, M. J. Kim, S. Kubono, M. S. Kawag, J. Liang, J. Y. Moon, S. Nishimura, S. Oka, S. Y. Park, A. Psaltis, T. Teranishi, Y. Ueno, L. Yang, “Isomeric  $^{26}\text{Al}$  beam production with CRIB,” *EPJ Web Conf.* **184**, 02013 (2018). \*
- M. Gulino, S. Cherubini, G. G. Rapisarda, S. Kubono, L. Lamia, M. L. Cognata, R. G. Pizzone, H. Yamaguchi, S. Hayakawa, Y. Wakabayashi, N. Iwasa, S. Kato, T. Komatsubara, T. Teranishi, A. Coc, N. Sereville, F. Hammache, G. Kiss, S. Bishop, D. N. Binh, B. Roeder, L. Trache, R. Tribble, R. Sparta, I. Indelicato, C. Spitaleri, “Trojan Horse Method experiments with radioactive ion beams,” *EPJ Web Conf.* **184**, 01008 (2018). \*
- E. Strano, M. Mazzocco, A. Boiano, C. Boiano, M. La Commara, C. Manea, C. Parascandolo, D. Pierroutsakou, C. Signorini, D. Torresi, H. Yamaguchi, D. Kahl, L. Acosta, P. Di Meo, J. P. Fernandez-Garcia, T. Glodariu, J. Grebosz, A. Guglielmetti, N. Imai, Y. Hirayama, H. Ishiyama, N. Iwasa, S. C. Jeong, H. M. Jia, N. Keeley, Y. H. Kim, S. Kimura, S. Kubono, J. A. Lay, C. J. Lin, G. Marquinez-Duran, I. Marte, H. Miyatake, M. Mukai, T. Nakao, M. Nicoletto, A. Pakou, K. Rusek, Y. Sakaguchi, A. M. Sanchez-Benitez, T. Sava, O. Sgouros, C. Stefanini, F. Soramel, V. Soukeras, E. Stiliaris, L. Stroe, T. Teranishi, N. Toniolo, Y. Wakabayashi, Y. X. Watanabe, L. Yang, Y. Y. Yang, “ $^7\text{Be}$  and  $^8\text{B}$  reaction dynamics at Coulomb barrier energies,” *EPJ Web Conf.* **184**, 02015 (2018). \*
- M. Mazzocco, A. Boiano, C. Boiano, M. La Commara, C. Manea, C. Parascandolo, D. Pierroutsakou, C. Signorini, E. Strano, D. Torresi, H. Yamaguchi, D. Kahl, L. Acosta, P. Di Meo, J. P. Fernandez-Garcia, T. Glodariu, J. Grebosz, A. Guglielmetti, N. Imai, Y. Hirayama, H. Ishiyama, N. Iwasa, S. C. Jeong, H. M. Jia, N. Keeley, Y. H. Kim, S. Kimura, S. Kubono, J. A. Lay, C. J. Lin, G. Marquinez-Duran, I. Marte, H. Miyatake, M. Mukai, T. Nakao, M. Nicoletto, A. Pakou, K. Rusek, Y. Sakaguchi, A. M. Sanchez-Benitez, T. Sava, O. Sgouros, F. Soramel, V. Soukeras, E. Stiliaris, L. Stroe, T. Teranishi, N. Toniolo, Y. Wakabayashi, Y. X. Watanabe, L. Yang, Y. Y. Yang, “Reaction Dynamics for the Systems  $^{7}\text{Be}$ ,  $^8\text{B} + ^{208}\text{Pb}$  at Coulomb Barrier Energies,” *IOP Conf. Series: J. Phys. Conf. Ser.* **1078**, 012013 (2018). \*
- N. Tsunoda, T. Otsuka, N. Shimizu, “Structure of exotic nuclei based on nuclear force,” Proceedings of the Ito International Research Center Symposium “Perspectives of the Physics of Nuclear Structure,” **23**, 012014. (2018). \*
- T. Abe, “Advances in the Monte Carlo Shell Model for Understanding Nuclear Structure,” *JPS Conf. Proc.* **23**, 012009 (2018). \*
- J. Menéndez, “Towards reliable nuclear matrix elements for neutrinoless  $\beta\beta$  decay,” Proceedings of the “Symposium on Perspectives of the Physics of Nuclear Structure,” *JPS Conf. Proc.* **23**, 012036 (2018). \*

T. Miyagi, T. Abe, M. Kohno, P. Navrátil, R. Okamoto, T. Otsuka, N. Shimizu, S. R. Stroberg, “Nuclear Ab Initio Calculations with the Unitary-Model-Operator Approach,” JPS Conf. Proc. **23**, 013007 (2018). \*

## Oral Presentations

### [International Conference etc.]

- S. Shimoura (Invited), “Tetra-neutron and few-body correlations studied by RI-beam experiments,” New Frontiers in Nuclear Physics and Astrophysics (NNPA), Antalya, Turkey, June 1–May 28, 2018.
- S. Shimoura (Invited), “Tetraneutron system populated by double-charge exchange reactions using RI beam,” The 13th International Conference on Hypernuclear and Strange Particle Physics (HYP2018), Portsmouth, Virginia, USA, June 24–29, 2018.
- S. Shimoura (Invited), “Tetra-neutron system populated by RI-beam induced reactions,” The 22nd International Conference on Few-Body Problems in Physics (FB22), Caen, France, July 9–13, 2018.
- S. Shimoura (Invited), “Nuclear Reaction Data for Long-Lived Fission Products,” IMPACT International Symposium on “New Horizons of Partitioning and Transmutation Technologies with Accelerator System,” The University of Tokyo, December 2–3, 2018.
- S. Shimoura (Invited), “Tetra-neutron system populated by exothermic double-charge exchange reaction,” 13th International Conference on Nucleus-Nucleus Collisions (NN2018), Omiya, Saitama, December 4–8, 2018.
- N. Imai (Invited), “Experimental studies with the energy-degraded RI beams,” 20th Northeastern Asia symposium, Nagoya, Japan, September 19, 2018.
- S. Michimasa (Invited), “Overview of OEDO,” International OEDO Workshop 2018, Wako, Japan, June 11, 2018.
- M. Dozono (Invited), “Status report of ImPACT17-02-01/02,” International OEDO Workshop 2018, Wako, Japan, June 11, 2018.
- N. Imai (Oral), “Measurement of  $^{77,79}\text{Se}(d, p)$  reactions in inverse kinematics at OEDO,” The 10th international conference on Direct Reaction with Exotic Beams (DREB2018), Matsue, Japan, June 4–8, 2018.
- S. Michimasa (Oral), “New energy-degrading beam line for in-flight RI beams, OEDO,” The International Conference on Electromagnetic Isotope Separators and Related Topics (EMIS), CERN Geneva, Switzerland, September 16–21, 2018.
- S. Michimasa (Oral), “Construction of Low-energy RI Beam Line at RIBF and Nuclear Reaction Data on Low-energy LLFPs,” Fifteenth NEA Information Exchange Meeting on Actinide and Fission Product Partitioning and Transmutation, Manchester Hall, Manchester, UK, September 30–October 3, 2018.
- S. Michimasa (Invited), “Recent Achievements using OEDO-SHARAQ at RIBF,” The 10th China-Japan Joint Nuclear Physics Symposium (CJNP2018), Sheraton Bailuhu Resort Hotel, Houzhou, China, November 18–23, 2018.
- S. Ota (Invited), “Active target technique with medium-energy high-intensity heavy-ion beams,” The 10th China-Japan Joint Nuclear Physics Symposium (CJNP2018), Sheraton Bailuhu Resort Hotel, Huizhou, China, November 18–23, 2018.
- N. Imai (Invited), “Surrogate reaction of  $^{79}\text{Se}(n, \gamma)$ ,” The 5th Joint Meeting of the APS Division of Nuclear Physics and the Physical Society of Japan, Waikoloa, Hawaii, USA, October 23–27, 2018.
- S. Michimasa (Oral), “Direct mass measurements of very neutron-rich calcium isotopes beyond  $N = 34$ ,” The 5th Joint Meeting of the APS Division of Nuclear Physics and the Physical Society of Japan, Waikoloa, Hawaii, USA, October 23–27, 2018.
- M. Dozono (Oral), “Nuclear reaction study for long-lived fission products in nuclear waste: Proton- and deuteron-induced reactions on  $^{107}\text{Pd}$  and  $^{93}\text{Zr}$  at 20–30 MeV/u,” The 5th Joint Meeting of the APS Division of Nuclear Physics and the Physical Society of Japan, Waikoloa, Hawaii, USA, October 23–27, 2018.
- S. Ota (Invited), “Experimental study of the isospin dependence of nuclear incompressibility,” The 5th Joint Meeting of the APS Division of Nuclear Physics and the Physical Society of Japan, Waikoloa, Hawaii, USA, October 23–27, 2018.
- S. Masuoka (Oral), “Re-measurement of  $^4\text{He}(^8\text{He}, ^8\text{Be})$  reaction,” The 5th Joint Meeting of the APS Division of Nuclear Physics and the Physical Society of Japan, Waikoloa, Hawaii, USA, October 23–27, 2018.
- R. Tsunoda (Oral), “Proton resonance scattering of a shape-coexistence nucleus  $^{118}\text{Sn}$ ,” The 5th Joint Meeting of the APS Division of Nuclear Physics and the Physical Society of Japan, Waikoloa, Hawaii, USA, October 23–27, 2018.
- K. Kawata (Oral), “Production of isomers around  $^{52}\text{Fe}$  nucleus via projectile fragmentation,” The 5th Joint Meeting of the APS Division of Nuclear Physics and the Physical Society of Japan, Waikoloa, Hawaii, USA, October 23–27, 2018.
- L. Stuhl (Oral), “Study of spin-isospin responses of radioactive nuclei with background free neutron spectrometer, PANDORA International Conference on Electromagnetic Isotope Separators and Related Topics (EMIS2018),” CERN, Geneva, Switzerland, September 16–21, 2018.
- L. Stuhl (Invited), “Detector development for  $(p, n)$  measurements at RIKEN RIBF,” Nuclear Physics In Stellar Explosions Workshop, Debrecen, Hungary, September 12–14, 2018.
- L. Stuhl (Oral), “Overview of campaign type experiments at SAMURAI—The  $^{18}\text{O}$  campaign,” SAMURAI International Workshop 2018, RIKEN Nishina Center, Wako, Japan, September 3–4, 2018.
- L. Stuhl (Oral), “Status of  $(p, n)$  measurements at SAMURAI,” SAMURAI International Workshop 2018, RIKEN Nishina Center, Wako, Japan, September 3–4, 2018.
- L. Stuhl (Oral), “Study of spin-isospin responses of light nuclei along the drip line with PANDORA,” The 10th international conference on Direct Reactions with Exotic Beams (DREB2018), Matsue, Japan, June 4–8, 2018.
- H. Tokieda (Oral), “CNS Active Target (CAT) for high-intensity heavy-ion beam experiment,” The 5th Joint Meeting of the APS Division of Nuclear Physics and the Physical Society of Japan, Waikoloa, Hawaii, USA, October 23–27, 2018.
- C. Iwamoto (Oral), “Performance evaluation of Dual Gain Multi-layer Thick GEM for CAT with high-intensity heavy-ion beams,” The 5th Joint Meeting of the APS Division of Nuclear Physics and the Physical Society of Japan, Waikoloa, Hawaii, USA, October 23–27,

2018.

- S. Ota (Oral), “Giant resonances in Tin-region nuclei,” 6th International Conference on Collective Motion in Nuclei under Extreme Conditions, Cape town, South Africa, October 29–November 2, 2018.
- Y. Sekiguchi (Oral), “Long-range two-particle correlations,” Second internal workshop on Collectivity in Small Collision Systems (CSCS2018), Wuhan, China, June 13–15, 2018.
- Y. Sekiguchi for the ALICE Collaboration (Oral), “Long range angular correlations in  $p$ -Pb collisions with ALICE,” The 5th Joint Meeting of the APS Division of Nuclear Physics and the Physical Society of Japan, Waikoloa, Hawaii, USA, October 23–27, 2018.
- S. Hayashi for the ALICE Collaboration (Oral), “ $J/\psi$  production in  $p$ -Pb collisions with the ALICE detector,” The 5th Joint Meeting of the APS Division of Nuclear Physics and the Physical Society of Japan, Waikoloa, Hawaii, USA, October 23–27, 2018.
- S. Hayashi for the ALICE Collaboration (Oral), “ $J/\psi$  production in  $p$ -Pb collisions with the ALICE detector,” The 7th Asian Triangle Heavy Ion Conference (ATHIC2018), Hefei, China, November 3–6, 2018.
- Y. Sekiguchi for the ALICE Collaboration (Oral), “Two-particle correlations with ALICE,” The 7th Asian Triangle Heavy Ion Conference (ATHIC2018), Hefei, China, November 3–6, 2018.
- S. Hayashi for the ALICE Collaboration (Oral), “Quarkonium production in pp, pA, and AA collisions,” Quark and Nuclear Physics 2018 (QNP2018), Tsukuba, Japan, November 13–17, 2018.
- T. Gunji (Oral), “Extension of Forward Physics beyond 2030,” International workshop on Forward Physics and Forward Calorimeter upgrade in ALICE, Tsukuba, Japan. March 7–9, 2019.
- L. Yang (Oral), “Reaction mechanisms of  $^{17}\text{F} + ^{58}\text{Ni}$  at energies around the Coulomb barrier,” DREB2018, Kunibiki Messe, Matsue, Shimane, Japan, June 4–8, 2018.
- H. Yamaguchi (Oral), “Study on explosive nuclear synthesis with low-energy RI beams at CRIB,” 15th International Symposium on Nuclei in the Cosmos, LNGS, Assergi, Italy, June 24–29, 2018.
- S. Hayakawa (Oral), “Cross section measurements of the  $^7\text{Be}(n, p)^7\text{Li}$  and the  $^7\text{Be}(n, \alpha)^4\text{He}$  reactions covering the Big-Bang nucleosynthesis energy range by the Trojan Horse method at CRIB,” 15th International Symposium on Nuclei in the Cosmos, LNGS, Assergi, Italy, June 24–29, 2018.
- H. Yamaguchi (Oral), “Activities at the low-energy RI beam separator CRIB,” RIBF Users Meeting 2018, RIKEN, Wako, Saitama, Japan, September 5–6, 2018.
- H. Yamaguchi (Invited), “Indirect method application for RI-beam experiments,” ECT\* Workshop “Indirect Methods in Nuclear Astrophysics,” ECT\*, Trento, Italy, November 5–9, 2018.
- H. Yamaguchi (Invited), “Studies on nuclear astrophysics and nuclear clustering with low-energy RI beams at CRIB,” 13th International Conference on Nucleus-Nucleus Collisions (NN2018), Omiya, Saitama, Japan, December 4–8, 2018.
- H. Yamaguchi (seminar), “Study on cluster states in unstable nuclei with alpha-resonant scattering,” RIBF Nuclear Physics Seminar, RIKEN, Wako, Saitama, Japan, January 8, 2019.
- K. Harada (Oral), “Magneto-optical trapping of radioactive francium atoms: toward search for electron electric dipole moment,” 11<sup>th</sup> Fundamental Physics using Atoms, OIST, Okinawa, Japan, March 1–4, 2019.
- H. Nagahama (Oral), “A new approach to high-precision measurements of the electron EDM using francium atoms,” The 5th Joint Meeting of the APS Division of Nuclear Physics and the Physical Society of Japan, Waikoloa, Hawaii, USA, October 23–27, 2018.
- H. Nagahama (Invited), “High-precision measurements for testing CP and CPT symmetry,” 3<sup>rd</sup> ETH Zurich-The University of Tokyo Strategic Partnership Symposium on the UN Sustainable Development Goals and Innovation, The University of Tokyo, Japan, January 21–22, 2019.
- T. Abe (Oral), “Recent advances of the no-core Monte Carlo shell model,” GANIL Workshop on Nuclear Structure and Reactions for the 2020s, GANIL, Caen, France, July, 2018.
- T. Abe (Oral), “Large-scale computation of the no-core Monte Carlo shell model for nuclear many-body problems,” The 5th Joint Meeting of the APS Division of Nuclear Physics and the Physical Society of Japan, Waikoloa, Hawaii, USA, October 23–27, 2018.
- T. Abe (Oral), “Recent results and implications of no-core MCSM calculations for nuclear structure,” The 5th Joint Meeting of the APS Division of Nuclear Physics and the Physical Society of Japan, Waikoloa, Hawaii, USA, October 23–27, 2018.
- T. Abe (Oral), “No-core Monte Carlo shell model calculations with Daejeon16 NN interaction,” International Conference “Nuclear Theory in the Supercomputing Era – 2018” (NTSE-2018), IBS, Daejeon, Korea, November, 2018.
- T. Abe (Oral), “Recent advances in the no-core Monte Carlo shell model for the alpha clustering nature in light nuclei,” International workshop on “Recent advances in nuclear structure physics 2018” (RANSP2018), YITP, Kyoto, Japan, November 2018.
- T. Abe (Oral), “Alpha-cluster structure from no-core Monte Carlo shell model (oral),” The 50th Reimei workshop on Universal Physics in Many-Body Quantum Systems —From Atoms to Quarks—, JAEA, Ibaraki, Japan, December 2018.
- T. Abe (Oral), “Alpha-cluster structure from no-core Monte Carlo shell model,” TRIUMF Theory Workshop on “Progress in Ab Initio Techniques in Nuclear Physics,” TRIUMF, Vancouver, Canada, March 2019.
- N. Shimizu (Oral), “Large-scale shell model calculations and chiral doublet of  $^{128}\text{Cs}$ ,” International Conference, Nuclear Theory in the Supercomputing Era 2018 (NTSE-2018), November 2018.
- N. Shimizu (Oral), “Double Gamow Teller transition and its relation to neutrinoless double beta decay matrix element,” The 5th Joint Meeting of the APS Division of Nuclear Physics and the Physical Society of Japan, Waikoloa, Hawaii, USA, October 23–27, 2018.
- N. Shimizu (Oral), “Shell-model study in  $A \sim 130$  nuclei and chiral doublet of  $^{128}\text{Cs}$ ,” The 9th international workshop “Quantum Phase Transitions in Nuclei and Many-body Systems,” Padova, Italy, May, 2018.
- 角田佑介 (Invited), “Shapes of Medium-mass Nuclei Studied by Monte Carlo Shell Model Calculations,” Nuclear Structure 2018

(NS2018), Michigan State University, Michigan, USA, August 2018.

角田佑介 (Invited), “Large-scale shell model calculations for structure of Ni and Cu isotopes,” The 5th Joint Meeting of the APS Division of Nuclear Physics and the Physical Society of Japan, Waikoloa, Hawaii, USA, October 23–27, 2018.

N. Tsunoda (Oral), “Physics in the island of inversion starting from the first principle,” Shapes and Symmetries in Nuclei: from Experiment to Theory (SSNET’18 conference), Gif-Sur Yvette, France, October 2018.

N. Tsunoda (Oral), “Study of neutron-rich nuclei via nuclear force and microscopic theory,” The 5th Joint Meeting of the APS Division of Nuclear Physics and the Physical Society of Japan, Waikoloa, Hawaii, USA, October 23–27, 2018.

J. Menéndez (Invited), “Double Gamow-Teller transitions in connection to neutrinoless double-beta decay,” ECT\* Workshop “Exploring the role of electro-weak currents, in Atomic Nuclei,” Trento, Italy, April 2018.

J. Menéndez (Invited), “Current status of neutrinoless double beta decay matrix elements,” 13th Conference on the Intersections of Particle and Nuclear Physics (CIPANP 2018), Indian Wells, USA, May 2018.

J. Menéndez (Invited), “Neutrinoless double-beta decay and direct dark matter detection,” INT Workshop “From nucleons to nuclei: enabling discovery for neutrinos, dark matter and more,” Seattle, USA, June 2018.

J. Menéndez (Invited), “Double charge exchanges for double beta decays,” Symposium “Neutrinos and Dark Matter in Nuclear Physics (NDM18),” Daejeon, South Korea, July 2018.

J. Menéndez (Invited), “Recent progress on neutrinoless double-beta decay nuclear matrix elements,” “Double-Beta Decay and Underground Science,” The 5th Joint Meeting of the APS Division of Nuclear Physics and the Physical Society of Japan, Waikoloa, Hawaii, USA, October 23–27, 2018.

J. Menéndez (Invited), “Nuclear observables to constrain neutrinoless double-beta decay,” The 5th Joint Meeting of the APS Division of Nuclear Physics and the Physical Society of Japan, Waikoloa, Hawaii, USA, October 23–27, 2018.

J. Menéndez (Invited), “Nuclear matrix elements to unveil the nature of neutrinos and dark matter,” Conference “Shapes and Symmetries in Nuclei: from Experiment to Theory (SSNET’18),” Gif-sur-Yvette, France, November 2018.

T. Miyagi (Oral), “Recent progress in the unitary-model-operator approach,” TRIUMF workshop on Progress in Ab Initio Techniques in Nuclear Physics, Vancouver, Canada, February–March 2018.

#### [Domestic Conference]

下浦享 (Oral), 「核変換：新たな核変換の方法を探る」, ImPACT プログラム「核変換による高レベル放射性廃棄物の大幅な低減・資源化」公開成果報告会—新たな選択肢の提案, 未来に向けて—品川インターシティホール, 2019年3月9日.

D. Dozono (Invited), “r-process study with OEDO,” 研究会「重力波観測時代の r プロセスと不安定核」, Wako, Japan, June 20, 2018.

S. Michimasa (Invited), “Closed-shell property at  $N = 34$  seen in the masses of neutron-rich Ca isotopes,” 日本物理学会第 74 回年次会, 九州大学, 伊都キャンパス, 福岡, 2019年3月14日–17日.

M. Dozono (Oral), 「低速 RI ビームを用いた  $^{107}\text{Pd}$  の陽子・重陽子誘起反応測定」, 日本物理学会第 7 回年次会, 九州大学, 伊都キャンパス, 福岡, 2019年3月14日–17日.

S. Masuoka (Oral), 「二重荷電交換反応  $^4\text{He}(^8\text{He}, ^8\text{Be})$  反応の再測定 (II)」, 日本物理学会第 74 回年次会, 九州大学, 伊都キャンパス, 福岡, 2019年3月14日–17日.

J. W. Hwang (Oral), “Angle-tunable Degradar for a low-energy beamline,” 日本物理学会第 74 回年次会, 九州大学, 伊都キャンパス, 福岡, 2019年3月14日–17日.

M. Dozono (Oral), 「低速 RI ビームを用いた LLFP 核の核反応データ測定」, 日本原子力学会 2018 年秋の大会, 岡山大学, 津島キャンパス, 岡山, 2018年9月5日–7日.

N. Imai (Oral), 「核変換による高レベル放射性廃棄物の大幅な低減・資源化 (4-2) 代理反応を用いた  $^{79}\text{Se}(n, \gamma)^{80}\text{Se}$  反応断面積評価」, 日本原子力学会 2019 年春の年会, 茨城大学, 水戸キャンパス, 水戸, 2019年3月20日–22日.

M. Dozono (Oral), 「核変換による高レベル放射性廃棄物の大幅な低減・資源化 (4-3) 低速 RI ビームを用いた LLFP 核の陽子・重陽子誘起反応測定」, 日本原子力学会 2019 年春の年会, 茨城大学, 水戸キャンパス, 水戸, 2019年3月20日–22日.

Y. Sekiguchi (Oral), 「 $p + p$  や  $p/d/\text{He} + A$  衝突 (小さい系) における集団運動」, 35th Heavy Ion Café and 27th Heavy Ion Pub, June 30, 2018. Nagoya, Japan.

T. Gunji (Oral), 「EM プローブ」, 35th Heavy Ion Café and 27th Heavy Ion Pub, Nagoya, Japan, June 30, 2018.

Y. Sekiguchi for the ALICE Collaboration (Oral), “Pseudorapidity dependence of anisotropic flow in  $p$ -Pb collisions with the ALICE detector,” The Physical Society of Japan 2019 annual meeting, Fukuoka, Japan, March 14–17, 2019.

T. Gunji for the ALICE Collaboration (Oral), “Low mass dielectron measurements in  $pp$  and Pb-Pb collisions at LHC-ALICE,” The Physical Society of Japan 2019 annual meeting, Fukuoka, Japan, March 14–17, 2019.

酒見泰寛 (Invited), 「人工 RI 結晶による基本対称性の研究」, 超重元素研究の新展開 (研究会), 九州大学, 福岡, 2018年7月30–31日.

酒見泰寛 (Invited), 「光格子重元素干渉計による基本対称性の研究」, 物質階層原理&ヘテロ界面 (研究報告会), 理化学研究所, 和光キャンパス, 和光, 2019年2月5–6日.

酒見泰寛 (Invited), “Fundamental physics with laser cooled heavy elements,” 2019 重元素化学ワークショップ, 理化学研究所, 和光キャンパス, 和光, 2019年3月27–28日.

長濱弘季 (Invited), 「基本対称性の高精度検証」, RIBF 若手放談会: エキゾチック核物理の将来, 理研神戸, 日本, 2019年2月.

早水友洋 (Oral), 「電子の永久電気双極子モーメント探索へ向けたフランシウム原子の生成とトラップ」, 日本物理学会第 74 回年次会, 伊都キャンパス, 九州大学, 福岡, 2019年3月14日–17日.

角田佑介 (Oral), 「モンテカルロ殻模型による中重核の構造の研究」, 素粒子・原子核・宇宙「京からポスト京に向けて」シンポジウム, 筑波大学東京キャンパス文京校舎, 東京, January 2019.

- N. Tsunoda (Oral), “Physics in neutron-rich nuclei with the effective interaction for the shell model based on nuclear force,” 日本物理学会第 73 回年次大会, 福岡, 2019 年 3 月.
- 角田直文, 「原子核殻模型の統計力学的理解」, 若手放談会: エキゾチック核物理の将来, 理研神戸, 2019 年 2 月,
- 角田直文, 「中性子過剰原子核の存在限界とその新しい原理—核力に基づく大規模計算による解析」, 素粒子・原子核・宇宙「京からポスト京に向けて」シンポジウム, 筑波大学東京キャンパス文京校舎, 東京, 2019 年 1 月.
- 阿部喬 (Invited), 「大規模数値計算の現在と未来」, RIBF 若手放談会: エキゾチック核物理の将来, 理研神戸, 2019 年 2 月.
- 清水則孝 (Oral), 「制限ボルツマンマシンによる殻模型波動関数の記述」, 日本物理学会第 73 回年次大会, 福岡, 2019 年 3 月.
- 清水則孝 (Oral), 「殻模型計算による中重核高スピン状態の記述とカイラル二重項バンド」, 素粒子・原子核・宇宙「京からポスト京に向けて」シンポジウム, 東京, 2019 年 1 月.
- 大城幸光 (Oral), 「CNS イオン源の現状」, 第 16 回 AVF 合同打ち合わせ, 2018 年 10 月 30–31 日. 高崎量子応用研究所.
- 小高康熙 (Oral), 「AVF 入射軌道解析の現状」, 第 16 回 AVF 合同打ち合わせ, 高崎量子応用研究所, 2018 年 10 月 30–31 日.

## Posters Presentations

### [International Conference etc.]

- M. Dozono (Poster), “Proton- and deuteron-induced reactions on  $^{107}\text{Pd}$  and  $^{93}\text{Zr}$  at 20–30 MeV/nucleon,” The 10th international conference on Direct Reaction with Exotic Beams (DREB2018), Matsue, Japan, June 4–8, 2018.
- J. W. Hwang (Poster), “Study on performance of the OEDO beamline,” The 10th international conference on Direct Reaction with Exotic Beams (DREB2018), Matsue, Japan, June 4–8, 2018.
- S. Shimoura (Poster), “Reduction and resource recycling of high-level liquid radioactive wastes through nuclear transmutation—Nuclear Reaction Data of long-lived fission products,” Fifteenth NEA Information Exchange Meeting on Actinide and Fission Product Partitioning and Transmutation, Manchester Hall, Manchester, UK, September 30–October 3, 2018.
- K. Kawata (Poster), “Production of isomer beam around  $^{52}\text{Fe}$  nucleus via projectile fragmentation,” The 10th international conference on Direct Reaction with Exotic Beams (DREB2018), Matsue, Japan, June 4–8, 2018.
- S. Hayashi for the ALICE Collaboration (Poster), “Inclusive  $J/\psi$  measurement at mid-rapidity in  $p$ -Pb collisions with the ALICE detector,” Quark Matter 2018 (QM2018), Venice, Italy, May 13–19, 2018.
- H. Shimizu (Poster), “Isomeric RIB Production of Aluminum-26,” 15th International Symposium on Nuclei in the Cosmos, LNGS, Assergi, Italy, June 24–29, 2018.
- N. Ozawa (Poster), “Development of a New Surface Ionizer for the FrEDM Experiment,” The 11<sup>th</sup> International Workshop on Fundamental Physics Using Atoms, OIST, Okinawa, Japan, March 1–4, 2019.

### [Domestic Conference]

- 下浦享 他 (Poster), 「PJ2-1 低速 RI ビーム開発」, ImPACT プログラム「核変換による高レベル放射性廃棄物の大幅な低減・資源化」公開成果報告会—新たな選択肢の提案, 未来に向けて—, 品川インターシティホール, 東京, 2019 年 3 月 9 日.
- T. Abe, “Alpha-cluster structure from no-core Monte Carlo shell model (poster),” The 1st R-CCS International Symposium on K and Post-K: Simulation, Big Data and AI supporting Society 5.0, Kobe, Japan, February 2019.
- 阿部喬, “Alpha-cluster structure from no-core Monte Carlo shell model (ポスター発表),” 新学術領域「量子クラスターで読み解く物質の階層構造」, キックオフシンポジウム, 東工大, 2018 年 11 月.

## Awards

- 大津秀暁, 藤田玲子, 松崎禎市郎, 櫻井博儀, 下浦享, 水口浩司, 大井川宏之, 小澤正基, 仁井田浩二, 平成 30 年度全国発明表彰「21 世紀発明賞」, 「放射性廃棄物の処理方法の発明」, (特許第 6106892 号), 2018 年 6 月.

## Partner Institution

Wako Nuclear Science Center, IPNS (Institute of Particle and Nuclear Studies)  
KEK (High Energy Accelerator Research Organization)

### 1. Abstract

The Wako Nuclear Science Center (WNSC) of KEK aims to promote low-energy nuclear physics and nuclear astrophysics research as well as interdisciplinary studies using short-lived radioactive nuclei. WNSC operates the KEK Isotope Separation System (KISS) which is an electro-magnetic isotope separator featuring elemental selectivity from the use of resonance laser ionization in a gas catcher. The KISS facility provides various neutron-rich nuclei via multinucleon transfer reactions. Of particular significance is its provision of nuclei in the vicinity of the neutron magic number  $N = 126$ . Optical and  $\beta$ - $\gamma$  spectroscopy have been applied to these neutron-rich nuclear beams, for nuclear structure and nuclear astrophysical studies. Several new developments—a rotating target, a donut-shaped gas cell, and in-jet laser ionization scheme—have been performed to improve the performance of KISS facility. The WNSC has also developed multi-reflection time of flight mass spectrographs (MRTOF-MS) for precision mass measurements of short-lived nuclei in collaboration with the RIKEN SLOWRI team and the Institute of Basic Science (IBS), Korea. After successful mass measurements in combination with the GARIS-II at RILAC, the existing MRTOF-MS setup has been renewed for use with the GARIS-II relocated after the ring cyclotron, and additional MRTOF-MS setups are being fabricated and placed at KISS and at F11 of the ZeroDegree Spectrometer for comprehensive mass measurements of more than one thousand nuclides.

### 2. Major Research Subjects

- (1) Production and manipulation of radioactive isotope beams for nuclear experiments.
- (2) Explosive nucleosynthesis (r- and rp-process).
- (3) Heavy ion reaction mechanism for producing heavy neutron-rich nuclei.
- (4) Development of MRTOF mass spectrographs for short-lived nuclei.
- (5) Comprehensive mass measurements of short-lived nuclei including superheavy elements.

### 3. Summary of Research Activity

KISS is an element-selective isotope separator, combining the use of a magnetic mass separator with in-gas-cell resonant laser ionization. The gas cell, filled with argon gas at 75 kPa, is a central component of KISS, from which only the elements of interest are extracted as an ion beam, and subsequently mass separated. In the cell, nuclei primarily produced by low-energy heavy-ion reactions are stopped (thermalization and neutralization), transported by a buffer gas (gas flow of  $\sim 75$  kPa argon in the present case), and then re-ionized by laser irradiation just before the exit. The gas cell was fabricated to efficiently collect the reaction products produced by multi-nucleon transfer (MNT) reactions. For higher primary beam intensities and a higher extraction efficiency, a doughnut-shaped gas cell with a rotating target wheel setup has been developed. The mass separated isotope beams are guided to a tape transport setup where a low-background beta telescope counter is setup and surrounded by an array of germanium detectors consisting of four super-clover germanium crystals. The system has successfully performed  $\beta$ - $\gamma$  spectroscopy of isotopes of Pt, Ir and Os.

An important feature of KISS is the capability to perform laser spectroscopy by scanning the resonant ionization laser frequency. The hyperfine structure constants of  $^{196,197,198}\text{Ir}$  and  $^{199}\text{Pt}$  have been measured at KISS. However, due to pressure broadening of the resonance line in the gas cell, the linewidths were as large as 12 GHz. To determine electromagnetic moments and isotope shifts with much higher precision, an “in-gas-jet” laser ionization method has been implemented at KISS. A high repetition rate, narrowband laser radiation irradiates the atoms within the gas jet after the nozzle of the cell and an S-shaped radiofrequency quadrupole structure guides resonantly ionized ions toward the mass separator. With this new setup, a narrow line width of 0.6 GHz has been achieved for the hyperfine splitting spectrum of  $^{194}\text{Pt}$ .

The multi-reflection time-of-flight mass spectrograph (MRTOF-MS) has been developed for direct mass measurements of short-lived heavy nuclei. After successful mass measurements of more than 80 nuclides, including short-lived ( $T_{1/2} = 10$  ms) isotopes of Ra and several isotopes of the trans-uranium elements Es and Md at GARIS-II in collaboration with the SLOWRI team and the Super Heavy Element Synthesis team of RIKEN, multiple MRTOF setups are being installed at different facilities of RIBF.

The first MRTOF was connected directly to the new GARIS-II in the E6 experimental room (after the ring cyclotron) in a manner expected to yield a total efficiency of more than 10%. This device will be used for precise mass measurements of Db isotopes produced in cold fusion reactions, as well for measurements of Mc and Nh isotopes produced in hot fusion reactions. In 2018, a short online commissioning experiment was performed for testing the newly developed “alpha-ToF” detector which can correlate the time-of-flight signal to alpha-decay signals. The test experiment with a Ra isotope showed that the background rate was highly reduced and, in addition, the life-time of the isotope could be determined from the correlation data.

A mini-MRTOF with a so-called “gas-cell cooler buncher” setup has been installed at KISS and offline commissioning is in progress. Efficient trapping of a 30 keV ion beam from KISS has been confirmed. A third-prototype SLOWRI gas catcher with a “gutter structure” RF-carpet has been developed for a new MRTOF setup, referred to as the ZD-MRTOF, for use at the beam dump of the ZeroDegree spectrometer. This setup will be used for “symbiotic” experiments with other experimental groups who use the ZeroDegree spectrometer to perform efficient mass measurements in parallel to the other experiments.

## Members

### Group Leader

Hiroari MIYATAKE

### Researchers

Michiharu WADA  
Yutaka WATANABE

Yoshikazu HIRAYAMA  
Peter SCHURY

### Technical Staff

Yutaka KAKIGUCHI

Michihiro OYAIZU

### Visiting Researchers

Jun-young Moon (IBS)  
Jin-hyung Park (IBS)

Hyun-suk CHOI (Seoul National University)

### Student Trainees

Momo MUKAI (PhD. Student, Tsukuba Univ.)  
Sota KIMURA (PhD. Student, Tsukuba Univ.)

Md MURAD AHMED (PhD. Student, Tsukuba Univ.)

### Assistant

Machiko IZAWA

## List of Publications & Presentations

### Publications

#### [Journal]

#### (Original Papers) \*Subject to Peer Review

- Y. Watanabe, Y. Hirayama, H. Miyatake, “KEK Isotope Separation System (KISS),” *Nucl. Phys. News* **28**, 2–28 (2018).
- M. Reponen, V. Sonnenschein, T. Sonoda, H. Tomita, M. Oohashi, D. Matsui, M. Wada, “Towards in-jet resonance ionization spectroscopy: An injection-locked Titanium: Sapphire laser system for PALIS-facility,” *Nucl. Instrum. Methods Phys. Res. A* **908**, 236–243 (2018). \*
- P. Schury, Y. Ito, M. Rosenbusch, H. Miyatake, H. Wollnik, “Improving wide-band mass measurements in a multi-reflection time-of-flight mass spectrograph by usage of a concomitant measurement scheme,” *Int. J. Mass Spectrom.* **433**, 40–46 (2018). \*
- M. Wada, “超重元素の質量測定—革新的質量分光器 MRTOF-MS による—,” *Radiotopes* **67**, 299–308 (2018).
- M. La Commara, M. Mazzocco, A. Boiano, C. Boiano, C. Manea, C. Parascandolo, D. Pierrousakou, C. Signorini, E. Strano, D. Torresi, H. Yamaguchi, D. Kahl, P. Di Meo, J. Grebosz, N. Imai, Y. Hirayama, H. Ishiyama, N. Iwasa, S. C. Jeong, H. M. Jia, Y. H. Kim, S. Kimura, S. Kubono, C. J. Lin, H. Miyatake, M. Mukai, T. Nakao, M. Nicoletto, Y. Sakaguchi, A. M. Sánchez-Benítez, F. Soramel, T. Teranishi, Y. Wakabayashi, Y. X. Watanabe, L. Yang, Y. Y. Yang, “ $^{8}\text{B} + ^{208}\text{Pb}$  elastic scattering at Coulomb barrier energies,” *J. Phys. Conf. Ser.* **966**, 012010 (2018). \*
- Y. Hirayama, Y. X. Watanabe, M. Mukai, M. Ahmed, S. C. Jeong, Y. Kakiguchi, S. Kimura, M. Oyaizu, J. H. Park, P. Schury, M. Wada, H. Watanabe, H. Miyatake, “ $\beta$ - and  $\gamma$ -decay spectroscopy of  $^{197,198}\text{Os}$ ,” *Phys. Rev. C* **98**, 014321 (2018). \*
- S. Kimura, Y. Ito, D. Kaji, P. Schury, M. Wada, H. Haba, T. Hashimoto, Y. Hirayama, M. MacCormick, H. Miyatake, J. Y. Moon, K. Morimoto, M. Mukai, I. Muary, A. Ozawa, M. Rosenbusch, H. Schatz, A. Takamine, T. Tanaka, Y. X. Watanabe, H. Wollnik, “Atomic masses of intermediate-mass neutron-deficient nuclei with relative uncertainty down to 35-ppb via multireflection time-of-flight mass spectrograph,” *Int. J. Mass Spectrom.* **430**, 134–142 (2018). \*
- E. Strano, M. Mazzocco, A. Boiano, C. Boiano, M. La Commara, C. Manea, C. Parascandolo, D. Pierrousakou, C. Signorini, D. Torresi, H. Yamaguchi, D. Kahl, L. Acosta, P. Di Meo, J. P. Fernandez-Garcia, T. Glodariu, J. Grebosz, A. Guglielmetti, N. Imai, Y. Hirayama, H. Ishiyama, N. Iwasa, S. C. Jeong, H. M. Jia, N. Keeley, Y. H. Kim, S. Kimura, S. Kubono, J. A. Lay, C. J. Lin, G. Marquinez-Duran, I. Marte, H. Miyatake, M. Mukai, T. Nakao, M. Nicoletto, A. Pakou, K. Rusek, Y. Sakaguchi, A. M. Sanchez-Benitez, T. Sava, O. Sgouros, C. Stefanini, F. Soramel, V. Soukeras, E. Stiliaris, L. Stroe, T. Teranishi, N. Toniolo, Y. Wakabayashi, Y. X. Watanabe, L. Yang, Y. Y. Yang, “ $^{7}\text{Be}$  and  $^{8}\text{B}$  reaction dynamics at Coulomb barrier energies,” *J. Phys. Conf. Ser.* **184**, 02015 (2018).
- M. Rosenbusch, Y. Ito, P. Schury, M. Wada, D. Kaji, K. Morimoto, H. Haba, S. Kimura, H. Koura, M. MacCormick, H. Miyatake, J. Y. Moon, K. Morita, I. Murray, T. Niwase, A. Ozawa, M. Reponen, A. Takamine, T. Tanaka, H. Wollnik, “New mass anchor points for neutron-deficient heavy nuclei from direct mass measurements of radium and actinium isotopes,” *Phys. Rev. C* **97**, 064306 (2018).\*
- H. Miyatake, M. Wada, X. Y. Watanabe, Y. Hirayama, P. Schury, M. Ahmed, H. Ishiyama, S. C. Jeong, Y. Kakiguchi, S. Kimura, J. Y. Moon, M. Mukai, M. Oyaizu, J. H. Park, “Present status of the KISS project,” *AIP Conf. Proc.* **1947**, 020018 (2018).\*
- Y. Ito, P. Schury, M. Wada, F. Arai, H. Haba, Y. Hirayama, S. Ishizawa, D. Kaji, S. Kimura, H. Koura, M. MacCormick, H. Miyatake, J. Y. Moon, K. Morimoto, K. Morita, M. Mukai, I. Murray, T. Niwase, K. Okada, A. Ozawa, M. Rosenbusch, A. Takamine, T. Tanaka, Y. X. Watanabe, H. Wollnik, S. Yamaki, “First direct mass measurements of nuclides around  $Z = 100$  with a multireflection Time-of-flight mass spectrograph,” *Phys. Rev. Lett.* **120**, 152501 (2018).\*
- M. Mukai, Y. Hirayama, Y. X. Watanabe, P. Schury, H. S. Jung, M. Ahmed, H. Haba, H. Ishiyama, S. C. Jeong, Y. Kakiguchi, S. Kimura, J. Y. Moon, M. Oyaizu, A. Ozawa, J. H. Park, H. Ueno, M. Wada, H. Miyatake, “High-efficiency and low-background multi-segmented proportional gas counter for be-ta-decay spectroscopy,” *Nucl. Instrum. Methods Phys. Res. A* **884**, 1–10 (2018).\*

T. Sonoda, H. Iimura, M. Reponen, M. Wada, I. Katayama, V. Sonnenschein, T. Takamatsu, H. Tomita, T. M. Kojima, "The laser and optical system for the RIBF-PALIS experiment," Nucl. Instrum. Methods Phys. Res. A **877**, 118–123 (2018).\*

**[Proceedings]**

**(Original Papers) \*Subject to Peer Review**

M. Mazzocco, A. Boiano, C. Boiano, M. La Commara, C. Manea, C. Parascandolo, D. Pierroutsakou, C. Signorini, E. Strano, D. Torresi, H. Yamaguchi, D. Kahl, L. Acosta, P. Di Meo, J. P. Fernandez-Garcia, T. Glodariu, J. Grebosz, A. Guglielmetti, N. Imai, Y. Hirayama, H. Ishiyama, N. Iwasa, S. C. Jeong, H. M. Jia, N. Keeley, Y. H. Kim, S. Kimura, S. Kubono, J. A. Lay, C. J. Lin, G. Marquinez-Duran, I. Martel, H. Miyatake, M. Mukai, T. Nakao, M. Nicoletto, A. Pakou, K. Rusek, Y. Sakaguchi, A. M. Sánchez-Benítez, T. Sava, O. Sgouros, F. Soramel, V. Soukeras, E. Stiliaris, L. Stroe, T. Teranishi, N. Toniolo, Y. Wakabayashi, Y. X. Watanabe, L. Yang, Y. Y. Yang, " $^{8}\text{B} + ^{208}\text{Pb}$  elastic scattering at Coulomb barrier energies," J. Phys. Conf. Ser. **1078**, 012013 (2018).\*

**Oral Presentations**

**[International Conference etc.]**

- M. Wada, "Mass measurements with MRTO at RIKEN RIBF," NUSTAR Week 2018, Milan, Italy, September 27, 2018.
- M. Wada, "Mass measurements of heavy elements at GARIS," SSNET18 Conference, Paris, France, November 5–11, 2018.
- M. Wada, "MRTOF mass spectrographs at RIKEN RIBF — toward comprehensive mass measurements of >1000 nuclides including superheavy nuclides —," 13th Int. Conf. on Nucleus Nucleus Collisions (NN2018), Omiya, Japan, December 4, 2018.
- P. Schury, "KISS and MRTOF project of KEK," 10th China Japan Joint Nuclear Physics Symposium (CJNP2018), Huizhou, China, November 18–23, 2018.
- Y. Hirayama, "Nuclear spectroscopy of r-process nuclei using KEK isotope separation system," International Conference on Electromagnetic Isotope Separators and Related Topics (EMIS2018), CERN Geneva, Switzerland, September 16–21, 2018.
- M. Mukai, "Development of a multi-segmented proportional gas counter for beta-decay spectroscopy at KISS," International Conference on Electromagnetic Isotope Separators and Related Topics (EMIS2018), CERN Geneva, Switzerland, September 16–21, 2018.
- Y. X. Watanabe, "Production of neutron-rich nuclei by multinucleon transfer reactions at KISS project," IX Int. Symp. On Exotic Nuclei (EXON2018), Petrozavodsk, Russia, September 10–15, 2018.

**[Domestic Conference]**

- H. Miyatake, 「r-過程の第三ピークと終焉領域-KEK-WNSCのアプローチ」, 重力波観測時代の r プロセスと不安定核研究会, 2018 年 6 月 20–22 日.
- H. Miyatake, "RNB project on the astrophysical element synthesis," TGSW2018, 筑波大学, 2018 年 9 月 21 日.
- M. Wada, 「核データと重元素合成を中心とする宇宙核物理研究会, 札幌, 2019 年 3 月 6–8 日.
- Y. Hirayama, "Nuclear spectroscopy of r-process nuclei in the vicinity of  $N = 126$  at KISS," 日本物理学会年次大会 Joint Symposium on Nuclear structure studies through the magic numbers, 九州大学, 福岡, 2019 年 3 月 14–17 日.

## Events (April 2018 — March 2019)

## RNC

Apr. 21	Wako Open Campus
Jun. 12	The 24th RBRC Management Steering Committee (MSC)
Jun. 29	The 8th Industrial Program Advisory Committee (In-PAC)
Jul. 20	The 16th Program Advisory Committee for Materials and Life Science Researches at RIKEN Nishina Center (ML-PAC)
Jul.24–Aug.3	Nishina School
Nov.29–Dec.3	The 19th Program Advisory Committee for Nuclear Physics Experiments at RI Beam Factory (NP-PAC)
Jan	The 17th Program Advisory Committee for Materials and Life Science Researches at RIKEN Nishina Center (ML-PAC)P-PAC)
Jan. 11	Interim Review of the Chief Scientist, Tomohiro UESAKA

## CNS

Aug. 22–28	17th CNS International Summer School CNSSS18 <a href="https://indico2.cns.s.u-tokyo.ac.jp/event/30/">https://indico2.cns.s.u-tokyo.ac.jp/event/30/</a>
------------	---

## KEK

Sept. 4	2018 SSRI-PNS Collaboration meeting. <a href="http://research.kek.jp/group/wncs/workshop/2018_SSRI-PNS_201809/">http://research.kek.jp/group/wncs/workshop/2018_SSRI-PNS_201809/</a>
---------	--

## Press Releases (April 2018–March 2019)

RNC		
Apr. 13	Spectroscopy of pionic atoms in $^{122}\text{Sn}(d,3\text{He})$ reaction and angular dependence of the formation cross sections	T. Nishi, Spin isospin Laboratory K. Itahashi, Meson Science Laboratory
May. 24	Most Strange Dibaryon from Lattice QCD	S. Gongyo, T. Doi, Quantum Hadron Physics Laboratory
May. 29	Termination of Electron Acceleration in Thundercloud by Intra/Inter-cloud Discharge	Y. Wada, High Energy Astrophysics Laboratory
May. 31	A per-cent-level determination of the nucleon axial coupling from quantum chromodynamics	E. Rinaldi, Computing Group, RIKEN BNL Research Center
Jul. 10	Magic Nature of Neutrons in $^{54}\text{Ca}$ : First Mass Measurements of $^{55-57}\text{Ca}$	T. Uesaka, Spin isospin Laboratory
Jul. 12	Discovery of $^{60}\text{Ca}$ and Implications For the Stability of $^{70}\text{Ca}$	O. B. Tarasov, D. Ahn, N. Suzuki, BigRIPS Team
Aug. 3	Development of Ferromagnetic Fluctuations in Heavily Overdoped $(\text{Bi}, \text{Pb})_2\text{Sr}_2\text{CuO}_{6+\delta}$ Copper Oxides	I. Watanabe, Meson Science Laboratory
Aug. 11	Novel shape evolution in Sn isotopes from magic numbers 50 to 82	T. Otsuka, Nuclear Spectroscopy Laboratory
Oct. 2	Characterization of the shape-staggering effect in mercury nuclei	T. Otsuka, Nuclear Spectroscopy Laboratory
Oct. 19	Extraction of the Landau-Migdal Parameter from the Gamow-Teller Giant Resonance in $^{132}\text{Sn}$	M. Sasano, T. Uesaka, Spin isospin Laboratory
Dec. 11	Creation of quark-gluon plasma droplets with three distinct geometry	Y. Akiba, Experimental Group, RIKEN BNL Research Center
Jan. 30	Interplay between nuclear shell evolution and shape deformation revealed by the magnetic moment of $^{75}\text{Cu}$	Y. Ichikawa, H. Ueno, Nuclear Spectroscopy Laboratory
Feb. 28	First spectroscopy of the Near Drip-line Nucleus $^{40}\text{Mg}$	P. Doornenbal, H. Sakurai, Radioactive Isotope Physics Laboratory
CNS		
Jul. 10	希少原子核の高効率・高分解能質量測定による新しい魔法数 34 の確証	道正新一郎、小林幹、下浦亨、他



## **VII. LIST OF PREPRINTS**



## List of Preprints (April 2018 — March 2019)

## RIKEN NC-NP

188	Nascent fragment shell effects on the nuclear fission processes in semiclassical periodic orbit theory	K. Arita <i>et al.</i>
189	S-shaped heat capacity in an odd-odd deformed nucleus	B. Deya <i>et al.</i>
190	Interplay between nuclear shell evolution and shape deformation revealed by the magnetic moment of $^{75}\text{Cu}$	Y. Ichikawa <i>et al.</i>

## RIKEN NC- AC

	Not Applicable	
--	----------------	--

## RIKEN MP

	Not Applicable	
--	----------------	--

## RIKEN QHP

373	Many Fermi polarons at nonzero temperature	H. Tajima, S. Uchino
374	Quantitative analysis of tensor effects in the relativistic Hartree-Fock theory	Z. Wang <i>et al.</i>
375	Side-jump induced spin-orbit interaction of chiral fluids from kinetic theory	D. Yang
376	High precision nuclear mass predictions towards a hundred kilo-electron-volt accuracy	Z. Niu <i>et al.</i>
377	Non-equilibrium quantum transport of chiral fluids from kinetic theory	Y. Hidaka <i>et al.</i>
378	Asymptotic behavior of Nambu-Bethe-Salpeter wave functions for scalar systems with a bound state	S. Gongyo, S. Aoki
379	Holographic $J/\psi$ production near threshold and the proton mass problem	Y. Hatta, D. Yang
380	Diffusive Nambu-Goldstone modes in quantum time crystals	T. Hayata, Y. Hidaka
381	QCD sum rule for open strange meson $K_{1}^{\pm}$ in nuclear matter	T. Song <i>et al.</i>
382	Coulomb exchange functional with generalized gradient approximation for self-consistent Skyrme Hartree-Fock calculations	T. Naito <i>et al.</i>
383	$N\Omega$ dibaryon from lattice QCD near the physical point	T. Iritani <i>et al.</i>
384	Linear confinement and stress-energy tensor around static quark and anti-quark pair —Lattice simulation with Yang-Mills gradient flow—	R. Yanagihara <i>et al.</i>
385	Thermodynamics in the quenched QCD — EMT with NNLO coefficients in gradient flow formalism	T. Iritani <i>et al.</i>
386	HAL QCD method and Nucleon-Omega interaction with physical quark masses	T. Iritani (HAL QCD Collaboration)
387	Functional-renormalization-group aided density-functional analysis for the correlation energy of the two-dimensional homogeneous electron gas	T. Yokota, T. Naito
388	Measurement of time-dependent $CP$ Asymmetries in $B_0 \rightarrow K_s^0 \eta \gamma$ decays	H. Nakano (Belle Collaboration)
389	Search for $\Upsilon(1S, 2S) \rightarrow Z_c^+ Z_c^{(0)-}$ and $e^+e^- \rightarrow Z_c^+ Z_c^{(0)-}$ at $\sqrt{s} = 10.52, 10.58, \text{ and } 10.867$ GeV	S. Jia (Belle Collaboration)
390	Observation of an excited $\Omega^-$ baryon	J. Yelton (Belle Collaboration)
391	Observation of $\Upsilon(4S) \rightarrow \eta^* \Upsilon(1S)$	E. Guido (Belle Collaboration)

392	Inclusive study of bottomonium production in association with an $\eta$ meson in $e^+e^-$ annihilations near $\Upsilon(5S)$	U. Tamponi (Belle Collaboration)
393	Search for the lepton-flavor-violating decay $B^0 \rightarrow K^{*0} \mu^\pm e^\mp$	S. Sandilya (Belle Collaboration)
394	Measurement of $\eta_c(1S), \eta_c(2S)$ and non-resonant $\eta' \pi^+ \pi^-$ production via two-photon collisions	Q. N. Xu (Belle Collaboration)
395	Evidence of a structure in $\bar{K}^0 \Lambda_c^+ \Lambda_c^-$ consistent with a charged $\Xi_c(2930)^+$ , and updated measurement of $\bar{B}^0 \rightarrow \bar{K}^0 \Lambda_c^+ \Lambda_c^-$ at Belle	Y. B. Li (Belle Collaboration)
396	Observation of $e^+e^- \rightarrow \pi^+ \pi^- \pi^0 \chi_{b1,2}(1P)$ and search for $e^+e^- \rightarrow \phi \chi_{b1,2}(1P)$ at $\sqrt{s} = 10.96\text{--}11.05$ GeV	J. H. Yin (Belle Collaboration)
397	Observation of $\Upsilon(2S) \rightarrow \gamma \eta_b(1S)$ decay	B. G. Fulsom (Belle Collaboration)
398	Observation of $e^+e^- \rightarrow \gamma \chi_{c1}$ and search for $e^+e^- \rightarrow \gamma \chi_{c0}, \gamma \chi_{c2},$ and $\gamma \eta_c$ at $\sqrt{s}$ near 10.6 GeV at Belle	S. Jia (Belle Collaboration)
399	Measurement of the branching fraction and time-dependent $CP$ asymmetry for $B^0 \rightarrow J/\psi \pi^0$ decays	B. Pal (Belle Collaboration)
400	Consistency between Luescher's finite volume method and HAL QCD method for two-baryon systems in lattice QCD	T. Iritani <i>et al.</i>
401	Multi-body correlations in SU(3) Fermi gases	H. Tajima, P. Naidon
402	Thermal crossover, transition, and coexistence in Fermi polaronic spectroscopies	H. Tajima, S. Uchino
403	Improvement of functionals in density functional theory by the inverse Kohn-Sham method and density functional perturbation theory	D. Ohashi <i>et al.</i>
404	Distribution of solutions of the fastest apparent convergence condition in optimized perturbation theory and its relation to anti-Stokes lines	S. Tsutsui, T. M. Doi
405	Heavy quark spin multiplet structure of $P_c$ -like pentaquark as P-wave hadronic molecular state	Y. Shimizu <i>et al.</i>
406	Enhanced critical temperature, pairing fluctuation effects, and BCS-BEC crossover in a two-band Fermi gas	H. Tajima <i>et al.</i>
407	Anomaly-induced transport phenomena from the imaginary-time formalism	M. Hongo, Y. Hidaka
408	Chiral kinetic theory for massive fermions	K. Hattori <i>et al.</i>
409	Topological order in the color-flavor locked phase of (3+1)-dimensional $U(N)$ gauge-Higgs system	Y. Hidaka <i>et al.</i>
410	Universal crossover in interacting fermions within the low-energy expansion	H. Tajima

## CNS-REP

97	CNS Annual Report 2017	T. Gunji, Y. Kishi
----	------------------------	--------------------

*Nishina Center Preprint server* (not including Partner Institution) can be found at <http://nishina-preprints.riken.jp/>

## **VIII. LIST OF SYMPOSIA, WORKSHOPS & SEMINARS**



## List of Symposia &amp; Workshops (April 2018—March 2019)

RNC			
1	26th International Workshop on Deep Inelastic Scattering and Related Topics (DIS2018)	Convention Hall of Kobe University	Apr. 16–20
2	Workshop on r-Process and Unstable Nuclei in Multi-Messenger Astronomy (重力波観測時代の r プロセスと不安定核)	RIBF Conf. Hall, RIKEN Wako Campus	Jun. 20–22
3	Tesla Technology Collaboration Meeting 2018 (TTC2018)	RIKEN Wako Campus	Jun. 26–29
4	Nishina School 2018	RIBF Conf. Hall, RIKEN Wako Campus	Jul. 24 –Aug. 4
5	8th International Conference on Quarks and Nuclear Physics (QNP2018)	Tsukuba International Congress Center	Nov. 13–17
6	13th International Conference on Nucleus-Nucleus Collision (NN2018)	Omiya Sonic City	Dec. 4–8
7	The public symposium “Significance of Basic Science Research and its Impact on Society (in physics)”	Auditorium at Science Council of Japan	Dec. 17
8	The 1st Symposium on Heavy and Cluster Ions Mutagenesis of Microorganisms for finding Solutions to The Issue of Hyper-productivity, Energy and Environment	University of Tsukuba	Jan. 29
9	The 2nd RIBF “Hodan-kai” Meeting: Future of Exotic Nuclear Physics (第2回 RIBF 若手放談会 : エキゾチック核物理の将来)	Integrated Innovation Building, RIKEN Kobe Campus	Feb. 18–20
10	The International Year of the Periodic Table of Chemical Elements and activities supporting the Year (国際周期表年 2019 記念シンポジウム「周期表が拓く科学と技術国際周期表年を迎えて」)	Auditorium at Science Council of Japan	Feb. 23

CNS			
1	International OEDO Workshop	CNS	Jun. 11

## List of Seminars (April 2018—March 2019)

Nuclear Physics Monthly Colloquium			
1	Masaaki Hashimoto (Kyushu U.)	Stellar evolution and nucleosynthesis in massive stars <a href="https://indico2.riken.jp/event/2881/">https://indico2.riken.jp/event/2881/</a>	Oct. 3

RIBF Nuclear Physics Seminar			
1	Itaru Nakagawa (RIKEN)	Surprising forward neutron asymmetries observed in polarized proton + nucleus collision at RHIC <a href="https://indico2.riken.jp/event/2754/">https://indico2.riken.jp/event/2754/</a>	Apr. 10
2	Takahiro Kawabata (Kyoto U.)	Direct measurement of the ${}^7\text{Be}(n, \alpha){}^4\text{He}$ reaction cross section for the cosmological Li problem <a href="https://indico2.riken.jp/event/2753/">https://indico2.riken.jp/event/2753/</a>	Apr. 17
3	Takehiko Saito (GSI)	Hypernuclear spectroscopy with heavy ion beams: past, present and future <a href="https://indico2.riken.jp/event/2772/">https://indico2.riken.jp/event/2772/</a>	May 10

4	Koji Yoshimura (RIIS, Okayama U.)	Hunting for mysterious ultra-low energy isomer of Thorium-229 –to realize ultimate "nuclear clock"– <a href="https://indico2.riken.jp/event/2773/">https://indico2.riken.jp/event/2773/</a>	May 22
5	Newcomers to Nishina Center in 2018	Newcomers' seminar <a href="https://indico2.riken.jp/event/2774/">https://indico2.riken.jp/event/2774/</a>	May 29
6	Hironobu Ishiyama (RNC)	SLOWRI and related topics <a href="https://indico2.riken.jp/event/2788/">https://indico2.riken.jp/event/2788/</a>	Jul. 3
7	Noritaka Shimizu (U. Tokyo)	Double Gamow Teller transition and its relation to neutrinoless double beta decay matrix element <a href="https://indico2.riken.jp/event/2789/">https://indico2.riken.jp/event/2789/</a>	Jul. 10
8	Michiharu Wada (KEK)	The multi-reflection time-of-flight mass spectrographs at RIBF: Present and future <a href="https://indico2.riken.jp/event/2825/">https://indico2.riken.jp/event/2825/</a>	Jul. 31
9	Karlheinz Langanke (GSI)	Progress and scientific perspectives for the Facility of Antiproton <a href="https://indico2.riken.jp/event/2844/">https://indico2.riken.jp/event/2844/</a>	Sep. 21
10	Shinya Gongyo (RIKEN)	Dibaryon candidates in decuplet baryons from lattice QCD <a href="https://indico2.riken.jp/event/2877/">https://indico2.riken.jp/event/2877/</a>	Oct. 2
11	Sachio Komamiya /Hitoshi Hayano (Waseda U./KEK)	Introduction of ILC ~The physics, the accelerator, and the project status <a href="https://indico2.riken.jp/event/2878/">https://indico2.riken.jp/event/2878/</a>	Oct. 12
12	Hiroyuki Sagawa (U. Aizu)	The nuclear symmetry energy and the breaking of the isospin symmetry: how do they reconcile with each other? <a href="https://indico2.riken.jp/event/2906/">https://indico2.riken.jp/event/2906/</a>	Nov. 20
13	Shin'ichiro Michimasa (CNS)	First mass measurements of $^{55-57}\text{Ca}$ <a href="https://indico2.riken.jp/event/2945/">https://indico2.riken.jp/event/2945/</a>	Dec. 11
14	Hidetoshi Yamaguchi (CNS)	Study on cluster states in unstable nuclei with alpha-resonant scattering <a href="https://indico2.riken.jp/event/2954/">https://indico2.riken.jp/event/2954/</a>	Jan. 8
15	Masaki Sasano (RNC)	Gamow-Teller giant resonance in $^{132}\text{Sn}$ <a href="https://indico2.riken.jp/event/2973/">https://indico2.riken.jp/event/2973/</a>	Jan. 22
16	Yuichi Ichikawa (RNC)	Interplay between nuclear shell evolution and shape deformation revealed by the magnetic moment of $^{75}\text{Cu}$	Feb. 26
17	Fedor Šimkovic (Comenius U./ BLTP)	Massive neutrinos in nuclear processes <a href="https://indico2.riken.jp/event/2992/">https://indico2.riken.jp/event/2992/</a>	Mar. 5
18	Ali Al-adili (Uppsala U.)	Angular momenta in atomic nuclei – investigated by the population of nuclear isomers <a href="https://indico2.riken.jp/event/3003/">https://indico2.riken.jp/event/3003/</a>	Mar. 8
19	Shinya Wanajo (NAOJ)	R-process and kilonova <a href="https://indico2.riken.jp/event/3004/">https://indico2.riken.jp/event/3004/</a>	Mar. 12
20	Epelbaum Evgeny (Ruhr-U.)	Chiral EFT and the three-nucleon force problem <a href="https://indico2.riken.jp/event/3005/">https://indico2.riken.jp/event/3005/</a>	Mar. 25
21	Ushasi Datta (SINP)	A journey from light neutron rich-nuclei to heavier nuclei near proton-drip line <a href="https://indico2.riken.jp/event/3007/">https://indico2.riken.jp/event/3007/</a>	Mar. 29
22	Timo Dickel (JLU/GSI)	Experiments with thermalized RIB at the FRS <a href="https://indico2.riken.jp/event/3008/">https://indico2.riken.jp/event/3008/</a>	Mar. 29

## Seminar by Each Laboratory

### Nuclear Science and Transmutation Research Division

1	Susumu Inoue (ITHEMS)	The dawning of electroweak astronomy: interpreting electromagnetic +neutrino observations of blazars	Sep. 27
---	--------------------------	--	---------

2	Shin Watanabe (ISAS, JAXA)	Si/CdTe 半導体コンプトンカメラの開発研究と高感度 MeV ガンマ線観測実現に向けた展望	Sep. 27
3	Minoru Tanaka (Osaka U.)	同位体シフトで探る素粒子の新しい相互作用	Jan. 24
4	Takaya Nozawa (NAOJ)	Formation of dust and molecules in supernovae	Feb. 6

### Subnuclear System Research Division

1	Matthias Berwein (RIKEN)	QHP Seminar: Applications of effective field theories for heavy quarks	May 7
2	Yoshiko Kanada-En'yo (Kyoto U.)	SNP Seminar: Isoscalar monopole and dipole excitations in light nuclei	May 17
3	Kazuya Mameda (Fudan U.)	QHP Seminar: Rotational effects on quantum field theory for quark and hadron	May 22
4	Hiromichi Nishimura (RIKEN, RBRC)	QHP Seminar: On thermal effective potential of pure gauge theory at large $N$	May 30
5	Yuki Fujimoto (U. Tokyo)	QHP Seminar: Methodology study of machine learning for the neutron star equation of state	Jun. 18
6	Yusuke Namekawa (U. Tsukuba)	SNP Seminar: Successful prediction to charmed single hadrons and attempt on two-hadron by lattice QCD	Jun. 18
7	Nodoka Yamanaka (IPN Orsay))	SNP Seminar: The AFTER project, and the gluon and charm content of the deuteron	Jun. 20
8	Daisuke Kadoh (Keio U.)	QHP Seminar: Tensor network approach to lattice field theory	Jun. 25
9	Noriyuki Sogabe (Keio U.)	QHP Seminar: Does the chiral magnetic effect affect the dynamic critical phenomena in QCD?	Jul. 2
10	Yuki Kamiya (Kyoto U.)	SNP Seminar: Model-independent determination of structure of exotic hadrons with the scattering amplitude	Jul. 25
11	Kazuo Fujikawa (RIKEN, iTHEMS)	QHP Seminar: Chiral anomaly and Berry's phase	Sep. 10
12	Shunsuke Yabunaka (Kyoto U.)	QHP Seminar: Surprises in the $O(M)$ models: nonperturbative fixed points, large $N$ limit and multi-criticality	Sep. 21
13	Takahiro Ohgoe (U. Tokyo)	QHP Seminar: Resummation of diagrammatic series with zero convergence radius for the unitary Fermi gas	Oct. 1
14	Michele Viviani (INFN Pisa & U. of Pisa)	SNP Seminar: Theoretical study of three and four neutron resonances	Oct. 11
15	Takeru Yokota (Kyoto U.)	QHP Seminar: Functional renormalization group-aided density-functional theory -application to one-dimensional nuclear matter and two-dimensional electron gas-	Oct. 15
16	Akihiko Monnai (KEK)	QHP Seminar: The quark-gluon plasma fluid at finite density	Nov. 5
17	Huseyin Bahtiyar (Mimar Sinan Fine Arts U. )	SNP Seminar: Radiative transitions of singly - and doubly-charmed baryons in lattice QCD	Nov. 20
18	GuangJuan Wang (Peking U.)	SNP Seminar: The strong decay patterns of $Z_c$ and $Z_b$ states in the relativized quark model	Dec. 3

19	Akio Tomiya (RIKEN-BNL)	QHP Seminar: Deep Learning and Holographic QCD	Dec. 10
20	Hiromasa Takaura (Kyushu U.)	QHP Seminar: Renormalon and gluon condensate	Dec. 17
21	Masahiro Nozaki (RIKEN)	QHP Seminar: Signature of quantum chaos in operator entanglement in 2d CFTs	Jan. 21
22	Toshiaki Fujimori (Keio U.)	QHP Seminar: Bions and resurgence in $\mathbb{C}P^N$ model	Jan. 28
23	René Meyer (U. Würzburg)	QHP Seminar: Hydrodynamics & black holes in anti de sitter space-time	Mar. 25
24	Andreas Schmitt (U. Southampton)	Nuclear Theory/RIKEN Seminar: Dense nuclear and quark matter from holography	Apr. 6
25	Bernd-Jochen Schaefer (U. Giessen)	Nuclear Theory/RIKEN Seminar: Exploring the QCD phase structure with functional methods	Apr. 27
26	Peter Love (Tufts)	HET/RIKEN Lunch Seminar: Quantum simulation from quantum chemistry to quantum chromodynamics	May 10
27	HET/RIKEN Lunch Discussions	HET/RIKEN Lunch Discussions: Localized 4-sigma and 5-sigma dijet mass excesses in ALEPH LEP2 four-jet events	May 11
28	Stanley Brodsky (SLAC, Stanford U.)	Joint Nuclear Theory/RIKEN/CFNS Seminar: Novel QCD physics at an Electron-Ion Collider	May 25
29	Vladimir Skokov (BNL)	Nuclear Theory/RIKEN Seminar: Liouville action, high multiplicity tail and shape of proton	Jun. 1
30	Rasmus Larsen (BNL)	RIKEN Lunch Seminar: Topological structures in finite temperature QCD	Jul. 12
31	Matt Luzum (U. Sao Paulo)	Nuclear Theory/RIKEN Seminar: Confronting hydrodynamic predictions with Xe-Xe heavy-ion collision data	Jul. 13
32	Alessandro Roggero (U. Washington)	RIKEN Lunch Seminar/Special Nuclear Theory Seminar: Neutrino scattering on quantum computers	Jul. 19
33	Zhongbo Kang (UCLA)	Nuclear Theory/RIKEN Seminar: Jets as a probe of transverse spin physics	Jul. 27
34	Shigemi Ohta (IPNS, KEK)	RIKEN Lunch Seminar: Nucleon isovector axial charge in 2+1-flavor domain-wall QCD with physical mass	Aug. 2
35	Masanori Hanada (YITP)	RIKEN Lunch Seminar: Universality in classical and quantum chaos	Aug. 16
36	Andreas Weichselbaum (BNL)	RIKEN Lunch Seminar: Non-abelian symmetries and applications in tensor networks	Aug. 23
37	Joaquin Drut (UNC)	Special Nuclear Theory/RIKEN Lunch Seminar: Signal-to-noise issues in non-relativistic quantum matter: from entanglement to thermodynamics	Aug. 30
38	Ivan Horvath (U. Kentucky)	RIKEN/NT & Quantum Computing Seminar: Quantum uncertainty and quantum computation	Sep. 6
39	Julien Baglio (Tuebingen U.)	Joint BNL/RIKEN HET Seminar: Higgs pair production via gluon fusion at NLO QCD	Sep. 12
40	Yuta Kikuchi (RBRC)	RIKEN Lunch Seminar: Giant photocurrent in asymmetric Weyl semimetals from the helical magnetic effect	Sep. 13
41	Ilkka Helenius (U. Tubingen)	Nuclear Theory/RIKEN Seminar: Status of Pythia 8 for an Electron-Ion Collider	Sep. 21

42	Jordy De Vries (UMass Amherst)	Nuclear Theory/RIKEN Seminar: Neutrinoless double beta decay in effective field theory	Sep. 28
43	Shaouly Bar-Shalom (Technion)	HET/RIKEN Seminar: A universally enhanced light-quarks Yukawa couplings paradigm	Oct. 10
44	Nikhil Karthik (BNL)	RIKEN Lunch Seminar: Valence parton distribution function of pion using lattice	Oct. 18
45	Aleksas Mazeliauskas (U. Heidelberg)	Nuclear Theory/RIKEN Seminar: Studying out-of-equilibrium Quark-Gluon Plasma with QCD kinetic theory	Oct. 19
46	Kiminad Mamo (Stony Brook U.)	RIKEN Lunch Seminar: DIS on ""Nuclei"" using holography	Nov. 1
47	Alfred Mueller (Columbia U.)	Nuclear Theory / RIKEN Seminar: Diffractive electron-nucleus scattering and ancestry in branching random walks	Nov. 2
48	Ajit Srivastava (IOPB)	Nuclear Theory / RIKEN Seminar: Towards laboratory detection of superfluid phases of QCD	Nov. 9
49	Renaud Boussarie (BNL)	RIKEN Lunch Seminar: Exclusive $p$ meson production in $eA$ collisions: collinear factorization and the CGC	Nov. 15
50	Dimitra Karabali (CUNY)	Nuclear Theory / RIKEN: Casimir effect in Yang-Mills theory	Nov. 16
51	Juan Rojo (VU U.)	Nuclear Theory / RIKEN Seminar: Novel probes of small- $x$ QCD	Nov. 30
52	Mario Mitter (BNL)	RIKEN Lunch Seminar: On QCD and its phase diagram from a functional RG perspective	Dec. 6
53	Micheal Wagman (MIT)	NT/RIKEN Seminar: Lattice QCD input for fundamental symmetry tests	Dec. 14
54	Alba Soto Ontoso (BNL)	RIKEN Lunch Seminar: A novel background subtraction method for jet studies in heavy ion collisions	Jan. 10
55	Jun-sik Yoo (Stony Brook U.)	RIKEN Lunch Seminar: Proton decay matrix elements on lattice	Jan. 17
56	Andrey Sadofyev (Los Alamos National Lab)	Nuclear Theory / RIKEN Seminar: Chiral vortical effect for an arbitrary spin	Jan. 18
57	Xiaojun Yao (Duke U.)	RIKEN Lunch Seminar: Quarkonium production in heavy ion collisions: open quantum system, effective field theory and transport equations	Jan. 24
58	Paolo Glorioso (U. Chicago)	Nuclear Theory / RIKEN Seminar: Effective field theory of hydrodynamics	Jan. 25
59	Jasmine Brewer (MIT)	RIKEN Lunch Seminar: Sorting out jet quenching in heavy-ion collisions	Jan. 31
60	Juan M. Torres-Rincon (Stony Brook U.)	RIKEN Lunch Seminar: Modification of the nucleon-nucleon potential and nuclear correlations due to the QCD critical point	Feb. 7
61	Eden Figueroa (Stony Brook U.)	NT / RIKEN Seminar: Realizing relativistic dynamics with slow light polaritons at room temperature	Feb. 8
62	Sahal Kaushik (Stony Brook U.)	RIKEN Lunch Seminar: Chiral photocurrents and terahertz emission in Dirac and Weyl materials	Feb. 14
63	Jacobus Verbaarschot (Stony Brook U.)	NT / RIKEN Seminar: Quantum chaos, wormholes and the Sachdev-Ye-Kitaev model	Feb. 22
64	Ana-Maria Raclariu (Harvard U.)	Joint NT/RIKEN/CFNS Seminar: Measuring color memory in a color glass condensate	Feb. 28

65	Zohar Komargodski (Stony Brook U.)	NT/RIKEN Seminar: Baryons as Quantum Hall Droplets	Mar. 15
66	Hosted by Sally Dawson	High Energy / Nuclear Theory / RIKEN Seminars: Lattice Workshop for US-Japan Intensity Frontier Incubation	Mar. 25–27
67	Jamal Jalilian-Marian (CUNY)	NT/RIKEN Seminar: Toward a unified description of both low and high $p_T$ particle production in high energy collisions	Mar. 29

## CNS

1	Marco Mazzocco (U. of Padova / INFN)	Reaction dynamics studies with light weakly-bound radioactive ion beams at near-barrier energies <a href="https://indico2.riken.jp/event/2970/">https://indico2.riken.jp/event/2970/</a>	Dec. 10
2	Christian Smorra (CERN)	High-precision measurements of the antiproton's fundamental properties <a href="https://indico2.riken.jp/event/2969/">https://indico2.riken.jp/event/2969/</a>	Dec. 12
3	Afnasjev Anatoli (Mississippi State U.)	Covariant density functional theoretical studies across the nuclear landscape <a href="https://indico2.riken.jp/event/2968/">https://indico2.riken.jp/event/2968/</a>	Dec. 13
4	Ken'ichi Nakano (Tokyo Tech)	Measurement of flavor asymmetry of light antiquarks in proton via Drell-Yan process at Fermilab SeaQuest <a href="https://indico2.riken.jp/event/2967/">https://indico2.riken.jp/event/2967/</a>	Jan. 29
5	Fedor Šimkovic (Comenius U./BLTP JINR)	Massive neutrinos in nuclear processes <a href="https://indico2.riken.jp/event/2992/">https://indico2.riken.jp/event/2992/</a>	Mar. 5

## KEK WNSC

1	Ryan Ringle (Michigan State U.)	Advancing Penning trap mass spectrometry of rare isotopes at the LEBIT facility	Jul. 2
---	------------------------------------	---	--------



**理化学研究所**

埼玉県 和光市 広沢

RIKEN 2019-045